ROCK STRESS AND ITS MEASUREMENT

ROCK STRESS AND ITS MEASUREMENT

Bernard Amadei

Professor, Department of Civil, Environmental and Architectural Engineering, University of Colorado, Boulder, USA

and

Ove Stephansson

Professor, Department of Civil and Environmental Engineering, Royal Institute of Technology, Stockholm, Sweden

SPRINGER-SCIENCE+BUSINESS MEDIA, B.V.

First edition 1997

Originally published by Chapman & Hall in 1997
Softcover reprint of the hardcover 1st edition 1997

Typeset in 10/12 Palatino by Blackpool Typesetting Services Limited, UK

ISBN 978-94-010-6247-3 ISBN 978-94-011-5346-1 (eBook)
DOI 10.1007/978-94-011-5346-1

A catalogue record for this book is available from the British Library

Library of Congress Catalog Card Number: 96-86755

From Bernard to Robin, Liz-Ann and Alex
and
from Ove to Eija

for their patience, love and encouragement.

CONTENTS

PREFACE

Rock masses are initially stressed in their natural state. Whether one is interested in the formation of geological structures (folds, faults, intrusions, etc.), the stability of artificial structures (tunnels, caverns, mines, surface excavations, etc.), or the stability of boreholes, a knowledge of the *in situ* or virgin stress field, along with other rock mass properties, is needed in order to predict the response of rock masses to the disturbance associated with those structures. Stress in rock is usually described within the context of continuum mechanics. It is defined at a point and is represented by a second-order Cartesian tensor with six components. Because of its definition, rock stress is an enigmatic and fictitious quantity creating challenges in its characterization, measurement and application in practice. Stresses in rock cannot be measured directly and can only be inferred by disturbing the rock. Furthermore, rock stresses cannot be determined accurately due to the complex nature of rocks and rock masses. At best, and in good to very good rock conditions where the rock is essentially linearly elastic, homogeneous and continuous, and between well-defined geological boundaries, rock stresses can be determined with an error of $\pm$ 10–20% for their magnitude and an error of $\pm$ 10–20° for their orientation. On the other hand, in poor (weathered, weak, soft and heavily fractured) quality rocks, the measurement of rock stresses is extremely difficult. In such rocks the success rate of stress measurements is usually low.

This book focuses on the problem of *in situ* stresses in the Earth's crust, the methods for measuring and monitoring those stresses, and their importance in rock engineering, geology and geophysics. The emphasis is mostly on the current *in situ* state of stress and to a lesser extent on the monitoring of stress change. The subject of paleostresses is only briefly discussed.

The last 30 years have seen a major advance in our knowledge and understanding of rock stress. A large body of data is now available on the state of stress in the near surface of the Earth's crust (upper 3–4 km of the crust). Various theories have been proposed regarding the origin of *in situ* stresses and how gravity, tectonics, erosion, lateral straining, rock fabric, glaciation and deglaciation, topography, curvature of the Earth and other active geological features and processes contribute to the current *in situ* stress field. The techniques of stress measurement have evolved over the years, starting with the surface relief methods of the 1930s and 1940s, the flat jack method in the 1950s, the borehole relief methods of the 1950s and 1960s, and the engineering applications of hydraulic fracturing in the 1970s. Today, innovative methods are available for measuring rock stresses within the upper 3–4 km of the Earth's crust. At greater depths, very specialized techniques need to be used. The deepest reliable stress measurements ever made were reported in 1995 by scientists at the KTB (German Continental Deep Drilling Project) hole in Germany. Successful hydraulic fracturing stress measurements at a depth of 9 km gave maximum and minimum horizontal *in situ* stress values of 285 and 147 MPa, respectively. In general, the measurement of *in situ* stresses at depths below 9 km remains an unexplored territory where, in the future, new techniques will have to be developed and/or existing ones greatly improved.

Today, a large body of literature is available on the subject of *in situ* stresses. In writing this

book we have made a special attempt to refer to as many relevant publications and authors as possible. In general, the reader will find a comprehensive list of references spread over a total of 12 chapters, including the most recent contributions presented at the 8th Congress of the International Society for Rock Mechanics (ISRM) in Tokyo in September 1995.

This book is directed toward graduate students, teachers and practitioners in civil, mining and petroleum engineering, geology and geophysics. It can be used as a textbook in advanced graduate courses in rock mechanics and rock engineering, structural geology and geophysics. This book can also be used as a reference manual by practitioners who are faced with the challenge of rock stress. Actual case studies presented in this book should be of great interest to students, teachers and practitioners. The book has been written for someone who is familiar with the basic concepts of mechanics, geology and rock mechanics.

The 12 chapters in this book are presented in a logical order starting with the methods for estimating *in situ* stresses, followed by the techniques for measuring and monitoring rock stresses, and finally the importance of rock stresses in rock engineering, geology and geophysics. Several case studies of comparison of stress measurements are also presented, ranging in scale from local measurements to the World Stress Map. Throughout this book we have emphasized the role of geology when estimating and analyzing the results of stress measurements. We have also emphasized that the disciplines of engineering, geology and geophysics share many complementary similarities when it comes to understanding the state of stress in the Earth's crust.

This book satisfies the need to complement and update the information presented at the International Symposium on Rock Stress and Rock Stress Measurements organized by the second author and held in Stockholm on 1–3 September 1986. The conference revealed the broad range of interest in rock stress and its measurement in both the scientific and engineering communities. Despite its enigmatic nature, rock stress was recognized as a critical factor in a wide range of activities in rock engineering, geology and geophysics. Following the Stockholm meeting, the late 1980s and early 1990s witnessed an explosion in the number of publications dealing with the subject of rock stress and its measurement. The research program conducted at the Underground Research Laboratory (URL) in Canada and the stress compilation of the World Stress Map Project were instrumental in our understanding of the state of stress and its variation in the upper part of the Earth's crust. It was therefore decided that a book complementing the proceedings of the Stockholm meeting was timely and that an in-depth discussion of rock stress would be of great benefit to rock engineers, geologists and geophysicists, and others interested in that subject. Although this book deals mostly with the *in situ* or virgin stress field and its measurement, we have included one chapter (Chapter 10) dealing with the monitoring of stress change. We feel that such a chapter should be included as many of the techniques used for monitoring stress change are similar to those used for measuring virgin stresses. Furthermore, stress monitoring plays a crucial role in the different phases of development of nuclear waste repositories that are now being considered in different countries in the world.

Most of the chapters in this book have a lead author. The first author was responsible for the development of Chapters 2 (except section 2.14.2), 3, 5, 6 and 10, and the appendices. The second author was responsible for Chapters 4, 7 and 8, and section 2.14.2. Chapters 1, 9, 11 and 12 were jointly written. Questions and comments from the reader should be directed to the appropriate author(s).

In writing this book we have made every attempt to be comprehensive in our literature search. However, we may have inadvertently omitted some references. We hope that the reader will forgive such a transgression.

ACKNOWLEDGEMENTS

The writing of this book could not have been possible without the help of several of our colleagues. The first author is grateful to Russell Jernigan for reading the entire manuscript. The financial support of the US National Science Foundation under NSF grant no. MS-9215397 contributed to the development of several sections in Chapter 2 dealing with the role of rock fabric and topography on stress. The second author is grateful to the Swedish National Science Research Council for financial support under grant P3447-331. Both authors would like to thank Professor John A. Hudson for reviewing this book. His illuminating and inspiring comments are greatly appreciated. Many thanks go to Robert Walton from MINDATA (Australia), Jean-François Cappelle and Pierre Choquet from ROCTEST (Canada), and Helmut Bock from INTERFELS (Germany) for providing photographs and technical documentation. Discussions with Derek Martin were of great help in understanding the URL stress results and the nature of rock stress in general. We are grateful to J. Lauterjung for sending us a photograph of the KTB drilling site, to Mary-Lou Zoback and Birgir Müller for providing us with originals of maps of the World Stress Map Project, to Maria Ask for providing stress data from the Danish sector of the North Sea, and to David Ferrill for sending us illustrations regarding slip-tendency analysis and its application at the Yucca Mountain project in Nevada. A first draft of this book was used in a doctoral course at KTH in the fall of 1994. Valuable comments from the participants are acknowledged. Ann-Charlotte Åkerblom is acknowledged for typing the first version of Chapter 4. The illustrations in this book were made by William Semann at the University of Colorado in Boulder and by Mathias Lindahl at KTH in Stockholm.

INTRODUCTION 1

1.1 STRESS AT A POINT

Unlike artificial materials such as concrete and steel, natural materials such as rocks and soils are subject to natural (virgin) stresses called *in situ* stresses. Stress is an enigmatic quantity which, according to classical mechanics, is defined at a point in a continuum and is independent of the constitutive behavior of the medium. The concept of stress used in rock mechanics is consistent with that formulated by Cauchy and generalized by St Venant in France during the 19th century (Timoshenko, 1983). A summary of the continuum mechanics description of stress is presented below. More details can be found in Appendix A or in Mase (1970).

In continuum mechanics, stress is a fictitious quantity that is defined through a limiting process by considering the interaction between two parts of a continuum across a small oriented surface at a point. Consider for instance, the continuum shown in Fig. 1.1 occupying a region R of space and subjected to body forces $\boldsymbol{b}$ and surface forces $\bar{f}$. Let x, y, z be a Cartesian coordinate system with unit vectors e_1, e_2, e_3. Consider a volume V in the continuum, an infinitesimal surface element ΔS located on the outer surface S of V, a point P located on ΔS, and a unit vector $\boldsymbol{n}$ normal to ΔS at P.

Under the effect of the body and surface forces, the material within volume V interacts with the material outside of V. Let $\Delta \boldsymbol{f}$ and $\Delta \boldsymbol{m}$ be respectively the resultant force and moment exerted across ΔS by the material outside of V upon the material within V. The Cauchy stress principle asserts that the average force per unit area $\Delta f / \Delta S$ tends to a limit $\boldsymbol{t}_{(n)} = \mathrm{d}f / \mathrm{d}S$ as ΔS tends to zero, whereas $\Delta \boldsymbol{m}$ vanishes in the limiting process. The limit $\boldsymbol{t}_{(n)}$ is called the stress vector and has three components in the x, y, z coordinate system which are expressed in units of force per unit area (MPa, psi, psf, etc.). It is noteworthy that the components of the stress vector depend on the orientation of the surface element ΔS which is defined by the coordinates of its normal unit vector $\boldsymbol{n}$.

The stress vector $\boldsymbol{t}_{(n)}$ at point P in Fig. 1.1 is associated with the action of the material outside of V upon the material within V. Let $\boldsymbol{t}_{(-n)}$

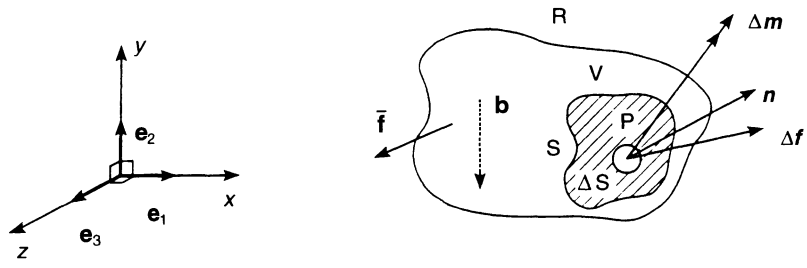

Fig. 1.1 Material continuum subjected to body and surface forces.

be the stress vector at point P corresponding to the action across ΔS of the material within V upon the material outside of V. By Newton's law of action and reaction, $\boldsymbol{t}_{(-n)} = -\boldsymbol{t}_{(n)}$. This remark implies that the stress vectors acting on opposite sides of a same surface are equal in magnitude but opposite in direction.

The state of stress at point P in Fig. 1.1 can be defined by calculating $\boldsymbol{t}_{(n)}$ for all possible infinitesimal surfaces ΔS having point P as an interior point. Another alternative is to consider the stress vectors $\boldsymbol{t}_{(e1)}$, $\boldsymbol{t}_{(e2)}$ and $\boldsymbol{t}_{(e3)}$ acting on three orthogonal planes normal to the x-, y- and z-axes and with normal unit vectors $\boldsymbol{e}_1$, $\boldsymbol{e}_2$ and $\boldsymbol{e}_3$, respectively. The three planes form an infinitesimal stress element around point P (Fig. 1.2a). Vector $\boldsymbol{t}_{(e1)}$ has components σ_x, τ_{xy} and τ_{xz}, vector $\boldsymbol{t}_{(e2)}$ has components τ_{yx}, σ_y and τ_{yz}, and vector $\boldsymbol{t}_{(e3)}$ has components τ_{zx}, τ_{zy} and σ_z.

The nine components of vectors $\boldsymbol{t}_{(e1)}$, $\boldsymbol{t}_{(e2)}$ and $\boldsymbol{t}_{(e3)}$ form the components of a second-order Cartesian tensor also known as the stress tensor σ_{ij}. The components consist of three normal stresses σ_x, σ_y, σ_z and six shear stresses τ_{xy}, τ_{yx}, τ_{xz}, τ_{zx}, τ_{yz}, τ_{zy}. As shown in Appendix A, the force and moment equilibrium yield the equations of equilibrium and symmetry of the stress tensor with $\tau_{xy} = \tau_{yx}$, $\tau_{xz} = \tau_{zx}$ and $\tau_{yz} = \tau_{zy}$. Thus three normal stresses and three shear stresses define the state of stress at a point in a continuum. Alternatively, the state of stress can be represented by three principal stresses σ_1, σ_2 and σ_3 and their orientation in the x, y, z coordinate system (Fig. 1.2b), which represent the eigenvalues and eigenvectors of the stress tensor. The principal stresses act on three principal planes on which shear stresses vanish.

As shown in Appendix A, knowing the stress tensor representing the state of stress at a point P, the components of the stress vector on any plane passing by P, and of known orientation with respect to the x-, y- and z-axes can be determined by using coordinate transformation laws for second-order tensors.

The reader should be aware that two sign conventions are used in engineering stress analysis. For rock mechanics problems, and throughout this book, normal stresses are taken as positive when compressive, and the direction of positive shear stresses is as shown in Fig. 1.2a. Note that this convention is opposite to that adopted in classical mechanics.

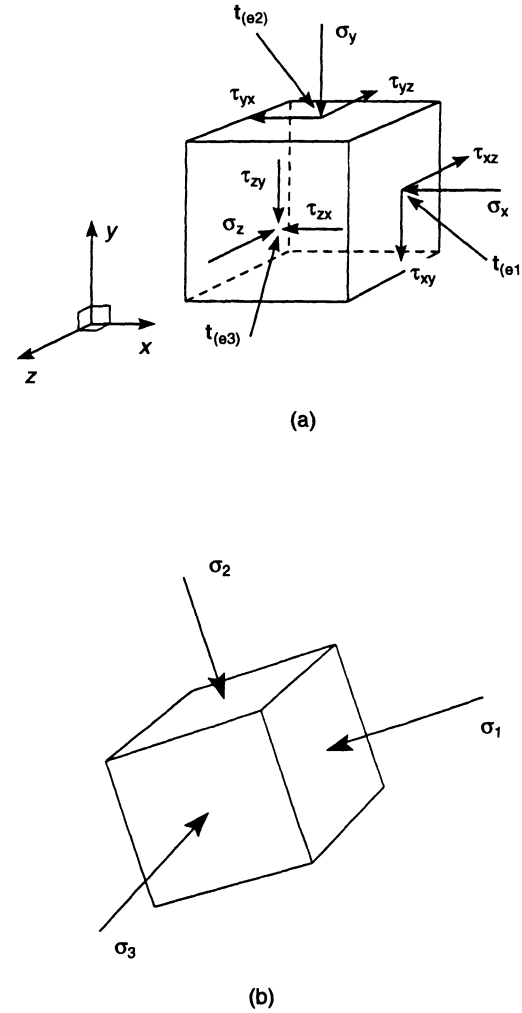

Fig. 1.2 (a) Infinitesimal stress element defining the state of stress at a point; (b) principal stress element. Direction of positive normal and shear stresses used in rock mechanics.

1.2 IMPORTANCE OF ROCK STRESS

Knowledge of the *in situ* state of stress in the Earth's crust is very important in many problems dealing with rocks in civil, mining and petroleum engineering and energy development, as well as in geology and geophysics. A list of activities for which *in situ* stresses play a critical role is given in Table 1.1. An overview of these activities is presented below. A more detailed discussion is given in Chapter 12.

In civil and mining engineering, *in situ* stresses control the distribution and magnitude of the stresses around underground openings such as tunnels, mines, shafts or caverns (Hoek and Brown, 1980). Stress concentrations in the excavation walls may be large enough to overstress the rock, mobilize the strength of the rock mass locally or at large, and create failure. They can also induce excessive deformation in the form of roof closure, sidewall movement and/or ground subsidence. On the other hand, tensile stresses in excavation walls may open existing fractures or create new ones which could result in block stability problems.

Table 1.1 Activities requiring knowledge of *in situ* stresses

Civil and mining engineering
Stability of underground excavations (tunnels, mines, caverns, shafts, stopes, haulages)
Drilling and blasting
Pillar design
Design of support systems
Prediction of rock bursts
Fluid flow and contaminant transport
Dams
Slope stability
Energy development
Borehole stability and deviation
Borehole deformation and failure
Fracturing and fracture propagation
Fluid flow and geothermal problems
Reservoir production management
Energy extraction and storage
Geology/geophysics
Orogeny
Earthquake prediction
Plate tectonics
Neotectonics
Structural geology
Volcanology
Glaciation

In general, stress-related stability problems increase with depth but can also be found in excavations at shallow depths (0–200 m) due to high horizontal *in situ* stresses such as in southern Ontario and upper New York State (Adams and Bell, 1991; Franklin and Hungr, 1978; Lee, 1981; Lee and Lo, 1976; Lo, 1978; Lo and Morton, 1976), Fennoscandia (Carlsson and Olsson, 1982; Hast, 1958; Myrvang, 1993; Stephansson, 1993; Stephansson, Särkkä and Myrvang, 1986) and Australia (Enever, Walton and Windsor, 1990). High stresses can also be found when conducting underground excavation in mountainous regions near steep valley walls (Myrvang, 1993). In general, excavation in highly stressed rock is more difficult and special strategies need to be followed to minimize the impact of high stresses. Potential stability problems associated with the relief of high stresses may include floor buckling, spalling, squeezing, inward movement of excavation walls and rock bursts. Detrimental effects of high stresses can be found in canals, bridges, surface excavations, shafts, tunnels and mining excavations. Furthermore, drilling in highly stressed rock is more difficult. Myrvang, Hansen and Sørensen (1993) found, for instance, a significant negative correlation between the rate of penetration in rotary drilling with increasing stress. A positive aspect of high stresses, however, is that the rock is tighter, which implies less water inflow in underground works and shorter pathways for contaminant transport.

In the engineering of underground construction, *in situ* stresses enter into excavation design and critical decision making. The distribution and magnitude of *in situ* stresses affect the geometry, shape, dimensioning, excavation sequence and orientation of underground excavations. They also help in the

selection and design of support systems. From a practical point of view, when designing underground openings in rocks where the virgin stresses are low compared with the rock strength, the goal is to minimize stress concentration problems, create a compressive stress field as uniformly distributed as possible in the excavation walls (the 'harmonic hole' concept) and avoid tensile stress regions. For instance, a circular excavation is better suited in a hydrostatic stress field than in any other stress fields. Horizontal caverns with large spans require horizontal stresses higher than the vertical stress. As an illustrative example, the feasibility of the 61 m span, 91 m long and 24 m high underground Olympic ice hockey hall in Lillehammer, Norway, was made possible due to not only a good geological setting but also because of the existence of large horizontal stresses in the order of 4–5 MPa at shallow depths ranging between 40 and 100 m (Myrvang, 1993). It is noteworthy that the 'harmonic hole' concept is not recommended when the virgin stresses are high (Hoek and Brown, 1980). In that case, the excavation shape should be selected in such a way that the zones of overstressed rock are concentrated in sharp corners and are limited in extent (Fairhurst, 1968).

Figure 1.3 shows a case study where stresses were critical in the layout of a penstock manifold for the Helms pumped storage project in the Sierra Nevada (Haimson, 1977, 1984). In this project, the penstock bifurcation branch was rotated 90° from its original orientation of N30°E in order to avoid opening of discontinuities in a direction parallel to the major horizontal *in situ* stress σ_{Hmax} measured (by hydraulic fracturing) in the N25°E direction. Mimaki (1976) and Mimaki and Matsuo (1986) give two examples of design of large underground caverns in Japan where it was decided to orient the caverns with their long axes parallel to the maximum horizontal *in situ* stress. In general, aligning caverns in rocks with their long axis perpendicular to the largest *in situ* stress component should be avoided (Broch, 1993).

Over the past 10 years, rock mechanics has become more of a practical tool for surface and underground mine operators. The acceptance of rock mechanics techniques in underground mining is largely due to rapid advancement in numerical modeling techniques, the use of

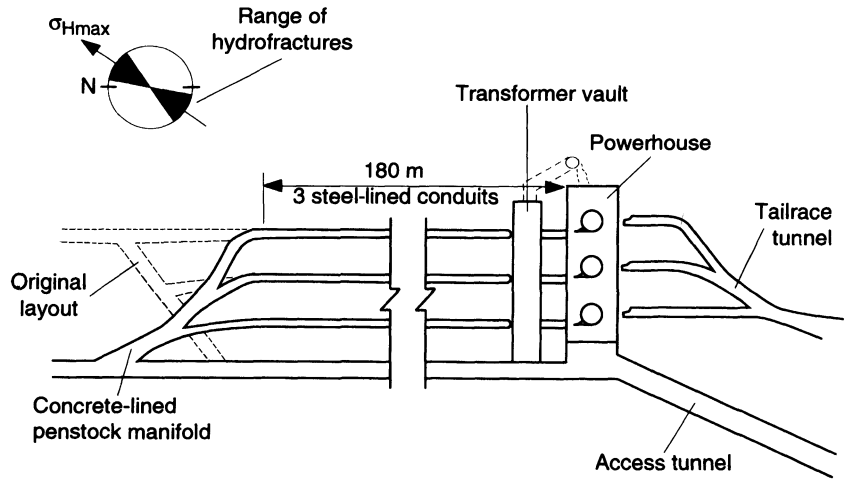

Fig. 1.3 Plan of Helms project powerplant complex showing the original and the redesigned penstock manifolds. (After Haimson, 1984.)

rock mass classification systems and more reliable methods for rock stress measurements. The state of the art in rock engineering for underground mine use is presented by Brady and Brown (1985). *In situ* stresses form the loading system for the underground excavations (Bawden, 1993). It is the redistribution of these stresses due to mining activity that causes deformation and failure of the rock mass. The adverse effects of mine failure are fatalities, injuries and damage to equipment which overall translate into a loss in production. In room and pillar mining, stresses in pillars affect the overall mine extraction ratio and control the overall mine stability and layout. Enever (1993) discussed the impact of *in situ* stresses in Australia for deciding on the location of new coal mine developments and mine layouts as well as the location and stability of coal seam methane extraction wells.

Several mining factors, including the depth of mining, mine geometry and the rate and volume extracted, can influence the redistribution of stresses and hence the occurrence of rockbursts and mine seismicity (Cook, 1976; McGarr and Wiebols, 1977). Mine seismicity is essentially rock failure due to the alteration of the virgin stress state by mining an opening in rock. Over the years, mining engineers have had to deal with higher *in situ* stress fields associated with increasingly deep mines. A combination of deeper mines and larger mine openings has increased the occurrence and severity of mine seismicity and collapse of mine openings. An *a priori* knowledge of the characteristics of pre-existing zones of weakness in rock masses and the *in situ* stress field can assist mining engineers in identifying areas where large mining-induced failure and seismic events are likely to occur. Several case histories which emphasize the importance of seismological analyses to characterize the sources of mine seismicity and the effects of geological discontinuities and *in situ* stresses are discussed by Gay and Van der Heever (1982) and Wong (1993).

Rock stress measurements are often performed to provide input to numerical modeling of mine design and deformability, strength and reinforcement of mine openings. For mine design applications, the common practice is to locate the measuring sites remote from the mining stopes, so that the measured stresses are unaffected by the mining activity. In old underground mines, where mining occurs at great depths below the ground surface, stress measurements have to be made in disturbed rock masses. As an illustrative example, in the design of the Zinkgruvan mine in central Sweden, an approach was adopted in which the stress measurement sites were located in the roofs of open stopes in different mine panels (Borg *et al.*, 1984). The location of the sites is shown in Fig. 1.4a and the results of the overcoring stress measurements in the roof of two stopes are presented in Fig. 1.4b, c. No stress gradients were found in the vicinity of the stopes, and very small differences in magnitude and direction of stresses were recorded for the measuring points at each site. The average value of the major principal stress was found to be equal to 40 MPa, and to be oriented perpendicular to the tabular orebody. These results were used in the design of mining sequences and rock reinforcement of the stopes. Stress data from the stopes together with stress measurements in an undisturbed region at the deepest point accessible in the mine (site no. 4 in Fig. 1.4a) were used by Borg *et al.* (1984) to estimate the variation of the virgin vertical and horizontal stresses with depth. Then, the estimated stresses were applied in the numerical modeling for design and stability prediction of mining at depths below 800 m.

Knowledge of *in situ* stresses is also critical for the storage of nuclear waste in rock. The US Nuclear Regulatory Commission (10CFR60), Sections 60.10 and 60.21, specifies that *in situ* stresses should be measured at the site, before and during the construction of a repository (Kim, 1992). *In situ* stresses are taken into account in repository site suitability,

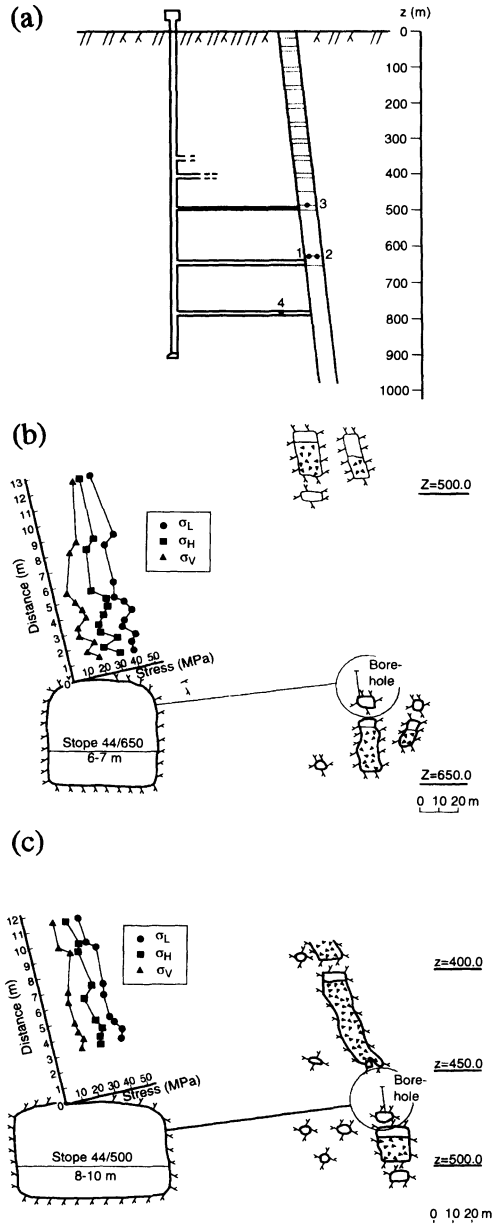

Fig. 1.4 Stress measurements at the Zinkgruvan mine in central Sweden. (a) Stress measurement sites with overcoring technique, (b) results of stress measurements at site no. 1 in the roof of stope 44/650, (c) results of stress measurements at site no. 3 in the roof of stope 44/500. σ_L = stress perpendicular to the local strike of the orebody, σ_H = stress parallel to the local strike of the orebody and σ_V = vertical stress. (After Borg *et al.*, 1984.)

selection and characterization and the repository design and construction (Kim, 1992; Kim *et al.*, 1986). As an example, Fig. 1.5 shows the layout of the underground nuclear waste facility that was proposed (and later abandoned) at Hanford, Washington (Rockwell Hanford Operations, 1982). Based on the results of hydraulic fracturing tests conducted at the depth of the proposed repository (about 1000 m), it was decided to align the placements rooms in a direction parallel to the minimum horizontal *in situ* stress and the storage holes parallel to the maximum horizontal stress (Kim *et al.*, 1986).

One of the most comprehensive and best documented case studies on rock stress and its measurement was conducted at the Underground Research Laboratory (URL) in the Lac du Bonnet granite batholith on the western edge of the Canadian Shield in the province of Manitoba in Canada. This research facility is used by Atomic Energy of Canada Limited (AECL) to investigate the permanent disposal of nuclear waste fuel in plutonic rock. The field studies conducted at the URL since the early 1980s have been used to answer many of the fundamental questions with regard to rock stress in hard and competent rock (Martin and Simmons, 1993), e.g. are *in situ* stresses dependent on the scale of the method used; what is the effect of geological structures on *in situ* stresses; what is the importance of residual stresses; do different methods yield comparable *in situ* stress fields? The four questions were answered by using a wide range of methods of *in situ* stress measurements.

The performance of unlined pressure tunnels, shafts and storage caverns is also strongly dependent on the magnitude and orientation of *in situ* stresses. Pressure tunnels and shafts which are unlined over most of their lengths have been used in various hydroelectric schemes around the world and have been called upon to perform under increasingly higher heads, now approaching 1000 m (Benson, 1988). The first and foremost consideration in the safe design of unlined

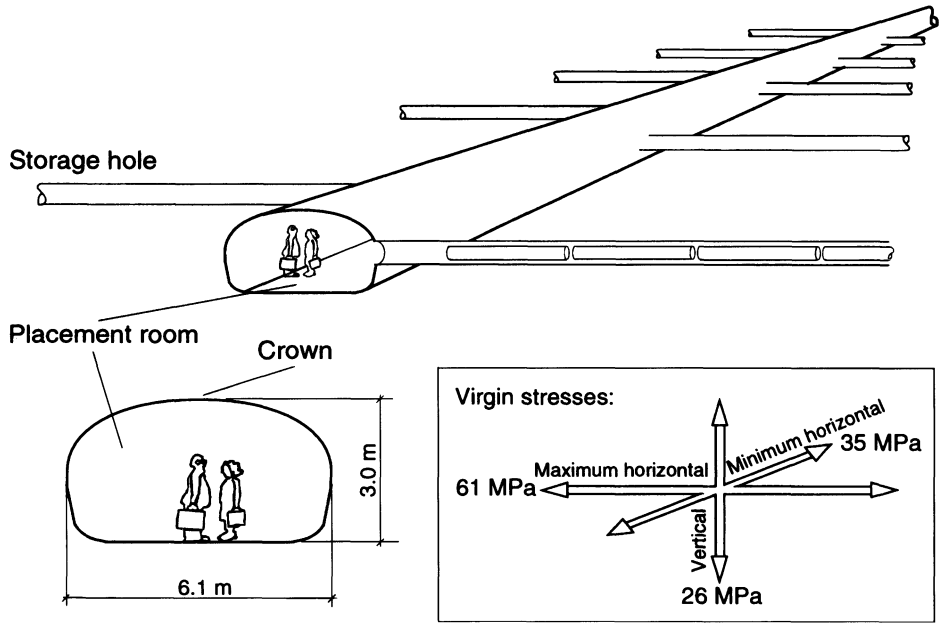

Fig. 1.5 Suggested layout of underground nuclear waste disposal facility at Hanford, Washington. The virgin stress values, shown in the insert, were determined by hydraulic fracturing on the candidate repository horizon at a depth of about 1000 m. (Adapted from Rockwell Hanford Operations, 1982.)

pressure tunnels and shafts is to avoid water leakage by hydraulic opening (also called hydraulic jacking) of the rock mass. Water leakage may lead to disastrous and costly consequences, as illustrated in many case studies (Brekke and Ripley, 1993; Broch, 1984a, b; Sharma *et al.*, 1991). Hydraulic jacking of the rock mass can be prevented by positioning unlined pressure tunnels and shafts in competent rock and under enough rock cover to provide adequate confinement and watertight conditions. One criterion used for positioning unlined pressure tunnels and shafts in valley sides is that nowhere along the opening alignment should the internal water pressure exceed the minimum *in situ* principal stress in the surrounding rock mass (Selmer-Olsen, 1974). Large enough *in situ* stresses can help in reducing the need for liners in pressure tunnels and shafts, thus creating substantial cost savings.

Myrvang (1993) discussed the importance of having sufficiently high rock stresses for the storage of gas in unlined rock caverns in Norway. The minimum *in situ* principal stress must be large enough to prevent leakage under minimum gas pressures of the order of 8–10 MPa. Construction cost of storage caverns can be reduced if confinement due to large enough horizontal stresses can be found at shallow depths. The importance of *in situ* stresses in critical decision making for gas storage was illustrated by Enever (1993) regarding a horizontal abandoned coal mine in Australia which was considered for storage. Horizontal fractures obtained during hydraulic fracturing tests in the rock above the mine showed lower vertical stresses than expected, indicating cracking of a large part of the overburden rock, thus making the site unsuitable for gas storage. Tightness of a rock mass due to large enough *in situ* stresses is also important for the storage of compressed air, cryogenic liquids (LNG, LPG), oil, etc.

The effective utilization of oil and gas resources on land and offshore and the applications of diverging wellboring technology have increased over the past 20 years. In particular, in order to determine the direction of a wellbore and reduce borehole deviations and breakouts, a clear understanding of *in situ* stresses is vital. Borehole stability, which is of major concern to petroleum engineers, is controlled by stress concentrations along borehole walls. Overbreaks due to mobilization of the rock strength may create large borehole stability problems (Maury, 1987). Knowledge of the *in situ* stress field is also important for the fracturing of formations of oil and gas fields to stimulate production (Teufel, 1986). Reservoir management also requires that changes in the *in situ* stress field be known during reservoir depletion. For instance, in the Ekofisk field (which is the largest of nine chalk reservoirs in the southern part of the Norwegian sector of the North Sea), Teufel, Rhett and Farrell (1991) reported a 21–24 MPa reduction in reservoir pore pressure and changes in the total minimum horizontal stress of about 80% of the changes in pore pressure, as a follow-up of 20 years of petroleum production. As the pore pressure decreases, more of the overburden load has to be carried out by the weak chalk matrix, which in turn may cause reservoir compaction and seafloor subsidence. Such subsidence may require oil and gas platforms to be jacked up in order to prevent breaking of sea waves. Figure 1.6 shows a plan view of the Ekofisk field, and the role played by natural fractures and the dome shape of the reservoir on the *in situ* stress distribution. In this figure, the maximum horizontal stress is parallel to the long axis of the reservoir near the dome crest. It becomes perpendicular to the dome structural contour and parallel to a radial fracture pattern on the flanks of the structure (Teufel and Farrell, 1990).

The new global geology and plate tectonics form the fundamentals of modern Earth sciences. Here, geologists and geophysicists are trying to gain knowledge of the role played by *in situ* stresses in the overall understanding of the mechanism of plate movement, collision and divergence, the dynamics of faulting along plate boundaries and intraplate regions, mountain building, basin formation, earthquakes and other active geological processes (M. D. Zoback, 1993). For that purpose, ultradeep continental drilling programs have been initiated in various parts of the world. For

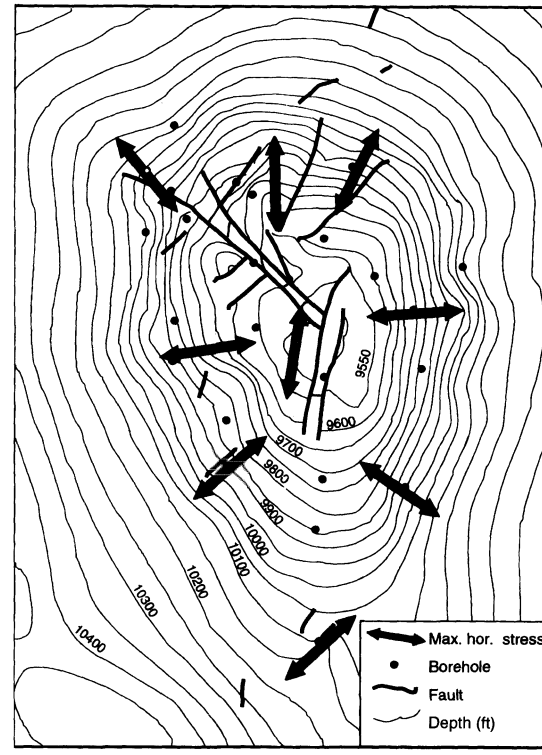

Fig. 1.6 Structure contour map for top of the Ekofisk formation in the North Sea showing the azimuth of the maximum horizontal stress determined from anelastic strain recovery measurements of oriented cores from nine wells in the Ekofisk field. On the crest of the dome structure, located at a depth of about 9500 ft (2.9 km), the maximum horizontal stress is parallel to the long axis of the reservoir. It becomes perpendicular to the dome structural contour and parallel to a radial fracture pattern on the flanks of the structure. (After Teufel and Farrell, 1990.)

instance, *in situ* stresses have been measured in the mid-crust at depths ranging between 0.8 and 9.0 km at the KTB (German Continental Deep Drilling Project) hole in Germany (Baumgärtner *et al.*, 1993; Brudy *et al.*, 1995; Te Kamp, Rummel and Zoback, 1995), and in the vicinity of the San Andreas fault at depths ranging between 0.9 and 3.5 km at the Cajon Pass drill site (Baumgärtner *et al.*, 1993; Zoback and Healy, 1992). Deep stress measurements were also reported by Batchelor and Pine (1986) and Pine and Kwakwa (1989) at depths up to 2.6 km in the Carnmenellis granite in Cornwall, England. Other deep stress measurements were conducted by Haimson (1978) at depths ranging between 3 and 5 km in the Michigan Basin.

Analysis of over 7300 data points collected as part of the World Stress Map Project has revealed some major stress patterns and stress regimes in the Earth's crust (Zoback *et al.*, 1989; M. L. Zoback, 1992). Multiple broad-scale regional stress provinces with uniform horizontal stress orientation have been identified. Also, there is clear evidence that the directions of plate movement for several major plates seem to coincide with the directions of maximum horizontal stresses. Other findings from the World Stress Map Project include dominant compressive stress regimes (thrust or combined thrust and strike-slip faulting) in most mid-plate or intraplate continental regions, and continental extensional stress regimes (normal or combined normal and strike-slip faulting) in topographically high areas. As an example, Fig. 1.7 shows the stress directions for Europe as compiled by Müller *et al.* (1992). Note the consistent NW–SE horizontal stress orientation in Western Europe.

In situ stresses are important to geologists in order to understand various geological processes. Over the years, several theories of faulting, folding, thrusting, tectonic fabrics, boudinage and pinch-and-swell structures, intrusions, subsidence and so on have been proposed. The formation, emplacement and extent of such structures depend largely on the *in situ* stress field that existed prior to their existence.

In situ stresses are usually determined along with rock mass properties such as deformability, strength and permeability. *In situ* stress measuring techniques can be seen as providing samples of the stress field over a certain volume of interest. Like many rock mass properties, *in situ* stresses may vary from point to point in a rock mass and may have different values when measured over different volumes. Such variations are intrinsic and should not always be seen as anomalies or errors in the measurements themselves.

In situ stresses are rarely uniform in a rock mass. Their distribution depends largely on the rock mass structure (discontinuities, heterogeneities, folds, faults, dikes, fabric, etc.) and on the loads applied to the rock mass throughout its entire geological history. For instance, competent rock layers tend to carry larger stresses than weak layers. A strong correlation has also been observed between rock fabric and stresses. The stress distribution in a rock mass can be so complex that local stresses may be quite different from the average stress.

In situ stresses interact with other rock mass properties. For instance, rock mass strength increases with *in situ* confinement. Stress fields alter the permeability of rock masses since compressive stresses tend to close natural fractures whereas tensile stresses tend to open them. The coupling existing between stress and flow and pressure in fractures is particularly important in understanding fluid flow and contaminant transport in rock masses, and in predicting the effectiveness of hydraulic injections which are common in the exploitation of hydrocarbon formations and geothermal energy systems and for liquid waste disposal (Evans, 1966; Grant, Donaldson and Bixley, 1982; Pine and Batchelor, 1984). On the other hand, rock mass structures such as joints or foliation planes affect the distribution of *in situ* stresses. In some recent papers, Hudson (1991, 1992a) presented compilations of rock engineering mechanisms showing the

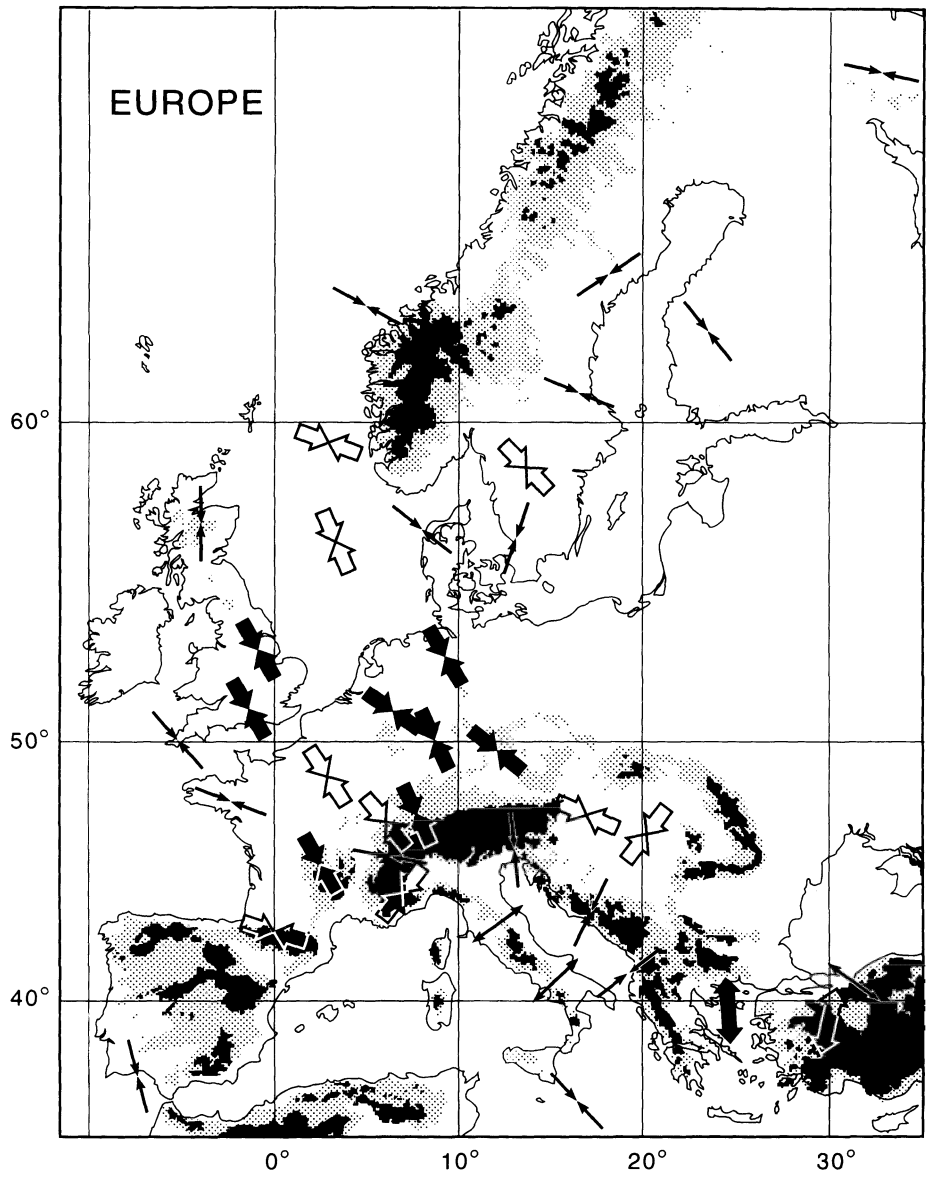

Fig. 1.7 Generalized stress map of Europe showing maximum horizontal compression directions in regions of dominantly compressive stress regimes (inward directed arrows) and least horizontal stresses in regions of extension (outward directed arrows). Thick arrows are shown for average stress directions which are based on at least ten stress observations with uniform orientations, open arrows are used for means based on five to ten consistent orientations and thin arrows are for average directions based on less than five observations. (After Müller *et al.*, 1992.)

importance of *in situ* stresses in the stability of underground excavations and rock slopes and how *in situ* stresses interact with other rock mass properties. *In situ* stress is an integral part of the theory of rock engineering systems (Hudson, 1992b; Jiao and Hudson, 1995).

1.3 HISTORY

The previous discussion shows clearly that modern rock mechanics engineers, geologists and geophysicists have to be well acquainted with the basics of rock stresses and rock stress measurements. The need to understand *in situ* stresses in rocks has been recognized by geologists, geophysicists and engineers for a long time and many methods to measure those stresses have been proposed since the early 1930s. The most common methods today include hydraulic and relief methods. The growing interest in *in situ* stresses and stress measurements has been reflected in the number of meetings dealing with the subject. The first international meeting devoted to *in situ* stresses was held in Santa Monica, California, in 1963 and was organized by Judd. This meeting took place at the time of the establishment of the International Society for Rock Mechanics (ISRM) and the *International Journal for Rock Mechanics and Mining Sciences.* Overcoring and flat jack methods were the most popular and reliable methods at that time. Since then, overcoring methods have been improved and are now used on a standard basis in both mining and civil engineering.

The subject of *in situ* stresses received quite a large amount of attention at the first ISRM congress held in Lisbon in 1966 with a special session on *in situ* stresses (see Theme 4: Residual stresses in rock masses). Various methods were presented and a lot of discussion was conducted on what *in situ* stresses actually are and their classification. Many of the questions raised in Lisbon in 1966 were further explored at another meeting in 1969 devoted exclusively to *in situ* stress and sponsored by the ISRM and the Laboratorio Nacional de Engenharia Civil (LNEC) in Lisbon.

Hydraulic fracturing research activities followed later in the mid-1960s. One of the first opportunities to test the method in the field came with the Rangely oil field (Colorado) experiment where water injection could be correlated with low-level earthquakes in the area, and the crustal stresses could be determined (Haimson, 1973). Soon after its introduction, hydraulic fracturing was used to measure rock stresses from tunnels and shafts as well as holes drilled from the ground surface for the design of underground structures and to increase our understanding of rock stresses in gas and oil fields. By the late 1970s the hydraulic fracturing method was also used in geophysical and geological research, for hot dry rock geothermal extraction, and for the design of potential repositories for storage of radioactive wastes. A state-of-the-art review of the *in situ* stress methods available in the mid-1970s can be found in the Proceedings of the ISRM Symposium on Investigation of Stress in Rock and Advances in Stress Measurement organized by the Australian Geomechanics Society in Sydney in 1976.

Another meeting dedicated to rock stress and rock stress measurements was the First Workshop on Hydraulic Fracturing Stress Measurement held in Monterey, California, in 1981 and organized by Zoback and Haimson. This workshop brought together the experts in the field of hydraulic fracturing. Existing equipment, test procedures and data interpretation were discussed. Borehole breakouts and pressurization of existing fractures for rock stress determination (HTPF method) were two new stress determination techniques introduced at the workshop.

The next meeting dealing with *in situ* stresses was held in Stockholm in 1986 and organized by Stephansson. That symposium was sponsored by the ISRM and its major themes concerned the state of stress in the Earth's crust, the methods for rock stress measurements, the interpretation of rock stresses, and the applications of stress measurements in mining and underground construction.

The Second Workshop on Hydraulic Fracturing Stress Measurements (HFSM '88) was held in Minneapolis, Minnesota, in 1988 under

the auspices of the US National Science Foundation and the Gas Research Institute and was organized by Haimson. This workshop was unique in that it convened scientists and engineers specializing in both hard rocks and permeable rocks found in oil and gas reservoirs. The major objective of the workshop was to review the progress made in the last decade in the interpretation of the data obtained during hydraulic fracturing testing. About 30 contributions were presented, including results from laboratory testing and field experience on granitic and sedimentary rocks.

A workshop dealing with stresses in the Earth's crust was held at the 7th ISRM Congress in Aachen in 1991 and was organized by Stephansson. The workshop was divided into three sessions: stress measurements in deep boreholes, stress measurements from underground openings and new methods and techniques.

Another workshop on rock stress measurement at great depth was held in conjunction with the recent 8th ISRM Congress in Tokyo in 1995. The workshop was organized by Matsuki and Sugawara. Eleven contributions were presented covering a wide variety of topics such as rock stress and rock stress measurements in Japan and South Korea, borehole breakouts and core disking, compressive and tensile failure in boreholes, integration of hydraulic data and focal plane solutions, and comparison of core base methods of stress measurements with overcoring methods.

In situ stress has often been the subject of technical sessions in recent US Rock Mechanics Symposia and other rock mechanics specialty conferences or workshops. *In situ* stresses were of particular interest at the 1990 ISRM-sponsored meeting on Rock at Great Depth in Pau (France), Eurock '94 in Delft (Holland) co-sponsored by the ISRM and the Society of Petroleum Engineers, and more recently at the 1995 Workshop on Rock Stresses in the North Sea in Trondheim (Norway) organized by NTH and SINTEF. This last workshop was held in response to the needs for continuous development of the oil and gas fields in the North Sea.

1.4 CLASSIFICATION OF ROCK STRESSES

Stresses in rock can be divided into *in situ* stresses and induced stresses. *In situ* stresses, also called natural, primitive or virgin stresses, are the stresses that exist in the rock prior to any disturbance. On the other hand, induced stresses are associated with artificial disturbance (excavation, drilling, pumping, loading, etc.) or are induced by changes in natural conditions (drying, swelling, consolidation, etc.).

In general, the current *in situ* stresses in a rock mass are the cumulative product of events in its geological history. A rock mass may have experienced several cycles of physicochemical, thermal and mechanical geological processes which have all contributed to the current *in situ* stress field, some more than others.

Several authors have proposed different classifications for *in situ* stresses and the terminology currently used to describe those stresses shows some diversity. Voight (1966) classified *in situ* (virgin) stresses into two groups: gravitational and tectonic. The tectonic stresses were themselves decomposed into current and residual components. Obert (1968) divided *in situ* stresses into external stresses composed of gravitational and tectonic stresses, and internal stresses composed of residual stresses. External stresses have also been called regional stresses (Fairhurst, 1968).

We present in Fig. 1.8 a terminology for rock stresses which is based on those proposed by Bielenstein and Barron (1971), Hyett, Dyke and Hudson (1986) and more recently by Price and Cosgrove (1990). For instance, we have retained the following definitions proposed by Bielenstein and Barron (1971):

Induced stresses are man made stress components due to removal or addition of

material. They are superimposed on *natural* stresses which exist prior to excavation. The natural stress field can be composed of *gravitational* stresses (due to mass of overburden); *tectonic* stresses and *residual* stresses (a much used and abused term, taken to mean 'stress components that remain in the structure if external forces and moments are removed'). Tectonic stresses may be *active tectonic* stresses (due to active present day straining of the Earth's crust) or *remnant tectonic* stresses (due to past tectonic events which have only been partially relieved by natural processes).

In Fig. 1.8, induced stresses have been broadened to include artificially induced stresses as well as those stresses induced by

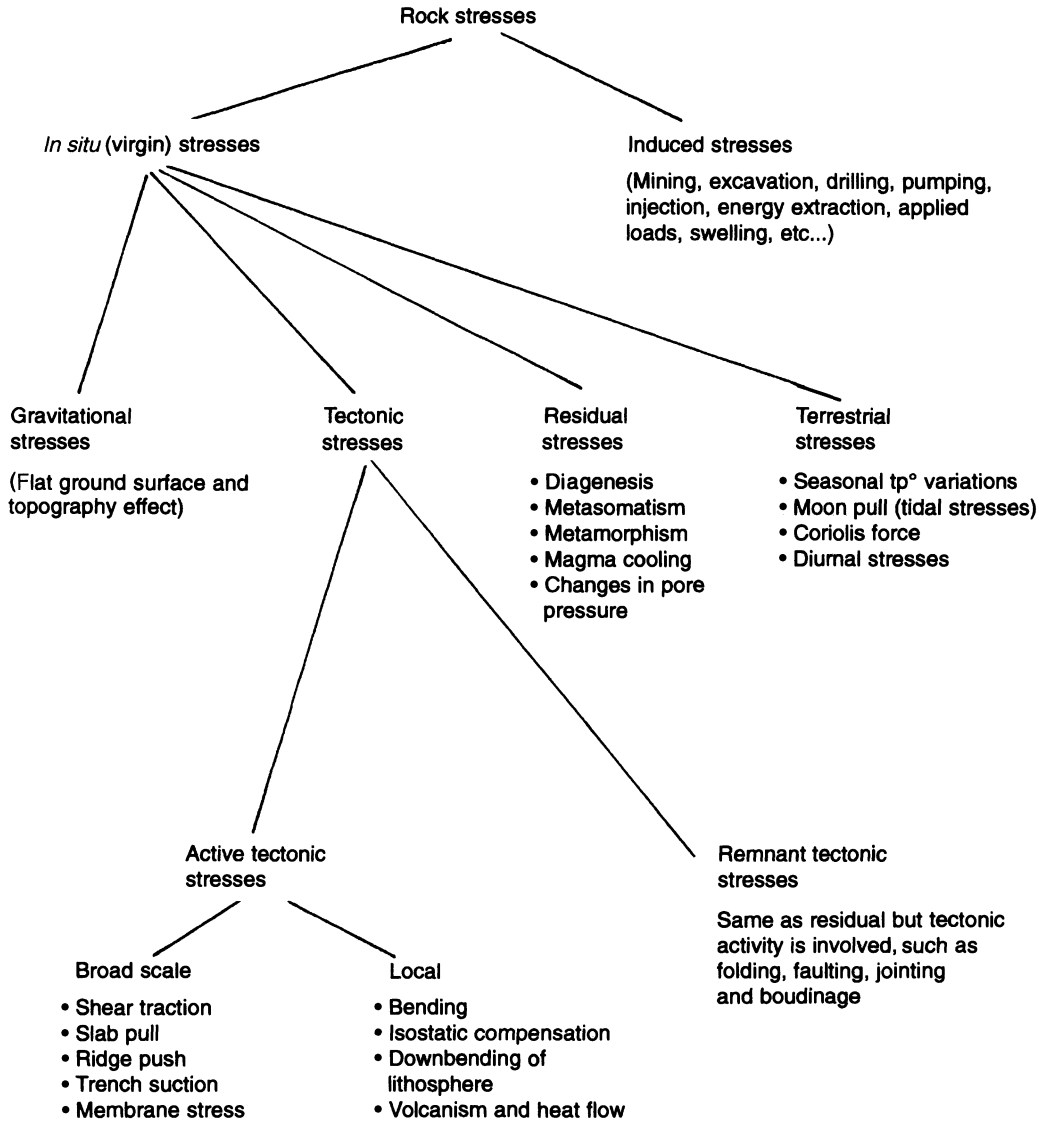

Fig. 1.8 Proposed stress terminology.

changes in natural conditions such as swelling, consolidation and other physico-chemical phenomena. We have also added a list of broad-scale and local plate tectonic phenomena that could induce active tectonic stresses such as ridge push, slab pull, trench suction, mantle drag, membrane stress, volcanism and heat flow and stress migration. These phenomena are in accordance with what are thought to be the driving mechanisms of plate movement in the World Stress Map Project (Zoback *et al.*, 1989). The remnant tectonic stresses are defined here as residual stresses for which tectonic activity is involved through folding, faulting, jointing or boudinage. Finally, in our classification, we have included terrestrial stresses as a distinct group among *in situ* stresses. They are induced by diurnal and seasonal variations of temperatures, Moon pull, and the Coriolis force. The contribution of these stress components to *in situ* stress measurements is often neglected but can be important, in particular, for stress measurements at shallow to very shallow depths (Berest, Blum and Durup, 1992; Clark and Newman, 1977; Hooker and Duvall, 1971; Sbar, Richardson and Flaccus, 1984; Scheidegger, 1982; Swolfs, pers. comm.; Swolfs and Walsh, 1990; Voight, 1966).

1.5 CONTENT OF THE BOOK

This book focuses on the problem of *in situ* stresses in the Earth's crust, the methods for measuring and monitoring those stresses and their importance in rock engineering, geology and geophysics. The emphasis is mostly on the current *in situ* state of stress and to a lesser extent on the monitoring of stress change. The subject of paleostresses, i.e. *in situ* stresses previously active in rock and no longer in existence, is only briefly discussed in Chapter 2 (section 2.14) as it could be, in itself, the topic of a separate book. The reader interested in the topic of paleostresses may want to consult the recent book by Engelder (1993).

The last 30 years have seen a major advance in our knowledge and understanding of *in situ* stresses in rock. A large body of data is now available on the state of stress in the near surface of the Earth's crust (the upper 3–4 km of the crust). Various theories have been proposed regarding the origin of *in situ* stresses and innovative techniques have been developed for their measurement. As a consequence, a large body of literature is available on the subject of *in situ* stresses. In writing this book, we have made a special attempt to refer to as many relevant publications and authors as possible. In general, the reader will find a comprehensive list of references spread over a total of 12 chapters, including the most recent contributions presented at the 8th Congress of the International Society for Rock Mechanics in Tokyo in September 1995.

This book is directed toward graduate students, teachers and practitioners in civil, mining and petroleum engineering, geology and geophysics. It can be used as a textbook in advanced graduate courses in rock mechanics and rock engineering, structural geology and geophysics. The book can also be used as a reference manual by practitioners who are faced with the challenge of rock stress. Actual case studies presented in this book should be of great interest to students, teachers and practitioners. The book has been written for someone who is familiar with the basic concepts of mechanics, geology and rock mechanics.

The 12 chapters in this book are presented in a logical order starting with the methods for estimating *in situ* stresses, followed by the techniques for measuring and monitoring rock stresses, and finally the importance of rock stresses in engineering, geology and geophysics. Several case studies of comparison of stress measurements are also presented, ranging in scale from local measurements to the World Stress Map. Throughout this book, we emphasize the role of geology when estimating and analyzing the results of stress measurements. We also emphasize that the

disciplines of engineering, geology and geophysics share many complementary similarities when it comes to understanding the state of stress in the Earth's crust.

Chapter 2 presents various methods to estimate the *in situ* stress field. This can be done, for instance, from stress versus depth relationships or observations obtained from stress measurements made in the past in the region of interest, or by extrapolation from regions with similar geological and tectonic settings. Information can also be derived from the topography, the geology, the rock fabric, the rock loading history, the first motion analysis of earthquakes, the occurrence of stress release phenomena, breakouts in boreholes, tunnels and shafts, and the presence of stratification, heterogeneities or geological structures. Estimating *in situ* stresses should be the first step when determining the state of stress *in situ* as it is useful in the early stage of engineering design, for planning process and when selecting stress measuring methods and the location of those measurements.

Chapter 3 gives an overview of the various techniques available for measuring *in situ* stresses in rock. The advantages and disadvantages and the range of application of each technique are outlined. This chapter also addresses the accuracy of *in situ* stress measurements, the sources of uncertainty in stress determination, and the range of rock volumes involved in stress measurements. This chapter gives the reader a quick tour of the techniques available for measuring *in situ* stresses and an appreciation of the margins of error associated with stress measurements.

The various methods of *in situ* stress measurements are covered in Chapters 4–8. Chapter 4 focuses on hydraulic methods such as the hydraulic fracturing method, the sleeve fracturing method and the hydraulic tests on pre-existing fractures (HTPF) method. Chapter 5 focuses on a large body of methods called relief methods. These methods are divided into three groups: surface, borehole and rock mass relief methods. Chapter 6 deals mostly with the flat jack method. Chapters 7 and 8 are concerned respectively with strain recovery core base methods and the borehole breakout methods, two groups of techniques that have been used for the measurement of stresses at large depths. After a brief history, each method is described with regard to techniques, equipment and procedures. Theories for the analysis of test results are presented. When appropriate, data presentation and analysis are discussed.

Several case studies of stress measurements are presented in Chapter 9. The objective of this chapter is to show how different techniques in the same rock environment may or may not yield different stress measurements and how some techniques may be complementary to each other. It is shown that for medium to good rock conditions, various techniques are able to give comparable stress pictures of a rock mass (within the uncertainty expected in stress measurements). In poor (weak, weathered and fractured) rock conditions, however, the agreement is usually not as good.

Chapter 10 deals with the monitoring of stress change in civil and mining engineering. In this chapter various techniques are presented. Their respective advantages and disadvantages are discussed and several examples of stress monitoring are presented. Stress monitoring is important when assessing the performance of engineering structures and the rock response to loading and unloading with time. Over the past 15 years, stress monitoring has also received considerable interest with regard to the storage of nuclear wastes in rock.

Chapter 11 presents first the 'big picture' of the state of stress in the Earth's crust with a summary of the recent findings of the World Stress Map Project. The effect of scale on *in situ* stresses and *in situ* stress measurements is also addressed, and in particular the relationship between local stress measurements and the global stress field.

Finally, Chapter 12 presents several examples of applications showing the role played by *in situ* stresses in civil and mining rock engineering, energy development and geology and geophysics. Here it is shown how *in situ* stresses are an integral part in design and stability assessment, and how they can help in understanding the formation of various basic geological structures.

1.6 GENERAL OBSERVATIONS

From the information presented in this book, several general observations can be made with regard to *in situ* stresses in the upper part of the Earth's crust and their measurements.

In situ stresses cannot be measured directly but can be measured by disrupting the rock. Today, stresses can be measured within the upper 3–4 km of the Earth's crust. At greater depths (down to 9 km), very specialized techniques need to be used. The measurement of *in situ* stresses at depths below 9 km remains an unexplored territory where, in the future, new techniques will have to be developed and/or existing ones greatly improved.

An accurate measurement of *in situ* stresses is an overstatement. At best, and in good to very good rock conditions where the rock is essentially linearly elastic, homogeneous and continuous, and between well-defined geological boundaries, *in situ* stresses can be determined with an error of ±10–20% for their magnitude and an error of ±10–20° for their orientation. On the other hand, in poor quality rocks (weathered, weak, soft and heavily fractured), the measurement of *in situ* stresses is extremely difficult. In such rocks the success rate of stress measurements is usually low.

Knowledge of site geology and rock mass structure at all scales is extremely critical when estimating *in situ* stresses, when planning stress measurement programs, and in the interpretation of stress measurement results.

In most cases, and in the absence of topography, the assumption that vertical and horizontal stresses are principal stresses is good as long as we accept that the principal stresses can deviate from the vertical and horizontal directions by as much as 30°. The magnitude of the vertical stress can be explained in most cases by the overburden weight only (although localized departures from this assumption are common). This is not true for horizontal stresses where the uniform $K_0 = \nu/(1-\nu)$ assumption is rarely found *in situ*. Many phenomena other than tectonics could result in high and unequal horizontal stresses, in particular near the ground surface. Such phenomena include residual and thermal stresses, erosion, lateral straining, anisotropy, glaciation and deglaciation, topography, curvature of the Earth and other active geological features and processes. This is not to say that tectonic stresses do not exist, but simply that their contribution to the measured stress fields may not be as large as previously thought.

The World Stress Map Project provides today the most comprehensive survey of *in situ* stress data in the upper lithospheric part of the Earth's crust. The stress measurements carried out in various parts of the world have been found to be consistent with plate movement and within the framework of plate tectonics. The World Stress Map Project shows clearly the existence of broad-scale tectonic stress provinces and various first- and second-order stress patterns in the upper and middle part of the Earth's crust.

The only comprehensive study on the effect of scale on *in situ* stresses was conducted at the Underground Research Laboratory site in Canada and involved rock volumes ranging between 0.1 m^3 and 10^5 m^3. This study shows that for a similar rock condition and within a well-defined geological domain, different stress measurement techniques give (on average) comparable stress values within the uncertainty expected in stress measurements. The non-uniformity of *in situ* stresses in rock masses at various scales creates, in itself, a natural local scale effect which is independent of the method of stress measurement and is

related to the geology and the applied boundary conditions. The effect of scale on rock properties involved in the analysis of stress measurements such as the Young's modulus, tensile strength and compressive strength must be taken into account, as it has potential for influencing the interpretation of various stress measurements.

Comparison of stress measurements obtained with different techniques at the same site shows that, in good rock conditions, and assuming that sufficient reliable tests are conducted, surprisingly similar results can be obtained (again within the uncertainty expected in stress measurements) despite differences in scale between the different techniques. For other rock conditions, the consistency in stress determination is still open to question.

REFERENCES

Adams, J. and Bell, J.S. (1991) Crustal stresses in Canada, in *The Geology of North America*, Decade Map Vol. 1, *Neotectonics of North America*, Geological Society of America, Boulder, Colorado, pp. 367–86.

Batchelor, A.S. and Pine, R.J. (1986) The results of *in situ* stress determinations by seven methods to depths of 2500 m in the Carnmenellis granite, in *Proc. Int. Symp. on Rock Stress and Rock Stress Measurements*, Stockholm, Centek Publ., Luleå, pp. 467–78.

Baumgärtner, J. *et al.* (1993) Deep hydraulic fracturing stress measurements in the KTB (Germany) and Cajon Pass (USA) scientific drilling projects – a summary, in *Proc. 7th Cong. Int. Soc. Rock Mech. (ISRM)*, Aachen, Balkema, Rotterdam, Vol. 3, pp. 1685–90.

Bawden, W.F. (1993) The use of rock mechanics principles in Canadian underground hard rock mine design, in *Comprehensive Rock Engineering* (ed. J.A. Hudson), Pergamon Press, Oxford, Chapter 11, Vol. 5, pp. 247–90.

Benson, R.P. (1988) Design of unlined and lined pressure tunnels, unpublished keynote paper presented at the International Symposium on Tunnelling for Water Resources and Power Projects, New Delhi.

Berest, P., Blum P.-A. and Durup, G. (1992) Effects of the moon on underground caverns, in *Proc. 33rd US Symp. Rock Mech.*, Santa Fe, Balkema, Rotterdam, pp. 421–8.

Bielenstein, H.U. and Barron, K. (1971) In-situ stresses. A summary of presentations and discussions given in Theme I at the Conference of Structural Geology to Rock Mechanics Problems. Dept. of Energy, Mines and Resources, Mines Branch, Ottawa, Internal Report MR71. Also published in *Proc. 7th Can. Symp. Rock Mech.*, Edmonton.

Borg, T. *et al.* (1984) Stability prediction for the Zinkgruvan Mine, Central Sweden, in *Proc. ISRM Symp. on Design and Performance of Underground Excavations*, Cambridge, British Geotechnical Society, London, pp. 113–21.

Brady, B.H.G. and Brown, E.T. (1985) *Rock Mechanics for Underground Mining*, Allen & Unwin, London.

Brekke, T. and Ripley, B.D. (1993) Design of pressure tunnels and shafts, in *Comprehensive Rock Engineering* (ed. J.A. Hudson), Pergamon Press, Oxford, Vol. 2, Chapter 14, pp. 349–69.

Broch, E. (1984a) Development of unlined pressure shafts and tunnels in Norway. *Underground Space*, **8**, 177–84.

Broch, E. (1984b) Unlined high pressure tunnels in areas of complex topography. *Water Power and Dam Constr.*, **36**, 21–3.

Broch, E. (1993) General report: caverns including civil defense shelters, in *Proc. 7th Cong. Int. Soc. Rock Mech. (ISRM)*, Aachen, Balkema, Rotterdam, Vol. 3, pp. 1613–23.

Brudy, M. *et al.* (1995) Application of the integrated stress measurement strategy to the 9 km depth in the KTB boreholes, in *Proc. Workshop on Rock Stresses in the North Sea*, Trondheim, Norway, NTH and SINTEF Publ., Trondheim, pp. 154–64.

Carlsson, A. and Olsson, T. (1982) Rock bursting phenomena in a superficial rock mass in southern Central Sweden. *Rock Mech.*, **15**, 99–110.

Clark, B.R. and Newman, D.B. (1977) Modeling of non-tectonic factors in near-surface in-situ stress measurements, in *Proc. 18th US Symp. Rock Mech.*, Golden, Johnson Publ., pp. 4C3-1–4C3-6.

Cook, N.G.W. (1976) Seismicity associated with mining. *Eng. Geol.*, **10**, 99–122.

Enever, J.R. (1993) Case studies of hydraulic fracture stress measurements in Australia, in *Comprehensive Rock Engineering* (ed. J.A. Hudson), Pergamon Press, Oxford, Chapter 20, Vol. 3, pp. 498–531.

Enever, J.R., Walton, R.J. and Windsor, C.R. (1990) Stress regime in the Sydney basin and its implication for excavation design and construction, in

Proc. Tunnelling Conf., Sydney, The Institution of Engineers, Australia, pp. 49–59.

Engelder, T. (1993) *Stress Regimes in the Lithosphere*, Princeton University Press, Princeton, New Jersey.

Evans, D.M. (1966) Man-made earthquakes in Denver. *Geotimes*, **10**, 11–18.

Fairhurst, C. (1968) Methods of determining in-situ rock stresses at great depths. Tech. Report No. 1-68, Corps of Engineers, Omaha, Nebraska.

Franklin, J.A. and Hungr, O. (1978) Rock stresses in Canada: their relevance to engineering projects. *Rock Mech.*, Suppl. **6**, 25–46.

Gay, N.C. and Van der Heever, P.J. (1982) In situ stresses in the Klerksdrop gold mining district, South Africa – a correlation between geological structure and seismicity, in *Proc. 23rd US Symp. Rock Mech.*, Berkeley, SME/AIME, pp. 176–82.

Grant, M.A., Donaldson, I.G. and Bixley, P.F. (1982) *Geothermal Reservoir Engineering*, Academy Press, London, 253–63.

Haimson, B.C. (1973) Earthquake related stresses at Rangely, Colorado, in *Proc. 14th US Symp. Rock Mech.*, University Park, ASCE Publ., pp. 689–708.

Haimson, B.C. (1977) Design of underground powerhouses and the importance of pre-excavation stress measurements, in *Proc. 16th US Symp. Rock Mech.*, Minneapolis, ASCE Publ., pp. 197–204.

Haimson, B.C. (1978) Crustal stresses in the Michigan Basin. *J. Geophys. Res.*, **83**, 5857–67.

Haimson, B.C. (1984) Pre-excavation in situ stress measurements in the design of large underground openings, in *Proc. ISRM Symp. on Design and Performance of Underground Excavations*, Cambridge, British Geotechnical Society, London, pp. 183–190.

Hast, N. (1958) The measurement of rock pressures in mines. *Sveriges Geologiska Undersokning, Ser. C*, No. 560.

Hoek, E. and Brown, E.T. (1980) *Underground Excavations in Rock*, Inst. of Mining and Metallurgy, London.

Hooker, V.E. and Duvall, W.I. (1971) In situ rock temperature: stress investigations in rock quarries. US Bureau of Mines Report of Investigation RI 7589.

Hudson, J.A. (1991) Atlas of rock engineering mechanisms: underground excavations, Technical Note. *Int. J. Rock Mech. Min. Sci. & Geomech. Abstr.*, **28**, 523–6.

Hudson, J.A. (1992a) Atlas of rock engineering mechanisms: part 2: slopes, Technical Note. *Int. J. Rock Mech. Min. Sci. & Geomech. Abstr.*, **29**, 523–6.

Hudson, J.A. (1992b) *Rock Engineering Systems, Theory and Practice*, Ellis Horwood Publ.

Hyett, A.J., Dyke, C.G. and Hudson, J.A. (1986) A critical examination of basic concepts associated with the existence and measurement of in-situ stress, in *Proc. Int. Symp. on Rock Stress and Rock Stress Measurements*, Stockholm, Centek Publ., Luleå, pp. 387–96.

Jiao, Y. and Hudson, J.A. (1995) The fully-coupled model for rock engineering systems. *Int. J. Rock Mech. Min. Sci. & Geomech. Abstr.*, **32**, 491–512.

Kim, K. (1992) In-situ stress in rock engineering projects, in Lecture Notes, *Short Course on Modern In Situ Stress Measurement Methods*, University of Wisconsin, Madison.

Kim, K. *et al.* (1986) Characterization of the state of in situ stress by hydraulic fracturing for a nuclear waste repository in basalt, in *Proc. Int. Symp. on Rock Stress and Rock Stress Measurements*, Stockholm, Centek Publ., Luleå, pp. 657–67.

Lee, C.F. (1981) In-situ stress measurements in southern Ontario, in *Proc. 22nd US Symp. Rock Mech.*, Cambridge, MIT Publ., pp. 465–72.

Lee, C.F. and Lo, K.Y. (1976) Rock squeeze of two deep excavations at Niagara Falls, in Rock Engineering for Foundations and Slopes, in *Proc. ASCE Specialty Conference*, Boulder, pp. 116–40.

Lo, K.Y. (1978) Regional distribution of in-situ horizontal stresses in rocks in southern Ontario. *Can. Geotech. J.*, **15**, 371–81.

Lo, K.Y. and Morton, J.D. (1976) Tunnels in bedded rock with high horizontal stresses. *Can. Geotech. J.*, **13**, 216–30.

Martin, C.D. and Simmons, G.R. (1993) The Atomic Energy of Canada Limited Underground Research Laboratory: an overview of geomechanics characterization, in *Comprehensive Rock Engineering* (ed. J.A. Hudson), Pergamon Press, Oxford, Chapter 38, Vol. 3, pp. 915–50.

Mase, G.E. (1970) *Continuum Mechanics*, Schaum's Outline Series, McGraw-Hill.

Maury, V. (1987) Oservations, researches and recent results about failure mechanisms around single galleries, in *Proc. 6th Cong. Int. Soc. Rock Mech. (ISRM)*, Montreal, Balkema, Rotterdam, Vol. 2, pp. 1119–28.

McGarr, A. and Wiebols, G.A. (1977) Influence of mine geometry and closure volume on seismicity in deep-level mine. *Int. J. Rock Mech. Min. Sci. & Geomech. Abstr.*, **14**, 139–45.

Mimaki, Y. (1976) Design and construction of a large underground power station, in *Design and Construction of Underground Structures*, The Japan Society of Civil Engineers, Tokyo, pp.115–52.

Mimaki, Y. and Matsuo, K. (1986) Investigation of asymmetrical deformation behavior at the horseshoe-shaped large cavern opening, in *Proc. Int. Symp. on Large Rock Caverns*, Helsinki, Pergamon Press, Oxford, Vol. 2, pp. 1337–48.

Müller, B. *et al.* (1992) Regional patterns of tectonic stress in Europe. *J. Geophys. Res.*, **97**, 11783–803.

Myrvang, A.M. (1993) Rock stress and rock stress problems in Norway, in *Comprehensive Rock Engineering* (ed. J.A. Hudson), Pergamon Press, Oxford, Chapter 18, Vol. 3, pp. 461–71.

Myrvang, A., Hansen, S.E. and Sørensen, T. (1993) Rock stress redistribution around an open pit mine in hardrock. *Int. J. Rock Mech. Min. Sci. & Geomech. Abstr.*, **30**, 1001–4.

Obert, L. (1968) Determination of stress in rock. A state of the art report. Appendix 5 in report by Fairhurst titled: Methods of determining in-situ rock stresses at great depths. Tech. Report No. 1-68, Corps of Engineers, Omaha, Nebraska.

Pine, R.J. and Batchelor, A.S. (1984) Downward migration of shearing in jointed rock during hydraulic injections. *Int. J. Rock Mech. Min. Sci. & Geomech. Abstr.*, **21**, 249–63.

Pine, R.J. and Kwakwa, K.A. (1989) Experience with hydrofracture stress measurements to depths of 2.6 km and implications for measurements to 6 km in the Carnmenellis granite. *Int. J. Rock Mech. Min. Sci. & Geomech. Abstr.*, **26**, 565–71.

Price, N.J. and Cosgrove, J.W. (1990) *Analysis of Geological Structures*, Cambridge University Press, Cambridge.

Rockwell Hanford Operations (1982) Site Characterization Report for the Basalt Waste Isolation Project. Report DOE/RL 82-3, Vol. II, 10.5-4.

Sbar, M.L., Richardson, R.M. and Flaccus, C. (1984) Near surface in-situ stress; strain relaxation measurements along the San Andreas fault in southern California. *J. Geophys. Res.*, **89**, 9323–32.

Scheidegger, A.E. (1982) *Principles of Geodynamics*, 3rd edn, Springer-Verlag.

Selmer-Olsen, R. (1974) Underground openings filled with high pressure water or air. *Bull. Int. Ass. Eng. Geol.*, **9**, 91–5.

Sharma, V.M. *et al.* (1991) In-situ stress measurement for design of tunnels, in *Proc. 7th Cong. Int. Soc. Rock Mech. (ISRM)*, Aachen, Balkema, Rotterdam, Vol. 2, pp. 1355–8.

Stephansson, O. (1993) Rock stress in the Fennoscandian shield, in *Comprehensive Rock Engineering* (ed. J.A. Hudson), Pergamon Press, Oxford, Chapter 17, Vol. 3, pp. 445–59.

Stephansson, O., Särkkä, P. and Myrvang, A. (1986) State of stress in Fennoscandia, in *Proc. Int. Symp. on Rock Stress and Rock Stress Measurements*, Stockholm, Centek Publ., Luleå, pp. 21–32.

Swolfs, H.S. and Walsh, J.B. (1990) The theory and prototype development of a stress-monitoring system. *Seism. Soc. Am. Bull.*, **80**, 197–208.

Te Kamp, L., Rummel, F. and Zoback, M.D. (1995) Hydrofrac stress profile to 9 km at the German KTB site, in *Proc. Workshop on Rock Stresses in the North Sea*, Trondheim, Norway, NTH and SINTEF Publ., Trondheim, pp. 147–53.

Teufel, L.W. (1986) In situ stress and natural fracture distribution at depth in the Piceance Basin, Colorado: implications to stimulation and production of low permeability gas reservoirs, in *Proc. 27th US Symp. Rock Mech.*, Tuscaloosa, SME/AIME, pp. 702–8.

Teufel, L.W. and Farrell, H.E. (1990) In Situ Stress and Natural Fracture Distribution in the Ekofisk Field, North Sea. Sandia National Labs. Report No. SAND-90-1058C.

Teufel, L.W., Rhett, D.W. and Farrell, H.E. (1991) Effect of reservoir depletion and pore pressure drawdown on in-situ stress and deformation in the Ekofisk Field, North Sea, in *Proc. 32nd US Symp. Rock Mech.*, Norman, Balkema, Rotterdam, pp. 63–72.

Timoshenko, S.P. (1983) *History of Strength of Materials*, Dover Publications.

Voight, B. (1966) Interpretation of in-situ stress measurements, in *Proc. 1st Cong. Int. Soc. Rock Mech. (ISRM)*, Lisbon, Lab. Nac. de Eng. Civil, Lisbon, Vol. III, pp. 332–48.

Wong, I.G. (1993) The role of geological discontinuities and tectonic stresses in mine seismicity, in *Comprehensive Rock Engineering* (ed. J.A. Hudson), Pergamon Press, Oxford, Chapter 15, Vol. 5, pp. 393–410.

Zoback, M.D. (1993) In situ stress measurements and geologic processes, in Lecture Notes, *Short Course on Modern In Situ Stress Measurement Methods*, University of Wisconsin, Madison.

Zoback, M.D. and Healy, J.H. (1992) In-situ stress measurements to 3.5 km depth in the Cajon Pass scientific research borehole: implications for the mechanics of crustal faulting. *J. Geophys. Res.*, **97**, 5039–57.

Zoback, M.L. (1992) First- and second-order

patterns of stress in the lithosphere: The World Stress Map project. *J. Geophys. Res.*, **97**, 11703–28.
Zoback, M.L. *et al.* (1989) Global patterns of tectonic stress. *Nature*, **341**, 291–8.

Conferences and Workshops on In Situ *Stresses*

International Conference on State of Stress in the Earth's Crust, Santa Monica, California, June 13–14, 1963. Proceedings published by American Elsevier Publishing Company, New York, 1964.
International Symposium on the Determination of Stresses in Rock Masses, Lisbon, Portugal, May 19–21, 1969. Proceedings published by Lab. Nac. de Eng. Civil (LNEC), Lisbon, 1971.
ISRM Symposium on Investigation of Stress in Rock: Advances in Stress Measurement, Sydney, Australia, August 11–13, 1976. Proceedings published by The Institution of Engineers, Australia, 1976.
Workshop on Hydraulic Fracturing Stress Measurements, Monterey, California, December 2–5, 1981, US National Commission on Rock Mechanics, Washington, DC. Proceedings published by National Academy Press, 1983.
International Symposium on Rock Stress and Rock Stress Measurements, Stockholm, Sweden, September 1–3, 1986. Proceedings published by Centek Publishers, Luleå, Sweden, 1986.
Second International Workshop on Hydraulic Fracturing Stress Measurements (HFSM'88), Minneapolis, Minnesota, June 15–18, 1988. Proceedings published by Pergamon Press in *Int. J. Rock Mech. Min. Sci. & Geomech. Abstr.*, **26**(6), 1989.
Specialty Conference on Stresses in Underground Structures, October 2–3, 1990, Ottawa, Canada. Proceedings available through Canada Center for Mineral and Energy Technology (CANMET), Ottawa, Canada, 1990.
Workshop on Stresses in the Earth's Crust, Aachen, Germany, 1991. Published in Vol. 3 of *Proceedings of 7th ISRM Congress*, Balkema, Rotterdam, 1993.
Workshop: Seminaire Formation: Mesure des Sollicitations et des Contraintes dans les Ouvrages et dans les Terrains (in French). Ecole des Mines, Nancy, France, September 12–16, 1994.
Workshop on Rock Stresses in the North Sea, Trondheim, Norway, February 13–14, 1995. Proceedings published by NTH and SINTEF Publ., Trondheim, Norway, 1995.
Workshop on Rock Stress Measurements at Great Depth, Tokyo, Japan, September 30, 1995. Published in Vol. 3 of *Proceedings of 8th ISRM Congress*, Balkema, Rotterdam, in press.

Major Sessions in Conferences

Session on Residual Stresses in Rock Masses (Theme 4) at 1st ISRM Congress, Lisbon, 1966. See Vol. III of Proceedings of the Congress.
Session on Rock Pressure Measurements and Interpretation of the Results at the Int. Symp. on Underground Openings, Luzern, 1972. In proceedings published by the Swiss Society for Soil Mechanics and Foundation Engineering.
Session on Basic Considerations for Field Instrumentation at the Int. Symp. on Field Measurements in Rock Mechanics, Zurich, 1977. In proceedings published by Balkema, Rotterdam.
Session on In-Situ State of Stress at the 20th US Symp. Rock. Mech., Austin, 1979. In proceedings published by Center for Earth Sciences and Eng., Austin.
Session on Stress Measurements at the 13th Canadian Rock Mechanics Symp., Toronto, 1980. In proceedings published by the Canadian Institute of Mining and Metallurgy, CIM Volume 22.
Session on Stresses at the 23rd US Symp. Rock Mech., Berkeley, 1982. In proceedings published by SME/AIME, Colorado.
Session on Fundamentals of Field Instrumentation at the 1st Int. Symp. on Field Measurements in Geomechanics, Zurich, Switzerland, 1983. In Vol. 1 of the proceedings published by Balkema, Rotterdam.
Session on In-Situ Stress at the 25th US Symp. Rock Mech., Evanston, 1984. In proceedings published by SME/AIME, Colorado.
Sessions on Hydraulic Fracture and New Stress Measurement Methods at 26th US Symp. Rock Mech., Rapid City, 1985. In proceedings published by Balkema, Rotterdam.
Session on Hydrofracture and Borehole Stability at 28th US Symp. Rock Mech., Tucson, 1987. In proceedings published by Balkema, Rotterdam.
Session on Fundamentals at the 2nd Int. Symp. on Field Measurements in Geomechanics, Kobe, Japan, 1987. In Vol. 1 of the proceedings published by Balkema, Rotterdam.
Session on Estimating Regional Stress Fields at Int. Symp. on Rock at Great Depth, Pau, France, 1989. In Vol. 2 of the proceedings published by Balkema, Rotterdam.
Sessions on Assessment of Stress and Hydrofracturing at the 30th US Symp. Rock Mech.,

Morgantown, West Virginia, 1990. In proceedings published by Balkema, Rotterdam.

Session on In-Situ Stresses at 32nd US Symp. Rock Mech., Norman, Oklahoma, 1991. In proceedings published by Balkema, Rotterdam.

Session on Origin of Stresses in the Lithosphere at 33rd US Symp. Rock Mech., Santa Fe, New Mexico, 1992. In proceedings published by Balkema, Rotterdam.

Sessions on In-Situ Stress Measurements and Borehole Instability and Breakouts at 34th US Symp. Rock Mech., Madison, Wisconsin, 1993. In proceedings published by Pergamon Press in *Int. J. Rock Mech. Min. Sci. & Geomech. Abstr.*, **30**(7).

Session on In-Situ Stresses at 1st North American Rock Mechanics Symposium, Austin, Texas, 1994. In proceedings published by Balkema, Rotterdam.

Session on In-Situ Measurement at Eurock '94: Int. Symp. on Rock Mechanics in Petroleum Engineering, Delft, The Netherlands, 1994. In proceedings published by Balkema, Rotterdam.

ESTIMATING *IN SITU* STRESSES 2

2.1 INTRODUCTION

Before measuring virgin stresses with some of the methods discussed in the following chapters, an attempt should be made to obtain an estimate of the *in situ* stress field. This can be done, for instance, from stress versus depth relationships or observations obtained from stress measurements made in the past in the region of interest or by extrapolation from regions with similar geological and tectonic settings. Information can also be derived from the topography, the geology, the rock fabric, the rock loading history, the first motion analysis of earthquakes, the occurrence of stress release phenomena (squeezing, pop-ups, buckling, etc.), breakouts in boreholes, tunnels and shafts, rock bursts, and the presence of stratification, heterogeneities or geological structures (faults, folds, shear zones, uncomformities, volcanic vents and dikes). Estimating *in situ* stresses can be useful in the early stage of engineering design, for the planning process and when selecting stress measuring methods and the location of those measurements.

An exact prediction of *in situ* stresses in rock and their spatial variation is very difficult and for all practical purpose impossible, since, as discussed in the previous chapter and as shown in Fig. 1.8, the current stress state is the end product of a series of past geological events and is the superposition of stress components of several diverse types. Further, since rock masses are rarely homogeneous and continuous, stresses can be expected to vary from place to place in a rock mass. *In situ* stresses not only vary in space but also with time due to tectonic events, erosion, glaciation, etc. The problem is further complicated in that the present rock fabric may or may not be correlated at all with the current *in situ* stress field (Terzaghi, 1962). Further, assumptions can only be made about the load history and the rock's constitutive model. This limitation can best be summarized as follows: 'In any case, it seems clear that it is impossible to know all the events in sufficient detail to ascertain the *in situ* stress state from a knowledge of geology' (Voight, 1971).

To date, no rigorous methods are available to predict *in situ* stresses exactly. Virgin stresses can be estimated to the best of our knowledge or determined using various techniques discussed in this book. It is noteworthy that the process of estimating *in situ* stresses should not be considered as a substitute for their measurement.

In general, estimating *in situ* stresses requires a detailed characterization of the site geology and considerable judgement. Models (physical or numerical) can be developed to explore the effect of parameters such as the constitutive model of the rock, its loading history, critical geological structures, the topography and the boundary conditions on *in situ* stresses. In this chapter we explore different natural processes that can generate *in situ* stresses in rocks and give a review of various models that have been proposed in the literature to predict those stresses.

It is common practice to make two basic assumptions when estimating the state of stress at any depth, z, in a rock mass. The first assumption is that the state of stress can be described by two components: a vertical

component, σ_v, due to the weight of the overlying rock at that depth and equal to γz (where $\gamma = \rho g$ is the average unit weight of the rock in N/m^3), and a uniform horizontal component, $\sigma_h = \sigma_H$ equal to K times σ_v. The second assumption is that both σ_v and σ_h are principal stresses. In general, σ_v and σ_h are taken as total stresses*.

Different expressions have been proposed in the literature for the coefficient K. Talobre (1967) suggested that K could be taken (as a working hypothesis) equal to unity, a proposal that has come to be known in the literature as Heim's rule (based on the work published by the Swiss geologist Heim in 1878). A state of stress where all three principal stress components are equal to γz is often referred to as *lithostatic* in the literature.

Another expression that is often used in the literature for the coefficient K is $K_0 = \nu/(1 - \nu)$ where ν is the rock's Poisson's ratio. This expression was derived assuming (1) that the rock mass is an ideal, homogeneous, linearly isotropic continuous half-space with horizontal surface, (2) that the rock mass is under gravity alone with vanishing horizontal displacements, and (3) that the loading history has no influence on how *in situ* stresses build up. It also implies that horizontal and vertical stresses vanish at the Earth's surface. The coefficient K_0 is often called in the geotechnical literature the *coefficient of Earth pressure at rest*.

Terzaghi and Richart (1952) suggested that the K_0 condition may be approximately satisfied 'for strata of sedimentary rocks in geologically undisturbed regions, provided these strata have never carried a heavy temporary load'. They also emphasized that many conditions in nature do not correspond to the K_0 condition and suggested that K may depend on the rock fabric and the geological history of the rock mass, vary with depth and have different values in different horizontal directions at a given depth. For instance, Terzaghi (1962) suggested that for columnar basalts with vertical open joints, K should be equal to zero since the rock mass is free to deform laterally. He also suggested that in a granitic intrusion, K is initially equal to unity until most of the substance is solidified, after which K is less than unity and larger than K_0. In a basin, one can expect K to vary during the process of sedimentation, diagenesis and erosion (Voight, 1966a).

In general, the assumptions that $K = 1$ or $K = K_0$ and that K is uniform in the horizontal plane, have been found inadequate to describe properly *in situ* stress fields in rock when compared with actual field measurements (Hast, 1958). An exception to this observation is for salt domes for which stresses have been found to be essentially hydrostatic to within 2 MPa (Eriksson and Michalski, 1986). For other rocks, measured horizontal stresses have been found to differ substantially from those predicted by the aforementioned assumptions. Indeed, measured horizontal stress levels at the surface of the Earth have been found to have an average maximum value of about 10 MPa (Swolfs, 1984). According to Aytmatov (1986), stress measurements conducted in different parts of the world show that for 65–70% of the cases, the horizontal stresses exceed the vertical stress. Non-uniform horizontal stresses have been found in most parts of the world. Li (1986) reported that in China 70% of the stress measurements show a ratio between maximum horizontal stress and minimum horizontal stress ranging between 1.4 and 3.3.

The differences between predicted and measured stresses were first attributed to tectonic stresses. The effect of other equally important phenomena has been inferred, such as residual and thermal stresses, erosion, lateral straining, anisotropy, glaciation and deglaciation, topography, curvature of the Earth and other active geological features and

* Throughout this book, σ_v or S_v denotes the vertical stress; σ_H, S_H, σ_{Hmax} or S_{Hmax} denotes the maximum horizontal stress; and σ_h, S_h, σ_{hmin} or S_{hmin} denotes the minimum horizontal stress. The major, intermediate and minor *in situ* principal stresses are denoted as σ_1, σ_2 and σ_3, respectively.

processes (Engelder, 1993; Engelder and Sbar, 1984; Fairhurst, 1986; Jaeger and Cook, 1976; McGarr, 1988; McGarr and Gay, 1978; Sheorey, 1994). Several of these different phenomena are discussed in this chapter. The reader should be aware that no agreement has yet been reached with certainty on this matter and that there is still room for discussion.

2.2 VARIATION OF *IN SITU* STRESSES WITH DEPTH

Several authors have proposed expressions for the variation of the magnitude of the vertical and horizontal *in situ* stresses with depth at specific sites or for different regions of the world. Most data are for depths of less than 3000 m. Examples of stress profiles and stress variations with depth can be found in Hast (1958, 1967, 1969, 1973, 1974), Voight (1966a), Bulin (1971), Kropotkin (1972), Herget (1974, 1980, 1986, 1987, 1993), Orr (1975), Jaeger and Cook (1976), Worotnicki and Denham (1976), Van Heerden (1976), Lindner and Halpern (1977), Haimson and Voight (1977), McGarr and Gay (1978), Brown and Hoek (1978), Blackwood (1979), Zoback and Zoback (1980), Lee (1981), Haimson (1977, 1980, 1981), Haimson and Lee (1980), Doe *et al.* (1981), Swolfs (1984), Stephansson, Särkkä and Myrvang (1986), Aytmatov (1986), Batchelor and Pine (1986), Li (1986), Rummel, Höhring-Ermann and Baumgärtner (1986), Cooling, Hudson and Tunbridge (1988), Pine and Kwakwa (1989), Arjang (1989), Herget and Arjang (1990), Adams and Bell (1991), Zoback and Healy (1992), Baumgärtner *et al.* (1993), Stephansson (1993), Burlet and Cornet (1993), Haimson, Lee and Herrick (1993), Sugawara and Obara (1993), Martin and Simmons (1993), Engelder (1993), Te Kamp, Rummel and Zoback (1995) and Lim and Lee (1995), among many others. Rummel (1986) presented an extensive literature review of stress variations with depth from deep hydraulic fracturing stress measurements conducted in various parts of the world. As an illustrative example, Figs 2.1a and 2.1b show, respectively, the variations of the vertical stress and the ratio between the mean horizontal stress and the vertical stress with depth for different regions of the world, as proposed by Brown and Hoek (1978).

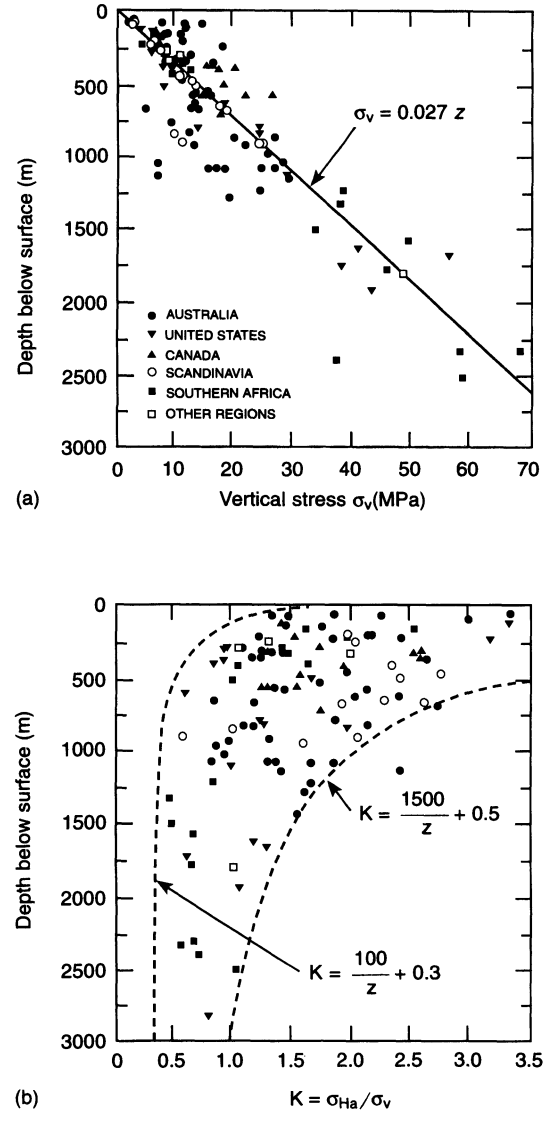

Fig. 2.1 (a) Plot of vertical stress against depth, z, below surface, (b) variation of average horizontal to vertical stress ratio with depth, z, below surface. (Adapted from Brown and Hoek, 1978.)

Tables 2.1 and 2.2 give several stress magnitude versus depth relationships reported in the literature for various regions of the world. The stress variations with depth are given for the vertical stress, σ_v, the maximum and minimum horizontal stresses, σ_H and σ_h, the mean horizontal stress $\sigma_{Ha} = (\sigma_H + \sigma_h)/2$, and/or the horizontal to vertical stress ratios $K_H = \sigma_H/\sigma_v$, $K_h = \sigma_h/\sigma_v$ and $K_{Ha} = \sigma_{Ha}/\sigma_v$. All stresses are total stresses. In some recent papers, the variation of *in situ* stresses with depth has also been presented in terms of

Table 2.1 Variation of horizontal stress components with depth

References	*Variation of* σ_H, σ_h, σ_{Ha} *(MPa) and* K *with depth* z *(m)*	*Location and depth range (m)*
Voight (1966a)	$\sigma_{Ha} = 8.0 + 0.043z$	World data (0–1000)
Herget (1974)	$\sigma_{Ha} = (8.3 \pm 0.5) + (0.0407 \pm 0.0023)z$	World data (0–800)
Van Heerden (1976)	$K_{Ha} = 0.448 + 248/z$ ($r = 0.85$)	Southern Africa (0–2500)
Worotnicki and Denham (1976)	$\sigma_{Ha} = 7.7 + (0.021 \pm 0.002)z$ ($r = 0.85$)	Australia (0–1500)
Haimson (1977)	$\sigma_H = 4.6 + 0.025z$ $\sigma_h = 1.4 + 0.018z$ ($r = 0.95$)	Michigan Basin (0–5000)
Lindner and Halpern (1977)	$\sigma_{Ha} = (4.36 \pm 0.815) + (0.039 \pm 0.0072)z$	North America (0–1500)
Brown and Hoek (1978)	K_{Ha} varies between $0.3 + 100/z$ and $0.5 + 1500/z$	World data (0–3000)
Aytmatov (1986)	$(\sigma_H + \sigma_h)$ between $9.5 + 0.075z$ and $5.0 + 0.058z$	World data (mostly former USSR) (0–1000)
Li (1986)	$\sigma_{Ha} = 0.72 + 0.041z$; K_{Ha} between $0.3 + 100/z$ and $0.5 + 440/z$	China (0–500)
Rummel (1986)	$K_H = 0.98 + 250/z$; $K_h = 0.65 + 150/z$	World data (500–3000)
Herget (1987)	$\sigma_{Ha} = 9.86 + 0.0371z$ $\sigma_{Ha} = 33.41 + 0.0111z$ $K_{Ha} = 1.25 + 267/z$ $K_H = 1.46 + 357/z$ $K_h = 1.10 + 167/z$	Canadian Shield (0–900) (900–2200) (0–2200)
Pine and Kwakwa (1989)	$\sigma_H = 15 + 0.028z$ $\sigma_h = 6 + 0.012z$	Carnmenellis granite Cornwall, UK (0–2000)
Arjang (1989)	$\sigma_H = 8.8 + 0.0422z$ $\sigma_h = 3.64 + 0.0276z$ $\sigma_{Ha} = 5.91 + 0.0349z$	Canadian Shield (0–2000)
Baumgärtner *et al.* (1993)	$\sigma_H = 30.4 + 0.023z$; $\sigma_h = 16.0 + 0.011z$ $\sigma_h = 1.75 + 0.0133z$	KTB pilot hole (800–3000) Cajon Pass hole (800–3000)
Sugawara and Obara (1993)	$\sigma_{Ha} = 2.5 + 0.013z$	Japanese Islands (0–1200)
Hast (in Stephansson, 1993)	$\sigma_H = 9.1 + 0.0724z$ ($r = 0.78$) $\sigma_h = 5.3 + 0.0542z$ ($r = 0.83$)	Fennoscandia overcoring (0–1000)
Stephansson (1993)	$\sigma_H = 10.4 + 0.0446z$ ($r = 0.61$) $\sigma_h = 5 + 0.0286z$ ($r = 0.58$) $\sigma_H = 6.7 + 0.0444z$ ($r = 0.61$) $\sigma_h = 0.8 + 0.0329z$ ($r = 0.91$) $\sigma_H = 2.8 + 0.0399z$ ($r = 0.79$) $\sigma_h = 2.2 + 0.0240z$ ($r = 0.81$)	Fennoscandia Leeman–Hiltscher overcoring (0–700) Leeman-type overcoring (0–1000) Hydraulic fracturing (0–1000)
Te Kamp, Rummel and Zoback (1995)	$\sigma_H = 15.83 + 0.0302z$ $\sigma_h = 6.52 + 0.01572z$	KTB hole (0–9000)
Lim and Lee (1995)	$\sigma_{Ha} = 1.858 + 0.018z$ ($r = 0.869$) $\sigma_{Ha} = 2.657 + 0.032z$ ($r = 0.606$)	South Korea overcoring (0–850) Hydraulic fracturing (0–250)

Table 2.2 Variation of vertical stress component with depth

References	*Variation of vertical stress* σ_v *(MPa) with depth* z *(m)*	*Location and depth range (m)*
Herget (1974)	$(1.9 \pm 1.26) + (0.0266 \pm 0.0028)z$	World data (0–2400)
Lindner and Halpern (1977)	$(0.942 \pm 1.31) + (0.0339 \pm 0.0067)z$	North America (0–1500)
Brown and Hoek (1978)	$0.027z$	World data (0–3000)
McGarr and Gay (1978)	$0.0265z$	World data (100–3000)
Herget (1987)	$0.026z$–$0.0324z$	Canadian Shield (0–2200)
Arjang (1989)	$(0.0266 \pm 0.008)z$	Canadian Shield (0–2000)
Baumgärtner *et al.* (1993)	$(0.0275$–$0.0284)z$	KTB pilot hole (800–3000)
Herget (1993)	$0.0285z$	Canadian Shield (0–2300)
Sugawara and Obara (1993)	$0.027z$	Japanese Islands (0–1200)
Te Kamp, Rummel and Zoback (1995)	$(0.0275$–$0.0284)z$	KTB hole (0–9000)
Lim and Lee (1995)	$0.233 + 0.024z$	South Korea (0–850)

principal stresses, in particular when the stresses are determined by techniques other than hydraulic fracturing or when the principal *in situ* stress components are not in the vertical or horizontal directions. Table 2.3 gives, for instance, the major, intermediate and minor *in situ* stress magnitude versus depth relationships for the Canadian Shield (Herget, 1993) and Sweden (Stephansson, 1993). In Tables 2.1–2.3, r indicates the accuracy of the fit. It should be noted that it is common practice, when presenting the distribution of stresses with depth, to assume that each stress component increases linearly with the depth, z, and that the horizontal to vertical stress ratios depend on $1/z$.

The unit weight $\gamma = \rho g$ of rocks varies, in general, between 0.025 and 0.033 MN/m^3. Thus the gravitational vertical stress γz should increase linearly with depth with a gradient ranging between 0.025 and 0.033 MPa/m. An average value for the rock unit weight of 0.027 MN/m^3 (quartz has a specific gravity of 2.65) is often assumed, giving an average vertical stress gradient of 0.027 MPa/m. Taking a value for the Poisson's ratio $\nu = 0.25$ gives $K_0 = \nu/(1 - \nu) = 1/3$. In other words, if the K_0 condition were true, the horizontal stress should increase with a gradient of 0.009 MPa/m. Note that K_0 can only vary between 0 and 1 as the Poisson's ratio ν varies between 0 and 0.5.

Comparison of the vertical stress gradient of 0.027 MPa/m with those reported in Table 2.2 and in the literature shows that, in most cases, the magnitude of the vertical stress can be explained by the overburden weight only. Localized departures from this assumption are

Table 2.3 Variation of major, intermediate and minor principal stress components with depth

References	*Variation of* σ_1, σ_2 and σ_3 *(MPa) with depth* z *(m)*	*Location and depth range (m)*
Herget (1993)	$\sigma_1 = 12.1 + (0.0403 \pm 0.002)z$ $(r = 0.84)$	Canadian Shield (0–2300)
	$\sigma_2 = 6.4 + (0.0293 \pm 0.0019)z$ $(r = 0.77)$	
	$\sigma_3 = 1.4 + (0.0225 \pm 0.0015)z$ $(r = 0.75)$	
Stephansson (1993)	$\sigma_1 = 10.8 + 0.037z$ $(r = 0.68)$	Sweden (0–1000)
	$\sigma_2 = 5.1 + 0.029z$ $(r = 0.72)$	
	$\sigma_3 = 0.8 + 0.020z$ $(r = 0.75)$	

not uncommon, however, and have been observed due to local geological features or active tectonic zones (Herget, 1980, 1986). Bulin (1971) reported values of the vertical stress measured at depths of 600 and 900 m (in the Donets–Makeyekva area in the former Soviet Union) three to four times higher than those predicted by gravity due to complex geological structures. Localized departure can also be due to shear stresses as suggested by Voight (1966a) and Howard (1966).

Comparison of the horizontal stress gradient of 0.009 MPa/m with those reported in Table 2.1 and in the literature shows much more discrepancy. The stress ratio, K, measured in the field is rarely equal to $\frac{1}{3}$, especially at shallow depths, and is often larger than unity. For instance, Herget (1974) noted that 75% of his world stress data (at the time) showed higher horizontal than vertical stresses. Table 2.1 also shows that within a single region of the world, such as Fennoscandia, several distributions of horizontal stress with depth can be obtained with different stress measurement methods (Stephansson, 1993).

Generic stress versus depth relationships such as those reported in Tables 2.1–2.3 can be useful in estimating the magnitude of the stress field at a given depth. They also provide an overall idea of the stress regime (normal, strike-slip, thrust) in a given area of interest, and how the stress regime varies with depth. For instance, in Fennoscandia one can expect the maximum and minimum horizontal stresses to exceed the vertical stress (Stephansson, 1993). The hydraulic fracturing tests at the KTB hole in Germany revealed a strike-slip stress regime at depths ranging between 800 and 3000 m (Baumgärtner *et al.*, 1993). This conclusion has recently been extended to a depth of 9000 m by Te Kamp, Rummel and Zoback (1995). For more information about the KTB hole, the reader is referred to section 12.4.7.

Adams and Bell (1991) concluded that for Canada, high horizontal stresses are widely present and that both maximum and minimum horizontal stresses often exceed the vertical stress at the depth of measurement. Also, within the Canadian Shield the difference between the maximum and minimum principal stresses seems to increase with depth and the major and intermediate principal stresses tend to be aligned in the horizontal plane (Herget, 1993; Martin and Chandler, 1993). Rummel (1986) concluded that the maximum shear stress in the upper crust of the Earth is determined by the two horizontal *in situ* stresses; however, at shallow depths the maximum shear stress is determined by the maximum horizontal stress and the vertical stress. He also concluded that stike-slip faulting would be the dominant fault mechanism in a randomly fractured Earth's crust if the empirical friction law proposed by Byerlee (1978) was satisfied.

The conclusions reached by Rummel (1986) reveal that the ordering of *in situ* stresses (i.e. the stress regime) is not necessarily constant with depth. Adams and Bell (1991) reported stress measurements conducted in the Beaufort Sea showing a change in stress regime from strike-slip faulting ($\sigma_H > \sigma_v > \sigma_h$) to thrust faulting ($\sigma_H > \sigma_h > \sigma_v$) at a depth of 3 km. A similar observation was made by Dey and Brown (1986) in a deep borehole at the Hot Dry Rock Project in New Mexico. They found using the differential strain curve analysis method a change of stress regime from normal faulting ($\sigma_v > \sigma_H > \sigma_h$) at a depth of 2.8 km to strike-slip faulting ($\sigma_H > \sigma_v > \sigma_h$) at a depth of 3.8 km. In a 5110 m ultradeep oil well near the center of the Michigan Basin, hydraulic fracturing tests conducted by Haimson (1977) revealed a change in stress regime with depth: thrust faulting ($\sigma_H > \sigma_h > \sigma_v$) from 0 to 200 m, strike-slip faulting ($\sigma_H > \sigma_v > \sigma_h$) from 200 to 4500 m and normal faulting ($\sigma_v > \sigma_H > \sigma_h$) at depths larger than 4500 m. Finally, using a recent survey of 1000 measurements of the least principal stress measured by hydraulic fracturing, Plumb (1994) concluded that in sedimentary basins, thrust faulting

seems to be dominant in the upper 1 km, but changes to strike-slip or normal faulting at greater depths.

It must be emphasized that the generic stress versus depth relationships presented in Tables 2.1–2.3 should be used with caution as they are usually associated with scatter. Local stresses can vary locally due, for instance, to stratification and heterogeneities (section 2.6), geological structures such as faults, dikes, shear zones and folds (section 2.7) or topography (section 2.8). When the effect of these parameters is important, assuming a linear variation of stress components with depth can be misleading. As an illustrative example, hydraulic stress measurements conducted adjacent to a postglacial fault at Lansjärv, Sweden, gave a maximum horizontal *in situ* stress of 12 MPa and a minimum horizontal stress of 6 MPa at a depth of 500 m (Stephansson, 1993). Using the best-fit stress versus depth relationships for hydraulic fracturing in Table 2.1 at that depth would give values of 22.8 and 14.2 MPa for the maximum and minimum stresses, respectively, As discussed by Stephansson (1993), the discrepancy between predicted and observed stresses can be attributed to stress relief associated with 10 m of displacement along the fault about 8000 years ago (section 12.4.5). Large variations in the horizontal stress that did not fit the model of linear increase with depth were also found at the URL site in Canada and were attributed to major thrust faults (Martin and Chandler, 1993). For more information about the URL project, the reader is referred to section 9.1.

Stress measurements have also revealed that, within a given stress regime, the orientation of *in situ* stresses may or may not change with depth. Stephansson (1993) gives examples of stress measurements by hydraulic fracturing in a deep well where the maximum horizontal stress was found to be approximately E–W from the surface down to 200 m depth and to rotate by 30° to N60°W from 200 to 500 m. Variations in the orientation of the maximum horizontal stress of 60° over a distance of 500 m were observed by Haimson and Rummel (1982) in lava flows in Iceland. Martin and Chandler (1993) reported a 90° rotation of the maximum *in situ* stress component across fault zone no. 2 at the URL site. This large rotation was attributed in part to stress release associated with slip along the fault. At the Cajon Pass well in California, the direction of the maximum horizontal stress determined by breakouts was found to vary widely over depths ranging between 2700 and 3500 m (Shamir and Zoback, 1992). On the other hand, Pine and Kwakwa (1989) found a relatively consistent orientation of the principal stresses measured by hydraulic fracturing at depths up to 2.6 km in the Carnmenellis granite in Cornwall, England. Adams and Bell (1991) reported that in Canada, most wells show breakouts implying little changes in stress orientation with depth, rock type or rock age. An example of breakout orientation in an offshore well in eastern Canada reported by Adams and Bell (1991) is shown in Fig. 2.2. This figure shows consistency in the orientation of the breakout azimuths over a depth ranging from 800 to 5000 m and in rocks ranging in age from Jurassic to Miocene.

Some measured variations of stresses with depths have also revealed that over the length of a vertical hole, stresses at shallow depths may be entirely different (in magnitude, orientation or both) from those at deeper depths. This phenomenon, sometimes referred to as 'stress decoupling', usually indicates separate stress regimes with depth and has been found at several sites (Haimson, 1979, 1980; Haimson and Lee, 1980). For instance, the hydraulic fracturing tests conducted by Haimson and Lee (1980) at depths up to 303 m in southwestern Ontario, have revealed that the anomalously high stresses measured in the overlying Paleozoic sedimentary rock units (30–210 m in depth) were not necessarily continuous in the underlying Precambrian granite gneiss (220–300 m in depth). There the stress distributions were markedly different in the

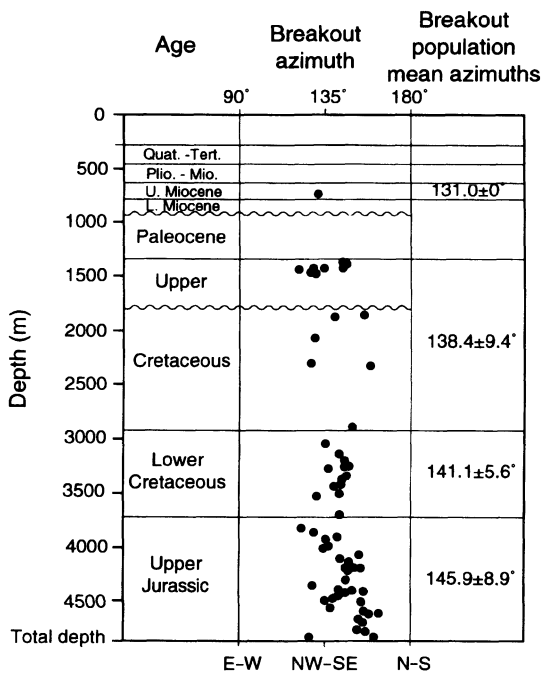

Fig. 2.2 Mean azimuth of 64 breakouts measured in the Sachem D-76 well, Scotian Shelf, offshore eastern Canada. (After Adams and Bell, 1991.)

Paleozoic and Precambrian units, with a shift in direction in the horizontal principal stresses of about 45°. In this example, stress decoupling was likely to be associated with the marked change in lithology. As remarked by Haimson (1990b), several examples of stress decoupling due to lithology have been reported with oil wells traversing sedimentary formations.

Stress decoupling can also be due to topography effects where the shallow stresses align themselves with the local topography (and away from regional trends), whereas the stresses at larger depths align themselves with the regional trends. Several case studies clearly showing this effect can be found in Haimson (1979), and in particular stress measurements at the site of the Kerckoff-2 project showing alignment of measured shallow stresses with the local Sierra Nevada topography. In general, the phenomenon of stress decoupling should be seen as a reminder that extrapolation of the stress field from one depth range or geological unit to another must be used with caution.

2.3 VERTICAL AND HORIZONTAL STRESSES AS PRINCIPAL STRESSES

In areas of smooth topography, it is often assumed that horizontal and vertical stress components are principal stresses. McGarr and Gay (1978) checked the validity of that assumption by plotting on a lower hemisphere stereographic projection net the orientation of principal stresses measured in several mines in southern Africa. They found a loose cluster of points around the center of the net with most of the points falling within a circle of radius of 30° about the vertical axis, thus indicating some deviation from the vertical and horizontal assumption. McGarr and Gay (1978) suggested that the observed scatter could be attributed to complex geology in the areas of stress measurements. They also suggested that for sedimentary basins the scatter should be less.

The conclusions reached by McGarr and Gay (1978) seem to be consistent with the analysis of 165 overcoring stress measurements in the Canadian Shield reported by Herget (1993). The orientation of the major, intermediate and minor principal *in situ* stresses was plotted on the lower hemisphere of an equal area net and concentration contour diagrams were constructed as shown in Figs 2.3a, 2.3b and 2.3c, respectively. It can be seen from these figures that the maximum concentration for the major principal stress, σ_1, is 5% for a dip direction/dip of 248°/10°. The intermediate principal stress, σ_2, shows a maximum concentration of 5% at 300–340°/00° and the minor principal stress, σ_3, shows a concentration of 8% in the vertical direction and the smallest amount of scatter. As pointed out by Herget (1993), the direction of σ_1 seems to coincide with the NE to ENE maximum

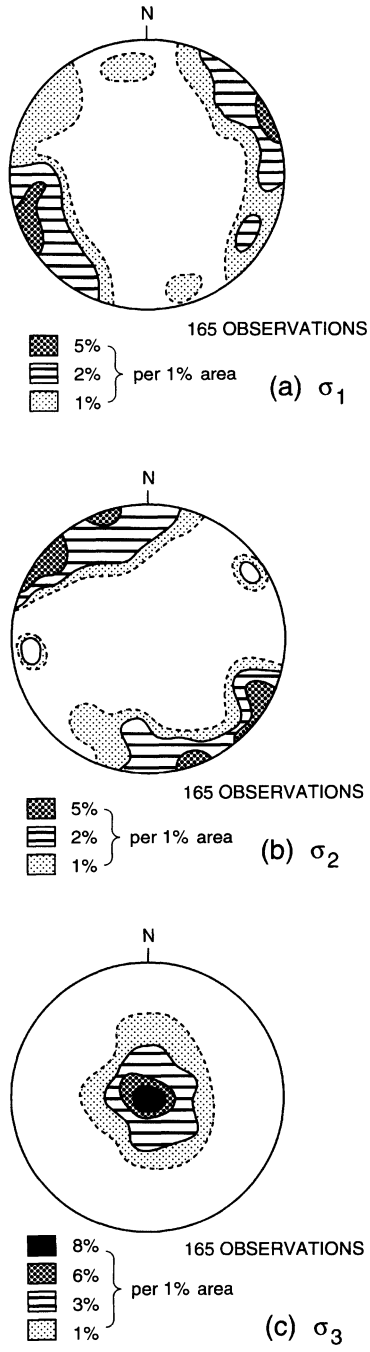

Fig. 2.3 Orientation of principal *in situ* stresses based on 165 overcoring measurements in the Canadian Shield. Lower hemisphere projection, equal area net. Orientation of σ_1, σ_2 and σ_3 in (a)–(c), respectively. (After Herget, 1993.)

horizontal stress direction in North America reported by Sbar and Sykes (1973), and more recently by M.L. Zoback *et al.* (1989) and Zoback (1992) in the World Stress Map Project.

Bulin (1971) analyzed a large amount of *in situ* stress measurements conducted around the world at depths ranging between 25 and 2700 m (with many measurements in the former Soviet Union). He found that for over 60% of the cases, the principal stresses were inclined at less than 30° to the horizontal and vertical directions. Similar conclusions were reached for the stresses measured in various parts of China (Li, 1986). Myrvang (1993) reported that, in Norway, the horizontal and vertical stresses coincide relatively well with the principal stress directions and that at depths down to 500 m the vertical stress is the minor principal stress. Stephansson (1993) concluded that for the majority of test sites in Fennoscandia, one of the intermediate or minor principal stresses is vertical and its magnitude is equal to the weight of the overburden. Klein and Brown (1983) also concluded that the principal stress directions in the UK are near vertical and horizontal with the maximum principal stress being horizontal and trending NW–SE, the minimum principal stress being horizontal and the intermediate principal stress being vertical (Klein and Barr, 1986). Observation of crustal earthquake focal mechanisms around the world seem also to support the assumption of vertical and horizontal stresses as principal stresses (Zoback *et al.*, 1989). Finally, Worotnicki and Walton (1976) concluded, from stress measurements in Australia, that the assumption that vertical and horizontal stresses are principal stresses is quite good with horizontal stresses in excess of the vertical stress with a stress ratio of about 1.5:1. The major horizontal stress was found to be close to the E–W direction for most of the Australian continent, except in the southern-central portion where it was found to be N–S. More recent *in situ* stress data analyzed by Brown and Windsor (1990) have

revealed that, in Australia, the stress orientation may not be as consistent as originally described by Worotnicki and Walton (1976) and shows more scatter (section 11.1.3).

2.4 LIMITS OF *IN SITU* STRESSES WITH DEPTH

The domains of variation for horizontal *in situ* stress components are restricted by the strength of the rock mass. Stresses in the Earth's crust may build up until failure occurs. This failure could occur either by the formation of new faults or by reactivation and slip on pre-existing discontinuities. Limits on crustal stresses have been proposed using different models based on various assumptions regarding the brittle or ductile behavior of rocks at depth. As pointed out by Rummel (1986), '. . . there is no consensus whatsoever among Earth scientists about the magnitude of shear stress, its variation with depth or about the depth of brittle–ductile transition in crustal deformation behavior. Stresses at depths greater than 3 km can only be estimated from empirical results of rock mechanics laboratory fracture and deformation studies, or by extrapolating existing stress data measured at shallow depth'. Since 1986 the deep stress measurements in the KTB boreholes in Germany, down to a depth of 9 km, have revealed that stress magnitudes are limited by the frictional equilibrium on pre-existing optimally oriented faults (Brudy *et al.*, 1985).

2.4.1 INTACT ROCK STRENGTH MODEL

Consider an intact rock mass whose strength can be described by a Mohr–Coulomb criterion with internal cohesion, S_0, and internal friction angle ϕ. In selecting this failure criterion, we are assuming here (1) that the rock strength is independent of the intermediate principal stress, and (2) that fracture takes place in one or both of a pair of conjugate planes which pass through the direction of the intermediate principal stress and are equally inclined at angles of less than 45° to the direction of the greatest principal stress (Jaeger and Cook, 1976). For the Mohr–Coulomb criterion, the major and minor principal stresses at failure, σ_1 and σ_3, are related as follows (Goodman, 1989):

$$\sigma_1 - \sigma_3 = C_0 + \sigma_3 \left[\tan^2\left(\frac{\pi}{4} + \frac{\phi}{2}\right) - 1 \right] \quad (2.1)$$

where C_0 is the unconfined compressive strength equal to

$$C_0 = 2S_0 \cdot \tan\left(\frac{\pi}{4} + \frac{\phi}{2}\right) \quad (2.2)$$

Equation (2.1) indicates that, in this model, the maximum shear stress is proportional to the minimum principal stress σ_3.

Let us assume that at a given depth, z, the state of stress consists of a vertical stress component, $\sigma_v = \gamma z$ and two non-equal horizontal stresses. Due to straining of the rock mass, the horizontal stresses may increase or decrease (at different rates or not) until failure of the rock mass takes place. Three cases can be considered at failure (Anderson, 1951):

- case 1: $\sigma_v > \sigma_H > \sigma_h$ (normal dip-slip faulting);
- case 2: $\sigma_H > \sigma_v > \sigma_h$ (horizontal-slip faulting);
- case 3: $\sigma_H > \sigma_h > \sigma_v$ (reverse dip-slip faulting);

where σ_H and σ_h are the maximum and minimum horizontal stress components, respectively.

(a) Case 1

This case corresponds to normal faulting which is characteristic of an extensional tectonic environment. Substituting $\sigma_v = \sigma_1$ and $\sigma_h = \sigma_3$ into equation (2.1) and rearranging gives the following expression for the minimum horizontal to vertical stress ratio $K_{min} = \sigma_h / \sigma_v$:

$$K_{min} = \cot^2\left(\frac{\pi}{4} + \frac{\phi}{2}\right) - \frac{C_0}{\gamma z} \cdot \cot^2\left(\frac{\pi}{4} + \frac{\phi}{2}\right) \quad (2.3)$$

In this case, fracturing of the rock will be parallel to the largest horizontal stress component, σ_H, as shown in Fig. 2.4a.

(b) Case 2

This case corresponds to a strike-slip stress regime. Substituting $\sigma_H = \sigma_1$ and $\sigma_h = \sigma_3$ into equation (2.1) and rearranging gives the following expression between the horizontal stress ratios $K_h = \sigma_h / \sigma_v$ and $K_H = \sigma_H / \sigma_v$ at failure:

$$K_H = \frac{C_0}{\gamma z} + K_h \cdot \tan^2\left(\frac{\pi}{4} + \frac{\phi}{2}\right) \quad (2.4)$$

Fracturing of the rock will be parallel to the vertical stress component, σ_v, as shown in Fig. 2.4b.

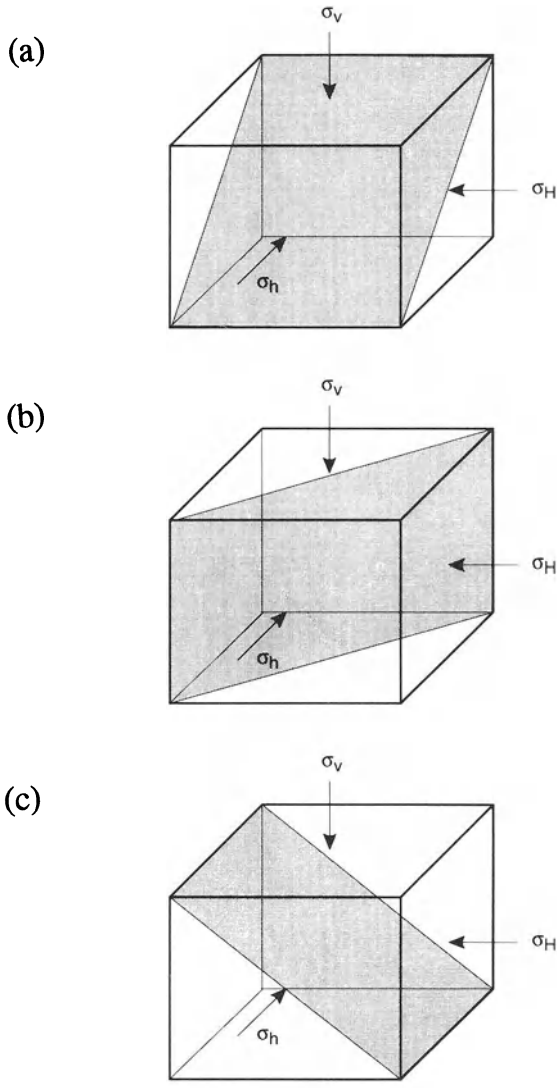

Fig. 2.4 Rock fracturing under σ_v, σ_H and σ_h loading. (a) Case 1: $\sigma_v > \sigma_H > \sigma_h$, normal dip-slip faulting; (b) case 2: $\sigma_H > \sigma_v > \sigma_h$, horizontal-slip faulting; (c) case 3: $\sigma_H > \sigma_h > \sigma_v$, reverse dip-slip faulting.

(c) Case 3

This case corresponds to a thrust faulting stress regime which is characteristic of a compressional tectonic environment. Substituting $\sigma_v = \sigma_3$ and $\sigma_H = \sigma_1$ into equation (2.1) and rearranging gives the following expression for the maximum horizontal to vertical stress ratio $K_{max} = \sigma_H / \sigma_v$:

$$K_{max} = \tan^2\left(\frac{\pi}{4} + \frac{\phi}{2}\right) + \frac{C_0}{\gamma z} \quad (2.5)$$

Fracturing of the rock will be parallel to the smallest horizontal stress component, σ_h, as shown in Fig. 2.4c.

The two stress ratios K_{max} and K_{min} represent the two extreme values for the horizontal to vertical stress ratio, assuming that the rock behaves in a brittle manner. They are analogous to the coefficients of passive and active pressure in soils (Lambe and Whitman, 1969). In general, the domain of variation $K_{min} < K < K_{max}$ is quite large. As an illustrative example, consider a rock mass with $\phi = 40°$, $S_0 = 5\,\text{MPa}$ and $\gamma = 0.027\,\text{MPa/m}$. This gives $C_0 = 21.44\,\text{MPa}$. According to equation (2.3), K_{min} is positive at depths larger than 794 m. At a depth of 10 m, $-16.83 < K < 84.00$ and at a depth of 2000 m, $0.13 < K < 4.99$. It is noteworthy that in view of the expression of K_{min} and K_{max} in (2.3) and (2.5), an increase in the rock mass cohesion would result in a wider domain of variation for K at a given depth.

Note that the analysis conducted above can also be done with other rock failure criteria

such as the Hoek and Brown (1980b) criterion or more complex criteria that involve all three principal stresses (Lade, 1993).

2.4.2 EFFECT OF PLANES OF WEAKNESS

Compared with intact rock, fractured rock has reduced shear strength and essentially zero tensile strength. In general, planes of weakness will reduce the possible range for K due to joint slip or joint opening. The effect of joint slip on *in situ* stresses is illustrated below for a regularly jointed rock mass with the geometry of Fig. 2.5a. The rock mass is assumed to be subject to an axisymmetric and compressive state of stress σ_1, σ_3. The joints are oriented at an angle δ with respect to σ_1. The intact rock shear strength is assumed to be described by

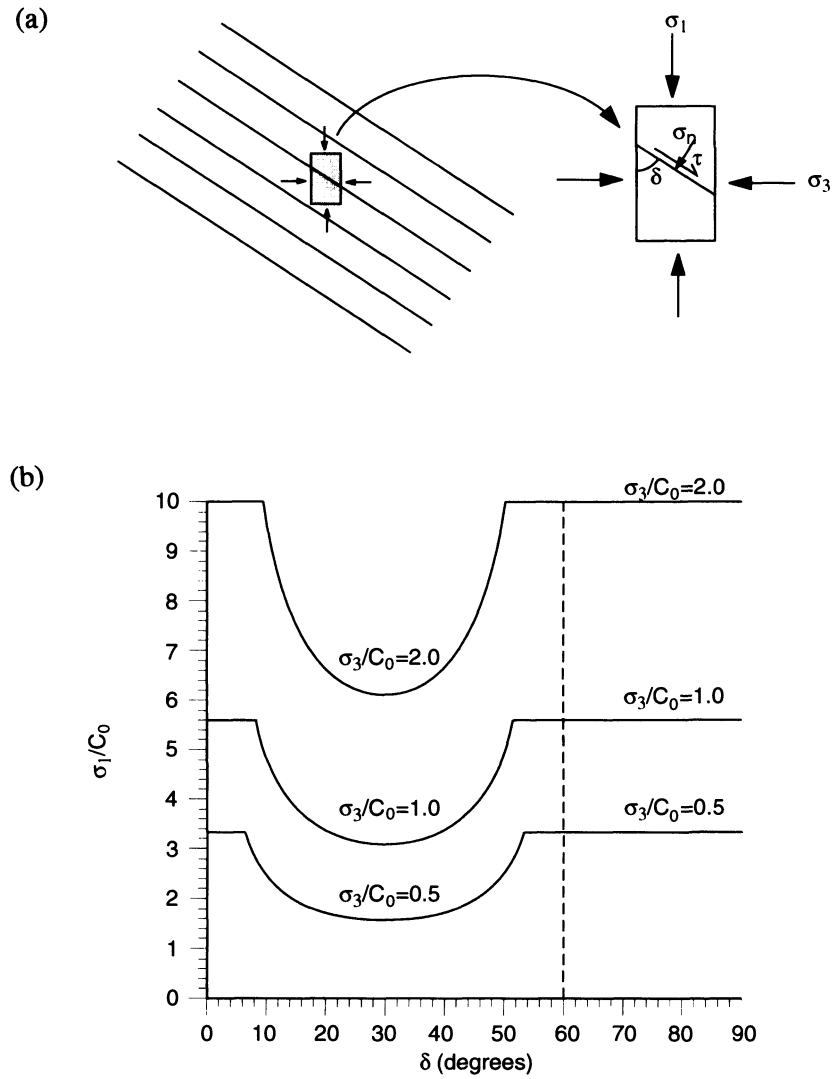

Fig. 2.5 (a) Regularly jointed rock mass subject to an axisymmetric state of stress σ_1, σ_3. (b) Variation of σ_1/C_0 with δ showing joint strength for different values of σ_3/C_0. The intact rock strength is shown as a series of horizontal lines.

the Mohr–Coulomb criterion with expression given in equation (2.1). On the other hand, the joint shear strength is defined by a Coulomb criterion with zero cohesion and a friction angle ϕ_j. In terms of principal stresses (σ_1, σ_3), the joint shear strength takes the following form (Goodman, 1976):

$$\sigma_1 = \sigma_3 \cdot \frac{\tan(\delta + \phi_j)}{\tan \delta} \tag{2.6}$$

Equations (2.1) and (2.6) have been plotted on the same diagram (σ_1 / C_0 versus δ) in Fig. 2.5b for $\phi = 40°$, $S_0 = 5$ MPa and $\phi_j = 30°$. It can be seen that for values of the orientation angle δ ranging essentially between 15 and 45°, slip along the joints takes place before the intact rock strength is mobilized. This, in turn, decreases the possible domain of variation for K. Starting with an initial state of stress ($\sigma_v = \gamma z$, σ_h) and using equation (2.6), K_{min} and K_{max} are independent of the depth z and are now equal to

$$K_{min} = \frac{\tan \delta}{\tan(\delta + \phi_j)};$$

$$K_{max} = \frac{\tan(\delta + \phi_j)}{\tan \delta} \tag{2.7}$$

Equations (2.6) and (2.7) indicate that the smallest domain of variation for K always occurs when $\delta = \pi/4 - \phi_j/2$. For instance, for $\phi_j = 30°$, $0.33 < K < 3.00$ when $\delta = \pi/4 - \phi_j/2 = 30°$.

Expressions for the maximum and minimum values of K can also be derived if the joint planes are located in a non-axisymmetric stress field. In that case the joint failure criterion is more complex, as discussed by Amadei and Savage (1989, 1993), and involves all three principal stresses. Also, expressions for the limiting values of K can be derived for other joint failure criteria, such as that of Barton (1976) as demonstrated by Pine and Batchelor (1984).

Note that if several joint sets exist in a given rock mass, the possible range for K will be further reduced as joint strength dominates more and more the rock mass strength. Sugawara and Obara (1993) give a good example of a tunnel project in Japan for which the joint system was found to play an important role in the magnitude and distribution of the *in situ* stress field. In particular, they showed how rock bursts, created by joint slip and monitored *in situ*, could be predicted knowing the *in situ* stress field and the joint orientation and by assuming a simple Coulomb criterion for joint slip.

2.4.3 GEOPHYSICAL MODELS

Equation (2.1) was derived using a simple model for intact rock strength assuming brittle response and no effect of strain rate or temperature on rock behavior. Many researchers in the geophysics literature have proposed upper limits to the stresses in the Earth's crust based on laboratory experiments conducted on intact core samples at very large confining pressures (up to 1000 MPa) and high temperatures (up to 900°C); (Brace and Kohlstedt, 1980; Goetze and Evans, 1979; Kirby, 1983; McGarr, 1980; McGarr, 1988; McGarr and Gay, 1978; Meissner and Strehlau, 1982; Smith and Bruhn, 1984). Rummel (1986) concluded that most experimental data on rock strength reported in the literature could be fitted by an equation of the form

$$(\sigma_1 - \sigma_3)_c = A + B(\sigma_3')^{1/2} \tag{2.8}$$

where σ_3' is the effective confining stress, $(\sigma_1 - \sigma_3)_c$ is the peak differential strength, and A and B are constants which depend on the temperature. By substituting σ_v, σ_H or σ_h for σ_1 or σ_3, Rummel (1986) was able to derive limits for $\sigma_H - \sigma_v$ (reverse faulting) and $\sigma_v - \sigma_h$ (normal faulting) as a function of depth for dry or wet conditions and for a normal geothermal gradient in the upper 30 km of the crust (Fig. 2.6). As mentioned by Rummel (1986), equation (2.8) can be applied for strain rates of the order of 10^{-6}/s. For smaller strain rates, he suggested that rock creep could create *in situ*

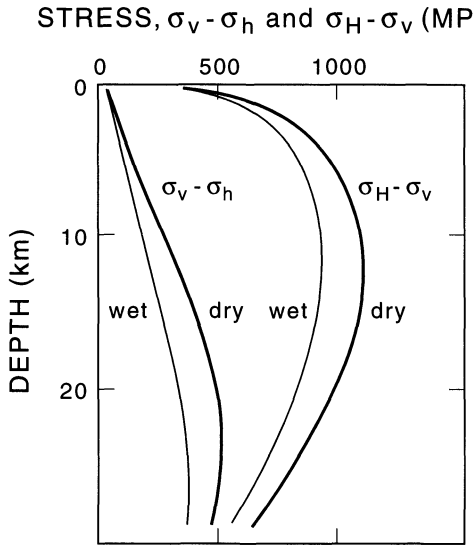

Fig. 2.6 Differential stresses required for normal faulting ($\sigma_v - \sigma_h$) and reverse faulting ($\sigma_H - \sigma_v$) in an intact dry and wet granitic crust with normal temperature gradient. (After Rummel, 1986.)

stresses to relax with time and proposed an empirical power law equation where the maximum shear stress is a nonlinear function of the creep rate.

In the geophysics literature, the limits on crustal stresses induced by slip along discontinuities are usually derived assuming Byerlee's (1978) empirical friction law. Experimental results obtained by Byerlee revealed that at normal stresses $\sigma_n < 200$ MPa, the critical shear stress τ to initiate slip is equal to $0.85\sigma_n$, and that at normal stresses $200 < \sigma_n < 2000$ MPa, $\tau = 0.5 + 0.6\sigma_n$. In general, Byerlee's law applies for temperatures less than 400°C and strain rates less than 10^{-7}/s. Examples of application of Byerlee's law can be found in Brace and Kohlstedt (1980), Rummel (1986), Zoback and Healy (1992), Zoback *et al.* (1993) and Brudy *et al.* (1995).

More recently, Savage, Swolfs and Amadei (1992) proposed a two-dimensional plasticity model to predict the limit of *in situ* stresses in brittle crustal rock. In this model, both frictional and intact rock strengths were assumed to be described by a Coulomb criterion with cohesion and friction. Strain rates were related to stresses assuming associated plasticity. It was found that rock strength constrains *in situ* stresses and that those stresses become independent of strain rates once failure has occurred during plastic flow of the crust. The plasticity model also predicted non-zero horizontal *in situ* stresses at the Earth's surface for plastically deforming rocks having cohesion.

2.5 EFFECT OF ANISOTROPY

The expression for the horizontal to vertical stress ratio $K_0 = \nu/(1 - \nu)$ applies to a semi-infinite continuum with linear elastic, homogeneous and isotropic properties. In this section we will explore the effect of anisotropy on the value of K in the absence of topography.

Many rocks are anisotropic, meaning that their properties vary with direction. This variation is often related to the existence of well-defined rock fabric elements in the form of bedding, layering, schistosity planes, foliation, fissuring and jointing. Anisotropy is a general characteristic of foliated metamorphic rocks (schists, slates, gneisses and phyllites), stratified sedimentary rocks (shales, limestones, sandstones and coal) and rocks cut by one or several regular, closely spaced joint sets. All these rocks display clear evidence of anisotropy and show one or several apparent directions of symmetry (Turner and Weiss, 1963). Mostly, orthotropy and transverse isotropy are used to describe the symmetry of anisotropic rocks. The discussion below is limited to *in situ* stresses in transversely isotropic rock masses.

Transverse isotropy is often used to describe the symmetry of rocks with one dominant system of layers, such as foliated and sedimentary rocks or rock masses with one joint set. In that case, five elastic constants are used to describe the rock deformability in a coordinate system attached to the layers (assumed

to coincide with the plane of transverse isotropy). These constants will be called E, E', ν, ν' and G' with the following definitions: (1) E and E' are Young's moduli in the plane of transverse isotropy and in the direction normal to it, respectively, (2) ν and ν' are Poisson's ratios characterizing the lateral strain response in the plane of transverse isotropy to a stress acting parallel or normal to it, respectively, and (3) G' is the shear modulus in planes normal to the plane of transverse isotropy. The shear modulus G in the plane of transverse isotropy is equal to $0.5E/(1+\nu)$.

In general, rocks are not too strongly anisotropic compared with wood or composite materials. For most transversely isotropic and intact rocks, E/E' and G/G' vary between 1 and 3 and the Poisson's ratios ν and ν' vary between 0.15 and 0.35 (Amadei, Savage and Swolfs 1987; Gerrard, 1975). For regularly jointed rock masses, the ratio of anisotropy can be much larger and in general depends on the stress level across the joint planes. Consider for instance a joint set with spacing S and normal stiffness k_n. As shown by Duncan and Goodman (1968), the ratio E/E' is equal to

$$\frac{E}{E'} = 1 + \frac{E}{k_n S} \tag{2.9}$$

Using the expression for the normal stiffness, k_n, proposed by Bandis, Lumsden and Barton (1983), equation (2.9) becomes

$$\frac{E}{E'} = 1 + \frac{E}{k_{ni} S} \cdot \left(\frac{k_{ni} V_m}{\sigma_n + k_{ni} V_m} \right)^2 \tag{2.10}$$

where k_{ni} is the initial normal stiffness of the joint planes and V_m is the maximum closure. At zero normal stress ($\sigma_n = 0$), E/E' is equal to $1 + E/(k_{ni} S)$ and can be large for joints with small values of the spacing and/or initial stiffness. As more compression is applied across the joints (due for instance to an increase in confinement with depth), the ratio E/E' approaches unity and the joint-induced anisotropy decreases.

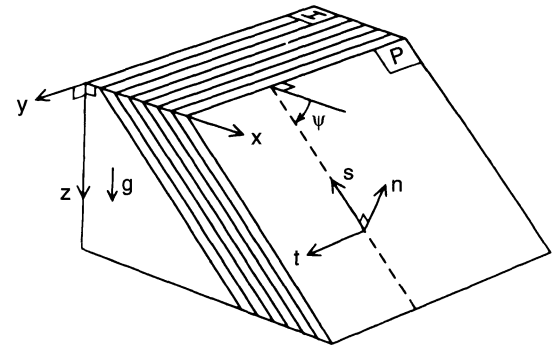

Fig. 2.7 Stress determination in anisotropic rock mass with inclined layers. Layers are parallel to plane P. (After Amadei and Pan, 1992.)

The effect of anisotropy on gravitational stresses in homogeneous rock masses with a horizontal ground surface has been addressed by Amadei, Savage and Swolfs (1987) and Amadei and Pan (1992). They proposed expressions for the coefficient K in transversely isotropic, orthotropic and generally anisotropic rock masses. Consider, for instance, the geometry of Fig. 2.7 where a rock mass is assumed to be transversely isotropic in a plane P. Let n, s, t be a coordinate system attached to P and inclined with respect to a global x, y, z coordinate system such that the x- and y-axes are horizontal and the z-axis is vertical downward. Plane P dips at an angle ψ and strikes parallel to the y-axis. The rock mass is subject to gravity only and the displacement components in the x and y directions are assumed to be independent of x and y and to depend on z only. This assumption leads to a condition of no lateral strain where the normal strains ε_x, ε_y and the shear strain γ_{xy} vanish.

As shown by Amadei and Pan (1992), for the geometry of Fig. 2.7 and the condition of no lateral strain, the stresses in the x, y and z directions are principal stresses with $\sigma_z = \rho g z$, $\sigma_x = K_x \rho g z$ and $\sigma_y = K_y \rho g z$. In general, the two stress ratios K_x and K_y are not equal and depend on the dip angle ψ and the ratios E/E', G/G', ν and ν'. If $\psi = 0°$ (horizontal plane of

transverse isotropy), K_x and K_y take simpler forms and reduce to

$$K_x = K_y = \frac{\sigma_x}{\rho g z} = \frac{\sigma_y}{\rho g z}$$

$$= \nu' \frac{E}{E'} \cdot \frac{1}{1-\nu} \qquad (2.11)$$

If the plane of transverse isotropy is vertical ($\psi = 90°$), equation (2.11) is replaced by

$$K_x = \frac{\sigma_x}{\rho g z} = \frac{\nu'(1+\nu)}{1-\nu'^2(E/E')};$$

$$K_y = \frac{\sigma_y}{\rho g z} = \frac{\nu + \nu'^2(E/E')}{1-\nu'^2(E/E')} \qquad (2.12)$$

For an isotropic rock mass, equations (2.11) and (2.12) reduce to $K_x = K_y = K_0 = \nu/(1-\nu)$. When $\psi = 0$ or 90°, it can be shown that the shear strains γ_{xz} and γ_{yz} vanish in addition to ε_x, ε_y and γ_{xy} and that the condition of no lateral strain reduces to a condition of no lateral displacement.

As a numerical example, Figs 2.8a–c show respectively the variations of $K_x = \sigma_x/\rho g z$, $K_y = \sigma_y/\rho g z$ and σ_x/σ_y for a transversely isotropic rock mass with E/E' and G/G' ranging between 1 and 3, $\nu = \nu' = 0.25$ and for a dip angle ψ equal to 30°. Compared with the isotropic solution, e.g. $\sigma_x/\rho g z = \sigma_y/\rho g z = 0.333$, which is represented by point I in Figs 2.8a and 2.8b, both σ_x and σ_y increase with E/E' and G/G'. For a fixed value of G/G', the stresses increase as E/E' increases, that is, as the rock mass becomes more deformable in directions normal to the plane of transverse isotropy. Note that for a fixed value of E/E', the stress σ_x parallel to the dip direction of the plane of transverse isotropy depends strongly on the value of G/G'. On the other hand, the stress σ_y parallel to the strike of the plane of transverse isotropy is not much affected by the value of G/G'. An increase of G/G' indicates that the rock mass becomes more deformable in shear

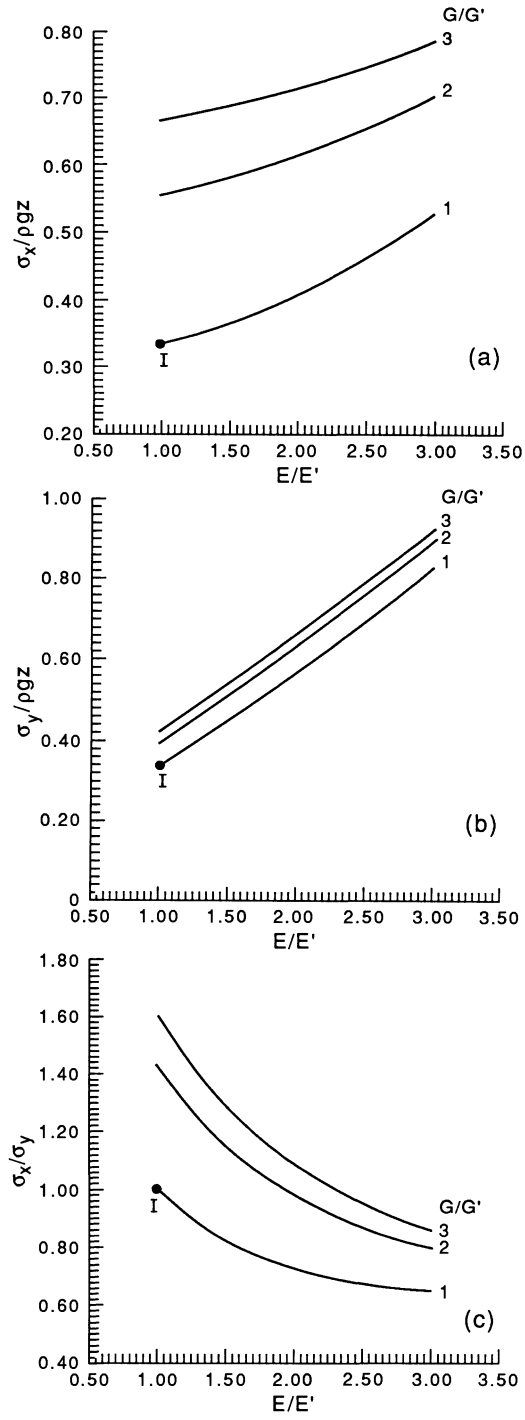

Fig. 2.8 Variation of (a) $\sigma_x/\rho g z$, (b) $\sigma_y/\rho g z$ and (c) σ_x/σ_y with E/E', G/G' for $\nu = \nu' = 0.25$ and $\psi = 30°$. (After Amadei and Pan, 1992.)

in planes normal to the plane of transverse isotropy. For a fixed value of G/G', the stress ratio σ_x/σ_y decreases as E/E' increases.

The models of Amadei, Savage and Swolfs (1987) and Amadei and Pan (1992) show that for anisotropic rock masses, the gravity-induced stress field is multiaxial and is strongly correlated to the rock mass structure. The vertical stress is always a principal stress and is equal to the weight of the overlying rock. Its magnitude is independent of anisotropy. The two horizontal principal stress components are, in general, not equal and their magnitude and orientation in the horizontal plane depend on the anisotropic character of the rock mass. Note that the solutions of Amadei, Savage and Swolfs (1987) and Amadei and Pan (1992) should not be used to estimate gravitational stresses in rock masses with rigid lateral boundaries (no horizontal lateral displacement) when the dip angle ψ is not equal to 0 or 90°. For those cases it has been shown by Dolezalova (1974), using the finite element method, that the principal stresses are inclined with respect to the vertical and horizontal directions. The analyses of Dolezalova (1974) and Amadei and Pan (1992) show the importance of lateral boundary conditions when estimating gravitational *in situ* stresses, which will be discussed further in section 2.13.

Compared with the isotropic solution, the range of permissible values of gravity-induced horizontal stresses in transversely isotropic rock masses is much wider. Indeed for isotropic elastic rock, since $\nu < 0.5$, $K = \nu/(1-\nu)$ is always less than 1. Thus horizontal stresses larger than the vertical stress are not possible under gravity loading only. On the other hand, for a transversely isotropic rock mass, the five elastic properties E, E', ν, ν' and G' must satisfy the following thermodynamic constraints (Amadei, Savage and Swolfs, 1987; Pickering, 1970):

$$E, E', G' > 0 \tag{2.13}$$

$$-1 < \nu < 1 \tag{2.14}$$

$$-\left(\frac{E'}{E}\cdot\frac{(1-\nu)}{2}\right)^{1/2} < \nu' < \left(\frac{E'}{E}\cdot\frac{(1-\nu)}{2}\right)^{1/2} \tag{2.15}$$

Considering only the positive part of the domains of variations for the Poisson's ratios ν and ν', the inequalities (2.13) to (2.15) provide constraints on the types of stress fields that are admissible in transversely isotropic rock masses. Figure 2.9 shows, for instance, the variation of the horizontal stress ratio $\sigma_h/\rho gz = \sigma_x/\rho gz = \sigma_y/\rho gz$ defined in equation (2.11) with $\nu' E/E'$ and ν for a horizontally transverse isotropic rock mass. The horizontal stress can vary over a large region compared to the isotropic solution since the domains of variation for ν and ν' in inequalities (2.13) to (2.15) are not as restrictive as the domain of variation for ν in the isotropic model. The region is bounded by a curve that depends on the value of E/E' and whose equation is

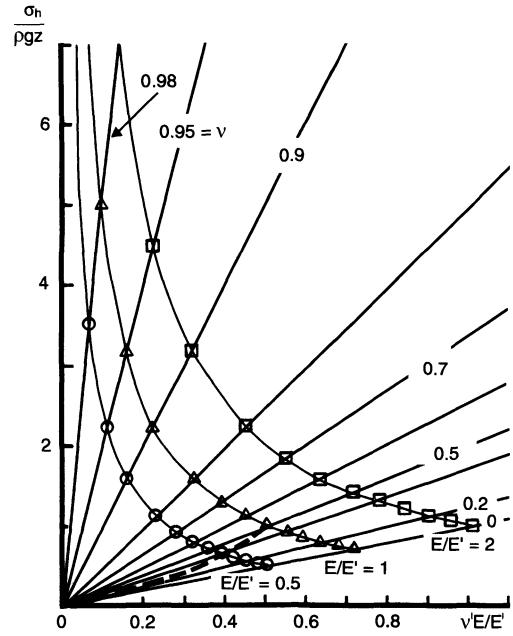

Fig. 2.9 Variation of the horizontal stress ratio $\sigma_h/\rho gz = \sigma_x/\rho gz = \sigma_y/\rho gz$ with $\nu' E/E'$ and ν for a horizontally transverse isotropic rock mass ($\psi = 0°$). The isotropic solution is shown as a dotted line. (After Amadei, Savage and Swolfs, 1987.)

obtained by combining the positive part of inequality (2.15) with equation (2.11). Figure 2.9 shows that horizontal stresses larger than the vertical stress are admissible for horizontally layered rock masses.

Figures 2.10a–d show, for comparison, the domains of variation of $\sigma_x/\rho gz$ and $\sigma_y/\rho gz$ with E/E' and ν' for transversely isotropic rock masses with planes of transverse isotropy dipping at angles ψ of 30, 45, 60 and 90°, respectively. In this numerical example, E/E' varies between 1 and 4, $\nu = 0.25$, $G/G' = 1$ and ν' varies between 0.1 and 0.4. In Fig. 2.10a–d the constraint associated with the positive part of inequality (2.15) is indicated as dotted dashed lines. These figures indicate that the stress component σ_y acting parallel to the plane of transverse isotropy is in general larger than σ_x. However, as ψ increases, values of σ_x larger than σ_y become possible for values

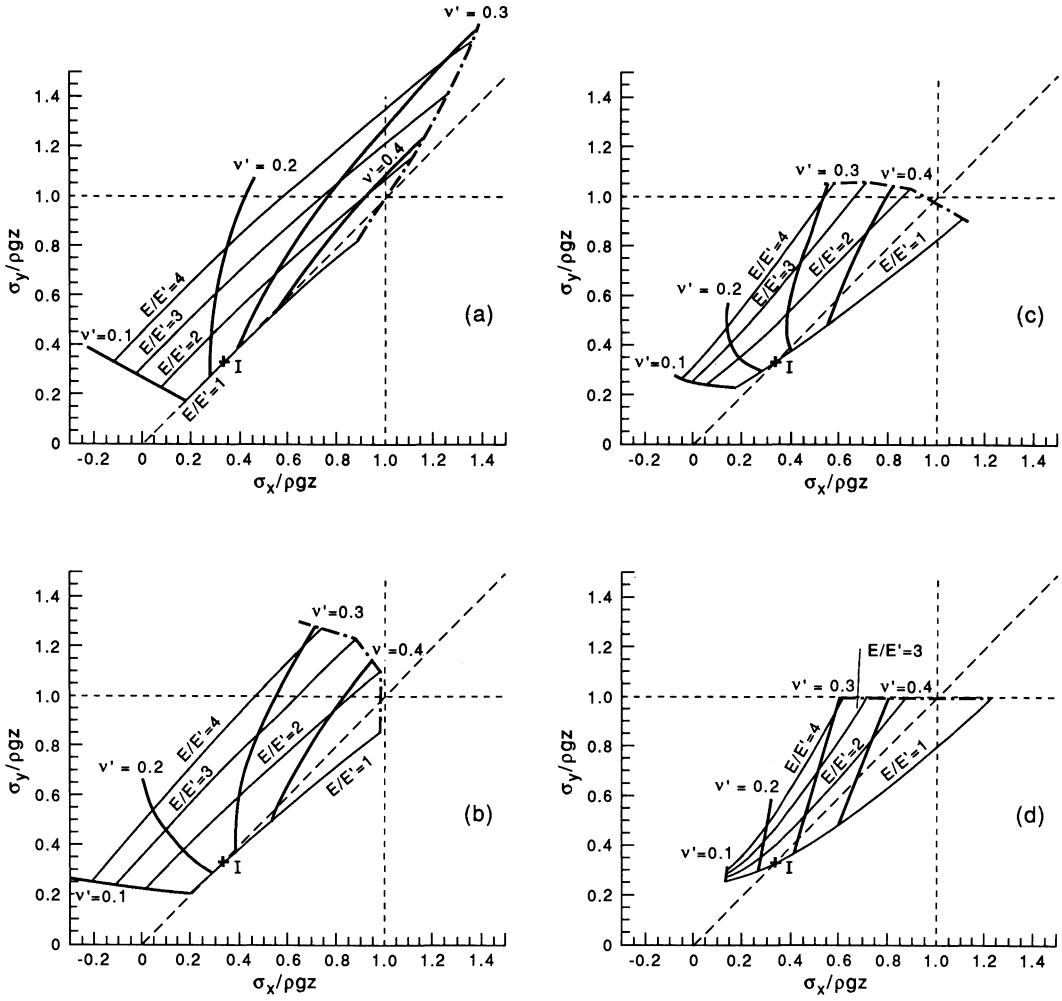

Fig. 2.10 Domains of variation of $\sigma_x/\rho gz$ and $\sigma_y/\rho gz$ with E/E' and ν' for transversely isotropic rock masses with inclined layers dipping at angles ψ of 30, 45, 60 and 90° in (a)–(d), respectively. E/E' varies between 1 and 4, $\nu = 0.25$, $G/G' = 1$ and ν' varies between 0.1 and 0.4. The constraint associated with the positive part of inequality (2.15) is indicated as dotted dashed lines. (After Amadei and Pan, 1992.)

of E/E' between 1 and 2 and for Poisson's ratio v' larger than 0.3. Compared with the isotropic solution represented by point I, horizontal stresses larger than the vertical stress ρgz are thermodynamically admissible. However, this becomes less admissible as ψ increases, that is, as the plane of transverse isotropy becomes steeper. Note also that for low values of v' and large values of E/E', tensile stresses can develop in the x direction. As shown by Amadei and Pan (1992), the trends observed in Fig. 2.10a–d can also be found for larger values of G/G'. However, the likelihood of having tensile stresses in the x direction when E/E' ranges between 1 and 4, diminishes as G/G' increases. Also, it was found that for values ranging between 0.15 and 0.35, the Poisson's ratio v has little effect on the stress variations shown in Fig. 2.10a–d.

2.6 EFFECT OF STRATIFICATION

The expressions for $K_x = \sigma_x/\rho gz$ and $K_y = \sigma_y/\rho gz$ proposed by Amadei, Savage and Swolfs (1987) and Amadei and Pan (1992) apply only to rock masses that are homogeneous. Stratification, which is common in sedimentary as well as volcanic rock masses, creates heterogeneities. Depending on the lithology and the relative stiffness between the different layers, *in situ* stresses may vary substantially from one layer to another. In general, abrupt changes in horizontal stress can take place across contacts between strata with different properties.

The influence of lithology on the distribution of horizontal stresses at depth has been demonstrated by numerous measurements in sedimentary rocks (Burlet and Ouvry, 1989; Enever, Walton and Wold, 1990; Evans, 1989; Evans, Engelder and Plumb, 1989; Hansen and Purcell, 1986; Jeffery and North, 1993; Lo, 1978; Plumb, 1994; Plumb, Evans and Engelder, 1991; Swolfs, 1984; Szymanski and Harper, 1979; Teufel, 1986; Warpinski, 1989; Warpinski, Branagan and Wilmer, 1985; Warpinski and Teufel, 1987; Whitehead, Hunt and Holditch, 1987) and volcanic rocks (Haimson and Rummel, 1982; Warpinski and Teufel, 1991). As an example, Fig. 2.11a shows the variation of the minimum horizontal *in situ* stress with depth measured by hydraulic fracturing through perforations by Warpinski, Branagan and Wilmer (1985) at the DOE's Multiwell Experiment site in the Mesaverde sedimentary formation of western Colorado. This figure shows higher stresses in the shale layers compared with the surrounding sandstones and siltstones. Similar conclusions were reached by Teufel (1986) who measured sharp differences in the *in situ* stress field in sandstone and shale layers at depths of about 2 km using both hydraulic fracturing tests and anelastic strain recovery tests on oriented cores. In the sandstone layers the average ratios of the minimum and maximum horizontal stresses to the overburden stress were found to be equal to 0.82 and 0.96, respectively. On the other hand, the shale formations bounding the sandstone were found to be under a lithostatic stress field (see also Warpinski, 1989; Warpinski and Teufel, 1987). Another interesting observation made by Teufel (1986) is that major joint sets in the sandstone layers were found to be aligned with the maximum horizontal stress direction. Another example, shown in Fig. 2.11b, corresponds to hydraulic stress measurements conducted by Haimson and Rummel (1982) in lava flows in Iceland. Here, both horizontal stress components vary from one lava flow to the next.

Stress measurements by hydraulic fracturing conducted by Warpinski and Teufel (1991) in welded tuff in Rainier Mesa at the Nevada Test Site have also revealed large stress contrasts due to changes in material properties, beddings and faults. Such contrasts were found to occur sometimes on a scale of less than 1 m if the contrast in rock properties was sufficient. The minimum horizontal stress determined from the instantaneous shut-in pressure of hydraulic fracturing tests was found to be lower in layers with a high Young's modulus and low Poisson's ratio and

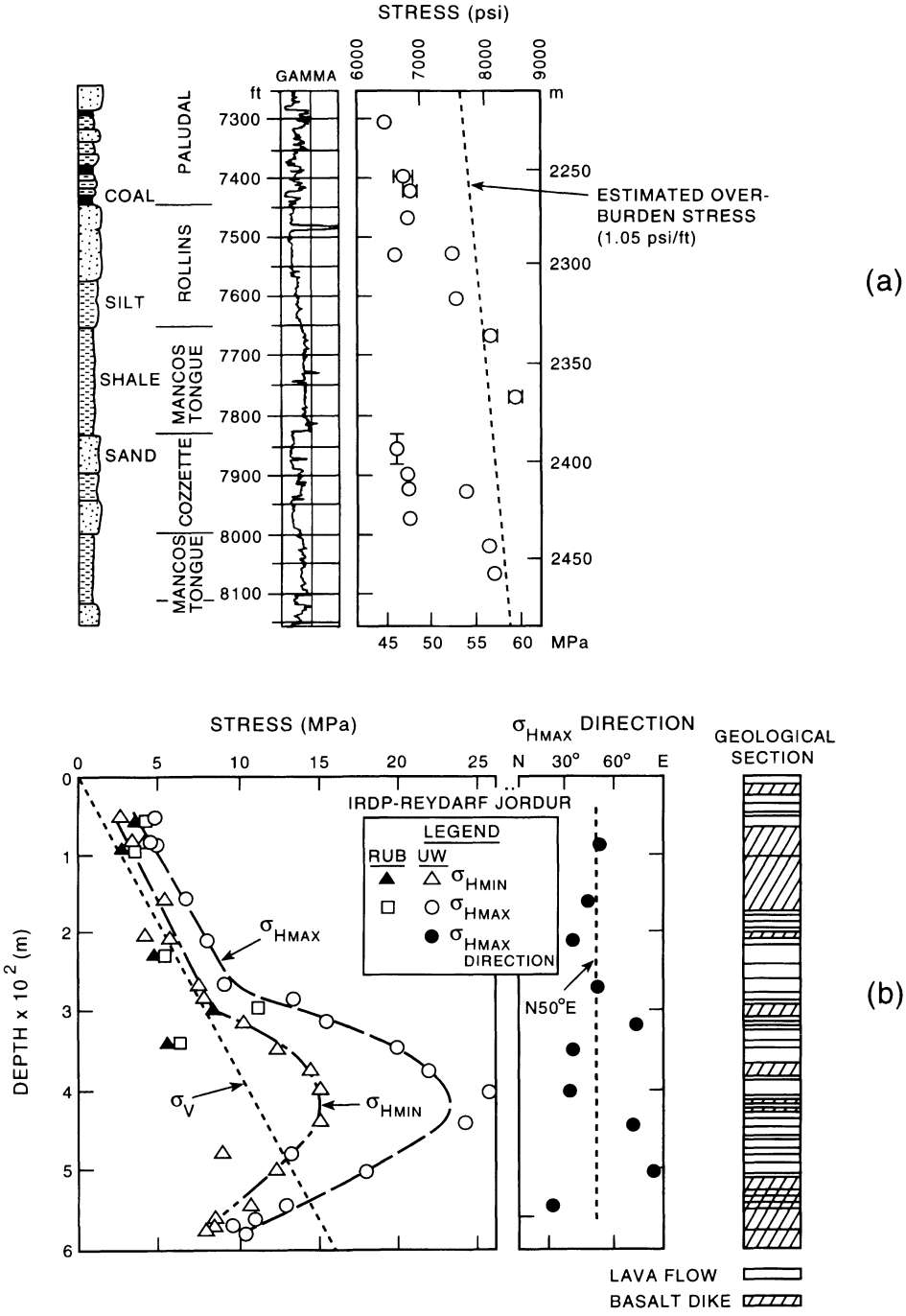

Fig. 2.11 Two examples showing the influence of lithology on *in situ* stress distribution. (a) Variation of the minimum horizontal *in situ* stress with depth measured by hydraulic fracturing through perforations in lower Mesaverde Formation. (Adapted from Warpinski, Branagan and Wilmer, 1985.) (b) *In situ* stress measurements in layered lava flows in Iceland. (After Haimson and Rummel, 1982.)

higher in layers with a low Young's modulus and high Poisson's ratio.

Swolfs (1984) compiled data on the variation of ratio of the minimum horizontal stress to vertical stress with depth measured by hydraulic fracturing in sedimentary basins. He concluded that, at depths greater than 600 m, the effect of lithology in basins is important and that at shallower depths, other near-surface phenomena may predominate in affecting the stress distribution. In a recent survey of 1000 least principal stress measurements in various sedimentary basins in the world, Plumb (1994) found high values of the ratio of minimum horizontal stress to vertical stress for depths less than 1 km. He found that the effect of lithology varied with the type of basin. For relaxed-state basins, values of the stress ratio for softer rocks such as shales were found to be 4 to 15% higher than stiffer rocks such as sandstones. On the other hand, in compressed-state basins, stiffer rocks were found to show higher values of the stress ratio with values in carbonate rocks 40% greater than in sandstones and values in sandstones 20% higher than in shale. Plumb (1994) also concluded that, despite its importance, lithology has less influence on stresses than changes in rock pore pressure. Finally, analysis of overcoring and hydraulic fracturing stress measurements conducted by Enever, Walton and Wold (1990) in the northern coalfields of New South Wales in Australia revealed higher stresses in the stiffer sedimentary strata.

Figure 2.11a, b and the examples mentioned above clearly indicate that when lithology affects the distribution of *in situ* stresses, stress differences (sometimes large) should be expected across layers of different rock types. Thus, for such geological environments, using linear regression analyses to describe the variation of individual stress components with depth (Tables 2.1–2.3) becomes meaningless. The field measurements of stress in stratified rock masses also indicate that, although higher modulus rocks are more likely to carry higher than average stresses (Voight, 1966a), softer rock layers have sometimes been found to carry higher stresses. This remark must be taken with caution as several phenomena may be responsible for that observation. For instance, Franklin and Hungr (1978) attributed that trend to the fact that weaker rocks are more difficult to sample, tend to deteriorate more quickly and therefore appear to be softer when tested in the laboratory. Another possible explanation is that the modulus of the apparently stiffer rock units may not be as large *in situ* as it is when measured in the laboratory, due to natural fractures or other planes of weakness present in the field. Also, the range of elastic behavior for weaker rocks is more limited than for stiffer rocks. Nonlinear, time-dependent and pore pressure-related phenomena may occur as the rock is disturbed during *in situ* measurements. Such phenomena are not necessarily accounted for in the analysis of the field tests.

As a possible explanation for the role of lithology on *in situ* stresses, Amadei, Savage and Swolfs (1988) proposed analytical solutions based on the theory of linear elasticity for the stresses in horizontal strata under a condition of no lateral displacement. In the model, each stratum can be isotropic or horizontally layered with moduli E_i, E_i', G_i and G_i' and Poisson's ratios ν_i and ν_i'. For the geometry of Fig. 2.12, and assuming continuity along the

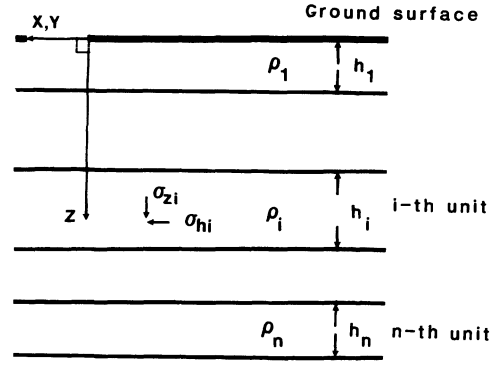

Fig. 2.12 Horizontally layered rock mass with different strata. (After Amadei, Savage and Swolfs, 1988.)

stratum contacts, the state of stress at depth z in the ith stratum is given by

$$\sigma_{hi} = \nu_i' \frac{E_i}{E_i'} \cdot \frac{1}{1-\nu_i} \cdot \sigma_{zi}$$
$$\sigma_{zi} = \rho_i g z + \sum_{j=1}^{i} (\rho_j - \rho_i) g h_j \qquad (2.16)$$

In each stratum (as for a homogeneous horizontally layered rock mass), the nature and magnitude of the stress field depend on the anisotropic character of the stratum deformability. Jumps in the magnitude of the horizontal stress occur across stratum contacts due to contrasts in deformability from one stratum to the next. The ratio σ_{hi}/σ_{zi} can be larger than, less than or equal to unity. If a stratum is isotropic, that ratio can only vary between 0 and 1. If a stratum is layered and a representative sample consisting of m layers can be identified, then the ratio σ_{hi}/σ_{zi} in that stratum is equal to

$$\frac{\sigma_{hi}}{\sigma_{zi}} = \sum_{j=1}^{m} \Phi_j \nu_j' \frac{E_j}{E_j'} \cdot \frac{1}{1-\nu_j} \qquad (2.17)$$

In equation (2.17) $\Phi_j = h_j/L$ where h_j is equal to the thickness of layer j in a representative sample of edge dimension L. In writing equation (2.17) it is assumed that the multilayered stratum can be replaced by an equivalent anisotropic continuum using the model proposed by Salamon (1968).

It is noteworthy that if all strata in Fig. 2.12 are isotropic, according to equation (2.16), the horizontal stress in each stratum depends only on the Poisson's ratio of the stratum and not on its elastic modulus. It is then clear that the model of Amadei, Savage and Swolfs (1988) alone is not enough to explain some of the observed variations of horizontal stress with lithology.

Equations (2.11) and (2.12) were derived for transversely isotropic rock masses with anisotropic elastic properties that are constant. Laboratory and field tests have shown that rock anisotropy is affected by confinement. Thus the degree of rock mass anisotropy must decrease with depth as more confinement takes place in the rock mass. For intact anisotropic rocks the increase in confinement may close preferred oriented microcracks and make the material more isotropic with depth. For regularly jointed rock masses the stiffness of the joints that create the rock mass anisotropy increases with the normal stress acting across their surfaces. As shown in equations (2.9) and (2.10), the ratio E/E' approaches a value of unity as the normal stress increases. Thus as the elastic properties change with the state of stress, so does the state of stress change because of the reduction in rock mass anisotropy. This closely interrelated phenomenon was investigated by Amadei and Savage (1985) for the stress distribution in horizontally and vertically regularly jointed rocks. Using the equivalent concept proposed by Duncan and Goodman (1968) and the expression for the variation of joint normal stiffness with stress proposed by Bandis, Lumsden and Barton (1983), it was shown that stress distributions similar to those observed by Brown and Hoek (1978) and others could be generated. For instance, for a jointed rock mass cut by horizontal joints with spacing S, combining equations (2.10) and (2.11) with $\sigma_n = \rho g z$, the horizontal to vertical stress ratio can be expressed as follows:

$$\frac{\sigma_h}{\rho g z} = \frac{\nu'}{1-\nu}\left[1 + \frac{E}{k_{ni} S} \cdot \left(\frac{k_{ni} V_m}{\rho g z + k_{ni} V_m}\right)^2\right] \qquad (2.18)$$

As z approaches infinity, the stress ratio defined in equation (2.18) approaches its value for the isotropic case (assuming that ν' converges toward ν). As a numerical example, Fig. 2.13 shows the variation of $\sigma_h/\rho g z$ with depth z for $V_m k_{ni} = 1.71$ MPa, $\nu = \nu' = 0.25$ and $E/k_{ni}S$ varying between 0 and 20. The isotropic case corresponds to $E/k_{ni}S = 0$. As $E/k_{ni}S$ increases, or in other words as E increases or k_{ni} and/or S decreases, the joints affect the stress field near the ground surface only. Stress distributions similar to those shown in Fig. 2.13 could also be obtained by

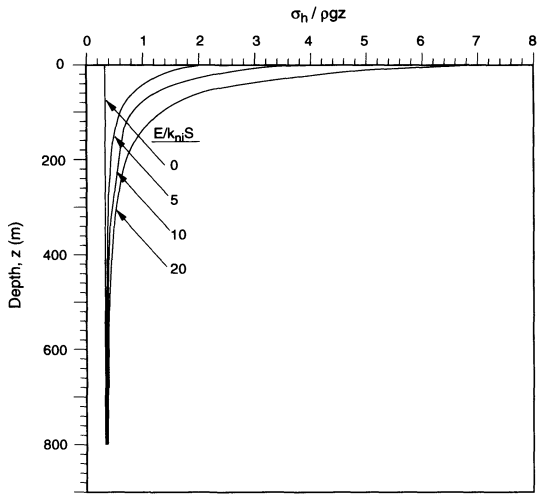

Fig. 2.13 Variation of $\sigma_h/\rho gz$ with depth z for $V_m k_{ni} = 1.71$ MPa, $\nu = \nu' = 0.25$ and $E/k_{ni}S$ varying between 0 and 20. The isotropic case corresponds to $E/k_{ni}S = 0$. Jointed rock mass cut by horizontal joints with spacing S.

making the moduli E and E' appearing in equation (2.11) functions of depth. Linear variations of modulus with depth were proposed by Gibson (1974) for soils and could be applied to rock masses as well.

2.7 EFFECT OF GEOLOGICAL STRUCTURES AND HETEROGENEITIES

Rock masses are rarely uniform, in particular in the continental crust. Variations in rock mass geology and the existence of geologic structures and heterogeneities may affect the distribution and magnitude of *in situ* stresses and contribute, in part, to the scatter often observed in field measurements (Fairhurst, 1986). For instance, as discussed in the previous section, the horizontal *in situ* stress may vary substantially from one layer to the next in stratified rock formations due to changes in rock stiffness. When crossing a persistent discontinuity, local changes in the *in situ* stress field can be expected (Hudson and Cooling, 1988; Pollard and Segall, 1987). Hudson and Cooling (1988) identified several cases depending on the relative stiffness of the material in the discontinuity versus the material in the surrounding rock: (1) if the discontinuity is open, the major principal stress is diverted parallel to the discontinuity, (2) if the discontinuity is made of a material with similar properties as the surrounding rock, the principal stresses are unaffected, and (3) if the material in the discontinuity is rigid, the major principal stress is diverted perpendicular to the discontinuity. In general, geological structures and heterogeneities disturb the regional stress field and make the local stress field quite different from the regional stress field.

Many cases of stress jumps and nonhomogeneous stress fields occurring while crossing or due to the vicinity of discontinuities, dikes, faults, shear zones, uncomformities, heterogeneities, orebodies and folds have been reported in the literature. Judd (1964) cites several examples of underground cavern projects, such as the Picote power station in Portugal and the Snowy Mountain Authority T1 power station in Australia, where major faults resulted in asymmetric stresses measured in the walls of the underground caverns. Large stress jumps of the order of tens of MPa measured in Fennoscandia across faults and shear zones were reported by Stephansson, Särkkä and Myrvang (1986) and Stephansson (1993). A survey of stress measurements conducted in salt domes in the southeastern USA by Eriksson and Michalski (1986) revealed generally hydrostatic *in situ* stresses. Locally, deviatoric stresses were found to occur due to the presence of layers of impure salt, geological structures and other heterogeneities. Aleksandrowski, Inderhaug and Knapstad (1992) found that structural features ranging between small faults and major fault systems could cause some major deflection of borehole breakouts, thus making local measurements of stress orientation different from regional stress trends. Enever, Walton and Wold (1990) presented various case studies of stress measurements with the overcoring and hydraulic

fracturing methods in Australia that showed how geological structures at various scales (ranging between regional and local scales) interact with *in situ* stresses. Other instances of stress anomalies due to discontinuities have been reported by Herget (1973, 1980), Tinchon (1987), Evans (1989), Haimson (1990a), Teufel and Farrell (1990), Teufel, Rhett and Farrell (1991) and Obara *et al.* (1995).

It is not uncommon for *in situ* stresses and the rock fabric to align. Sugawara and Obara (1993) give an example of overcoring measurements conducted 1.25 km from the Atotsugawa fault in Japan showing the effect of the fault on the *in situ* stress field (Fig. 2.14a). There, the measured major and intermediate *in situ* stresses were found to be parallel to the fault plane and the minor principal stress was found to be normal to the fault plane and strongly reduced in magnitude compared with the other two principal stress components (Fig. 2.14b). Multiple *in situ* stress determinations conducted in the granite at the Underground Research Laboratory (URL) in Pinawa, Manitoba, Canda, have also revealed the strong dependence of the *in situ* stress field on rock geological structures ranging in scale from microcracks in the intact rock to major thrust faults (Martin and Simmons, 1993). Martin and Chandler (1993) give an example of reorientation of *in situ* stresses in the vicinity of a discrete fracture near room 209 at the URL site (Fig. 9.9). The minimum *in situ* principal stress was found to be subhorizontal and perpendicular to the fracture, and to rotate and become vertical over a short distance of 30 m. Clear domain boundaries (separated by major faults) in which stresses are uniform were observed (section 9.1). The alignment of *in situ* principal stresses with rock fabric was also reported by Carlsson and Olsson (1982) regarding the state of stress at the site of the Forsmark power plant in Sweden. There, a clear correlation was found between joint orientation, joint opening and foliation orientation on one hand, and the directions of the principal stresses measured *in situ* by overcoring on the other hand. Overcoring measurements conducted by Mills, Pender and Depledge (1986) in coal mines in New Zealand revealed close alignment of the measured horizontal stresses with nearby faults and the major cleat system in the coal. Other cases of alignment of *in situ* stresses with faults and joint sets have been reported by Preston (1968), Lee, Nichols and Abel (1969), Eisbacher and Bielenstein (1971), Hast (1972), Lee, Abel and Nichols (1976), Kim and Smith (1980), Gay and Van Der Heever (1982), Leijon (1986), Enever, Walton and Windsor (1990) and Wong (1993).

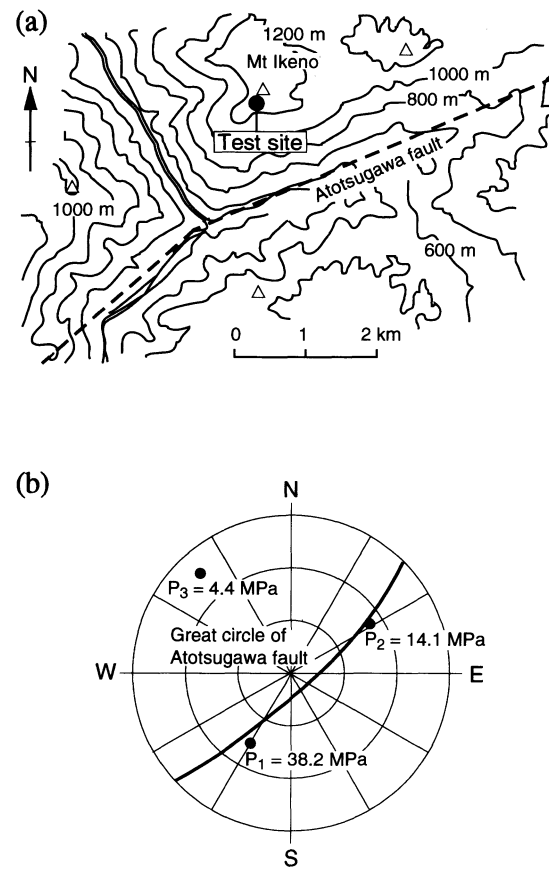

Fig. 2.14 (a) Overcoring measurements near the Atotsugawa fault in Japan, (b) relation between principal *in situ* stresses and fault plane. Lower hemisphere stereographic projection. (After Sugawara and Obara, 1993.)

At a much larger scale, Engelder *et al.* (1978), Sbar *et al.* (1979), Mount and Suppe (1987) and Zoback *et al.* (1987) have reported clear evidence of stress reorientation near and across the San Andreas fault (Fig. 2.15). Similar phenomena have been identified near faults in Canada by Adams and Bell (1991). Stress distortions near plate margins are believed to be due to slip occurring along the faults defining those boundaries (Zoback, 1989; Zoback, 1991). On a very large scale, the distribution of tectonic stresses in Europe was found to be affected by geological structures such as the western Alps (Müller *et al.*, 1992). As part of their study, Müller *et al.* (1992) also found that not all major geological structures can be expected to affect stress distributions. For instance, the distribution of the maximum

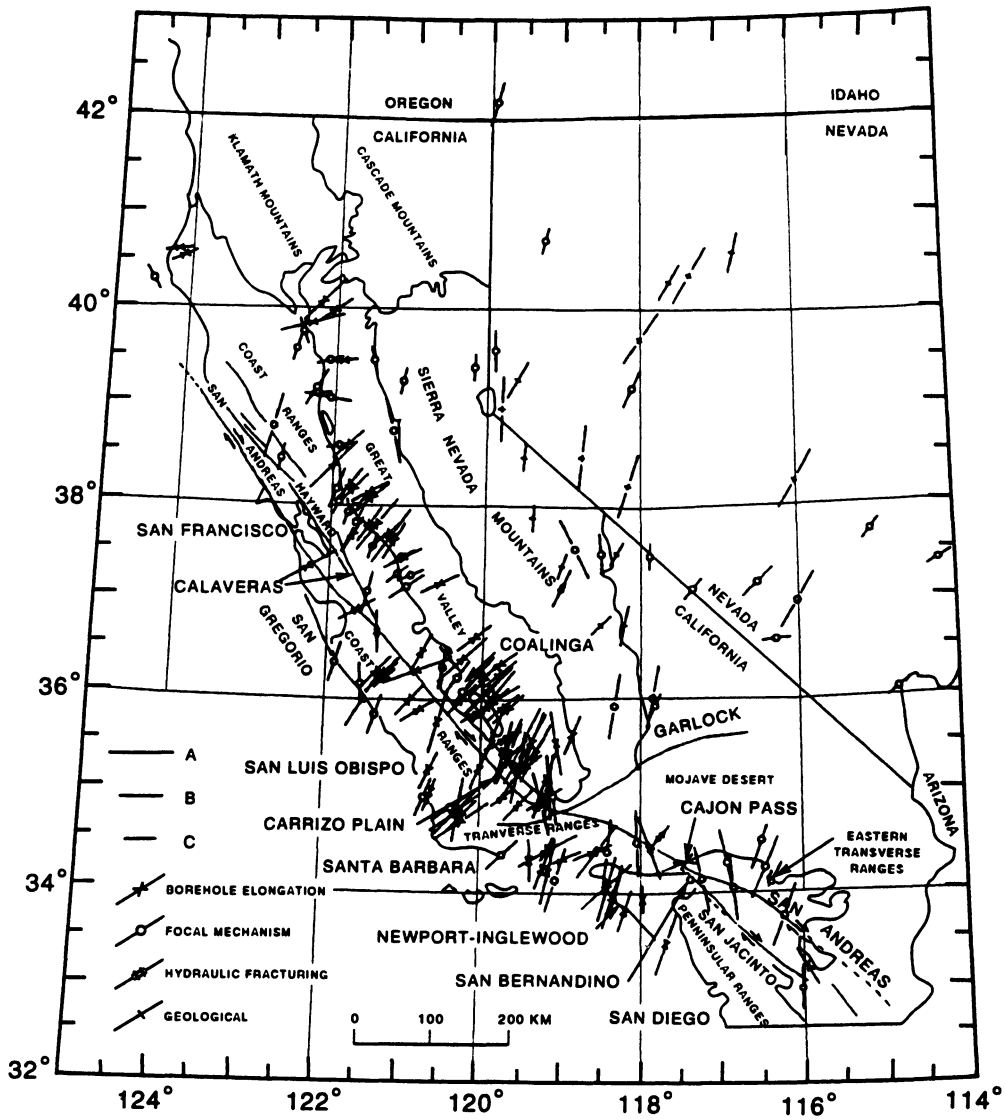

Fig. 2.15 Generalized geological map of California with data points showing the direction of maximum horizontal compression in the crust. (After Zoback *et al.*, 1987.)

horizontal stress was found to be continuous in the near vicinity of the Rhine Graben rift zone.

Figure 2.16 shows an example of stress distribution in a 6000 m × 4000 m rock mass consisting of three distinct blocks. The analysis was conducted by Stephansson, Ljunggren and Jing (1991) using the two-dimensional distinct element method. It indicates clearly that, despite uniform stresses applied on the boundaries of the domain, non-uniform stresses develop in each block of the rock mass

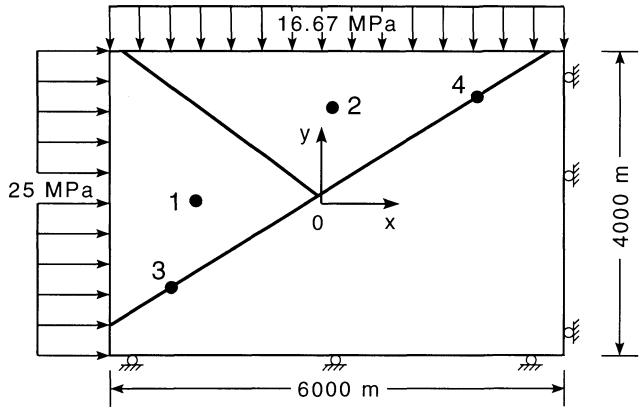

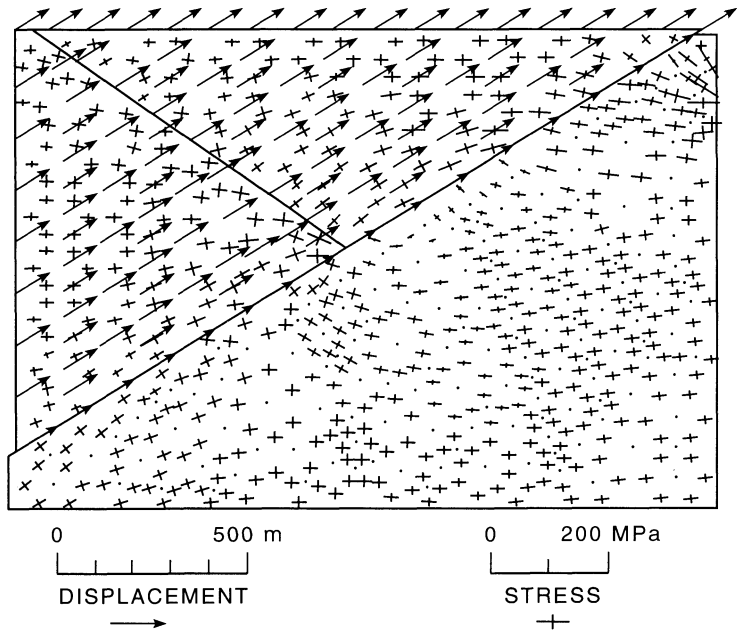

Fig. 2.16 Displacements and stresses in a distinct element model with three blocks. (After Stephansson, Ljunggren and Jing, 1991.)

and stress discontinuities occur due to sliding along the block boundaries. Similar conclusions were reported by Brown, Leijon and Hustrulid (1986) in their numerical analysis of block tests conducted at the Colorado School of Mines experimental mine in Idaho Springs, Colorado, and by Martin and Chandler (1993) in their numerical analysis of the granite at the URL site in Canada. The non-uniformity of load distribution in granular assemblies was clearly demonstrated by Cundall and Strack (1979) using the discrete element method. All these examples show that stresses in rock depend on the boundary loading conditions and the rock structure and that, even though the boundary conditions may be well defined, the local stress field can be quite complex.

In addition to discontinuities, stresses in rock masses can also change due to local heterogeneities such as strata, dikes and orebodies. Arjang (1989) conducted a survey on the orientation of the maximum and minimum horizontal *in situ* stresses in mines near several vertical orebodies in the Canadian Shield. It was found that the maximum horizontal stress often acts perpendicular to the strike of orebodies whereas the minimum stress acts parallel to their strike. Alignment of principal *in situ* stresses with orebodies has also been reported by Enever, Walton and Wold (1990) for various mines in Australia.

Disturbance of the *in situ* stress field due to heterogeneities can be understood using the analogy of a solid inclusion embedded into an infinite medium. It can be shown, using the theory of elasticity, that the stresses in a solid inclusion perfectly bonded to a continuum differ from those in the surrounding host material (Coutinho, 1949; Donnell, 1941; Sezawa and Nishimura, 1931). In particular, if the medium is infinite (isotropic or anisotropic), the stresses and strains in the inclusion are uniform (Amadei, 1983; Babcock, 1974a; Eshelby, 1957; Niwa and Hirashima, 1971). On the other hand, if the medium is finite, stresses in the inclusion vary from point to point.

As an example, Fig. 2.17 shows the stress concentration in a circular inclusion perfectly bonded to an infinite isotropic plate subjected to uniaxial compression (Leeman, 1964). It can be seen from this figure that the vertical stress in the inclusion can be as large as 1.5 times that in the host material provided the inclusion has a modulus four to five times that of the host material. A detailed study on stress concentrations in single inclusions of elliptical, ovaloid and rectangular shapes under uniaxial and biaxial loading and their applications to mining problems can be found in Oudenhoven, Babcock and Blake (1972) and Babcock (1974b). Inclusions also have a zone of influence on the encapsulating medium. For instance, work conducted by Stephen and Pirtz (1963) revealed that an inclusion with a

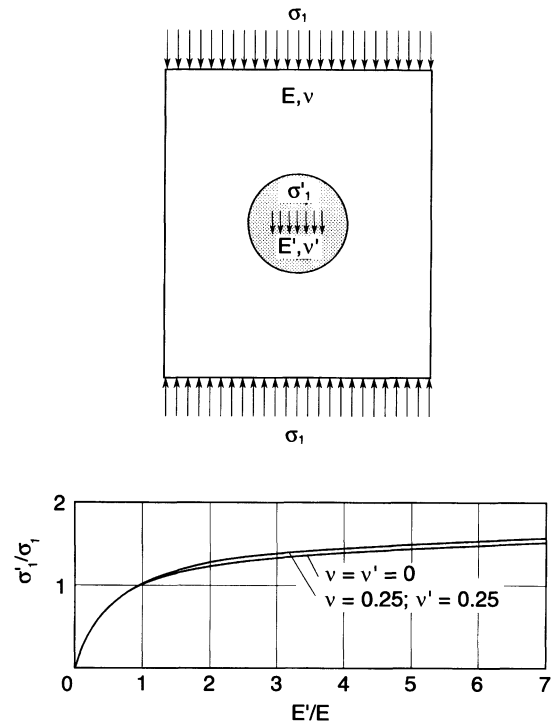

Fig. 2.17 Stress concentration in a circular inclusion (with elastic properties E', ν') perfectly bonded to an infinite isotropic plate (with elastic properties E, ν) subjected to uniaxial compression. (After Leeman, 1964.)

modulus four times that of the surrounding material has an area of influence roughly one diameter from the edge of the hole in which the inclusion is placed.

Gay (1979) gives an example of stress measurements in a quartz dolerite dike in South Africa showing much higher stresses in the dike than in the host quartzitic rock. Gay (1979) invoked residual tectonic and thermal stresses to explain the observations. The difference in stiffness between the dike (the inclusion) with a Young's modulus of 91 GPa and that in the surrounding rock (the host medium) with a modulus ranging between 75 and 86 GPa may well be responsible, in part, for the observed stress concentration. The inclusion analogy was also used by Germain and Bawden (1989) to explain the stress distribution near a sulfide orebody in an underground mine in Quebec. The softer nature of the orebody compared to the stiffer andesite/rhyolite surrounding rock was believed to be responsible for the observed diversion of the *in situ* stresses away from the orebody and for stress concentrations in the surrounding rock. In general, and from a practical point of view, heterogeneities may create stress concentrations that could lead to rockbursts and local stability problems during excavations.

The effect of heterogeneities on stresses in rock can also be illustrated using the simple model of Fig. 2.18. Here, a medium consisting of N juxtaposed and connected elements with Young's moduli E_i ($i = 1, N$) is subject to a normal force F. The force is applied over an area $A = \sum A_i = L \times 1$ where $A_i = w_i \times 1$ is the area of each element i. Using the basic strength of materials and assuming uniform displacement over the area A (or length L), the average stress σ_i in each element is equal to

$$\sigma_i = \frac{E_i L}{\sum_{k=1}^{N} w_k E_k} \cdot \sigma_{av} \qquad (2.19)$$

where σ_{av} is the average stress and is equal to F/A. Equation (2.19) shows that the local stress in each element can differ from the

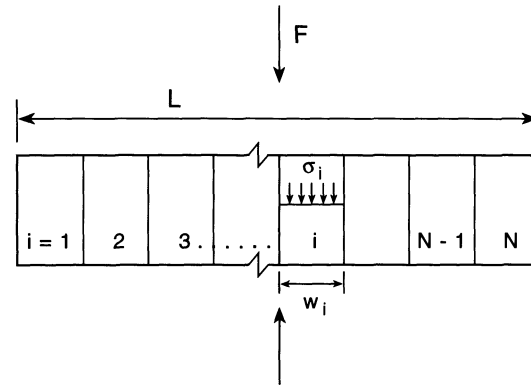

Fig. 2.18 Stresses in an idealized rock mass consisting of N juxtaposed elements with different moduli E_i ($i = 1, N$).

average stress, and that it is controlled by the value of the modulus in that element. Stiffer elements give higher stresses whereas softer elements give lower stresses. If, for instance, all the elements in Fig. 2.18 are horizontal and are located at a depth z with $\sigma_{av} = \gamma z$, excavation through those elements can be expected to take place under a changing vertical stress whose magnitude depends on the local rock stiffness.

Another example showing that the vertical average stress at a given depth may not always be representative at the local level is shown in Fig. 2.19 and is associated with folding (Goodman, 1989). Here we consider tunneling at two different depths z (defined as AA′ and BB′ in Fig. 2.19) in a folded sedimentary rock formation consisting of stiffer (more competent) beds such as sandstone or limestone surrounded by softer beds such as shale. Along AA′ the two right and left anticlines create shielding and divert the stresses toward the center syncline. The local vertical stresses almost vanish below the anticlines and increase above the average value ($\sigma_v = \gamma z$) in the syncline. Along BB′ the shielding still holds, but the vertical stress in the trough of the syncline is now higher than for AA′ due to the additional weight of the stiffer layers. Figure 2.19 illustrates that in folded rock

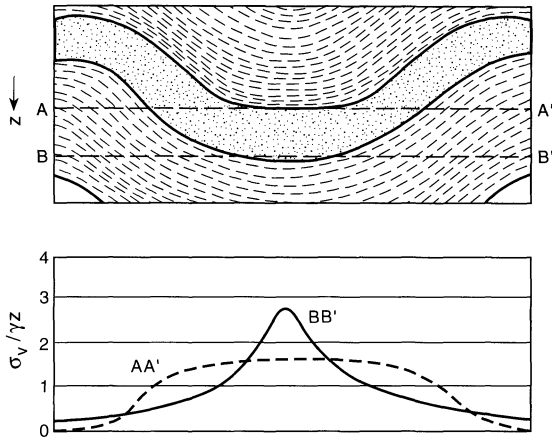

Fig. 2.19 Variation of vertical stress along tunnel alignment at two different depths along AA' and BB' in a folded sedimentary rock formation consisting of stiffer beds surrounded by softer beds. (After Goodman, 1989.)

masses, the *in situ* stress field at a given depth should not be expected to be uniform even though the ground surface is horizontal (Voight, 1966a).

2.8 EFFECT OF TOPOGRAPHY

2.8.1 MODELING THE EFFECT OF TOPOGRAPHY

The simplifying assumption that the principal stresses are vertical and horizontal with depth breaks down when the ground surface is not horizontal. Consider, for instance, a semi-infinite isotropic, homogeneous rock mass with a complex topography consisting of a series of hills and valleys and no surface loads, as shown in Fig. 2.20. The rock mass is under gravity alone with no lateral displacements. Because of the traction-free boundary conditions, the principal stresses are parallel and normal to the ground surface. With depth the principal stresses approach the same directions as when the ground surface is horizontal.

Knowledge of the effect of topography on stress distributions is of particular interest when conducting excavation in mountainous

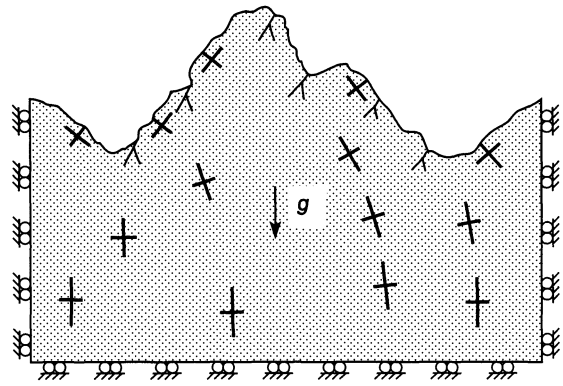

Fig. 2.20 Rock mass with a complex topography consisting of a series of hills and valleys and no surface loads.

regions, near valley slopes or near large open pit mines. Slopes and valley walls create unbalanced stress concentrations in the walls of nearby underground excavations (Chaplow and Eldred, 1984; Haimson, 1984; Judd, 1964), which may result in overstressed phenomena such as rockbursts, spalling, squeezing or fracturing. Examples of such phenomena have been reported by Brekke and Selmer-Olsen (1966), Broch and Sorheim (1984), Martna and Hansen (1986), Martna (1988), Ahola (1990), Myrvang, Hansen and Sørensen (1993) and Myrvang (1993), among others.

The effect of topography on *in situ* stresses is also very important when selecting the safe position of pressure tunnels and shafts near slopes and valley walls (Broch, 1984). The aim in pressure tunnel and shaft design is to maximize the opening length which stays unlined with a minimum risk of water leakage. Selmer-Olsen (1974) proposed a criterion, which uses the finite element method, to determine the *in situ* state of stress in valley sides. Then, the pressure tunnel or shaft location is aligned such that the internal water pressure is always less than the minimum *in situ* principal stress in the surrounding rock mass.

Other examples of the effect of topography on *in situ* stresses can be found in Hooker, Bickel and Aggson (1972), Brückl and

Scheidegger (1974), Myrvang (1976), Clark and Newman (1977), Scheidegger (1977), White, Hoskins and Nilssen (1978), Haimson (1979), Bauer, Holland and Parrish (1985), Swolfs and Savage (1985) and Kanagawa *et al.* (1986), among others. For instance, before construction of the Eisenhower Memorial Tunnel in Colorado, White, Hoskins and Nilssen (1978) found that the measured principal stresses were essentially parallel and perpendicular to the continental divide ridge crossing the tunnel axis. Similar examples of alignment of measured stresses at shallow depth with the topography can be found in Haimson (1979). Finally, Bauer, Holland and Parrish (1985) and Swolfs and Savage (1985) showed that the combined effect of topography, stratigraphy and rock mass structure needs to be considered when predicting *in situ* stresses at the Yucca Mountain site in Nevada.

It is difficult to determine analytically the *in situ* stress field in a rock mass with an irregular surface using the theory of elasticity. The effect of surface irregularities on stresses has been addressed in the literature using different analytical methods. Ling (1947) used a bipolar coordinate transformation method to determine stresses in an elastic and isotropic continuum with a notch in the form of an arc of a circle (representing a valley or a hill) and subjected to lateral loading only. Another method is the exact conformal mapping method as studied by Akhpatelov and Ter-Martirosyan (1971), Ter-Martirosyan, Akhpatelov and Manvelyan (1974), Ter-Martirosyan and Akhpatelov (1972), Savage, Swolfs and Powers (1985) and Savage (1994) for gravity loading only, and by Savage and Swolfs (1986) for gravity and tectonic loading. Chiu and Gao (1993) also used that method to predict stress concentrations in an elastic continuum with a cycloid rough surface subject to lateral loading only. The exact conformal mapping method is limited to isotropic media, to a very few smooth topographic profiles for which conformal mapping functions can be found exactly, and to two-dimensional problems. A third approach for two- and three-dimensional problems in isotropic media is the perturbation method discussed by McTigue and Mei (1981, 1987), McTigue and Stein (1984), Srolovitz (1989), Gao (1991), and Liu and Zoback (1992). Liao, Savage and Amadei (1992) also used the perturbation method for two-dimensional problems in anisotropic rock masses. The advantage of the perturbation method is that it can handle any smooth topographic features. However, the solutions derived with that method are restricted to topographies with slopes not exceeding 10%.

In spite of their limitations, all the solutions derived with the bipolar coordinate transformation method, the exact conformal mapping method and the perturbation method clearly show that topography can have a major effect on the magnitude and distribution of *in situ* stresses. For instance, the expressions in Savage, Swolfs and Powers (1985) for gravitational stresses in long, symmetric, isotropic ridges and valleys clearly depend on the geometry of the topography and on the Poisson's ratio of the rock. It was found that non-zero horizontal compressive stresses develop at and near ridge crests and that horizontal tensile stresses develop under valleys. The horizontal compressive stresses in ridge crests decrease and the horizontal tensile stresses in valleys become more compressive with increasing Poisson's ratio. Also the tensile region under valleys increases laterally as valleys broaden. Savage, Swolfs and Powers (1985) also found that broader ridges affect the stress field to greater depths. On the other hand, for valleys the topography-induced stresses were found to approach the far-field stresses more rapidly.

As shown by Savage and Swolfs (1986), superposing the effect of a uniaxial tectonic compression acting normal to the axial planes of isolated symmetric ridges and valleys on the gravitational stresses results in a slight increase in the lateral component of the compressive stresses at the ridge crests. Under the

valley bottoms, this superposition results in a decrease in the tensile stresses. The opposite effects occur when a far-field tectonic tension is superposed on the gravitational stress field.

McTigue and Mei (1981, 1987) and Liao, Savage and Amadei (1992) showed that topography affects gravitational stress distributions even in areas of low regional slopes of less than 10%. Liao, Savage and Amadei (1992) also concluded that the magnitude of the horizontal stress in transversely isotropic and orthotropic ridges and valleys depends strongly on the rock's elastic properties and the orientation of the rock mass fabric with respect to the ground surface. For instance, for horizontally layered rock masses, the horizontal stress at a given depth below a ridge was found to increase with the ratio of horizontal to vertical Young's moduli E_h / E_v (or, in other words, as the rock mass becomes more deformable in the vertical direction). For a given value of $E_h / E_v > 1$, the horizontal stress is the greatest for ridges that are horizontally layered and the smallest for ridges that are vertically layered. For valleys with horizontal layers, it was found that the tensile region at the bottom of the valleys decreases as the ratio of horizontal to vertical moduli increases (or, in other words, as the rock mass becomes more deformable in the vertical direction).

Because of the limitations of the conformal mapping and perturbation methods, numerical methods such as the finite element and boundary element methods were, until recently, the only other alternative to determine *in situ* stresses in rock masses with complex topographies. As an example, Fig. 2.21 shows the results of a finite element analysis conducted for the Hochkonig massif in Austria by Sturgul, Scheidegger and Greenshpan (1976). Another example of finite element analysis to study the effect of topography on *in situ* stresses was reported by Kohlbeck, Scheidegger and Sturgul (1979).

Recently, the limitations of the conformal mapping and perturbation methods have been overcome with a new analytical method proposed by Pan and Amadei (1994) to determine the stress field in homogeneous, general anisotropic and elastic half-spaces subject to gravity, surface loads and far-field uniform stresses associated with tectonic loading under a condition of generalized plane strain and limited by an irregular (but smooth) outer boundary such as that shown in Fig. 2.22. In the analytical solutions, the stresses are expressed in terms of three analytical functions that can be determined using a numerical conformal mapping method and an integral equation method. The solutions have been used to determine the stresses induced by gravity in long symmetric and asymmetric ridges and valleys (Pan and Amadei, 1993; Pan and Amadei, 1994; Pan, Amadei and Savage, 1994), and the stresses induced by gravity or combined gravity and uniaxial horizontal tectonic loading in symmetric and asymmetric ridges and valleys (Pan, Amadei and Savage, 1995). Parametric studies were conducted for transversely isotropic ridges and valleys with planes of anisotropy striking parallel to the ridge or valley axis. The effect of (1) topography, (2) orientation of anisotropy and (3) degree of anisotropy on the magnitude and distribution of gravitational stresses was investigated. A summary of the parametric study is presented below.

2.8.2 SYMMETRIC RIDGES AND VALLEYS UNDER GRAVITY ONLY

Consider a long, isolated, symmetric ridge with the geometry of Fig. 2.23a. The medium in the half-space is assumed to be linearly elastic, homogeneous, anisotropic and continuous with a uniform density ρ. An x, y, z coordinate system is attached to the half-space such that the x- and z-axes are in the horizontal plane and the y-axis points upward. The half-space geometry and the medium's elastic properties are assumed to be independent of the z direction. The medium is assumed to deform under a condition of generalized plane

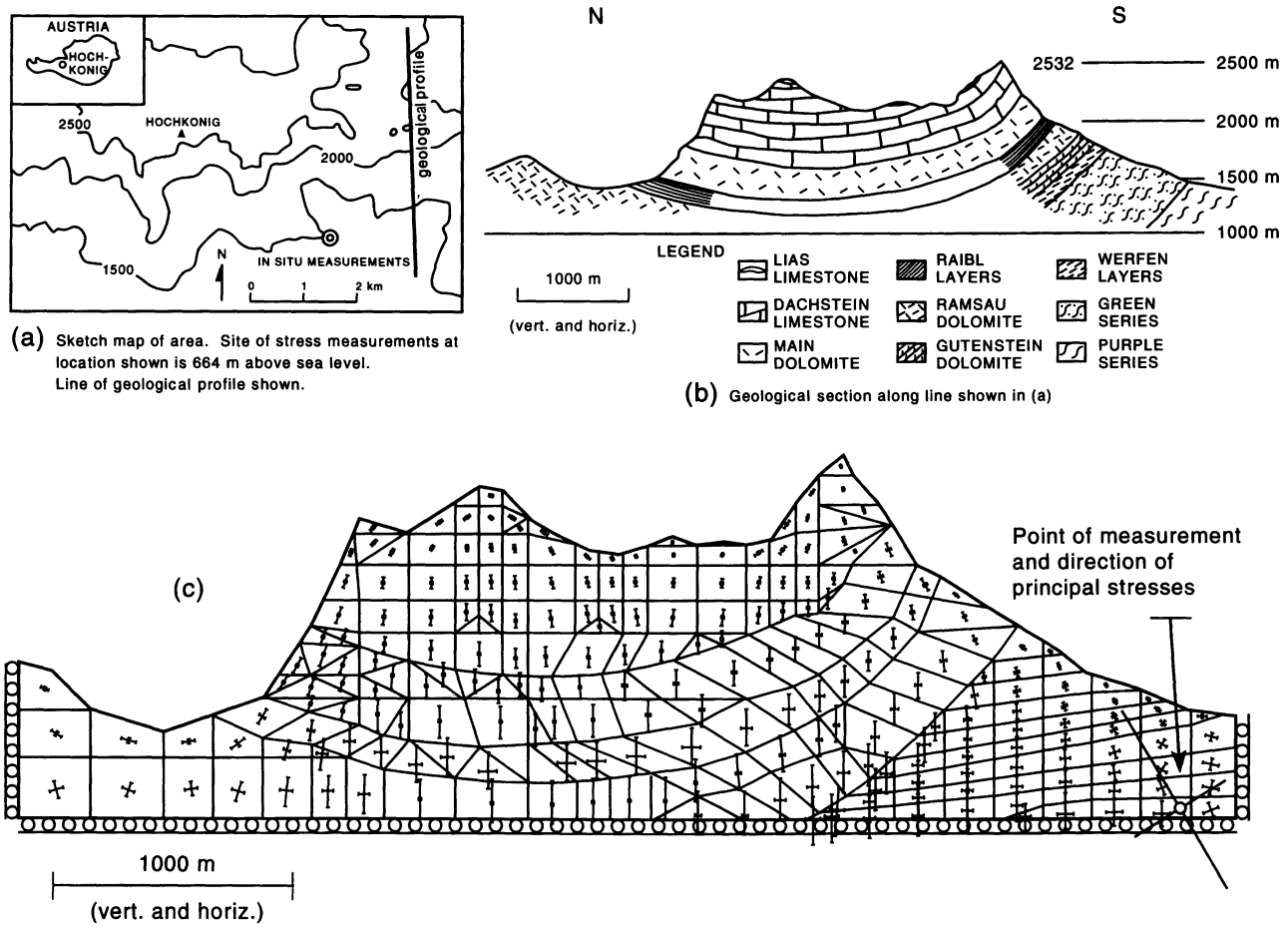

Fig. 2.21 Finite element analysis conducted for the Hochkonig massif in Austria. (a) Sketch of the area; (b) geological section along line shown in (a); (c) principal stresses determined with finite element analysis. (After Sturgul, Scheidegger and Greenshpan, 1976.)

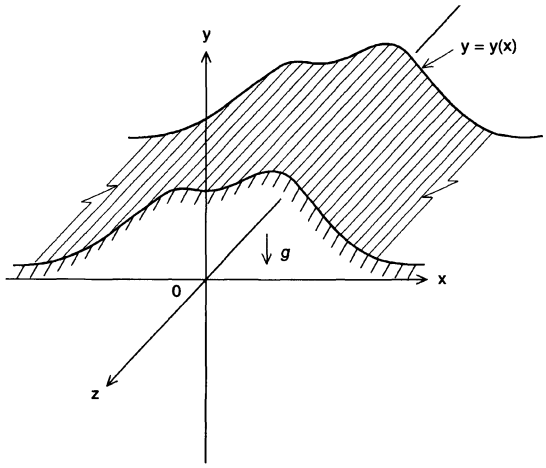

Fig. 2.22 Half-space limited by a boundary curve $y = y(x)$ and subject to gravity.

strain, e.g. all planes normal to the z-axis are assumed to warp identically with $\varepsilon_z = 0$. As $x \to \pm\infty$, the lateral horizontal strains ε_x and γ_{xz} approach zero. The boundary curve of the half-space is defined by an analytic function $y = y(x)$ or in parametric form

$$\begin{aligned} x(t) &= t \qquad (-\infty < t < +\infty) \\ y(t) &= a^2 b/(t^2 + a^2) \end{aligned} \tag{2.20}$$

where b is the ridge height and is assumed to be positive. If b is negative, equation (2.20) corresponds to a long, isolated, symmetric valley where $|b|$ is the depth of the valley (Fig. 2.23b). The parameter a in equation (2.20) is defined by the inflection points of the boundary curve. They are located at $x = \pm a/(3)^{1/2}$ and $y = 0.75b$ at which the slopes are equal to $\pm (3b(3)^{1/2})/(8a)$. For instance, for $a/|b| = 0.5, 1$ and 2, the slopes at the inflection points of the ridges and valleys are equal to ± 1.30 (52.4°), ± 0.65 (33.0°) and ± 0.32 (18°), respectively.

Using the analytical solution of Pan and Amadei (1994), the stresses can be determined at each point (x, y) in the ridge and valley of Figs 2.23a and 2.23b, respectively. The rock mass can be orthotropic or transversely isotropic in an n, s, t coordinate system inclined with respect to the x-, y- and z-axes. The orientation of the n, s, t coordinate system with respect to the x-, y- and z-axes is defined by a dip azimuth β and a dip angle ψ as shown in Fig. 2.24. The t-axis is located in the x, z plane.

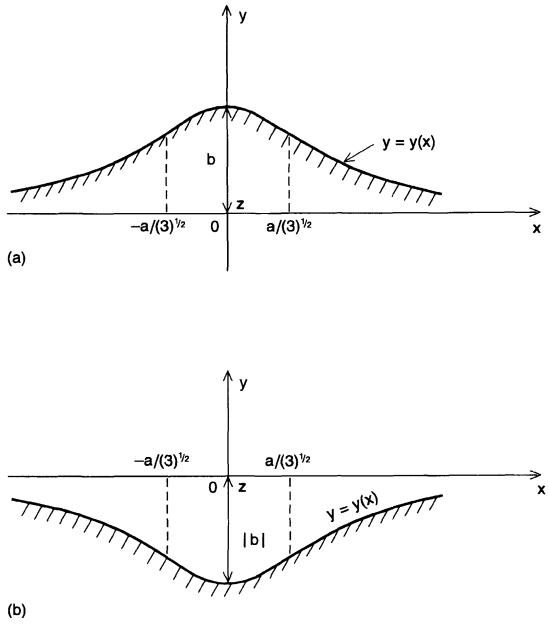

Fig. 2.23 (a) Symmetric ridge of height b; (b) symmetric valley of depth $|b|$.

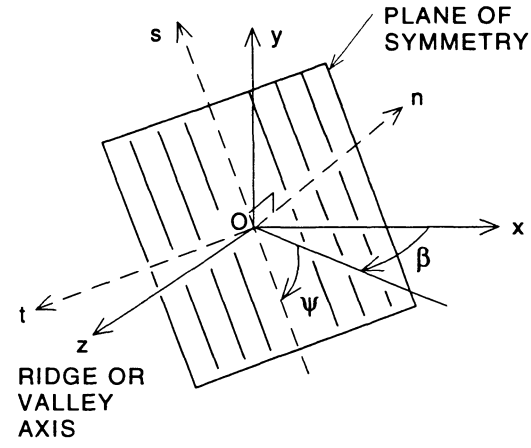

Fig. 2.24 Orientation of planes of symmetry with respect to the x, y, z coordinate system attached to the ridge or valley.

As shown by Pan and Amadei (1994) and Pan, Amadei and Savage (1994), the ratios between the six stress components σ_{ij} $(i, j = x, y, z)$ and a characteristic stress $\rho g|b|$ depend on the dimensionless ratios of elastic constants such as E/E', G/G', ν and ν' for transversely isotropic rocks. The stress ratios $\sigma_{ij}/\rho g|b|$ also depend on (1) the orientation angles β and ψ of the planes of anisotropy with respect to the x-, y- and z-axes attached to the ridge or valley, (2) the coordinates $(x/|b|, y/|b|)$ of the points at which the stresses are calculated and (3) the ratios $a/|b|$ and $b/|b|$ describing the geometry of the ridge or valley.

In general, at each point in the ridge and valley of Figs 2.23a, b, the stress field is three-dimensional and the principal stress components are inclined with respect to the x-, y- and z-axes attached to the ridge or valley. For the special case when there is a plane of elastic symmetry normal to the z-axis of Figs 2.23a, b, it can be shown that two of the three principal stresses induced by gravity are located in the x, y plane normal to the ridge or valley axis and that the longitudinal stress σ_{zz} is the third principal stress. This special case takes place (1) when the dip azimuth β in Fig. 2.24 is zero and the dip angle ψ varies between 0 and 90°, or (2) when both β and ψ are equal to 90°.

As a numerical example, Figs 2.25a–h show the gravitational stress regime for a ridge and a valley with $a/|b| = 1$ in a transversely isotropic rock mass with $E/E' = G/G' = 3$, $\nu = 0.25$ and $\nu' = 0.15$ with vertical anisotropy ($\psi = 90°$). In this example, the geometry of Figs 2.23a, b and 2.24 is adopted with planes of transverse isotropy parallel to the ridge or valley axis ($\beta = 0°$). In Figs 2.25a–f the stress distributions are presented using trajectories and contours of dimensionless stresses $\sigma_1/\rho g|b|$ and $\sigma_2/\rho g|b|$ where σ_1 and σ_2 are the maximum and minimum in-plane principal stresses in the x, y plane normal to the ridge or valley axis. Only the right halves of the plots of stress trajectories and contours are presented because of symmetry. As expected, the principal stresses in Figs 2.25a, b are no longer horizontal and vertical as for flat ground but are oriented parallel and normal to the ground surface along the boundary of the ridge and valley and gradually turn to become horizontal and vertical with depth. Figure 2.25c indicates that the largest value of the maximum compressive principal stress $\sigma_1/\sigma g|b|$ is reached on the sides of the ridge (0.33 at $x/|b| = \pm 0.94$). For the ridge, the contours of the minimum compressive stress $\sigma_2/\rho g|b|$ tend to follow the ridge shape (Fig. 2.25d). For the valley, Figs 2.25e–f indicate that there is a concentration of tensile stress $\sigma_2/\rho g|b|$ at the valley bottom (-0.51 at $x/|b| = 0$) and that the maximum stress $\sigma_1/\rho g|b|$ is compressive with contours that follow the valley shape. Figures 2.25g, h show the variation of the vertical stress $\sigma_{yy}/\rho g|b|$ and the horizontal stresses $\sigma_{xx}/\rho g|b|$ and $\sigma_{zz}/\rho g|b|$ with $y|b|$ along the ridge and valley centerline $(x/|b| = 0)$. The short dashed lines in those two figures represent the variation of the standard vertical and horizontal stresses for the case when $b = 0$; that is, when the ground surface is flat. The topographically induced stresses in the ridge and valley become, with increasing depth, asymptotic to the standard stresses. The stress regime is $\sigma_{xx} < \sigma_{zz} < \sigma_{yy}$.

Several major trends were observed by Pan, Amadei and Savage (1994) after conducting a parametric study with E/E' and G/G' varying between 1 and 3, $\nu = 0.25$ and ν' ranging between 0.15 and 0.35. The topographic ratio $a/|b|$ was taken equal to 0.5, 1 or 2, corresponding to ridges and valleys with slopes at their inflection points equal to ± 1.30 (52.4°), ± 0.65 (33.0°) and ± 0.32 (18°), respectively. The dip angle ψ varied between 0° (horizontal anisotropy) and 90° (vertical anisotropy).

(a) Effect of dip angle and degree of anisotropy

At a given depth, the horizontal stress $\sigma_{xx}/\rho g|b|$ decreases as the dip angle ψ increases. This stress is the greatest for ridges and valleys with horizontal anisotropy and the smallest

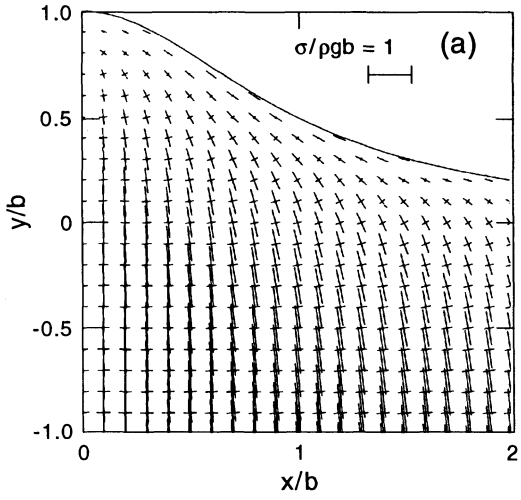
σ/ρgb = 1
(a)
y/b
x/b

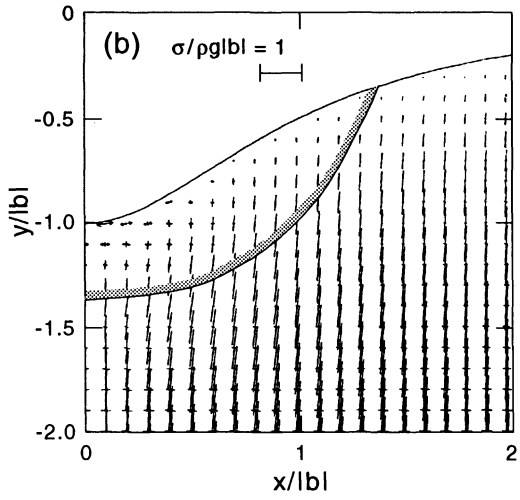
(b)
σ/ρg|b| = 1
y/|b|
x/|b|

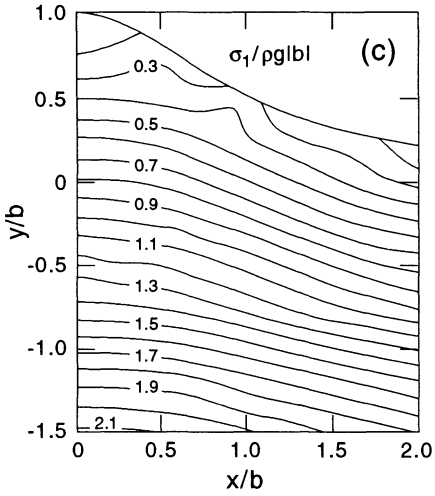
σ1/ρg|b|
(c)
0.3
0.5
0.7
0.9
1.1
1.3
1.5
1.7
1.9
2.1
y/b
x/b

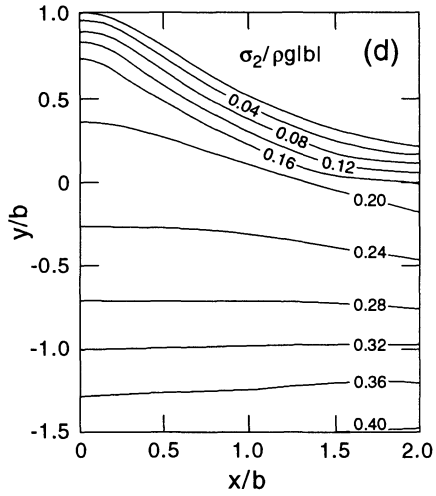
σ2/ρg|b|
(d)
0.04
0.08
0.12
0.16
0.20
0.24
0.28
0.32
0.36
0.40
y/b
x/b

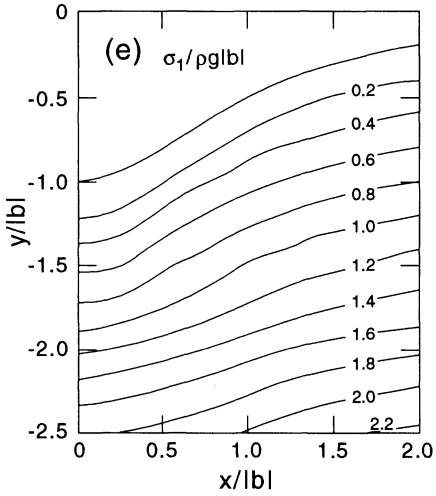
(e)
σ1/ρg|b|
0.2
0.4
0.6
0.8
1.0
1.2
1.4
1.6
1.8
2.0
2.2
y/|b|
x/|b|

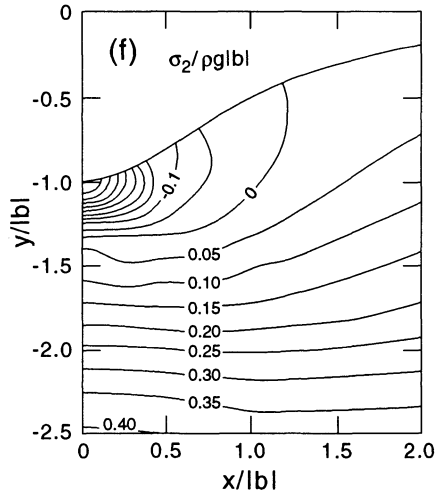
(f)
σ2/ρg|b|
-0.1
0
0.05
0.10
0.15
0.20
0.25
0.30
0.35
0.40
y/|b|
x/|b|

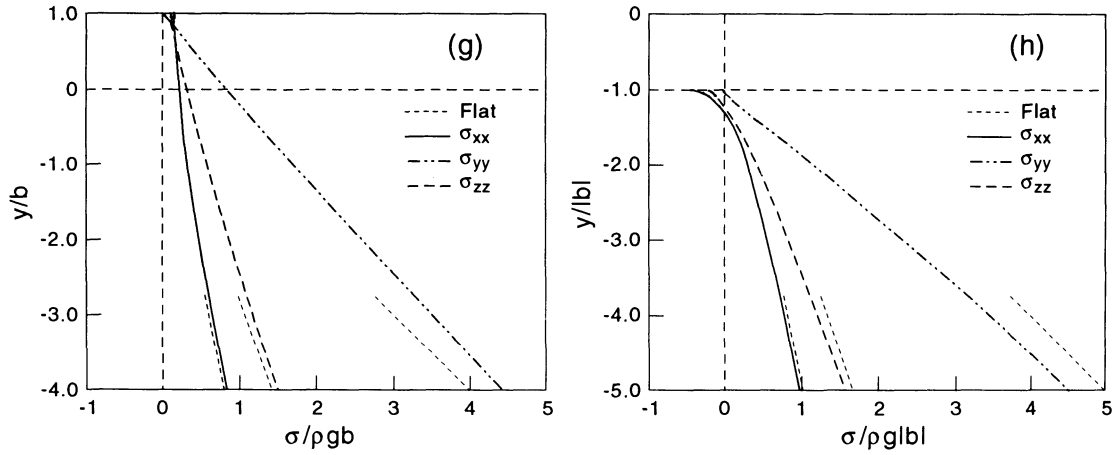

Fig. 2.25 Gravitational stress regime for a ridge and a valley with $a/|b| = 1$ in a strongly transversely isotropic rock mass ($E/E' = G/G' = 3$, $\nu = 0.25$, $\nu' = 0.15$ and $\psi = 90°$). Stress trajectories for the ridge in (a) and the valley in (b), $\sigma_1/\rho g|b|$ and $\sigma_2/\rho g|b|$ stress contours for the ridge in (c) and (d) and for the valley in (e) and (f), and variation of $\sigma_{xx}/\rho g|b|$, $\sigma_{zz}/\rho g|b|$ and $\sigma_{yy}/\rho g|b|$ with $y/|b|$ along the ridge and valley centerline ($x/|b| = 0$) in (g) and (h). The short dashed lines in (g) and (h) represent the variation of the standard stresses in the absence of topography for this case of anisotropy. The shaded region in (b) represents the extent of the tensile region at the valley bottom. (After Pan, Amadei and Savage, 1994.)

for ridges and valleys with vertical anisotropy. The principal stresses adjust to the horizontal and vertical directions more rapidly with depth for vertical planes of anisotropy ($\psi = 90°$) than when the planes of anisotropy are horizontal ($\psi = 0°$). For rocks with inclined planes of anisotropy, the principal stress trajectories and the tensile region are no longer symmetric with respect to the vertical axial planes of the ridge and valley. For a fixed value of E/E', the value of the ratio G/G' has no effect on the variation of $\sigma_{xx}/\rho g|b|$ with depth for rock masses with horizontal and vertical anisotropy. On the other hand, for inclined planes of anisotropy, the ratio G/G' has a strong effect where an increase in G/G' (as the rock mass becomes more deformable in shear in planes normal to the planes of transverse isotropy) results in an increase in $\sigma_{xx}/\rho g|b|$ and a decrease of the tensile region at the valley bottom. For a fixed value of G/G', E/E' affects the value of $\sigma_{xx}/\rho g|b|$ the most for horizontal anisotropy where $\sigma_{xx}/\rho g|b|$ increases with E/E' (or in other words as the rock mass becomes more deformable in the vertical direction). For vertical anisotropy the effect of E/E' on the magnitude of $\sigma_{xx}/\rho g|b|$ is small. For inclined planes of anisotropy, an increase in E/E' results in a decrease in $\sigma_{xx}/\rho g|b|$.

(b) Effect of ridge and valley geometry

The maximum value of $\sigma_1/\rho g|b|$ along the ground surface increases with $a/|b|$. The location where the stress maximum is reached on the sides of the ridge moves farther away from the ridge axis as $a/|b|$ increases or, in other words, as the ridge broadens. Also, the variation of $\sigma_1/\rho g|b|$ along the ground surface becomes gentler as $a/|b|$ increases. The lateral extent of the tensile region at the valley bottom increases with $a/|b|$ or, in other words, as the valley slope decreases.

(c) Depth of influence of topography

Broader ridges and valleys affect the stress field to a greater depth and to a wider area. For a given ridge geometry, the effect of the topography on the stresses at depth is the strongest

for ridges and valleys in rock masses with vertical planes of anisotropy.

(d) Tensile region at valley bottoms

The maximum tensile stress is at the valley bottom and the zone of tension is symmetric for isotropic rocks and for transversely isotropic rocks with vertical and horizontal planes of anisotropy. If the planes of anisotropy are inclined, the tension zone is no longer symmetric and extends on the side of the valley that is dipping in the same direction as the planes of anisotropy. The other side of the valley experiences a compressive state of stress. For a given valley geometry and a given value of the dip angle ψ, the extent of the tensile region depends on the value of the elastic properties. For a fixed value of G/G', the size of the tensile region decreases as E/E' increases. It also decreases as G/G' increases for a fixed value of E/E'. The size of the tensile region decreases significantly as ν' increases. For given values of the rock elastic properties and the dip angle of the planes of transverse isotropy, the extent of the tensile region decreases as the topography ratio $a/|b|$ decreases, that is, as the valley becomes narrower.

2.8.3 ASYMMETRIC RIDGES AND VALLEYS UNDER GRAVITY ONLY

As shown by Pan and Amadei (1993, 1994), asymmetric topographies can be obtained by superposition of the topography of several symmetric ridges and valleys. The topography is assumed to be smooth and to be expressed in parametric form as follows:

$$\begin{aligned} x(t) &= t \qquad (-\infty < t < +\infty) \\ y(t) &= \sum_{i=1}^{N} y_i(t) \end{aligned} \tag{2.21}$$

with

$$y_i(t) = \frac{a_i^2 b_i}{(t - x_i)^2 + a_i^2} \tag{2.22}$$

Equations (2.21) and (2.22) correspond to the geometric superposition of $i = 1, N$ symmetric ridges or valleys $x(t), y_i(t)$ centered at $x = x_i$. If b_i is positive, equation (2.22) corresponds to a ridge with height b_i. If b_i is negative, equation (2.22) corresponds to a valley with depth $|b_i|$. The parameter a_i controls the lateral extent of each ridge or valley with inflection points located at $x = x_i \pm a_i/(3)^{1/2}$, $y = 0.75b_i$ at which the slopes are equal to $\pm 3b_i(3)^{1/2}/(8a_i)$. Thus different complex and smooth topographies can be obtained by choosing different positive or negative values of a_i, b_i and x_i for $i = 1, N$. As an example, Figs 2.26a, b show asymmetric topographies obtained by superposition of $N = 2$ symmetric ridges or valleys, respectively.

For geometries such as those of Figs 2.26a, b, Pan and Amadei (1993) have shown that the ratios between the six stress components σ_{ij} $(i, j = x, y, z)$ and a characteristic stress $\rho g|d|$ (where $|d|$ is a characteristic elevation) depend on the dimensionless ratios of elastic constants such as E/E', G/G', ν and ν' for transversely isotropic rocks. The stress ratios $\sigma_{ij}/\rho g|d|$ also depend on (1) the orientation angles β and ψ of the planes of anisotropy with respect to the x-, y- and z-axes attached to the ridge or valley (Fig. 2.24), (2) the coordinates $(x/|d|, y/|d|)$ of the points at which the stresses are calculated, and (3) the ratios $a_i/|d|$, $b_i/|d|$ and $x_i/|d|$ for $i = 1N$ describing the geometry of the asymmetric ridge or valley.

As a numerical example, Fig. 2.27a shows the contours of maximum principal stress $\sigma_1/\rho g|d|$ (with $d = b_2$) for the ridge of Fig. 2.26a and for a rock mass with $E/E' = 1$, $G/G' = 3$, $\nu = 0.25$, $\nu' = 0.15$ and $\psi = 90°$. Figure 2.27b shows the variation of $\sigma_1/\rho g|d|$ along the ground surface for $E/E' = 1$, 2 and 3. We note from Fig. 2.27a that near the ground surface, the distribution of $\sigma_1/\rho g|d|$ is complicated with local maxima and minima. As shown in Fig. 2.27b, the location of those extrema is controlled by the surface topography and their magnitude decreases as E/E' increases.

2.8.4 RIDGES AND VALLEYS UNDER GRAVITY AND TECTONIC LOADING

The effect of horizontal tectonic loading on *in situ* stresses in rock masses with smooth and irregular topographies constructed by the superposition of multiple long and symmetric ridges and valleys was analyzed recently by Pan, Amadei and Savage (1995). It was found that addition of a horizontal uniaxial compression to gravity increases slightly the horizontal compression at the crests of ridges and diminishes the horizontal tension in valley bottoms.

Let σ_{xx}^{∞} be a uniform tectonic stress acting in the x direction of Fig. 2.22. For the geometry of Figs 2.26a, b, the ratios between the six stress components σ_{ij} ($i, j = x, y, z$) and a characteristic stress $\rho g|d|$ (where $|d|$ is a characteristic elevation) depend on the ratio $\sigma_{xx}^{\infty}/\rho g|d|$ in addition to the same parameters as under gravity alone.

As a numerical example, Figs 2.28a–f show stress contour diagrams below a complex (asymmetric) topography similar to that analyzed by Swolfs and Savage (1985). Here, $y(0)$ is the characteristic height equal to the elevation of the topography at $x = 0$. The rock is transversely isotropic with planes of transverse isotropy striking parallel to the z-axis of Fig. 2.24 ($\beta = 0°$) and dipping at an angle $\psi = 30°$ in the $+x$ direction. The rock mass elastic properties are such that $E/E' = 2$, $G/G' = 1$ and $\nu = \nu' = 0.25$.

The contour diagrams of $\sigma_{xx}/\rho g y(0)$, $\sigma_{yy}/\rho g y(0)$ and $\sigma_{xy}/\rho g(0)$ in Figs 2.28a–c were obtained assuming that the rock mass is under

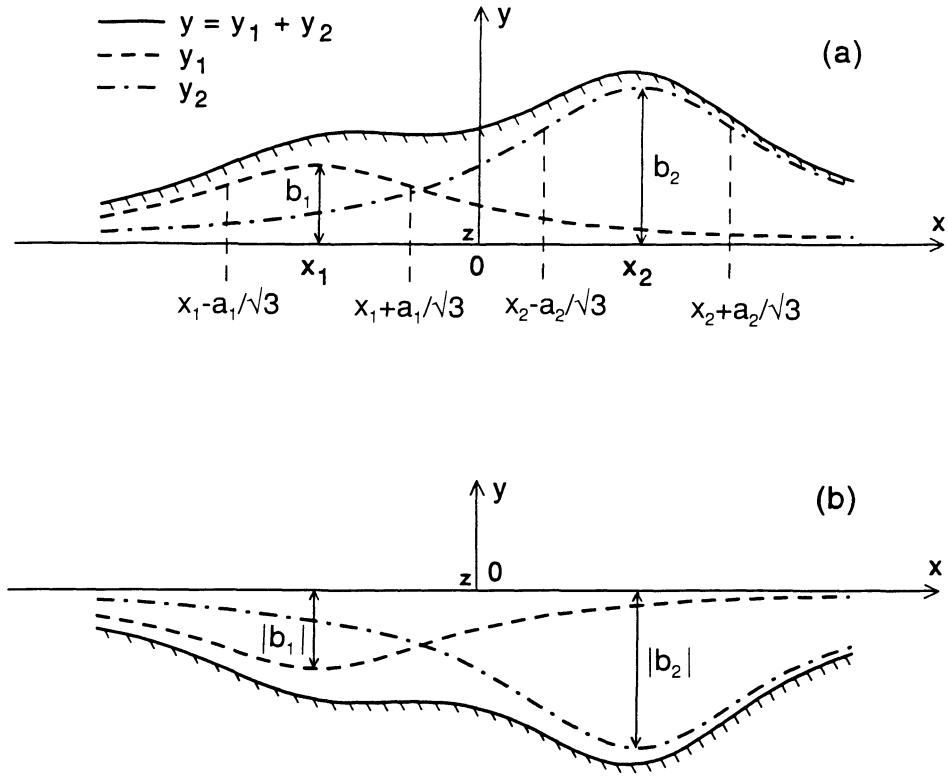

Fig. 2.26 Asymmetric topographies obtained by superposition of two separate symmetric ridges and valleys (a) $b_1/|d| = 0.5$ and $b_2/|d| = 1$, (b) $b_1/|d| = -0.5$ and $b_2/|d| = -1$. In (a) and (b) $a_1/|d| = 1$, $a_2/|d| = 1$, $x_1/|d| = -1$ and $x_2/|d| = 1$. (After Pan and Amadei, 1993.)

gravity alone. For comparison, Figs 2.28d–f show the corresponding stress contour diagrams when the rock mass is now subjected to combined gravitational loading and far-field horizontal tectonic loading $\sigma_{xx}^{\infty} = \rho g y(0)$. The contours of $\sigma_{yy}/\rho g y(0)$ nearly follow the ridge and valley shape (Figs 2.28b, e). Also, concentrations of compressive stress $\sigma_{xx}/\rho g y(0)$ and shear stress $\sigma_{xy}/\rho g y(0)$ can be seen in the valley at $x/y(0) = 1.6$ in Figs 2.28a, 2.28c, 2.28d and 2.28f. Comparing Figs 2.28a–c with Figs 2.28d–f shows that addition of a far-field horizontal tectonic stress $\rho g y(0)$ increases the magnitude of $\sigma_{xy}/\rho g y(0)$ near the ground surface and, to a greater extent, increases the magnitude of the horizontal stress $\sigma_{xx}/\rho g|b|$. For instance at $x/y(0) = 1.6$, the magnitude of the concentration of $\sigma_{xx}/\rho g y(0)$ is about 0.86 under gravity alone and is 2.5 if horizontal tectonic loading is added. Also, addition of the far-field horizontal tectonic stress has little effect on the magnitude of the vertical stress $\sigma_{yy}/\rho g y(0)$ (Fig. 2.28b, e).

2.8.5 TENSILE STRESSES IN VALLEY BOTTOMS

All the aforementioned analytical solutions predict tensile stresses in valley bottoms. There is field evidence to support that prediction. For instance, Knill (1968) found that there is usually a zone near the valley surface in which the rock mass is loose and discontinuous. Because of this, Knill (1968) suggested that underground excavation, tunneling or dam foundation should be carried out well below this zone. Another piece of evidence for valley bottom tensile stress is rebound near valley bottoms and valley walls, as noted by Matheson and Thomson (1973). This up-warping phenomenon may be considered as a result of tensile stresses (Matheson and

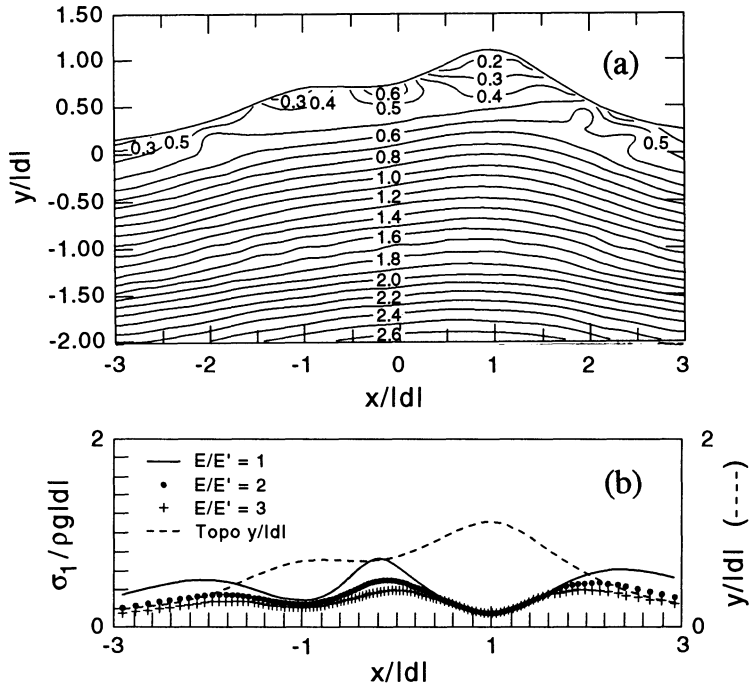

Fig. 2.27 (a) Contours of $\sigma_1/\rho g|d|$ for the ridge of Fig. 2.26a with $\psi = 90°$, $E/E' = 1$, $G/G' = 3$, $\nu = 0.25$ and $\nu' = 0.15$. (b) Variation of $\sigma_1/\rho g|d|$ along the ground surface. (After Pan and Amadei, 1993.)

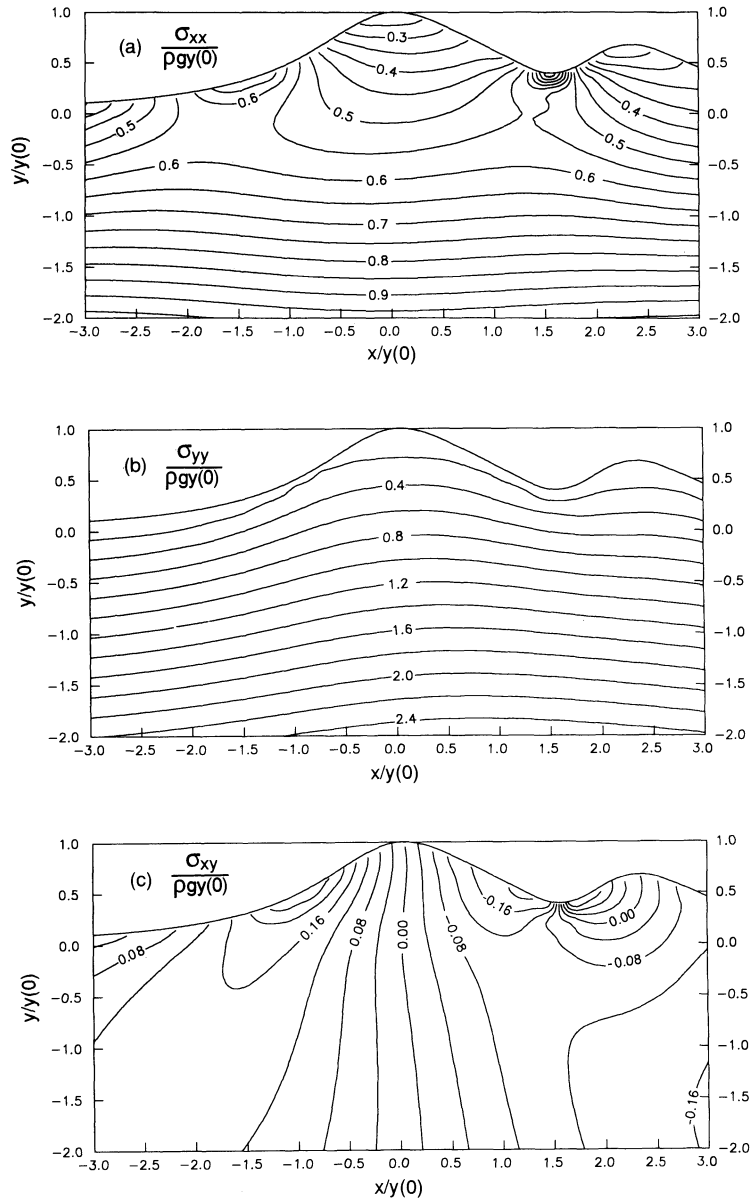

Fig. 2.28 Contour diagrams of $\sigma_{xx}/\rho gy(0)$, $\sigma_{yy}/\rho gy(0)$ and $\sigma_{xy}/\rho gy(0)$ in a transversely isotropic rock mass ($E/E' = 2$, $G/G' = 1$, $\nu = \nu' = 0.25$, $\beta = 0°$ and $\psi = 30°$) under gravity only in (a), (b) and (c), respectively, and under combined gravitational and tectonic loading with $\sigma^{\infty}_{xx} = \rho gy(0)$ in (d), (e) and (f), respectively. Topography obtained by superposition of $N = 4$ ridges and valleys with $a_i/y(0) = 1$ for $i = 1$–4, $b_1/y(0) = 0.8983$, $b_2/y(0) = 1.2657$, $b_3/y(0) = -2.1186$, $b_4/y(0) = 1.3438$, $x_1/y(0) = 0$, $x_2/y(0) = 1.35$, $x_3/y(0) = 1.6$, $x_4/y(0) = 2.1$. (After Pan, Amadei and Savage, 1995.)

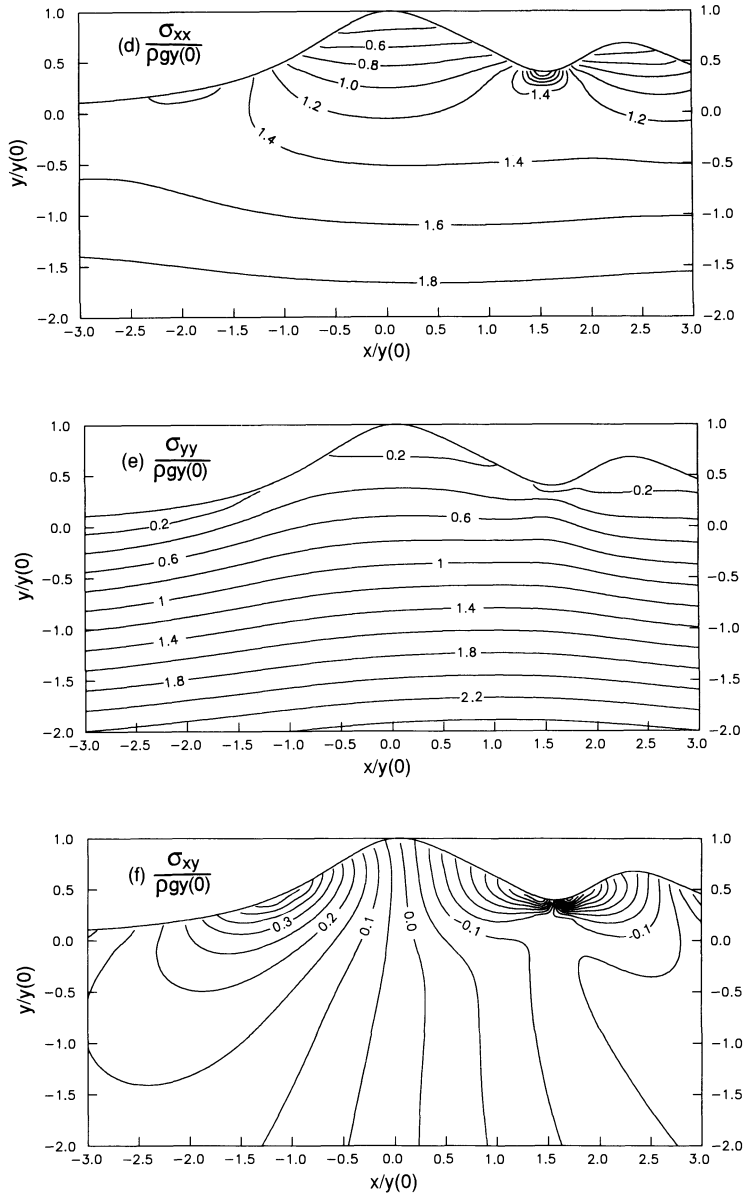

Fig. 2.28 *Continued*

Thomson, 1973; Silvestri and Tabib, 1983a, b). James (1991) also described the evidence of tensile stresses near valley bottoms, such as bed separation and bedding fractures at the toes of deep valleys and open (tension) joints deep into valley sides. By conducting a survey on the nature and frequency of coal mine roof failure beneath valleys, Molinda *et al.* (1992) found that 52% of the unstable roof cases in the surveyed mines occurred directly beneath the bottom-most part of the valleys. The survey also showed that broad, flat-bottomed

valleys were more likely to be sites of hazardous roof conditions than narrow-bottomed valleys.

2.9 TECTONIC AND RESIDUAL STRESSES

2.9.1 TECTONIC STRESSES

Current geological structures and their observations provide incontestable evidence of past and current tectonic activities. Several mechanisms related to plate tectonics have been proposed to model tectonic stresses (Solomon, Richardson and Bergman, 1980; Solomon, Sleep and Richardson 1975; Sykes and Sbar, 1973; Turcotte, 1973; Turcotte and Oxburgh, 1973; Voight, 1971; Voight and Hast, 1969). More recently, the World Stress Map Project was able to outline some global patterns of tectonic stresses in the lithosphere (Zoback, 1992; Zoback, 1993; Zoback *et al.*, 1989). Two groups of forces shown in Fig. 2.29 were identified as being responsible for tectonic stresses: (1) broad-scale tectonic forces acting on lithospheric plate boundaries such as shear tractions at the base of the lithosphere, slab pull at subduction zones, ridge push from oceanic ridges and trench suction; and (2) local tectonic stresses related to bending of the lithosphere due to surface loads, isostatic compensation and downbending of oceanic lithosphere. Tectonic stresses related to plate tectonics are typically very uniform over areas larger than 10 000 km^2 (Herget, 1993). Voight (1966a) also suggested classifying (in a broader sense) stresses due to erosion and overconsolidation as tectonic; the rationale being that such stresses can be responsible for the formation of deformational elements such as fractures.

In general, it is difficult to differentiate between active and remnant tectonic stresses by looking at geological structures alone. Although this distinction may not be of major concern to engineers, it is important to geologists and geophysicists. The current state of stress in an area may not always be related to the geological structures that we see today. It is likely that it has changed during past tectonic events such as folding and faulting. This emphasizes the importance of stress history which can be inferred, only in part, from kinematic analysis.

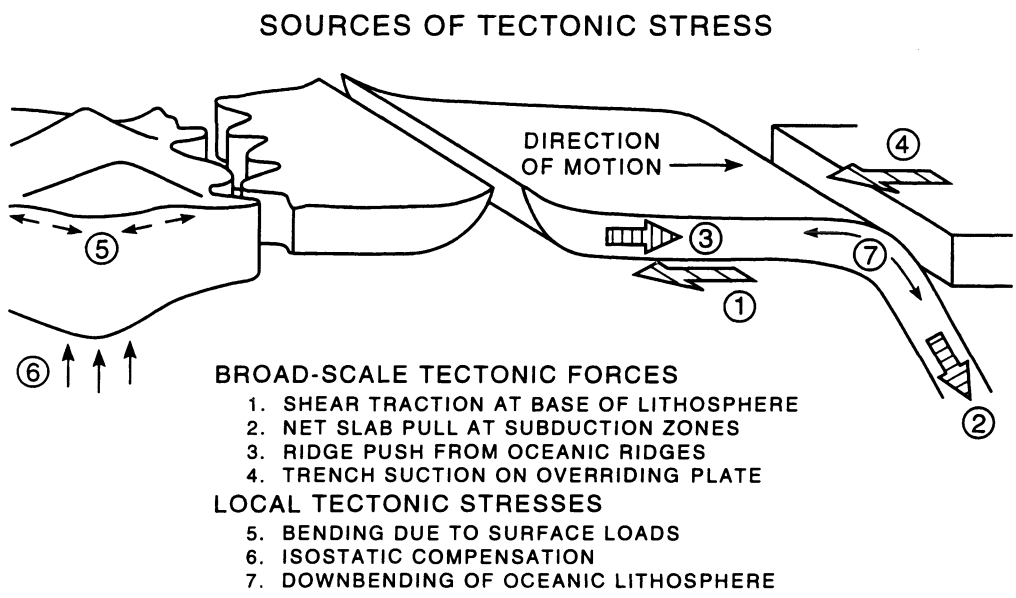

Fig. 2.29 Forces responsible for tectonic stresses. (After Zoback *et al.*, 1989.)

It is noteworthy that normal horizontal tectonic stresses do not have to be necessarily equal on opposite sides of a region. If this is the case, boundary shear stresses are needed in order to satisfy static equilibrium. This may create rotation of the principal stresses in the region of interest (Voight, 1966a).

2.9.2 RESIDUAL STRESSES

Residual stresses are 'self equilibrating stresses that remain in a structure if external forces and moments are removed' (Voight, 1966a). In rock mechanics they are also called internal or 'locked-in' stresses. Residual stresses appear to be related to a system of balanced (and not necessarily zero) tensile and compressive forces which are contained in domains ranging from the micro-scale (grains and crystals) to the macro-scale. The presence of residual stresses and strains leads to the existence of internal residual strain energy which can be critical for the stability of underground openings and surface excavations in rock. Residual stresses are believed to be responsible (in part) for phenomena such as rockbursts, rock surface spalling and sheet jointing (Varnes, 1970) and time-dependent movements of excavations such as those encountered in the Niagara Falls area (Lo *et al.*, 1975).

Although there is a large amount of evidence for residual stresses in metals (McClintock and Argon, 1966; Orowan, 1948), their existence and contribution to the virgin stress field in rock is still the subject of extensive discussion by geologists, geophysicists and engineers. The terms 'residual stresses' and 'residual strains' are often used interchangeably in the literature.

Hyett, Dyke and Hudson (1986) have suggested three fundamental requirements for generating residual stresses in rock: '(1) a change in the energy level, e.g., a stress or temperature change, (2) a heterogeneity caused by different constituent parts of the material, and (3) compatibility (at least partial) of these constituent parts'. Upon rock excavation, drilling or coring, some of the residual stresses contribute to instantaneous deformation and the rest to time-dependent deformation (Voight, 1966a; Nichols and Savage, 1976; Bielenstein and Barron, 1971). In order to separate the short-term deformations associated with residual stresses from the short-term deformations associated with active tectonic and gravitational stresses, overcoring or undercoring of overcored or undercored specimens or specimens cut from a rock mass can be carried out (Bielenstein and Barron, 1971; Friedman, 1972; Gentry, 1973; Lang, Thompson and Ng, 1986; Nichols, 1975; Nichols and Savage, 1976; Russell and Hoskins, 1973; Sbar *et al.*, 1979).

Residual stresses can remain in rock masses which have been subject in the past to higher stresses than they are subject to today or to different conditions. As those rock masses tend to relax under reduced load (due to erosion or uplift, for instance) or temperature changes (due to cooling), restraints are created by the interlocking fabric of the rock itself. The rock then reaches a new equilibrium with balanced internal (tensile and compressive) forces. For instance, Savage (1978) was able to show, using a thermoelastic bisphere model (spherical inclusion surrounded by an infinite host material), that residual stresses of the order of 23 MPa could be induced in granitic magmas during cooling from 300°C to 0°C. Haxby and Turcotte (1976) have shown that large residual thermal stresses could be induced in rocks by changes in the ambient temperature.

For metals, Orowan (1948) distinguishes two types of residual stresses: (1) stresses associated with inhomogeneous external conditions (mostly at the macroscopic scale), and (2) stresses associated with inhomogeneities within the material itself (mostly at the microscopic scale). Similar mechanisms producing residual stresses in rock were suggested by Russell and Hoskins (1973) and were classified as macro- and micro-mechanisms.

An example of the micro-thermoelastic mechanism is when a rock containing minerals with different coefficients of thermal expansion undergoes a uniform change in temperature resulting in non-uniform strains. Residual stresses can also be created at the microscopic level by elastic deformation when grains in a sedimentary rock, for instance, are cemented under load and then unloaded. This can be modeled as shown in Fig. 2.30a. Two springs (grains) with different elastic constants are subject to a same load, *P*, and deform by different amounts. Following deformation, the two springs are connected by a bar (cement) that can only move parallel to itself. As the load is removed and because of the bond that now exists between the two springs, the springs cannot regain their original position. Residual tension develops in one spring and compression is created in the other spring. Another example of micro-mechanism is when an undisturbed sample of saturated rock or soil is taken from the ground (Voight, 1966a). The external load vanishes and the intergranular stress becomes equal to the fluid pressure according to the effective stress principle. Figure 2.30b shows an example of a micro-elastoplastic mechanism where loading of a frictional element creates sliding. Upon unloading, residual tension and compression

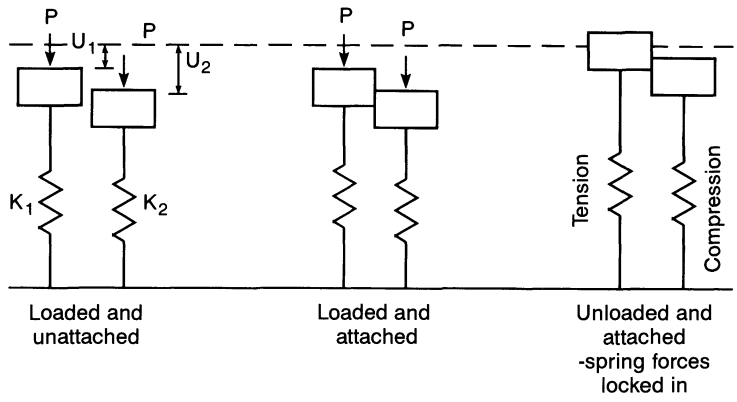

Fig. 2.30 Models of residual stresses. (a) Micro-elastic mechanism and (b) micro-elastoplastic mechanism. (After Russell and Hoskins, 1973.)

develop in the springs. If the frictional element is replaced by a viscous element, time-dependent residual strain recovery can be modeled. Numerical simulations of locked-in stresses created by non-recoverable slip along disconnected (non-continuous) discontinuities were proposed by Brady, Lemos and Cundall (1986) using a couple discrete element–boundary element program. A physical model explaining the concept of residual stresses in rock was proposed by Varnes (1970).

Figure 2.31 shows an example of the macro-mechanism that could take place in a sedimentary layer upon bending and folding. Residual tension and compression remain in the layer because yielding has taken place during the loading phase. Another example of macro-mechanism is when several sedimentary layers, some stiff and others soft, are cemented together under load. Upon unloading, residual compression and tension develops in the softer and stiffer layers, respectively, and large shear stresses are likely to develop at the layer interfaces (Holzhausen and Johnson, 1979). A similar phenomenon is found in 'pre-tension' reinforced concrete beams where the steel is in tension and the concrete in compression (Engelder, 1993).

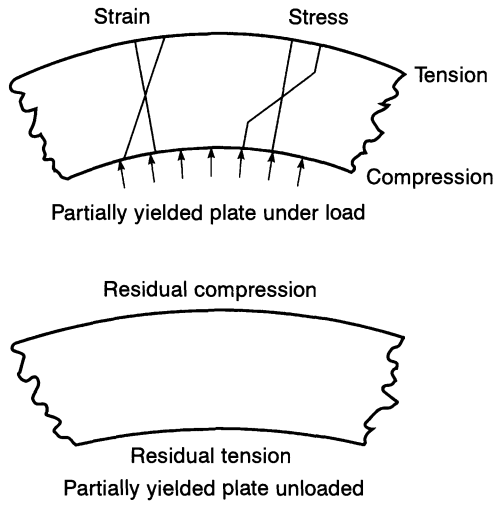

Fig. 2.31 Macro-mechanism of residual stresses. (After Russell and Hoskins, 1973.)

There seems to be a consensus in the literature that the importance of residual stresses in rock engineering is related to the size of the volume of rock in which the residual stresses are locked in (i.e. the volume of rock for which equilibrium is reached) versus the size of the problem of interest (Bielenstein and Barron, 1971; Holzhausen and Johnson, 1979; Hyett, Dyke and Hudson, 1986; Nichols and Savage, 1976; Russell and Hoskins, 1973; Tullis, 1977; Varnes and Lee, 1972). According to Hyett, Dyke and Hudson (1986), the amount of residual stress should increase as the volume of rock decreases from the macro- to the micro-scale. This trend can be attributed to the fact that as the volume increases, discontinuities are more likely to be found and those discontinuities are not able to transmit the residual stresses if they are in tension.

As discussed by Cuisiat and Haimson (1992), various authors have used different terms to define the volume of rock over which residual stresses are stored, such as equilibrium volume, self-equilibrium volume, locking domain, residual stress domain or strain energy storage volume. The volume dependency of residual strains was clearly emphasized by Swolfs, Handin and Pratt (1974) who measured residual strains on blocks of quartz diorite freed from their surroundings. The strains were found to range between 1400×10^{-6} (expansion) in small conventional overcores and -700×10^{-6} (contraction) on large blocks with volumes of up to 15 m^3.

How significant are residual stresses compared with other *in situ* stress components? The answer to that question varies. For instance, Lang, Thompson and Ng (1986) measured residual stresses of less than 1.0 MPa, and ranging between 1.5 and 2.5% of the total stresses, in the granitic rock at the URL in Pinawa, Canada. Sbar *et al.* (1979) found no significant residual stresses near the San Andreas fault. Lindner (1985) measured residual stresses of the order of ± 2 MPa in sedimentary rocks in the southeastern part of Lake Ontario. These stresses were found to be

relatively small compared to the high horizontal stresses (up to 12 MPa) measured at shallow depths in that area. Finally, Bock (1979) measured significant residual stresses up to 15.2 MPa in compression and 12.6 MPa in tension in a plane across a single basaltic column using the central hole drilling method. This study is interesting in that Bock was able to show concentric zoning of the residual stresses in the cross-section of the column, with compression in the inner and outer parts of the column and tension in the intermediate part. He also showed that the measured residual compressive and tensile stresses were approximately balanced.

2.10 EFFECT OF EROSION, OVERCONSOLIDATION, UPLIFT AND GLACIATION

Erosion or denudation was proposed by Voight (1966b) as a mechanism that could be responsible for high horizontal stresses at shallow crustal levels. As summarized by Goodman (1989), let K_0 be the initial horizontal to vertical stress ratio at a point located at a depth z_0 in a rock mass. The rock mass is subjected to unloading by removal of a layer of thickness Δz. Using the theory of elasticity, it can be shown that the new stress ratio at depth $z = z_0 - \Delta z$ is equal to

$$K = K_0 + \left[K_0 - \frac{v}{1-v}\right] \cdot \frac{\Delta z}{z_0 - \Delta z} \quad (2.23)$$

As an example, let $K_0 = 0.8$, $v = 0.25$ and $z_0 = 5000$ m. For values of Δz larger than 1500 m, K is larger than unity. For instance, for $\Delta z = 2000$ m, $K = 1.11$.

Voight and St Pierre (1974) included the combining mechanical and thermal effects associated with removal of rock by erosion. They concluded that for normal thermal gradients the thermal effect predominates, resulting in a reduction and not in an increase in the horizontal stress. Haxby and Turcotte (1976) showed that the state of stress induced by erosion comprises three components: a component due to the reduction in the overburden pressure, a component due to the associated uplift by isostatic readjustment and a thermal component due to a temperature decrease. They also found that the net effect is a reduction instead of an increase in the horizontal stresses which could result in dominantly tensional stresses.

Overconsolidation of sediments was also proposed by Voight (1966a) as another phenomenon capable of creating high horizontal stresses. For soils, it has been observed that the stress ratio K_0 depends on the past history of loading and unloading of the soils, and can be related to a so-called overconsolidation ratio, OCR, which is the ratio of past maximum horizontal stress to vertical stress (Kulhawy, Jackson and Mayne, 1989; Lambe and Whitman, 1969; Skempton, 1961). Both Steiner (1992) and Kim and Schmidt (1992) invoked overconsolidation to explain large K_0 values measured in sedimentary rocks in Germany and Texas, respectively. Voight (1966a) used the results of uniaxial strain tests conducted by Brooker (1964) on shale to demonstrate that large K_0 values can be induced upon unloading. The test results are shown in Fig. 2.32. If, in this figure, the radial and axial stresses are taken as the horizontal and vertical stress components respectively, the slope of the unloading curve indicates an increase in

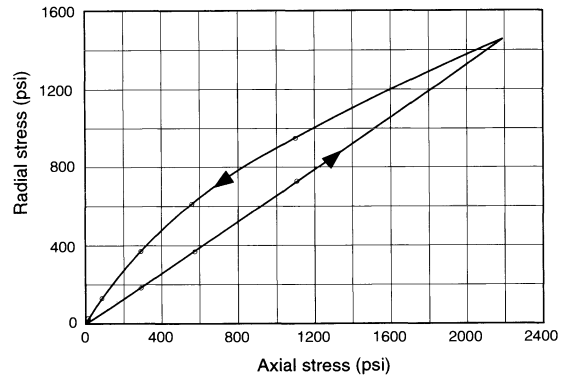

Fig. 2.32 Radial stress versus axial stress for Bearpaw shale tested under uniaxial strain condition by Brooker. (After Voight, 1966a.)

the stress ratio K_0 during unloading. Also, it shows that K_0 can be large near the surface and decreases with increasing depth.

Price (1966, 1974) presented another explanation for the development of high horizontal stresses in sedimentary basins using a complex geological history consisting of first accumulation of sediments, downwarp and burial followed by uplift and concomitant dewatering.

It has been suggested that high *in situ* stresses could be induced in rocks by a sequence of glacier loading, isostatic movements and postglacial uplift (Adams and Bell, 1991; Artyushkov, 1971; Asmis and Lee, 1980; Hast, 1958; Rosengren and Stephansson, 1990, 1993; Stephansson, 1988; Turcotte and Schubert, 1982). Here, bending stresses in the lithosphere stresses are created by subsidence under ice loads. Following the melting of the ice and gradual rebound, locked-in stresses remain because of incomplete isostatic recovery.

2.11 HIGH HORIZONTAL STRESSES

Unusually high horizontal stresses have been observed in certain regions of the world. High horizontal stresses were first measured by Hast in Fennoscandia in granite, leptite, limestone and quartzite in the period 1957–1966 (Hast, 1958, 1973, 1974). Hast found horizontal pressures as large as 1.5–3.5 times the overburden stress. Locally, values as great as eight times the vertical stress were obtained. Hooker and Duvall (1966) reported high horizontal stresses ranging between 3.5 and 21 MPa at depths of only a few meters in a rock outcrop near Atlanta, USA. More recent stress measurements in Fennoscandia have been reported by Stephansson, Ljunggren and Jing (1991), Stephansson (1993) and Myrvang (1993). High horizontal stresses were also found in northern Ontario, Canada, by Herget (1974, 1980, 1987), Australia (Enever, Walton and Windsor, 1990) and the Soviet Union (Bulin, 1971). Palmer and Lo (1976), Lo (1978) and Lee (1981) also reported high horizontal stresses ranging between 5 and 15 MPa at depths less than 25 m in sedimentary Paleozoic rocks in southern Ontario. The horizontal to vertical stress ratio was found to be large at shallow depths (0–100 m), sometimes reaching values as high as 10 : 100 (Franklin and Hungr, 1978). Similar trends were observed in upper New York State and the southeastern shore of Lake Ontario (Lindner, 1985). Figure 2.33 shows some of the high horizontal stresses measured around Lake Ontario.

High horizontal stresses can usually be inferred from field and core observations. In the field, high horizontal stresses can manifest themselves in different ways. For instance, thrust faulting might be dominant. Franklin and Hungr (1978) reported that in southern Ontario and in the northern part of New York State, natural evidence of high horizontal

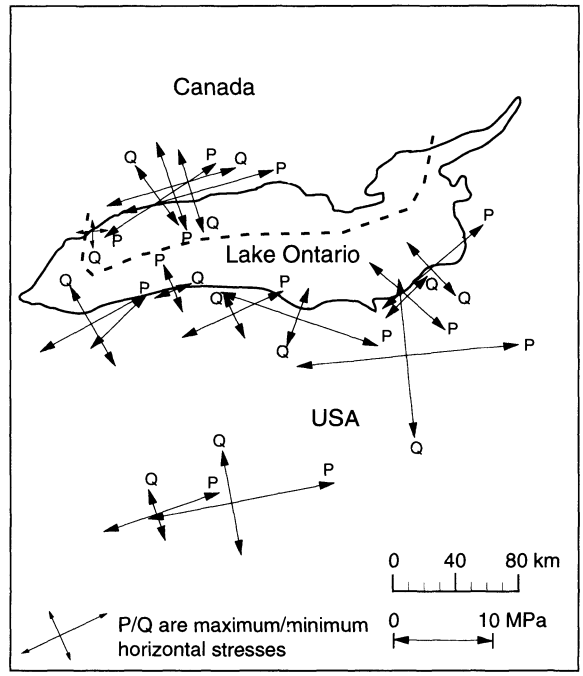

Fig. 2.33 Stress measurements around Lake Ontario showing high horizontal stresses. (Adapted from Lindner, 1985.)

stresses has been in the form of post- Pleistocene folds and faults in near-surface foundations and quarry floors; both phenomena having been documented as early as 1886. In addition, features such as heave of quarry floors, natural pop-ups, rock squeeze, rockbursts and cracking of tunnel concrete linings and/or movement of the walls of unsupported excavations (tunnels, shafts and canals) can be observed. Such phenomena were observed, for instance, in Ontario by Coates (1964) and in the Niagara Falls area by Lee and Lo (1976), Lo and Morton (1976) and Lo (1978). Rockbursts can also occur as reported by Carlsson and Olsson (1982) for some shallow tunnels at the Forsmark power plant in southern-central Sweden where horizontal stresses as large as 20 MPa were encountered for rock covers of only 5 to 15 m. Note that rockbursts depend on many parameters beside *in situ* stresses such as excavation geometry, rate of excavation and rock properties. They are not always indicative of high horizontal stresses (Herget, 1980). In Norway, evidence of high horizontal stresses can be seen on rock surfaces in the form of exfoliation, spalling and buckling (Myrvang, 1993) or, in the form of rockbursts in tunnels, in particular in mountainous areas (Myrvang, 1976).

High horizontal stresses are often accompanied by horizontal core disking, as noted by Hast (1958). The core breaks up into disks that are usually curved (saddle shaped) with a center of curvature being towards the collar of the hole. The size of the core disks can be a crude measure of the magnitude of horizontal stresses. For instance, Obert and Stephenson (1965) showed from laboratory triaxial tests on six different rock types that core disking occurs if the radial stress exceeds half the compressive strength of the rock. They also found a linear relationship between the axial and radial stresses required for disking. Obert and Stephenson (1965), Hast (1979) and more recently Haimson and Lee (1995) suggested that thinner disks are indicative of higher horizontal stresses. Recent work has shown that the morphology of the disks could be used as an indicator of the direction and approximate ratio of the horizontal stresses, and as a way to check whether the vertical stress is a principal stress (Dyke, 1989). Natau, Borm and Rockel (1989) and Haimson and Lee (1995) found that the trough axis of saddle-shaped core disks is essentially aligned with the direction of the maximum horizontal *in situ* stress. The problem of core disking can be enhanced in the case of layered, bedded or foliated rocks where the disks tend to follow the rock fabric.

The mechanism of disking has been a subject of discussion, in particular failure initiation (on the exterior or interior of the core) and the mode of failure (tension/extension versus shear). Experimental work by Jaeger and Cook (1963) showed that (1) the failure surfaces of rock disks are clean, indicating tension breakage instead of shear, (2) the thickness of the disks is inversely proportional to the stresses, (3) fracturing of the disks starts at the center of the core and not on the outside, and (4) the failure surfaces are convex toward the top of the core. Obert and Stephenson (1965) suggested that disking is initiated by, or is completely the result of, shear stresses. Hast (1979) also suggested that the disks are formed in shear and that failure starts on the exterior of the core. Stacey (1982) emphasized the discrepancy between the experimental observations of Jaeger and Cook (1963) and the assumption of shear failure. He postulated that disking is the result of extension fracturing that can be predicted using a criterion of extension–strain fracture. Numerical analysis carried out by Ingraffea (1984, personal communication) using fracture mechanics seems to indicate that an alternate hypothesis for disking is a combination of microcrack formation parallel to the horizontal stress and unloading of the core in the vertical direction. Based on recent experimental results in the laboratory, and analysis of disk surfaces with a scanning electron microscope, Haimson and

Lee (1995) concluded that core disking is the result of subhorizontal extensile cracks developing at the root of drill cores.

It should be emphasized first, that core disking is just an indicator of high horizontal stresses and that disking does not automatically imply high horizontal stresses. Disking depends on many parameters, such as the *in situ* state of stress, the strength properties of the rock and the stress parallel to the borehole (Stacey, 1982). Second, the information inferred from core disking is only qualitative (i.e. the potential for having high horizontal stresses). Third, core disking can also occur due to poor drilling when, for instance, too much thrust is applied to the drill bit and the rock (Kutter, 1993).

In general, core disking makes overcoring difficult and thus creates a depth threshold beyond which stresses cannot be measured. According to Hast (1979), 'it would appear that the highest stress that can at present be recorded in competent rock is of the order of 100 MPa; for rocks of greater strengths it is somewhat higher'. Herget (1980) reported successful stress determinations in the Canadian Shield at stresses up to 130 MPa and at a depth of 2100 m.

High horizontal stresses may also result in difficulties in drilling, excavation and shaft sinking and may create borehole stability problems such as borehole breakouts and borehole collapse. Breakouts can be used to estimate the orientation of *in situ* stresses, as discussed in Chapter 8.

2.12 SPHERICAL SHELL MODELS OF STRESSES IN THE EARTH

A more global approach for the analytical prediction of *in situ* stresses in rock has been suggested in the literature by modeling the Earth as a self-gravitating spherical shell consisting of one or several concentric slices or layers (McCutchen, 1982; Sheorey, 1994).

McCutchen (1982) considered an isotropic spherical shell (representing the Earth's crust) of outer radius R consisting of material with unit weight γ and subject to gravity g. The shell was assumed to be situated on an unyielding massive interior body. Using the equations of equilibrium, the stress–strain relations and the constitutive equations, the radial stress σ_r (also equal to the vertical stress), the tangential stress σ_θ (assumed the same in all tangential directions and equal to the horizontal stress), and the tangential strain u/r (where u is the outward radial displacement) were found to be equal to

$$\sigma_r = \frac{\gamma R}{4}\left[-4(1-\beta)x + (3-4\beta)\mathrm{A} - \frac{4\beta\mathrm{B}}{x^3}\right]$$

$$\sigma_\theta = \frac{\gamma R}{4}\left[-2(2-3\beta)x + (3-4\beta)\mathrm{A} + \frac{2\beta\mathrm{B}}{x^3}\right]$$

$$\frac{u}{r} = \frac{gR}{4P^2}\left[-x + \mathrm{A} + \frac{\mathrm{B}}{x^3}\right] \tag{2.23}$$

In equations (2.23) x is the ratio between the distance r from the center of the sphere and the sphere's outer radius R and is also equal to $1 - z/R$ where z is the depth below the surface. The constant β is equal to $0.5(1-2\nu)/(1-\nu)$ and to $(S/P)^2$ where S is the velocity of secondary seismic waves and P the velocity of primary seismic waves. Finally, A and B are two constants of integration that can be determined from the boundary condition $\sigma_r = 0$ at $x = 1$ and by assuming that at a distance r_0 (or a depth z_0), corresponding to the crust–mantle interface, the tangential strain is equal to zero. Substituting these two conditions into equations (2.23a) gives a horizontal to vertical stress ratio $K = \sigma_\theta/\sigma_r$ that varies in a nonlinear manner between $K_0 = 1\text{–}2\beta = \nu/(1-\nu)$ at $z = z_0$ and infinity at $z = 0$. McCutchen (1982) showed that, by using the upper and lower bounds for K proposed by Brown and Hoek (1978) and shown in Fig. 2.1b, the depth z_0 corresponding to the base of the crust would vary between 33.73 and 138.37 km, which is considerably greater than

the accepted value of about 15 km over young oceanic areas and 40–50 km over shield areas.

An interesting aspect of the model of McCutchen (1982) is that, despite its relative simplicity, the model leads to a predicted variation of K with depth which is consistent with the expressions reported in the literature. In particular, at shallow depths (less than 3 km), K is found to be proportional to $1/z$. Also, the model assumes that the tangential (horizontal) strain u/r does not vanish. Finally, the model shows that the horizontal stress depends on the depth z_0 of the base of the crust, producing larger stresses in a thicker crust. The main drawback of the model of McCutchen (1982) is that the elastic constant and density of the rock in the crust do not vary with depth and the model does not account for the effect of the geothermal gradient.

Sheorey (1994) extended McCutchen's model to account for the effect of the geothermal gradient, the variations of the coefficient of thermal expansion, the unit weight and the elastic properties with depth, and possible displacement within the mantle, on *in situ* stresses. Figure 2.34a shows the geometry of the Earth modeled by Sheorey (1994). It consists of a series of 12 annular slices, six in the mantle and six in the crust. The crust has an average thickness of 35 km and the radius of the Earth is equal to 6371 km. No displacement is allowed to occur at the mantle–core interface located at a depth of 2900 km. The state of stress in the mantle is assumed to be hydrostatic. Table 2.4 gives the values of the coefficient of thermal expansion α_i, the Young's modulus E_i, the radius R_i and the unit weight γ_i for each slice $i = 1, 12$. The temperature in the Earth is assumed to vary between 0°C at the ground surface and 3961°C at the base of the mantle, with three temperature gradients of 0.0008°C/m (for slices 1–5), 0.0003°C/m (for slice 6) and 0.024°C/m (for slices 7–12). The mantle is assumed to have a uniform Poisson's ratio ν_m equal to 0.27 and the crust has a uniform Poisson's ratio ν_c equal to 0.2.

Figure 2.34b shows the variation of the stress ratio $K = \sigma_\theta / \sigma_r$ with depth and Fig. 2.34c shows the variation of the horizontal stress σ_θ and the vertical stress σ_r with depth predicted by Sheorey's model. Figures 2.34b, c indicate that the model predicts large values of K at shallow depths and a value of 11 MPa for the horizontal stress at the ground surface, which is in agreement with maximum *in situ* stress values of about 10 MPa measured at the surface of the Earth (Swolfs, 1984).

A parametric study conducted by Sheorey (1994) revealed several important trends. First, the magnitude of the horizontal stress depends on the elastic modulus, with softer slices producing less horizontal stresses than harder slices. Variations in the modulus of the top slice of Fig. 2.34a showed that the stress ratio K in that slice is essentially proportional to the value of the modulus. This finding is in perfect agreement with the finding of large-magnitude horizontal stresses in old shield areas with hard competent rocks, as reported by Stephansson (1988) and Müller *et al.* (1992). Another trend found by Sheorey (1994) is that inclusion of the thermal gradient keeps the magnitude of horizontal stresses within reasonable limits. For instance, if the coefficient of thermal expansion is assumed to vanish, the model of Sheorey (1994) gives an unrealistic horizontal stress of 132.4 MPa at the ground surface. Inclusion of the coefficient of thermal expansion reduces that stress component to a more reasonable value of 11 MPa. Finally, the model of Sheorey (1994) seems to indicate that larger horizontal stresses could be expected in areas where the crust is thicker, e.g. in the continental crust.

The models of both McCutchen and Sheorey reveal that the curvature of the Earth could be responsible for large values of K and large values of the horizontal stress near the Earth's surface, particularly in old granitic shield areas. The model of Sheorey (1994) predicts that horizontal stresses vary between zero if the curvature of the Earth is ignored and 11 MPa if the curvature is taken into account.

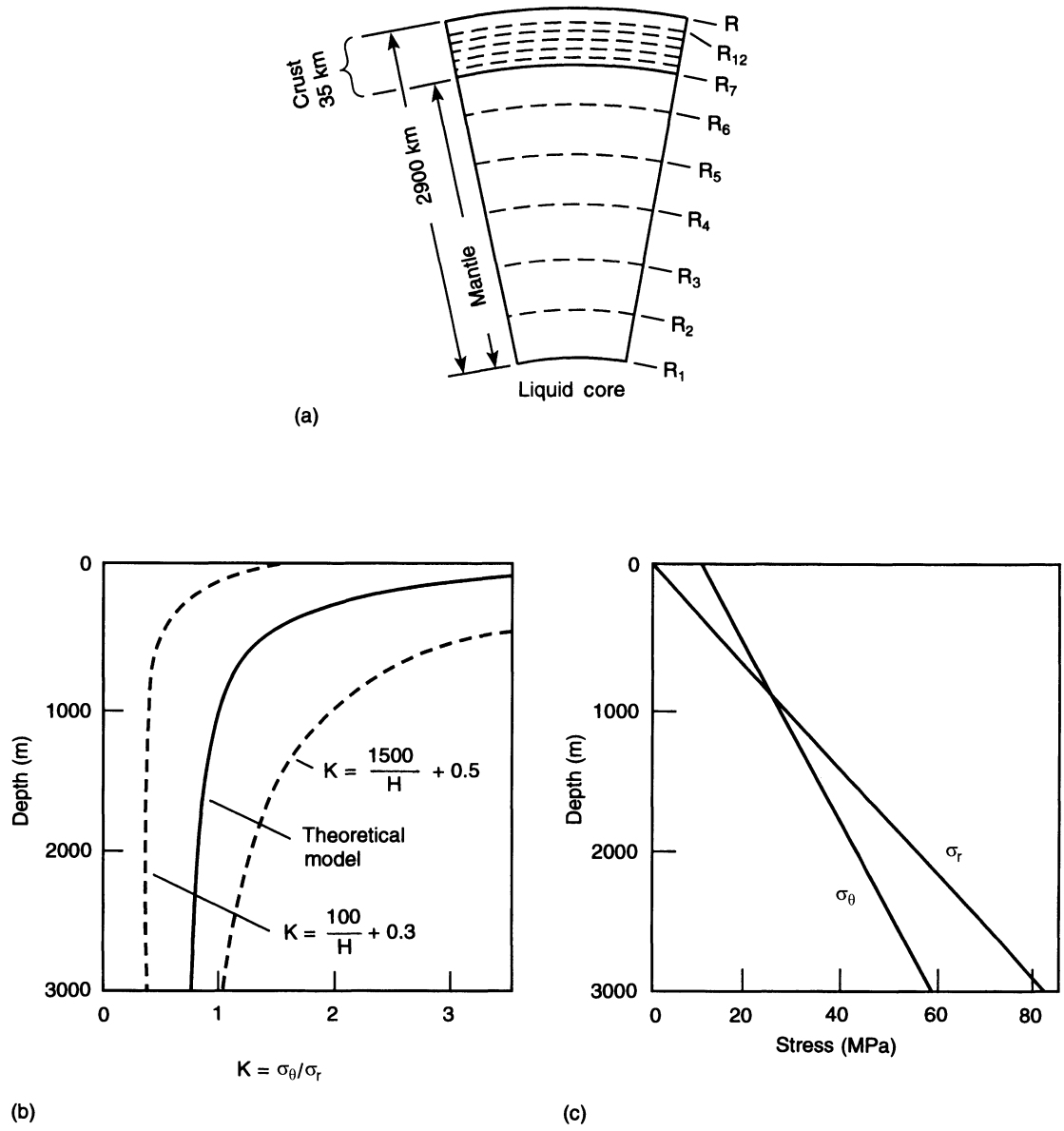

Fig. 2.34 Spherical shell model of Sheorey. (a) Geometry of the Earth consisting of 12 annular slices; (b) predicted variation of K with depth, H, and comparison with upper and lower bounds of Brown and Hoek (1978); (c) predicted variation of vertical stress σ_r and horizontal stress σ_θ with depth. (After Sheorey, 1994.)

In a recent contribution, Sugawara and Obara (1995) extended McCutchen's model to account for the geothermal gradient and the vertical displacement of the ground surface due to tectonic forces. By assuming a vertical displacement of 2.0 km and 13.0 km, constant thermal expansion, geothermal gradient and Poisson's ratio, and a stress-dependent Young's modulus, Sugawara and Obara (1995) were able to predict upper and lower limits for the variation of the

Table 2.4 Values of coefficient of thermal expansion α_i, the Young's modulus E_i, the radius R_i and the unit weight γ_i for each slice $i = 1$–12 in the spherical shell model of Sheorey (1994). Slices $i = 1$–6 correspond to the mantle and slices $i = 7$–12 correspond to the crust

Slice no.	*Radius* $R_i \times 10^6$ *(m)*	$\alpha_i \times 10^{-5}$ *(/C)*	E_i *(GPa)*	*Unit weight* γ_i *(MPa/m)*
1	3.470	2.4	760	0.052
2	3.870	1.9	700	0.048
3	4.370	1.6	610	0.045
4	4.870	1.35	520	0.043
5	5.370	1.25	360	0.040
6	5.958	1.2	200	0.037
7	6.335	0.77	20	0.027
8	6.340	0	30	0.027
9	6.436	2.2	40	0.027
10	6.352	1.5	45	0.027
11	6.358	0.9	50	0.027
12	6.364	0.6	50	0.027

stress ratio K with depth. They observed that most stress observations in Japan fell in between those limits, which led them to conclude that near-surface stresses in Japan are sensitive to the vertical displacement (upheaval) caused by the plate tectonics at the collision boundaries of merging plates.

The reader should be aware that more complex spherical and multilayered models of the Earth that include the crust, core and mantle rheology have been proposed in the geophysics literature. A review of these models can be found in a recent paper by Aydan (1995), who used the finite element method to predict *in situ* stresses for the following models of the Earth: (1) the crust and mantle are elastic solids and the core is in a liquid state, (2) the crust and mantle are elastoplastic solids and the core is in a liquid isothermic state, and (3) the crust and mantle are thermo-elastoplastic solids and the core is in a non-isothermic state. All these different models yield different *in situ* stress distributions and magnitudes.

2.13 EFFECT OF BOUNDARY CONDITIONS AND TIME ON *IN SITU* STRESS

Little is known about the precise nature of lateral restraints to be found at the geological scale. A large amount of discussion has been placed on the validity of the no lateral displacement assumption. Some authors have argued that since rocks are deformable, the hypothesis of no horizontal displacement is non-realistic (Cornet, 1993; McGarr, 1988).

It is well known that the stress field within a certain volume of rock will depend on the applied loads (body and surface forces), and the constitutive model of the rock, as well as the boundary conditions applied along the boundaries of the domain under consideration. In fact, by varying these parameters, various *in situ* stress regimes can be predicted (Denkhaus, 1966). This can be demonstrated using numerical methods for complex rock masses (e.g. Figs 2.16 and 2.21) or analytical solutions for simpler cases.

Consider, for instance, the simple case of a homogeneous isotropic rock mass with Young's modulus E and Poisson's ratio ν, and unit weight $\gamma = \rho g$, subject to gravity only. The rock mass has the geometry of Fig. 2.7 with the x- and y-axes being horizontal and the z-axis vertical downward. The vertical stress at depth z is equal to $\sigma_v = \rho g z$. If the rock mass is free to deform laterally with no lateral stress, the state of stress will be uniaxial in the vertical direction and the horizontal stresses will be zero. This condition could take place for instance in rock masses with vertical and open joints. Consider now another special case where the rock mass is under gravity and is also strained (due to tectonics) in the x and y directions by an amount ε_x and ε_y, respectively. As shown by Savage, Swolfs and Amadei (1992), and assuming Hooke's law, the horizontal stress components are equal to

$$\sigma_x = \frac{E}{(1-\nu^2)}(\varepsilon_x + \nu\varepsilon_y) + \frac{\nu}{(1-\nu)}\rho g z$$
$$\sigma_y = \frac{E}{(1-\nu^2)}(\varepsilon_y + \nu\varepsilon_x) + \frac{\nu}{(1-\nu)}\rho g z \qquad (2.24)$$

These expressions for the horizontal stress components include the combining effect of gravity and horizontal straining due to tectonics. They also predict non-zero horizontal stresses at the Earth's surface. Various three-dimensional stress regimes can be predicted depending on the vanishing or non-vanishing character of the lateral strains and their respective values. If the horizontal strains vanish, equations (2.24) reduce to the K_0 condition mentioned at the beginning of this chapter. As shown by Savage, Swolfs and Amadei (1992), equations (2.24) can be generalized to anisotropic rock masses. For horizontally layered rock masses modeled as transversely isotropic, equations (2.24) are replaced by

$$\sigma_x = \frac{E}{(1-\nu^2)}(\varepsilon_x + \nu\varepsilon_y) + \frac{E}{E'}\frac{\nu'}{(1-\nu)}\rho g z$$
$$\sigma_y = \frac{E}{(1-\nu^2)}(\varepsilon_y + \nu\varepsilon_x) + \frac{E}{E'}\frac{\nu'}{(1-\nu)}\rho g z \qquad (2.25)$$

It is noteworthy that the strains ε_x and ε_y entering into equations (2.24) and (2.25) must be small since the theory of elasticity is used in deriving these equations. According to Savage, Swolfs and Amadei (1992), equations (2.24) and (2.25) would apply for strains as large as 1 to 5% which could take place during tectonic processes of relatively short duration and with strain rates of the order of 1.0×10^{-15}/s (0.03 μ-strain/year) to 1.0×10^{-14}/s (0.32 μ-strain/year). Such strain rates have been reported by Savage (1983) and Savage, Proscott and Lisowski (1987) in geodetic measurements in various parts of the western United States.

Equations (2.24) and (2.25) and other elastic models presented in this chapter for the prediction of the effect of anisotropy, stratification and topography on *in situ* stresses imply that loads *in situ* are applied instantly and that the rock response to those loads is elastic. This cannot be the case for tectonic processes of relatively long durations. Failure may occur in brittle rocks either by creating new fault planes or by slip along existing fractures as discussed in section 2.4. Stress relaxation by creep may also occur in more ductile rocks (Rummel, 1986; Savage, Swolfs and Amadei, 1992).

Since rocks show some form of viscoelastic behavior (Goodman, 1989; Jaeger and Cook, 1976), stresses might be expected to relax over time in the more ductile parts of the crust when subject to a constant level of strain. This phenomenon was modeled by Savage, Swolfs and Amadei (1992), assuming that the crustal rock is isotropic and behaves elastically under hydrostatic loading, and as a Maxwell viscoelastic substance (a spring and a dashpot in series) under deviatoric loading. The short-term Young's modulus and Poisson's ratio of the rock are E_0 and ν_0 and the relaxation time is denoted as η. For a Maxwell substance, the time-dependent Young's modulus $E(t)$ and Poisson's ratio $\nu(t)$ are equal to

$$E(t) = E_0 \, e^{-(t/\eta)};$$
$$\nu(t) = 0.5(1 - e^{-(t/\eta)}) + \nu_0 \, e^{-(t/\eta)} \qquad (2.26)$$

Note that, in this model, the modulus approaches zero and the Poisson's ratio approaches 0.5 for large times. The crust is assumed to be strained uniformly in the horizontal x, y plane by an amount $\varepsilon_x = \varepsilon_y = \bar{\varepsilon}t$ where $\bar{\varepsilon}$ is a constant strain rate. Also, the initial strains in the x and y directions at time $t = 0$ are assumed to vanish. For these conditions, Savage, Swolfs and Amadei (1992) found that the vertical stress at depth z is equal to γz and that the horizontal stress depends on the time t and is equal to

$$\sigma_h = [2\eta E_0 \bar{\varepsilon} + \gamma z][1 - e^{-\tau}] + \frac{\nu_0}{1-\nu_0}\gamma z \, e^{-\tau} \qquad (2.27)$$

where $\tau = t/[2\eta(1-\nu_0)]$ is a dimensionless time. Equation (2.27) consists of a gravitational

part and a strain rate-dependent part. For $t \to 0$,

$$\sigma_h \to \frac{\nu_0}{1-\nu_0}\gamma z \tag{2.28}$$

which corresponds to a K_0 condition before initiation of lateral straining in the crust. On the other hand, for $t \to \infty$

$$\sigma_h \to \gamma z + 2\eta\bar{\varepsilon}E_0 \tag{2.29}$$

For large times, the gravitational part of the stress field becomes hydrostatic and the strain rate-dependent part becomes constant. Note that, in that case, a purely hydrostatic stress state (lithostatic stress field) would exist when the strain rate or the relaxation time is zero. A similar conclusion was reached by Jaeger and Cook (1976) in the modeling of a continuum which behaves elastically under hydrostatic loading and as a Maxwell viscoelastic substance in distortion, and is subject to a vertical stress at time $t = 0$ and no lateral displacement. Furthermore, this conclusion is in agreement with the hypotheses of Heim (1878) and Anderson (1951) that long-term rock creep could lead to a hydrostatic state of stress in the Earth's crust.

At the Earth's surface the variation of the horizontal stress with time is obtained by taking $z = 0$ in equation (2.27), which gives

$$\sigma_h = 2\eta E_0 \bar{\varepsilon}(1 - e^{-\tau}) \tag{2.30}$$

For large times, relaxation causes the horizontal stress to approach a constant value equal to $2\eta\bar{\varepsilon}E_0$. This is in contrast with the elastic model where stresses would continue to increase linearly with time if a constant strain rate was applied. Using a value of 10 MPa for $2\eta\bar{\varepsilon}E_0$ (Swolfs, 1984), $E_0 = 0.5$ GPa, a strain rate of 1.0×10^{-14}/s (0.32 μ-strain/year), the relaxation time η is found to be equal to 31 746 years. Assuming that $\nu_0 = 0.25$, equation (2.30) gives a horizontal stress of 0 at $t = 0$, a stress of 4.87 MPa at $t = 31\,746$ years, and a stress of 9.9 MPa at $t = 238\,095$ years. In comparison, the elastic model would give a horizontal stress of 50 MPa after 238 095 years.

As mentioned by Savage, Swolfs and Amadei (1992), the time-dependent model summarized above applies for strain accumulation in a homogeneous isothermal viscoelastic crust subjected to non-deviatoric strain rates. It does not apply when large temperature gradients exist, nor does it apply near major active faults where shear strain rates are dominant.

2.14 ESTIMATING STRESS ORIENTATION

Various methods have been proposed in the literature to estimate the orientation of *in situ* stresses. These methods can be divided into three major groups: (1) methods based on the orientation, distribution, deformation and fracturing of geological features ranging in size between rock crystals and mountain ranges, (2) methods that rely on the analysis of first motion of earthquakes, and (3) breakout methods. Other methods that use geomorphological features will not be discussed here and can be found, for instance, in the books of Scheidegger (1982) and Mattauer (1973).

2.14.1 STRESS ORIENTATION FROM GEOLOGICAL STRUCTURES

Geological structures such as faults, folds, joints, dikes, sills, volcanoes, fault striations or slickensides, etc. have been used by geologists and geophysicists as indicators of paleostresses, i.e. stresses previously active and no longer in existence (Anderson, 1951; Arthaud and Mattauer, 1969; Buchner, 1981; Engelder, 1993; Ode, 1957; Parker, 1973; Price, 1966, 1974; Price and Cosgrove, 1990; Scheidegger, 1982). Friedman (1964) presented various petrographic techniques that could be used to determine the direction of *in situ* stresses at the time of deformation. Some of these techniques range between analysis of orientation and distribution of fractures and folds at the macro-scale, and intercrystalline gliding,

rotation phenomena such as kink bands and recrystallization at the micro-scale.

Using petrographic techniques to estimate the orientation of the current state of stress should be approached with caution, since the stresses that created the geological structures may have been modified over time due to additional tectonic events, erosion, glaciation, etc. Hence the current rock fabric may or may not be correlated at all with the current *in situ* stress field (Terzaghi, 1962). Therefore, it is necessary to seek out the most recent geological structures (Parker, 1973). A study on the relationship between geological structures and hydrofracture direction by Towse and Heuze (1983), for tight gas reservoirs in the USA, concluded that geological structures are helpful but not always sufficient in predicting hydrofracture orientation and therefore the orientation of the horizontal principal stresses. When inferring both the orientation and magnitude of *in situ* stresses from geological structures, a model of rock behavior must be assumed (elasticity, plasticity, Coulomb friction, Mohr-type fracturing, etc.).

Examples of determination of paleostresses from fault orientation can be found in Friedman (1964), Gresseth (1964), Chappell (1973), Spicak (1988), Zoback *et al.* (1987) and Zoback (1993). The rationale is that the ordering and orientation of *in situ* stress components can be inferred by comparing a given fault with one of the three faulting modes shown in Fig. 2.4. The orientation of *in situ* stresses has also been estimated from joint sets in a given area. The principal stresses are assumed to be oriented in directions bisecting the angles between major joint sets (Mattauer, 1973; Scheidegger, 1982, 1995).

The orientation of sheet intrusions such as dikes and sills has also been used to determine principal stress directions (Eisbacher and Bielenstein, 1971; Muller and Pollard, 1977; Pollard, 1978). Parker (1973) suggested that veins or dikes are commonly emplaced parallel to the maximum compressive stress as they follow the path of least resistance. Ode (1957) and more recently Nakamura (1977) and Nakamura, Jacob and Davies (1977) suggested using the orientation of flank volcanoes formed by radial dikes originating from the central conduit of a main volcano, to determine the orientation of *in situ* stresses. The rationale is (1) that the propagation of dikes is comparable to a large hydraulic fracturing test with magma instead of water, and (2) that the dikes are more likely to propagate in a direction normal to the minimum *in situ* principal stress.

The use of slickensides (striae) on fault planes to determine not only the orientation but also the magnitude of the *in situ* stress field has received a lot of attention in the geology and geophysics literature over the past 15 years. The method (sometimes called fault-slip analysis) was first proposed by Carey and Brunier (1974) and extended by others such as Angelier (1979, 1984, 1989), Etchecopar, Vasseur and Daignieres (1981), Angelier *et al.* (1982), Michael (1984), Reches (1987) and Huang (1989). Both graphical and more recently numerical techniques have been used. The methodology consists, first, of recording the orientation and direction of motion of slickensides on a given population of non-parallel fault planes. Several basic assumptions are made in the analysis of the field measurements: (1) all the slickensides on the faults in the population are related to a given and uniform but unknown stress tensor, (2) motion on each fault plane is parallel to the acting shear stress on that plane, and (3) fault motions are independent and there is no fault interaction. These assumptions are important since they somewhat limit the range of application of the method. The third step in the method is to assume Coulomb friction. This slip condition is then expressed in terms of the six components of the *in situ* stress field in an arbitrary coordinate system using the expression for the normal and shear stress components on each plane (see for instance equations (A.18) and (A.19) in Appendix A). Finally, using a large number of faults (10 to

100), the *in situ* stress field that best fits the field measurements is determined by least squares. Figure 2.35 gives an example of *in situ* stress determination proposed by Reches (1987) and obtained by analysis of slickensides on 22 faults in Dixie Valley, Nevada.

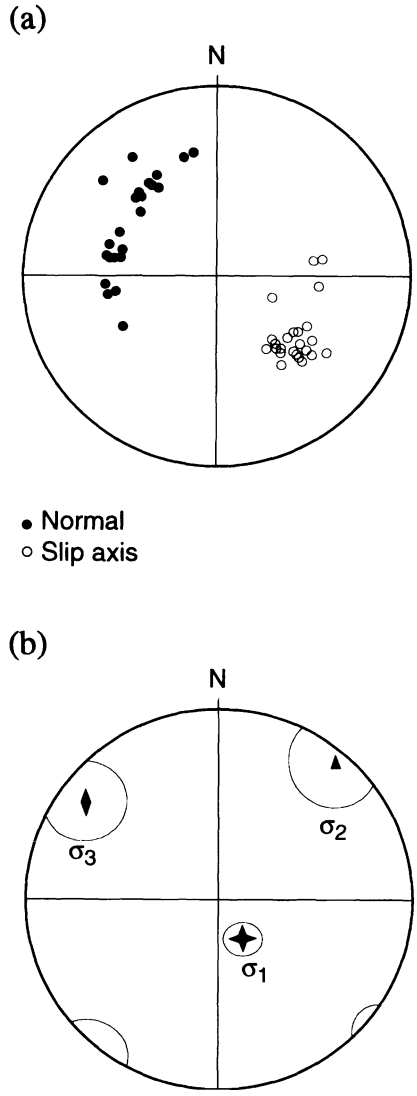

Fig. 2.35 Example of stress determination from fault slip data, Dixie Valley, Nevada. (a) Normal to 22 faults and direction of striations, (b) orientation of *in situ* principal stress components. The circles around the principal stresses indicate the standard deviations of orientations of the principal stresses. The stresses were determined assuming a coefficient of Coulomb friction equal to 0.8 (friction angle = 38.6°). (After Reches, 1987.)

The orientation of slickensides on fracture surfaces in oriented core samples can also be used to determine the *in situ* stress field. This method was suggested in a recent paper by Hayashi and Masuoka (1995). It is essentially an extension of the method of Angelier and co-workers (1982) to fractures on core samples instead of rock outcrops, and relies on the same assumptions. Hayashi and Masuoka (1995) applied that technique to determine the state of stress in two different geothermal fields in Japan. The results were found to compare well with anelastic strain recovery stress measurements.

Some recent geological structures can be used to infer the orientation of *in situ* stresses, in particular in regions where horizontal stresses are known to be high. For instance, Franklin and Hungr (1978) noted that in Ontario, post- Pleistocene folds and faults tend to align themselves in directions perpendicular to the NE–E trending maximum principal stress. They also observed that there were many exceptions to that trend.

Two very good examples showing how geological structures and *in situ* stress measurements can be combined to determine the *in situ* stress field in underground mines were reported by Allen, Chan and Beus (1978) and Bunnell and Ko (1986). Allen, Chan and Beus (1978) used a combination of CSIR Doorstopper measurements and detailed geological mapping of faults, folds and joint and fracture patterns to determine the *in situ* stress field at the Lucky Friday mine in the Coeur d'Alene mining district in Idaho. It was found that the current stress field measured with the Doorstopper paralleled the older stress field which was thought to be responsible for the existing geological structures.

Bunnell and Ko (1986) presented a clear description on how they estimated the *in situ* stress orientation from geological structures such as faults, dikes and photolineation for an

underground coal mine in central Utah. Data collected on the faults included fault strike and dip, fault slickenside orientation and slip direction. In general it was found that high stresses existed in the mine area in the recent geological past with a strong horizontal stress component in the E–W direction. A good correlation was found between that trend and the results of overcoring stress measurements.

2.14.2 STRESS ORIENTATION FROM FAULT-PLANE SOLUTIONS

By careful study of earthquake waves recorded by seismographs, it is possible to tell the direction of motion of the fault that caused an earthquake. The information that is needed is contained in the arrival records of the seismic body waves. Construction of the fault-plane solution is based on the principle that motion on a fault controls the pattern of seismic wave radiation, particularly the first motion of the compressional P-wave recorded at distant seismographs. Because earthquakes are essentially stress release phenomena, seismologists have suggested that the preferred orientation of earthquake faults over a large region could be used as a tool to determine the stress orientation in that region. By analyzing the earthquake fault-plane solutions in the region, a best-fit regional stress tensor can be determined by means of an inversion technique. Sometimes the term 'earthquake focal mechanism' is used instead of fault-plane solution.

Consider a P-wave record from an earthquake (Fig. 2.36a). If the first arrival is a compressive pulse, the stress release and the fault motion must be toward the seismograph. If, on the other hand, it is a dilational pulse, the fault motion must be away from the seismograph. The effect of an earthquake caused by displacement on a strike-slip fault is presented in Fig. 2.36b. The model for earthquake motion has two nodal planes separating the four quadrants. One nodal plane is the fault plane itself and the other is an auxiliary plane having no geological significance.

In general, a second (auxiliary) plane can be found, besides the fault plane, giving exactly the same P-wave radiation pattern, i.e. identical sets of recorded compressions and dilatations. In Fig. 2.36b, for example, the auxiliary plane is the hatched nodal plane assuming left-lateral displacement. The supplementary information needed to discriminate between the true fault plane and the auxiliary plane (which has no geological significance) can be mapped in the field or determined from the distribution of several earthquake foci on the same fault surface.

The most convenient fault-plane solution uses the stereographic projection of the seismic ray path as they emerge from the hypocenter of an earthquake. This method assumes that the earthquake hypocenter is located at the center of the stereographic projection representing the focal sphere. Following the methodology presented by Engelder (1993), a fault-plane solution is constructed from a stereographic projection which shows where the ray paths to distant seismic stations cut the focal sphere. The so-called extended position of a seismic station is determined from data about the azimuth of the earthquake, the travel time for the wave and the so-called angle of emergence. The extended positions for a number of stations recording the same earthquake are plotted in either lower or upper hemisphere projection. Compressional first arrivals of P-waves are plotted as solid circles and dilational first arrivals are plotted as open circles (Fig. 2.37). The two nodal planes that distinguish compressional from extensional regimes are drawn and geological data or distribution of aftershocks are used to identify the actual fault plane. When the main shock is small, so-called 'composite fault-plane solutions' are constructed by superimposing data from aftershocks associated with microearthquakes. Alternative techniques for fault-plane solutions consist of using surface waves and the amplitude of free oscillations (Engelder, 1993).

Fault-plane solutions are a representation of

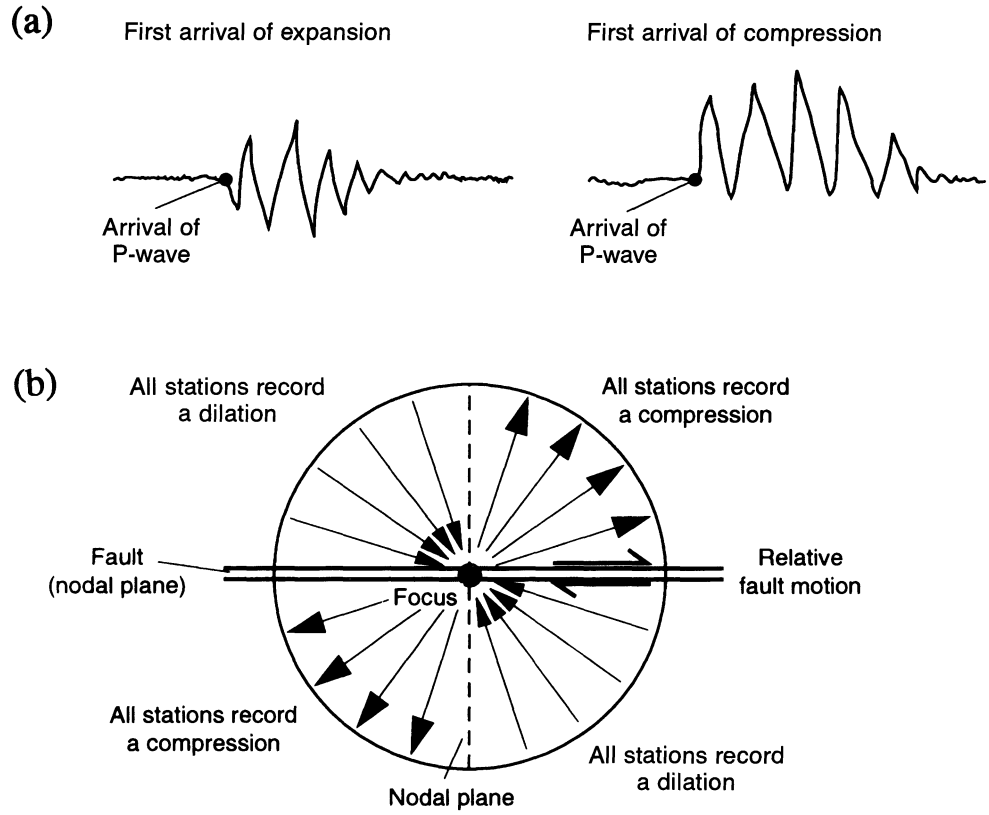

Fig. 2.36 Fault-plane solution of a strike-slip fault. (a) Motion of a P-wave detected by a seismograph, (b) plot of the first motion detected at a number of seismograph stations (arrows) and determination of right-lateral displacement of the fault.

slip on a fault and the pressure (P) and tension (T) axes represent the axes of maximum shortening and maximum extension. The P-axis is located in the middle of the quadrants with dilations and the T-axis is in the middle of the quadrants with compressions. The so-called B-axis is located at the intersection of the fault plane and the auxiliary plane.

An early assumption made by seismologists was that earthquakes were due to the failure of intact rock, which justified using the P-axis as the direction of σ_1, T as σ_3 and B as σ_2 (Engelder, 1993). However, laboratory and field data have shown that stress drops accompanying fracture of intact rock can be more than ten times higher than those associated with earthquakes. McKenzie (1969) noted that the proposed model of using P-, T- and B-axes as the directions of principal stresses did not apply to earthquakes associated with slip along pre-existing faults. Hence, according to McKenzie (1969), the fault-plane solution method could not be used to infer precisely stress orientations in the crust. In fact, McKenzie (1969) showed that the only restriction for mapping stress orientation based on fault-plane solutions is that σ_1 must lie in a quadrant associated with dilations, whereas σ_3 must lie in a quadrant related to compression. In order to activate slip along a fault, the shear stress along the fault must exceed a critical stress. In an area of pre-existing faults, the fault planes oriented such that they have the highest resolved shear stress will slip.

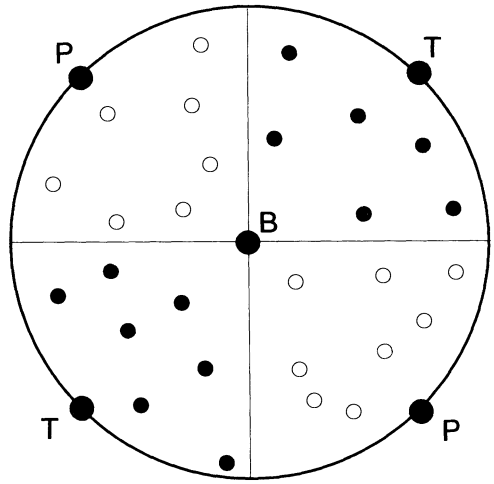

Fig. 2.37 Stereographic projection of fault-plane solutions presented in Fig. 2.36. Compressional first arrivals of P-waves are plotted as solid circles and dilational first arrivals as open circles. The *P*-, *T*- and *B*-axes are shown.

Nevertheless, despite those limitations, fault-plane solutions are important components in our understanding of regional stress fields (Engelder, 1993).

From the field of structural geology and tectonics, and in particular the constraint that fault slip occurs in the direction of the maximum resolved shear stress, Gephart and Forsyth (1984) proposed an averaging technique which was more quantitative for the determination of stress orientation from fault-plane solutions. An inversion method similar to that proposed by Angelier (1979) for the analysis of fault-plane striations (section 2.14.1) was applied to search for all possible stress tensors which could satisfy the fault-plane solution over a region. The method allows for an error analysis and the establishment of confidence limits for the preferred regional stresses. It also uses an objective means for identifying which of the two possible nodal planes corresponds to the plane that has slipped (Engelder, 1993).

Largely as a result of seismic waveform modeling made possible by digital seismic acquisition networks placed all over the world, more and better-constrained fault-plane solutions or focal mechanisms are now available. The data form the major input (54%) to the establishment of the World Stress Map (Zoback, 1992; Zoback *et al.*, 1989) most of them in the depth range 5–20 km. Because of the uncertainty in inferring stress directions from fault-plane solutions, no single-event focal mechanism receives the highest ranking in the World Stress Map Project, regardless of the magnitude of the event and whether it is well constrained or not. The highest ranking is reserved for stress directions determined from mean *P*- and *T*-axis orientations or formal inversions for best-fitting stress axes of groups of moderate-size earthquakes occurring within close geographical proximity, and with a variety of focal mechanisms (Chapter 11).

2.14.3 BREAKOUTS

The rock around circular excavations such as boreholes, tunnels or shafts may not be able to sustain the compressive stress concentration associated with the process of excavation itself. Breakage of the rock results in two diametrically opposed zones of enlargement called 'breakouts'. There is experimental evidence that breakouts occur along the direction of the least *in situ* stress component. They can therefore be an indicator of *in situ* stress orientation. Several attempts have been made in the literature to use the depth and width of borehole breakouts in order to determine the magnitude of *in situ* stresses (see review by Haimson and Lee, 1995).

Borehole breakouts for the purpose of stress determination were first reported by Leeman (1964). They have been used extensively to determine the orientation of horizontal *in situ* stresses in the World Stress Map Project (Zoback, 1992; Zoback *et al.*, 1989), and other more specific projects such as the KTB hole in northeastern Bavaria, Germany (Baumgärtner *et al.*, 1993; Te Kamp, Rummel and Zoback, 1995), the Cajon Pass hole in the vicinity of the

San Andreas fault in southern California (Shamir and Zoback, 1992; Vernik and Zoback, 1992), the borehole for deep-Earth gas in the Precambrian rocks of Sweden (Stephansson, Savilahti and Bjarnason, 1989), and the Ocean Drilling Program (Kramer *et al.*, 1994; Moos and Zoback, 1990). Borehole breakouts give information about the stress field at depths ranging between 1 and 4 km (and in some cases as deep as 5–7 km), and provide a valuable link between overcoring and hydraulic fracturing data and focal mechanism data (Zoback *et al.*, 1989).

Breakouts in galleries, tunnels and shafts have also been reported in the literature (Hoek and Brown, 1980a; Ortlepp and Gay, 1984). In some cases they have been used to determine the orientation of *in situ* stresses such as at the URL site in Canada (Martin, Martino and Dzik, 1994) and elsewhere (Maury, 1987). The breakout method is discussed further in Chapter 8.

2.15 SUMMARY

This chapter shows that many phenomena can contribute to the build-up of *in situ* stresses in rock. In particular, rock mass structure associated with discontinuities, anisotropy and heterogeneities may result in complex stress regimes, and scatter and perturbation in the stress field at all scales. As pointed out by Hudson and Cooling (1988), study of the scatter should assist in understanding better possible variations in the *in situ* stress field rather than being regarded as a nuisance. Further, for a given rock mass, different boundary conditions may result in different stress regimes. Likewise, for given boundary conditions, different stress regimes can be predicted for different rock mass constitutive behavior. Finally, topography can create rotation of the *in situ* stress field that is far from being negligible.

In general, the process of estimating *in situ* stresses in rocks requires a large amount of judgement and is very much site specific. The relative importance of various phenomena when estimating the *in situ* stress field at a given site can be assessed by carrying out parametric studies using analytical or numerical models. Predictions can also be improved by combining the results of previous or current *in situ* stress measurements.

This chapter also emphasizes that many phenomena other than tectonics could result in high horizontal stresses, in particular near the ground surface. This is not to say that tectonic stresses do not exist but simply that their contribution to the measured stress fields may not be as large as previously thought.

In general, this chapter shows how critical it is to have a clear picture of the geology of a site before estimating *in situ* stresses and before embarking on any stress measurement program. A clear description of the rock mass will help in developing an optimal stress sampling strategy and in the interpretation of field measurements (Hudson and Cooling, 1988). It will also help in selecting the techniques that best fit the geological environment of interest.

REFERENCES

Adams, J. and Bell, J.S. (1991) Crustal stresses in Canada, in *The Geology of North America*, Decade Map Vol. 1, *Neotectonics of North America*, Geological Society of America, Boulder, Colorado, pp. 367–86.

Ahola, M.P. (1990) Geomechanical evaluation of escarpments subjected to mining induced subsidence, in *Proc. 31st US Symp. Rock. Mech.*, Golden, Balkema, Rotterdam, pp. 129–36.

Akhpatelov, D.M. and Ter-Martirosyan, Z.G. (1971) The stressed state of ponderable semi-infinite domains. *Armenian Acad. Sci. Mech. Bull.*, **24**, 33–40.

Aleksandrowski, P., Inderhaug, O.H. and Knapstad, B. (1992) Tectonic structures and wellbore breakout orientation, in *Proc. 33rd US Symp. Rock Mech.*, Santa Fe, Balkema, Rotterdam, pp. 29–37.

Allen, M.D., Chan, S.S.M. and Beus, M.J. (1978) Correlation of in-situ stress measurement and geologic mapping in the Lucky Friday Mine, Mullan, Idaho, in *Proc. 16th Annual Symp. of Eng.*

Geol. and Soils Eng., Idaho Transportation Dept. of Highways, pp. 1–22.

Amadei, B. (1983) *Rock Anisotropy and the Theory of Stress Measurements*, Lecture Notes in Engineering, Springer-Verlag.

Amadei, B. and Pan, E. (1992) Gravitational stresses in anisotropic rock masses with inclined strata. *Int. J. Rock Mech. Min. Sci. & Geomech. Abstr.*, **29**, 225–36.

Amadei, B. and Savage, W.Z. (1985) Gravitational stresses in regularly jointed rock masses. A keynote lecture, in *Proc. Int. Symp. on Fundamentals of Rock Joints*, Bjorkliden, Centek Publ., Luleå, 463–73.

Amadei, B. and Savage, W.Z. (1989) Anisotropic nature of jointed rock mass strength. *ASCE J. Eng. Mech.*, **115**, 525–42.

Amadei, B. and Savage, W.Z. (1993) Effect of joints on rock mass strength and deformability, in *Comprehensive Rock Engineering* (ed. J.A. Hudson), Pergamon Press, Oxford, Chapter 14, Vol. 3, pp. 331–65.

Amadei, B., Savage, W.Z. and Swolfs, H.S. (1987) Gravitational stresses in anisotropic rock masses. *Int. J. Rock Mech. Min. Sci. & Geomech. Abstr.*, **24**, 5–14.

Amadei, B., Savage, W.Z. and Swolfs, H.S. (1988) Gravity-induced stresses in stratified rock masses. *Rock Mech. Rock Eng.*, **21**, 1–20.

Anderson, E.M. (1951) *The Dynamics of Faulting and Dyke Formation with Applications to Britain*, Oliver and Boyd, Edinburgh.

Angelier, J. (1979) Determination of the mean principal directions of stresses for a given fault population. *Tectonophysics*, **56**, T17–26.

Angelier, J. (1984) Tectonic analysis of fault slip data sets. *J. Geophys. Res.*, **89**, 5835–48.

Angelier, J. (1989) From orientation to magnitudes in paleostress determinations using fault slip data. *J. Struct. Geol.*, **11**, 37–50.

Angelier, J., *et al.* (1982) Inversion of field data in fault tectonics to obtain the regional stress – I. Single phase fault populations: a new method of computing the stress tensor. *Geophys. J. Roy. Astron. Soc.*, **69**, 607–21.

Arjang, B. (1989) Pre-mining stresses at some hard rock mines in the Canadian shield, in *Proc. 30th US Symp. Rock Mech.*, Morgantown, Balkema, Rotterdam, pp. 545–51.

Arthaud, F. and Mattauer, M. (1969) Exemples de stylolites d'origine tectonique dans le Languedoc. *Bull. Soc. Geol. France*, **11**, 738–44.

Artyushkov, E.V. (1971) Rheological properties of the crust and upper mantle according to data on isostatic movements. *J. Geophys. Res.*, **76**, 1376–90.

Asmis, H.W. and Lee, C.F. (1980) Mechanistic modes of stress accumulation and relief in Ontario rocks, in *Proc. 13th Can. Symp. Rock Mech.*, Toronto, Canadian Institute of Mining and Metallurgy, CIM Special Vol. 22, pp. 51–5.

Aydan, Ö. (1995) The stress state of the Earth and the Earth's crust due to the gavitational pull, in *Proc. 35th US Symp. Rock Mech.*, Lake Tahoe, Balkema, Rotterdam, pp. 237–43.

Aytmatov, I.T. (1986) On virgin stress state of a rock mass in mobile folded areas, in *Proc. Int. Symp. on Rock Stress and Rock Stress Measurements*, Stockholm, Centek Publ., Luleå, pp. 55–9.

Babcock, C.O. (1974a) A new method of analysis to obtain exact solutions for stresses and strains in circular inclusions. US Bureau of Mines Report of Investigation RI 7967.

Babcock, C.O. (1974b) A geometric method for the prediction of stresses in inclusions, orebodies, and mining systems. US Bureau of Mines Report of Investigation RI 7838.

Bandis, S.C., Lumsden, A.C. and Barton, N. (1983) Fundamentals of rock joint deformation. *Int. J. Rock Mech. Min. Sci. & Geomech. Abstr.*, **20**, 249–68.

Barton, N. (1976) The shear strength of rock and rock joints. *Int. J. Rock Mech. Min. Sci. & Geomech. Abstr.*, **13**, 255–79.

Batchelor, A.S. and Pine, R.J. (1986) The results of in-situ stress determinations by seven methods to depths of 2500 m in the Carnmenellis granite, in *Proc. Int. Symp. on Rock Stress and Rock Stress Measurements*, Stockholm, Centek Publ., Luleå, pp. 467–78.

Bauer, S.J., Holland, J.F. and Parrish, D.K. (1985) Implications about in-situ stress at Yucca Mountain, in *Proc. 26th US Symp. Rock Mech.*, Rapid City, Balkema, Rotterdam, pp. 1113–20.

Baumgärtner, J. *et al.* (1993) Deep hydraulic fracturing stress measurements in the KTB (Germany) and Cajon Pass (USA) scientific drilling projects – a summary, in *Proc. 7th Cong. Int. Soc. Rock Mech. (ISRM)*, Aachen, Balkema, Rotterdam, Vol. 3, pp. 1685–90.

Bielenstein, H.U. and Barron, K. (1971) In-situ stresses. A summary of presentations and discussions given in Theme I at the Conference of Structural Geology to Rock Mechanics Problems. Dept. of Energy, Mines and Resources, Mines Branch, Ottawa, Internal Report MR71.

Blackwood, R.L. (1979) An inference of crustal rheology from stress observations, in *Proc. 4th Cong. Int. Soc. Rock Mech. (ISRM)*, Montreux, Balkema, Rotterdam, Vol. 1, pp. 37–44.

Bock, H. (1979) Experimental determination of the residual stress field in a basaltic column, in *Proc. 4th Cong. Int. Soc. Rock Mech. (ISRM)*, Montreux, Balkema, Rotterdam, Vol. 1, pp. 45–9.

Brace, W.F. and Kohlstedt, D.L. (1980) Limits on lithospheric stress imposed by laboratory experiments. *J. Geophys. Res.*, **85**, 6248–52.

Brady, B.H.G., Lemos, J.V. and Cundall, P.A. (1986) Stress measurement schemes for jointed and fractured rock, in *Proc. Int. Symp. on Rock Stress and Rock Stress Measurements*, Stockholm, Centek Publ., Luleå, pp. 167–76.

Brekke, T. and Selmer-Olsen, R. (1966) A survey of the main factors influencing the stability of underground constructions in Norway, in *Proc. 1st Cong. Int. Soc. Rock Mech. (ISRM)*, Lisbon, Lab. Nac. de Eng. Civil, Lisbon, Vol. II, 257–60.

Broch, E. (1984) Development of unlined pressure shafts and tunnels in Norway. *Underground Space*, **8**, 177–84.

Broch, E. and Sorheim, S. (1984) Experiences from the planning, construction and supporting of a road tunnel subjected to heavy rockbursting. *Rock Mech. Rock Eng.*, **17**, 15–35.

Brooker, E.W. (1964) The influence of stress history on certain properties of remolded cohesive soils, unpublished PhD Thesis, Univ. of Illinois, 218 pp.

Brown, E.T. and Hoek, E. (1978) Trends in relationships between measured in situ stresses and depth. *Int. J. Rock Mech. Min. Sci. & Geomech. Abstr.*, **15**, 211–15.

Brown, E.T. and Windsor, C.R. (1990) Near surface in-situ stresses in Australia and their influence on underground construction, in *Proc. Tunnelling Conf.*, Sydney, The Institution of Engineers, Australia, pp. 18–48.

Brown, S.M., Leijon, B.A. and Hustrulid, W.A. (1986) Stress distribution within an artificially loaded, jointed block, in *Proc. Int. Symp. on Rock Stress and Rock Stress Measurements*, Stockholm, Centek Publ., Luleå, pp. 429–39.

Brückl, E. and Scheidegger, A.E. (1974) In situ stress measurements in the copper mine at Mitterberg, Austria, *Rock Mechanics*, **6**, 129–39.

Brudy, M. *et al.* (1995) Application of the integrated stress measurements strategy to 9 km depth in the KTB boreholes, in *Proc. Workshop on Rock Stresses in the North Sea*, Trondheim, Norway, NTH and SINTEF Publ., Trondheim, pp. 154–64.

Buchner, F. (1981) Rhinegraben: horizontal stylolites indicating stress regimes of earlier stages of rifting. *Tectonophysics*, **73**, 113–18.

Bulin, N.K. (1971) The present stress field in the upper parts of the crust. *Geotectonics* (Engl. Transl.), **3**, 133–9.

Bunnell, M.D. and Ko, K.C. (1986) In situ stress measurements and geologic structures in an underground coal mine in the Northern Wasatch Plateau, Utah, in *Proc. 27th US Symp. Rock Mech.*, Tuscaloosa, SME/AIME, pp. 333–7.

Burlet, D. and Cornet, F.H. (1993) Stress measurements at great depth by hydraulic tests in boreholes, in *Proc. 7th Cong. Int. Soc. Rock Mech. (ISRM)*, Aachen, Balkema, Rotterdam, Vol. 3, pp. 1691–7.

Burlet, D. and Ouvry, J.F. (1989) In situ stress inhomogeneity in deep sedimentary formations relative to material heterogeneity, in *Proc. Int. Symp. on Rock at Great Depth*, Pau, Balkema, Rotterdam, Vol. 2, 1065–71.

Byerlee, J. (1978) Friction of rocks. *Pure Appl. Geophys.*, **116**, 615–26.

Carey, E. and Brunier, B. (1974) Analyse théorique et numérique d'un modele mécanique élémentaire appliqué à l'étude d'une population de failles. *CR Hebd. Seanc. Acad. Sci. Paris, D*, **279**, 891–94.

Carlsson, A. and Olsson, T. (1982) Rock bursting phenomena in a superficial rock mass in southern Central Sweden. *Rock Mech.*, **15**, 99–110.

Chaplow, R. and Eldred, C.D. (1984) Geotechnical investigations for the design of an extension to the Kariba South underground power station, Zimbabwe, in *Proc. ISRM Symp. on Design and Performance of Underground Excavations*, Cambridge, British Geotechnical Society, London, pp. 213–19.

Chappell, J. (1973) Stress field associated with a dense fault pattern in New Guinea. *J. Geol.*, **81**, 705–16.

Chiu, C.H. and Gao, H. (1993) Stress singularities along a cycloid rough surface. *Int. J. Solids and Structures*, **30**, 2983–3012.

Clark, B.R. and Newman, D.B. (1977) Modeling of non-tectonic factors in near-surface in-situ stress measurements, in *Proc. 18th US Symp. Rock Mech.*, Golden, Johnson Publ., 4C3-1–4C3-6.

Coates, D.F. (1964) Some cases of residual stress effects in engineering work, in *Int. Conf. on State of Stress in the Earth's Crust*, Santa Monica, Elsevier, New York, pp. 679–88.

Cooling, C.M., Hudson, J.A. and Tunbridge, L.W.

(1988) In-situ rock stresses and their measurements in the UK – Part II. Site experiments and stress field interpretation. *Int. J. Rock Mech. Min. Sci. & Geomech. Abstr.*, **25**, 371–82.

Cornet, F.H. (1993) Stresses in rocks and rock masses, in *Comprehensive Rock Engineering* (ed. J.A. Hudson), Pergamon Press, Oxford, Chapter 17, Vol. 3, pp. 297–324.

Coutinho, A. (1949) A theory of an experimental method for determining stresses not requiring an accurate knowledge of the elastic modulus. *Int. Ass. Bridge and Structural Eng. Cong.*, **83**(9), Paris.

Cuisiat, F.D. and Haimson, B.C. (1992) Scale effects in rock mass stress measurements. *Int. J. Rock Mech. Min. Sci. & Geomech. Abstr.*, **29**, 99–117.

Cundall, P.A. and Strack, O.D.L. (1979) A discrete numerical model for granular assemblies. *Geotechnique*, **29**, 47–75.

Denkhaus, H. (1966) General report of Theme IV, in *Proc. 1st Cong. Int. Soc. Rock Mech. (ISRM)*, Lisbon, Lab. Nac. de Eng. Civil, Lisbon, Vol. III, pp. 312–19.

Dey, T.N. and Brown, D.W. (1986) Stress measurements in a deep granitic rock mass using hydraulic fracturing and differential strain curve analysis, in *Proc. Int. Symp. on Rock Stress and Rock Stress Measurements*, Stockholm, Centek Publ., Luleå, pp. 351–7.

Doe, T. *et al.* (1981) Hydraulic fracturing and overcoring stress measurements in a deep borehole at the Stripa test mine, Sweden, in *Proc. 22nd US Symp. Rock Mech.*, MIT Publ., Cambridge, pp. 403–8.

Dolezalova, M. (1974) Geostatic stress state in cross-anisotropic soil deposits, in *Proc. 4th Danube–European Conf. on Soil Mech. and Found. Eng.*, Bled, Yugoslavia, pp. 155–60.

Donnell, L.H. (1941) Stress concentrations due to elliptical discontinuities in plates under edge forces, *T.V. Karman Anniversary Volume*, Cal. Inst. of Tech., pp. 293–309.

Duncan, J.M. and Goodman, R.E. (1968) Finite element analysis of slopes in jointed rocks. Corps of Engineers Report No. CR S-68-3.

Dyke, C.G. (1989) Core discing: its potential as an indicator of principal in situ stress directions, in *Proc. Int. Symp. on Rock at Great Depth*, Pau, Balkema, Rotterdam, Vol. 2, 1057–64.

Eisbacher, G.H. and Bielenstein, H.U. (1971) Elastic strain recovery in Proterozoic rocks near Elliot Lake, Ontario. *J. Geophys. Res.*, **76**, 2012–21.

Enever, J.R., Walton, R.J. and Windsor, C.R. (1990) Stress regime in the Sydney basin and its implications for excavation design and construction, in *Proc. Tunnelling Conf.*, Sydney, The Institution of Engineers, Australia, 49–59.

Enever, J.R., Walton, R.J. and Wold, M.B. (1990) Scale effects influencing hydraulic fracture and overcoring stress measurements, in *Proc. Int. Workshop on Scale Effects in Rock Masses*, Loen, Balkema, Rotterdam, pp. 317–26.

Engelder, T. (1993) *Stress Regimes in the Lithosphere*, Princeton University Press, Princeton, New Jersey.

Engelder, T. and Sbar, M.L. (1984) Near-surface in-situ stress: introduction. *J. Geophys. Res.*, **89**, 9321–2.

Engelder, T. *et al.* (1978) Near surface in-situ stress pattern adjacent to the San Andreas fault, Palmdale, California, in *Proc. 19th US Symp. Rock Mech.*, Reno, Univ. of Nevada Publ., pp. 95–101.

Eriksson, L.G. and Michalski, A. (1986) Hydrostatic conditions in salt domes – a reality or a modeling simplification?, in *Proc. Int. Symp. on Rock Stress and Rock Stress Measurements*, Stockholm, Centek Publ., Luleå, pp. 121–32.

Eshelby, J.D. (1957) The determination of the elastic field of an ellipsoidal inclusion and related problems, in *Proc. Roy. Soc. A*, **241**, 376–96.

Etchecopar, A., Vasseur, G. and Daignieres, M. (1981) An inverse problem in microtectonics for the determination of stress tensors from fault striation analysis. *J. Struct. Geol.*, **3**, 51–65.

Evans, K.F. (1989) Appalachian stress study, 3, regional scale stress variations and their relation to structure and contemporary tectonics. *J. Geophys. Res.*, **94**, 17619–45.

Evans, K.F., Engelder, T. and Plumb, R.A. (1989) Appalachian stress study, 1. A detailed description of in-situ stress variations in Devonian shale of the Appalachian Plateau. *J. Geophys. Res.*, **94**, 7129–54.

Fairhurst, C. (1986) In-situ stress determination – an appraisal of its significance in rock mechanics, in *Proc. Int. Symp. on Rock Stress and Rock Stress Measurements*, Stockholm, Centek Publ., Luleå, pp. 3–17.

Franklin, J.A. and Hungr, O. (1978) Rock stresses in Canada: their relevance to engineering projects. *Rock Mech.*, Suppl. **6**, 25–46.

Friedman, M. (1964) Petrographic techniques for the determination of principal stress directions in rocks, in *Proc. Int. Conf. on State of Stress in the Earth's Crust*, Santa Monica, Elsevier, New York, pp. 451–550.

Friedman, M. (1972) Residual elastic strain in rocks. *Tectonophysics*, **15**, 297–330.

Gao, H. (1991) Stress concentrations at slightly undulating surfaces. *J. Mech. Phys. Solids*, **39**, 443–58.

Gay, N.C. (1979) The state of stress in a large dyke on E.R.P.M., Boksburg, South Africa. *Int. J. Rock Mech. Min. Sci. & Geomech. Abstr.*, **16**, 179–85.

Gay, N.C. and Van Der Heever, P.J. (1982) In situ stresses in the Klerksdrop gold mining district, South Africa – a correlation between geological structure and seismicity, in *Proc. 23rd US Symp. Rock Mech.*, Berkeley, SME/AIME, pp. 176–82.

Gentry, D.W. (1973) Horizontal residual stresses in the vicinity of a breccia pipe. *Int. J. Rock Mech. Min. Sci. & Geomech. Abstr.*, **10**, 19–36.

Gephart, J.W. and Forsyth, D.W. (1984) An improved method for determining the regional stress tensor using earthquake focal mechanism data: application to San Fernando earthquake sequence. *J. Geophys. Res.*, **89**, 9305–20.

Germain, P. and Bawden, W.F. (1989) Interpretation of abnormal in situ stress at great depth, in *Proc. Int. Symp. on Rock at Great Depth*, Pau, Balkema, Rotterdam, Vol. 2, pp. 999–1004.

Gerrard, C.M. (1975) Background to mathematical modeling in geomechanics: the roles of fabric and stress history, in *Proc. Int. Symp. on Numerical Methods*, Karlsruhe, Balkema, Rotterdam, pp. 33–120.

Gibson, R.E. (1974) The analytical method in soil mechanics. 14th Rankine Lecture. *Geotechnique*, **24**, 115–40.

Goetze, C. and Evans, B. (1979) Stress and temperature in the bending lithosphere as constrained by experimental rock mechanics. *Geophys. J. Roy. Astron. Soc., London*, **59**, 463–78.

Goodman, R.E. (1976) *Methods of Geological Engineering*, West Publ.

Goodman, R.E. (1989) *Introduction to Rock Mechanics*, 2nd edn, Wiley.

Gresseth, E.W. (1964) Determination of principal stress directions through an analysis of rock joint and fracture orientation, Star Mine, Burke, Idaho. US Bureau of Mines Report of Investigation RI 6413.

Haimson, B.C. (1977) Recent in-situ stress measurements using the hydrofracturing technique, in *Proc. 18th US Symp. Rock Mech.*, Golden, Johnson Publ., pp. 4C2-1–4C2-6.

Haimson, B.C. (1979) New hydrofracturing measurements in the Sierra Nevada mountains and the relationship between shallow stresses and surface topography, in *Proc. 20th US Symp. Rock Mech.*, Austin, Center for Earth Sciences and Eng. Publ., Austin, pp. 675–82.

Haimson, B.C. (1980) Near surface and deep hydrofracturing stress measurements in the Waterloo quartzite. *Int. J. Rock Mech. Min. Sci. & Geomech. Abstr.*, **17**, 81–8.

Haimson, B.C. (1981) Confirmation of hydrofracturing results through comparisons with other stress measurements, in *Proc. 22nd US Symp. Rock Mech.*, MIT Publ., Cambridge, pp. 409–15.

Haimson, B.C. (1984) Pre-excavation in situ stress measurements in the design of large underground openings, in *Proc. ISRM Symposium on Design and Performance of Underground Excavations*, Cambridge, British Geotechnical Society, London, pp. 183–90.

Haimson, B.C. (1990a) Stress measurements in the Sioux Falls quartzite and the state of stress in the Midcontinent, in *Proc. 31st US Symp. Rock Mech.*, Golden, Balkema, Rotterdam, pp. 397–404.

Haimson, B.C. (1990b) Scale effects in rock stress measurements, in *Proc. Int. Workshop on Scale Effects in Rock Masses*, Leon, Norway, Balkema, Rotterdam, pp. 89–101.

Haimson, B.C. and Lee, C.F. (1980) Hydrofracturing stress determinations at Darlington, Ontario, in *Proc. 13th Can. Symp. Rock Mech.*, Toronto, Canadian Institute of Mining and Metallurgy, CIM Special Vol. 22, pp. 42–50.

Haimson, B.C. and Lee, M.Y. (1995) Estimating *in situ* stress conditions from borehole breakouts and core disking – experimental results in granite, in *Proc. Int. Workshop on Rock Stress Measurement at Great Depth*, Tokyo, Japan, 8th ISRM Cong., pp. 19–24.

Haimson, B.C. and Rummel, F. (1982) Hydrofracturing stress measurements in the Iceland drilling project drillhole at Reydasfjordur, Iceland. *J. Geophys. Res.*, **87**, 6631–49.

Haimson, B.C. and Voight, B. (1977) Crustal stress in Iceland. *Pure and Appl. Geophys.*, **115**, 153–90.

Haimson, B.C., Lee, M. and Herrick, C. (1993) Recent advances in in-situ stress measurements by hydraulic fracturing and borehole breakouts, in *Proc. 7th Cong. Int. Soc. Rock Mech. (ISRM)*, Aachen, Balkema, Rotterdam, Vol. 3, pp. 1737–42.

Hansen, K.S. and Purcell, W.R. (1986) Earth stress measurements in the South Belridge oil field, Kern County, California. Paper SPE 15641 presented at 61st Annual Tech. Conf. of SPE, New Orleans.

Hast, N. (1958) The measurement of rock pressures in mines. *Sveriges Geol. Undersokning, Ser. C*, No. 560.

Hast, N. (1967) The state of stress in the upper part of the Earth's crust. *Eng. Geol.*, **2**, 5–17.

Hast, N. (1969) The state of stress in the upper part of the Earth's crust. *Tectonophysics*, **8**, 169–211.

Hast, N. (1972) Stability of stress distributions in the Earth's crust during geologic times and the formation of iron ore lenses at Malmberget. *Phys. Earth Planet. Inter.*, **6**, 221–8.

Hast, N. (1973) Global measurements of absolute stress. *Phil. Trans. Roy. Soc. London, A*, **274**, 409–19.

Hast, N. (1974) The state of stress in the upper part of the Earth's crust as determined by measurements of absolute rock stress. *Naturwissenschaften*, **61**, 468–75.

Hast, N. (1979) Limit of stresses in the Earth's crust. *Rock Mech.*, **11**, 143–50.

Haxby, W.F. and Turcotte, D.L. (1976) Stresses induced by the addition or removal of overburden and associated thermal effects. *Geology*, **4**, 181–4.

Hayashi, K. and Masuoka, M. (1995) Estimation of tectonic stress from slip data from fractures in core samples, in *Proc. Int. Workshop on Rock Stress Measurement at Great Depth*, Tokyo, Japan, 8th ISRM Cong., pp. 35–9.

Heim, A. (1878) Untersuchungen über den Mechanismus der Gebirgsbildung, in *Anschluss and die Geologische Monographie der Tödi-Windgälen-Gruppe, B. Schwabe*, Basel.

Herget, G. (1973) Variation of rock stresses with depth at a Canadian iron mine. *Int. J. Rock Mech. Min. Sci.*, **10**, 37–51.

Herget, G. (1974) Ground stress determinations in Canada. *Rock Mech.*, **6**, 53–74.

Herget, G. (1980) Regional stresses in the Canadian shield, in *Proc. 13th Can. Symp. Rock Mech.*, Toronto, Canadian Institute of Mining and Metallurgy, CIM Special Vol. 22, pp. 9–15.

Herget, G. (1986) Changes of ground stresses with depth in the Canadian shield, in *Proc. Int. Symp. on Rock Stress and Rock Stress Measurements*, Stockholm, Centek Publ., Luleå, pp. 61–8.

Herget, G. (1987) Stress assumptions for underground excavations in the Canadian shield. *Int. J. Rock Mech. Min. Sci. & Geomech. Abstr.*, **24**, 95–7.

Herget, G. (1993) Rock stresses and rock stress monitoring in Canada, in *Comprehensive Rock Engineering* (ed. J.A. Hudson), Pergamon Press, Oxford, Chapter 19, Vol. 3, pp. 473–96.

Herget, G. and Arjang, B. (1990) Update on ground stresses in the Canadian shield, in *Proc. Conf. on Stresses in Underground Structures*, Ottawa, CANMET, pp. 33–47.

Hoek, E. and Brown, E.T. (1980a) *Underground Excavations in Rock*, Institution of Mining and Metallurgy, London.

Hoek, E. and Brown, E.T. (1980b) Empirical strength criterion for rock masses. *ASCE J. Geotech. Eng.*, **106**, 1013–35.

Holzhausen, G.R. and Johnson, A.M. (1979) The concept of residual stress in rock. *Tectonophysics*, **58**, 237–67.

Hooker, V.E. and Duvall, W.I. (1966) Stresses in rock outcrops near Atlanta, GA. US Bureau of Mines Report of Investigation RI 6860.

Hooker, V.E., Bickel, D.L. and Aggson, J.R. (1972) In situ determination of stresses in mountainous topography. US Bureau of Mines Report of Investigation RI 7654.

Howard, J.H. (1966) Vertical normal stress in the Earth and the weight of the overburden. *Geol. Soc. Am. Bull.*, **77**, 657–60.

Huang, Q. (1989) Modal and vectorial analysis for determination of stress axes associated with fault slip data. *Math. Geol.*, **21**, 543–58.

Hudson, J.A. and Cooling, C.M. (1988) In situ rock stresses and their measurement in the UK – Part I. The current state of knowledge. *Int. J. Rock Mech. Min. Sci. & Geomech. Abstr.*, **25**, 363–70.

Hyett, A.J., Dyke, C.G. and Hudson, J.A. (1986) A critical examination of basic concepts associated with the existence and measurement of in-situ stress, in *Proc. Int. Symp. on Rock Stress and Rock Stress Measurements*, Stockholm, Centek Publ., Luleå, pp. 387–91.

Jaeger, J.C. and Cook, N.G.W. (1963) Pinching off and discing of rocks. *J. Geophys. Res.*, **86**, 1757–65.

Jaeger, J.C. and Cook, N.G.W. (1976) *Fundamentals of Rock Mechanics*, 2nd edn, Chapman & Hall, London.

James, P. (1991) Stress and strain during river downcutting. *Austr. Geomech.*, 28–31.

Jeffery, R.I. and North, M.D. (1993) Review of recent hydrofracture stress measurements made in the Carboniferous coal measures of England, in *Proc. 7th Cong. Int. Soc. Rock Mech. (ISRM)*, Aachen, Balkema, Rotterdam, Vol. 3, pp. 1699–1703.

Judd, W.R. (1964) Rock stress, rock mechanics and research, in *Proc. Int. Conf. on State of Stress in the Earth's Crust*, Santa Monica, Elsevier, New York, pp. 5–54.

Kanagawa, T. *et al.* (1986) In situ stress measure-

ments in the Japanese Islands: overcoring results from a multi-element gauge at 23 sites. *Int. J. Rock Mech. Min. Sci. & Geomech. Abstr.*, **23**, 29–39.

Kim, K. and Schmidt, B. (1992) Characterization of the state of in situ stress for the design of the Superconducting Super Collider interaction hall, in *Proc. Eurock '92: Int. Symp. on Rock Characterization*, Chester, UK, British Geotechnical Society, London, pp. 462–7.

Kim, K. and Smith, C.S. (1980) Hydraulic fracturing stress measurements near the Keneenaw fault in upper Michigan, in *Proc. 13th Can. Symp. Rock Mech.*, Toronto, Canadian Institute of Mining and Metallurgy, CIM Special Vol. 22, pp. 24–30.

Kirby, S.H. (1983) Rheology of the lithosphere. *Rev. Geophys. Space Phys.*, **21**, 1458–87.

Klein, R.J. and Barr, M.V. (1986) Regional state of stress in western Europe, in *Proc. Int. Symp. on Rock Stress and Rock Stress Measurements*, Stockholm, Centek Publ., Luleå, pp. 33–44.

Klein, R.J. and Brown, E.T. (1983) The state of stress in British rocks. Report DOE/RW/83.8.

Knill, J.L. (1968) Geotechnical significance of some glacially induced rock discontinuities. *Bull. Assoc. Eng. Geol.*, **5**, 49–62.

Kohlbeck, F., Scheidegger, A.E. and Sturgul, J.R. (1979) Geomechanical model of an Alpine valley. *Rock Mech.*, **12**, 1–4.

Kramer, A. *et al.* (1994) Borehole televiewer data analysis from the New Hebrides Island Arc: the state of stress at holes 829A and 831B, in *Proc. ODP, Science Results*, Ocean Drilling Program, College Station, Texas.

Kropotkin, P.N. (1972) The state of stress in the Earth's crust as based on measurements in mines and on geophysical data. *Phys. Earth Planet. Inter.*, **6**, 214–18.

Kulhawy, F.H., Jackson, C.S. and Mayne, P.W. (1989) First order estimation of K_o in sands and clays, in *Proc. Foundation Engineering Cong.*, Evanston, ASCE, pp. 121–34.

Kutter, H.K. (1993) Influence of drilling method on borehole breakouts and core disking, in *Proc. 7th Cong. Int. Soc. Rock Mech. (ISRM)*, Aachen, Balkema, Rotterdam, Vol. 3, pp. 1659–64.

Lade, P.V. (1993) Rock strength criteria: the theories and evidence, in *Comprehensive Rock Engineering* (ed. J.A. Hudson), Pergamon Press, Oxford, Chapter 11, Vol. 3, pp. 255–82.

Lambe, T.W. and Whitman, R.V. (1969) *Soil Mechanics*, Wiley, New York.

Lang, P.A., Thompson, P.M. and Ng, L.K.W. (1986) The effect of residual stress and drill hole size on the in situ stress determined by overcoring, in *Proc. Int. Symp. on Rock Stress and Rock Stress Measurements*, Stockholm, Centek Publ., Luleå, pp. 687–94.

Lee, C.F. (1981) In-situ stress measurements in southern Ontario, in *Proc. 22nd US Symp. Rock Mech.*, MIT Publ., Cambridge, pp. 465–72.

Lee, C.F. and Lo, K.Y. (1976) Rock squeeze of two deep excavations at Niagara Falls, in Rock Engineering for Foundations and Slopes, in *Proc. ASCE Specialty Conf.*, Boulder, 116–40.

Lee, F.T., Nichols, T.C. and Abel, J.F. (1969) Some relations between stress, geologic structure, and underground excavation in a metamorphic rock mass West of Denver, Colorado. *US Geol. Surv. Prof. Pap.*, **650-C**, pp. C127–39.

Lee, F.T., Abel, J. and Nichols, T.C. (1976) The relation of geology to stress changes caused by underground excavation in crystalline rocks at Idaho Springs, Colorado. *US Geol. Surv. Prof. Pap.*, **965**, Washington.

Leeman, E.R. (1964) The measurement of stress in rock. *J. South Afr. Inst. Mining Metall.*, **65**, 45–114.

Leijon, B.A. (1986) Application of the LUT triaxial overcoring techniques in Swedish mines, in *Proc. Int. Symp. on Rock Stress and Rock Stress Measurements*, Stockholm, Centek Publ., Luleå, pp. 569–79.

Li, F. (1986) In situ stress measurements, stress state in the upper crust and their application to rock engineering, in *Proc. Int. Symp. on Rock Stress and Rock Stress Measurements*, Stockholm, Centek Publ., Luleå, pp. 69–77.

Liao, J.J., Savage, W.Z. and Amadei, B. (1992) Gravitational stresses in anisotropic ridges and valleys with small slopes. *J. Geophys. Res.*, **97**, 3325–36.

Lim, H.-U. and Lee, C.-I. (1995) Fifteen years' experience on rock stress measurements in South Korea, in *Proc. Int. Workshop on Rock Stress Measurement at Great Depth*, Tokyo, Japan, 8th ISRM Cong., pp. 7–12.

Lindner, E.N. (1985) In situ stress indications around Lake Ontario, in *Proc. 26th US Symp. Rock Mech.*, Rapid City, Balkema, Rotterdam, pp. 575–90.

Lindner, E.N. and Halpern, E.N. (1977) In-situ stress: an analysis, in *Proc. 18th US Symp. Rock Mech.*, Johnson Publ., Golden, pp. 4C1-1–4C1-7.

Ling, C.B. (1947) On the stresses in a notched plate under tension. *J. Math. Phys.*, **26**, 284–9.

Liu, L. and Zoback, M.D. (1992) The effect of topography on the state of stress in the crust:

application to the site of the Cajon Pass Scientific Drilling Project. *J. Geophys. Res.*, **97**, 5095–108.

Lo, K.Y. (1978) Regional distribution of in-situ horizontal stresses in rocks in southern Ontario. *Can. Geotech. J.*, **15**, 371–81.

Lo, K.Y., *et al.* (1975) Stress relief and time-dependent deformation of rocks, in Final Report to National Research Council of Canada, Special Project S-7307.

Lo, K.Y. and Morton, J.D. (1976) Tunnels in bedded rock with high horizontal stresses. *Can. Geotech. J.*, **13**, 216–30.

Martin, C.D. and Chandler, N.A. (1993) Stress heterogeneity and geological structures. *Int. J. Rock Mech. Min. Sci. & Geomech. Abstr.*, **30**, 993–9.

Martin, C.D. and Simmons, G.R. (1993) The Atomic Energy of Canada Limited Underground Research Laboratory: an overview of geomechanics characterization, in *Comprehensive Rock Engineering* (ed. J.A. Hudson), Pergamon Press, Oxford, Chapter 38, Vol. 3, pp. 915–50.

Martin, C.D., Martino, J.B. and Dzik, E.J. (1994) Comparison of borehole breakouts from laboratory and field tests, in *Proc. Eurock' 94*, Delft, Balkema, Rotterdam, pp. 183–90.

Martna, J. (1988) Distribution of tectonic stresses in mountainous areas, in *Proc. Int. Symp. on Tunneling for Water Resources and Power Projects*, New Delhi.

Martna, J. and Hansen, L. (1986) Initial rock stresses around the Vietas headrace tunnels no. 2 and 3, Sweden, in *Proc. Int. Symp. on Rock Stress and Rock Stress Measurements*, Stockholm, Centek Publ., Luleå, pp. 605–13.

Matheson, D.S. and Thomson, S. (1973) Geological implications of valley rebound. *Can. J. Earth Sci.*, **10**, 961–78.

Mattauer, M. (1973) *Les Déformations des Matériaux de l'Ecorce Terrestre*, Herman Publ., Paris.

Maury, V. (1987) Observations, researches and recent results about failure mechanisms around single galleries, in *Proc. 6th Cong. Int. Soc. Rock Mech. (ISRM)*, Montreal, Balkema, Rotterdam, Vol. 2, pp. 1119–28.

McClintock, F.A. and Argon, A.S. (1966) *Mechanical Behavior of Materials*, Addison-Wesley.

McCutchen, W.R. (1982) Some elements of a theory for in-situ stress. *Int. J. Rock Mech. Min. Sci. & Geomech. Abstr.*, **19**, 201–3.

McGarr, A. (1980) Some constraints on levels of shear stress in the crust from observation and theory. *J. Geophys. Res.*, **85**, 6231–8.

McGarr, A. (1988) On the state of lithospheric stress in the absence of applied tectonic forces. *J. Geophys. Res.*, **93**, 609–17.

McGarr, A. and Gay, N.C. (1978) State of stress in the Earth's crust. *Ann. Rev. Earth Planet. Sci.*, **6**, 405–36.

McKenzie, D.P. (1969) The relation between fault plane solutions for earthquakes and the directions of the principal stresses. *Seism. Soc. Am. Bull.*, **50**, 595–601.

McTigue, D.F. and Mei, C.C. (1981) Gravity induced stresses near topography of small slopes. *J. Geophys. Res.*, **86**, 9268–78.

McTigue, D.F. and Mei, C.C. (1987) Gravity induced stresses near axisymmetric topography of small slopes. *Int. J. Num. Anal. Math. Geomech.*, **11**, 257–68.

McTigue, D.F. and Stein, R.S. (1984) Topographic amplification of tectonic displacement: Implications for geodetic measurement of strain changes. *J. Geophys. Res.*, **89**, 1123–31.

Meissner, R. and Strehlau, J. (1982) Limits of stresses in the continental crust and their relation to the depth–frequency distribution of shallow earthquakes. *Tectonics*, **1**, 73–89.

Michael, A.J. (1984) Determination of stress from slip data: faults and folds. *J. Geophys. Res.*, **89**, 11517–26.

Mills, K.W., Pender, M.J. and Depledge, D. (1986) Measurement of in situ stress in coal, in *Proc. Int. Symp. on Rock Stress and Rock Stress Measurements*, Stockholm, Centek Publ., Luleå, pp. 543–49.

Molinda, M. *et al.* (1992) Effects of horizontal stress related to stream valleys on the stability of coal mine openings. US Bureau of Mines Report of Investigation RI 9413.

Moos, D. and Zoback, M.D. (1990) Utilization of observations of well bore failure to constrain the orientation and magnitude of crustal stresses: application to continental, deep sea drilling project and ocean drilling program boreholes. *J. Geophys. Res.*, **95**, 9305–25.

Mount, V.S. and Suppe, J. (1987) State of stress near the San Andreas fault; implications for wrench tectonics. *Geology*, **15**, 1143–6.

Müller, B. *et al.* (1992) Regional patterns of tectonic stress in Europe. *J. Geophys. Res.*, **97**, 11783–803.

Muller, O. and Pollard, D.D. (1977) The stress state near Spanish Peaks, Colorado determined from a dike pattern. *Pure Appl. Geophys.*, **115**, 69–86.

Myrvang, A.M. (1976) Practical use of rock stress measurements in Norway, in *Proc. ISRM Symp. on Investigation of Stress in Rock, Advances in Stress*

Measurement, Sydney, The Institution of Engineers, Australia, pp. 92–9.

Myrvang, A.M. (1993) Rock stress and rock stress problems in Norway, in *Comprehensive Rock Engineering* (ed. J.A. Hudson), Pergamon Press, Oxford, Chapter 18, Vol. 3, pp. 461–71.

Myrvang, A., Hansen, S.E. and Sørensen, T. (1993) Rock stress redistribution around an open pit mine in hard rock. *Int. J. Rock Mech. Min. Sci. & Geomech. Abstr.*, **30**, 1001–4.

Nakamura, K. (1977) Volcanoes as possible indicators of tectonic stress orientation – principle and proposal. *J. Volcanol. Geotherm. Res.*, **2**, 1–16.

Nakamura, K., Jacob, K.H. and Davies, J.N. (1977) Volcanoes as possible indicators of tectonic stress orientation – Aleutians and Alaska. *Pure and Appl. Geophys.*, **115**, 87–112.

Natau, O., Borm, G. and Rockel, Th. (1989) Influence of lithology and geological structure on the stability of the KTB pilot hole, in *Proc. Rock at Great Depth*, Pau, Balkema, Rotterdam, pp. 1487–90.

Nichols, T.C. (1975) Deformations associated with relocation of residual stresses in a sample of Barre granite from Vermont. *US Geol. Surv. Pap.*, **875**.

Nichols, T.C. and Savage, W.Z. (1976) Rock strain recovery – factor in foundation design, in *Rock Engineering for Foundations and Slopes, ASCE Specialty Conf.*, Boulder, Vol. 1, pp. 34–54.

Niwa, Y. and Hirashima, K.I. (1971) The theory of the determination of stress in an anisotropic elastic medium using an instrumented cylindrical inclusion, in *Mem. Faculty Eng., Kyoto University*, **33**, 221–32.

Obara, Y. *et al.* (1995) Measurement of stress distribution around fault and considerations, in *Proc. 2nd Int. Conf. on the Mechanics of Jointed and Faulted Rock*, Vienna, Balkema, Rotterdam, pp. 495–500.

Obert, L. and Stephenson, D.E. (1965) Stress conditions under which core discing occurs. *SME Trans.*, **232**, 227–35.

Ode, H. (1957) Mechanical analysis of the dike pattern of the Spanish Peaks area, Colorado. *Geol. Soc. Am. Bull.*, **38**, 567–76.

Orowan, E. (1948) Classification and nomenclature of internal stresses, in *Proc. Symp. on Internal Stresses, Inst. Metals*, 47–59.

Orr, C.M. (1975) High horizontal stresses in near surface rock masses, in *Proc. 6th Regional Conf. for Africa on Soil Mech. Found. Engr.*, Durban, pp. 201–6.

Ortlepp, W.D. and Gay, N.C. (1984) Performance of an experimental tunnel subjected to stresses ranging between 50 MPa and 230 MPa, in *Proc. ISRM Symp. on Design and Performance of Underground Excavations*, Cambridge, British Geotechnical Society, London, 337–46.

Oudenhoven, M.S., Babcock, C.O. and Blake, W. (1972) A method for the prediction of stresses in an isotropic inclusion or orebody of irregular shape. US Bureau of Mines Report of Investigation RI 7645.

Palmer, J.H.L. and Lo, K.Y. (1976) In situ stress measurements in some near-surface rock formations – Thorold, Ontario. *Can. Geotech. J.*, **13**, 1–7.

Pan, E. and Amadei, B. (1993) Gravitational stresses in long asymmetric ridges and valleys in anisotropic rock. *Int. J. Rock Mech. Min. Sci. & Geomech. Abstr.*, **30**, 1005–8.

Pan, E. and Amadei, B. (1994) Stresses in an anisotropic rock mass with irregular topography. *ASCE J. Eng. Mech.*, **120**, 97–119.

Pan, E., Amadei, B. and Savage, W.Z. (1994) Gravitational stresses in long symmetric ridges and valleys in anisotropic rock. *Int. J. Rock Mech. Min. Sci. & Geomech. Abstr.*, **31**, 293–312.

Pan, E., Amadei, B. and Savage, W.Z. (1995) Gravitational and tectonic stresses in anisotropic rock with irregular topography. *Int. J. Rock Mech. Min. Sci. & Geomech. Abstr.*, **32**, 201–14.

Parker, J. (1973) The relationship between structure, stress, and moisture. *Eng. and Mining J.*, October, 91–5.

Pickering, D.J. (1970) Anisotropic elastic parameters for soils. *Geotechnique*, **20**, 271–6.

Pine, R.J. and Batchelor, A.S. (1984) Downward migration of shearing in jointed rock during hydraulic injections. *Int. J. Rock Mech. Min. Sci. & Geomech. Abstr.*, **21**, 249–63.

Pine, R.J. and Kwakwa, K.A. (1989) Experience with hydrofracture stress measurements to depths of 2.6 km and implications for measurements to 6 km in the Carnmenellis granite. *Int. J. Rock Mech. Min. Sci. & Geomech. Abstr.*, **26**, 565–71.

Plumb, R.A. (1994) Variations of the least horizontal stress magnitude in sedimentary rocks, in *Proc. 1st North Amer. Rock Mech. Symp.*, Austin, Balkema, Rotterdam, pp. 71–8.

Plumb, R.A., Evans, K.F. and Engelder, T. (1991) Geophysical log responses and their correlation with bed-to-bed stress contrasts in Paleozoic rocks, Appalachian Plateau, NY. *J. Geophys. Res.*, **96**, 14509–28.

Pollard, D.D. (1978) Forms of hydraulic fractures as deduced from field studies of sheet intrusions, in

Proc. 19th US Symp. Rock Mech., Reno, Univ. of Nevada Publ., pp. 1–9.

Pollard, D.D. and Segall, P. (1987) Theoretical displacements and stresses near fractures in rock: with applications to faults, joints, veins, dikes, and solution surfaces, in *Fracture Mechanics of Rock*, Academic Press, London, pp. 277–349.

Preston, D.A. (1968) Photoelastic measurement of elastic strain recovery in outcropping rocks. *Trans. AGU*, Abstract, **49**, p. 302.

Price, N.J. (1966) *Fault and Joint Development in Brittle and Semi-Brittle Rocks*, Pergamon Press, London.

Price, N.J. (1974) The development of stress systems and fracture patterns in undeformed sediments, in *Proc. 3rd Cong. Int. Soc. Rock Mech. (ISRM)*, Denver, Nat. Academy of Sciences, Washington, DC, 487–96.

Price, N.J. and Cosgrove, J.W. (1990) *Analysis of Geological Structures*, Cambridge University Press.

Reches, Z. (1987) Determination of the tectonic stress tensor from slip along faults that obey the Coulomb yield condition. *Tectonics*, **6**, 849–61.

Rosengren, L. and Stephansson, O. (1990) Distinct element modelling of the rock mass response to glaciation at Finnsjön, Central Sweden. SKB Technical Report 90-40, Stockholm.

Rosengren, L. and Stephansson, O. (1993) Modelling of rock mass response to glaciation at Finnsjön, Central Sweden. *Tunnelling and Underground Space Technol.*, **8**, 75–82.

Rummel, F. (1986) Stresses and tectonics of the upper continental crust – a review, in *Proc. Int. Symp. on Rock Stress and Rock Stress Measurements*, Stockholm, Centek Publ., Luleå, pp. 177–86.

Rummel, F., Höhring-Ermann, G. and Baumgärtner, J. (1986) Stress constraints and hydrofracturing stress data for the continental crust. *Pure Appl. Geophys.*, **124**, 875–95.

Russell, J.E. and Hoskins, E.R. (1973) Residual stresses in rock, in *Proc. 14th US Symp. Rock Mech.*, University Park, ASCE Publ., pp. 1–24.

Salamon, M.D.G. (1968) Elastic moduli of a stratified rock mass. *Int. J. Rock Mech. Min. Sci.*, **5**, 519–27.

Savage, J.C. (1983) Strain accumulation in the western United States. *Ann. Rev. Earth Planet. Sci.*, **11**, 11–43.

Savage, J.C., Proscott, W.H. and Lisowski, M. (1987) Deformation along the San Andreas fault 1982–1986 as indicated by frequent geodolite measurements. *J. Geophys. Res.*, **92**, 4785–97.

Savage, W.Z. (1978) The development of residual stress in cooling rock bodies. *Geophys. Res. Lett.*, **5**, 633–6.

Savage, W.Z. (1994) Gravity induced stresses in finite slopes. *Int. J. Rock Mech. Min. Sci. & Geomech. Abstr.*, **31**, 471–83.

Savage, W.Z. and Swolfs, H.S. (1986) Tectonic and gravitational stress in long symmetric ridges and valleys. *J. Geophys. Res.*, **91**, 3677–85.

Savage, W.Z., Swolfs, H.S. and Powers, P.S. (1985) Gravitational stress in long symmetric ridges and valleys. *Int. J. Rock Mech. Min. Sci. & Geomech. Abstr.*, **22**, 291–302.

Savage, W.Z., Swolfs, H.S. and Amadei, B. (1992) On the state of stress in the near surface of the Earth's crust. *Pure Appl. Geophys.*, **138**, 207–28.

Sbar, M.L. and Sykes, L.R. (1973) Contemporary compressive stress and seismicity in eastern North America: an example of intra-plate tectonics. *Geol. Soc. Am. Bull.*, **84**, 1861–82.

Sbar, M.L. *et al.* (1979) Stress pattern near the San Andreas fault, Palmdale, California, from near-surface in situ measurements. *J. Geophys. Res.*, **84**, 156–64.

Scheidegger, A.E. (1977) Geotectonic stress determination in Austria, in *Proc. Int. Symp. on Field Measurements in Rock Mechanics*, Zurich, Balkema, Rotterdam, Vol. 1, pp. 197–208.

Scheidegger, A.E. (1982) *Principles of Geodynamics*, 3rd edition, Springer-Verlag.

Scheidegger, A.E. (1995) Geojoints and geostresses, in *Proc. 2nd Int. Conf. on the Mechanics of Jointed and Faulted Rock*, Vienna, Balkema, Rotterdam, pp. 3–35.

Selmer-Olsen, R. (1974) Underground openings filled with high pressure water or air. *Bull. Int. Ass. Eng. Geol.*, **9**, 91–5.

Sezawa, K. and Nishimura, G. (1931) Stresses under tension in a plate with heterogeneous insertions. *Aero. Res. Inst.* (Tokyo, Japan), **6**, 25–45.

Shamir, G. and Zoback, M.D. (1992) Stress orientation profile to 3.5 km depth near the San Andreas fault at Cajon Pass, California. *J. Geophys. Res.*, **97**, 5059–80.

Sheorey, P. R. (1994) A theory for in-situ stresses in isotropic and transversely isotropic rock. *Int. J. Rock Mech. Min. Sci. & Geomech. Abstr.*, **31**, 23–34.

Silvestri, V. and Tabib, C. (1983a) Exact determination of gravity stresses in finite elastic slopes: Part I. Theoretical considerations. *Can. Geotech. J.*, **20**, 47–54.

Silvestri, V. and Tabib, C. (1983b) Exact determination of gravity stresses in finite elastic slopes: Part II. Applications. *Can. Geotech. J.*, **20**, 55–60.

Skempton, A. (1961) Horizontal stresses in an overconsolidated Eocene clay, in *Proc. 5th Int. Cong. Soil Mech.*, Paris, Vol. 1, pp. 531–37.

Smith, R.B. and Bruhn, R.L. (1984) Intraplate extensional tectonics of the Eastern Basin Range. *J. Geophys. Res.*, **89**, 5733–62.

Solomon, S.C., Sleep, N.H. and Richardson, R.M. (1975) On the forces driving plate tectonics: inferences from absolute plate velocities and intraplate stresses. *Geophys. J. Roy. Astron. Soc.*, **42**, 769–801.

Solomon, S.C., Richardson, R. and Bergman, E.A. (1980) Tectonic stress: models and magnitudes. *J. Geophys. Res.*, **85**, 6086–92.

Spicak, A. (1988) Interpretation of tectonic stress orientation on the basis of laboratory model experiments. *Phys. Earth Planet. Inter.*, **51**, 101–6.

Srolovitz, D.J. (1989) On the stability of surfaces of stressed solids. *Acta Metall.*, **37**, 621–5.

Stacey, T.R. (1982) Contribution to the mechanism of core discing. *J. South Afr. Inst. Mining Metall.*, 269–74.

Steiner, W. (1992) Swelling rock in tunnels: characterization and effect of horizontal stresses, in *Proc. Eurock '92: Int. Symp. on Rock Characterization*, Chester, UK, British Geotechnical Society, London, pp. 163–73.

Stephansson, O. (1988) Ridge push and glacial rebound as rock stress generators in Fennoscandia, in *Geological Kinematics and Dynamics: From Molecules to the Mantle* (ed. C. Talbot), *Bull. Geol. Inst. Upps.*, Spec. Issue, NS, **14**, 39–48.

Stephansson, O. (1993) Rock stress in the Fennoscandian shield, in *Comprehensive Rock Engineering* (ed. J.A. Hudson), Pergamon Press, Oxford, Chapter 17, Vol. 3, pp. 445–59.

Stephansson, O., Särkkä, P. and Myrvang, A. (1986) State of stress in Fennoscandia, in *Proc. Int. Symp. on Rock Stress and Rock Stress Measurements*, Stockholm, Centek Publ., Luleå, pp. 21–32.

Stephansson, O., Savilahti, T. and Bjarnason, B. (1989) Rock mechanics of the deep borehole at Gravberg, Sweden, in *Proc. Int. Symp. on Rock at Great Depth*, Pau, Balkema, Rotterdam, Vol. 2, pp. 863–70.

Stephansson, O., Ljunggren, C. and Jing, L. (1991) Stress measurements and tectonic implications for Fennoscandia. *Tectonophysics*, **189**, 317–22.

Stephen, R.M. and Pirtz, D. (1963) Application of birefringent coating to the study of strains around circular inclusions in mortar prisms. *SESA Experimental Mech.*, **3**, 91–7.

Sturgul, J.R., Scheidegger, A.E. and Greenshpan, Z. (1976) Finite element model of a mountain massif. *Geology*, **4**, 439–42.

Sugawara, K. and Obara, Y. (1993) Measuring rock stress, in *Comprehensive Rock Engineering* (ed. J.A. Hudson), Pergamon Press, Oxford, Chapter 21, Vol. 3, pp. 533–52.

Sugawara, K. and Obara, Y. (1995) Rock stress and rock stress measurements in Japan, in *Proc. Int. Workshop on Rock Stress Measurement at Great Depth*, Tokyo, Japan, 8th ISRM Cong., pp. 1–6.

Swolfs, H.S. (1984) The triangular stress diagram – a graphical representation of crustal stress measurements. *US Geol. Surv. Prof. Pap.*, **1291**, Washington, 19 pp.

Swolfs, H.S. and Savage, W.Z. (1985) Topography, stresses, and stability at Yucca Mountain, Nevada, in *Proc. 26th US Symp. Rock Mech.*, Rapid City, Balkema, Rotterdam, pp. 1121–9.

Swolfs, H.S., Handin, J. and Pratt, H.R. (1974) Field measurement of residual strain in granitic rock masses, in *Proc. 3rd Cong. Int. Soc. Rock Mech. (ISRM)*, Denver, National Academy of Sciences, Washington, DC, 2A, pp. 563–568.

Sykes, L.R. and Sbar, M.L. (1973) Intraplate earthquakes, lithosphere stresses and the driving mechanisms of plate tectonics. *Nature*, **245**, 298–302.

Szymanski, J.C. and Harper, T.R. (1979) Interpretation of in-situ strain relief measurements: stress redistribution associated with heterogeneity, in *Proc. 20th US Symp. Rock Mech.*, Austin, pp. 691–4.

Talobre, J.A. (1967) *La Mecanique des Roches*, 2nd edn, Dunod, Paris.

Te Kamp, L., Rummel, F. and Zoback, M.D. (1995) Hydrofrac stress profile to 9 km at the German KTB site, in *Proc. Workshop on Rock Stresses in the North Sea*, Trondheim, Norway, NTH and SINTEF Publ., Trondheim, pp. 147–53.

Terzaghi, K. (1962) Measurement of stresses in rock. *Geotechnique*, **12**, 105–24.

Terzaghi, K. and Richart, F.E. (1952) Stresses in rock about cavities. *Geotechnique*, **3**, 57–90.

Ter-Martirosyan, Z.G. and Akhpatelov, D.M. (1972) The stressed state of an infinite slope with a curvilinear boundary object to a field of gravity and percolation. *J. Probl. Geomech.*, **5**, 81–91.

Ter-Martirosyan, Z.G., Akhpatelov, D.M. and Manvelyan, R.G. (1974) The stressed state of rock masses in a field body forces, in *Proc. 3rd Cong. Int. Soc. Rock Mech. (ISRM)*, Denver, National Academy of Sciences, Washington DC, Part A, pp. 569–74.

Teufel, L.W. (1986) In situ stress and natural fracture distribution at depth in the Piceance Basin, Colorado: implications to stimulation and production of low permeability gas reservoirs, in *Proc. 27th US Symp. Rock Mech.*, Tuscaloosa, SME/AIME, pp. 702–8.

Teufel, L.W. and Farrell, H.E. (1990) In situ stress and natural fracture distribution in the Ekofisk field, North Sea. Sandia National Lab. Report No. SAND-90-1058C.

Teufel, L.W., Rhett, D.W. and Farrell, H.E. (1991) Effect of reservoir depletion and pore pressure drawdown on in-situ stress and deformation in the Ekofisk Field, North Sea, in *Proc. 32nd US Symp. Rock Mech.*, Balkema, Rotterdam, pp. 63–72.

Tinchon, L. (1987) Evolution des contraintes naturelles en fonction de la profondeur et de la tectonique aux Houillères du bassin de Lorraine. *Revue de l'Industrie Minerale – Mines et Carrières – les Techniques*, **69**, 281–8.

Towse, D.F. and Heuze, F.E. (1983) Estimating in-situ stresses and rock mass properties from geological and geophysical data: applications in the hydraulic fracturing of tight gas reservoirs. Lawrence Livermore National Laboratory Report UCRL-53443.

Tullis, T.E. (1977) Reflections on measurement of residual stress in rock. *Pure Appl. Geophys.*, **115**, 57–68.

Turcotte, D.L. (1973) Driving mechanisms for plate tectonics. *Geofisica Internac.*, **13**, 309–15.

Turcotte, D.L. and Oxburgh, E.R. (1973) Mid-plate tectonics. *Nature*, **244**, 337–9.

Turcotte, D.L. and Schubert, G. (1982) *Geodynamics: Applications of Continuum Physics to Geological Problems*, Wiley.

Turner, F.J. and Weiss, L.E. (1963) *Structural Analysis of Metamorphic Tectonites*, McGraw-Hill.

Van Heerden, W.L. (1976) Practical application of the CSIR triaxial strain cell for rock stress measurements, in *Proc. ISRM Symposium on Investigation of Stress in Rock, Advances in Stress Measurement*, Sydney, The Institution of Engineers, Australia, pp. 1–6.

Varnes, D.J. (1970) Model for simulation of residual stress in rock, in *Proc. 11th US Symp. Rock Mech.*, Berkeley, SME/AIME, 415–26.

Varnes, D.J. and Lee, F.T. (1972) Hypothesis of mobilization of residual stress in rock. *Geol. Soc. Am. Bull.*, **83**, 2863–6.

Vernik, L. and Zoback, M.D. (1992) Estimation of maximum horizontal principal stress magnitude from stress-induced well bore breakouts in the Cajon Pass scientific research borehole. *J. Geophys. Res.*, **97**, 5109–19.

Voight, B. (1966a) Interpretation of in-situ stress measurements. Panel Report on Theme IV, in *Proc. 1st Cong. Int. Soc. Rock Mech. (ISRM)*, Lisbon, Lab. Nac de Eng. Civil, Lisbon, Vol. III, pp. 332–48.

Voight, B. (1966b) Beziehung Zwischen grossen Horizontalen Spannungen im Gebirge und der Tektonik und der Abtragung, in *Proc. 1st Cong. Int. Soc. Rock Mech. (ISRM)*, Lisbon, Lab. Nac. de Eng. Civil, Lisbon, Vol. II, pp. 51–6.

Voight, B. (1971) Prediction of in-situ stress patterns in the Earth's crust, in *Proc. Int. Symp. on the Determination of Stresses in Rock Masses*, Lab. Nac. de Eng. Civil, Lisbon, pp. 111–31.

Voight, B. and Hast, N. (1969) The state of stresses in the upper part of the Earth's crust: a discussion. *Eng. Geol.*, **3**, 335–44.

Voight, B. and St. Pierre, B.H.P. (1974) Stress history and rock stress, in *Proc. 3rd Cong. Int. Soc. Rock Mech. (ISRM)*, Denver, National Academy of Sciences, Washington DC, 2A, pp. 580–82.

Warpinski, N.R. (1989) Determining the minimum in-situ stress from hydraulic fracturing through perforations. *Int. J. Rock Mech. Min. Sci. & Geomech. Abstr.*, **26**, 523–31.

Warpinski, N.R. and Teufel, L.W. (1987) In-situ stresses in low permeability, nonmarine rocks, in *Proc. SPE/DOE Joint Symp. on Low Permeability Reservoirs*, Denver, Paper SPE/DOE 16402, pp. 125–38.

Warpinski, N.R. and Teufel, L.W. (1991) In-situ stress measurements at Rainier Mesa, Nevada Test Site – influence of topography and lithology on the stress state in tuff. *Int. J. Rock Mech. Min. Sci. & Geomech. Abstr.*, **28**, 143–61.

Warpinski, N.R., Branagan, P. and Wilmer, R. (1985) In situ stress measurements at US DOE's multiwell experiment site, Mesaverde group, Rifle, Colorado. *J. Petrol. Technol.*, **37**, 527–36.

White, J.M., Hoskins, E.R. and Nilssen, T.J. (1978) Primary stress measurement at Eisenhower Memorial Tunnel, Colorado. *Int. J. Rock Mech. Min. Sci. & Geomech. Abstr.*, **15**, 179–82.

Whitehead, W.S., Hunt, E.R. and Holditch, S.A. (1987) The effects of lithology and reservoir pressure on the in-situ stresses in the Waskon (Travis Peak) field, in *Proc. SPE/DOE Joint Symp. on Low Permeability Reservoirs*, Denver, Paper SPE/DOE 16403, pp. 139–52.

Wong, I.G. (1993) The role of geological discontinuities and tectonic stresses in mine seismicity, in *Comprehensive Rock Engineering* (ed. J.A. Hudson), Pergamon Press, Oxford, Chapter 15, Vol. 5, pp. 393–410.

Worotnicki, G. and Denham, D. (1976) The state of stress in the upper part of the Earth's crust in Australia according to measurements in mines and tunnels and from seismic observations, in *Proc. ISRM Symposium on Investigation of Stress in Rock, Advances in Stress Measurement*, Sydney, The Institution of Engineers, Australia, pp. 71–82.

Worotnicki, G. and Walton, R.J. (1976) Triaxial hollow inclusion gauges for determination of rock stresses in-situ, Supplement to *Proc. ISRM Symposium on Investigation of Stress in Rock, Advances in Stress Measurement*, Sydney, The Institution of Engineers, Australia, pp. 1–8.

Zoback, M.D. (1991) State of stress and crustal deformation along weak transform faults. *Phil. Trans. Roy. Soc. London, A*, **337**, 141–50.

Zoback, M.D. (1993) In situ stress measurements and geologic processes, in *Lecture Notes of the Short Course on Modern* In-Situ *Stress Measurement Methods*, 34th US Symp. Rock Mech., Madison, Wisconsin.

Zoback, M.D. and Healy, J.H. (1992) In-situ stress measurements to 3.5 km depth in the Cajon Pass scientific research borehole: implications for the mechanics of crustal faulting. *J. Geophys. Res.*, **97**, 5039–57.

Zoback, M.D. *et al.* (1987) New evidence of the state of stress of the San Andreas fault system. *Science*, **238**, 1105–11.

Zoback, M.D. *et al.* (1993) Upper-crustal strength inferred from stress measurements to 6 km depth in the KTB borehole. *Nature*, **365**, 633–5.

Zoback, M.L. (1989) State of stress and modern deformation of the Northern Basin and Range province. *J. Geophys. Res.*, **94**, 7105–28.

Zoback., M.L. (1992) First- and second-order patterns of stress in the lithosphere: The World Stress Map project. *J. Geophys. Res.*, **97**, 11703–28.

Zoback, M.L. and Zoback, M.D. (1980) State of stress in the conterminous United States. *J. Geophys. Res.*, **85**, 6113–56.

Zoback, M.L. *et al.* (1989) Global patterns of tectonic stress. *Nature*, **341**, 291–8.

METHODS OF *IN SITU* STRESS MEASUREMENT

3

3.1 INTRODUCTION

Compared with other rock mass properties, rock stress is a difficult quantity to measure. As pointed out by Leeman (1959), 'It is impossible to measure stress directly since, in fact, it is a fictitious quantity. It is only possible to deduce the stresses in a solid body from the results of measurements using some indirect method'. Since stress can be represented by a secondorder Cartesian tensor, determination of the complete *in situ* stress field in three dimensions requires at least six independent pieces of information.

In general, all *in situ* stress measuring techniques consist of disrupting the rock. The response associated with the disturbance is measured (in the form of strain, displacement or hydraulic pressure record) and analyzed by making several assumptions about the rock's constitutive behavior, etc. The process of disturbance itself is usually accounted for in the analysis. A prerequisite when measuring the virgin stress field is that the rock's response to disturbance must be measured in regions far away from natural or artificial excavation boundaries. For underground openings, a distance of at least 1.5–2 times the opening span or diameter is suggested. Also, it is recommended that the measurements should be carried out away from major rock mass heterogeneities or fault zones unless the measurements are intentionally carried out to study the stress disturbance associated with such features.

Several factors need to be considered when planning a program of *in situ* stress measurements.

(1) The site geology and environmental aspects (and their variations) must be properly identified including topography, rock type, geological structures, anisotropy, heterogeneities and the likelihood of high stresses. Such factors are important since they will help, among other things, in selecting the methods of stress measurement that are the most suitable and the location of the measurements. They will also help in the interpretation of the measurements themselves. Other important factors involved in the decision process include the presence of water, the temperature of the rock and the water, and the possible influence of external conditions.

(2) The objectives of the stress measurements must be clearly identified and in particular how they will be integrated into the project of interest. This affects the selection of the stress measurement technique, the location of the measurements, how many measurements need to be carried out, and in what directions and depths.

(3) Equipment and personnel needs have to be assessed. (4) Available access and services need to be identified. (5) The budget and time available for stress measurements must be assessed.

(6) Finally, it must be kept in mind that, for a given project, stresses can be determined using several (direct or indirect) methods at the same location or at different locations. This approach is highly recommended since it will provide a measure of consistency and reliability. The

data obtained with each method may be analyzed separately and checked to see if the simplifying assumptions associated with each method are met. The data from different methods may also be combined in order to impose more rigorous constraints on the *in situ* stresses. The combination of data is also vital when a limited number of tests from each method is available. Also, stress measurements can be done in several stages with one or several methods. The idea here is to use the best attributes of different methods for a given project. For instance, Enever (1993) recommends using hydraulic fracturing for the initial planning of engineering projects and then conducting overcoring measurements to obtain a more refined description of the *in situ* state of stress. In general, combining several methods based on their respective attributes can help in obtaining a more reliable assessment of the *in situ* stress field. The benefits of using hybrid stress methods are discussed in Haimson (1988), Cornet (1993) and Brudy *et al.* (1995).

Over the past 30 years, various techniques for measuring *in situ* stresses have been developed and improved. As shown in Table 3.1, these techniques can be divided into six main groups: hydraulic methods, relief methods, jacking methods, strain recovery methods, borehole breakout methods and others. This chapter gives an overview of the different methods and presents a summary of their respective advantages and disadvantages and their range of application. Each one of the first five techniques is a subject of a chapter in this book. This chapter also presents a discussion on the volume of rock involved in the different methods of rock stress measurement and reviews the sources of uncertainties in stress determination.

Table 3.1 Methods of *in situ* stress measurement and estimates of rock volume involved in each method

	Method	*Volume (m^3)*
Hydraulic methods	Hydraulic fracturing	0.5–50
	Sleeve fracturing	10^{-2}
	Hydraulic tests on pre-existing fractures (HTPF)	1–10
Relief methods	Surface relief methods	1–2
	Undercoring	10^{-3}
	Borehole relief methods (overcoring, borehole slotting, etc.)	10^{-3}–10^{-2}
	Relief of large rock volumes (bored raise, under-excavation technique, etc.)	10^{2}–10^{3}
Jacking methods	Flat jack method	0.5–2
	Curved jack method	10^{-2}
Strain recovery methods	Anelastic strain recovery (ASR)	10^{-3}
	Differential strain curve analysis (DSCA)	10^{-4}
Borehole breakout method	Caliper and dipmeter analysis	10^{-2}–10^{2}
	Borehole televiewer analysis	10^{-2}–10^{2}
Other methods	Fault slip data analysis	10^{8}
	Earthquake focal mechanisms	10^{9}
	Indirect methods (Kaiser effect, etc.)	10^{-4}–10^{-3}
	Inclusions in time-dependent rock	10^{-2}–1
	Measurement of residual stresses	10^{-5}–10^{-3}

3.2 HYDRAULIC METHODS

Hydraulic methods measure the state of stress *in situ* in boreholes. Pressure is applied along a section of a borehole isolated by packers and is increased until existing fractures are open or new fractures are created. The fluid pressure required to open, generate, propagate, sustain and reopen fractures in rock at a given depth is measured and is related to the existing *in situ* stress field. The direction of the *in situ* stresses is inferred by observing or measuring the orientation of the hydraulically induced or open fractures.

Hydraulic methods can be divided into three subgroups: the hydraulic fracturing method, the sleeve fracturing method, and the hydraulic tests on pre-existing fractures (HTPF) method. All three types have the main advantage that they do not require advanced knowledge of the rock deformability properties and that they can be carried out without much difficulty below the water table. Hydraulic methods are discussed in more detail in Chapter 4.

3.2.1 HYDRAULIC FRACTURING

Hydraulic fracturing is by far the most popular of the three hydraulic methods. Fairhurst (1964) was the first to recommend such a method for stress measurement. The methodology has been tested in deep to very deep vertical holes and in various (but continuous) rock conditions. The deepest hydraulic fracturing tests conducted to date have been at depths between 6 and 9 km (Te Kamp, Rummel and Zoback, 1995). The vertical and horizontal stresses are assumed to be principal stresses and the vertical stress is assumed to be due to the weight of the overburden rock. The rock is cracked by pumping water or drilling mud in a section of a borehole. The orientation of the resulting fracture is obtained using televiewers or impression packers. By far the largest proportion of *in situ* stress measurements by hydraulic fracturing has been obtained when vertical fractures are formed. In that case, the least horizontal stress is inferred from the pressure (also called shut-in pressure) at which the induced fractures close in the pressure–time record. Several interpretation procedures have been proposed on this subject. The largest horizontal stress is determined from the pressure–time record, the stress concentrations around a circular hole in an isotropic medium and knowledge of the rock tensile strength. Various interpretation procedures have been proposed in the literature with regard to what value of the tensile strength should be used, the type of stress analysis (Kirsch solution or fracture mechanics) to be employed for different rock types, and the effect of temperature, fluids and poroelasticity. Both horizontal stress components are determined by hydraulic fracturing if the measurements are made in vertical open holes. In cased holes with perforations, which are more popular in the oil and gas industry, only the minimum horizontal stress can be determined accurately.

In general the interpretation of hydraulic fracturing tests in very porous rocks can be difficult. Also, in sedimentary rock formations, hydraulic fracturing requires relatively thick formations of at least 2–3 m and preferably larger. The applicability of hydraulic fracturing under hostile conditions such as under very high stresses and very high temperatures (above 200°C), which are found in ultradeep boreholes, is very limited. There it is difficult to crack the rock and special equipment (valves, tubings and packers) is required. Also, the rock may show nonlinear as well as ductile behavior with possible borehole wall breakouts.

3.2.2 SLEEVE FRACTURING

Sleeve fracturing is similar to hydraulic fracturing except that it has the major advantage that no fluid penetrates the rock upon fracturing. The method was first proposed by Stephansson (1983). A neoprene (hard rubber) membrane is inserted into the borehole and

pressurized. As in conventional hydraulic fracturing, a fracture is initiated at the borehole wall once the pressure exceeds the rock tensile strength and the fracture propagates in the direction perpendicular to the least horizontal *in situ* stress. The maximum and minimum principal stresses in the plane perpendicular to the borehole are determined from the breakdown and reopening pressures of an induced single or double fracture at the borehole wall, and by using Kirsch solution. The fracture orientation is determined using impression packers. Until fracturing, the test is essentially a dilatometer test which can be used to determine the rock mass modulus of deformation, by assuming a value for the rock's Poisson's ratio. A drawback of the sleeve fracturing method is that, compared with hydraulic fracturing, the breakdown pressure is not well defined, thus complicating the interpretation of the field test results. Another limitation is that the induced fractures do not propagate far from the borehole wall.

3.2.3 HTPF METHOD

The HTPF method is the only hydraulic method and the only *in situ* stress determination method at great depth, where the borehole does not have to be assumed to be vertical and perpendicular to a principal *in situ* stress component. The method was first proposed by Cornet (1986) and consists of reopening an existing fracture of known orientation that has previously been isolated in between two packers. From that point of view, it is the opposite of hydraulic fracturing where sections of boreholes with competent rock are sought. By using a low flow rate of injection, the fluid pressure which balances exactly the normal stress across the fracture is measured. The method is then repeated for other non-parallel fractures of known orientation. Since the normal stress across a fracture depends on the six components of the *in situ* stress field and the orientation of the fracture with respect to that stress field, a system of equations can be created to determine the six *in situ* stress components without making any assumption with regard to the orientation of the principal stresses and the rock's constitutive behavior. The system can account for the lateral and vertical variations of the *in situ* stress field in the volume of rock involved in the HTPF tests. Further, the method does not require determination of the rock's tensile strength and is independent of pore pressure effects. The HTPF method requires the same equipment as the hydraulic fracturing method. However, when conducting HTPF tests, special attention must be placed on the fracture itself as it must be of a size for which the normal stress can be assumed to be uniform and its geometry must be planar. The HTPF method requires a large number of tests on fractures of various dips and strikes in a region where the stress field can be assumed to be continuous. Further, the rock mass cannot be too fractured since each fracture needs to be isolated. Finally, it has been found that the HTPF method does not work well in heterogeneous (stratified) rock formations, but works well in homogeneous rock formations (Burlet, Cornet and Feuga, 1989).

3.3 RELIEF METHODS

The main idea behind relief methods is to isolate (partially or wholly) a rock sample from the stress field in the surrounding rock mass and monitor its response. This can be done by different methods such as over- or undercoring holes, cutting slots or underexcavation. The stresses are not related to applied pressures such as in hydraulic methods. Instead, the stresses are inferred from strains or displacements created by the relief (unloading) process and measured on isolated rock samples, in boreholes or on the surrounding rock associated with the relief process. The successful interpretation of stress relief tests depends to a great extent on the ability (1) to establish a stress–strain (or displacement)

relationship for the rock, (2) to be able to determine rock mass properties from tests on samples, and (3) to have instrumentation sensitive enough to capture small strains or displacements. It is common practice to relate strains or displacements to the *in situ* stress components through equations derived from the theory of linear elasticity. Borehole and surface relief methods require rock volumes to be fracture-free. Other techniques, such as under-excavation, do not have those limitations. In general, relief methods originally developed for hard rocks have been tested for use in less ideal materials such as weak and soft rocks, as well as evaporitic rocks such as rock salt and potash. The success rate in such rock conditions has been found to vary a lot.

Several stress relief methods have been proposed since the early 1930s. They can be divided into three major groups: (1) the methods that involve strain or displacement measurements on rock surfaces in underground or surface excavations, (2) the methods that use instruments in boreholes, and, (3) the methods that involve the response of large volumes of rock. Relief methods are discussed in more detail in Chapter 5.

3.3.1 SURFACE RELIEF METHODS

Surface relief methods were the very first techniques used to determine *in situ* stresses on underground excavation walls. Rock surfaces are first instrumented with gages or pins. Then, the rock response to stress relief (by cutting or drilling) is obtained by recording the gages and pins before and after the relief process. A well-known surface relief method is that of stress relief by center hole or undercoring of Duvall (1974), where a hole 6 inches (152 mm) diameter is drilled at the center of a circle 10 inches (254 mm) in diameter along which six pins have been installed 60° apart. The pin displacements induced by drilling are related to the *in situ* stress components in the plane of the rock surface.

Surface relief methods suffer from many limitations. First, the performance of the gages or pins can be affected by humidity and dust. Second, the strains or displacements are measured on a rock that may have been disturbed and damaged by weathering and the excavation process itself. Third, stress concentration factors have to be assumed in order to relate the stresses measured locally in the walls of the excavation to the far-field stress components.

3.3.2 BOREHOLE RELIEF METHODS

The methods that use instruments in boreholes, also known as overcoring methods, are by far the most commonly used relief methods. They can be classified as total relief methods. First, a large-diameter hole is drilled to the required depth in the volume of rock in which stresses have to be determined. In some techniques, a small pilot hole is drilled at the end of the previous hole. An instrumented device that can measure strains or displacements is inserted into the pilot hole. Then, drilling of the large-diameter hole is resumed and resulting changes of strain or displacement within the instrumented device are recorded. A variety of instrumented devices are available. Devices that seem to have had a high success rate in the field include the South African CSIR triaxial strain cell (Leeman and Hayes, 1966), the Australian CSIRO Hollow Inclusion (HI) Cell (Worotnicki and Walton, 1976), and the US Bureau of Mines (USBM) gage (Merrill, 1967). Most of these devices work well at distances not exceeding 10–50 m from existing free surfaces and in good rock conditions. They usually require unbroken cores at least 150 to 300 mm in length. Several modified versions of the CSIR triaxial strain cell and USBM gage have been proposed in the literature and some of them have recently been tested in vertical water-filled boreholes down to a depth of 500–1000 m.

Another technique consists of attaching an instrumented device at the bottom of the large-diameter hole which is then overcored.

This approach does not require a pilot hole and has been used with the South African CSIR 'Doorstopper' (Leeman, 1971) at distances from free surfaces not exceeding 60 m. Furthermore, the overcore does not have to be long as for the other overcoring methods. A length of core of as little as 50 mm is required for successful overcoring, thus making this instrument very useful for measuring stresses in weak and broken ground and in rocks under high stresses for which core disking is common.

A third and more recent technique was developed in Japan and consists of attaching a spherical or conical strain cell to the bottom of a pilot hole which is then overcored (Kobayashi *et al.*, 1991; Sugawara and Obara, 1995). After drilling the hole, its bottom surface is reshaped into a spherical or conical shape using special drill bits. Thereafter, the bottom surface is ground and polished before the strain cell is bonded onto the rock. During the overcoring operation, changes in strain are recorded continuously. Like the CSIR Doorstopper, a small volume of rock is required for overcoring.

Depending on the instrument used to monitor the rock during overcoring, the complete state of stress can be determined in one, two or three non-parallel boreholes. No assumption needs to be made regarding the *in situ* stress field as with the hydraulic fracturing method. Some problems may arise, however, with the installation of some of the instrumented devices *in situ*, in particular in wet and dusty environments and poor rock conditions. However, many of those problems seem to have been remedied over the past 5 to 10 years. Furthermore, when using more than one borehole, the stress field needs to be somewhat homogeneous throughout the volume of interest.

The success rate with overcoring methods rarely exceeds 50% (Herget, 1993). The overcoring method is also limited by the magnitude of the *in situ* stresses themselves. It can only be used at depths for which the strength of the rock in the wall and bottom of the borehole is not exceeded. Phenomena such as core disking or shearing off of thin flakes of rock may make strain or displacement measurements during overcoring very difficult and the analysis meaningless. Hast (1979) suggested that with overcoring, and because of these phenomena, the maximum recordable stress is about 100 MPa. Herget (1986) reported measured stresses in high-strength rocks in the Canadian Shield as high as 130 MPa, and at a depth of 2100 m.

An innovative but different borehole relief method called 'borehole slotting' was proposed by Bock and Foruria (1983) and Bock (1986). It consists of cutting three longitudinal slots, 120° apart, into the wall of a borehole. Tangential strains induced by release of tangential stresses are measured on the borehole surface in the near vicinity of each slot. This is a partial relief method which does not require any overcoring. The method is fast, and the instrument is reusable and is self-contained in both its stress release operations and strain measuring capabilities. However, the method is limited to two-dimensional analysis.

3.3.3 RELIEF OF LARGE ROCK VOLUMES

The main drawback with surface and borehole relief methods is that they involve small rock volumes. Thus the measured stresses can be sensitive to changes in the mineral composition of the rock and to the rock grain size. Relief methods involving much larger rock volumes have been proposed. One method consists of overcoring several strain gages on the surface of a large-diameter bored raise and at different levels in the bored raise (Brady, Friday and Alexander, 1976; Brady, Lemos and Cundall, 1976; Chandler, 1993). The data can be analyzed to determine the local stresses or to determine the average stress over the entire volume of rock involved in all the measurements.

Other techniques consist of using measurements made while excavating an underground opening. This approach was proposed

simultaneously by Zajic and Bohac (1986) and Sakurai and Shimizu (1986). The rationale of this approach is to measure displacements in one or several cross-sections of an opening following excavation. The displacements are related to the *in situ* stress field using analytical methods or numerical methods (finite element or boundary element method). Simplifying assumptions are usually made about the mechanical properties of the rock. Another back-analysis approach, called the under-excavation technique by Wiles and Kaiser (1994), uses measurements in the near vicinity of an advancing excavation. Combined measurements, such as strains from CSIR or CSIRO HI cells and displacements measured with convergence gages, extensometers, closure meters, tiltmeters or inclinometers, are used simultaneously to determine the three-dimensional *in situ* stress field. The *in situ* stress field is determined (using a three-dimensional boundary element method) as the stress field that gives the 'best fit' to the measured displacements and strain changes associated with the advancing excavation.

3.4 JACKING METHODS

Jacking methods are sometimes called 'stress compensating methods'. The equilibrium of a rock mass is disturbed by cutting slots (planar or circular) on rock surfaces. This in turn creates deformations that are measured with reference pins or strain gages placed in the near vicinity of the slots. Equilibrium is restored by inserting a device such as a jack in the slots. Then the jack is pressurized until all deformations have vanished. *In situ* stresses are determined from the rock response during pressurizing assuming the rock response to be elastic.

The flat jack method is by far the most popular of all jacking methods. When using flat jacks, the cancellation pressure is used as a direct estimate of the stress normal to the jack. Since each flat jack test yields one component of the *in situ* stress field, a total of six tests need to be carried out to obtain the complete *in situ* stress field.

The flat jack method represents one of the first techniques used in rock mechanics for measuring *in situ* stresses (Mayer, Habib and Marchand, 1951). It was very popular in the 1950s and 1960s. The main advantage of the flat jack method is that it does not require knowledge of the elastic constants of the rock in order to determine the tangential stress at points in the wall of an excavation, and the stresses are measured directly. Furthermore, the equipment used in flat jack tests is rugged and stable. Also, relatively large rock volumes can be involved in the tests and the stresses can be determined over large areas. Nevertheless, flat jacks have many disadvantages and limitations that limit their range of application. Jacking methods are discussed more extensively in Chapter 6.

3.5 STRAIN RECOVERY METHODS

Strain recovery methods are based on monitoring the response of core samples following drilling. In many ways they can be seen as relief methods.

One method, called the anelastic strain recovery (ASR) method, consists of instrumenting an oriented core sample following its removal from a borehole and monitoring its strain response as it continues to recover (or relax) from the *in situ* state of stress (Teufel, 1982). It is assumed that the direction of the principal recovery strains coincides with the direction of the *in situ* principal stresses. Determination of *in situ* stress magnitudes using the ASR method requires a viscoelastic model for the rock response to unloading. In the analysis, the vertical stress is usually assumed.

Another technique, called the differential strain curve analysis (DSCA) method, consists of applying a hydrostatic pressure to a cubic sample cut from an oriented drill core following its removal from the ground (Strickland and Ren, 1980). Microcracks which developed during drill core removal and its expansion

are then closed under pressure. The response of the cubic sample to hydrostatic loading is monitored using strain gages previously attached to its surfaces. Using a minimum of six strain gages, the principal strains due to microcrack closure and their orientation can be determined. The principal directions of the current *in situ* stress field and ratios between the three principal *in situ* stresses can be determined assuming (1) that most of the microcracks in the core samples are due to the relief of the current *in situ* stress field, (2) that the *in situ* stress tensor has the same orientation as the strain tensor due to crack closure, and (3) that the cracks are proportional volumetrically to the *in situ* stress magnitude in any direction.

Strain recovery methods have been found to be very well suited for stress measurements in deep to very deep wells for which many of the other techniques do not work and for which only small core samples are available. Several examples proposed in the literature have shown that those methods can give reasonable measurements of *in situ* stresses, especially when combined with hydraulic methods. Strain recovery methods are discussed in more detail in Chapter 7.

3.6 BOREHOLE BREAKOUT METHOD

The rock around boreholes may not be able to sustain the compressive stress concentration associated with the process of drilling itself. Breakage of the rock results in two diametrically opposed zones of enlargement called 'breakouts'. In vertical boreholes, the smallest horizontal *in situ* stress component is assumed to coincide with the breakout direction. When logged in vertical boreholes, using tools such as dipmeters or borehole televiewers, breakouts can give an estimate of the orientation of the maximum and minimum horizontal principal stresses and the variation of that orientation with depth.

Breakouts have been used as an indicator of *in situ* stress orientation in boreholes several kilometers deep and in all rock types. The deepest breakouts analyzed have been at a depth of about 11.6 km in the Kola Peninsula hole in the former Soviet Union (Zoback, Mastin and Barton, 1986). In general, breakouts have helped to bridge the gap between near-surface stress indicators and deep stress indicators from earthquake focal mechanisms. They are useful as stress indicators at large depths for which it is difficult to conduct direct measurements of stress.

In general, it is difficult to use borehole breakouts to estimate the magnitude of *in situ* stresses (although several attempts have been proposed using the breakout geometry). Several models have been proposed for the formation of breakouts. In these models the principal *in situ* stresses are assumed to be horizontal and vertical. A conventional approach is to assume that breakouts are formed in shear and that their location can be predicted using the Kirsch solution for the stresses around a circular hole drilled in a linear elastic, isotropic and homogeneous continuum subject to a three-dimensional stress field at infinity. A Mohr–Coulomb failure criterion is superimposed on the elastic stress field in order to determine where failure takes place. This theory may have limited value if the rock is anisotropic or time dependent and/or yielding of the borehole wall takes place. Despite these limitations, borehole breakouts have played a major role in defining stress provinces in the World Stress Map Project, and are reliable indicators of the direction of horizontal principal stresses in vertical boreholes. The borehole breakout method is discussed further in Chapter 8.

3.7 OTHER METHODS

3.7.1 FAULT-SLIP DATA ANALYSIS

As discussed in section 2.14.1, measurement of slickensides on a population of faults can be used to determine the orientation as well as the magnitude of the *in situ* stress field. This method, which involves large rock volumes

(at the outcrop scale), is based on three assumptions: (1) all the slickensides on the faults in the population are related to a given but unknown stress tensor, (2) motion on each fault plane is parallel to the acting shear stress on that plane, and (3) fault motions are independent. These provisos are important since they somewhat limit the range of application of the method.

This method has the main advantage that advance knowledge of the rock deformability properties is not required. However, Coulomb friction and the aforementioned assumptions are implied in the analysis. If the method is used to determine the current *in situ* stress field, there must be enough evidence that the striations used in the analysis are related to that stress field only. The same limitations apply if striations on fractures in core samples are used instead of striations on outcrop fractures, as suggested by Hayashi and Masuoka (1995). It is noteworthy that using striations on oriented core samples to determine *in situ* stresses has great potential in rock engineering.

3.7.2 EARTHQUAKE FOCAL MECHANISMS

As discussed in section 2.14.2, the first motion analysis of earthquakes can provide the sense of faulting, and the relative magnitudes of the three *in situ* principal stress components and their orientation. It is the only method that provides data about *in situ* stresses at mid-crustal or greater depths (5–20 km) and involves very large rock volumes. The method is most effective for large earthquakes that occur deep within the crust at plate boundaries, but is also applicable to small earthquakes within the interior of lithospheric plates and in the vicinity of mines and oil and gas fields.

3.7.3 INDIRECT METHODS

Indirect methods measure stresses by looking at changes in some physical, mechanical or other rock properties as a result of a change in stress. Beside relief methods that use strains and displacements, other techniques include monitoring of opening displacement and convergence measurements (Martin, 1989), the acoustic method (Rivkin, Zapolskiy and Bogdanov, 1956), seismic and microseismic methods (Bridges *et al.*, 1976; Martin, Read and Lang, 1990; Swolfs and Handin, 1976; Talebi and Young, 1989), sonic and ultrasonic methods (Aggson, 1978; Mao *et al.*, 1984; Pitt and Klosterman, 1984; Sun and Peng, 1989), the radioisotope method (Riznichanko *et al.*, 1967), the atomic magnetic resonance method (Cook, 1972) and electromagnetic methods (Petukhov, Marmorshteyn and Morozov, 1961). The *in situ* state of stress can also be measured by using holographic methods (Smither, Schmitt and Ahrens, 1988; Smither and Ahrens, 1991; Schmitt and Li, 1993) where displacements induced by the drilling of a small (stress-relieving) hole at three different locations in the wall of a borehole are measured using double-exposure optical holograms. The reader should note that these various techniques are listed here for completeness but will not be the subject of discussion in this book since they have not yet gained much popularity in practice.

Some remarks need to be made, however, about a method called the Kaiser effect method which has been investigated over the past 10 years as a potential method for determining *in situ* stresses. Research originally conducted by Kaiser (1950) on the acoustic emission of metal revealed that when the stress on metal is relaxed from a certain level and then increased, there is a significant increase in the rate of acoustic emission as the stress exceeds its previous higher value. Several attempts have been made to use this observation, also known as the Kaiser effect, as a method for determining *in situ* stresses in rock. In particular, it has been hypothesized for a long time that the stress experienced by a rock *in situ* could be inferred by monitoring acoustic emission on core samples cut from

different directions and loaded cyclically in uniaxial compression in the laboratory. An extensive review of the different studies conducted on the Kaiser effect can be found in Holcomb (1993). Despite encouraging results obtained by several authors showing a fairly good correlation between stresses determined with the Kaiser effect and with other methods, research carried out by Holcomb (1993) revealed that using the acoustic emission emitted during uniaxial compression laboratory tests to infer *in situ* stresses could not be justified.

3.7.4 INCLUSIONS IN TIME-DEPENDENT MATERIALS

Inserting and casting an inclusion in a borehole drilled in an already stressed material with creep properties can theoretically be a technique to measure *in situ* stresses in rock. Indeed, viscoelasticity theory tells us that with time the steady state of stress in the inclusion will approach the absolute stress in the rock (Peleg, 1968). Thus if the creep characteristics of the rock are known, stresses can be deduced from inclusion readings over shorter periods of time (Berry and Fairhurst, 1966; Leeman, 1971).

This concept has been used in the literature for measuring *in situ* stresses in viscoelastic rocks such as rock salt or potash for which other methods of stress measurements have had a limited amount of success. Inclusions such as the vibrating wire stressmeter, flat jacks and other borehole pressure cells such as the Glötzl (or Gloetzl) cell have been installed in rock masses or in boreholes to measure absolute stresses, and thereafter monitor stress changes. An interesting application of this method was demonstrated by Natau, Lempp and Borm (1986) in Germany and by Lu (1986) from the US Bureau of Mines in Denver, Colorado. Lu (1986) used a system of three pressure cells (one cylindrical cell and two flat cells) to determine absolute stresses and stress changes in salt and coal.

3.7.5 MEASUREMENT OF RESIDUAL STRESSES

As discussed in Chapter 2, residual stresses represent a class on their own. There seems to be a consensus in the literature that they exist on at least two different scales: the microscopic scale and the macroscopic scale. Depending on the scale that is being considered, the methods used for the measurement of residual stresses are different. At the microscopic scale (crystal or grain scale), possible methods include the calorimetric technique, the X-ray technique and the spot-drilling or center hole-drilling technique. A review of these methods can be found, for instance, in Voight (1966) and Bock (1979). It is noteworthy that all these methods were borrowed from the study of residual stresses in metals. At the macroscopic level (specimen to rock mass), overcoring of overcored specimens (double overcoring) or undercoring of undercored specimens is highly recommended.

3.8 ROCK VOLUME IN STRESS MEASUREMENTS

All the techniques mentioned above involve rock volumes that differ by several orders of magnitude. A list of volume estimates is given in Table 3.1. According to this table, very few of the stress measurement methods involve large volumes of rocks. The earthquake focal mechanism method provides stress information at mid-crustal or greater depths and includes by far the largest rock volumes, of the order of 10^9 m^3. The fault-slip data analysis method comes next with slightly smaller rock volumes, of the order of 10^8 m^3, because of its surface nature. This is followed by the large rock volume relief methods. For instance, the overall volume of rock involved in the bored raise tests of Brady, Lemos and Cundall (1986) has been estimated to be about 100 m^3 (Fig. 3.1a). According to Zou and Kaiser (1990) and Wiles and Kaiser (1994), the under-excavation technique involves several hundred or thousand cubic meters of rock (Fig. 3.1b). All these methods

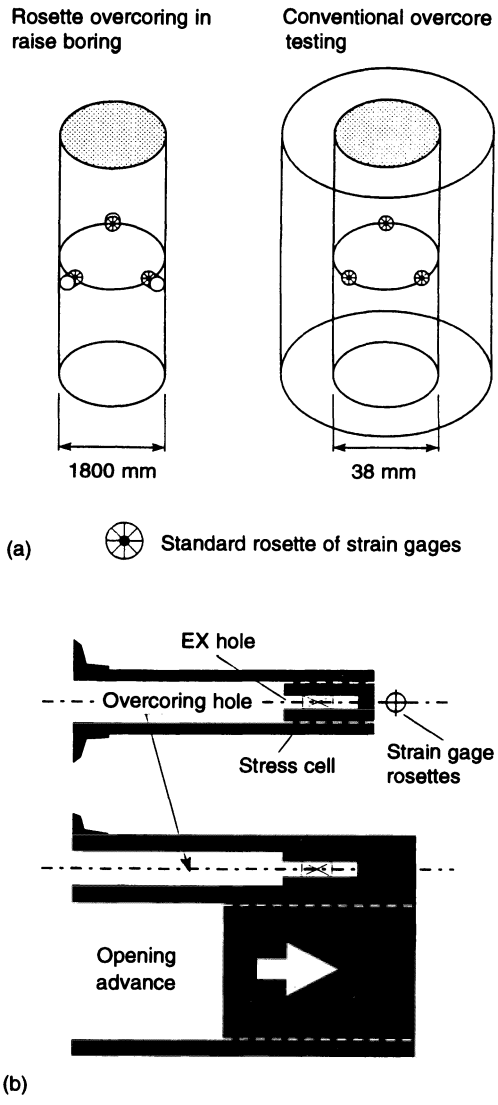

Fig. 3.1 Examples of stress measurement methods involving larger rock volumes than conventional overcoring. (a) Bored raise method where strain rosettes are installed on the wall of a 1.8 m diameter bored raise (adapted from Martin, Read and Lang, 1990); and (b) under-excavation technique where rock mass deformation or strain is measured in the near vicinity of an advancing opening. (Adapted from Zou and Kaiser, 1990.)

give average values of the *in situ* stress field and eliminate the effect of local rock mass irregularities on the stress measurements.

Most other stress measurement methods, in particular those that use borehole devices, involve small rock volumes and provide only pointwise measurements of the *in situ* stress field (Leijon, 1989). For instance, overcoring methods involve rock volumes ranging between only 10^{-3} and $10^{-2}\,m^3$, depending on the size of the overcore diameter. Hydraulic tests, and in particular hydraulic fracturing tests, involve somewhat larger rock volumes (0.5–50 m^3) than the overcoring techniques since the borehole is pressurized over a distance of the order of ten borehole diameters. Flat jacks and other surface relief methods can involve volumes as large as 0.5–2 m^3. The strain recovery methods and all the techniques based on measurements on small core samples involve small rock volumes not exceeding $10^{-3}\,m^3$. Finally, borehole breakouts involve rock volumes (10^{-2}–$10^{2}\,m^3$) intermediate between those of the deep stress methods and those of the near-surface stress methods.

In general, the methods that involve small volumes are more likely to capture local distortions of the regional stress field. With such methods, wide variations in stress magnitude and orientation among closely spaced measurements are common. Due to the localized nature of the measurements, the measured stresses can be sensitive to changes in the mineral composition of the rock, the microstructures of the rock and the rock grain size (Leijon, 1989).

3.9 ACCURACY AND UNCERTAINTY IN STRESS MEASUREMENTS

A basic question that is often raised in practice is: can we measure stresses in rock with sufficient accuracy? In the literature there is a general consensus that stress measurements are seldom accurate. Accuracy, being a measure of deviation from a known value (Holman, 1989), becomes meaningless when measuring stresses *in situ* since we do not have beforehand a known value with which to compare the measurements. The accuracy of an

instrument to measure stresses can only be assessed by controlled laboratory tests where the measured stresses are compared with the applied stresses.

It is common practice to present *in situ* stress measurements with a plus or minus range or confidence interval which relates to the uncertainty in the measurements. Three types of uncertainty are considered below: (1) natural (intrinsic, inherent) uncertainty, (2) uncertainty related to the process of stress measurement itself, and (3) uncertainty associated with the analysis of the stress measurement data.

3.9.1 NATURAL (INTRINSIC, INHERENT) UNCERTAINTY

Natural (or intrinsic, inherent) uncertainty stems from the fact that, by definition, *in situ* stresses vary from point to point in a rock mass, can change over short distances, are volume dependent and depend on the mechanical properties, the geological structures and the fabric of the rock mass (Chapter 2). As discussed in section 2.6, the local stresses in a rock mass consisting of different units with different elastic properties can be quite different from the average stress. Contrast in stress with depth in a single hole or laterally from one hole to the next can be expected in most sedimentary rock formations and lava flow deposits. They can also be found randomly in uniform hard rock conditions as shown in Fig. 3.2 (Leijon, 1989). Such local variations are intrinsic and should not always be seen as anomalies or errors in the measurements themselves.

Rock properties entering into the analysis of stress measurements can themselves vary throughout a rock mass, along the length of a borehole, or even over the length of an overcore. Enever, Walton and Wold (1990) reported variations in Young's modulus of sedimentary rocks in a coal field in New South Wales, Australia by a factor of up to 2 within a core length of 0.2 m. Such extreme variations

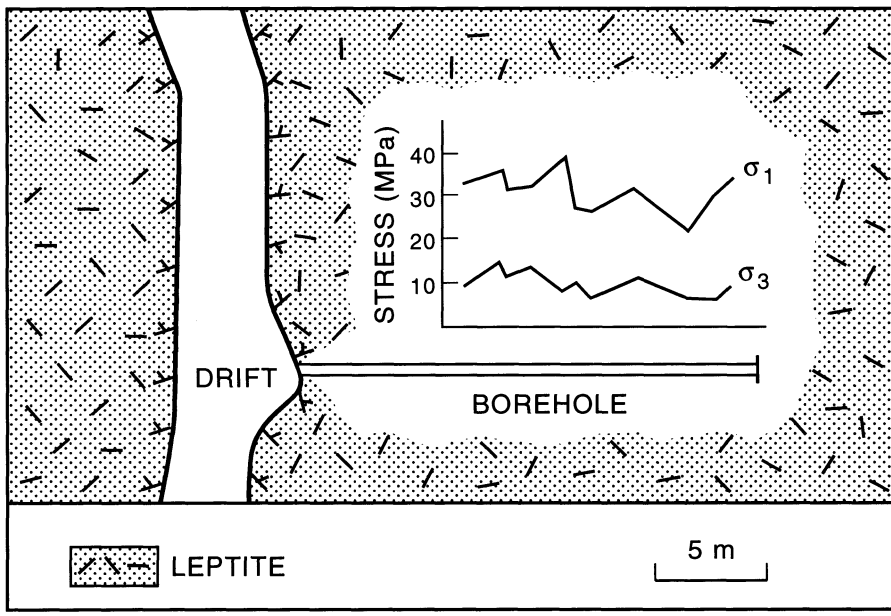

Fig. 3.2 Random variations of principal stresses measured along a borehole in uniform rock conditions. (Source: Leijon, B.A., Copyright 1989, with kind permission from Elsevier Science Ltd, The Boulevard, Langford Lane, Kidlington, UK.)

were found to be critical in the analysis of overcoring tests. Figure 3.3 shows, for instance, the variation in the Young's modulus of a granitic rock, over a borehole length of 5 m, reported by Aytmatov (1986). Here the modulus shows cyclical variations and varies by 20 to 25% over short distances. If this modulus enters into the calculation of the stresses, such as in overcoring, one would expect large variations in the calculated stresses. In overcoring, the Young's modulus enters as a multiplier between *in situ* stresses and measured strains or displacements. Thus a 5% error in the Young's modulus would result in a 5% error in all the stress components provided all other factors are constant. As far as the Poisson's ratio is concerned, the problem is more complicated. For the CSIR cell, Van Heerden (1973) found that errors in the Poisson's ratio yielded much smaller errors in the stresses compared with errors in the Young's modulus.

Uncertainty can also be created by rock anisotropy, heterogeneities and grain and pore size (Cyrul, 1983). Local stresses at the grain size level can be quite different from the average stress. This needs to be taken under consideration, in particular if the scale of the measurements (such as with strain gages) is comparable to the average grain size.

3.9.2 MEASUREMENT-RELATED UNCERTAINTY

Uncertainty when measuring *in situ* stresses may be associated with errors due to blunders in the construction of the apparatus or instrument used to measure stresses. Errors may also come from the experimental procedure itself.

In overcoring tests, possible errors may arise due to creep of the glue or creep of the instrument itself, malfunctions and idiosyncrasies of strain gages or other sensing elements, movement of the measuring cell in the pilot hole, poor instrument installation, breaking of overcore samples due to inherent cracks, temperature of drilling water, heat generated by drilling, humidity effects, electrical problems, borehole eccentricity, borehole oversize, etc. At the Underground Research Laboratory (URL) site in Canada, it was estimated that an error of ±5° in the installation of overcoring measuring devices would result in principal stress trend errors of ±15° (Martin, Read and Chandler, 1990).

The accuracy of instruments which use strain gages as measuring devices depends greatly on changes in temperature (rock, drilling water or environment). This is a complex problem because of the transient nature of the temperature gradients in the overcore

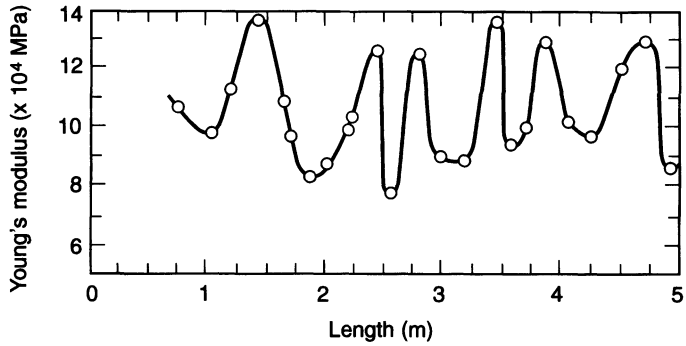

Fig. 3.3 Variation of modulus of elasticity along a borehole in granitic rock. (After Aytmatov, 1986.)

samples. Martin, Read and Chandler (1990) concluded that temperature variations of less than 2°C do not significantly affect the overcoring test results. On the other hand, variations of 8°C can change principal stress magnitudes by as much as 25%. The accuracy of the instruments can also vary with the type of temperature compensation scheme used (Cai, 1990) and if a quarter-bridge, half-bridge or full bridge is used (Garritty, Irvin and Farmer, 1985).

Tsur-Lavie and Van Ham (1974) investigated different sources of error when measuring stresses with the undercoring method. They found that errors in the readings of the pin displacements of 0.001 mm would result in small errors in the calculated stresses if the stresses are high. They also found that hole eccentricity and errors in measuring pin location would only result in small errors when calculating the stresses. The conclusions of Tsur-Lavie and Van Ham (1974) should probably apply to other surface methods as well.

All the problems mentioned above are even more critical when conducting measurements at shallow depths, for which the measured strains or displacements are in general small and the measuring instruments work near their limit of resolution. In such conditions, slight changes in the experimental conditions, such as changes in temperature during overcoring, could drastically affect the measurements (Cooling, Hudson and Tunbridge, 1988; Garritty, Irvin and Farmer, 1985). Furthermore, as discussed in Chapter 1, stresses at shallow depths may also be affected by phenomena such as diurnal and seasonal variations in temperature, and Moon pull, which may add to the observed scatter.

When using more than one borehole to determine the *in situ* state of stress such as with the USBM gage or the CSIR Doorstopper, errors may arise if the volume of rock involved with all the boreholes is too large. The volume must be kept to a minimum and within the size of the stress domain. On the other hand, when measuring *in situ* stresses, we want a volume large enough to obtain a representative sample of the *in situ* stress field.

In hydraulic fracturing tests, errors may arise if the borehole is inclined and is not vertical. Even if it is vertical, hydraulic fractures may initially (or not) propagate in the vertical direction and then turn to become parallel to most favorably oriented preexisting natural cracks, joints or partings in the rock. This phenomenon can create a major source of error in the analysis of hydraulic fracturing tests (Brown, 1989). According to Haimson (1988), the conventional theory for the analysis of hydraulic fracturing tests assuming a vertical fracture gives reliable estimates of the *in situ* stress field as long as the fracture deviates only several degrees from the vertical (less than 20°). Additional sources of uncertainty when measuring *in situ* stresses with hydraulic fracturing might be related to the malfunction of packers, valves and pumps or to the use of cased instead of open holes.

3.9.3 DATA ANALYSIS-RELATED UNCERTAINTY

Uncertainty can be associated with errors in the selection of data to be analyzed, such as strains or deformations in overcoring tests. For instance, neglecting strain gage length when analyzing overcoring results may create some error. Natau (1974) and Amadei (1986) reported errors of 2 and 5% for the CSIR and CSIRO HI cells placed in 38 mm diameter holes. Mills and Pender (1986) recommended using smaller strain gages of the order of 5 mm in length rather than 10 mm. They found that for longer gages, the average strain could be quite different from the strain at the middle of the gage. When analyzing strains obtained in overcoring, special attention must be placed on the size of the strain gages with respect to the size, shape and distribution of rock grains and pores (Cyrul, 1983). It has been found that consistent strain readings in rock are usually obtained when strain gages have a length

greater than or equal to ten times the average crystal dimension (Garritty, Irvin and Farmer, 1985).

In hydraulic fracturing, uncertainty may arise in the interpretation of the fluid pressure versus flow behavior during crack initiation and propagation (Fairhurst, 1986). For instance, errors may arise when selecting the shut-in and reopening pressures, and the rock tensile strength. Using the results of hydraulic fracturing tests at the Basalt Waste Isolation Project in Hanford, Washington, Aggson and Kim (1987) compared five different methods of determining the shut-in pressure and analyzed their effect on stress determination. They found that for their specific set of data, and depending on the method used, the calculated minimum and maximum horizontal stresses could vary as much as 4.9 MPa (14%) and 14.7 MPa (23%), respectively.

Errors may arise when assumptions associated with individual measuring techniques are not fulfilled or are partially fulfilled. For instance, overcoring tests are often analyzed by assuming that the rock is a linearly elastic, isotropic and homogeneous continuum. Errors may be created due to nonlinear or inelastic response, time-dependent response, overstressing (yielding) of the rock after drilling, anisotropy, and inhomogeneities at the scale of the overcore sample.

Errors may arise in the analysis of hydraulic fracturing tests by assuming that the vertical stress is a principal stress. For flat jack tests the stresses across the jacks may not be uniform, as is often assumed. Using flat jacks in areas of high stress gradients or in sections of underground openings that have been disturbed may yield erroneous stress measurements. If the rock shows a viscous behavior, substantial errors may arise by analyzing field test results using the theory of linear elasticity.

Another source of uncertainty is associated with errors in the mechanical properties entering into the calculation of the stresses such as the Young's modulus and Poisson's ratio in overcoring tests or tensile strength in hydraulic fracturing tests. As discussed in Chapter 5, determination of the elastic properties through biaxial testing is subject to some errors, in particular when dealing with complex cells such as the CSIRO HI cell (Worotnicki, 1993). The other alternative, which is to test rock cores, may also yield errors. Tests on overcore samples containing either a CSIRO HI cell or a LuH gage conducted by Leijon and Stillborg (1986) revealed that markedly different rock properties could be determined by using biaxial tests or triaxial tests (biaxial plus longitudinal loading) on the overcores. Triaxial testing was found to increase the values of the Young's modulus by as much as 20% compared with biaxial loading. Also, the biaxial test values for the Poisson's ratio were found to be on average more than twice as large and more scattered than those obtained by triaxial testing. It is noteworthy that this discrepancy in the elastic properties must come from the rock since Leijon and Stillborg (1986) reported that biaxial and triaxial tests on an aluminum cylinder yielded similar properties. As remarked by Leijon and Stillborg (1986), such discrepancies in the elastic properties have a strong effect on the *in situ* stresses, as illustrated in Fig. 3.4. This figure shows the effect of varying the Poisson's ratio on the magnitude of the principal stresses. It can be seen that the effect is moderate for low values of the Poisson's ratio and increases as the Poisson's ratio approaches the limiting value of 0.5.

Another source of error can be created when analyzing the results of stress measurements conducted at several locations and when determining the average principal stresses for a certain region of interest. As remarked by Hudson and Cooling (1988) and Walker, Martin and Dzik (1990), the magnitude and orientation of the average principal stresses cannot be determined by simply calculating the average of the magnitudes and the average of the orientations of the principal stresses. This approach may lead to non-orthogonal average principal stresses. All stress tensors

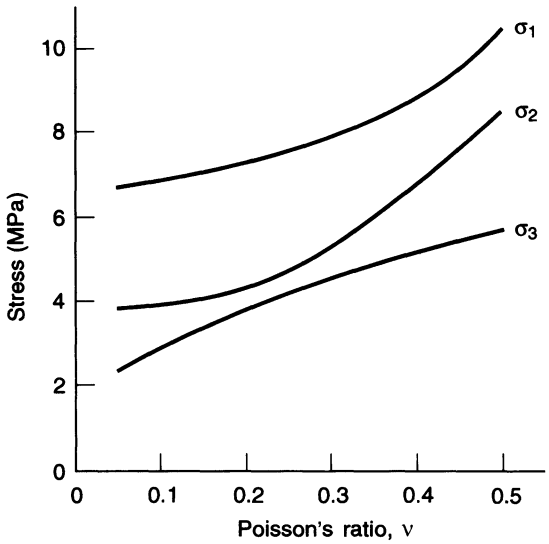

Fig. 3.4 Effect of the value of Poisson's ratio on magnitude of *in situ* stresses determined by overcoring. (After Leijon and Stillborg, 1986.)

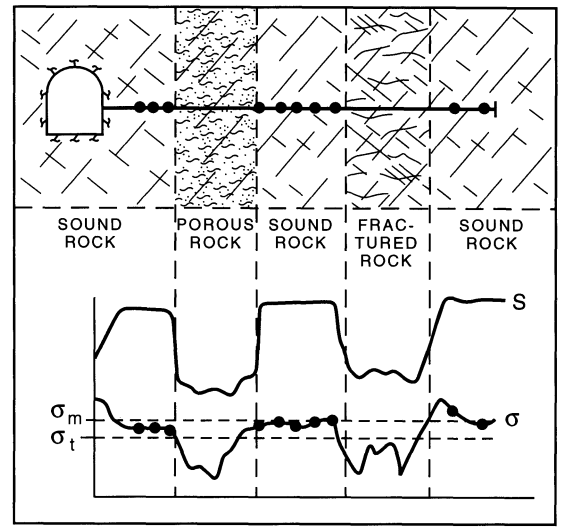

Fig. 3.5 Schematic example illustrating sampling bias due to variable rock conditions. Diagram shows variation of the rock mass stiffness S and the mean stress σ. In this diagram, σ_m and σ_t denote the measured and true borehole averages, respectively. (Source: Leijon, B.A. Copyright 1989, with kind permission from Elsevier Science Ltd, The Boulevard, Langford Lane, Kidlington, UK.)

must first be expressed in the same coordinate system. Then the average stress tensor is calculated by determining the average of each of the six stress components. Finally, the average principal stresses and their orientation are determined from the eigenvalues and eigenvectors of the average stress tensor.

It must also be kept in mind that most stress measurements are carried out in good and competent rock conditions. Among engineers, geologists and geophysicists there is a maxim that *in situ* stresses cannot be determined in fractured or weak rocks. Since, as discussed in sections 2.6 and 2.12, stiffer and harder rocks seem to be able to carry higher than average *in situ* stresses, a significant error in measuring *in situ* stresses may result (Voight, 1966), with a bias toward an overestimation of *in situ* stresses (Leijon, 1989). This is illustrated schematically in Fig. 3.5 for a borehole traversing a series of porous, fractured and sound rock sections with different stiffnesses. Thus significant errors may arise due to indiscriminate selection of sites for stress measurements.

Another source of bias is associated with the determination of elastic properties of weak rocks, such as shales or other clay-bearing rocks, which are included in the analysis of overcoring tests. When subject to unloading, such rocks often expand and deteriorate relatively quickly. Thus the rocks tested later in the laboratory will appear softer than *in situ*. According to Franklin and Hungr (1978), this phenomenon may be responsible for the observation made by some authors that softer rocks carry higher horizontal stresses. In general, errors in stress determination with methods such as overcoring can be expected even in medium- to good-quality rocks due to the sampling process itself and possible alteration associated with coring and core handling.

3.9.4 UNDERSTANDING AND REDUCING UNCERTAINTIES

Many of the uncertainties listed above can be overcome or at least understood (or even

quantified) by using one or several of the following steps.

(1) Conduct laboratory tests where instruments are subjected to known stress fields and simulated field conditions. The orientation and magnitude of the measured stresses are then compared with those applied. Such laboratory experiments can help, among other things, in identifying the limitations of the instruments, their performance and accuracy, and their suitability in various geological environments. They can also help in assessing if the rock responds during overcoring in a linearly elastic manner or if it has any nonlinear or time-dependent characteristics requiring the rock to be treated as viscoelastic or with more complex constitutive behavior.

An example of an extensive experimental study conducted to verify the suitability of the USBM gage, the CSIRO HI cell, the CSIR cell and a solid inclusion cell for rock stress measurements was reported by Cai (1990). Full-scale overcoring tests under biaxial loads were carried out in rock (coal, sandstone and marble) and rock-like materials (cement mortar and cement concrete) with Young's moduli ranging between 3 and 40 GPa. Such tests were able to reveal the performance of various instruments in materials ranging from ideal linearly elastic, homogeneous and isotropic continua to less ideal nonlinearly elastic, heterogeneous and anisotropic discontinua. All the tests on ideal media revealed that all the instruments were reliable with a difference between applied and measured stresses of less than 10%. On non-ideal materials, the differences were found to be much larger (Cai, Qiao and Yu, 1995).

Simulated field conditions can also be done by conducting block tests *in situ*, a good example of which can be found in Gregory *et al.* (1983) in relation to the Near-Surface Test Facility at the Basalt Waste Isolation Project in Hanford, Washington. There, five overcoring techniques were tested and all were found unsuitable for the closely jointed rock found at the site.

(2) Discard bad (erroneous) data resulting from obvious blunders in the measurements. Bad data points that fall outside the range of normally expected random deviations may be discarded, based on statistical analysis, response to loads or simple compatibility tests. This must be done in a consistent and unbiased manner. For instance, in overcoring tests, strain gage readings may be discarded because of obvious debonding (partial or complete), low sensitivity or core breakage. Such phenomena usually create anomalies and irregularities in the strain or displacement relief curves recorded during overcoring. Such curves can therefore be used as a diagnostic tool to evaluate the quality of the measurements (Blackwood, 1978). Good relief curves are usually regular and stabilize after the depth of overcoring is beyond the plane of measurement. Compatibility checks between the strains in a given strain rosette or in between separate rosettes may also help in eliminating bad data. Biaxial (radial) tests or uniaxial tests on the overcore after core recovery may also indicate deficient and malfunctioning strain gages. Another simple test that can be used with USBM-type gages and the CSIR Doorstopper (in order to identify bad data) is to check if the sum of two normal strains or two diametral deformations in two orthogonal directions is close to being invariant. In hydraulic fracturing tests the absence of a distinct breakdown pressure in the pressure–time record may indicate reopening of an existing fracture or joint.

(3) Compare stress measurements in the same borehole obtained with the same method or compare parallel measurements obtained with different methods. Such comparisons provide a measure of consistency of the stress measurements. Repeating tests a number of times along one, or occasionally more than one hole, can be used to quantify and smooth out apparent scatter of the results obtained. Multiple boreholes can also be used as a crosscheck. In general, it is believed that using hybrid stress methods can reduce

uncertainties in stress determination (Brudy *et al.*, 1995; Cornet, 1993; Haimson, 1988).

(4) Analyze the results of stress measurements using statistical techniques (Cornet and Valette, 1984; Dey and Brown, 1986; Gray and Toews, 1968, 1975; Panek, 1966; Walker, Martin and Dzik, 1990; Worotnicki, 1993). Methods such as least squares and Monte Carlo analysis can be used to determine the magnitude and orientation of mean principal stresses, as well as their domain of variation for different confidence intervals.

(5) Monitor (if possible) as many *in situ* and laboratory test conditions as possible, such as humidity, rock and air temperatures, and drilling fluid temperature. Figure 3.6 shows an example of continuous monitoring of *in situ* conditions obtained with a data logger during overcoring of a CSIR-type of triaxial strain cell at the URL site. The advantage of monitoring test conditions is that adjustments can be made to reduce uncertainties. Also, corrections can be applied to the various measurements. Discussion of the importance of applying corrections to account for the effect of temperature in the analysis of strain measurements with a modified CSIR Doorstopper can be found in Corthesy, Gill and Nguyen (1990).

(6) Investigate whether the observed scatter in stress measurements can be related to the effect of topography, anisotropy,

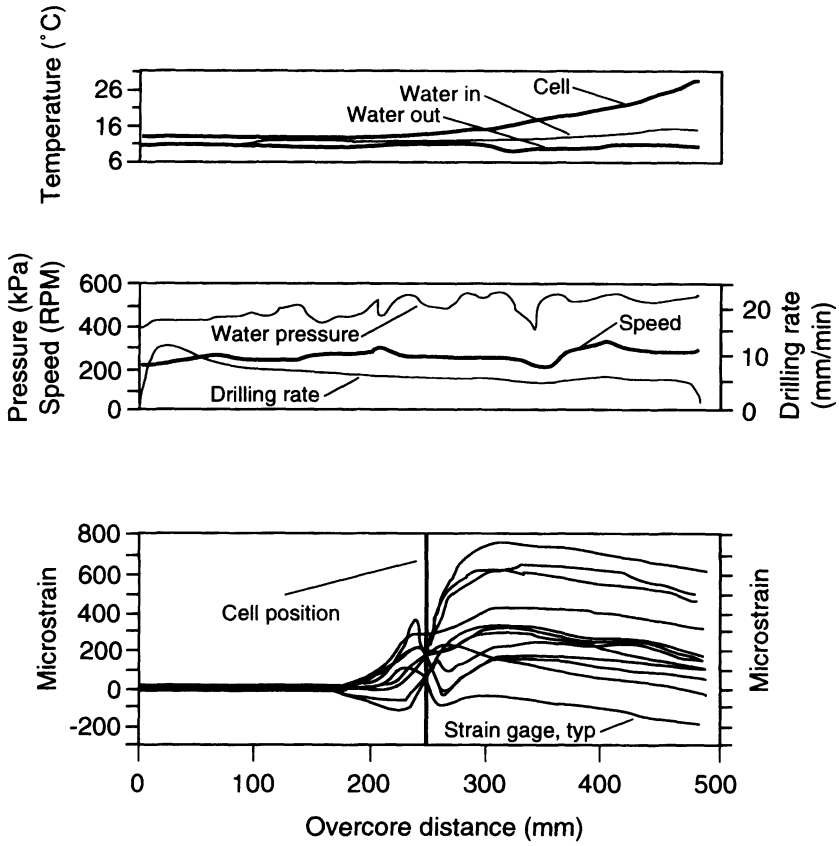

Fig. 3.6 Typical example of continuous monitoring of *in situ* conditions during overcoring of a CSIR-type strain cell at the URL site in Canada. (After Martin, Read and Chandler, 1990.)

heterogeneities or any geological structures. Such effects can be simulated using analytical or numerical techniques.

3.9.5 EXPECTED UNCERTAINTIES

Although the accuracy varies with the method employed, a natural scatter in *in situ* stress measurements should be expected as for any other rock properties. According to Gonano and Sharp (1983) for borehole strain devices, '. . . confidence intervals of the order of ±20% are generally the limit of accuracy obtainable, even with rock masses that can be described as linear elastic'. Herget (1986) mentioned that errors of ±10–15% for stress components are common. Rocha (1968) concluded that *in situ* stresses could be determined with flat jack tests with an error of less than 10%. When estimating *in situ* stresses at large depths in the Carnmenellis granite, Pine and Kwakwa (1989) reported errors of the order of ±15% for the maximum horizontal stress, ±5–10% for the minimum horizontal stress, and ±5% for the vertical stress. The results of hydraulic fracturing tests by Haimson (1990) in the Sioux Falls quartzite were presented with errors of ±10% for the vertical stress, and ±15% and ±25% for the minimum and maximum horizontal stresses, respectively. The orientation of the latter was measured with an error of ±15°. This is comparable with the 5–20° variation in hydrofracture orientation reported by Baumgärtner *et al.* (1993) and Brudy *et al.* (1995) for the KTB and Cajon Pass holes. Finally, Warpinski and Teufel (1991) suggested that in hydraulic fracturing, the minimum *in situ* principal stress determined from the shut-in pressure could be determined with an accuracy of 0.1–0.2 MPa in clear pressure records and 1–2 MPa for more obscure pressure records.

The answers to what can be considered an acceptable *in situ* stress measurement and how many reliable stress measurements need to be carried out are somewhat subjective. They largely depend on the type of technique used, the site geology and the difficulties encountered when conducting measurements in the geological environment of interest. According to Goodman (1989), results are usually considered satisfactory if they are consistent and give stress values to within about 0.3 MPa. Leijon (1986) found that four to five overcoring tests with the LuH gage in a homogeneous granite in the Malmberget mine in Sweden were sufficient to determine the principal stress magnitudes with an accuracy of 14% (±3 MPa) at a depth of 600 m. For five tests, the accuracy on the stress orientation was about 15°. The same number of tests conducted in a highly foliated and jointed leptite at the same depth, but at a different location in the mine, increased the uncertainty to 35% (±8 MPa) for the stress magnitude and 40° for the stress orientation. In the granite it was found that the confidence was not improved by conducting additional tests. On the other hand, for the leptite it was found that the confidence could be somewhat improved by doubling the number of tests.

In general, it is recommended that the presentation of stress measurement data includes error bars or confidence intervals (with mean value and standard deviation) for both stress magnitude and stress orientation. For instance, Fig. 3.7 gives the orientation and magnitude of the three mean principal stresses based on the results of six measurements conducted in a single borehole at the URL site in Canada (Walker, Martin and Dzik, 1990). The 90% confidence intervals for stress magnitude and orientation obtained using a Monte Carlo analysis are also shown. As a second example, Figs 3.8a, b show the uncertainty on the magnitude and orientation of principal stresses determined with the DSCA method obtained by Dey and Brown (1986) down to a depth of 4 km at the Fenton Hill Hot Dry Rock site in New Mexico. These figures indicate rotation of the principal stresses with depth and depth-dependent uncertainty. Finally, as a last illustrative example, Figs 3.9a, b show the magnitude of the horizontal principal stresses

	Confidence intervals (MPa)		
Principal stress	Lower 90%	Mean	Upper 90%
σ_1	30.97	34.03	37.59
σ_2	16.01	17.74	21.02
σ_3	11.94	15.15	16.26

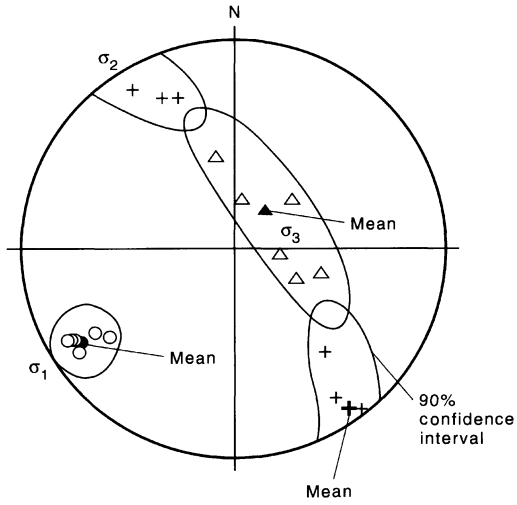

Fig. 3.7 Confidence intervals for principal stress magnitude (table) and orientation (hemispherical projection). *In situ* stress measurements from borehole 209-056-OC1 at the URL site in Canada. (After Walker, Martin and Dzik, 1990.)

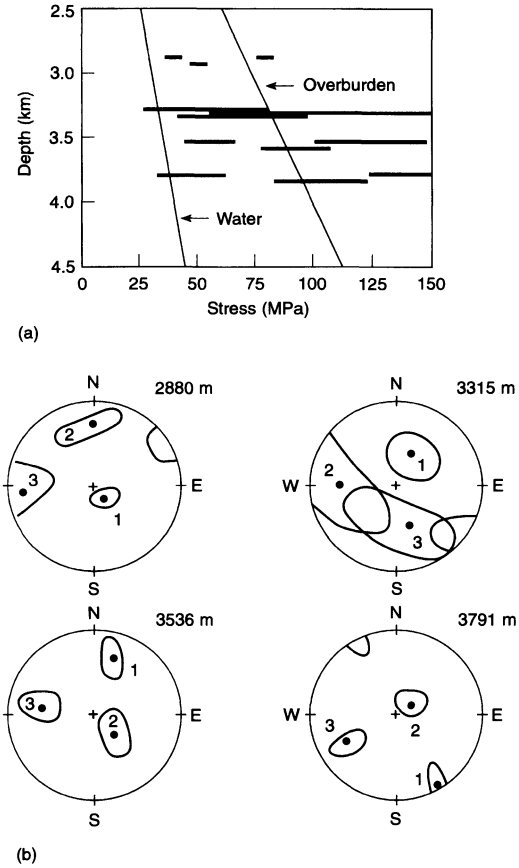

Fig. 3.8 Stress measurements determined with the DSCA method down to a depth of 4 km at the Fenton Hill Hot Dry Rock site in New Mexico. (a) Stress magnitude versus depth. The horizontal bars represent an error of one standard deviation on the estimates. At a given depth, the bars represent from left to right the minimum, intermediate and maximum principal stresses. (b) Stress orientation and uncertainty at different depths using lower hemisphere stereographic projection. (After Dey and Brown, 1986.)

and the orientation of the maximum horizontal stress with depth obtained by Haimson (1982) by hydraulic fracturing of three holes near Anna, Ohio. The stresses were measured at depths from 0 to 200 m. Several tests resulted in horizontal fractures due to horizontal bedded partings in the rock, thus giving an estimate of the vertical stress (Fig. 3.9a). Linear regression analysis of the hydraulic fracturing test results gave the following variations with depth z (at depths larger than 50 m) for the vertical stress, σ_v (determined from the horizontal hydraulic fractures), the vertical stress, σ_v^{wt} (estimated from the weight of the overlying rock), and the maximum and minimum horizontal stresses σ_{Hmax} and σ_{Hmin}

$$\sigma_v^{wt} = 0.026z; \qquad \sigma_v = 0.4 + 0.029z$$

$$\sigma_{Hmin} = 5.1 + 0.014z \quad \text{at N20°W} \qquad (3.1)$$

$$\sigma_{Hmax} = 10.1 + 0.014z \quad \text{at N70°E}$$

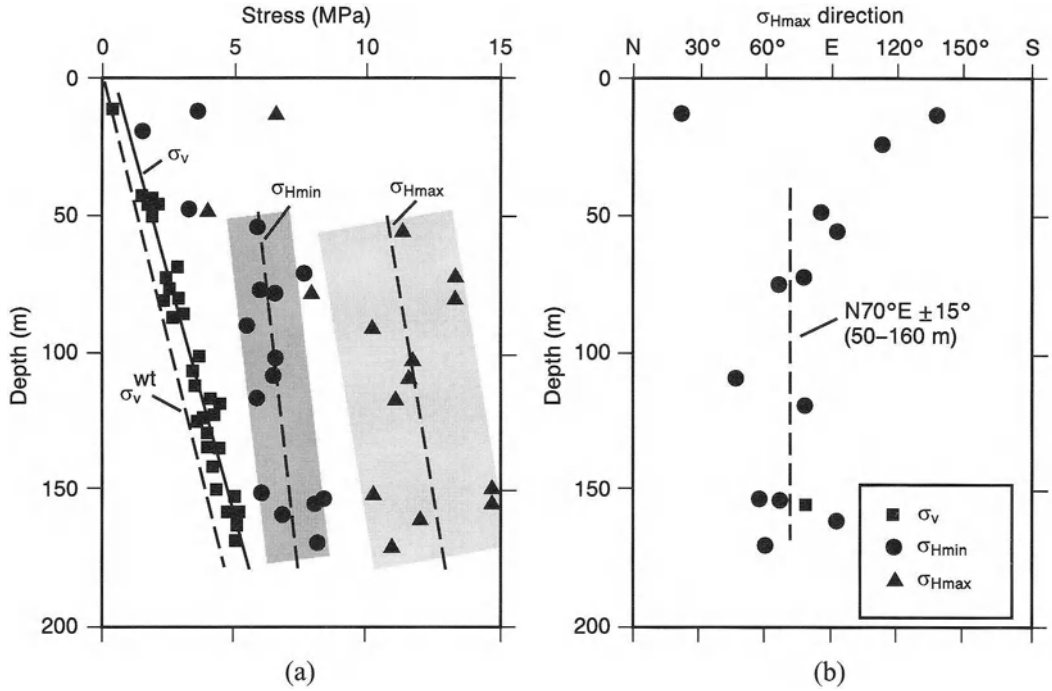

Fig. 3.9 Stress data in three quarries near Anna, Ohio. (a) Variation of principal stresses with depth and (b) variation of major horizontal stress direction with depth. (Adapted from Haimson, 1982.)

As remarked by Haimson (1982), the variations of σ_v and σ_v^{wt} with depth in Fig. 3.9a confirm the reliability of estimating the vertical stress from the weight of the overlying rock. Here σ_v is slightly larger than σ_v^{wt} by an average of 0.7 MPa. Figure 3.9a also shows the scatter in the horizontal stresses around the best-fit lines defined by equations (3.1). The minimum and maximum horizontal stresses can deviate by as much as ±1.25 and ±2.50 MPa, respectively. The standard deviation in the direction of the maximum horizontal stress is ±15° around the N70°E direction.

The combined effect of volume and the errors associated with each technique may create discrepancies when comparing stress measurements obtained with different methods. Gonano and Sharp (1983) estimated that errors in both hydraulic fracturing and overcoring methods may lead to 5–10% differences in the magnitude of the stresses determined. Doe (1983) gives differences of the order of 20% for the stress magnitudes obtained with those two methods. Haimson (1981) compared hydraulic fracturing test results with overcoring test results at several sites in North America and in Sweden. He found that (1) the directions of the horizontal stresses determined by the two methods were within ±10°, (2) the magnitudes of the minimum horizontal stress were within ±2 MPa (equivalent to a discrepancy of up to 30% of the stresses determined by hydraulic fracturing), (3) the magnitudes of the maximum horizontal stress were within ±5 MPa (equivalent to a discrepancy of up to 50% of the stresses determined by hydraulic fracturing) and (4) the principal stress axes between the two methods were less than 30° apart. According to Haimson (1981), the larger discrepancy for the maximum horizontal stress arises from

errors created when selecting the rock tensile strength in hydraulic fracturing, and the rock elastic properties for the analysis of overcoring tests. Other examples of comparison between different stress measurement methods are presented in Chapter 9.

REFERENCES

Aggson, J.R. (1978) The potential application of ultrasonic spectroscopy to underground site characterization. Presented at the 48th Annual Int. Meeting Soc. of Exploration Geophysicists.

Aggson, J.R. and Kim, K. (1987) Analysis of hydraulic fracturing pressure histories: a comparison of five methods used to identify shut-in pressure. *Int. J. Rock Mech. Min. Sci. & Geomech. Abstr.*, **24**, 75–80.

Amadei, B. (1986) Analysis of data obtained with the CSIRO cell in anisotropic rock masses. CSIRO Division of Geomechanics, Technical Report No. 141.

Aytmatov, I.T. (1986) On virgin stress state of a rock mass in mobile folded area, in *Proc. Int. Symp. on Rock Stress and Rock Stress Measurements*, Stockholm, Centek Publ., Luleå, pp. 55–9.

Baumgärtner, J. *et al.* (1993) Deep hydraulic fracturing stress measurements in the KTB (Germany) and Cajon Pass (USA) scientific drilling projects – a summary, in *Proc. 7th Cong. Int. Soc. Rock Mech. (ISRM)*, Aachen, Balkema, Rotterdam, Vol. 3, pp. 1685–90.

Berry, D.S. and Fairhurst, C. (1966) Influence of rock anisotropy and time dependent deformation on the stress relief and high modulus inclusion techniques of in situ stress determination. *ASTM STP*, **42**.

Blackwood, R.L. (1978) Diagnostic stress-relief curves in stress measurement by overcoring. *Int. J. Rock Mech. Min. Sci. & Geomech. Abstr.*, **15**, 205–9.

Bock, H. (1979) Experimental determination of the residual stress field in a basaltic column, in *Proc. 4th Cong. Int. Soc. Rock Mech. (ISRM)*, Montreux, Balkema, Rotterdam, Vol. 1, pp. 45–9.

Bock, H. (1986) In-situ validation of the borehole slotting stressmeter, in *Proc. Int. Symp. on Rock Stress and Rock Stress Measurements*, Stockholm, Centek Publ., Luleå, pp. 261–70.

Bock, H. and Foruria, V. (1983) A recoverable borehole slotting instrument for in-situ stress measurements in rock, in *Proc. Int. Symp. on Field Measurements in Geomechanics*, Zurich, Balkema, Rotterdam, pp. 15–29.

Brady, B.H.G., Friday, R.G. and Alexander, L.G. (1976) Stress measurement in a bored raise at the Mount Isa Mine, in *Proc. ISRM Symposium on Investigation of Stress in Rock, Advances in Stress Measurement*, Sydney, The Institution of Engineers, Australia, pp. 12–16.

Brady, B.H.G., Lemos, J.V. and Cundall, P.A. (1986) Stress measurement schemes for jointed and fractured rock, in *Proc. Int. Symp. on Rock Stress and Rock Stress Measurements*, Stockholm, Centek Publ., Luleå, pp. 167–76.

Bridges, M.C. *et al.* (1976) Monitoring of stress, strain and displacement in and around a vertical pillar at Mount Isa Mine, in *Proc. ISRM Symposium on Investigation of Stress in Rock, Advances in Stress Measurement*, Sydney, The Institution of Engineers, Australia, pp. 44–9.

Brown, D.W. (1989) The potential for large errors in the inferred minimum Earth stress when using incomplete hydraulic fracturing results. *Int. J. Rock Mech. Min. Sci. & Geomech. Abstr.*, **26**, 573–7.

Brudy, M. *et al.* (1995) Application of the integrated stress measurements strategy to 9 km depth in the KTB boreholes, in *Proc. Workshop on Rock Stresses in the North Sea*, Trondheim, Norway, NTH and SINTEF Publ., Trondheim, pp. 154–64.

Burlet, D., Cornet, F.H. and Feuga, B. (1989) Evaluation of the HTPF method of stress determination in two kinds of rock. *Int. J. Rock Mech. Min. Sci. & Geomech. Abstr.*, **26**, 673–9.

Cai, M. (1990) Comparative tests and studies of overcoring stress measurement devices in different rock conditions, unpublished PhD Thesis, University of New South Wales, Australia.

Cai, M., Qiao, L. and Yu, J. (1995) Study and tests of techniques for increasing overcoring stress measurement accuracy. *Int. J. Rock Mech. Min. Sci. & Geomech. Abstr.*, **32**, 375–84.

Chandler, N.A. (1993) Bored raise overcoring for in situ stress determination at the Underground Research Laboratory. *Int. J. Rock Mech. Min. Sci. & Geomech. Abstr.*, **30**, 989–92.

Cook, J.C. (1972) Semi-annual report on electronic measurements of rock stress. US Bureau of Mines Technical Report No. 72-10.

Cooling, C.M., Hudson, J.A. and Tunbridge, L.W. (1988) In-situ rock stresses and their measurements in the UK – Part II. Site experiments and stress field interpretation. *Int. J. Rock Mech. Min. Sci. & Geomech. Abstr.*, **25**, 371–82.

Cornet, F.H. (1986) Stress determination from hydraulic tests on pre-existing fractures, in *Proc. Int. Symp. on Rock Stress and Rock Stress Measurements*, Stockholm, Centek Publ., Luleå, pp. 301–12.

Cornet, F.H. (1993) The HTPF and the integrated stress determination methods, in *Comprehensive Rock Engineering* (ed. J.A. Hudson), Pergamon Press, Oxford, Chapter 15, Vol. 3, pp. 413–32.

Cornet, F.H. and Valette, B. (1984) In-situ stress determination from hydraulic injection test data. *J. Geophys. Res.*, **89**, 11527–37.

Corthesy, R., Gill, D.E. and Nguyen, D. (1990) The modified Doorstopper cell stress measuring technique, in *Proc. Conf. on Stresses in Underground Structures*, CANMET Publ., Ottawa, pp. 23–32.

Cyrul, T. (1983) Notes on stress determination in heterogeneous rocks, in *Proc. Int. Symp. on Field Measurements in Geomechanics*, Zurich, Balkema, Rotterdam, pp. 59–70.

Dey, T.N. and Brown, D.W. (1986) Stress measurements in a deep granitic rock mass using hydraulic fracturing and differential strain curve analysis, in *Proc. Int. Symp. on Rock Stress and Rock Stress Measurements*, Stockholm, Centek Publ., Luleå, pp. 351–7.

Doe, W.T. (1983) Determination of the state of stress at the Stripa Mine, Sweden, in *Proc. Workshop on Hydraulic Fracturing Stress Measurements*, Monterey, National Academy Press, Washington, DC, pp. 305–31.

Duvall, W.I. (1974) Stress relief by center hole. Appendix in US Bureau of Mines Report of Investigation RI 7894.

Enever, J.R. (1993) Case studies of hydraulic fracture stress measurements in Australia, in *Comprehensive Rock Engineering* (ed. J.A. Hudson), Pergamon Press, Oxford, Chapter 20, Vol. 3, pp. 498–531.

Enever, J.R., Walton, R.J. and Wold, M.B. (1990) Scale effects influencing hydraulic fracture and overcoring stress measurements, in *Proc. Int. Workshop on Scale Effects in Rock Masses*, Loen, Norway, Balkema, Rotterdam, pp. 317–26.

Fairhurst, C. (1964) Measurement of in-situ rock stresses with particular reference to hydraulic fracturing. *Rock Mech. Eng. Geol.*, **2**, 129–47.

Fairhurst, C. (1986) In-situ stress determination – an appraisal of its significance in rock mechanics, in *Proc. Int. Symp. on Rock Stress and Rock Stress Measurements*, Stockholm, Centek Publ., Luleå, pp. 3–17.

Franklin, J.A. and Hungr, O. (1978) Rock stresses in Canada: their relevance to engineering projects. *Rock Mech.*, Suppl. **6**, 25–46.

Garritty, P., Irvin, R.A. and Farmer, I.W. (1985) Problems associated with near surface in-situ stress measurements by the overcoring method, in *Proc. 26th US Symp. Rock Mech.*, Rapid City, Balkema, Rotterdam, pp. 1095–1102.

Gonano, L.P. and Sharp, J.C. (1983) Critical evaluation of rock behavior for in-situ stress determination using the overcoring method, in *Proc. 5th Cong. Int. Soc. Rock Mech. (ISRM)*, Melbourne, Balkema, Rotterdam, pp. A241–50.

Goodman, R.E. (1989) *Introduction to Rock Mechanics*, 2nd edn, Wiley.

Gray, W.M. and Toews, N.A. (1968) Analysis of accuracy in the determination of the ground stress tensor by means of borehole devices, in *Proc. 9th US Symp. Rock Mech.*, Golden, SME/AIME, pp. 45–72.

Gray, W.M. and Toews, N.A. (1975) Analysis of variance applied to data obtained by means of a six element borehole deformation gage for stress determination, in *Proc. 15th US Symp. Rock Mech.*, Rapid City, ASCE Publ., pp. 323–56.

Gregory, E.C. *et al.* (1983) In situ stress measurement in a jointed basalt, in *Proc. Rapid Excavation and Tunneling (RETC) Conf.*, Chicago, Vol. 1, SME/AIME, pp. 42–61.

Haimson, B.C. (1981) Confirmation of hydrofracturing results through comparisons with other stress measurements, in *Proc. 22nd US Symp. Rock Mech.*, MIT Publ., Cambridge, pp. 409–15.

Haimson, B.C. (1982) Deep stress measurements in three Ohio quarries and their comparison to near surface tests, in *Proc. 23rd US Symp. Rock Mech.*, Berkeley, SME/AIME, pp. 190–202.

Haimson, B.C. (1988) Status of in-situ stress determination methods, in *Proc. 29th US Symp. Rock Mech.*, Minneapolis, Balkema, Rotterdam, pp. 75–84.

Haimson, B.C. (1990) Stress measurements in the Sioux Falls quartzite and the state of stress in the mid-continent, in *Proc. 31st US Symp. Rock Mech.*, Golden, Balkema, Rotterdam, pp. 397–404.

Hast, N. (1979) Limit of stresses in the Earth's crust. *Rock Mech.*, **11**, 143–50.

Hayashi, K. and Masuoka, M. (1995) Estimation of tectonic stress from slip data from fractures in core samples, in *Proc. Int. Workshop on Rock Stress Measurement at Great Depth*, Tokyo, Japan, 8th ISRM Cong., pp. 35–9.

Herget, G. (1986) Changes of ground stresses with depth in the Canadian shield, in *Proc. Int. Symp. on Rock Stress and Rock Stress Measurements*, Stockholm, Centek Publ., Luleå, pp. 61–8.

Herget, G. (1993) Rock stresses and rock stress monitoring in Canada, in *Comprehensive Rock Engineering* (ed. J.A. Hudson), Pergamon Press, Oxford, Chapter 19, Vol. 3, pp. 473–96.

Holcomb, D.J. (1993) Observations of the Kaiser effect under multiaxial stress states: implications for its use in determining in-situ stress. *Geophys. Res. Lett.*, **20**, 2119–22.

Holman, J.P. (1989) *Experimental Methods for Engineers*, 5th edn, McGraw-Hill.

Hudson, J.A. and Cooling, C.M. (1988) In situ rock stresses and their measurement in the UK – Part I. The current state of knowledge. *Int. J. Rock Mech. Min. Sci. & Geomech. Abstr.*, **25**, 363–70.

Kaiser, J. (1950) An investigation into the occurrence of noises in tensile tests or a study of acoustic phenomena in tensile tests, unpublished Doctoral Thesis, Tech. Hosch, Munich.

Kobayashi, S. *et al.* (1991) In-situ stress measurement using a conical shaped borehole strain gage plug, in *Proc. 7th Cong. Int. Soc. Rock Mech. (ISRM)*, Aachen, Balkema, Rotterdam, Vol. 1, pp. 545–8.

Leeman, E.R. (1959) The measurement of changes in rock stress due to mining. *Mine and Quarry Eng.*, **25**, 300–304.

Leeman, E.R. (1971) The measurement of stress in rock: a review of recent developments (and a bibliography), in *Proc. Int. Symp. on the Determination of Stresses in Rock Masses*, Lab. Nac. de Eng. Civil, Lisbon, pp. 200–229.

Leeman, E.R. and Hayes, D.J. (1966) A technique for determining the complete state of stress in rock using a single borehole, in *Proc. 1st Cong. Int. Soc. Rock Mech. (ISRM)*, Lisbon, Lab. Nac. de Eng. Civil, Lisbon, Vol. II, pp. 17–24.

Leijon, B.A. (1986) Application of the LUT triaxial overcoring techniques in Swedish mines, in *Proc. Int. Symp. on Rock Stress and Rock Stress Measurements*, Stockholm, Centek Publ., Luleå, pp. 569–79.

Leijon, B.A. (1989) Relevance of pointwise rock stress measurements – an analysis of overcoring data. *Int. J. Rock Mech. Min. Sci. & Geomech. Abstr.*, **26**, 61–8.

Leijon, B.A. and Stillborg, B.L. (1986) A comparative study between two rock stress measurement techniques at Luossavaara mine. *Rock Mech. Rock Eng.*, **19**, 143–63.

Lu, P.H. (1986) A new method of rock stress measurement with hydraulic borehole pressure cells, in *Proc. Int. Symp. on Rock Stress and Rock Stress Measurements*, Stockholm, Centek Publ., Luleå, pp. 237–45.

Mao, N. *et al.* (1984) Using a sonic technique to estimate in-situ stresses, in *Proc. 25th US Symp. Rock Mech.*, Evanston, SME/AIME, pp. 167–75.

Martin, C.D. (1989) Characterizing in-situ stress domains at AECL's underground research laboratory, in *Proc. 42nd Can. Geotech. Conf.*, Winnipeg, pp. 1–14.

Martin, C.D., Read, R.S. and Chandler, N.A. (1990) Does scale influence in situ stress measurements? – some findings at the Underground Research Laboratory, in *Proc. 1st Int. Workshop on Scale Effects in Rock Masses*, Loen, Norway, Balkema, Rotterdam, pp. 307–16.

Martin, C.D., Read, R.S. and Lang, P.A. (1990) Seven years of in situ stress measurements at the URL, in *Proc. 31st US Symp. Rock Mech.*, Golden, Balkema, Rotterdam, pp. 15–26.

Mayer, A., Habib, P. and Marchand, R. (1951) Underground rock pressure testing, in *Proc. Int. Conf. Rock Pressure and Support in the Workings*, Liege, pp. 217–21.

Merrill, R.H. (1967) Three component borehole deformation gage for determining the stress in rock. US Bureau of Mines Report of Investigation RI 7015.

Mills, K.W. and Pender, M.J. (1986) A soft inclusion instrument for in-situ stress measurement in coal, in *Proc. Int. Symp. on Rock Stress and Rock Stress Measurements*, Stockholm, Centek Publ., Luleå, pp. 247–51.

Natau, O. (1974) The influence of the length of strain gages in the CSIR stress cell on results of measurements. *Rock Mech.*, **6**, 117–18.

Natau, O., Lempp, Ch. and Borm, G. (1986) Stress relaxation monitoring prestressed hard inclusions, in *Proc. Int. Symp. on Rock Stress and Rock Stress Measurements*, Stockholm, Centek Publ., Luleå, pp. 509–14.

Panek, L.A. (1966) Calculation of the average ground stress components from measurements of the diametral deformation of a drillhole. US Bureau of Mines Report of Investigation RI 6732.

Peleg, N. (1968) The use of high modulus inclusions for in-situ stress determination in viscoelastic rocks. Corps of Engineers Technical Report 22-268, Missouri River Division, Nebraska.

Petukhov, I.M., Marmorshteyn, L.M. and Morozov, G.I. (1961) Use of changes in electrical conductivity of rock to study the stress state in the rock mass and its aquifer properties. *Trudy VNIMI*, **42**, 110–18.

Pine, R.J. and Kwakwa, K.A. (1989) Experience with hydrofracture stress measurements to depths of 2.6 km and implications for measurements to 6 km in the Carnmenellis granite. *Int. J. Rock Mech. Min. Sci. & Geomech. Abstr.*, **26**, 565–71.

Pitt, J.M. and Klosterman, L.A. (1984) In-situ stress by pulse velocity monitoring of induced fractures, in *Proc. 25th US Symp. Rock Mech.*, Evanston, SME/AIME, pp. 186–93.

Rivkin, I.D., Zapolskiy, V.P. and Bogdanov, P.A. (1956) *Sonometric Method for the Observation of Rock Pressure Effects*, Ketallurgizdat Press, Moscow.

Riznichanko, Y.V. *et al.* (1967) *Study of Rock Stress by Geophysical Methods*, Nauka Press, Moscow.

Rocha, M. (1968) New techniques for the determination of the deformability and state of stress in rock masses, in *Proc. Int. Symp. on Rock Mechanics*, Madrid, pp. 289–302.

Sakurai, S. and Shimizu, N. (1986) Initial stress back analyzed from displacements due to underground excavations, in *Proc. Int. Symp. on Rock Stress and Rock Stress Measurements*, Stockholm, Centek Publ., Luleå, pp. 679–86.

Schmitt, D.R. and Li, Y. (1993) Influence of a stress relief hole's depth on induced displacements: application in interferometric stress determinations. *Int. J. Rock Mech. Min. Sci. & Geomech. Abstr.*, **30**, 985–88.

Smither, C.L. and Arhens, T.J. (1991) Displacements from relief of in situ stress by a cylindrical hole. *Int. J. Rock Mech. Min. Sci. & Geomech. Abstr.*, **28**, 175–86.

Smither, C.L., Schmitt, D.R. and Ahrens, T.J. (1988) Analysis and modelling of holographic measurements of in-situ stress. *Int. J. Rock Mech. Min. Sci. & Geomech. Abstr.*, **25**, 353–62.

Stephansson, O. (1983) Rock stress measurement by sleeve fracturing, in *Proc. 5th Cong. Int. Soc. Rock Mech. (ISRM)*, Melbourne, Balkema, Rotterdam, pp. F129–37.

Strickland, F.G. and Ren, N.-K. (1980) Use of differential strain curve analysis in predicting the *in-situ* stress state for deep wells, in *Proc. 21st US Symp. Rock Mech.*, Rolla, University of Missouri Publ., pp. 523–32.

Sugawara, K. and Obara, Y. (1995) Rock stress and rock stress measurements in Japan, in *Proc. Int. Workshop on Rock Stress Measurement at Great Depth*, Tokyo, Japan, 8th ISRM Cong., pp. 1–6.

Sun, Y.L. and Peng, S.S. (1989) Development of in-situ stress measurement technique using ultrasonic wave attenuation method – a progress report, in *Proc. 30th US Symp. Rock Mech.*, Morgantown, Balkema, Rotterdam, pp. 477–84.

Swolfs, H.S. and Handin, J. (1976) Dependence of sonic velocity on size and in-situ stress in a rock mass, in *Proc. ISRM Symposium on Investigation of Stress in Rock, Advances in Stress Measurement*, Sydney, The Institution of Engineers, Australia, pp. 41–3.

Talebi, S. and Young, R.P. (1989) Failure mechanism of crack propagation induced by shaft excavation at the Underground Research Laboratory, in *Proc. Int. Symp. Rock Mech. and Rock Physics at Great Depth*, Pau, Balkema, Rotterdam, Vol. 3, 1455–61.

Te Kamp, L., Rummel, F. and Zoback, M.D. (1995) Hydrofrac stress profile to 9 km at the German KTB site, in *Proc. Workshop on Rock Stresses in the North Sea*, Trondheim, Norway, NTH and SINTEF Publ., Trondheim, pp. 147–53.

Teufel, L.W. (1982) Prediction of hydraulic fracture azimuth from anelastic strain recovery measurements of oriented core, in *Proc. 23rd US Symp. Rock Mech.*, Berkeley, SME/AIME, pp. 238–45.

Tsur-Lavie, Y. and Van Ham, F. (1974) Accuracy of strain measurements by the undercoring method, in *Proc. 3rd Cong. Int. Soc. Rock Mech. (ISRM)*, Denver, National Academy of Sciences, Washington, DC, Vol. 2A, pp. 474–80.

Van Heerden, W.L. (1973) The influence of various factors on the triaxial strain cell results. South African Council for Scientific and Industrial Research (CSIR) Technical Report ME 1178.

Voight, B. (1966) Interpretation of in-situ stress measurements, in *Proc. 1st Cong. Int. Soc. Rock Mech. (ISRM)*, Lisbon, Lab. Nac. de Eng. Civil, Lisbon, Vol. III, Theme 4, pp. 332–48.

Walker, J.R., Martin, C.D. and Dzik, E.J. (1990) Confidence intervals for in-situ stress measurements. *Int. J. Rock Mech. Min. Sci. & Geomech. Abstr.*, **27**, 139–41.

Warpinski, N.R. and Teufel, L.W. (1991) In-situ stress measurements at Rainier Mesa, Nevada Test Site – influence of topography and lithology on the stress state in tuff. *Int. J. Rock Mech. Min. Sci. & Geomech. Abstr.*, **28**, 143–61.

Wiles, T.D. and Kaiser, P.K. (1994) In-situ stress determination using the under-excavation

technique – I: theory. *Int. J. Rock Mech. Min. Sci. & Geomech. Abstr.*, **31**, 439–46.

Worotnicki, G. (1993) CSIRO triaxial stress measurement cell, in *Comprehensive Rock Engineering* (ed. J.A. Hudson), Pergamon Press, Oxford, Chapter 13, Vol. 3, pp. 329–94.

Worotnicki, G. and Walton, R.J. (1976) Triaxial hollow inclusion gauges for determination of rock stresses in-situ, Supplement to *Proc. ISRM Symposium on Investigation of Stress in Rock, Advances in Stress Measurement*, Sydney, The Institution of Engineers, Australia, pp. 1–8.

Zajic, J. and Bohac, V. (1986) Gallery excavation method for the stress determination in a rock mass, in *Proc. Int. Symp. on Large Rock Caverns*, Helsinki, Pergamon Press, Oxford, Vol. 2, pp. 1123–31.

Zoback, M.D., Mastin, L. and Barton, C. (1986) In-situ stress measurements in deep boreholes using hydraulic fracturing, wellbore breakouts, and stonely wave polarization, in *Proc. Int. Symp. on Rock Stress and Rock Stress Measurements*, Stockholm, Centek Publ., Luleå, pp. 289–99.

Zou, D. and Kaiser, P.K. (1990) In situ stress determination by stress change monitoring, in *Proc. 31st US Symp. Rock Mech.*, Golden, Balkema, Rotterdam, pp. 27–34.

HYDRAULIC METHODS 4

4.1 INTRODUCTION

The main objective of hydraulic methods is to measure *in situ* stresses by isolating a section of a borehole and applying a hydraulic pressure on its wall. The applied pressure is increased until existing fractures open or new fractures are formed. The fluid pressure required to open, generate, propagate, sustain and reopen fractures in rock at the test horizon is measured and is related to the existing stress field. The direction of the measured stresses is usually obtained by observing and measuring the orientation of the hydraulically induced or opened fractures.

Hydraulic methods can be divided into three subgroups: the hydraulic fracturing method, the sleeve fracturing method and the hydraulic tests on pre-existing fractures (HTPF) method. All three techniques are discussed in this chapter. These methods have found application in site characterization and investigation using holes drilled from the surface or underground from tunnels, shafts and rock chambers. They have the advantage that they do not require advance knowledge of the rock deformability properties and that they can be carried out without much difficulty below the water table. Hydraulic methods are, in general, most suited for *in situ* stress measurements at depths larger than about 50 m. Hydraulic fracturing is the only rock stress determination technique that has been successfully applied for measuring stresses in deep and very deep boreholes.

In applying hydraulic fracturing and sleeve fracturing, the drillhole direction is assumed to be a principal stress direction. Usually, this assumption is considered valid for vertical holes drilled from the surface, in which case the vertical stress is calculated from the weight of the overburden. The HTPF method is the only hydraulic method and the only *in situ* stress determination method at great depth, where the drillhole does not have to be assumed to be vertical and oriented perpendicular to principal *in situ* stress components.

Before embarking on the description of the various hydraulic methods, the reader should be aware that hydraulic methods have not yet reached maturity and that there is a far from universal consensus about which approaches, analyses and interpretations work best. In this chapter we have tried to give a balanced view of the various techniques and methods of interpretation presented in the literature.

4.2 HYDRAULIC FRACTURING

4.2.1 HISTORY

The hydraulic fracturing technique used in boreholes began as well stimulation in the petroleum industry. The technique of applying a pressure in a borehole to fracture a rock formation was first introduced by Clark (1949). The 'hydrofrac' process, as it was called at that time, consisted of two steps: (1) injection of a viscous liquid containing a granular material, such as sand for a propping agent, under high hydraulic pressure to fracture the formation, and (2) causing the viscous liquid to change from high to low viscosity so that it could be readily displaced from the formation. In the 1940s the most popular interpretation of hydraulic fracturing was that the pressure had parted the formation along a bedding plane

and lifted the overburden, notwithstanding the fact that the fracturing pressures were significantly less than the total weight of the overburden. A few years later, Scott, Bearden and Howard (1953) conducted laboratory tests on hollow cylindrical cores of rock and observed that, with penetrating fluids, the fractures occurred parallel to the rock bedding whereas with non-penetrating fluids, the fractures tended to be parallel to the axis of the core.

A critical re-examination of the fracturing of rocks by means of pressure applied in boreholes led Hubbert and Willis (1957) to the conclusion that, regardless of whether the fracturing fluid was of the penetrating type or not, the fractures produced should be approximately perpendicular to the axis of the least applied stress. They presented strong arguments that the general stress condition underground is not hydrostatic (which was the general opinion at that time), but instead consists of three unequal, mutually perpendicular principal stresses. Hubbert and Willis (1957) used sandbox experiments, the results of triaxial tests on sandstone and anhydrite, and applied Mohr diagrams to prove that the shearing mechanism of faulting and its use when estimating the state of stress underground is quite distinct from the mechanism of producing hydraulic fractures. After a clear and thorough presentation of the stress distortion caused by a borehole and the effect of the pressure applied in a borehole, Hubbert and Willis (1957) discussed the rupture pressure (or breakdown pressure) to initiate fractures and in particular the properties of the rocks being fractured. They write: 'In any section of a wellbore a few tens of feet in length, it is probable that many such joints have been intersected. It appears likely, therefore, that the tensile strength of most rocks that are to be subjected to hydraulic fracturing by pressure applied in wellbores is effectively zero, and that the pressure required to produce a parting in the rocks is only that required to reduce the compressive stresses across some plane in the walls of the hole to zero' (Hubbert and Willis, 1957, p. 160).

To support their postulate about the breakdown pressure, Hubbert and Willis (1957) presented an idealized diagram of two possible types of pressure behavior during fracture treatment (Fig. 4.1). In one case the breakdown pressure is substantially higher than the injection pressure. They thought that this would probably correspond to either the formation of a horizontal fracture or to a condition in which the two horizontal principal stresses were nearly equal. In the second case there is no pressure breakdown and this would correspond to a horizontal or vertical fracture starting from a pre-existing opening, or to a vertical fracture in a situation of great contrast between the two horizontal stresses.

Many authors in the hydraulic fracturing literature often refer to the classical paper by Hubbert and Willis (1957) in their introduction to the theory of hydraulic fracturing of wellbores. Sometimes the development of the classical equation for hydraulic fracturing is credited to them. This is not correct because Hubbert and Willis (1957) never introduced a tensile strength term in their equations. Furthermore, they limited themselves to discussing the general state of stress underground in which the three principal stresses are unequal.

Once a fracture has been initiated at the borehole wall, the fluid penetrates the parting of the rocks and the pressure is applied to the walls of the fracture. Hubbert and Willis (1957) were of the correct opinion that minimum injection pressures depend solely upon the magnitude of the least principal regional stress and are not affected by the hole geometry or the penetrating quality of the fluid. Therefore the minimum downhole injection pressure required to hold open and extend a fracture is slightly in excess of the original undisturbed regional stress normal to the plane of the fracture.

Based on the observation that the majority of fracturing operations in the petroleum

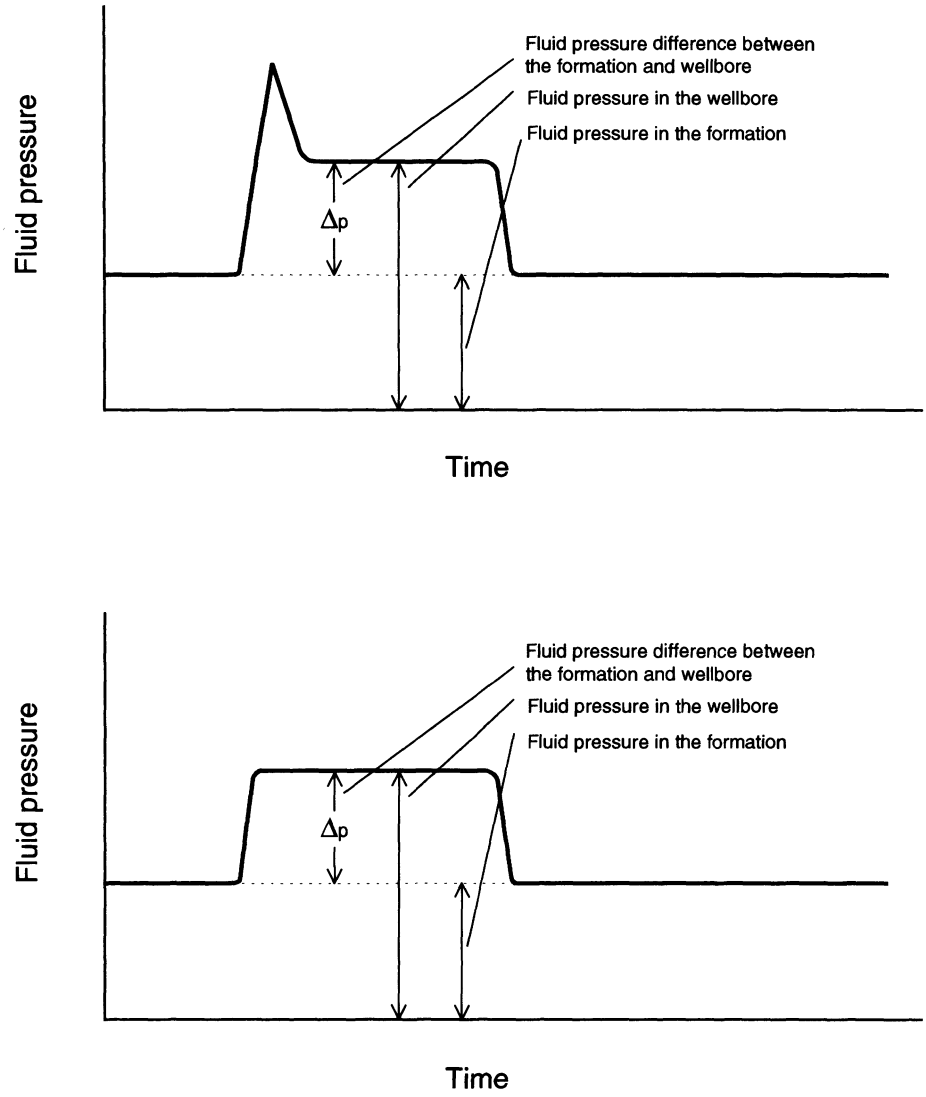

Fig. 4.1 First idealized diagram of stress determination by hydraulic fracturing showing two possible types of pressure behavior during fracture treatment depending upon various underground conditions. (Redrawn after Hubbert and Willis, 1957.)

industry in the Gulf Coast, mid-continental and West Texas–New Mexico areas of the United States required injection pressures less than the overburden pressure, Hubbert and Willis (1957) concluded that most of these fractures were vertical and controlled by the pre-existing stress field of the rocks into which the fluid was injected.

Scheidegger (1962) was the first scientist to propose a method for determining the three principal stresses in the Earth's upper crust directly by analyzing the bottom hole pressure charts obtained from the hydra-fracturing (old term for hydrofracturing) process of oil wells. He investigated the connection between fracturing in wells and the prevalent regional

stress for penetrating and non-penetrating fluids. He also introduced the finite strength of the rock into the equations for hydraulic fracturing. Furthermore, Scheidegger (1962) noted that the bottom hole pressure during a fracturing job usually settles to a value which is less than the fracture pressure. Like Hubbert and Willis (1957), he assumed that this pressure is just able to keep the fracture open and therefore must be equal to the least principal stress acting in the plane perpendicular to the induced fracture. Scheidegger (1962) calculated the regional stresses and the apparent tensile strength for five wells in Canada for which bottom hole pressure charts were available at that time during a fracturing operation. The stress state was found to correspond to incipient wrench faulting, and to be in agreement with the transcurrent faulting postulated by seismologists from their fault-plane solutions of earthquakes in the same region.

Kehle (1964) provided the next significant step in the development of hydraulic fracturing by analyzing the stress distribution around the packed-off section of a well and the shear stresses caused by the packers. The shortcoming of Kehle's model is the oversimplification of the shear stress bands produced by the rubber packers. Later, Haimson (1968) pointed out that rubber is incompressible, so that axial compression results in a considerable lateral expansion which applies a normal load to the wellbore wall and thereby reduces the stress concentration at the corners between the rubber packers and the open hole. This will diminish the possibility of horizontal fracture initiation at these corners. Later, Stephansson (1983a) presented the results of laboratory tests of packers installed in steel tubes where he demonstrated the very low risk of fracture initiation at the packer ends of a straddle packer with a steel mandrel.

Hubbert and Willis (1957), Scheidegger (1962), Kehle (1964) and others discussed the implications of pump pressure records in wellbores with regard to the regional tectonic stresses and the orientation of fractures, but Fairhurst (1964) was the first to recommend hydraulic fracturing for the primary purpose of stress measurement. He listed several attractive features of hydraulic fracturing not possessed by the other stress measurement techniques available at that time, such as the flat jack and overcoring methods. Fairhurst (1964) also adopted the theory developed by Kehle (1964) to study the stresses developed around the wall of the pressurized interval between two packers and developed a simple theory to determine the stress distribution around a hole in orthotropic rock subjected to a far-field stress. He also stressed the possibility of determining fracture orientation by using an inflatable lining extruded slightly into the fracture, similar to the technique demonstrated by Fraser and Pettitt (1962). The impression packer technique is still extensively used today for determining hydraulic fracture orientation.

The process of hydraulic fracturing as a method for determining *in situ* stresses in brittle elastic formations at great depths was analyzed both theoretically and experimentally in the doctoral thesis by Haimson (1968). This work represents a milestone in the history of hydraulic fracturing as Haimson (1968) was the first to point out the importance of investigating whether or not the fluid used to induce and extend the fracture penetrates and flows into rock strata. Haimson (1968) showed that the pumped flow raises the pore fluid pressure in porous formations and creates additional stresses and displacements. This in turn lowers the critical pressure required to initiate the fracture and reduces the width of the newly formed fracture.

In a joint paper, Haimson and Fairhurst (1967) proposed a criterion for the initiation of vertical fractures, taking into consideration the contribution of the following three stress fields around a wellbore: (1) the non-hydrostatic regional stresses in the Earth's crust, (2) the difference between the fluid pressure in the wellbore and the formation fluid pressure, and

(3) the radial fluid flow through the porous rock from the wellbore into the formation due to the pressure difference.

Despite the extensive theoretical work on the subject of hydraulic fracturing that had been carried out by the mid-1960s, the amount of experimental work had thus far been very limited. In Haimson's thesis (1968), about 400 tests on hollow cylindrical and cubical specimens of five different porous and non-porous rocks were conducted under constant triaxial external loading and increasing borehole fluid pressure. In all of the samples tested, the induced hydraulic fractures were always tensile and no shear failure was observed. The fractures in all the rock types were either vertical or horizontal depending on the applied stresses. Later, Haimson and Fairhurst (1970) made the statement that hydraulic fracturing may soon cease to be a potential method and become a practical tool of stress determination.

Two of the first opportunities to test the hydraulic fracturing method in the field were made in an underground mine and a granite quarry, both in Minnesota, by Von Schonfeldt and Fairhurst (1970). The tests were carried out in open holes, 2.25 inches (57.1 mm) in diameter, with specially designed equipment. Fractures extending in the direction perpendicular to the least compressive stress were reported. The opportunity to test the applicability of the method at greater depths came with the experiment in the Rangely oil field, Colorado (Haimson, 1973; Raleigh, Healy and Bredehoeft, 1976). Intense seismic activity centered in and around the Rangely field in the vicinity of a strike-slip fault had been recorded and a research program was initiated to determine whether a correlation existed between earthquake triggering and the pore pressure of the formation. The hydrofracturing tool (down to a depth of 1900 m) showed that the vertical principal stress was intermediate in magnitude and that the remaining stresses were in accordance with a strike-slip fault stress regime. The stress measurements were considered very successful and a flurry of hydrofracturing research activities followed. Soon hydraulic fracturing was used to measure rock stresses from inside tunnels and shafts, as well as from boreholes drilled at the surface, to solve engineering problems. At the same time, hydraulic fracturing increased our understanding of the state of stress in the Earth's crust (Bredehoeft *et al.*, 1976; Haimson, 1976, 1978a, b, 1980; Rummel and Jung, 1975; Zoback, Healy and Rolles, 1977; Zoback, Tsukahara and Hickmann, 1980).

(a) First workshop on hydraulic fracturing

The first workshop on hydraulic fracturing for stress determination was held in Monterey, California, in 1981. Scientists and engineers interested in the technique convened for the first time to compare the different approaches, and also to learn from colleagues in order to improve the method. At that time, stress measurements with hydraulic fracturing had been introduced: (1) in North America by Haimson (1978a, b, 1983), Barton (1983), Hickman and Zoback (1983), and Haimson and Doe (1983); (2) in Germany by Rummel and Jung (1975) and Rummel, Baumgärtner and Alheid (1983); (3) in Iceland by Haimson and Voight (1977); (4) in the United Kingdom by Pine, Ledingham and Merrifield (1983); (5) in France and Belgium by Cornet (1983); (6) in Japan by Tsukahara (1983); (7) in China by Li *et al.* (1983); and (7) in Australia by Enever and Wooltorton (1983). In addition to hydraulic fracturing case histories, major issues addressed at the workshop included: interpretation techniques, innovation methods and technological improvements, and comparison between different stress measurement techniques. Haimson (1983), Doe *et al.* (1981, 1983), and Li *et al.* (1983) demonstrated good to excellent agreement between the results of deep hole hydrofracturing stress measurements and overcoring stress measurements,

with respect to both stress magnitudes and directions.

(b) International Symposium on Rock Stress and Rock Stress Measurements in Stockholm

The next major event where hydraulic fracturing was discussed in depth was the International Symposium on Rock Stress and Rock Stress Measurements held in Stockholm, in 1986. At that time, several countries had started (or were about to start) deep continental drilling programs in hard rocks. Rock stresses became a major issue in the research programs of the 1980s as it became clearer that stresses at great depths in the crust control the stability of borehole walls and the possible depth of drilling and extraction of heat (Batchelor and Pine, 1986; Dey and Brown, 1986). Questions of borehole stability and state of stress brought up the issue of the state of stress in different tectonic environments. Zoback, Mastin and Barton (1986) found that the limit of the commercially available equipment at that time was such that hydraulic fracturing in deep boreholes could reach depths of about 3 km for reverse faulting conditions, 8 km for strike-slip faulting and only 2 km in a situation with normal faulting. All these estimates were based on an assumption of $\mu = 0.6$ for the frictional coefficient of faults in geological formations.

The application of stress measurements to the solution of problems in tectonics is not as easy as in engineering design. Whereas the engineer is concerned with the current stress field affecting the rock, the geologist attempts to deduce the process that might have caused the stress. Representatives of the two schools met at the international symposium in Stockholm in 1986 and were able to exchange ideas about the role played by *in situ* stresses in both geological and engineering disciplines.

At that time several review articles had been published that summarized many of the stress observations known to us about the contemporary state of stress in continental areas. Haimson (1977) was the first to summarize stresses within the United States using the hydraulic fracturing technique. Later, McGarr and Gay (1978) presented results of stress versus depth from a compilation of stress data from Canada, southern Africa and sedimentary basins in the United States. They found that, in the United States, most of the measurements conducted using the hydrofrac technique in the upper 2.3 km in basins fell remarkably close to a gradient of 15 MPa/km. The measurements in granitic rocks did not show such a regular increase of stress with depth as the measurements in sandstone and shale. This conclusion was derived from the results of stress measurements in granitic rocks conducted in old shield areas such as Fennoscandia, Canada, South Africa and Australia. The scatter in the direction of the maximum horizontal stress was demonstrated by Stephansson, Särkkä and Myrvang (1986) using the stress measurements compiled in the Fennoscandian Rock Stress Data Base. Hydraulic fracturing methods were found to give the smallest stress magnitudes of all stress measuring techniques used in Fennoscandia.

Based on the results from deep continental drilling projects, the constraints imposed by experimental rock mechanics and existing *in situ* stress data from deep hydraulic fracturing borehole profiles, Rummel (1986) proposed the following expressions for the variation of the magnitude of the horizontal stresses with depth in the upper continental crust:

$$S_h/S_V = 0.15/z + 0.65$$

$$S_H/S_V = 0.25/z + 0.98$$

where S_H and S_h are the maximum and minimum horizontal stresses, S_V is the vertical stress and z is the depth in kilometers.

Stress orientations are intrinsically much more amenable to analysis than magnitudes because measurements of stress direction at all

depths can be meaningfully compared. In addition, hydrofracturing stress orientations can be compared with directions from earthquake focal mechanisms and the directions inferred from geological stress indicators. Raleigh (1974) and Sbar and Sykes (1973) presented results of the stress direction in eastern North America and concluded that S_H trends east to northeast from west of the Appalachian mountain system to the middle of the continent. They related this phenomenon to plate tectonics and seismicity. Later, Haimson (1978a) compiled all existing hydraulic fracturing results and showed a consistent NE–SW orientation for the horizontal principal stress direction in the continental United States based on the orientation of vertical hydrofractures. Zoback and Zoback (1980) made a compilation of the state of stress in the conterminous United States, including information from focal mechanisms, overcoring and the orientation of major geological features.

At the symposium in Stockholm, Stephansson, Särkkä and Myrvang (1986) and Bjarnason *et al.* (1986) presented results from a compilation of the orientation of the maximum horizontal stress for the Baltic Shield. A large scatter was observed in the orientation of the maximum horizontal stress, although there seemed to be a slight tendency for a NW–SE direction for the deepest stress measurements. This was contradictory to the results presented by Klein and Barr (1986) in which they stated that there existed a regional and uniform NW–SE directed maximum horizontal state of stress in western Europe. Most of their data came from borehole breakouts. Hence the results obtained by different research groups with different stress measuring techniques indicated that the state of stress in Europe was less consistent and clear compared with that in the United States. This was one of the driving forces behind the establishment of the World Stress Map Project of the International Lithosphere Program (Zoback, 1992; Zoback *et al.*, 1989).

(c) Second International Workshop on Hydraulic Fracturing Stress Measurements in Minnesota

Two years after the symposium in Stockholm and 7 years after the first workshop on hydraulic fracturing in Monterey, the Second International Workshop on Hydraulic Fracturing Stress Measurements was convened in Minneapolis, Minnesota, USA, in 1988. By that time the method of hydraulic fracturing had been introduced in many countries around the world and especially in those institutions having research programs in rock mechanics and geophysics. The number of testing projects had increased from a few per year during the 1970s to ten or more per year. Hydraulic fracturing had now been used for geophysical and earthquake research, for design of underground openings in civil and mining engineering, for oil and gas field stimulation and for geothermal extraction from hot dry rocks.

About 30 contributions to the workshop were later published as a special issue of the *International Journal of Rock Mechanics and Mining Sciences* with Haimson as coordinator (1989). The major objective of the workshop was to review the progress made in the last decade in the interpretation of the data recorded during testing. The outcome became very successful, partly because it convened some of the most experienced scientists and engineers interested in both hard rock and the more permeable rock masses typically encountered in oil and gas reservoirs.

More than half of the presented papers dealt with the interpretation of pressure versus time plots and traces of hydraulic fracture intersection with borehole walls. Lee and Haimson (1989) applied statistical techniques to hydraulic fracturing field data in order to enhance the objectivity of determining the shut-in pressure, the fracture reopening pressure and fracture orientation. An interactive interpretation system to allow quick access to different presentation types of pressure and flow data from field experiments was

presented by Baumgärtner and Zoback (1989). Poroelastic effects in the determination of the maximum horizontal principal stress were presented by Schmitt and Zoback (1989) and Detournay *et al.* (1989). Schmitt and Zoback (1989) also developed a new expression for the breakdown pressure based on a modified effective stress law for tensile fracturing. Warpinski (1989) reported stress determination from fracturing through perforations of cased boreholes. Other contributions related to oil and gas reservoirs were presented by Holzhausen *et al.* (1989) and Shlyapobersky (1989).

Doe and Boyce (1989), Wawersick and Stone (1989), and Bush and Barton (1989) all reached the conclusion that the interpretation of hydraulic fracturing records for rock salt using the classical approach (Haimson and Fairhurst, 1970) was not valid because of the ductile properties of rock salt. Improvements of hydrofracturing equipment were presented by Li (1989) and Bjarnason, Ljunggren and Stephansson (1989), among others. New data from the application of fracture pressurization tests and the HTPF method were presented by Baumgärtner and Rummel (1989) and Burlet, Cornet and Feuga (1989).

(d) Workshop on Stresses in the Earth's Crust at the 7th ISRM Congress, Aachen, Germany

The objective of the Workshop on Stresses in the Earth's Crust at the 7th ISRM Congress in Aachen in 1991 was to review the progress made over the last 3 years. The fact that the workshop was held only 3 years after the previous one demonstrated, in a way, the fast-growing interest in the field of rock stress and in the techniques to measure stresses. The number of data points about stresses in the Earth's crust had grown to a stage where it was meaningful to compile all existing data into the database of the whole world within the World Stress Map Project (Zoback, 1992; Zoback *et al.*, 1989). In late 1989 the database contained 3574 entries of which 3% came from hydraulic fracturing tests. Three years later, the number of hydraulic fracturing data had increased to more than 5000, as discussed in Chapter 11.

In response to the growing interest in the state of stress in the Earth's crust, the organizers of the 7th ISRM Congress in 1991 decided to devote one session of the workshop to stress measurements in deep boreholes. Hydraulic fracturing was, and still is so far, the only geophysical method applicable to determining absolute *in situ* stresses along deep vertical profiles in different tectonic environments. When the German Continental Drilling Project (KTB) and the US Deep Continental Drilling Project at Cajon Pass were initiated (Baumgärtner *et al.*, 1993), hydraulic fracturing became the obvious choice for determining the state of stress at depth. The KTB project is a basic geoscience research project aimed at exploring the mid-crust at the western margin of the Bohemian Massif in the center of a Variscan suture zone in eastern Europe. During the first phase of the KTB project, a 4 km deep pilot hole with a diameter of 6 inches (152 mm) was drilled and 14 depth intervals were selected for hydrofrac testing. The classical data analysis was applied in the stress evaluation procedure and poroelastic effects were assumed to be negligible due to the low rock porosity.

Baumgärtner *et al.* (1993) reported that within the depth range between 800 m and 3000 m, the stress magnitudes at KTB follow a linear trend with a stike-slip type of stress regime. The linearized stress profiles indicate that below about 5 km, the maximum horizontal stress S_H may become the intermediate stress and thus creates a stress environment which is in agreement with normal faulting. The orientation of S_H as determined by hydraulic fracturing and borehole breakouts was found to be N149° ± 15°, which is in general agreement with the global pattern of tectonic stress in central Europe. In the second phase of the KTB project, conducted between 1990 and 1994, drilling was conducted down

to a depth of 9 km and hydraulic fracturing tests were carried out at depths of 6 and 9 km (section 12.4.7). The average stress orientation at depths ranging between 3.2 and 8.6 km inferred from borehole breakouts was also found to agree with the NW–SE direction of maximum horizontal stress in central Europe (Brudy *et al.*, 1995).

The complex state of stress near the San Andreas fault (SAF) was first reported by Zoback, Healy and Rolles (1977), Zoback, Tsukahara and Hickman (1980) and Zoback *et al.* (1987). Hydrofracturing stress measurements at the Cajon Pass clearly reflected the structural complexity of the local geology in the vicinity of the SAF. The majority of the measurements of S_H were found to follow a linear trend with depth and the overall stress state was found to cause normal faulting or strike-slip faulting. The stress orientations, surprisingly, suggest a left-lateral shear stress on planes parallel to the SAF and do not correlate with the right-lateral slip movement of the fault. On the other hand, the results of the stress measurements at Cajon Pass support the idea of a weak SAF which moves under very small shear stresses, implying theoretical fault friction coefficients of about 0.1 (Baumgärtner *et al.*, 1993).

During 1990 a program of downhole hydrofracture stress measurements was undertaken in surface boreholes throughout the coalfields of England and the results were reported by Jeffery and North (1993). The depth of the tests ranged from 320 m to 1123 m and the tests were conducted in silty mudstones, siltstones and fine-grained sandstones. Conventional test equipment and data recording and evaluation techniques were employed. In general, in non-faulted areas, the ratio of horizontal principal stresses S_H/S_h was found to be 2 : 1 and the majority of test data indicated a reverse slip faulting tectonic stress pattern (Fig. 2.4). Other stress measurements conducted in the Ruhr region of Germany were presented by Müller (1993).

Interpretation of rock stresses obtained with various measuring techniques was an important issue at the 1991 workshop and the contributions to this workshop clearly demonstrated the strong activity in the field. The contribution by Klasson, Ljunggren and Öberg (1991) presented a new graphical interpretation technique for determining the shut-in pressure P_s. This method was similar to the one developed by Tunbridge (1989) and made use of the rate of pressure decay after pump shut-off, which was represented by two exponential functions. The technique was applied to a site investigation for nuclear waste in Finland and was found to work better than the conventional tangent divergence and tangent intersecting methods of interpretation.

Interpretation of the state of stress in inclined boreholes is a classical problem in the field of rock stress measurement and hydrofracturing in particular. The only available method directly suitable for stress calculations from hydrofracturing data in arbitrarily inclined holes is the HTPF method (Cornet, 1986; Cornet and Valette, 1984). Klasson, Ljunggren and Öberg (1991) presented a new method for the interpretation of the orientation of S_H from measurements in inclined boreholes and applied the method with good results to hydrofracturing data in a borehole in Finland inclined at 60–63°.

At the 7th ISRM Congress, Haimson, Lee and Herrick (1993) presented a special case of the conventional elastic method for stress determination in arbitrarily inclined boreholes. The induced hydrofracture must meet the requirements of being both vertical and axial with respect to the test hole. If so, the maximum horizontal stress is determined from the classical hydraulic fracturing equations (Haimson and Fairhurst, 1967, 1970) with a term that considers the vertical stress and the hole inclination. This is a very useful and simple approach with many applications, particularly in site locations for underground structures where inclined boreholes are commonly drilled.

In a general report on the workshop to the delegates of the 7th ISRM Congress, Stephansson (1993) concluded that the science of rock stress and rock stress measurements, in general, is still evolving and that its applications are very dynamic.

4.2.2 TECHNIQUES, EQUIPMENT AND PROCEDURES

Hydraulic fracturing involves the isolation of part of a borehole using an inflatable straddle packer and the subsequent pressurization of the hole until the wall rock fractures (Fig. 4.2a). If an axial fracture is produced, the pressure record obtained during the test can be used to determine the magnitude of the secondary principal stresses in the plane normal to the borehole axis. During a hydraulic fracture test, pressure versus time is recorded. The magnitude of the minor secondary principal stress component can be determined directly from the recorded shut-in pressure. The magnitude of the major secondary principal stress can be calculated from relationships involving the fracture initiation pressure, the fracture reopening pressure and the tensile strength of the rock (section 4.2.3).

An impression packer together with a compass or a borehole scanner can be used to determine the orientation of the fracture (Fig. 4.2b). This in turn gives the orientation of the major principal stress in the plane normal to the borehole axis. An impression packer consists of an inflatable element wrapped with a replaceable soft rubber film. When the packer is inflated, the film is extruded into the fracture, which leaves a permanent impression on the surface. With a known orientation of the impression packer in the borehole, the direction of the stress field can be inferred.

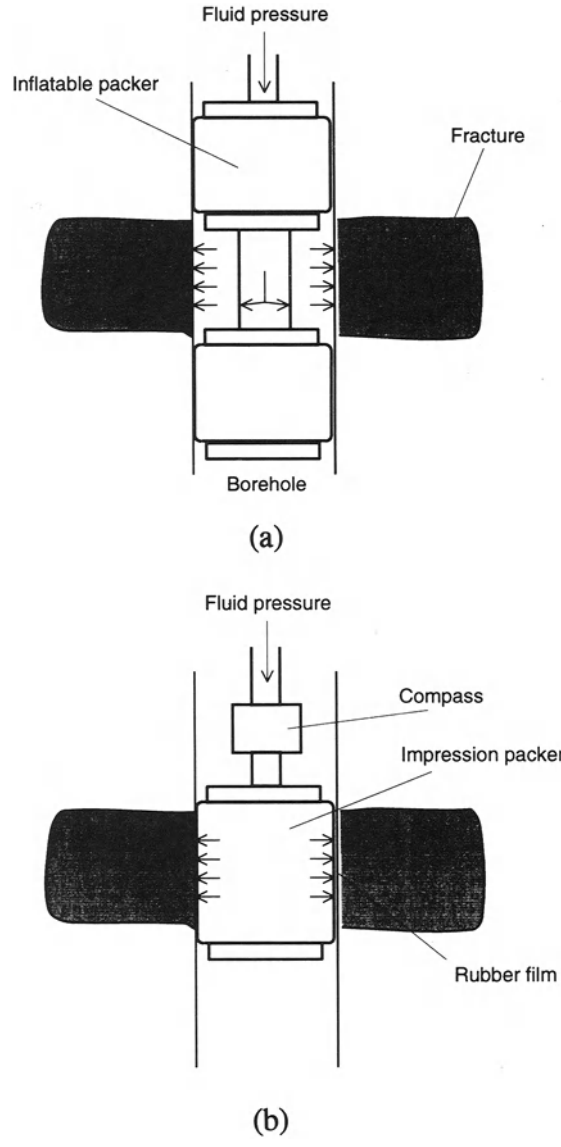

Fig. 4.2 Basic steps of hydraulic fracturing. (a) Pressurization of borehole until fracturing of the rock in the borehole wall, (b) determination of fracture orientation with impression packer and compass.

(a) Equipment

The first field experiments on hydraulic fracturing for the purpose of determining *in situ* stresses were carried out by Von Schonfeldt and Fairhurst (1970). The tests were conducted in open holes, 56 mm in diameter, with specially designed equipment consisting of fracturing tools and pressurizing systems. The packed-off interval was either 1 ft (0.3 m) or 2 ft (0.6 m) long and a light oil was used for the fracturing fluid. High-pressure motorized

pumps capable of delivering a flow rate of about 1 l/min at 70 MPa were used to inject the fracturing fluid. Breakdown pressures of up to 40 MPa were recorded at two underground locations and one near-surface location in igneous and shale formations. Even during these very first hydraulic fracturing tests, some of the problems (which still exist even today) were explored, such as the rate effect of pumping, the reduction of breakdown pressure in subsequent tests and the formation of horizontal fractures in high stress regions.

The introduction of the hydrofracturing technique for stress measurement of deep wells had some definite initial drawbacks as it required heavy equipment such as a drill rig and drill rods for lowering the probe downhole (Haimson and Fairhurst, 1970; Haimson and Stahl, 1970). Currently, the oil industry service companies can provide a straddle packer system and special pipes which permit control of packer inflation and test zone pressurization with valves which operate by varying the weight on the rods, rotating the rods, or by dropping bars or balls down the drill string. In 1989 Tunbridge, Cooling and Haimson proposed a new system for hydraulic fracturing stress measurement in deep boreholes within the United Kingdom. The system, shown in Fig. 4.3, is simple, robust and reliable.

An improvement in the conventional technique used in the 1970s and thereafter came with the introduction of a flexible, high-pressure hose solely for the inflation of the downhole packers (Haimson, 1978a, b). The hose was lowered strapped to the outside of the drill rod, and was instrumental in making hydrofracturing a continuous method without the need to retrieve the straddle packer after each test.

An improvement which dramatically contributed to enhancing the cost efficiency of stress measurements was the introduction of wireline hydrofracturing (Rummel, Baumgärtner and Alheid, 1983). By replacing conventional drilling with a lightweight tripod and a portable hoist, and replacing the drill rods with a slim, continuous high-pressure hose and wireline, the system becomes considerably lighter to operate, substantially faster and thus more economical (Fig. 4.4). The wireline conductors and downhole instrumentation attached to the straddle packer and impression packer allow hydrofracturing and packer pressure readings to be taken at the depth of testing. Wireline hydrofracturing has been used extensively in Europe by Rummel, Baumgärtner and Alheid (1983) and Rummel, Höhring-Erdmann and Baumgärtner (1986), in the United States by Haimson and Lee (1984) and Haimson (1988), and in Australia by Enever and Chopra (1986). These measurements have been conducted in 56 mm and 75 mm diameter drillholes down to a depth of 1000 m in many different rock types.

(b) Multihose system

The multihose system field unit constructed at the Luleå University of Technology in 1981–1982 was the first of its kind for hydrofracturing application in which pressure lines, signal cable and load-carrying wire were combined into a single umbilical cable (Stephansson, 1983a). Due to very good experience with the first multihose system, a second system was built and permanently installed on a new field truck (Figs 4.5 and 4.6). A detailed description of the system is presented by Bjarnason, Ljunggren and Stephansson (1989), and a summary of the experience with the multihose system for hydraulic fracturing stress measurement is discussed below.

The main advantages of the multihose system are independence of drill rig, and simplicity and efficiency during operation. The same independence can be achieved without the expensive multihose using loose component wireline systems in which pressure tubing is clamped to the wire. The operation of a loose component wireline system is, however, more cumbersome and the risk of getting stuck is probably larger. Rigging up at the test

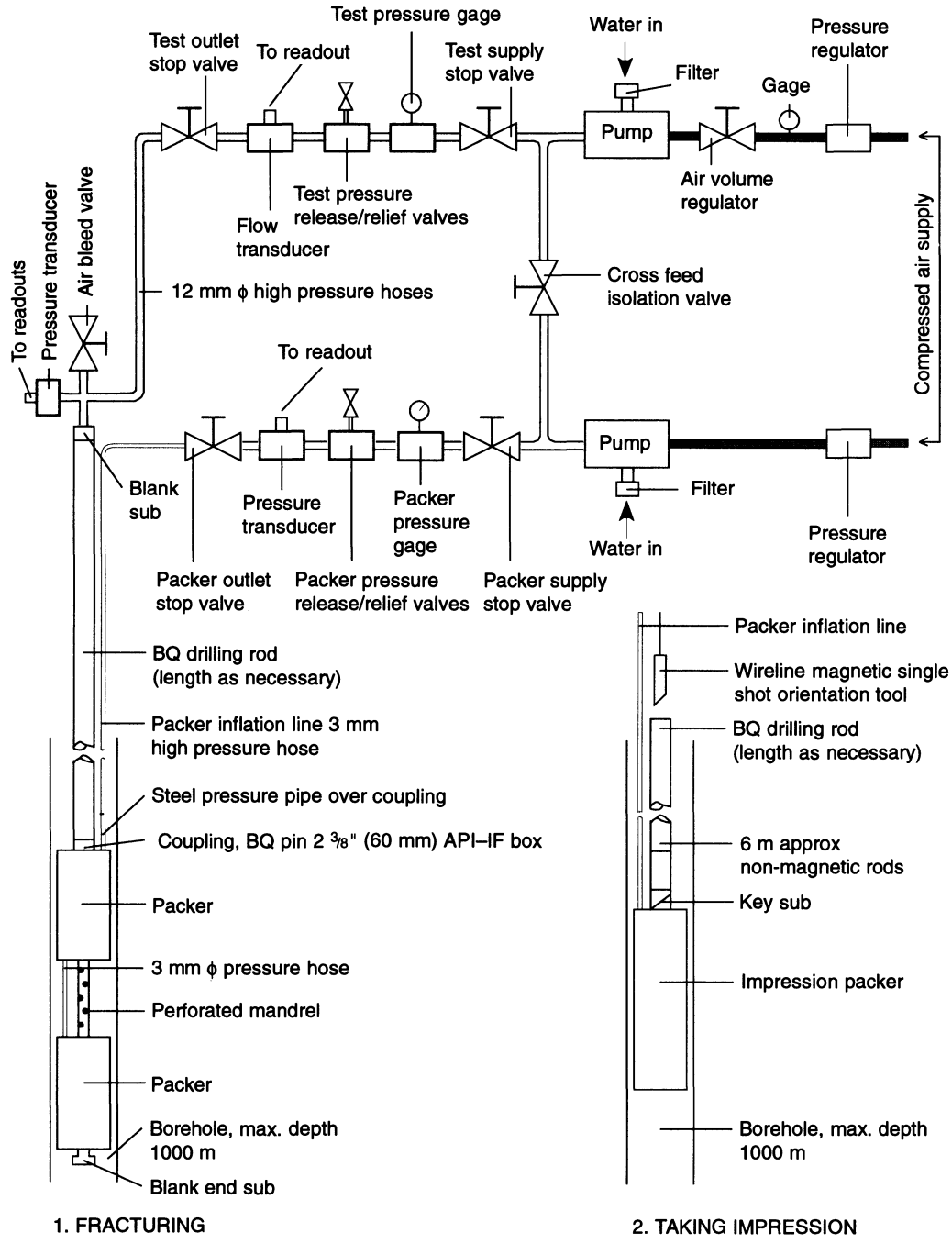

Fig. 4.3 System for hydraulic fracturing stress measurement in deep boreholes. (After Tunbridge, Cooling and Haimson, 1989, Courtesy of the National Academy Press, Washington, DC.)

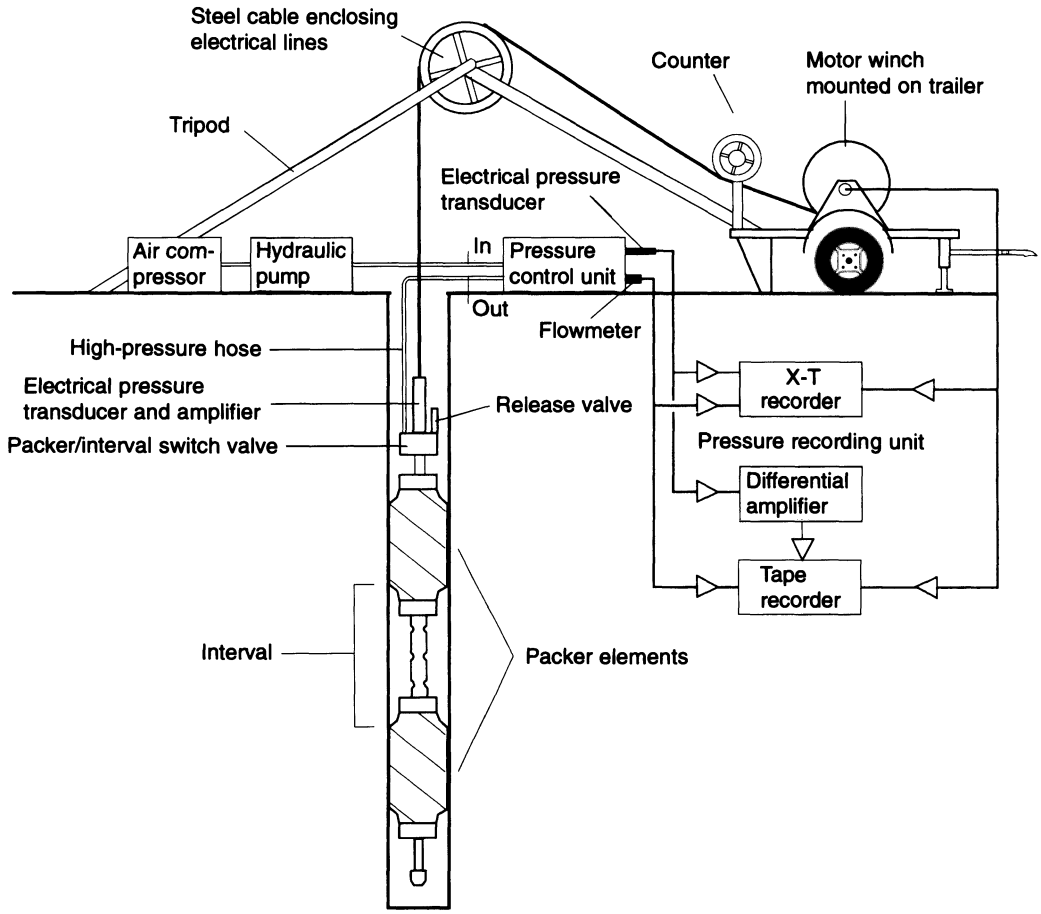

Fig. 4.4 The Ruhr University Bochum wireline hydraulic fracturing system mounted on a trailer. (After Rummel, Baumgärtner and Alheid, 1983.)

site takes 2 h. All fracturing work and impression work can be operated by one person, with the exception of installing and removing the packers from the borehole, which requires two persons. Travel times in the hole are short; the 1000 m hose is run from the surface down to the bottom within 15 min and up again in less than 30 min. This is particularly important in deep boreholes with a large number of test points (40–50 test points in a 1000 m deep borehole) where the application of the conventional impression method for fracture orientation would otherwise result in excessively long and expensive field periods.

The latest version of the system has the option of a flowmeter and a shut-in valve located downhole and close to the straddle packer. The installation of a downhole valve takes care of the problems with flow-dependent pressure drop and recording of multihose stiffness. This version of the system allows determination of rock mass stiffness and the stiffness of single fractures (Rutqvist *et al.*, 1992).

Disadvantages of the multihose system on a truck include the high initial cost, the fact that manufacturing of the multihose is highly specialized work, and once finished, it is not possible to change its design or performance. To benefit fully from the advantages of a

Fig. 4.5 Photograph of first-generation hydrofracturing field truck at Luleå University of Technology, Sweden.

multihose system, a wide range of auxiliary components are needed which are not readily available on the market. Auxiliaries include everything from vital components, such as a drum and a hose feeder, up to a full-size truck for permanent installation of the instrumentation. The risk of the equipment getting stuck in the borehole is greater than for conventional drillstring operated instruments. The chance of recovering equipment stuck downhole by means of the multihose is small. The hose should therefore be designed with a weak tension link at the cable head to be torn off in an emergency, leaving only the packer assembly in the hole.

A cross-section of a 1000 m long multihose with three high-pressure hoses, two electrical cables, a stress member and filler compound is presented in Fig. 4.7. The multihose is designed to be slightly denser than water to minimize loading on the stress member. The pumping system consists of three different units and each unit is remotely controlled and computerized (Fig. 4.8). The data measuring and logging system, comprising transducers, chart recorder and data logger, is used to measure and record the data during the tests.

(c) Borehole tools

The most common downhole tools for hydrofracturing stress measurements are (1) a straddle packer, (2) an impression packer, and (3) a single-shot magnetic orientation tool (Fig. 4.9). The straddle packer system comprises heavy-duty inflatable rubber packer elements on a specially designed and constructed hollow mandrel. The connecting piece between the packers is perforated to transmit hydraulic pressure in the hose to the test zone. The packers are inflated by hydraulic pressure in a separate system. An example of the straddle packer assembly is shown in Fig. 4.10.

Tangential and axial tensile stresses at the ends of a pressurized straddle packer with and without a connecting piece have been studied theoretically and experimentally by Stephansson (1983a). The calculated circumferential stresses at the ends of a pressurized straddle packer in a steel tube were

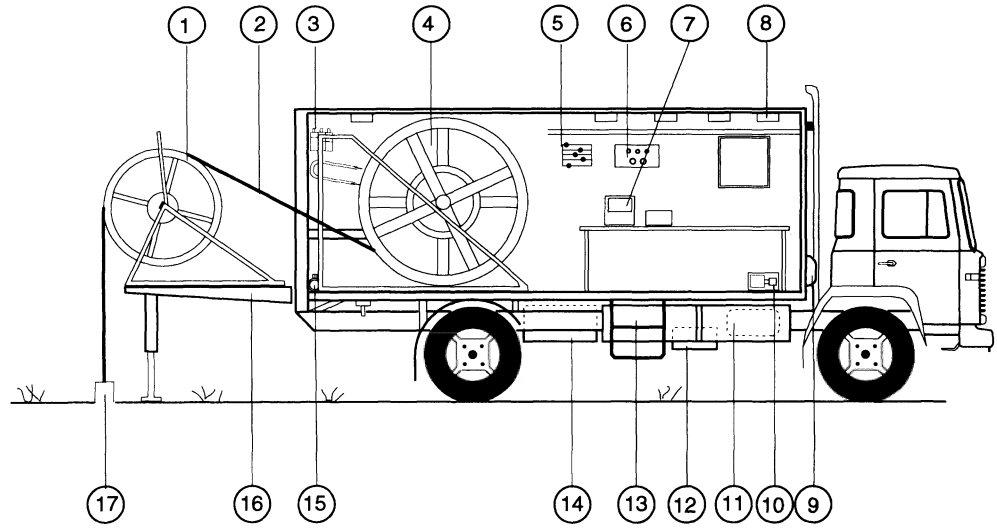

Fig. 4.6 Components of the hydrofracturing field truck at Luleå University of Technology, Sweden. 1, Guidewheel for multihose; 2, multihose; 3, control unit of the hydraulic system, remote controlled proportional valves; 4, drum for multihose, 1000 m; 5, flowmeters; 6, manifold for control of fracturing flow and packer pressure; 7, data acquisition system; 8, working lights, 24 V DC and 220 V AC; 9, cabin heater, 7 kW; 10, high-pressure water pump; 11, compressed air tubes; 12, hydraulic pump; 13, diesel fuel tanks, 400 l for long field periods; 14, hydraulic tank; 15, winch; 16, working platform, adjustable height and inclination; 17, borehole. (Source: *Int. J. Rock. Mech. Min. Sci. & Geomech. Abstr.*, **26**, Bjarnason, B., Ljunggren, C. and Stephansson, O., New developments in hydrofracturing stress measurements at Luleå University of Technology, p. 582, Copyright 1989, with kind permission from Elsevier Science Ltd, The Boulevard, Langford Lane, Kidlington, UK.)

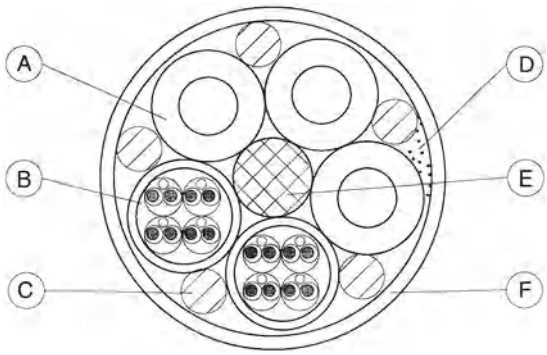

Fig. 4.7 Cross-section of a 1000 m long multihose: A, 0.25 inches (6 mm) hose, proof pressure 70 MPa; B, signal cable, four-screened twisted pair; C, filler wires; D, filler compound; E, Kevlar stress member; and F, polyurethane jacket. Outer diameter of the multihose is 40 mm. (After Bjarnason, Ljunggren and Stephansson, 1989.)

found to be in close agreement with experimental results. Although an inflated element of a straddle packer is supposed to generate only radial stresses to the borehole wall, it also causes tensile stresses in the connecting mandrel piece between the packers.

The impression packer is used to determine the orientation and morphology of fractures on the borehole wall and was first introduced by Anderson and Stahl (1967). The impression packer is a heavy-duty long packer element mounted on a specially designed and manufactured mandrel. A soft uncured rubber is glued around the packer element. The packer is inflated through the high-pressure hydraulic hose. In order to keep track of the orientation of the impression packer, a single- or multiple-shot magnetic borehole compass is mounted together with the impression packer

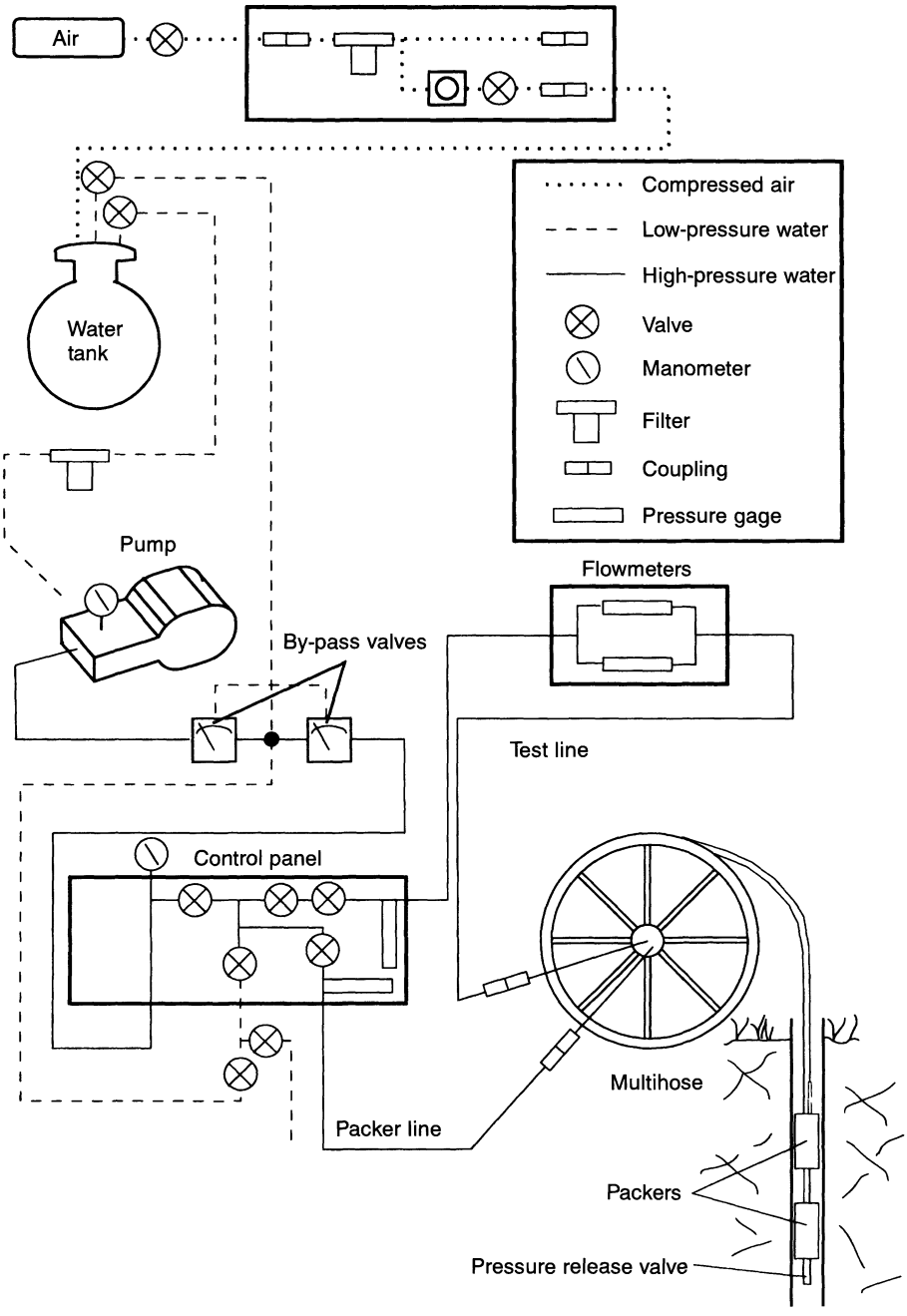

Fig. 4.8 Pumping system and control unit for hydraulic fracturing at Luleå University of Technology. (After Bjarnason, Ljunggren and Stephansson, 1989.)

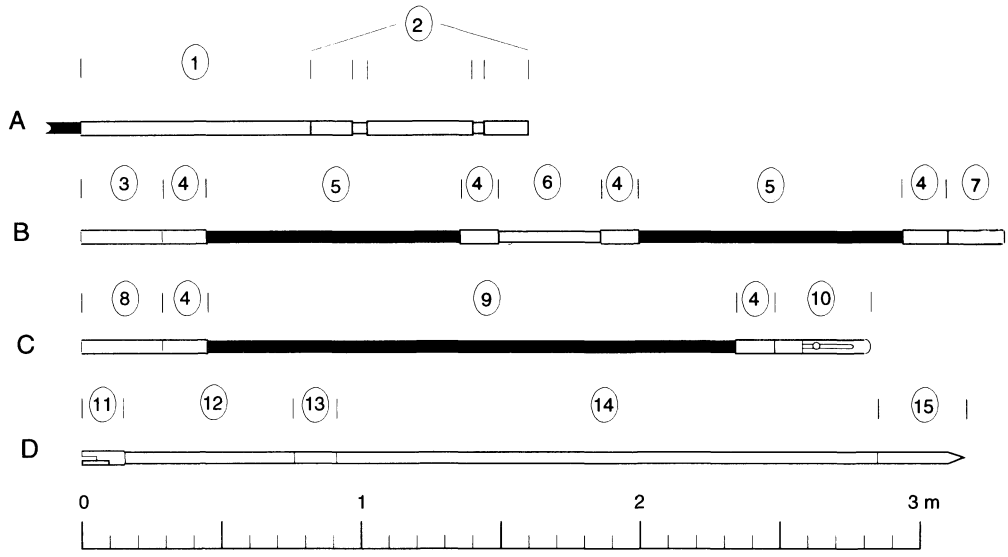

Fig. 4.9 Borehole tools for hydraulic fracturing with multihose system. A, Multihose and cable head; B, straddle packer for fracturing and injection testing; C, impression packer; D, single-shot magnetic borehole compass. 1, Cable head connection to multihose; 2, cable head; 3, upper end of fracturing tool, connects to (2); 4, packer end, pressed-on steel binding to the inflatable rubber; 5, inflatable packer rubber; 6, mandrel; 7, bottom end of fracturing tool; 8, upper end of impression tool, connects to (2); 9, inflatable part of impression packer, covered with uncured rubber; 10, bottom end of impression tool; 11, connection of orientation tool to the impression packer, connects to (10); fixed orientation against packer; 12, extension rod, aluminum; 13, upper end plug to single-shot barrel; 14, stainless steel barrel to single-shot compass camera; 15, bottom end plug to the barrel, fixes the orientation of the single-shot compass camera.

(Fig. 4.9). After a certain time allowed for lowering the equipment into the borehole, the instrument shoots a picture of an inclinometer and a compass and this allows the tracing of the fracture orientation. To facilitate proper recording of the fracture impression on the packer element, a transparent celluloid sheet is normally wrapped around the packer and the impression is marked with permanent ink.

The fracture azimuth can also be recorded with an ultrasonic borehole televiewer (Zemanek *et al.*, 1970) or more modern borehole scanners. The televiewer displays, as brightness, the amplitude of an acoustic pulse reflected off the borehole wall, and the induced fracture is viewed as a dark line on the image, as demonstrated by Zoback, Tsukahara and Hickmann (1980). The application of borehole scanners such as FACSIMILE for the analysis of fractures in boreholes is discussed in Chapter 8 in relation to the borehole breakout method.

(d) Minifrac system

The growing demand for rock stress data in mining and underground construction, and the need for developing smaller and easier systems to use instead of the large-scale equipment, have led to the manufacturing of self-contained and portable systems, such as the CSIRO Minifrac system (Enever, Walton and Wold, 1990). The equipment is made for 38 mm diameter boreholes and a maximum packer pressure of 35 MPa (Fig. 4.11). Hand pumps allow for a maximum pressure of 40 MPa and a maximum flow rate of 200 ml/min. An intrinsically safe version is available, suitable for use in hazardous areas such as underground coal mines.

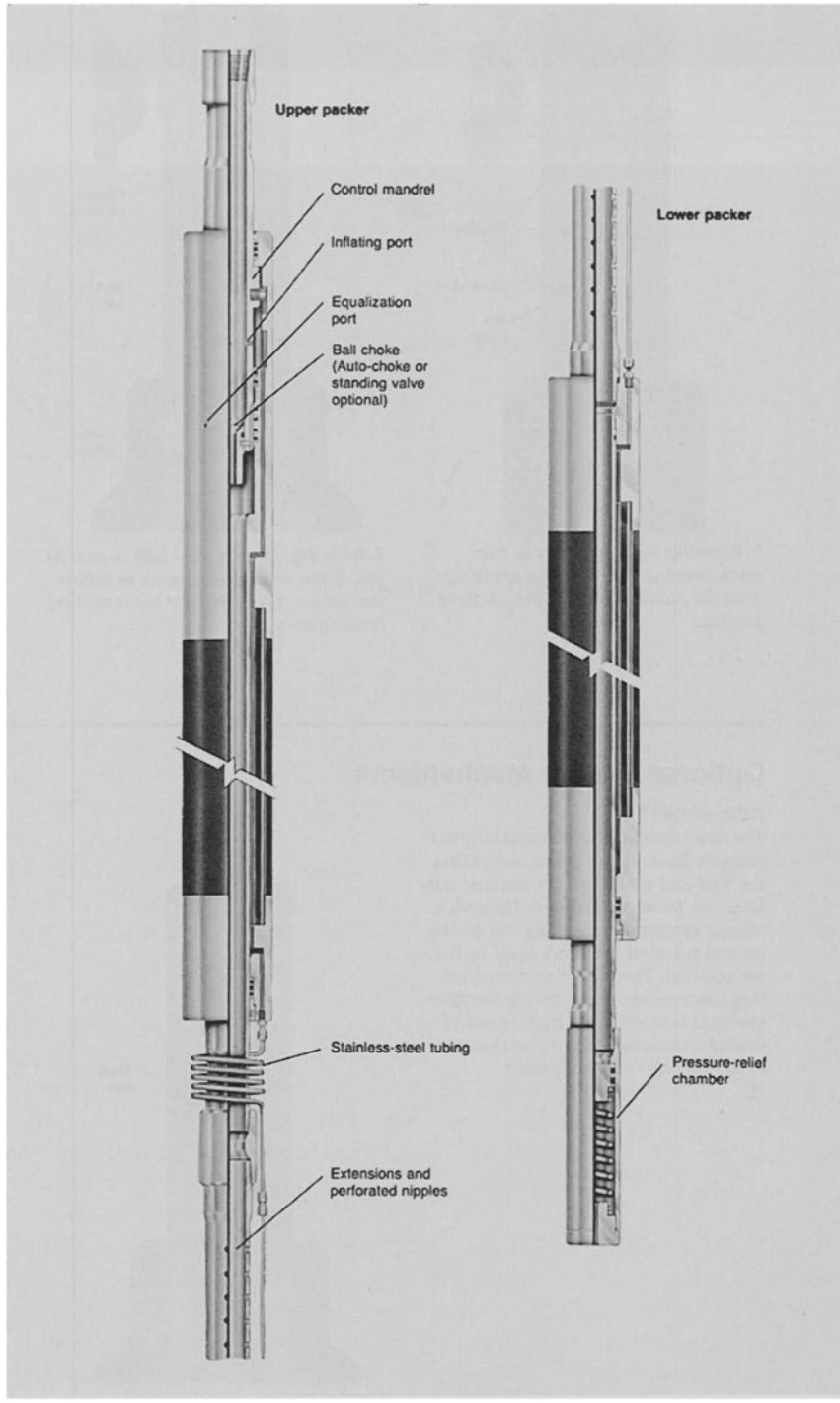

Fig. 4.10 Example of straddle packer assembly. The upper and lower packers inflate and deflate simultaneously and are separated by perforated tubing nipples. (Courtesy of TAM International.)

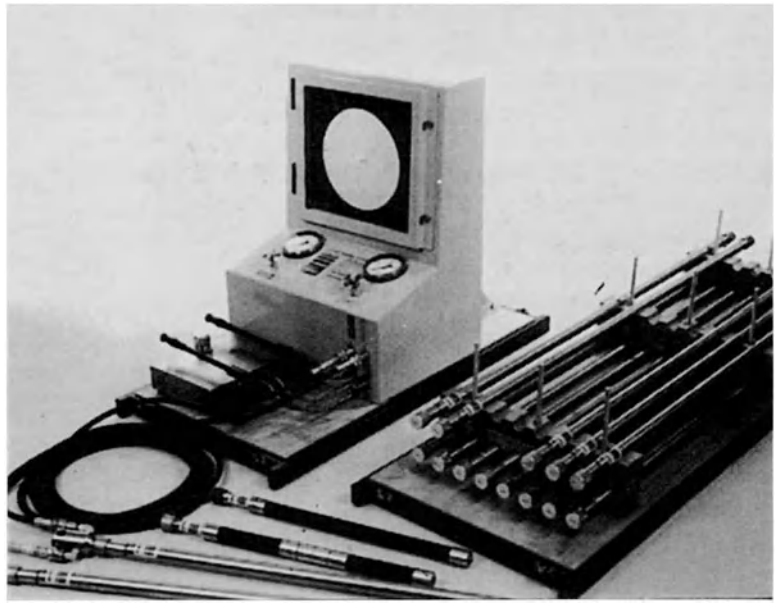

Fig. 4.11 The CSIRO Minifrac system supplied with two transportation modules comprising installation and test tools and a pressurization and recording system. (Courtesy of MINDATA, Australia.)

(e) Testing procedures

The Commission on Testing Methods of the ISRM proposed suggested methods for rock stress determination using the hydraulic fracturing technique (Kim and Franklin, 1987). We present below a summary of the ISRM recommendations with regard to drilling and inspection and testing. In principle, we recommend following the ISRM-suggested methods.

Drilling and inspection

1. The choice of a hole diameter and size of downhole hydraulic fracturing equipment may be made based on the equipment available and the budget of the project. Following determination of the test location and depth, a drillhole should be sunk below that depth to provide the test intervals. The final choice of the test zone length and depth is made based upon the fracture characteristics of recovered cores or on the inspection of the drillhole wall by an optical or acoustic logging tool or impression packer.
2. Rock cuttings and/or cores are examined in detail to determine rock characteristics at the test horizons. The choice of packers and inflation pressures may be affected by rock hardness and the roughness of the drillhole wall.
3. The hole should be flushed to remove debris and/or the drill bit may be lowered to the test depth to clear the passage for the packer assembly.
4. The position, orientation and aperture of geological discontinuities within the test section should be estimated and recorded, using the core, impression packers, a downhole camera and an acoustic televiewer or a borehole scanner, if practical. This investigation also serves as a pre-test run of the fracture orientation measurement.
5. It may sometimes be advisable to run a drillhole caliper log to avoid placing packers in oversized sections of the hole.

6. The packer assembly is inserted to the predetermined depth, the depth is recorded and the packers are inflated to a pressure sufficient to contain the applied fluid pressure.
7. When filling the injection tubing, care must be taken to eliminate air from the system. Trapped air greatly increases the compressibility of the system and has an adverse effect on the rate of pressure build-up during test interval pressurization.

Testing

8. When pressure is monitored at the ground surface, the pressure in the test interval is increased slowly to ensure minimal pressure losses in the tubing. When pressure is monitored within the test section, pressure losses are unimportant. No standard for the pressurization rate of flow exists; however, a common range of pressurization rate is about 0.1–2.0 MPa/s. The pressurization rate is controlled by the constant flow rate selected. The appropriate flow rate to achieve the desired pressurization rate will vary depending on the overall compressibility of the test system, which largely reflects the elasticity of the tubing, the length of the tubing, the fluid compressibility and the volume of fluid in the test system. In general, deep tests with large-diameter tubing will require higher flow rates than short-hole tests with smaller diameter tubing. The packer pressure should be initially set well below the anticipated breakdown pressure; the packer pressure should be increased at the same rate as the injection pressure. This procedure reduces the possibility of fracture initiation caused by the packer pressure. The test interval pressure is recorded against time. As pressure increases, both tangential and vertical effective stresses can become tensile. Fracture will occur if the induced tensile stress reaches the drillhole rupture strength. Evidence of failure may be obtained from the pressure–time curve. The drillhole fluid pressure at the moment of drillhole rupture is termed the 'fracture initiation pressure' or breakdown pressure.
9. After injecting a volume sufficient to propagate a fracture of length equal to about three times the drillhole diameter, injection is stopped and the hydraulic system is sealed or 'shut in', yielding the shut-in pressure, also called the 'instantaneous shut-in pressure'.
10. The test section pressure is vented to atmosphere and venting is continued until pressure rebound no longer occurs when the system is sealed. A lack of rebound indicates that the fracture is closed and can be reopened.
11. Several additional repressurizations are normally sufficient and they should be conducted at similar, constant flow rates.
12. If the instantaneous shut-in pressure is ill-defined, subsequent pressurizations with a stepwise increase of injection pressure are recommended. The level of constant pressure during pressure build-up defines the shut-in pressure and the minimum normal stress across the fracture.
13. The straddle packer is deflated and the equipment is removed from the drillhole. Care should be taken to deflate the packers fully before attempting to move them.
14. The impression packer is inserted into the test location and inflated to a pressure in excess of the fracture reopening pressure. An impression of the fracture will be left on the soft rubber film. The orientation of the fracture can be obtained from the known orientation of the impression packer in the borehole. Another option is to log the borehole with a borehole televiewer or borehole scanner.
15. The tensile strength of the rock mass may be estimated from laboratory tests on core samples or may be obtained *in situ* by comparing the fracture breakdown pressure with subsequent fracture reopening

pressures. The difference between the two pressures is taken as the tensile strength.

The purpose of the suggested methods presented by Kim and Franklin (1987) is to achieve some degree of standardization without inhibiting the development or improvement of techniques. The increasing need for accurate and reliable rock stress determinations will ensure that measurement techniques and equipment will continue to evolve.

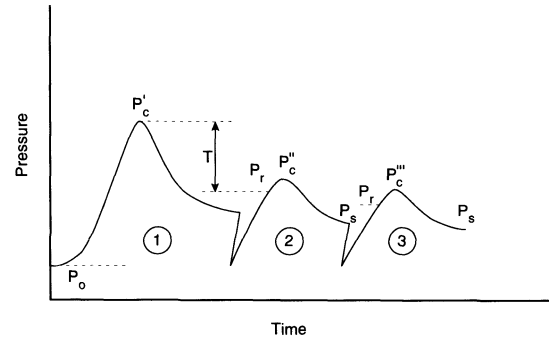

Fig. 4.12 Typical recording of pressure versus time for a hydraulic fracturing operation in a poroelastic rock formation. P_o = pore pressure, P'_c = first breakdown pressure, P''_c and P'''_c = second and third breakdown pressures, P_r = reopening pressure and P_s = shut-in pressure or fracture closure pressure.

4.2.3 THEORY OF HYDRAULIC FRACTURING

The hydraulic fracturing method makes possible the determination of the state of stress in boreholes at considerable depth, and in almost any rock formation. The principal idea is that when a fluid is pumped into a section of a borehole that is sealed off by packers, the initial pressure on the wall of the borehole is reduced and at some points becomes tensile. When the stresses at the borehole wall exceed the tensile strength of the rock (which is low and typically one-tenth to one-twentieth of the rock uniaxial compressive strength), a fracture is formed. The fracture will propagate in the direction perpendicular to the minimum *in situ* principal stress. Repeated pumping and recording of the pressure versus time allows determination of the principal stresses around the borehole at a particular depth. Depending upon the type of rock tested in a borehole and the orientation of the borehole, different analytical expressions can be derived for the analysis of hydraulic fracturing tests. Figure 4.12 shows a typical recording of pressure versus time for a hydraulic fracturing operation in a poroelastic rock formation.

(a) Breakdown pressure P_c

In this section the basic equations for the breakdown pressure are derived for the most general case of hydrofracturing of a linearly elastic, porous, isotropic and homogeneous rock formation. A second assumption is that the rock formation is subjected to a non-hydrostatic state of stress with one of the three principal stresses acting parallel to the vertical direction and along the axis of the borehole. In deriving the basic equations, first presented by Haimson and Fairhurst (1967, 1970), we assume that the total principal regional stress field acting at a point in the Earth's crust has the following components:

$$\begin{aligned} S_H &= \sigma_{11} + P_o \\ S_h &= \sigma_{22} + P_o \\ S_V &= \sigma_{33} + P_o \end{aligned} \tag{4.1}$$

where S_H, S_h are the maximum and minimum horizontal total principal *in situ* stresses, S_V is the vertical total principal stress, σ_{11}, σ_{22} and σ_{33} are the effective principal regional stresses with $\sigma_{11} \geq \sigma_{22}$, and P_o is the formation pore fluid pressure. Note that here we consider compressive stresses to be positive whereas Haimson and Fairhurst (1967) defined tensile stresses to be positive.

When a vertical borehole of radius r_w is drilled into the formation, the original state of stress is disturbed and the new resulting total stress field $S_{ij}^{(1)}$ $(i, j = r, \theta)$ around the borehole has components

$$\begin{aligned} S_{rr}^{(1)} &= \sigma_{rr}^{(1)} + P_o \\ S_{\theta\theta}^{(1)} &= \sigma_{\theta\theta}^{(1)} + P_o \\ S_{r\theta}^{(1)} &= \sigma_{r\theta}^{(1)} \end{aligned} \tag{4.2}$$

where $S_{rr}^{(1)}$, $S_{\theta\theta}^{(1)}$ and $S_{r\theta}^{(1)}$ are the radial, tangential and shear stresses acting on the borehole wall, respectively. The Kirsch solution (Jaeger and Cook, 1976) can be used to determine the expression for the radial effective stress $\sigma_{rr}^{(1)}$, the tangential effective stress $\sigma_{\theta\theta}^{(1)}$ and the shear stress $\sigma_{r\theta}^{(1)}$. These stress components vary with the distance r from the center of the borehole and the angle θ measured counterclockwise from the direction of S_H.

When fluid is pumped into the borehole, two additional stress fields are introduced. The increase in pressure from the original pressure P_o to P_w at the borehole wall introduces a stress field $S_{ij}^{(2)}$ $(i,j = r,\theta)$ at any distance r with components

$$\begin{aligned} S_{rr}^{(2)} &= \frac{r_w^2}{r^2} p_w \\ S_{\theta\theta}^{(2)} &= -\frac{r_w^2}{r^2} p_w \\ S_{r\theta}^{(2)} &= 0 \end{aligned} \tag{4.3}$$

where p_w is the pressure difference between the injected fluid P_w and the pore fluid in the formation P_o. Provided that the rock formation is permeable to the injected fluid, that difference will cause an outward radial flow. If the injected fluid has properties similar to those of the formation pore fluid and the fluid flow is assumed to be axisymmetric, the theory of poroelasticity holds and the third stress field $S_{ij}^{(3)}$ $(i,j = r,\theta)$ can be expressed as

$$\begin{aligned} S_{rr}^{(3)} &= \frac{\alpha(1-2\nu)}{r^2(1-\nu)} \int_{r_w}^{r} p(r) r \, dr \\ S_{\theta\theta}^{(3)} &= \frac{-\alpha(1-2\nu)}{1-\nu} \left[\frac{1}{r^2} \int_{r_w}^{r} p(r) r \, dr - p(r) \right] \\ S_{r\theta}^{(3)} &= 0 \end{aligned} \tag{4.4}$$

In equation (4.4) $p(r)$ is the increase in pressure above P_o at any distance r, ν is the Poisson's ratio of the formation and α is the Biot coefficient equal to

$$\alpha = 1 - K/K_s \tag{4.5}$$

where K_s and K are the bulk moduli of the rock constituents (grains) and the rock (grains, pores and microcracks), respectively. The parameters α and ν are thus characteristics of the porous solid only.

The distribution of stresses around the borehole is then obtained by superposition of the three different stress fields, e.g.

$$S_{ij} = S_{ij}^{(1)} + S_{ij}^{(2)} + S_{ij}^{(3)} \tag{4.6}$$

At the borehole wall $(r = r_w)$, it can be shown that, at the two points aligned with the direction of the maximum horizontal principal stress S_H (corresponding to $\theta = 0°$ and 180°), the total stress components are equal to

$$\begin{aligned} S_{rr} &= P_o + p_w = P_w \\ S_{\theta\theta} &= \sigma_{\theta\theta} + P_w = 3\sigma_{22} - \sigma_{11} + P_o \\ &\quad - p_w + \alpha p_w \left(\frac{1-2\nu}{1-\nu} \right) \\ S_{r\theta} &= 0 \end{aligned} \tag{4.7}$$

Rearranging equation (4.7) gives the expression of the tangential effective stress $\sigma_{\theta\theta}$ in the direction of S_H, e.g.

$$\sigma_{\theta\theta} = 3\sigma_{22} - \sigma_{11} - p_w \left(2 - \frac{\alpha(1-2\nu)}{1-\nu} \right) \tag{4.8}$$

which is the first to become tensile around the borehole wall.

We now postulate that the breakdown of the borehole wall and fracture initiation take place when the tangential effective stress given by equation (4.8) is equal to the tensile strength T of the rock, e.g.

$$\sigma_{\theta\theta} = -T \tag{4.9}$$

and that the hydraulic fracture extends in a vertical plane perpendicular to S_h. Combining equations (4.8) and (4.9), the minimum pressure at the borehole wall to induce fracture,

also known as the breakdown pressure P_c, is given by the equation

$$P_c = \frac{T + 3\sigma_{22} - \sigma_{11}}{2 - \alpha\left(\frac{1-2\nu}{1-\nu}\right)} + P_o \qquad (4.10)$$

Since α varies between 0 (for stiff, low-porosity rocks) and 1 (compliant rocks), and ν varies between 0 and 0.5, the denominator in equation (4.10) can vary between 1 and 2. Typical poroelastic constants for water-saturated rocks are presented in Table 4.1. For hard rocks with typical values of $\nu = 0.25$ and $\alpha = 0.25$, the denominator in equation (4.10) becomes equal to 1.8. A porous sandstone with $\alpha = 0.85$ and $\nu = 0.2$ gives a denominator of 1.37. Hence if poroelastic constants are available, they should be regarded in the calculation of the effective stresses σ_{11} and σ_{22}.

In the case of a non-penetrating fluid, the total stress $S_{\theta\theta}$ in (4.7) is replaced by

$$S_{\theta\theta} = \sigma_{\theta\theta} + P_o = 3\sigma_{22} - \sigma_{11} + P_o - p_w \qquad (4.11)$$

Combining equations (4.9) and (4.11), the breakdown pressure P_c reduces to

$$P_c = T + 3\sigma_{22} - \sigma_{11} + P_o \qquad (4.12)$$

Equations (4.10) and (4.12) can be expressed in terms of the maximum and minimum horizontal *in situ* stresses S_H and S_h by using equation (4.1). This gives

$$P_c = \frac{T + 3S_h - S_H - 2\eta P_o}{2(1-\eta)} \qquad (4.13)$$

and

$$P_c = T + 3S_h - S_H - P_o \qquad (4.14)$$

In equation (4.13), η is the poroelastic coefficient equal to

$$\eta = \frac{\alpha(1-2\nu)}{2(1-\nu)} \qquad (4.15)$$

Calculated values of η for different water-saturated rocks are presented in Table 4.1.

Equations (4.1)–(4.15) represent the 'classical theory' for the analysis of hydraulic fracturing tests as presented by Haimson and Fairhurst (1967, 1970). Although poroelasticity is used in the derivation of equation (4.10), the coupled diffusion–deformation phenomena which exist in fluid-saturated porous rocks are not taken into account. A complete analysis of the problem also has to consider how the state of stress around the borehole and near the hydraulic fracture is altered by diffusion of the fracturing fluid in the rock and how the fluid-saturated rock responds due to the flow. Both issues were addressed analytically by Detournay and Cheng (1988) and Detournay *et al.* (1989). In particular, they emphasized how the tangential stress due to the difference

Table 4.1 Poroelastic constants for water-saturated rocks (Source: Detournay, E. *et al.* Copyright 1989, with kind permission from Elsevier Science Ltd, The Boulevard, Langford Lane, Kidlington, UK.)

Rock type	G (N/m^2)	ν	ν_u	B	C (m^2/s)	η	α
Ruhr sandstone	1.3×10^{10}	0.12	0.31	0.88	5.3×10^{-3}	0.28	0.65
Tennessee marble	2.4×10^{10}	0.25	0.27	0.51	1.3×10^{-5}	0.06	0.19
Charcoal granite	1.9×10^{10}	0.27	0.30	0.55	7.0×10^{-6}	0.09	0.27
Berea sandstone	6.0×10^{9}	0.20	0.33	0.62	1.6×10^{0}	0.30	0.79
Westerly granite	1.5×10^{10}	0.25	0.34	0.85	2.2×10^{-5}	0.16	0.47
Weber sandstone	1.2×10^{10}	0.15	0.29	0.73	2.1×10^{-2}	0.26	0.64
Ohio sandstone	6.8×10^{9}	0.18	0.28	0.50	3.9×10^{-2}	0.29	0.74
Pecos sandstone	5.9×10^{9}	0.16	0.31	0.61	5.4×10^{-3}	0.34	0.83
Boise sandstone	4.2×10^{9}	0.15	0.31	0.61	4.0×10^{-1}	0.35	0.85

in pressure between the borehole and the rock formation (e.g. $S^{(3)}_{\theta\theta}$ in equation (4.4)), evolves with time. They also discussed how rapid drainage of the rock mass near the borehole has a direct impact on the stress concentration. At the borehole wall, the rock is characterized by the drained elastic modulus, while the rock farther away is characterized by the stiffer undrained modulus. As a result of this stiffness contrast, the borehole is partially shielded from the stress concentration during the period soon after drilling. This short-term stress concentration at the point of fracture initiation of the borehole wall was derived by Detournay and Cheng (1988) and is given by

$$\lim_{t\to 0} \sigma_{\theta\theta}(r_w, t) = (3\sigma_{22} - \sigma_{11})\left(\frac{1-\nu_u}{1-\nu}\right) \quad (4.16)$$

where ν and ν_u are the drained and undrained Poisson's ratios, respectively, and t is the time elapsing from drilling a borehole with radius r_w. At very small times the peak of the tangential stress is actually located inside the rock and not at the wall of the borehole as predicted by the elastic analysis. At greater times the tangential stress decreases monotonically with distance and the stress concentration at the wall increases toward the long-term elastic values of $3\sigma_{22} - \sigma_{11}$ in the direction of the maximum horizontal stress S_H. The characteristic time to reach this stage is about $\tau \approx r_w^2/C$, where C is the diffusivity constant given by the following expression:

$$C = \frac{2\kappa B^2 G(1-\nu)(1+\nu_u)^2}{9(1-\nu_u)(\nu_u-\nu)} \quad (4.17)$$

where κ is the mobility coefficient defined as the ratio of the permeability to the fluid viscosity, B is the Skempton coefficient and G is the shear modulus. The radial stress component is reported to experience little variation as a function of time and distance from the borehole wall.

As remarked first by Haimson and Fairhurst (1967) and more extensively by Detournay *et al.* (1989), it is not correct to apply the breakdown expression (4.13) to the limiting case of zero porosity. It is noteworthy that equation (4.13) does not reduce to equation (4.14) as the porosity (or the poroelastic coefficient η) approaches zero. In the diffusion phenomenon of the fluid, it is assumed that one can always locate an arbitrary small distance near the wall where the pore pressure is a significant portion of the borehole pressure, no matter how small the porosity. This assumption breaks down at zero porosity when there is no pore pressure anywhere.

Equations (4.13) and (4.14) also apply for the reopening pressure P_r defined in Fig. 4.12, provided that the tensile strength is set at zero. Sometimes the reopening pressure P_r coincides with the second and successive breakdown pressures P_c'' and P_c''' also shown in Fig. 4.12. The reopening pressure is a reliable measure of the stress concentration when a sharp drop in pressure is obtained in the pressure–time record (Detournay *et al.*, 1989).

(b) Tensile strength from field testing, T

Bredehoeft *et al.* (1976) first suggested that the tensile strength of the formation could be determined from the difference in pressure between the first breakdown pressure P_c' and the borehole reopening (refrac) pressure P_r necessary to open an existing hydraulic fracture, so that

$$T = P_c' - P_r \quad (4.18)$$

The assumption here is that the fracture closes completely between each cycle of pressurization and that P_r is the pressure level at which the pre-existing hydrofracture just begins to open, i.e. it is equal to the minimum compressive hoop stress at the hole wall induced by the far-field stresses. Notice that the value of P_r is not necessarily the peak of the pressure–time curve during the second and subsequent cycles but the point where a sudden slowdown in pressure increases with time (Fig. 4.12). Combining equations (4.14) and

(4.18), the maximum horizontal *in situ* stress S_H is equal to

$$S_H = 3S_h - P_r - P_o \tag{4.19}$$

From about 1978 onward, the above method of determining the tensile strength of rock formations in hydrofracturing stress measurements has been commonly used (Haimson, 1978a, b; Hickman and Zoback, 1983; Lee and Haimson, 1989; Zoback, Tsukahara and Hickman, 1980). If equation (4.13) is used to determine the reopening pressure P_r, equation (4.18) is now replaced by $T = 2(1 - \eta)(P'_c - P_r)$, and the maximum horizontal *in situ* stress S_H is now equal to

$$S_H = 3S_h - 2(1 - \eta)P_r - 2\eta P_o \tag{4.20}$$

(c) Breakdown pressures in poorly consolidated strata

Analytical solutions for stresses and strains around a circular borehole in an impermeable and permeable unconsolidated medium during drilling and hydraulic fracturing were derived by Wang and Dusseault (1991a, b). Their theories also account for the effect of stress path and strain weakening yield before injection of a fluid into the borehole. They demonstrated that the breakdown pressure in a plastically deformed medium cannot be used to predict the *in situ* state of stress by the conventional breakdown pressure analysis since unconsolidated rocks such as oil sand or weak shale display hysteresis in their deformation response to external loading. A simple elastoplastic model was used where the material is linearly elastic until the yield criterion is reached, weakens instantly and thereafter behaves perfectly plastically.

The equations for the breakdown pressure presented above assume tensile rupture (equation (4.9)). As this type of rupture might be the case in elastic impermeable media, it is reasonable to assume that in weak permeable media, either during borehole drilling or borehole injection, shear failure of the borehole wall may occur before tensile failure, and may even affect tensile failure by reducing the tensile strength of the rock. Wang and Dusseault (1991b) analyzed that problem by assuming that shear failure of the rock is governed by a Mohr–Coulomb criterion, which in terms of effective stresses can be expressed as follows:

$$\tau = c_o + \sigma'_n \tan \phi_p \tag{4.21}$$

where c_o and ϕ_p are the peak cohesion and friction angle of the rock, respectively. The Mohr–Coulomb criterion can be rewritten in terms of the major and minor (effective) principal stresses, σ'_1 and σ'_3 as follows:

$$\sigma'_1 - N\sigma'_3 + M = 0 \tag{4.22}$$

where

$$N = \frac{1 + \sin \phi_p}{1 - \sin \phi_p} \tag{4.23}$$

$$M = -\frac{2c_o \cos \phi_p}{1 - \sin \phi_p} \tag{4.24}$$

Two shear rupture modes were considered by Wang and Dusseault (1991a, b): active and passive. The active shear rupture can occur during drilling of the borehole and along the minimum principal *in situ* stress axis (Fig. 4.13a). No tensile fractures are normally created in this load path unless there is an exceptionally large stress difference, and even then the tensile fractures are of limited length. For active shear rupture, $\sigma'_\theta = \sigma'_1$ and $\sigma'_r = \sigma'_3$. Substituting into equation (4.22) the expressions for the effective tangential and radial stresses at the borehole wall in the direction of S_h, Wang and Dusseault (1991b) determined the expression for the borehole pressure P_{sa} when active shearing is initiated, e.g.

$$P_{sa} = \frac{3S_H - S_h + M_a - 2\eta P_o}{(1 + \alpha_s) + N_a(1 - \alpha_s) - 2\eta} \tag{4.25}$$

where $M_a = M$ and $N_a = N$, η is defined in equation (4.15), and α_s is a poroelastic constant.

The passive shear rupture can occur during borehole injection and at right angles to the minimum principal *in situ* stress axis (Fig.

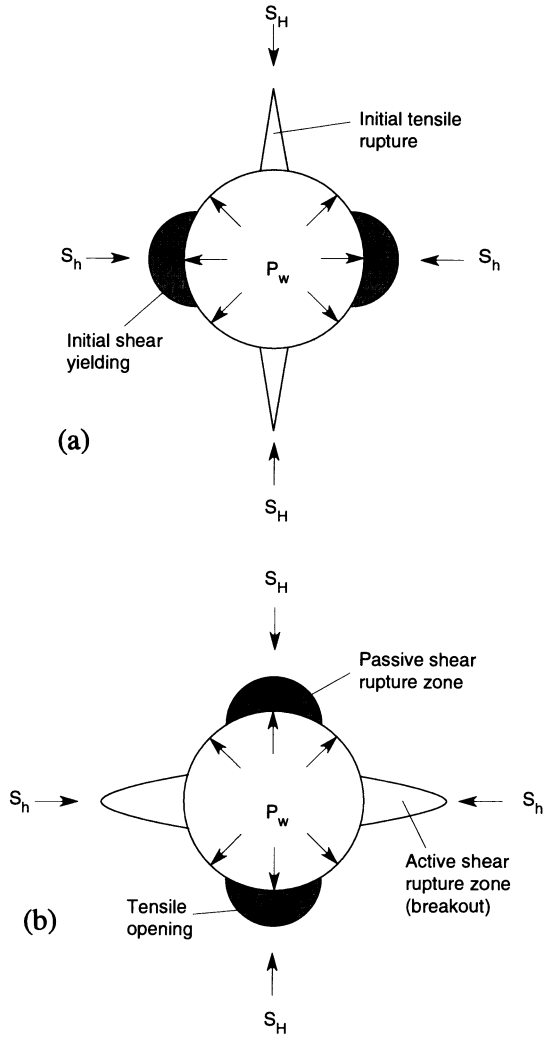

Fig. 4.13 Active shear rupture in (a) and passive shear rupture in (b) before tensile fracturing of the wall of a borehole in poorly consolidated rock. (After Wang and Dusseault, 1991b.)

4.13b). In this case, $\sigma'_\theta = \sigma'_3$ and $\sigma'_r = \sigma'_1$. Substituting into equation (4.22) the expressions for the effective tangential and radial stresses at the borehole wall in the direction of S_H, Wang and Dusseault (1991b) determined the expresssion for the borehole pressure P_{sp} when passive shearing is initiated, e.g.

$$P_{sp} = \frac{N_p(3S_h - S_H - 2\eta P_o) - M_p}{(1 - \alpha_s) + N_p(1 + \alpha_s - 2\eta)} \quad (4.26)$$

where $N_p = 1/N$ and $M_p = -M/N$. Rearranging equation (4.26) by dividing the numerator and denominator by N_p, using $M_p/N_p = -M$ and letting $\alpha_s = 1$, gives

$$P_{sp} = \frac{3S_h - S_H - 2\eta P_o + M}{2(1 - \eta)} \quad (4.27)$$

Coexisting with the Mohr–Coulomb criterion for shear failure, there is a criterion for tensile failure similar in form to equation (4.9), e.g.

$$\sigma_{\theta\theta} = -T_s \quad (4.28)$$

where T_s is the 'damaged' value of the tensile resistance. Substituting T_s into (4.13) gives

$$P_{tp} = \frac{3S_h - S_H - 2\eta P_o + T_s}{2(1 - \eta)} \quad (4.29)$$

Comparison of equation (4.27) with equation (4.29) indicates that $P_{sp} < P_{tp}$ and therefore shear rupture initiates before tensile fracture.

In many cases of poorly consolidated rock masses, true effective tension is never attained since shear yield always occurs first. Further, if passive shear rupture takes place in the borehole wall it will create redistribution of the tangential stress around the borehole wall and create a reduction in the tensile strength T_s of the material, particularly in the type of materials considered here. Thus a tensile rupture can immediately follow shear rupture, as shown in Fig. 4.13b. This phenomenon is referred to as 'shear tensile rupture' by Wang and Dusseault (1991a, b).

Wang and Dusseault (1991a, b) also concluded that in weakly consolidated strata, one has to be careful in trying to relate breakdown pressure to the tensile resistance of the intact rock. In the same way, one has to be careful when interpreting the tensile strength from the difference in pressure between the first breakdown pressure and the borehole reopening pressure necessary to open an existing hydraulic fracture.

The stress distribution during fluid injection in the plastic zone close to the borehole wall and the elastic zone outside the area of influence of the borehole was presented by Wang

and Dusseault (1991b). They found that the minimum radial stress is located inside the porous medium rather than at the borehole wall. This may force the radial stress to be zero inside the porous medium before a tensile fracture is initiated at the borehole wall. Under these conditions, the initial breakdown pressure does not reflect the *in situ* stress in a proper manner and the difference between the first breakdown pressure and the fracture reopening pressure cannot be used to estimate T_s. At this stage of knowledge, we must question the possibility of reaching closed-form analytical solutions in the near future for all the complicated processes developed around a borehole in weakly consolidated sedimentary rocks during hydraulic fracturing. What can be said, however, is that in the limit of slow pressurization, i.e. when the fluid pressure both in the pores and the defects in a boundary layer of a given thickness is the same as the borehole pressure, the general equation of Haimson and Fairhurst (1967) applies (Detournay, personal communication, 1995).

(d) Breakdown pressure for low-porosity rocks

In the derivation of the breakdown equations (4.13) and (4.14), it is assumed that the hydraulic fracture initiates when the circumferential (Terzaghi) effective stress at the borehole wall first exceeds the rock tensile strength T. Schmitt and Zoback (1989) found major differences between the computed values of S_H associated with three existing breakdown equations, especially for low-compressibility rocks at great depths for which the Biot coefficient α is small. They considered (1) the breakdown equation for a porous material with fluid penetration (equation (4.13)), (2) the breakdown equation when the fluid is non-penetrating (equation (4.14)), and (3) the breakdown equation for the case of a non-porous medium without pore pressure (equation (4.14) with $P_o = 0$). In order to resolve the discrepancy between the computed values of S_H, Schmitt and Zoback (1989) proposed a breakdown equation based on a modified effective stress failure criterion in which the tensile strength is dependent on an effective stress law of the type

$$\sigma = S - \beta P_o \tag{4.30}$$

where S is the total stress, P_o is the pore pressure and β is a constant that varies between 0 and 1. In rock masses with vanishing porosity, we expect β to approach zero. Using the modified effective stress law, Schmitt and Zoback (1989) rederived the breakdown pressure equations. For a porous material with penetrating fluid, equation (4.13) is replaced by

$$P_c = \frac{T + 3S_h - S_H - 2\eta P_o}{1 + \beta - 2\eta} \tag{4.31}$$

For the case of non-penetrating fluid, equation (4.14) becomes

$$P_c = T + 3S_h - S_H - \beta P_o \tag{4.32}$$

As remarked by Schmitt and Zoback (1989), both equations (4.31) and (4.32) have the advantage that, for non-porous rocks (for which η and β are zero), they reduce to the same equation, e.g.

$$P_c = T + 3S_h - S_H \tag{4.33}$$

The introduction of the modified effective stress law by Schmitt and Zoback (1989) lends support to the elimination of the pore pressure term in the interpretation of hydrofracturing stress measurements in low-permeability, hard, granitic rocks which have been applied by researchers such as Pine, Ledingham and Merrifield (1983), Rummel, Baumgärtner and Alheid (1983) and Bjarnason, Ljunggren and Stephansson (1989).

It is noteworthy that in low-porosity/ permeability crystalline rocks, in which most of the scientific hydraulic fracturing stress measurements are performed, there exist at least three breakdown pressure criteria on which the interpretation of S_H is based, corresponding to equations (4.13), (4.14) and (4.31).

According to the classical approach, breakdown characterizes the end of the elastic regime and the immediate initiation of tensile failure. Detournay and Carbonell (1994) pointed out that hydraulic fracturing could initiate significantly before the borehole pressure attains its peak. Thus the aforementioned three breakdown pressure criteria may be more appropriately characterized as fracture initiation criteria rather than breakdown criteria. Further, none of the equations for breakdown pressure include expressions of size effect and rate of pressurization, although this has been reported in the literature. Finally, the fact that there exist three different breakdown pressure criteria for low-porosity/permeability rocks makes it very important to state very clearly in the reporting of *in situ* stress measurements which criterion was applied in the determination of the maximum horizontal stress S_H.

(e) Breakdown pressure for rock salt

Based on finite element analyses of the normalized tangential stress distribution around a borehole in salt subjected to an isotropic far-field stress state, Wawersick and Stone (1989) demonstrated that the inelastic properties of rock salt could result in pronounced stress relaxation at the borehole wall. The inelastic rock behavior involves both rate-independent and rate-dependent permanent deformations. Therefore the strong time dependency of the tangential stress distribution obtained in the finite element analyses suggests that the shapes of the pressure versus time records of hydraulic fracturing tests in rock salt might change with the time delay between drilling and hydraulic fracturing. This change should lead to pronounced progressive reduction in breakdown and reopening pressures. From hydraulic fracturing tests in salt formation at the Waste Isolation Pilot Plant in New Mexico, USA, Wawersick and Stone (1989) found that stable pressure versus time records, with little or no pressure drop between peak and driving pressures, could be obtained in isotropic stress fields. Unstable pressure records were found to be characteristic of anisotropic stress conditions. Conclusions about the existence of either isotropic or anisotropic *in situ* stress were supported by the patterns of the hydraulic fractures. The fact that the records of hydraulic fracturing tests could not be interpreted uniquely led Wawersick and Stone (1989) to introduce a factor M, equal to the ratio of the relaxed stress concentration to the instantaneous elastic stress concentration at the borehole boundary, in the equation for the breakdown pressure for rock salt. Equation (4.14) becomes

$$P_{rs} = M(3S_h - S_H) - P_o(2M - 1) + T \quad (4.34)$$

Likewise, the equation for the fracture reopening pressure for rock salt is obtained by setting $T = 0$ in equation (4.34).

Computed magnitudes of M after 55 days were found to be $M = 0.41$ when $S_H/S_h = 1$, $M = 0.61$ when $S_H/S_h = 1.4$ and $M = 1.3$ when $S_H/S_h = 2$, assuming $S_h = 13.85$ MPa. It is important to recognize that the factor M is not only stress path-dependent but is likely to vary for different types of rock salt. Estimates of S_h were obtained from the fracture driving process.

Based on the results of hydraulic fracturing tests in salt beds in Texas, USA, Bush and Barton (1989) claimed that the measurement of S_h is applicable in salt using the pressure decline method after shut-in. With the reduction of the tangential stresses at the borehole and the solubility or erosion of salt along the fracture interface, they claimed that neither the calculated maximum stress S_H nor the values of tensile strength T could be considered realistic of the *in situ* conditions.

In summary, the elastic interpretation of hydraulic fracturing test records in salt is suspect. Due to the non-elastic properties of salt and its solubility, the classical equations for breakdown pressure are not valid. Nevertheless, the form and propagation of the induced hydraulic fractures are good indicators of

hydrostatic or non-hydrostatic stress conditions. Laboratory experiments conducted by Doe and Boyce (1989) proved that hydraulic fractures with strong preferred orientations could be indicators of stress ratios $S_H/S_h > 1.1$–1.3. Thus proximity to hydrostatic conditions can be determined from the form of the hydraulic fracture alone, regardless of the ambiguities in the interpretation of the pressure versus time records from the field tests.

(f) Fracture mechanics approach to determine breakdown pressure

Fracture mechanics provides the tools necessary to account for the presence of pre-existing flaws or cracks in the borehole wall rock, and to correlate transient pressure recordings during a hydrofracturing test with fracture propagation. The pressurization of cracks in the rock contributes to the stress intensity at their tips. Thus hydraulic fracturing can be defined in terms of the critical condition leading to crack growth, rather than in terms of fracture initiation in an idealized continuum as in the 'classical theory'.

The use of fracture mechanics principles to analyze results from hydraulic fracturing stress measurements was initiated by Hardy (1973) and Hardy and Fairhurst (1974). The fact that the effect of pressurizing the borehole wall with pre-existing cracks had been neglected, and that the method of Haimson and Fairhurst (1967) appeared to overestimate the prediction of the maximum horizontal stress S_H, led Abou-Sayed, Brechtel and Clifton (1978) to follow a fracture mechanics approach to *in situ* stress determination by hydrofracturing. The fracture mechanics analysis was applied to determine the stress field at a depth of 837 m in a shale formation in West Virginia, USA. The analysis suggested that uncertainties associated with crack geometry (size and shape) could be reduced greatly by modifying hydrofracturing tools to include the cutting of narrow notches of known depth into the borehole wall in order to determine S_H and the principal stress direction.

A linear relationship between the breakdown pressure and the *in situ* stress components can be derived using a linear elastic fracture mechanics (LEFM) approach. We present below a summary of that approach. More details of the mathematical derivations can be found in the papers by Winther (1983) and Rummel (1987).

We consider the geometry of Fig. 4.14 showing a symmetrical double crack of half-length a extending on each side of a borehole with radius r. The borehole is drilled in an infinite plate subjected to compressive far-field horizontal stresses S_H and S_h. When the pressure P_w in the borehole is such that the tensile strength of the rock is exceeded, a vertical fracture is formed parallel to the direction of S_H. The fluid is then allowed to penetrate into the crack and the pressure inside the fracture is denoted as P_a. Since we are using an LEFM approach, the stress intensity in the vicinity of the crack tips can now be expressed by using the principle of superposition of stress intensity factors for each of the four loading sources depicted in Fig. 4.15, e.g.

$$K_I(S_H, S_h, P_w, P_a) = K_I(S_H) + K_I(S_h) + K_I(P_w) + K_I(P_a) \quad (4.35)$$

where K_I is the stress intensity factor for mode I crack propagation. The general formula of the stress intensity factor for a tension crack of half-length a, in an infinite plate of the type shown in Fig. 4.14 has the form

$$K_I = \frac{1}{(\pi a)^{1/2}} \int_{-a}^{a} \sigma_{\theta\theta}(x, 0) \left(\frac{a+x}{a-x}\right)^{1/2} dx \quad (4.36)$$

where $\sigma_{\theta\theta}(x, 0)$ is the tangential stress in the crack plane $y = 0$. For each of the four loading sources of Fig. 4.15, K_I can be determined once we have an analytical expression for $\sigma_{\theta\theta}(x, 0)$.

Derivation of K_I *for loading source* S_H

Using the Kirsch solution for the stresses around a circular hole in an infinite plate

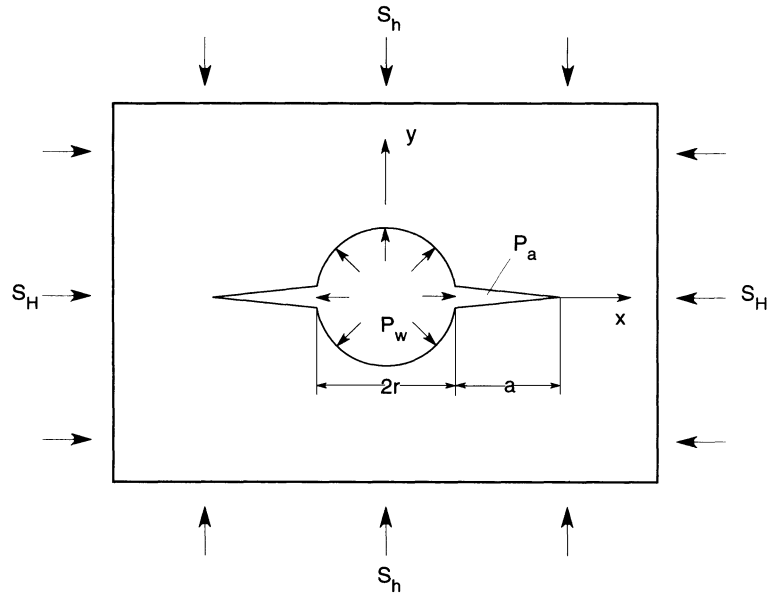

Fig. 4.14 Fracture mechanics model of hydraulic fracturing in an infinite plate subjected to a far field state of stress. (After Rummel, 1987.)

subjected to far-field stresses S_H and S_h (Jaeger and Cook, 1976), the tangential stress $\sigma_{\theta\theta}(x, 0)$ due to the effect of S_H only can be expressed as follows:

$$\sigma_{\theta\theta} = \frac{S_H}{2}\left[\left(\frac{r}{x}\right)^2 - 3\left(\frac{r}{x}\right)^4\right] \qquad (4.37)$$

Substituting equation (4.37) into equation (4.36) and integrating yields

$$K_I(S_H) = -S_H(r)^{1/2} f(b) \qquad (4.38)$$

where $f(b)$ is a dimensionless stress intensity function of the normalized crack length $b = 1 + a/r$.

Derivation of K_I *for loading source* S_h

Again, using the Kirsch solution, the tangential stress $\sigma_{\theta\theta}(x, 0)$ due to the effect of S_h only can be expressed as follows:

$$\sigma_{\theta\theta} = \frac{S_h}{2}\left[2 + \left(\frac{r}{x}\right)^2 + 3\left(\frac{r}{x}\right)^4\right] \qquad (4.39)$$

Substituting equation (4.39) into equation (4.36) and after integration yields

$$K_I(S_h) = -S_h(r)^{1/2} g(b) \qquad (4.40)$$

where $g(b)$ is another dimensionless stress intensity function of $b = 1 + a/r$.

Derivation of K_I *for loading sources* P_w *and* P_a

The stress intensity function due to fluid penetration depends on both the pressure P_w in the borehole and the pressure distribution P_a along the fracture. Assuming zero fluid penetration into the fracture gives the stress intensity factor

$$K_I(P_w) = P_w(r)^{1/2} h(b) \qquad (4.41)$$

where $h(b)$ is a dimensionless stress intensity function of b. The stress intensity factor for the crack pressure has the same form as equation (4.41), e.g.

$$K_I(P_a) = P_w(r)^{1/2} i(b) \qquad (4.42)$$

The dimensionless stress intensity function $i(b)$ depends on the pressure distribution

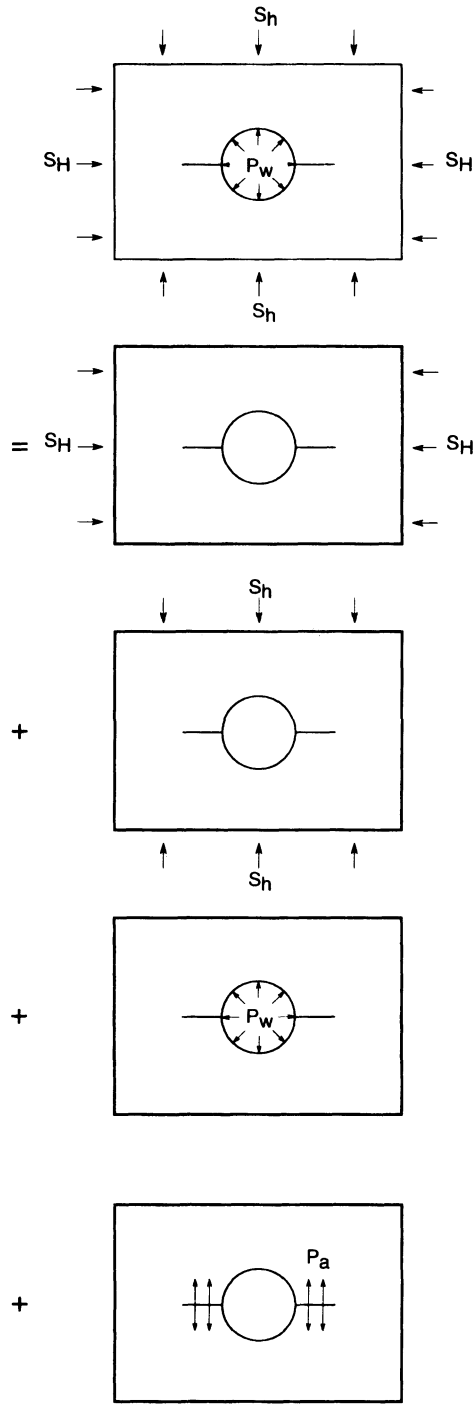

Fig. 4.15 Superposition of loading sources to derive the stress intensity factor for crack growth by hydraulic fracturing. (After Rummel, 1987.)

$P_a(x,0)$ along the crack surface. Different expressions for that function were derived by Rummel (1987) for different pressure distributions (constant pressure, reduced constant pressure, reciprocal pressure drop, linear pressure drop and quadratic pressure drop). Variations of $h(b) + i(b)$ with the normalized crack length $b = 1 + a/r$ are presented in Fig. 4.16 for these different types of pressure distribution.

Substituting equations (4.38) and (4.40)–(4.42) into equation (4.35) yields the following expression for the borehole pressure at unstable crack extension, or the breakdown pressure, e.g.:

$$P_c = \frac{K_{IC}}{(h+i)(r)^{1/2}} + k_1 S_h + k_2 S_H \quad (4.43)$$

where K_{IC} is the fracture toughness of the rock material in mode I, and k_1 and k_2 are equal to

$$k_1 = \frac{g}{h+i} \quad (4.44)$$

and

$$k_2 = \frac{f}{h+i} \quad (4.45)$$

The first term in equation (4.43) corresponds to the borehole pressure under zero external

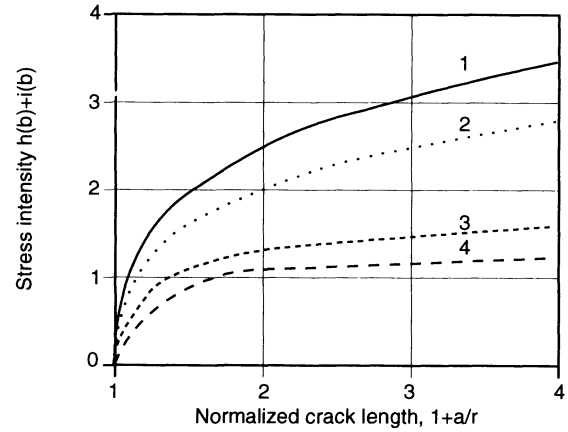

Fig. 4.16 Variation of dimensionless stress intensity function $h(b) + i(b)$ with normalized crack length $b = 1 + a/r$ for various crack pressure distributions. 1, $P_a(x,0) = P_w$; 2, $P_a(x,0) = 0.75\ P_w$; 3, linear pressure drop; 4, quadratic pressure drop. (After Rummel, 1987.)

stresses ($S_H = S_h = 0$). It can be interpreted as the hydraulic fracturing tensile strength of the rock equal to

$$P_{co} = \frac{K_{IC}}{(h+i)(r)^{1/2}} \tag{4.46}$$

which depends on the fracture toughness of the rock K_{IC}, the radius of the borehole r, the half-crack length a, and the fluid pressure distribution $P_a(x)$ within the crack. The latter is somewhat related to the pumping rate or to fluid pressurization during a test.

It is interesting to note that equation (4.43) is similar in form to equation (4.14) with no initial pore pressure. In fact, it can be shown that k_1 and k_2 take values of 3 and -1, respectively, for zero crack length (crack-free rock).

For the specific case of $S_H = S_h$, Rummel (1987) and Rummel and Hansen (1989) used equation (4.43) to estimate the so-called '*in situ* fracture gradient', k^*, with respect to depth, defined as follows:

$$k^* = g^*(k\rho - \rho_f) \tag{4.47}$$

where g^* is the gravitational acceleration and ρ and ρ_f are the rock density and fluid density, respectively, and k is equal to

$$k = k_1 + k_2 = \frac{f+g}{h+i} \tag{4.48}$$

The variation of k^* as a function of the normalized crack length $b = 1 + a/r$, for water-filled cracks and constant crack pressure ($P_a = P_w$), and for rocks with density ρ ranging between 2.3 and 2.7 g/cm^3 is presented in Fig. 4.17. The gradient k^* enters into a relationship between the *in situ* breakdown pressure and depth z, e.g.

$$P_c = k^* z + P_{co} \tag{4.49}$$

where P_{co} is the tensile strength of the rock defined in equation (4.46). In view of Fig. 4.17 and equation (4.48), it appears that increases in rock density, depth and rock tensile strength or fracture toughness all result in increasing the breakdown pressure. Note that using equation (4.48) and Fig. 4.17, the length of pre-existing cracks can be determined from fracture gradients derived from *in situ* hydrofracturing tests.

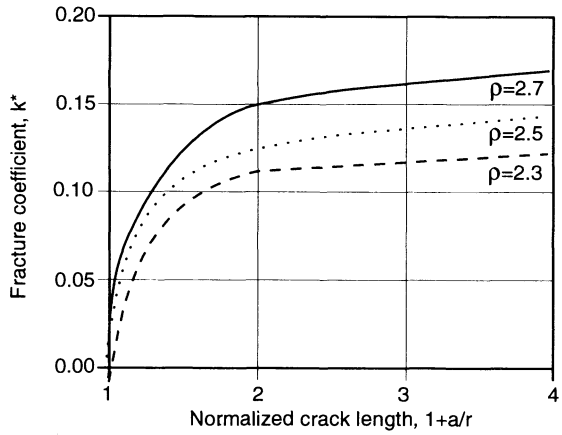

Fig. 4.17 Variation of fracture coefficient k^* with normalized crack length in a rock mass subjected to isotropic horizontal stress and various rock densities (in g/cm^3). The cracks are assumed to be fluid filled with $P_a = P_w$. (After Rummel, 1987.)

The fracture mechanics model presented in this section was used by Rummel (1987) to analyze the results of hydrofracturing tests on granite conducted at different scales (Table 4.2). Cylindrical cores, 3 cm in diameter, of Falkenberg granite from Germany were tested in a biaxial chamber and 1 m^3 rectangular specimens were loaded triaxially in the laboratory. The fluid pressure was applied at a low pumping rate to sealed-off boreholes in the samples and pressure versus time was recorded. At the Falkenberg geothermal test site, fractures were initiated at a depth of 250 m using a pumping rate of 20 l/min. From the laboratory and field tests, the intrinsic microcrack length a was calculated using equation (4.46) and the value of the rock tensile strength. The latter was found to decrease with the volume of rock considered in the tests. That observation was attributed to the fact that the larger the volume of rock, the greater the probability of finding larger microcracks. The back-calculated crack lengths were found to vary between 2 and 8 mm, which was

Table 4.2 Parameters for hydraulic fracturing tests of different sizes in granite (after Rummel, 1987)

Type of test	*Type of granite*	*Borehole radius* r *(mm)*	*Maximum horizontal stress* S_H *(MPa)*	*Minimum horizontal stress* S_h *(MPa)*	*Breakdown pressure* P_c *(MPa)*	*Tensile strength* P_{co} *(MPa)*	*Fracture toughness* K_{IC} *($MN/m^{3/2}$)*	*Estimated crack length* a *(mm)*	*Fracture coefficient* k
Core diameter 3 cm	Falkenberg	1.25	0–80.0	0–80.0	16–100	16.6 ± 1.5	1.79 ± 0.22	2–3	1.04 ± 0.04
Block 1 m^3	Epprechstein	15	5.0	2.0	15.5	13.5	2.47 ± 0.20	4	–
Borehole 250 m depth	Falkenberg	48/66	7.0	5.0	10–17	4–9	1.79 ± 0.22	7–8	–

considered perfectly acceptable if one assumes that grain boundaries of coarse granites can act as potential microcracks under tensile loading (Table 4.2). The fracture coefficient k defined in equation (4.48) was calculated only for the laboratory tests on cylindrical cores. With the assumption of constant crack pressure ($P_a = P_w$), that coefficient was calculated to be $k = 1.04$. This should be compared with the value of $k = 2$, as predicted by the 'classical theory' which neglects the existence of microcracks.

The application of linear elastic fracture mechanics for estimating the breakdown pressure and tensile strength of rock masses in hydrofracture stress measurements accounts for the presence of pre-existing microfractures and flaws in the borehole wall. However, the major problem in the application of fracture mechanics to hydrofracturing as a whole, and hydraulic stress measurement in particular, is to assume a realistic pressure distribution within the propagating fracture. Despite these problems, Rummel and Hansen (1989) have developed a simulation program called FRAC that allows the estimation of the pressure drop at the fracture inlet and the pressure distribution within the hydraulic fracture. The program also calculates the energy consumption during discrete crack growth as well as rock mass permeability data away from the disturbed zone around the borehole. As pointed out by Detournay and Carbonell (1994), the breakdown criterion proposed by Rummel and co-workers is based on an approximation which can only be justified for crack lengths that are large compared with the borehole radius.

Theoretical analysis and experimental results were presented by Bruno and Nakagawa (1991) to describe the influence of pore pressure on tensile fracture initiation and propagation direction. From the application of fracture mechanics to the problem, these authors found that the fracture is influenced by both pore pressure magnitude on a local scale around the crack tip and by the orientation and distribution of pore pressure gradients on a global scale. If we consider a situation in which fluid flows inwards towards an extending fracture tip, the induced pores are compressive and almost perpendicular to the fracture plane. Their effect will be to reduce the effective stress and strain energy available for crack extension. The opposite will result where fluid flow is directed outwards along a potential fracture path, such as along the line connecting two pressure sources. In controlled fracture experiments conducted on porous limestone and sandstone samples, Bruno and Nakagawa (1991) were able to demonstrate that fractures propagate toward regions of higher local pore pressure.

Detournay and Carbonell (1994) showed that a fracture mechanics approach, which considers a length scale of the induced fractures at the wall of the borehole, appears to remove many of the ambiguities and problems that afflict the classical interpretation of the breakdown pressure. Some of the observations

and predictions of their approach still need to be corroborated by experiments. More generally, these authors demonstrated that a better understanding of the breakdown process could be gained by re-examining the problem from a more rigorous point of view than has been done so far. Progress in understanding the breakdown process by the application of fracture mechanics is then likely to lead to the development of a more reliable methodology to determine far-field stresses from the pressure measurements recorded during a hydraulic fracturing experiment.

(g) Shut-in pressure, P_s

After injecting a volume of fluid sufficient to propagate a fracture length equal to about three times the drillhole diameter, injection is stopped and the hydraulic system is sealed or 'shut in'. The instantaneous shut-in pressure P_s is the pressure when the hydrofracture closes, preventing further flow in the rock formation. If the hydrofracture extends in a vertical plane perpendicular to S_h, it is assumed that the pressure at the time of fracture closing is equal to S_h, e.g.

$$S_h = P_s \tag{4.50}$$

Combining equation (4.50) with any of the breakout equations mentioned above gives a system of two equations that can be solved for the major and minor horizontal *in situ* stresses S_H and S_h.

The determination of the shut-in pressure P_s in the pressure–time record of the hydrofracturing test is straightforward when a sharp break occurs after the initial fast pressure decline following pump shut-off. For most cases, however, the pressure decay is gradual and P_s is indistinct.

In the early days of hydraulic fracturing for stress measurements, the determination of P_s was simply done by observing a break or a knee in the curve obtained with the recording unit, typically a conventional chart recorder. Later, graphical methods were employed for estimating P_s from pressure–time curves. Today, statistical analysis of hydraulic fracturing field data enhances the objectivity of determining the shut-in pressure, together with the fracture reopening pressure and fracture orientation (Haimson, 1989; Lee and Haimson, 1989). The different methods of analysis are discussed in section 4.2.4.

When there is a risk that the induced vertical fractures at the borehole wall tend to 'roll over' and propagate horizontally away from the borehole, it is necessary to separate clearly the shut-in pressure values for the different propagation stages. For that purpose, Baumgärtner and Zoback (1989) have developed a computer-based interactive analysis method where P_s is determined from a handful of additional parameter combinations from a test, such as pressure versus injection rate.

Using an LEFM approach, Hayashi and Sakurai (1989) developed a theory to demonstrate that the pressure decay characteristics of shut-in curves are governed by (1) the rate of leak-off to the formation, (2) the compliance of the equipment and (3) the partial crack closure. The general conclusions that can be drawn from the study of Hayashi and Sakurai (1989) are as follows.

1. The downhole pressure corresponding to the onset of the closure at the crack tip is very close to the compressive *in situ* stress acting perpendicularly to the crack plane. The point representing this pressure appears as the point of maximum curvature on each shut-in curve.
2. Crack lengths have almost no effect on the shut-in pressure, provided the cracks are longer than the wellbore diameter. The rate of pressure decay increases with the crack height, the stress ratio and the fluid loss coefficient, making the point of maximum curvature more difficult to define. Compliance of the tubes located between the shut-in valve and the downhole straddle packers has a large effect on the shape of the shut-in curves, larger compliances

being more helpful to the determination of the point of maximum curvature.

3. The methods using pressure versus log (time) plots, log (pressure) versus log (time) plots, and the pressure versus log (time/time after shut-in) plots give essentially the same instantaneous shut-in pressure result, a value which is very close to the minimum compressive *in situ* stress. When the point of maximum curvature is not clear on the original shut-in curves, these methods are recommended.

(h) Using the Hoek and Brown failure criterion to determine *in situ* stresses

The classical strength criterion used in hydraulic fracturing states that once the tangential stress at the borehole wall exceeds the tensile strength of the rock mass, a fracture will initiate and propagate away from the borehole in the direction of the maximum principal stress. If we consider the case of a vertical borehole, the state of stress at the two points on the borehole wall aligned with the direction of the maximum horizontal principal stress (corresponding to $\theta = 0°$ and 180°) has the following components (Jaeger and Cook, 1976):

$$\begin{aligned} \sigma_{rr} &= P_w \\ \sigma_{\theta\theta} &= 3S_h - S_H - P_w \\ \sigma_{zz} &= S_V - 2\nu(S_H - S_h) \end{aligned} \tag{4.51}$$

where S_H and S_h are the principal horizontal *in situ* stresses, S_V is the vertical stress equal to ρgz, P_w is the borehole pressure and ν is the rock Poisson's ratio.

The classical tensile strength criterion for hydraulic fracturing that we have used so far does not take into account the confining effect of the vertical stress σ_{zz} and the borehole pressure. Furthermore, it cannot be used to explain the creation of horizontal fractures in the borehole wall, a situation that is not too rare in hydraulic stress measurements. When horizontal fractures are formed in a field test, the data are usually omitted because they oppose the theoretical assumption that only vertical fractures can be initiated.

In order to overcome these two limitations, Ljunggren, Amadei and Stephansson (1988) and Ljunggren and Amadei (1989) replaced the tensile strength criterion by the nonlinear empirical failure criterion developed by Hoek and Brown (1980). For intact rock, this criterion involves the major and minor principal stresses σ_1 and σ_3 at failure, as follows:

$$\sigma_1 = \sigma_3 + (m\sigma_c\sigma_3 + \sigma_c^2)^{1/2} \tag{4.52}$$

where m is an empirical constant that depends on the rock type and σ_c is the unconfined compressive strength of the rock. Figure 4.18 shows the failure envelope associated with the criterion in the (σ_1, σ_3) space. Substituting $\sigma_1 = 0$ and $\sigma_3 = -T$ in equation (4.52), the failure criterion gives the following expression for the uniaxial tensile strength T of the rock:

$$T = \sigma_t = \frac{\sigma_c}{2}((m^2 + 4)^{1/2} - m) \tag{4.53}$$

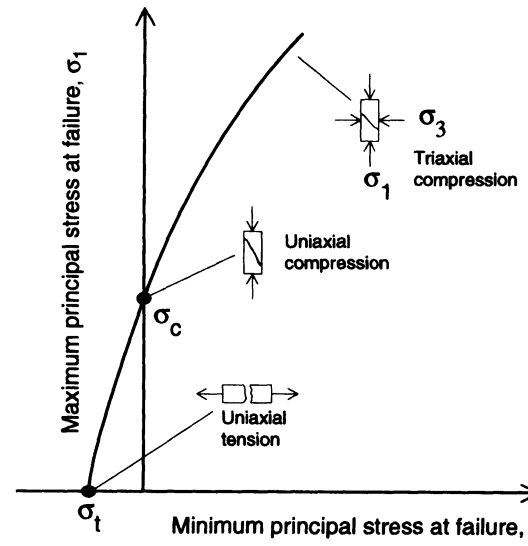

Fig. 4.18 Failure envelope associated with the empirical criterion of Hoek and Brown (1980).

When the two horizontal stresses S_H and S_h are not equal, tensile cracking can take place in the vertical or horizontal plane since according to equation (4.51), $\sigma_{\theta\theta}$ or σ_{zz} can be tensile. Of the six possible forms that can be assumed by equation (4.52) only four of them, for which $\sigma_{\theta\theta}$ or σ_{zz} could be the minor principal stress, are of interest here. These are

$$\sigma_{zz} > \sigma_{rr} > \sigma_{\theta\theta} \qquad \sigma_{zz} = \sigma_{\theta\theta} + (m\sigma_c\sigma_{\theta\theta} + \sigma_c^2)^{1/2} \tag{4.54}$$

$$\sigma_{rr} > \sigma_{zz} > \sigma_{\theta\theta} \qquad \sigma_{rr} = \sigma_{\theta\theta} + (m\sigma_c\sigma_{\theta\theta} + \sigma_c^2)^{1/2} \tag{4.55}$$

$$\sigma_{rr} > \sigma_{\theta\theta} > \sigma_{zz} \qquad \sigma_{rr} = \sigma_{zz} + (m\sigma_c\sigma_{zz} + \sigma_c^2)^{1/2} \tag{4.56}$$

$$\sigma_{\theta\theta} > \sigma_{rr} > \sigma_{zz} \qquad \sigma_{\theta\theta} = \sigma_{zz} + (m\sigma_c\sigma_{zz} + \sigma_c^2)^{1/2} \tag{4.57}$$

Substituting the expression for the stress components in equation (4.51) into equations (4.54)–(4.57) gives the following relationships that need to be satisfied between the borehole pressure P_c and the *in situ* stress components S_H, S_h and S_V for fracturing to occur:

$$S_V - 2\nu(S_H - S_h) > P_c > 0 > 3S_h - S_H - P_c$$
$$S_V - 2\nu(S_H - S_h) = 3S_h - S_H - P_c + (m\sigma_c(3S_h - S_H - P_c) + \sigma_c^2)^{1/2} \tag{4.58}$$

$$P_c > S_V - 2\nu(S_H - S_h) > 3S_h - S_H - P_c$$
$$P_c = 3S_h - S_H - P_c + (m\sigma_c(3S_h - S_H - P_c) + \sigma_c^2)^{1/2} \tag{4.59}$$

$$P_c > 3S_h - S_H - P_c > S_V - 2\nu(S_H - S_h)$$
$$P_c = S_V - 2\nu(S_H - S_h) + (m\sigma_c(S_V - 2\nu(S_H - S_h)) + \sigma_c^2)^{1/2} \tag{4.60}$$

$$3S_h - S_H - P_c > P_c > 0 > S_V - 2\nu(S_H - S_h)$$
$$3S_h - S_H - P_c = S_V - 2\nu(S_H - S_h) + (m\sigma_c(S_V - 2\nu(S_H - S_h)) + \sigma_c^2)^{1/2} \tag{4.61}$$

The failure envelopes representing equations (4.58)–(4.61) are shown in Figs 4.19a–d along with the stress paths followed as the borehole pressure P_w increases. In order to obtain vertical tensile fracturing, the paths in Figs 4.19a, b must intersect the failure envelopes representing equations (4.58) and (4.59) in the $\sigma_{\theta\theta} < 0$ regions of the $(\sigma_{zz}, \sigma_{\theta\theta})$ and $(\sigma_{rr}, \sigma_{\theta\theta})$ spaces, respectively. This takes place as long as σ_{zz} and σ_{rr} are less than the unconfined compressive strength σ_c. On the other hand, horizontal fracturing takes place when the path in Fig. 4.19c intersects the failure envelope representing equation (4.60) in the $\sigma_{zz} < 0$ region of the $(\sigma_{rr}, \sigma_{zz})$ space. In view of the expression of σ_{zz} in equation (4.51), horizontal fracturing can occur if there is a large differential horizontal stress field $(S_H - S_h)$ in comparison to the vertical stress component S_V. Note that the case shown in Fig. 4.19d is not of interest here since as P_w increases, σ_θ decreases and the path followed in the $(\sigma_{\theta\theta}, \sigma_{zz})$ space does not intersect the failure envelope representing equation (4.61).

In their contribution, Ljunggren and Amadei (1989) focused their discussion on equation (4.60) which, unlike the traditional equations for hydraulic fracturing, can explain the initiation of horizontal hydrofractures. It can be seen that it is not possible to solve equation (4.60) for the maximum horizontal stress S_H, since the shut-in pressure P_s, in the case of horizontal fractures, does not give any information on the smallest horizontal *in situ* stress component. The shut-in pressure is instead equal to the *in situ* vertical stress S_V. However, equation (4.60) can be solved for the horizontal stress difference $(S_H - S_h)$. By using the value of this difference and the inequalities associated with equation (4.60), the possible domains of variation for $(S_H - S_h)$ can also be determined.

Laboratory experiments reported by Ljunggren, Amadei and Stephansson (1988) seem to show that horizontal hydrofracturing occurs when the *in situ* principal horizontal stresses are significantly larger than the vertical stress. Horizontal fractures can also be created due to the opening of horizontal rock

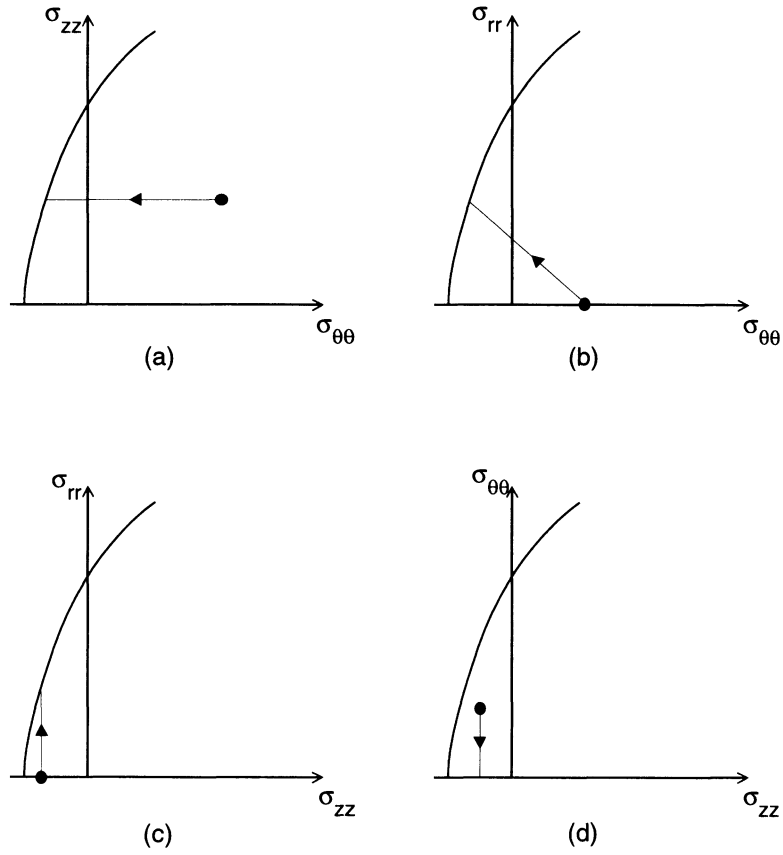

Fig. 4.19 Hoek and Brown failure envelopes and stress paths for the four cases representing equations (4.58)–(4.61). (After Ljunggren and Amadei, 1989.)

partings, bedding planes, foliation planes, joints or microcrack planes.

(i) Determination of *in situ* stresses from measurements in inclined boreholes

In the derivation of the equations for the breakdown and shut-in pressures, it has been assumed that one of the principal stresses is oriented parallel to the borehole axis. For this case the problem reduces to the two-dimensional plane strain situation of a circular hole in an infinite plate subjected to far-field boundary stresses. For the case when none of the *in situ* principal stresses are parallel to the borehole wall, Fairhurst (1968) derived mathematical expressions for the stress components on the borehole wall in isotropic and transversely isotropic media. Using experiments, Von Schonfeldt (1970) and Daneshy (1970) independently observed that under isotropic conditions the fracture orientation is influenced by the borehole and its vicinity. The trace of inclined hydraulic fractures at the wellbore was found to be misleading if used for the purpose of determining the overall fracture orientation. The inclined fractures are usually rough and very seldom perpendicular to the maximum tensile stresses induced on the borehole wall.

These observations, together with the existence of shear stresses around the borehole, suggest that inclined hydraulic fractures are initiated as a result of shear as well as tensile

fracture of the rock. Starting with the basic equations for the state of stress around a cylindrical borehole with internal pressure applied on its wall, Daneshy (1973) derived the equation for the maximum tensile stress at a point on the borehole wall. This point has to lie in a plane tangent to the borehole axis. One decade later, Richardson (1983) presented an analytical solution for stresses around a borehole arbitrarily oriented with respect to the principal stress axes, and solved for the angular error between predicted hydraulic fractures and the direction of the minimum compressive *in situ* principal stress. Finally, Ljunggren and Nordlund (1990) presented a method to determine the orientation of horizontal *in situ* stresses from hydrofracturing in inclined boreholes. Their method is, in essence, similar to that proposed by Richardson (1983).

In the method of Ljunggren and Nordlund (1990), σ_1, σ_2 and σ_3 are three principal *in situ* stresses oriented in the vertical and horizontal planes as shown in Fig. 4.20a. The rock is assumed to be linearly elastic, isotropic and homogeneous. Consider an $(S1, S2, S3)$ coordinate system where $S1$, $S2$ and $S3$ are parallel to the directions of σ_1, σ_2 and σ_3 (S_H, S_h and S_V), respectively. S_H and S_h are the horizontal *in situ* stresses ($S_H > S_h$), and S_V is the vertical stress. The borehole orientation is defined by the unit vector $\boldsymbol{b}$ (Fig. 4.20b) parallel to the borehole axis. In Fig. 4.20b γ is the vertical angle between vector $\boldsymbol{b}$ and the vertical axis $S3$, and ϕ is the horizontal angle between $S1$ and the projection of vector $\boldsymbol{b}$ onto the $S1, S2$ plane.

We now consider a local coordinate system $(\overline{S1}, \overline{S2}, \overline{S3})$ attached to the borehole such that the $\overline{S1}$ axis is parallel to the borehole axis and the $\overline{S2}$ axis is contained in the $S1, S2$ horizontal plane (Fig. 4.20b). Finally, a global coordinate system (N, E, V) is defined where N and E lie in the $S1, S2$ plane and V is vertical. A horizontal angle α is introduced which measures the angle from north (N) to the horizontal projection of $\boldsymbol{b}$.

The (N, E, V) and $(\overline{S1}, \overline{S2}, \overline{S3})$ coordinate systems are related to each other by the coordinate transformation matrix $[B]$ such that

$$\{\overline{S}\} = [B]\{S\} \tag{4.62}$$

where

$$\begin{aligned} b_{11} &= \cos\alpha \cdot \sin\gamma & b_{12} &= \sin\alpha \cdot \sin\gamma & b_{13} &= \cos\gamma \\ b_{21} &= -\sin\alpha & b_{22} &= \cos\alpha & b_{23} &= 0 \\ b_{31} &= -\cos\alpha \cdot \cos\gamma & b_{32} &= -\sin\alpha \cdot \cos\gamma & b_{33} &= \sin\gamma \end{aligned} \tag{4.63}$$

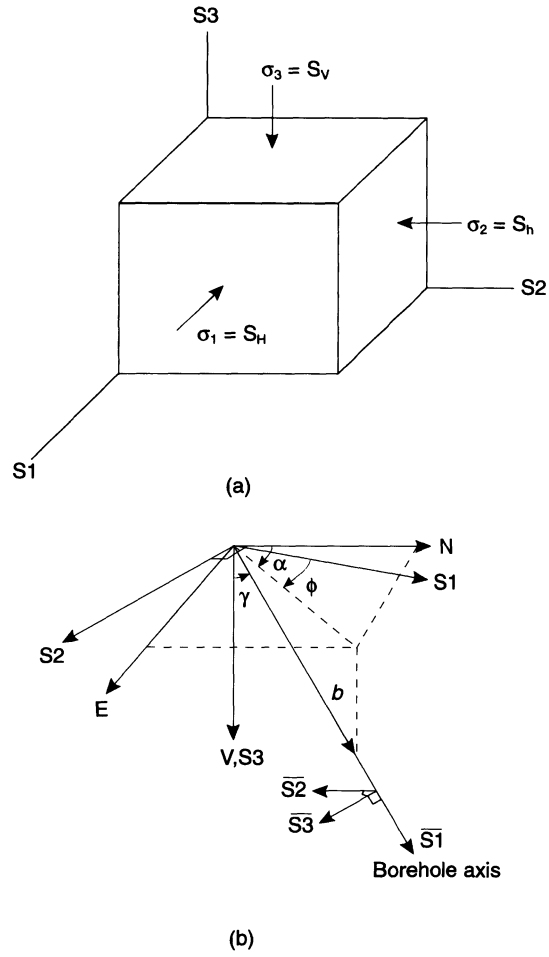

Fig. 4.20 Problem geometry and coordinate systems to calculate the stress distribution around an inclined borehole. (a) *In situ* stresses, (b) definition of angles. (After Ljunggren and Nordlund, 1990.)

If the angle α in (4.63) is replaced by the angle ϕ, we obtain instead the expressions that describe how the borehole coordinate system is related to the *in situ* principal stress coordinate system and matrix $[B]$ is replaced by matrix $[C]$. Using the coordinate transformation rule for the coordinate transformation of second-order Cartesian tensors, the components of the stress tensor $[\sigma_b]$ in the borehole coordinate system can then be determined from the following expression:

$$[\sigma_b] = \begin{bmatrix} \sigma_{\overline{S1}} & \tau_{\overline{S1}\,\overline{S2}} & \tau_{\overline{S1}\,\overline{S3}} \\ \tau_{\overline{S1}\,\overline{S2}} & \sigma_{\overline{S2}} & \tau_{\overline{S2}\,\overline{S3}} \\ \tau_{\overline{S1}\,\overline{S3}} & \tau_{\overline{S2}\,\overline{S3}} & \sigma_{\overline{S3}} \end{bmatrix}$$

$$= [C]\begin{bmatrix} S_H & 0 & 0 \\ 0 & S_h & 0 \\ 0 & 0 & S_V \end{bmatrix}[C]^T \qquad (4.64)$$

which after expansion gives

$$\begin{aligned}
\sigma_{\overline{S1}} &= (S_H \cos^2\phi + S_h \sin^2\phi)\sin^2\gamma \\
&\quad + S_V \cos^2\gamma \\
\sigma_{\overline{S2}} &= S_H \sin^2\phi + S_h \cos^2\phi \\
\sigma_{\overline{S3}} &= (S_H \cos^2\phi + S_h \sin^2\phi)\cos^2\gamma \\
&\quad + S_V \sin^2\gamma \qquad (4.65) \\
\tau_{\overline{S1}\,\overline{S2}} &= \tfrac{1}{2}(S_h - S_H)\sin 2\phi \sin\gamma \\
\tau_{\overline{S1}\,\overline{S3}} &= \tfrac{1}{2}(S_V - S_H \cos^2\phi - S_h \sin^2\phi) \\
&\quad \times \sin 2\gamma \\
\tau_{\overline{S2}\,\overline{S3}} &= \tfrac{1}{2}(S_H - S_h)\sin 2\phi \cos\gamma
\end{aligned}$$

The presence of the borehole will cause stress concentrations in the rock mass. Using cylindrical polar coordinates (r, θ, z) where z is directed along the borehole axis, and a plane strain formulation, the total stress state at the borehole wall can be described as follows (Jaeger and Cook, 1976):

$$\begin{aligned}
\sigma_r &= P_w \\
\sigma_\theta &= (\sigma_{\overline{S2}} + \sigma_{\overline{S3}}) - 2(\sigma_{\overline{S2}} - \sigma_{\overline{S3}})\cos 2\theta \\
&\quad - 4\tau_{\overline{S2}\,\overline{S3}}\sin 2\theta - P_w \\
\sigma_z &= \sigma_{\overline{S1}} - 2\nu(\sigma_{\overline{S2}} - \sigma_{\overline{S3}})\cos 2\theta \qquad (4.66) \\
&\quad - 4\nu\tau_{\overline{S2}\,\overline{S3}}\sin 2\theta \\
\tau_{\theta z} &= 2(\tau_{\overline{S1}\,\overline{S3}}\cos\theta - \tau_{\overline{S1}\,\overline{S2}}\sin\theta) \\
\tau_{r\theta} &= \tau_{rz} = 0
\end{aligned}$$

where ν is the Poisson's ratio of the rock mass, P_w is the fluid pressure acting at the borehole wall and θ is the angle from the $\overline{S2}$ direction. The stresses of particular interest here are the tangential stress σ_θ, the axial stress σ_z and the shear stress $\tau_{\theta z}$ acting in the plane tangent to the borehole wall as shown in Fig. 4.21a. Since $\tau_{\theta z}$ is the only non-zero tangential shear stress and σ_r is always zero or positive, the maximum tensile stress σ_p acts in a plane tangent to the borehole at some angle θ. This tensile stress has the following expression:

$$\sigma_p = \tfrac{1}{2}(\sigma_\theta + \sigma_z - ((\sigma_\theta - \sigma_z)^2 + 4\tau_{\theta z}^2)^{1/2}) \qquad (4.67)$$

According to Ljunggren and Nordlund (1990), fracture will initiate at an oblique angle λ_p measured from the borehole axis, given by

$$\lambda_p = \tfrac{1}{2}\tan^{-1}\left(\frac{2\tau_{\theta z}}{\sigma_\theta - \sigma_z}\right) \qquad (4.68)$$

Combining equations (4.66) and (4.67), it is clear that σ_p is a function of θ and that there are two values of θ (180° apart) between 0° and 360°, where σ_p has its minimum value. These angles can be found by using a minimizing routine on $\sigma_p(\theta)$ for a set of *in situ* stress components. By substituting into equation (4.68) the angle θ that makes σ_p minimum, the inclination angle λ_p of the initial fracture can be determined. In reality, however, the fracture with an inclination λ_p never fully develops around the borehole wall. Since σ_p becomes less negative in either direction from its minimum points, these fractures will only appear as short dipping traces at the borehole wall. The points along the circumference of the borehole at which σ_p reaches a minimum form

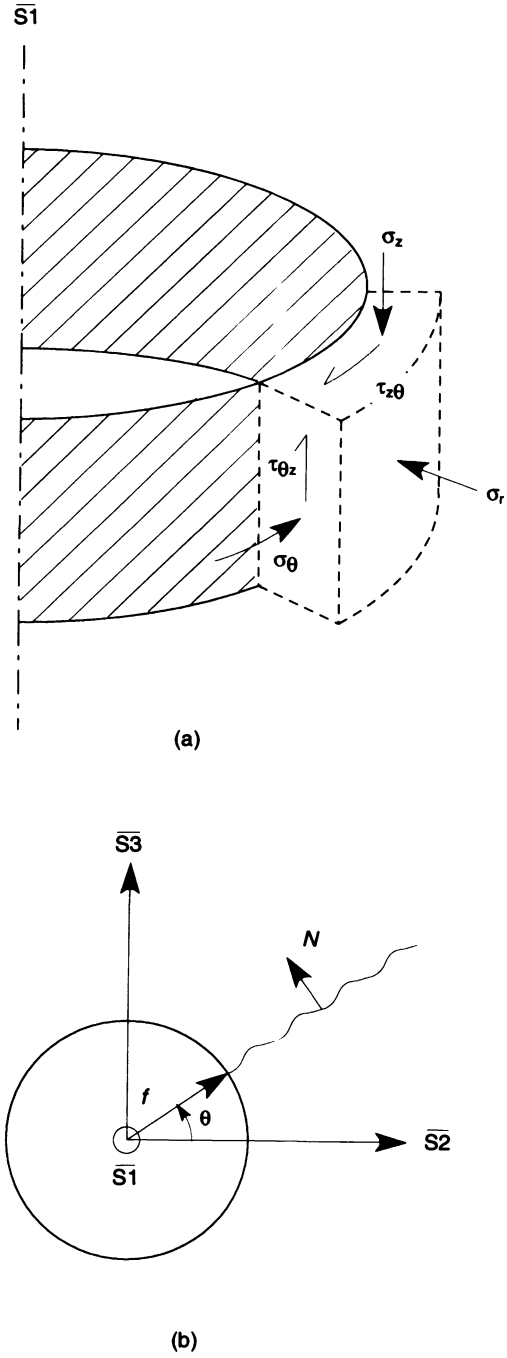

Fig. 4.21 (a) Stress distribution at borehole wall, (b) definition of the normal N to the fictitious fracture in the $\overline{S2}$, $\overline{S3}$ plane. (After Ljunggren and Nordlund, 1990.)

two lines parallel to the borehole axis, and 180° apart. Thus when the borehole is pressurized by a fluid, the macroscopic hydraulic fracture will develop in a direction parallel to these lines. The direction where the fracture initiates in the $\overline{S2}$, $\overline{S3}$ plane is then given by

$$f = e_{\overline{S2}} \cos\theta + e_{\overline{S3}} \sin\theta \qquad (4.69)$$

where $e_{\overline{S2}}$ and $e_{\overline{S3}}$ are the unit vectors along the $\overline{S2}$ and $\overline{S3}$ axes, respectively (Fig. 4.21b). Their components in the (N, E, V) coordinate system are given by the second and third lines of (4.63). The unit vector, N, normal to the fictitious fracture, and also shown in Fig. 4.21b, is such that

$$N = e_{\overline{S1}} \times f \qquad (4.70)$$

where $e_{\overline{S1}}$ is the unit vector parallel to the $\overline{S1}$ hole axis, with components in the (N, E, V) coordinate system given by the first line of (4.63). The components (N_1, N_2, N_3) of the unit vector N in the (N, E, V) coordinate can therefore be found.

The next step is to define the normal to the hydrofracture obtained from actual hydrofracturing measurements. Fracture orientations are usually given in the form of strike and dip. In the case of coaxial hydrofractures in inclined boreholes, the fracture dip is the same as the dip of the borehole if the fracture strikes perpendicular to the dip direction of the borehole. For all other fracture strikes, the true dip of the fracture is obtained by stereographic analysis. In the global (N, E, V) coordinate system, the strike vector of the fracture has components

$$s = (\cos\varepsilon, -\sin\varepsilon, 0) \qquad (4.71)$$

and the dip vector has components

$$d = (\cos\eta \sin\varepsilon, \cos\eta \cos\varepsilon, \sin\eta) \qquad (4.72)$$

where ε is the angle between the strike vector and N (north), and η is the inclination of the fracture with respect to the horizontal plane (Fig. 4.22). Since the strike and dip vectors are orthogonal to each other, the orientation of the

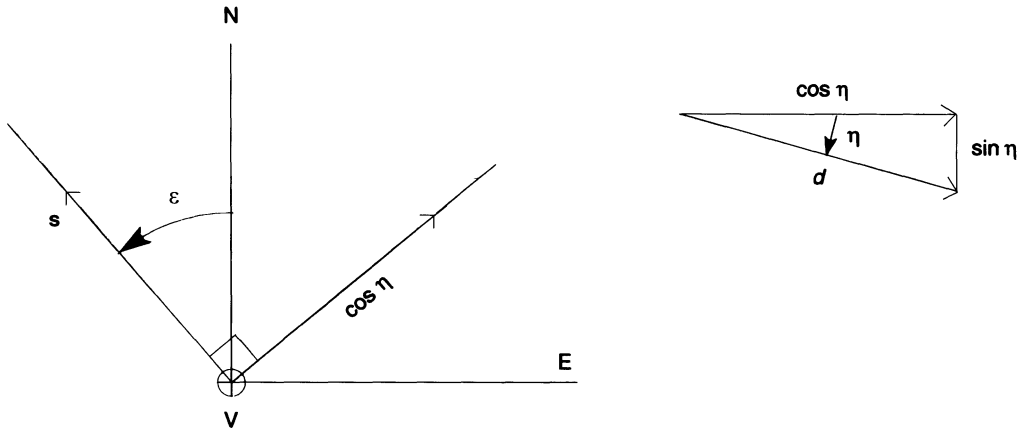

Fig. 4.22 Definition of strike vector s and dip vector d for a hydrofracture in the global (N, E, V) coordinate system. (Adapted from Ljunggren and Nordlund, 1990.)

unit vector normal to the true fracture plane can be determined as follows:

$$\boldsymbol{n} = \boldsymbol{s} \times \boldsymbol{d} = (n_1, n_2, n_3)$$
$$= (-\sin\varepsilon \sin\eta, -\cos\varepsilon \sin\eta, \cos\eta) \quad (4.73)$$

The angular difference β between the normal to the fictitious fracture and the normal to the true fracture plane can be obtained by using the scalar product, which is written as

$$\boldsymbol{N} \cdot \boldsymbol{n} = N_1 n_1 + N_2 n_2 + N_3 n_3 = \cos\beta \quad (4.74)$$

The angle β represents the angular error between the two normals $\boldsymbol{n}$ and $\boldsymbol{N}$.

Let us consider coaxial hydrofractures obtained from measurements in an inclined borehole. Assume that the orientation of the fractures is controlled only by the far-field *in situ* stresses (S_H, S_h and S_V). The rock is considered to be impermeable and no anisotropy exists. The *in situ* stress magnitude is assumed to be known, as well as the breakdown pressure and the orientations of the borehole and hydrofracture. Assuming a given orientation for the horizontal stress field, equations (4.62)–(4.70) give the orientation of the fictitious hydrofracture. The latter is then compared with the orientation from *in situ* measurements (equation (4.74)). When the angular error is zero ($\beta = 0$), the true orientation of the horizontal stresses is the same as that used as input to calculate the orientation of the fictitious fracture. If the error is non-zero, a new assumption for the orientation of the horizontal stress field must be made. This procedure is repeated until the magnitude of the error becomes zero and the complete stress field is obtained.

The method presented above was tested by Ljunggren and Nordlund (1990) on three field cases in Sweden and Finland. The boreholes had inclinations ranging between 62° and 69° from the horizontal plane. At each site, the *in situ* stress field was known from measurements in adjacent vertical holes and coaxial hydrofractures were created. It was found that the orientation of S_H differed between 0 and 9° from the strikes of the hydrofractures. Ljunggren and Nordlund (1990) concluded that the most important factors that seem to control the orientation of axially induced fractures from hydrofracturing tests in inclined boreholes, beside the angles γ and ϕ of Fig. 4.20b, are (1) the magnitude of the horizontal stress difference $S_H - S_h$; (2) the difference in magnitude between the three principal *in situ* stresses; and (3) the magnitude of the breakdown pressure required to initiate the hydrofractures.

The maximum and minimum *in situ* horizontal stresses S_H and S_h can be determined by

hydrofracturing of the walls of an inclined borehole for certain borehole orientations and assumptions. Consider, for instance, the case when the borehole of Fig. 4.20b is inclined in the direction of S_H (e.g. $\phi = 0°$). Combining equations (4.65) and (4.66), the tangential stress around the borehole wall has the following expression:

$$\sigma_\theta = S_h + S_H \cos^2\gamma + S_V \sin^2\gamma - 2(S_h - S_H \cos^2\gamma - S_V \sin^2\gamma) \times \cos 2\theta - P_w \quad (4.75)$$

As the pressure increases in the borehole, σ_θ becomes tensile in the borehole wall at $\theta = 90°$ and 270°, i.e. in the direction parallel to S_H. For those angles the shear stress $\tau_{\theta z}$ vanishes, which means that the tangential stress is a principal stress. Assuming that, for those values of the angle θ, hydrofracturing takes place when the tangential stress is equal to the rock tensile strength T (as for vertical boreholes), the breakdown pressure when the crack propagates is equal to

$$P_c = 3S_h - S_H \cos^2\gamma - S_v \sin^2\gamma + T \quad (4.76)$$

Assuming that the hydrofracture propagates in the vertical plane parallel to S_H, the horizontal stress S_h can again be estimated from the shut-in pressure P_s.

4.2.4 DATA ANALYSIS AND INTERPRETATION

The basic data collected during hydraulic fracturing are essentially of two types: pressure data and hydrofracture data. Pressure data are obtained from the records of pressure versus time and volume of fluid injected and recovered versus time during multiple pumping cycles. An idealized hydraulic fracturing pressure record for two cycles of pressurization and venting is shown in Fig. 4.23. From that record it is possible to extract the data necessary to determine the *in situ* state of stress, e.g.

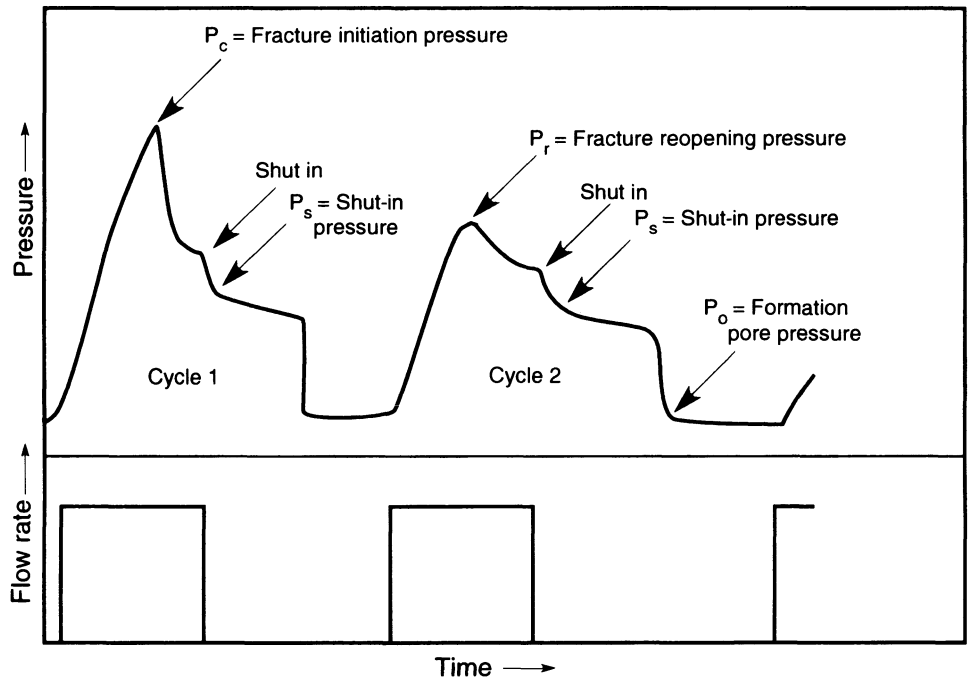

Fig. 4.23 Idealized hydraulic fracturing pressure record for two cycles of pressurization and venting. (Source: Enever, J.R., Cornet, F. and Roegiers, J.C. Copyright 1992, with kind permission from Elsevier Science Ltd, The Boulevard, Langford Lane, Kidlington, UK.)

the fracture initiation (breakdown) pressure P_c, the shut-in pressure or instantaneous shut-in pressure P_s and the fracture reopening pressure P_r. The second set of data obtained from hydraulic fracturing tests includes the hydrofracture delineation and orientation. The reader should be aware of the existence of the ISRM commission on interpretation of hydraulic fracture records (Enever, Cornet and Roegiers, 1992), whose role is to provide a basis for the systematic interpretation of hydraulic fracture records. We present below a review of the various methods available for the interpretation of hydraulic fracturing data.

(a) Fracture breakdown pressure, P_c

The fracture breakdown pressure is determined as the sharp pressure peak on the pressure versus time record during the initial (first) pressurization cycle. The pumping is carried out at a constant flow rate, about 3.5 l/min for slim-hole conditions in hard granitic rocks (Bjarnason, Ljunggren and Stephansson, 1989).

(b) Shut-in pressure, P_s

The shut-in pressure is the pressure at which a hydrofracture stops propagating and closes following pump shut-off. The determination of the shut-in pressure P_s is straightforward when a sharp break is observed in the pressure–time curve after the initial fast pressure decline following pump shut-off. However, in many situations the pressure decay is gradual with no obvious breaks or kinks and the shut-in pressure cannot be readily defined. In the early days of hydraulic fracturing stress measurements, pressure versus time was recorded by analog instruments, and the recording instruments provided a graph. Today the recording of pressure versus time is computerized, which allows for more elaborate data interpretation and statistical analysis.

Over the years, a number of methods (mostly graphical) have been proposed for estimating P_s from pressure versus time curves. A review of these various methods can be found in Tunbridge (1989) and Lee and Haimson (1989), among others. Gronseth and Kry (1983) proposed the inflection point method which consists of first drawing a tangent to the pressure versus time curve following shut-in. The shut-in pressure is then defined as the point at which the response curve (or the tangent to the curve) diverges from this tangent. Another more frequently used method is the tangent intersection method (Enever and Chopra, 1986), where P_s is represented by the point of intersection between the tangent to the pressure curve immediately after pump shut-off and that to the late stable section of the pressure curve (Fig. 4.24a). A third method to determine P_s consists of finding the point of maximum curvature on the pressure versus time record. This method was first suggested by Hardy (1973) and later applied by Hayashi and Sakurai (1989).

When using the aforementioned methods, it is common practice to determine the shut-in pressure after two or three pressurization cycles (Hickman and Zoback, 1983). In general, the shut-in pressure determined in the first cycle is usually higher and decreases somewhat in repeated pressurization cycles as the hydrofracture propagates away from the hole. As an illustrative example, Fig. 4.25a shows the interpretation of a pressure decay versus time record (for the third pressurization cycle) from borehole KAS03 at the Äspö Hard Rock Laboratory for nuclear waste disposal in southeast Sweden. It can be seen that the tangent intersection method gives the lowest shut-in pressure of the three methods applied.

The shut-in pressure can also be determined from semi-log and log–log plots of pressure versus time such as those shown in Figs 4.25b,c for the Äspö project. The semi-logarithmic representation was first suggested by Doe *et al.* (1983). The rationale for using such a representation is based on the analogy

between the post-breakdown pressure decay and the response of a pulse permeability test on a single fracture where the permeability decreases when the pressure in the fracture falls below the minimum *in situ* stress. The logarithmic curves typically have a break-in slope which is used to define P_s. An alternative method is to use the inflection point after shut-in to determine P_s, as suggested by Klasson (1989). The use of the log–log representation to determine the shut-in pressure was first suggested by Zoback and Haimson (1982).

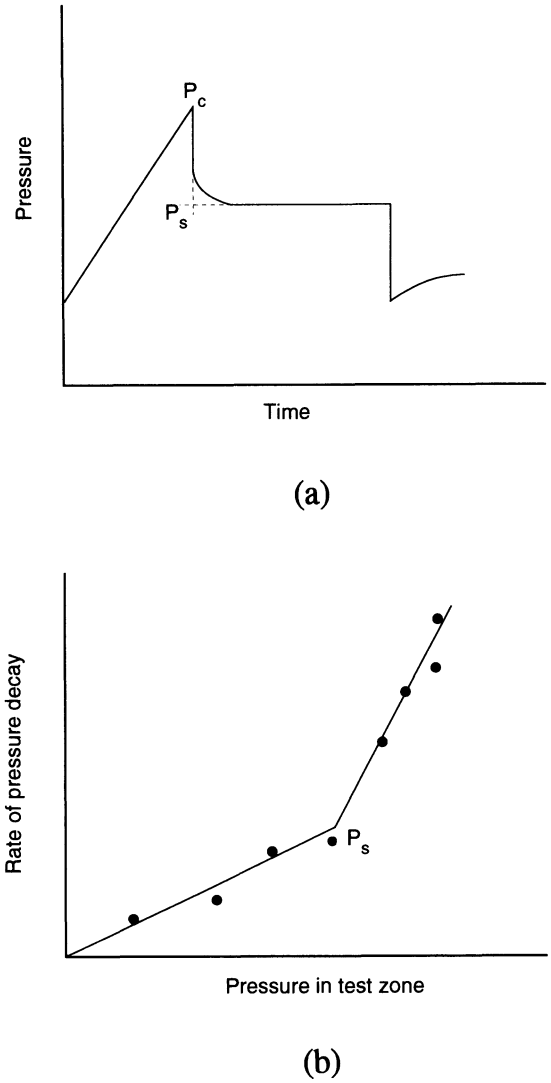

Fig. 4.24 Determination of shut-in pressure from hydrofracturing pressure versus time records. (a) Tangent intersection method, (b) bilinear pressure decay rate method.

Figures 4.25a–c indicate that, for the Äspö Hard Rock Laboratory data, the shut-in pressure determined with the tangent intersection method increases in magnitude when going from the linear to semi-log and log–log representations. If the inflection method is used instead, one notices the opposite trend.

Another method of interpretation of the shut-in pressure, called the exponential pressure decay method or Muskat method, assumes that the pressure decay after fracture closure approaches an asymptotic value in an exponential fashion (Aamodt and Kuriyagawa, 1983). The shut-in pressure is determined by plotting $\ln(P - P_\infty)$ versus time where P_∞ is the asymptotic pressure (presumably the rock formation pore pressure). The pressure decay data are fitted by a straight line. The intercept of that line at time $t = 0$ (time of pump shut-off) is taken as an estimate of P_s for a given value of the asymptotic pressure P_∞. Figure 4.26a shows an example of application of the Muskat method for the Äspö Hard Rock Laboratory data. The value of $\ln(P - P_\infty)$ at $t = 0$ is equal to $\ln(P_s - P_\infty) = 0.95$, which gives a shut-in pressure of 5.1 MPa for $P_\infty = 2.5$ MPa.

McLennan and Roegiers (1983) suggested another graphical method to determine the shut-in pressure. The method consists of plotting, using a semi-log representation, the pressure as a function of $(t + \Delta t)/\Delta t$, where t is the time of pressurization and Δt is the time since shut-in. The inflection point of the plot gives the shut-in pressure. This is shown in Fig. 4.26b for the Äspö Hard Rock Laboratory data.

As remarked by Tunbridge (1989), the shut-in pressure decay curve can also be expressed as a flow rate out of the borehole since the drop in pressure following shut-in must be

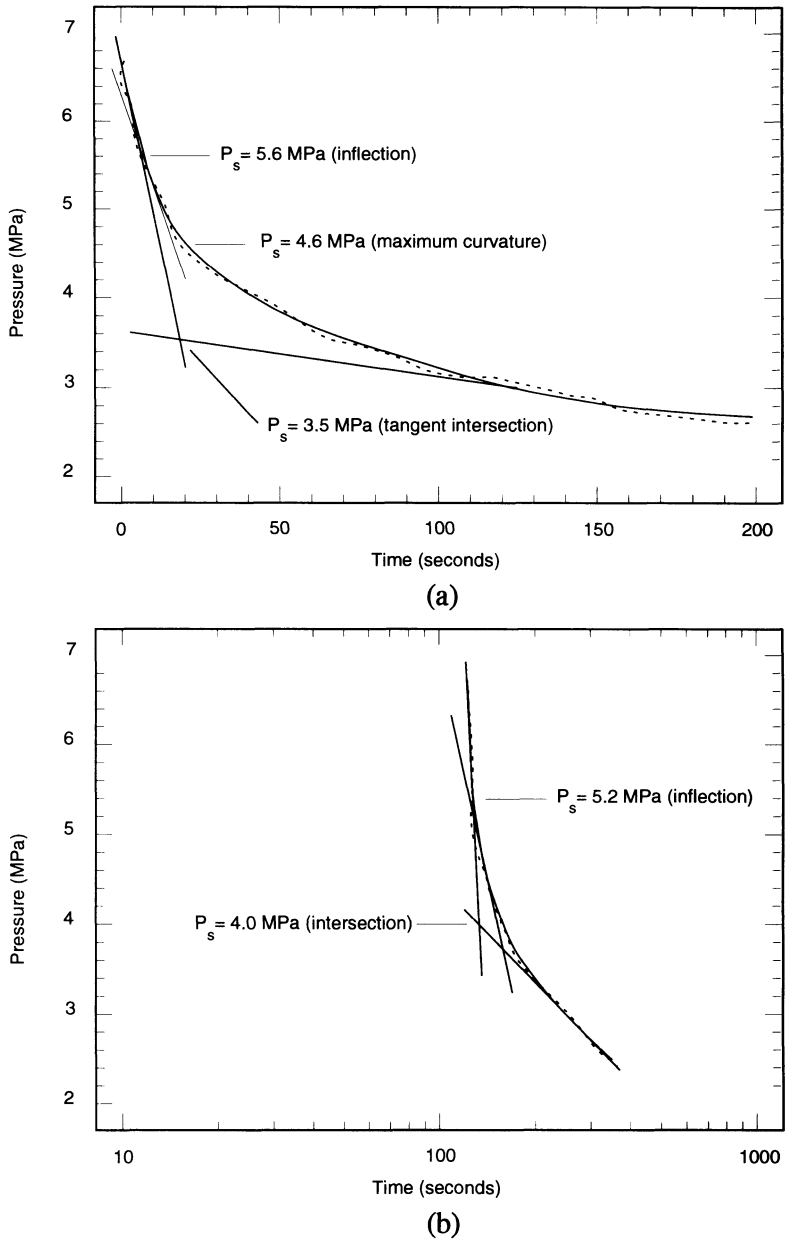

Fig. 4.25 Determination of shut-in pressure P_s from pressure decay records in borehole KAS03, depth 132.5 m at Äspö Hard Rock Laboratory, Sweden. (a) Linear pressure versus time; (b) pressure versus log(time); and (c) log(pressure) versus log(time). (After Klasson, 1989.)

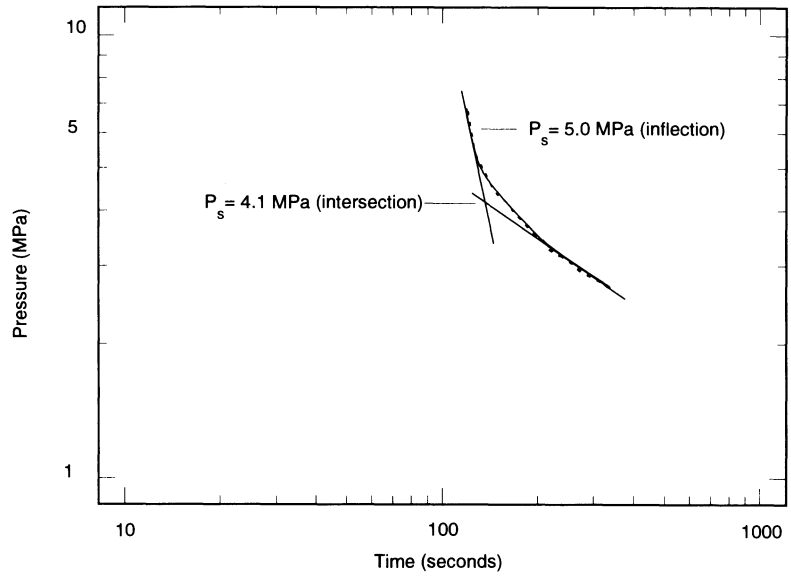

(c)

Fig. 4.25 *Continued.*

related to the quantity of fluid flowing out of the system into the hydrofracture, and to the quantity of fluid from other sources of leakage. Tunbridge (1989) observed that the relationship between pressure in the borehole and rate of flow into the hydrofracture appears to be bilinear. He suggested a similar bilinear relationship between the rate of pressure decay and pressure in the shut-in phase of a hydrofracturing test (Fig. 4.24b). Assuming that following pump shut-off the pressure decay is composed of two exponential curves, Tunbridge (1989) showed mathematically that the plot of rate of pressure decay versus pressure should consist of two linear segments. The intersection of those segments gives an estimate of the shut-in pressure P_s. Thus by plotting the tangent dP/dt to the pressure decay curve versus the pressure P, the shut-in pressure can be determined. Figure 4.26c shows an example of application of that method for the Äspö Hard Rock Laboratory data where the two segments were determined by linear regression analysis.

The bilinear pressure decay rate method of Tunbridge (1989) has now become the most reliable and therefore the most popular method for the determination of the shut-in pressure among the various groups conducting hydrofracturing stress measurements. In order to single out the shut-in pressure more rigorously, Lee and Haimson (1989) determined the best-fitting bilinear curve by applying a nonlinear regression analysis to the set of dP/dt versus P data. The same approach was also used by Lee and Haimson (1989) for the analysis of data with the exponential pressure decay method.

The values of the shut-in pressure at different depths determined by the various graphical methods for the Äspö Hard Rock Laboratory data (third pressurization cycle) are summarized in Table 4.3. Analysis of that table reveals that the inflection method in the pressure versus time and pressure versus log(time) plots gives the highest values of the shut-in pressure. The exponential pressure decay method yields the next largest. On the other hand, the intersection method gives the smallest values of the shut-in pressure.

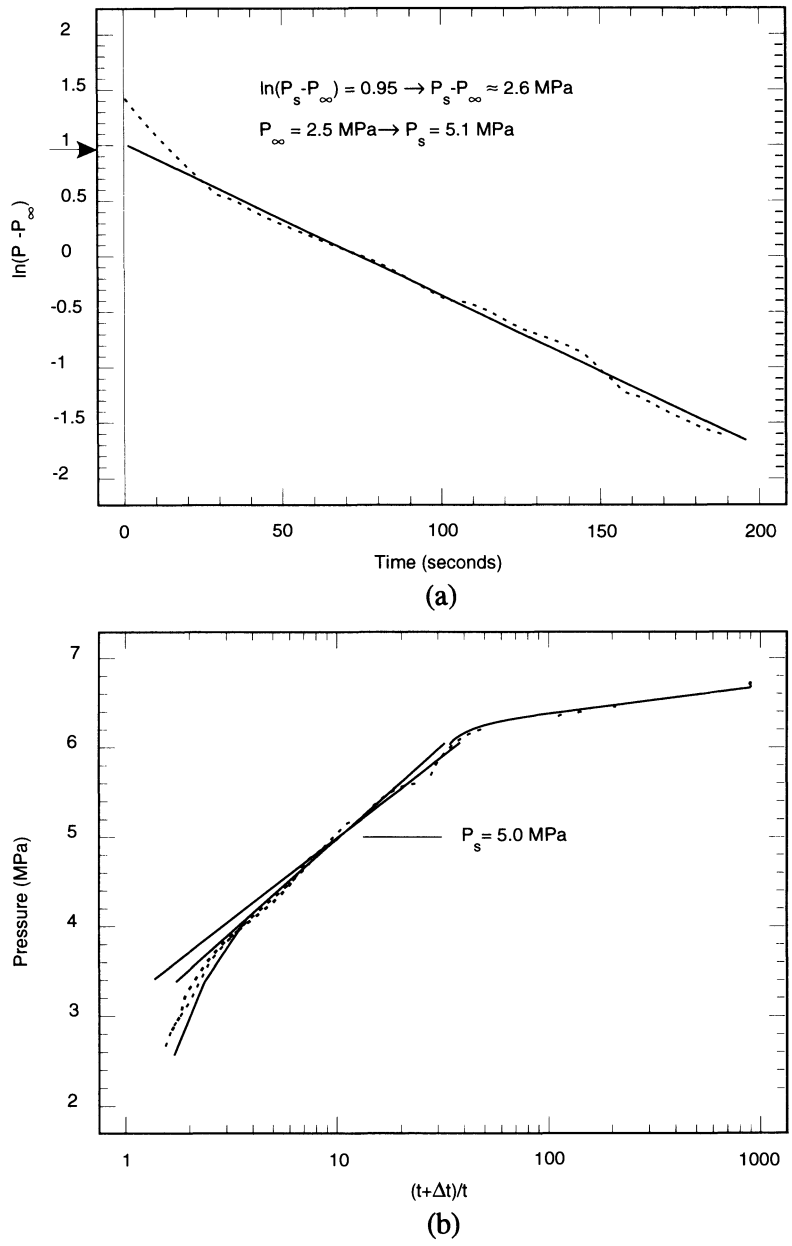

Fig. 4.26 Determination of shut-in pressure P_s from pressure decay records in borehole KAS03, depth 132.5 m at Äspö Hard Rock Laboratory, Sweden. (a) Exponential pressure decay method, (b) method of McLennan and Roegiers, (c) bilinear pressure decay rate method. (After Klasson, 1989.)

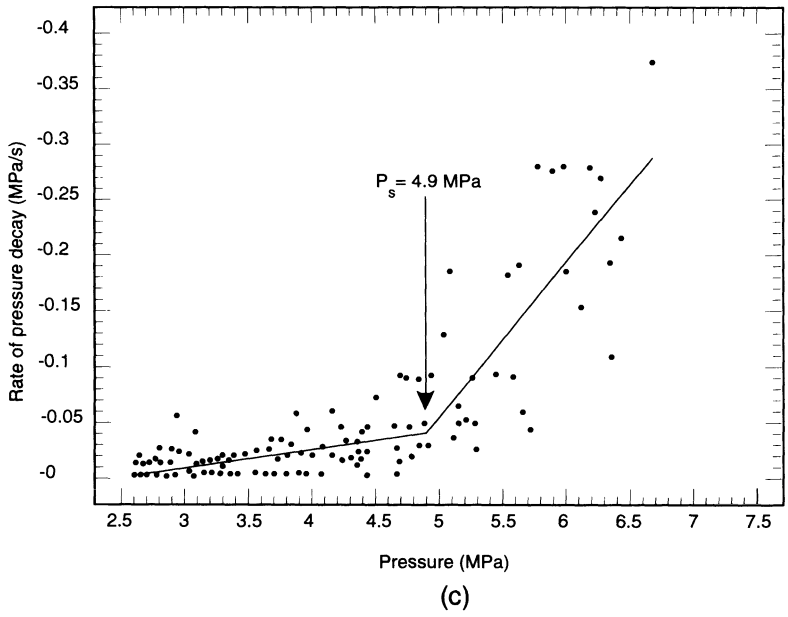

Fig. 4.26 *Continued.*

The variability of the shut-in pressure for the Äspö project is somewhat comparable to that reported by Aggson and Kim (1987) at the Basalt Waste Isolation Project in Hanford, Washington. These authors found that for a specific set of hydraulic fracturing data, and depending on the method of analysis, the shut-in pressure (also equal to the minimum

Table 4.3 Values of the shut-in pressure at different depths in borehole KAS03 determined by various graphical methods for the Äspö Hard Rock Laboratory data (third pressurization cycle; after Klasson, 1989)

		Test depth (m)					
		132.5	485.0	519.0	552.0	630.0	887.0
Relationship	*Method*	P_s *(MPa)*	P_s *(MPa)*	P_s *(MPa)*	P_s *(MPa)*	P_s *(MPa)*	P_s *(MPa)*
P vs. t	Intersection	3.5	10.8	12.0	9.7	10.1	21.5
	Curvature	4.6	11.2	13.1	10.2	11.1	21.9
	Inflection	5.6	11.7	14.1	11.0	11.5	22.5
P vs. $\log(t)$	Intersection	4.0	11.0	12.3	9.8	10.5	21.6
	Inflection	5.2	11.3	13.4	10.5	11.0	22.0
$\log(P)$ vs. $\log(t)$	Intersection	4.1	11.1	12.3	9.7	10.7	21.6
	Inflection	5.0	11.3	13.2	10.3	11.1	22.2
$\ln(P - P_\infty)$ vs. t	Exponential decay	5.1	10.9	13.2	10.8	11.0	21.8
P vs. $\log[(t + \Delta t)/t]$		5.0	10.9	13.3	10.1	11.0	21.9
dP/dt vs. P	Bilinear decay	4.9	11.3	12.9	10.1	10.7	22.0
Mean value		4.7	11.2	13.0	10.2	10.9	21.6
Standard deviation		0.60	0.30	0.60	0.40	0.40	0.30

horizontal stress) could vary by as much as 4.9 MPa (14%). For the Äspö project, the variation is about 2.1 MPa (38%).

(c) Reopening pressure, P_r and tensile strength, T

The hydraulic fracture tensile strength is critical in the analysis of hydrofracturing tests as it enters into the relationship between the breakdown pressure and the maximum and minimum *in situ* stresses. Several methods have been suggested in the literature for determining the hydraulic fracture tensile strength. According to Ratigan (1990), five approaches are available:

1. perform fracture reopening in subsequent pressurization cycles following the first cycle (Bjarnason, Ljunggren and Stephansson, 1989; Bredehoeft *et al.*, 1976; Hickman and Zoback, 1983);
2. use the tensile strength obtained from laboratory hydraulic fracture tests (Bjarnason, Ljunggren and Stephansson, 1989; Haimson, 1978a, b);
3. use a statistical fracture mechanics model formulated from laboratory experiments to estimate the *in situ* hydraulic fracture tensile strength (Doe *et al.*, 1983; Ratigan, 1982);
4. incorporate a slotting of the packed-off section of the borehole to enable a deterministic fracture mechanics interpretation of the test (Abou-Sayed, Brechtel and Clifton, 1978);
5. use an LEFM approach and estimate the crack size from known rock grain size and laboratory data of fracture toughness (Rummel, 1987).

In general, these techniques yield different values of the rock tensile strength. Thus it appears that the hydraulic fracture tensile strength is not a unique material property of the rock.

The first two techniques are by far the most common when determining the hydraulic fracture tensile strength. In the first technique the pressure necessary to reopen the hydrofracture is determined by conducting a second or third pressurization cycle. That pressure is defined as the reopening (or 'refrac') pressure P_r (Figs 4.12 and 4.23). If the classical theory of hydraulic fracturing is used, and assuming a non-penetrating fluid, the hydraulic fracture tensile strength T is obtained by calculating the difference between the breakdown pressure and the reopening pressure (Bredehoeft *et al.*, 1976), as described by equation (4.18).

As remarked by Lee and Haimson (1989) and Ratigan (1992), the method suggested by Bredehoeft *et al.* (1976) was developed under the assumptions that (1) the hydrofracture closes completely between pressurization cycles, (2) the reopening pressure is the pressure level at which the pre-existing hydrofracture just begins to open, (3) the tensile strength of the rock with the hydrofracture is zero and (4) the stress state in the borehole wall is the same with or without the hydrofracture. The last assumption is very much open to question since the hoop stresses for the fractured and unfractured borehole walls cannot be the same. The importance of that effect on the determination of the hydraulic fracture tensile strength and the *in situ* stresses was investigated by Ratigan (1992) using an LEFM approach and for the case of hydraulic fracturing of an impermeable rock formation. Ratigan (1992) derived an equation for the reopening pressure which, for the variables defined in Fig. 4.14, can be expressed as follows:

$$P_r = S_H F_1(a, \lambda) + S_h F_2(a, \lambda) \qquad (4.77)$$

where λ is the ratio between the pressure in the hydrofracture (assumed uniform) and that in the borehole, a is the fracture length and F_1 and F_2 are two complex functions. As remarked by Ratigan (1992), equation (4.77) has a functional form similar to equation (4.43) derived by Rummel (1987) without the first term associated with the fracture toughness. Ratigan also concluded that the relationship of Bredehoeft *et al.* (1976), which uses equation

(4.77) with $F_1 = -1$ and $F_2 = 3$, is only appropriate for interpreting hydraulic fracture stress measurements for two specific cases:

1. $\lambda = 1$ (slow pumping and low-viscosity fluid), the initial crack length is at least four to five times the borehole radius and the ratio $S_H/S_h \approx 2$.
2. $\lambda = 0$ (fast pumping and high-viscosity fluid), the initial crack length is less than about one borehole radius.

For other conditions, Ratigan (1992) concluded that the relationship of Bredehoeft *et al.* (1976) could not be used and that the hydraulic fracturing tensile strength should be estimated from laboratory tests.

As for the shut-in pressure, the determination of the fracture reopening pressure from pressure–time records can be subjective. By definition the fracture reopening pressure is the pressure in a subsequent pressurization cycle (second or third cycle) where the slope of the ascending portion of the pressure–time curve departs from that of the pressure–time curve in the first fracture-inducing cycle. A conventional way of determining P_r is to superimpose the first cycle fracture-inducing curve onto the pressure–time curves for the other pressurization cycles. However, as remarked by Lee and Haimson (1989), this graphical technique can be misleading. They proposed instead a more rigorous statistical technique of superimposing the pressure–time curves and selecting P_r.

The method of Lee and Haimson (1989), called the 'reference threshold' method and shown in Figs 4.27a,b for hydrofracturing data at the Waterloo site in Wisconsin, consists of comparing the digitized pressure–time data for a segment of the ascending portion in the fracturing cycle with the data points in the repressurization cycle over the same elapsed

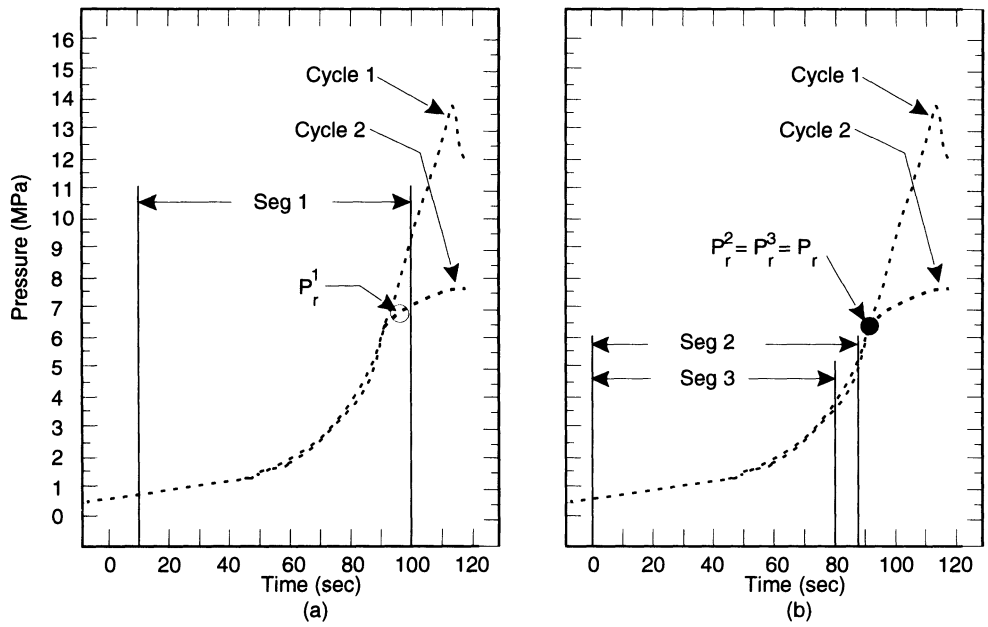

Fig. 4.27 Fracture reopening pressure determination using 'reference threshold' method. (a) Initial segment 1 yields unsatisfactory matching, since P_r^1 is inside the segment; (b) segment 2 determines P_r and reduced segment 3 confirms P_r. Data from borehole W1 in quartzite, depth 81.5 m at Waterloo, Wisconsin, USA. (Source: Lee, M.Y. and Haimson, B.C. Copyright 1989, with kind permission from Elsevier Science Ltd, The Boulevard, Langford Lane, Kidlington, UK.)

time. The average pressure difference between the two pressure–time curves and its standard deviation are determined by statistical techniques. The reference threshold is defined as the average pressure difference plus two standard deviations. The onset of deviation between the ascending portions of the pressure–time curves for the first and subsequent cycles is interpreted as the starting point of continuous pressure difference larger than the reference threshold. If the onset of deviation is inside the segment (Seg 1 in Fig. 4.27a), the segment is reduced in size at the high end and the procedure is repeated until the onset of deviation pressure is just on the upper edge of the segment (Seg 2 in Fig. 4.27b). The value of that pressure is then defined as the reopening pressure P_r.

The second approach for determining the hydraulic fracture tensile strength is to conduct hydraulic fracture tests on core samples in the laboratory. This approach raises another concern, which is how to interpolate the tensile strength measured in the laboratory to that in the field. As discussed below, although several recommendations have been proposed on that subject, it is still open for discussion.

According to Ratigan (1982, 1990), three observations are invariably made when intact rock samples are taken into the laboratory and tested to determine the tensile strength. First, the apparent tensile strength depends upon the sample size, with larger specimens giving smaller tensile strengths. This phenomenon is referred to as 'size effect' in the rock mechanics literature. Second, the apparent tensile strength depends upon the type of test being performed. Finally, with any given test and specimen size, a scatter about the mean value is often observed. Within the context of strength of (continuous) materials, none of these laboratory observations could be attributed to the inherent behavior of the material. Instead, they must be attributed to the testing methods and/or sample inhomogeneity. As shown by Ratigan (1982), the first two observations can be explained with deterministic fracture mechanics, and all three observations can be explained with statistical fracture mechanics using a method such as the weakest link theory proposed by Weibull in the late 1930s.

Laboratory hydraulic fracture tests used for the determination of the hydraulic fracture tensile strength T are usually carried out on rock specimens obtained from nominal-size cores taken from boreholes where field hydraulic fracture tests are conducted. The specimens contain an inner drillhole along their axis in which two small-diameter packers are inserted (Fig. 4.28). If the rock is porous, a membrane is placed around the test samples. Axisymmetric and axial pressures are then applied to simulate the virgin conditions. The small-diameter drillhole is pressurized until rupture occurs at a pressure P_c. The procedure is repeated for different levels of confining pressure P. An example of variation of fracturing pressure versus confinement is shown in Fig. 4.29 for tests conducted on drillcore samples of granitic gneiss from Forsmark in central Sweden. The core samples had an inner drillhole diameter of 10 mm and an outer diameter of 65 mm. For those tests the membrane was omitted and the confining oil pressure was in direct contact with the low-permeability rock. Using the least squares method, the data points in Fig. 4.29 were fitted by a straight line with equation

$$P_c = kP + T \tag{4.78}$$

with slope $k = 1.2$ and intercept, $T = 17.4$ MPa, taken as the tensile strength. It is interesting to note that coefficient $k = 1.2$ is quite different from the value predicted with the theory of linear elasticity. Indeed, for the geometry of the core samples used in the tests, k should be equal to 1.95 and a coefficient of 0.95 (instead of 1.0) should be applied to T. Test results reported by various authors have shown the same discrepancy (Ljunggren, 1984; Rummel, 1987). For instance, in the laboratory hydraulic fracture tests on drillcores of Falkenberg granite reported by Rummel (1987), the coefficient

k was found to be as small as 1.04. As discussed in section 4.2.3, LEFM can predict, in part, such smaller values for k by using equations (4.43) and (4.48) with $S_H = S_h = P$. The viscosity of the penetrating fluid and the rate of penetration also seem to be important factors in controlling the value of k.

Another observation often reported in laboratory hydraulic fracture tests is that the measured hydraulic fracture tensile strength depends on the drillhole diameter. More specifically, the tensile strength decreases with an increase in the central drillhole diameter (Cuisiat and Haimson, 1992; Enever, Walton and Wold, 1990; Haimson, 1968, 1990; Haimson and Zhao, 1991; Ljunggren, 1984). As an example, Haimson and Zhao (1991) conducted laboratory hydraulic fracture tests on core samples of Lac du Bonnet granite and Indiana limestone under no confinement and containing a drillhole with a diameter ranging between 3.4 and 50.8 mm. According to equation (4.78), the breakdown pressure was therefore a direct measurement of the hydraulic fracture tensile strength. The tests were conducted under either controlled flow rate or pressurization rate. The tests showed a negative exponential decrease in tensile strength with an increase in borehole diameter up to 20 mm. Beyond that, the tensile strength was essentially constant. The tests also revealed that the breakdown pressure, and therefore the tensile strength, almost doubled as the pressurization rate increased from 0.05 MPa/s to 10 MPa/s. Haimson and Zhao (1991) concluded however that, for the borehole diameters and pressurization rates used in the field, the hydraulic fracture tensile strength

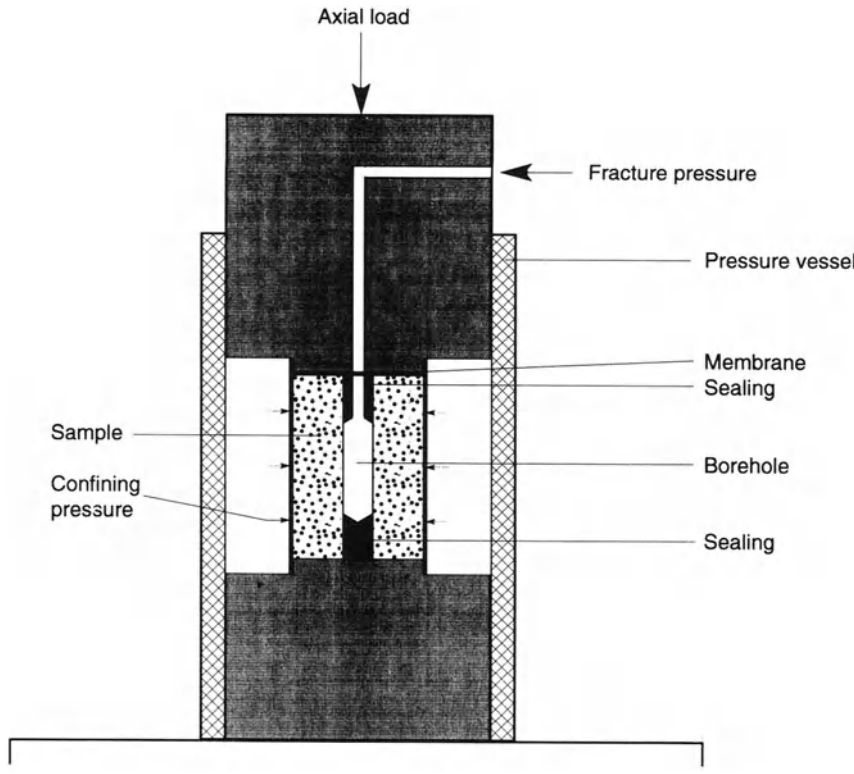

Fig. 4.28 Laboratory simulation of hydraulic fracturing for determination of the hydraulic tensile strength of a rock sample.

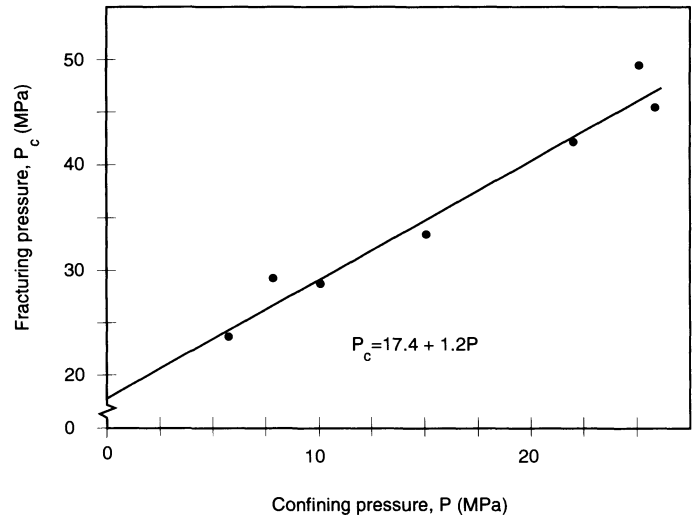

Fig. 4.29 Variation of fracturing pressure with confinement for hydraulic fracture laboratory tests conducted on 65 mm diameter core samples of granitic gneiss from Forsmark, central Sweden. The core samples have a 10 mm diameter drillhole.

measured in the laboratory was directly usable for the analysis of field data.

From an intuitive point of view, the observation that the tensile strength decreases as the borehole diameter increases makes sense since, as the borehole diameter becomes larger (and therefore the borehole wall surface increases), the probability of finding larger potential critical microcracks also increases. The models that have been proposed to predict the effect of the hole diameter on the tensile strength include the point stress criterion of Whitney and Nuismer (1974), the poroelastic model of Detournay and Carvalho (1989), and the LEFM models of Abou-Sayed, Brechtel and Clifton (1978) and Rummel (1987). We discuss below the fracture mechanics models only.

As shown in section 4.2.3 (equation (4.46)), the model of Rummel (1987) predicts that the hydraulic fracture tensile strength depends on the inverse of the square root of the borehole radius. As reported by Cuisiat and Haimson (1992), this model has been found to reproduce well the variations of hydraulic fracture tensile strength with borehole diameter observed in the laboratory by Haimson and Zhao (1991).

In the model of Abou-Sayed, Brechtel and Clifton (1978), for zero confinement ($P = 0$) the tensile strength (also equal to the breakdown pressure) is such that

$$P_c = T = \frac{K_{IC}}{F(L/r)(L\pi)^{1/2}} \tag{4.79}$$

where K_{IC} is the fracture toughness, L is the initial fracture length and r is the drillhole radius. In equation (4.79) $F(L/r)$ is a complex function whose values were determined by Paris and Sih (1965). Here again, the tensile strength should decrease as the borehole diameter increases.

The model of Abou-Sayed, Brechtel and Clifton (1978) was used by Ljunggren (1984) as a technique to predict the hydraulic fracture tensile strength in the field from the results of laboratory hydraulic fracture tests. The rationale used by Ljunggren was that, according to equation (4.79), the tensile strengths for two boreholes with radii r_1 and r_2 are related as follows:

$$\frac{T(r_1)}{T(r_2)} = \frac{F(L/r_2)}{F(L/r_1)} \tag{4.80}$$

Laboratory hydraulic fracturing tests were conducted on core samples of two Swedish rocks: Stidsvig gneiss (62 and 45 mm outer diameter) and Forsmark granitic gneiss (62 mm outer diameter). The core samples had an inner drillhole with radius $r = 5$ mm. Using equation (4.80), the hydraulic fracture tensile strength was predicted for 56 and 76 mm diameter boreholes, for initial fracture lengths $L = 0.5$ and 5 mm, and for the case of one or two fractures emanating from the borehole. The results are summarized in Table 4.4.

The results in Table 4.4 indicate that a longer initial fracture length reduces the tensile strength for the same number of fractures initiated at the borehole wall. For a large fracture length, the tensile strength is sensitive to the number of fractures initiated at the borehole wall. For a 76 mm diameter borehole, the predicted mean tensile strengths for the Stidsvig gneiss and Forsmark granitic gneiss were 14.0 MPa and 13.5 MPa, respectively. For the 56 mm diameter borehole, the predicted mean tensile strength for the Stidsvig gneiss was 12.6 MPa. In general, these predicted values were found not to correlate well with the mean values of tensile strength determined from the difference between the first and second breakdown pressures in the field, e.g. $T = 1.0$ MPa for the Stidsvig gneiss (76 mm borehole), $T = 2.1$ MPa for the Stidsvig gneiss (56 mm borehole) and $T = 5.4$ MPa for the Forsmark granitic gneiss (76 mm borehole). No satisfactory explanation was proposed by Ljunggren (1984) to explain such a large discrepancy between predicted and measured field values.

(d) Fracture delineation and orientation

The orientation of the hydrofractures that have formed on borehole walls is crucial when defining the *in situ* stress field. Theoretically, the fracture planes are oriented parallel to the axis of the borehole.

The images of induced vertical hydrofractures obtained on impression packers or on borehole televiewer pictures are rarely found in the form of two straight lines 180° apart.

Table 4.4 Determination of tensile strength of Swedish granitic rocks from laboratory hydraulic fracturing tests (after Ljunggren, 1984)

		Fracture length L = *0.5 mm*				*Fracture length* L = *5 mm*				
Rock type	*Core diameter* ϕ *(m)*	*Hole diameter (mm)*	L/r	F(L/r)	T *(MPa)*	*Hole diameter (mm)*	L/r	F(L/r)	T *(MPa)*	*Mean* T *(MPa)*
		One fracture initiated at the wall								
Stidsvig gneiss	62	10	0.1	1.98	18.0[a]	10	1.0	1.22	18.0[a]	
		76	0.013	2.22	16.0	76	0.13	1.93	11.0	13.5
Stidsvig gneiss	45	10	0.1	1.98	16.0[a]	10	1.0	1.22	16.0[a]	
		56	0.018	2.21	14.0	56	0.18	1.85	10.5	12.3
Forsmark granitic gneiss	62	10	0.1	1.98	17.4[a]	10	1.0	1.22	17.4[a]	
		76	0.013	2.22	15.5	76	0.13	1.93	11.0	13.3
		Two fractures initiated at the wall								
Stidsvig gneiss	62	76	0.013	2.22	16.0	76	0.13	1.94	13.0	14.5
Stidsvig gneiss	45	56	0.018	2.21	14.0	56	0.18	1.86	12.0	13.0
Forsmark granitic gneiss	62	76	0.013	2.22	15.5	76	0.13	1.94	12.0	13.8

[a] Experimental data.

More common are discontinuous traces that are oriented off-center, en echelon and irregular. In order to remove subjectivity in the determination of fracture orientation, Lee and Haimson (1989) introduced circular statistics to delineate coaxial hydrofractures more rigorously.

Figure 4.30a illustrates the main steps needed to delineate a coaxial hydrofracture from the image on an impression packer. First, the fracture traces are defined in terms of the azimuth with respect to a reference direction, typically north. The angle E_i $(i = 1, n)$ corresponding to the center of each digitized trace is represented by a unit vector on a circle. This results in two groups of vectors representing the two halves of the coaxial fracture. Following the presentation by Lee and Haimson (1989), since the strike of a fracture is such that $E_i = E_i + 180°$, the range of possible strikes can be reduced by rotating one of the groups by 180°. If X and Y are the mean components of the resultant vector along the 0° and 90° directions, the mean length of the resultant vector is $L = (X^2 + Y^2)^{1/2}$. The mean orientation angle of the hydrofracture E_o, defined as the resultant vector direction of n digitized trace data, is such that

$$E_o = \cos^{-1}(X/L) \tag{4.81}$$

where

$$X = \frac{\sum_{i=1}^{n} \cos E_i}{n} \qquad Y = \frac{\sum_{i=1}^{n} \sin E_i}{n} \tag{4.82}$$

The standard deviation (SD) of the mean direction is obtained from the length of the resultant vector L and is equal to

$$\mathrm{SD} = 0.5(-2 \ln L)^{-2} \tag{4.83}$$

An example of application of the above method for a typical en echelon hydrofracture trace is shown in Fig. 4.31a. The mean fracture strike direction based on equation (4.82) was determined as 48° ± 4.5°.

If the hydrofracture is not coaxial and is inclined with respect to the hole, a different approach needs to be used. In general, an inclined fracture intersecting a borehole appears as a sinusoidal curve on the unwrapped image of an impression packer or on a

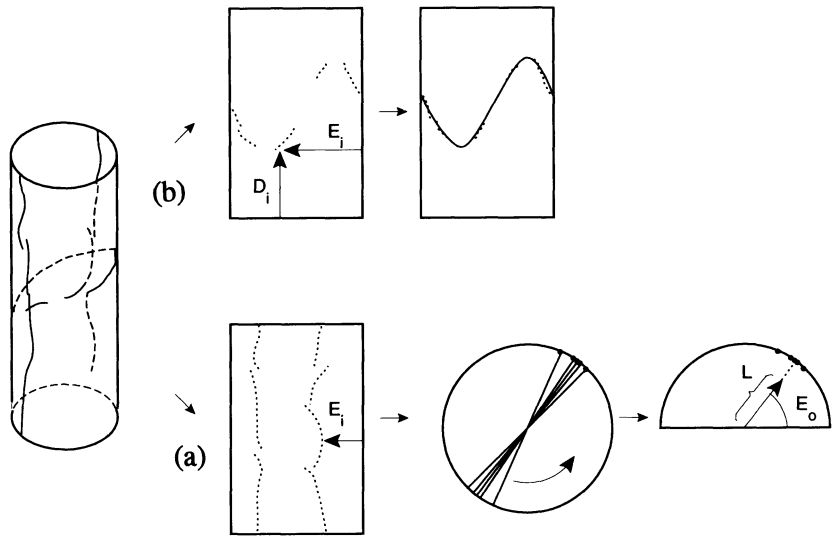

Fig. 4.30 Fracture delineation from an impression packer. (a) Circular statistics applied to sets of vertical fractures, (b) sinusoidal regression method applied to an inclined fracture. (After Lee and Haimson, 1989.)

formation microscanner (FMS) and borehole televiewer picture. The dip direction of the fracture can be determined by the azimuth of the lower hinge of the curve, and the dip angle can be calculated from the arctangent of the amplitude of the curve divided by the borehole radius. As for coaxial fractures, it is sometimes difficult to delineate inclined fractures, in particular if their traces are partially visible. In order to overcome this difficulty, Lee and Haimson (1989) introduced a sinusoidal curve-fitting regression method shown in Fig. 4.30b. If D and E are the coordinates of the fracture trace (in terms of depth and azimuthal angle) along the axis of the borehole, the following relation represents the geometry of the trace:

$$D = e_1 + e_2 \sin(E + e_3) \qquad (4.84)$$

where e_1, e_2 and e_3 are unknown parameters. By using nonlinear regression analysis, the digitized data of the traces obtained in the hydrofracturing experiment are fitted to equation (4.84). The average dip direction and its uncertainty are calculated from parameter e_3 and its standard deviation. The average dip angle and its uncertainty are calculated from parameters e_1 and e_2 and their standard deviations. An example of application of that method is shown in Fig. 4.31b.

The general experience of most research and engineering groups conducting hydrofracturing is that most impression tests or FMS and televiewer photographs yield less than ideal fracture traces. Therefore, the statistical techniques described by Lee and Haimson (1989) and summarized in this section are highly recommended as they remove subjectivity and offer confidence and uniformity.

4.3 SLEEVE FRACTURING

As discussed in the previous section, the build-up in pore pressure in the rock mass

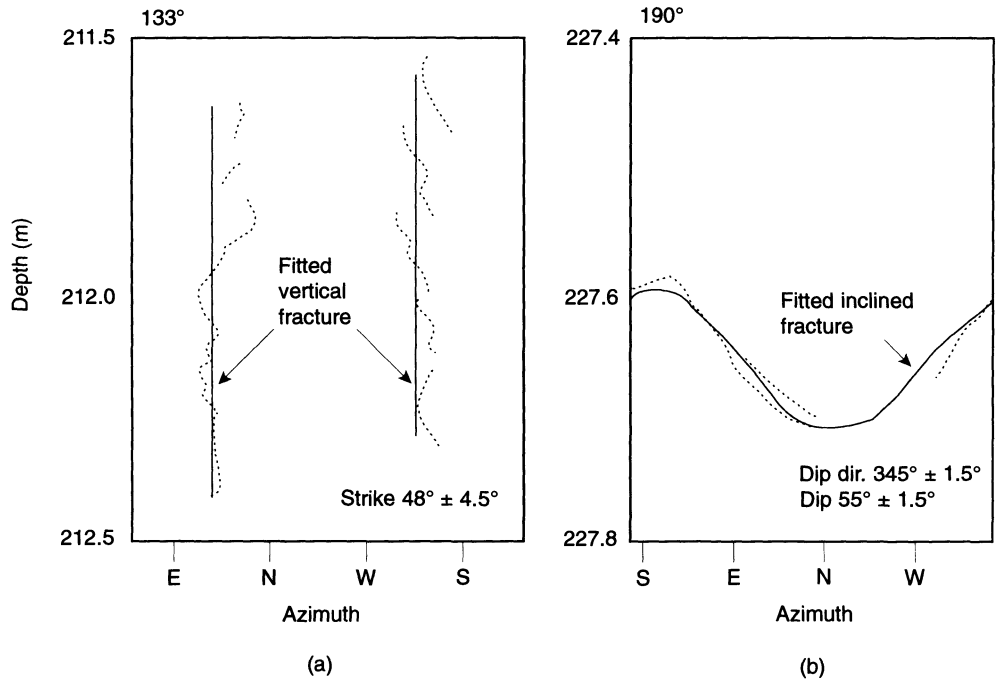

Fig. 4.31 Image of fractures from an unwrapped impression packer. (a) Mean direction of fracture determined by circular statistics, (b) optimum dip and dip direction of inclined fracture plane obtained by sinusoidal curve fitting. (After Lee and Haimson, 1989.)

adjacent to a borehole during conventional hydraulic fracturing stress measurements has an effect on the breakdown pressure and the determination of *in situ* stresses. Sleeve fracturing is an alternative technique to hydrofracturing whereby axial fractures are created at the borehole wall by expansion of the membrane of a high-capacity type of dilatometer. As in conventional hydraulic fracturing in vertical holes, a fracture is initiated at the borehole wall once the pressure exceeds the tensile strength of the rock and the fracture propagates in the direction perpendicular to the minimum horizontal principal *in situ* stress. However, unlike hydraulic fracturing, no fluid penetrates the rock mass during the fracturing process. The maximum and minimum principal stresses S_H and S_h in the plane perpendicular to the axis of the borehole are determined from the breakdown pressure and the pressure required to reopen the induced fractures.

4.3.1 HISTORY

The sleeve fracturing method was first proposed by Stephansson (1983b, c). It was essentially based on the concept of pressuremeter testing in soils and dilatometer testing in rocks. The sleeve fracturing system of Stephansson was an extension of the so-called Colorado School of Mines flexible dilatometer (also known as the CSM cell) developed by Hustrulid and Hustrulid (1975). The method was tested first in the laboratory in loaded and unloaded blocks of mortar, Indiana limestone and Colorado sandstone. Additional laboratory tests in blocks of granite and diabase were later on reported by Ljunggren and Stephansson (1986) using a stiffer system. Field testing of the sleeve fracturing method was conducted at four sites and in four different rock types related to the US program of storage of radioactive waste in geological formations (Stephansson, 1983b, c).

In the sleeve fracturing method of Stephansson and co-workers, the magnitude of the horizontal principal *in situ* stresses perpendicular to the borehole axis is determined from recorded pressure versus volume curves. The direction of the maximum horizontal principal stress is found from the orientation of the axial fracture plane in the borehole. The fracture orientation is determined from impression on black vinyl electrical tape wrapped around the surface of the sleeve.

Another sleeve fracturing system was proposed by Serata and Kikuchi (1986) and Serata *et al.* (1992). In their method of *in situ* stress measurement, called the 'double fracture' method, the pressure of the sleeve is raised to create a set of two mutually perpendicular fractures at the borehole wall. The magnitude of the *in situ* principal stresses in the plane normal to the borehole axis is deduced from sleeve pressure versus borehole diametral deformation recordings. The orientation of the maximum and minimum *in situ* stresses is determined from the diametral deformation of the borehole measured by four deformation sensors placed inside the sleeve. The double fracture method has been tested in both laboratory and field.

The reader should be aware of the recent development of a new dilatometer for rocks, called the 'directional dilatometer'. That instrument was designed and built by ROCTEST and was developed at the University of Colorado at Boulder (Amadei *et al.*, 1994). Unlike conventional dilatometers, the directional dilatometer is divided into four sectors, each containing an inflating membrane and a displacement transducer. Directional loading or uniform loading can be applied on the borehole wall. In principle, the directional dilatometer can be used for sleeve fracturing of borehole walls and the measurement of *in situ* stresses together with the measurement of both the Young's modulus and Poisson's ratio of the rock. This equipment is still under testing.

The main advantage of sleeve fracturing, in general, is that it provides a method of inducing axial fractures in boreholes and at any

depth without introducing fluids into the rock mass during the fracturing process. The sleeve breakdown pressure should be more representative of the *in situ* stress field than the breakdown pressure obtained in hydraulic fracturing since there is no fluid interacting with microfissures, flaws and other rock discontinuities in the vicinity of the borehole.

However, compared with hydraulic fracturing, sleeve fracturing has a couple of drawbacks. First, existing microfractures and flaws in rocks often make it difficult to obtain sharp and consistent elastic breakdown points in the recorded pressure versus volume curves or pressure versus diametral deformation curves. Second, compared with hydraulic fracturing, the induced fractures do not propagate far from the borehole wall. Both of these limitations remain to be overcome. As a closing note, attempts have been made to combine the sleeve fracturing and hydraulic fracturing techniques. For instance, Thiercelin and Desroches (1993) and Thiercelin, Desroches and Kurkjian (1994) recommended using such an approach in order to obtain reliable stress determinations in weak rocks such as shale.

4.3.2 TECHNIQUES, EQUIPMENT AND PROCEDURES

The sleeve fracturing stress measurement methods make use of modified high-capacity flexible dilatometers. In principal, there are two types of dilatometer used in rock mechanics. The first type measures borehole volume changes from which radial displacements can be calculated. The second type measures radial displacements directly using displacement transducers mounted in the dilatometer itself. Both types are flexible in that they can apply a uniform distributed pressure to the borehole wall throughout a flexible membrane of neoprene or adiprene (hard rubber). The sleeve fracturing system used by Stephansson (1983b, c), which is a slight modification of the CSM cell developed by Hustrulid and Hustrulid (1975), is shown in Fig. 4.32. The system was further modified by Ljunggren

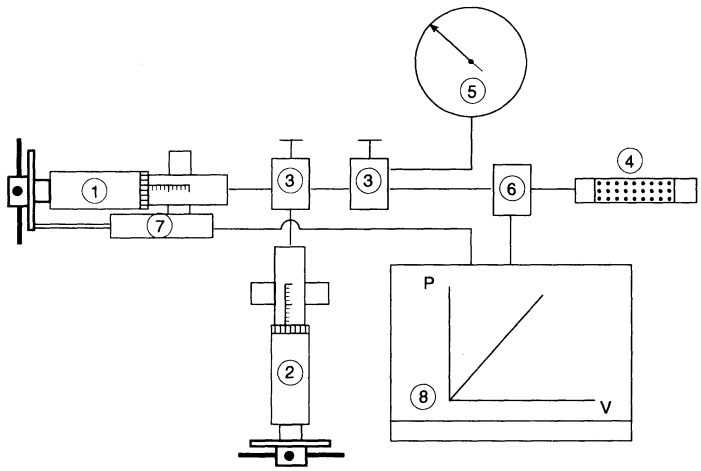

Fig. 4.32 Sleeve fracturing system of Stephansson (1983b, c) used to determine rock mass deformability and *in situ* stresses. 1, High-pressure generator with vernier indicator rated at a pressure capacity of 70 MPa and a fluid capacity of 30 cm^3; 2, high-pressure generator with vernier indicator rated at a pressure capacity of 35 MPa and a fluid capacity of 60 cm^3; 3, three-way high-pressure valve; 4, CSM borehole cell; 5, pressure gage rated at 0–140 MPa; 6, high line differential pressure transducer of diaphragm type ranging from 35 kPa to 85 MPa and readout unit; 7, linear displacement transducer with a resolution of 0.05–0.08 mm; 8, X–Y recorder.

and Stephansson (1986) by placing a pressure intensifier next to the CSM cell. This addition was able to make the sleeve fracturing system much stiffer than the CSM system.

The main component of the sleeve fracturing system of Stephansson and co-workers is the CSM borehole cell. The cell fits into EX (38 mm) boreholes and consists of three parts: (1) a membrane made of adiprene, (2) a central steel mandrel with an end cup and (3) a removable steel end cup. The membrane has a self-sealing construction so that when the pressurizing fluid enters the cavity between the mandrel and the inner membrane wall, the pressure seals the flange of the membrane against the mandrel and the ends against the end cup. A minimum of tubing should be applied and water should be used as the pressurizing fluid in order to obtain a stiff system. Figure 4.33 shows a laboratory set-up for sleeve fracturing testing used at the Colorado School of Mines in Golden, Colorado.

The sleeve fracturing method of Stephansson offers the possibility of determining two parameters *in situ* in one and the same test in a vertical borehole. The system is first pressurized to a level where no fractures are initiated and the modulus of rigidity of the rock mass is determined. If the Poisson's ratio ν of the rock is known or can be estimated, its Young's modulus E can also be found. By increasing the pressure further, a borehole fracture is induced and a sleeve breakdown pressure is recorded. If the fracture is vertical, its direction indicates the direction of the maximum horizontal principal *in situ* stress. By recording the pressure necessary for reopening the fracture during a second pressurization cycle, and knowing the tensile strength of the rock, the magnitude of the horizontal principal *in situ* stresses can be determined from the classical equation for hydraulic fracturing. Fracture orientation in the borehole is determined by impression on black vinyl electrical tape wrapped around the surface of the sleeve. The tape is somewhat sticky, causing the loose particles from the fracture

Fig. 4.33 Laboratory set-up for sleeve fracturing testing used at the Colorado School of Mines, Golden, Colorado.

to stick to the tape. At the same time, the tape can deform plastically as the sleeve is inflated and it penetrates into the fracture opening and gives a distinct print with the topography of the fracture. By knowing the orientation of the sleeve in the borehole and the fracture orientation, the direction of the maximum horizontal principal *in situ* stress is determined from the impression on the surface of the sleeve.

Serata *et al.* (1992) developed a special instrument called the Stressmeter (S-200) as a necessary tool to implement the double fracture method of *in situ* stress measurement. The sleeve of the Stressmeter probe consists of two compartments, pressure-loading and non-pressurized sections, within a single cylindrical housing. The plastic tube of the pressure-loading section is constructed of urethane. The sleeve diameter is 100 mm, its length is 100 cm and it is pressurized using an electrical power pump. Four diameter-sensing transducers, arranged at 45° angular and 110 mm intervals inside the Stressmeter, measure changes in borehole diameter with a high resolution in relation to the applied sleeve pressure. Signal outputs from the electronic compartments represent diametral deformation and loading pressure, and are transferred by an electronic cable to a laptop computer and disk storage for later post-processing offsite.

In the double fracture method, after a first cycle of loading, fracturing and unloading of the borehole wall, the sleeve pressure is increased again to a level where a second fracture is formed.

The initiation and reopening of the first and second fractures are recorded by the four diametral transducers in relation to the applied sleeve pressure. From the plots of applied pressure versus borehole diametral deformation across each fracture plane, the two reopening pressures can be extracted and the maximum and minimum horizontal principal *in situ* stresses can be calculated. Orientation of the principal *in situ* stresses is determined from the diametral deformation (strain ellipse) of the borehole wall. When applying the double fracture method, the borehole is preloaded (or 'pretreated') with the sleeve. The increased loading pressure allows simultaneous consolidation of the rock mass and creation of the double fractures around the borehole.

Thiercelin and Desroches (1993) developed a new and interesting downhole method for hydraulic stress measurements. The method combines the sleeve fracturing technique with the conventional hydraulic fracturing technique. First a sleeve fracturing is carried out at the test location in the borehole and two fractures are formed with the fracture planes oriented parallel with the axis of the borehole. The fractures are generated by inflating one of the packers of the straddle packer equipment. After generating the fractures, the straddle packer is deflated and moved such that the straddle packer interval is located at the depth of the initiated fractures. Thereafter, the fractures can be pressurized with any fluid and allowed to propagate. This technique establishes the location of the fractures to be tested and significantly reduces the reopening pressure for the hydraulic testing. The latest version of the wireline tool for conducting combined sleeve fracturing and hydraulic fracturing in deep boreholes is entirely software controlled (Thiercelin, Desroches and Kurkjian, 1994). It consists of a downhole pump to pressurize both the packers and the fluid in the test interval, which reduces the wellbore storage and increases the overall stiffness of the system.

4.3.3 THEORY OF SLEEVE FRACTURING

(a) Determination of rock modulus

The complete derivation of the equations required for the calculation of the rock elastic modulus from pressure versus volume curves obtained with borehole dilatometers such as the CSM cell was presented by Hustrulid and

Hustrulid (1975). We present below a summary of that derivation when applied to the analysis of sleeve fracturing tests.

Prior to conducting sleeve fracturing tests, the stiffness of the entire system (i.e. pressure generators, fluid, valves, membrane and pressure gages), must be determined. This is accomplished by inserting the cell in a metal cylinder of known geometry and elastic properties, and then pressurizing it. During pressurization a pressure versus volume curve is recorded. The slope of that curve M_m combines the stiffness of the system M_s and that of the calibration cylinder, M_c. The stiffness of the calibration cylinder alone can be calculated using the following equation:

$$M_c = \frac{\gamma G_c}{\pi L r_{ic}^2 \left(\frac{1 + \beta_c - 2\nu_c \beta_c}{1 - \beta_c} \right)} \tag{4.85}$$

where γ is the volume of fluid injected from pressure generator per turn of pressure pump (0.361 cm^3/turn for CSM cell), L is the effective length of the rubber sleeve (cm), r_{ic} is the radius of the hole in the calibration cylinder (cm), r_{oc} is the outside radius of the calibration cylinder (cm), $\beta_c = (r_{ic}/r_{oc})^2$, G_c is the modulus of rigidity of the calibration cylinder (MPa) and ν_c is the Poisson's ratio of the calibration cylinder.

For the units selected here, M_c is determined in MPa/turn. Once M_c is known, the system stiffness M_s (in MPa/turn) can now be computed as follows:

$$M_s = \frac{M_c M_m}{M_c - M_m} \tag{4.86}$$

After calibration, the cell can now be inserted into a borehole in a rock with unknown elastic properties. The slope M_T of the linear portion of the pressure versus volume curve is determined over the same pressure range as in the calibration phase. The rock stiffness M_R is then determined from

$$M_R = \frac{M_S M_T}{M_S - M_T} \tag{4.87}$$

For testing in a borehole in an infinite rock mass, the rock modulus of rigidity G_R is related to M_R as follows:

$$G_R = \frac{M_R \pi L r_i^2}{\gamma} \tag{4.88}$$

where L is the length of the sleeve, r_i is the radius of the borehole and γ is the volume of fluid injected per turn of the pressure pump. If the Poisson's ratio of the rock mass ν_R is known, then the Young's modulus of the rock E_R can be calculated from

$$E_R = 2(1 + \nu_R) G_R \tag{4.89}$$

For deformability determination using a flexible dilatometer with radial displacement measurements, the resulting hole expansion is measured directly by displacement transducers mounted in the sleeve. If for a given change in applied pressure Δp, a change in diametral deformation ΔU is measured in a borehole of initial radius r_i, the modulus of rigidity of the rock is equal to

$$G_R = r_i \frac{\Delta p}{\Delta U} \tag{4.90}$$

The Young's modulus of the rock is again determined using equation (4.89). An advantage in using measurements of diametral deformations instead of volume changes is that rock anisotropy may be inferred from the variation in diametral deformation around the borehole wall.

(b) Determination of *in situ* stresses

Consider again the same geometry used for the derivation of the hydraulic fracturing equations, that is a circular vertical hole of radius R subjected to an internal pressure P and to far-field stresses S_H and S_h. Again, using the Kirsch solution (Jaeger and Cook, 1976), at the borehole wall and at an angle θ from S_H, the radial stress σ_r is equal to P, the shear stress $\sigma_{r\theta}$ vanishes and the tangential stress σ_θ is equal to

$$\sigma_\theta = (S_H + S_h) - 2(S_H - S_h)\cos 2\theta - P \tag{4.91}$$

As the sleeve pressure P increases, the tangential stress σ_θ decreases linearly until fracturing of the borehole wall. The first fracture occurs at $\theta = 0$ and 180°, i.e. in the direction of the maximum *in situ* principal stress S_H, when σ_θ is equal to the rock tensile strength T. The sleeve pressure or breakdown pressure P_1^C necessary to initiate the first fracture in a direction parallel to the maximum principal stress S_H is equal to

$$P_1^C = 3S_h - S_H + T \tag{4.92}$$

The extension of the first fracture plane is short due to the limited amount of force generated by the sleeve. The extent of the fracture is usually about the size of the borehole diameter. This is different from conventional hydraulic fracturing where the fluid pressure in the fracture planes generates enough loading to propagate the fractures over long distances.

Equation (4.92) provides one equation for determining the two unknowns S_H and S_h. When using the method of Stephansson, the second equation is obtained by repressurizing the fractured borehole wall. The minimum horizontal stress S_h is then determined as the pressure when the first fracture reopens.

It is noteworthy that the application of equation (4.92) to sleeve fracturing is valid, assuming that the breakdown pressure is equal to the contact stress at the interface between the borehole wall and the sleeve. This is however not true since there is a reduction in contact stress caused by the membrane. Stephansson (1983c) studied this problem and showed that the error in stress magnitude is less than 1% for stresses in the order of tens of megapascals. For sleeve pressures less than a few megapascals, however, the reduction due to contact stresses needs to be considered. The equations necessary for calculating the amount of stress reduction can be found in Stephansson (1983c).

After the first fracture has developed, further increase of the borehole pressure directly increases tension at $\theta = 90°$ and 270°. According to Serata *et al.* (1992), the second fracture generally originates in a direction perpendicular to the first fracture, i.e. in the direction of the minimum horizontal *in situ* stress S_h.

Serata *et al.* (1992) followed a different approach from Stephansson for the analysis of sleeve fracturing tests. They suggested that the *in situ* stresses S_H and S_h could be determined by measuring the sleeve pressures at the reopening of the first and second fractures. These reopening pressures can best be determined from the pressure versus deformation diagrams that relate the borehole diametral deformation across each fracture plane to the sleeve pressure. At the time of reopening of each fracture, the tangential stress at the borehole wall is assumed to vanish as in hydraulic fracturing, e.g.

$$\begin{aligned} \sigma_\theta(\theta = 0°) &= 3S_h - S_H - P_1^R = 0 \\ \sigma_\theta(\theta = 90°) &= 3S_H - S_h - P_2^R = 0 \end{aligned} \tag{4.93}$$

where P_1^R and P_2^R are the reopening pressures for the first and second fractures, respectively. Solving equations (4.93) for S_H and S_h gives

$$\begin{aligned} S_H &= (P_1^R + 3P_2^R)/8 \\ S_h &= (P_2^R + 3P_1^R)/8 \end{aligned} \tag{4.94}$$

Equations (4.93) and (4.94) imply that the rock is linearly elastic up to the point of fracture. This also implies that the first fracture has no effect on the stress distribution around the borehole wall or on the initiation and propagation of the second fracture.

4.3.4 RECORDINGS AND INTERPRETATION

Figure 4.34 shows a summary of the different steps necessary to determine the rock modulus and *in situ* stresses by sleeve fracturing in a vertical hole using the method of Stephansson (1983b, c). The pressure versus volume (P versus V) curve is recorded and a single vertical fracture is assumed to be induced at the borehole wall. As before, the *in situ* stress field

in the horizontal plane is characterized by two principal components, S_H and S_h (Fig. 4.34a).

The rock modulus is first determined from the slope M_T of the linear portion of the pressure versus volume recording obtained before fracturing of the borehole wall (Fig. 4.34b). Equations (4.85)–(4.89) are used to analyze the recording taking into account the stiffness of the system. As the sleeve pressure increases, a fracture will form in the direction of the maximum principal stress, S_H. The initiation and propagation of the fracture will cause a change in the stiffness of the rock mass. The sharp break in the pressure–volume curve defines the breakdown pressure P_1^C (Fig. 4.34c).

As discussed in section 4.2, in hydraulic fracturing the magnitude of the least principal stress S_h is determined from the shut-in pressure. In sleeve fracturing this method cannot be used due to the absence of penetrating fluid. Instead, S_h is determined as the fracture reopening pressure P_1^R corresponding to a break point on the pressure versus volume curve (Fig. 4.34d). This is based on the assumption that the rate of volume change for the pressurized sleeve is different before and after reopening of the fracture. Substituting $S_h = P_1^R$ into equation (4.92), the value of S_H can be determined once the rock tensile strength T is known.

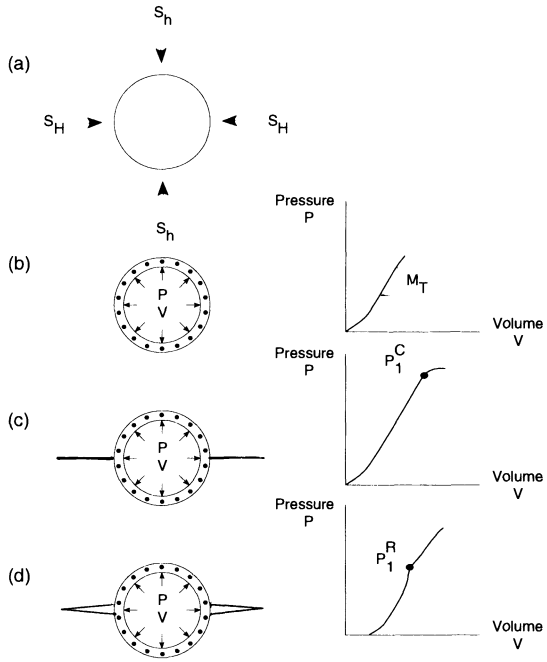

Fig. 4.34 Different steps when determining the rock modulus and *in situ* stresses by sleeve fracturing in a vertical hole using the CSM cell. (a) Virgin state of stress in the rock mass; (b) pressurization and determination of rock modulus from the slope M_T of the linear portion of the pressure versus volume recording; (c) determination of breakdown pressure P_1^C; (d) repressurization and determination of fracture reopening pressure P_1^R. (After Stephansson, 1983b.)

Figures 4.35a, b show idealized pressure versus borehole diametral deformation response curves obtained during cyclic loading with the double fracture method. Figure 4.35a corresponds to the first fracture and Fig. 4.35b corresponds to the second fracture. Upon loading, the breakdown pressures P_1^C and P_2^C for the first and second fractures are defined as sharp breaks in the response curves of Figs 4.35a and 4.35b, respectively, following a linear elastic response. After fracturing, unloading of the borehole wall gives non-recoverable deformation reflecting a permanent diametral expansion caused by both consolidation and fracture development. Upon reloading, the rock first deforms elastically until reaching the fracture reopening pressures P_1^R and P_2^R, at which there is a marked change in the pressure versus borehole diametral deformation curves. Substituting the values of P_1^R and P_2^R into equation (4.94) gives the values of S_H and S_h.

The pressure differences between the breakdown pressures P_1^C and P_2^C on one hand and the reopening pressures P_1^R and P_2^R on the other hand give estimates of the tensile strength T of the rock in the borehole wall. This method, which is identical to that suggested by Bredehoeft *et al.* (1976) for hydraulic fracturing, should give reasonable estimates of the tensile strength in view of the recommendations made by Ratigan (1992; section 4.2.4) since, in sleeve fracturing, there is no fluid

penetrating into the rock and the induced fractures are small.

4.3.5 DATA ANALYSIS AND PRESENTATION

Field testing of the sleeve fracturing method with the CSM cell has been conducted at four sites and in four different rock types related to the US program of storage of radioactive waste in geological formations (Stephansson, 1983b, c). Tests were carried out in migmatitic gneiss (CSM Experimental Mine, Idaho Springs, Colorado), latitic lava (USGS Test Site, Golden, Colorado), granite (Nevada Test Site, Nevada) and basalt (NSTF Test Site, Hanford, Washington). Some of the results of

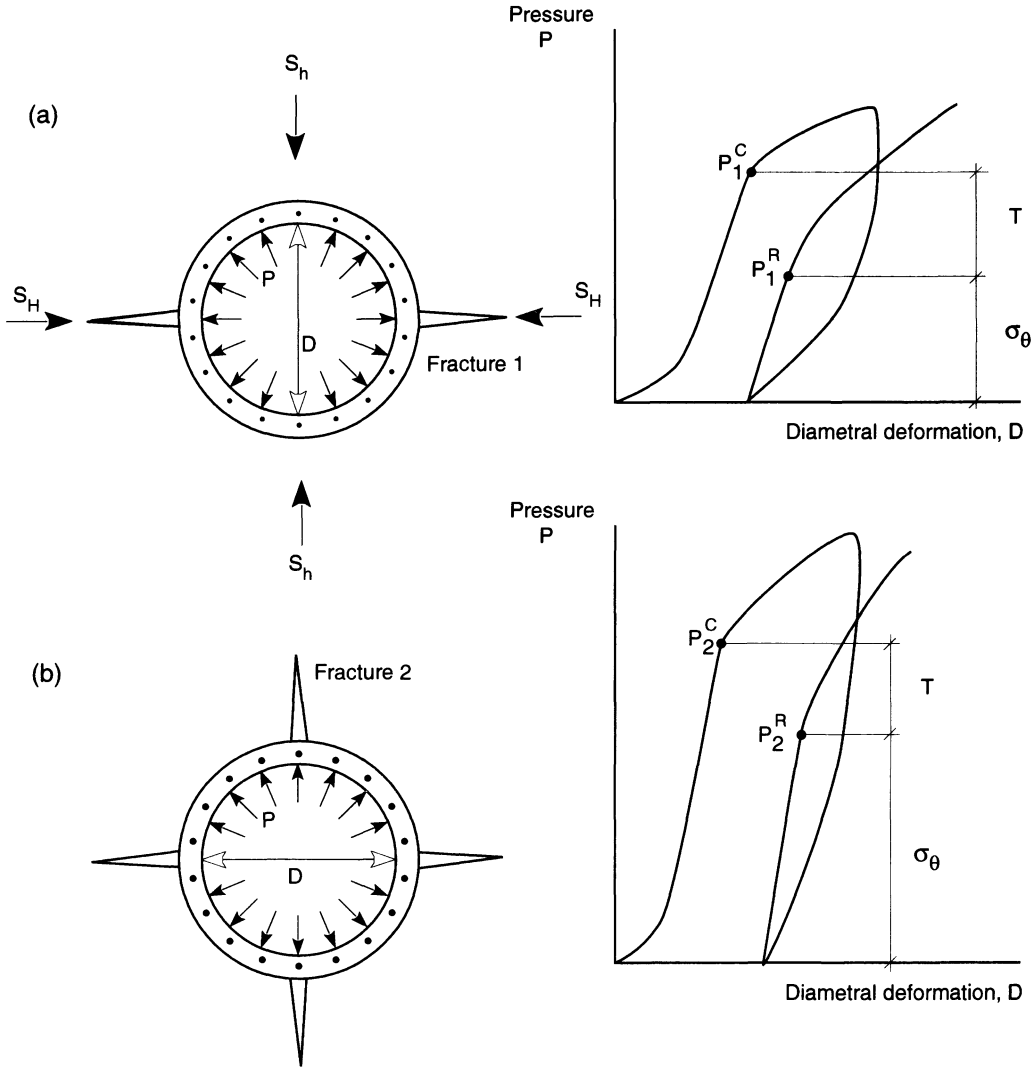

Fig. 4.35 Idealized pressure versus borehole diametral deformation response curves obtained during cyclic loading with the double fracture method. (a) Response curve for first fracture and determination of breakdown pressure P_1^C and reopening pressure P_1^R. (b) Response curve for second fracture and determination of breakdown pressure P_2^C and reopening pressure P_2^R. (Modified from Serata *et al.*, 1992.)

the field tests conducted in three vertical boreholes in the Pomona basalt at the NSTF Hanford Test Site are presented below. Other results can be found in Stephansson (1983b, c).

At the Hanford site, most of the test procedure consisted of pressurizing the sleeve up to the breakdown pressure where a fracture first appeared. Following fracturing, a pressure drop was recorded. After unloading of the system, a second pressurization cycle was imposed until a pressure drop was recorded for the second time. Repeated loading and unloading indicated minor changes in rock mass stiffness as indicated in the pressure versus number of turns (volume) curves of Fig. 4.36.

Fracture initiation and propagation in the hard basalt was also recorded from clear and in most cases loud sounds transmitted from the fracture via the extension rod to the pressure equipment. The pressure for reopening the fracture in subsequent pressurizations (also equal to the minimum horizontal principal *in situ* stress) was determined by overlapping the pressure–volume curves from the first and later pressurizations. The point where the curves diverged indicated a change in stiffness and hence reopening of the fracture. For the response curves of Fig. 4.36, the rock was found to have a Young's modulus of 4.1 GPa, and the breakdown and reopening pressures were found to be equal to 11.7 and 5.2 MPa, respectively. The maximum and minimum horizontal *in situ* stress components were equal to $S_H = 21.2$ MPa and $S_h = 5.2$ MPa, respectively, for a tensile strength of 17.4 MPa (determined by a modified borehole jacking method).

Fracturing in basalt gave clear and distinct impressions that could be distinguished from existing rock joints. Most fractures recorded at Hanford were oriented 180° apart and were visible along the full length of the surface of the sleeve. The direction of the maximum horizontal principal *in situ* stress for the test results presented in Fig. 4.36 ranged between N70°W and S75°E. As discussed by Stephansson (1983b), at the NSTF Hanford test site the rock stress measurements by hydraulic fracturing, overcoring and sleeve fracturing were found to be in close agreement despite

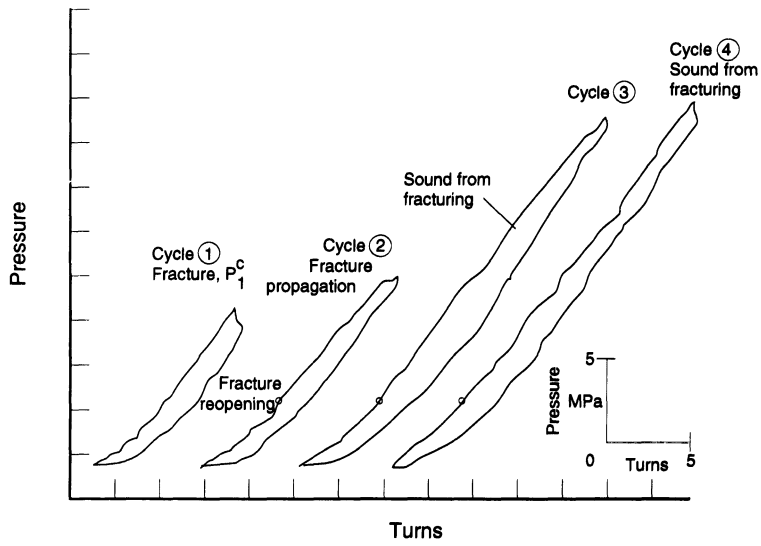

Fig. 4.36 Determination of rock modulus and *in situ* stresses by sleeve fracturing in the Pomona basalt at the NSTF Hanford Test Site in Washington. Pressure versus number of turns (volume) curves for four cycles of pressurization. (After Stephansson, 1983b.)

the difficulties encountered in the test conditions associated with the jointed basalt.

Figure 4.37 shows two sleeve pressure versus diametral deformation response curves obtained by Serata *et al.* (1992) using the double fracture method in a tuff formation. The diametral deformations were measured across the first and second fracture planes and in the directions of S_h and S_H, respectively.

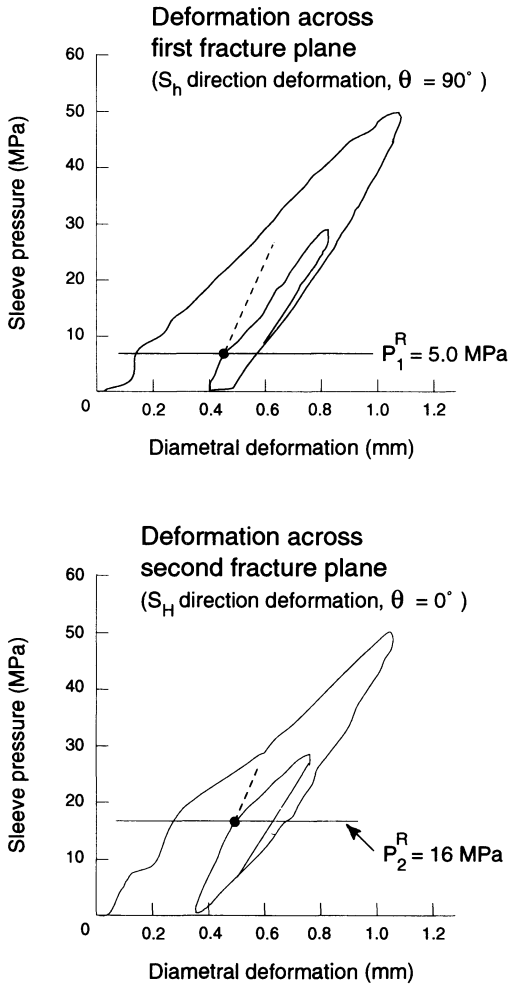

Fig. 4.37 Sleeve pressure versus borehole diametral deformation curves obtained with the double fracture method in tuff. The diametral deformations were measured across the first and second fracture planes and in the directions of S_h and S_H, respectively. (Modified after Serata *et al.*, 1992.)

According to Serata *et al.* (1992), those directions of diametral measurements yielded the highest resolution for the stresses. Substituting $P_1^R = 5.0$ MPa and $P_2^R = 16.0$ MPa into equation (4.94) gave $S_H = 6.6$ MPa and $S_h = 3.9$ MPa.

4.4 HTPF

When a hydraulic pressure is applied in a straddled borehole section and increased, either a new fracture is created or a pre-existing fracture is reopened. Assuming the reopened fracture is long enough, hydraulic pumping tests can be conducted to determine the normal stress supported by the fracture plane (Fig. 4.38). By using a low flow rate of injected fluid, the pressure which balances exactly the normal stress supported by the fracture can be measured. If several fracture

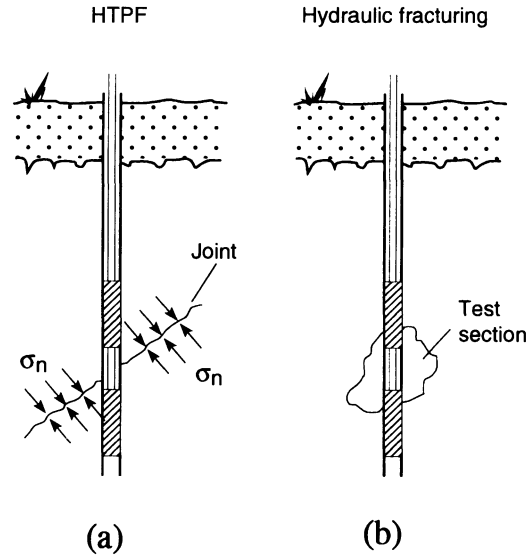

Fig. 4.38 Rock stress measurement with the hydraulic tests on pre-existing fractures (HTPF) method in (a), compared with hydraulic fracturing in (b). (Source: *Int. J. Rock. Mech. Min. Sci. & Geomech. Abstr.*, **24**, Ljunggren C. and Raillard, G., Rock stress measurements by means of hydraulic tests on pre-existing fractures at Gideå test site, Sweden, p. 340, Copyright 1987, with kind permission from Elsevier Science Ltd, The Boulevard, Langford Lane, Kidlington, UK.)

planes with known orientation in a borehole are identified and pressurized, the regional stress field can be calculated. The main advantage of this method, called the HTPF method, over the classical hydraulic fracturing method is the limited number of conditions constraining its domain of validity (Cornet, 1986). Further, it is the only stress determination method available at great depths when the borehole does not need to be parallel to an *in situ* principal stress direction. Another very attractive aspect of the HTPF method is that it does not rely on strength determination and is independent of pore pressure effects (Cornet, 1993).

4.4.1 HISTORY

Cornet (1983) was able to demonstrate that the reopening pressure of a fracture in rock is strongly dependent on the flow rate because the fracture permeability is usually much larger than that of the rock matrix. As a consequence, some percolation may occur before the fracture opens. This percolation induces a change in the tangential stress magnitude at the borehole wall. For this reason, Cornet (1983) suggested that two different types of reopening pressure tests should be considered in hydraulic stress measurement methods, namely (1) tests at flow rates large enough such that no percolation occurs before fracture opening, and (2) tests at slow flow rates so that percolation occurs before the fracture opens. Thus for planar fractures and impervious rocks, slow flow rate reopening tests may provide measurements of the normal stress supported by the fracture. As a method to determine this normal stress, Cornet (1983) suggested the 'constant pressure steps' test where the pressure is raised in a series of steps, and the flow rate necessary to maintain constant the borehole pressure at each step is measured. As soon as the fracture opens, the flow rate necessary to maintain the borehole pressure constant increases markedly. Plots of pressure level versus corresponding flow rate give an accurate determination of the pressure required to ensure fracture opening.

By combining instantaneous shut-in pressure measurements (section 4.2.4), and the reopening tests based on the step by step procedure, Cornet and Valette (1984) presented a new stress determination method which was based on normal stress measurements. Later Cornet (1986) named that method the hydraulic tests on pre-existing fractures (HTPF) method.

After completing a number of tests in a borehole where the orientation of the hydraulically tested fractures and their normal stress have been recorded, the regional stress field can be determined from a set of nonlinear equations which may be solved by a method of least squares. A method of solving the inverse problem was suggested by Tarantola and Valette (1982) and applied to field results by Cornet and Valette (1984), Ljunggren and Raillard (1987), Cornet (1988, 1993) and Cornet and Burlet (1992). Baumgärtner and Rummel (1989) used a Monte Carlo method for solving the inverse problem.

4.4.2 TECHNIQUES, EQUIPMENT AND PROCEDURES

The equipment required for stress determination with the HTPF method is essentially the same as that used in classical hydraulic fracturing tests (section 4.2.2). The main difference between HTPF tests and the classical hydraulic fracturing tests is that special attention must be given to the size of that part of each fracture which is opened. The opened section must be long enough such that the normal stress which is acting across the fracture is not affected by the borehole stress concentration. At the same time, the fracture must be of a size such that the normal stress can be assumed to be uniform across its surface. Finally, the fracture geometry must remain planar.

For the HTPF method performed with conventional hydraulic fracturing equipment, the following test procedure was adopted by

Ljunggren and Raillard (1987). After selection of pre-existing single fractures with different strike and dip in the core log or from the drillcore, the impression packer is lowered to the depth of each pre-existing fracture and hydraulically pressurized for 25–30 min. Careful examination of the packer will define the impression of the joint or fracture. The orientation of the packer, found by magnetic compass during the inflation period, enables the determination of the strike and dip angle of the joint or fracture. A straddle packer is then lowered to the fracture depth and hydraulically pressurized to a predetermined value slightly above the estimated reopening pressure. The sealed-off interval between the packers is then pressurized by water at a low flow rate (constant pressure steps test) to avoid the initiation of axial fracture. The fluid pressure acting on the borehole wall in the sealed-off section will ultimately reach the tensile strength of the joint and open up the joint. A breakdown pressure is then recorded and the flow is shut off. The shut-in pressure is then recorded. This corresponds to a state of equilibrium between the hydraulic pressure in the joint and the stress acting across the fracture plane. The pressure in the test section is then released, after which three or four additional cycles are conducted.

The orientation (dip and azimuth) of the hydraulically tested fractures can be determined with the impression packer technique developed for hydraulic fracturing (section 4.2.2). Other tools such as the Mosnier azimuthal laterolog (Mosnier and Cornet, 1989) and the Schlumberger FMS (section 8.3.3) can be applied to orient the fractures. The use of borehole televiewers and borehole TV cameras does not give enough resolution to detect standard hydraulic fractures.

Mosnier and Cornet (1989) developed a piece of equipment, called the HTPF tool, which combines the possibility of running hydraulic tests through a wireline-activated straddle packer with that of obtaining electrical images of the fractures intersecting the borehole (Fig. 4.39). An alternating electric voltage is applied between a distant electrode and a number of electrodes set in various azimuths on a ring placed at the center of the tool. The electric current emitted or received by each of the electrodes on the central ring is proportional to the conductance of the part of the borehole wall facing the electrode. Planar fractures intersecting the borehole are easily detected by their characteristic elliptical shape. Since the tool orientation is known, both the strike and dip of each fracture can be determined.

The HTPF tool is used first as a standard logging tool in order to produce a complete image of the borehole. The tool imaging function is then used to position precisely the straddle packer over the selected interval for hydraulic testing. When the test is run, the fractures which are being opened by the pressurization are identified by the tool and a very detailed interpretation of the pressure versus

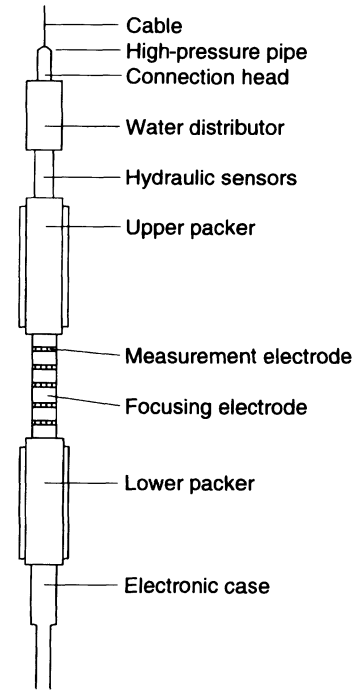

Fig. 4.39 Schematic diagram of the HTPF tool. (After Cornet, 1992.)

time record is possible. After the packers have been deflated, the tool is used again for logging the complete tested interval. This provides a better resolution of the fracture geometry, and makes it possible to investigate and identify the packer zone for possible fractures outside the domain scanned during hydraulic testing (Cornet, 1992, 1993).

4.4.3 THEORY

Both the instantaneous shut-in pressure and the quasi-static reopening pressure recorded during an HTPF test are considered to be measurements of the normal stress σ_n exerted on a fracture plane by the *in situ* stress field. Once the orientation of the fracture has been determined by the impression packer or the HTPF tool, the problem is to determine the complete stress field at all points where a test has been conducted. A stress determination method based only on the recorded normal stresses and fracture orientations was developed by Cornet and Valette (1984) and later refined by Cornet (1986, 1993). A condensed version of the theory based on these references is presented below.

Let N be the total number of fractures tested with the HTPF method at a given site. Each fracture i $(i = 1, N)$ is characterized by its normal $\boldsymbol{n}_i$ whose orientation is defined by an azimuth ϕ_i and an angle θ_i with respect to the vertical direction. The angle θ_i is also the dip angle of the fracture. The problem here is to determine the components of the stress tensor $\boldsymbol{\sigma}(\boldsymbol{X})$ acting in the volume of rock in which the N normal stress measurements have been conducted. Mathematically, the normal stress measurement σ_{ni} across the ith fracture plane is related to the stress tensor as follows:

$$\sigma_{ni} = \boldsymbol{\sigma}(\boldsymbol{X}_i)\boldsymbol{n}_i \cdot \boldsymbol{n}_i \qquad (4.95)$$

where $\boldsymbol{\sigma}(\boldsymbol{X}_i)$ is the local stress tensor which exists at the center $\boldsymbol{X}_i$ on the ith fracture plane. Note that equation (4.95) holds regardless of the constitutive behavior of the rock mass.

When many boreholes are drilled from an underground excavation, allowing measurements to be made on planes located roughly in the same rock volume, the stress can be assumed to be the same at all points so that equation (4.95) provides a system of N linear equations with six unknowns. A more common situation is when $\boldsymbol{\sigma}(\boldsymbol{X}_i)$ is not constant and varies in the vertical and horizontal directions. Assuming that $\boldsymbol{\sigma}(\boldsymbol{X}_i)$ varies linearly in both directions, Cornet (1993) has shown that using the equations of equilibrium, 22 parameters are required to determine the *in situ* stress field and its variation. Thus a minimum of 22 independent measurements would have to be conducted, which is impractical. As discussed by Cornet (1993), that number can be reduced if some simplifying assumptions are made.

As simplifying assumptions, consider the case when the stress field $\boldsymbol{\sigma}(\boldsymbol{X})$ does not vary laterally, varies linearly with depth x_3, is continuous up to the surface (assumed to be horizontal), and its principal components are in the vertical direction x_3 and the horizontal plane (x_1, x_2). The x_1- and x_2-axes are parallel to the north and east directions, respectively. For the aforementioned assumptions, the stress field can be expressed as follows:

$$\boldsymbol{\sigma}(\boldsymbol{X}) = \boldsymbol{\sigma}(x_3) = \boldsymbol{S} + x_3\boldsymbol{\alpha} \qquad (4.96)$$

where $\boldsymbol{S}$ and $\boldsymbol{\alpha}$ are two second-order symmetrical Cartesian tensors. For the above assumptions, Cornet (1993) showed that seven parameters are required to determine the stress field. Three of those parameters are associated with $\boldsymbol{S}$ and include two eigenvalues S_1 and S_2, and the orientation λ of the eigenvector with respect to north (positive in the east direction) associated with the eigenvalue S_1 in the horizontal plane. Four parameters are associated with $\boldsymbol{\alpha}$ and include the eigenvectors $\alpha_1, \alpha_2, \alpha_3$ and the angle η between the directions of α_1 and S_1 in the horizontal plane. Note that the number of parameters can be reduced further from seven to six if α_3 is taken as the unit weight of the overlying rock at depth x_3.

As shown by Cornet (1993), combining equations (4.95) and (4.96) gives, for the ith normal stress measurement on the ith fracture with orientation angles θ_i and ϕ_i and at depth x_{3i},

$$\sigma_{ni} - \alpha_3 x_{3i}\cos^2\theta_i - \tfrac{1}{2}\sin^2\theta_i[S_1 + S_2 + (\alpha_1 + \alpha_2)x_{3i} + (S_1 - S_2)\cos 2(\phi_i - \lambda) + (\alpha_1 - \alpha_2)x_{3i} \times \cos 2(\phi_i - \lambda - \eta)] = 0 \quad (4.97)$$

In order to determine the seven unknown parameters (S_1, S_2, λ, α_1, α_2, α_3, η), a minimum of seven independent measurements of normal stress are needed. However, because of the uncertainty on the measurements, Cornet and co-workers recommend a minimum of nine or ten measurements. Using equation (4.97) for each of the N measurements, a system of N nonlinear equations and seven unknowns can be constructed. Solution of that inverse problem can be obtained by the generalized least squares procedure for solving nonlinear problems presented by Tarantola and Valette (1982). That method is based on a fixed point algorithm, and is iterative. After several iterations, the seven non-zero components of tensors $\boldsymbol{S}$ and $\boldsymbol{\alpha}$ are determined. Knowing the depth of interest, the principal components (eigenvalues) of $\boldsymbol{\sigma}(\boldsymbol{X})$ and their orientation (eigenvectors) can also be determined.

The method of Tarantola and Valette (1982) assumes that all measurements obey a Gaussian law and can be described by their expected values, variances and covariances with other measurements. When applied to the HTPF method, the least squares procedure takes into account the uncertainties on the depth, normal stress measurements and fracture plane orientation. As an output, it yields an *a posteriori* estimate of the unknowns as well as their variance and covariance. It also provides *a posteriori* values of the measurements of normal stress and fracture plane orientation, which when compared with their *a priori* values gives a measure of quality of the inversion process.

Since it is iterative, the method of Tarantola and Valette (1982) requires an *a priori* guess of each unknown and its variance in order to be initiated. As discussed by Cornet (1993), that guess can be obtained from the results of hydraulic fracturing tests conducted at the same site. For instance, the *a priori* value for the angle λ could be taken as the mean orientation of the hydrofractures. An *a priori* variance for that angle could be computed from the scatter in hydrofracture orientation. Likewise, an *a priori* value for the angle η could be zero.

4.4.4 RECORDINGS AND INTERPRETATION

Cornet and Burlet (1992) presented the results of *in situ* stress measurements conducted by hydraulic tests at eight different sites in France. For seven of those sites, the stress field was determined using the HTPF inversion method. Results from Auriat, a site located east of Limoges in the northern Massif Central of France, are summarized below. For more details about that site and the other sites, the reader is referred to the papers by Cornet (1986) and Cornet and Burlet (1992).

Two wells are available at Auriat. The first one is 1000 m deep and the second, located 20 m away from the first, is 500 m deep. Both wells are vertical and have been drilled in granite. Elevation of the well head is reported to be 440 m above sea level in a landscape with minor topography. Twenty-one zones were tested at depths ranging between 115 and 972 m with a wireline straddle packer system of the type presented in Fig. 4.4. Orientation of the fractures was determined with an oriented impression packer. Eighteen tests were reported to yield satisfactory shut-in and reopening pressures. However, only 14 tests with successful impressions were chosen for the HTPF stress determination. Shut-in pressure measurements were combined with the reopening data for the determination of the expected value of the normal stress σ_n and its standard deviation ε_σ (Table 4.5).

Since the Auriat site is located in a fairly flat landscape, it was assumed that, in the HTPF

inversion method, the vertical stress was a principal stress. The stress field was assumed to be described by equation (4.96) with seven parameters: S_1, S_2, λ, α_1, α_2, α_3 and η. Furthermore, from density measurements of samples taken at various depths, α_3 was taken equal to 0.0263 MPa/m.

Using equation (4.97), inversion of the data for eight tests (for which only one fracture was observed) yielded the following results: $S_1 = -4.0$ MPa, $S_2 = 1.4$ MPa, $\lambda = $ N11°E, $\alpha_1 = 0.0295$ MPa/m, $\alpha_2 = 0.016$ MPa/m, $\alpha_3 = 0.0265$ MPa/m and $\eta = -30°$. Using equation (4.96), the maximum and minimum horizontal principal *in situ* stresses σ_H and σ_h were computed for four different depths ranging between 250 and 1000 m. The values and orientation of those stresses as well as their *a posteriori* standard deviations are listed in Table 4.6. This table indicates that the value of σ_H is better constrained than that of σ_h.

Another inversion was run with 12 of the 14 tests, where the two shallowest tests were omitted in order to reduce the effect of possible near-surface stress relaxation phenomena. The analysis yielded the following results: $S_1 = -3.9$ MPa, $S_2 = 1.2$ MPa, $\lambda = $ N1°E, $\alpha_1 = 0.0319$ MPa/m, $\alpha_2 = 0.0133$ MPa/m, $\alpha_3 =$

Table 4.5 Results of hydraulic tests at Auriat, France (after Cornet and Burlet, 1992)

x_3 (m)	ϕ	ε_ϕ	ϕ_c	θ	ε_θ	θ_c	σ_n (MPa)	ε_σ (MPa)	σ_{nc} (MPa)
115	333	4		35	3		2.6	0.4	
153	27	5		90	3		2.8	0.3	
	190	3		67	5				
235	88		88	79	5	79	5.1	0.5	5.1
277	339	3	339	90	3	90	5.6	0.4	5.6
	91	4		34	4				
288	65	6	65	89	3	89	4.1	0.2	4.1
331	182	12	182	67	7	67	5.9	0.4	5.9
361	199	8	201	33	5	34	8.0	0.2	8.0
	36	10	122	39	4				
379	122	3	4	80	3	80	9.8	0.5	9.8
413	3	5	198	90	3	90	7.4	0.5	7.5
491	199	5	1	90	3	90	8.0	0.5	8.0
525	2	6		81	3	81	11.2	1.2	11.0
	14	7		90	3				
562							9.9	0.5	
585	181	5	180	90	3	90	12.9	0.5	12.8
	257	5		76	4				
808	183	8	183	81	3	81	18.7	0.2	18.7
922							16.9	0.5	
928							20.3	0.2	
968					3		17.0	1.0	
973	21	2	21	70	3	70	19.0	1.2	19.2
	158	10		83	7				
	56	3		76	7				

x_3 is the depth of test; ϕ is the strike, positive eastward, of the normal n to the fracture plane; θ is the angle of n with the vertical axis (also fracture dip angle); σ_n is the normal stress measurement for the corresponding depth interval; ε_ϕ, ε_θ and ε_σ are the standard deviations associated with ϕ, θ and σ_n, respectively. The standard deviation for x_3 is equal to 0.5 m. When multiple fractures were observed, the first one shown is that considered for the final solution. ϕ_c, θ_c and σ_{nc} are the *a posteriori* values of ϕ, θ and σ_n which yield the best fit according to the least squares criterion.

Table 4.6 Stress determination at Auriat, France (after Cornet and Burlet, 1992)

x_3 (m)	σ_H (MPa)	ε_{σ_H} (MPa)	σ_h (MPa)	ε_{σ_h} (MPa)	ω_{σ_H} (deg)	$\varepsilon_{\omega_{\sigma_H}}$ (deg)
250	6.8	0.8	1.8	1.1	121	5
500	13.0	1.0	7.2	1.2	136	8
750	19.8	2.2	12.0	3.0	145	11
1000	26.8	3.1	16.7	4.7	150	14

Only those depth intervals where one single fracture has been observed are considered in this inversion. ε_{σ_H}, ε_{σ_h} and $\varepsilon_{\omega_{\sigma_H}}$ are the *a posteriori* standard deviations of σ_H, σ_h and ω_{σ_H} (the orientation angle of σ_H), respectively.

0.0264 MPa/m and $\eta = -26°$. The *a posteriori* values of the measured normal stress, defined as σ_{nc}, and fracture orientation angles, defined as ϕ_c and θ_c, are listed in Table 4.5. It can be seen that the *a posteriori* values are very close to the *a priori* values, thus giving confidence on the quality of the inversion process used in the stress analysis.

Figure 4.40 shows the variation of the magnitude and orientation of the maximum and minimum horizontal principal *in situ* stresses, σ_H and σ_h, and the vertical stress σ_V with depth. This figure shows a rotation of σ_H with increasing depth. Below 600 m the maximum stress orientation is N145°E with a 9° standard deviation. Figure 4.40 also indicates that at the Auriat site, a strike-slip stress regime is dominant where σ_H is the maximum stress, σ_V is the intermediate stress and σ_h is the minimum stress.

The results presented here and those from other investigations conducted by Cornet (1993), Cornet and Burlet (1992), Cornet and Julien (1989) and Cornet (1986) at different sites in France, as well as measurements conducted in Sweden by Ljunggren and Raillard (1987), have shown that in homogeneous rock masses the HTPF stress determination method yields satisfactory values. This is supported by the good fits usually observed between *a priori* and *a posteriori* values for the input data, by the generally satisfactory standard deviations computed for the solutions, and by the general agreement with the results obtained with the classical hydraulic fracturing method except, perhaps, for the magnitude of the maximum horizontal principal stress. This misfit in stress magnitude has been attributed to the effect of fluid percolation prior to the actual opening of

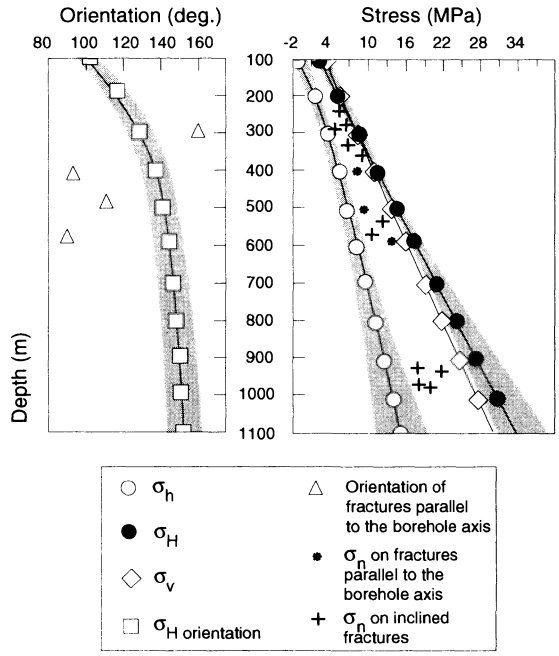

Fig. 4.40 Variation of stress with depth measured with the HTPF method at Auriat, France. σ_V is the vertical stress, σ_H and σ_h are the maximum and minimum horizontal stresses, and σ_n is the measured normal stress on the fracture planes. The shaded area indicates the 68% confidence interval of the stress components. (After Cornet and Burlet, 1992.)

the fractures (Cornet and Burlet, 1992). Examples of comparison between the results of hydraulic fracturing tests and those obtained with the HTPF method can be found in section 9.4.

4.5 INTEGRATED STRESS DETERMINATION METHOD

A program of stress determination often involves several types of hydraulic methods conducted in one or several boreholes at a given site. Hydraulic methods can also be complemented with other methods discussed in this book. The data obtained with each method may be analyzed separately and checked to see if the simplifying assumptions associated with each method are met. The data from different methods may also be combined in order to impose more rigorous constraints on the *in situ* stress field. The combination of data is also vital when only a limited number of tests from each method are available. The use of hybrid methods to determine the *in situ* stress field was recently demonstrated by Brudy *et al.* (1995) regarding the KTB deep borehole in Germany (section 12.4.7). They were able to integrate the results of hydraulic fracturing, modified hydraulic fracturing, drilling-induced fractures and borehole breakouts in order to determine the state of stress down to a depth of 9 km.

The approach of integrating the results of various methods in order to obtain a better assessment of the *in situ* stress field has been explored quite extensively by Cornet (1993). The approach was named the 'integrated stress determination' method. In that method the results of different stress measurement methods are integrated into the least squares inversion process associated with the HTPF method, either in the form of equations that are then combined with those associated with the HTPF method, or in the form of *a priori* guesses for the unknowns in the HTPF method and their variances (section 4.4.3). In his paper, Cornet (1993) shows how the integrated stress determination method is well suited for combining HTPF data with data from hydraulic fracturing, borehole breakout orientations, microseismic focal mechanisms and conventional overcoring.

Finally, it is obvious that the integrated stress determination procedure should become very helpful in future stress determination campaigns. It provides a method of integration of all the data available from different measuring techniques for constraining the *in situ* stress field. Further, the generalized least squares inversion procedure of the HTPF method is certainly well adapted for appraising the confidence level associated with the final solution, provided the errors can be represented by a normal law. Therefore the procedure is well suited for taking into account the errors on pressure and strain readings, as well as those on the orientation measurements from different stress measurement techniques.

4.6 TECHNICAL INFORMATION

Additional information about the different instrument devices presented in this chapter and any related equipment can be obtained directly from the following manufacturers:

1. VATTENFALL Hydropower AB, PO Box 50120, S-973 24 Luleå, Sweden: hydraulic fracturing stress measurements in slim holes to a depth of 1500 m and hydraulic fracturing equipment;
2. MINDATA Pty. Ltd, Unit 2, 10–12 Peninsula Boulevard, Seaford, Victoria 3198, Australia: hydraulic fracturing in slim holes, Minifrac equipment and service;
3. MeSy, Meesmannstrasse 49, G-4630 Bochum, Germany: hydraulic fracturing measurements and straddle packer technology;
4. TAM INTERNATIONAL, Inc., 4620 Southerland, Houston, Texas 77092, USA:

inflatable packers for hydraulic fracturing and hydrological applications.

REFERENCES

Aamodt, L. and Kuriyagawa, M. (1983) Measurement of instantaneous shut-in pressure in crystalline rock, in *Proc. Hydraulic Fracturing Stress Measurements*, Monterey, USA, National Academy Press, Washington, DC, pp. 139–42.

Abou-Sayed, A.S., Brechtel, C.E. and Clifton, R.J. (1978) In situ stress determination by hydrofracturing: a fracture mechanics approach. *J. Geophys. Res.*, **83**, 2851–62.

Aggson, J.R. and Kim, K. (1987) Analysis of hydraulic fracturing pressure history: a comparison of five methods used to identify shut-in pressure. *Int. J. Rock Mech. Min. Sci. & Geomech. Abstr.*, **24**, 75–80.

Amadei, B., *et al.* (1994) A new dilatometer to determine rock mass deformability, in *Proc. ISRM Symp. on Integral Approach to Applied Rock Mechanics*, Santiago, Chile, Vol. 1, pp. 155–67.

Anderson, T.O. and Stahl, E.J. (1967) A study of induced fracturing using an instrumental approach. *J. Petrol. Technol.*, **64**, 261–7.

Barton, N. (1983) Hydraulic fracturing to estimate minimum stress and rock mass stability at a pumped hydro project, in *Proc. Hydraulic Fracturing Stress Measurements*, Monterey, National Academy Press, Washington, DC, pp. 61–7.

Batchelor, A.S and Pine, R.J. (1986) The results of in situ stress determinations by seven methods to depths of 2500 m in the Carnmenellis granite, in *Proc. Int. Symp. on Rock Stress and Rock Stress Measurements*, Stockholm, Centek Publ., Luleå, pp. 467–78.

Baumgärtner, J. and Rummel, F. (1989) Experience with 'Fracture pressurization tests' as a stress measuring technique in a jointed rock mass. *Int. J. Rock Mech. Min. Sci. & Geomech. Abstr.*, **26**, 661–71.

Baumgärtner, J. and Zoback, M.D. (1989) Interpretation of hydraulic fracturing pressure. Time records using interactive analysis methods. *Int. J. Rock Mech. Min. Sci. & Geomech. Abstr.*, **26**, 461–9.

Baumgärtner, J. *et al.* (1993) Analysis of deep hydraulic fracturing stress measurements in the KTB (FRG) and Cajon Pass (USA) scientific drilling projects – a summary, in *Proc. 7th Cong. Int. Soc. Rock Mech. (ISRM)*, Aachen, Balkema, Rotterdam, Vol. 3, pp. 1685–90.

Bjarnason, B., Ljunggren, C. and Stephansson, O. (1989) New developments in hydrofracturing stress measurements at Luleå University of Technology. *Int. J. Rock Mech. Min. Sci. & Geomech. Abstr.*, **26**, 579–86.

Bjarnason, B. *et al.* (1986) Four years of hydrofracturing rock stress measurements in Sweden, in *Proc. Int. Symp. on Rock Stress and Rock Stress Measurements*, Stockholm, Centek Publ., Luleå, pp. 421–7.

Bredehoeft, J.D. *et al.* (1976) Hydraulic fracturing to determine the regional in-situ stress, Piceance Basin, Colorado. *Geol. Soc. Am. Bull.*, **87**, 250–58.

Brudy, M. *et al.* (1995) Application of the integrated stress measurement strategy to 9 km depth in the KTB boreholes, in *Proc. Workshop on Rock Stresses in the North Sea*, Trondheim, Norway, NTH and SINTEF Publ., Trondheim, pp. 154–64.

Bruno, M.S. and Nakagawa, F.M. (1991) Pore pressure influence on tensile fracture propagation in sedimentary rock. *Int. J. Rock Mech. Min. Sci. & Geomech. Abstr.*, **28**, 261–73.

Burlet, D., Cornet, F.H. and Feuga, B. (1989) Evaluation of the HTPF method of stress determination in two kinds of rock. *Int. J. Rock Mech. Min. Sci. & Geomech. Abstr.*, **26**, 673–9.

Bush, D.D. and Barton, N. (1989) Application of small-scale hydraulic fracturing for stress measurements in bedded salt. *Int. J. Rock Mech. Min. Sci & Geomech. Abstr.*, **26**, 629–35.

Clark, J.B. (1949) A hydraulic process for increasing the productivity of wells. *Petrol. Trans. Am. Institute of Mining Eng. T.P. 2510*, **186**, 1–8.

Cornet, F.H. (1983) Interpretation of hydraulic injection tests for in situ stress determination, in *Proc. Hydraulic Fracturing Stress Measurements*, Monterey, National Academy Press, Washington, DC, pp. 149–58.

Cornet, F.H. (1986) Stress determination from hydraulic tests on preexisting fractures – the HTPF method, in *Proc. Int. Symp. on Rock Stress and Rock Stress Measurements*, Stockholm, Centek Publ., Luleå, Sweden, pp. 301–12.

Cornet, F.H. (1988) Two examples of stress measurements by the HTPF method; key questions in rock mechanics, in *Proc. 29th US Symp. Rock Mech.*, Minneapolis, Balkema, Rotterdam, pp. 615–24.

Cornet, F.H. (1992) In situ stress heterogeneity identification with the HTPF tool, in *Proc. 33rd US Symp. Rock Mech.*, Santa Fe, Balkema, Rotterdam, pp. 39–48.

Cornet, F.H. (1993) The HTPF and the integrated stress determination methods, in *Comprehensive*

Rock Engineering (ed. J.A. Hudson), Pergamon Press, Oxford, Chapter 15, Vol. 3, pp. 413–32.

Cornet, F.H. and Burlet, D. (1992) Stress field determinations in France by hydraulic tests in boreholes. *J. Geophys. Res.*, **97**, 11829–49.

Cornet, F.H. and Julien, P. (1989) Stress determination from hydraulic test and focal mechanisms of induced seismicity. *Int. J. Rock Mech. Min. Sci. & Geomech. Abstr.*, **26**, 235–8.

Cornet, F.H. and Valette, B. (1984) In situ stress determination from hydraulic injection test data. *J. Geophys. Res.*, **89**, 11527–37.

Cuisiat, F.D. and Haimson, B.C. (1992) Scale effects in rock mass stress measurements. *Int. J. Rock Mech. Min. Sci. & Geomech. Abstr.*, **29**, 99–117.

Daneshy, A.A. (1970) True and apparent direction of hydraulic fractures, in *Proc. 5th Conf. on Drilling and Rock Mechanics*, Austin, Texas, Soc. Petrol. Engineers, pp. 1234–64.

Daneshy, A.A. (1973) A study of inclined hydraulic fractures, in *47th SPE Annual Fall Meeting*, San Antonio, Texas, Soc. Petrol. Engineers, pp. 346–57.

Detournay, E. and Carbonell, R. (1994) Fracture mechanics analysis of the breakdown process in minifrac or leak-off tests, in *Proc. Eurock '94: Int. Symp. on Rock Mech. in Petrol. Eng.*, Delft, Holland, Balkema, Rotterdam, pp. 399–407.

Detournay, E. and Carvalho, J.L. (1989) Application of the pressurized hollow poroelastic cylinder solution to the interpretation of laboratory burst experiments, in *Proc. 30th US Symp. Rock Mech.*, Morgantown, Balkema, Rotterdam, pp. 377–83.

Detournay, E. and Cheng, A.H.-D. (1988) Poroelastic response of a borehole in a non-hydrostatic stress field. *Int. J. Rock Mech. Min. Sci. & Geomech. Abstr.*, **25**, 171–82.

Detournay, E. *et al.* (1989) Poroelasticity considerations in in situ stress determination by hydraulic fracturing. *Int. J. Rock Mech. Min. Sci & Geomech. Abstr.*, **26**, 507–13.

Dey, T.N. and Brown, D.W. (1986) Stress measurements in a deep granite rock mass using hydraulic fracturing and differential strain curve analysis, in *Proc. Int. Symp. on Rock Stress and Rock Stress Measurements*, Stockholm, Centek Publ., Luleå, pp. 351–7.

Doe, T.W. and Boyce, G. (1989) Orientation of hydraulic fractures in salt under hydrostatic and non-hydrostatic stresses. *Int. J. Rock Mech. Min. Sci. & Geomech. Abstr.*, **26**, 605–11.

Doe, T. *et al.* (1981) Hydraulic fracturing and overcoring stress measurements in a deep borehole at the Stripa test mine, in *Proc. 22nd US Symp. Rock Mech.*, MIT Publ., Cambridge (US), pp. 373–8.

Doe, T.W. *et al.* (1983) Determination of the state of stress at the Stripa Mine, Sweden, in *Proc. Hydraulic Fracturing Stress Measurements*, Monterey, National Academy Press, Washington, DC, pp. 119–29.

Enever, J. and Chopra, P.N. (1986) Experience with hydraulic fracture stress measurements in granites, in *Proc. Int. Symp. on Rock Stress and Rock Stress Measurements*, Stockholm, Centek Publ., Luleå, pp. 411–20.

Enever, J.R. and Wooltorton, B.A. (1983) Experience with hydraulic fracturing as a means of estimating in situ stress in Australian coal basin sediments, in *Proc. Hydraulic Fracturing Stress Measurements*, Monterey, National Academy Press, Washington DC, pp. 28–43.

Enever, J.R., Walton, R.J. and Wold, M.B. (1990) Scale effects influencing hydraulic fracture and overcoring stress measurements, in *Proc. Int. Workshop on Scale Effects in Rock Masses*, Loen, Norway, Balkema, Rotterdam, pp. 317–26.

Enever, J.R., Cornet, F. and Roegiers, J.C. (1992) ISRM commission on interpretation of hydraulic fracture records. *Int. J. Rock Mech. Min. Sci. & Geomech. Abstr.*, **29**, 69–72.

Fairhurst, C. (1964) Measurement of in situ rock stresses with particular references to hydraulic fracturing. *Rock Mech. Eng. Geol.*, **2**, 129–47.

Fairhurst, C. (1968) Methods of determining in-situ rock stresses at great depths. Corps of Engineers, Tech. Report No. 1–68, Omaha, Nebraska.

Fraser, C.D. and Pettitt, B.E. (1962) Results of a field test to determine the type and orientation of a hydraulically induced formation fracture. *J. Petrol. Technol.*, **14**, 463–8.

Gronseth, J.M. and Kry, P.R. (1983) Instantaneous shut-in pressure and its relationship to the minimum in-situ stress, in *Proc. Hydraulic Fracturing Stress Measurements*, Monterey, National Academy Press, Washington, DC, pp. 55–60.

Haimson, B.C. (1968) Hydraulic fracturing in porous and nonporous rock and its potential for determining in situ stresses at great depth, unpublished PhD Thesis, University of Minnesota, 234 pp.

Haimson, B.C. (1973) Earthquake related stresses at Rangely, Colorado, in *Proc. 14th US Symp. Rock Mech.*, University Park, ASCE, pp. 689–708.

Haimson, B.C. (1976) Preexcavation deep-hole stress measurements for design of underground

chambers – case histories, in *Proc. Rapid Excavation and Tunneling (RETC) Conf.*, New York, SME/AIME, pp. 699–714.

Haimson, B.C. (1977) Recent in-situ stress measurements using the hydrofracturing technique, in *Proc. 18th US Symp. Rock Mech.*, Golden, Johnson Publ., pp. 4C2-1–4C2-6.

Haimson, B.C. (1978a) The hydrofracturing stress measuring method and recent field results. *Int. J. Rock Mech. Min. Sci. & Geomech. Abstr.*, **15**, 167–78.

Haimson, B.C. (1978b) Near-surface and deep hydrofracturing stress measurements in the Waterloo quartzite, in *Proc. 19th US Symp. Rock Mech.* Univ. of Nevada Publ., Reno, pp. 345–61.

Haimson, B.C. (1980) Near-surface and deep hydrofracturing stress measurements in the Waterloo quartzite. *Int. J. Rock Mech. Min. Sci. & Geomech. Abstr.*, **17**, 81–8.

Haimson, B.C. (1983) A comparative study of deep hydrofracturing and overcoring stress measurements at six locations with particular interest to the Nevada test site, in *Proc. Hydraulic Fracturing Stress Measurements*, Monterey, National Academy Press, Washington, DC, pp. 107–18.

Haimson, B. (1988) New developments in stress measurements for the design of underground openings, in *Proc. 2nd Int. Symp. on Field Measurements in Geomechanics*, Oslo, pp. 723–39.

Haimson, B. (1989) Hydraulic fracturing stress measurements. Introductions to Part I and II. *Int. J. Rock Mech. Min. Sci. & Geomech. Abstr.*, **26**, 445, 563.

Haimson, B. (1990) Scale effects in rock stress measurements, in *Proc. Int. Workshop on Scale Effects in Rock Masses*, Loen, Norway, Balkema, Rotterdam, pp. 89–101.

Haimson, B.C. and Fairhurst, C. (1967) Initiation and extension of hydraulic fractures in rocks. *Soc. Petrol. Eng. J.*, Sept., 310–18.

Haimson, B.C. and Fairhurst, C. (1970) In situ stress determination at great depth by means of hydraulic fracturing, in *Proc. 11th US Symp. Rock Mech.*, Berkeley, SME/AIME, pp. 559–84.

Haimson, B.C. and Lee, M.Y. (1984) Development of a wireline hydrofracturing technique and its use at a site of induced seismicity, in *Proc. 25th US Symp. Rock Mech.*, Evanston, SME/AIME, pp. 194–203.

Haimson, B. and Stahl, E.J. (1970) Hydraulic fracturing and the extraction of minerals through wells, in *Proc. 3rd Symp. on Salt*, Cleveland, pp. 421–32.

Haimson, B.C. and Voight, B. (1977) Crustal stress in Iceland. *Pure Appl. Geophys.*, **115**, 153–90.

Haimson, B.C. and Zhao, Z. (1991) Effect of borehole size and pressurization rate on hydraulic fracturing breakdown pressure, in *Proc. 31st US Symp. Rock Mech.*, Norman, Balkema, Rotterdam, pp. 191–9.

Haimson, B.C., Lee, M. and Herrick, C. (1993) Recent advances in in situ stress measurements by hydraulic fracturing and borehole breakout, in *Proc. 7th Cong. Int. Soc. Rock Mech. (ISRM)*, Aachen, Balkema, Rotterdam, Vol. 3, pp. 1737–42.

Hardy, M.P. (1973) Fracture mechanics applied to rock, unpublished PhD Thesis, University of Minnesota, Minneapolis.

Hardy, M.P. and Fairhurst, C. (1974) Analysis of fracture in rock and rock masses, in *Proc. 14th Annual Symp. New Mexico Section of ASME, Engineering for the Materials/Energy Challenge*, New Mexico, pp. 73–80.

Hayashi, K. and Sakurai, I. (1989) Interpretation of hydraulic fracturing shut-in curves for tectonic stress measurements. *Int. J. Rock Mech. Min. Sci. & Geomech. Abstr.*, **26**, 477–82.

Hickman, S.H. and Zoback, M.D. (1983) The interpretation of hydraulic fracturing pressure–time data for in-situ stress determination, in *Proc. Hydraulic Fracturing Stress Measurements*, Monterey, National Academy Press, Washington, DC, pp. 44–54.

Hoek, E. and Brown, E.T. (1980) Empirical strength criterion for rock masses. *ASCE J. Geotech. Division*, **106**, 1013–33.

Holzhausen, G. *et al.* (1989) Fracture closure pressures from free-oscillation measurements during stress testing in complex reservoirs. *Int. J. Rock Mech. Min. Sci. & Geomech. Abstr.*, **26**, 533–40.

Hubbert, K.M. and Willis, D.G. (1957) Mechanics of hydraulic fracturing. *Petrol. Trans. AIME, T.P. 4597*, **210**, 153–66.

Hustrulid, W. and Hustrulid, A. (1975) The CSM cell – a borehole device for determining the modulus of rigidity of rock, in *Proc. 15th US Symp. Rock Mech.*, Custer State Park, ASCE, pp. 181–225.

Jaeger, J.C. and Cook, N.G.W. (1976) *Fundamentals of Rock Mechanics*, 2nd edn, Chapman & Hall, London.

Jeffery, R.I. and North, M.D. (1993) Review of recent hydro fracture stress measurements made in the Carboniferous coal measures of England, in *Proc.*

7th Cong. Int. Soc. Rock Mech. (ISRM), Aachen, Balkema, Rotterdam, Vol. 3, pp. 1699–703.

Kehle, R.O. (1964) Determination of tectonic stresses through analysis of hydraulic well fracturing. *J. Geophys. Res.*, **69**, 252–73.

Kim, K. and Franklin, J.A. (coordinators) (1987) Suggested methods for rock stress determination. *Int. J. Rock Mech. Min. Sci. & Geomech. Abstr.*, **24**, 53–73.

Klasson, H. (1989) Interpretation of presure versus time in hydrofracturing stress measurements, unpublished MSc Thesis, Luleå University of Technology, Luleå, 53 pp.

Klasson, H., Ljunggren, C. and Öberg, A. (1991) Computerized interpretation techniques for hydrofracturing field data, in *Proc. 7th Cong. Int. Soc. Rock Mech. (ISRM)*, Aachen, Balkema, Rotterdam, Vol. 1, pp. 533–7.

Klein, R.J. and Barr, V.M. (1986) Regional state of stress in Western Europe, in *Proc. Int. Symp. on Rock Stress and Rock Stress Measurements*, Stockholm, Centek Publ., Luleå, pp. 33–44.

Lee, M.Y. and Haimson, B.C. (1989) Statistical evaluation of hydraulic fracturing stress measurement parameters. *Int. J. Rock Mech. Min. Sci. & Geomech. Abstr.*, **26**, 447–56.

Li, F. (1989) Improvements of hydrofracturing technology and its interpretation of data. *Int. J. Rock Mech. Min. Sci. & Geomech. Abstr.*, **26**, 681–5.

Li, F.-Q. *et al.* (1983) Experiments of in-situ stress measurements using stress relief and hydraulic fracturing techniques, in *Proc. Hydraulic Fracturing Stress Measurements*, Monterey, National Academy Press, Washington, DC, pp. 130–34.

Ljunggren, C. (1984) Laboratory testing of tensile strength of rocks by means of hydraulic fracturing and sleeve fracturing, unpublished MSc Thesis, Luleå University of Technology, Luleå, 54 pp. (in Swedish).

Ljunggren, C. and Amadei, B. (1989) Estimation of virgin rock stresses from horizontal hydrofractures. *Int. J. Rock Mech. Min. Sci. & Geomech. Abstr.*, **26**, 69–78.

Ljunggren, C. and Nordlund, E. (1990) A method to determine the orientation of the horizontal in-situ stresses from hydrofracturing measurements in inclined boreholes, in unpublished Doctoral Thesis of C. Ljunggren, Luleå University of Technology, Luleå also submitted for publication to *Computers and Geotechnics*.

Ljunggren, C. and Raillard, G. (1987) Rock stress measurements by means of hydraulic tests on pre-existing fractures at Gideå test site, Sweden. *Int. J. Rock Mech. Min. Sci. & Geomech. Abstr.*, **24**, 339–45.

Ljunggren, C. and Stephansson, O. (1986) Sleeve fracturing – a borehole technique for in situ determination of rock deformability and rock stresses, in *Proc. Int. Symp. on Rock Stress and Rock Stress Measurements*, Stockholm, Centek Publ., Luleå, pp. 323–30.

Ljunggren, C., Amadei, B. and Stephansson, O. (1988) Use of Hoek and Brown failure criterion to determine in-situ stresses from hydraulic fracturing measurements, in *Proc. Int. Conf. Applied Rock Engineering, CARE 88*, Newcastle upon Tyne, Institution of Mining and Metallurgy, London, pp. 133–41.

McGarr, A and Gay, N.C. (1978) State of stress in the Earth's crust. *Ann. Res. Earth Planet. Sci.*, **6**, 405–36.

McLennan, J.D. and Roegiers, J.C. (1983) Do instantaneous shut-in pressures accurately represent the minimum principal stresses, in *Proc. Hydraulic Fracturing Stress Measurements*, Monterey, National Academy Press, Washington, DC, pp. 181–207.

Mosnier, J. and Cornet, F.H. (1989) Apparatus to provide an image of the wall of a borehole during a hydraulic fracturing experiment, in *Proc. 4th European Geothermal Update*, Florence, Kluwer Academic Publ., Dordrecht, Holland, pp. 205–12.

Müller, W. (1993) The stress state in the Ruhr coalfield, in *Proc. 7th Cong. Int. Soc. Rock Mech. (ISRM)*, Aachen, Balkema, Rotterdam, Vol. 3, pp. 1707–11.

Paris, P.C. and Sih, G.C. (1965) Stress analysis of cracks, in *Fracture Toughness Testing and Its Application*, ASTM Publication 381, Philadelphia, pp. 30–83.

Pine, R.J., Ledingham, P. and Merrifield, M. (1983) In-situ stress measurement in the Carnmenellis granite 2 – hydrofracture tests at Rosemanowes Quarry to depths of 2000 m. *Int. J. Rock Mech. Min. Sci. & Geomech. Abstr.*, **20**, 63–72.

Raleigh, C.B. (1974) Crustal stress and global tectonics, in *Proc. 3rd Cong. Int. Soc. Rock Mech. (ISRM)*, Denver, National Academy of Sciences, Washington, DC, pp. 487–96.

Raleigh, C.B., Healy, J.H. and Bredehoeft, J.D. (1976) An experiment in earthquake control at Rangely, Colorado. *Science*, **191**, 1230–37.

Ratigan, J.L. (1982) An examination of the tensile strength of brittle rock, in *Proc. 23rd US Symp. Rock Mech.*, Berkeley, SME/AIME, pp. 423–40.

Ratigan, J.L. (1990) Scale effects in the hydraulic fracture test associated with the estimation of tensile strength, in *Proc Int. Workshop Scale Effects in Rock Masses*, Loen, Norway, Balkema, Rotterdam, pp. 297–306.

Ratigan, J.L. (1992) The use of fracture reopening pressure in hydraulic fracturing stress measurements. *Rock Mech. Rock Eng.*, **25**, 225–36.

Richardson, R.M. (1983) Hydraulic fracture in arbitrarily oriented boreholes: an analytical approach, in *Proc. Hydraulic Fracturing Stress Measurements*, Monterey, National Academy Press, Washington, DC, pp. 167–75.

Rummel, F. (1986) Stresses and tectonics of the upper continental crust – a review, in *Proc. Int. Symp. on Rock Stress and Rock Stress Measurements*, Stockholm, Centek Publ., Luleå, pp. 177–86.

Rummel, F. (1987) Fracture mechanics approach to hydraulic fracturing stress measurements, in *Fracture Mechanics of Rocks*, Academic Press, London, pp. 217–39.

Rummel, F. and Hansen, J. (1989) Interpretation of hydrofrac pressure recordings using a simple fracture mechanics simulation model. *Int. J. Rock Mech. Min. Sci. & Geomech. Abstr.*, **26**, 483–8.

Rummel, F. and Jung, R. (1975) Hydraulic fracturing stress measurements near the Hohenzollern-Graben structure, S.W. Germany. *Pure Appl. Geophys.*, **113**, 321–30.

Rummel, F., Baumgärtner, J. and Alheid, H.J. (1983) Hydraulic fracturing stress measurements along the eastern boundary of the SW-German Block, in *Proc. Hydraulic Fracturing Stress Measurements*, Monterey, National Academy Press, Washington, DC, pp. 3–17.

Rummel, F., Höhring-Erdmann, G. and Baumgärtner, J. (1986) Stress constraints and hydrofracturing stress data for the continental crust. *Pure Appl. Geophys.*, **124**, 875–95.

Rutqvist, J. *et al.* (1992) Theoretical and field studies of coupled hydromechanical behaviour of fractured rocks – 2. Field experiment and modelling. *Int. J. Rock Mech. Min. Sci. & Geomech. Abstr.*, **29**, 411–19.

Sbar, M.L. and Sykes, L.R. (1973) Contemporary compressive stress and seismicity in eastern North America; an example of intraplate tectonics. *Geol. Soc. Am. Bull.*, **84**, 1861–82.

Scheidegger, A.E. (1962) Stresses in the Earth's crust as determined from hydraulic fracturing data. *Geologie und Bauwesen*, **27**, 45–53.

Schmitt, D.R. and Zoback, M.D. (1989) Poroelastic effects in the determination of the maximum horizontal principal stress in hydraulic fracturing tests – a proposed breakdown equation employing a modified effective stress relation for tensile failure. *Int. J. Rock Mech. Min. Sci. & Geomech. Abstr.*, **26**, 499–506.

Scott, P.P., Jr, Bearden, W.G. and Howard, G.C. (1953) Rock rupture as affected by fluid properties. *Petrol. Trans. Am. Inst. Mining Eng., TP 3540*, **198**, 111–24.

Serata, S. and Kikuchi, S. (1986) A diametral deformation method for in situ stress and rock property measurement. *Int. J. Min. Geol. Eng.*, **4**, 15–38.

Serata, S. *et al.* (1992) Double fracture method of *in situ* stress measurement in brittle rock. *Rock Mech. Rock Eng.*, **25**, 89–108.

Shlyapobersky, J. (1989) On-site interactive hydraulic fracturing procedures for determining the minimum in situ stress from fracture closure and reopening pressures. *Int. J. Rock Mech. Min. Sci. & Geomech. Abstr.*, **26**, 541–8.

Stephansson, O. (1983a) State of the art and future plans about hydraulic fracturing stress measurements in Sweden, in *Proc. Hydraulic Fracturing Stress Measurements*, Monterey, National Academy Press, Washington, DC, pp. 260–67.

Stephansson, O. (1983b) Rock stress measurement by sleeve fracturing, in *Proc. 5th Cong. Int. Soc. Rock Mech. (ISRM)*, Melbourne, Balkema, Rotterdam, pp. F129–37.

Stephansson, O. (1983c) Sleeve fracturing for rock stress measurement in boreholes, in *Proc. Int. Symp. Essais en Place, In Situ Testing*, Paris, Vol. 2, pp. 571–8.

Stephansson, O. (1993) General report of Workshop W2: stresses in the Earth's crust, in *Proc. 7th Cong. Int. Soc. Rock Mech. (ISRM)*, Aachen, Balkema, Rotterdam, Vol. 3, pp. 1667–81.

Stephansson, O., Särkkä, P. and Myrvang, A. (1986) State of stress in Fennoscandia, in *Proc. Int. Symp. on Rock Stress and Rock Stress Measurements*, Stockholm, Centek Publ., Luleå, pp. 21–32.

Tarantola, A. and Valette, B. (1982) Generalized non-linear inverse problem solved using the least squares criterion. *Rev. Space Phys.*, **20**, 219–32.

Thiercelin, M. and Desroches, J. (1993) Improving the performance of open hole stress tools. *Int. J. Rock Mech. Min. Sci.. & Geomech. Abstr.*, **30**, 1249–52.

Thiercelin, M., Desroches, J. and Kurkjian, A. (1994)

Open hole stress tests in shale, in *Proc. Eurock '94: Int. Symp. on Rock Mech. in Petrol. Eng.*, Delft, Balkema, Rotterdam, pp. 921–8.

Tsukahara, H. (1983) Stress measurements utilizing the hydraulic fracturing technique in the Kanto–Tokai area, Japan, in *Proc. Hydraulic Fracturing Stress Measurements*, Monterey, National Academy Press, Washington, DC, pp. 18–27.

Tunbridge, L.W. (1989) Interpretation of the shut-in pressure from the rate of pressure decay. *Int. J. Rock Mech. Min. Sci. & Geomech. Abstr.*, **26**, 457–9.

Tunbridge, L.W., Cooling, C.M. and Haimson, B. (1989) Measurement of rock stress using the hydraulic fracturing method in Cornwall, UK – Part I. *Int. J. Rock Mech. Min. Sci. & Geomech. Abstr.*, **26**, 351–60.

Von Schonfeldt, H. (1970) An experimental study of open-hole hydraulic fracturing as a stress measurement method with particular emphasis on field tests, unpublished Doctoral Thesis, University of Minnesota.

Von Schonfeldt, H. and Fairhurst, C. (1970) Field experiments on hydraulic fracturing, *Soc. Petrol. Eng. J.*, Am. Inst. Min. Eng., 1234–9.

Wang, Y. and Dusseault, M.B. (1991a) Borehole yield and hydraulic fracture initiation in poorly consolidated rock strata – Part I. Impermeable media. *Int. J. Rock Mech. Min. Sci. & Geomech. Abstr.*, **28**, 235–46.

Wang, Y. and Dusseault, M.B. (1991b) Borehole yield and hydraulic fracture initiation in poorly consolidated rock strata – Part II. Permeable media. *Int. J. Rock Mech. Min. Sci. & Geomech. Abstr.*, **28**, 246–60.

Warpinski, N.R. (1989) Determining the minimum in situ stress from hydraulic fracturing through perforation. *Int. J. Rock Mech. Min. Sci. & Geomech. Abstr.*, **26**, 523–31.

Wawersick, W.R. and Stone, C.M. (1989) A characterization of pressure records in inelastic rock demonstrated by hydraulic fracturing measurements in salt. *Int. J. Rock Mech. Min. Sci. & Geomech. Abstr.*, **26**, 613–27.

Whitney, J.M. and Nuismer, R.J. (1974) Stress fracture criterion for laminated composites containing stress concentration. *J. Composite Materials*, **84**, 156–265.

Winther, R.B. (1983) Bruchmechanische Gesteinsuntersuchungen mit dem Bezug zu hydraulischen Frac-Versuchen in Tiefbohrungen, *Bericht Inst. Geophysik, Ruhr-Universität Bochum, Reihe A*, No. 13.

Zemanek, J. *et al.* (1970). Formation evaluation by inspection with the borehole televiewer. *Geophysics*, **35**, 254–69.

Zoback, M.D. and Haimson, B.C. (1982) Status of hydraulic fracturing method for in situ stress measurements, in *Proc. 23rd US Symp. Rock Mech.*, Berkeley, SME/AIME, pp. 143–56.

Zoback, M.D., Healy, J.H. and Rolles, J.C. (1977) Preliminary stress measurements in Central California using the hydraulic fracturing technique. *Pure Appl. Geophys.*, **115**, 135–52.

Zoback, M.D., Tsukahara, H. and Hickmann, S. (1980) Stress measurements at depth in the vicinity of the San Andreas fault: implications for the magnitude of shear stress with depth. *J. Geophys. Res.*, **85**, 6157–73.

Zoback, M.D., Mastin, L. and Barton, C. (1986) In-situ stress measurements in deep boreholes using hydraulic fracturing wellbore breakouts and stonely wave polarization, in *Proc. Int. Symp. on Rock Stress and Rock Stress Measurements*, Stockholm, Centek Publ., Luleå, pp. 289–99.

Zoback, M.D. *et al.* (1987) New evidence on the state of stress on the San Andreas fault system. *Science*, **238**, 1105–11.

Zoback, M.L. (1992) First- and second-order patterns of stress in the lithosphere: The World Stress Map project. *J. Geophys. Res.*, **97**, 11703–28.

Zoback, M.L. and Zoback, M.D. (1980) State of stress in the conterminous United States. *J. Geophys. Res.*, **85**, 6113–56.

Zoback, M.L. *et al.* (1989) Global patterns of tectonic stress. *Nature*, **341**, 291–8.

RELIEF METHODS 5

5.1 INTRODUCTION

The main idea behind relief methods is to isolate (partially or wholly) a rock sample from the stress field in the surrounding rock mass and monitor its response (Merrill, 1964). This can be achieved by different methods such as overcoring or undercoring holes and cutting slots. The stresses are not related to applied pressures such as in hydraulic methods. Instead, the stresses are inferred from strains or displacements created by the relief process and measured on isolated rock samples, in boreholes or on the surrounding rock associated with the relief process. The successful interpretation of stress relief tests depends to a great extent on the ability (1) to establish a stress–strain (or displacement) relationship for the rock, (2) to be able to determine rock mass properties from tests on samples and (3) to have instrumentation sensitive enough to capture small strains or displacements. It is common practice to relate strains or displacements to the stress field components through equations derived from the theory of linear elasticity for isotropic media.

Since strains and displacements are recorded in the vicinity of the point at which the state of stress is to be determined, the stress field needs to be homogeneous throughout the volume of interest before conducting any measurement; a reasonable assumption in the absence of major heterogeneities or geological features in a rock mass. In this chapter we will limit ourselves to the techniques used for measuring the absolute state of stress. Many of the same techniques can be used for monitoring stress changes, as discussed in Chapter 10.

5.2 HISTORY

A large variety of total or partial stress relief methods have been proposed since the early 1930s. They can be divided into three major groups: (1) the methods that involve strain or displacement measurements on rock surfaces, (2) the methods that use instruments in boreholes and (3) the methods that involve the response of large volumes of rock. The different types of relief methods are listed in Table 5.1.

5.2.1 SURFACE RELIEF METHODS

As early as the 1910s, several surface relief methods were used by civil engineers for determining the inherent stresses in structural components. The methods consisted of disturbing the stress equilibrium with some mechanical device and measuring the resulting deformations. For instance, holes were drilled in structural parts and deformations were measured at selected points. The deformations were then related to the loads through calibration or by using the theory of elasticity. A review of the different methods can be found in Mathar (1934).

One of the earliest measurements of *in situ* stresses using surface relief methods was reported by Lieurance (1933, 1939) from the US Bureau of Reclamation in Denver. The tests were carried out on the walls of a drainage tunnel (5×6 ft or 1.5×1.8 m in cross-section) in the foundation rock of the Hoover (Boulder) dam in Nevada, USA, prior to construction of the dam. Measurements were made at several stations along the axis of the tunnel and located about 50 ft (15 m) apart. The geometry

of the test at each station is shown in Fig. 5.1. Four sets of two brass pins (20 inches or 508 mm apart) were first placed in the wall of the tunnel. After measuring the distances between the pins, a slot consisting of overlapping holes (30 inches or 762 mm deep) was cut around the pins thus isolating a 4 ft (1.22 m) square of rock. The change in distance between the pins was monitored as the slot was cut. The secondary principal stresses parallel to the wall of the tunnel were first determined. Then, values for the stress concentration factors for the shape of the tunnel were assumed and the *in situ* stress field was calculated. Specimens were cut from the blocks and tested in the laboratory to determine their deformability. Lieurance (1933) also recommended using his measuring technique to monitor stress changes in the rock foundation during construction of the dam and reservoir filling. Talobre (1964) made reference to a method similar to that of Lieurance used by Oberti in Europe in the late 1930s.

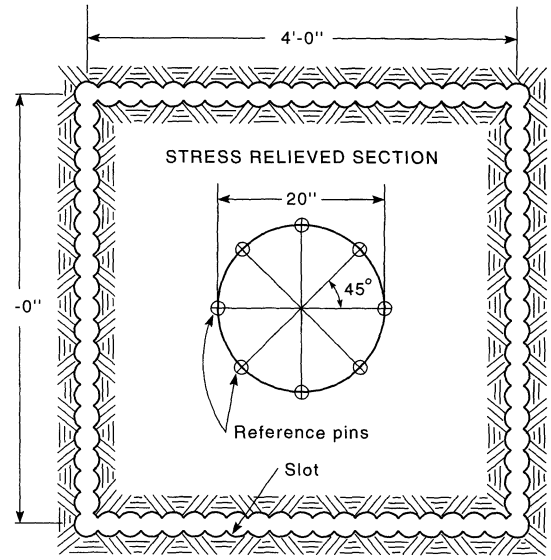

Fig. 5.1 Relieved section of rock and instrumented points used by Lieurance. Dimensions are in feet (') and inches ("). (After Merrill, 1964.)

Table 5.1 Types of relief methods

Surface relief methods	• Isolate a block of rock from surrounding rock mass and monitor its surface strain or deformation response: • Monitor hole deformation due to drilling of parallel hole • Center hole drilling or undercoring
Borehole relief methods	• Overcoring of prestressed cells • Overcoring of deformation-type gages such as the USBM gage • Overcoring of a gage attached to the flat end of a borehole: Doorstopper and photoelastic disks • Overcoring of CSIR-type triaxial strain cells • Overcoring of triaxial strain cells attached to the end of a borehole (spherical and conical cells) • Overcoring of stiff, solid or hollow inclusion-type gages • Borehole jack fracturing, or slotting, or deepening • Holographic methods • Undercoring of borehole wall • Borehole tapercoring
Rock mass relief methods	• Bored raise method • Back-analysis • Under-excavation technique

In 1949 Olsen studied the need for reinforcement in the concrete lining in the Prospect Mountain tunnel in Colorado. In order to determine the load-carrying capacity of the rock, Olsen (1949) improved Lieurance's method by overdrilling, with a 6 inch (152 mm) diameter core bit, several areas on the surface of the tunnel wall on which electric resistance strain gages had first been mounted in four directions 45° apart. A 5 inch (127 mm) depth of cut was found to be the minimum necessary to produce complete strain relief. Again, the method allowed determination of the principal stresses in the plane parallel to the tunnel walls. The method was validated in the laboratory by overcoring blocks under uniaxial compression (Olsen, 1957). A technique similar to that of Olsen was also used by Sipprelle and Teichman (1950) in

an underground oil shale mine near Rifle, Colorado.

Other surface (or near-surface) relief methods were proposed by Talobre in France as early as 1950 (Talobre, 1967), and by Habib, Phong and Pakdaman (1971), Shemyakin, Kurlenya and Popov (1983) and Duvall (1974) in the USA. The method of Talobre consists of placing three 200 mm long extensometers in a triangular pattern defining a central region in which a 56 mm hole is drilled. Upon drilling, deformations are measured with the three extensometers and the stresses in the plane of measurement are determined. In the methods of Habib, Phong and Pakdaman (1971) and Shemyakin, Kurlenya and Popov (1983), holes are drilled in the vicinity of an existing hole whose deformation is monitored at a short distance into the rock mass.

The method of Duvall (1974) is called 'stress relief by center hole' and can be seen as an undercoring method. It consists of drilling on a rock surface, a 6 inch (152 mm) diameter hole at the center of a circle 10 inches (254 mm) in diameter along which six pins have been installed 60° apart. Comparison between the three diameters formed by the six pins before and after drilling allows determination of the state of stress in the plane of measurement. A slightly different methodology was proposed by Ivanov, Parashkevov and Popov (1983) where 12 instead of six pins were used. The stresses were determined from ten diametral and diagonal displacement measurements.

5.2.2 BOREHOLE RELIEF METHODS

Surface relief methods suffer from many limitations. First, the gages or pins are subject to aggressive conditions such as humidity and dust. Second, the strains or displacements are measured on a rock that may have been disturbed and damaged by weathering and the excavation process itself. Third, stress concentration factors have to be assumed in order to relate the stresses measured in the walls of the excavation to the far-field stress components. These limitations have led to the development of the overcoring method where stresses are measured in boreholes away from any excavation surfaces. Complete destressing (total stress relief) of the rock is accomplished by drilling (overcoring) a large hole concentric with an existing borehole (also called a pilot hole). In the earlier papers the overcoring method was sometimes referred to as the trepanning method. Borehole relief methods can be divided into several groups as indicated in Table 5.1.

(a) Overcoring of prestressed cells

Hast (1958) seems to have been the first to have proposed overcoring an instrument placed in a 26 mm diameter borehole at points located away (10–20 m) from rock faces in drifts. The instrument, whose development started in the early 1940s (Hast, 1943), consists of a magnetostrictive nickel cell that measures stress directly by measuring changes in the magnetic permeability of the nickel alloy when subjected to loads. The cell is prestressed in a borehole to a desired value. Upon overcoring, the load in the cell is measured and the absolute stress in the direction of measurement determined. By placing the cell in three directions and at three different locations (at least 100 mm apart) in a borehole, the state of stress in a plane normal to the borehole axis can be determined. By repeating the process in two other perpendicular holes, the complete state of stress can be calculated. The magnetostrictive cell of Hast was used extensively in the 1950s and early 1960s for stress measurements in mines in Sweden, Norway and Finland. More recently, a modified version of Hast's cell has been proposed by Wang *et al.* (1986).

(b) Overcoring of deformation-type gages

Several authors have proposed deformation-type rock stress measuring instruments that

could be installed in boreholes and later overcored. These instruments measure one or several changes in borehole diameter during the process of overcoring. Talobre (1967) refers to an early method proposed by Berthier in 1950 in France to determine the state of stress by measuring three changes in the diameter of a borehole using an optical system. Another method was developed at the US Bureau of Mines (USBM) which led to the first version of the well-known USBM gage (Obert, Merrill and Morgan, 1962). This gage could only measure one change in diameter of an EX (38 mm) borehole during overcoring. Hence several diameter measurements had to be conducted at different depths in a borehole in order to determine the state of stress in a plane perpendicular to the hole. This shortcoming required interpolation between measurements and could be a source of error, in particular when high stress gradients were present. Subsequently, a three-component deformation gage was developed (Merrill, 1967) that could monitor hole diameter changes along three diameters 60° apart located in a single plane normal to the hole axis. By using the gage in two or three boreholes, the complete state of stress can be determined.

Having gone through several phases of improvement (Bickel, 1978; Hooker, Aggson and Bickel, 1974; Hooker and Bickel, 1974), the USBM gage is still extensively used today. It is still regarded as one of the most reliable and accurate instruments for determining *in situ* stresses in rock by overcoring. A more recent modified version of the gage called the deep borehole deformation gage (DBDG) was proposed by Thompson (1990) from the Atomic Energy of Canada Limited. The DBDG gage is one of only a few overcoring techniques capable of measuring stresses at great depths. It has been designed to operate at depths to 1000 m in water-filled boreholes.

At the same time as Merrill introduced the USBM gage, Suzuki (1966, 1971) developed another borehole deformation-type gage with three diametral measurements. Griswold (1963) proposed another gage consisting of three small beryllium–copper transducer rings placed next to each other over a distance of 0.75 inches (19 mm) along the borehole axis. Contact between the rings and the rock was achieved using pairs of $\frac{1}{8}$ inch (3.2 mm) steel balls. This instrument is interesting in that it is smaller than any of the other deformation gages as it was designed to fit into $\frac{5}{8}$ inch (15.9 mm) pilot holes and can be overcored with a 2.25 inch (57.2 mm) hole.

Royea (1969) developed a six-component borehole deformation-type gage that fits into 1.16 inch (29.5 mm) holes. The diametral measurements are not contained in one plane but are distributed over a 2.25 inch (57.2 mm) length of borehole. Crouch and Fairhurst (1967) proposed a four-component deformation-type gage that fits into 2.25 inch (57.2 mm) pilot holes. Crouch and Fairhurst tested their instrument in a quarry in central Minnesota at depths less than 1 m. Their gage was somewhat similar to that of Merrill (1967) but the pistons were pushed against the rock using air pressure. Furthermore, four instead of three diametral measurements could be carried out, thus allowing for some redundancy in the measurements. Crouch and Fairhurst (1967) also suggested that their gage could be modified to measure longitudinal displacements along with the diameter changes, thus allowing determination of the complete state of stress in a single borehole. This idea was later followed by Bonnechere (1971) and Bonnechere and Cornet (1977) who developed a cell called the 'University of Liege' cell capable of measuring the complete state of stress from four diametral and three longitudinal displacement measurements in 76 mm diameter pilot holes.

Other deformation-type gages have been proposed in the literature. For instance, in Japan Kanagawa *et al.* (1986) have worked (since the early 1970s) on the development of a gage that allows four diametral and one longitudinal deformation measurements in 56 mm diameter pilot holes. Three non-parallel

boreholes are necessary to obtain the complete state of stress. The gage of Kanagawa *et al.* (1986) has been extensively used in Japan for the past 20 years but is not popular elsewhere in the world. In a recent paper, Sugawara and Obara (1993) referred to another borehole deformation-type gage, again developed by Kanagawa and co-workers in the 1980s, consisting of four diametral and four diagonal measurements in 48 mm diameter pilot holes, which can be used to determine the complete state of stress in a single borehole. Again, this cell is not well known outside Japan.

In Switzerland Kovari, Amstad and Grob (1972) proposed a gage (called the L6 gage) that measures changes in diameter in six directions in 56 mm diameter holes. Another gage (called the D3 gage) that measures three longitudinal deformations in a pilot hole of the same diameter was also constructed. Both gages can be used in series. In Germany Pahl (1977) developed a gage, called the BRG gage, that can measure four changes in diameter in 46 mm diameter pilot holes. More recent information about this gage can be found in Pahl and Heusermann (1993). Finally, in France, the CERCHAR developed a 500 mm long cell that fits into 97 mm pilot holes and measures three diametral deformations (Helal and Schwartzmann, 1983). The cell can be seen as a combination of dilatometer and USBM gages. A total of six induction displacement transducers allow the measurement of three diameter changes in three planes 40 mm apart. The head of each transducer is attached to the inflatable membrane of the apparatus. A constant pressure of 0.2 MPa is applied in order to keep the transducers in contact with the rock during overcoring. The CERCHAR cell can also be used to determine the rock modulus of rigidity prior to overcoring.

(c) Overcoring of gages attached to the flat end of a borehole

In South Africa Leeman (1964a, b) experimented with cementing strain gages directly on the flat end of a borehole. Similar methods had been previously proposed by Mohr (1956) in Germany and Slobodov (1958) in Russia. The strains were read at the end of the overcoring process. However, this technique was quickly abandoned due to the sensitivity of the gages to water. Subsequently, Leeman (1964a) developed a cell that could be cemented on the bottom of BX (60 mm) boreholes and overcored. This cell consists of a silicone rubber plug at the bottom of which a strain rosette consisting of three (or more recently four) strain gages is attached. The cell is often referred to as the CSIR (Council for Scientific and Industrial Research) Doorstopper (Leeman, 1971b). The strains measured with the cell are related to some of the *in situ* stress components.

Although the Doorstopper was initially developed to determine the principal stresses in a plane perpendicular to a borehole oriented parallel to an already known principal stress direction (Leeman, 1971b), it has also been used to determine the complete state of stress. In that case, three (or two) non-parallel holes are required. The Doorstopper is useful when measuring stresses in weak and soft rocks or in hard but jointed and foliated rocks for which it is difficult to obtain long overcores. The Doorstopper method has also been used successfully in highly stressed ground. Improvements to the original Doorstopper have been reported by Gregory *et al.* (1983), and more recently by Gill *et al.* (1987), Corthesy, Gill and Nguyen (1990) and Myrvang and Hansen (1990), thus making the Doorstopper a valuable instrument for measuring *in situ* stresses at small or large depths.

A technique similar to that of Leeman (1964a, b) was proposed by Hawkes and Moxon (1965). Instead of using electric strain gages, a 'biaxial gage' consisting of an annular disk of photoelastic material is bonded onto the end of a borehole 3 in (76 mm) in diameter and overcored. Upon overcoring, isochromatic fringe patterns in the gage are viewed by

polarized light. The pattern is then interpreted directly in terms of the strains and stresses in the plane normal to the borehole (Hawkes, 1968, 1971). The method is inexpensive, fairly reliable and requires short overcore samples (Roberts, 1971). Its main disadvantages are (1) cementing problems can arise in wet conditions, (2) three holes are necessary, (3) no continuous monitoring is available, (4) analysis of the field tests requires knowledge of stress concentrations at the end of the borehole and (5) stress measurements can only be made not too far from existing free surfaces. The use of different photoelastic devices to measure stresses by overcoring was very popular in the 1960s and was later abandoned. The reader interested in such devices will find a good review in Leeman (1971a), Hawkes (1971) and Voight (1967).

(d) Overcoring of CSIR-type triaxial strain cells

In 1966 Leeman and Hayes proposed a new cell called the South African CSIR triaxial strain cell to measure the complete state of stress in a single EX (38 mm) size borehole. The cell allows the direct measurement of strains on the wall of a borehole by gluing three triple-strain gage rosettes at known orientations and positions (Leeman, 1971b). Strains are measured before and after overcoring. Improvements of the CSIR triaxial strain cell were proposed by Van Heerden (1976). He found that the cell was capable of determining stresses with reasonable accuracy if the magnitude of the stresses was above 5 MPa. The layout of the original cell of Leeman was changed, e.g. the strain rosettes were located at different positions and each strain rosette had four instead of three strain gages.

Various devices that operate on the same principle as the original CSIR triaxial strain cell have been proposed in the literature. In Switzerland, Kovari, Amstad and Grob (1972) and Grob, Kovari and Amstad (1975) proposed a cell which was tested in various projects in the Alps. A modified version of the CSIR triaxial strain cell initially reported by Myrvang (1976) has been used extensively throughout Scandinavia. INTERFELS, in Germany, developed a CSIR-type triaxial strain cell for boreholes with a depth up to 200 m. The cell can be seen as a combination of the conventional cell of Leeman and the CSIRO HI cell discussed below, as the strain rosettes are located just inside an epoxy strain gage body. The INTERFELS cell has been mostly used in central Europe.

Another version of the CSIR triaxial strain cell which can be used for measuring stresses in deep boreholes was developed by the Swedish State Power Board (Hiltscher, Martna and Strindell, 1979). The cell (called the SSPB cell) was initially tested in vertical water-filled boreholes down to a depth of 500 m and has been more recently tested in a 45° inclined borehole 90 m in length (Hallbjörn, 1986). Another version of the probe has been used in horizontal and upward-inclined boreholes up to 45 m in length. The SSPB cell is one of only a few overcoring instruments capable of measuring stresses at great depths now reaching 1000 m (Ljunggren, personal communication, 1995). Modified versions of the CSIR cell have also been proposed by Thompson, Lang and Snider (1986) (AECL-modified CSIR cell) and Gill *et al.* (1987) which allow continuous strain measurement during overcoring.

Leijon (1986) and Leijon and Stillborg (1986) proposed another CSIR-type triaxial strain cell called the Luleå University of Technology (LuH or LuT) gage. This cell has been under development since 1979 and is mostly used for water-free holes in mining environments. It contains three four-component strain rosettes (120° apart) with 5 mm long strain gages that are glued onto the wall of the hole and oriented in ten different directions. Unlike the current CSIR cell, the body of the LuH gage is recoverable, and is reusable after reconditioning. The strain gages embedded into

small epoxy resin pieces are lost. Also, improvements were made in the hole cleaning technique, the installation tool and the readout equipment.

In New Zealand, Mills and Pender (1986) proposed another cell (called the ANZSI cell) which is more flexible than the CSIR triaxial strain cell. The instrument fits into 38 mm pilot holes and has an inflatable rubber membrane on which nine 5 mm long strain gages are mounted. The membrane, which is cast on a cylindrical aluminum body, is inflated and glued to the wall of a borehole and overcored. Prior to overcoring, the rubber membrane is inflated and works essentially as a low-pressure dilatometer (up to 1 MPa). It can be used to determine the modulus of the rock *in situ* and to check the functioning of the strain gages. This instrument has been found to perform well in weak rocks, such as coal, for which it is very difficult to obtain intact overcores.

Finally, the most recent CSIR-type triaxial strain cell is that proposed by Cai (1990). It consists of a 36.5 mm thin-walled hollow tube, 200 mm in length, consisting of a 0.05 mm thick stainless shim steel plate cemented onto two Araldite or aluminum cylindrical heads. A total of 12 strain gages are glued on the inner surface of the tube with the same orientation as the CSIR cell. To the authors' knowledge, this cell has only been tested in the laboratory.

(e) Overcoring of triaxial strain cells attached to the end of a borehole

Sugawara *et al.* (1986) proposed a new strain cell that can be glued at the end of a 75 mm diameter hemispherically-ended borehole and overcored. The cell consists of a plug of hemispherical shape made from epoxy resin with 16 spherical strain gages mounted on its outer surface. The strain gages are in direct contact with the rock and the complete state of stress can be determined from the overcoring data obtained in one borehole. The cell has been found to work well in rock formations with a joint spacing less than 40 mm. Several examples of stress measurements with that cell have been reported by Obara *et al.* (1991) and Sugawara and Obara (1993). The cell is mostly popular in Japan. It is noteworthy that the concept of overcoring of strain gages mounted on the end of hemispherically ended boreholes is not new as it was initially suggested by Berents and Alexander (1965) and Hoskins (1968) 30 years ago.

A modification of the hemispherically-ended borehole technique was proposed by Kobayashi *et al.* (1991) and consists of gluing strain gages at the end of a conical borehole. A conical strain gage plug (or conical strain cell) having 12 strain components is cemented onto the end of a borehole. The complete *in situ* state of stress can be determined by strain measurements in a single hole. The stress concentration factors required for the strain analysis have been computed using the three-dimensional boundary element method. Recent measurements with the conical borehole technique can be found in Tamai, Kaneda and Mimaki (1994). The latest version of the conical strain cell, equipped with 16 strain components, has been successfully tested by Obara *et al.* (1995), Sugawara and Obara (1995) and Matsuki and Sukaguchi (1995). The conical borehole technique (also known as the 'conical-ended borehole' method) has been found to be a viable method for measuring *in situ* stresses in a single borehole and in various rock types.

(f) Overcoring of inclusion-type gages

Rock stresses can also be measured by placing inclusion-type measuring instruments in boreholes that are then overcored. A first group of such inclusions called stiff (or rigid) inclusions was proposed in the 1950s and 1960s. One example is the photoelastic glass inclusion stressmeter (Chapter 10) of Roberts *et al.* (1964) which had a limited amount of success for measuring absolute *in situ* stresses. Separation problems due to tensile stresses upon stress

relief were often encountered. Hawkes (1971) reported that the rock–stressmeter interface could only take tensile stresses as large as 450 psi (3.1 MPa).

Another stiff inclusion proposed to determine *in situ* stresses during overcoring is that of Nichols, Abel and Lee (1968). The inclusion consists of a 1 inch (25.4 mm) diameter steel (or aluminum or brass) ball upon which three 45° strain rosettes are bonded in orthogonal directions. Rock strains occurring during overcoring are transferred to the ball through a waterproof epoxy infilling that bonds the ball to the borehole wall. The complete state of stress can then be determined from the strains measured in a single borehole. Thermal gages are also bonded on the steel ball to monitor changes in temperature during overcoring. More recent developments on this probe can be found in Lee, Abel and Nichols (1976) and Nichols (1983). As for the photoelastic stressmeter, this inclusion has had a limited amount of success for measuring absolute stresses due to possible debonding between the rock and the epoxy. On the other hand, it has worked quite successfully for the monitoring of stress changes (Chapter 10).

Another, more recent, technology consists of directly embedding strain gages into solid or hollow inclusions that are glued either to the wall or the bottom of a borehole. The difference between those inclusions compared with the aforementioned stiff inclusions is that they are much more compliant and deform with the rock. This methodology prevents the strain gages from being affected by water and dust. By having enough independent strain measurements (at least six) in the inclusion, the complete state of stress can be determined in a single borehole. Solid inclusions have been proposed by Rocha and Silverio (1969) and Blackwood (1977).

The solid inclusion of Rocha and Silverio (1969) is 440 mm long and 35 mm in diameter. It contains ten 20 mm long strain gages embedded in nine different directions along the middle of the probe. The cell was abandoned due to frequent debonding problems (Rocha *et al.*, 1974). The inclusion of Blackwood, also known as the University of New South Wales (UNSW) SI cell, whose development started in the early 1970s, consists of an epoxy resin cylinder in which ten electrical strain gages have been embedded. It is similar to the cell of Rocha and Silverio (1969) except that the modulus of the inclusion has been reduced, which makes it more applicable for measurements in coal and soft rocks (Blackwood, 1982a, b).

Another type of solid inclusion was proposed by Riley, Goodman and Nolting (1977). An inclusion is created by first pouring a liquid epoxy resin into a pilot hole. After hardening of the epoxy resin, the hole is overcored and the overcored section cut into slices. Finally, the stress-relieved epoxy inclusion is analyzed for the stresses perpendicular to the hole using the theory for biaxial photoelastic strain gages (Hawkes, 1968; Hawkes and Fellers, 1969). Another approach is to drill a small hole in the center of a three-component strain gage rosette initially glued on the inclusion (Nolting, 1980). The method of Nolting is analogous to the undercoring or stress relief by the center hole method of Duvall (1974) discussed earlier in this chapter and the central hole technique used to measure residual stresses in metal (Beaney and Procter, 1974). One advantage of this methodology is that it is simple and no cable or electrical devices are necessary. Another advantage is that the method works well in weak rocks (since the epoxy serves as a reinforcing agent). The disadvantages include the following: (1) no continuous monitoring during overcoring, (2) creep, moisture and temperature problems, and (3) the method is two-dimensional.

In general, the major problem with solid inclusions is that they tend to offer resistance to the borehole wall deformation during overcoring. Tensile stresses are created along the rock–inclusion interface during overcoring because of the difference in modulus between the rock and the inclusion material. According

to the theory of elasticity, these residual stresses can be large enough to break the bond between the rock and the inclusion. Hence according to Rocha *et al.* (1974) and Duncan-Fama (1979), solid inclusions should behave poorly especially in soft rocks. This theoretical prediction has more recently been questioned by Blackwood, Sandström and Leijon (1986) who emphasized that field and laboratory experience with solid inclusions have shown otherwise, even in weak rocks. The overall controversy about the bond between solid inclusions and rock has led to the development of thin-walled hollow inclusions gages such as the Portuguese LNEC (Labatorio Nacional de Engenharia Civil, Lisbon) gage of Rocha *et al.* (1974) and the Australian CSIRO (Commonwealth Scientific and Industrial Research Organization) hollow inclusion (HI) cell of Worotnicki and Walton (1976).

The LNEC gage is a 2 mm thick hollow inclusion with an inner diameter of 31 mm and an outer diameter of 35 mm. The inclusion has three triple-strain gage rosettes embedded in the middle of the inclusion. It has not been used very much except in Portugal in the 1970s. On the other hand, the CSIRO HI cell is a more widely known instrument that has been used in a wide variety of rock conditions throughout the world for the past 20 years. The cell has an inner diameter of 32 mm and an outer diameter of 36 mm. The CSIRO HI cell is usually not reusable after overcoring. However, more recently Cai and Blackwood (1991) presented a method to recover that gage after overcoring. The CSIRO HI cell does not perform well in very weak rocks due to tensile stresses developing along the gage–rock interface. For instance, Mills and Pender (1986) reported separation problems along the interface between the CSIRO HI cell and coal with tensile stresses of the order of 800 kPa along that interface. This problem can be avoided by using a thin-walled version of the gage proposed by Walton and Worotnicki (1986).

(g) Other borehole relief methods

An innovative but different borehole relief method called 'borehole jack fracturing' was proposed by De la Cruz (1977). It is based on using the modified borehole (Goodman) jack proposed by the same author (De la Cruz, 1978). The method consists of applying friction strain gages on two opposite quadrants of a borehole and applying a uniaxial load in the other two quadrants using two steel platens. Fracturing of the rock releases the borehole wall tangential strains which are then measured with the friction gages. The process is repeated in three different sections at different depths. This is a partial stress relief method that does not require any overcoring. According to the literature, the borehole jack fracturing method has not been much used despite very good initial field performance reported by De la Cruz (1977).

Another innovative method, which is somewhat based on the same idea as the borehole jack fracturing method, is called 'borehole slotting' and was proposed by Bock and Foruria (1983) and Bock (1986). It consists of cutting three longitudinal slots, 120° apart, into the wall of a borehole. Tangential strains induced by release of tangential stresses are measured on the borehole surface in the near vicinity of each slot. This is also a local and partial relief method which does not require any overcoring. The method is fast, and the instrument is reusable and is self-contained in both its stress release operations and strain measuring capabilities (Bock, 1993). However, the method is two-dimensional. An attempt was made in the late 1980s to determine the complete state of stress in a single hole using the so-called 3D borehole slotter (Yeun and Bock, 1988). The idea is to overdrill three strain rosettes initially glued on a borehole wall. The method is, in principle, similar to some of the surface methods described in section 5.2.1.

Other partial relief methods that have been proposed in the literature, which should be mentioned here for completeness, include the

'borehole deepening' method of De la Cruz and Goodman (1971), the undercoring of friction bonded strain gages on the bottom or sidewall of a borehole (Hoskins and Oshier, 1973), and more recently the use of holographic techniques by Bass, Schmitt and Ahrens (1986), Smither, Schmitt and Ahrens (1988) and Smither and Ahrens (1991). Despite being innovative, these techniques have not (yet) received much attention in practice.

Finally, the reader should be aware of a new borehole relief method called the 'tapercoring' method which was recently proposed by De la Cruz (1995). It differs from the conventional overcoring method in that overcoring is entirely replaced by cutting an inclined, outwardly tapering circular slot around a borehole. Therefore no pilot hole is necessary. The borehole can be of any size with larger boreholes being preferable. Any larger diameter versions of the classical instrumented devices used in conventional overcoring methods can be used with the tapercoring method. Analysis of the field tests is the same as with overcoring. This partial relief method seems to be promising and hopefully will be used in the near future.

5.2.3 ROCK MASS RELIEF METHODS

The surface and borehole methods discussed above can be used to determine the state of stress only in small volumes of rock. Overcoring of surface strain rosettes as a method for measuring stresses in large rock volumes has been reported by Brady, Friday and Alexander (1976) and Brady, Lemos and Cundall (1986). The technique consisted of overcoring a large number of strain rosettes glued on the wall of a 1.81 m bored raise at the Mount Isa mine in Australia. Each rosette consisted of ten measuring pins arranged in five diametric pairs on the circumference of a 250 mm diameter circle. The rosettes were overcored using a 360 mm diameter thin-walled diamond bit. A total of 14 measurement stations were established at different elevations in the bored raise. At each station, four rosettes were installed and five strain measurements were obtained per rosette. The strain data were analyzed to determine the state of stress at each station and the average stress in the volume of rock encompassing the 14 stations. The overall volume of rock involved in the test was estimated to be 100 m^3. Another bored raise overcoring test similar to that of Brady and co-workers was conducted at the AECL Underground Research Laboratory (URL) in Canada. The results of that test were reported by Chandler (1993; Figs 3.1a and 9.6a).

The state of stress in large rock volumes can also be calculated, by back-analysis, using the displacements measured during excavation of an underground opening as the excavation proceeds. This approach was proposed simultaneously by Zajic and Bohac (1986) and Sakurai and Shimizu (1986). The displacements are measured in one or several cross-sections and are related to the *in situ* stress field using analytical methods (finite element or boundary element method). This approach requires that simplifying assumptions be made with regard to the rock mass material properties and their variations with depth. More recently, Sakurai and Akutagawa (1994) extended the methodology to account for non-elastic rock behavior.

Another back-analysis approach, called the under-excavation technique, was initially proposed by Zou and Kaiser (1990) for two-dimensional problems and later extended to three-dimensional problems by Wiles and Kaiser (1994a). In this approach (Figs 3.1b and 9.6b), the three-dimensional *in situ* stress field is determined by back-analysis of the rock mass response resulting from an advancing excavation. Measurements with several types of instrumentation can be used simultaneously, such as strains from CSIR or CSIRO HI cells, and displacements measured with convergence gages, extensometers, closure meters, tiltmeters or inclinometers. The *in situ* stress field is determined (using the three-dimensional boundary element method) as

the stress field that gives the 'best fit' to the measured displacements and strain changes associated with the advancing excavation. This can be done for each step in the excavation process. Thus this technique can provide as many predictions of the *in situ* stress field as there are of excavation steps over a large rock volume (several hundred or thousand cubic meters of rock). The applicability of the UET method was demonstrated for stress measurements at two locations in the URL in Canada (Kaiser, Zou and Lang, 1990; Wiles and Kaiser, 1994b). At both locations, the *in situ* state of stress was inferred from measurements of stress changes carried out with a minimum of eight CSIRO HI cells placed ahead of the advancing excavations.

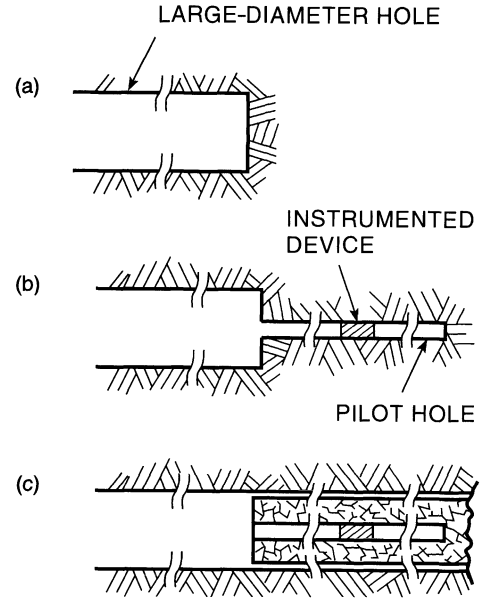

Fig. 5.2 Steps commonly followed during overcoring. See explanation in the text.

5.3 TECHNIQUES, EQUIPMENT AND PROCEDURES

This section presents the techniques, equipment and procedures for the most commonly used stress relief methods only: (1) overcoring with the USBM gage, Doorstopper, CSIR triaxial strain cell and CSIRO HI cell, (2) borehole slotting and (3) surface relief by undercoring.

5.3.1 BASIC STEPS IN BOREHOLE OVERCORING

Figure 5.2 illustrates the three steps that are commonly followed in borehole overcoring.

(1) In Fig. 5.2a a large-diameter hole (ranging between 60 and 220 mm in diameter) is drilled in the volume of rock where stresses are determined. The hole is drilled to a distance sufficiently large from any excavation or ground surface such that the effect of the excavation or ground surface on the stress measurements can be neglected. For underground excavations, a distance of at least 1.5 to 2.5 opening diameters or spans should be used as a rule of thumb. The diameter of the large-diameter hole varies a great deal with each overcoring method and where the tests are conducted in the world. Investigators in the USA, Canada and United Kingdom seem to prefer using a 150 mm diameter. In Sweden and Norway, a 76 or 88 mm diameter is often chosen. In the Canadian Shield a 96 mm diameter has often been preferred (Lang, Thompson and Ng, 1986). In Japan, overcores with diameters as large as 220 mm have often been used. As remarked by Lang, Thompson and Ng (1986), large overcores have several advantages since they are less likely to break in weak rocks, the heat generated by overcoring has less effect on the measurements and small-scale inhomogeneities have a lesser effect on the results. On the other hand, small overcores are more economical since more tests can be carried out.

(2) In Fig. 5.2b a small pilot hole (usually EW or 38 mm in size and sometimes larger) is drilled at the end of the previous one. The pilot and large-diameter holes must be as concentric as possible. In order to centralize the pilot hole, the bottom of the large hole is often flattened. The core of the pilot hole can be used

for inspection of rock quality and in deciding on the location of the instrumented device. It can also be used for testing in order to determine the elastic properties of the rock. The pilot hole must be long enough to neglect the effects of its own ends on the measurements and the disturbance in stress caused by the larger hole. Pilot hole lengths vary between 300 and 500 mm. An instrumented device is then inserted into the pilot hole. This device must be capable of measuring small displacements or strains. The instrumented device, such as the Doorstopper, can also be positioned directly onto a flat surface at the end of the large-diameter hole. In that case, no pilot hole is necessary but careful preparation of the borehole bottom is required.

(3) In Fig. 5.2c the large-diameter hole is resumed, partially or totally relieving stresses and strains within the hollow cylinder of rock that is formed. Changes in strains or displacements are then recorded with the instrumented device as the overcoring front proceeds beyond the plane of measurements. Note that not all existing procedures provide continuous monitoring.

Following overcoring, the recovered overcore (containing the instrumented device) is often tested in a biaxial (radial) chamber to determine the elastic properties of the rock. These properties can also be obtained by axial loading of the overcore. Another option is to test core samples in uniaxial compression. For instance, some authors use the core obtained by drilling of the pilot hole. Another option is to conduct dilatometer tests or to test core samples taken in the near vicinity of the stress measurements. This last approach is somewhat less desirable since the core samples are remote from the points of stress measurement and may be different from the rock undergoing relaxation by overcoring. Finally, an option that has sometimes been used is to keep the overcore *in situ* and measure the rock elastic properties by inserting and pressurizing curved jacks around the overcore (Helal and Schwartzmann, 1983).

5.3.2 USBM GAGE

Figure 5.3a shows a schematic of the principal parts of the gage originally proposed by Merrill (1967). The gage fits into EW holes (38 mm or 1.5 inches) and is made out of stainless steel. Provisions have been taken to protect the gage from corrosion and water and dust. During overcoring with usually a 150 mm diameter bit, deformation is measured across three diameters spaced 60° apart in a plane normal to the EW hole. For each diametral measurement, two pistons press against two beryllium strips (transducers) mounted as a cantilever, on each of which are mounted two resistance strain gages. Two opposing transducers constitute a single component in the gage. The cantilevers also produce a contact force of 10–30 lb (45–135 N) for each piston, hence ensuring perfect contact between the piston and the rock. Clamping springs (located 150 mm behind the pistons) hold the gage into position during overcoring. Three strain indicators are normally used to measure the three diametral deformations. Tests conducted by Merrill (1967) on blocks of various materials revealed that the USBM gage accuracy is 50×10^{-6} inches (1.3×10^{-3} mm). This corresponds to a stress accuracy of 20 psi (0.14 MPa) for a rock with a modulus of 10^6 psi (7 GPa), 60 psi (0.42 MPa) for a modulus of 3×10^6 psi (21 GPa) and 200 psi (1.4 MPa) for a modulus of 10^7 psi (70 GPa). This accuracy is sufficient in order to obtain an estimate of *in situ* stresses in rock.

The original design of the gage suffered from several different flaws. The gage was subsequently modified to reduce creep and the gage sensitivity to temperature (Hooker, Aggson and Bickel, 1974). Tapered mounted transducers replaced those originally proposed by Merrill (Fig. 5.3b). The current USBM gage has a sensitivity of 10^{-6} inches/inch and a temperature sensitivity of 2×10^{-6} inches/inch/°F (Herget, 1993). Figure 5.4 shows a photograph of the assembled gage and readout unit. A reverse version of the gage was

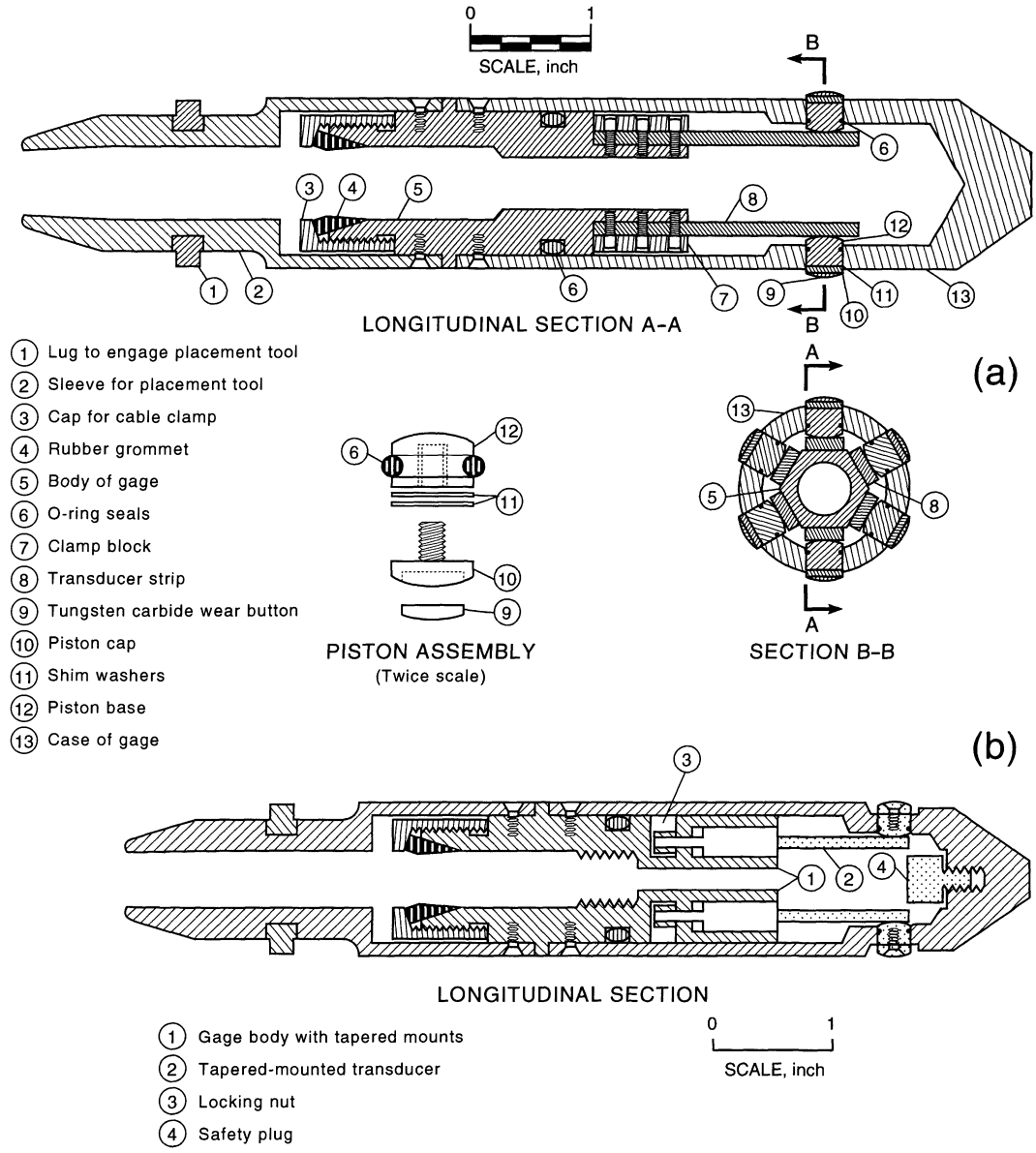

Fig. 5.3 (a) Drawing of principal parts of the three-component USBM gage. (After Merrill, 1967.) (b) Three-component gage with tapered mounted transducers. (After Hooker, Aggson and Bickel, 1974.)

developed by Hooker, Aggson and Bickel (1974) where stabilizing springs are placed in front of the measuring pistons and an extended placement end is placed at the back of the gage. This reverse version is particularly useful in fractured rocks for which it is difficult to obtain long overcores. It also helps in reducing vibration effects of overcoring in highly fractured rocks. A detailed description of the drilling equipment, accessories and testing procedures for the USBM gage can be found in Hooker and Bickel (1974). Standards for

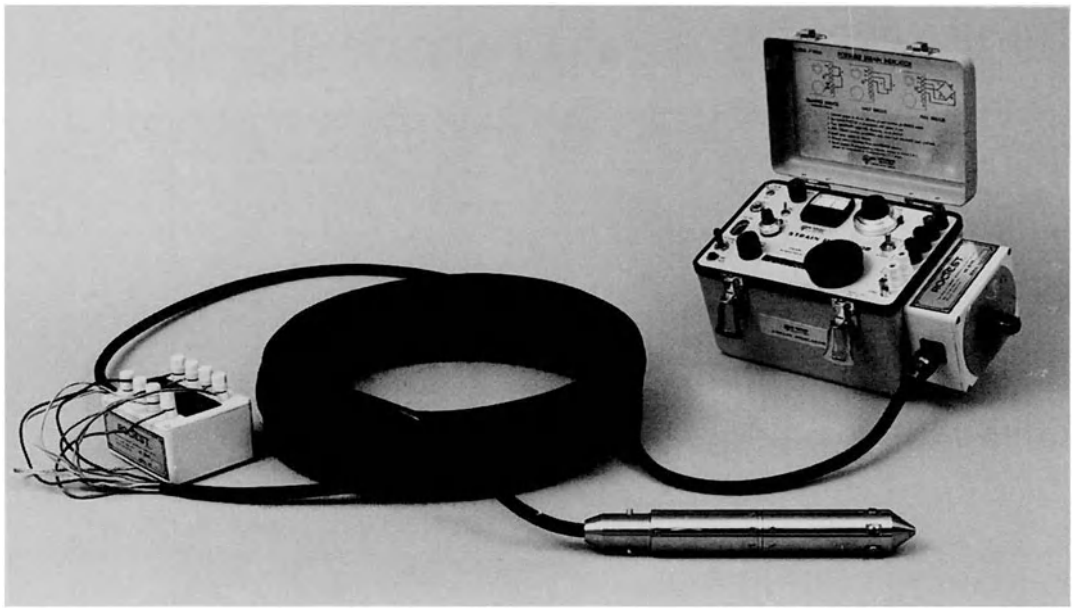

Fig. 5.4 Photograph of the assembled USBM gage, cable and readout unit. (Courtesy of ROCTEST.)

determining *in situ* stresses with the USBM gage have been proposed by the American Society for Testing of Materials (ASTM D 4623-86) and the International Society for Rock Mechanics (Kim and Franklin, 1987). Adaptations of those standards to heterogeneous and fractured rock masses have been suggested more recently by Odum, Lee and Stone (1992).

Overcoring with the USBM is generally performed at depths within 30 m of working faces, although measurements have been made to depths of 70 m in vertical boreholes. Overcoring should proceed until the overcoring bit has passed the measuring pistons for a distance of at least 150 mm (equivalent to about one overcoring hole diameter). Thus the overcore must be at least 300 mm long. However, the method is difficult in rocks with joint spacings less than 130 mm. In fractured rock, the reverse version of the gage can be used and the minimum overcore length is reduced to 150 mm. The method does not require a dry drillhole and can be used in holes filled with groundwater or water from drilling. A typical plot illustrating the variation of the three diametral measurements with depth of overcoring is shown in Fig. 5.5 for tests conducted by Walton and Worotnicki (1978) at the CSA mine in Australia. Note that after 400 mm of overcoring, the diametral measurements do not change much with further drilling.

The advantages of the USBM gage are multiple: (1) the gage is recoverable and reusable, (2) no cementing or gluing is required, (3) the gage has been used over a long period of time, has a proven record and has had a high success rate in the field, (4) the gage is designed to be monitored continuously during overcoring, (5) the gage has essentially no effect on the stress in the rock, (6) the installation process is straightforward, (7) a relatively large number of measurements can be carried out in a single day, (8) the gage is more or less unaffected by temperature changes in the rock or the drilling water since the gage is a full-bridge instrument, and (9) the gage can be regularly calibrated to ensure accuracy.

When using the deep borehole deformation gage (DBDG) developed by Thompson (1990),

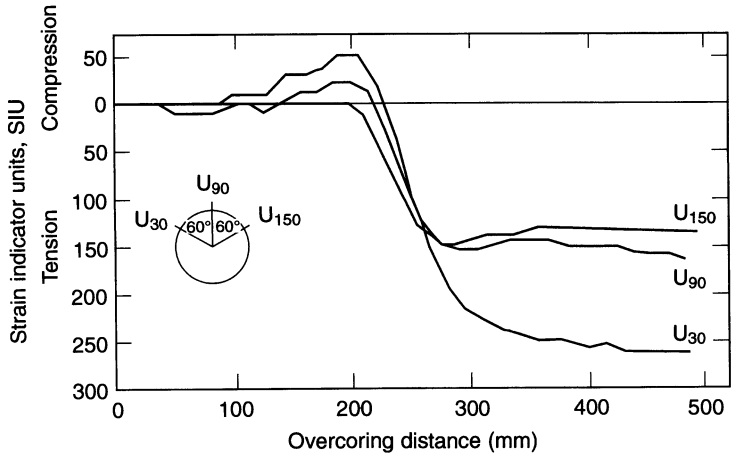

Fig. 5.5 Typical response curves for a USBM gage. (After Walton and Worotnicki, 1978.)

another advantage is that the gage can be tested in deep water-filled boreholes. According to Thompson (1990), the DBDG gage is designed to operate at depths up to 1000 m. Furthermore, by using wireline overcoring instead of conventional overcoring, the time required to conduct one overcore test can be greatly reduced, in particular for deep holes (from 12 to 8 h for tests conducted by Thompson at the URL site in Canada).

The success ratio of relief tests with the USBM gage has been 80% for good rocks and 5% in highly stressed rocks (Cai, 1990). Laboratory work by Cai (1990) has revealed that the USBM gage works well in isotropic, homogeneous and continuous media. Its performance has been found to be not as good in heterogeneous media. Also, problems may arise in longitudinally bedded overcores where the measuring pins can be in contact with softer beds or cracks. Under ideal conditions, a total of two or three stress measurements can be made per day (Choquet, 1994).

The major disadvantages of the USBM gage are (1) it requires an unbroken core of at least 300 mm in length, (2) the gage can be damaged if the core breaks, (3) three non-parallel holes are necessary to calculate the *in situ* stress field, (4) the response of the gage depends largely on the minerals in contact with the gage pistons, (5) the gage needs to be calibrated before and after installation, and (6) the gage relies on point contact with the borehole wall and is more liable to be affected by discontinuity, inhomogeneities and grain size of the rock (Cai, 1990).

The Young's modulus of the rock can be determined by biaxial testing of the recovered overcore in the laboratory or in the field. Figure 5.6 shows the biaxial test apparatus set-up with the USBM gage in place recommended by the ASTM.

5.3.3 CELLS OF BONNECHERE AND KANAGAWA

The cell of Bonnechere (1971) was designed to measure, in a continuous manner, both diametral and longitudinal displacements during overcoring. The cell fits into 76 mm diameter pilot holes. Although the cell has been used in only very few cases (Buyle Bodin in Bertrand and Durand, 1983) and is not much used today, it has potential for determining the complete state of stress in a single borehole by measuring deformations only. It has also the advantage of being fully recoverable. Figure 5.7a shows a cross-section of the cell. Four diametral displacements are measured using eight cantilever beams with strain gages

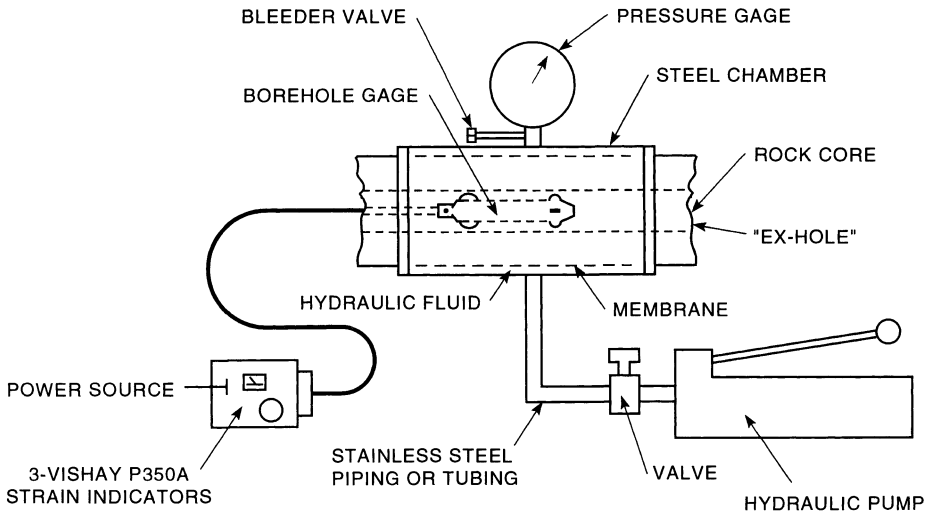

Fig. 5.6 Schematic of the biaxial test apparatus with USBM gage. (After ASTM D 4623-86, 1994. Copyright ASTM. Reprinted with permission.)

mounted on both sides. The free end of each cantilever is held against the rock using nitrogen pressure. The three longitudinal displacements are measured by means of six DCDTs (direct current differential transformers). Each of these DCDTs is fixed at one end onto the core of the cell while the other end is attached to a small flexible plate that is free to move longitudinally. At the middle of each plate, a hardened steel cone is pressed against the borehole walls using nitrogen pressure.

The cell of Kanagawa and co-workers (Sugawara and Obara, 1993) is shown in Fig. 5.7b and fits into 48 mm diameter pilot holes. The complete state of stress can be determined in a single borehole using measurements obtained with four diagonal gages and four diametral gages. The overcore diameter varies between 180 and 218 mm. Little information is available about that cell outside Japan. In a recent paper, Sugawara and Obara (1995) briefly mentioned the cell of Kanagawa in their review of overcoring techniques used in Japan. They mentioned that the strain gages of the cell are attached to the wall of the pilot hole using a cement milk, and that special laboratory calibrations are required to convert the diametral and diagonal measurements into stresses. Finally, they emphasized that the cell has worked well in rock masses with joint spacing larger than 400 mm.

5.3.4 CSIR DOORSTOPPER

Figures 5.8 and 5.9 show a schematic cross-section and a photograph of the Doorstopper, respectively. The gage is 35 mm in diameter and works in BW holes (60 mm in diameter) or NW holes (76 mm in diameter). At the base of the instrument, a 45° strain rosette consisting of three (or four) strain gages is cemented upon a circular piece of shim. The leads from the strain gages are connected to four (or five) pins in an insulated connector plug. The shim and the connector are molded into a rubber plug which acts as a protection against water and dust. The connector can be plugged into an installing tool which in turn can be connected by lead wires to a strain indicating instrument. The cell is pushed by compressed air and cemented on a smooth surface at the base of a drillhole. Before and following overcoring, strains are recorded in the three (or four) strain gages. By knowing the elastic

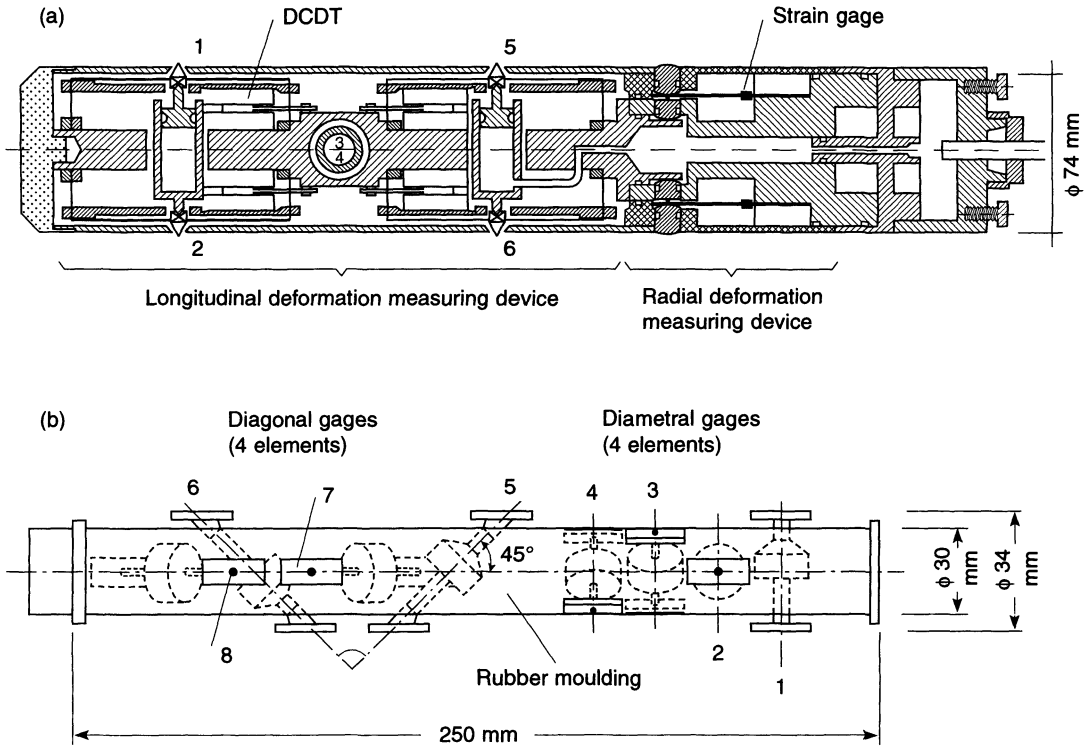

Fig. 5.7 (a) Cross-section of the cell of Bonnechere. (After Bonnechere and Cornet, 1977.) (b) Cross-section of the cell of Kanagawa. (Source: Sugawara, K. and Obara, Y. Copyright 1993, with kind permission from Elsevier Science Ltd, The Boulevard, Langford Lane, Kidlington, UK.)

properties of the rock, the stresses at the end of the hole can be determined and are then related to the *in situ* stress field. The Doorstopper was given its name because of its resemblance with red rubber cylindrical blocks used as doorstops in the home (Leeman, 1971a). The sensitivity of the Doorstopper strain gages is $5\text{–}10 \times 10^{-6}$ inches/inch (Herget, 1993).

Figure 5.10 shows the different steps when measuring stresses with the Doorstopper. More detailed description of the Doorstopper

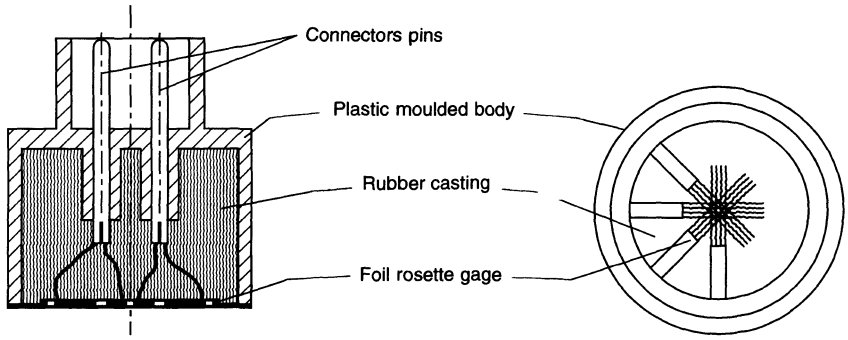

Fig. 5.8 Schematic cross-section and bottom view of the Doorstopper. (From ROCTEST documentation.)

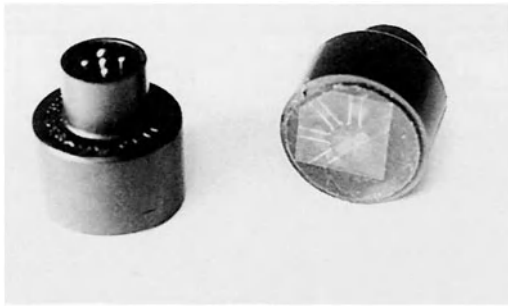

Fig. 5.9 Photograph of the Doorstopper. (Courtesy of ROCTEST.)

equipment and field testing procedure can be found in Leeman (1971b). The method requires that the end of the borehole be ground smooth, extremely flat and preferably dry. Water repellant can also be used to glue the Doorstopper (Leeman, 1971a). The overcore length does not have to be long as for the other overcoring methods. A length of core as little as 50 mm is required for successful overcoring (Leeman, 1971b). An extreme value for the core length of 5 mm has also been reported (Choquet, 1994). Thus the Doorstopper is very useful when measuring stresses in weak and fractured rock masses or in rock masses with high stresses for which long overcores are not always available. Also, temperature compensation is accounted for by placing another Doorstopper glued to a 12 mm length of BX core in the installing tool. Overcoring with the Doorstopper is usually carried out at distances not exceeding 50 to 60 m from free surfaces.

The standard Doorstopper measuring procedure does not allow continuous monitoring of the three (or four) strain gages during overcoring since the strains are measured at the start and at the end of overcoring. Gregory *et al.* (1983) modified the Doorstopper set-up to allow continuous monitoring. Figure 5.11 shows typical overcoring response curves obtained with the modified Doorstopper by Gregory *et al.* (1983) on basalt at the Basalt Waste Isolation Project in Hanford, Washington. Additional modifications to the Doorstopper for that project include selection of an adhesive to attach the Doorstopper in hot and humid environments and a new installation tool (Stickney, Senseny and Gregory, 1984). The Doorstopper was also modified for continuous monitoring by White, Hoskins and Nilssen (1978) and Jenkins and McKibbin (1986). More recent modifications to the Doorstopper have been carried out by Gill *et al.* (1987) and Corthesy, Gill and Nguyen (1990). Their modified Doorstopper cell provides continuous monitoring, can be attached to the rock in water-filled boreholes and monitors the temperature at the rock–cell interface.

The main advantage of the CSIR Doorstopper is that it only requires short overcore lengths. Another advantage is that it can be placed in smaller diameter boreholes. Under ideal conditions, a total of two or three stress measurements can be made per day (Choquet, 1994). The elastic properties of the rock can be determined by testing the overcore on which the Doorstopper is glued in a biaxial chamber and subsequently by applying a diametral load perpendicular to the direction of maximum strain measured during biaxial loading (Corthesy *et al.*, 1994a, b).

The main disadvantages of the Doorstopper are (1) the end of the large-diameter hole must be smooth and flat, (2) cementing problems may arise if the hole is wet, although new glues are now available that reduce that disadvantage, (3) three boreholes are required to determine the complete state of stress, (4) curing of the glue can vary between 1 and 20 h depending on the glue used and the borehole conditions, and (5) for the standard CSIR cell, no continuous monitoring of strains is possible during overcoring.

5.3.5 CSIR TRIAXIAL STRAIN CELL

Since it was first proposed in 1966 by Leeman and Hayes, the CSIR triaxial strain cell has undergone several modifications, in particular

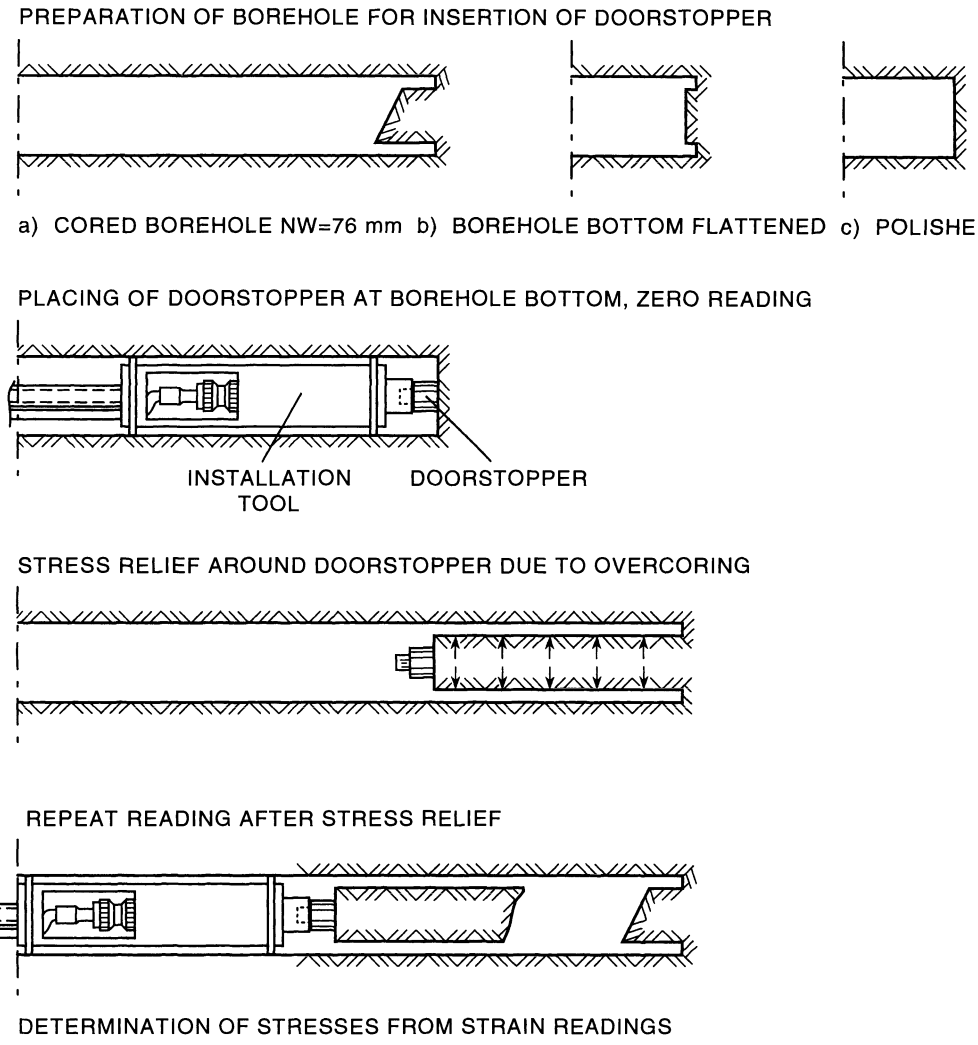

Fig. 5.10 Steps involved in installing the Doorstopper. (From INTERFELS documentation.)

with regard to the number and position of the strain gages. Figure 5.12a shows a photograph and Fig. 5.12b an exploded view of the cell after modifications made by Van Heerden (1976), following recommendations by Gray and Toews (1974). The new cell consists of a nylon body which contains three four-component strain rosettes 120° apart. The location and configuration of the rosettes are shown in Figs 5.13a and 5.13b, respectively. Each strain gage is 10 mm long. In addition to the measuring gages, a dummy strain gage used for temperature compensation is located at the front of the cell. The cell fits into EX size (38 mm) holes. Overcoring is usually carried out with a 90 mm (or larger) diameter bit (NXCU holes).

Figure 5.14 shows the different steps when measuring stresses with the CSIR cell. After bonding a 6 mm thick disk of EX core on the dummy gage, the cell is plugged into an installing tool. A 1 mm thick layer of glue is applied at the surface of the gages. After pushing the assembly into the pilot hole and keeping track

of its orientation, compressed air is used to push the strain rosettes against the walls of the EX hole. When the glue has set, initial strain readings are taken, the installing tool is removed and the pilot hole is plugged. The strain cell is then overcored, the core is broken off the end of the borehole and is removed from the borehole. The plug is then removed and the installing tool plugged again into the triaxial cell. The final strain readings are taken. The strain relief, which resulted during overcoring, is the difference between the final and initial strain readings. Following overcoring,

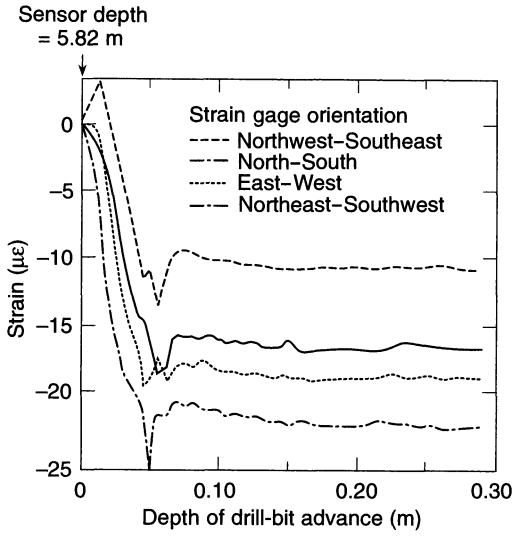

Fig. 5.11 Typical overcoring response curves with modified Doorstopper. (After Gregory *et al.*, 1983.)

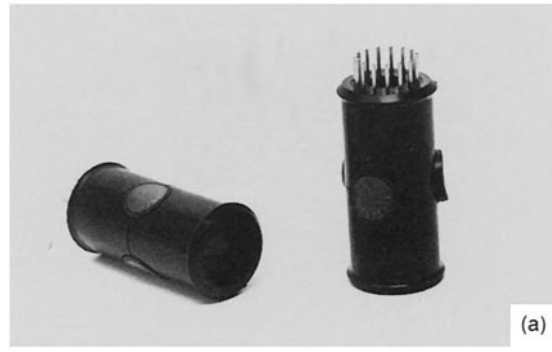

Fig. 5.12 (a) Photograph of the CSIR triaxial strain cell. (Courtesy of ROCTEST.) (b) Exploded view of the CSIR triaxial strain cell. (Source: Kim, K. and Franklin, J.A. Copyright 1987, with kind permission from Elsevier Science Ltd, The Boulevard, Langford Lane, Kidlington, UK.)

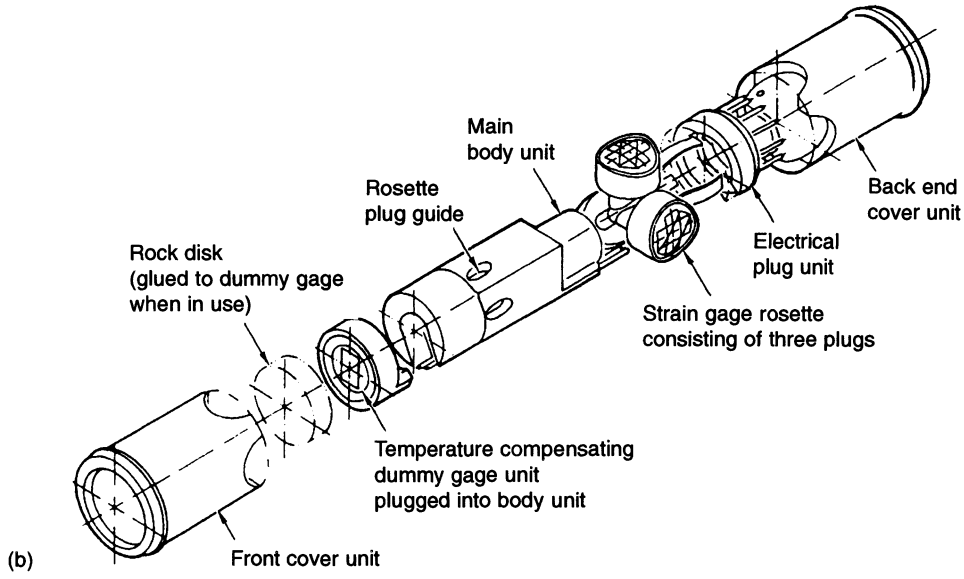

Fig. 5.12 *Continued.*

twelve strain measurements are recorded. Standards for determining *in situ* stresses with the CSIR strain cell have been proposed by the International Society for Rock Mechanics (Kim and Franklin, 1987). Procedures for drilling, installation and measurement can also be found in those standards as well as in Herget (1993).

Using the standard CSIR triaxial strain cell, continuous monitoring of the strain gages is not possible since the strains are measured before and after overcoring. Modifications to the CSIR cell have been made by Thompson, Lang and Snider (1986) and Gill *et al.* (1987) in order to provide continuous strain monitoring. The modified cells allow the identification of any strain gage debonding during overcoring. Figure 5.15 shows an example of response curves obtained with the AECL-modified CSIR cell of Thompson, Lang and Snider (1986) on URL granite (Martin and Christiansson, 1991). In that modified CSIR cell, the dummy strain gage used for temperature compensation has been replaced by a thermistor enabling the monitoring of the temperature at the interface between the cell and the rock during overcoring.

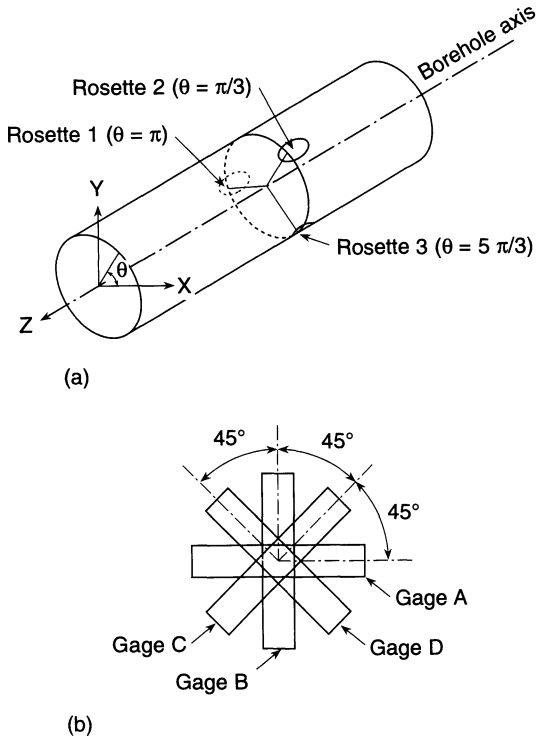

Fig. 5.13 Position of the CSIR triaxial strain cell rosettes in (a) and strain gage configuration in (b). (After Van Heerden, 1976.)

Note that the CSIR triaxial strain cell requires that the wall of the EX pilot hole should be clean and preferably free of water. The overcore must be at least 500 mm long. Since 12 strain readings are made, six of them are redundant and are used to assess the precision of the data. Three of the 12 strain gages are parallel to the hole axis and three are in the tangential direction. Various gage cements are available, depending on whether the wall of the hole is dry or moist and on the temperature (Herget, 1993). Under ideal conditions, a total of two stress measurements can be made per day (Choquet, 1994).

Overcoring with the CSIR triaxial strain cell is generally performed at distances ranging between 30 and 50 m from working faces. In order to avoid water problems, the boreholes are drilled slightly upwards and dip toward the opening. The modified CSIR cell of Hiltscher, Martna and Strindell (1979) has been tested in vertical water-filled boreholes down to a depth of 500 m and more recently to a depth of 1000 m (Ljunggren, personal communication, 1995).

Laboratory tests conducted by Cai (1990) have revealed that the performance of the CSIR triaxial strain cell is very satisfactory and reliable in isotropic and homogeneous materials and acceptable in moderately non-homogeneous and medium-grained rock. It has also been found that the CSIR triaxial strain cell is more suitable when used in longitudinally bedded rocks. In bedded rocks the performance of the cell may be affected by the location of the strain gages with respect to the beds or layers and possible cracks because the strain gages are glued directly onto the rock and the strain gages provide point measurements. In weaker rocks, large scatter has been

observed with the CSIR triaxial strain cell (Van Heerden, 1973).

The main advantage of the CSIR triaxial strain cell is that it can be used to determine the complete stress field in one borehole only. Since 12 measurements are made and there are six unknowns, redundant measurements are available, and a least squares estimate of the *in situ* stress field components can be determined. Also, laboratory tests on blocks of aluminum in uniaxial compression carried out by Herget (1973) revealed that the accuracy of the CSIR triaxial strain cell is within 5%, which is acceptable for the measurement of stresses *in situ*.

Upon overcoring, both the Young's modulus and Poisson's ratio of the rock can be determined by biaxial (radial) loading of the recovered overcore containing the CSIR triaxial strain cell. The biaxial test apparatus set-up

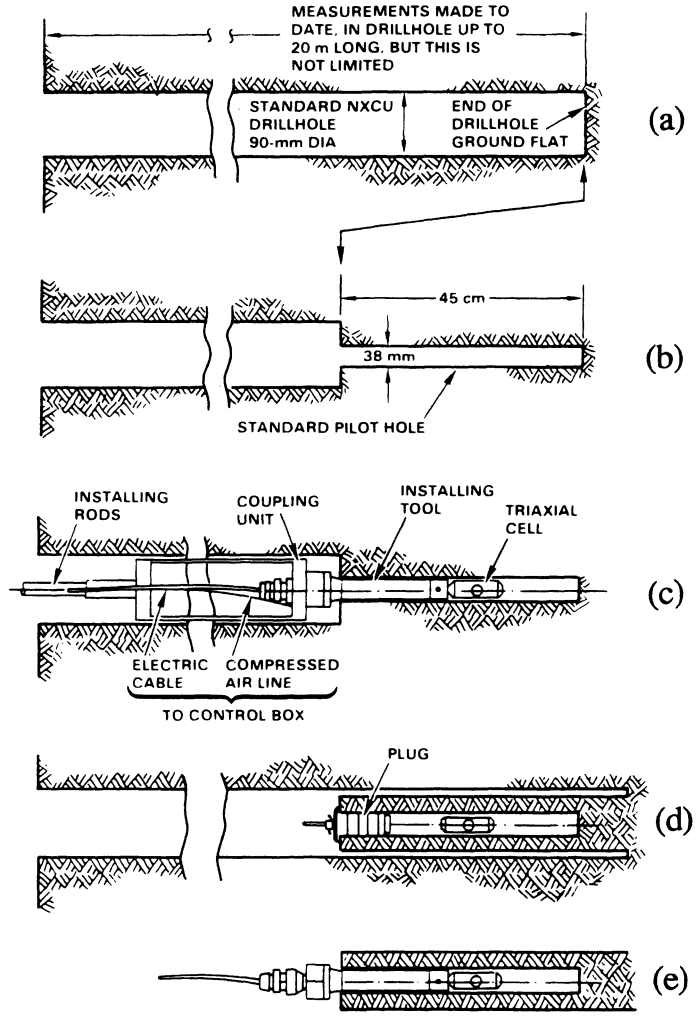

Fig. 5.14 Different steps when measuring stresses with the CSIR triaxial strain cell. (Source: Kim, K. and Franklin, J.A. Copyright 1987, with kind permission from Elsevier Science Ltd, The Boulevard, Langford Lane, Kidlington, UK.)

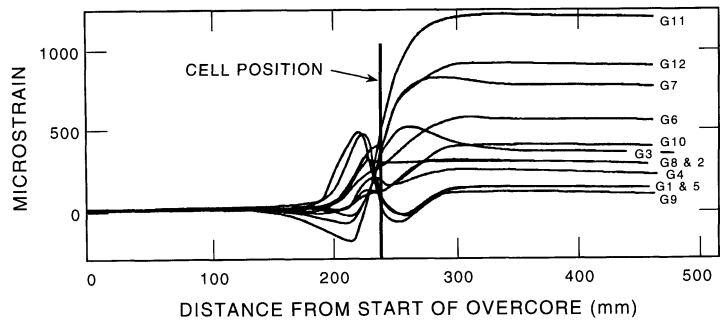

Fig. 5.15 Response curves obtained with the AECL-modified CSIR triaxial cell. (After Martin and Christiansson, 1991.)

is similar to that shown in Fig. 5.6. Both elastic properties can also be determined by axial loading of the overcore (Herget, 1993) or by uniaxial loading of EX core samples.

The main disadvantages of the CSIR triaxial strain cell are that (1) the cell requires cleaning of the pilot hole walls, (2) in the standard CSIR cell no monitoring of the strain gages during overcoring is possible, (3) the cell is not recoverable unless one uses the recovery method of Cai and Blackwood (1991), (4) it is a quarter-bridge instrument, (5) the time required for curing of the glue can vary from 1 to 10 or even 20 h depending on the hole conditions and the type of glue being used, and (6) long overcores are necessary, which may be difficult in weak or bedded rocks and rocks under high stresses.

5.3.6 CSIRO HI CELL

The CSIRO HI cell was developed in the early 1970s and was first reported by Worotnicki and Walton (1976). Since that time, the cell has undergone several modifications but its basic design has remained essentially the same. Detailed characteristics of the CSIRO HI cell and its performance over the past 20 years can be found in Worotnicki (1993). Figure 5.16 shows a photograph of the cell and the associated installation equipment. The cell fits into an EX 38 mm diameter hole. It is an epoxy (Araldite) thin-walled pipe with outer and inner diameters equal to 36 and 32 mm, respectively. The cell is glued to the wall of the pilot hole using a 1 mm thick layer of epoxy cement. More recently, a thin-walled version of the CSIRO HI cell (one-third the thickness of the regular cell) has been developed by Walton and Worotnicki (1986) for stress measurements in weak rocks.

The cell contains three triple-strain gage rosettes 120° apart. All strain gages are 10 mm in length and are located 0.5 mm below the cell outer surface. Figure 5.17 shows the orientation of the nine strain gages in the epoxy pipe. Two strain gages are parallel to the axis of the cell, three gages measure tangential strains and four gages measure strains at $\pm 45°$. Because the strain gages are fully encapsulated in the epoxy, the performance of the cell is not affected by moisture and dust. Note that a three four-component strain rosette version of the HI cell containing 12 strain gages instead of nine is also available. The three additional strain gages (two circumferential and one at 45°) provide additional strain measurement redundancy.

One of the major differences between the CSIRO HI cell and the CSIR triaxial strain cell is that (like the USBM gage) the CSIRO cell is permanently attached to the readout cable. Thus stress relief data are obtained and can be monitored during overcoring using a multiple channel strain indicator. Grouting of the cell in the EX hole is achieved by filling the epoxy tube shown in Fig. 5.16 with epoxy cement. Then the cement is extruded by displacement

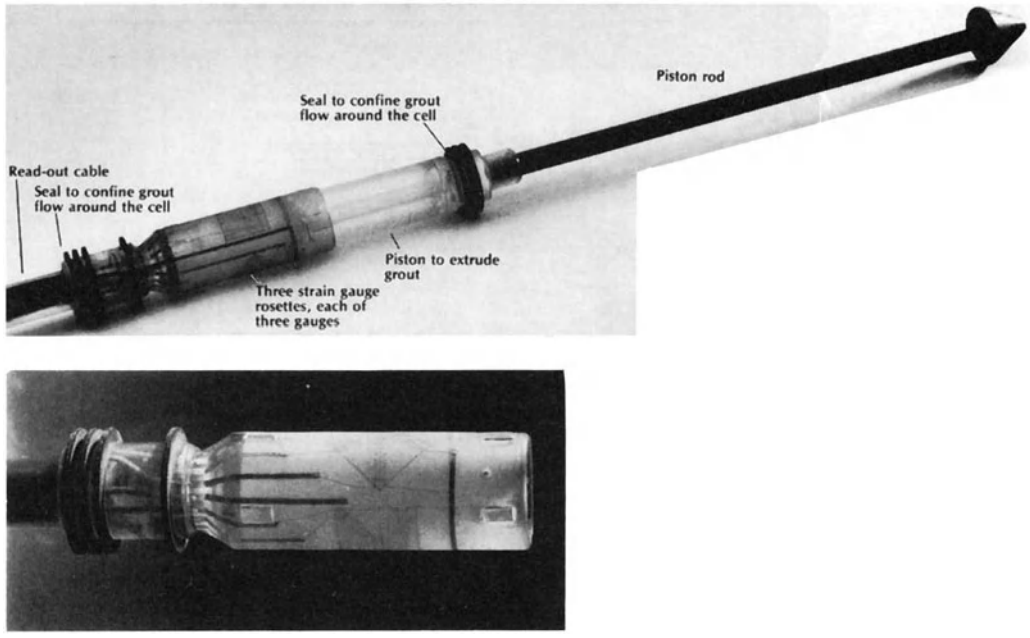

Fig. 5.16 Photograph of the CSIRO HI cell. (From GEOKON documentation.)

with a piston. Piston activation is done either by forcing a protruding rod (Fig. 5.16) against the end of the borehole or by manually pulling the piston into the epoxy shell. Seals are used to confine the grout around the cell. Three types of epoxy cement are now available depending on the ambient rock temperature (Worotnicki, 1993). A bond strength of about 4 MPa is assumed for field conditions with the regular HI cell and about 8 MPa for the thin-walled version of the cell (Worotnicki, 1993).

Overcoring of the CSIRO HI cell is usually done with a 150 mm diameter bit. A 100 mm bit is also satisfactory in good coring conditions. Satisfactory results are usually obtained with 200 to 400 mm long overcores. Changes

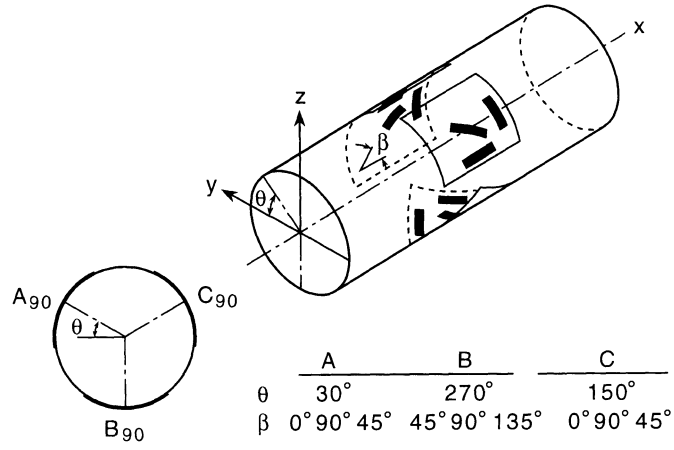

Fig. 5.17 Orientation of strain gages in the CSIRO HI cell. (After Worotnicki and Walton, 1976.)

in temperature during overcoring can be measured using an additional thermistor installed in the HI cell. Overcoring with the CSIRO HI cell is generally performed at depths within 30 m of working faces. Under ideal conditions, one or two stress measurements can be made per day (Choquet, 1994).

Standards for determining *in situ* stresses with the CSIRO HI cell have been proposed by the International Society for Rock Mechanics (Kim and Franklin, 1987). The procedures for drilling, installation and measurement are essentially the same as for the USBM gage and can be found in the ISRM standards. Figure 5.18 shows a typical set of response curves obtained by Worotnicki and Walton (1976). Laboratory tests of the CSIRO HI cell under uniaxial and biaxial loading conditions and in ideal materials have given stress estimates within 4–5% of their correct magnitudes and within a few degrees of the directions of applied loads (Cai, 1990; Walton and Worotnicki, 1986). The tests of Cai (1990) have shown that, like the CSIR cell, the performance of the CSIRO HI cell is very satisfactory and reliable in isotropic and homogeneous materials and acceptable in moderately non-homogeneous and medium-grained rock. It was also found that, like the CSIR triaxial strain cell, the CSIRO HI cell is more suitable when used in longitudinally bedded rocks. However, unlike the CSIR cell, the CSIRO HI cell is little influenced by rock inhomogeneities and grain size.

The main advantage of the CSIRO HI cell is that it can be used to determine the complete stress field in one borehole only. Since nine (or 12) measurements are made and there are six unknowns, redundant measurements are available and a least squares estimate of the *in situ* stress field components can be carried out. Further, the cell provides continuous monitoring during overcoring and the bond stresses are low. The CSIRO HI cell has shown a high success rate in the field, in particular in isotropic rocks and at rock temperatures in the range 15–40°C, but only a limited success rate at low (< 10°C) and high (> 40°C) temperatures. Consistent results have been obtained in rocks with grain size up to 4–5 mm (Worotnicki, 1993). Finally, bonding of the cell to the rock tends to keep the overcore sample intact, particularly in bedded and layered rocks, which is not the case with the USBM gage.

The main disadvantages of the CSIRO HI cell are (1) the cost of the cell is about twice

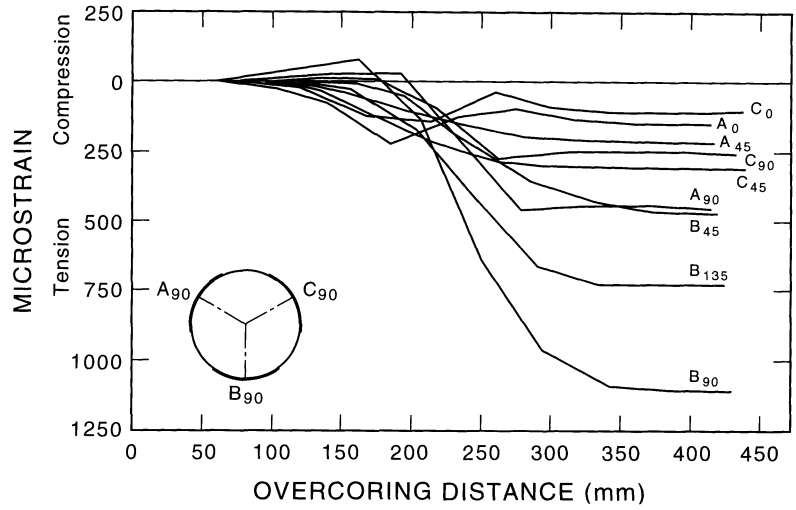

Fig. 5.18 Response curves obtained with the CSIRO HI cell. (After Worotnicki and Walton, 1976.)

that of the CSIR triaxial strain cell, (2) it requires long unbroken overcores, which may be difficult in weak or bedded rocks and rocks under high stresses, (3) it is a quarter-bridge instrument, (4) until recently, the cell has not been recoverable (Cai, 1990; Cai and Blackwood, 1991), (5) long periods of up to 10–20 h are required for the epoxy based adhesive to cure, the curing being quite difficult in wet and cool environments, and (6) in low-temperature environments (less than 10°C), softening of the epoxy adhesive at the cell–rock interface due to a slight increase in temperature may create yielding along the interface, which has been shown to result in high principal stresses parallel to the hole axis after analysis (Garritty, Irvin and Farmer, 1985; Irvin, Garritty and Farmer, 1987). This latter problem has been remedied in part (Worotnicki, 1993).

Upon overcoring, both the Young's modulus and Poisson's ratio of the rock are determined by biaxial testing of the recovered overcore containing the CSIRO HI cell. The biaxial test apparatus set-up is similar to that shown in Fig. 5.6.

5.3.7 BIAXIAL TESTING

As mentioned previously, the overcore samples containing the USBM gage, the CSIR triaxial strain cell or the CSIRO HI cell are tested in a biaxial chamber. The main objective of biaxial testing is to determine the deformability properties of the rock, in particular during unloading. The method was first suggested by Fitzpatrick (1962). Biaxial testing can also be used to assess rock grain size, anisotropy or heterogeneity, and borehole eccentricity. The biaxial cell can be used to check the response of the rock to cycles of loading and unloading and to determine whether or not the rock can be treated as linearly elastic within the stress range expected *in situ*. Monitoring the strains or displacements on the overcore can also help to identify the amount and rate of rock creep.

For the CSIR and CSIRO HI cells, the overcore can be sawn across the cells in order to check the quality of the bond between the cells and the rock. This can help (1) to identify defective strain gages and the presence of air bubbles in the cement at the location of the strain gages, (2) to check the hardness of the bond and its thickness around the circumference of the cell, (3) to check the actual strain gage orientation and (4) to check the size of the pilot hole, which may become oversized in softer rocks. The quality of the bond between the rock and the CSIRO HI cell can also be assessed if the cell is recovered with the technique proposed by Cai (1990).

A schematic of the biaxial cell is shown in Fig. 5.6. A photograph of the apparatus with pump and readout unit is shown in Fig. 5.19. The test shown in the photograph was conducted on an overcore sample containing a CSIRO HI cell. The biaxial cell essentially consists of a cylindrical steel jacket, a rubber membrane and seals. The rock overcore is placed in the biaxial cell. Oil is pumped into the space between the jacket and the rock. This applies a uniformly distributed biaxial pressure on the outer surface of the overcore sample while the strains or displacements in the USBM gage, CSIR triaxial strain cell or CSIRO HI cell are monitored. A rubber membrane is used to protect the rock from any ingress of oil into the pores or cracks that may be present in the rock. Biaxial cells can usually apply pressures up to 30–40 MPa. Some of the most recent cells have a multicore diameter capability and can be used to test core samples ranging between 40 and 150 mm in diameter. The overcore sample is subjected to several loading/unloading cycles.

The strains or displacements measured during biaxial tests are interpreted in terms of elastic properties of the rock comprising the overcore by using elastic solutions for the strains and displacements at the inner surface of a hollow cylinder under external axisymmetric pressure. An example of response curves for the CSIRO HI cell is shown in Fig.

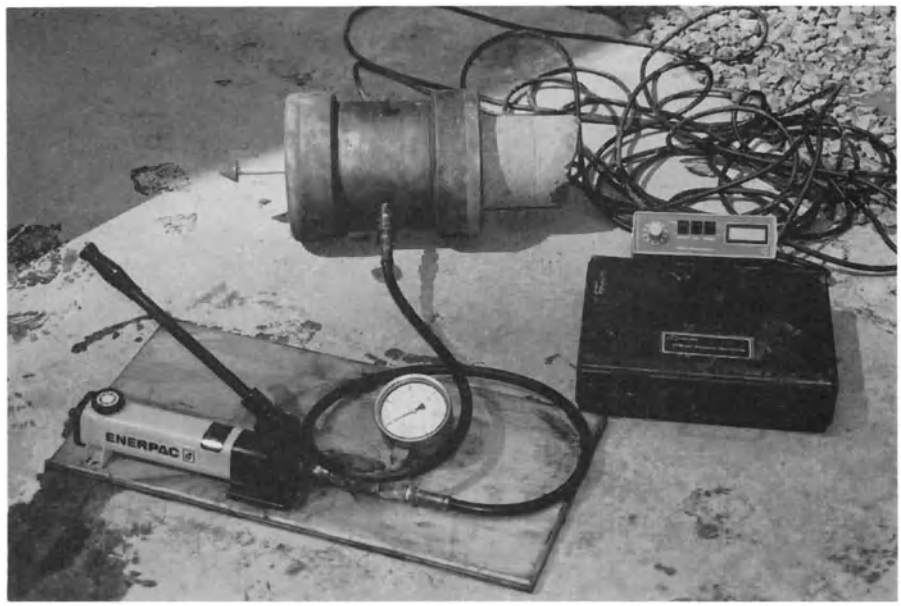

Fig. 5.19 Photograph of the biaxial test chamber with pump and readout unit. The test was done on an overcore instrumented with the CSIRO HI cell. (Courtesy of MINDATA.)

5.20 for tests conducted by Gale (1983) in Australia. These curves clearly show that the rock is linearly elastic over a 0–20 MPa pressure range. In order to obtain good results, the USBM gage, the CSIR triaxial strain cell or the CSIRO HI cell must be located close to the middle of the biaxial cell loading area (Worotnicki, 1993; Worotnicki and Walton, 1979).

5.3.8 BOREHOLE SLOTTING

The borehole slotter (available through INTERFELS) has been designed to work in boreholes with diameters ranging between 95 and 103 mm. Figures 5.21a and 5.21b show a picture and a schematic cross-section of the instrument, respectively. The stresses are relieved locally by cutting half-moon shaped radial slots into the borehole wall using a small, pneumatically driven saw. Each slot is usually 1.0 mm wide and up to 25 mm deep. Before, during and after cutting the slot, the tangential strain is measured at the borehole wall in the near vicinity (within a 15° arc) of the slot using a contact strain sensor, which is part of the slotter. The strains are converted into stresses using the theory of linear elasticity and using the Kirsch solution for the stresses and strains around a circular opening. A minimum of three longitudinal cuts (usually 120° apart) in three different directions is necessary to determine the stresses in the plane perpendicular to the hole. Figure 5.22 shows typical tangential strain response curves for eight slots cut 45° apart in a single borehole. Detailed description of the borehole slotter can be found in Bock (1993).

The borehole slotter has several advantages. The method provides quick measurements of stresses. For instance, the time span of a single slotting test is only 5 min. A total of 10–15 measurements can be carried out in a single 8 h shift. The instrument is fully recoverable, self-sufficient and provides continuous monitoring of strain during slot cutting. No borehole preparation is necessary. Also, cutting of additional slots besides the three basic ones can provide redundancy. Comparison of the

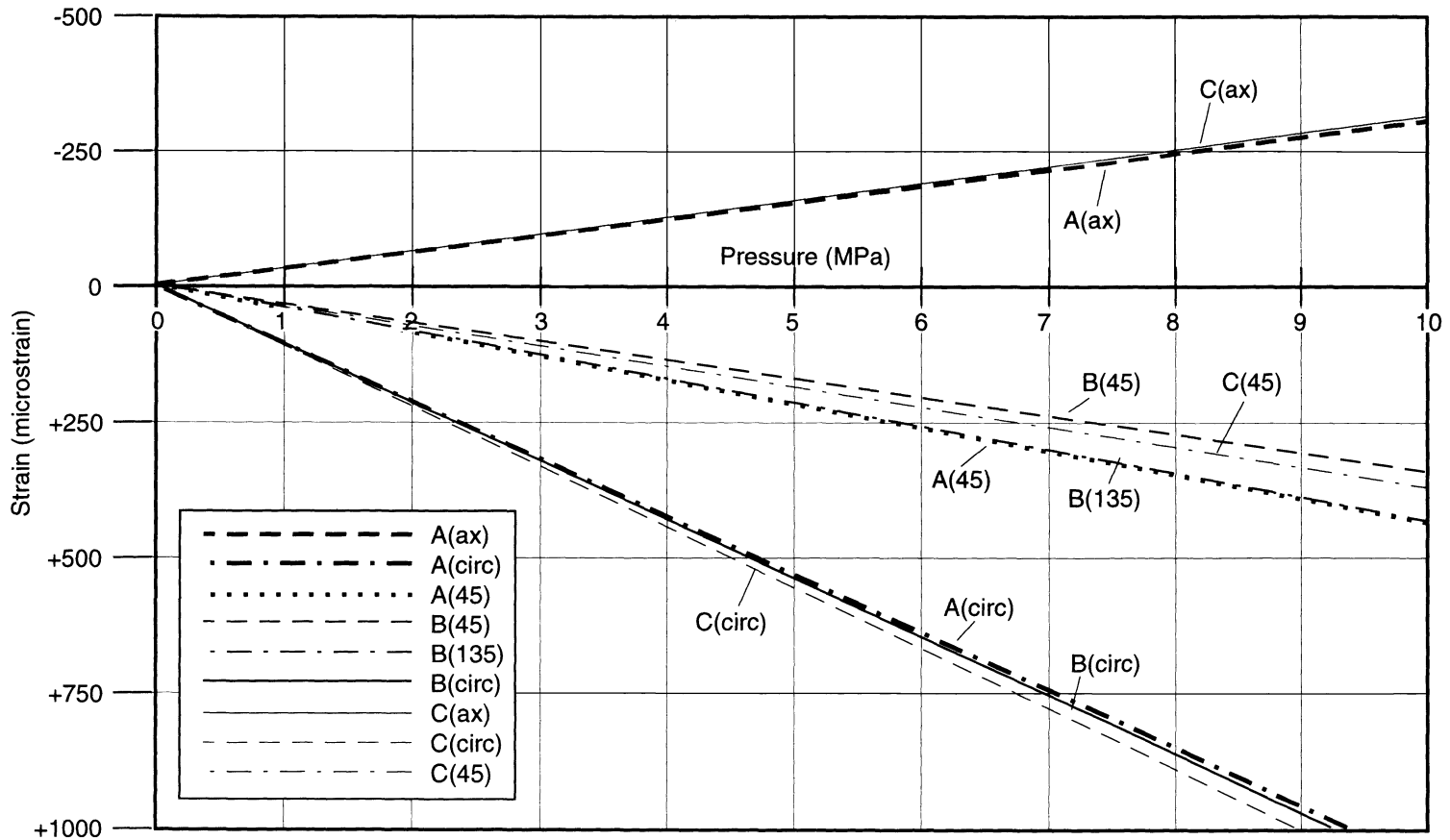

Fig. 5.20 Biaxial test response curves obtained with CSIRO HI cell. A, B and C correspond to the cell strain rosettes shown in Fig. 5.17. (After Gale, 1983.)

response curves of two slots 180° apart can give an appreciation of the degree of rock homogeneity.

The borehole slotter has several limitations: (1) it has only been tested at shallow depths less than 30 m, (2) the borehole must be dry and (3) the stress parallel to the borehole axis must be assumed since the tangential strain along the borehole wall depends on four stress components (for isotropic rock): three in the

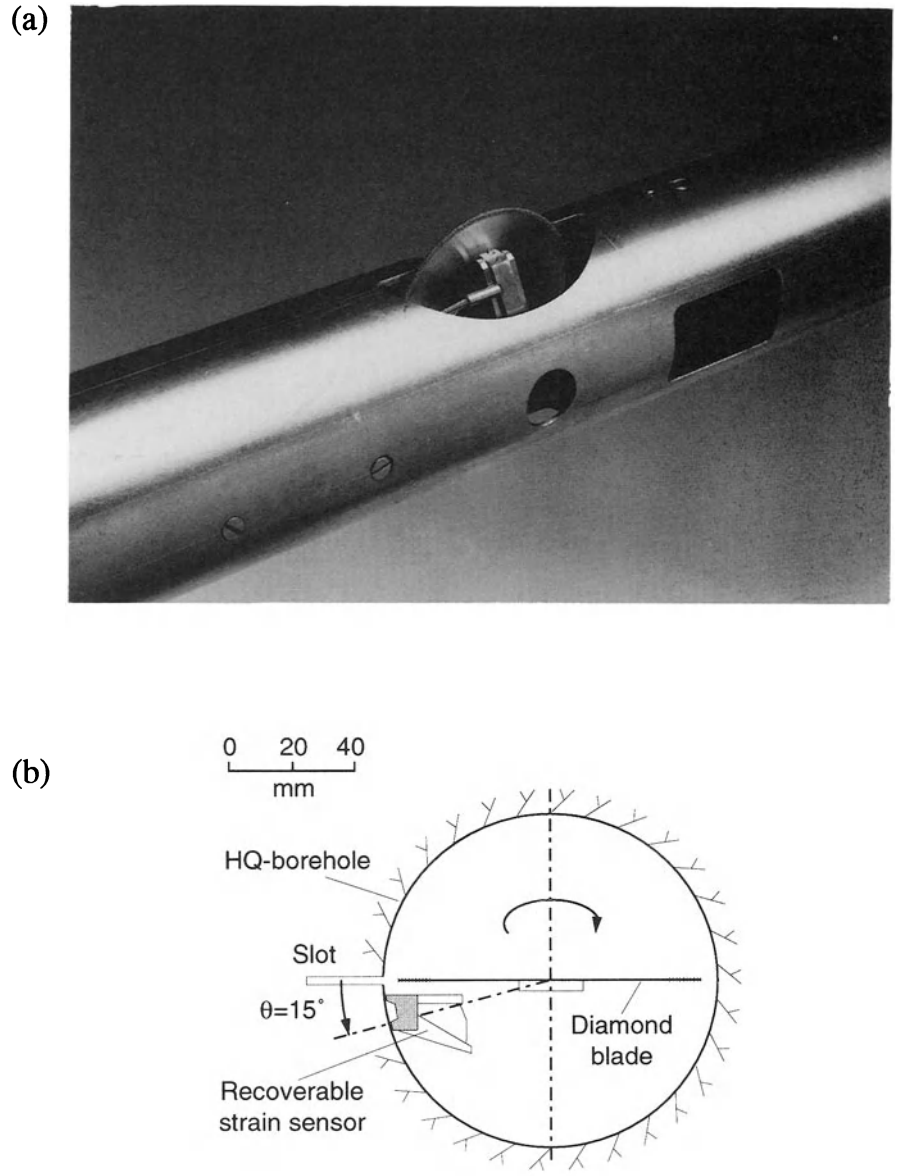

Fig. 5.21 The borehole slotter. (a) Photograph. (Courtesy of INTERFELS.) (b) Cross-section. (Source: Bock, H. Copyright 1993, with kind permission from Elsevier Science Ltd, The Boulevard, Langford Lane, Kidlington, UK.)

plane normal to the borehole axis and one parallel to the borehole axis.

In general, very good agreement has been found between stress measurements with the borehole slotter and measurements with other techniques. This seems to show that the borehole slotter is a very promising device for measuring stresses in rock.

5.3.9 STRESS RELIEF BY CENTER HOLE

The stress relief by center hole method (or undercoring method) was first proposed by Duvall (1974) to measure the state of stress on exposed rock surfaces. The idea behind the method is to monitor the radial displacements of points located around a center hole as the hole is being drilled. The geometry of the test is shown in Fig. 5.23. The procedure consists of two steps. First, six measuring pins $\frac{3}{8}$ inch (9.5 mm) in diameter, $\frac{1}{4}$ inch (6.3 mm) long and 60° apart are cemented (using a quick-setting epoxy) on a rock surface along a circle 10 inches (254 mm) in diameter with a metal platen. The distance across diametrically opposed pins is measured. The second step consists of drilling a 6 inch (152 mm) diameter hole in the center of the pins with a thin-walled masonry bit. The distance across diametrically opposed pins is again measured. From the three measured diametral measurements, the secondary principal stresses and their orientation in the rock surface are determined. The displacements are usually measured using a micrometer with an accuracy of 0.001 mm.

5.4 THEORY

This section presents the theory to analyze the results obtained with the following stress relief methods: (1) overcoring with the USBM gage, Doorstopper, CSIR and CSIR-type triaxial strain cells, and the CSIRO HI cell, (2) surface relief by undercoring and (3) borehole slotting. The theory for the analysis of biaxial tests to determine rock elastic properties is also presented.

5.4.1 ASSUMPTIONS IN THE ANALYSIS OF OVERCORING TESTS

Several assumptions are made when analyzing the results of overcoring tests in boreholes.

(1) The stresses that are relieved during overcoring are equal to the stresses when the rock was in its precoring environment.

Recalling the general procedure described in Fig. 5.2, the process of overcoring can be seen as canceling the components of initial stress acting across a cylindrical surface in the

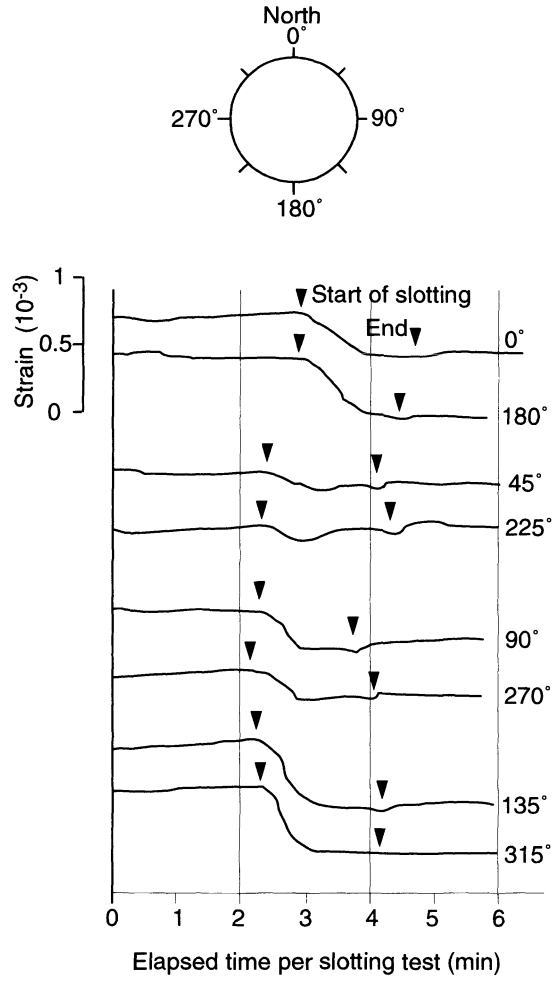

Fig. 5.22 Typical tangential strain response curves for eight slots cut 45° apart in a single borehole using the borehole slotter. (After Bock, 1986.)

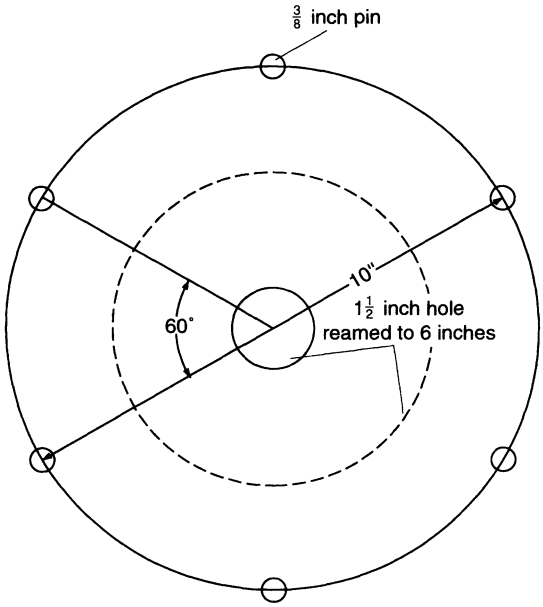

Fig. 5.23 Geometry of stress relief by center hole method. (After Duvall, 1974.)

rock. Hence overcoring is equivalent to adding tractions equal in magnitude but opposite in sign to those that existed across the cylindrical overcore surface before it was drilled.

(2) The size of the overcoring diameter does not influence the stress measurements.

The analysis of the displacements and strains generated during overcoring depends to a great extent on the type of instrumented device. If the instrumented device in contact with the rock does not interfere with the deformation of the rock during overcoring, then the overcore sample will be completely free of any stress and strain (complete relief) at the end of the overcoring process. This is true regardless of the overcore sample size and shape. Overcoring releases strains, displacements and stresses due not only to the *in situ* stresses but also those induced by the introduction of the pilot hole and the large-diameter hole. Instrumented devices that allow stress relief with little or no interference include the USBM gage, the CSIR Doorstopper, the CSIR triaxial strain cell and other CSIR-type triaxial strain cells. Lang, Thompson and Ng (1986) conducted an extensive field study on the effect of overcore diameter on the magnitude and orientation of *in situ* stresses in the granitic rock at the URL in Pinawa, Canada. They found that for the USBM gage and the AECL-modified CSIR cell, the stress results from overcoring with a 96 mm diameter bit were not significantly different from those with 150 and 200 mm diameter bits.

If on the other hand, the instrumented device does interfere with the deformation of the rock, then overcoring does not produce a total stress relief (partial relief) since the presence of an inclusion attached to the rock results in the retention of residual stresses and strains in both the inclusion and the rock. This is the case with solid and hollow inclusion probes. The partial relief implies that the size of the overcoring diameter must influence the distribution of stresses and strains within the inclusion probes. Therefore the overcoring diameter must be accounted for when analyzing strains and displacements induced by overcoring. The imposition of negative stresses at the overcore surface will not produce, in general, a uniform state of stress within a solid probe, as is the case for an infinite medium. Furthermore, the release of compressive stresses on the boundaries of the overcore may create tensile stresses along the inclusion–rock interface and break the bond, particularly for solid inclusions.

For a solid inclusion in an isotropic medium, Duncan-Fama (1979) showed that the error induced in neglecting the finiteness of the overcoring diameter is not significant when the ratio between the shear modulus of the inclusion to that of the rock is less than 0.05 and for overcoring diameters that are at least three times the pilot hole diameter. If the inclusion is hollow, it must also be thin walled for the approximation to be valid (Duncan-Fama and Pender, 1980). For anisotropic rocks, Amadei (1985) has shown that for very low-modulus solid inclusions and low-modulus thin-walled inclusions, stresses and strains are

only disturbed in a region very close to the rock–inclusion interface. In particular, it was found that the residual stresses decay rapidly and become negligible at distances less than three to four times the radius of the pilot hole. This seems to apply regardless of the type and orientation of the anisotropy. Hence, provided that overcoring is conducted beyond those limits, the errors involved in neglecting the finiteness of the overcore diameter become insignificant and the overcore diameter can be set equal to infinity.

(3) The rock response is elastic and its elastic properties are the same under loading and unloading.

As discussed by Bielenstein and Barron (1971), the strains and displacements measured during overcoring can be divided into two categories: short term (within 2 h of overcoring) and long term (relief occurring after 2 h). Each category can in turn be divided into those attributable to the relief of residual stresses and those attributable to the relief of gravitational and/or tectonic stresses. This is summarized in Fig. 5.24. In general, standard overcoring techniques measure short-term (elastic) strains due to the relief of active stresses such as gravitational and tectonic stresses. The short-term relief of residual stresses can be obtained by 'double overcoring', i.e. overcoring existing overcores (e.g. Lang, Thompson and Ng, 1986). The long-term strain relief can be observed by instrumenting overcores over longer periods of time. Borecki and Kidybinski (1966) found that instantaneous (elastic) strains constitute 55–87% of the total strains for rocks such as sandstone, mudstone and coal, the remainder being in the form of viscoelastic, plastic and viscoplastic components. Palmer and Lo (1976) conducted overcoring stress measurements in southwestern Ontario. They found that in shaly zones of the local Gasper formation, continuous strains could still be measured on overcore samples over a long period after overcoring, with additional strains after 18 h being of the same order as the elastic strains used in the analysis of the overcoring tests.

(4) The rock is continuous and homogeneous.

The importance of continuity and homogeneity when measuring *in situ* stresses depends on the scale at which the measurement is made and the relative size of the geological structures and rock heterogeneities with respect to the size of the pilot hole.

(5) The borehole is circular with smooth surfaces.

When drilling a hole for the placement of an instrumented device, hole eccentricity cannot be ruled out. Also, borehole surfaces are not always smooth since rock pieces may detach during drilling. This will depend on the rock type, the rock structure and the orientation of the rock fabric with respect to the borehole. Agarwal (1968) showed that for a circular hole in an isotropic medium subjected to a uniaxial stress field, a small ellipticity created during drilling of the hole can be neglected if the device that measures changes in borehole diameter has a precision of $\pm 50 \times 10^{-6}$ inches (1.3×10^{-3} mm).

(6) The rock deforms in plane strain or plane stress.

Plane strain (or generalized plane strain) is assumed to relate strains and displacements to the stresses. This applies to measurements with the USBM gage, the CSIR and CSIR-type triaxial strain cells, and the CSIRO HI cell. Plane strain requires that the pilot holes are long enough and that the measurements are carried out in cross-sections remote from the ends of the pilot holes and the ends of the measuring instrument, in order to neglect end effects (Blackwood, 1982a). In general, the plane strain assumption is met if the measurements are in a plane distant from the ends of a pilot hole by at least three to four times the hole diameter. Thus for a 38 mm diameter hole, the minimum distance is 114 to 152 mm, which means that the overcore must be at least 300 mm in length. Based on the results of a finite element analysis, Van Heerden (1973) recommended using 500 mm long overcores when overcoring the CSIR triaxial strain cell.

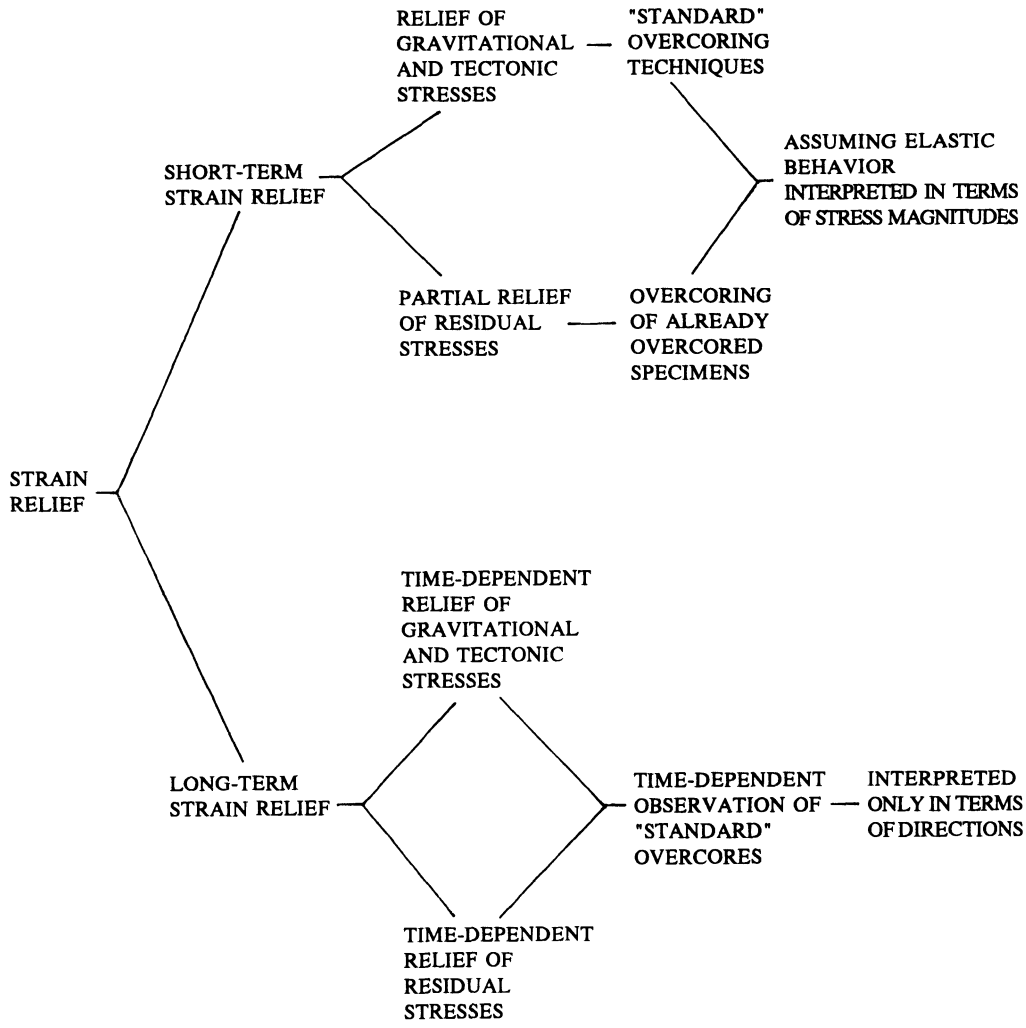

Fig. 5.24 Strain relief components defined by Bielenstein and Barron (1971).

Plane stress is used only for the analysis of the CSIR Doorstopper.

(7) The *in situ* stress field is three-dimensional.

The rock is assumed to be subjected to a three-dimensional stress field with components σ_{xo}, σ_{yo}, σ_{zo}, τ_{yzo}, τ_{xzo} and τ_{xyo} acting at infinity and defined in an x, y, z coordinate system attached to the pilot hole. Let $[\sigma_o]$ be the stress matrix such that

$$[\sigma_o]^t = [\sigma_{xo} \quad \sigma_{yo} \quad \sigma_{zo} \quad \tau_{yzo} \quad \tau_{xzo} \quad \tau_{xyo}] \quad (5.1)$$

In a global X, Y, Z coordinate system inclined with respect to the local x, y, z coordinate system (Fig. 5.25a), the *in situ* stress field has components σ_{Xo}, σ_{Yo}, σ_{Zo}, τ_{YZo}, τ_{XZo} and τ_{XYo}, and the stress matrix $[\sigma_o]_{XYZ}$ is related to $[\sigma_o]$ as follows:

$$[\sigma_o] = [T_\sigma][\sigma_o]_{XYZ} \quad (5.2)$$

where $[T_\sigma]$ is a (6×6) stress transformation matrix defined in equation (A.13) in Appendix A. The components of this matrix depend on the direction cosines of the x-, y- and z-axes with respect to the global X, Y, Z coordinate system. As an example, for a pilot hole with

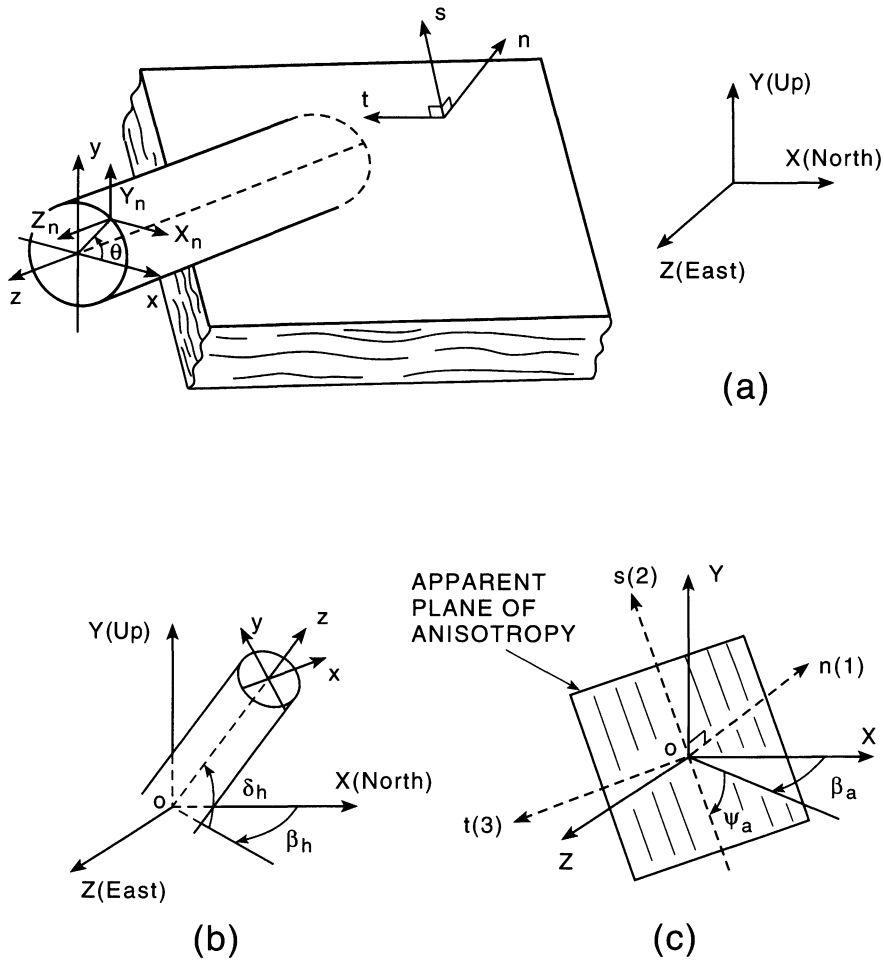

Fig. 5.25 (a) Problem geometry, (b) orientation of pilot hole, (c) orientation of the anisotropy.

the geometry of Fig. 5.25b whose orientation is defined by two angles β_h and δ_h, the direction cosines of the x-, y- and z-axes are equal to

$$\begin{aligned} l_x &= \sin\beta_h & m_x &= 0 & n_x &= -\cos\beta_h \\ l_y &= -\sin\delta_h \cos\beta_h & m_y &= \cos\delta_h & n_y &= -\sin\delta_h \sin\beta_h \\ l_z &= \cos\delta_h \cos\beta_h & m_z &= \sin\delta_h & n_z &= \cos\delta_h \sin\beta_h \end{aligned} \quad (5.3)$$

5.4.2 ANALYSIS OF USBM GAGE MEASUREMENTS

Analysis of USBM gage diametral measurements requires that a relationship should be derived between the diametral measurements recorded during overcoring and the components of the *in situ* stress field $[\sigma_o]$. This can be done using the theory of elasticity for isotropic or anisotropic media. Isotropic solutions for the analysis of USBM gage measurement have been proposed by Leeman (1967) and Hiramatsu and Oka (1968). Anisotropic solutions have been proposed by Berry and Fairhurst (1966), Berry (1968), Becker and Hooker (1967), Becker (1968), Hooker and Johnson (1969) and Hirashima and Koga (1977). Most of these anisotropic solutions make some assumptions about the type of rock anisotropy

and the orientation of the pilot holes with respect to the planes of rock anisotropy and symmetry. The solution presented below is general and can be used for the analysis of USBM gage measurements in orthotropic, transversely isotropic or isotropic rock masses. Furthermore, the pilot holes can be inclined with respect to the planes of rock anisotropy.

(a) Diametral deformation of a hole in a three-dimensional stress field

Consider the equilibrium of a rock mass modeled as infinite, linearly elastic, anisotropic, continuous and homogeneous. Let X, Y, Z be a global coordinate system such that the X- and Z-axes are pointing in the north and east directions, respectively. The Y-axis is positive upward. The rock is bounded internally by a cylindrical surface of circular cross-section and radius a that represents a borehole (pilot hole). Consider the geometry of Fig. 5.25a and let x,y,z be a coordinate system attached to the hole with the z-axis defining the longitudinal axis of the hole. The orientation of the borehole and that of the x-, y- and z-axes are defined with respect to the X, Y, Z coordinate system by two angles β_h (borehole azimuth) and δ_h (borehole rise) such that the x-axis lies in the X, Z plane (Fig. 5.25b). The direction cosines l, m and n of the unit vectors in the x, y and z directions are defined in equation (5.3).

The rock mass is assumed to be orthotropic in an n,s,t coordinate system attached to a clearly defined plane of rock anisotropy (Fig. 5.25a). For rocks, this plane may be an apparent direction of rock symmetry such as foliation, schistosity or bedding planes. In any case, the n-axis is taken normal to the plane, the t-axis is horizontal and the s- and t-axes are contained within the plane. The orientation of the n,s,t coordinate system with respect to the X-, Y- and Z-axes, is defined by a dip direction angle β_a and a dip angle ψ_a (Fig. 5.25c). The direction cosines l, m and n of the unit vectors in the n, s and t (1, 2 and 3) directions are respectively equal to

$$\begin{aligned} l_1 &= \cos\beta_a \sin\psi_a & m_1 &= \cos\psi_a & n_1 &= \sin\beta_a \sin\psi_a \\ l_2 &= -\cos\beta_a \cos\psi_a & m_2 &= \sin\psi_a & n_2 &= -\sin\beta_a \cos\psi_a \\ l_3 &= -\sin\beta_a & m_3 &= 0 & n_3 &= \cos\beta_a \end{aligned} \tag{5.4}$$

The constitutive equation of the medium in the n,s,t coordinate system is given by (Lekhnitskii, 1977)

$$\begin{bmatrix} \varepsilon_n \\ \varepsilon_s \\ \varepsilon_t \\ \gamma_{st} \\ \gamma_{nt} \\ \gamma_{ns} \end{bmatrix} = \begin{bmatrix} \frac{1}{E_n} & -\frac{\nu_{sn}}{E_s} & -\frac{\nu_{tn}}{E_t} & 0 & 0 & 0 \\ -\frac{\nu_{ns}}{E_n} & \frac{1}{E_s} & -\frac{\nu_{ts}}{E_t} & 0 & 0 & 0 \\ -\frac{\nu_{nt}}{E_n} & -\frac{\nu_{st}}{E_s} & \frac{1}{E_t} & 0 & 0 & 0 \\ 0 & 0 & 0 & \frac{1}{G_{st}} & 0 & 0 \\ 0 & 0 & 0 & 0 & \frac{1}{G_{nt}} & 0 \\ 0 & 0 & 0 & 0 & 0 & \frac{1}{G_{ns}} \end{bmatrix} \times \begin{bmatrix} \sigma_n \\ \sigma_s \\ \sigma_t \\ \tau_{st} \\ \tau_{nt} \\ \tau_{ns} \end{bmatrix} \tag{5.5}$$

or in a more compact matrix form

$$[\varepsilon]_{nst} = [H][\sigma]_{nst} \tag{5.6}$$

Nine independent elastic constants are needed to describe the deformability of the rock in the n,s,t coordinate system. The quantities E_n, E_s and E_t are the Young's moduli in the n, s and t directions, respectively. The moduli G_{ns}, G_{nt} and G_{st} are the shear moduli in planes parallel to the n,s, n,t and s,t planes, respectively. Finally, ν_{ij} $(i,j = n,s,t)$ are the Poisson's ratios that characterize the normal strains in the symmetry directions j when a stress is applied

in the symmetry directions i. Because of symmetry of the compliance matrix $[H]$, Poisson's ratios ν_{ij} and ν_{ji} are such that $\nu_{ij}/E_i = \nu_{ji}/E_j$.

Equations (5.5) and (5.6) still apply if the rock mass is transversely isotropic in one of the three n,s,n,t or s,t planes. In that case, only five independent elastic constants are needed to describe the deformability of the rock in the n,s,t coordinate system. In this book (see also section 2.5), these constants are called E, E', ν, ν' and G' with the following definitions: (1) E and E' are Young's moduli in the plane of transverse isotropy and in the direction normal to it, respectively, (2) ν and ν' are Poisson's ratios characterizing the lateral strain response in the plane of transverse isotropy to a stress acting parallel or normal to it, respectively, and (3) G' is the shear modulus in planes normal to the plane of transverse isotropy. Relationships exist between E, E', ν, ν', G and G' and the coefficients of matrix $[H]$ in equation (5.6). For instance, for transverse isotropy in the s,t plane

$$\frac{1}{E_n}=\frac{1}{E'};\quad \frac{1}{E_s}=\frac{1}{E_t}=\frac{1}{E};\quad \frac{1}{G_{ns}}=\frac{1}{G_{nt}}=\frac{1}{G'}$$

$$\frac{\nu_{ns}}{E_n}=\frac{\nu_{nt}}{E_n}=\frac{\nu'}{E'};\quad \frac{\nu_{st}}{E_s}=\frac{\nu_{ts}}{E_t}=\frac{\nu}{E};\quad \frac{1}{G_{st}}=\frac{1}{G}=\frac{2(1+\nu)}{E} \tag{5.7}$$

For known orientation of the plane of rock anisotropy with respect to the hole, the constitutive relation of the rock in the x,y,z coordinate system can be obtained by using second-order Cartesian tensor coordinate transformation rules (e.g. Amadei, 1983a). This gives

$$[\varepsilon]_{xyz} = [A][\sigma]_{xyz} \tag{5.8}$$

where $[\varepsilon]^t_{xyz} = [\varepsilon_x, \varepsilon_y, \varepsilon_z, \gamma_{yz}, \gamma_{xz}, \gamma_{xy}]$ and $[\sigma]^t_{xyz} = [\sigma_x, \sigma_y, \sigma_z, \tau_{yz}, \tau_{xz}, \tau_{xy}]$ are the strain and stress matrices, respectively. As shown by Amadei (1983a), $[A]$ is a (6×6) symmetric compliance matrix whose components a_{ij} $(i,j = 1,6)$ depend on the elastic properties of the rock mass in the n,s,t coordinate system and the four orientation angles β_h, δ_h, β_a and ψ_a defined in Figs 5.25b, c. Matrix $[A]$ can be expressed as follows:

$$[A] = [T_\varepsilon][T'_\sigma]^t[H][T'_\sigma][T_\varepsilon]^t \tag{5.9}$$

where $[T_\varepsilon]$ and its transpose $[T_\varepsilon]^t$ are (6×6) matrices with components that depend only on the direction cosines of the unit vectors parallel to the x-, y- and z-axes attached to the borehole. Also, $[T'_\sigma]$ and its transpose $[T'_\sigma]^t$ are (6×6) matrices with components that depend on the direction cosines of the unit vectors parallel to the n-, s- and t-axes attached to the plane of anisotropy.

The existence of any planes of symmetry in the x,y,z coordinate system depends on the values of the four orientation angles β_h, δ_h, β_a and ψ_a and the transversely isotropic or orthotropic nature of the rock in the n,s,t coordinate system. In particular, the borehole is perpendicular to a plane of elastic symmetry (1) when the rock mass is orthotropic in the x,y,z coordinate system (Fig. 5.26a) or has one of its three planes of symmetry normal to the z-axis (Fig. 5.26b), (2) when the rock mass is transversely isotropic and the hole axis is either

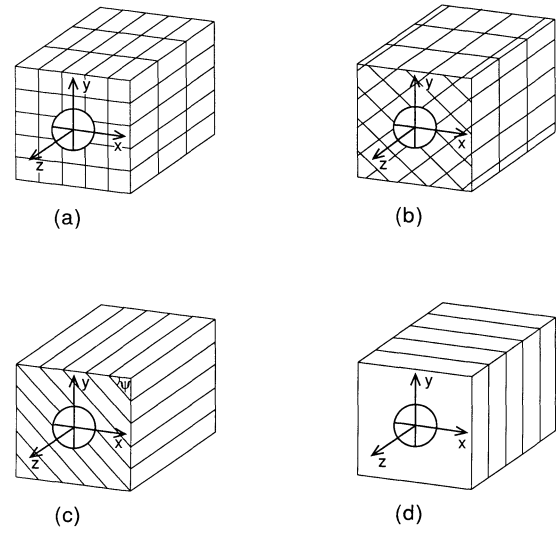

Fig. 5.26 Four cases of anisotropy for which the hole axis is normal to a plane of elastic symmetry. (a), (b) Orthotropic medium; (c), (d) transversely isotropic medium.

parallel (Fig. 5.26c) or perpendicular (Fig. 5.26d) to the plane of transverse isotropy or (3) when the rock mass is isotropic.

As shown in Fig. 5.25a, the borehole is loaded along its contour by surface tractions. Let X_n, Y_n and Z_n be the components in the x, y and z directions of the surface stress vector acting along the contour of the hole. Since we are using the geomechanics sign convention for stress, strain and displacement in this book, the positive directions of the stress vector components are in the negative x, y and z directions, respectively. In addition X_n, Y_n and Z_n are assumed not to vary along the z-axis, to be periodic functions with period 2π, and to be expressed as Fourier series in $\cos\theta$ and $\sin\theta$ as follows:

$$\begin{aligned} X_n &= a_{1x}\cos\theta + b_{1x}\sin\theta \\ Y_n &= a_{1y}\cos\theta + b_{1y}\sin\theta \\ Z_n &= a_{1z}\cos\theta + b_{1z}\sin\theta \end{aligned} \tag{5.10}$$

The angle θ assumes all values from 0 to 2π for a complete circuit along the contour of the borehole. In writing equation (5.10), it is assumed that the resultants of X_n, Y_n and Z_n along the contour of the hole vanish. This assumption leads to an absence of constant terms. In this analysis it is also assumed that, under the influence of the stress vectors with components given by equation (5.10), the rock deforms under a condition of generalized plane strain in the x,y plane (Amadei, 1983a; Lekhnitskii, 1977). In other words, all planes parallel to the x, y plane are assumed to warp in the same way and the longitudinal deformation induced by X_n, Y_n and Z_n does not vanish and depends only on the x and y coordinates. Finally, body forces are neglected in the present analysis.

General expressions for the components of stress, strain and displacement at any point in the medium induced by X_n, Y_n and Z_n with the general form of equation (5.10) can be found in Lekhnitskii (1977) and Amadei (1983a). Closed-form solutions for the displacements, when the hole is either inclined or at right angles to a plane of elastic symmetry in the rock, are summarized in Appendix B. For all cases shown in Fig. 5.26, the hole deforms in plane strain in the x,y plane instead of generalized plane strain and the longitudinal deformation always vanishes.

Drilling a circular hole in an already stressed medium is equivalent to applying at an angle θ along the contour of the hole a stress vector with components X_n, Y_n and Z_n such that (Amadei, 1983a)

$$\begin{aligned} X_n &= \sigma_{xo}\cos\theta + \tau_{xyo}\sin\theta \\ Y_n &= \tau_{xyo}\cos\theta + \sigma_{yo}\sin\theta \\ Z_n &= \tau_{xzo}\cos\theta + \tau_{yzo}\sin\theta \end{aligned} \tag{5.11}$$

As shown in Appendix B (equation (B.13)), the change in hole diameter $U_{dh} = 2u_{rh}$ at an angle θ from the x-axis induced by the stress vector components defined in equation (5.11) is equal to

$$\frac{U_{dh}}{2a} = f_{1h}\sigma_{xo} + f_{2h}\sigma_{yo} + f_{3h}\sigma_{zo} + f_{4h}\tau_{yzo} + f_{5h}\tau_{xzo} + f_{6h}\tau_{xyo} \tag{5.12}$$

where $f_{1h}\cdots f_{6h}$ depend on the elastic properties of the anisotropic rock mass in the n,s,t coordinate system and the orientation of its planes of anisotropy with respect to the hole. Note that f_{3h} always vanishes. General expressions for $f_{1h}\cdots f_{6h}$ are given in Appendix B (equation (B.14)).

As shown in Appendix B (equation (B.19)), the change in distance $U_{do} = 2u_{ro}$ between two points (originally a distance $2a$ apart and located at an angle θ from the x-axis) induced by applying the *in situ* stress field on the anisotropic medium without a borehole can be expressed as follows:

$$\frac{U_{do}}{2a} = f_{1o}\sigma_{xo} + f_{2o}\sigma_{yo} + f_{3o}\sigma_{zo} + f_{4o}\tau_{yzo} + f_{5o}\tau_{xzo} + f_{6o}\tau_{xyo} \tag{5.13}$$

where $f_{1o}\cdots f_{6o}$ depend on the elastic properties of the anisotropic rock in the n,s,t coordinate system and the orientation of its planes

of anisotropy with respect to the hole. General expressions for $f_{1o} \cdots f_{6o}$ are given in equation (B.20). Adding equations (5.12) and (5.13), the total borehole diametral deformation at an angle θ from the x-axis is such that

$$\frac{U_d}{2a} = f_1\sigma_{xo} + f_2\sigma_{yo} + f_3\sigma_{zo} + f_4\tau_{yzo} + f_5\tau_{xzo} + f_6\tau_{xyo} \quad (5.14)$$

with $f_1 = f_{1h} + f_{1o} \cdots f_6 = f_{6h} + f_{6o}$. Equation (5.14) can also be written as follows

$$\frac{U_d}{2a} = M_1 + M_2\cos 2\theta + M_3 \sin 2\theta \quad (5.15)$$

where M_1, M_2 and M_3 depend on the six stress components, the elastic properties of the anisotropic rock mass in the n,s,t coordinate system, and the orientation of its planes of anisotropy with respect to the hole. Equation (5.14) shows that for a general anisotropic rock mass, the borehole diametral deformation depends on all six *in situ* stress components.

When there is a plane of elastic symmetry normal to the hole axis z, such as in Figs 5.26a–d, $f_{4h} = f_{5h} = f_{4o} = f_{5o} = 0$ and therefore f_4 and f_5 vanish. Then equation (5.14) becomes

$$\frac{U_d}{2a} = f_1\sigma_{xo} + f_2\sigma_{yo} + f_3\sigma_{zo} + f_6\tau_{xyo} \quad (5.16)$$

and M_1, M_2 and M_3 in equation (5.15) depend only on σ_{xo}, σ_{yo}, σ_{zo} and τ_{xyo} and are independent of τ_{xzo} and τ_{yzo}. The expressions for f_{1h}, f_{2h} and f_{6h} and f_{1o}, f_{2o}, f_{3o} and f_{6o} are given in equations (B.15) and (B.21) in Appendix B, respectively. If, in addition, the x, y- and z-axes attached to the borehole are also perpendicular to planes of elastic symmetry (Figs 5.26a, 5.26d and 5.26c with $\psi = 0°$ or 90°), then f_1, f_2, f_3 and f_6 in equation (5.16) take the following form:

$$f_1 = \sin^2\theta(\beta_{12} + (\beta_{11}\beta_{22})^{1/2}) - \cos^2\theta\,\beta_{11}\left(\frac{2\beta_{12} + \beta_{66}}{\beta_{11}} + 2\left(\frac{\beta_{22}}{\beta_{11}}\right)^{1/2}\right)^{1/2} - a_{11}\cos^2\theta - a_{21}\sin^2\theta \quad (5.17)$$

$$f_2 = \cos^2\theta(\beta_{12} + (\beta_{11}\beta_{22})^{1/2}) - \sin^2\theta(\beta_{11}\beta_{22})^{1/2} \times \left(\frac{2\beta_{12} + \beta_{66}}{\beta_{11}} + 2\left(\frac{\beta_{22}}{\beta_{11}}\right)^{1/2}\right)^{1/2} - a_{12}\cos^2\theta - a_{22}\sin^2\theta \quad (5.18)$$

$$f_3 = -a_{13}\cos^2\theta - a_{23}\sin^2\theta \quad (5.19)$$

$$f_6 = -\sin 2\theta(\beta_{12} + (\beta_{11}\beta_{22})^{1/2}) - \frac{\sin 2\theta}{2}(\beta_{11} + (\beta_{11}\beta_{22})^{1/2}) \times \left(\frac{2\beta_{12} + \beta_{66}}{\beta_{11}} + 2\left(\frac{\beta_{22}}{\beta_{11}}\right)^{1/2}\right)^{1/2} - \frac{\sin 2\theta}{2}a_{66} \quad (5.20)$$

For this special case, M_1, M_2 and M_3 are given in equation (B.26) in Appendix B. In equations (5.17)–(5.20) $\beta_{ij} = a_{ij} - a_{i3}a_{j3}/a_{33}$ $(i,j = 1\text{–}6)$ and a_{ij} are the coefficients of matrix $[A]$ in equation (5.8). Finally, if the medium is isotropic with Young's modulus E and Poisson's ratio ν, substituting $\beta_{11} = \beta_{22} = (1 - \nu^2)/E$, $\beta_{12} = -\nu(1 + \nu)/E$ and $\beta_{66} = a_{66} = 2(1 + \nu)/E$ into equations (5.17)–(5.20), f_1, f_2, f_3 and f_6 are now equal to

$$f_1 = \frac{1}{E}(2\cos 2\theta(\nu^2 - 1) - 1);$$

$$f_2 = \frac{1}{E}(2\cos 2\theta(1 - \nu^2) - 1) \quad (5.21)$$

$$f_3 = \frac{\nu}{E}; \quad f_6 = \frac{4}{E}\sin 2\theta(\nu^2 - 1)$$

The expressions of M_1, M_2 and M_3 for the isotropic case are given in equation (B.27) in Appendix B.

The derivation of equation (5.14) for the total diametral deformation U_d implies that the rock without the borehole is free to deform in the z direction when subjected to the *in situ* stress field. If this is not the case and the rock cannot deform in the z direction, i.e. $\varepsilon_{zo} = 0$, then the stress component σ_{zo} is now related to

the other five *in situ* stress components. Using equation (5.8), we have

$$\sigma_{zo} = -\frac{1}{a_{33}}(a_{31}\sigma_{xo} + a_{32}\sigma_{yo} + a_{34}\tau_{yzo} + a_{35}\tau_{xzo} + a_{36}\tau_{xyo}) \quad (5.22)$$

Substituting equation (5.22) into equation (5.14) or (5.16) and into the expressions of M_1, M_2 and M_3, the diametral deformation now depends only on five *in situ* stress components for the general case of anisotropy. When there is a plane of elastic symmetry normal to the borehole axis, the diametral deformation depends on only three stress components, e.g. σ_{xo}, σ_{yo} and τ_{xyo}. In particular, when the borehole axes are at right angles to planes of elastic symmetry, M_1, M_2 and M_3 in equation (5.15) take the form

$$M_1 = A_1\sigma_{xo} + B_1\sigma_{yo} \quad (5.23)$$

with

$$A_1 = 0.5\left[\beta_{12} + (\beta_{11}\beta_{22})^{1/2} - \beta_{11}\left(\frac{2\beta_{12}+\beta_{66}}{\beta_{11}} + 2\left(\frac{\beta_{22}}{\beta_{11}}\right)^{1/2}\right)^{1/2} - a_{11} - a_{21} + \frac{a_{31}}{a_{33}}(a_{13}+a_{23})\right];$$

$$B_1 = 0.5\left[\beta_{12} + (\beta_{11}\beta_{22})^{1/2} - (\beta_{11}\beta_{22})^{1/2}\left(\frac{2\beta_{12}+\beta_{66}}{\beta_{11}} + 2\left(\frac{\beta_{22}}{\beta_{11}}\right)^{1/2}\right)^{1/2} - a_{12} - a_{22} + \frac{a_{32}}{a_{33}}(a_{13}+a_{23})\right]$$

$$M_2 = A_2\sigma_{xo} + B_2\sigma_{yo} \quad (5.24)$$

with

$$A_2 = 0.5\left[-\beta_{12} - (\beta_{11}\beta_{22})^{1/2} - \beta_{11}\left(\frac{2\beta_{12}+\beta_{66}}{\beta_{11}} + 2\left(\frac{\beta_{22}}{\beta_{11}}\right)^{1/2}\right)^{1/2} - a_{11} + a_{21} + \frac{a_{31}}{a_{33}}(a_{13}-a_{23})\right]$$

$$B_2 = 0.5\left[\beta_{12} + (\beta_{11}\beta_{22})^{1/2} + (\beta_{11}\beta_{22})^{1/2} \times \left(\frac{2\beta_{12}+\beta_{66}}{\beta_{11}} + 2\left(\frac{\beta_{22}}{\beta_{11}}\right)^{1/2}\right)^{1/2} - a_{12} + a_{22} + \frac{a_{32}}{a_{33}}(a_{13}-a_{23})\right]$$

and

$$M_3 = A_3\tau_{xyo} \quad (5.25)$$

with

$$A_3 = -\left[\beta_{12} + (\beta_{11}\beta_{22})^{1/2} + 0.5(\beta_{11} + (\beta_{11}\beta_{22})^{1/2}) \times \left(\frac{2\beta_{12}+\beta_{66}}{\beta_{11}} + 2\left(\frac{\beta_{22}}{\beta_{11}}\right)^{1/2}\right)^{1/2} + 0.5a_{66}\right]$$

For the isotropic case, equations (5.23) to (5.25) become

$$M_1 = -\frac{1}{E}(1-\nu^2)(\sigma_{xo} + \sigma_{yo});$$

$$M_2 = -\frac{2}{E}(1-\nu^2)(\sigma_{xo} - \sigma_{yo}); \quad (5.26)$$

$$M_3 = -\frac{4}{E}(1-\nu^2)\tau_{xyo}$$

(b) Analysis of *in situ* stress measurements with the USBM gage

Pilot hole diametral deformations recorded with the USBM gage during overcoring are assumed to be equal in magnitude but opposite in sign to those that would be developed if the pre-existing *in situ* stresses were applied at a large distance from a central hole already drilled and instrumented in the rock mass. From an analytical point of view, this means that if σ_{xo}, σ_{yo}, σ_{zo}, τ_{yzo}, τ_{xzo} and τ_{xyo} are the components of the *in situ* stress field (in the coordinate system attached to the pilot hole) to be determined with the USBM gage, equation (5.14) or (5.16) can be used to relate the changes in pilot hole diameters measured with the gage to the components of the *in situ* stress

field with U_d replaced by $-U_d$. Note that in analyzing the results of USBM gages, the effect of the tangential and longitudinal displacements is neglected. Each change in diameter is assumed to be equal to two times the radial displacement.

Equation (5.14) shows that, in general, the borehole diametral deformation is a linear function of all six components of the *in situ* stress field. Therefore, determination of those components requires that we set up a system of six independent equations from the results of six independent diametral measurements. However, such measurements will not provide any information as to the precision of the calculated stress values. In order to improve the accuracy of these results, additional measurements are required and a least squares estimate of the stress components must be carried out (Gray and Toews, 1968, 1975; Panek, 1966). Least squares estimates can be treated in the same way as the problem of multilinear regression analysis.

Equation (5.15) implies that, in a single pilot hole, there are at most three independent measurements of diameter changes. Therefore it would seem possible to use two non-parallel boreholes to determine the six components of the *in situ* stress field as proposed by Panek (1966) and Leeman (1967). Let U_{d1}, U_{d2} and U_{d3} be three diametral measurements in borehole no. 1 and U_{d4}, U_{d5} and U_{d6} be three other diametral measurements in borehole no. 2. For each one of the six diametral measurements U_{di} $(i = 1,6)$, an equation similar to equation (5.14) can be written. Since the two boreholes are not parallel, the local x-, y- and z-axes in borehole no. 1 are different to those attached to borehole no. 2. Therefore, the six components of the *in situ* stress field in the global X,Y,Z coordinate system need to be related to the six diametral measurements. This can be done by combining equation (5.14) with equation (5.2) for each borehole. After rearrangement, this gives an equation of the form

$$[UD] = [T][\sigma_o]_{XYZ} \tag{5.27}$$

where $[UD]$ is a (6×1) column matrix containing the six diametral measurements U_{di} $(i = 1,6)$. $[T]$ is a (6×6) matrix whose components depend on the f_i $(i = 1,6)$ coefficients of equation (5.14) and the orientation angles β_h and δ_h of boreholes 1 and 2. It can be shown that if the rock mass of interest is isotropic, the six equations relating diametral deformations to the stress components are dependent and matrix $[T]$ in equation (5.27) is singular. Therefore, a third non-parallel borehole is always required to determine the complete state of stress. Then nine diametral measurements U_{di} $(i = 1,9)$ are made. In equation (5.27), $[UD]$ is now a (9×1) matrix and $[T]$ is a (9×6) matrix. The corresponding system of nine equations and six unknowns must be solved for the components of matrix $[\sigma_o]_{XYZ}$ by multilinear regression analysis. As shown by Draper and Smith (1966) and as summarized in section 5.5, the regression analysis gives the following system of six equations and six unknowns:

$$[T]^t[T][\sigma_o]_{XYZ} = [T]^t[UD] \tag{5.28}$$

By having nine measurements and six unknowns, it is also possible to estimate the confidence limits for the six *in situ* stress components.

As shown by Berry (1968) and Amadei (1983b), if the medium is anisotropic, the minimum number of boreholes can be reduced to two depending on the orientation of the boreholes with respect to the axes and planes of symmetry in the medium. Amadei (1983b) found, for instance, that two boreholes could be used (1) when none of the boreholes are perpendicular to planes of symmetry, or (2) when one of the boreholes is perpendicular to a plane of symmetry but is not at right angles to the other borehole.

The analysis presented above was implemented into a Fortran program called USBMA.FOR. The program runs on PCs and can be used to determine *in situ* stresses in isotropic, transversely isotropic or orthotropic rocks by overcoring a USBM gage in two or

three boreholes. The boreholes can be inclined with respect to the planes of rock anisotropy. The program calculates the least squares estimates of the principal components of the three-dimensional *in situ* stress field and their orientation with respect to a fixed X,Y,Z coordinate system such that the X- and Z-axes point in the north and east directions, respectively. The orientation of each borehole and the planes of rock anisotropy in that coordinate system are defined in Figs 5.25b and 5.25c, respectively. The program also calculates the domain of variation of each of the *in situ* stress components for different confidence limits following the statistical analysis summarized in section 5.5. Program USBMA.FOR is available (for a fee) by directly contacting B. Amadei.

(c) Determining stresses with the USBM gage in a single borehole

If there are planes of elastic symmetry normal to the x-, y- and z-axes of the pilot hole, equation (5.16) relates the change in hole diameter to four of the six *in situ* stress components. If an assumption can be made regarding one of those components, the other three stress components can be determined. As an example, consider the case when the borehole is vertical and the z-axis points downward. Assuming σ_{zo} to be equal to the overburden stress at the depth of the overcoring measurements, a system of three equations and three unknowns can be assembled to solve for the three *in situ* stress components σ_{xo}, σ_{yo} and τ_{xyo}.

With only one borehole, the three stress components σ_{xo}, σ_{yo} and τ_{xyo} in the x,y plane normal to the borehole axis can be determined exactly without making any other assumptions on the other *in situ* stress components: (1) if the x-, y- and z-axes are normal to planes of elastic symmetry in the medium, and (2) if no longitudinal strain takes place during overcoring. If those two conditions are satisfied then equation (5.15), with M_1, M_2 and M_3 defined in equations (5.23)–(5.25), can be used in the interpretation of the overcoring measurements.

For instance, let U_1, U_2 and U_3 be the values of $U_d/2a$ measured with the USBM gage at $\theta = 0°$, 60° and 120° from the x-axis, respectively (Fig. 5.27). In order to avoid introducing negative terms in all the equations derived above, a positive value of U_d now corresponds to a reduction in the pilot hole diameter. Substituting $\theta = 0°$, 60° and 120° and U_1, U_2 and U_3 into equation (5.15) gives a system of three linear equations that can be solved for M_1, M_2 and M_3, with

$$\begin{aligned} M_1 &= \frac{1}{3}(U_1 + U_2 + U_3) \\ M_2 &= \frac{1}{3}(2U_1 - U_2 - U_3) \\ M_3 &= \frac{1}{(3)^{1/2}}(U_2 - U_3) \end{aligned} \tag{5.29}$$

Note that this equation can be used for both isotropic and anisotropic media. The determination of the three stress components σ_{xo}, σ_{yo} and τ_{xyo} depends, however, on the isotropic or anisotropic nature of the medium as shown below.

For the anisotropic cases shown in Figs 5.26a, 5.26c and 5.26d (with $\psi = 0°$ and 90°), combining equations (5.29) with equations (5.23), (5.24) and (5.25), after rearrangement the three stress components σ_{xo}, σ_{yo} and τ_{xyo} are equal to

$$\begin{aligned} \sigma_{xo} &= \frac{B_1(2U_1 - U_2 - U_3)}{3(A_2B_1 - A_1B_2)} \\ &\quad - \frac{B_2(U_1 + U_2 + U_3)}{3(A_2B_1 - A_1B_2)} \\ \sigma_{yo} &= -\frac{A_1(2U_1 - U_2 - U_3)}{3(A_2B_1 - A_1B_2)} \\ &\quad + \frac{A_2(U_1 + U_2 + U_3)}{3(A_2B_1 - A_1B_2)} \\ \tau_{xyo} &= \frac{(U_2 - U_3)}{A_3(3)^{1/2}} \end{aligned} \tag{5.30}$$

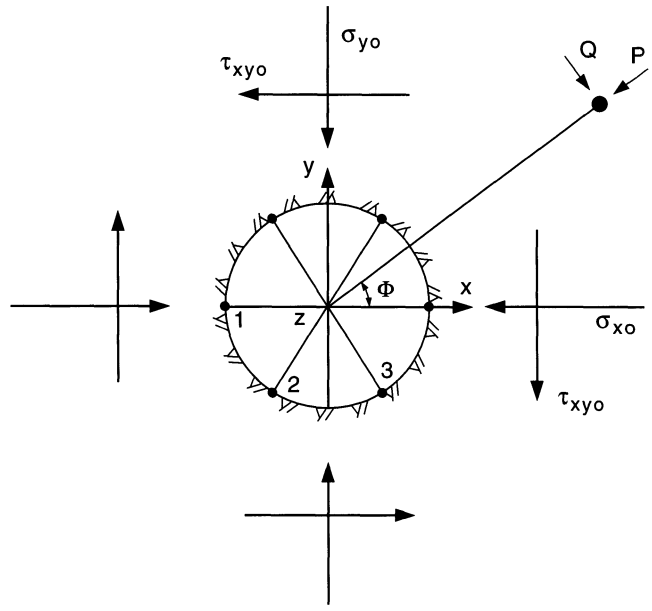

Fig. 5.27 Measurements U_1, U_2 and U_3 across diameters 1, 2 and 3 at 0°, 60° and 120° from the x-axis, respectively. The major and minor principal *in situ* stresses defined as P and Q are inclined at an angle Φ from the x-axis.

If the medium is isotropic, substituting into equation (5.29) the expressions of M_1, M_2 and M_3 defined in equation (5.26), the three stress components are now equal to

$$\begin{aligned}
\sigma_{xo} &= \frac{E}{6(\nu^2-1)}[U_1+U_2+U_3+0.5 \\
&\quad \times (2U_1-U_2-U_3)] \\
\sigma_{yo} &= \frac{E}{6(\nu^2-1)}[U_1+U_2+U_3-0.5 \\
&\quad \times (2U_1-U_2-U_3)] \\
\tau_{xyo} &= \frac{E}{4(3)^{1/2}(\nu^2-1)}[U_2-U_3]
\end{aligned} \tag{5.31}$$

The magnitude of the major and minor principal stresses P and Q in the x,y plane (Fig. 5.27) can be determined as follows:

$$\begin{aligned}
P &= \frac{(\sigma_{xo}+\sigma_{yo})}{2} + \left(\frac{(\sigma_{xo}-\sigma_{yo})^2}{4}+\tau_{xyo}^2\right)^{1/2} \\
Q &= \frac{(\sigma_{xo}+\sigma_{yo})}{2} - \left(\frac{(\sigma_{xo}-\sigma_{yo})^2}{4}+\tau_{xyo}^2\right)^{1/2}
\end{aligned} \tag{5.32}$$

and the orientation angle Φ between the major principal stress P and the x-axis is such that

$$\begin{aligned}
\cos 2\Phi &= \frac{0.5(\sigma_{xo}-\sigma_{yo})}{\left(\frac{(\sigma_{xo}-\sigma_{yo})^2}{4}+\tau_{xyo}^2\right)^{1/2}} \\
\sin 2\Phi &= \frac{\tau_{xyo}}{\left(\frac{(\sigma_{xo}-\sigma_{yo})^2}{4}+\tau_{xyo}^2\right)^{1/2}}
\end{aligned} \tag{5.33}$$

As a numerical example, consider a transversely isotropic rock mass with a plane of transverse isotropy parallel to the s,t plane of Fig. 5.25a. Tables 5.2 and 5.3 give the expressions of the coefficients a_{ij} and β_{ij} appearing in equations (5.23)–(5.25) when the plane of transverse isotropy is also parallel to the y,z plane (Fig. 5.26c with $\psi = 90°$), the x,z plane (Fig. 5.26c with $\psi = 0°$) or the x,y plane (Fig. 5.26d). These coefficients are expressed in terms of the five elastic rock properties E, E', ν, ν' and G' defined earlier in this chapter.

The modulus of elasticity E and Poisson's

Table 5.2 Expressions of coefficients a_{ij} for three orientations of the plane of transverse isotropy

	Transverse isotropy parallel to		
a_{ij}	y, z *plane*	x, z *plane*	x, y *plane*
a_{11}	$1/E'$	$1/E$	$1/E$
a_{13}	$-\nu'/E'$	$-\nu/E$	$-\nu'/E'$
a_{33}	$1/E$	$1/E$	$1/E'$
a_{22}	$1/E$	$1/E'$	$1/E$
a_{23}	$-\nu/E$	$-\nu'/E'$	$-\nu'/E'$
a_{12}	$-\nu'/E'$	$-\nu'/E'$	$-\nu/E$
a_{66}	$1/G'$	$1/G'$	$1/G$

ratio ν in the plane of transverse isotropy are taken equal to 20.0 GPa and 0.25, respectively. The ratios E/E' and G/G' are assumed to vary respectively between 1 and 4 and 1 and 3, and ν' is assumed to vary between 0.15 and 0.35. Let $U_1 = -2.343750 \times 10^{-4}$, $U_2 = -1.749399 \times 10^{-4}$ and $U_3 = -0.125601 \times 10^{-4}$ be the values of $U_d/2a$ at $\theta = 0°$, 60° and 120° measured during overcoring (negative values indicate outward radial borehole displacements). The isotropic solution for the *in situ* stress field gives $P = 2.21$ MPa, $Q = 0.79$ MPa and $\Phi = 22.5°$. Figures 5.28a, 5.28b and 5.28c show, respectively, the variations of the principal stress components P and Q and the orientation angle Φ with E/E' for different values of G/G' when $\nu = \nu' = 0.25$.

Figures 5.28a–c indicate that for a fixed value of the ratio G/G', and compared to the isotropic solution (represented by point I in those figures), P and Q decrease and Φ increases as E/E' increases when the plane of transverse isotropy is parallel to the y,z plane. When the plane of transverse isotropy is parallel to the x,z plane, P increases only slightly with E/E' whereas Q and Φ decrease. For a fixed value of E/E', P, Q and Φ always decrease as G/G' increases when the plane of transverse isotropy is parallel to either the y,z plane or the x,z plane. On the other hand, when the plane of transverse isotropy is parallel to the x,y plane, P and Q are independent of G/G' and increase with E/E'. For that orientation, it can be shown that the angle Φ is independent of the degree of rock anisotropy.

Table 5.4 gives the values of P, Q and Φ for $\nu' = 0.15$, 0.25 and 0.35, $E/E' = 3$, $G/G' = 1$ and when the plane of transverse isotropy is parallel to the y,z, x,z or x,y planes. P and Q are found to increase with ν'. The orientation angle Φ decreases as ν' increases when the plane of transverse isotropy is parallel to the y,z plane but increases with ν' when the plane of transverse isotropy is parallel to the x,z plane. It is independent of ν' when the plane of transverse isotropy is parallel to the x,y plane.

This example shows that neglecting rock anisotropy when analyzing USBM gage measurements may result in substantial errors in the magnitude and orientation of the calculated *in situ* stresses. Similar conclusions were reached by Amadei (1983a) for the analysis of

Table 5.3 Expressions of coefficients β_{ij} for three orientations of the plane of transverse isotropy

	Transverse isotropy parallel to		
β_{ij}	y, z *plane*	x, z *plane*	x, y *plane*
β_{11}	$(1 - \nu'^2 E/E')/E'$	$(1 - \nu^2)/E$	$(1 - \nu'^2 E/E')/E$
β_{22}	$(1 - \nu^2)/E$	$(1 - \nu'^2 E/E')/E'$	$(1 - \nu'^2 E/E')/E$
β_{12}	$-\nu'(1 + \nu)/E'$	$-\nu'(1 + \nu)/E'$	$-(\nu + \nu'^2 E/E')/E$
β_{66}	$1/G'$	$1/G'$	$1/G$

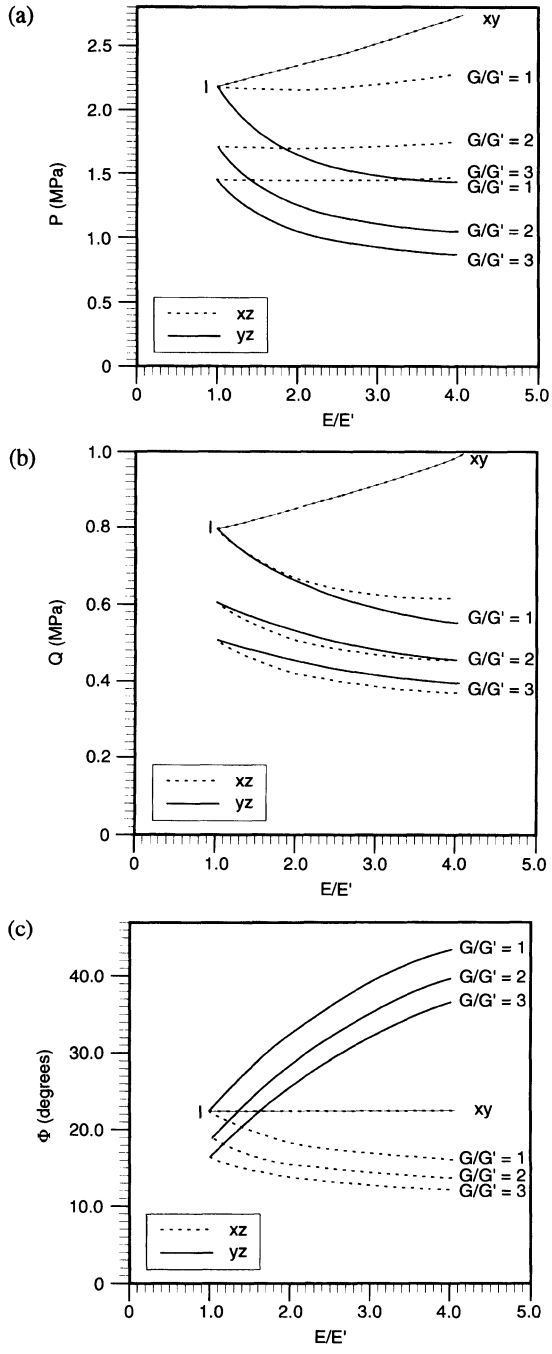

Fig. 5.28 Variation of (a) principal stress P and (b) principal stress Q with E/E' and G/G' for $\nu = \nu' = 0.25$. (c) Variation of the orientation angle Φ with E/E' and G/G' for $\nu = \nu' = 0.25$.

USBM measurements with two or three boreholes. The effect of rock anisotropy on *in situ* stress measurements by overcoring will be discussed further in section 5.7.

5.4.3 ANALYSIS OF CSIR DOORSTOPPER MEASUREMENTS

The analysis of Doorstopper measurements requires the strains measured with the three or four strain gages mounted on the bottom surface of the Doorstopper to be related to the components of the *in situ* stress field. The strains are first related to the stresses at the bottom of the hole. Then those stresses are themselves related to the *in situ* stress field components using stress concentration factors derived using photoelastic methods or three-dimensional numerical models. Both isotropic and anisotropic solutions exist for the analysis of Doorstopper measurements.

(a) Isotropic solution

Consider the geometry of Fig. 5.29 showing the end surface of a borehole on which three 45° strain gages A, B, C are glued. Let x, y, z be a coordinate system attached to the hole with the z-axis being parallel to the hole axis. If ε_A, ε_B and ε_C are respectively the strains measured in gages A, B and C, then

$$\varepsilon_x = \varepsilon_A; \quad \varepsilon_y = \varepsilon_B; \quad \gamma_{xy} = 2\varepsilon_C - (\varepsilon_A + \varepsilon_B) \tag{5.34}$$

If the rock is isotropic with Young's modulus E and Poisson's ratio ν, the stresses σ'_x, σ'_y *and* τ'_{xy} at the end of the borehole are equal to

$$\begin{aligned}
\sigma'_x &= \frac{E}{2}\left[\frac{\varepsilon_A + \varepsilon_B}{1-\nu} + \frac{\varepsilon_A - \varepsilon_B}{1+\nu}\right];\\
\sigma'_y &= \frac{E}{2}\left[\frac{\varepsilon_A + \varepsilon_B}{1-\nu} - \frac{\varepsilon_A - \varepsilon_B}{1+\nu}\right];\\
\tau'_{xy} &= \frac{E}{2}\left[\frac{2\varepsilon_C - (\varepsilon_A + \varepsilon_B)}{1+\nu}\right]
\end{aligned} \tag{5.35}$$

If a four-element 45° strain gage is used instead and ε_A, ε_B, ε_C and ε_D are the measured

Table 5.4 Values of P (in MPa), Q (in MPa) and Φ (in degrees) for different values of ν'

	Transverse isotropy parallel to								
	y, z *plane*			x, z *plane*			x, y *plane*		
	P	Q	Φ	P	Q	Φ	P	Q	Φ
$\nu' = 0.15$	1.25	0.51	40.1	1.98	0.53	15.0	2.22	0.79	22.5
$\nu' = 0.25$	1.49	0.59	39.2	2.22	0.62	16.7	2.55	0.91	22.5
$\nu' = 0.35$	1.99	0.75	37.2	2.67	0.81	20.1	3.27	1.17	22.5

strains in the 0°, 45°, 90° and 135° directions, then equation (5.35) is replaced by

$$\begin{aligned}
\sigma'_x &= \frac{E}{2}\left[\frac{\varepsilon_A + \varepsilon_C}{1-\nu} + \frac{\varepsilon_A - \varepsilon_C}{1+\nu}\right];\\
\sigma'_y &= \frac{E}{2}\left[\frac{\varepsilon_A + \varepsilon_C}{1-\nu} - \frac{\varepsilon_A - \varepsilon_C}{1+\nu}\right];\\
\tau'_{xy} &= \frac{E}{2}\frac{(\varepsilon_B - \varepsilon_D)}{1+\nu}
\end{aligned} \tag{5.36}$$

The stresses σ'_x, σ'_y and τ'_{xy} are related to the *in situ* stress components σ_{xo}, σ_{yo}, σ_{zo} and τ_{xyo} as follows (Leeman, 1971a)

$$\begin{aligned}
\sigma'_x &= a\sigma_{xo} + b\sigma_{yo} + c\sigma_{zo}\\
\sigma'_y &= a\sigma_{yo} + b\sigma_{xo} + c\sigma_{zo}\\
\tau'_{xy} &= d\tau_{xyo}
\end{aligned} \tag{5.37}$$

and are independent of the shear stresses τ_{xzo} and τ_{yzo}. Values for the coefficients a, b and c have been proposed by Galle and Wilhiot (1962), Leeman (1964c), Hoskins (1967), Bonnechere and Fairhurst (1968), Van Heerden (1969), Hiramatsu and Oka (1968), Hiltscher (1971), Coates and Yu (1970), Bonnechere (1972), Hocking (1976) and Rahn (1984), and are summarized in Table 5.5. A value of 1.25 for coefficient d was proposed by Van Heerden (1969) and Bonnechere (1967). Coefficients a, b, c and d have been determined by photoelasticity, experimentally or through finite or boundary element models. Those coefficients seem to depend slightly on the elastic constants of the rock, at least in a region not too far from the center of the hole. Hocking (1976) found that these coefficients are approximately constant over a concentric circular region on the flat end of a borehole whose radius is half that of the hole. Leeman (1971a) recommended that all strain measurements must be made in the middle third of the end of the borehole.

Combining equations (5.35), (5.37) and (5.2) and knowing the orientation of the borehole with respect to a global coordinate system, the three (or four) Doorstopper strain measurements can be linearly related to the six components of the *in situ* stress field. Since there are at most three independent strain measurements per borehole, a second borehole nonparallel to the first one is necessary to determine the *in situ* stress field. A system of six equations, similar in form to equation (5.27), can be constructed where matrix $[UD]$ is now replaced by a matrix of strain measurements. However, it can be shown that, for isotropic media, matrix $[T]$ is again singular and that a third borehole is necessary to determine the *in situ* stress field as for the USBM gage (Gray and Toews, 1968).

As for the USBM gage, if one of the four stress components σ_{xo}, σ_{yo}, σ_{zo} and τ_{xyo} is known, the other three components can be determined from overcoring the Doorstopper in a single borehole. Determination of these four components in one hole can also be achieved by following a new methodology, called the 'recovered to peak ratio' (RPR) method, proposed recently by Corthesy *et al.* (1994a, b).

A fourth independent equation was derived relating the mean recovered and peak strain invariants measured with the recovery curves and the normal stresses σ_{xo}, σ_{yo} and σ_{zo}. It can be shown that when using the RPR methodology, two instead of three boreholes can be used to determine the complete *in situ* stress field.

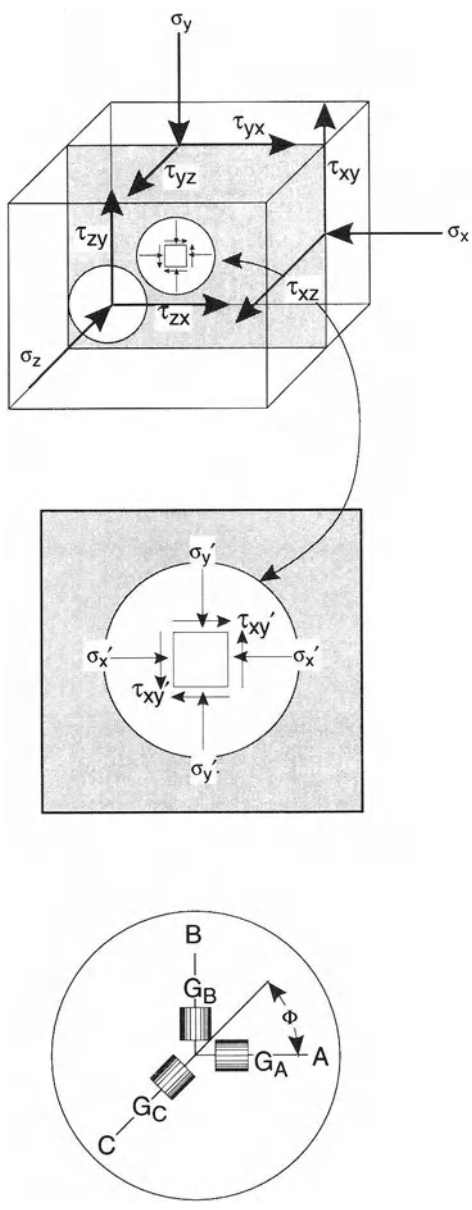

Fig. 5.29 Borehole end on which three strain gages are attached. (After Leeman, 1971a.)

(b) Anisotropic solution

For anisotropic rock masses, equation (5.34) still holds but equations (5.35) and (5.36) must be replaced by equations that depend on the symmetry of the rock mass and the orientation of its planes of anisotropy with respect to the end of the hole. For anisotropic rock masses, the stress concentration factors are more complex and depend on the elastic constants of the rock as well as on the orientation of its anisotropy planes. They cannot be determined once and for all but can be determined for each case using three-dimensional numerical models. Rahn (1984) proposed stress concentration factors for boreholes in transversely isotropic ground when the boreholes are either parallel or normal to the plane of transverse isotropy. The stress concentration factors were obtained using three-dimensional finite element analysis. Borsetto, Martinetti and Ribacchi (1984) showed that in the general case of anisotropy, ten stress concentration factors, instead of four for the isotropic solution, need to be determined using numerical methods. They also showed that, like the USBM gage, two boreholes instead of three can sometimes be used to determine the *in situ* stress field with the Doorstopper in anisotropic ground if the boreholes are properly oriented with respect to the rock anisotropy. A recent breakthrough in the analysis of Doorstopper measurements was made by Corthesy and Gill (1990) and Corthesy, Gill and Leite (1993). These authors developed a mathematical model to account for both nonlinearity and transverse isotropy in the analysis of overcoring measurements with the CSIR Doorstopper.

5.4.4 ANALYSIS OF MEASUREMENTS WITH CSIR-TYPE TRIAXIAL STRAIN CELLS

The analysis of measurements obtained with the original CSIR triaxial strain cell or modified versions of it, such as the LuT (or LuH)

Table 5.5 Summary of stress concentration factors for the Doorstopper. (Source: Rahn, W. Copyright 1984, with kind permission from Elsevier Science Ltd, The Boulevard, Langford Lane, Kidlington, UK.)

References	*Methods*	*v*	a	b	c
Galle and Wilhiot (1962)	Photoelastic experiment	0.47	1.56	0	–
Leeman (1964c)	Photoelastic experiment	0.48	1.55	0	–
		0.29	1.51	0	–
		0.26	1.53	0	–
Hoskins (1967)	Experiment	0.22	1.56	0	–
Bennechere and Fairhurst (1968)	Experiment	0.38	1.25	0	–
Van Heerden (1969)	Photoelastic experiment	0.48	1.25	−0.07	−0.85
		0.35	1.28	−0.02	−0.74
		0.30	1.24	−0.07	−0.71
		0.26	1.22	−0.10	−0.67
Hiramatsu and Oka (1968)	Experiment	0.44	1.42	−0.06	−1.10
		0.37	1.39	−0.20	−0.98
		0.29	1.32	−0.29	−0.82
		0.24	1.36	−0.30	−0.69
Coates and Yu (1970)	FEM (axisymmetric)	0.4	1.45	0.0	–0.91
		0.3	1.41	−0.04	−0.84
		0.2	1.40	−0.08	−0.75
		0.0	1.36	−0.12	−0.52
Hiltscher (1971)	Dynamic relaxation	0.45	1.45	–	−0.85
		0.4	1.35	–	−0.81
		0.3	1.28	–	−0.71
		0.2	1.25	–	−0.60
		0.1	1.21	–	−0.51
		0.0	1.19	–	−0.41
Hocking (1976)	BIEM (3D)	0.475	1.39	0.08	−0.91
		0.4	1.38	0.03	−0.82
		0.3	1.36	−0.03	−0.70
		0.2	1.35	−0.07	−0.58
		0.1	1.34	−0.10	−0.48
		0.0	1.33	−0.13	−0.37
Rahn (1984)	FEM (annular elements)	0.475	1.37	0.06	−0.86
		0.4	1.36	0.02	−0.80
		0.3	1.35	−0.03	−0.68
		0.2	1.24	−0.07	−0.57
		0.1	1.33	−0.10	−0.47
		0.0	1.32	−0.13	−0.37

gage of Leijon (1986), the SSPB cell of Hiltscher, Martna and Strindell (1979), the ANZSI cell of Mills and Pender (1986) and the AECL-modified CSIR cell of Thompson, Lang and Snider (1986) requires that the strains measured with the instrument on the pilot hole wall must be related to the six components of the *in situ* stress field. Both isotropic and anisotropic solutions have been proposed in the literature. The isotropic solution can be found in Leeman and Hayes (1966) and Hiramatsu and Oka (1968). Anisotropic solutions can be found in Berry (1968), Hirashima and Koga (1977), Van Heerden (1983) and Amadei (1983a). A general solution is presented below that can be used for the

analysis of CSIR-type triaxial strain cell measurements in orthotropic, transversely isotropic or isotropic rock masses. Furthermore, the boreholes can be inclined with respect to the planes of rock anisotropy.

The geometry of the problem being analyzed here is the same as that used for the USBM gage (Figs 5.25a–c). The rock's constitutive model is defined by equation (5.5). The *in situ* state of stress is defined by matrix $[\sigma_o]$ in the x,y,z coordinate system attached to the pilot hole and matrix $[\sigma_o]_{XYZ}$ in the global X,Y,Z coordinate system.

Let r,θ,z be a cylindrical coordinate system attached to the pilot hole. The strain components in that system are related to those in the x,y,z coordinate system as follows:

$$[\varepsilon]_{r\theta z} = [T_{r\theta z}][\varepsilon]_{xyz} \tag{5.38}$$

where $[\varepsilon]^t_{xyz} = [\varepsilon_x, \varepsilon_y, \varepsilon_z, \gamma_{yz}, \gamma_{xz}, \gamma_{xy}]$, $[\varepsilon]^t_{r\theta z} = [\varepsilon_r, \varepsilon_\theta, \varepsilon_z, \gamma_{\theta z}, \gamma_{rz}, \gamma_{r\theta}]$ and $[T_{r\theta z}]$ is a (6×6) coordinate transformation matrix for strains (equation (B.53) in Appendix B). Consider a CSIR-type triaxial strain cell as shown in Fig. 5.30a. For each strain gage i ($i = 1,N$) whose center is located at an angle θ_i from the x-axis (or α_i from the y-axis) and whose longitudinal axis is inclined at an angle ψ_i with respect to the z-axis (Fig. 5.30b), the longitudinal strain ε_{li} is related to the local strain components ε_θ, ε_z and $\gamma_{\theta z}$ as

$$\varepsilon_{li} = [0 \sin^2\psi_i \cos^2\psi_i \cos\psi_i \sin\psi_i 0\ 0][\varepsilon]_{r\theta z} \tag{5.39}$$

As shown in equation (B.36), the stress field at each point $P(a,\theta)$ along the contour of the borehole is related to the *in situ* stress field as follows:

$$[\sigma]_{xyz} = [F][\sigma_o] \tag{5.40}$$

where $[F]$ is a (6×6) matrix whose components depend on the elastic properties of the medium in the n,s,t coordinate system, the four orientation angles β_h, δ_h, β_a and ψ_a defined in Figs 5.25b and 5.25c, and the angle θ. Expressions for the coefficients of matrix $[F]$ can be found in Appendix B for both anisotropic and isotropic rocks.

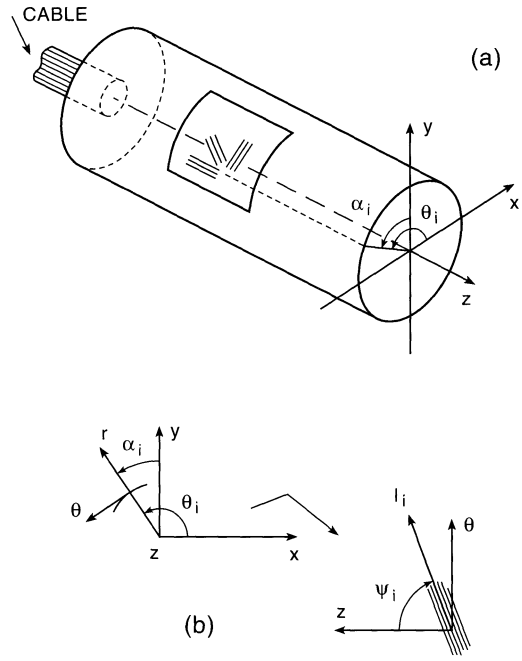

Fig. 5.30 (a) Geometry of a CSIR-type triaxial strain cell, (b) orientation of strain gages.

Combining equations (5.38), (5.39), (5.40), (5.8) and (5.2), the longitudinal strain ε_{li} in strain gage i is linearly related to the *in situ* stress field components in the X,Y,Z coordinate system as

$$\varepsilon_{li} = [0 \sin^2\psi_i \cos^2\psi_i \cos\psi_i \sin\psi_i 0\ 0] \times [T_{r\theta z}][A][F][T_\sigma][\sigma_o]_{XYZ} \tag{5.41}$$

The strains recorded with the CSIR-type cell during overcoring are assumed to be equal in magnitude but opposite in sign to those that would be developed if the pre-existing *in situ* stresses were applied at a large distance from a central hole already drilled and instrumented in the rock mass. Thus equation (5.41) can be used to relate the measured strains to the components of the *in situ* stress field with ε_{li} replaced by $-\varepsilon_{li}$.

Equation (5.41) represents the basic equation for the analysis of overcoring measurements with CSIR-type triaxial strain cells in

anisotropic or isotropic rocks. It also implies that the length of strain gage is neglected in the analysis. Equation (5.41) shows that, in general, each strain is a linear function of all six components of the *in situ* stress field. Therefore determination of those components requires that we set up a system of six independent equations from the results of six independent strain measurements. However, any additional measurements can be used to obtain a least squares estimate of the stress components. This can be done by multilinear regression analysis (Draper and Smith, 1966). Let N ($N \geq 6$) be the number of strain gages in the cell. Equation (5.41) can be written for each of the N strain gages. This leads to the following system of N equations and six unknowns:

$$[E] = [T_e][\sigma_o]_{XYZ} \tag{5.42}$$

where $[E]$ and $[T_e]$ are $(N \times 1)$ and $(N \times 6)$ matrices, respectively. As shown in Draper and Smith (1966) and as summarized in section 5.5, the least squares solution of equation (5.42) is the solution of the following system of six equations and six unknowns:

$$[T_e]^t[T_e][\sigma_o]_{XYZ} = [T_e]^t[E] \tag{5.43}$$

The analysis presented above was implemented in a Fortran program called CSIRA.FOR. The program runs on PCs and can be used to determine *in situ* stresses in isotropic, transversely isotropic or orthotropic rocks by overcoring a CSIR-type triaxial strain cell in a single borehole. The borehole can be inclined with respect to the planes of rock anisotropy. The program has been written for CSIR-type triaxial strain cells with a maximum of four strain rosettes and up to four strain gages per rosette ($N \leq 16$ in equations (5.42) and (5.43)). The program calculates the least squares estimates of the principal components of the three-dimensional *in situ* stress field and their orientation with respect to a fixed X, Y, Z coordinate system such that the X- and Z-axes point in the north and east directions, respectively. The orientation of the borehole and the planes of rock anisotropy in that coordinate system are defined in Figs 5.25b and 5.25c, respectively. The program also calculates the domain of variation of each of the *in situ* stress components for different confidence limits using the statistical analysis summarized in section 5.5. Program CSIRA.FOR is available (for a fee) by directly contacting B. Amadei. Examples of application of the program can be found in section 5.7.

5.4.5 ANALYSIS OF MEASUREMENTS WITH THE CSIRO HI CELL

The analysis of measurements obtained with the CSIRO HI cell is somewhat similar to that for the CSIR triaxial strain cell. The main difference is that the strains are no longer on the borehole surface but are embedded into the hollow epoxy. This makes the analysis more complicated. When analyzing strain measurements with the CSIRO HI cell, the geometry of Fig. 5.31 is used. The cell is assumed to have an inner diameter of 32 mm and an outer diameter of 38 mm (36 mm plus 2 mm of glue assumed to have the same elastic properties as the cell material). The strain gages are located 1.5 mm away from the borehole wall. Referring to Figs 5.17 and 5.31, the three strain rosettes A, B and C are spaced 120° along the circumference of the cell.

As for the CSIR triaxial strain cell, the position of each strain gage i ($i = 1,9$) in the CSIRO HI cell is defined by two angles defined in Fig. 5.31c: an angle θ_i between the x-axis and the center of the gage, and an angle ψ_i between the z-axis and the longitudinal axis of the gage. For the conventional CSIRO HI cell, the arrangement of strain gages gives three circumferential strain measurements ($\psi_i = 90°$), two axial strain measurements ($\psi_i = 0°$) and four additional strain measurements, three with $\psi_i = 45°$ and one with $\psi_i = 135°$.

Duncan-Fama and Pender (1980) proposed an isotropic analytical solution to relate ε_θ, ε_z and $\gamma_{\theta z}$ at any point (ρ, θ) in the cell to the six components of the *in situ* stress field $[\sigma_o]$ as

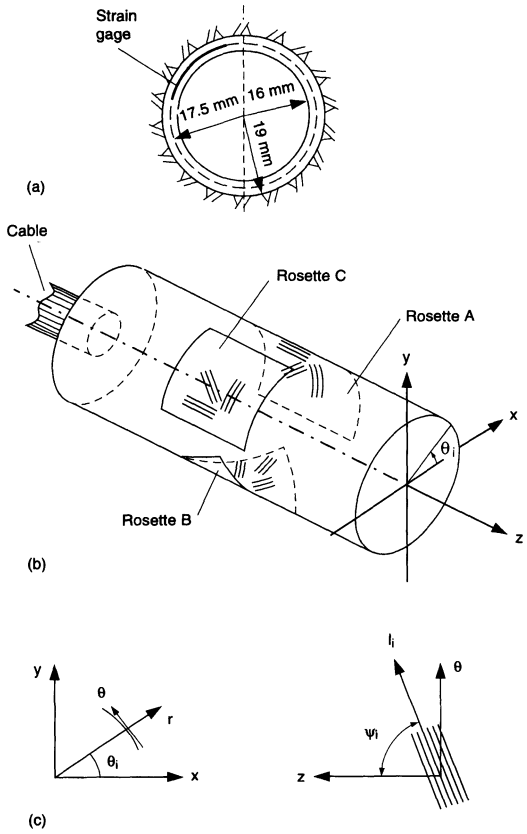

Fig. 5.31 Geometry of the CSIRO HI cell. (a) Cross-section, (b) orientation of the nine strain gages, (c) orientation angles for each strain gage.

follows:

$$
\begin{aligned}
E_2\varepsilon_\theta &= (\sigma_{xo} + \sigma_{yo})K_1(\rho) \\
&\quad - \nu_2\sigma_{zo}K_4(\rho) - 2(1-\nu_2^2) \\
&\quad \times [(\sigma_{xo} - \sigma_{yo})\cos 2\theta \\
&\quad + 2\tau_{xyo}\sin 2\theta]K_2(\rho) \qquad (5.44) \\
E_2\varepsilon_z &= \sigma_{zo} - \nu_2(\sigma_{xo} + \sigma_{yo}) \\
E_2\gamma_{\theta z} &= 4(1+\nu_2)[\tau_{yzo}\cos\theta \\
&\quad - \tau_{xzo}\sin\theta]K_3(\rho)
\end{aligned}
$$

where ρ is equal to 17.5 mm and E_2 and ν_2 are the Young's modulus and Poisson's ratio of the rock, respectively. Coefficients $K_i(\rho)$ $(i = 1,4)$ have complex analytical expressions. In general, they depend on the Poisson's ratio of the epoxy ν_1 $(=0.4)$, the inner radius of the cell R_1 $(=16\,\text{mm})$, the Poisson's ratio of the rock ν_2, the ratio between the inner and outer radii of the cell, R_1/R_2 $(=0.842)$, and the ratio between the shear modulus of the epoxy G_1 $(=1.25\,\text{GPa})$ and the shear modulus of the rock G_2. Note that approximate values of $K_i(\rho)$ were proposed by Worotnicki and Walton (1976) several years before the analytical solution of Duncan-Fama and Pender (1980) was available. Comparing equation (5.44) for the CSIRO HI cell with equation (B.54) for the CSIR cell, it can be seen that the CSIRO solution converges to the CSIR solution by simply taking $K_i(\rho) = 1$ for $i = 1,4$.

Combining equation (5.44), (5.39) and (5.2), each strain measurement in the CSIRO HI cell can then be linearly related to the six components of the *in situ* stress field in the global X,Y,Z coordinate system. Combining the results of all nine strain gages, a system of nine equations and six unknowns can be written similar to equation (5.42) where $[E]$ is now a (9×1) column matrix containing the nine strain measurements ε_{1i} $(i = 1,9)$ and $[T_e]$ is now a (9×6) matrix. The system of nine equations and six unknowns can be solved for the components of matrix $[\sigma_o]_{XYZ}$ by multilinear regression analysis (equation (5.43) and section 5.5). Note that if the four strain rosette version of the CSIRO HI cell is used instead, $[E]$ and $[T_e]$ are now (12×1) and (12×6) matrices, respectively.

An analytical solution for the analysis of strain measurements with the CSIRO HI cell in anisotropic rocks was proposed by Amadei (1983a). The solution was implemented into a mainframe computer program called ANISS.FOR developed at the CSIRO in Australia. A user's manual of the program can be found in a report by Amadei (1986).

5.4.6 MEASUREMENT OF ELASTIC PROPERTIES ON OVERCORE SAMPLES

If the rock behaves in a linearly elastic manner during biaxial tests on overcore samples (i.e.

the response curves are linear), the elastic properties of the rock can be determined using elastic solutions for the strains and displacements at the inner surface of a hollow cylinder under external axisymmetric pressure. Most of the solutions have been derived for isotropic media.

When using the USBM gage, the Young's modulus of the rock can be determined by biaxial (radial) loading of the overcore samples. Let d and D be the inner and outer diameters of an overcore. For each diametral measurement U_i $(i = 1,3)$ made with the USBM gage, the modulus is determined as follows:

$$E = 2p \cdot \frac{d}{U_i} \cdot \frac{D^2}{D^2 - d^2} \qquad (5.45)$$

where p is the pressure applied on the outer boundary of the overcore. In equation (5.45) U_i is positive for a decrease in pilot hole diameter. Equation (5.45) was derived for a hollow cylinder subject to outside axisymmetric loading in plane stress condition (e.g. Obert and Duvall, 1967).

If the CSIR triaxial strain cell or a CSIR-type cell is used instead, both the Young's modulus E and Poisson's ratio ν can be determined for each strain rosette in the cell. Let $\varepsilon_{\theta i}$ and ε_{zi} be the tangential and longitudinal strains measured in rosette i $(i = 1,2,3)$ when the pressure applied on the outer boundary of the overcore is equal to p. For that rosette, E and ν are such that

$$E = \frac{2p}{\varepsilon_{\theta i}} \cdot \frac{D^2}{D^2 - d^2}; \quad \nu = -\frac{\varepsilon_{zi}}{\varepsilon_{\theta i}} \qquad (5.46)$$

For the CSIRO HI cell, equation (5.46) is also used to obtain an estimate of the Young's modulus and Poisson's ratio. However, since the strain gages are not directly in contact with the wall of the pilot hole, correction factors for both the Young's modulus and Poisson's ratio must be introduced. Worotnicki and Walton (1979) suggested that the modulus calculated using equation (5.46) is 20–25% lower than the true rock modulus and that the Poisson's ratio is likely to be higher than the true value. A correction factor of 12% instead of 20–25% was initially proposed by Walton and Worotnicki (1978). A numerical study published more recently by Worotnicki (1993) has revealed that the correction factors can be quite complex and that the two-dimensional loading assumption inherent in the derivation of equation (5.46) may not be necessarily correct. The interaction between the CSIRO HI cell, the rock overcore and the finite loading area of the biaxial cell has been found to be quite complex.

Equations (5.45) and (5.46) were derived assuming that the rock is isotropic and linearly elastic. It is common practice to determine the elastic properties for each diametral measurement or strain rosette and average the three sets of results to obtain average values for the rock's Young's modulus and Poisson's ratio. For instance, analysis of the biaxial response curves of Fig. 5.20 (assuming the CSIRO strain rosettes are in direct contact with the rock and there are no correction factors) gives, at an applied pressure of 5 MPa, values of the Poisson's ratio of 0.25, 0.28 and 0.24 for strain rosettes A, B and C, respectively, and an average Poisson's ratio of 0.26. The corresponding Young's moduli are 20.0, 19.6 and 19.2 GPa with an average value of 19.6 GPa.

Variations in the three values of the Young's modulus and Poisson's ratio measured during biaxial testing can serve as a qualitative indicator of rock anisotropy. Rock anisotropy can also be assessed qualitatively in two other ways.

(1) For the USBM gage, variations in pilot hole diameters can be used as an indicator of rock anisotropy. The gage can be rotated in the pilot hole and tested under different cycles of biaxial loading and unloading. The variation of diametral measurements along the circumference of the pilot hole can be compared with any fabric orientation on the overcore sample. Aggson (1977) recommended using 15° rotation increments and plotting the inverse of the square root of the

diametral deformations. If the plot is close to an ellipse, the major and minor axes of the ellipse may indicate the direction and degree of rock anisotropy.

(2) For the CSIR and CSIRO HI cells, an indicator of rock anisotropy is given by comparing the strains measured with strain gages of same orientation and by comparing the strains measured at 45° to the core axis with the values of the circumferential and axial strains (Worotnicki and Walton, 1979). If the rock is isotropic, the circumferential strains ε_{cir} must be equal and the longitudinal strain gages must show equal strain ε_{ax}. Further, the following relationship must hold:

$$\varepsilon_{45} = 0.5(\varepsilon_{ax} + \varepsilon_{cir}) \qquad (5.47)$$

e.g. the strains ε_{45} measured with the $\pm 45°$ inclined strain gages must be the same and equal to the average of the longitudinal and tangential strains. On the other hand, if the rock is anisotropic, the tangential or longitudinal strains may be different from one rosette to the other, and biaxial loading will induce a shear strain equal to $\pm 0.5\gamma_{\theta z}$ which needs to be added to the right-hand side of equation (5.47).

The anisotropic character of the rock in an overcore sample can also be inferred directly by examining the distribution of the strain–pressure or displacement–pressure curves obtained during biaxial loading. For instance, when using the USBM gage, the displacement–pressure curves should be close to each other if the rock is isotropic. If the curves are far enough apart, anisotropy may be inferred. Figure 5.32a shows a set of three response curves published by Cai, Qiao and Yu (1995) for tests carried out in the laboratory on sandstone specimens. The curves clearly indicate that the material is not isotropic, and furthermore that it has a nonlinear elastic behavior with hysteresis.

For an ideal isotropic medium and instruments such as the CSIRO HI cell, the CSIR triaxial strain cell and CSIR-type triaxial strain cells, the response curves must be grouped for strain gages of similar orientation. Further, if equation (5.47) is satisfied, the response curves for the $\pm 45°$ inclined strain gages must bisect those in the axial and circumferential directions. In practice, however, these rules are never strictly satisfied (even if the rock is isotropic) due to other phenomena such as gage debonding and gage orientation which may create deviation. As pointed out by Worotnicki (1993), deviations up to $\pm 20\%$ should be expected before inferring rock anisotropy. As an illustrative example, the distribution of the response curves in Fig. 5.20 shows that the rock under consideration can be treated for all practical purposes as isotropic. On the other hand, Fig. 5.32b shows a

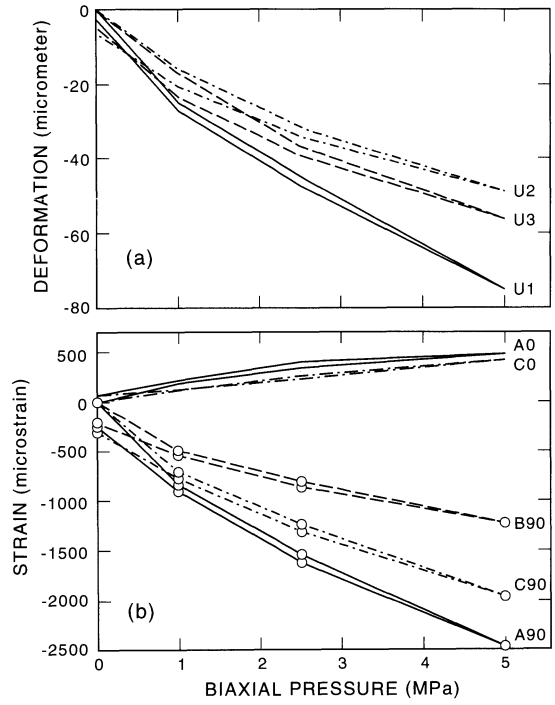

Fig. 5.32 (a) Biaxial response curves obtained with USBM gage in sandstone overcore, (b) biaxial response curves obtained with CSIRO HI cell in sandstone overcore (A, B and C correspond to the cell strain rosettes shown in Fig. 5.31). (After Cai, Qiao and Yu, 1995.)

set of biaxial response curves obtained by Cai (1990) in the laboratory using the CSIRO HI cell in a sandstone overcore. In this figure, the three tangential strains A90, B90 and C90 differ greatly, thus indicating a potential for anisotropy.

Several attempts have been described in the literature to determine quantitatively the elastic properties of anisotropic rocks during biaxial tests. The problem is complicated since the number of elastic properties is now five (transverse isotropy) or nine (orthotropy), instead of two for the isotropic case. Becker and Hooker (1967) and Becker (1968) proposed a methodology whereby the overcore sample is tested under a combination of axisymmetric loading (with internal and outer pressures) and axial loading. The overcore sample axis must be parallel and perpendicular to planes of elastic symmetry in the rock. In addition to this limitation, several approximations and simplifications were made on the elastic constants in order to reduce the number of unknowns. Recent examples of application of this methodology can be found in Cai (1990) and Worotnicki (1993).

To date, no analytical solution has been proposed for a complete determination of the elastic properties of anisotropic rocks by biaxial testing. An attempt was proposed by Amadei (1986). The idea is to use cells such as the CSIRO HI cell or the CSIR triaxial strain cell or CSIR-type triaxial strain cells with the number of independent strain measurements at least equal to the number of unknown elastic constants, i.e. five if the rock can be treated as transversely isotropic or nine if the rock can be treated as orthotropic. If the orientation of the anisotropy also needs to be inferred, additional strain measurements are required. It is noteworthy that this remark has led to the manufacture of a version of the CSIRO HI cell with 12 strain gages. A system of equations is then formed to relate the strain measurements to the five or nine elastic constants. It can be shown that the system is highly nonlinear since, unlike in isotropic elasticity, stress concentrations in anisotropic media also depend on the elastic properties. Furthermore, the system is constrained since the elastic properties of anisotropic media can only vary over certain intervals (e.g. equations (2.13)–(2.15) for transversely isotropic media). This approach is still under investigation by Amadei and co-workers using the generalized reduced gradient method, which is essentially a constrained optimization technique (Amadei, 1996).

The determination of elastic properties by biaxial testing can be complemented by borehole expansion tests (dilatometer and borehole jack) and conventional tests on core samples. The rule is to obtain core samples as close as possible to the area where the stress measurements are carried out. The core sample obtained by drilling the pilot hole can be used for that purpose. A review of different laboratory tests for the determination of elastic properties of anisotropic rocks can be found in a recent paper by Amadei (1996).

5.4.7 ANALYSIS OF SURFACE RELIEF BY UNDERCORING MEASUREMENTS

Analysis of displacement measurements obtained with the undercoring method (or stress relief by center hole method) requires that the displacements must be related to the three components of the *in situ* stress field acting parallel to the surface on which the test is conducted. Let σ_{xo}, σ_{yo} and τ_{xyo} be these stress components in an x,y coordinate system attached to the rock surface (Fig. 5.33). The rock is also assumed to be isotropic and linearly elastic with Young's modulus E and Poisson's ratio ν. Assuming plane stress condition, it can be shown that the radial displacement u_{rh} at point (r,θ) induced by drilling a hole of radius a is equal to

$$\frac{u_{rh}}{a} = f_1\sigma_{xo} + f_2\sigma_{yo} + f_3\tau_{xyo} \qquad (5.48)$$

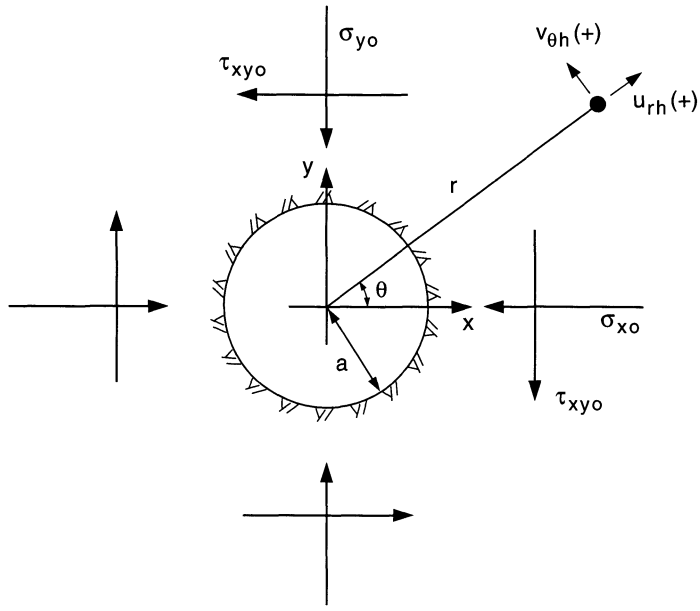

Fig. 5.33 Geometry used in the analysis of undercoring tests.

with

$$f_1 = -\frac{1}{2E}\frac{a}{r}[1 + v + H\cos 2\theta]$$

$$f_2 = -\frac{1}{2E}\frac{a}{r}[1 + v - H\cos 2\theta] \quad (5.49)$$

$$f_3 = -\frac{1}{E}\frac{a}{r}H\sin 2\theta$$

In equation (5.49), H is equal to $4 - (1 + v)a^2/r^2$.

Let U_1, U_2 and U_3 be three diametral measurements at $\theta = \theta_1$, θ_2 and θ_3 induced by drilling of the center hole. A system of three equations and three unknowns can be written as follows:

$$\begin{bmatrix} \frac{U_1}{2a} \\ \frac{U_2}{2a} \\ \frac{U_3}{2a} \end{bmatrix} = \begin{bmatrix} f_{11} & f_{21} & f_{31} \\ f_{12} & f_{22} & f_{32} \\ f_{13} & f_{23} & f_{33} \end{bmatrix} \cdot \begin{bmatrix} \sigma_{xo} \\ \sigma_{yo} \\ \tau_{xyo} \end{bmatrix} \quad (5.50)$$

This system can then be solved for the three stress components with (for the geometry of Fig. 5.23), a = 3 inch (76.2 mm) and r = 5 inch (127 mm). The magnitude of the principal stresses and their orientation with respect to the x,y coordinate system can be determined using equations (5.32) and (5.33).

A solution for the analysis of undercoring tests in anisotropic rocks was proposed by Amadei (1983a) for the situation when the planes of rock anisotropy strike either parallel or normal to the rock surface.

5.4.8 ANALYSIS OF BOREHOLE SLOTTING MEASUREMENTS

The analysis of measurements obtained with the borehole slotter requires each tangential strain measured with the instrument on the borehole wall to be related to the six components of the *in situ* stress field. The equations used for the analysis of measurements with CSIR-type triaxial strain cells can also be used for the borehole slotter.

Consider again the geometry of Figs 5.25a–c and 5.30. The rock is assumed to be anisotropic. At each point P(a,θ) along the contour

of the hole where a strain measurement i is made with the borehole slotter, the measured tangential strain $\varepsilon_{\theta i}$ is linearly related to the six components of the *in situ* stress field in the x,y,z coordinate system through an equation obtained by combining equations (5.38)–(5.40) and (5.8) with $\psi_i = 90°$. This equation can be rewritten as follows:

$$\varepsilon_{\theta i} = f_{1\theta}\sigma_{xo} + f_{2\theta}\sigma_{yo} + f_{3\theta}\sigma_{zo} + f_{4\theta}\tau_{yzo} + f_{5\theta}\tau_{xzo} + f_{6\theta}\tau_{xyo} \quad (5.51)$$

or

$$\varepsilon_{\theta i} = M_{1\theta} + M_{2\theta}\cos 2\theta + M_{3\theta}\sin 2\theta \quad (5.52)$$

It is noteworthy that equations (5.51) and (5.52) are similar in form to equations (5.14) and (5.15) for the USBM gage, respectively. They indicate that, for a general anisotropic rock, each tangential strain measurement with the borehole slotter depends on all six components of the *in situ* stress field and that there are at most three independent strain measurements per borehole. Equations (5.51) and (5.52) can be used to relate each measured tangential strain during slotting to the six components of the *in situ* stress field by simply substituting $-\varepsilon_{\theta i}$ for $\varepsilon_{\theta i}$.

When there is a plane of elastic symmetry normal to the hole axis z, such as in Figs 5.26a–d, it can be shown that $f_{4\theta}$ and $f_{5\theta}$ in equation (5.51) vanish. Thus equation (5.51) reduces to

$$\varepsilon_{\theta i} = f_{1\theta}\sigma_{xo} + f_{2\theta}\sigma_{yo} + f_{3\theta}\sigma_{zo} + f_{6\theta}\tau_{xyo} \quad (5.53)$$

If, in addition, the rock is isotropic with Young's modulus E and Poisson's ratio ν, $f_{1\theta}$, $f_{2\theta}$, $f_{3\theta}$ and $f_{6\theta}$ are equal to

$$f_{1\theta} = \frac{1}{E}[1 - 2(1+\nu^2)\cos 2\theta]$$

$$f_{2\theta} = \frac{1}{E}[1 + 2(1+\nu^2)\cos 2\theta] \quad (5.54)$$

$$f_{3\theta} = -\frac{\nu}{E}; \quad f_{6\theta} = -\frac{4}{E}(1+\nu^2)\sin 2\theta$$

Equation (5.53) indicates that for isotropic rocks or anisotropic rocks with the borehole orientation of Figs 5.26a–d, determination of the stress components in the x,y plane normal to the hole axis using the strains resulting from three cuts with the borehole slotter requires that an assumption must be made about the fourth stress component σ_{zo}. For instance, if the hole is vertical, σ_{zo} can be related to the weight of the overlying rock at the depth of measurement.

Equation (5.52) indicates that there are at most three independent strain measurements per borehole. Therefore, it would seem possible to use two non-parallel boreholes to determine the six components of the *in situ* stress field. Let $\varepsilon_{\theta 1}$, $\varepsilon_{\theta 2}$ and $\varepsilon_{\theta 3}$ be three strain measurements obtained by slotting in borehole no. 1 and $\varepsilon_{\theta 4}$, $\varepsilon_{\theta 5}$ and $\varepsilon_{\theta 6}$ be three other strain measurements obtained by slotting in borehole no. 2. For each of the six strain measurements, $\varepsilon_{\theta i}$ $(i = 1,6)$, an equation similar to equation (5.51) can be written. Since the two boreholes are not parallel, the local x-, y- and z-axes attached to borehole no. 1 differ from those attached to borehole no. 2. Therefore, the six components of the *in situ* stress field in the global X,Y,Z coordinate system need to be related to the six strain measurements. This can be done by combining equation (5.51) with equation (5.2) for each borehole. After rearrangement, this yields a system of six equations and six unknowns similar in form to equation (5.42). It can be shown that if the rock is isotropic, that system cannot be solved. A third non-parallel hole is then necessary with at least one more slotting cut. The *in situ* stress field is then determined by multilinear regression analysis of a system of N equations $(N > 6)$ and six unknowns.

Due to the similarities between the analysis of borehole slotting test results and those with the USBM gage, it would seem possible to determine the complete *in situ* stress field with two boreholes when the rock is anisotropic and the boreholes are inclined with respect to the planes of rock anisotropy (Amadei, 1983a, b).

5.5 STATISTICAL ANALYSIS OF OVERCORING MEASUREMENTS

5.5.1 LEAST SQUARES ANALYSIS

The statistical analysis of overcoring measurements is usually treated as a problem of multilinear regression analysis since we often have more measurements (in one or several boreholes) than the six *in situ* stress unknowns. The use of least squares methods for multilinear regression analysis is well documented in the mathematical statistics literature (e.g. Draper and Smith, 1966). Its application to stress measurements has been explored by Panek (1966), Gray and Toews (1968, 1975), Gray and Barron (1971) and Duvall and Aggson (1980). The highlights of the method are summarized below for the analysis of overcoring measurements. Note that the same mathematics also applies to the analysis of borehole slotting measurements.

Consider a total of N strains or displacements measured during overcoring. Using the theory of linear elasticity, these N observations are linearly related to the six *in situ* stress components (in an arbitrary global coordinate system) through the following equation:

$$[Y] = [X][b] + [\varepsilon] \tag{5.55}$$

where $[Y]$ is an $(N \times 1)$ matrix of observations, $[X]$ is an $(N \times 6)$ matrix of known form, $[b] = [\sigma_o]_{XYZ}$ is a (6×1) matrix containing the six *in situ* stress components, and $[\varepsilon]$ is an $(N \times 1)$ matrix of residual errors associated with the measurements. Possible sources of error in stress measurements were discussed in section 3.9. In least squares analysis it is further assumed that the components of matrix $[\varepsilon]$ are uncorrelated (independent) variables with zero means and common variance, an assumption that is often made but has not been properly checked when applied to the analysis of overcoring measurements (Worotnicki, 1993).

It can be shown that the least squares estimate of the stress matrix minimizes the quantity $Q = [\varepsilon]^t[\varepsilon]$ and is the solution of the following system of six equations and six unknowns:

$$[X]^t[X][b] = [X]^t[Y] \tag{5.56}$$

Solution of equation (5.56) gives the most probable values of the normal and shear stresses in the test area which best fit the observed displacement or strain data at the test site. From these six components, the most probable principal stresses and their orientation can be determined in the global coordinate system.

Knowing the most probable stress components, the expected values of the strains or displacements defined by matrix $[Y']$ can be calculated as follows:

$$[Y'] = [X][b] \tag{5.57}$$

The components of $[Y']$ are defined as Y_i' $(i = 1, N)$. The matrix of residuals $[e]$ is obtained as the difference between $[Y]$ and $[Y']$. A measure of how good the linear regression analysis is can be obtained by calculating the coefficient of multiple correlation R. The square of this quantity is called the coefficient of multiple determination and is equal to

$$R^2 = \frac{\sum_{i=1}^{N}(Y_i' - \bar{Y})^2}{\sum_{i=1}^{N}(Y_i - \bar{Y})^2} = \frac{[b]^t[X]^t[Y] - N\bar{Y}^2}{[Y]^t[Y] - N\bar{Y}^2} \tag{5.58}$$

where $\bar{Y}$ is the average of the Y_i $(i = 1, N)$ measurements. If $[e]$ is equal to $[0]$, then $R^2 = 1$. Let Q' be the minimum value of Q, which is defined as the sum of the squares about the regression. Dividing Q' by $N - 6$ gives an estimate of the variance about the regression S^2, with

$$S^2 = \frac{Q'}{N-6} = \frac{[Y]^t[Y] - [b]^t[X]^t[Y]}{N-6} \tag{5.59}$$

As long as the coefficients of matrix $[X]$ in equation (5.55) are accurately known, the value of S^2 is related to the errors associated with the strain or displacement measurements

only. The quantity S, defined as the standard deviation about the regression, enters into the calculation of the error and confidence limits for each stress component. The variance covariance matrix $[V]$ for the stress components is equal to

$$[V] = [[X]^t[X]]^{-1}S^2 \tag{5.60}$$

Using equation (5.59) as the estimated value of S^2, the square roots of the diagonal terms of $[V]$ provide the estimated standard errors s_{bi} of each stress component b_i $(i = 1,6)$ in the global coordinate system. Each off-diagonal term in matrix $[V]$ gives the estimated covariance between stress components b_i and b_j $(i \neq j)$.

If it is assumed that the error matrix $[\varepsilon]$ follows an N-dimensional multivariate normal distribution, we can then assign $100(1-\alpha)\%$ confidence limit for each stress component b_i separately by calculating $b_i + t(N-6, 1-\alpha/2)s_{bi}$ where $t(N-6, 1-\alpha/2)$ is the $1-\alpha/2$ percentage point of a Student's t-distribution with $N-6$ degrees of freedom. In other words, the true value of each stress component is between $b_i + t(N-6,1-\alpha/2)s_{bi}$ and $b_i - t(N-6,1-\alpha/2)s_{bi}$, and this statement can be made with $100(1-\alpha)\%$ confidence.

The statistical analysis presented above was incorporated into the computer programs CSIRA.FOR and USBMA.FOR mentioned earlier. A review of other programs available in the literature, which make use of the same statistical analysis, can be found in Worotnicki (1993). Unlike the programs mentioned in this book, most previous computer programs have been limited to the analysis of overcoring tests in isotropic rock. The reader should be aware that some of those programs have the capability of rejecting abnormal observations (also known as outliers) during the analysis. Following rejections of some of the data, and as long as the number of remaining measurements is larger than six, the statistical analysis is repeated until judged acceptable by the user. As remarked by Worotnicki (1993), special caution must be taken when following such a procedure as it must be done in an unbiased manner by the user. A blind approach in removing data could result in a distorted estimate of the *in situ* stress field.

5.5.2 REMARKS

The least squares analysis summarized above provides a valuable tool for determining the best estimate of the average *in situ* stress field which best fits the measured strains or displacements. As remarked by Gray and Toews (1968), using equation (5.59) to determine the standard deviation about the regression S, and subsequently the confidence limits for each stress component, must however be taken with caution. Indeed, this can only be done if the components of matrix $[X]$ are accurately known. If this is not the case, due for instance to variability in the rock elastic constants, the quantity S can be expected to differ from its value defined in equation (5.59). As shown by Gray and Toews (1968), a better estimate of S can then be obtained by grouping and analyzing replicate measurements made in the same borehole and in the same measurement direction. An alternative method to the least squares method was then proposed by Gray and Toews (1974) to account for variability of rock conditions at three different scales: (1) at the scale of the measurements due to local inhomogeneities ('within location'), (2) from one location of measurement to the next in a single borehole ('between locations'), and (3) from one borehole to the next ('between boreholes') due to large-scale inhomogeneities.

For USBM gage and Doorstopper measurements, Gray and Toews (1968) also showed that, once the standard deviation about the regression S is determined, the precision with which stresses are determined depends greatly on the orientation of the boreholes (when three holes are required). It can be shown that the orientation of the three boreholes affects the coefficients of matrix $[[X]^t[X]]^{-1}$ in equation (5.60) and in particular

its diagonal components. Analysis of various borehole configurations has revealed that three orthogonal boreholes provide the best configuration for measuring the six *in situ* stress components with uniform precision. Four measurements in each hole at 45° from each other or three measurements at 60° from each other seem to give comparable precision. It was also observed that three coplanar boreholes at 45° from each other could also give good results. All these conclusions were reached assuming the rock to be isotropic. No such studies have been carried out for anisotropic ground, where the problem is more complex due to the directional character of the rock and also because the number of holes can sometimes be reduced from three to two (Amadei, 1983b).

The least squares approach has been, for a long time, the sole approach used in the statistical analysis of overcoring tests. More recently, alternative statistical techniques have been sought. For instance, Chambon and Revalor (1986) proposed various best-fit criteria as a substitute for the original least squares method. A more promising method was proposed by Walker, Martin and Dzik (1990) who used a Monte Carlo analysis to determine the confidence intervals for the magnitude and orientation of the average principal stresses from a group of stress measurements. The method uses a sampling of the normal probability distribution function (or pdf) estimated from several measurements carried out within a borehole. An example of Monte Carlo analysis of six stress measurements conducted at the URL in Canada is shown in Fig. 3.7. More recently, an alternative approach to the method of Walker, Martin and Dzik (1990) has been proposed by Jupe (1994) who uses a statistical technique called 'jacknifing'. This approach differs from the Monte Carlo analysis in that, among other things, no assumption is necessary regarding the form of the pdf. An example conducted by Jupe (1994) showed that his approach did not yield large differences in the prediction of *in situ* stresses compared with the Monte Carlo solution.

5.6 EFFECT OF NONLINEARITY ON OVERCORING RESULTS

The analysis of overcoring tests relies on the assumption that the response of the rock is linearly elastic during the unloading process associated with overcoring. This may not always be true in practice and will depend greatly on the rock type and the rock condition, as well as on the magnitude of the *in situ* stress field. In addition to elastic deformation, rocks may experience plastic flow and/or time-dependent response. The problem is further complicated if the measuring instrument is attached to the rock and also experiences plastic flow and/or creep (Motahed *et al.*, 1990; Spathis, 1988).

Different types of non-ideal rock behavior may be observed during overcoring. In fact, rocks may behave quite differently during unloading than during loading. The rock may show, for instance, elastic but nonlinear behavior. Some anisotropic rocks whose anisotropy is derived from preferential microcracks may show such behavior. These rocks show stiffening and a decrease in anisotropy with increasing confinement as cracks are being closed. This phenomenon has been well documented in the literature over the past 20 years (see review by Amadei, 1996). Microcracks may also develop in the overcore rock if it has been subjected to high stresses. Martin, Read and Lang (1990), Martin and Chandler (1993) and Martin and Simmons (1993) discuss the importance of this phenomenon in the analysis of overcoring measurements in the granite at the URL in Canada. Another option for the rock is to be elastic and show hysteresis with an unloading curve different from the loading curve. The rock may also show plastic behavior during loading and elastic behavior upon unloading.

Departure from linear elastic behavior with plastic and time-dependent response has been

observed in rocks containing microcracks, weak and soft clay-bearing rocks, porous rocks and evaporitic rocks such as salt or potash. The response of such rocks during overcoring depends not only on the stress level *in situ*, but also on the stress path and stress history, the loading and unloading rate, time, temperature, moisture, etc. Unless the effect of all these parameters can be quantified, *in situ* stresses cannot be expected to be determined with much accuracy. Neglecting altogether the complex constitutive behavior of a rock by assuming that it behaves as linearly elastic (as has often been done in the past) may yield erroneous stress predictions when analyzing overcoring results.

Plastic deformation of borehole walls may create problems in addition to the analysis of the overcoring measurements themselves. For instance, stress measurements may become impossible if yielding of the borehole wall and borehole end occur. This may result in flaking of the borehole wall or core disking, thus creating a depth threshold beyond which stresses cannot be measured (Hast, 1979). Yielding of borehole walls also represents a challenge to the assumption made in section 5.4 that the size of the overcoring diameter does not affect the analysis of overcoring tests. Even if the measuring instrument can be considered as soft, one can say with certainty that if yielding of the rock occurs in the wall of the pilot hole, the size of the overcore diameter will have an effect. Based on elastoplastic finite element studies, Grob, Kovari and Amstad (1975) concluded that the effect of yielding is considerably smaller for large overcores than for small overcores.

Analytical solutions for the analysis of overcoring tests in non-ideal media are limited. In fact, very few analytical or semi-analytical solutions exist in the literature that can predict the response of a circular hole in a medium that is not linearly elastic. Existing solutions often make approximations and assumptions in order to reduce the complexity of the problem (Barla and Wane, 1968; Brown, Bray and Santarelli, 1989; Detournay and Fairhurst, 1987; Popov, 1979; Rechsteiner and Lombardi, 1974; Sulem, Panet and Guenot, 1987; Yamatomi *et al.*, 1988), and are therefore of limited value as far as the analysis of overcoring tests is concerned.

Some authors have proposed using an iterative (quasi-linear) algorithm when analyzing overcoring tests in nonlinear elastic rocks. Starting with a first set of (secant) elastic properties, the stresses are determined assuming linear elasticity. Knowing the stress range, new (secant) elastic properties are calculated from the nonlinear stress–strain unloading curves. The process is repeated until successful convergence is reached. Examples of application of this iterative method can be found in Martinetti, Martino and Ribacchi (1975), Aggson (1977), and Gonano and Sharp (1983).

Leeman and Denkhaus (1969) proposed an analytical solution to analyze CSIR Doorstopper and CSIR triaxial strain cell measurements in nonlinear elastic and isotropic media. In their solution the nonlinearity is handled by taking the bulk and shear moduli of the rock as power series functions of octahedral normal and shear strains. An extension to this approach was proposed more recently by Corthesy and Gill (1990) and Corthesy, Gill and Leite (1993) where a mathematical model (including both numerical and analytical components) was developed to handle both nonlinearity and transverse isotropy in the analysis of overcoring measurements with the CSIR Doorstopper. Nonlinear functions were used to relate mean strains and mean stresses, deviatoric strains and deviatoric stresses, and also the interaction between mean strains and deviatoric stresses and deviatoric strains and mean stresses which need to be accounted for in anisotropic media. A procedure was described to determine those functions in the field by biaxial loading tests on core samples still attached to the CSIR Doorstopper. The methodology has been applied to the analysis of stress measurements on samples of Barre granite and rock salt. For both rocks, Corthesy

and Gill (1991) reported that errors ranging between 5 and 10% could result if the anisotropic and nonlinear rock behavior was ignored in the analysis of overcoring measurements with the CSIR Doorstopper.

In general, the analysis of overcoring tests in rocks whose behavior departs from linear elasticity is difficult. No recommended methodology is available. A careful and thoughtful approach must be followed in order to decide whether, for the time separating drilling, overcoring and the measurements themselves, the rock can be treated as (linearly or nonlinearly) elastic or not (Corthesy and Gill, 1990; Heusermann and Pahl, 1983; Worotnicki, 1993). This can be decided based on the results of laboratory tests conducted on the rock material, and numerical simulations using various three-dimensional numerical methods.

5.7 EFFECT OF ANISOTROPY ON OVERCORING RESULTS

5.7.1 LITERATURE REVIEW

Most analyses of overcoring measurements presented in the literature assume the rock to be isotropic. However, when dealing with rocks that are clearly anisotropic, such as foliated metamorphic rocks (schists, slates, gneisses and phyllites) or stratified sedimentary rocks (shales, limestones, sandstones and coal), their directional character needs to be accounted for in the analysis of overcoring tests. Neglecting anisotropy may reduce the accuracy of stress measurements.

A basic question that has often been asked in practice is: how large an error is involved when neglecting rock anisotropy in the analysis of overcoring measurements? Several authors have tried to answer that question with various models based on the theory of linear elasticity for anisotropic media, and by treating the rock either as a transversely isotropic or orthotropic medium. Depending on the model, further assumptions have been made on the orientation of the *in situ* stress field with respect to the directions of measurements and on the orientation of the planes of rock anisotropy with respect to the boreholes in which the measurements take place. Only a limited number of models have been proposed where the anisotropy and the three- dimensional *in situ* stress field can be inclined in different directions with respect to the boreholes.

Berry and Fairhurst (1966) seem to have been the first to have considered the role of anisotropy in overcoring measurements. They presented an analytical solution for the radial displacement at the surface of a circular hole in an infinite transversely isotropic medium. The hole was assumed to be in a principal stress direction and to lie perpendicular or parallel to the planes of rock anisotropy. They found that the error in neglecting anisotropy was largest (over 50% error) when the hole was parallel to the planes of rock anisotropy and was much less when the hole was perpendicular to the planes of rock anisotropy.

The model of Berry and Fairhurst (1966) was extended by Berry (1968) who proposed a more general analytical solution for the radial displacement and strains at the surface of a circular hole in an infinite transversely isotropic medium. The hole could be inclined with respect to the *in situ* stress components and the anisotropy. However, the manner in which the orientation of the anisotropy was defined was somewhat cumbersome. Nevertheless, Berry (1968) was able to show that when using diametral deformations to measure *in situ* stresses, there are at most three independent measurements per borehole, as in the isotropic case. Furthermore, it was found that for strongly anisotropic rocks and for certain orientations of the planes of rock anisotropy, two instead of three boreholes could be used to determine the complete *in situ* stress field. These conclusions were later confirmed by Amadei (1983a, b).

The effect of anisotropy on overcoring measurements was a subject of interest to the

US Bureau of Mines in the 1960s. Becker and Hooker (1967) and Becker (1968) proposed an analytical expression for the radial displacement at the surface of a circular hole in an orthotropic medium subject to a biaxial stress field in a plane normal to the hole axis, and to a principal stress parallel to the hole axis. The planes of symmetry of the medium were assumed to be parallel and perpendicular to the hole axis. Other restrictive approximations and simplifications of the elastic constants (which may not be true) previously proposed by Kawamoto (1963) were also used in deriving the analytical solution. It was shown that the magnitude and orientation of principal stresses normal to a borehole axis (assuming an axial stress) could be determined from the results of three changes in borehole diameter during overcoring with an instrument such as the USBM gage. This procedure was used by Hooker and Johnson (1969) to determine near-surface horizontal stresses in several quarries in orthotropic rock. They concluded that isotropic versus anisotropic stress determination could differ by as much as 25% in magnitude and 25° in orientation.

Berry (1970) proposed a general solution for the stresses and strains in a solid and isotropic inclusion perfectly bonded to an anisotropic rock. Berry (1970) claimed that the solution could be used to monitor stress changes and could also be used for measuring absolute stresses by overcoring only if the inclusion was soft. A similar solution was derived by Niwa and Hirashima (1971).

Hirashima and Koga (1977) presented a general solution for the analysis of diametral measurements or strains along the surface of a borehole in anisotropic ground. They recommended using three boreholes if diametral measurements are used. Van Heerden (1983) proposed a simplified version of Hirashima and Koga's solution for the analysis of overcoring tests with the CSIR triaxial strain cell. The rock is transversely isotropic and the hole is either perpendicular or parallel to the plane of transverse isotropy. Ribacchi (1977) derived a general solution for the analysis of CSIR triaxial strain cells in generally anisotropic rocks. Numerical examples presented by Hirashima and Koga (1977), Ribacchi (1977) and Van Heerden (1983) clearly show that neglecting rock anisotropy by assuming the rock to be isotropic could lead to erroneous *in situ* predictions.

New and more general analytical solutions for the analysis of overcoring tests in anisotropic ground were proposed by Amadei (1983a, 1984, 1986). The solutions can be used for the interpretation of overcoring measurements with the USBM gage, the CSIR triaxial strain cell, the CSIRO HI cell and any other instrument that can be modeled either as a solid or a hollow inclusion. The rock can be isotropic, transversely isotropic, orthotropic or have a general type of anisotropy. The boreholes can be inclined with respect to the planes of rock anisotropy. Several (mainframe) computer programs were written. New versions of the programs (which can now be used on microcomputers) for the USBM gage, the CSIR cell and other CSIR-type triaxial strain cells called USBMA.FOR and CSIRA.FOR are now available. Large errors in the analysis of stress measurements were found if rock anisotropy was neglected. In one of his illustrative examples, Amadei (1984) reported an error of 110% for the principal stress magnitudes and 50° for their orientation. Some numerical examples showing various degrees of error are presented in section 5.7.3.

More recently, Worotnicki (1993) addressed the issue of rock anisotropy and its role in the analysis of overcoring measurements with the CSIRO HI cell. Anisotropic rocks were classified into four groups: (1) quartzofeldspathic rocks (e.g. granites, quartz and arkose sandstones, granulites and gneisses), (2) basic/lithic rocks (e.g. basic igneous rocks such as basalt; lithic and graywacke sandstones and amphibolites), (3) pelitic clay and pelitic micaceous rocks (e.g. mudstones, slates, phyllites and schists), and (4) carbonate rocks (e.g. limestones, marbles and dolomites).

Based on 200 sets of test results, Worotnicki (1993) concluded that quartzofeldspathic and basic/lithic rocks show low to moderate degrees of anisotropy, with a ratio of maximum to minimum values of the Young's modulus E_{max}/E_{min} of less than 1.3 for about 70% of the rocks analyzed and less than 1.5 in about 80%. This ratio was found not to exceed 3.5. Pelitic clay and pelitic micaceous rocks were found to show the highest degree of anisotropy, with E_{max}/E_{min} less than 1.5 for about 33% of the rocks analyzed and less than 2 in about 50%. The modulus ratio was found not to exceed 6, with most cases below 4. Finally, carbonate rocks were found to show an intermediate degree of rock anisotropy with E_{max}/E_{min} not exceeding 1.7.

Worotnicki (1993) used the equations derived by Berry (1968) for the strains at the surface of a borehole and considered the special case of a borehole directed normal or parallel to the plane of transverse isotropy of a transversely isotropic medium. By varying the ratios of the Young's and shear moduli for the rock, Worotnicki (1993) concluded that serious errors could result by neglecting rock anisotropy for rocks with a ratio of maximum to minimum Young's moduli, E_{max}/E_{min}, exceeding 1.3–1.5 (depending on the anisotropy of the shear moduli). These critical values apply when the borehole is parallel to the plane of transverse isotropy. The role of anisotropy was found to be less when the borehole is perpendicular to the plane of transverse isotropy. For comparison, Amadei (1983a, b) recommended, as a rule of thumb, a critical value $E_{max}/E_{min} = 2$ beyond which anisotropy could not be ignored. Thus based on the aforementioned classification of anisotropic rocks of Worotnicki (1993), it would seem that neglecting rock anisotropy by assuming isotropy could be justified somewhat for most (but not all) quartzofeldspathic and basic/lithic rocks. On the other hand, for pelitic and carbonate rocks, neglecting rock anisotropy may yield in most cases (but not in all cases) unacceptable errors.

The role of anisotropy on stress measurements with the CSIR Doorstopper was investigated by Barla and Wane (1970), Ribacchi (1977), Rahn (1984) and Borsetto, Martinetti and Ribacchi (1984). Because of the three-dimensionality of the problem, the stress concentration factors necessary to relate the stresses at the end of the hole on which the Doorstopper is located to the *in situ* stress field need to be determined using three-dimensional numerical models. This needs to be done for each case of anisotropy (orientation and magnitude). For transversely isotropic rocks, ten stress concentration factors are required (Borsetto, Martinetti and Ribacchi 1984). Large errors were reported on case studies conducted by the authors if the rock anisotropy was ignored. For instance, Rahn (1984) reported errors on the magnitude of principal stresses ranging between 45 and 116% and up to 20° for their orientation. Borsetto, Martinetti and Ribacchi (1984) also showed that, like the USBM gage, two boreholes instead of three can sometimes be used to determine the *in situ* stress field with the Doorstopper in anisotropic ground if the boreholes are properly oriented with respect to the rock anisotropy.

5.7.2 LABORATORY AND FIELD STUDIES

In general, overcoring in anisotropic rock formations is more difficult than in isotropic rocks. Major difficulties can be encountered for instance during drilling, coring and preparation of samples of anisotropic rocks, in particular if the rock is weak and possesses planes of weakness. Cracks may also develop along the fabric during unloading of the overcore, thus invalidating the stress measurements altogether. In highly stressed ground, and boreholes perpendicular to the rock fabric, core disking parallel to the rock fabric may prevent stress measurements altogether.

Compared with isotropic rocks, determination of the elastic properties of the rock is also more complex. In order to reduce the number of elastic properties that need to be

determined (five for transversely isotropic rocks and nine for orthotropic rocks), an approximation is sometimes made in order to calculate the rocks' shear moduli. The approximation is sometimes called the St Venant approximation (e.g. Amadei, 1996) and should be used with caution. In a recent survey of elastic constants of anisotropic rocks, Worotnicki (1993) concluded that most of the published experimental data support the validity of the St Venant approximation, though with major exceptions. In the same paper Worotnicki (1993) showed that using that approximation when it was not valid, could result in large errors when determining *in situ* stresses.

In addition, anisotropic rocks tend to be heterogeneous and therefore affect the response of instruments that rely on point measurements, such as the USBM gage, the CSIR triaxial strain cell and other CSIR-type triaxial strain cells where the sensing elements are in direct contact with the rock. Finally, as discussed in section 5.6, anisotropic rocks tend to show nonlinear behavior under stress. Thus the combination of anisotropy, heterogeneity and nonlinearity may add to the inaccuracy of stress measurements and contribute to the scatter in *in situ* stress data.

An excellent experimental study of overcoring in isotropic and anisotropic (natural and synthetic) rocks under applied biaxial loads was recently conducted by Cai (1990). The latter tested in the laboratory various rocks such as coal, sandstone and marble, and rock-like materials such as cement mortar and cement concrete. Some of the synthetic overcores had artificially created longitudinal and transverse bedding planes of various thicknesses ranging between 20 and 120 mm. The stresses were calculated using the solution of Becker and Hooker (1967) and Becker (1968). The elastic properties of the different materials were determined by a combination of biaxial testing of the overcores and uniaxial testing of core samples. The tests showed that anisotropy can have a strong effect on the response of the rock to overcoring. For instance, the

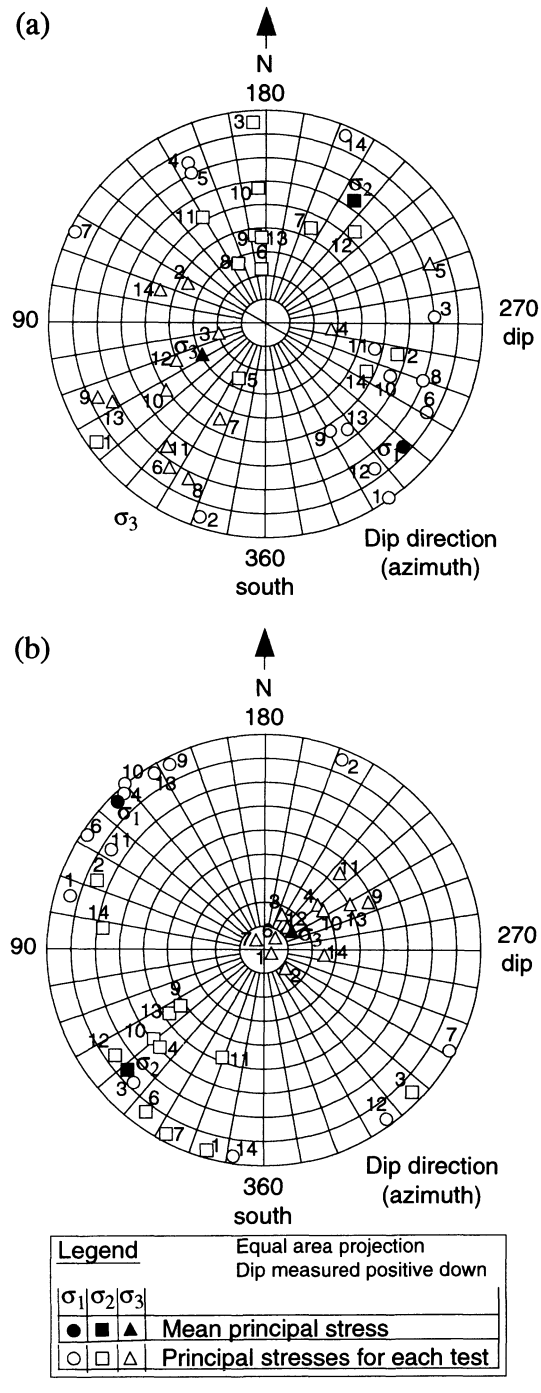

Fig. 5.34 Principal stress directions assuming isotropy in (a) and transverse isotropy in (b). Equal area lower hemisphere projection. (After Gonano and Sharp, 1983.)

relief curves in anisotropic rocks are not as predictable as for isotropic rocks with undulating shapes. The test results also showed that inclusion of rock anisotropy in the determination of the *in situ* stresses always resulted in stresses much closer to the applied stresses than with the isotropic solution.

Gonano and Sharp (1983) conducted a series of overcoring tests in weak and bedded sedimentary formations in South Africa. The *in situ* stress results were integrated into the design of a pumped storage scheme. The stresses were determined using the CSIR triaxial strain cell assuming the rock to be anisotropic (transversely isotropic) and nonlinearly elastic. A special effort was placed in reducing uncertainties in the stress determination by careful examination of the input data and monitoring of *in situ* conditions (temperature, moisture, etc.). Figures 5.34a and 5.34b show the principal stress directions determined assuming isotropy and anisotropy, respectively. The average stresses are also shown for comparison. It can be seen that inclusion of anisotropy changes the direction of the average stresses and reduces the dispersion in the data. In the anisotropic solution the average principal stresses are essentially subhorizontal

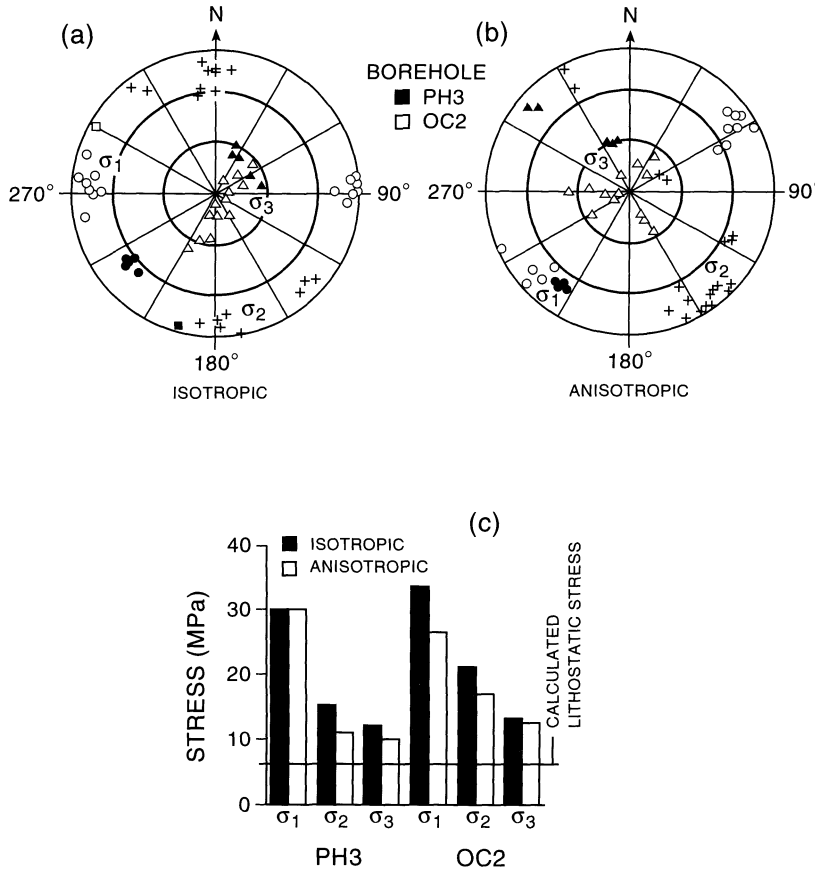

Fig. 5.35 Comparison of principal stresses obtained from overcore tests in boreholes PH3 and OC2 at the 240 level of the URL site. (a) Stress orientation assuming isotropic rock properties, (b) stress orientation assuming anisotropic rock properties, (c) comparison between stress magnitudes obtained with isotropic and anisotropic analyses. (After Martin and Simmons, 1993.)

and vertical. Gonano and Sharp (1983) also found the magnitudes to be different, with the mean principal stresses equal to 12.5, 10.6 and 8.3 MPa for the isotropic solution versus 8.7, 7.5 and 5.9 MPa for the anisotropic solution.

Another illustrative example showing the importance of anisotropy in the analysis of overcoring tests is associated with the URL site located 100 km northeast of Winnipeg, Manitoba (Canada), in the Lac du Bonnet granite batholith. An overview of the geomechanics aspects of the URL site can be found in section 9.1. A more comprehensive up-to-date review of this project can be found in Martin and Simmons (1993).

Table 5.6 Orientation of strain gages and measured strains during overcoring using a CSIR-type triaxial strain cell. The orientation angles α_i and ψ_i are defined in Fig. 5.30b

Rosette	*Strain*	α_i *(deg)*	ψ_i *(deg)*
1	-0.4565×10^{-4}	300	0
	0.6149×10^{-4}	300	90
	0.7654×10^{-4}	300	45
	-0.6070×10^{-4}	300	135
2	-0.1661×10^{-3}	180	45
	-0.9939×10^{-4}	180	135
	-0.2198×10^{-3}	180	90
	-0.4569×10^{-4}	180	0
3	-0.4565×10^{-4}	60	0
	-0.1637×10^{-3}	60	90
	-0.1400×10^{-3}	60	45
	-0.6935×10^{-4}	60	135

At the 240 Level of the URL site, the granite was found to be anisotropic due to pervasive (stress relief-induced) microcracks which were found to be aligned with a major joint set. The rock was modeled as transversely isotropic with the plane of transverse isotropy parallel to the plane of the microcracks. The rock's secant Young's modulus in the direction perpendicular to the plane of rock anisotropy was 30 GPa, which was about 50% of that in the direction parallel to the plane. The Poisson's ratios parallel and perpendicular to the plane of rock anisotropy were equal to 0.25 and 0.15, respectively. Overcoring results obtained in two boreholes OC2 and PH3, 20 m apart, were analyzed assuming isotropic and anisotropic conditions. The isotropic and anisotropic analyses are shown in Figs 5.35a and 5.35b, respectively. These two figures indicate that inclusion of anisotropy creates a 45° rotation of the stress field and yields consistent results in both boreholes. Inclusion of anisotropy also results in less scatter, which is consistent with that reported by Gonano and Sharp (1983). Further, as discussed by Martin and Simmons (1993) and as shown in Fig. 5.35c, the magnitude of each principal stress was found to be reduced if the anisotropy was taken into account.

5.7.3 NUMERICAL EXAMPLES

Numerical examples are presented below to illustrate further the role of anisotropy in the analysis of overcoring measurements. The examples were run using program CSIRA.FOR mentioned earlier. The geometry

Table 5.7 Magnitude of the three *in situ* principal stresses (in MPa) for different values of E/E' and G/G'; first numerical example; the case $E/E' = G/G' = 1$ corresponds to isotropy

	G/G′ = *1*				G/G′ = *2*			
	E/E′ = *1*	E/E′ = *1.5*	E/E′ = *2*	E/E′ = *3*	E/E′ = *1*	E/E′ = *1.5*	E/E′ = *2*	E/E′ = *3*
σ_1	3.83	3.87	3.93	4.14	3.04	3.08	3.15	3.34
σ_2	3.07	3.26	3.42	3.78	2.57	2.65	2.74	2.93
σ_3	0.24	0.32	0.38	0.51	0.33	0.37	0.41	0.48

used in all the examples is that of Figs 5.25a–c. The rock is assumed to be transversely isotropic with the five elastic properties E, E', ν, ν' and G' defined in section 5.4.2.

A CSIR-type triaxial strain cell is placed in a borehole assumed to be parallel to the Z (east) direction of Figs 5.25a–c ($\beta_h = 90°$; $\delta_h = 0°$). The cell is assumed to contain three rosettes at 120° from each other. Each rosette contains four strain gages. The orientation of the 12 strain gages and the magnitude of the strains recorded during overcoring are given in Table 5.6. The *in situ* stress field was determined using program CSIRA.FOR by solving equation (5.43) with $N = 12$.

In the first numerical example, the plane of rock anisotropy (or plane of transverse isotropy) is assumed to be horizontal ($\psi_a = 0°$ in Fig. 5.25c), and to be parallel to the borehole. The rock elastic properties are such that $E = 35$ GPa, $\nu = 0.25$ and $G = 14$ GPa. The ratio E/E' was taken equal to 1, 1.5, 2 or 3. The ratio G/G' was taken equal to 1 or 2. The Poisson's ratio ν' was taken equal to 0.25 (for the isotropic case) or 0.27 (for the anisotropic cases). Table 5.7 and Fig. 5.36 give respectively the magnitude and orientation of the three principal stresses for different values of E/E' and G/G'.

Table 5.7 indicates that for a given value of G/G', the magnitude of the stresses increases with E/E' or, in other words, as the rock becomes more deformable in the direction perpendicular to the plane of rock anisotropy (vertical direction in the present case). The error involved in neglecting anisotropy by assuming isotropy can be large. For instance, Table 5.7 shows that when $E/E' = 3$ and $G/G' = 1$, the errors in σ_1, σ_2 and σ_3 are 8, 23 and 112%, respectively.

Figures 5.36a and 5.36b give the orientation of the principal stresses using the lower hemisphere stereographic projection when $G/G' = 1$ and 2, respectively. For a given value of G/G', both σ_1 and σ_2 rotate as E/E' increases, whereas the orientation of σ_3 is essentially unaffected by the rock anisotropy.

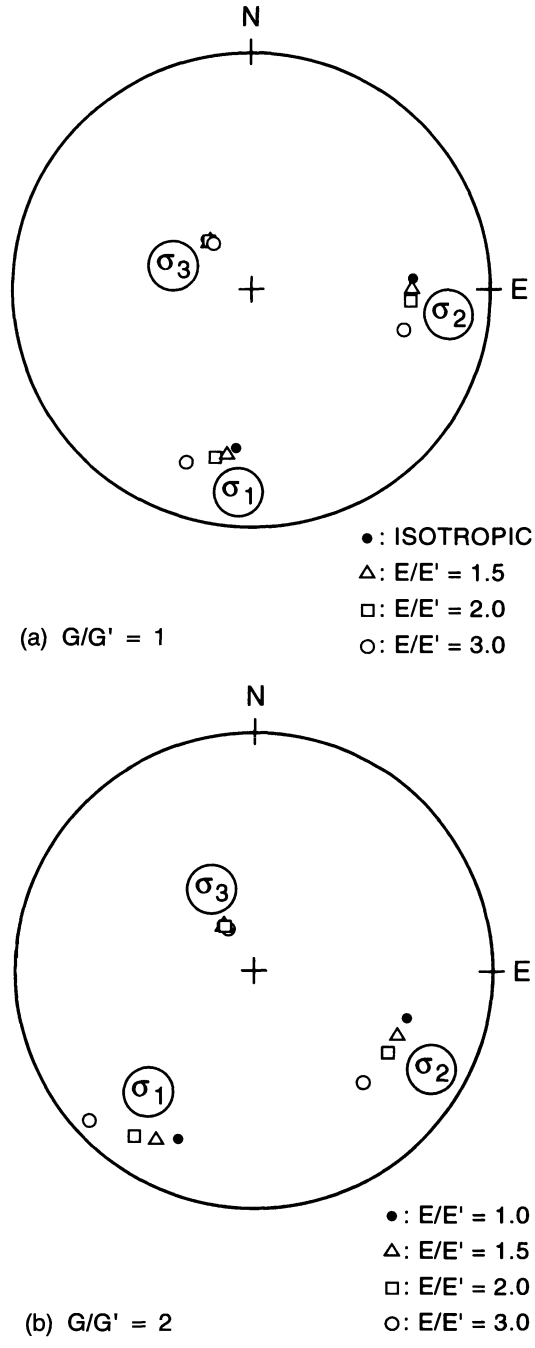

Fig. 5.36 Orientation of principal stresses σ_1, σ_2 and σ_3 for $E/E' = 1$, 1.5, 2 and 3 and $G/G' = 1$ and 2 in (a) and (b), respectively. The isotropic case corresponds to $E/E' = G/G' = 1$. Lower hemisphere stereographic projection, first numerical example.

Table 5.8 Magnitude of the three *in situ* principal stresses (in MPa) for different values of β_a ranging between 0 and 90°. Second numerical example with $E/E' = G/G' = 2$; the isotropic case is shown for comparison; the plane of rock anisotropy dips at an angle $\psi_a = 30°$

	Isotropic	$\beta_a = 0°$	$\beta_a = 15°$	$\beta_a = 30°$	$\beta_a = 45°$	$\beta_a = 60°$	$\beta_a = 75°$	$\beta_a = 90°$
σ_1	3.83	3.08	3.10	3.14	3.20	3.28	3.36	3.44
σ_2	3.07	2.38	2.47	2.58	2.71	2.84	2.96	3.06
σ_3	0.24	0.29	0.33	0.38	0.43	0.47	0.49	0.49

Figure 5.36a shows that when $G/G' = 1$, neglecting rock anisotropy by assuming isotropy results in a maximum error of 15° for the bearing of σ_1, 18° for σ_2 and 3° for σ_3.

In the second numerical example, the rock is transversely isotropic with $E = 35$ GPa, $E' = 17.5$ GPa, $\nu = 0.25$, $\nu' = 0.27$, G = 14 GPa and G′ = 7 GPa. Thus both E/E' and G/G' are equal to 2. The plane of rock anisotropy (plane of transverse isotropy) dips at an angle $\psi_a = 30°$ and its dip direction angle β_a varies between 0° (anisotropy parallel to the borehole) and 90° (anisotropy perpendicular to the borehole). Table 5.8 and Fig. 5.37 give respectively the magnitude and orientation of the three principal stresses for different values of β_a. The isotropic case is also shown for comparison.

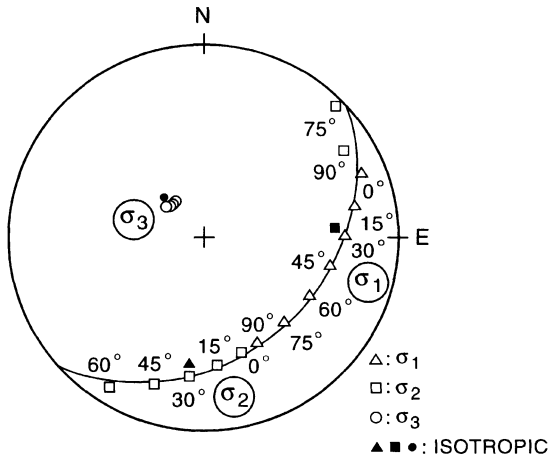

Fig. 5.37 Orientation of principal stresses σ_1, σ_2 and σ_3 when the plane of rock anisotropy dips at an angle $\psi_a = 30°$ and its dip direction angle β_a varies between 0 and 90°. The isotropic solution is also shown for comparison. Lower hemisphere stereographic projection, second numerical example.

Table 5.8 indicates that the magnitude of σ_1, σ_2 and σ_3 depends greatly on the orientation of the plane of rock anisotropy with respect to the borehole. Neglecting rock anisotropy by assuming isotropy results in a maximum error of 19% for σ_1 (when $\beta_a = 0°$), 22% for σ_2 (when $\beta_a = 0°$) and 104% for σ_3 (when $\beta_a = 90°$). Figure 5.37 indicates that both σ_1 and σ_2 rotate with the plane of rock anisotropy. The rotation takes place essentially in a plane perpendicular to σ_3, which is represented by a great circle in Fig. 5.37. Note that the orientation of σ_3 is essentially unaffected by the value of β_a. Neglecting rock anisotropy by assuming isotropy results in a maximum error of 120° for the bearing of σ_1 (when $\beta_a = 0°$), 125° for σ_2 (when $\beta_a = 60°$) and 12° for σ_3 (when $\beta_a = 90°$).

5.8 TECHNICAL INFORMATION

Additional information about the different instrument devices presented in this chapter and any related equipment can be obtained by contacting directly the following manufacturers:

1. INTERFELS GMbH, Deilmanstraße 5, D-48455 Bad Bentheim, Germany: borehole slotter, CSIR-type triaxial cell, Doorstopper, dilatometers;
2. VATTENFALL, Hydropower AB, PO Box 800, S-771 28 Ludvika, Sweden: modified CSIR triaxial strain cell for large depths;
3. MINDATA Pty. Ltd., 115 Seaford Road, Seaford 3198, Victoria, Australia: CSIRO HI

cells, biaxial chamber, ANZSI cell (also available in the USA through Reliable Geo L.L.C., 241 Lynch Road, Yakima, Washington 98908-9512);

4. Rogers Arms & Machine Co., Inc., 1246 Ute Avenue, Grand Junction CO 81501, USA: USBM gage;
5. ROCTEST, 665 Pine Street, St Lambert, Quebec, Canada J4P 2P4, Canada: CSIR triaxial strain cell, AECL-modified CSIR strain cell, Doorstopper, USBM gage, dilatometers, biaxial chamber;
6. GEOKON, Inc., 48 Spencer St, Lebanon, NH 03766, USA: USBM gage.

REFERENCES

Agarwal, R. (1968) Sensitivity analysis of borehole deformation measurements of in-situ determination when affected by borehole eccentricity, in *Proc. 9th US Symp. Rock Mech.*, Golden, SME/AIME, pp. 79–83.

Aggson, J.R. (1977) Test procedures for nonlinearly elastic stress-relief overcores.US Bureau of Mines Report of Investigation RI 8251.

Amadei, B. (1983a) *Rock Anisotropy and the Theory of Stress Measurements*, Lecture Notes in Engineering, Springer-Verlag.

Amadei, B. (1983b) Number of boreholes to measure the state of stress in-situ by overcoring, in *Proc. 24th US Symp. Rock Mech.*, College Station, Association of Eng. Geologists Publ., pp. 87–98.

Amadei, B. (1984) In situ stress measurements in anisotropic rock. *Int. J. Rock. Mech. Min. Sci. & Geomech. Abstr.*, **21**, 327–38.

Amadei, B. (1985) Applicability of the theory of hollow inclusions of overcoring stress measurements in rock. *Rock Mech. Rock Eng.*, **18**, 107–30.

Amadei, B. (1986) Analysis of data obtained with the CSIRO cell in anisotropic rock masses. CSIRO Division of Geomechanics, Technical Report No. 141.

Amadei, B. (1996) Importance of anisotropy when estimating and measuring in-situ stresses in rock. *Int. J. Rock Mech. Min. Sci. & Geomech. Abstr.*, **33**, 293–325.

ASTM D 4623-86 (1994) Standard test method for determination of in-situ stress in rock mass by overcoring method – USBM borehole deformation gage. *1994 Annual Book of ASTM Standards*, Vol. 04–08, pp. 746–58.

Barla, G. and Wane, M.T. (1968) Analysis of the borehole stress-relief method in rocks with rheological properties. *Int. J. Rock Mech. Min. Sci.*, **5**, 187–93.

Barla, G. and Wane, M.T. (1970) Stress relief method in anisotropic rocks by means of gauges applied to the end of a borehole. *Int. J. Rock Mech. Min. Sci.*, **7**, 171–82.

Bass, J., Schmitt, D.R. and Ahrens, T.J. (1986) Holographic in situ stress measurements. *Geophys. J. Roy. Astron. Soc.*, **85**, 13–14.

Beaney, E.M. and Procter, E. (1974) A critical evaluation of the center hole technique for the measurement of residual stresses. *Strain*, **10**, 7–14.

Becker, R.M. (1968) An anisotropic elastic solution for testing stress relief cores. US Bureau of Mines Report of Investigation RI 7143.

Becker, R.M. and Hooker, V.E. (1967) Some anisotropic considerations in rock stress determinations. US Bureau of Mines Report of Investigation RI 6965.

Berents, H.P. and Alexander, L.G. (1967) Rock measurements and drilling techniques. *Contracting Const. Equip.*, **19**, 64–6.

Berry, D.S. (1968) The theory of stress determination by means of stress relief techniques in transversely isotropic medium. Missouri River Division, US Corps of Engineers Technical Report 5-68.

Berry, D.S. (1970) The theory of determination of stress changes in a transversely isotropic medium, using an instrumented cylindrical inclusion. Corps of Engineers, Missouri River Division, Omaha District, Technical Report MRD-1-70.

Berry, D.S. and Fairhurst, C. (1966) Influence of rock anisotropy and time dependent deformation on the stress relief and high modulus inclusion techniques of in-situ stress determination, in *Testing Techniques for Rock Mechanics, ASTM STP 402*, pp. 190–206.

Bertrand, L. and Durand, E. (1983) In situ stress measurements: comparison of different methods, in *Proc. Int. Symp. on Soil and Rock Investigations by In-Situ Testing*, Paris, Vol. 2, pp. 449–70.

Bickel, D.L. (1978) Transducer preparation and gage assembling of the Bureau of Mines three-component borehole deformation gage. US Bureau of Mines IC No. 8764.

Bielenstein, H.U. and Barron, K. (1971) In-situ stresses. A summary of presentations and discussions given in Theme I at the Conference of Structural Geology to Rock Mechanics Problems. Dept. of Energy, Mines and Resources, Mines Branch, Ottawa.

Blackwood, R.L. (1977) An instrument to measure the complete stress field in soft rock or coal in a single operation, in *Proc. Int. Symp. on Field Measurements in Rock Mechanics*, Zurich, Balkema, Rotterdam, Vol. 1, pp. 137–50.

Blackwood, R.L. (1982a) A three dimensional study of an overcored solid inclusion rock stress instrument by the Boundary Integral Equation Method, in *Proc. 4th Int. Conf. in Australia on Finite Element Methods*, Melbourne, pp. 109–13.

Blackwood, R.L. (1982b) Experience with the solid inclusion stress measurement cell in coal in Australia, in *Proc. 23rd US Symp. Rock Mech.*, Berkeley, SME/AIME, pp. 168–75.

Blackwood, R.L., Sandström, S. and Leijon, B.A. (1986) A study of the bond strength in cemented epoxy solid inclusion stress cell installations, in *Proc. Int. Symp. on Rock Stress and Rock Stress Measurements*, Stockholm, Centek Publ., Luleå, pp. 523–8.

Bock, H. (1986) In-situ validation of the borehole slotting stressmeter, in *Proc. Int. Symp. on Rock Stress and Rock Stress Measurements*, Stockholm, Centek Publ., Luleå, pp. 261–70.

Bock, H. (1993) Measuring in-situ rock stress by borehole slotting, in *Comprehensive Rock Engineering* (ed. J.A. Hudson), Pergamon Press, Oxford, Chapter 16, Vol. 3, pp. 433–43.

Bock, H. and Foruria, V. (1983) A recoverable borehole slotting instrument for in-situ stress measurements in rock, in *Proc. Int. Symp. on Field Measurements in Geomechanics*, Zurich, Balkema, Rotterdam, pp. 15–29.

Bonnechere, F.J. (1967) A comparative study of in-situ rock stress measurements, unpublished MS Thesis, University of Minnesota.

Bonnechere, F.J. (1971) The University of Liege borehole deformation cell, in *Proc. Int. Symp. on the Determination of Stresses in Rock Masses*, Lab. Nac. de Eng. Civil, Lisbon, pp. 300–306.

Bonnechere, F.J. (1972) Stress of the central region of a flat ended borehole, in *Proc. Int. Symp. on Underground Openings*, Luzern, Swiss Society for Soil Mechanics and Foundation Engineering, pp. 447–56.

Bonnechere, F.J. and Cornet, F.H. (1977) In-situ stress measurements in a borehole deformation cell, in *Proc. Int. Symp. on Field Measurements in Rock Mechanics*, Zurich, Balkema, Rotterdam, Vol. 1, pp. 151–9.

Bonnechere, F.J. and Fairhurst, C. (1968) Determination of the regional stress field from doorstopper measurements. *J. S. Afr. Inst. Min. Metall.*, **69**, 520–44.

Borecki, M. and Kidybinski, A. (1966) Problems of stress measurements in rocks taken in the Polish coal mining industry, in *Proc. 1st Cong. Int. Soc. Rock Mech. (ISRM)*, Lisbon, Lab. Nac. de Eng. Civil, Lisbon, Vol. 2, pp. 9–16.

Borsetto, M., Martinetti, S. and Ribacchi, R. (1984) Interpretation of in situ stress measurements in anisotropic rocks with the Doorstopper method. *Rock Mech. Rock Eng.*, **17**, 167–82.

Brady, B.H.G., Friday, R.G. and Alexander, L.G. (1976) Stress measurement in a bored raise at the Mount Isa Mine, in *Proc. ISRM Symposium on Investigation of Stress in Rock, Advances in Stress Measurement*, Sydney, The Institution of Engineers, Australia, pp. 12–16.

Brady, B.H.G., Lemos, J.V. and Cundall, P.A. (1986) Stress measurement schemes for jointed and fractured rock, in *Proc. Int. Symp. on Rock Stress and Rock Stress Measurements*, Stockholm, Centek Publ., Luleå, pp. 167–76.

Brown, E.T., Bray, J.W. and Santarelli, F.J. (1989) Influence of stress dependent elastic moduli on stresses and strains around axisymmetric boreholes. *Rock Mech. Rock Eng.*, **22**, 189–203.

Cai, M. (1990) Comparative tests and studies of overcoring stress measurement devices in different rock conditions, unpublished PhD Thesis, University of New South Wales, Australia.

Cai, M. and Blackwood, R.L. (1991) A technique for the recovery and re-use of CSIRO hollow inclusion cells. *Int. J. Rock Mech. Min. Sci. & Geomech. Abstr.*, **28**, 225–9.

Cai, M., Qiao, L. and Yu, J. (1995) Study and tests of techniques for increasing overcoring stress measurement accuracy. *Int. J. Rock Mech. Min. Sci. & Geomech. Abstr.*, **32**, 375–84.

Chambon, C. and Revalor, R. (1986) Statistic analysis applied to rock stress measurements, in *Proc. Int. Symp. on Rock Stress and Rock Stress Measurements*, Stockholm, Centek Publ., Luleå, pp. 397–410.

Chandler, N.A. (1993) Bored raise overcoring for in situ stress determination at the Underground Research Laboratory. *Int. J. Rock Mech. Min. Sci. & Geomech. Abstr.*, **30**, 989–92.

Choquet, P. (1994) La mesure des contraintes par la méthode du surcarottage, in *Proc. Seminaire Formation: Mesure des sollicitations et des contraintes dans les ouvrages et dans les terrains*, Ecole des Mines, Nancy, Sept. 12–16.

Coates, D.F. and Yu, Y.S. (1970) A note on the stress concentrations at the end of a cylindrical hole. *Int. J. Rock Mech. Min. Sci.*, **7**, 585–8.

Corthesy, R. and Gill, D.E. (1990) A novel approach to stress measurements in rock salt. *Int. J. Rock Mech. Min. Sci. & Geomech. Abstr.*, **27**, 95–107.

Corthesy, R. and Gill, D.E. (1991) The influence of non-linearity and anisotropy on stress measurement results, in *Proc. 7th Cong. Int. Soc. Rock Mech. (ISRM)*, Aachen, Balkema, Rotterdam, Vol. 1, pp. 451–4.

Corthesy, R., Gill, D.E. and Nguyen, D. (1990) The modified Doorstopper cell stress measuring technique, in *Proc. Conf. on Stresses in Underground Structures*, Ottawa, CANMET Publ., pp. 23–32.

Corthesy, R., Gill, D.E. and Leite, M.H. (1993) An integrated approach to rock stress measurement in anisotropic non-linear elastic rock. *Int. J. Rock Mech. Min. Sci. & Geomech. Abstr.*, **30**, 395–411.

Corthesy, R. *et al.* (1994a) First application of the RPR method of field measurements, in *Proc. 1st North Am. Rock Mech. Symp.*, Austin, Balkema, Rotterdam, pp. 385–92.

Corthesy, R. *et al.* (1994b) The RPR method for the Doorstopper technique: four or six stress components from one or two boreholes. *Int. J. Rock Mech. Min. Sci. & Geomech. Abstr.*, **31**, 507–16.

Crouch, S.L. and Fairhurst, C. (1967) A four component borehole deformation gauge for the determination of in-situ stresses in rock masses. *Int. J. Rock Mech. Min. Sci.*, **4**, 209–17.

De la Cruz, R.V. (1977) Jack fracturing technique of stress measurement. *Rock Mech.*, **9**, 27–42.

De la Cruz, R.V. (1978) Modified borehole jack method for elastic property determination in rocks. *Rock Mech.*, **10**, 221–39.

De la Cruz, R.V. (1995) Tapercoring method of determining in situ rock stresses, in *Proc. 35th US Symp. Rock Mech.*, Lake Tahoe, Balkema, Rotterdam, pp. 895–900.

De la Cruz, R.V. and Goodman, R.E. (1971) The borehole deepening method of stress measurement, in *Proc. Int. Symp. on the Determination of Stresses in Rock Masses*, Lab. Nac. de Eng. Civil, Lisbon, pp. 230–44.

Detournay, E. and Fairhurst, C. (1987) Two dimensional elastoplastic analysis of a long, cylindrical cavity under non-hydrostatic loading. *Int. J. Rock Mech. Min. Sci. & Geomech. Abstr.*, **24**, 197–211.

Draper, N.R. and Smith, H. (1966) *Applied Regression Analysis*, Wiley.

Duncan-Fama, M.E. (1979) Analysis of a solid inclusion in-situ stress measuring device, in *Proc. 4th Cong. Int. Soc. Rock Mech. (ISRM)*, Montreux, Balkema, Rotterdam, Vol. II, pp. 113–20.

Duncan-Fama, M.E. and Pender, M.J. (1980) Analysis of the hollow inclusion technique for measuring in-situ rock stress. *Int. J. Rock Mech. Min. Sci. & Geomech. Abstr.*, **17**, 113–46.

Duvall, W.I. (1974) Stress relief by center hole. Appendix in US Bureau of Mines Report of Investigation RI 7894.

Duvall, W.I. and Aggson, J.R. (1980) Least square calculation of horizontal stresses from more than three diametral deformations in vertical boreholes. US Bureau of Mines Report of Investigation RI 8414.

Fitzpatrick, J. (1962) Biaxial device for determining the modulus of elasticity of stress relief cores. US Bureau of Mines Information Circular 6128.

Gale, W.J. (1983) Measurements of the stress field in Appin and Corrimal Collieries, NSW, Australia. CSIRO Division of Geomechanics, Technical Report No. 11.

Galle, E.M. and Wilhiot, J. (1962) Stresses around a well bore due to internal pressure and unequal geostatic stresses. *J. Soc. Petrol. Eng. (AIME)*, **2**, 145–55.

Garritty, P., Irvin, R.A. and Farmer, I.W. (1985) Problems associated with near surface in-situ stress measurements by the overcoring method, in *Proc. 26th US Symp. Rock Mech.*, Rapid City, Balkema, Rotterdam, pp. 1095–102.

Gill, D.E. *et al.* (1987) Improvements to standard doorstopper and Leeman cell stress measuring techniques, in *Proc. 2nd Int. Symp. on Field Measurements in Geomechanics*, Kobe, Balkema, Rotterdam, Vol. 1, pp. 75–83.

Gonano, L.P. and Sharp, J.C. (1983) Critical evaluation of rock behavior for in-situ stress determination using overcoring methods, in *Proc. 5th Cong. Int. Soc. Rock Mech. (ISRM)*, Melbourne, Balkema, Rotterdam, pp. A241–50.

Gray, W.M. and Barron, K. (1971) Stress determination from strain relief measurements on the ends of boreholes: planning, data evaluation and error assessment, in *Proc. Int. Symp. on the Determination of Stresses in Rock Masses*, Lab. Nac. de Eng. Civil, Lisbon, pp. 183–99.

Gray, W.M. and Toews, N.A. (1968) Analysis of accuracy in the determination of the ground stress tensor by means of borehole devices, in *Proc. 9th US Symp. Rock Mech.*, Golden, SME/AIME, pp. 45–72.

Gray, W.M. and Toews, N.A. (1974) Optimization of the design and use of a triaxial strain cell for stress determination, in *Field Testing and Instrumentation of Rock*, ASTM STP 554, pp. 116–33.

Gray, W.M. and Toews, N.A. (1975) Analysis of variance applied to data obtained by means of a six element borehole deformation gage for stress determination, in *Proc. 15th US Symp. Rock Mech.*, Custer State Park, South Dakota, ASCE Publ., pp. 323–56.

Gregory, E.C. *et al.* (1983) In-situ stress measurement in a jointed basalt: the suitability of five overcoring techniques, in *Proc. Rapid Excavation and Tunneling (RETC) Conf.*, Chicago, Vol. 1, SME/AIME, pp. 42–61.

Griswold, G.N. (1963) How to measure rock pressures: new tools. *Eng. Mining J.*, **164**, 90–95.

Grob, H., Kovari, K. and Amstad, C. (1975) Sources of error in the determination of in-situ stresses by measurements. *Tectonophysics*, **29**, 29–39.

Habib, P., Phong, L.M. and Pakdaman, K. (1971) Natural stress measurements with a relaxation method, in *Proc. Int. Symp. on the Determination of Stresses in Rock Masses*, Lab. Nac. de Eng. Civil, Lisbon, pp. 135–44.

Hallbjörn, L. (1986) Rock stress measurements performed by Swedish State Power Board, in *Proc. Int. Symp. on Rock Stress and Rock Stress Measurements*, Stockholm, Centek Publ., Luleå, pp. 197–205.

Hast, N. (1943) Measuring stresses and deformations in solid materials. Centraltryckeriet, Esselte AB, Stockholm.

Hast, N. (1958) The measurement of rock pressure in mines. *Sveriges Geol. Undersokning, Ser. C*, No. 560.

Hast, N. (1979) Limit of stresses in the Earth's crust. *Rock Mech.*, **11**, 143–50.

Hawkes, I. (1968) Theory of the photoelastic biaxial strain gauge. *Int. J. Rock Mech. Min. Sci.*, **5**, 57–63.

Hawkes, I. (1971) Photoelastic strain gages and in-situ rock stress measurements, in *Proc. Int. Symp. on the Determination of Stresses in Rock Masses*, Lab. Nac. de Eng. Civil, Lisbon, pp. 359–75.

Hawkes, I. and Fellers, G.E. (1969) Theory of the determination of the greatest principal stress in a biaxial stress field using photoelastic hollow cylinder inclusions. *Int. J. Rock Mech. Min. Sci.*, **6**, 143–58.

Hawkes, I. and Moxon, S. (1965) The measurement of in situ rock stress using the photoelastic biaxial gauge with the core-relief technique. *Int. J. Rock Mech. Min. Sci.*, **2**, 405–19.

Helal, H. and Schwartzmann, R. (1983) In situ stress measurements with the CERCHAR dilatometric cell, in *Proc. Int. Symp. on Field Measurements in Geomechanics*, Zurich, Balkema, Rotterdam, pp. 127–36.

Herget, G. (1973) First experiences with the CSIR triaxial strain cell for stress determinations. *Int. J. Rock Mech. Min. Sci.*, **10**, 509–22.

Herget, G. (1993) Overcoring techniques, in *Lecture Notes of the Short Course on Modern In-Situ Stress Measurement Methods* at the 34th US Symp. Rock Mech., Madison, Wisconsin.

Heusermann, S. and Pahl, A. (1983) Stress measurements in underground openings by the overcoring method and by the flatjack method with compensation, in *Proc. Int. Symp. on Field Measurements in Geomechanics*, Zurich, Balkema, Rotterdam, pp. 1033–45.

Hiltscher, R. (1971) On the strain rosette relief method of measuring rock stresses, in *Proc. Int. Symp. on the Determination of Stresses in Rock Masses*, Lab. Nac. de Eng. Civil, Lisbon, pp. 245–64.

Hiltscher, R., Martna, J. and Strindell, L. (1979) The measurement of triaxial rock stresses in deep holes and the use of rock stress measurements in the design and construction of rock openings, in *Proc. 4th Cong. Int. Soc. Rock Mech. (ISRM)*, Montreux, Balkema, Rotterdam, Vol. 2, pp. 227–34.

Hiramatsu, Y. and Oka, Y. (1968) Determination of the stress in rock unaffected by boreholes or drifts from measured strains or deformations. *Int. J. Rock Mech. Min. Sci.*, **5**, 337–53.

Hirashima, K. and Koga, A. (1977) Determination of stresses in anisotropic elastic medium unaffected by boreholes from measured strains or deformations, in *Proc. Int. Symp. on Field Measurements in Rock Mechanics*, Zurich, Balkema, Rotterdam, Vol. 1, pp. 173–82.

Hocking, G. (1976) Three dimensional elastic stress distribution around the flat end of a cylindrical cavity. *Int. J. Rock Mech. Min. Sci. & Geomech. Abstr.*, **13**, 331–7.

Hooker, V.E. and Bickel, D.L. (1974) Overcoring equipment and techniques used in rock stress determination. US Bureau of Mines Report of Investigation RI 8618.

Hooker, V.E. and Johnson, C.F. (1969) Near surface horizontal stresses including the effects of rock anisotropy. US Bureau of Mines Report of Investigation RI 7224.

Hooker, V.E., Aggson, J.R. and Bickel, D.L. (1974) Improvements in the three component borehole deformation gage and overcoring techniques. US Bureau of Mines Report of Investigation RI 7894.

Hoskins, E. (1967) An investigation of strain relief methods of measuring rock stress. *Int. J. Rock Mech. Min. Sci.* **4**, 155–64.

Hoskins, E.R. (1968) Strain rosette relief measurements in hemispherically ended boreholes. *Int. J. Rock Mech. Min. Sci.*, **5**, 551–9.

Hoskins, E.R. and Oshier, E.H. (1973) Development of deep hole stress measurement device, in *Proc. 14th US Symp. Rock Mech.*, University Park, ASCE Publ., pp. 299–310.

Irvin, R.A., Garritty, P. and Farmer, I.W. (1987) The effect of boundary yield on the results of in-situ stress measurements using overcoring techniques. *Int. J. Rock Mech. Min. Sci. & Geomech. Abstr.*, **24**, 89–93.

Ivanov, V., Parashkevov, R. and Popov, S.N. (1983) Deformations measurement with the method of partial stress relief and geomechanical processing of the results, in *Proc. Int. Symp. on Field Measurements in Geomechanics*, Zurich, Balkema, Rotterdam, pp. 1057–61.

Jenkins, F.M. and McKibbin, R.W. (1986) Practical considerations of in-situ stress determination, in *Proc. Int. Symp. on Application of Rock Characterization Techniques in Mine Design*, AIME Publ., pp. 33–9.

Jupe, A.J. (1994) Confidence intervals for in-situ stress measurements. *Int. J. Rock Mech. Min. Sci. & Geomech. Abstr.*, **31**, 743–7.

Kaiser, P.K., Zou, D. and Lang, P.A. (1990) Stress determination by back-analysis of excavation-induced stress changes – a case study. *Rock Mech. Rock Eng.*, **23**, 185–200.

Kanagawa, T. *et al.* (1986) In-situ stress measurements in the Japanese Islands: overcoring results from a multi-element gauge used at 23 sites. *Int. J. Rock Mech. Min. Sci. & Geomech. Abstr.*, **23**, 29–39.

Kawamoto, T. (1963) On the state of stress and deformation around tunnel in orthotropic elastic ground. *Mem. Faculty of Eng., Kumamoto Univ.*, Japan, **10**, 1–30.

Kim, K. and Franklin, J.A. (coordinators) (1987) Suggested methods for rock stress determination. *Int. J. Rock Mech. Min. Sci. & Geomech. Abstr.*, **24**, 53–73.

Kobayashi, S. *et al.* (1991) In-situ stress measurement using a conical shaped borehole strain gage plug, in *Proc. 7th Cong. Int. Soc. Rock Mech. (ISRM)*, Aachen, Balkema, Rotterdam, Vol. 1, pp. 545–8.

Kovari, K., Amstad, Ch. and Grob, H. (1972) Contribution to the problem of stress measurements in rock, in *Proc. Int. Symp. on Underground Openings*, Luzern, Swiss Society for Soil Mechanics and Foundation Engineering, pp. 501–12.

Lang, P.A., Thompson, P.M. and Ng, L.K.W. (1986) The effect of residual stress and drill hole size on the in-situ stress determined by overcoring, in *Proc. Int. Symp. on Rock Stress and Rock Stress Measurements*, Stockholm, Centek Publ., Luleå, pp. 687–94.

Lee, F.T., Abel, J. and Nichols, T.C. (1976) The relation of geology to stress changes caused by underground excavation in crystalline rocks at Idaho Springs, Colorado. *US Geol. Surv. Prof. Pap.*, **965**, Washington.

Leeman, E.R. (1964a) Rock stress measurements using the trepanning stress-relieving technique. *Mine Quarry Eng.*, **30**, 250–55.

Leeman, E.R. (1964b) Absolute rock stress measurements using a borehole trepanning stress-relieving technique, in *Proc. 6th US Symp. Rock Mech.*, Rolla, University of Missouri Publ., pp. 407–26.

Leeman, E.R. (1964c) The measurement of stress in rock – Parts I, II and III. *J. S. Afr. Min. Metall.*, **65**, 45–114 and 254–84.

Leeman, E.R. (1967) The borehole deformation type of rock stress measuring instrument. *Int. J. Rock Mech. Min. Sci.*, **4**, 23–44.

Leeman, E.R. (1971a) The CSIR Doorstopper and triaxial rock stress measuring instruments. *Rock Mech.*, **3**, 25–50.

Leeman, E.R. (1971b) The measurement of stress in rock: a review of recent developments (and a bibliography), in *Proc. Int. Symp. on the Determination of Stresses in Rock Masses*, Lab. Nac. de Eng. Civil, Lisbon, pp. 200–229.

Leeman, E.R. and Denkhaus, H.G. (1969) Determination of stress in rock with linear or non-linear elastic characteristics. *Rock Mech.*, **1**, 198–206.

Leeman, E.R. and Hayes, D.J. (1966) A technique for determining the complete state of stress in rock using a single borehole, in *Proc. 1st Cong. Int. Soc. Rock Mech. (ISRM)*, Lisbon, Lab. Nac. de Eng. Civil, Lisbon, Vol. II, pp.17–24.

Leijon, B.A. (1986) Application of the LUT triaxial overcoring techniques in Swedish mines. *Proc. Int. Symp. on Rock Stress and Rock Stress Measurements*, Stockholm, Centek Publ., Luleå, pp. 569–79.

Leijon, B.A. and Stillborg, B.L. (1986) A comparative study between two rock stress measurement techniques at Luossavaara mine: *Rock Mech. Rock Eng.*, **19**, 143–63.

Lekhnitskii, S.G. (1977) *Theory of Elasticity of an Anisotropic Body*, Mir Publ., Moscow.

Lieurance, R.S. (1933) Stresses in foundation at Boulder (Hoover) dam. US Bureau of Reclamation Technical Memorandum No. 346.

Lieurance, R.S. (1939) Boulder canyon project final report, Part V (technical investigation), *Bull.*, **4**, 265–8.

Martin, C.D. and Chandler, N.A. (1993) Stress heterogeneity and geological structures. *Int. J. Rock Mech. Min. Sci. & Geomech. Abstr.*, **30**, 993–9.

Martin, C.D. and Christiansson, R. (1991) Overcoring in highly stressed granite; comparison between the USBM and CSIR devices. *Rock Mech. Rock Eng.*, **24**, 207–35.

Martin, C.D. and Simmons, G.R. (1993) The Atomic Energy of Canada Limited Underground Research Laboratory: an overview of geomechanics characterization, in *Comprehensive Rock Engineering* (ed. J.A. Hudson), Pergamon Press, Oxford, Chapter 38, Vol. 3, pp. 915–50.

Martin, C.D., Read, R.S. and Lang, P.A. (1990) Seven years of in-situ stress measurements at the URL. An overview, in *Proc. 31st US Symp. Rock Mech.*, Golden, Balkema, Rotterdam, pp. 15–25.

Martinetti, S., Martino, D. and Ribacchi, R. (1975) Determination of the original stress state in an anisotropic rock mass. *Revista de Geotecnica*, **9**, 84–98.

Mathar, J. (1934) Determination of initial stresses by measuring the deformations around drilled holes. *Trans. ASME*, **56**, 249–54.

Matsuki, K. and Sakaguchi, K. (1995) Comparison of results of in-situ stresses determined by core-based methods with those by overcoring technique, in *Proc. Int. Workshop on Rock Stress Measurement at Great Depth*, Tokyo, Japan, 8th ISRM Cong., pp. 52–7.

Merrill, R.H. (1964) In situ determination of stress by relief techniques, in *Proc. Int. Conf. State of Stress in the Earth's Crust*, Santa Monica, Elsevier, New York, pp. 343–69.

Merrill, R.H. (1967) Three component borehole deformation gage for determining the stress in rock. US Bureau of Mines Report of Investigation RI 7015.

Mills, K.W. and Pender, M.J. (1986) A soft inclusion instrument for in-situ stress measurement in coal, in *Proc. Int. Symp. on Rock Stress and Rock Stress Measurements*, Stockholm, Centek Publ., Luleå, pp. 247–51.

Mohr, H.F. (1956) Measurement of rock pressure. *Mine Quarry Eng.*, **22**, 178–89.

Motahed, P. *et al.* (1990) Stress measurement in potash by overcoring CSIRO hollow inclusion stress meters, in *Proc. 31st US Symp. Rock Mech.*, Golden, Balkema, Rotterdam, pp. 413–20.

Myrvang, A.M. (1976) Practical use of rock stress measurements in Norway, in *Proc. ISRM Symposium on Investigation of Stress in Rock, Advances in Stress Measurement*, Sydney, The Institution of Engineers, Australia, pp. 92–9.

Myrvang, A.M. and Hansen, S.E. (1990) Use of the modified doorstoppers for rock stress change measurements, in *Proc. 31st US Symp. Rock Mech.*, Golden, Balkema, Rotterdam, pp. 999–1004.

Nichols, T.C. (1983) In-situ geomechanics of crystalline and sedimentary rocks, Part IV: continued field testing of the modified USGS 3-D borehole stress probe. US Geological Survey Open File Report, Denver.

Nichols, T.C., Abel, J.F. and Lee, F.T. (1968) A solid inclusion probe to determine three dimensional stress changes at a point in a rock mass. *US Geol. Surv. Bull.*, **1258-C**.

Niwa, Y. and Hirashima, K.I. (1971) The theory of the determination of stress in an anisotropic elastic medium using an instrumented cylindrical inclusion. *Mem. Faculty of Eng., Kyoto Univ.*, Japan, **33**, 221–32.

Nolting, R.M. (1980) Absolute stress measurement in rock by overcoring cast-in-place epoxy inclusions, unpublished PhD Thesis, University of California, Berkeley.

Obara, Y. *et al.* (1991) Application of hemispherical-ended borehole technique to hot rock, in *Proc. 7th Cong. Int. Soc. Rock Mech. (ISRM)*, Aachen, Balkema, Rotterdam, Vol. 1, pp. 587–90.

Obara, Y. *et al.* (1995) Measurement of stress distribution around fault and considerations, in *Proc. 2nd Int. Conf. on the Mechanics of Jointed and Faulted Rock*, Vienna, Balkema, Rotterdam, pp. 495–500.

Obert, L. and Duvall, W.I. (1967) *Rock Mechanics and the Design of Structures in Rock*, Wiley.

Obert, L., Merrill, R.H. and Morgan, T.A. (1962) Borehole deformation gauge for determining the

stress in mine rock. US Bureau of Mines Report of Investigation RI 5978.

Odum, J.K., Lee, F.T. and Stone, J.W. (1992) Adaptations to standard drilling equipment and procedures for a USBM overcore in situ stress determination under unique conditions. *Int. J. Rock. Mech. Min. Sci. & Geomech. Abstr.*, **29**, 73–6.

Olsen, O.J. (1949) Residual stresses in rock as determined from strain relief measurements on tunnel walls, unpublished MS Thesis, Univ. of Colorado, Boulder.

Olsen, O.J. (1957) Measurement of residual stress by the strain relief method. *Quarterly Colorado School of Mines*, **52**, 183–204.

Pahl, A. (1977) In situ stress measurements by overcoring inductive gages, in *Proc. Int. Symp. on Field Measurements in Rock Mechanics*, Zurich, Balkema, Rotterdam, Vol. 1, pp. 161–71.

Pahl, A. and Heusermann, S. (1993) Determination of stress in rock salt taking time-dependent behavior into consideration, in *Proc. 7th Cong. Int. Soc. Rock Mech. (ISRM)*, Aachen, Balkema, Rotterdam, Vol. 3, pp. 1713–18.

Palmer, J.H.L. and Lo, K.Y. (1976) In situ stress measurements in some near-surface rock formations – Thorold, Ontario. *Can. Geotech. J.*, **13**, 1–7.

Panek, L.A. (1966) Calculation of the average ground stress components from measurements of the diametral deformation of a drillhole. US Bureau of Mines Report of Investigation RI 6732.

Popov, S.N. (1979) Use of elastoplastic analysis in the relief method. *Sov. Min. Sci.* (Engl. translation), **15**, 65–9.

Rahn, W. (1984) Stress concentration factors for the interpretation of Doorstopper stress measurements in anisotropic rocks. *Int. J. Rock Mech. Min. Sci. & Geomech. Abstr.*, **21**, 313–26.

Rechsteiner, G.F. and Lombardi, G. (1974) Une méthode de calcul élasto-plastique de l'état de tension et de déformation autour d'une cavité souterraine, in *Proc. 3rd Cong. Int. Soc. Rock Mech. (ISRM)*, Denver, National Academy of Sciences, Washington, DC, 1049–54.

Ribacchi, R. (1977) Rock stress measurements in anisotropic rock masses, in *Proc. Int. Symp. on Field Measurements in Rock Mechanics*, Zurich, Balkema, Rotterdam, Vol. 1, pp. 183–97.

Riley, P.B., Goodman, R.E. and Nolting, R.M. (1977) Stress measurement by overcoring cast photoelastic inclusions, in *Proc. 18th US Symp. Rock Mech.*, Golden, Johnson Publ., 4C4-1–4C4-5.

Roberts, A. (1971) In situ stress determination in rock masses. A review of progress in the application of some techniques, in *Proc. Int. Symp. on the Determination of Stresses in Rock Masses*, Lab. Nac. de Eng. Civil, Lisbon, pp. 265–79.

Roberts, A. *et al.* (1964) A laboratory study of the photoelastic stressmeter. *Int. J. Rock Mech. Min. Sci.*, **1**, 441–57.

Rocha, M. and Silverio, A. (1969) A new method for the complete determination of the state of stress in rock masses. *Geotechnique*, **19**, 116–32.

Rocha, M. *et al.* (1974) A new development of the LNEC stress tensor gauge, in *Proc. 3rd Cong. Int. Soc. Rock Mech. (ISRM)*, Denver, National Academy of Sciences, Washington, DC, Vol. IIA, pp. 464–7.

Royea, M.J. (1969) Rock stress measurement at the Sullivan mine, in *Proc. 5th Canadian Rock Mech. Symp.*, Toronto, pp. 59–74.

Sakurai, S. and Akutagawa, S. (1994) Back analysis of in-situ stresses in a rock mass taking into account its non-elastic behavior, in *Proc. ISRM Int. Symp. Integral Approach to Applied Rock Mechanics*, Santiago, Chile, Vol. 1, pp. 135–43.

Sakurai, S. and Shimizu, N. (1986) Initial stress back analyzed from displacements due to underground excavations, in *Proc. Int. Symp. on Rock Stress and Rock Stress Measurements*, Stockholm, Centek Publ., Luleå, pp. 679–86.

Shemyakin, E.I., Kurlenya, M.V. and Popov, S.N. (1983) Elaboration of parallel borehole method for investigation of stress state and deformation properties in rock masses, in *Proc. Int. Symp. on Field Measurements in Geomechanics*, Zurich, Balkema, Rotterdam, pp. 349–58.

Sipprelle, E.M. and Teichman, H.L. (1950) Roof studies and mine structure stress analysis, Bureau of Mines Oil Shale Mine, Rifle, Colorado. *Trans. AIME.*, **187**, 1031–6.

Slobodov, M.A. (1958) Test application of the load relief method for investigating stresses in deep rock. *Ugal*, **7**, 30–35.

Smither, C.L. and Arhens, T.J. (1991) Displacements from relief of in situ stress by a cylindrical hole. *Int. J. Rock Mech. Min. Sci. & Geomech. Abstr.*, **28**, 175–86.

Smither, C.L., Schmitt, D.R. and Ahrens, T.J. (1988) Analysis and modelling of holographic measurements of in situ stress. *Int. J. Rock Mech. Min. Sci. & Geomech. Abstr.*, **25**, 353–62.

Spathis, A.T. (1988) A biaxial viscoelastic analysis of hollow inclusion gauges with implication for stress monitoring. *Int. J. Rock Mech. Min. Sci. & Geomech. Abstr.*, **25**, 473–7.

Stickney, R.G., Senseny, P.E. and Gregory, E.C. (1984) Performance testing of the Doorstopper biaxial strain cell, in *Proc. 25th US Symp. Rock Mech.*, Evanston, SME/AIME, pp. 437–44.

Sugawara, K. and Obara, Y. (1993) Measuring rock stress, in *Comprehensive Rock Engineering* (ed. J.A. Hudson), Pergamon Press, Oxford, Chapter 21, Vol. 3, pp. 533–52.

Sugawara, K. and Obara, Y. (1995) Rock stress and rock stress measurements in Japan, in *Proc. Int. Workshop on Rock Stress Measurement at Great Depth*, Tokyo, Japan, 8th ISRM Cong., pp. 1–6.

Sugawara, K. *et al.* (1986) Hemispherical-ended borehole technique for measurement of absolute rock stress, in *Proc. Int. Symp. on Rock Stress and Rock Stress Measurements*, Stockholm, Centek Publ., Luleå, pp. 207–16.

Sulem, J., Panet, M. and Guenot, A. (1987) An analytical solution for time-dependent displacements in a circular tunnel. *Int. J. Rock Mech. Min. Sci. & Geomech. Abstr.*, **24**, 155–64.

Suzuki, K. (1966) Fundamental study on the rock stress measurement by borehole deformation method, in *Proc. 1st Cong. Int. Soc. Rock Mech. (ISRM)*, Lisbon, Lab. Nac. de Eng. Civil, Lisbon, Vol. II, pp. 35–9.

Suzuki, K. (1971) Theory and practice of rock stress measurement by borehole deformation method, in *Proc. Int. Symp. on the Determination of Stresses in Rock Masses*, Lisbon, Lab. Nac. de Eng. Civil, Lisbon, pp. 173–82.

Talobre, J.A. (1964) Discussion of the paper by Merrill, in *Proc. Int. Conf. on State of Stress in the Earth's Crust*, Santa Monica, Elsevier, New York, pp. 369–71.

Talobre, J.A. (1967) *La Mecanique des Roches*, 2nd edn, Dunod, Paris.

Tamai, A., Kaneda, T. and Mimaki, T. (1994) Measurement of in-situ initial stress and excavation-induced stress changes in the vicinity of underground opening, in *Proc. 1st North Amer. Rock Mechanics Symp.*, Austin, Balkema, Rotterdam, pp. 377–84.

Thompson, P.M. (1990) A borehole deformation gauge for stress determinations in deep borehole, in *Proc. 31st US Symp. Rock Mech.*, Balkema, Rotterdam, pp. 579–86.

Thompson, P.M., Lang, P.A. and Snider, G.R. (1986) Recent improvements to in-situ stress measurements using the overcoring method, in *Proc. 39th Canadian Geotechnical Conf.*, Ottawa.

Van Heerden, W.L. (1969) Stress concentration factors for the flat borehole end for use in rock stress measurements. *Eng. Geol.*, **3**, 307–23.

Van Heerden, W.L. (1973) The influence of various factors on the triaxial strain cell results. South African Council for Scientific and Industrial Research (CSIR) Technical Report ME 1178.

Van Heerden, W.L. (1976) Practical application of the CSIR triaxial strain cell for rock stress measurements, *Proc. ISRM Symp. on Investigation of Stress in Rock, Advances in Stress Measurement*, Sydney, The Institution of Engineers, Australia, pp. 1–6.

Van Heerden, W.L. (1983) Stress strain relations applicable to overcoring techniques in transversely isotropic rocks. *Int. J. Rock Mech. Min. Sci. & Geomech. Abstr.*, **20**, 277–82.

Voight, B. (1967) On photoelastic techniques, in situ stress and strain measurement, and the field geologist, *J. Geol.*, **75**, 46–58.

Walker, J.R., Martin, C.D. and Dzik, E.J. (1990) Confidence intervals for in-situ stress measurements. *Int. J. Rock Mech. Min. Sci. & Geomech. Abstr.*, **27**, 139–41.

Walton, R.J. and Worotnicki, G. (1978) Rock stress measurements in the 18CC/12CZ2 crown pillar area of the CSA mine, NSW. CSIRO Technical Report No. 38.

Walton, R.J. and Worotnicki, G. (1986) A comparison of three borehole instruments for monitoring the change of rock stress with time, in *Proc. Int. Symp. on Rock Stress and Rock Stress Measurements*, Stockholm, Centek Publ., Luleå, pp. 479–88.

Wang, L. *et al.* (1986) The type YG-73 piezomagnetic stress gauge for rock stress measurement, in *Proc. Int. Symp. on Rock Stress and Rock Stress Measurements*, Stockholm, Centek Publ., Luleå, pp. 227–35.

White, J.M., Hoskins, E.R. and Nilssen, T.J. (1978) Primary stress measurement at Eisenhower Memorial Tunnel, Colorado. *Int. J. Rock Mech. Min. Sci. & Geomech. Abstr.*, **15**, 179–82.

Wiles, T.D. and Kaiser, P.K. (1994a) In-situ stress determination using the under-excavation technique – I: theory. *Int. J. Rock Mech. Min. Sci. & Geomech. Abstr.*, **31**, 439–46.

Wiles, T.D. and Kaiser, P.K. (1994b) In-situ stress determination using the under-excavation technique – II: applications. *Int. J. Rock Mech. Min. Sci. & Geomech. Abstr.*, **31**, 447–56.

Worotnicki, G. (1993) CSIRO triaxial stress measurement cell, in *Comprehensive Rock Engineering* (ed.

J.A. Hudson), Pergamon Press, Oxford, Chapter 13, Vol. 3, pp. 329–94.

Worotnicki, G. and Walton, R.J. (1976) Triaxial hollow inclusion gauges for determination of rock stresses in-situ, Supplement to *Proc. ISRM Symp. on Investigation of Stress in Rock, Advances in Stress Measurement*, Sydney, The Institution of Engineers, Australia, Suppl. 1–8.

Worotnicki, G. and Walton, R.J. (1979) Virgin rock stress measurements at the Warrego mine. CSIRO Division of Geomechanics, Technical Report No. 93.

Yamatomi, J. *et al.* (1988) An analytical method of stress and displacement around a circular tunnel excavated in rock mass with non-linear time dependency, in *Proc. 29th US Symp. Rock Mech.*, Minneapolis, Balkema, Rotterdam, pp. 317–24.

Yeun, S.C.K. and Bock, H.F. (1988) Analytical evaluation for the design and operation of new recoverable 3D stressmeter for rock, in *Proc. 5th Australia–New Zealand Conf. on Geomechanics*, Sydney, pp. 207–13.

Zajic, J. and Bohac, V. (1986) Gallery excavation method for the stress determination in a rock mass, in *Proc. Int. Symp. on Large Rock Caverns*, Helsinki, Pergamon Press, Oxford, Vol. 2, pp. 1123–31.

Zou, D. and Kaiser, P.K. (1990) In situ stress determination by stress change monitoring, in *Proc. 31st US Symp. Rock Mech.*, Golden, Balkema, Rotterdam, pp. 27–34.

JACKING METHODS 6

6.1 INTRODUCTION

Jacking methods are sometimes called 'stress compensating' methods. The equilibrium of a rock mass is disturbed by cutting slots on the surfaces of rock excavations (quarries, galleries, pillars, etc.). This in turn creates deformations that are measured with reference pins or strain gages placed on either side of the slots. Finally, equilibrium is restored by inserting a device such as a jack in the slots. Then the jack is pressurized until all deformations have vanished. One of the most widely used jacking methods is the flat jack (or flatjack) method.

In general, jacking methods are intended for the determination of surface or near-surface rock stresses (at depths not exceeding 5–7 m). In many aspects they can be classified as partial surface relief methods. Jacking methods can also be used for the monitoring of stress changes, as discussed in Chapter 10.

6.2 HISTORY

The flat jack method represents one of the first techniques used in rock mechanics for measuring *in situ* stresses in rock. Initially proposed to characterize the deformability of rock masses, the method gained popularity in the 1950s and 1960s for measuring stresses as well. Numerous records of stress measurements with flat jacks can be found in the literature (see for instance the *Proceedings of the First ISRM Congress* in 1966 (Theme No. 4: Residual stresses in rock masses) and those of the Symposium on State of Stress in the Earth's Crust in 1963 (Judd, 1964)). Stresses determined with flat jacks have often been compared with those determined with the early version of the USBM gage (e.g. Judd, 1964; Merrill, 1964).

The use of flat jacks to measure absolute stresses was first investigated in the 1950s in France. The method called flat jack method was proposed by Mayer, Habib and Marchand (1951) and Tincelin (1951) and was later modified by Panek (1961), Panek and Stock (1964), Hoskins (1966), Merrill *et al.* (1964) and Rocha, Lopes and Silva (1966, 1971). Since the 1960s, stress measurements with flat jacks have been reported for a wide variety of rock conditions ranging between hard rocks and weak and soft rocks and evaporitic rocks. Examples can be found in Wareham and Skipp (1974), Bonvallet and Dejean (1977), Froidevaux, Paquin and Souriau (1980), Borsetto, Guiseppetti and Mandfredini (1983), Faiella, Mandfredini and Rossi (1983), Heusermann and Pahl (1983), Bertrand and Durand (1983), Tinchon (1986), Grossman and Camara (1986), Pinto and Cunha (1986), Zimmerman *et al.* (1989), Bertrand (1994) and Piguet (1994). Beside a few technological improvements, the flat jack method used today is essentially the same as it was 30 years ago.

In general, the flat jack method consists of measuring the displacement between one or several sets of pins or strain gages placed on the surface (or near the surface) of an excavation created by cutting a nearby slot. A flat jack (consisting of two thin metal plates welded together) is inserted into the slot, grouted in place and pressurized until the pin or strain gage readings have returned to their original position. This 'cancellation pressure' is used as

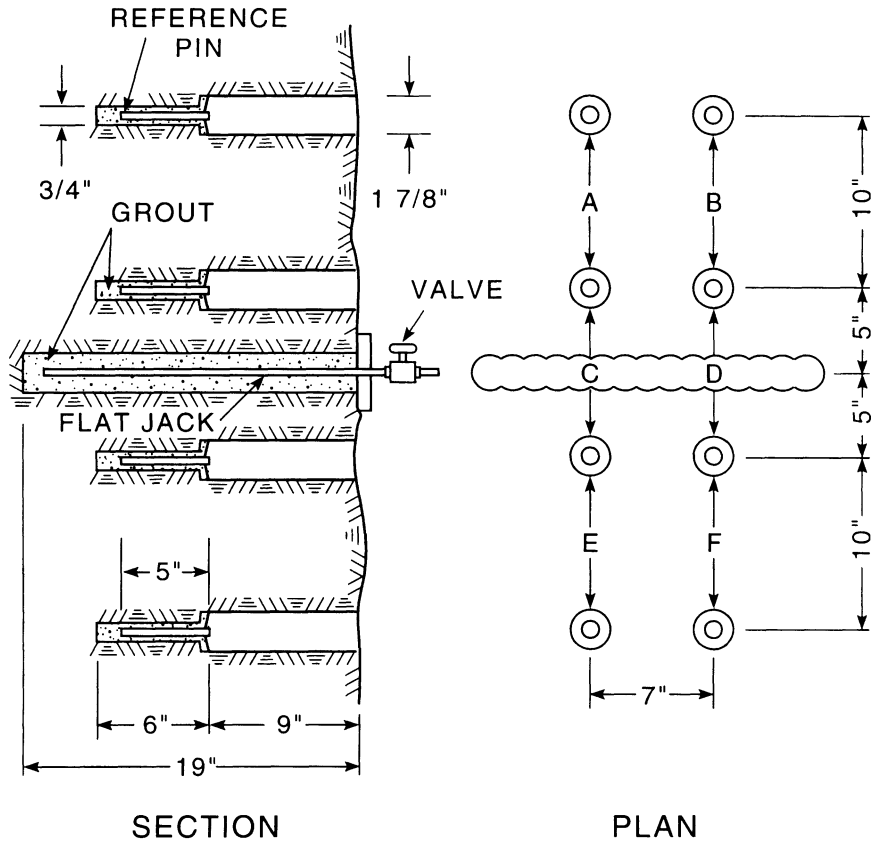

Fig. 6.1 Flat jack set-up used by Merrill and co-workers (1964).

an estimate of the tangential stress normal to the jack also called 'skin stress'. Figure 6.1 shows an example of the flat jack set-up used by Merrill and co-workers (1964) in the early 1960s.

From a mechanical point of view, the path followed by the rock during a flat jack test can be represented as shown in Fig. 6.2. Here it is assumed that the rock is elastic (linear or nonlinear) and is under compression in a direction perpendicular to the jack surface. The initial distance between two reference pins is taken as d_o and the unknown normal stress is defined as σ (point A). As a result of cutting the slot, the normal stress across the slot is reduced from σ to zero (free surface) and the distance between the pins is reduced by an amount $2\Delta d$ (point B). Pressurization of the jack up to the cancellation pressure p_c brings the pins to their original position. Figure 6.3 shows an illustrative example of stress measurement reported by Bertrand (1994) showing three sets of unloading–reloading response curves similar to the theoretical curve shown in Fig. 6.2. In this example the rock shows a very good linear elastic behavior. The measurements were made with three sets of reference pins placed across one slot 590 mm long, 190 mm deep and 5 mm thick. The three cancellation pressures give an average normal stress equal to 1.66 MPa.

Bowling (1976) proposed using a cylindrical rather than a flat jack to determine the stresses parallel to a rock surface. The jack consists of a solid steel core onto which fits a rubber sleeve. Eight reference pins are first grouted around

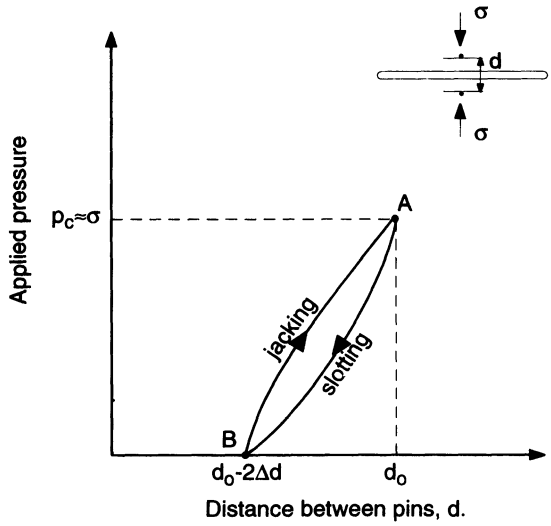

Fig. 6.2 Path followed by a rock during a flat jack test. The rock is assumed to be elastic (linear or non-linear) and under compression in a direction perpendicular to the jack surface.

the circumference of a circle 250 mm in diameter on a rock surface. The pins form four reference diameters spaced 45° apart. Then a hole 150 mm in diameter and 500 mm deep is drilled at the center of the circle, as in the stress relief by center hole method of Duvall (1974). The four diameter changes are monitored. Finally, a cylindrical jack is inserted into the hole and pressurized and the pin movements are measured. The principal stresses and their orientation in the plane parallel to the rock surface, as well as the rock's Young's modulus, are determined from the response curves of the reference pins obtained during drilling and pressurizing.

Curved jacks have also been proposed by Jaeger and Cook (1964) for measuring stresses in boreholes, at distances of 3 to 6 m into rock masses, thus eliminating the main disadvantages associated with flat jacks. Several pairs of jacks need to be used, however. The method is complex and requires a combination of fracturing, pressurizing, destressing and pressure restoration. It has the advantage of being able to determine the secondary principal stresses perpendicular to the boreholes. A method similar to that of Jaeger and Cook (1964) has also been suggested by Helal (1982).

6.3 TECHNIQUES, EQUIPMENT AND PROCEDURES

Standards for determining *in situ* stresses with flat jacks have been proposed by the American Society for Testing of Materials (ASTM D 4729-87, 1993) and the International Society for Rock Mechanics (Kim and Franklin, 1987). Figure 6.4 shows the flat jack set-up recommended by the ASTM.

Flat jacks consist of two plates of metal that are welded together. They can operate at pressures of several thousand psi (tens of MPa). They are usually square or rectangular with widths not less than 0.6 m (2 ft). The slots can be cut by overlapping holes or by using a large diamond disk saw giving a smooth surface (Rocha, Lopes and Silva, 1966). Overlapping holes seem to be more suitable for deep slots (deeper than 1.5 m) whereas the saw is used for cutting slots less than 1.5 m in depth. Grout such as mortar, epoxy resins or plaster is used to hold the jack in place. The grout must have similar strength and deformability as the surrounding rock. Grouting of the jack may not be necessary if the slots are cut with a large saw (Rocha, Lopes and Silva, 1966). In that case the jack is also reusable. The method of Rocha, Lopes and Silva (1966) requires the use of flat jacks with boundaries in the shape of an arc of a circle instead of the more conventional square or rectangular jacks. The pressure is applied using hydraulic pumps and the pressure should be able to remain constant over a period of 5 min. The reader should note that more than one coplanar flat jack can be installed in a slot, thus increasing the volume of rock involved in the test.

Rock surface deformations or strains must be measured in the near vicinity of the slots, otherwise the deformations or strains would be too small to be measured with enough precision. Rocha, Lopes and Silva (1966)

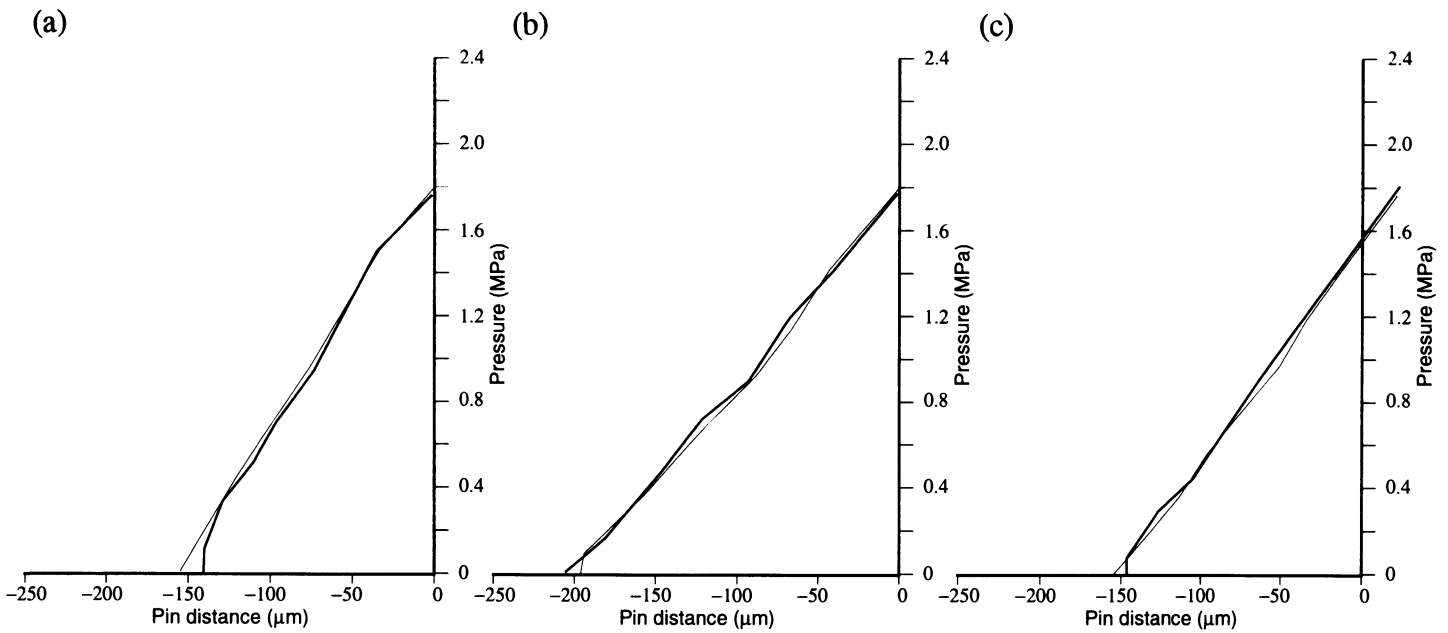

Fig. 6.3 Example of field measurements with a flat jack. Three response curves are shown here corresponding to three sets of reference pins 1, 2 and 3 placed next to each other. (a) Base pins no. 1, $p_c = 1.70$ MPa, (b) base pins no. 2, $p_c = 1.70$ MPa, (c) base pins no. 3, $p_c = 1.58$ MPa. (After Bertrand, 1994.)

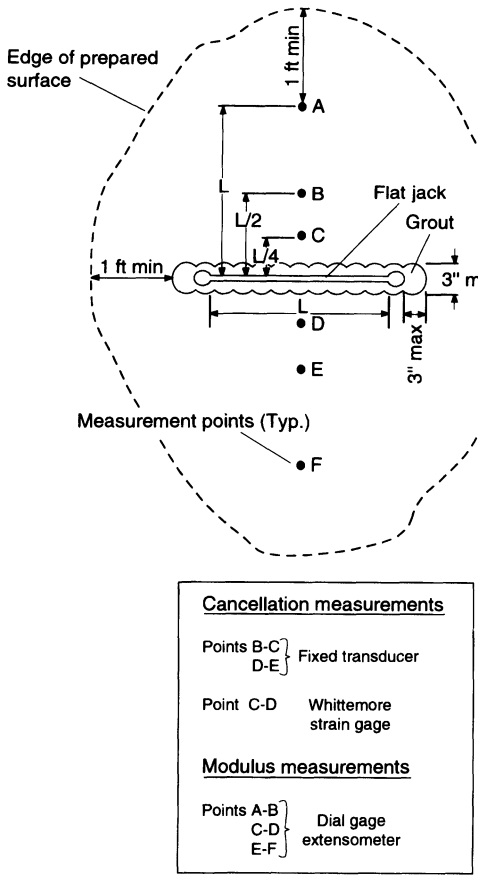

Fig. 6.4 Flat jack set-up and surface measurements. (After ASTM D 4729-87, 1993. Copyright ASTM. Reprinted with permission.)

suggested a distance of less than 300 mm. According to ASTM D 4729-87, the measurement points should be installed within a distance, $L/2$ of the flat jack slot, where L is the flat jack width. Deformation transducers must be located on the centerline normal to the flat jacks and include dial gages, Whittemore-type strain gages and electronic transducers such as LVDTs or linear potentiometers. The displacements are usually measured with an accuracy of 0.001 mm.

Figure 6.5a shows an ideal and generic variation of pin separation measured across a slot during a jack test, where d_o is the initial distance between two reference pins and p_c is the cancellation pressure (Goodman, 1989). For comparison, Fig. 6.5b shows a typical record reported by Hoskins (1966) for a flat jack test carried out in a $19 \times 24 \times 30$ inch ($0.5 \times 0.6 \times 0.76$ m) block of Wombeyan marble with $d_o = 6$ inch (152 mm). In this figure, it can be seen that some creep took place over a period of 6 days in between slot cutting and slot jacking.

A system of three flat jacks at 45° from each other in a given plane normal to the axis of an underground opening can be used to determine the three components of the *in situ* stress field acting in that plane. If the complete three-dimensional state of stress needs to be determined with flat jacks alone, a minimum of six jack tests need to be conducted in six different directions and at different locations around the periphery of the opening. Any additional measurements can serve as a measure of redundancy. As an example, Fig. 6.6a shows the orientation of 16 flat jack tests conducted in coal by Tinchon (1986). Figure 6.6b shows another set-up recommended by Pinto and Cunha (1986) where a total of 12 slots are cut along the wall of an underground opening.

In general, the flat jack method has several disadvantages that may limit its range of applications.

(1) The flat jack method is limited to stress measurements near the surface of an opening and therefore may be influenced by the disturbance associated with the process of excavation of the opening. This disturbance could invalidate the stress measurements altogether. The disturbance can however be reduced by using tunnel boring machines or smooth blasting excavation techniques rather than the conventional drill and blast method. Also, flat jack tests should not be conducted near open natural fractures and major rock heterogeneities.

(2) When using flat jacks to determine the *in-situ* stresses around an underground gallery, knowledge of the stress concentrations along the wall of the opening is required in order to relate the measured cancellation

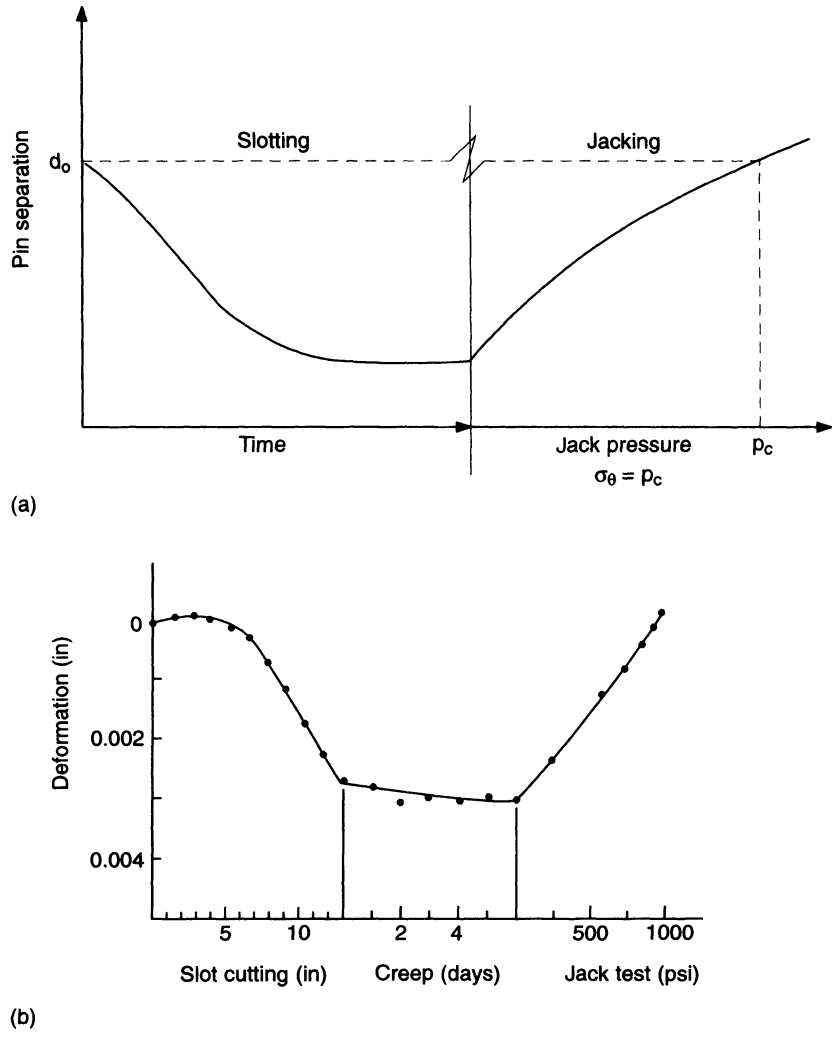

Fig. 6.5 (a) Theoretical variation of pin separation during a flat jack test. (After Goodman, 1989.) (b) Record of a test conducted in a block of Wombeyan marble. (Source: Hoskins, E.R. Copyright 1966, with kind permission from Elsevier Science Ltd, The Boulevard, Langford Lane, Kidlington, UK.)

pressure to the virgin stresses at infinity. In general, the stress concentration factors depend on the shape of the opening as well as the rock's constitutive behavior.

(3) The results of flat jack tests may be disturbed by atmospheric conditions (humidity and temperature) and dust (Fidler, 1964).

(4) Many jack tests are necessary to determine the complete *in situ* state of stress acting at infinity. Theoretically, a minimum of six measurements in six different directions are required to determine the complete stress tensor. The rock mass must have similar mechanical characteristics in the volume encompassing those measurements.

(5) The pressure may not be entirely transmitted over the whole surface of the jack, in particular in the vicinity of the jack welded edges. The contact area may change during loading. Differences between applied pressure

and actual overall pressure acting against the rock surfaces as large as 18% were reported by Rocha, Lopes and Silva (1966). Jaeger and Cook (1976) suggested that a region of the order of 0.25 inches (6.3 mm) wide is inoperative around the periphery of a jack due to the welding joint. Another problem with flat jacks is that the stresses across the jacks may not be uniform, as is often assumed. This is particularly problematic when using large flat jacks (Grossman and Camara, 1986). Indeed, using flat jacks (in particular large flat jacks) in areas of high stress gradients or in sections of underground openings that have been disturbed may yield erroneous stress measurements.

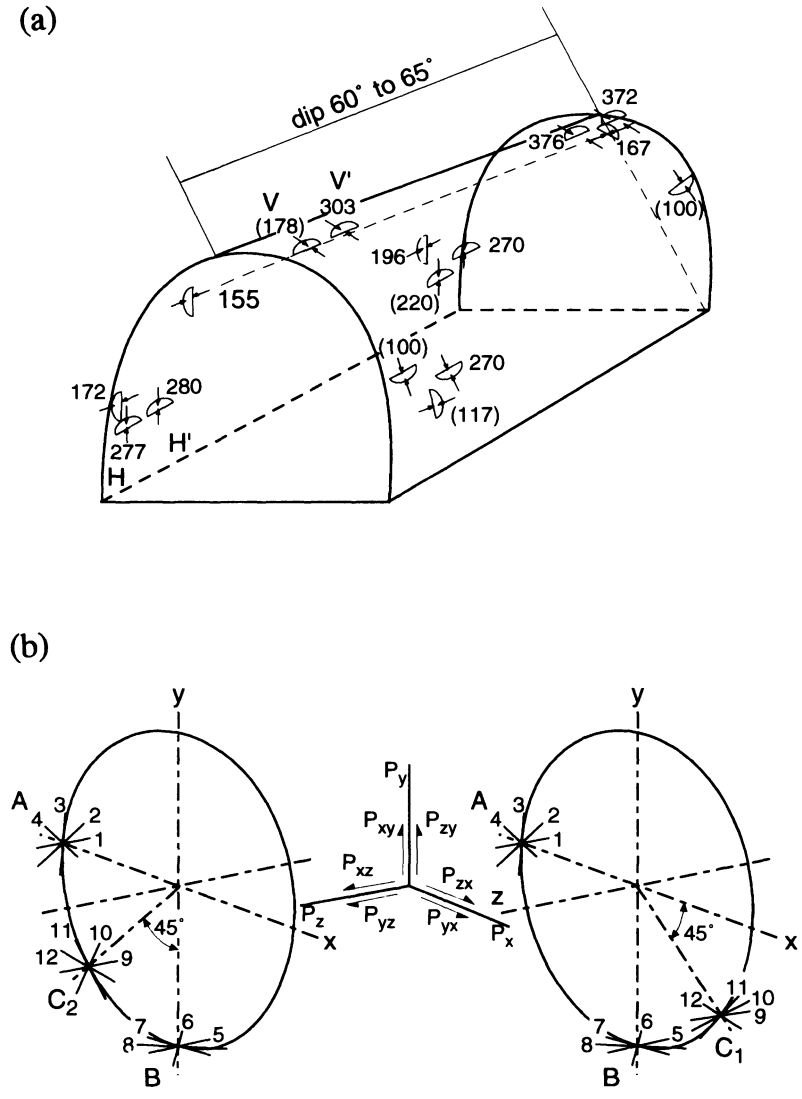

Fig. 6.6 (a) Orientation of 16 flat jack tests in coal. (After Tinchon, 1986.) (b) Orientation of flat jack tests recommended by Pinto and Cunha (1986). In both cases, the three-dimensional stress field can be determined from the test results.

(6) When conducting flat jack tests in soft rocks, or in swelling or flaking media, the water used for the mortar or plaster to grout the jacks in place may soften the rock and give incoherent stress results. Mayer and Bernede (1966) identified that problem in chalk and clay shales and suggested using special precautions (such as plastic bags in the slot) in order to avoid the problem.

(7) Some creep may take place following cutting of the slot (Heusermann and Pahl, 1983; Hoskins, 1966; Panek and Stock, 1964). This phenomenon may occur in soft and weak rocks as well as in evaporitic rocks such as rock salt and potash. If creep is allowed to occur over a long period of time, the cancellation pressure will give an overestimate of the tangential stress.

On the other hand, the flat jack method has several advantages. The first and foremost advantage is that the elastic constants of the rock do not have to be known in order to determine the tangential stress at points in the walls of an excavation. Second, the stresses are measured directly. Third, the equipment used in flat jack tests is rugged and stable. Fourth, the measured stress is an average over an area (Panek, 1961). Fifth, relatively large rock volumes can be tested (0.5–2 m^3), especially when one or several coplanar large flat jacks are used. Finally, as pointed out by Rocha, Lopes and Silva (1971), the flat jack method creates only a partial relief of the rock mass, thus less disturbance to the mechanical properties of the rock is induced compared with other methods. This aspect is particularly important when dealing with weak rock masses.

In addition to measuring *in situ* stresses, flat jacks can also be used to determine the modulus of deformation of the rock by measuring displacements which occur when the slot is cut or by relating the applied pressure to displacements during the pressurizing phase (e.g. Hoskins, 1966; Jaeger and Cook, 1976; Rocha, Lopes and Silva, 1966; Vogler, Deffur and Bieniawski, 1976; Zimmerman *et al.*, 1989). The relative displacement of the two slot surfaces is measured using deformation sensors or transducers embedded in the jacks or in direct contact with the slot surfaces. Equations for the determination of the rock's modulus of deformation can be found in Rocha and Da Silva (1970) and Loureiro-Pinto (1986).

6.4 THEORY

The analysis of flat jack tests is based on several major assumptions.

(1) The pressure in the jack at cancellation is equal to the tangential stress in the rock (before the slot was cut) normal to the plane of the jack. This assumes that the stress before the slot was cut was uniform. The effect of stress gradients across the jack surface is therefore neglected.

(2) The rock is elastic (linear or nonlinear) and therefore the stress relief process is assumed to be completely reversible. No creep is assumed to occur. This may be of limited value in weak and soft rocks, and in rocks that show plastic and/or time-dependent deformation.

(3) The rock is isotropic. No anisotropic solution has been derived for the analysis of flat jack tests. Anisotropy should have some effect on the displacement or strain measurements if the planes of rock anisotropy are neither parallel to the rock surface nor strike parallel or perpendicular to the jack surface. Shear stresses could be generated in the rock near the slot if the anisotropy strikes at an angle to the jack surface.

(4) Flat jacks are assumed to be aligned with the principal stresses on the surface of the opening. Shear stresses cannot be measured with flat jacks. The presence of shear stresses can however be detected by measuring variation in diagonal lengths between different sets of surface pins. The effect of the rock stress parallel to the slot is usually assumed to be negligible. Bonvallet and Dejean (1977) concluded that the effect of that stress component

could be disregarded for magnitudes up to 5 MPa and that neglecting the effect of the shear stresses could cause an error of 9%. Alexander (1960) presented a more complex theory which relates the cancellation pressure to the rock stresses normal and parallel to the jack. The stress parallel to the jack was found to have a negligible effect.

(5) Flat jacks are assumed to be 100% efficient over their surfaces.

(6) Flat jacks are mostly used to measure compressive stresses. However, the method could also be used to measure tensile stresses (Bernede, 1974; R.E. Goodman, personal communication, 1982). If the rock is under a tensile stress, σ, before cutting the slot (point A), the response shown in Fig. 6.2 is replaced by that shown in Fig. 6.7. Instead of getting closer, the pins move further apart from each other by an amount $2\Delta d$ upon cutting the slot (point B). Further pressurization of the jack increases the distance between the pins. Using the tangent to the pressure–displacement curve at point B, the tensile stress σ can be estimated.

In view of the above assumptions, the analysis of flat jack tests is not as straightforward as initially thought. A correct analysis requires several correction factors (Alexander, 1960) which are often overlooked in practice. Since many of the problems with flat jacks cannot be quantified, the cancellation pressure p_c is often used as a direct measurement of the normal stress acting across the slots.

Jaeger and Cook (1976) proposed a simple correction factor to account for the fact that the cancellation pressure does not act over the whole slot area or even over the whole jack area (edge effect). If $2c$ and $2c_j$ are the widths of the slot and the jack, respectively and if e is the distance along the edge of the jack (of the order of 0.25 inches (6.3 mm) wide) that is not operative due to the welding joint, the normal stress σ_n is related to the cancellation stress p_c as follows:

$$\sigma_n = p_c \frac{(c_j - e)}{c} \tag{6.1}$$

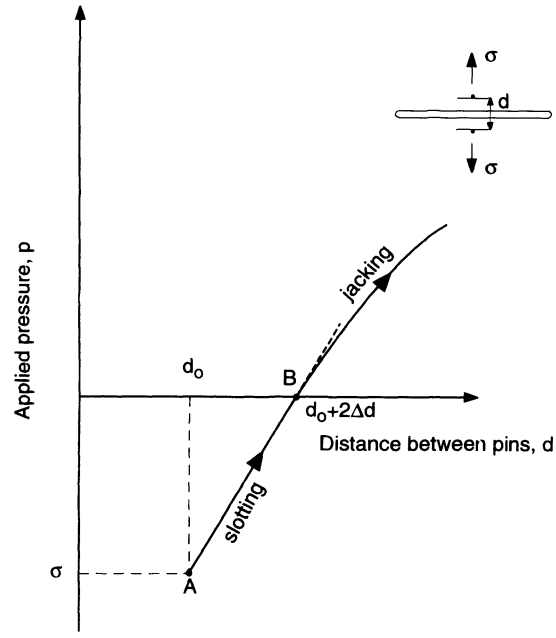

Fig. 6.7 Measuring tensile normal stresses with flat jacks.

Let $\sigma_{\theta 1}$, $\sigma_{\theta 2}$ and $\sigma_{\theta 3}$ be three tangential stresses measured with three flat jacks in the wall of an underground opening subjected to a two-dimensional *in situ* stress field with components σ_{xo}, σ_{yo} and τ_{xyo}. The three flat jacks are oriented parallel to the axis of the opening and are perpendicular to the x,y plane. If the rock is elastic and isotropic, the three tangential stresses will be linearly related to the *in situ* stress components in a general form as follows:

$$\begin{bmatrix} \sigma_{\theta 1} \\ \sigma_{\theta 2} \\ \sigma_{\theta 3} \end{bmatrix} = \begin{bmatrix} f_{11} & f_{12} & f_{13} \\ f_{21} & f_{22} & f_{23} \\ f_{31} & f_{32} & f_{33} \end{bmatrix} \cdot \begin{bmatrix} \sigma_{xo} \\ \sigma_{yo} \\ \tau_{xyo} \end{bmatrix} \tag{6.2}$$

where the coefficients f_{ij} $(i,j = 1,3)$ depend on the geometry of the excavation. Then equation (6.2) can be solved for the three *in situ* stress components. For a circular opening with the geometry of Fig. 6.8, equation (6.2) becomes

$$\begin{bmatrix} \sigma_{\theta 1} \\ \sigma_{\theta 2} \\ \sigma_{\theta 3} \end{bmatrix} = \begin{bmatrix} 1-\cos 2\theta_1 & 1+\cos 2\theta_1 & -4\sin 2\theta_1 \\ 1-\cos 2\theta_2 & 1+\cos 2\theta_2 & -4\sin 2\theta_2 \\ 1-\cos 2\theta_3 & 1+\cos 2\theta_3 & -4\sin 2\theta_3 \end{bmatrix} \cdot \begin{bmatrix} \sigma_{xo} \\ \sigma_{yo} \\ \tau_{xyo} \end{bmatrix} \tag{6.3}$$

where θ_i $(i = 1,2,3)$ is the angle defining the location of the ith flat jack test from the x-axis of Fig. 6.8.

In the more general case when the slots are cut at an angle to the axes of the underground excavation of interest, each cancellation pressure can be related to the six components of the *in situ* stress field by knowing the orientation of each slot and the stress concentration factors associated with the shape of the excavation. The *in situ* stress components are then determined by solving a system of six equations and six unknowns based on six measurements. If more measurements are available, a multilinear regression analysis or optimization approach can be carried out on the measurements (e.g. Pinto and Cunha, 1986). Since the stress concentrations are themselves functions of the *in situ* stresses and can have complex expressions (in particular for openings with complex geometries), determination of the three-dimensional *in situ* stress field can be carried out in an iterative manner by coupling a numerical model for stress determination and an optimization model (Piguet, 1994; Tinchon, 1986). In doing so, any rock constitutive behavior can be introduced.

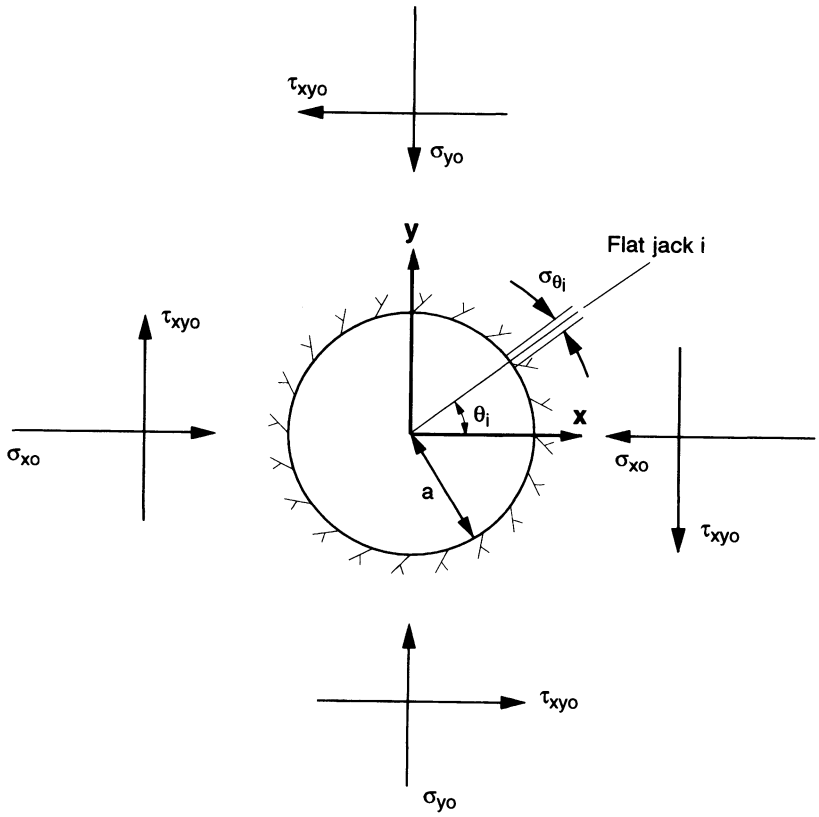

Fig. 6.8 Circular opening in which flat jack test i $(i = 1,2,3)$ is conducted.

6.5 TECHNICAL INFORMATION

Additional information about flat jacks, large flat jacks and associated equipment can be obtained by contacting directly the following groups:

1. INTERFELS GMbH, Deilmanstraße 5, D-48455 Bad Bentheim, Germany.
2. Laboratorio Nacional de Engenharia Civil (LNEC), 101 Avenida do Brasil, P-1799 Lisboa (Lisbon) Codex, Portugal.
3. ROCTEST, 665 Pine Street, St Lambert, Quebec, Canada J4P 2P4.

REFERENCES

Alexander, L.G. (1960) Field and laboratory tests in rock mechanics, in *Proc. 3rd Australia–New Zealand Conf. on Soil Mechanics*, pp. 161–8.

ASTM D 4729-87 (1993) Standard test method for in-situ stress and modulus of deformation using the flatjack method, in *1993 Annual Book of ASTM Standards*, Vol. 04-08.

Bernede, J. (1974) New developments in the flat jack test, in *Proc. 3rd Cong. Int. Soc. Rock Mech. (ISRM)*, Denver, National Academy of Sciences, Washington, DC, Vol. 2A, pp. 433–8.

Bertrand, L. (1994) Mesure des contraintes in-situ par la méthode du verin plat, in *Proc. Seminaire Formation: Mesure des sollicitations et des contraintes dans les ouvrages et dans les terrains*, Ecole des Mines, Nancy, Sept. 12–16.

Bertrand, L. and Durand, E. (1983) In situ stress measurements: comparison of different methods, in *Proc. Int. Symp. on Soil and Rock Investigations by In-Situ Testing*, Paris, Vol. 2, pp. 449–70.

Bonvallet, J. and Dejean, M. (1977) Flat jack test and determination of mechanical characteristics, in *Proc. Int. Symp. on Field Measurements in Rock Mechanics*, Zurich, Balkema, Rotterdam, Vol. 1, pp. 361–74.

Borsetto, M., Guiseppetti, G. and Mandfredini, G. (1983) Recent advances in the interpretation of the flat jack test, in *Proc. 5th Cong. Int. Soc. Rock Mech. (ISRM)*, Melbourne, Balkema, Rotterdam, pp. A143–50.

Bowling, A.J. (1976) Surface rock stress measurement with a new cylindrical jack, in *Proc. ISRM Symposium on Investigation of Stress in Rock, Advances in Stress Measurement*, Sydney, The Institution of Engineers, Australia, pp. 7–11.

Duvall, W.I. (1974) Stress relief by center hole. Appendix in US Bureau of Mines Report of Investigation RI 7894.

Faiella, D., Manfredini, G. and Rossi, P.P. (1983) In situ flat jack test: analysis of results and critical assessment, in *Proc. Int. Symp. on Soil and Rock Investigations by In-Situ Testing*, Paris, Vol. 2, pp. 507–12.

Fidler, J. (1964) Discussion of the paper by Merrill, in *Proc. Int. Conf. on State of Stress in the Earth's Crust*, Santa Monica, Elsevier, New York, pp. 375–6.

Froidevaux, C., Paquin, C. and Souriau, M. (1980) Tectonic stresses in France: in-situ measurements with a flatjack. *J. Geophys. Res.*, **85**, 6342–6.

Goodman, R.E. (1989) *Introduction to Rock Mechanics*, 2nd edn, Wiley.

Grossman, N.F. and Camara, R.J.C. (1986) About the rock stress measurement using the LFJ (large flat jack) technique, in *Proc. Int. Symp. on Rock Stress and Rock Stress Measurements*, Stockholm, Centek Publ., Luleå, pp. 375–83.

Helal, H.M. (1982) Etude et développement d'une méthode de mesure des contraintes par surcarottage, unpublished PhD Thesis, Ecole des Mines, Nancy (France).

Heusermann, S. and Pahl, A. (1983) Stress measurements in underground openings by the overcoring method and by the flatjack method with compensation, in *Proc. Int. Symp. on Field Measurements in Geomechanics*, Zurich, Balkema, Rotterdam, pp. 1033–45.

Hoskins, E.R. (1966) An investigation of the flatjack method of measuring rock stress. *Int. J. Rock Mech. Min. Sci.*, **3**, 249–64.

Jaeger, J.C. and Cook, N.G.W. (1964) Theory and application of curved jacks for measurement of stresses, in *Proc. Int. Conf. on State of Stress in the Earth's Crust*, Santa Monica, Elsevier, New York, pp. 381–95.

Jaeger, J.C. and Cook, N.G.W. (1976) *Fundamentals of Rock Mechanics*, 2nd edn, Chapman & Hall, London.

Judd, W. (1964) Rock stress, rock mechanics and research, in *Proc. Int. Conf. on State of Stress in the Earth's Crust*, Santa Monica, Elsevier, New York, pp. 5–53.

Kim, K. and Franklin, K.A. (coordinators) (1987) Suggested methods for rock stress determination. *Int. J. Rock Mech. Min. Sci. & Geomech. Abstr.*, **24**, 53–73.

Loureiro-Pinto, J. (1986) Suggested method for deformability determination using a large

flatjack technique. *Int. J. Rock Mech. Min. Sci. & Geomech. Abstr.*, **23**, 131–40.

Mayer, A. and Bernede, J. (1966) Mesures des contraintes dans le terrain en place en roches tendres ou sensibles a l'humidité, in *Proc. 1st Cong. Int. Soc. Rock Mech. (ISRM)*, Lisbon, Lab. Nac. de Eng. Civil, Lisbon, Vol. 2, pp. 41–4.

Mayer, A., Habib, P. and Marchand, R. (1951) Underground rock pressure testing, in *Proc. Int. Conf. Rock Pressure and Support in the Workings*, Liege, pp. 217–21.

Merrill, R.H. (1964) In-situ determination of stress by relief techniques, in *Proc. Int. Conf. on State of Stress in the Earth's Crust*, Santa Monica, Elsevier, New York, pp. 343–69.

Merrill, R.H. *et al.* (1964) Stress determination by flatjack and borehole deformation methods. US Bureau of Mines Report of Investigation RI 6400.

Panek, L.A. (1961) Measurement of rock pressure with a hydraulic cell. *Trans. Am. Inst. Mining Eng.*, **220**, 287–90.

Panek, L.A. and Stock, J.A. (1964) Development of a rock stress monitoring station based on the flat slot method of measurement. US Bureau of Mines Report of Investigation RI 6537.

Piguet, J.P. (1994) Mesure des contraintes par la methode du verin plat, in *Proc. Seminaire Formation: Mesure des sollicitations et des contraintes dans les ouvrages et dans les terrains*, Ecole des Mines, Nancy, Sept. 12–16.

Pinto, J.L. and Cunha, A.P. (1986) Rock stress determinations with the STT and SFJ techniques, in *Proc. Int. Symp. on Rock Stress and Rock Stress Measurements*, Stockholm, Centek Publ., Luleå, pp. 253–60.

Rocha, M. and Da Silva, J.N. (1970) A new method for the determination of the deformability of rock masses, in *Proc. 2nd Cong. Int. Soc. Rock Mech. (ISRM)*, Belgrade, Jaroslav Cerni Inst., Belgrade, Vol. 1, pp. 423–37.

Rocha, M., Lopes, J.J.B. and Silva, J.N. (1966) A new technique for applying the method of the flat jack in the determination of stresses inside rock masses, in *Proc. 1st Cong. Int. Soc. Rock Mech. (ISRM)*, Lisbon, Lab. Nac. de Eng. Civil, Lisbon, Vol. 2, pp. 57–65.

Rocha, M., Lopes, J.J.B. and Silva, J.N. (1971) A new technique for applying the method of the flatjack in the determination of stresses inside rock masses, in *Proc. Int. Symp. on the Determination of Stresses in Rock Masses*, Lab. Nac. de Eng. Civil, Lisbon, pp. 431–50.

Tincelin, E. (1951) Research on rock pressure in the Iron Mines of Lorraine, in *Proc. Int. Conf. Rock Pressure and Support in the Workings*, Liege, pp. 158–75.

Tinchon, L. (1986) Evolution des contraintes naturelles en fonction de la profondeur et de la tectonique aux Houillères du Bassin de Lorraine, in *Proc. Int. Symp. on Rock Stress and Rock Stress Measurements*, Stockholm, Centek Publ., Luleå, pp. 111–20.

Vogler, U.W., Deffur, R.D. and Bieniawski, Z.T. (1976) CSIR large flat jack equipment for determining rock mass deformability, in *Proc. Symp. on Exploration for Rock Engineering*, Johannesburg, pp. 105–11.

Wareham, B.F. and Skipp, B.O. (1974) The use of the flatjack installed in a sawcut slot in the measurement of in situ stress, in *Proc. 3rd Cong. Int. Soc. Rock Mech. (ISRM)*, Denver, National Academy of Sciences, Washington, DC, pp. 481–7.

Zimmerman, R. *et al.* (1989) Results of pressurized-slot measurements in the G-tunnel underground facility, in *Proc. 30th US Symp. Rock Mech.*, Morgantown, Balkema, Rotterdam, pp. 697–704.

STRAIN RECOVERY METHODS 7

7.1 INTRODUCTION

When a piece of rock is removed from the *in situ* state of stress, it tends to relax and thereby deform. The relaxation consists of an instantaneous elastic component and a time-dependent (anelastic) recovery. Field measurements have shown that anelastic strain recovery occurs in drill cores after drilling and coring and is usually accompanied by the opening and propagation of preferential microcracks. Upon relief from an anisotropic *in situ* stress field, core samples tend to expand most in the direction of maximum stress relief and least in the direction of minimum stress relief. Thus by proper instrumentation of recovered oriented cores, the orientation of the principal *in situ* stresses can be inferred from the directions of measured maximum and minimum strains (Fig. 7.1a). Determination of the magnitude of the stresses is more difficult and requires a constitutive model for the rock. This relatively recent stress measurement method is called the 'anelastic strain recovery' (ASR) method.

Another recent technique which also uses the response of oriented core samples following drilling and coring is called the 'differential strain curve analysis' (DSCA) method. It is based on the concept that careful monitoring of the strain behavior of a rock specimen upon reloading can reflect its past stress history. After an oriented drill core is brought up to the surface, and the microcracks have had time to develop and to align themselves in the direction of the original stresses, the expansion of the core is reversed by subjecting it to hydrostatic loading in a pressure vessel (Fig. 7.1b). By instrumenting the core with strain gages, the strains due to microcrack closure can be

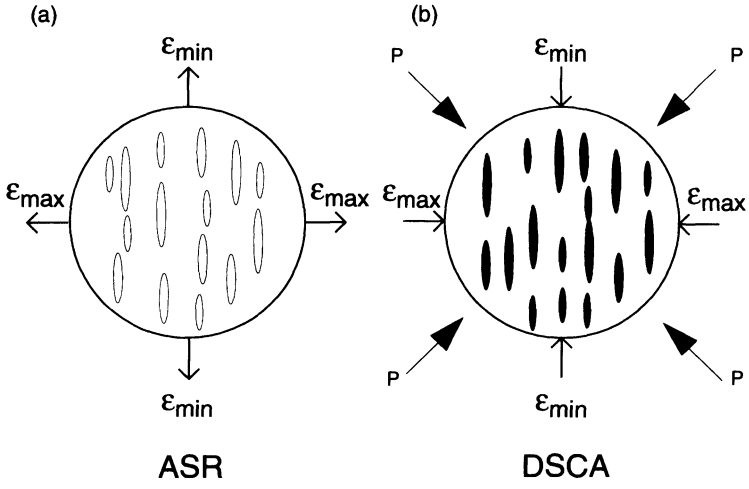

Fig. 7.1 Principle behind (a) the anelastic strain recovery (ASR) method and (b) the DSCA method.

determined by subtracting the average intact rock strains from the measured total strains. In the analysis of DSCA data it is assumed (among other things) that the principal directions of the current *in situ* stress field coincide with the principal directions of the strains due to microcrack closure. Further, the ratios between the three principal *in situ* stresses are assumed to be related to the ratios between the three principal strains due to crack closure. Specific stress values can be assigned by using, for instance, the hydrofracturing shut-in pressure as a measure of the minimum stress. Another assumption is to take the vertical stress as a principal stress due to the weight of the overlying rock. Once one principal stress is known, the other two principal stresses can be determined.

7.2 HISTORY

7.2.1 ASR METHOD

Voight (1968) suggested that if it can be assumed that partial recoverable strains are proportional to total recoverable strains, an estimate of the virgin state of stress at depth can be obtained by instrumenting an oriented drill core immediately following its removal from a borehole. Voight (1968) noted that there is a need for an empirical justification when considering that the recovered anelastic strains are proportional to the total recoverable strains and that the strains are related to the virgin stress state. If the rock is assumed to be isotropic and homogeneous and the relaxation is linearly viscoelastic, then the strain relief along the principal strain directions will be uniform with time, and the directions of principal strain relief will correspond to the initial *in situ* strain conditions. Thus the principal strain directions determined with ASR measurements will coincide with the principal *in situ* stress directions.

The first successful use of ASR measurements on oriented cores from deep wells as a method of determining the directions and ratios of *in situ* stresses was reported by Teufel (1982). Prior to that time, ASR measurements had been carried out but the results had been found inconsistent due to the measuring technique used where conventional strain gages had been attached onto the surfaces of unsealed core samples (e.g. Enever and McKay, 1976). Teufel (1982) used clip-on disk gages placed on sealed cores to measure displacements across their entire diameter. Three disk gages mounted at 45° to each other were able to record core deformation with a sensitivity of 2 to 8 microstrains over a period of about 40 h and at a fixed time interval of 1 h. Good agreement was obtained between the principal stress directions inferred from ASR measurements and the azimuth of hydraulic fractures measured as part of a mineback operation in volcanic tuff at the Nevada Test Site in the USA. Later, Smith *et al.* (1986), Lacy (1987), Warpinski and Teufel (1989a), Perreau, Heugas and Santarelli (1989) and Teufel and Farrell (1990) applied the same technique to other geological formations and found good agreement between horizontal principal stress directions determined from ASR and other methods such as hydraulic fracturing, borehole breakouts, core disking and DSCA.

The determination of stress magnitudes using the ASR method is more difficult and requires a constitutive viscoelastic model for strain relaxation. Blanton (1983) derived equations to solve the problem for isotropic and transversely isotropic rocks. Later, Blanton and Teufel (1983) included the effect of pore pressure in the viscoelastic recovery model and applied the model to stress measurements in Devonian shales. To date, the most extensive published ASR data set comes from the Multiwell Experiment site in the Piceance Basin near Rifle, Colorado (Warpinski and Teufel, 1989a). The horizontal principal stress magnitudes and directions determined from open-hole hydraulic fracturing experiments and ASR measurements in the Rollins Sandstone Formation were found to be in relatively good agreement (Teufel and Warpinski, 1984).

Strain recovery methods are well suited for stress measurements in deep wells. The time-dependent strain recovery was investigated on drill cores of two rock types from the German Continental Deep Drilling Project (KTB) by Wolter and Berckhemer (1989). The strains were measured with inductive displacement transducers along the core axis and in three different radial directions under constant conditions of temperature and moisture (Fig. 7.2). Time-dependent strain recovery was recorded for several days and distinct differences in magnitude and duration of anelastic recovery processes were observed for lithologically different samples.

Several studies have been conducted by Teufel and co-workers in order to understand the mechanism involved in the ASR process (Lacy, 1987; Teufel, 1982, 1993). In general, it has been found that upon coring and subsequent stress relief, core samples acquire a new microfabric due to the opening and propagation of microcracks that are aligned in the directions of the principal stresses. As summarized by Teufel (1993), the new fabric can be confirmed by acoustic emission and anisotropy of various petrophysical properties of the rock, such as compressional velocity, elastic modulus and permeability. Genesis of microcracks during ASR has been supported, indirectly, by laboratory studies which have shown that, in totally relaxed sandstone cores, compressional wave velocities and elastic modulus are lowest in the direction of maximum strain recovery and stress relief (Lacy, 1987; Teufel, 1982).

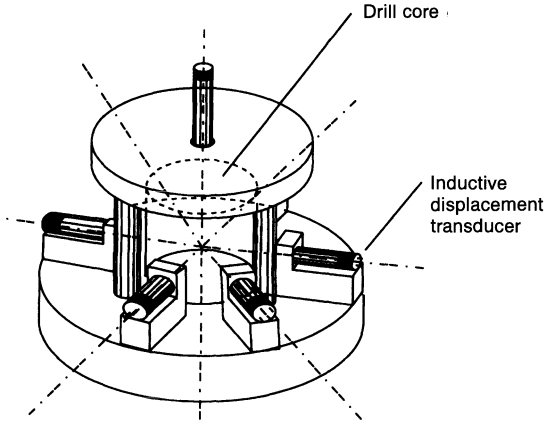

Fig. 7.2 Instrument for ASR measurements of a drill core. Three pairs of radial inductive displacement transducers and one axial transducer are used to measure the anelastic response of a core sample. (After Wolter and Berckhemer, 1989.)

Teufel (1993) also analyzed the various parameters that could affect ASR measurements and the analysis of ASR data. He concluded that nine parameters could significantly limit the application of the ASR method for determining *in situ* stresses: (1) temperature variations yielding thermal strains, (2) dehydration of core samples, (3) pore fluid pressure diffusion, (4) non-homogeneous recovery deformation, (5) rock anisotropy, (6) drilling mud–rock interaction, (7) residual strains, (8) core recovery time and (9) accuracy of core orientation.

Recently, Matsuki (1991) and Matsuki and Takeuchi (1993) developed a three-dimensional theory that can be used to determine both the magnitude and orientation of *in situ* stresses from measurements of anelastic normal strain recovery on oriented core samples. The rock is assumed to be isotropic and viscoelastic. Normal strains are measured using strain rosettes glued on the faces of cubical specimens cut from the core samples. The theory was applied successfully to field measurements carried out at the Yunomori geothermal field in Japan. The same technique was also applied by Matsuki and Sakaguchi (1995) on core samples of a hard limestone at the Kamaishi mine in Japan. The results of the differential strain analysis method were compared with those obtained with the conical-ended borehole overcoring method (section 5.2.2). The stress orientations obtained with the ASR method did not coincide well with those determined by overcoring. The difference was attributed to difficulties in measuring small strains, thus indicating a need for more accurate measuring systems when using the ASR method on hard rocks.

7.2.2 DSCA METHOD

Core specimens recovered from deep boreholes typically exhibit a large, reversible nonlinear behavior when subjected to hydrostatic loading in the laboratory. At sufficiently high stress levels, however, the nonlinear deformation is replaced by a linear response. The nonlinear part of the response is commonly attributed to the closure of microcracks in the rock, the linear portion being observed once the microcracks are completely closed (Walsh, 1965).

In the 1970s, Simmons, Siegfried and Feves (1974) and Siegfried and Simmons (1978) developed an experimental laboratory method to characterize microcrack porosity in a rock sample for various closing pressures. The method, called differential strain analysis, consisted of applying hydrostatic pressure to a rectangular prism of rock which had previously been jacketed and instrumented with strain gages. A fused silica sample was prepared similarly to the rock sample and was subjected to the same pressure as the rock sample. Differential strains (rock strains minus the fused silica strains) were measured. By measuring the longitudinal strain in six directions on the rock prism at different pressures, the six components of a crack strain tensor could be determined. It was also shown that the principal values and axes of that tensor could provide information regarding crack orientation in the rock sample and its variation with confining pressure.

Experimental studies reported by Simmons and Richter (1974), Simmons, Siegfried and Feves (1974) and Strickland, Feves and Sorrells (1979) all seemed to confirm that microcracks in core samples are the result of core relaxation during the drilling process. Based on that observation, Strickland and Ren (1980) modified the differential strain analysis method in order to be able to predict *in situ* stresses. Their method, called the differential strain curve analysis method, was based on four critical assumptions: (1) microcracks are induced as the rock expands by relief from the *in situ* stress field, (2) the microcracks are aligned in the direction of the original stresses, (3) the cracks are proportional volumetrically to the *in situ* stress magnitude in any direction and (4) under hydrostatic loading, contraction of the rock in any specific direction is analogous to the original strain in that direction. By measuring the response to hydrostatic loading of a cubical rock sample on which a minimum of six strain gages are glued, the three principal strains due to crack closure can be determined. These strains are then related to the *in situ* stresses. Strickland and Ren (1980) reported several examples of stress measurements with the DSCA method on oriented and nonoriented core samples of sandstone and shale from Texas, Louisiana and Pennsylvania.

Extensive laboratory and field investigations led Ren and Roegiers (1983) to validate further the DSCA method for determining the *in situ* stress field from measurements performed on oriented rock cores. The DSCA method was applied to three different rocks (fine-grained sandstone, medium-grained sandstone and fine-grained granite). Good agreement was found between the stresses predicted with the DSCA method and other direct and indirect methods of stress measurement for the two sandstones. The stresses determined with the DSCA method on granite did not agree well with the stresses determined with other methods. Ren and Roegiers (1983) concluded that the quality and reliability of DSCA data depend strongly on experience, and that the DSCA method is a cost-effective measurement technique which does not require any assumption regarding the orientation of the *in situ* stress field with respect to the borehole.

Thiercelin *et al.* (1986) improved the DSCA technique and applied it to core samples from the Multiwell Experiment site in the Piceance Basin of Colorado. They presented two possible approaches to derive information on the *in situ* stress tensor. One approach consists of computing the crack density in the core

sample as a function of spatial direction. Assuming that one preferential microcrack orientation exists, knowledge of the principal directions of the compressibility tensor at a given pressure should indicate the crack distribution as a function of orientation. The maximum principal direction will show the direction of the largest crack density, and therefore should correspond to the direction of the maximum principal *in situ* stress. A better approach to understanding the crack pattern can be obtained, however, by determining the variation of the total strain tensor of the cracked rock as a function of hydrostatic pressure. Mathematically, this approach is similar to that proposed by Strickland and Ren (1980). Thiercelin *et al.* (1986) reported that the two approaches mentioned above to predict stress direction from microcracks induced by core relaxation yield good orientation predictions. Stresses determined with the DSCA method were also found to be in good agreement with measured values from hydraulic fracturing and borehole seismic tests.

Dey and Brown (1986) employed the DSCA method for deep stress measurements (down to a depth of 4 km) at the Fenton Hill Hot Dry Rock site in New Mexico, along with hydrofracturing tests. The DSCA performed on cubical samples 3 cm in size cut from oriented cores gave reasonable magnitudes and directions of principal stresses (Fig. 3.8). Determination of the stress field from laboratory measurements on oriented core samples was also investigated by Perreau, Heugas and Santarelli (1989). They presented results from ASR, DSCA and core disking analysis carried out on three cores retrieved at depths ranging between 1285 m and 4550 m in two wells. A comparison was made with data available from hydraulic fracturing, geophysical logs and regional tectonics. Their main conclusion was that the different methods gave a good idea of the horizontal principal stresses at the wellbore site.

More recently, Matsuki and Sakaguchi (1995) applied the DSCA method to core samples of a hard limestone at the Kamaishi mine in Japan. The results of the DSCA method were compared with those obtained with the conical-ended borehole overcoring method (section 5.2.2). In general, it was found that the *in situ* stress orientations determined with the DSCA method correlated poorly with those determined by overcoring. However, the stress magnitudes correlated better if the vertical stress determined by overcoring was used as an input into the DSCA analysis in order to determine the other principal stress components.

7.3 TECHNIQUES, EQUIPMENT AND PROCEDURES

7.3.1 ASR

ASR measurements are, in general, conducted on oriented drill cores from deep wells. Immediately upon retrieval from the core barrel, the oriented core is carefully examined to select samples without inhomogeneities and natural fractures. Cored samples are cut and sealed in order to prevent moisture changes. The displacements associated with ASR can be measured using various techniques such as spring-loaded clip-on gages, displacement transducers or strain rosettes.

If the core comes from a vertical borehole where the vertical stress is known to be one of the principal stresses, only three independent displacement measurements are required to determine the direction and magnitude of the two horizontal principal strains (Fig 7.2). Teufel (1993) suggested that, in that case, the best procedure is to use four clip-on gages or transducers mounted at 45° to each other in the horizontal plane of each core and to use the combination of any three gages to calculate the horizontal principal strains. The vertical strain is determined by mounting a gage or transducer parallel to the axis of the core. Displacement data for each gage, ambient temperature and temperature of the core are recorded. Teufel (1993) reported strain measurements with a resolution of 1 microstrain. During

testing, the temperature of the core must be kept constant, otherwise thermal corrections must be made.

If cores are obtained from deviated holes or the stress state is known to be inclined with respect to the borehole axis, the method requires at least six gages. Then it becomes more difficult to apply the method of clip-on gages as the number of gages increases. Instead, the core can be cut with a diamond saw to produce three perpendicular flat surfaces where a strain rosette with thermocouple is glued on each surface (Matsuki and Takeuchi, 1993). The specimen is then sealed to prevent changes in water content. The sealed sample is then set in a water bath with constant temperature and the anelastic normal strains in six independent directions are measured at constant time interval until the relaxation ceases (Matsuki and Takeuchi, 1993).

7.3.2 DSCA

The standard experimental procedure for the DSCA method described by Ren and Roegiers (1983) and Thiercelin *et al.* (1986) consists of the following steps.

1. A cubical sample is cut from the center of an oriented drill core in order to avoid the zone of core damage associated with drilling.
2. After cleaning the sample and drying it for a period of 24 h, the cube is instrumented with strain gages. Figure 7.3a shows an example of a nine strain gage arrangement used by Thiercelin *et al.* (1986). Strickland and Ren (1980) and Ren and Roegiers (1983) used 12 strain gages, four on each of three orthogonal faces of the cube (Fig. 7.3b). The entire assembly is then potted into a flexible silicone jacket to prevent fluid entering the rock during subsequent hydrostatic loading.
3. The assembly is placed in a pressure vessel and a hydrostatic pressure (up to 200 MPa) is applied at a constant high rate to avoid rock creep and temperature changes during compression. To avoid experimental errors due to secondary effects from pressure and temperature on the instrumentation used, a small sample of fused silica (prepared similarly to the rock sample) is put in the vessel as a reference following the differential strain analysis procedure of Simmons, Siegfried and Feves (1974) and Siegfried and Simmons (1978).

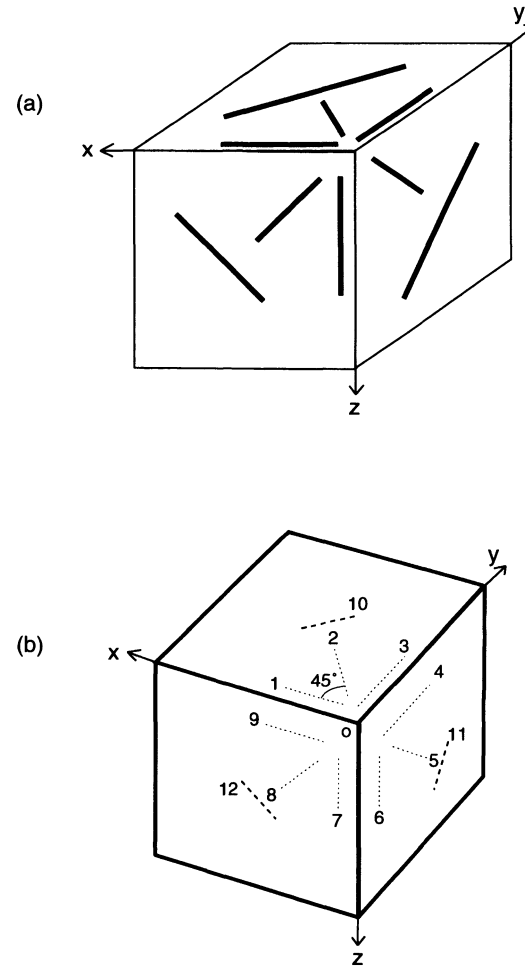

Fig. 7.3 Differential strain curve analysis. (a) Nine strain gage arrangement on a cubical sample. (After Thiercelin *et al.*, 1986.) (b) Twelve strain gage arrangement. (After Strickland and Ren, 1980.)

4. Output signals from the strain gages and pressure are continuously recorded by a data acquisition system during loading and subsequent unloading.
5. The strain versus applied pressure records are analyzed after correction for the strains measured in the fused silica sample (Siegfried and Simmons, 1978). Then the components of the crack strain tensor associated with microcrack closure, the ratio of principal stress magnitude and the principal stress orientation are determined.

In general, the number of strain gages glued at the surface of the cubical samples is more than the six required to determine the six components of the strain tensor. If one of the principal stresses (strains) is known and the rock is isotropic, only three strain measurements are needed to determine the other two principal strains. If more than the six or three strain measurements are available, several combinations of strain data can be analyzed, thus providing redundancy and a way to determine confidence intervals for the *in situ* stress components.

7.4 THEORY

7.4.1 ASR

Several models have been proposed to determine the orientation and magnitude of principal *in situ* stresses from ASR data. In the general three-dimensional theory of Matsuki and Takeuchi (1993), the ASR of an isotropic viscoelastic rock subjected to a general three-dimensional stress field is decomposed into two independent deformation modes: a shear mode and a volumetric mode. Let C_{as} and C_{av} be the ASR compliances for the shear and volumetric modes, respectively. The anelastic deviatoric strain tensor e_{ij} and the anelastic mean normal strain e_m after stress relief are related to the deviatoric stress tensor s_{ij} and the mean normal stress σ_m as follows:

$$e_{ij}(t) = C_{as}(t)s_{ij} \tag{7.1}$$

and

$$e_m(t) = C_{av}(t)\sigma_m \tag{7.2}$$

Consider now a rock subjected to a three-dimensional *in situ* stress field, a pore pressure P_o and a change in temperature ΔT. Using the correspondence principle of the theory of linear viscoelasticity, Matsuki and Takeuchi (1993) derived an expression for the anelastic normal strain recovery $\varepsilon_a(t)$ in any direction with direction cosines (l,m,n) in an arbitrary x,y,z coordinate system, when the stresses and pore pressure are released stepwise and for a given rate of temperature change, e.g.

$$\begin{aligned}\varepsilon_a(t) = {} & \tfrac{1}{3}[(3l^2-1)\sigma_x + (3m^2-1)\sigma_y \\ & + (3n^2-1)\sigma_z + 6lm\tau_{xy} \\ & + 6mn\tau_{yz} + 6nl\tau_{zx}]C_{as}(t) \\ & + (\sigma_m - P_o)C_{av}(t) + \alpha_T\Delta T(t)\end{aligned} \tag{7.3}$$

where α_T is the coefficient of linear thermal expansion of the rock. Equation (7.3) indicates that, in general, the anelastic normal strain depends on the six components of the *in situ* stress field, the pore pressure, the change in temperature and the two compliance terms.

Equations (7.1)–(7.3) provide the basis for the ASR method. The six components of the anelastic strain tensor in the x,y,z coordinate system can be determined if anelastic normal strains in (at least) six independent directions are measured with either displacement transducers or clip-on gages as described by Teufel (1982, 1993), or strain gages as suggested by Matsuki and Takeuchi (1993). The anelastic strain tensor can then be divided into a mean normal strain tensor and a deviatoric strain tensor. Because of the pore pressure and the change in temperature, the mean normal strain is equal to

$$e_m = (\sigma_m - P_o)C_{av}(t) + \alpha_T\Delta T \tag{7.4}$$

The components of the anelastic deviatoric strain tensor are equal to

$$\begin{aligned} e_x &= s_x C_{as}(t); & e_y &= s_y C_{as}(t); \\ e_z &= s_z C_{as}(t); & e_{xy} &= \tau_{xy} C_{as}(t); \\ e_{yz} &= \tau_{yz} C_{as}(t); & e_{zx} &= \tau_{zx} C_{as}(t) \end{aligned} \tag{7.5}$$

where $s_x = \sigma_x - \sigma_m$, $s_y = \sigma_y - \sigma_m$, etc. are the deviatoric stress components. From equation (7.5), it follows that the orientation of the principal stresses $(\sigma_1, \sigma_2, \sigma_3)$ can be determined from the orientation of the principal anelastic deviatoric strains (e_1, e_2, e_3). Also, the ratios of principal deviatoric stresses $(s_1/s_3,\ s_2/s_3)$ are given by the ratios of principal anelastic deviatoric strains $(e_1/e_3,\ e_2/e_3)$. These ratios are constant throughout the strain recording and can be determined without knowing the ASR compliances of the rock sample. This statement is valid as long as the rock sample is thermally and mechanically isotropic.

The magnitude of each principal stress σ_i $(i = 1,2,3)$ can be determined by combining equations (7.4) and (7.5), e.g.

$$\sigma_i(t) = \frac{e_i(t)}{C_{as}(t)} + \frac{1}{C_{av}(t)} \times [e_m(t) - \alpha_T \Delta T] + P_o \qquad (7.6)$$

Thus according to equation (7.6), in order to determine the magnitude of the principal *in situ* stress components, the ASR shear and volumetric compliances, C_{as} and C_{av}, must be determined along with the effect of pore pressure and temperature on the mean anelastic normal strain. As shown by Matsuki and Takeuchi (1993), the two compliances depend themselves on the magnitude of the mean normal stress. Therefore, several iterations must be performed in order to ensure that the stress condition used to calibrate the ASR compliances does not differ significantly from the determined values. Note that if the two compliances cannot be determined, the theory of Matsuki and Takeuchi (1993) yields only the orientation and ratios of the principal *in situ* stresses. If one of the three principal stresses can be estimated, the other two principal stresses can be determined.

Another theory was proposed by Blanton (1983), who developed an expression to calculate the magnitude of the principal stresses from the strain recovery of drill cores as long as the following assumptions are satisfied: (1) the rock is homogeneous, isotropic and linearly viscoelastic, (2) the wellbore is vertical, (3) the vertical stress is a principal stress and can be estimated, (4) the pore pressure in the formation is known and (5) a constant Poisson's ratio and poroelastic condition prevail throughout the relaxation process.

As shown by Blanton (1983), the two horizontal principal *in situ* stresses S_H and S_h can be calculated from the changes in the principal strains between any two times as

$$S_H = (S_v - \alpha P_o)\frac{(1-\nu)\Delta\varepsilon_H + \nu(\Delta\varepsilon_h + \Delta\varepsilon_v)}{(1-\nu)\Delta\varepsilon_v + \nu(\Delta\varepsilon_H + \Delta\varepsilon_h)} + \alpha P_o \qquad (7.7)$$

and

$$S_h = (S_v - \alpha P_o)\frac{(1-\nu)\Delta\varepsilon_h + \nu(\Delta\varepsilon_H + \Delta\varepsilon_v)}{(1-\nu)\Delta\varepsilon_v + \nu(\Delta\varepsilon_H + \Delta\varepsilon_h)} + \alpha P_o \qquad (7.8)$$

where $\Delta\varepsilon$ are changes in principal strain between any two times in the horizontal (H,h) and vertical (v) directions, ν is the Poisson's ratio, P_o is the pore pressure, α is the poroelastic constant and S_v is the vertical stress. The orientation of the horizontal principal stresses is determined from the directions of the horizontal principal anelastic strains.

A third type of strain model was developed by Warpinski and Teufel (1989b). It requires fitting a theoretical linear viscoelastic model to the measured strain history using a least squares fit of the entire strain data set to an expected relaxation behavior of the form

$$\varepsilon_r(t) = (2S_H\cos^2\theta + 2S_h\sin^2\theta - S_H\sin^2\theta - S_h\cos^2\theta - S_v)J_1(1 - e^{-t/t_1}) + (S_H + S_h + S_v - 3P_o)J_2(1 - e^{-t/t_2}) \qquad (7.9)$$

and

$$\varepsilon_v(t) = (2S_v - S_H - S_h)J_1(1 - e^{-t/t_1}) + (S_H + S_h + S_v - 3P_o)J_2(1 - e^{-t/t_2}) \qquad (7.10)$$

where θ is the orientation angle of the measuring gage with respect to the maximum horizontal stress; J_1 and J_2 are the distortional and dilatational creep compliance arguments (i.e. equilibrium values of the creep compliances); t represents time, t_1 and t_2 are deviatoric and dilatational creep time constants, respectively; and the subscripts r and v correspond to the radial direction in the horizontal plane and the vertical direction, respectively. This model is based on the assumptions that the rock is isotropic and linearly viscoelastic, the borehole is vertical and the vertical stress is a known principal stress. Again, the orientation of the horizontal principal stresses is determined from the directions of the horizontal principal anelastic strains.

7.4.2 DSCA

In general, a rock sample containing microcracks will experience a volume change when subjected to a hydrostatic pressure. Walsh (1965) proposed the following relationship relating the volumetric strain $\Delta V/V$ of a rock sample containing microcracks to the applied pressure p:

$$\frac{\Delta V}{V} = \beta p + \eta(p) \qquad (7.11)$$

where $\beta = 3(1 - 2\nu)/E$ is the (intrinsic) compressibility of the intact rock with Young's modulus E and Poisson's ratio ν, and $\eta(p)$ is the microcrack porosity. The first term in equation (7.11) is associated with the linear elastic deformation of the intact rock, while the second term reflects the contribution of the microcracks. Figure 7.4 schematically represents this relationship. As pointed out by Walsh (1965), the intercept η_o of the linear portion of the pressure versus volumetric strain curve with the strain axis of Fig. 7.4 represents the initial rock porosity due to the microcracks. In Fig. 7.4 the pressure p_c is a critical pressure beyond which all microcracks are completely closed and the rock sample responds in a linearly elastic manner to further pressure increase. At any given pressure p less than p_c, $\eta(p)$ is the zero pressure intercept of a line parallel to the linear portion of the pressure versus volumetric strain curve. It can also be understood as the microcrack porosity due to the presence of cracks closing completely at pressures less than p.

A three-dimensional generalization of equation (7.11) was proposed by Morlier (1971) and Siegfried and Simmons (1978) assuming linear crack closure and non-interacting cracks. Linear crack closure implies that strain of a rock with microcracks is linear over any pressure range in which no cracks close completely. A somewhat more practical version of the mathematical model of Siegfried and Simmons (1978) was presented by Strickland and Ren (1980) for the analysis of DSCA data and is summarized below.

For each strain gage i (i = 1–9 or 12) of Figs 7.3a, b, a pressure versus longitudinal strain curve is obtained during hydrostatic loading.

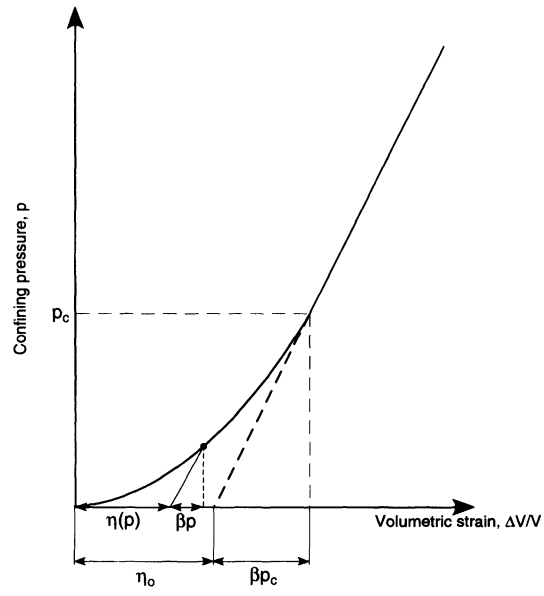

Fig. 7.4 Pressure versus volume change curve used in the DSCA method. In this figure, η_o is the microcrack porosity at zero pressure due to all the cracks that close completely once a critical pressure p_c has been reached.

The curve is in general similar to that shown in Fig. 7.4 where $\Delta V/V$ is now replaced by the longitudinal strain ε. Let β_i be the slope of the linear portion of that curve which represents the intrinsic compressibility of the rock sample in the direction of the ith strain gage. The contribution of microcrack closure, $\eta_i(p)$, to the longitudinal strain $\varepsilon_i(p)$ recorded in the ith strain gage at pressure p is equal to

$$\eta_i(p) = \varepsilon_i(p) - \beta_i p \tag{7.12}$$

In the pressure versus strain diagram, $\eta_i(p)$ is represented by the zero pressure intercept of a line of slope β_i passing by the point at pressure p (Fig. 7.4). Knowing the orientation of the strain gages with respect to an x,y,z coordinate system (Figs 7.3a, b), and using coordinate transformation rules for strains, the crack strain contribution to all strain gages can be resolved into a second-order crack strain tensor, $\eta_{ij}(p)$. The principal values of that tensor and their orientation in the x,y,z coordinate system can then be determined. By repeating this analysis at different pressures, any rotation in the microcrack orientation can be assessed, allowing one to identify the presence of more than one set of microcracks in the core samples (Thiercelin *et al.*, 1986).

The analysis of DSCA data is usually done by determining the crack strain tensor over a pressure range Δp, from strain measurements in the linear sections of the pressure versus strain curves and for pressures less than the closing pressure (Ren and Roegiers, 1983; Strickland and Ren, 1980). In that case, for each strain measurement, the following quantity is determined:

$$\begin{aligned} \varepsilon_i' &= \frac{\eta_i(p+\Delta p) - \eta_i(p)}{\Delta p} \\ &= \frac{\varepsilon_i(p+\Delta p) - \varepsilon_i(p)}{\Delta p} - \beta_i \\ &= \theta_i - \beta_i \end{aligned} \tag{7.13}$$

Using the coordinate transformation rules for strains, the values of ε_i' ($i = 1$–9 or 12) can be resolved into a second-order crack strain tensor. The principal values η_{p1}, η_{p2} and η_{p3} of that tensor and their orientation in the x,y,z coordinate system are then determined.

In DSCA the principal *in situ* stress directions are assumed to coincide with the principal directions of the crack strain tensor. Several suggestions have been proposed to calculate the ratios of the principal *in situ* stresses. Strickland and Ren (1980) use directly the ratios η_{p1}/η_{p3} and η_{p2}/η_{p3} as a measure of the principal stress ratios σ_1/σ_3 and σ_2/σ_3, respectively. Ren and Roegiers (1983) use the following relations:

$$\frac{\sigma_1}{\sigma_3} = \frac{\eta_{p1}(1-\nu) + \nu(\eta_{p2} + \eta_{p3})}{\eta_{p3}(1-\nu) + \nu(\eta_{p1} + \eta_{p2})} \tag{7.14}$$

and

$$\frac{\sigma_2}{\sigma_3} = \frac{\eta_{p2}(1-\nu) + \nu(\eta_{p1} + \eta_{p3})}{\eta_{p3}(1-\nu) + \nu(\eta_{p1} + \eta_{p2})} \tag{7.15}$$

which were derived based on Hooke's law for isotropic media. In equations (7.14) and (7.15) ν is the Poisson's ratio of the rock. Modified versions of equations (7.14) and (7.15) for transversely isotropic rocks can be found in Ren and Roegiers (1983).

7.5 DATA ANALYSIS AND INTERPRETATION

7.5.1 ASR

To date, the most extensive published ASR data set comes from the Multiwell Experiment site in the Piceance Basin of Colorado (Warpinski and Teufel, 1989a). ASR measurements were conducted on oriented sandstone and mudstone cores taken at depths ranging between 1400 m and 2500 m in three closely spaced wells. Figure 7.5 shows examples of ASR data for representative sandstones from three non-marine intervals. Data from four displacement gages (three horizontal and one vertical) taken at 1 h intervals and the strain history fits of the data determined with the strain history model represented by equations (7.9) and (7.10) are shown. All strains start at zero at the time the cores are first instrumented with the displacement gages. The

early negative strains represent anelastic strains that the cores experienced prior to instrumentation, as estimated by the strain history model.

Warpinski and Teufel (1989a) reported that the data quality for the Mesaverde sandstones was excellent and that the theoretical viscoelastic strain history model fitted the measured response very well. As shown in Fig. 7.5, the vertical strain relaxation is considerably greater than the horizontal strain relaxation, implying that the maximum principal stress

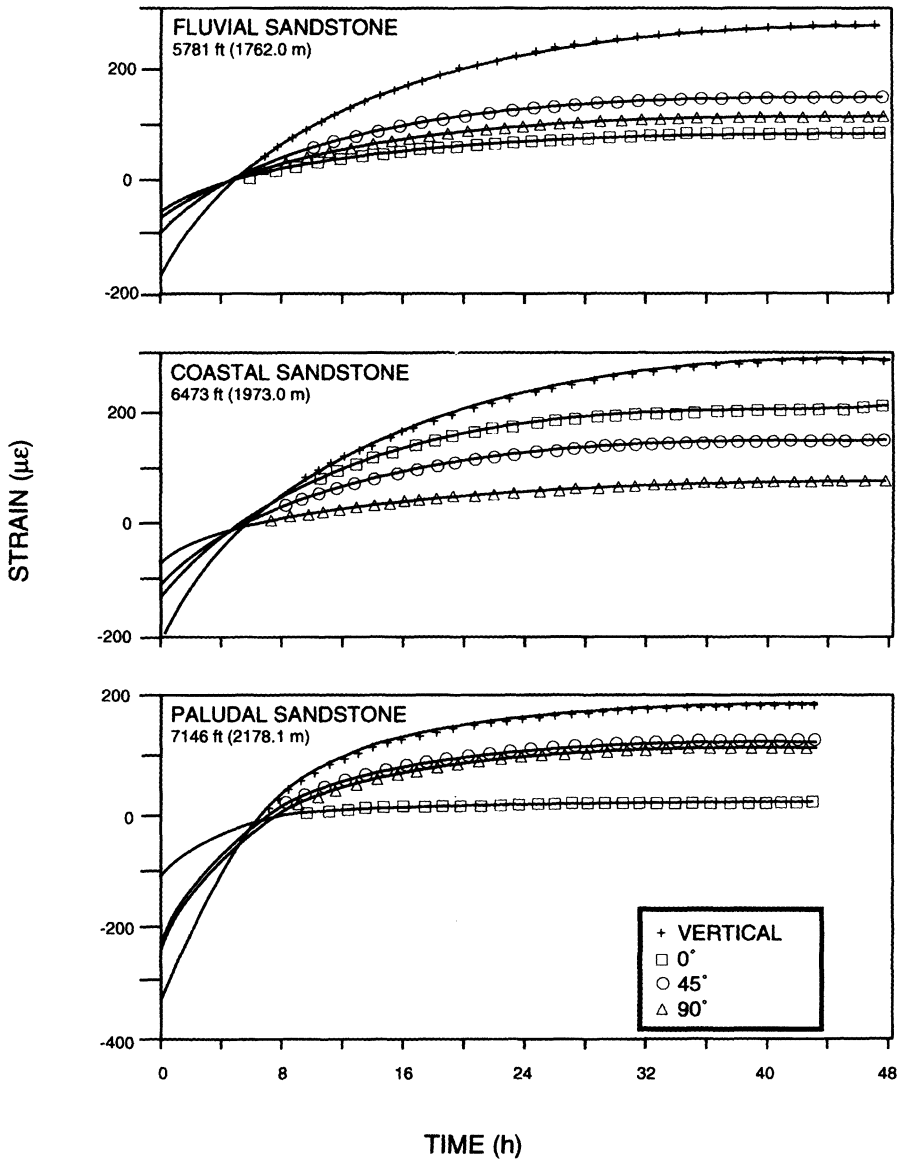

Fig. 7.5 ASR data and strain history fits for three types of Mesaverde sandstone of the Piceance Basin of Colorado. Strain recovery versus time is presented for three pairs of horizontal displacement gages and one vertical gage. (After Warpinski and Teufel, 1989a.)

Table 7.1 Maximum horizontal stress direction determined with four methods at the Multiwell Experiment site in the Piceance Basin of Colorado (after Teufel, 1993)

Method	*Maximum horizontal stress orientation*
Hydraulic fracturing – impression packer	N60°W ± 10°
Hydraulic fracturing – borehole seismic	N68°W ± 8°
Borehole breakouts	N74°W ± 11°
ASR measurements	N75°W ± 15°

is the overburden stress. Further, the total anelastic strain experienced by the rock in any gage direction increases with increasing depth. The calculated principal strain data and corresponding strain orientations were found to vary with the lithology but the largest source of error was estimated to be related to the core heterogeneities and orientation survey during core recovery, which at best was accurate to within 5–10°.

Teufel (1993) presented a summary of different methods used to determine the maximum horizontal stress direction at the Multiwell Experiment site in Colorado. The methods and recorded directions of S_H are listed in Table 7.1. All of the measurements are in good agreement and suggest that ASR can be a useful method for estimating the directions of horizontal principal *in situ* stresses.

The determination of horizontal principal stress magnitudes from ASR measurements requires implementation of a viscoelastic model for the rock material. According to Warpinski and Teufel (1989a), the state of stress can be calculated if the creep compliance J_1 in equations (7.9) and (7.10) is known or the minimum horizontal principal stress S_h can be determined separately (from the shut-in pressure of hydraulic fracturing tests). Using the direct model defined by equations (7.7) and (7.8) and the strain history model defined by equations (7.9) and (7.10) together with hydrofracturing data for the least horizontal principal stress, the maximum horizontal stresses were calculated for the fluvial, coastal and paludal examples presented in Fig. 7.5. The results are reported in Table 7.2. It can be seen that there is a relatively good agreement between the two ASR methods and between hydrofracturing and strain recovery.

7.5.2 DSCA

The results of DSCA of one typical sample from the Multiwell Experimental site in the Piceance Basin of Colorado tested by Thiercelin *et al.* (1986) are presented below as an illustrative example. The sample (a cube 3 cm in size) was cut from an oriented core of a massive sandstone originating from a depth of about 1980 m. The sample was instrumented with nine strain gages as shown in Fig. 7.3a. Typical principal strain versus hydrostatic pressure curves are shown in Fig. 7.6. The curves exhibit a somewhat linear behavior for pressures larger than about 50 MPa.

Following the DSCA analysis summarized above, the principal *in situ* stress directions

Table 7.2 Stress data from hydraulic fracturing and ASR in Mesaverde sandstones, Colorado (after Warpinski and Teufel, 1989a)

Type of sandstone	*Depth (m)*	*Hydraulic fracturing*		*ASR, direct model*[a]		*ASR, strain history model*[b]
		S_V *(MPa)*	S_h *(MPa)*	S_H *(MPa)*	S_h *(MPa)*	S_H *(MPa)*
Fluvial	1762	41.9	30.6	37.4	32.8	36.5
Coastal	1973	46.9	39.1	44.3	39.7	43.6
Paludal	2178	51.8	40.3	49.9	44.2	48.9

[a] See equations (7.7) and (7.8).
[b] See equations (7.9) and (7.10).

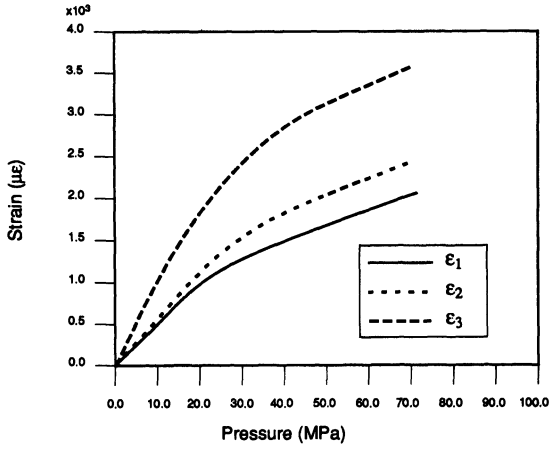

Fig. 7.6 DSCA principal strain versus pressure response curves for a sample of Mesaverde sandstone. (After Thiercelin *et al.*, 1986.)

were determined from the principal directions of the strains due to microcrack closure. Figure 7.7 shows those directions on a stereonet (lower hemisphere equal area projection) for different combinations of strain data and for pressures ranging between 28 and 35 MPa. It

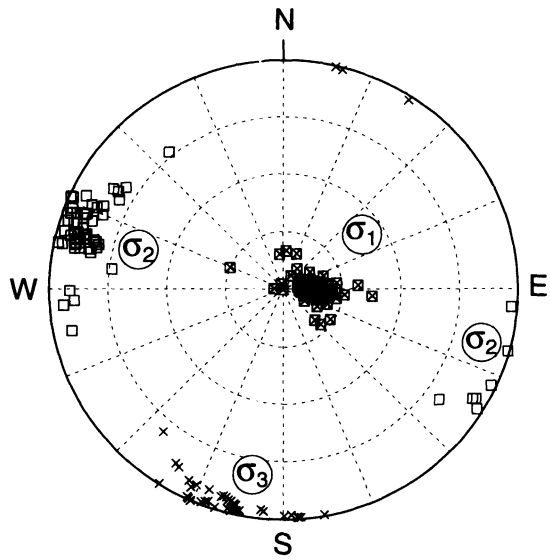

Fig. 7.7 Principal *in situ* stress directions determined from principal directions of the crack strain tensor for a sample of Mesaverde sandstone tested at hydrostatic pressures ranging between 28 and 35 MPa. (After Thiercelin *et al.*, 1986.)

can be seen that the *in situ* stresses predicted by the DSCA method are essentially horizontal and vertical. Thiercelin *et al.* (1986) also noted that the orientation of the major horizontal principal stress σ_2 in Fig. 7.7 was essentially parallel to the azimuth of hydrofractures induced by hydraulic fracturing in the same rock formation. For the sample considered here, the principal *in situ* stress ratios were found to be equal to $\sigma_1/\sigma_3 = 1.65$ and $\sigma_2/\sigma_3 = 1.37$ for applied hydrostatic pressures larger than 15 MPa.

REFERENCES

Blanton, T.L. (1983) The relation between recovery deformation and *in situ* stress magnitude, in *Proc. SPE/DOE Symp. Low Permeability Gas Reservoirs*, Denver, SPE Paper 11624, pp. 632–46.

Blanton, T.L. and Teufel, L.W. (1983) A field test of the strain recovery method of stress determination in Devonian shales, in *Proc. SPE/DOE Symp. Low Permeability Gas Reservoirs*, Denver, SPE Paper 12304, pp. 342–65.

Dey, T.N. and Brown, D.W. (1986) Stress measurements in a deep granitic rock mass using hydraulic fracturing and differential strain curve analysis, in *Proc. Int. Symp. on Rock Stress and Rock Stress Measurements*, Stockholm, Centek Publ., Luleå, pp. 351–7.

Enever, J. and McKay, J. (1976) A note on the relationship between anelastic strain recovery and virgin rock stresses – a possible method of stress measurement, in *Proc. ISRM Symp. on Investigation of Stress in Rock, Advances in Stress Measurement*, Sydney, The Institution of Engineers, Australia, pp. 37–40.

Lacy, L. (1987) Comparison of fracture diagnostic techniques. *SPE Prod. Eng.*, **3**, 66–78.

Matsuki, K. (1991) Three-dimensional *in situ* stress measurement with anelastic strain recovery of a rock core, in *Proc. 7th Cong. Int. Soc. Rock Mech. (ISRM)*, Aachen, Balkema, Rotterdam, Vol. 1, pp. 557–60.

Matsuki, K. and Sakaguchi, K. (1995) Comparison of results of in-situ stresses determined by core-based methods with those by overcoring technique, in *Proc. Int. Workshop on Rock Stress Measurement at Great Depth*, Tokyo, Japan, 8th ISRM Cong., pp. 52–7.

Matsuki, K. and Takeuchi, K. (1993) Three-dimensional *in situ* stress determination by

anelastic strain recovery of a rock core, in *Proc. 34th US Symp. Rock Mech.*, Madison, also published in *Int. J. Rock Mech. Min. Sci. & Geomech. Abstr.*, **30**, 1019–22.

Morlier, P. (1971) Description de l'état de fissuration d'une roche à partir d'essais non-destructifs simples. *Rock Mech.*, **3**, 125–38.

Perreau, P.J., Heugas, O. and Santarelli, F.J. (1989) Tests of ASR, DSCA, and core discing analyses to evaluate *in situ* stresses. SPE Paper 17960, pp. 325–36.

Ren, N.-K., and Roegiers, J.-C. (1983) Differential strain curve analysis – a new method for determining the pre-existing *in-situ* stress state from rock core measurements, in *Proc. 5th Cong. Int. Soc. Rock Mech. (ISRM)*, Melbourne, Balkema, Rotterdam, pp. F117–27.

Siegfried, R.W. and Simmons, G. (1978) Characterization of oriented cracks with differential strain analysis. *J. Geophys. Res.*, **83**, 1269–78.

Simmons, G. and Richter, D.A. (1974) Microcracks in rocks: a new petrographic tool (abstract). *EOS Trans.*, **55**, 478.

Simmons, G., Siegfried, R.W. and Feves, M.L. (1974) Differential strain analysis: a new method for examining cracks in rocks. *J. Geophys. Res.*, **79**, 4383–5.

Smith, M.B. *et al.* (1986) A comprehensive fracture diagnostic experiment: comparison of seven fracture azimuth measurements. *SPE Prod. Eng.*, **2**, 423–32.

Strickland, F.G. and Ren, N.-K. (1980) Use of differential strain curve analysis in predicting the *in-situ* stress state for deep wells, in *Proc. 21st US Symp. Rock Mech.*, Rolla, University of Missouri Publ., pp. 523–32.

Strickland, F.G., Feves, M.L. and Sorrells, D. (1979) Microstructural damage in Cotton Valley cores, in *Proc. SPE 54th Annual Tech. Conf.*, SPE Paper 8303, Las Vegas.

Teufel, L.W. (1982) Prediction of hydraulic fracture azimuth from anelastic strain recovery measurements of oriented core, in *Proc. 23rd US Symp. Rock Mech.*, Berkeley, SME/AIME, pp. 238–45.

Teufel, L.W. (1993) Determination of *in situ* stress from partial anelastic strain recovery measurements of oriented cores from deep boreholes, in *Lecture Notes of the Short Course in Modern In Situ Stress Measurement Methods at the 34th US Symp. Rock Mech.*, Madison, 19 pp.

Teufel, L.W. and Farrell, H.E. (1990) *In situ* stress and natural fracture distribution in the Ekofisk field, North Sea. Sandia National Labs Report No. SAND-90-1058C.

Teufel, L.W. and Warpinski, N.R. (1984) Determination of in-situ stress from anelastic strain recovery measurements of oriented core: comparison to hydraulic fracture stress measurements, in *Proc. 25th US Symp. Rock Mech.*, Evanston, SME/AIME, pp. 176–85.

Thiercelin, M.J. *et al.* (1986) Laboratory determination of the *in-situ* stress tensor, in *Proc. Int. Symp. on Engineering in Complex Rock Formations*, Beijing, Pergamon Press, Oxford, pp. 278–83.

Voight, B. (1968) Determination of the virgin state of stress in the vicinity of a borehole from measurements of a partial anelastic strain tensor in drill cores. *Felsmechanik und Ingenieurgeologi*, **6**, 201–15.

Walsh, J.B. (1965) The effects of cracks on the compressibility of rocks. *J. Geophys. Res.*, **70**, 381–9.

Warpinski, N.R. and Teufel, L.W. (1989a) *In situ* stress measurements in nonmarine rocks. *J. Petrol. Tech.*, **41**, 405–14.

Warpinski, N.R. and Teufel, L.W. (1989b) A viscoelastic constitutive model for determining *in situ* stress magnitudes from anelastic strain recovery of core. *SPE Prod. Eng.*, **4**, 272–80.

Wolter, K.E. and Berckhemer, H. (1989) Time dependent strain recovery of cores from KTB – deep drilling hole. *Rock Mech. Rock Eng.*, **22**, 273–87.

BOREHOLE BREAKOUT METHOD 8

8.1 INTRODUCTION

Spalling of the walls of boreholes or wellbores due to stress concentration produces elongated intervals with non-circular cross-sections whose long axes share common average direction. Such intervals are defined as breakouts or breakout zones when the shorter diameter of the borehole corresponds to, or is close to, the diameter of the drillbit. The orientation of the major and minor horizontal *in situ* stresses around a vertical borehole can be inferred from the orientation of breakouts as it is usually assumed that breakouts occur in two diametrically opposed zones along the direction of the minimum horizontal *in situ* stress (Fig. 8.1).

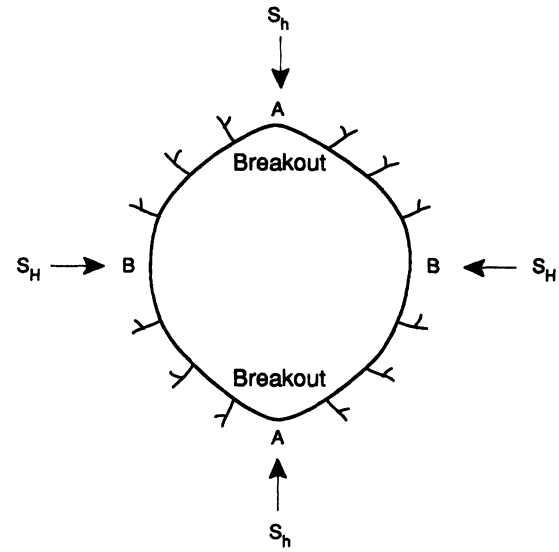

Fig. 8.1 Borehole breakout in the wall of a vertical borehole subjected to major and minor horizontal *in situ* stresses S_H and S_h, respectively. Maximum tangential stress at A and minimum tangential stress at B.

Breakout formation is a rupture phenomenon that has been found in almost all rock types. Numerous investigations have established that consistently oriented breakouts form within an individual well and in wells within a given stress field. This possibility of multiple determinations of stress in an individual well, and the ability to check for regional consistency among numerous wells, make breakout data valuable indicators of stress orientation. In addition, because wells for petroleum and thermal energy exploration and production often are drilled to depths of 3–4 km and even deeper, breakout data help to bridge the gap between near-surface stress indicators and deep stress indicators from earthquake focal mechanisms at depths of 5–15 km (Zoback *et al.*, 1989).

In general, breakouts are used to determine the orientation of *in situ* stresses but not their magnitude. However, it has been found that the shape and depth of breakouts in vertical holes depend on the magnitude of the major and minor horizontal *in situ* stresses. This dependency has led several authors to suggest that the geometry of borehole breakouts could be used to estimate the magnitude of *in situ* stresses. Nevertheless, this approach must be used with caution as breakouts can be enlarged because of various phenomena such as reduction of rock mass strength due to temperature fluctuations or the chemical composition of the drilling fluids, or weathering of the borehole wall especially in weak or weakly cemented rock masses. Breakouts can also be affected by the intensity of drilling (high or low thrust) and the drilling method selected

(Kutter, 1991). Furthermore, recent field tests by Martin, Martino and Dzik (1994) have revealed that breakout geometry is affected by the hole diameter, with an increase in breakout length and depth with increasing hole diameter. Also, when analyzing breakouts for stress analysis, breakouts must be clearly differentiated from other forms of borehole enlargements resembling breakouts (Dart and Zoback, 1987; Plumb and Hickman, 1985). Whether the width and depth of breakouts are clear indications of stress magnitudes is still an open question today.

8.2 HISTORY

8.2.1 OBSERVATIONS

Breakouts for stress determination were first reported by Leeman (1964), who stated that borehole spalling is the result of excessive compressive stress and that the degree of fracturing in the sidewall of a borehole gives quantitative information about the variation in rock stress along the length of the borehole. Further, Leeman (1964) suggested that the broken-out segments are perpendicular to the maximum principal stress in the plane perpendicular to the borehole axis.

The relationship between borehole elongation and fractures mapped on outcrops was first discussed by Babcock (1978) following some observations in deep boreholes with high-resolution dipmeter loggings by Cox (1970). Both Babcock and Cox observed that, in boreholes, zones with elongated cross-sections (over a large interval of borehole depth) show a constant preferential elongation direction which is independent of the stratigraphy. While Babcock (1978) interpreted this as a result of the interaction between the drill-bit and pre-existing joints (fracture intersection mechanism), Bell and Gough (1979) concluded that borehole elongations could be explained through shear fracturing in zones of amplified stress difference in the borehole wall. Concentration of breakouts in a given azimuth was shown to require unequal horizontal principal stresses, and appreciable initial shear strength (cohesion) in the rock mass. Gough and Bell (1982) applied the Mohr–Coulomb brittle fracture theory to determine the state of stress in a borehole wall, and found that shear fracturing could initially extend the hole by 8–10% of its original diameter.

The drilling of the Auburn geothermal well in the state of New York in the USA provided the first opportunity to study dipmeter, televiewer and stress orientation data collected from the same well. The data allowed Plumb and Hickman (1985) to test whether the breakout mechanism or the fracture intersection mechanism best explained the borehole elongation logged with the dipmeter, and to improve the ability to distinguish between breakouts and non-stress-related elongations. The well was logged twice with a four-arm dipmeter. Also, hydrofracturing stress measurements and televiewer loggings were performed by the US Geological Survey and the results were presented by Hickman, Healy and Zoback (1985) and Zoback *et al.* (1985), respectively. Comparison of the borehole geometry determined using the televiewer and the dipmeter showed that both tools gave the same orientation of borehole elongation, provided that the zone of elongation was longer than 30 cm, a restriction that was governed by the geometry of the dipmeter tool. As a result of the logging, Plumb and Hickman (1985) established criteria that had to be met when determining breakout zones from dipmeter caliper logs. Comparison of dipmeter caliper data with orientation of *in situ* stress and natural fractures (obtained from hydrofracturing tests and televiewer data) demonstrated that borehole elongations were symmetrical and aligned with the minimum horizontal stress, and were not associated with natural fractures intersecting the well (Plumb and Hickman, 1985). The results from logging and testing in the Auburn geothermal well were important as they demonstrated that

borehole elongations derived from dipmeters could be used to infer the directions of the least principal stress perpendicular to the borehole axis, and that these directions were comparable to those determined independently with the borehole televiewer.

The reliability of using breakouts as indicators of the direction of the major and minor horizontal *in situ* stresses was demonstrated further by Dart and Zoback (1987). They analyzed wellbore breakouts from four-arm dipmeter logs obtained from more than 200 petroleum exploration wells in 15 structurally diverse areas within the continental United States. Dart and Zoback (1987) concluded that (1) breakouts are elliptical in cross-section with their long axis parallel to the least horizontal *in situ* stress, (2) breakouts are found in all rock types and tectonic environments, (3) breakouts in wells within a given structural region have essentially the same azimuth, and (4) stress orientation inferred by breakouts is consistent with that determined with other methods such as earthquake focal mechanisms and hydraulic fracturing. Dart and Zoback (1987) also emphasized the need to differentiate between actual breakouts and other forms of wellbore enlargements and elongations not directly or indirectly related to stresses, such as washouts, enlargement in soft or poorly consolidated rocks, borehole deviation-induced elongations, drilling-induced (hydraulic) fracturing of the wellbore and opening of pre-existing vertical fractures. The differentiation can sometimes be done by examination of the dipmeter logs.

8.2.2 THEORIES OF BREAKOUT FORMATION

The analytical method commonly used for predicting the location and extent of borehole breakouts is that proposed by Zoback *et al.* (1985). It uses the Kirsch solution to calculate the stresses around a circular hole in a linearly elastic and isotropic continuum subjected to a three-dimensional stress field. The stresses are then included in a Mohr–Coulomb failure criterion with cohesion and angle of internal friction. This approach will be discussed in more detail in section 8.4. The role played by rock anisotropy on the formation of breakouts was addressed by Vernik and Zoback (1992) regarding breakouts at the Cajon Pass borehole near the San Andreas fault in California. They concluded that rock anisotropy at that site had only a minor effect on the breakouts. This assumption cannot, however, be generalized to other rocks or other tectonic settings.

Contrary to the model presented by Zoback *et al.* (1985) which predicts that excessive compressive stresses near the borehole wall may cause shear failure, Freudenthal (1977) suggested that extension or tensile fracturing may actually occur at the borehole wall. Extension modes of failure and spalling have also been suggested by Mastin (1984), Guenot (1989), Zheng, Kemeny and Cook (1989), Ewy and Cook (1990), Lee and Haimson (1993) and Haimson and Lee (1995).

The growth of borehole breakouts and the associated progressive failure process have been simulated by Zheng, Kemeny and Cook (1989) using the boundary element method combined with the rock tensile and compressive strengths. The boundary of the borehole is updated by removing failed segments around the borehole wall. Zheng, Kemeny and Cook (1989) predicted that breakouts deepen but do not widen as they grow and that they eventually reach a stabilized pointed V-shape.

Progressive failure can also be predicted using damage models (Onaisi, Sarda and Bouteca, 1990; Rutqvist *et al.*, 1990). In the continuum damage model used by Rutqvist *et al.* (1990), borehole breakouts are simulated by the propagation of active damage planes and/or planar localization bands. It is then found that the propagation of these planes follows that of the fracture planes commonly associated with borehole breakouts. The continuum damage model predicts that borehole breakouts initiate at the borehole wall and propagate into the rock mass in a direction parallel to the minimum compressive stress.

8.2.3 LABORATORY STUDIES

Laboratory investigations of borehole breakouts are numerous. Haimson and Edl (1972) tested hollow cylindrical specimens of dry Berea sandstone under axisymmetric horizontal loading and an independent vertical stress in a triaxial vessel. The observed breakouts extended throughout the circumference of the borehole and their depth showed a clear increase with an increase in confining pressure. Mastin (1984) subjected the same rock type to uniaxial loading and found spalling (extension cracking) to be an important mechanism in the development of borehole breakouts. An important observation was that the width of the breakouts remained basically unchanged regardless of the final depth of spalling.

Haimson and Herrick (1985, 1986) completed an experimental program studying the relationship between borehole breakout formation in cubical blocks of Indiana limestone and the *in situ* state of stress. Analysis of thin sections following failure suggested that the major breakout mechanism is tensile rupture along surfaces parallel to the borehole wall, aided by shear failure in the radial direction. Breakout depth and width were found to be directly proportional to the magnitude of the least applied principal stress. A series of physical simulations of borehole breakouts was conducted on large cubical specimens of model material simulating the behavior of weak sedimentary rocks (Maloney and Kaiser, 1989). Under most conditions, failure of the borehole wall was found to occur ultimately due to shearing concentrated in narrow bands parallel to the intermediate principal stress. Maloney and Kaiser (1989) suggested that this process initially causes apparent spalling due to the intersection of shallow shear surfaces with some extension zones.

A set of thick-walled hollow cylinder experiments was designed for careful measurement and observation of elastic and inelastic deformation, fracture and failure around cylindrical openings in clastic rocks by Santarelli and Brown (1989) and Ewy and Cook (1990). These hollow cylinder experiments revealed that the elastic behavior of the rock around cylindrical openings is of importance for fracture and failure development and in particular the increase in stiffness away from the borehole wall (Santarelli and Brown, 1989; Santarelli, Brown and Maury, 1986). For most clastic rock types, the deformation process starts with a process of plastic pore and crack closure followed by a phase of elastic deformation, and then a phase of microcrack development. The macroscopic failure is produced by the proliferation of microcracks and by their extension, clustering and bridging. Around unsupported holes, these cracks form macroscopic splitting fractures subparallel to the hole wall, and also form en echelon patterns that meet the wall. Slabs of fairly uniform thickness progressively detach from the surrounding rock, resulting in a triangular failure zone with a pointed tip. Initiation, growth and interaction of fractures have been well defined in the experiments by Ewy and Cook (1990).

Breakouts in Lac du Bonnet granite from the Underground Research Laboratory (URL) site in Canada were simulated in the laboratory by Lee and Haimson (1993) and Haimson and Lee (1995). In both cases, cubical specimens of granite were subjected to a three-dimensional stress field. In the experiments of Lee and Haimson (1993) the stresses were applied on predrilled specimens, whereas in the experiments of Haimson and Lee (1995) drilling was done under stress, thus simulating a loading path closer to actual field conditions. The extent and geometry (depth and width) of the breakouts were analyzed using thin sections.

The experimental study of Lee and Haimson (1993) revealed some important trends. First, it confirmed that in crystalline rock, breakouts are aligned in the direction of the minimum horizontal stress. Second, extensile cracking was found to be the basic mechanism of breakout initiation, followed by

progressive detachment of rock flakes bounded by the cracks, leading to V-shaped cross-sections. Third, the value of the maximum horizontal stress at which breakouts initiate was found to increase linearly with the magnitude of the minimum horizontal stress. Finally, breakout depth and angular width were found to increase linearly with the value of the maximum horizontal stress for fixed values of the vertical and minimum horizontal stresses. As remarked by Lee and Haimson (1993), this last conclusion would suggest that the geometry of borehole breakouts could be used to estimate the magnitude of *in situ* stresses.

In the more recent experimental study of Haimson and Lee (1995), acoustic emission was monitored for a period up to 1 h following borehole breakout in order to gain a better understanding of progressive rock failure. Thin sections were made at various cross-sections along the drill holes. In addition, vertical cross-sections of the core stems still attached to the drillcores were made in directions parallel to the maximum and minimum applied horizontal stresses.

The test results of Haimson and Lee (1995) confirmed many of the trends reported in the previous study, and provided additional information regarding the phenomenon of core disking (see discussion in section 2.11) and its relation to borehole wall failure. More specifically, it was found that V-shaped breakouts that develop in granite are smaller than those in sedimentary rocks. No substantial effect of the load path on borehole breakouts was observed. The test results provided a better description of the process of borehole wall failure with the development of small flakes in extension subparallel to the maximum horizontal stress followed by buckling of the flakes, and a decrease in the span of the V-shaped sections due to the cantilever effect of rock flake remnants. It was also found that the depth and angular width of breakouts could be used as constraining factors when determining the orientation and magnitude of *in situ* stresses, since they both depend on the applied stress level. However, extrapolation from laboratory conditions to field conditions is difficult due to an apparent increase in rock strength around smaller diameter boreholes in the laboratory. The results of the experiments of Haimson and Lee (1995) also revealed that core disking develops at stress levels considerably smaller than those required for borehole breakouts, and that the relative occurrence of core disking and borehole breakouts in a borehole could be used to set limits on the level of *in situ* stress.

8.2.4 RECENT DEVELOPMENTS

Over the last decade, the analysis of borehole wall breakouts has become a promising technique for estimating *in situ* stress orientation at all depths and in all geological conditions, and particularly at great depths where direct *in situ* stress measurements are difficult. Analysis of borehole breakouts has become routine work in deep continental drilling programs such as (1) the Cajon Pass drill hole located close to the San Andreas fault in southern California (Shamir and Zoback, 1992; Vernik and Zoback, 1992), (2) the German continental deep drilling project (KTB) in northeast Bavaria, Germany (Baumgärtner *et al.*, 1993; Te Kamp, Rummel and Zoback, 1995) and (3) the borehole for deep-Earth gas in the Precambrian rocks of Sweden (Stephansson, Savilahti and Bjarnason, 1989). Breakouts were also used as stress orientation indicators in boreholes intersecting deeply buried basalt flows at the Hanford site in Washington in the USA (Paillet and Kim, 1987). In many of these projects, breakout analysis was carried out in parallel with other stress measurement methods such as hydraulic fracturing. The use of borehole breakouts to constrain the orientation and magnitude of oceanic crustal stresses in the deep sea drilling projects like the Ocean Drilling Program has been reported by Moos and Zoback (1990) and Kramer *et al.* (1994).

In most studies of borehole breakouts, their origin and orientation are ascribed solely to large-scale tectonics and stress fields. The possible influence of local geological structures on the orientation and magnitude of borehole breakouts has been discussed by several authors (Aleksandrowski, Inderhaug and Knapstad, 1992; Brereton and Müller, 1991; Cowgill *et al.*, 1993; Zoback *et al.*, 1989). The observed low stresses and minor breakouts of crystalline rock masses at depth have been found to be located and confined to zones of faulting and dense fracturing (Koslovsky, 1987; Stephansson, Savilahti and Bjarnason, 1989; Vernik and Zoback, 1992).

The construction and research activities at the URL in Canada have provided a unique opportunity to study borehole breakouts, both in the laboratory and *in situ*. Martin, Martino and Dzik (1994) conducted a series of uniaxial load tests on blocks of sparsely fractured Lac du Bonnet granite containing boreholes with diameters ranging between 5 and 103 mm. For small-diameter boreholes, less than 20 mm, it was found that the tangential stress at the wall of the hole required to cause failure and breakouts was about 1.5 to 2.5 times the unconfined compressive strength determined in standard uniaxial compression tests. It was also found that the strength–scale dependence disappeared for boreholes with diameters larger than 75 mm. It is interesting to note that the apparent increase in rock compressive strength in the wall of small-diameter boreholes observed in the experiments of Martin, Martino and Dzik (1994) has also been reported by various authors for different rock conditions (see discussion in section 11.2.3).

In order to investigate further the strength–scale dependence, Martin, Martino and Dzik (1994) analyzed breakout phenomena in the walls of a series of vertical boreholes with diameters of 75, 150, 300, 600 and 1250 mm drilled in the floor of one of the test rooms at the URL site, and in the roof and floor of a 3500 mm diameter mine-by test tunnel excavated at the same site. Martin, Martino and Dzik (1994) reported that breakouts, if present, formed immediately during drilling of the boreholes and excavation of the test tunnel. Microseismic events were recorded during the mine-by test and were found to concentrate near the face of the tunnel and in areas where the breakouts were formed. A modest strength–scale dependence was observed for the field data compared with the laboratory data. This difference led Martin, Martino and Dzik (1994) to conclude that there is no unique strength–scaling law for laboratory and *in situ* failure, not even for a sparsely fractured granite such as the Lac du Bonnet granite. In a recent paper, Martin (1995) attributed the difference to the different load paths used in the laboratory and *in situ*.

8.3 TECHNIQUES, EQUIPMENT AND PROCEDURES

The orientation of borehole elongations can be measured using optical (borehole camera), mechanical (three- and four-arm dipmeters), acoustic (televiewer) or electrical resistivity (formation microscanner or FMS) methods. Borehole cameras and three-arm dipmeter caliper logs are known to provide the least reliable data for breakout analysis, as there is always a problem to center the borehole camera and to measure the depth of spalling at the borehole wall. The three-arm caliper measurements can provide reliable data if the borehole shape is not too irregular but poor pad contacts may occur in non-cylindrical holes (Cox, 1970). Four-arm dipmeters measure the borehole diameter in two orthogonal directions between two sets of opposing arms. The technique is robust, can be used at great depths, and the evaluation procedure is well established. Caliper logs were originally developed as tools for estimating cement grouting and casing in the petroleum industry. Therefore, a large amount of caliper data exists from oil and gas fields. The main drawback of caliper logs is that they do not provide information on the detailed shape of the breakouts.

On the other hand, existing acoustic and high-resolution microresistivity methods, and in particular modern FMSs, provide excellent data for breakout analysis. The basic principles and characteristics of four-arm dipmeter tools, televiewers and FMSs are reviewed below.

8.3.1 DIPMETER

The dipmeter is a logging tool initially designed to measure the orientation of beddings intersecting a borehole by continuous monitoring of the rock resistivity on four or more coplanar electrode pads pressed against the wall of a borehole. An example of a dipmeter with four arms and pads is shown in Fig. 8.2. The pads are pressed against the borehole wall by a controllable force and make measurements that depend upon the electrical conductivity of the rock. The reference pad (referred to as pad 1) is magnetically oriented and two independent calipers measure the borehole diameter between pads 1 and 3 and between pads 2 and 4. Deviations of the borehole from the vertical and the strike of the projection of the drilling at the surface are determined for every depth in the logging campaign.

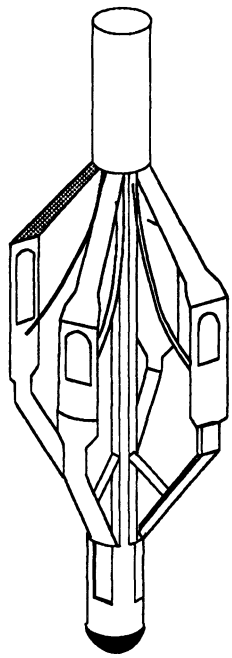

Fig. 8.2 Four-arm dipmeter for analysis of borehole breakouts.

Four-arm dipmeter measurements are carried out by winching the tool up the borehole. As the tool is winched up the hole, it rotates due to the twisting and tensioning of the cable. The borehole shape is recorded over the depth interval for which the tool rotates 90°. Close to the surface, the cable torque diminishes and slows the rotation, increasing the depth interval for the 90° rotation. This can result in poor accuracy in the determination of the breakout orientation.

8.3.2 TELEVIEWER

The borehole televiewer is a wireline logging tool that provides a continuous, oriented, ultrasonic image of a borehole wall (Zemanek *et al.*, 1970). The borehole televiewer consists of a transducer that is mounted on a motor-driven shaft and aimed at the borehole wall. The transducer rotates about three times per second and generates an ultrasonic (≈ 1.2 MHz) acoustic pulse 1800 times per second. The tool is winched up the hole at a speed of 1.5 m/min on a standard wireline logging cable. The reflected energy that returns to the transducer modulates the intensity of a trace on a cathode ray tube at the surface. Both travel time and amplitude of the sonic pulse are measured. A bright trace corresponds to a good reflection and a dark trace indicates a scattered or absorbed signal. Successive traces appear on the ray tube as the tool is pulled up the hole. This display is photographed, and the unprocessed sonic signals from the tool together with the flux-gate magnetometer recordings are stored on videotape for later processing.

Characteristic patterns on the borehole televiewer log are produced by fractures, voids, washouts and other borehole features. Planar

features such as natural fractures and joints produce a sinusoidal signature on the borehole televiewer log from which their strike and dip may be determined (Barton *et al.*, 1991). Zones of low reflectance (dark bands) on the televiewer log correspond to zones of borehole elongation or breakout as shown in Fig. 8.3.

8.3.3 FMS

The FMS (developed by Schlumberger) produces high-resolution microresistivity images or structural maps of the borehole wall that can be used for detailed sedimentological or structural interpretations and for determining fracture and breakout orientations. The tool consists of 16 electrode 'buttons' on each of four orthogonal pads that are pressed against the borehole wall. The focused current that flows from the buttons is recorded as a series of curves that reflect the microresistivity variations of the formation. Analog or digital processing converts the current intensity measurements into complete, spatially oriented images where black represents the most conductive areas of the borehole wall and white corresponds to the most resistive areas.

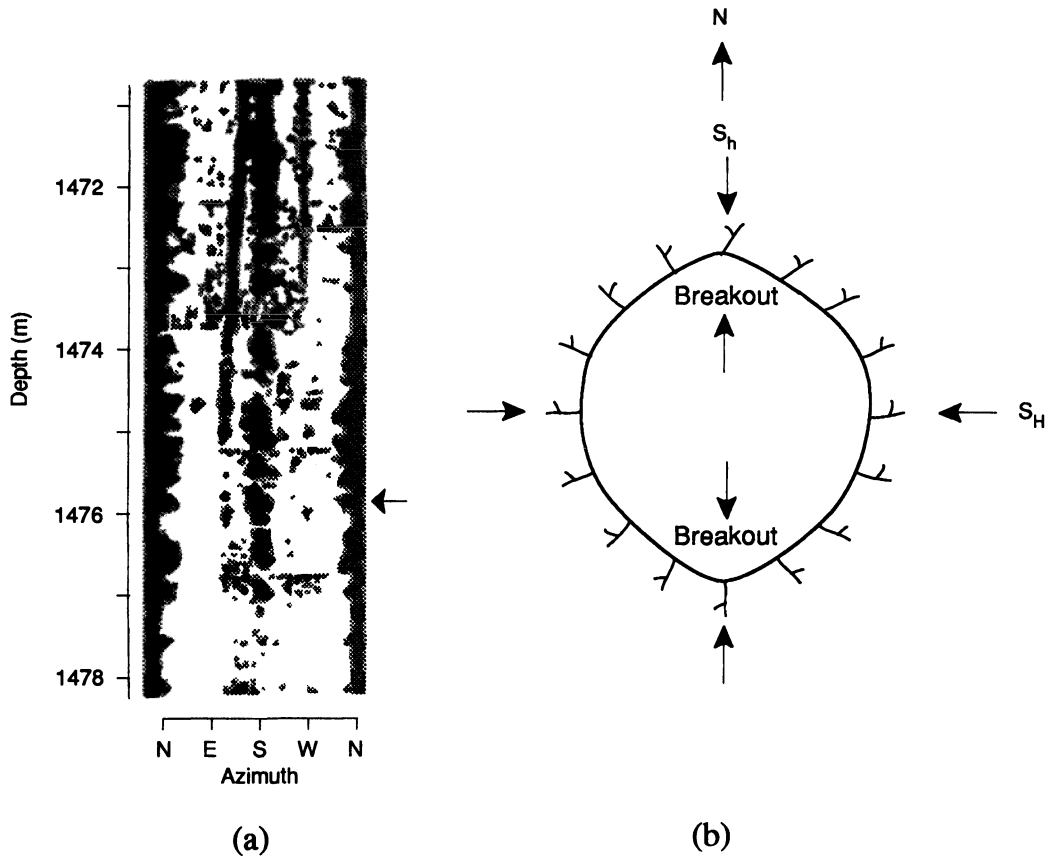

Fig. 8.3 (a) Section of borehole televiewer log from the Auburn well showing zones of borehole elongation or breakouts (dark patches), and (b) horizontal cross-section of breakout at a depth of 1475.8 m (arrow in Fig. 8.3a) obtained using a travel time modification to the basic televiewer tool. Also shown is the orientation of the horizontal principal stresses relative to the breakouts as determined from the hydraulic fracturing tests in the same well. (After Hickman, Healy and Zoback, 1985.)

Applications of FMS images include detailed correlation of coring and logging depths, orientation of cores and mapping of fractures, foliations, faults and formation structures as well as determining strikes and dips of bedding planes. The high-resolution images from FMS logging open up new approaches for log interpretation and allow quantitative data interpretation of borehole breakouts.

8.4 THEORY

The first analysis of breakout formation by Bell and Gough (1979) and Gough and Bell (1982) predicted that breakouts are spalled areas on either side of the borehole which are centered in the direction of the minimum horizontal principal stress (where the compressive stress concentration is the largest). They suggested that the breakouts were the result of localized compressive shear failure, and their analysis predicted that the region of failure would be triangular in cross-section, enclosed by flat conjugate shear planes. Those shear planes are tangential to the circumference of the borehole and are inclined to the direction of the maximum principal stress at an angle $\pi/4 - \phi/2$, where ϕ is the angle of internal friction of the rock. In the early 1980s, the primary source of information about borehole breakouts came from four-arm caliper logs. These instruments yielded only two orthogonal borehole diameters and no information about the detailed shape of the breakouts. Later, the use of borehole televiewers and FMSs called for a better theory to explain the initiation and mode of failure of borehole breakouts. We present below first the theoretical model developed by Zoback *et al.* (1985), followed by the continuum damage model of Singh and Digby (1989a,b). Both models can be used to predict the initiation, growth and geometry of breakouts.

Consider a vertical circular hole in a homogeneous, isotropic and linearly elastic rock mass subjected to effective minimum and maximum horizontal principal stresses S_h and S_H acting at infinity. According to the Kirsch solution (Jaeger and Cook, 1976), the stress components at any point (r,θ) in the horizontal plane around the hole can be expressed as

$$\sigma_r = \left(1 - \frac{R^2}{r^2}\right)\frac{(S_H + S_h)}{2} + \left(1 + 3\frac{R^4}{r^4} - 4\frac{R^2}{r^2}\right) \times \frac{(S_H - S_h)}{2}\cos 2\theta + \Delta P \frac{R^2}{r^2} \quad (8.1)$$

$$\sigma_\theta = \left(1 + \frac{R^2}{r^2}\right)\frac{(S_H + S_h)}{2} - \left(1 + 3\frac{R^4}{r^4}\right) \times \frac{(S_H - S_h)}{2}\cos 2\theta - \Delta P \frac{R^2}{r^2} \quad (8.2)$$

$$\tau_{r\theta} = -\left(1 - 3\frac{R^4}{r^4} + 2\frac{R^2}{r^2}\right)\frac{(S_H - S_h)}{2}\sin 2\theta \quad (8.3)$$

where σ_r is the radial stress, σ_θ is the circumferential stress, $\tau_{r\theta}$ is the tangential shear stress, R is the radius of the borehole, r is the distance from the center of the borehole, θ is the angle measured from the direction of S_H and ΔP is the difference between the fluid pressure in the borehole and that in the rock formation. Due to stress concentration, shear failure occurs along conjugate surfaces intersecting at $\theta = 90°$ and 270°, i.e. in the direction of the minimum horizontal principal stress. It is important to note that the magnitude of the shear and normal stresses along these potential failure surfaces varies as a function of the radius r and the angle θ.

It is now assumed that failure of the rock near the borehole wall occurs in accordance with the Mohr–Coulomb criterion. At each point (r,θ), it is assumed that the maximum and minimum principal stresses are in the horizontal plane and the failure surfaces are parallel to the borehole vertical axis. The rock is assumed to have a coefficient of internal friction $\mu = \tan\phi$ (where ϕ is an internal friction angle) and an internal cohesive strength (or cohesion) C. According to the Mohr–Coulomb criterion, the shear stress τ and the effective normal stress σ on the failure

surfaces are related as follows:

$$|\tau| = C + \mu\sigma \tag{8.4}$$

Rearrangement of equation (8.4) gives the following expression for the cohesive strength at failure in terms of μ and the stress components σ_r, σ_θ and $\tau_{r\theta}$:

$$C = (1+\mu^2)^{1/2}\left(\left(\frac{\sigma_\theta - \sigma_r}{2}\right)^2 + \tau_{r\theta}^2\right)^{1/2} - \mu\left(\frac{\sigma_\theta + \sigma_r}{2}\right) \tag{8.5}$$

Substituting equations (8.1)–(8.3) into equation (8.5), the cohesive strength can be expressed in terms of r and θ and the horizontal principal stresses S_h and S_H. Conversely, for given values of the stresses S_h and S_H, the cohesive strength C and the coefficient of internal friction μ, the extent of the breakout zone where shear failure occurs can be determined. As a numerical example, consider the case where $S_H = 45$ MPa, $S_h = 30$ MPa ($S_H/S_h = 1.5$), $\mu = 1.0$, $C = 12.5$ MPa and $\Delta P = 0$. Figure 8.4a shows the conjugate surfaces along which shear failure is expected to occur. The size of the region in which the rock shear strength is actually mobilized (breakout zone) is shown in Fig. 8.4b.

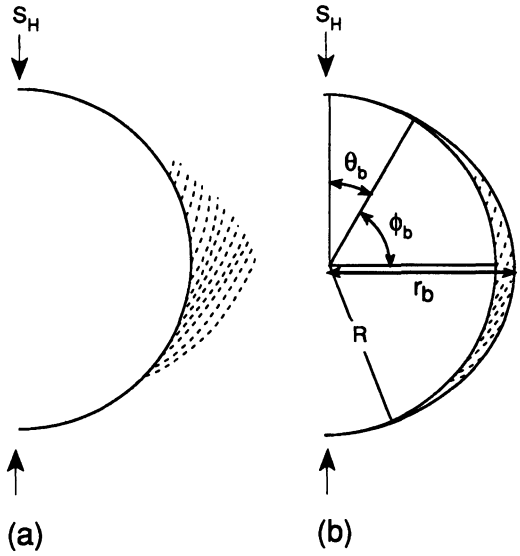

Fig. 8.4 (a) Orientation of potential shear failure surfaces adjacent to a wellbore for $S_H = 45$ MPa, $S_h = 30$ MPa, $\Delta P = 0$ and $\mu = 1.0$. (b) Area in which failure is expected for $C = 12.5$ MPa. θ_b, ϕ_b and r_b are defined in the text. (After Zoback *et al.*, 1985.)

Numerical analysis conducted by Zoback *et al.* (1985), assuming $\Delta P = 0$, revealed that for given values of μ and C, increasing the stress ratio S_H/S_h up to a value of 3 makes the breakouts much larger and with steeper edges. Similarly, for given values of the stress ratio and C, much smaller breakouts result for larger values of μ. Finally, for given values of the stress ratio and μ, the lower the value of C, the deeper and wider the breakouts become.

The theory presented above can be extended to consider the general problem of the initial size of breakouts in terms of the rock cohesive strength and coefficient of friction and the excessive fluid pressure. Let θ_b be the value of the angle θ at the point (R,θ) where the breakout intersects the borehole wall (Fig. 8.4b). The value of the cohesive strength at that point is defined as $C(R,\theta_b)$. Likewise, let r_b be the value of r at the deepest point at $\theta = \pi/2$ on the outer edge of the breakout (Fig. 8.4b). The value of the cohesive strength at that point is defined as $C(r_b, \pi/2)$. Using equations (8.1)–(8.3) and (8.5), assuming $\Delta P = 0$ and $S_H/S_h \leq 3$ (for which $\sigma_\theta > \sigma_r$ in the near vicinity of the borehole), $C(R,\theta_b)$ and $C(r_b, \pi/2)$ can be written as follows:

$$\begin{aligned} C(R,\theta_b) &= 0.5(aS_H + bS_h) \\ C(r_b,\pi/2) &= 0.5(cS_H + dS_h) \end{aligned} \tag{8.6}$$

where

$$a = [(1+\mu^2)^{1/2} - \mu][1 - 2\cos 2\theta_b]$$

$$b = [(1+\mu^2)^{1/2} - \mu][1 + 2\cos 2\theta_b]$$

$$c = -\mu + (1+\mu^2)^{1/2} - \frac{R^2}{r_b^2}[(1+\mu^2)^{1/2} + 2\mu] + 3\frac{R^4}{r_b^4}(1+\mu^2)^{1/2} \tag{8.7}$$

$$d = -\mu - (1+\mu^2)^{1/2} + \frac{R^2}{r_b^2}[3(1+\mu^2)^{1/2} + 2\mu] - 3\frac{R^4}{r_b^4}(1+\mu^2)^{1/2}$$

Consider now a breakout which follows a trajectory for a given value of the cohesive strength C such that $C(R,\theta_b) = C(r_b, \pi/2) = C$. Solving equations (8.6) for the stresses S_h and S_H gives

$$S_H = 2C\frac{d-b}{ad-bc}$$

$$S_h = 2C\frac{a-c}{ad-bc} \qquad (8.8)$$

$$\frac{S_H}{S_h} = \frac{d-b}{a-c}$$

Figure 8.5 shows the variation of the *in situ* stress ratio S_H/S_h (which is independent of C) with r_b/R for different values of the breakout half-width angle ϕ_b, where $\phi_b = \pi/2 - \theta_b$ as shown in Fig. 8.4b. The coefficient of friction μ is equal to 0.6. Figure 8.5 indicates that when S_H and S_h are almost equal, little spalling is anticipated. The breakouts become deeper and wider as S_H/S_h increases. For large values of the *in situ* stress ratio, up to 3, it can be seen that the borehole radius increases by only about 15% when ϕ_b is as large as 50° ($\theta_b = 40°$).

The theory mentioned above for the initial formation of breakouts can explain the broad, flat-bottomed breakouts observed in many boreholes, but cannot explain the deeper breakouts. In the analysis above, it was assumed that the excessive fluid pressure in the borehole was the same as that in the formation (i.e. $\Delta P = 0$). Analysis conducted by Zoback *et al.* (1985) revealed that by increasing the fluid pressure in the borehole ($\Delta P > 0$), the size of the breakouts is substantially diminished. On the other hand, a decrease in the fluid pressure in the borehole ($\Delta P < 0$) promotes breakout development as expected. The very strong influence of ΔP on the size and shape of the breakouts is due to the change in normal stress on the potential failure planes near the borehole wall. A practical example showing how positive ΔP inhibits failure is the common practice of using dense additives in drilling muds for stabilizing the borehole wall when drilling in low-cohesion rocks such as shale and siltstone.

The theory presented above is intended to explain the initial size and shape of borehole breakouts. Further, the calculations indicate

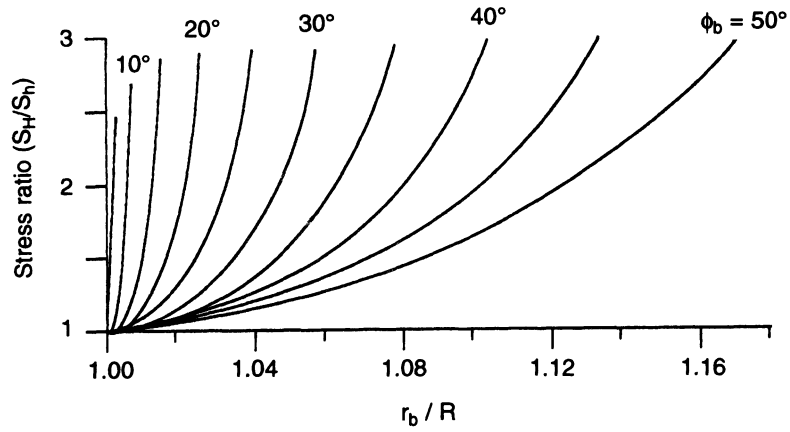

Fig. 8.5 Variation of the *in situ* stress ratio S_H/S_h with r_b/R for different values of the breakout half-width angle ϕ_b ranging between 5 and 50° when $\mu = 0.6$ and $\Delta P = 0$. (Adapted from Zoback *et al.*, 1985.)

that as the breakouts deepen, they do not become wider. However, the theory does not consider the inelastic deformation occurring as the rock around the borehole fails and the corresponding stress redistribution. Additional considerations are the possibility of time-dependent effects related to subcritical crack growth and the possibility that the circulation of mud with a temperature different from the formation may promote breakouts. Some of these issues and a general solution to the theory presented above for stress ratios S_H/S_h larger than 3 (and $\sigma_\theta < \sigma_r$) and non-zero values of ΔP can be found in Zoback *et al.* (1985).

Experimental studies of borehole breakouts by Ewy and Cook (1990) and others have demonstrated that the failure process can be described in an average sense by a degradation in the elastic stiffness of the rock. The progressive development of failure is illustrated in Fig. 8.6. Let us assume that the borehole breakout is due to the progressive growth and coalescence of microcracks. We can then quantify the process of progressive failure by introducing a continuous field variable called 'damage', which may be regarded as a continuous measure of the state of internal degradation of the rock. This approach was followed by Rutqvist *et al.* (1990) who presented a breakout prediction model where breakouts were simulated by the propagation of active damage planes and/or planar localization bands. This model is based on the continuum damage model of Singh and Digby (1989a, b). The continuum damage model simulates the progressive failure and accumulated damage (due to the growth of cracks), and the formation of localization bands in brittle rocks under both compressive and tensile loading and under plane strain condition.

The continuum damage model involves the definition of damage vectors that vary in a space populated with penny-shaped microcracks. The damage vectors are internal variables describing the state of the material considered. The magnitude of each vector in any direction depends on the number of

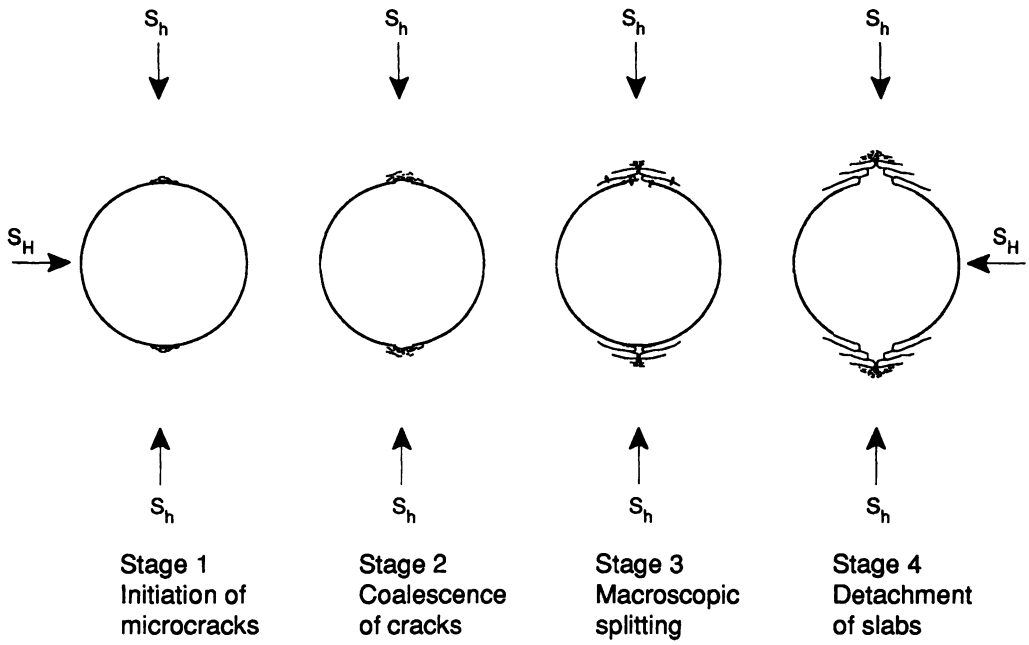

Fig. 8.6 Progressive development of borehole breakouts.

cracks in that direction. The model also requires, for each damage vector, the definition of damage surfaces (similar in concept to the yield surfaces in the theory of plasticity) and damage growth functions formulated in terms of strains. The initiation of damage growth occurs when the damage growth functions exceed some 'yield functions'. As the cracks grow in a body and damage planes exist simultaneously in the body, the stiffness of the damaged material varies and an effective compliance tensor can be determined.

In the continuum damage model of Singh and Digby (1989a, b), damage is assumed to be irreversible, unloading is purely elastic with no further damage, the damage surfaces are assumed to be parabolic and there is independence of damage growth in different directions. The input parameters required in the continuum damage model include (1) the Young's modulus and Poisson's ratio of the intact material, (2) the critical compressive stress for crack closure, (3) parameters describing how damage initiates in shear and in tension, and the damage growth rate, and (4) the initial damage in the material. Methods to determine those parameters and detailed derivations of the continuum damage model can be found in the paper by Singh and Digby (1989a).

Rutqvist *et al.* (1990) implemented the continuum damage model of Singh and Digby (1989a) into a finite element code to simulate borehole breakouts in hard crystalline rocks. Breakouts were predicted in the wall of a vertical borehole 200 mm in diameter loaded under plane strain condition by horizontal *in situ* stresses S_H and S_h. No internal pressure was applied on the borehole walls. Microcrack growth around the borehole wall was driven by increasing the compressive *in situ* boundary stresses stepwise, but the ratio S_H/S_h was maintained constant and equal to 1.5 throughout the numerical simulation. The rock was assumed to be linearly elastic, homogeneous and isotropic with a Young's modulus equal to 65 GPa and a Poisson's ratio equal to 0.26. Other parameters in the damage model were obtained from numerical simulations of laboratory uniaxial compressive tests on drill-cores of granitic rocks. In particular, the rock had a uniaxial compressive strength of 145 MPa. The results of the analysis are shown in Figs 8.7 and 8.8.

For the loading conditions just described, and for the first seven load increments, no evidence of fracture initiation was observed. Microfracturing first appeared at the eighth load increment when the maximum and minimum *in situ* stresses attained values of $S_H = 72$ MPa and $S_h = 48$ MPa, respectively. This is illustrated in Fig. 8.7b by the formation of damage planes in two elements adjacent to the borehole wall. These damage planes indicate that microcracks grow in two directions parallel to these damage planes. The isostress contours in Fig. 8.7a show that microfracturing starts in the region with the largest stress concentration. The largest compressive stress in this region was found to be about 130 MPa, which is less than the uniaxial compressive strength of the rock considered (145 MPa).

Further into the loading process and at load increment 11 ($S_H = 97$ MPa and $S_h = 64$ MPa) it was found that four elements of the finite element mesh localized (softened) at the borehole wall, forming a band, and that the microcrack concentration had increased sufficiently to enable the formation of macroscopic features by the process of crack coalescence. This creates failure of a splitting type where the rock spalls adjacent to the free surface created by extension fractures propagating parallel to the maximum applied compressive stress S_H.

Finally, at load increment 13 ($S_H = 114$ MPa and $S_h = 75$ MPa), the failure region around the borehole grows (Fig. 8.8b). The most highly stress concentrated regions move away from the borehole wall and into the rock behind the failure region (Fig. 8.8a). The maximum compressive stress is much higher than the uniaxial compressive strength of the rock considered. In the two black elements in Fig. 8.8b, the magnitude of the current damage has

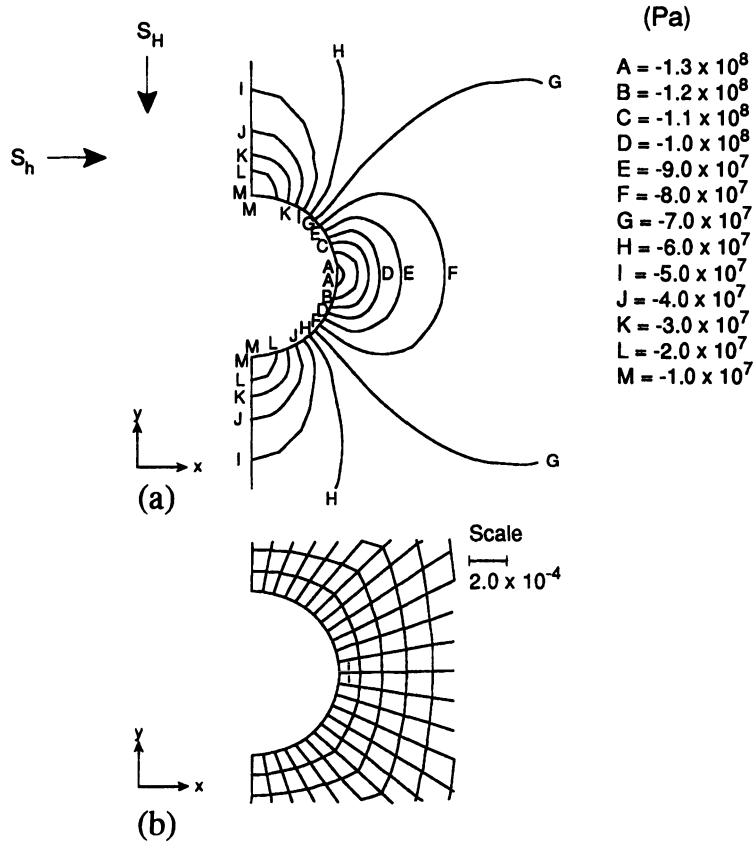

Fig. 8.7 Simulation of borehole breakouts with a damage model. Borehole response at the eighth load increment when $S_H = 72$ MPa and $S_h = 48$ MPa. (a) Isostress contours in Pascals (compressive stresses are negative), (b) damage planes in two elements. (After Rutqvist *et al.*, 1990.)

exceeded a certain predefined value. The simulation was stopped after 16 load increments when the damaged regions of the borehole showed the characteristic breakout pattern with detachment (completely failed elements) surrounded by elements of localized damage.

In general, the model of Rutqvist *et al.* (1990) represents a substitute for the simple model of Zoback *et al.* (1985). It predicts that breakouts initiate at borehole walls and propagate in a direction parallel to the minimum *in situ* compressive stress. The model is also able to explain the deep borehole breakouts with the typical 'dog ear' shape.

The models described in this section can only be used to determine the orientation and geometry of breakouts and therefore the orientation of the maximum and minimum stresses. If the geometry of breakouts was controlled by stresses only, measurement of their width and depth could be used for calculating the magnitude of the stresses, as some authors have suggested. For instance, if r_b and ϕ_b in Fig. 8.4b could be measured exactly, and knowing the value of the rock's friction angle, the ratio S_H/S_h could be determined using equation (8.8). Knowing, for instance, S_h from hydraulic fracturing, S_H could then be calculated. Such an approach has been suggested

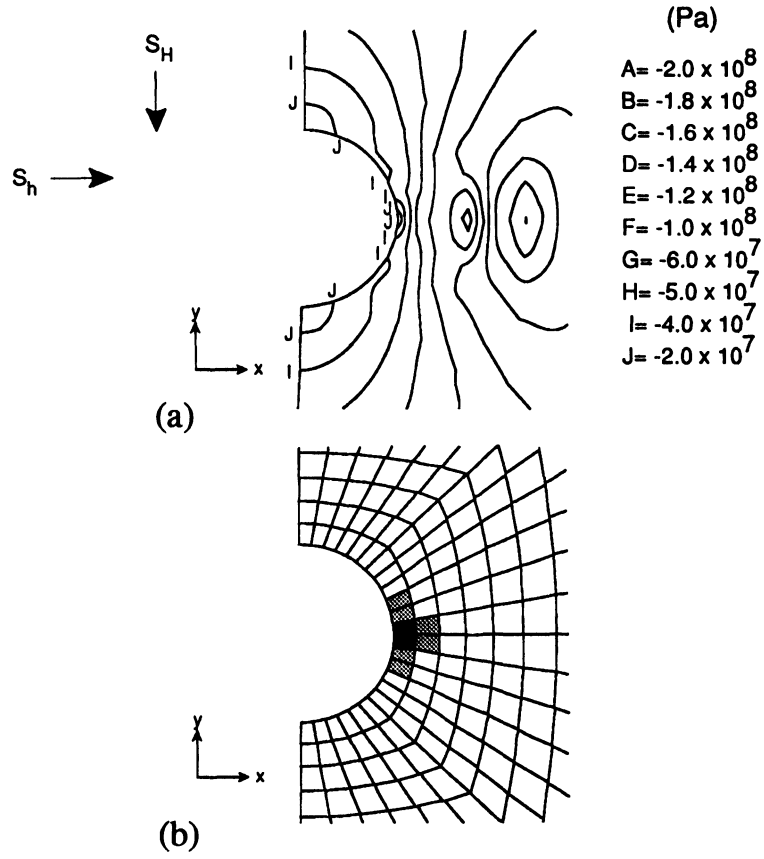

Fig. 8.8 Simulation of borehole breakouts with a damage model. Borehole response at the 13th load increment when $S_H = 114$ MPa and $S_h = 75$ MPa. Damage has exceeded a certain predefined value and caused failure at the wall of the borehole (black); localized damage (shaded) surrounds the failure zone. (a) Isostress contours in Pascals (compressive stresses are negative), (b) strain softening in six elements and damage in two elements. (After Rutqvist *et al.*, 1990.)

by Zoback *et al.* (1985). In a more recent paper, Vernik and Zoback (1992) proposed a theory where the magnitude of S_H was determined by using breakout widths, the strength of core samples, the strain energy criterion of Wiebols and Cook (1968), and an estimate (by hydraulic fracturing) of S_h. The method of Vernik and Zoback (1992) has been applied to determine stress magnitudes at the Cajon Pass drill site in California and at the KTB borehole in southern Germany (Zoback *et al.*, 1993). As mentioned at the beginning of this chapter, breakout geometry is controlled not only by stresses, but also by factors such as lithology, pre-existing fractures, formation consolidation, pore pressure and drilling (Dart and Zoback, 1987). Therefore relying on breakout geometry (wholly or partly) to predict the magnitude of stresses may be of limited value and misleading.

8.5 DATA ANALYSIS AND INTERPRETATION

Most boreholes drilled for hydrocarbon exploration purposes are logged using dipmeters. Thus the number of boreholes available for the analysis of breakouts in various lithologic environments is potentially large for

most parts of the world. In practice, the tendency is now to use televiewer instruments and FMSS more frequently, because they provide more detailed information about magnitude and orientation of borehole breakouts.

Breakout data are especially important for the evaluation of stress patterns in the upper part of the Earth's crust because they generally sample a depth interval intermediate between earthquake focal mechanisms and *in situ* stress measurements from overcoring, and other methods. They also provide multiple observations of stress orientation over considerable depth ranges. The large number of observations allows statistical determinations of stress orientation (mean orientation, angular or standard deviation) as demonstrated in the World Stress Map Project (Zoback *et al.*, 1989; Zoback, 1992). As discussed further in section 11.1, five qualities denoted A–E are used in ranking data in the World Stress Map Project. For breakouts, the ranking depends largely on the number and combined length of breakouts observed in a single well (or in wells in close proximity), and on the average and standard deviation of the breakout orientation (Table 11.1).

8.5.1 ANALYSIS OF FOUR-ARM DIPMETER LOGS

Borehole breakouts can be identified from four-arm caliper records collected routinely with conventional geophysical logs. The orientation of borehole breakouts recorded by the dipmeter in vertical boreholes is interpreted as the orientation of the minimum horizontal principal stress. Breakouts are characterized by their length, azimuth and depth.

The smallest breakout detectable by a dipmeter is determined by the electrode pad dimensions and borehole diameter. For instance, the dipmeter used by Plumb and Hickman (1985) at the Auburn well had a pad length of 30 cm and a pad width of 6 cm. Thus the calipers could only record borehole breakouts with a length greater than 30 cm and a width greater than 6 cm. A minimum difference in caliper readings of 0.6 cm (for a well diameter of about 220 mm) was found to be necessary to prevent the tool rotating as it was winched up the borehole. At Auburn, breakouts were selected from dipmeter caliper logs based on the following criteria:

1. the dipmeter tool comes to rest in the zone of elongation and the azimuth of pad 1 remains constant over the length of the breakout;
2. the caliper difference (difference in caliper readings) is greater than 0.6 cm;
3. the smallest of the two caliper readings is close to the size of the drillbit, or if the smaller caliper reading is greater than the bit size, it should exhibit less variation than the larger caliper;
4. the length of the breakout is greater than 30 cm;
5. the direction of elongation should not consistently coincide with the azimuth of the high side of the borehole when the hole deviates from vertical.

These conditions are essentially fulfilled in Fig. 8.9b. Other types of borehole geometries identified by Plumb and Hickman (1985) at Auburn, and shown in Figs 8.9a, c, d, include (1) in gage hole (both caliper readings are identical), (2) washout (both caliper readings are larger than the bit size with one dominant) and (3) key seat (one caliper reading is larger than the bit size). For each borehole geometry, Fig. 8.9 shows the configuration of the borehole with the location of the dipmeter arms, the caliper readings (where Cal 1–3 and Cal 2–4 indicate borehole diameters measured between pads 1 and 3 and pads 2 and 4, respectively), and the azimuth of pad 1 of the dipmeter.

Plumb and Hickman (1985) emphasized the need to separate borehole breakouts from asymmetric elongations. This can be done by using electrical conductivity anomalies

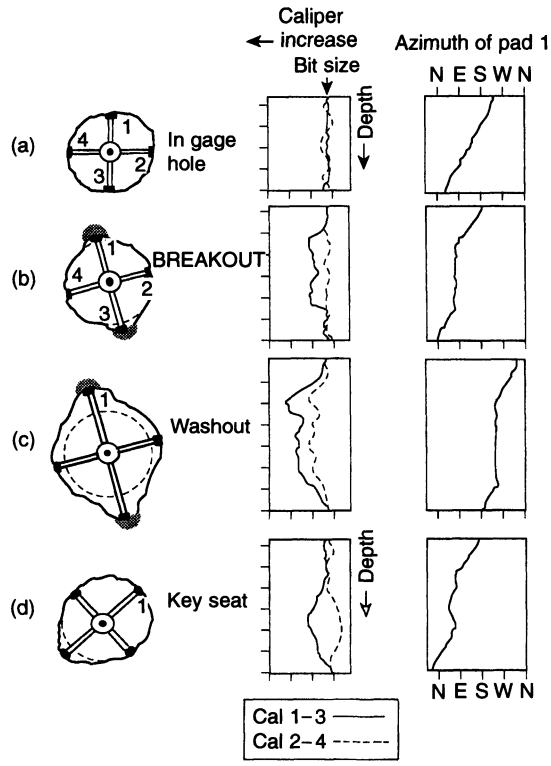

Fig. 8.9 Examples of four-arm dipmeter caliper logs and interpretation of borehole geometry. Cal 1–3 and Cal 2–4 indicate borehole diameter measured between opposite dipmeter arms. Tool rotation stops in the zone of borehole elongation resulting in constant azimuth of pad 1 of the dipmeter. The shaded regions in the direction of elongation in (b) and (c) represent zones of slightly higher electrical conductivity when compared to orthogonal directions. (Adapted from Plumb and Hickman, 1985.)

measured with the dipmeter pads in the direction of elongation. The anomalies are symmetric for breakouts and non-symmetric for asymmetric elongations.

At Auburn the zones of breakout determined with the four-arm dipmeter were confirmed with the borehole televiewer as long as the zones of elongation were at least 30 cm in length (Hickman, Healy and Zoback, 1985; Plumb and Hickman, 1985). In particular, a good correlation was observed between the difference in dipmeter readings and the definition in the televiewer reflectance logs, with large caliper differences (larger than 1 cm) being associated with clear definitions.

Breakout analysis of a borehole begins by inspection of the logs, with special notice of the recorded tool rotation and caliper difference. The most promising and interesting section of the borehole is selected for further analysis based on the readability of the logs, the competency of the rock at the borehole wall and the criteria for definition of breakouts (e.g. the five criteria suggested by Plumb and Hickman (1985) mentioned above). The caliper readings, the azimuth of pad 1 and the hole deviation are digitized. Typical breakout results are presented in Fig. 8.10 for borehole Pernille-1 located in Denmark, which is one of 20 boreholes selected for a study of the state of stress at the margin of the Baltic Shield (Ask, Müller and Stephansson, 1996). The data were analyzed using a program called Caliper 1.0 (B. Müller, personal communication) as briefly described below.

Caliper data for each set of dipmeter arms are loaded into the Caliper 1.0 program. First, the program converts the raw data and shows plots of caliper readings, pad 1 azimuth, the relative bearing of the instrument and borehole deviation. Borehole breakout candidates are selected by the cursor and a plotting routine produces a so-called contour differential plot. This plot comprises the azimuth of pad 1, the borehole deviation and the caliper readings Cal 1–3 and Cal 2–4. An example of such a plot is shown in Fig. 8.10a for the 1549–1599 m depth interval in borehole Pernille-1. Furthermore, the program displays a contour plot (Fig. 8.10b) and a difference plot (Fig. 8.10c).

The contour plot shows the borehole section as seen from above the selected interval. In this representation, the true drillbit size is represented as a circle, and the orientation and size of the caliper readings are shown by markers surrounding the borehole. The difference plot, introduced by Blümling (1986), is

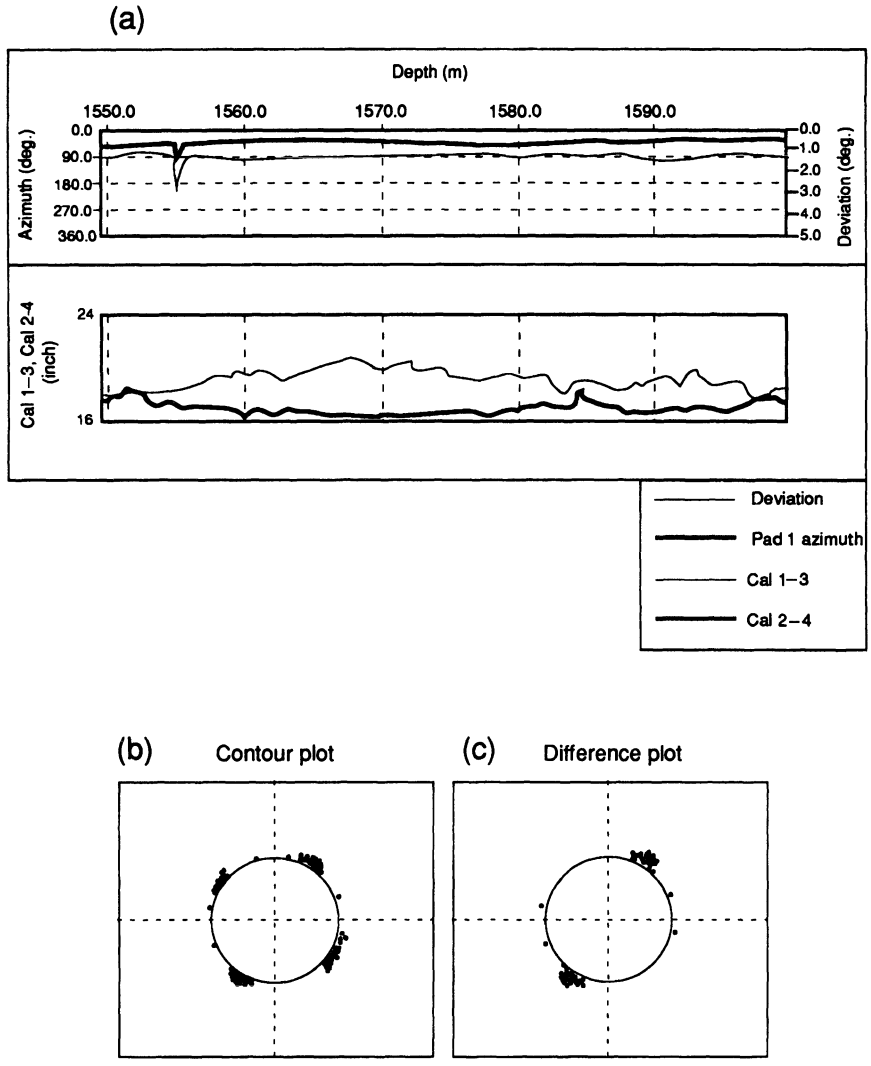

Fig. 8.10 Processing of dipmeter data for breakout analysis of borehole Pernille-1 located in Denmark. (a) Plots of azimuth of pad 1, caliper readings Cal 1–3 and Cal 2–4, and borehole deviation versus borehole depth; (b) contour plot; (c) difference plot. (After Ask, 1996.)

used to eliminate the influence of washouts in the representation of breakouts. Here, the difference between the minimum caliper reading and the bit size is subtracted from both caliper readings (Cal 1–3 and Cal 2–4), and the resulting values are plotted in the diagram. The orientation of the minimum horizontal stress is determined from the orientation of the borehole breakouts for the selected interval.

The variation of borehole breakouts and borehole elongations (corresponding to minor washouts) for different lithologies along the wall of borehole Pernille-1 is shown in Fig. 8.11. In order to compute the mean stress orientation for the complete borehole, the circular statistics of Mardia (1972) are used. In this procedure, each individual breakout is weighted by its length to enhance the

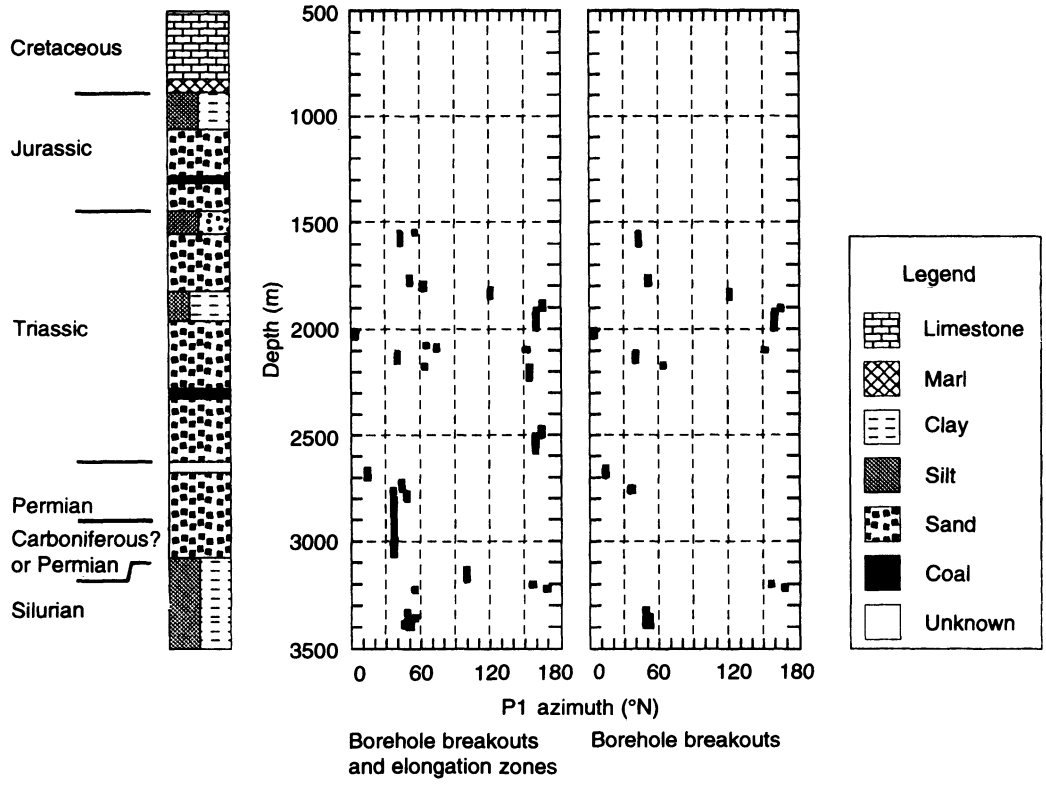

Fig. 8.11 Variation of borehole breakout zones and borehole elongation zones (corresponding to minor washouts) with depth for borehole Pernille-1 in Denmark. (After Ask, 1996.)

dominant breakout orientation and the mean horizontal stress azimuth. The quality of the breakout data was assessed according to the World Stress Map quality ranking system (Zoback, 1992), which considers the number of observations, the consistency of the results and the reliability of the data as a tectonic indicator.

8.5.2 ANALYSIS OF BOREHOLE TELEVIEWER AND FMS LOGS

The principle of the modern borehole televiewer is that a narrow pulsed acoustic beam scans the borehole wall in a tight helix as the tool moves up the borehole. To scan the borehole wall for breakouts, the acoustic beam generator is rotated by an electrical motor. During rotation of the beam, pulses of acoustic energy are sent toward the borehole wall. The acoustic energy is reflected from the borehole wall and the amplitude and the travel times of the reflected signal are measured with the same transducer that generates the acoustic beam. The most recent focused acoustic system, called FACSIMILE, measures up to 512 amplitude and travel time values per revolution and up to 12 revolutions per second can be realized. This instrument has been developed as a part of the KTB drilling project in Germany.

In the KTB drilling project, a pilot hole was drilled to a depth of 4 km for the purpose of obtaining continuous core and conducting extensive geophysical logs. As a part of the logging program, continuous FMS data were

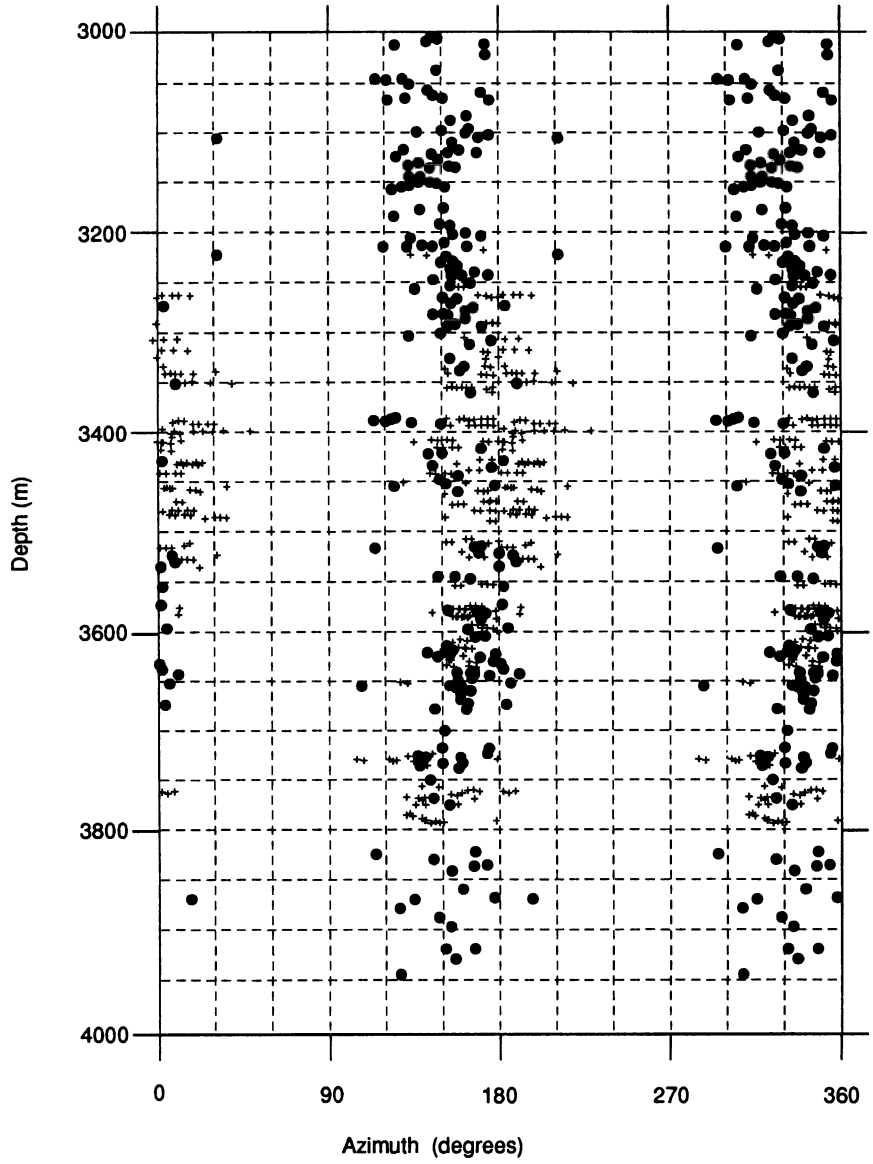

Fig. 8.12 Comparison of direction of the maximum horizontal stress inferred from drilling-induced tensile fractures (dots) and from breakouts (crosses) in the KTB pilot hole at depths ranging between 3000 and 4000 m. (After Apel, Zoback and Fuchs, 1993; reproduced by permission of K. Fuchs.)

obtained for the purpose of revealing numerous drilling-induced subvertical tensile fractures (Apel, Zoback and Fuchs, 1993; Zoback *et al.*, 1993). A detailed analysis of these data was conducted using an interactive image processing system developed at the University of Karlsruhe and based on an interactive borehole televiewer processing system developed at Stanford University by Barton *et al.* (1991). Analysis of the FMS data from the pilot hole revealed 200 drilling-induced near-vertical fractures at depths ranging between 3000 and

4000 m. Comparison of the direction of the maximum horizontal stress inferred from drilling-induced tensile fractures recorded by FMSs and from breakouts is shown in Fig. 8.12. This figure indicates a NNW direction of the maximum horizontal stress which is consistent with the general stress orientation in central Europe presented by Müller *et al.* (1992). The occurrence of the drilling-induced subvertical fractures was explained in terms of the combined effects of stress concentration (tension) around the borehole, the borehole fluid pressure during drilling, and thermally induced tensional stresses around the wellbore resulting from circulation of relatively cold mud into the hole during drilling (Apel, Zoback and Fuchs, 1993; Brudy *et al.*, 1995).

REFERENCES

Alexandrowski, P., Inderhaug, O.H. and Knapstad, B. (1992) Tectonic structures and wellbore breakout orientation, in *Proc. 33rd US Symp. Rock Mech.*, Santa Fe, Balkema, Rotterdam, pp. 29–37.

Apel, R., Zoback, M.D. and Fuchs, K. (1993) Drilling-induced tensile fractures in the KTB pilot hole: supplementary information in Zoback *et al.* (1993). Unpublished paper.

Ask, M.V.S. (1996) In-situ stress determination from borehole breakouts in Denmark, unpublished Licentiate Thesis, Royal Institute of Technology, Division of Engineering Geology, Dept. of Civil and Environmental Eng., Stockholm, Sweden.

Ask, M.V.S., Müller, B. and Stephansson, O. (1996) In situ stress determination from breakout analysis in the Tornquist Fan, Denmark. *Terra Nova* (in press).

Babcock, E.A. (1978) Measurement of subsurface fractures from dipmeter logs. *Am. Assoc. Petrol. Geol. Bull.*, **62**, 1111–26.

Barton, C.B. *et al.* (1991) Interactive image analysis of borehole televiewer data, in *Automated Pattern Recognition in Exploration Geophysics*, Springer-Verlag, New York, pp. 217–42.

Baumgärtner, J. *et al.* (1993) Analysis of deep hydraulic fracturing stress measurements in the KTB (FRG) and Cajon Pass (USA) scientific drilling projects – a summary, in *Proc. 7th Cong. Int. Soc. Rock Mech. (ISRM)*, Aachen, Balkema, Rotterdam, Vol. 3, pp. 1685–90.

Bell, J.S. and Gough, D.I. (1979) Northeast–southwest compressive stress in Alberta: evidence from oil wells. *Earth Planet. Sci. Lett.*, **45**, 475–82.

Blümling, P. (1986) In-situ Spannungsmessung in Tiefborungen mit Hilfe von Bohrlochrandausbruchen und die Spannungsverteilung in der Kruste Mitteleuropas und Australiens, unpublished Dissertation, University of Karlsruhe, Karlsruhe.

Brereton, R. and Müller, B. (1991) European stress: contributions from borehole breakouts. *Phil. Trans. Roy. Soc. London*, **337**, 165–79.

Brudy, M. *et al.* (1995) Application of the integrated stress measurement strategy to the 9 km depth in the KTB boreholes, in *Proc. Workshop on Rock Stresses in the North Sea*, Trondheim, Norway, NTH and SINTEF Publ., Trondheim, pp. 154–64.

Cowgill, S.M. *et al.* (1993) Crustal stresses in the North Sea from breakouts and other borehole data, in *Proc. 34th US Symp. Rock Mech.*, Madison, *Int. J. Rock Mech. Min. Sci. & Geomech Abstr.*, **30**, 113–16.

Cox, J.W. (1970) The high resolution dipmeter reveals dip-related borehole and formation characteristics, in *Proc. 11th Annual Logging Symp.*, Society of Professional Well Log Analysis, 25 pp.

Dart, R.L. and Zoback, M.L. (1987) Well-bore breakout-stress analysis within the continental United States, in *Proc. 2nd Int. Symp. on Borehole Geophysics for Minerals, Geotechnical, and Groundwater Applications*, Golden, Soc. of Prof. Well Log Analysts Publ., pp. 1–11.

Ewy, R.T. and Cook, N.G.W. (1990) Deformation and fracture around cylindrical openings in rock – I. Observations and analysis of deformation, II. Initiation, growth and interaction of fractures. *Int. J. Rock Mech. Min. Sci. & Geomech. Abstr.*, **27**, I. 387–407, II. 409–27.

Freudenthal, A.M. (1977) Stresses around spherical and cylindrical cavities in shear dilatant elastic media, in *Proc. 18th US Symp. Rock Mech.*, Keystone, Johnson Publishing Co., 4B1-1–4B1-6.

Gough, D.I. and Bell, J.S. (1982) Stress orientation from borehole wall fractures with examples from Colorado, East Texas, and northern Canada. *Can. J. Earth Sci.*, **19**, 1358–70.

Guenot, A. (1989) Borehole breakouts and stress fields. *Int. J. Rock Mech. Min. Sci. & Geomech. Abstr.*, **26**, 185–95.

Haimson, B.C. and Edl, J.N. (1972) Hydraulic fracturing of deep wells. SPE Paper No. SPE 4061.

Haimson, B.C. and Herrick, C.G. (1985) In-situ stress evaluation from borehole breakouts: experimental studies, in *Proc. 26th US Symp. Rock Mech.*, Rapid City, Balkema, Rotterdam, 1207–18.

Haimson, B.C. and Herrick, C.G. (1986) Borehole breakouts – a new tool for estimating *in situ* stress?, in *Proc. Int. Symp. on Rock Stress and Rock Stress Measurements*, Stockholm, Centek Publ., Luleå, pp. 271–80.

Haimson, B.C. and Lee, M.Y. (1995) Estimating *in situ* stress conditions from borehole breakouts and core disking – experimental results in granite, in *Proc. Int. Workshop on Rock Stress Measurement at Great Depth*, Tokyo, Japan, 8th ISRM Congress, pp. 19–24.

Hickman, S.H., Healy, J.H. and Zoback, M.D. (1985) In-situ stress, natural fracture distribution, and borehole elongation in the Auburn geothermal well. *J. Geophys. Res.*, **90**, 5497–512.

Jaeger, J.C. and Cook, N.G.W. (1976) *Fundamentals of Rock Mechanics*, 2nd edn, Chapman & Hall, London.

Koslovsky, Y.A. (ed.) (1987) *The Super Deep Well of the Kola Peninsula*, Springer-Verlag, New York.

Kramer, A. *et al.* (1994) Borehole televiewer data analysis from the New Hebrides Island Arc: the state of stress at Holes 829A and 831B, in *Proc. Ocean Drill. Proj., Science Results*, Ocean Drilling Program, College Station, Texas.

Kutter, H.K. (1991) Influence of drilling method on borehole breakouts and core disking, in *Proc. 7th Cong. Int. Soc. Rock Mech. (ISRM)*, Aachen, Balkema, Rotterdam, Vol. 3, pp. 1659–64.

Lee, M.Y. and Haimson, B.C. (1993) Borehole breakouts in Lac du Bonnet granite: a case of extensile failure mechanism. *Int. J. Rock Mech. Min. Sci. & Geomech. Abstr.*, **30**, 1039–45.

Leeman, E.R. (1964) The measurement of stress in rock – Part I. *J. S. Afr. Inst. Min. Metall.*, **65**, 45–114.

Maloney, S. and Kaiser, P.K. (1989) Results of borehole breakout simulation tests, in *Proc. Int. Symp. on Rock at Great Depth*, Pau, Balkema, Rotterdam, pp. 745–51.

Mardia, K.V. (1972) *Statistics of Directional Data*, Academic Press, London.

Martin, C.D. (1995) Brittle rock strength and failure: laboratory and *in situ*, in *Proc. 8th. Cong. Int. Soc. Rock Mech. (ISRM)*, Tokyo, Balkema, Rotterdam, Vol. 3 (in press).

Martin, C.D., Martino, J.B. and Dzik, E.J. (1994) Comparison of borehole breakouts from laboratory and field tests, in *Proc. Eurock '94: Int. Symp. on Rock Mech. in Petrol. Eng.*, Delft, Balkema, Rotterdam, 183–90.

Mastin, L.G. (1984) Development of borehole breakouts in sandstone, unpublished MSc Thesis, Stanford University, Palo Alto.

Moos, D. and Zoback, M.D. (1990) Utilization of observations of wellbore failure to constrain the orientation and magnitude of crustal stresses: application to continental, Deep Sea Drilling Project and Ocean Drilling Program boreholes. *J. Geophys. Res.*, **95**, 9305–25.

Müller, B. *et al.* (1992) Regional patterns of tectonic stress in Europe. *J. Geophys. Res.*, **97**, 11783–803.

Onaisi, A., Sarda, J.P. and Bouteca, M. (1990) Experimental and theoretical investigation of borehole breakouts, in *Proc. 31st US Symp. Rock Mech.*, Golden, Balkema, Rotterdam, pp. 703–10.

Paillet, F.L. and Kim, K. (1987) Character and distribution of borehole breakouts and their relationship to in situ stresses in deep Columbia river basalts. *J. Geophys. Res.*, **92**, 6223–34.

Plumb, R.A. and Hickman, S.H. (1985) Stress-induced borehole elongation: a comparison between the four-arm dipmeter and the borehole televiewer in the Auburn geothermal well. *J. Geophys. Res.*, **90**, 5513–21.

Rutqvist, J. *et al.* (1990) Simulation of borehole breakouts with a damage material model, in *Proc. Int. Symp. Rock at Great Depth*, Pau, Balkema, Rotterdam, Vol. 3, pp. 1439–45.

Santarelli, F.J. and Brown, E.T. (1989) Failure of three sedimentary rocks in triaxial and hollow cylinder compression tests. *Int. J. Rock Mech. Min. Sci. & Geomech. Abstr.*, **26**, 401–13.

Santarelli, F.J., Brown, E.T. and Maury, V. (1986) Analysis of borehole stresses using pressure dependent, linear elasticity. *Int. J. Rock Mech. Min. Sci. & Geomech. Abstr.*, **23**, 445–9.

Shamir, G. and Zoback, M.D. (1992) Stress orientation profile to 3.5 km depth near the San Andreas fault at Cajon Pass, California. *J. Geophys. Res.*, **97**, 5059–80.

Singh, U.K. and Digby, P.J. (1989a) A continuum damage model for simulation of the progressive failure of brittle rocks. *Int. J. Solids Structures*, **25**, 647–63.

Singh, U.K. and Digby, P.J. (1989b) The application of a continuum damage model in the finite element simulation of the progressive failure and localization of deformation in brittle rock structures. *Int. J. Solids Structures*, **25**, 1023–38.

Stephansson, O., Savilahti, T. and Bjarnason, B. (1989) Rock mechanics of the deep borehole at

Gravberg, Sweden, in *Proc. Int. Symp. Rock at Great Depth*, Pau, Balkema, Rotterdam, Vol. 2, pp. 863–70.

Te Kamp, L., Rummel, F. and Zoback, M.D. (1995) Hydrofrac stress profile to 9 km at the German KTB site, in *Proc. Workshop on Rock Stresses in the North Sea*, Trondheim, Norway, NTH and SINTEF Publ., Trondheim, pp. 147–53.

Vernik, L. and Zoback, M.D. (1992) Estimation of maximum horizontal principal stress magnitude from stress-induced well bore breakouts in the Cajon Pass scientific research borehole. *J. Geophys. Res.*, **97**, 5109–19.

Wiebols, G.A. and Cook, N.G.W. (1968) An energy criterion for the strength of rock in polyaxial compression. *Int. J. Rock Mech. Min. Sci.*, **5**, 529–49.

Zemanek, J. *et al.* (1970) Formation evaluation by inspection with the borehole televiewer. *Geophysics*, **35**, 254–69.

Zheng, Z., Kemeny, J. and Cook, N.G.W. (1989) Analysis of borehole breakouts. *J. Geophys. Res.*, **94**, 7171–82.

Zoback, M.D. *et al.* (1985) Well bore breakouts and in-situ stress. *J. Geophys. Res.*, **90**, 5523–30.

Zoback, M.D. *et al.* (1993) Upper-crustal strength inferred from stress measurements to 6 km depth in the KTB borehole. *Nature*, **365**, 633–5.

Zoback, M.L. (1992) First- and second-order patterns of stress in the lithosphere: The World Stress Map Project. *J. Geophys. Res.*, **97**, 11703–28.

Zoback, M.L. *et al.* (1989) Global pattern of tectonic stress. *Nature*, **341**, 291–8.

CASE STUDIES AND COMPARISON BETWEEN DIFFERENT METHODS

9

The previous five chapters have described various techniques of rock stress measurements. In this chapter we present several case studies where some of those techniques have been used at the same site either in a complementary manner or as a cross-check. Several examples of comparison between different methods are presented. Such comparisons are recommended in practice as they provide an additional measure of consistency and reliability with regard to the methods used and the stresses measured.

9.1 STRESS MEASUREMENTS AT THE URL PROJECT

The Underground Research Laboratory (URL) of Atomic Energy of Canada Limited (AECL) has been selected as it represents one of the most comprehensive and best-documented case studies on rock stress and its measurement. It provides a comparison between different methods and also answers many of the fundamental questions with regard to rock stress in hard and competent rock. The work conducted at the URL has been part of an assessment study conducted by AECL on the feasibility and safety of deep geological disposal of nuclear waste in plutonic rocks at depths ranging between 500 and 1000 m. This section is a summary of several papers published in the literature between 1987 and 1994. For more information, the reader is directed to the paper by Martin and Simmons (1993) which provides an overview of the geomechanics characterization of the URL project and an up-to-date literature review.

9.1.1 GEOLOGICAL SETTING

The URL is located within the Lac du Bonnet granite batholith on the western edge of the Canadian Shield in the province of Manitoba (Canada). The batholith is about 75 km × 25 km in surface area and extends to a depth of 10 km. It consists of medium- to coarse-grained porphyritic granite with relatively uniform texture and composition with local subhorizontal gneissic banding.

Figures 9.1a and 9.1b show respectively a map and a geological cross-section though the URL and Fig. 9.2 shows a three-dimensional layout of the URL project. The batholith consists of five major rock units: pink or gray granite, granite with xenolithic inclusions, leucocratic granitic segregations and subvertical granodiorite and pegmatitic dikes (Martin, Read and Lang, 1990). The batholith is cut by two major thrust faults dipping at 25–30° to the southeast which are referred to as Fracture Zones 2 and 3. Their splays are defined as Fracture Zones 2.5 and 1.9. Above Fracture Zone 2.5, the pink granite contains two vertical joint sets: one dominant striking 020–040° and a less dominant one striking 150–180°. Below Fracture Zone 2.5, the granite is gray and is essentially massive except in Fracture Zone 2 and its splays Fracture Zones 1.9 and 1.5, where the rock is more fractured. The differential displacement along Fracture Zone 2 has been estimated at 7 m.

In general, the gray granite was found (in the laboratory) to contain more microcracks than the pink granite (due to sample disturbance), thus making the gray granite more

nonlinear and anisotropic in its response to loading and unloading (Fig. 9.3). Table 9.1 gives a summary of the geotechnical properties of the intact pink and gray granites determined in the laboratory. Scale effect was

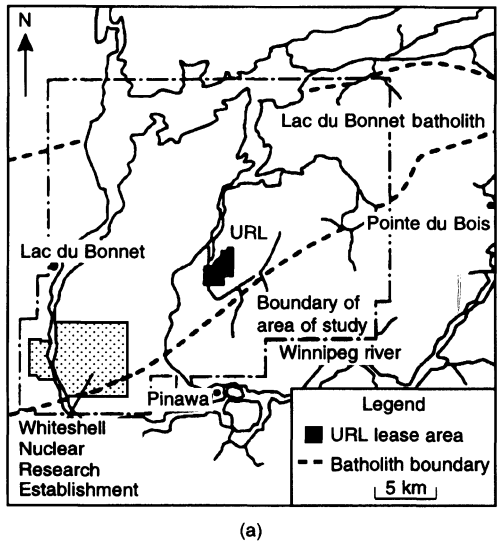

Fig. 9.1 (a) Map of the URL site, (b) generalized NW–SE cross-section of the URL geology. (After Martin, Read and Lang, 1990.)

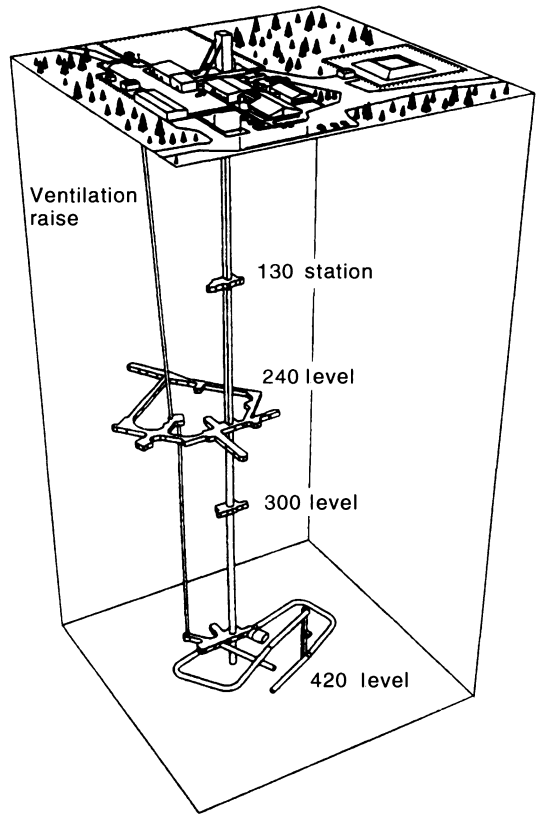

Fig. 9.2 Three-dimensional layout of the URL site. (After Martin and Simmons, 1993.)

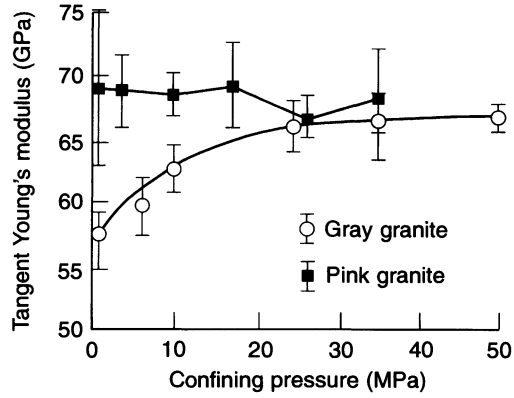

Fig. 9.3 Variation of tangent Young's moduli at 50% peak strength measured in triaxial compression on 45 mm diameter samples of Lac du Bonnet granite. (After Martin and Christiansson, 1991.)

Table 9.1 Summary of laboratory geotechnical properties of Lac du Bonnet granite at the URL (Source: Martin, C.D. and Simmons, G.R. Copyright 1993, with kind permission from Elsevier Science Ltd, The Boulevard, Langford Lane, Kidlington, UK.)

Property	*Pink granite*	*Gray granite*
Porosity (%)		
Range	0.16–0.28	0.32–0.67
Mean	0.24	0.50
Density (kg/m^3)		
Mean	2640	2630
Uniaxial compression strength (MPa)		
Range	134–248	147–198
Mean	200	167
Brazilian tensile strength (MPa)		
Range	6.17–12.07	6.22–11.52
Mean	9.32	8.72
Tangent Young's modulus (GPa)		
Range	53–86	46–64
Mean	69	55
Poisson's ratio		
Range	0.18–0.44	0.13–0.43
Mean	0.26	0.30
Hoek and Brown failure parameters		
m	31.17	30.54
s	1	1

observed on intact specimens ranging in size between 54 and 300 mm in diameter with a decrease in uniaxial compressive strength and tangent modulus of elasticity with increasing test sample diameter (Martin, Martino and Dzik, 1994). It is noteworthy that the microcracks have been observed in the laboratory and are believed to be induced by stress relief due to sampling. It is not clear if those same microcracks and the associated nonlinear and anisotropic behavior are prevalent *in situ* (Martin, 1989; Martin and Simmons, 1993).

A vertical shaft was constructed in two stages. The upper shaft was constructed to a depth of 255 m and is rectangular with a 2.8×4.9 m cross-section. The lower shaft is circular with a 4.6 m diameter cross-section and was excavated to a depth of 443 m. Shaft stations were excavated at the 130, 240, 300 and 420 m levels. Stress measurements were carried out from the 240 and 420 m levels and at various locations along the shaft.

9.1.2 STRESS MEASUREMENTS

Stress measurements at the URL have been conducted since 1982. Since then, an extensive research program has been carried out to address several fundamental questions dealing with *in situ* stresses in rock (Martin, Read and Lang, 1990): (1) are *in situ* stresses dependent on the scale of the method used, (2) what is the effect of geological structures on *in situ* stresses, (3) what is the importance of residual stresses, and (4) do different methods yield comparable *in situ* stress fields? These four questions were addressed by using several methods such as overcoring, hydraulic fracturing, borehole slotting, rock mass relief methods (under-excavation and bored

raise), borehole and shaft breakouts, microseismic measurements and other indirect measurements.

(a) Overcoring measurements

Overcoring measurements have been made with a variety of techniques such as the USBM, CSIR, CSIRO HI and SSPB gages. A total of about 1000 overcore measurements have been made, out of which 350 have been far-field triaxial measurements covering a volume of rock about $100 \times 100 \times 500$ m in size (Martin and Chandler, 1993). Most of the overcoring measurements were carried out above Fracture Zone 2. Below that fracture zone, core disking and microcracking were found to be limiting factors.

The USBM gage was modified by Thompson (1990). The new gage, called the deep borehole deformation gage (DBDG), was designed to operate at depths to 1000 m in water-filled boreholes. Tests could only be done to depths of 280 m below surface because of core disking (Martin, Read and Lang, 1990).

The CSIR gage was also modified for continuous monitoring of strains (Thompson, Lang and Snider, 1986). The new cell, called the AECL-modified CSIR cell, has been used extensively for measuring *in situ* stresses and has become the standard method of overcore testing at the URL. It was found to be less costly than other methods, could be overcored 1 h after installment, did not have the debonding problem of the CSIRO HI cell (due to low temperatures) and showed less scatter than with the SSPB gage (Martin, Read and Lang, 1990). Figure 9.4 shows the results of five consecutive overcoring tests carried out with the AECL-modified CSIR cell in one borehole on the 240 level at the URL. It can be seen that the cell gives similar and consistent results (within the expected range of accuracy).

Biaxial tests on overcore samples of the URL gray granite at the 240 m level have revealed that, due to the microcracks, the rock is elastic but nonlinear with an increasing Young's modulus with confining stress. For the stresses around the URL excavations, the Young's modulus is expected to vary from 55 to 70 GPa *in situ* (Martin, Read and Lang, 1990). The same microcracks have been found to create

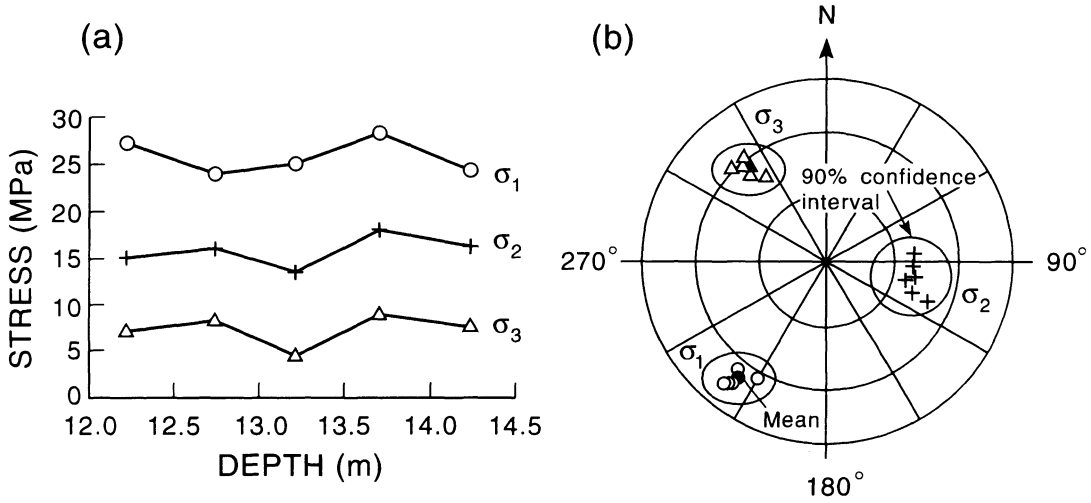

Fig. 9.4 Results of five consecutive overcoring tests conducted in borehole OC1 on the 240 level at the URL using an AECL-modified CSIR triaxial strain cell. (a) Principal stress magnitudes, (b) principal stress orientations. (After Martin and Simmons, 1993.)

planar anisotropy as well. The anisotropy was modeled as transverse isotropy with the plane of transverse isotropy parallel to the average plane of microcracking. The rock's secant Young's modulus in the direction perpendicular to the plane of rock anisotropy is 30 GPa, which is about 50% of that in the direction parallel to the plane. The Poisson's ratios parallel and perpendicular to the plane of anisotropy are equal to 0.25 and 0.15, respectively (Martin and Simmons, 1993).

It is interesting to note that, in this case study, the microcrack-induced anisotropy was quantified through both biaxial tests on overcores and uniaxial tests on core samples cut in different directions (Martin, 1989). For example, Fig. 9.5 shows the results of biaxial tests conducted on the gray granite. The rock's secant Young's modulus was determined by rotating the USBM gage in 15° increments and by repeating the biaxial test for each gage orientation. A good agreement was found between the directions of the maximum and minimum secant Young's moduli determined on the same rock by biaxial and uniaxial testing (Martin, 1989).

Lang, Thompson and Ng (1986) conducted an extensive field study on the effect of overcore diameter on the magnitude and orientation of *in situ* stresses at the URL. They found that for the USBM gage and the AECL-modified CSIR cell, the stress results from overcoring with a 96 mm diameter bit were not significantly different from those with 150 and 200 mm diameter bits. Furthermore, overcoring of overcores was also carried out to determine the existence of residual stresses in the granite and their relative proportion compared with the *in situ* stresses. The measured residual stresses were found to be less than 1.0 MPa and to range between 1.5 and 3.5% of the total stresses, thus making residual stresses negligible. This conclusion was confirmed with other measurements carried out by Read (Martin and Simmons, 1993) using concentric measurements for diameters of up to 600 mm.

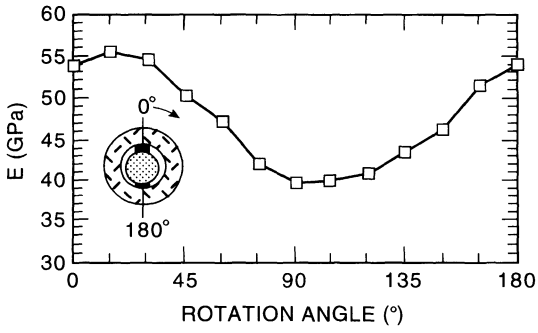

Fig. 9.5 Typical plot of the secant Young's modulus determined from biaxial tests using a USBM gage rotated in 15° increments in an overcore sample of Lac du Bonnet gray granite. (After Martin and Christiansson, 1991.)

(b) Rock mass relief methods

The rock mass relief methods used at the URL included the bored raise method and the under-excavation technique. Both methods involve the largest volume of rocks tested for *in situ* stress at the URL, with estimated values of the order of 10^3–10^4 m^3 (Martin, Read and Chandler, 1990). The results of those tests have been found particularly important in assessing the effect of scale on *in situ* stress.

The bored raise tests were reported by Chandler (1993). The *in situ* stresses were determined by overcoring strain rosettes located on the surface of the 1.8 m diameter ventilation raise of Fig. 9.2 in between Fracture Zones 2 and 2.5 and at an elevation of about 220 m. The test configuration is shown in Fig. 9.6a. Four strain rosettes consisting of 120 mm long strain gages were recessed 10–20 mm into the surface of the rock and overcored using a 300 mm diameter bit. In addition to these tests, overcoring of 17 AECL-modified CSIR cells was carried out in three nearby orthogonal holes, and four additional CSIR overcore stress measurements were conducted in boreholes drilled outward from the ventilation shaft (also shown in Fig. 9.6a).

The under-excavation technique was applied to determine *in situ* stresses during excavation of the 209 experimental drift at the

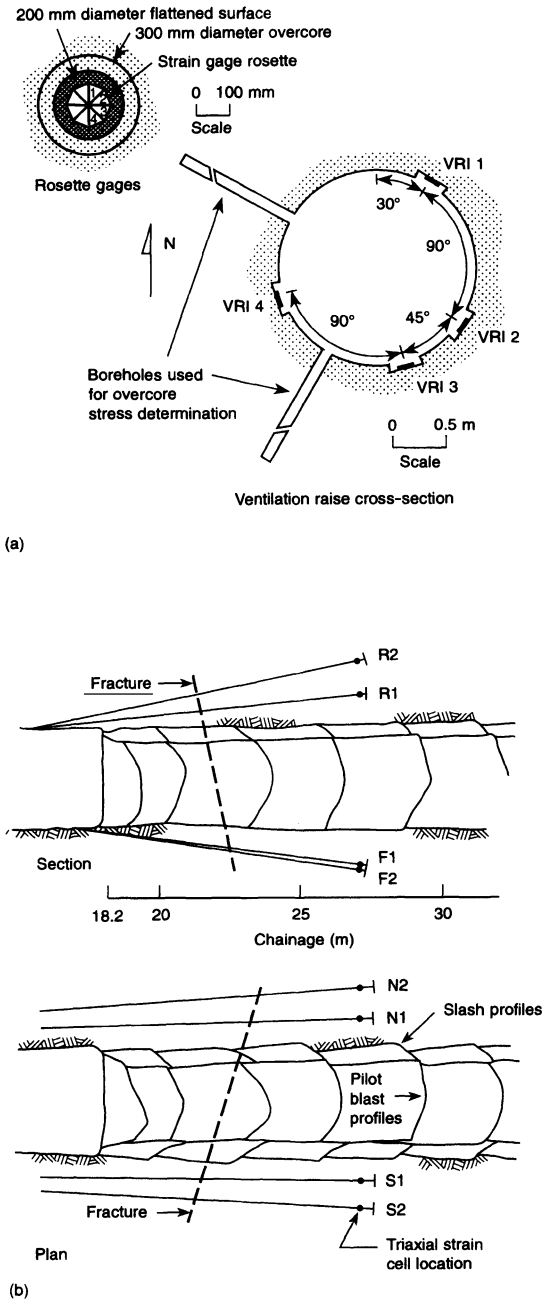

Fig. 9.6 Rock mass relief tests at the URL. (a) Plan view of bored raise test configuration. (After Chandler, 1993.) (b) Longitudinal and plan view of the under-excavation technique used in the excavation of the 209 experimental drift at the 240 m level. (After Kaiser, Zou and Lang, 1990.)

240 m level (Kaiser, Zou and Lang, 1990; Zou and Kaiser, 1990) and the ventilation shaft by raise boring from the 420 m to the 240 m level (Wiles and Kaiser, 1994a, b). Figure 9.6b shows the geometry of the test at the 240 m level. In this test, eight CSIRO HI cells (two in the roof, two in the floor, and two near each springline) were placed in a plane ahead of the advancing drift (3.9 m × 3.6 m finished) by drilling holes angled slightly outward. The distance from each cell to the wall of the opening varied between 0.85 and 2.28 m. The strains in the cells were monitored until the excavation had passed the instrument locations by about 25 m. The *in situ* stresses were determined using a two-dimensional analysis by Kaiser, Zou and Lang (1990) and a three-dimensional analysis by Wiles and Kaiser (1994a).

During excavation of the ventilation shaft, the *in situ* stresses were again determined using eight CSIRO HI cells placed ahead of the upward-advancing 1.8 m bored raise. Three-dimensional back-analysis of the *in situ* stresses was done on 1 m intervals as the raise borer passed within 10 m on either side of the instrument array (Wiles and Kaiser, 1994b).

The test results for the bored raise tests, the nearby AECL-modified CSIR overcoring tests and the two-dimensional under-excavation analysis for room 209 are summarized in Fig. 9.7. Except for the bored raise method, the orientations of the principal stresses are quite consistent. Also, the stresses determined with the bored raise method tend to be higher than those determined with the AECL-modified CSIR cells (except for the three orthogonal holes where they are similar). The magnitudes of the stresses determined with the two-dimensional underexcavation technique are in good agreement with those determined with the bored raise method and those determined with the CSIR cells in the three orthogonal holes.

(c) Borehole slotters

Borehole slotter tests at the URL were reported by Martin, Read and Lang (1990). It was

concluded that, based on the results in three intersecting and orthogonal boreholes, and compared with the stresses determined with the USBM gage and the AECL-modified CSIR cell, the borehole slotter gave inconsistent stress magnitudes but reasonable stress orientation.

(d) Hydraulic fracturing

Hydraulic fracturing tests represent some of the first *in situ* stress measurement techniques used at the URL. The test results have been found to be inconsistent due to difficulties in fracturing the rock. Also, horizontal fractures have been found below Fracture Zone 2, making the analysis of hydraulic tests difficult (Chandler and Martin, 1991).

(e) Microseismic monitoring

Monitoring of microseismic events has been used at the URL as a method to determine stress orientation (Talebi and Young, 1989, 1992). Monitoring of microseismic events caused by shaft excavation was carried out during excavation of the 4.6 m diameter shaft from the 324 m to the 443 m level (Fig. 9.8a). During and following excavation, it has been found that most of the microseismic activities occur within a zone about one shaft diameter thick around the shaft with preferred occurrence in the minimum horizontal stress direction (Fig. 9.8b). The clustering of microseismic events seems to indicate a NW–SE orientation for the maximum horizontal stress below Fracture Zone 2. Martin, Martino and Dzik (1994) reported the results of another microseismic monitoring study around a 3.5 m tunnel excavated at the 420 level. A very good correlation was found there between the regions of microseismic activity and the locations of the tunnel breakouts.

(f) Indirect measurements

Indirect inferences of *in situ* stresses were obtained through convergence measurements during excavation of the lower shaft, observations of shaft spalling and borehole core disking. Borehole and shaft breakouts were also valuable in estimating the orientation of the maximum horizontal stress (Martin, 1989; Martin, Martino and Dzik, 1994).

In particular it was found that above Fracture Zone 2, V-shaped notches due to spalling of the shaft wall were in the NW–SE direction, thus indicating a NE–SW direction for the maximum horizontal stress. On the other

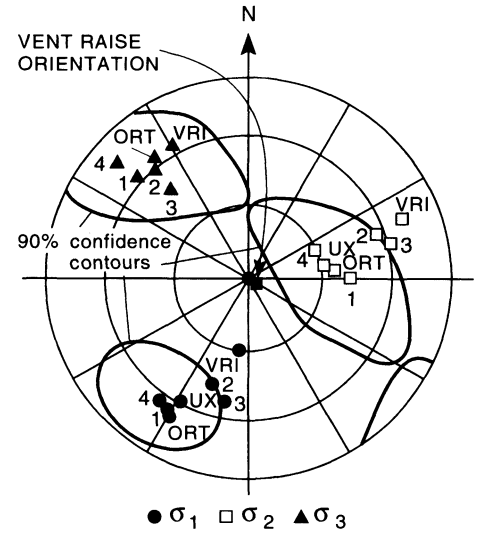

		Stress magnitudes (MPa) σ_1	σ_2	σ_3
VRI	Ventilation raise rosette overcoring	28.1	18.6	11.1
1	CSIR OC2 6.18 m	22.1	14.5	7.1
2	CSIR OC3 3.46 m	18.9	12.8	6.3
3	CSIR OC3 5.30 m	19.8	15.7	10.0
4	CSIR OC4 4.81 m	21.9	13.7	8.3
ORT	Average from CSIR tests in three orthogonal holes	30.1	14.9	10.6
UX	Under-excavation	29.3	14.1	—

Fig. 9.7 Comparison of *in situ* stress orientation and magnitude determined with the bored raise tests, the two-dimensional under-excavation technique in room 209 and AECL-modified CSIR cells. The 90% confidence contours for stress direction from the CSIR data are included. (After Chandler, 1993.)

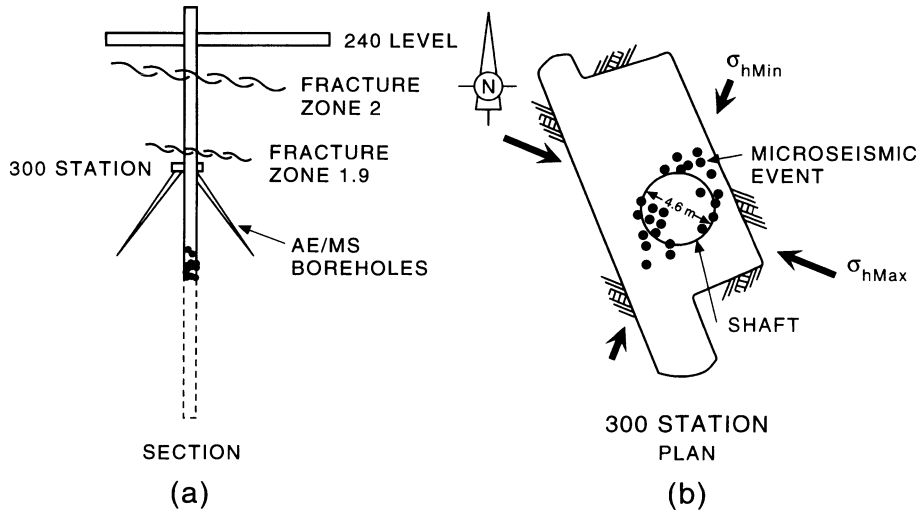

Fig. 9.8 (a) Layout of acoustic emission (AE) and microseismic (MS) monitoring system; (b) results from the monitoring of microseismic events for a shaft depth of 348.4 m. (After Talebi and Young, 1989.)

hand, below Fracture Zone 2, the V-shaped notches were found in the NE–SW direction, thus indicating a 90° rotation with the maximum horizontal stress now oriented in the NW–SE direction.

The convergence measurements were taken at 10 m intervals during excavation of the circular shaft from the 225 m to the 443 m depth. Back-analysis of the shaft convergence measurements using the Kirsch solution for the displacements around a circular opening were used to determine the orientation and magnitudes of the horizontal stresses below Fracture Zone 2 where hydraulic fracturing and overcoring tests had been found unsuccessful. The convergence measurements indicated a NW–SE direction for the maximum horizontal stress.

9.1.3 OBSERVATIONS

(a) Influence of geological structures

Geological structures at different scales, such as microcracks in the granite, single discrete fractures and the thrust faults of Fig. 9.1b, have been found to have a major impact on the *in situ* state of stress and the interpretation of the stress measurements at the URL site (Martin and Chandler, 1993).

Inclusion of microcrack-induced anisotropy in the analysis of stress measurements in the gray granite at the 240 level has been found to create less dispersion in the *in situ* stress results. Also, inclusion of anisotropy creates rotation of the *in situ* stress field compared with isotropy. Both trends have already been discussed in section 5.7.2. However, as mentioned earlier, it is not clear if the anisotropy observed in the laboratory is also present *in situ* under the stress field. Nonetheless, it is clear that if anisotropy is not accounted for in the analysis of overcoring tests, large errors would result.

Figure 9.9a, b shows the orientation of principal stresses measured by overcoring in the vicinity of a steeply dipping single discrete fracture intersecting room 209 at the 240 level. Near the fracture (Fig. 9.9a), the minimum principal stress is essentially subhorizontal and perpendicular to the fracture surface. On the other hand, 30 m away from the fracture (Fig. 9.9b), the same stress has rotated and is now vertical.

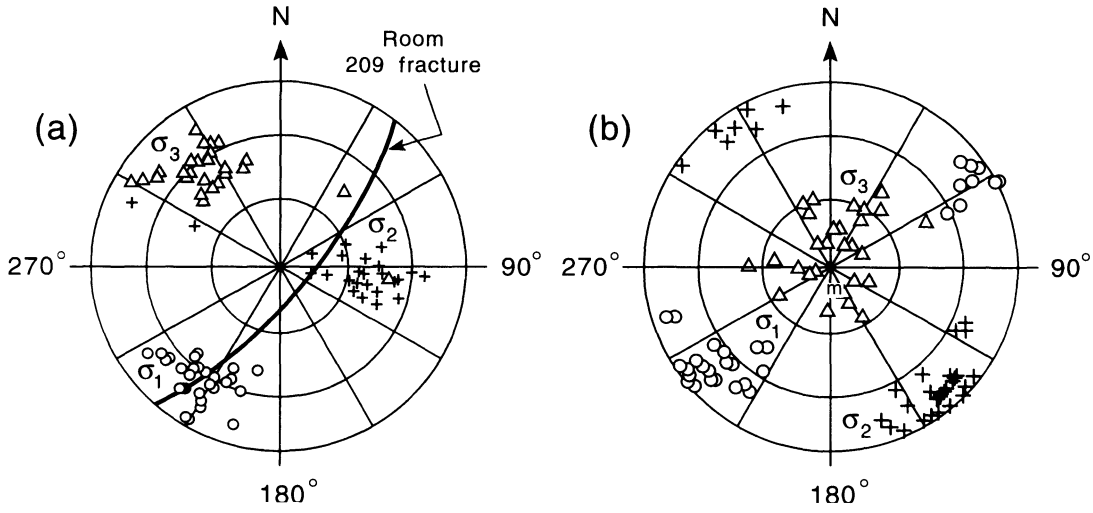

Fig. 9.9 Orientation of principal stresses measured by overcoring in the vicinity of a single discrete fracture intersecting room 209 at the 240 level at the URL site. (a) Stress orientation near the fracture, (b) stress orientation 30 m away from the fracture. (After Martin and Chandler, 1993.)

Well-defined domain boundaries have been found between the major thrust faults. In each domain the stress field is essentially continuous. In particular, above Fracture Zone 2 (which intersects the URL shaft at about 280 m) the major principal stress is horizontal with an azimuth of 040° and is parallel to the major joint set in the pink granite and the strike of Fracture Zone 2. Starting below Fracture Zone 2.5, and in particular after crossing Fracture Zone 2 and down to a depth of 429 m, the maximum horizontal stress increases and experiences a 90° turn with an azimuth of 130° to become parallel to the dip direction of Fracture Zone 2 (Fig. 9.10a, b). As remarked by Martin and Chandler (1993), the 130° orientation coincides with the overall orientation of the stresses in the western part of the Canadian Shield. Below Fracture Zone 2, the maximum horizontal stress is fairly constant with a value of about 55 MPa. The rotation of the maximum horizontal stress and the constant value below Fracture Zone 2 were predicted using a discrete element plane strain model of the rock mass at the URL which allows for slip along Fracture Zones 2, 2.5 and 3 (Chandler and Martin, 1994).

Figure 9.11 shows the effect of Fracture Zone 2 on the variation with depth of the minimum *in situ* stress component σ_3 (commonly equivalent to the vertical stress) normalized by the overburden stress γz (with $\gamma = 0.026$ MPa/m). Around Fracture Zone 2, the ratio $\sigma_3/\gamma z$ is about equal to 2 and approaches a value of 1 above and below that fracture zone. It has been suggested that this increase in vertical stress could be associated with a thinning and stiffening of Fracture Zone 2 near the URL shaft (Martin and Chandler, 1993).

(b) Consistency in stress measurements with different methods

In general, consistency was found between the stress measurements carried out with different direct and indirect methods at the URL site. Above Fracture Zone 2, a good agreement was found between the magnitudes of the maximum and minimum horizontal stresses

determined by hydraulic fracturing and overcoring (Fig. 9.12a). However, the stress orientations determined by the two methods did not agree (Fig. 9.12b). Below Fracture Zone 2, and because of many instances of horizontal hydraulic fractures, the agreement between overcoring and hydraulic fracturing was found to be not as good, in particular for the maximum horizontal stress. The 040° orientation of the maximum horizontal stress is consistent with the orientation of the shaft wall failure observed immediately above Fracture Zone 2 and continuing until Fracture Zone 1.9.

Below Fracture Zones 2 and 1.9, a very good agreement was found between the orientation of the maximum horizontal stress determined with the convergence method, the microseismic method and the shaft failure. All these methods indicate a rotation of the maximum horizontal stress of about 90°.

There is also consistency between the results of the rock mass relief methods and the borehole relief methods. This is shown in Fig. 9.10 where the results of the three-dimensional analysis conducted by Wiles and Kaiser (1994b) for room 209 and the ventilation shaft have been added to the other stress measurements. The consistency between the results of the bored raise tests and those of the borehole tests has already been discussed in relation to Fig. 9.7.

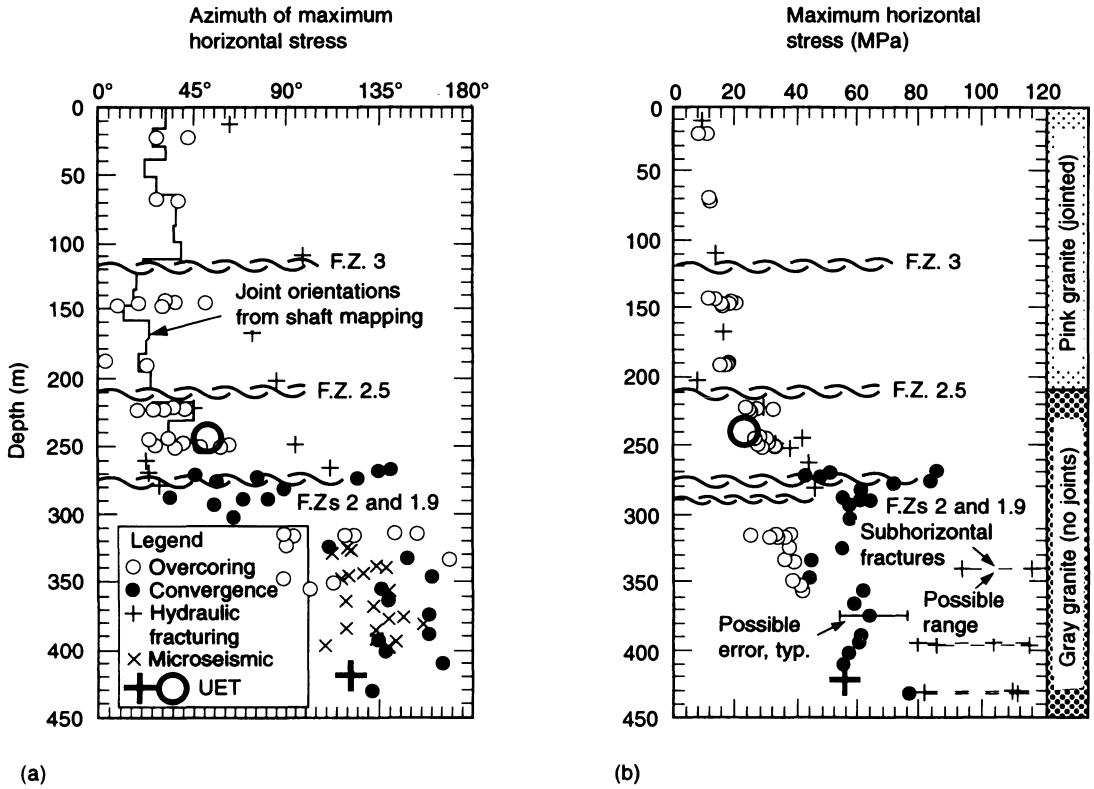

Fig. 9.10 Summary of maximum horizontal stress orientation in (a) and magnitude in (b) for different stress measuring techniques. (After Martin, Read and Lang, 1990.) The results of the under-excavation technique (UET) have been added (see Wiles and Kaiser, 1994b).

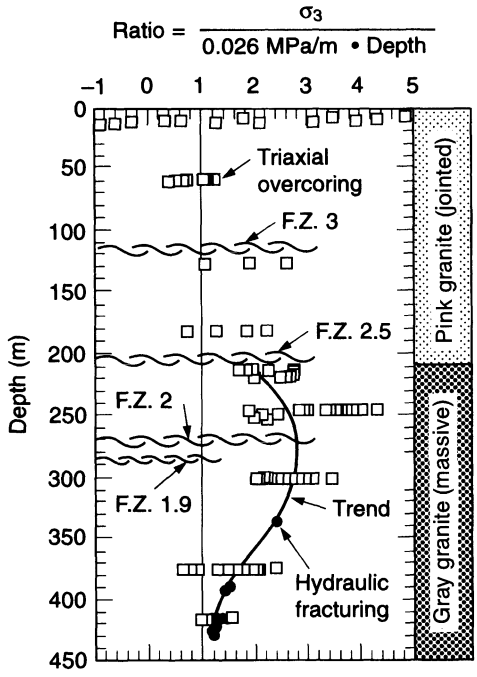

Fig. 9.11 Variation of $\sigma_3/\gamma z$ with depth at the URL site. (After Martin and Chandler, 1993.)

(c) Scale effects

All the stress measurements at the URL involve volumes ranging over several orders of magnitude from $0.1\,m^3$ to $10^5\,m^3$. The volume of rock involved in each test was calculated assuming that a hole of diameter D affects a cylinder of rock $6D$ in length and $3D$ in radius. Figure 9.13 shows the variation of the first stress invariant (sum of the principal stresses) versus rock volume for the different stress measurements carried out at the URL. This figure indicates that, on average, the magnitude of the stress field is not much affected by the rock volume, with more scatter for smaller volumes and less scatter for larger volumes (Martin, Read and Chandler, 1990).

Apart from the fact that there are fewer tests involving large rock volumes, the larger scatter for the smaller rock volumes can be attributed to variability in the material properties at the local scale. As remarked by Chandler (1993), the overcoring tests with the CSIR cells involved strain measurements over a length of 10 mm whereas the bored raise measurements

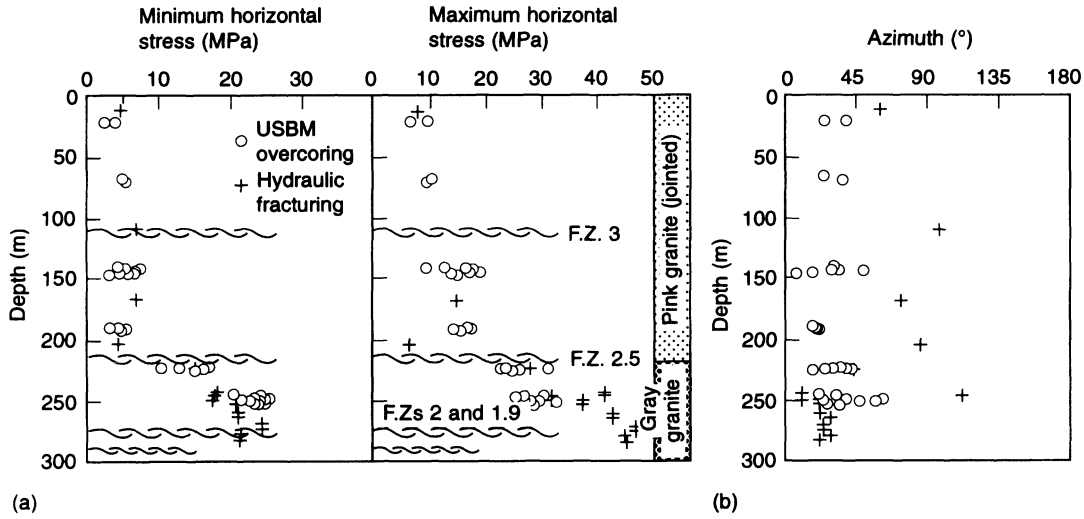

Fig. 9.12 Comparison between maximum and minimum horizontal stress magnitudes in (a) and orientation of maximum horizontal stress in (b) determined by hydraulic fracturing and overcoring above Fracture Zone 2 where the hydraulic fractures were coaxial with the borehole. (After Martin and Simmons, 1993.)

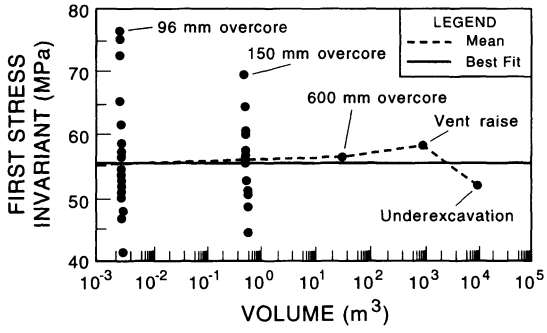

Fig. 9.13 Summary of effect of scale on first stress invariant. (After Martin, Read and Chandler, 1990.)

involved 120 mm strain gages. The longer the strain gages, the smaller the effect that can be expected from the 2–5 mm grain size of the granite.

(d) Stresses at the URL versus stresses in the Canadian Shield

Figure 9.14 shows the distribution of the maximum horizontal stress with depth measured at the URL compared with other stress measurements reported for the Canadian Shield. This figure clearly shows much higher stresses at shallow depths at the URL compared with the rest of the Canadian Shield. It also shows that below Fracture Zone 2 the maximum horizontal stress is essentially constant and approaches with depth the shield trend line. Martin and Chandler (1993) attributed the much higher horizontal stresses at the URL to the presence of Fracture Zone 2 and the contrast in rock mass deformation moduli between the softer jointed pink granite and the underlying stiffer gray granite.

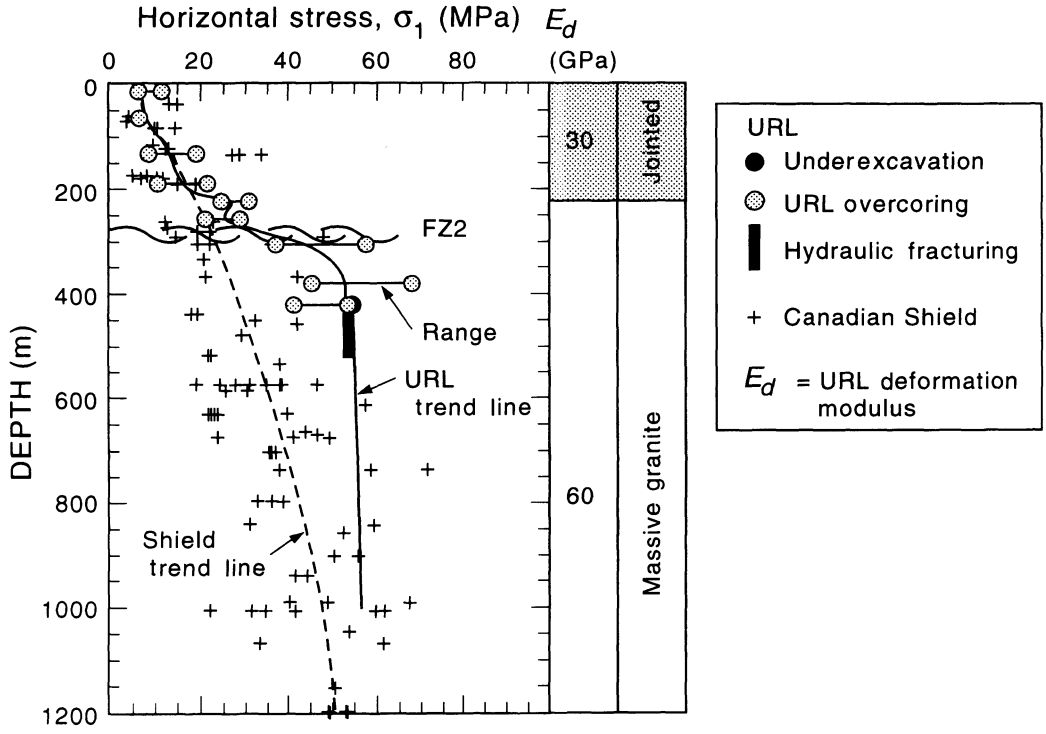

Fig. 9.14 Comparison of the maximum horizontal stress σ_1 measured in the Canadian Shield with the values determined at the URL. (After Martin and Chandler, 1993.)

9.1.4 SUMMARY

Analysis of the stress measurements conducted at the URL has revealed several interesting features for the kind of rock tested, i.e. hard and competent granitic rock (Martin, 1989; Martin and Simmons, 1993).

1. Unusually high *in situ* stresses can be found in large volumes of massive unfractured rock masses and at relatively shallow depths.
2. As long as the rock responds in an elastic manner, consistent stress measurements (on average) can be obtained with different methods and test geometries.
3. Consistent stress measurements can be obtained without much influence from residual stresses and with little scale effect.
4. Different rock structures can affect *in situ* stresses at different scales ranging from the micro-scale to the macro-scale. In particular, inclusion of anisotropy due to microcracks associated with unloading of the rock is required when analyzing stress measurements. Large errors can be created if the anisotropy is not taken into account. At the other extreme, large structures such as thrust faults can act as *in situ* stress domain boundaries and both stress magnitude and orientation can change while crossing those boundaries.
5. Direct stress measurements can be cross-checked with other indirect methods such as excavation convergence tests, microseismic tests, shaft and borehole breakouts and core disking.
6. Rock mass relief methods such as the bored raise method and the under-excavation technique represent valuable tools for determining *in situ* stresses in large rock volumes of interest to engineers.

9.2 COMPARISON BETWEEN DIFFERENT OVERCORING TECHNIQUES

Comparison between two overcoring techniques was conducted by Leijon and Stillborg (1986). Stress measurements were carried out at four locations, representing three different rock types (quartz porphyry, magnetite ore and syenite) in the Luossavaara mine within the Kiruna iron ore fields in northern Sweden. The stress measurements were part of a comprehensive geomechanical site characterization scheme.

The measurements were made with the CSIRO HI cell and the LuH (LuT) gage, which were both described in Chapter 5. Both instruments are triaxial devices that can be used for determining the complete state of stress in a single borehole. The stress measurements were concentrated in a small area at the 265 m level of the Luossavaara mine. A total of 34 tests were carried out in four boreholes penetrating the hard rocks in the hanging wall, the orebody and the footwall of the mine. Table 9.2 gives a summary of the stress results for each stress instrument and for each borehole. Figure 9.15 shows the corresponding orientation of the principal stresses.

Table 9.2 indicates that, except for holes 0-2 and F, both instruments yield comparable stress predictions with regard to magnitude and orientation. However, in each borehole of Fig. 9.15, considerable scatter can be noted. Leijon and Stillborg (1986) concluded that the stress measurements were consistent with those in adjacent mines. They also concluded (without statistical justification) that the stress measurements did not indicate any obvious discrepancy between the two methods of measurement, considering the uncertainty associated with the nonlinear and inhomogeneous character of the rock (in particular the magnetite ore). This emphasizes the fact that, regardless of the overcoring method used, the rock quality is a major factor when measuring *in situ* stresses. Finally, Leijon and Stillborg (1986) concluded that the choice of measuring technique should be governed by practical factors such as site-specific conditions and the availability of experienced personnel, rather than by minor technical differences between the techniques used.

Table 9.2 Summary of principal stress results from a comparative study between CSIRO HI cell and LuH gage at the Luossavaara mine in Sweden. (After Leijon and Stillborg, 1986)

Location	Gage type	No. tests	Maximum σ_1 (MPa)			Intermediate σ_2 (MPa)	Minimum σ_3 (MPa)
			Magnitude (MPa)	Azimuth (deg)	Dip (deg)		
Hanging wall	CSIRO	3	8.0	200	34	6.2	4.5
(Hole H)	LuH	4	8.6	180	31	4.9	1.3
Orebody	CSIRO	2	10.4	340	9	4.6	2.3
(Hole 0-1)	LuH	7	13.5	337	5	6.5	4.6
Orebody	CSIRO	2	5.7	9	11	4.7	1.4
(Hole 0-2)	LuH	6	9.5	331	17	5.1	4.0
Footwall	CSIRO	3	15.1	165	7	7.3	5.6
(Hole F)	LuH	7	8.3	162	10	5.3	2.4

An early example of comparison between two different overcoring techniques was presented by Van Heerden and Grant (1967). This case study is interesting as it represents one of the first records and experience with both the USBM gage and the CSIR Doorstopper. Both instruments were used to determine stresses in a Canadian uranium mine. Three horizontal and parallel holes, two with a length of 30 ft (9 m) and one with a length of 19 ft (6 m), were drilled in the sidewall of a drift located at a depth of 1400 ft (427 m) in the mine. Overcoring was carried out in two holes instrumented with the CSIR Doorstopper and one hole instrumented with the USBM gage. The distance between two consecutive measurements in each hole varied between 2 and 5 ft (0.6 and 1.5 m). Figures 9.16a and 9.16b show respectively the variation with distance of the major and minor principal stresses in the plane perpendicular to the holes, and Fig. 9.16c shows the variation with distance of the orientation of the major principal stress from the vertical. In general, Figs 9.16a–c indicate a relatively good agreement between the two stress measuring methods with greater scatter deeper within the rock mass. It should be noted that the measured stresses in this case study are not necessarily the *in situ* stresses since it does not seem that the authors separated the rock deformation induced by the excavation of the drift from the total rock deformation.

Several examples of comparison of overcoring stress measurements have also been reported as part of block tests associated with potential nuclear waste repositories. The main idea behind block tests is to apply known loads on the side of a large block of rock and measure the stresses at different points inside the block. The measured stresses are then compared with the applied stresses.

At the Near-Surface Test Facility of the Basalt Waste Isolation Project (BWIP) near Hanford, Washington, Gregory *et al.* (1983a, b) tested five different overcoring techniques (USBM gage, CSIRO HI cell, LuH gage, the CSIR cell and the photoelastic hollow inclusion gage) in a cubical block of fractured basalt 2.0 m in size cut in a vertical wall and loaded by flat jacks (Black and Cramer, 1983). The results of 42 overcoring tests showed that all five overcoring techniques were unsuitable for the closely jointed (joint spacing between 0.1 and 0.2 m) nature of the rock found at the site.

Another program of block test stress measurements was reported by Brown, Leijon and Hustrulid (1986) regarding an 8 m^3 block of jointed gneiss at the Colorado School of Mines Experimental Mine in Idaho Springs, Colorado. The block was in the floor of the

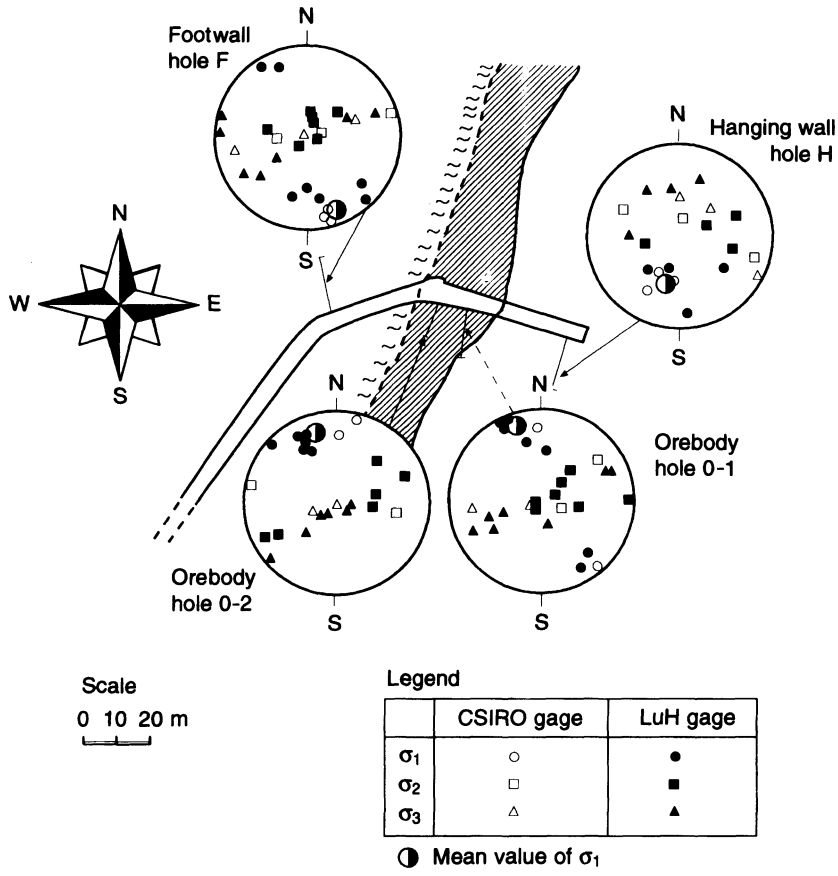

Fig. 9.15 Comparative study between CSIRO HI and LuH triaxial overcoring stress measurement techniques in the Luossavaara mine, northern Sweden. Measured principal stress directions are presented in lower hemisphere, equal area projections. (After Leijon and Stillborg, 1986.)

mine and was intersected by three major fractures. Stresses were measured in EX and NX boreholes using the USBM gage and the LuH triaxial strain gage under uniaxial side loading (in the E–W and N–S directions) and biaxial loading. Figures 9.17a and 9.17b give two examples of measured stresses with the USBM gage and LuH gage, respectively. Both figures show similarities in stress distribution (except for two circled points in Fig. 9.17b) and consistency between the direction of applied stress and the stress directions in each part of the block. Stress magnitudes were found to be more variable due to existing fractures in the block. It was also found that, on average and under uniaxial loading, the USBM gage stress results were at least 20% higher than those obtained with the LuH gage. Finally, three-dimensional analysis of the LuH gage measurements revealed that the tested block was indeed under a uniaxial or biaxial stress field and that the local principal stresses at the measurement points in the block were close to the vertical and horizontal directions.

9.3 COMPARISON BETWEEN HYDRAULIC FRACTURING AND OVERCORING TECHNIQUES

Haimson (1981) presented several case histories in which the results of stress

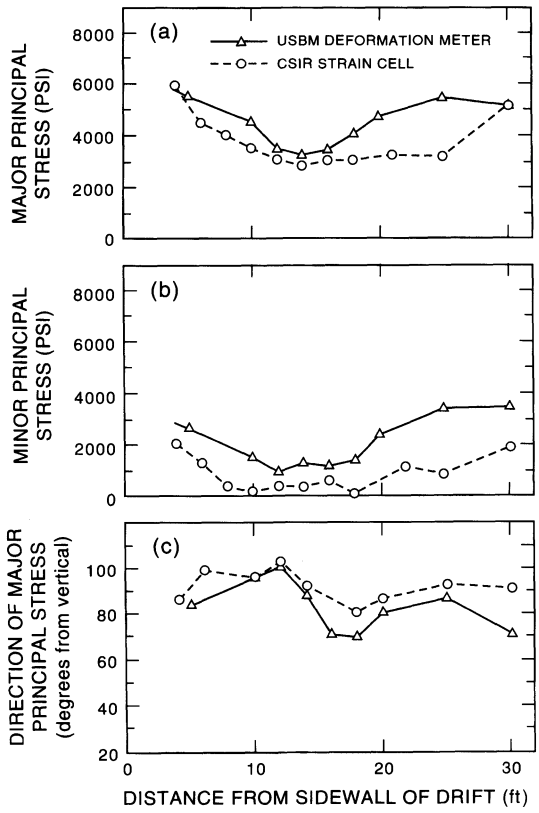

Fig. 9.16 Variation of major principal stress in (a), minor principal stress in (b), and orientation of the major principal stress from vertical in (c) with distance, measured with the USBM gage and the CSIR Doorstopper. (After Van Heerden and Grant, 1967.)

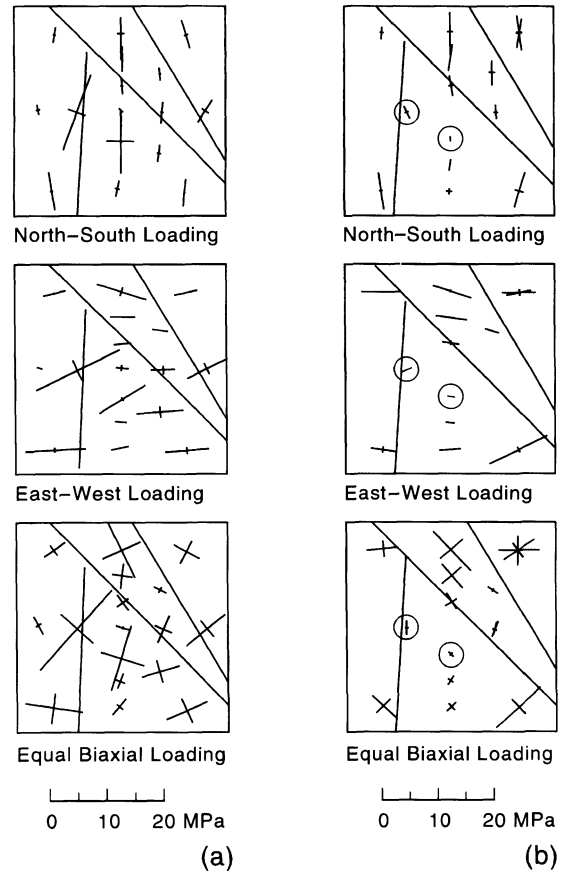

Fig. 9.17 Principal stress directions measured with the USBM gage in (a) and the LuH gage in (b), in a block at the Colorado School of Mines Experimental Mine in Idaho Springs, Colorado. (After Brown, Leijon and Hustrulid, 1986.)

measurements obtained by hydraulic fracturing were compared with those obtained by overcoring. The case studies discussed here include the Nevada Test Site, the Helms pumped storage project in California, the Bad Creek pumped storage project in South Carolina, the Near-Surface Test Facility of the BWIP at Gable Mountain near Hanford, Washington, and the Stripa project in Sweden. In general, stresses were measured at depths not exceeding 400 m.

For each site and at comparable depths, the orientation and magnitude of the *in situ* stresses determined by overcoring and hydraulic fracturing were found to compare relatively well. Table 9.3 gives a summary of the horizontal stress comparisons. Based on this table, the following conclusions were reached by Haimson (1981).

- The directions of the horizontal stresses determined by the two methods are within $\pm 10°$.
- The magnitudes of the minimum horizontal stress are within ± 2 MPa, which is equivalent to a discrepancy of up to 30% of the minimum horizontal stress determined by hydraulic fracturing.

Table 9.3 Comparison between overcoring and hydraulic fracturing measurements of horizontal stresses at five different sites (after Haimson, 1981)

Site	$\Delta\sigma$ (MPa)		$\Delta\sigma/\sigma_{HF}$ (%)		$\Delta\sigma_{Hmax}$ (direction) (deg)
	σ_{hmin}	σ_{Hmax}	σ_{hmin}	σ_{Hmax}	
Nevada Test Site	1	1	29	11	−10
Helms	−1.5	−5	−27	−50	8
Bad Creek	−2	−4.5	−13	−19	4
Gable Mountain	−0.5	7	−33	100	−6
Stripa[a]	−2/1	−7/−0.5	−19/10	−42/3	13/40

$\Delta\sigma$, hydrofrac stress–overcoring stress; σ_{HF}, hydrofrac stress; $\Delta\sigma_{Hmax}$ (direction): difference in σ_{Hmax} direction between hydrofrac and overcoring results.
[a] Two types of analysis were carried out at Stripa (Haimson, 1981).

- The magnitudes of the maximum horizontal stress are within ±5 MPa, which is equivalent to a discrepancy of up to 50% of the maximum horizontal stress determined by hydraulic fracturing. A high discrepancy was however observed in the stress measurements at Gable Mountain.
- The inclination of the overcoring principal stress axes is usually within 30° of the vertical and horizontal directions.

A more detailed comparison of stress measurements at the Nevada Test Site was presented later by Haimson (1983). The latter used the results of three sets of hydraulic fracturing stress measurements and two sets of overcoring stress measurements conducted by five different groups over a period of 10 years at different locations at the Nevada Test Site including Yucca Mountain, Rainier Mesa and the Yucca flat. Also, additional *in situ* stress-related information could be derived from borehole wall spalling, oriented cores and focal mechanisms. As a basis for comparison, Table 9.4 gives the results of the different stress measurements at the Nevada Test Site

Table 9.4 Comparison between all *in situ* stress measurements and indicators at the Nevada Test Site (normalized for a depth of 400 m; after Haimson, 1983)

Method	Site	σ_{Hmax}		σ_{hmin}		σ_v (MPa)
		Magnitude (MPa)	Direction (deg)	Magnitude (MPa)	Direction (deg)	
HF	RM-U12n	9.0	N35°E	3.5	N55°W	7.0
OC	RM-U12n	8.0	N45°E	2.5	N45°W	6.0
HF	RM-U12g	7.5	N40°E	3.0	N50°W	7.3
OC	RM-U12g	8.5	N22°E	2.6	N68°W	6.8
HF	YM	N.A.	N25°E	1.0	N65°W	8.0
ORC	YM	–	N20°E	–	N70°W	–
HS	YF	–	N30°E	–	N60°W	–
FMS	NTS	$<$ or $>\sigma_v$	N45°E	$<\sigma_{Hmax}$ and $<\sigma_v$	N45°W	–

HF, hydrofracturing; OC, overcoring; ORC, oriented core; HS, hole spalling; FMS, focal mechanism solution; RM, Rainier Mesa; YM, Yucca Mountain; YF, Yucca flat; NTS, Nevada Test Site.

normalized for a depth of 400 m and expressed in terms of maximum and minimum horizontal stresses and vertical stress.

Table 9.4 shows, first, good agreement between the different methods at a given site such as Rainier Mesa. There the average maximum horizontal stress is 8.25 MPa (±0.65 MPa) at N35°E (±10°). The minimum horizontal stress is equal to 2.9 MPa (±0.45 MPa) at N55°W (±10°) and the vertical stress is equal to 6.8 MPa (±0.55 MPa). The overall stress regime varies from normal to strike-slip faulting. Table 9.4 also shows that the stress measurements at Yucca Mountain are consistent with those of Rainier Mesa despite the 50 km distance between the two sites. At Yucca Mountain the minimum horizontal stress is oriented at N60°W (±10°), which is only 5° from the direction at Rainier Mesa. Finally, Table 9.4 indicates a good agreement between the measured horizontal stresses and those estimated from indirect methods such as the focal mechanism, oriented core and hole spalling techniques.

Another example of comparison of stress measurements by hydraulic fracturing and overcoring was reported by Enever and Chopra (1986). Hydraulic fracturing tests were carried out in granite at three sites in Australia and at depths not exceeding 170 m. The stress measurements were compared with independent overcoring measurements made at shallower depths with the USBM gage and CSIRO HI cell. At each site a good agreement was found between the orientation of the maximum horizontal principal stresses determined by overcoring and hydraulic fracturing. In a more recent paper, Enever, Walton and Wold (1990) again found good agreement between the overcoring and hydraulic fracturing test results for various low-permeability rocks, if the difference between the crack initiation and crack reopening pressures measured in the field (instead of small test holes in the laboratory) was used as a measure of tensile strength. Table 9.5 gives a summary of the average minimum *in situ* stress magnitudes determined during side by side comparison of overcoring and hydraulic fracturing test results.

Hudson and Cooling (1988) and Cooling, Hudson and Tunbridge (1988) reported an extensive program of *in situ* stress measurements by overcoring and hydraulic fracturing

Table 9.5 Summary of average minimum stress magnitude determined during side by side comparison of overcoring and hydraulic fracturing tests (after Enever, Walton and Wold, 1990)

	Average minimum stress magnitude (MPa)	
Rock type	*Hydraulic fracturing*	*Overcoring*
Sandstone	9.8	10.6
Sandstone	12.0	12.0
Sandstone	9.0	8.2
Sandstone	6.8	7.0
Sandstone	4.5	4.8
Sandstone/conglomerate	5.3	7.9
Sandstone	2.5	2.1
Serpentinite	20.2	18.5
Porphyry	16.5	20.0
Lead–zinc ore	9.5	9.0
Volcanic agglomerate	9.5	9.7

in the Carnmenellis granite in the extreme southwestern part of Britain. The overcoring tests were carried out in a drift mine at Carwynnen and the hydraulic fracturing tests were conducted in two boreholes (A and B) 100 m apart in an adjacent quarry. All tests were essentially carried out in competent granitic rock. The overcoring stress measurements were made with the CSIRO HI cell, the INTERFELS CSIR-type triaxial strain cell and the USBM gage at a depth of 34 m. The hydraulic fracturing tests were carried out at depths of 74, 122 and 642 m. The test results are summarized in Table 9.6 and are shown in Figs 9.18 and 9.19. In both figures, the measured stresses are compared with the results of two other campaigns of stress measurement conducted by Pine, Tunbridge and Kwakwa (1983a, b): overcoring tests with the CSIRO HI cell and the USBM gage in the South Crofty mine at a depth of 790 m and hydraulic fracturing tests at depths of 2000 m as part of a geothermal project at the Rosemanowes quarry.

Table 9.6 and Figs 9.18 and 9.19 indicate good agreement among the overcoring or hydraulic fracturing tests at the Carwynnen site, good agreement between the results of the overcoring and hydraulic fracturing tests at that site, and good agreement with the stress measurements at the other two sites reported by Pine, Tunbridge and Kwakwa (1983a, b). It is noteworthy that all test results show that the vertical and horizontal stresses are essentially

Table 9.6 Stress measurement results in the Carnmenellis granite (Source: Cooling, C.M., Hudson, J.A. and Tunbridge, L.W. Copyright 1988, with kind permission from Elsevier Science Ltd, The Boulevard, Langford Lane, Kidlington, UK)

Site	*Method*	*Depth (m)*	*Principal stress*	*Magnitude (MPa)*	*Trend (deg)*	*Plunge (deg)*
Carwynnen	Hydraulic fracturing	74	σ_1	16.5	141	00[a]
			σ_2	6.5	051	00[a]
			σ_3	2.0	–	90[a]
		122	σ_1	16.7	145	00[a]
			σ_2	7.2	055	00[a]
			σ_3	3.3	–	90[a]
		642	σ_1	34.9	145	00[a]
			σ_2	16.7	–	90[a]
			σ_3	12.3	055	00[a]
	USBM gage	34	σ_1	5.9	317	09
			σ_2	2.2	224	17
			σ_3	−0.2	075	71
	CSIRO HI cell	34	σ_1	5.9	331	01
			σ_2	4.9	241	09
			σ_3	2.2	055	81
	INTERFELS CSIR-type cell	34	σ_1	5.3	308	19
			σ_2	3.9	040	06
			σ_3	−0.6	146	70
South Crofty	Overcoring	790	σ_1	37.7	130	05
			σ_2	18.5	347	84
			σ_3	11.3	220	03
Rosemanowes	Hydraulic fracturing	2000	σ_1	70	130[a]	00[a]
			σ_2	52[a]	–[a]	90[a]
			σ_3	30	040[a]	00[a]

[a] Estimated for hydraulic fracturing tests.

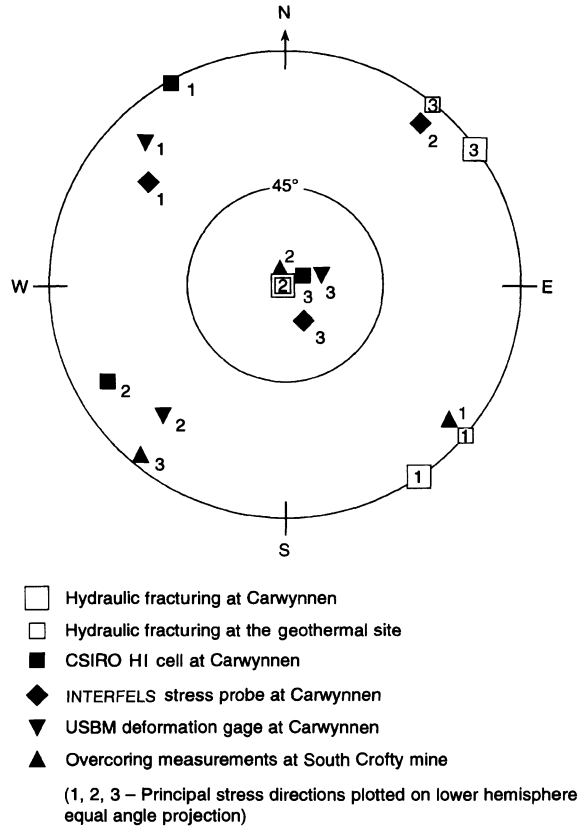

Fig. 9.18 Orientation of principal stresses measured in the Carnmenellis granite. (Source: Cooling, C.M., Hudson, J.A. and Tunbridge, L.W. Copyright 1988, with kind permission from Elsevier Science Ltd, The Boulevard, Langford Lane, Kidlington, UK.)

principal stresses and very consistent results are obtained for the horizontal principal stress orientation with dominant NW–SE and NE–SW directions. It is interesting to note also that the hydraulic fracturing tests at the Carwynnen site indicate a change in stress regime with depth, with the minimum principal stress being vertical at depths of 74 m and 122 m and becoming horizontal at 642 m.

Table 9.6 and Figs 9.18 and 9.19 also show that the consistency in stress magnitude is not as good as for the stress orientation but is however very acceptable considering the volume of rock involved. This consistency between overcoring and hydraulic stress measurements in the Carnmenellis granite has been confirmed further by additional measurements and analyses by Haimson *et al.* (1989) and Pine, Jupe and Tunbridge (1990).

9.4 COMPARISON BETWEEN HYDRAULIC METHODS

9.4.1 HYDRAULIC FRACTURING AND HTPF METHODS

As a validation of the hydraulic test on pre-existing fractures (HTPF) method for stress determination, Cornet and Valette (1984) used the results of hydraulic fracturing tests obtained by Haimson (1980) at the Waterloo test site in Wisconsin. That site was selected

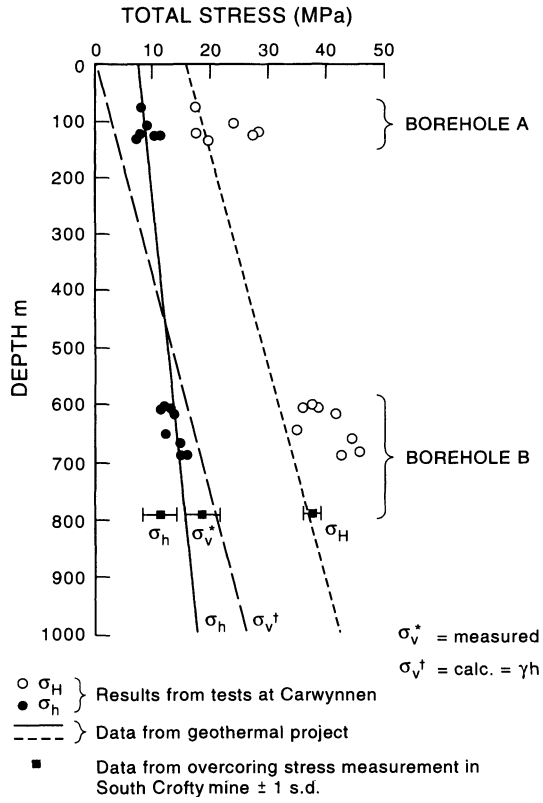

Fig. 9.19 Variation of principal stresses measured in the Carnmenellis granite with depth. (Source: Cooling, C.M., Hudson, J.A. and Tunbridge, L.W. Copyright 1988, with kind permission from Elsevier Science Ltd, The Boulevard, Langford Lane, Kidlington, UK.)

because of the large amount of data available and because the stress field was well known at depths ranging between 35 and 250 m. Following the prediction of the variation of the state of stress over that depth range, Cornet and Valette (1984) calculated the *a posteriori* shut-in pressures at nine locations and compared them with the measured shut-in pressures and those predicted by Haimson (1980). It was found that the standard deviation of the difference between the observed and computed shut-in pressures was 0.36 MPa with the HTPF inversion method and 0.54 MPa with Haimson's predictions. This close agreement was found to be very promising and slightly in favor of the HTPF method. On the other hand, the standard deviations for the magnitude and orientation of the maximum horizontal principal stress obtained with the HTPF inversion method were found to be large, thus making the stress determination not well constrained.

Ljunggren and Raillard (1987) made a detailed comparison between HTPF results and those obtained by conventional hydraulic fracturing in a vertical borehole at Gideå about 480 km north of Stockholm, Sweden. Gideå is one of the selected test sites for investigation of final disposal of Swedish high-level radioactive waste in crystalline rock. Conventional hydraulic fracturing stress measurements were conducted by Bjarnason and Stephansson (1986). Later, Ljunggren and Raillard (1986) conducted HTPF rock stress measurements in the same borehole at depths ranging between 90 and 270 m. The results of the field tests are reported in Table 9.7.

First, a two-dimensional analysis of the HTPF data was carried out assuming (1) that the *in situ* stress field varies with depth only, (2) that the principal *in situ* stresses are horizontal and vertical and (3) that the vertical stress is due to gravity. As seen in section 4.4.3, in that case the total number of unknowns in tensors S and $\boldsymbol{\alpha}$ in equation (4.96) is equal to six. The inversion process was found to converge (after nine iterations) only after omitting the results at depths of 238.3 m and 267.9 m. The horizontal principal *in situ* stress components σ_H and σ_h were then calculated for depths ranging between 100 and 250 m and are listed in Table 9.8.

Table 9.8 indicates a rotation of the maximum horizontal stress σ_H from N14°E at a depth of 100 m to N56°W at a depth of 250 m, and an almost isotropic horizontal state of stress for depths ranging between 100 and 150 m. At a depth of 250 m, the value of the maximum horizontal stress was found to be about 2 MPa higher than that measured with hydraulic fracturing. The values of the minimum horizontal stress determined with HTPF

Table 9.7 Test points and corresponding field results, borehole Gi-1, Gideå, Sweden; HTPF data according to Ljunggren and Raillard (1987) and hydrofracturing data according to Bjarnason and Stephansson (1986)

Method	No. of test points	Depth z (m)		Fracture strike ϕ (deg)[a]		Fracture dip θ (deg)[b]		Normal stress σ_n (MPa)[c]	
		z	ε_z[d]	ϕ	ε_ϕ[d]	θ	ε_θ[d]	σ_n	ε_σ[d]
HTPF	1	93.3	0.1	328	7	61	3	4.4	0.1
	2	129.7	0.1	92	7	40	3	4.5	0.1
	3	130.1	0.1	206	7	58	3	5.9	0.1
	4	178.4	0.1	308	7	28	3	6.5	0.1
	5	247.5	0.1	213	7	32	3	6.9	0.1
	6	238.3	0.1	204	7	22	3	8.7	0.1
	7	247.5	0.1	181	7	33	3	8.3	0.1
	8	252.5	0.1	248	7	26	3	7.6	0.1
	9	253.0	0.1	300	7	19	3	8.2	0.1
	10	260.1	0.1	258	7	20	3	7.4	0.1
	11	262.2	0.1	5	7	71	3	9.8	0.1
	12	267.9	0.1	240	7	83	3	10.0	0.1
HF	13	111.0	0.1	135	7	90	3	4.4	0.1
	14	122.5	0.1	168	7	90	3	5.2	0.1
	15	140.0	0.1	141	7	90	3	6.4	0.1
	16	183.0	0.1	42	7	90	3	8.0	0.1

[a] Orientation of the horizontal projection of the normal with respect to north.
[b] Angle between normal to a fracture plane and vertical axis.
[c] Normal stress acting across the fracture plane.
[d] ε: standard deviation.

and hydraulic fracturing were found to be almost identical.

A three-dimensional analysis was carried out assuming now that tensors S and $\boldsymbol{\alpha}$ in equation (4.96) each had six unknown components. Thus a minimum of 12 tests were required to reach a solution. In practice, a minimum of 15 tests are needed for the complete determination of the three-dimensional stress field. To fulfill this requirement, Ljunggren and Raillard (1986, 1987) selected four conventional hydraulic fracturing test data and included them in the HTPF analysis. From the results of the HTPF inversion process, the principal *in situ* stresses σ_1, σ_2 and σ_3 and their orientation were determined for depths ranging between 93.3 and 267.9 m. Comparison of σ_1, σ_2 and σ_3 with the principal stresses S_H, S_h and S_v determined by hydraulic fracturing is shown in Fig. 9.20. This figure shows the following trends: (1) the stresses σ_1 and S_H are nearly equal in magnitude with a maximum difference of about only 0.5 MPa, (2) the magnitudes of σ_2 and S_h are very close with a maximum difference of about 1.0 MPa, and (3) the vertical stress S_v calculated from the weight of the overburden does not agree perfectly with σ_3. However, as shown in Fig. 9.20, in the interval where σ_3 is almost vertical (i.e. 150–250 m), a good agreement in magnitude is obtained.

The variation with depth of the orientation of σ_1 and S_H from north for the Gideå borehole is presented in Fig. 9.21. For the three-dimensional HTPF model, the orientation of σ_1 is N60°E at a depth of 90 m and rotates

Table 9.8 Calculated *in situ* stress magnitude and orientation at borehole Gi-1, Gideå, Sweden. (Source: Ljunggren, C. and Raillard, G. Copyright 1987, with kind permission from Elsevier Science Ltd, The Boulevard, Langford Lane, Kidlington, UK)

Depth (m)	σ_H *(MPa)*	σ_h *(MPa)*	*Direction of* σ_H *(deg)*
100	6.5	4.5	14
125	7.1	6.0	−9
150	8.4	6.9	−40
175	10.1	7.3	−49
200	11.9	7.7	−53
225	13.6	8.1	−55
250	15.4	8.5	−56

clockwise to become N120°E at a depth of 250 m. This agrees fairly well with the orientation of the hydrofractures, particularly in the upper part of the profile. At a depth of 250 m, both the two-dimensional and three-dimensional HTPF models were found to give the same orientation for the maximum principal stress.

The orientation of the principal stresses from stress measurements in boreholes is usually presented using the stereographic projection where each individual stress vector is represented by a point on the stereonet. If the stress magnitude and orientation are to be presented together, the method used by Ljunggren and Raillard (1986, 1987) for the results obtained at Gideå is recommended (Fig. 9.22). The state of stress at a point in space is viewed from above and each stress vector is projected onto the horizontal plane. The length of the vector is proportional to the magnitude of the individual stress vector. The dip of the stress vector is governed by the fan-shaped symbol at the tip of the stress vector. An open fan indicates a vertical dip of the principal stress vector. A complete representation of the state of stress versus depth in the Gideå borehole is obtained by combining the information presented in Figs 9.20–9.22.

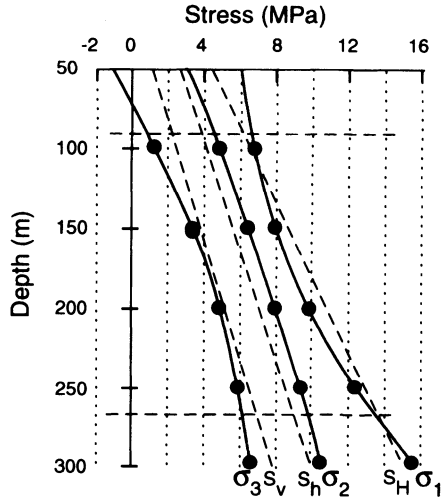

Fig. 9.20 The three-dimensional state of stress calculated from the HTPF method and hydraulic fracturing method. Measurements taken at depths between 93.3 and 267.9 m at borehole Gi-1, Gideå, Sweden. (After Bjarnason and Stephansson, 1986; Ljunggren and Raillard, 1987.)

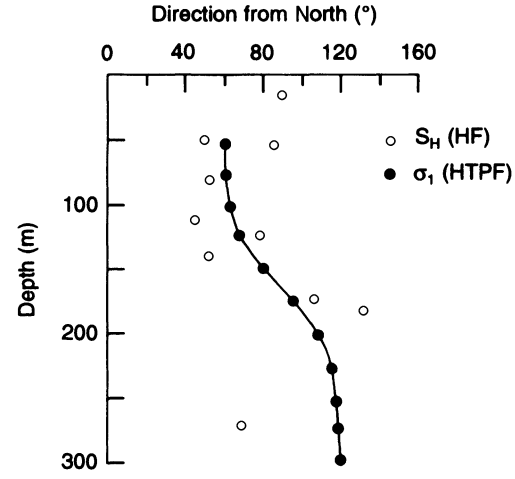

Fig. 9.21 Directions of σ_1 and S_H according to the three-dimensional HTPF evaluation and hydrofracture orientations at borehole Gi-1, Gideå, Sweden. (Source: Ljunggren, C. and Raillard, G. Copyright 1987, with kind permission from Elsevier Science Ltd, The Boulevard, Langford Lane, Kidlington, UK.)

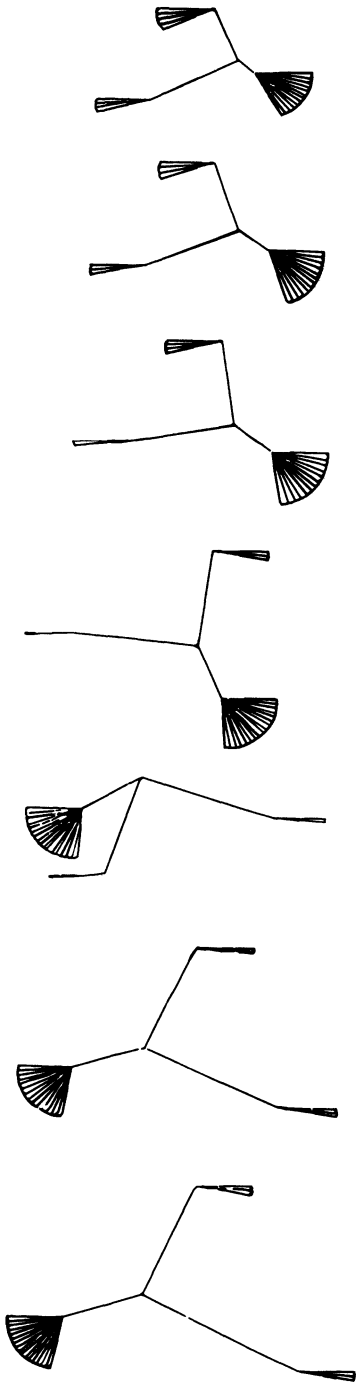

100 m

	magnitude (MPa)	bearing (°)	dip (°)
σ_1	6.8	242	15
σ_2	4.4	340	25
σ_3	1.5	125	61

125 m

	magnitude (MPa)	bearing (°)	dip (°)
σ_1	7.2	248	11
σ_2	5.5	341	18
σ_3	2.6	125	70

150 m

	magnitude (MPa)	bearing (°)	dip (°)
σ_1	7.7	259	7
σ_2	6.5	351	14
σ_3	3.5	128	79

175 m

	magnitude (MPa)	bearing (°)	dip (°)
σ_1	8.5	276	2
σ_2	7.5	7	9
σ_3	4.2	161	86

200 m

	magnitude (MPa)	bearing (°)	dip (°)
σ_1	9.8	109	4
σ_2	8.1	198	2
σ_3	4.8	240	84

225 m

	magnitude (MPa)	bearing (°)	dip (°)
σ_1	11.1	115	8
σ_2	8.7	24	6
σ_3	5.3	253	80

250 m

	magnitude (MPa)	bearing (°)	dip (°)
σ_1	12.6	118	11
σ_2	9.3	26	10
σ_3	5.8	255	76

Fig. 9.22 Three-dimensional state of principal stress and orientations at borehole Gi-1, Gideå, Sweden. (Source: Ljunggren, C. and Raillard, G. Copyright 1987, with kind permission from Elsevier Science Ltd, The Boulevard, Langford Lane, Kidlington, UK.)

Examples of comparisons of results and techniques between conventional hydraulic fracturing and HTPF tests have been reported for a fair number of different tectonic regimes and rock types, such as quartzite by Cornet and Valette (1984), granite by Ljunggren and Raillard (1987) and Cornet and Burlet (1992), migmatitic gneiss by Ljunggren (1990) and limestones interbedded with lignite and clay, sandstone and schist by Cornet and Burlet (1992). The results presented have shown that, in the majority of rock types, the HTPF method and the classical hydraulic fracturing method yield satisfactory agreements. However, it must be remembered that the field work required to collect data for the HTPF method is greater than that needed for hydrofracturing tests. Therefore, if time and cost are deciding factors, the HTPF method should replace the hydrofracturing technique only when none of the principal stresses are expected to be parallel to the borehole axis or when major planes of weakness exist in the rock mass.

9.4.2 HYDRAULIC FRACTURING, SLEEVE FRACTURING AND THE HTPF METHOD

A program of sleeve fracturing, conventional hydrofracturing and HTPF testing was reported by Ljunggren (1990). The tests were conducted in a 500 m deep vertical borehole with a diameter of 56 mm located on the campus of the Luleå University of Technology in Sweden. The main rock type is migmatitic gneiss with a steeply dipping foliation. Measurements were conducted at 33 locations using the hydrofracturing field truck presented in Fig. 4.6. The HTPF method was used at 15 test points where single pre-existing fracture planes with different strikes and dips had previously been mapped. The conventional hydraulic fracturing tests were conducted after the HTPF tests had been completed. A clear discrepancy in the orientation of the maximum horizontal principal stress was found between conventional hydrofracturing and the HTPF method. A probable explanation for this discrepancy is that the hydrofractures were controlled by the existing planes of foliation in the gneiss.

In order to constrain the orientation of the maximum horizontal principal stress, a couple of sleeve fracturing tests were also conducted by inflating an impression packer to a pressure where fractures were initiated and could be recorded. The tests created 2 m long vertical fractures, 180° apart. The orientations of the maximum horizontal stress determined by sleeve fracturing and the HTPF method were found to be in good agreement. Further, it was recorded that the strike of the existing steeply dipping foliation planes coincided with the average hydrofracture orientation.

From the tests conducted in the borehole on the campus of the Luleå University of Technology, it was concluded that the induced hydrofractures were influenced by the steeply dipping foliation planes in the rock mass and therefore did not reflect the true orientation of the maximum horizontal stress. Since the foliation also affected the results of indirect tensile strength laboratory tests, it is most likely that the inherent rock anisotropy should also affect the determination of the principal stresses by hydrofracturing.

The results of the comparative field study of Ljunggren (1990) yielded the following conclusions:

- if time and cost are deciding factors for a stress measurement campaign, the HTPF method should replace the hydrofracturing technique only when none of the principal stresses are expected to be parallel to the borehole axis or when marked weakness planes exist in the rock mass;
- the orientation of the maximum horizontal stress can be determined by the HTPF method and sleeve fracturing tests despite the existence of foliation in the rock mass;
- the hydraulic fracturing second breakdown method for stress evaluation and the HTPF method result in the same magnitude of the horizontal principal stresses;

- a source of error in the HTPF method is related to the assumption that the fracture orientation at the borehole wall corresponds to the fracture orientation further away into the rock mass.

9.4.3 CYCLIC HYDRAULIC TESTING

Based on the experience and results of different hydraulic tests conducted in the borehole at the Luleå University of Technology, Rutqvist and Stephansson (1996) concluded that existing procedures (shut-in test, hydraulic jacking test and constant flow rate test) used for determining the normal stress across an open fracture may yield inaccurate normal stress measurements due to near-wellbore effects. They recommended that methods such as hydraulic jacking and constant flow rate (which are based on flow between the wellbore and the fracture) should be avoided. For these methods, the nonlinear fracture stiffness behavior near the wellbore may dominate the pressure versus flow or pressure versus time response, and mask the true virgin normal stress across the fracture. The shut-in test works well if the shut-in pressure can be defined, and if it can be ensured that it represents the closure pressure and not the fracture propagation pressure. To overcome these problems, Rutqvist and Stephansson (1996) proposed cyclic hydraulic testing as a method to determine the virgin stress normal to a fracture plane. In this method, fracture closure and the virgin normal stress are determined from the zero-flow pressure in a well pressure versus well flow diagram.

Cyclic hydraulic jacking testing was conducted on six subhorizontal joints intersecting the vertical borehole at the Luleå University of Technology. The downhole equipment was of a multihose type (section 4.2.2) and consisted of a straddle packer with 0.65 m of packer separation, and a downhole pressure transducer. Flow from the hydraulic hose into the packer section could be shut off by a valve located immediately above the packer. Two hydraulic jacking tests were conducted on each joint with one day of venting in between. In the first jacking test, the pressure was increased to hydrofrac each joint and create a fracture. Fast pressure pulse injection testing was performed prior to and after fracturing to determine the hydraulic aperture of the fracture plane. Each pressure pulse test is conducted by injecting a small amount of water to the packer interval and the valve is closed. Thereafter the well pressure decreases as the fluid is discharged from the wellbore into the fracture and the hydraulic aperture of the fracture can be determined from the pressure decay (Rutqvist, 1995a). From the pressure decay it is also possible to judge whether the fracture is hydraulically closed or connected to other conducting joints.

The cyclic hydraulic jacking tests were conducted in cycles with stepwise increase of well pressure (forward step pressure) followed by stepwise decrease of well pressure (backward step pressure) as shown in Fig. 9.23. The pressure is kept constant for a few minutes in each step until a steady flow has been attained. The forward step pressure cycle is conducted up to a maximum flow rate of 5 l/min and the subsequent backward step pressure cycle is conducted until a backflow is obtained from the fracture into the wellbore. The well pressure P_w versus well flow Q_w for the second hydraulic jacking test of the subhorizontal fracture at a depth of 356 m depth is presented in Fig. 9.24. This figure also includes the breakup pressure P_b obtained during the first hydraulic jacking of the fracture. The zero-flow well pressure is taken as the virgin stress normal to the fracture plane. The results obtained with this method for determining the vertical stress have been found to be in close agreement with other stress data from the HTPF tests on randomly oriented fractures in the same borehole (Ljunggren, 1990). Therefore the cyclic hydraulic jacking method proposed by Rutqvist and Stephansson (1996) can be seen as an alternative to the traditional

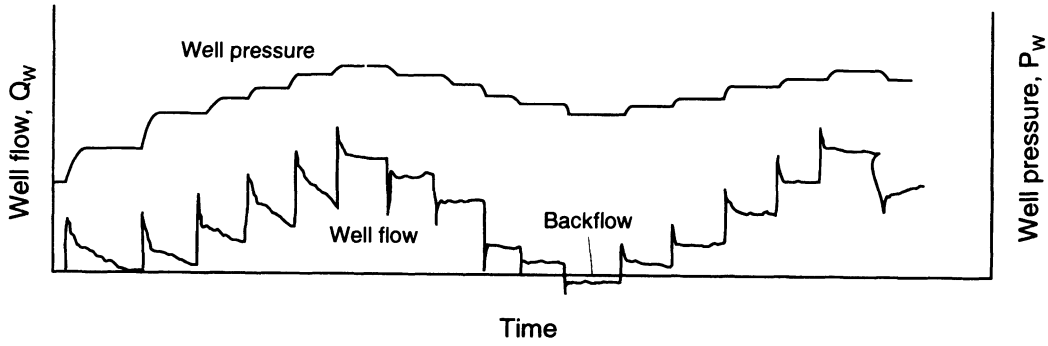

Fig. 9.23 Strip chart of well pressure and well flow versus time in a cyclic hydraulic jacking test for determination of virgin stress normal to a fracture. (After Rutqvist and Stephansson, 1996.)

shut-in analysis, in particular when it is difficult to determine the shut-in pressure. If the method is combined with a fast pressure pulse test and numerical modeling, the hydraulic aperture of the fracture, the fracture normal stiffness and the stress dependency of the fracture transmissivity can be determined more accurately (Rutqvist, 1995b).

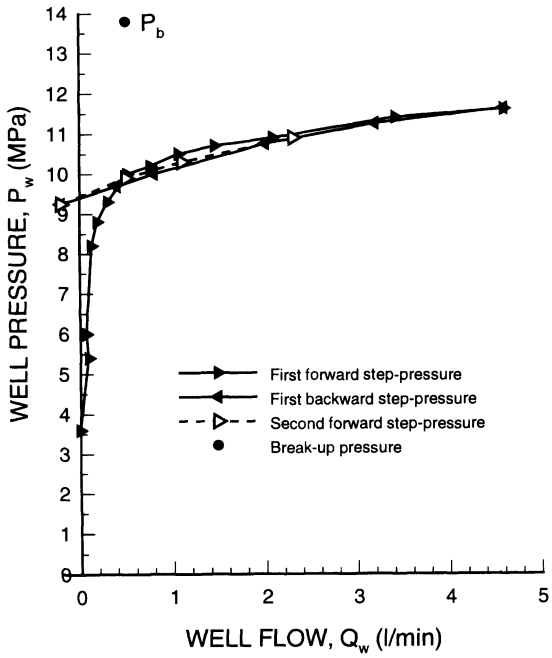

Fig. 9.24 Second hydraulic jacking test of a subhorizontal joint in granitic rock at a depth of 356 m in the vertical borehole at the Luleå University of Technology. Variation of well pressure P_w versus well flow rate Q_w. P_b is the break-up point obtained during the first jacking test. The zero-flow pressure (9.5 MPa) is taken as the virgin stress normal to the joint. (After Rutqvist and Stephansson, 1996.)

9.5 COMPARISON BETWEEN HYDRAULIC FRACTURING AND BOREHOLE BREAKOUT METHODS

Hydraulic fracturing stress measurements and borehole breakouts determined by geophysical logging are the two most commonly used techniques for determining stress orientation and stress magnitude at great depth. The first attempt to compare the two methods was relatively recent, as it was first reported by Hickman, Healy and Zoback (1985) at the Auburn Geothermal Well, New York. In this section we present three case studies of comparison between hydraulic fracturing and borehole breakouts for deep and very deep boreholes: (1) the Auburn Geothermal Well in New York State, which is 1.6 km deep in predominantly sedimentary rocks, (2) a series of boreholes penetrating some of the basalt flows of the Columbia River Basalt Group at the Hanford site in Washington State, which were logged and tested at depths of about 1000 m, and (3) the Cajon Pass scientific well which penetrates 0.5 km of Tertiary sediments and 3 km of Mesozoic granitic rocks, gneisses and

migmatites in the San Andreas and San Jacinto fault systems in southern California.

9.5.1 THE AUBURN GEOTHERMAL WELL, NEW YORK

An understanding of the nature and origin of the contemporary *in situ* stress field in the northeastern part of the United States was needed in the mid-1980s to develop constraining models of tectonic processes and driving mechanisms of plate motion. For that purpose, Hickman, Healy and Zoback (1985) conducted a series of hydraulic fracturing stress measurements and a borehole televiewer survey in the Auburn Geothermal Well in central New York State. The Auburn Geothermal Well is located in the Appalachian plateau, approximately 30 km southwest of Syracuse. The 1600 m deep well penetrates 1540 m of lower Paleozoic salts, carbonates, shales and sandstones and terminates 60 m into a Precambrian marble basement. The testing in this well is of special interest as it was the first one where breakouts were used to determine the orientation and magnitude of the *in situ* stress field.

After hydraulic fracturing, a borehole televiewer or impression packer was used to determine the orientation of the induced fractures at the borehole wall and hence the azimuth of the maximum horizontal stress. The magnitude of the minimum horizontal stress in three of four tests conducted in the well was determined from the repeatable instantaneous shut-in pressure obtained after conducting a number of pressurization cycles, together with low flow-rate pumping. The fracture reopening pressure in the third cycle was used to determine the maximum horizontal stress and the poroelastic correction was omitted. The magnitude of the minimum horizontal stress at Auburn has been found to increase in an almost linear fashion from 9.9 ± 0.2 MPa at 593 m to 30.6 ± 0.4 MPa at 1482 m. The magnitude of the maximum horizontal stress was found to increase in a less regular fashion from 13.8 ± 1.2 MPa to 49.0 ± 2.0 MPa over the same depth range (Hickman, Healy and Zoback, 1985). The magnitude of the overburden stress relative to the horizontal principal stresses indicates anomalously low horizontal stress magnitudes, with a strike-slip stress regime which at some depths converts into a normal stress regime. The maximum horizontal stress azimuths determined from the hydraulic fractures at depths of 593 and 919 m had an average direction of $N83°E \pm 15°$ which was in agreement with other stress field indicators for this region.

The borehole televiewer is a wireline logging tool that provides a continuous, oriented, ultrasonic image of a borehole wall (section 8.3.2). Characteristic patterns of the borehole televiewer log are produced by joints, fractures, voids, washouts and other wall features, and the orientation of these features relative to magnetic north may be determined from this log. At Auburn the borehole televiewer log revealed a large number of subhorizontal planar features, which were thought to be bedding plane washouts or drillbit scour marks (Hickman, Healy and Zoback, 1985). Also, steeply dipping natural fractures were found with a strike essentially random throughout much of the Auburn well, except in the lower sedimentary section where the fractures had a strongly developed E–W preferred orientation. Borehole elongations observed throughout the well were attributed to stress-induced spalling of the borehole wall and were classified as breakouts. The breakouts were found to trend in a consistent N–S direction perpendicular to the direction of maximum horizontal compression. This is shown in Fig. 9.25 in the form of a rose diagram plot of breakout length versus orientation. Figure 9.25 also shows a comparison between the average azimuth of the maximum horizontal stress S_H determined from the breakouts and that determined by hydraulic fracturing. It can be seen that the two directions agree quite well.

Comparison of borehole geometries determined using the televiewer and a four-arm

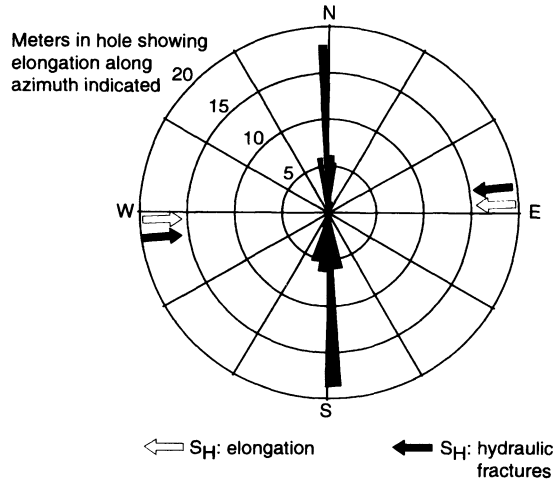

Fig. 9.25 Rose diagram showing the total length of breakouts in the Auburn Geothermal Well, New York, along a given azimuth as determined from a televiewer log. The average azimuths of the maximum horizontal stress S_H determined from hydraulic fracturing and inferred from borehole breakouts are also shown. (After Hickman, Healy and Zoback, 1985.)

dipmeter (section 8.3.1) in the Auburn well showed that both tools gave the same orientation of borehole elongation, provided that the zone of elongation was longer than 30 cm (Plumb and Hickman, 1985). The study demonstrated that the dipmeter could be used to determine the orientation of the minimum horizontal stress and provides a firm basis for mapping regional stress patterns using existing dipmeter data.

9.5.2 HANFORD TEST SITE, WASHINGTON

The character and distribution of borehole breakouts in deep basalt flows at the Hanford Test Site in south-central Washington State were examined in relation to hydraulic fracturing stress data by using acoustic televiewer and acoustic waveform logs (Paillet and Kim, 1987). The geophysical data were obtained in five boreholes penetrating different types of basalt flows of the Columbia River Basalt Group. Breakouts were found to occur discontinuously throughout the interior of most of the lava flow beds. Also, for several of the boreholes, the distribution of the breakouts was found to correlate closely with the incidence of core disking, i.e. the tendency for cylindrical core samples to break into saddle-shaped disks. Paillet and Kim (1987) observed basalt flow interiors with extensive breakouts surrounded by thin intervals of breakout-free flow tops and bottoms. Intersection of oblique fractures and changes in rock deformability due to basalt alteration were given as possible explanations for that transition. Homogeneous basalt beds with a low fracture frequency were found to have intervals (as much as 10 m in length) with continuous breakouts of uniform width. Many intervals of discontinuous breakouts were also observed in intervals with fractures, cooling joints and vesicles in the basalt. The breakouts were found to have a dominant E–W trend and an azimuthal width of 40–50°. Paillet and Kim (1987) suggested that the breakouts were formed in shear and that the distribution of the breakouts and core disking within the interior of individual basalt flows indicated that substantial stresses were being produced by concentration of regional stresses in relatively hard and thick basalt flows embedded within softer, more easily deformable sediments and altered flow-top breccia (section 2.6).

The variation of stress orientation with depth recorded from the geophysical logs was also found to be reflected in the stress measurements. Hydraulic fracturing stress measurement results obtained from four of the five boreholes indicated anisotropic horizontal principal stresses with a tendency for the maximum principal stress to be consistent and parallel to the N–S direction. That orientation was consistent with the east-trending orientation of the breakouts and the analysis of focal mechanism solutions in the central Columbia plateau.

9.5.3 CAJON PASS SCIENTIFIC DRILL SITE, CALIFORNIA

Knowledge of *in situ* stresses is very important when predicting shear stresses acting on major crustal faults such as the San Andreas fault. Zoback and Healy (1992) reported *in situ* stress measurements conducted in two holes at the Cajon Pass drill site in southern California. The stress measurements were made down to a depth of 1.3 km in one hole and to a depth of 3.5 km in the deepest hole. One of the main objectives of that project was to understand better how weak the San Andreas fault is in its southern part. Indeed, a large amount of data in central California had shown that the direction of maximum horizontal compression was almost perpendicular to the strike of the San Andreas fault, thus indicating that there is extremely little shear stress on the fault. Before the Cajon Pass project, no clear pattern of fault-normal compression had been seen in southern California. The Cajon Pass project was also designed to address the so-called 'San Andreas stress/heat flow paradox', i.e. the discrepancy between the shear stresses along the fault predicted by the Mohr–Coulomb faulting theory with laboratory-determined coefficients of friction of 0.6–1.0 and the shear stresses inferred from various heat flow measurements along the fault (Zoback and Healy, 1992).

Measurements of *in situ* stress magnitude and orientation were conducted at the Cajon Pass drill site using hydraulic fracturing and detailed observations of borehole breakouts at depths ranging between 907 and 3486 m. The hydrofrac tests consisted of open-hole hydraulic fracturing tests and pressurization tests on pre-existing fractures. Those tests provided 23 measurements of the minimum horizontal principal stress, six estimates of the maximum horizontal stress as a function of depth, and four measurements of the direction of maximum horizontal compression in crystalline basement rocks (Table 1 in Zoback and Healy, 1992). In addition, 12 estimates of the maximum horizontal stress were derived from the borehole breakouts.

The ultrasonic borehole televiewer was used to re-create precisely borehole shapes with a resolution of 1 cm vertically and 1 mm radially, when the data quality was good. A special study of 32 000 breakouts in the Cajon Pass well by Shamir and Zoback (1992) yielded the minimum horizontal principal stress orientation over a depth range of 1.7–3.5 km. The average direction of maximum horizontal stress S_{Hmax} determined from the ubiquitous borehole breakouts in the lower half of the deepest borehole at the Cajon Pass site was found to be N57°E ± 19° (Fig. 9.26). The breakouts were also found to be essentially orthogonal to the hydrofracs, thus giving consistent orientation for the horizontal principal *in situ* stresses. It is noteworthy that the average direction of the San Andreas fault in the region of the Cajon Pass is N60°W. According to Zoback and Healy (1992), these orientations indicate that the San Andreas fault is quite weak with a complete absence of right-lateral shear stress resolved on planes parallel to the N60°W-striking fault.

Figures 9.27a and 9.27b show respectively variations of the minimum and maximum horizontal stresses with depth obtained with the different stress measurement methods at the Cajon Pass drill site. In these figures (1) S_{HmaxHF} and S_{hminHF} are the maximum and minimum stresses determined with the open-hole hydraulic fracturing tests, (2) S_{hminPE} is the minimum stress determined from pressurization tests on pre-existing fractures and (3) S_{HmaxBO} is the maximum stress determined using the borehole breakout theory developed by Vernik and Zoback (1992).

Figures 9.27a and 9.27b also show expected values of the minimum stress S_{hmin} and the maximum stress S_{Hmax} for normal faulting and strike-slip faulting, respectively, on favorably oriented fault planes assuming Mohr–Coulomb faulting theory and Byerlee's law with laboratory-derived coefficients of friction between 0.6 and 1.0, and hydrostatic pore

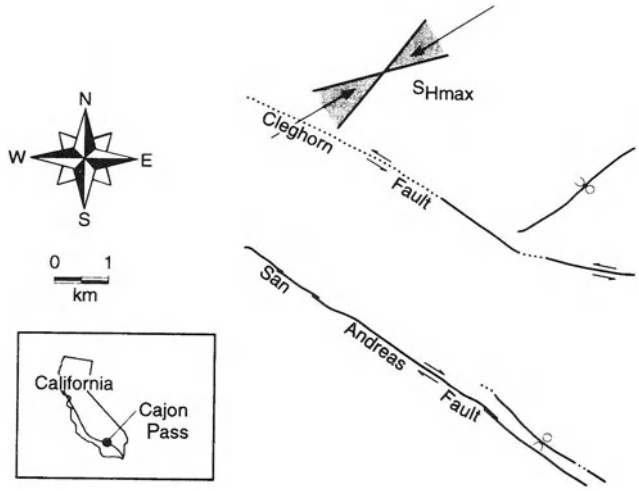

Fig. 9.26 Average direction and standard deviation of maximum horizontal principal stress in the Cajon Pass scientific research borehole in California. Active faults in the vicinity of the drill site are shown. (After Zoback and Healy, 1992.)

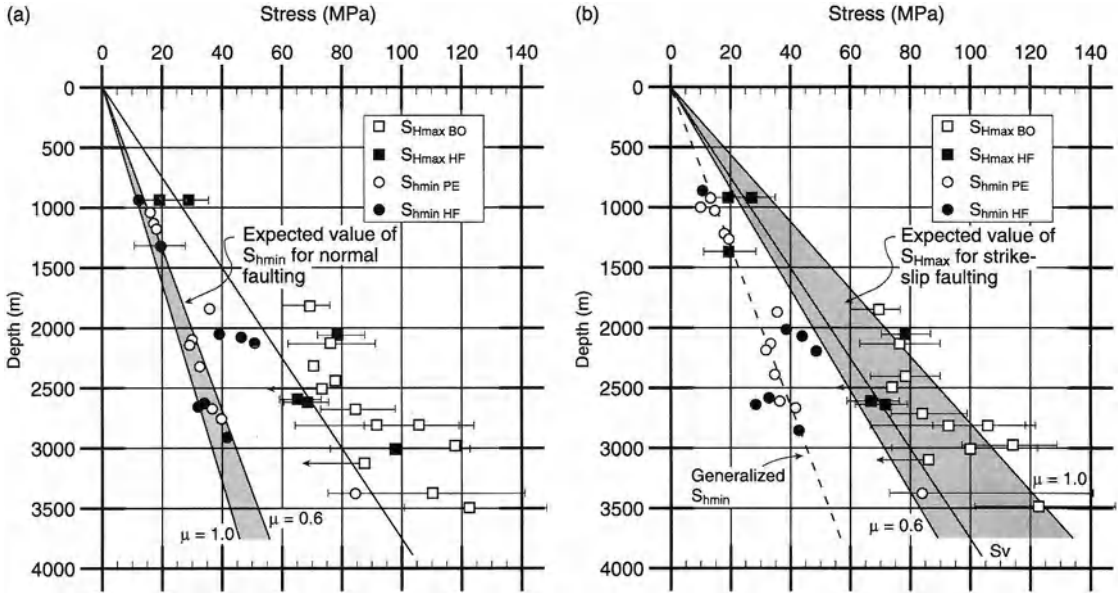

Fig. 9.27 Stress versus depth at the Cajon Pass drill site. Stress data are from open-hole hydraulic fracturing (S_{HmaxHF} and S_{hminHF}), pressurization tests on pre-existing fractures (S_{hminPE}), and borehole breakouts (S_{HmaxBO}). The gray areas indicate theoretical magnitude based on coefficients of friction between 0.6 and 1.0. (a) Expected values of S_{hmin} for the case of normal faulting, (b) expected values of S_{Hmax} for the case of strike-slip faulting. (After Zoback and Healy, 1992.)

pressure. It can be seen that the expected stress values are in agreement with those measured, except for anomalously high values of S_{hmin} at a depth of 2.1 km in Fig. 9.27a. Thus the difference between S_v and S_{hmin} in Fig. 9.27a is large enough to make favorably oriented normal faults move. Likewise, in Fig. 9.27b, the difference between S_{Hmax} and S_{hmin} is large enough to make favorably oriented strike-slip faults move.

Based on the stress measurements at the Cajon Pass drill site and the results shown in Figs 9.27a, b, Zoback and Healy (1992) concluded that the frictional strength of the crust adjacent to the San Andreas fault is high and consistent with laboratory-derived friction values, and that the level of shear stress in the crust adjacent to the fault is principally controlled by its frictional strength. The stress measurements also indicate that in the Cajon Pass area, the San Andreas fault is weak with respect to the surrounding crust.

REFERENCES

Bjarnason, B. and Stephansson, O. (1986) Hydraulic rock stress measurements in borehole Gi-1 Gideå study site, Sweden. Swedish Nuclear Fuel and Waste Management Company, Stockholm, SKB Technical Report 86-11.

Black, M.T. and Cramer, M.L. (1983) The design and construction of a block test in closely jointed rock. Rockwell International Report RHO-BW-SA-286 P.

Brown, S.M., Leijon, B.A. and Hustrulid, W.A. (1986) Stress distribution within an artificially loaded, jointed block, in *Proc. Int. Symp. on Rock Stress and Rock Stress Measurements*, Stockholm, Centek Publ., Luleå, pp. 429–39.

Chandler, N.A. (1993) Bored raise overcoring for in situ stress determination at the Underground Research Laboratory. *Int. J. Rock Mech. Min. Sci. & Geomech. Abstr.*, **30**, 989–92.

Chandler, N.A. and Martin, D. (1991) An examination of the conditions causing subhorizontal hydraulic fractures in a highly stressed granite batholith, in *Proc. 32nd US Symp. Rock Mech.*, Norman, Balkema, Rotterdam, pp. 251–60.

Chandler, N.A. and Martin, D. (1994) The influence of near surface faults on in-situ stresses in the Canadian shield, in *Proc. 1st North Amer. Rock Mech. Symp.*, Austin, Balkema, Rotterdam, pp. 369–76.

Cooling, C.M., Hudson, J.A. and Tunbridge, L.W. (1988) In-situ rock stresses and their measurement in the UK – Part II. Site experiments and stress field interpretation. *Int. J. Rock Mech. Min. Sci. & Geomech. Abstr.*, **25**, 371–82.

Cornet, F.H. and Burlet, D. (1992) Stress field determinations in France by hydraulic tests in boreholes. *J. Geophys. Res.*, **97**, 11829–49.

Cornet, F.H. and Valette, B. (1984) In situ stress determination from hydraulic injection test data. *J. Geophys. Res.*, **89**, 11527–37.

Enever, J.R. and Chopra, P.N. (1986) Experience with hydraulic fracture stress measurements in granite, in *Proc. Int. Symp. on Rock Stress and Rock Stress Measurements*, Stockholm, Centek Publ., Luleå, pp. 411–20.

Enever, J.R., Walton, R.J. and Wold, M.B. (1990) Scale effects influencing hydraulic fracture and overcoring stress measurements, in *Proc. Int. Workshop on Scale Effects in Rock Masses*, Loen, Norway, Balkema, Rotterdam, pp. 317–26.

Gregory, E.C. *et al.* (1983a) Applicability of borehole stress measurement instrumentation to closely jointed rock, in *Proc. 24th US Symp. Rock Mech.*, College Station, Association of Eng. Geologists Publ., pp. 283–6.

Gregory, E.C. *et al.* (1983b) In situ stress measurement in a jointed basalt, in *Proc. Rapid Excavation & Tunneling (RETC) Conf.*, Chicago, Vol. 1, SME/AIME, pp. 42–61.

Haimson, B. (1980) Near surface and deep hydrofracturing stress measurements in Waterloo quartzite. *Int. J. Rock Mech. Min. Sci. & Geomech. Abstr.*, **17**, 81–8.

Haimson, B.C. (1981) Confirmation of hydrofracturing results through comparisons with other stress measurements, in *Proc. 22nd US Symp. Rock Mech.*, Cambridge, MIT Publ., pp. 409–15.

Haimson, B.C. (1983) The state of stress at the Nevada Test Site: a demonstration of the reliability of hydrofracturing and overcoring techniques, in *Proc. Int. Symp. Field Measurements in Geomechanics*, Zurich, Balkema, Rotterdam, pp. 115–26.

Haimson, B.C. *et al.* (1989) Measurement of rock stress using the hydraulic fracturing method in Cornwall, UK – Part II. Data reduction and stress calculation. *Int. J. Rock Mech. Min. Sci. & Geomech. Abstr.*, **26**, 361–72.

Hickman, S.H., Healy, J.H. and Zoback, M.D. (1985) In situ stress, natural fracture distribution, and

borehole elongation in the Auburn Geothermal Well, Auburn, New York. *J. Geophys. Res.*, **90**, 5497–512.

Hudson, J.A. and Cooling, C.M. (1988) In situ rock stresses and their measurement in the UK – Part I. The current state of knowledge. *Int. J. Rock Mech. Min. Sci. & Geomech. Abstr.*, **25**, 363–70.

Kaiser, P.K., Zou, D. and Lang, P.A. (1990) Stress determination by back-analysis of excavation-induced stress changes – a case study. *Rock Mech. Rock Eng.*, **23**, 185–200.

Lang, P.A., Thompson, P.M. and Ng, L.K.W. (1986) The effect of residual stress and drill hole size on the in situ stress determined by overcoring, in *Proc. Int. Symp. on Rock Stress and Rock Stress Measurements*, Stockholm, Centek Publ., Luleå, pp. 687–94.

Leijon, B.A. and Stillborg, B.L. (1986) A comparative study between two rock stress measurement techniques at Luossavaara mine. *Rock Mech. Rock Eng.*, **19**, 143–63.

Ljunggren, C. (1990) Hydraulic fracturing and hydraulic tests on pre-existing fractures in a foliated rock – a comparison of results and techniques, in *Proc. 31st US Symp. Rock Mech.*, Golden, Balkema, Rotterdam, pp. 1027–34.

Ljunggren, C. and Raillard, G. (1986) *In situ* stress determination by hydraulic tests on pre-existing fractures at Gideå test site, Sweden. Luleå University of Technology, Sweden, Research Report TULEA 1986:22.

Ljunggren, C. and Raillard, G. (1987) Rock stress measurements by means of hydraulic tests on pre-existing fractures at Gideå test site, Sweden. *Int. J. Rock Mech. Min. Sci. & Geomech. Abstr.*, **24**, 339–45.

Martin, C.D. (1989) Characterizing in-situ stress domains at AECL's underground research laboratory, in *Proc. 42nd Can. Geotech. Conf.*, Winnipeg, pp. 1–14.

Martin, C.D. and Chandler, N.A. (1993) Stress heterogeneity and geological structures. *Int. J. Rock Mech. Min. Sci. & Geomech. Abstr.*, **30**, 993–9.

Martin, C.D. and Christiansson, R. (1991) Overcoring in highly stressed granite: comparison between USBM and CSIR devices. *Rock Mech. Rock Eng.*, **24**, 207–35.

Martin, C.D. and Simmons, G.R. (1993) The Atomic Energy of Canada Limited Underground Research Laboratory: an overview of geomechanics characterization, in *Comprehensive Rock Engineering* (ed. J.A. Hudson), Pergamon Press, Oxford, Chapter 38, Vol. 3, pp. 915–50.

Martin, C.D., Read, R.S. and Chandler, N.A. (1990) Does scale influence in-situ stress measurements? – Some findings at the Underground Research Laboratory, in *Proc. 1st Int. Workshop on Scale Effects in Rock Masses*, Loen, Norway, Balkema, Rotterdam, pp. 307–16.

Martin, C.D., Read, R.S. and Lang, P.A. (1990) Seven years of in-situ stress measurements at the URL. An overview, in *Proc. 31st US Symp. Rock Mech.*, Golden, Balkema, Rotterdam, pp. 15–26.

Martin, C.D., Martino, J.B. and Dzik, E.J. (1994) Comparison of borehole breakouts from laboratory and field tests, in *Proc. Eurock '94: Int. Symp. on Rock Mech. in Petrol. Eng.*, Delft, Balkema, Rotterdam, pp. 183–90.

Paillet, F.L. and Kim, K. (1987) Character and distribution of borehole breakouts and their relationship to in situ stresses in deep Columbia river basalts. *J. Geophys. Res.*, **92**, 6223–34.

Pine, R.J., Tunbridge, L.W. and Kwakwa, K. (1983a) In-situ stress measurement in the Carnmenellis granite – I. Overcoring tests at South Crofty Mine at a depth of 790 m. *Int. J. Rock Mech. Min. Sci. & Geomech. Abstr.*, **20**, 51–62.

Pine, R.J., Tunbridge, L.W. and Kwakwa, K. (1983b) In-situ stress measurement in the Carnmenellis granite – II. Hydrofracture tests at Rosemanowes quarry to depths of 2000 m. *Int. J. Rock Mech. Min. Sci. & Geomech. Abstr.*, **20**, 63–72.

Pine, R.J., Jupe, A. and Tunbridge, L.W. (1990) An evaluation of in-situ stress measurements affecting different volumes of rock in the Carnmenellis granite, in *Proc. 1st Int. Workshop on Scale Effects in Rock Masses*, Loen, Norway, Balkema, Rotterdam, pp. 269–77.

Plumb, R.A. and Hickman, S.H. (1985) Stress-induced borehole elongation: a comparison between the four-arm dipmeter and the borehole televiewer in the Auburn Geothermal Well. *J. Geophys. Res.*, **90**, 5513–21.

Rutqvist, J. (1995a) Determination of hydraulic normal stiffness of fractures in hard rock from well testing. *Int. J. Rock Mech. Min. Sci. & Geomech. Abstr.*, **32**, 513–23.

Rutqvist, J. (1995b) A method to determine stress–transmissivity relationship of joints from hydraulic testing, in *Proc. 8th Cong. Int. Soc. Rock Mech. (ISRM)*, Tokyo, Balkema, Rotterdam, Vol. 2, pp. 755–8.

Rutqvist, J. and Stephansson, O. (1996) A cyclic hydraulic jacking test to determine the in situ stress normal to a fracture. *Int. J. Rock Mech. Min. Sci. & Geomech. Abstr.*, **33**, 695–711.

Shamir, G. and Zoback, M.D. (1992) Stress orientation profile to 3.5 km depth near the San Andreas Fault at Cajon Pass, California. *J. Geophys. Res.*, **97**, 5059–80.

Talebi, S. and Young, R.P. (1989) Failure mechanism of crack propagation induced by shaft excavation at the Underground Research Laboratory, in *Proc. Int. Symp. Rock Mech. and Rock Physics at Great Depth*, Pau, Balkema, Rotterdam, Vol. 3, pp. 1455–61.

Talebi, S. and Young, R.P. (1992) Microseismic monitoring in highly stressed granite: relation between shaft-wall cracking and in situ stress. *Int. J. Rock Mech. Min. Sci. & Geomech. Abstr.*, **29**, 25–34.

Thompson, P.M. (1990) A borehole deformation gauge for stress determinations in deep boreholes, in *Proc. 31st US Symp. Rock Mech.*, Golden, Balkema, Rotterdam, pp. 579–86.

Thompson, P.M., Lang, P.A. and Snider, G.R. (1986) Recent improvements to in-situ stress measurements using the overcoring method, in *Proc. 39th Can. Geotech. Conf.*, Ottawa.

Van Heerden, W.L. and Grant, F. (1967) A comparison of two methods for measuring stress in rock. *Int. J. Rock Mech. Min. Sci.*, **4**, 367–82.

Vernik, L. and Zoback, M.D. (1992) Estimation of maximum horizontal principal stress magnitude from stress-induced well bore breakouts in the Cajon Pass scientific research borehole. *J. Geophys. Res.*, **97**, 5109–119.

Wiles, T.D. and Kaiser, P.K. (1994a) In-situ stress determination using the under-excavation technique – I: theory. *Int. J. Rock Mech. Min. Sci. & Geomech. Abstr.*, **31**, 439–46.

Wiles, T.D. and Kaiser, P.K. (1994b) In-situ stress determination using the under-excavation technique – I: applications. *Int. J. Rock Mech. Min. Sci. & Geomech. Abstr.*, **31**, 447–56.

Zoback, M.D. and Healy, J.H. (1992) In situ stress measurements to 3.5 km depth in the Cajon Pass scientific research borehole: implications for the mechanics of crustal faulting. *J. Geophys. Res.*, **97**, 5039–57.

Zou, D. and Kaiser, P.K. (1990) In situ stress determination by stress change monitoring, in *Proc. 31st US Symp. Rock Mech.*, Golden, Balkema, Rotterdam, pp. 27–34.

MONITORING OF STRESS CHANGE 10

10.1 INTRODUCTION

Monitoring of rock stress change with time is important when assessing the short- and long-term performance of a rock mass to the construction and exploitation of underground engineering structures such as tunnels, caverns and mines. A large amount of literature on stress change monitoring deals with the stability of mines and more particularly mine pillars. Of particular interest to mining engineers is the optimization of mine layout and pillar design and the prediction of rock loads, rockbursts and mine stability upon blasting (Maleki, 1990). The magnitude and distribution of stress changes in a rock mass due to excavation can be quite complex, as some regions in a rock mass experience stress increases and others experience stress decreases (Kaiser and Maloney, 1992). As an example, Fig. 10.1 shows a pattern of stress changes measured by Lee, Abel and Nichols (1976) in jointed and foliated gneiss ahead of an advancing crosscut at the Colorado School of Mines Experimental Mine in Idaho Springs, Colorado. They found that stress changes could be detected as far as 7.5 diameters ahead of the crosscut face.

Monitoring of stress changes can also be done when assessing the performance of a particular civil engineering design. For instance, field measurements assist in evaluating the need for adapting, modifying or, if necessary, reconsidering the design of underground structures in the light of the actual ground conditions as excavation proceeds. Stress changes can be determined at points in the rock mass and/or in the excavation lining (Barla and Rossi, 1983). In petroleum engineering, prediction of changes in stress due to reservoir depletion, compaction and resulting subsidence deformation is critical when assessing future reservoir productivity. This prediction was of particular concern for the case of the Ekofisk field in the North Sea (Teufel and Farrell, 1990). In geophysics, monitoring of stress changes can be useful when predicting the rupture of crustal rocks.

Over the past 15 years, stress monitoring has received a lot of attention with regard to the long-term performance of high-level nuclear waste in geological repositories. Here, engineers are interested in assessing the short- and long-term rock mass response to heating once nuclear waste has been emplaced. The measurement of absolute *in situ* stresses and the monitoring of stress change (along with rock deformation and temperature) has been an integral part of heater simulated experiments, block tests and mine-by experiments in the characterization phase of potential nuclear waste disposal sites (Fiore, Der and Montenyohl, 1984; Hustrulid and McClain, 1984; Patrick and Rector, 1983; St John and Hardy, 1982). More specific projects include (1) the Spent Fuel Test-Climax site in Nevada (Heuze, 1981; Heuze *et al.*, 1980; Mao, 1986; Patrick, 1986); (2) the Stripa mine project in Sweden (Lingle, Bakhtar and Barton, 1983; Lingle and Nelson, 1982); (3) *in situ* heated block tests at the Colorado School of Mines Experimental Mine (Hustrulid, 1983) and at the Basalt Waste Isolation Project (BWIP) in Hanford, Washington (Cramer *et al.*, 1987; Gregory and Kim, 1981; Hocking, Williams and Mustoe, 1990; Kim and McCabe, 1984); (4) the G Tunnel and

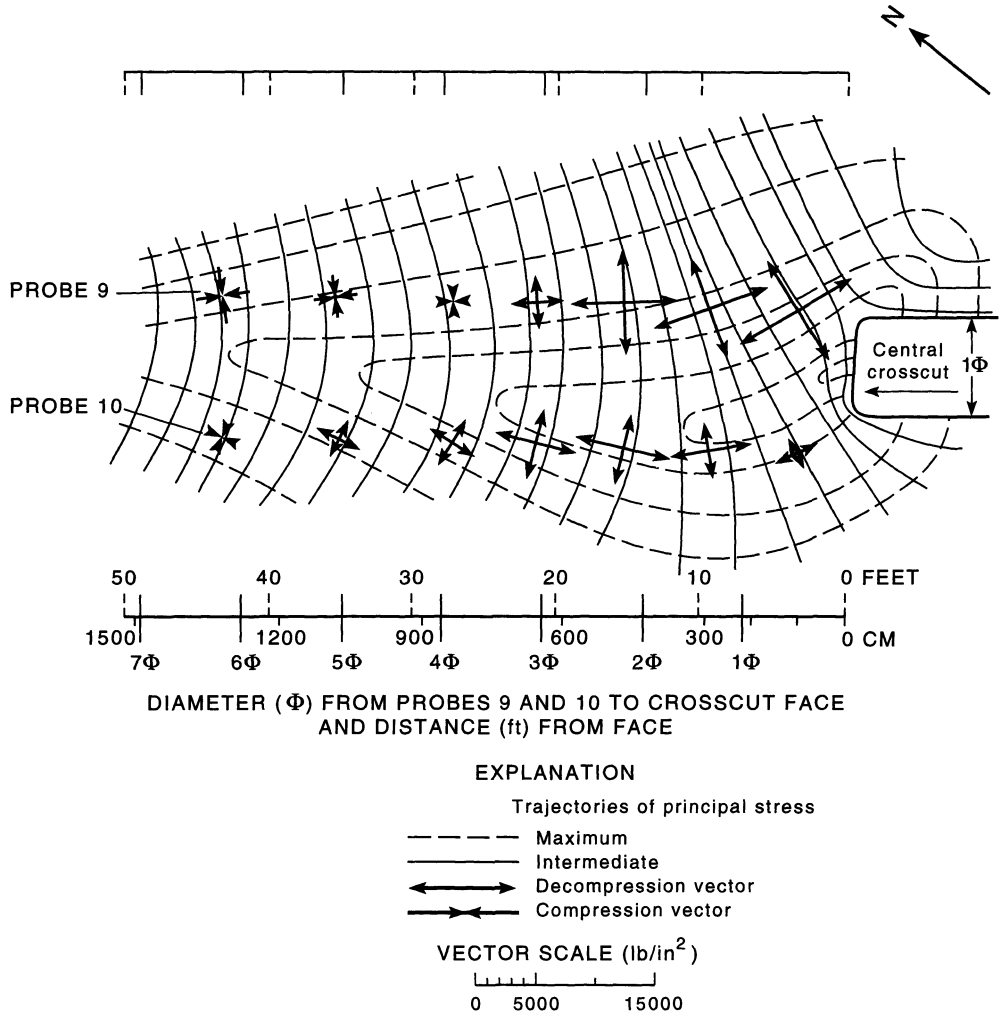

Fig. 10.1 Stress change trajectories determined based on stress change measurements in jointed and foliated gneiss ahead of an advancing crosscut at the Colorado School of Mines Experimental Mine in Idaho Springs, Colorado. (After Lee, Abel and Nichols, 1976.)

Yucca Mountain projects in tuff on the Nevada Test Site (Blejwas, 1987, 1989; Zimmerman, 1982); (5) various potential storage sites in bedded and dome salt in the US and in Germany; and (6) the Underground Research Laboratory (URL) site in granite in Canada (Martin and Simmons, 1993; Read and Martin, 1992). As an example, Fig. 10.2a shows the general layout of the Stripa project and Fig. 10.2b shows the location of the different boreholes and the corresponding instrumentation in the Stripa full-scale drift. It is most likely that monitoring of stress change will play a crucial role in one or several of the following phases of development of nuclear waste repositories: construction, waste emplacement and retrievable storage, decommissioning and post-decommissioning.

Stress changes in rock involve both virgin and induced stresses. Virgin stresses may vary,

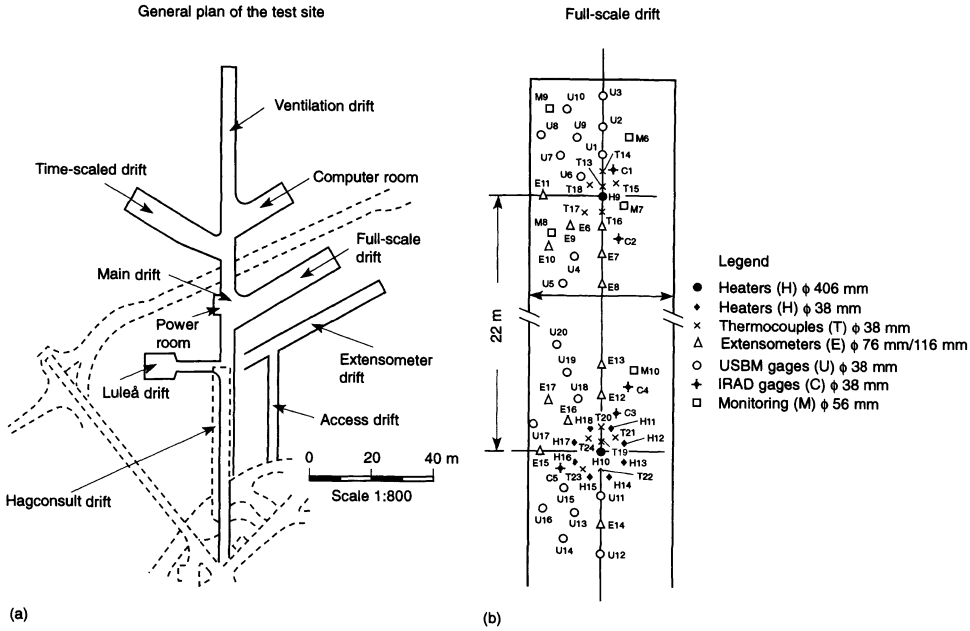

Fig. 10.2 General layout of the Stripa project in (a) and location of the different boreholes and the corresponding instrumentation in the Stripa full-scale drift in (b). (After Hustrulid, 1983.)

for instance, in the near vicinity of a major fault as the fault creeps and stress redistribution takes place. On the other hand, changes in induced stresses may occur due to nearby excavation, drilling, pumping, injection, energy extraction, applied loads, thermal loading, underground storage, blasting, etc. Monitoring stresses near an underground excavation may pick up the effect of the excavation itself (i.e. creation of a new free surface), thermal effects and any reaction of the rock to atmospheric conditions such as drying, swelling or slaking. In addition, stress monitoring at shallow depth may also be affected by such phenomena as diurnal and seasonal variations in temperature, Moon pull and the Coriolis force.

In principle, many of the techniques discussed in this book for measuring absolute stresses should apply to the measurement of stress changes. However, compared with the measurement of absolute stresses, stress monitoring is subject to additional constraints. First, monitoring of stress change involves time. Compared with absolute stress measurements which are relatively fast (1 to 2 h), measurements of stress changes may be conducted over longer periods of time of the order of days, months or even years. In general, the duration of stress change monitoring depends on the nature of the engineering activity responsible for the stress change and on the time required for the rock mass to reach a new state of equilibrium due to excavation and/or to volumetric phenomena (seepage, heating, cooling, consolidation, etc.). The longer the period of stress monitoring, the more critical is the stability of the measuring instruments. Monitoring stress changes around an advancing tunnel may not place as many constraints on the instruments compared with monitoring the stability of a mine pillar or a waste repository.

Over long periods, measurements of stress changes are more prone to time-dependent errors and failure. The instruments are likely

to be subject to adverse conditions of humidity, dust, temperature changes, pore pressure, etc. Moisture infiltration and internal corrosion are quite common. Thus instruments used for stress monitoring must be sensitive to load changes and their sensitivity should not change much with time. Their drift rates must be small. The instruments must be stable when subject to changes in moisture or temperature. Further, the instruments must be stable in areas subjected to vibration associated with blasting. Finally, the instruments must be able to monitor changes in tension as well as in compression.

A second concern when monitoring stress changes is that rock properties may change over the period of monitoring. This is of particular concern with rocks that show nonlinear or time-dependent behavior. Finally, a third concern for instruments that do not measure stress changes directly is that theoretical solutions are needed to relate strains or displacements monitored with the instruments to the components of the stress change occurring near the point of measurement. The solutions must account, as closely as possible, for the rock mass conditions and the process or processes responsible for the stress changes. These solutions can become particularly complex if time, flow, creep, nonlinearities and/or temperature effects have to be taken into account, thus causing stress monitoring to lose accuracy.

The three previous considerations have specifically been addressed in relation to the storage of nuclear wastes in rock (Hustrulid, 1983; Hustrulid and McClain, 1984). They also require that, before embarking on a program of stress change monitoring, laboratory tests under simulated field conditions or *in situ* block tests must be conducted to identify instrument performance with time under adverse conditions (humidity, dust, heat, etc.), the instrument limitations and how the rock of interest interacts with the instruments.

10.2 TECHNIQUES AND APPLICATIONS

There are essentially two ways of monitoring stress changes in rock (Obert and Duvall, 1967). One technique, called the discrete approach, consists of measuring absolute stresses at the same location and at two different times t and $t + \Delta t$. Thus some of the surface and borehole methods discussed in the previous chapters can theoretically be used for this approach. The difference between the components of the two stress tensors gives the components of the tensor of stress change. The major advantage of this procedure is that the measurements are not affected by drift, corrosion or creep phenomena since the initial and final stress measurements are of relatively short duration. The major disadvantage of this procedure is that the initial and final measurements must be made at the same location, which is physically impossible. An error may result, particularly when using instruments such as the USBM gage for which three holes are required. For other overcoring techniques that only require one hole, the error may not be as large.

Another approach consists of a continuous monitoring of the stress field. The idea is to place strain rosettes or pins permanently on a rock surface, or a cell into a hole or a slot. This can be done mechanically or using resin, epoxy or cement. After an initial reading, changes in load, strain or displacement are recorded as a function of time at the same location. Factors that may influence the response of a borehole cell to load changes include (1) the ratio between the modulus of the cell and that of the rock (cells can be divided into two groups: soft and rigid), (2) the ratio between the modulus of the encapsulating material and that of the rock and (3) the ratio between the diameter of the cell and that of the hole in which the cell is located (Bois, 1995). The major disadvantage of continuous monitoring of stress changes is related to time-dependent effects as mentioned in section 10.1. More demand is placed

on the instrumentation than in the discrete approach.

Many of the surface devices and borehole cells used for monitoring stress changes are similar to those discussed in Chapters 5 and 6. As long as the rock behaves in a linearly elastic manner, the equations derived for the interpretation of absolute stress measurements can be rewritten in terms of increments of stress, strain and displacement, and are directly applicable for the analysis of stress change measurements. Stress changes due to thermal loading and/or creep or other volumetric phenomena would, of course, require new solutions (Amadei, 1985).

Beside the devices described in Chapters 5 and 6, other cells have been developed for the sole purpose of monitoring stress changes. It is interesting to note that many of those cells can only determine changes in the secondary (apparent) principal stresses perpendicular to the hole in which the cells are located. Only a limited number of cells are available to determine the complete tensor of stress change. It is obvious that the latter are better suited since they can pick up not only changes in magnitude but also changes in the direction of principal stresses with time. The direction of the field stresses is likely to change with time (Pariseau, 1978). Table 10.1 gives a summary of the various techniques available for monitoring stress changes in rock.

Table 10.1 Types of stress change monitoring techniques

Deformation gages	USBM gage CSIRO Yoke gage
Strain cells	CSIR triaxial strain cell ANZSI triaxial strain cell Doorstoppers
Stiff cylindrical inclusions	Solid and hollow stressmeters Prestressed stressmeter Photoelastic stressmeter Vibrating wire stressmeter CIUS stressmeter Encapsulated spherical inclusion
Solid and hollow deformable inclusions	CSIRO HI cell Thin-walled CSIRO HI cell Solid inclusions
Flat jacks and hydraulic borehole pressure cells	Flat jacks Borehole pressure cell Borehole platened flatjack Slender flat cell CALIP gage Gloetzl (Glötzl) cells

10.2.1 DEFORMATION GAGES

Monitoring changes in borehole diameter to measure stress changes was first suggested by Leeman (1959) who proposed a cell that would fit into 1.5 inch (38 mm) diameter boreholes. The cell could measure diameter changes in the vertical and horizontal directions using a system of strain gages mounted onto a ring attached to a piston pushed against the rock. Another version of the same cell was proposed by Leeman (1960) where borehole deformation was measured directly using an LVDT. More recently, the conventional USBM gage discussed in Chapter 5 and the Yoke gage developed by the CSIRO in Australia (Walton and Worotnicki, 1986) have been used to determine stress changes. All these gages can be seen for all practical purposes as very soft cells that do not affect the borehole wall displacements. As for absolute stresses, determination of the six components of the tensor of stress change requires three holes.

The conventional USBM gage has been used for the monitoring of stress changes at potential nuclear waste disposal sites. The gage has been modified to reduce its creep and temperature sensitivity and moisture infiltration, and to improve its performance at elevated temperatures (Gregory *et al.*, 1983; Gregory and Kim, 1981; Hooker, Aggson and Bickel, 1974; Schrauf *et al.*, 1979). Lingle and Nelson (1982) reported measurements of borehole diameter changes due to thermal loads induced through *in situ* heater tests at Stripa, Sweden, over a period of 18 months in temperatures ranging between 10 and 120°C by

using USBM gages modified to function in wet and elevated temperature environments. The USBM gage did not perform well, with 22 of 30 gages failing due to long-term malfunctioning with water entering the gage body. In the full-scale heater tests at the BWIP site in Washington, Gregory and Kim (1981) reported a 25% failure with the USBM gage after 9 months of test operation.

Despite the measures taken in the past to make the USBM gage a more reliable instrument for monitoring stress changes, its long-term performance is still questionable. In addition to the effect of water and dust, another disadvantage is that the gage can move in a borehole with time, in particular during blasting events, thus making the gage inadequate for monitoring dynamic stress changes.

The Yoke gage developed by the CSIRO was designed specifically for the monitoring of stress changes in rock (Walton and Worotnicki, 1986). It is shown in Fig. 10.3a. The gage is somewhat similar to the conventional USBM gage and consists of a hollow PVC core with three cantilever transducers 60° apart and shaped in the form of a 'C' or a 'yoke'. The tips of the transducers protrude from the PVC pipe. When installed into a borehole (56 mm or 60 mm in diameter), they are compressed to match the diameter in the borehole. Once in place, an epoxy cement is then extruded into the space between the gage and the borehole wall using a system of spacer rod and rubber seals similar to those on the CSIRO HI cell. The cement keeps the instrument in place and works as a moisture barrier. Unlike the conventional USBM gage, the Yoke gage is not recoverable. It also contains a temperature sensor accurate to within 0.1°C. A major advantage is that the gage can be used in areas subjected to vibration associated with blasting. Finally, no hole cleaning is required.

The Yoke gage has been found to perform well. Figure 10.3b shows an example of the gage response placed in a vertical hole used to determine stress changes in a horizontal plane adjacent to a developing open stope of a metalliferous mine. In this example the gage performed well over a period of 60 days. Experiments conducted in the laboratory by Walton and Worotnicki (1986) showed that the Yoke gage is capable of measuring stress

(a)

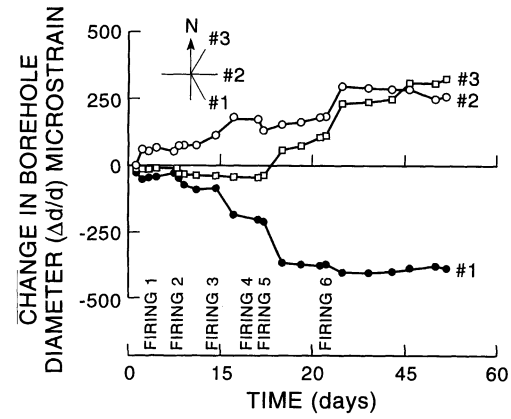

(b)

Fig. 10.3 (a) Photograph of CSIRO Yoke borehole deformation gage. (Courtesy of MINDATA.) (b) Output from a Yoke gage installed *in situ* showing response to stope firings; positive change is tensile. (After Walton and Worotnicki, 1986.)

changes of about ± 0.5 MPa (in a material with a 70 GPa elastic modulus) over a period of 250 days. In the field, a drift rate of about 1–2 $\mu\varepsilon$/day was observed due to moisture absorption of the epoxy cement encapsulating the instrument.

Another modified version of the USBM gage was proposed by Blackwood and Buckingham (1986) for the measurement of stress changes. This new gage works on the same principle as the USBM gage except that it uses an optical system (based on Moire fringes) to measure borehole deformation and a microprocessor control to transmit the data in digital form using an infrared signal to the operator. The cable of the original USBM gage is no longer necessary. Although this instrument is still at the research stage, it represents a step forward in the remote monitoring of stress changes in rock.

10.2.2 STRAIN CELLS

(a) CSIR triaxial and ANZSI cells

The CSIR triaxial strain cell of Leeman (1971) and the other CSIR-type triaxial strain cells discussed in Chapter 5 can be seen as soft cells. The long-term durability of the conventional CSIR triaxial strain cell has been found to be low. On the other hand, the flexible cell of Mills and Pender (1986), called the ANZSI cell, has been found to perform well for stress monitoring. Figure 10.4 shows an example of strain changes measured with the instrument over a period of 3 months following excavation of a tunnel. The complete tensor of stress change can be determined in a single borehole.

(b) Doorstoppers

The original CSIR Doorstopper of Leeman (1971) is not suitable for measuring stress changes since the strains cannot be monitored continuously. Some recent modifications of the Doorstopper for continuous strain monitoring and long-term measurement of temperature

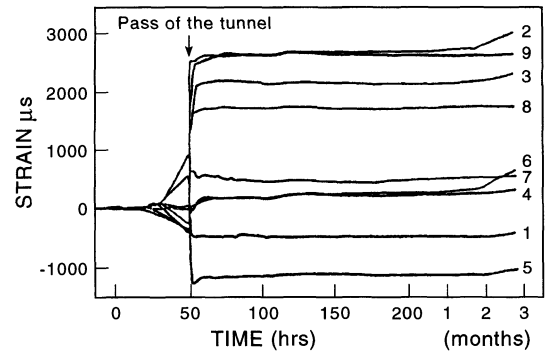

Fig. 10.4 Example of stress change monitoring using the ANZSI cell. The nine strains of the cell were recorded over a period of three months. (After Mills and Pender, 1986.)

(Corthesy and Gill, 1990; Gill *et al.*, 1987; Gregory *et al.*, 1983; Myrvang and Hansen, 1990) have made the Doorstopper a prime candidate for monitoring stress changes. Figure 10.5 shows an example of long-term stress monitoring with a modified Doorstopper cell conducted by Myrvang and Hansen (1990) in a mine in central Norway.

10.2.3 STIFF CYLINDRICAL INCLUSIONS

In the 1950s and 1960s it was thought that stiff cylindrical inclusions could be used as 'stressmeters' for measuring uniaxial or biaxial stress changes in rock in boreholes. Very

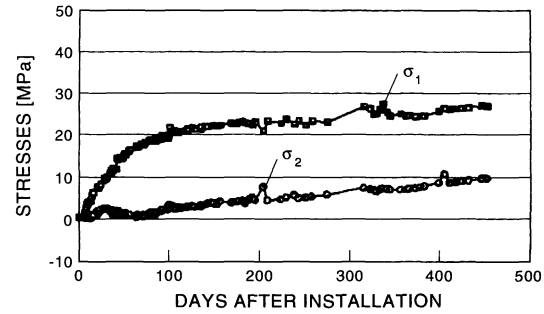

Fig. 10.5 Example of stress change monitoring with a modified Doorstopper. (After Myrvang and Hansen, 1990.)

few of those devices are still used today. These inclusions originated from the analytical prediction that if a rigid inclusion placed in a hole has an elastic modulus four to five times that of the host material, change in stress in the inclusion is proportional to the change in stress in the material irrespective of any change in the elastic modulus of the material. Thus such stressmeters are particularly attractive for measuring stresses in materials that do not always behave in a linearly elastic manner.

(a) Solid and hollow stressmeters

The use of stiff inclusions as stressmeters was first suggested by Coutinho (1949) for the measurement of stress changes in concrete. It was later extended to rock by Wilson (1961). The latter proposed a tapered brass borehole plug consisting of two halves with strain gages embedded in between using Araldite. The two halves of the plug are reassembled and the plug is prestressed into a 2 inch (50.8 mm) diameter borehole. Prestressing of the plug is done by making the instrument slightly tapered (1°) on its sides and by forcing the instrument into tapered sockets. Stress is measured normal to the interface. Prestressing is important in order to provide intimate contact between the stressmeter and the rock and to be able to measure a decrease in stress.

Other devices somewhat similar to that of Wilson (1961) were proposed in the literature to measure uniaxial stress changes across a plane. For instance, Potts (1954) and May (1962) proposed two instruments consisting of two steel plates between which a thin film of fluid is placed. After prestressing of the instrument in a borehole, changes in the space between the plates due to a change in applied pressure is transmitted by the fluid to a diaphragm on which strain gages are attached. The cell of May (1962) was able to measure stress changes with an error of ± 5 psi (35 kPa).

A more recent stressmeter was suggested by Peng, Su and Okubo (1982). Compared with the aforementioned inclusions which are essentially solid, the cell of Peng, Su and Okubo (1982) is hollow and consists of a thick steel pipe (1.25 inch or 31.75 mm OD, 0.75 inch or 19.05 mm ID) with a central partition on which a 45° strain gage rosette is mounted. The cell is cemented into a borehole. Another difference compared with other stressmeters is that changes in the three stress components acting in a plane perpendicular to the hole axis can be determined. It is noteworthy that the cell of Peng, Su and Okubo (1982) is quite similar in concept to the first CSIR strain cell proposed by Leeman (1958), where single strain gages mounted on both sides of several diametral diaphragms were used instead of strain rosettes.

Finally, Park (1986) proposed another stressmeter called the PAL borehole stressmeter. A plug instrumented with strain gages is placed in a shell with a tapered inner surface which is itself pushed into a borehole. Movement of the borehole walls creates movement of the shell and strains in the gages. According to Park (1986), the device responds to stress changes more rapidly than the vibrating wire stressmeter (discussed below), is less expensive, easier to install and has a higher resolution and sensitivity.

(b) Prestressed stressmeter

The cell of Hast (1958) discussed in Chapter 5 can also be used to determine changes in stress in one direction. The cell is prestressed in a borehole to a desired value. The load in the cell is measured as a function of time and the stress in the direction of measurement is determined. By placing the cell in three directions and at three different locations in a borehole, the change in the state of stress in a plane normal to the borehole axis can be determined. By repeating the process into two other perpendicular holes, the six components of the tensor of stress change can be determined.

(c) Photoelastic stressmeter

The photoelastic stressmeter was initially proposed by Roberts *et al.* (1964) as a device to measure stress changes in rock. Modifications of the initial stressmeter and field applications in rock, concrete and masonry can be found in Roberts *et al.* (1965). The instrument consists of a plug of optical glass in the form of a cylinder with an axial hole. As shown in Fig. 10.6, the plug is bonded around its periphery close to the end of a borehole. A light source with a polarizing filter and a quarter-wave plate is inserted through the hole of the plug to illuminate a reflector with circularly polarized light. The stressmeter is bonded to the rock in such a way that the face of the plug remote from the light source can be viewed by an observer looking downhole. The plug is observed through a viewer consisting of two filters, a linear analyzer and a quarter-wave plate. As the rock deforms and the plug is stressed, the shear strain in the glass can be inferred from the observed fringes (number and distribution) using the theory of photoelasticity.

The photoelastic stressmeter is essentially a stiff inclusion (with a Young's modulus of 10^7 psi or 70 GPa) and a biaxial system that can be used to determine principal stresses in a plane perpendicular to the hole. Roberts *et al.* (1964) showed that for rocks with a Young's modulus less than 5×10^6 psi (35 GPa), the response of the inclusion to stress is independent of the deformability of the rock and the plug has a high sensitivity to stress changes. For rocks with larger moduli, however, calibration of the instrument is required and the sensitivity of the plug decreases. Additional studies conducted by Barron (1965) have shown that the critical rock modulus should be lowered to 2.5×10^6 psi (17.5 GPa) or in other words, the ratio between the modulus of the glass stressmeter and that of the rock must be equal to at least 4. As pointed out by Bonnechere and Fairhurst (1971), the stressmeter cannot be used to monitor stress changes in excess of about 3000 psi (21 MPa), at which the glass breaks.

The photoelastic stressmeter has been found to perform well in materials that are not linearly elastic and in particular materials which creep (Hawkes, 1969; Skilton, 1971). The laboratory tests of Skilton (1971) on salt showed that the photoelastic stressmeter was able to maintain its calibration value to within $\pm 5\%$ under constant load and under increasing load. Tests were also conducted under uniaxial loading to show that insertion of a

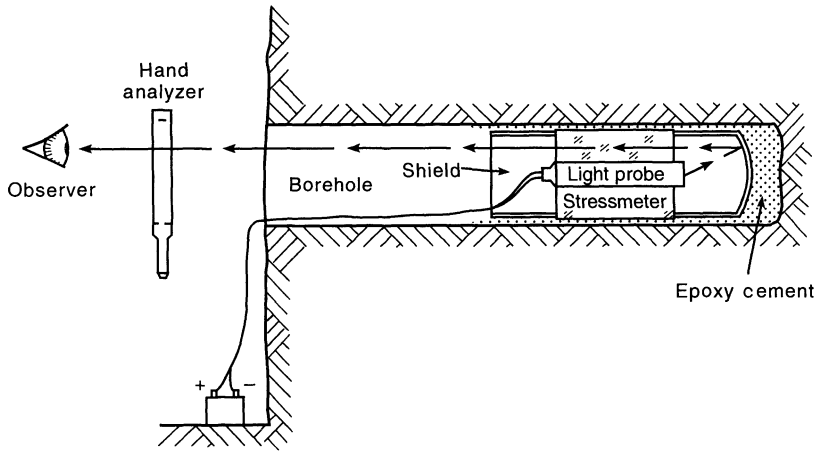

Fig. 10.6 Field set-up of the photoelastic stressmeter. (After Hawkes, 1969.)

photoelastic stressmeter in an already creeping material could give a measurement of the absolute state of stress with time.

(d) Vibrating wire stressmeter

One of the most commonly used devices to monitor stress changes in rock is the vibrating wire stressmeter (sometimes called the IRAD stressmeter). It was first proposed by Hawkes and Hooker (1974) as a low-cost tool to monitor long-term stress changes around underground excavations in rock. The stressmeter was originally intended to monitor stress changes in mine pillars subjected to uniaxial stress changes. Since then it has been used in various mining and civil engineering projects, in particular for the characterization and monitoring of rock mass response to excavation and heating at potential nuclear waste repositories in rock.

Figures 10.7a and 10.7b show respectively a photograph and a cross-section of the vibrating wire stressmeter. It can be considered for all practical purposes as a rigid (stiff) inclusion. It is robust and consists essentially of a thick-walled steel cylinder sealed at both ends with a pretensioned vibrating piano wire strain gage transducer mounted across a diameter at mid-length. The cylinder is 1.6 in (40.6 mm) long and fits into a 1.5 in (38 mm) hole. It is held in place by preloading using a sliding wedge and platen assembly. Changes in the wire frequency due to changes in hole diameter are related to changes in stress in the surrounding rock through a coefficient called 'stress sensitivity factor', which is determined by laboratory calibration for the host material of interest (Dutta, 1985). The vibrating stressmeter measures stresses directly and is unidirectional. By placing three gages inclined with respect to each other in a single borehole, changes in the state of stress in a plane normal to the borehole axis can be determined.

The performance of the vibrating wire stressmeter has been found to be quite good compared with other stress monitoring devices. It has been found to depend on the type of contact with the rock, the deformability of the rock and the amount of initial preloading. Calibration and performance of the vibrating wire stressmeter under various loading and temperature conditions have been reported by several authors including Sellers (1977), Fossum, Russell and Hansen (1977), Lingle and Nelson (1982), Jaworski *et al.* (1982), Lingle, Bakhtar and Barton (1983), Patrick and Rector (1983) and more recently by Dutta (1985), Mao (1986), Dutta and Hatfield

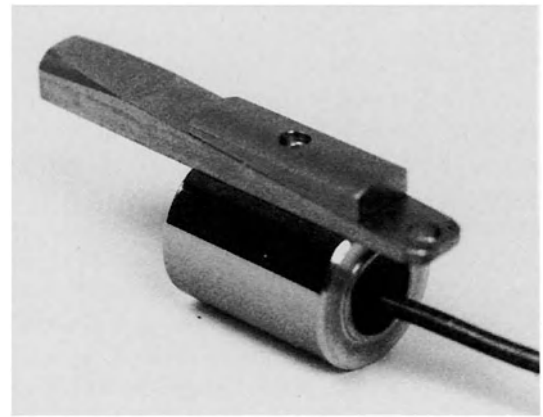

(a)

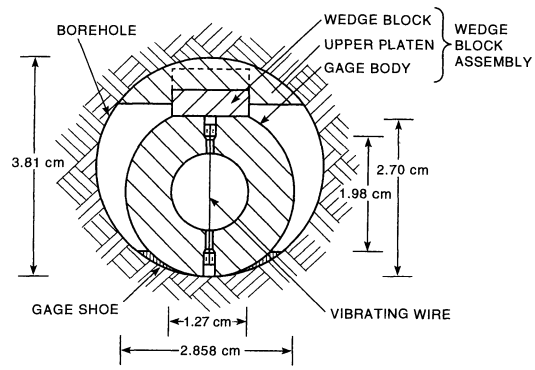

(b)

Fig. 10.7 The vibrating wire stressmeter (IRAD stressmeter). (a) Photograph of the instrument, (b) cross-section of the instrument. (Courtesy of ROCTEST.)

(1987), Tunbridge and Oien (1987) and Herget (1991).

One of the initial problems with the performance of the vibrating wire stressmeter *in situ* has been corrosion, in particular in moist and hot environments in relation to potential nuclear waste repository sites. For instance, in the field tests conducted by Lingle and Nelson (1982) at Stripa, out of 36 stressmeters installed, six failed. A lack of repeatability, found during calibration, was attributed to seating effects, changes in temperature and variability in the rock elastic modulus. It was concluded that errors as large as ± 33% could be expected. Similar problems of internal corrosion were found at the Spent Fuel Test-Climax Site in Nevada (Mao, 1986) and in some block tests at the Near-Surface Test Facility of the BIWP in Hanford, Washington (Gregory and Kim, 1981). Improvements conducted by Gregory *et al.* (1983) to prevent moisture infiltration resulted in considerable improvement of the reliability of the vibrating wire stressmeter.

Over the past 10 years, the design of the vibrating wire stressmeter has been improved, in particular to prevent internal corrosion. Another addition is the use of different seating platens for different rocks. In softer rocks, the platens are usually wider in order to reduce the contact stresses on the borehole wall. Overall, the vibrating wire stressmeter is still today a very attractive device for monitoring stress changes due to its long-term stability and low cost.

A variant of the vibrating wire stressmeter was proposed by Cook and Ames (1979) for stress monitoring in salt. The cell, called the strain gage stressmeter, differs from the vibrating wire stressmeter in that it is not as stiff and the deformation of the instrument is monitored by a strain gage instead of the vibrating wire. Calibration of the stressmeter in a block of salt is required. Numerical analysis of the stressmeter conducted by Morgan (1984) revealed that the stressmeter's performance in salt can be strongly affected by creep, which may be a source of error when determining actual stress changes.

A recent development based on the vibrating wire principle was proposed by Cox and Johnson (1987). The instrument, shown in Fig. 10.8, can be defined as a three-component

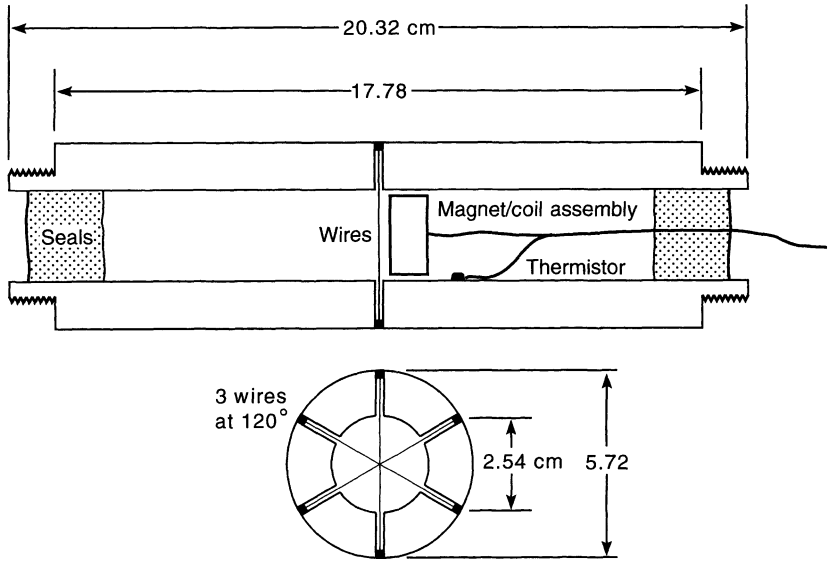

Fig. 10.8 Three-component vibrating wire biaxial stress sensor. (After Cox and Johnson, 1987.)

vibrating wire stressmeter which measures radial deformation of a hollow steel tube along three directions at 120° from each other using three tensioned wires. The instrument was tested in ice (a very nonlinearly elastic material with creep characteristics). The instrument was found to have a low temperature sensitivity (5 kPa/°C) and an accuracy of better than 15% under a variety of both uniaxial and biaxial loading conditions in the laboratory. Also, principal stresses could be determined to within 5°. The instrument can measure radial displacements as small as 10^{-6} mm. Figure 10.9 shows an example of stress determination and comparison with applied stresses for a block of ice under biaxial loading in the laboratory. This instrument is very promising, particularly for measuring stress changes in materials that behave in a nonlinearly elastic manner.

The vibrating wire technology was recently incorporated into a strain monitoring system developed at CANMET in Canada (Herget, 1990). The system consists of a vibrating wire sensor and a readout unit. The sensor itself consists of a steel ring supporting a vibrating wire that can fit in boreholes with diameters ranging between 76 and 153 mm. Deformation of the hole (as small as 0.0004 mm) can be determined by measuring changes in the resonant frequency of the wire. Changes in the maximum and minimum secondary (apparent) principal stresses normal to the hole are determined by measuring deformations in at least three sensors. The system has been found to perform well for monitoring stress changes in hard rocks.

Finally, a new cell consisting of six non-parallel vibrating wires has been proposed by Bois (1995). The cell, called the CIUS (cylindre instrumenté de l'Université de Sherbrooke), consists of a solid concrete inclusion 140 mm in diameter in which six vibrating wires have been embedded. The cell is sealed in a

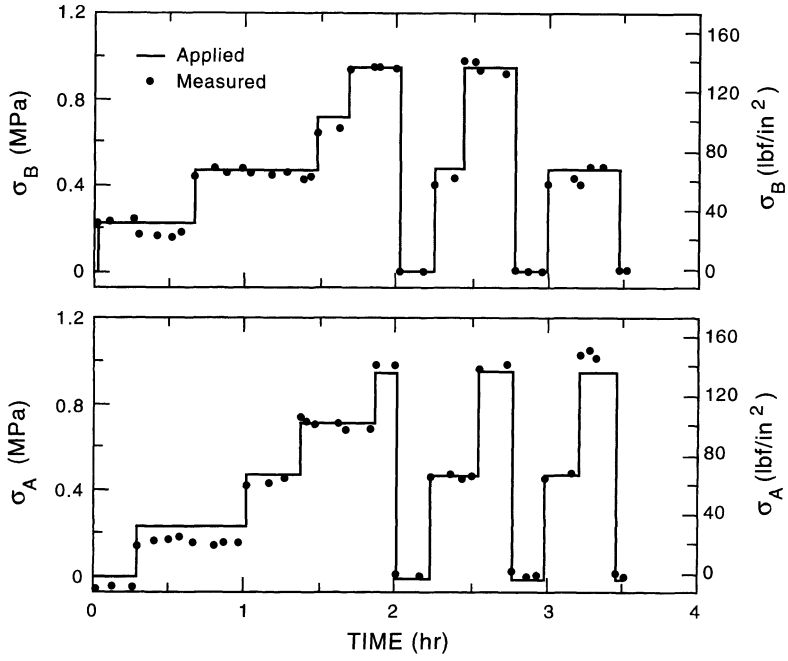

Fig. 10.9 Measured versus applied stresses for three-component vibrating wire biaxial stress sensor in saline ice under biaxial stresses σ_A and σ_B. (After Cox and Johnson, 1987.)

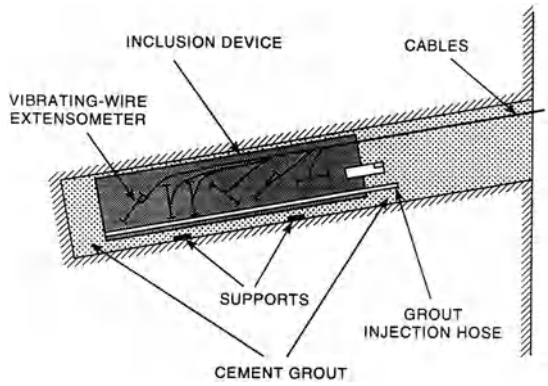

Fig. 10.10 Instrumented cylinder of University of Sherbrooke also known as the CIUS cell. (Source: Bois, A.-P., Ballivy, G. and Saleh, K. Copyright 1994, with kind permission from Elsevier Science Ltd, The Boulevard, Langford Lane, Kidlington, UK.)

borehole (152 mm in diameter) with cement grout (Fig. 10.10). It allows determination of all six components of the tensor of stress change. The cell has been found to perform well in rock and concrete. Examples of stress change monitoring can be found in Ballivy *et al.* (1991), Bois, Ballivy and Saleh (1994) and Bois (1995).

(e) Encapsulated spherical inclusion

Another stiff inclusion was proposed by Nichols, Abel and Lee (1968). Instead of being cylindrical, it is spherical and consists of a 1 inch (25.4 mm) diameter chrome alloy steel (or brass or aluminum) ball. Three 45° strain rosettes are bonded on the ball in orthogonal directions. The ball is then encapsulated into a waterproof epoxy grout (Fig. 10.11). Rock strain associated with stress changes is transferred to the ball through the epoxy. Using this instrument, the complete tensor of stress change can be determined from changes in strain measured in one borehole. Further development of this probe and measurement of stress changes in the laboratory and *in situ* can be found in Lee, Abel and Nichols (1976). In general, the probe has been found to work well for stress change monitoring.

10.2.4 SOLID AND HOLLOW DEFORMABLE INCLUSIONS

Solid and hollow deformable inclusions differ from the stiff inclusions mentioned above in that they are more compliant and deform with the rock. The inclusions are perfectly bonded to the rock. Unlike stiff inclusions, analysis of their response requires knowledge of the deformability properties of the host rock. Most of the inclusions discussed in Chapter 5 can theoretically be used for monitoring stress changes. They have the advantage that the strain gages are protected from adverse conditions. Furthermore, if strain changes can be measured in six different directions, the six components of the tensor of stress change can be determined in one hole only.

The use of solid inclusions for monitoring stress changes is based on the mathematical prediction that if an infinite linearly elastic isotropic medium containing a perfectly bonded single elliptical or ellipsoidal solid inclusion is subjected to stresses at infinity, the stress field in the inclusion is uniform (Babcock, 1974; Eshelby, 1957). This observation has been extended to inclusions in anisotropic media (Amadei, 1983; Berry, 1970; Niwa and Hirashima, 1971). The main problem with solid inclusions however is that, if they are too stiff, they will tend to interfere with the borehole deformation, thus causing possible debonding with time and making stress monitoring meaningless. This problem can be avoided or at least reduced (as for absolute stresses) by keeping the inclusions very soft with respect to the rock or by using thin-walled inclusions such as the CSIRO HI cell.

A limited amount of success has been obtained with the conventional CSIRO HI cell for stress monitoring (Kohlbeck and Scheidegger, 1986; Walton and Worotnicki, 1986; Wold and Pala, 1986). A thin-walled

version of the CSIRO HI cell has been developed by Walton and Worotnicki (1986) for monitoring stress changes in weak rocks in order to reduce potential debonding between the inclusion epoxy and the rock. A recent review of the use of the regular and thin-walled versions of the HI cell for stress monitoring and their respective performances can be found in Worotnicki (1993). The latter concluded that CSIRO HI cells are best suited to monitoring rapid changes in stress and are less suitable for monitoring gradual stress changes.

As pointed out by Walton and Worotnicki (1986), instrument-related problems when using the CSIRO HI cell over long time periods can be of four types: (1) breakdown of electrical insulation between the strain gages and the rock due to prolonged exposure of the instrument and its electrical connections to a moist and corrosive environment, (2) volume changes of the epoxy cement and the epoxy body of the cell due to continuous polymerization, (3) moisture absorption leading to swelling and (4) deterioration of the epoxy cement bond due to the effect of moisture or temperature changes. Spathis (1988) analyzed the effect of time on strain readings with the regular and thin-walled CSIRO HI cells, assuming that the epoxy resin in the cells is viscoelastic and the rock is elastic. He found that creep of the epoxy could altogether invalidate stress monitoring and that correction

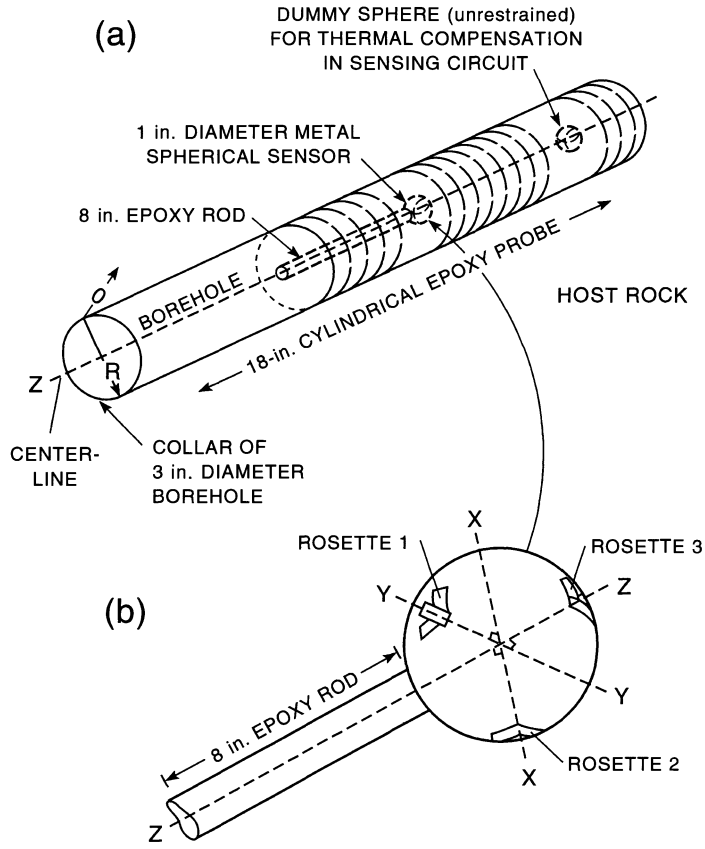

Fig. 10.11 US Geological Survey encapsulated spherical inclusion. (a) Relationship of spherical sensor to cylindrical epoxy probe and host rock, (b) location of strain gage rosettes on spherical sensor. (After Lee, Abel and Nichols, 1976.)

needs to be applied to the current analysis. He also found that the creep problem was strongly reduced with the thin-walled CSIRO HI cell.

Laboratory and field tests conducted by Walton and Worotnicki (1986) revealed drift rates of the order of $0.35\,\mu\varepsilon$/day for the conventional CSIRO HI cell and $0.05\,\mu\varepsilon$/day for the thin-walled version of the cell. Drift rates have been found to decrease with time and it has been suggested that HI cells should be installed 1 to 3 months prior to expected stress changes *in situ*. Accuracy of about 1 MPa can be achieved with rocks with an elastic modulus of 1 GPa and over monitoring periods of 1–1.5 months.

Figure 10.12 shows an example of stress change monitoring (magnitude and orientation) versus excavation sequence at the 240 level of the URL site in Canada (Martin and Simmons, 1993). Arrays of several CSIRO HI cells were placed ahead of the advancing excavation. Also shown in Fig. 10.12 are the predicted stress changes determined using a three-dimensional linear elastic finite element program. It can be seen that good agreement exists between measured and predicted stresses for each blast event and that the rock behaves for all practical purposes as linearly elastic.

10.2.5 FLAT JACKS AND HYDRAULIC BOREHOLE PRESSURE CELLS

In principle, the flat jacks discussed in Chapter 6 can also be used to monitor stress changes. Once in place, changes in flat jack pressure with time can be measured directly. Many of the problems discussed in Chapter 6 apply here as well. In particular, the problem of creep may make long-term stress measurements with flat jacks meaningless. In general, despite their limitations, flat jacks have been popular for monitoring changes in compressive stress in mine pillars or excavation walls. However, one should not expect the measurements to be very accurate.

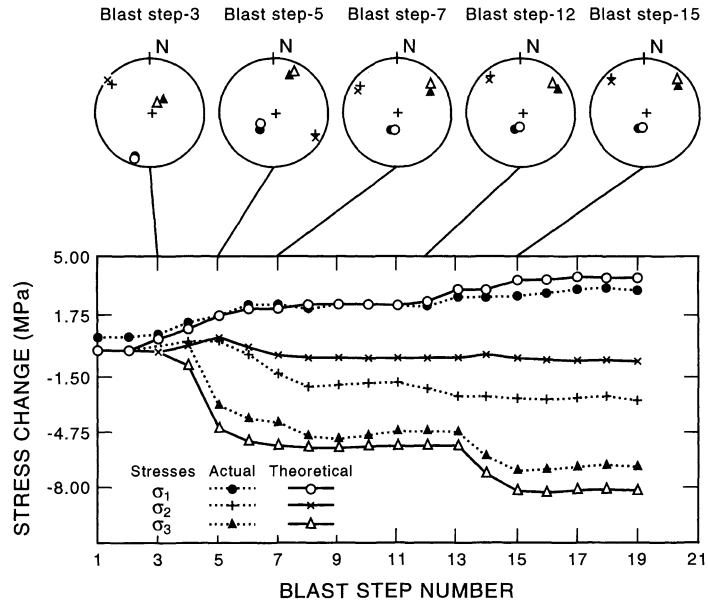

Fig. 10.12 Stress change monitoring at the 240 level at the URL site using CSIRO HI cells. Comparison of measured and predicted (orientation and magnitude) principal components of stress change versus excavation (blast step) from room 209 excavation response test. (After Martin and Simmons, 1993.)

Changes in normal stress can be measured directly using the change in hydraulic fluid pressure in flat and elongated cells left in place in a borehole drilled in a rock mass. Such instruments are known as hydraulic pressure cells and operate, for all practical purposes, very much like flat jacks. However, unlike the flat jacks, they are not limited to surface measurements and can be used to measure changes in stress well within a rock mass. After installing the cell in a borehole and following the application of an initial seating pressure, changes in pressure are recorded with time. The pressure changes are then related to the rock stress changes through calibration and/or mathematical or numerical models. The technique is simple, of low cost and reliable over long periods of time, but is limited to measurements of uniaxial stress changes in a direction perpendicular to the cell. One major problem with hydraulic pressure cells (beside their temperature sensitivity) is that they do not perform well under tensile stresses where separation between the cells and the rock is likely to occur. A standard for stress monitoring using hydraulic cells has been proposed by the International Society for Rock Mechanics (Franklin, 1980).

Various flat borehole pressure cell systems have been proposed in the literature, in particular for monitoring vertical stress changes in mine and mine pillars during extraction, the main objective being a control of rockburst phenomena. Some of the cells are placed directly in a borehole, the gap between the cells and the rock being grouted with epoxy or mortar or other infilling material. The cells can also be encapsulated in grout during construction, forming an inclusion (Fig. 10.13) which is then installed into a borehole.

One of the first hydraulic cells was the borehole pressure cell (BPC) developed at the US Bureau of Mines (Panek and Stock, 1964). The cell was designed for 2.25 inch (57.1 mm) boreholes and had an active length of 7 inches (178 mm). Theories for the analysis of BPC cell measurements can be found in Sellers (1970) and Babcock (1986). Devices similar to the BPC have also been proposed by Gilley, Sporcic and Zona (1964), Jeger (1971) and Schaller, McKay and Hargraves (1976). Figure 10.14 shows an example of stress monitoring obtained with the cell of Gilley, Sporcic and Zona (1964) in a room and pillar coal mine in West Virginia. Several cells installed at depths of 10, 15, 20 and 25 ft (3.0, 4.6, 6.1 and 7.6 m) into mine pillars were monitored during extraction and several rockburst events.

Instead of using grout, the hydraulic pressure cells can also be encapsulated in solid platens (Babcock, 1986). The borehole platened flatjack (BPF) developed by Bauer, Chekan and Hill (1985) is an example of such an instrument. It consists of a copper flat jack positioned between two aluminum platens. It was designed for installation in 2 inch (5.1 cm) boreholes. Theory for the analysis of the BPF

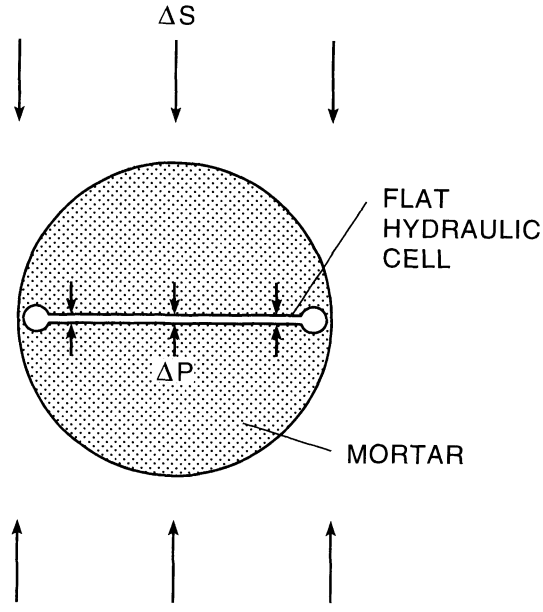

Fig. 10.13 Flat jack type of hydraulic cell grouted into a borehole. The measured change in pressure ΔP in the cell is related to the actual change in stress ΔS. (Adapted from: Sellers, J.B. Copyright 1970, with kind permission from Elsevier Science Ltd, The Boulevard, Langford Lane, Kidlington, UK.)

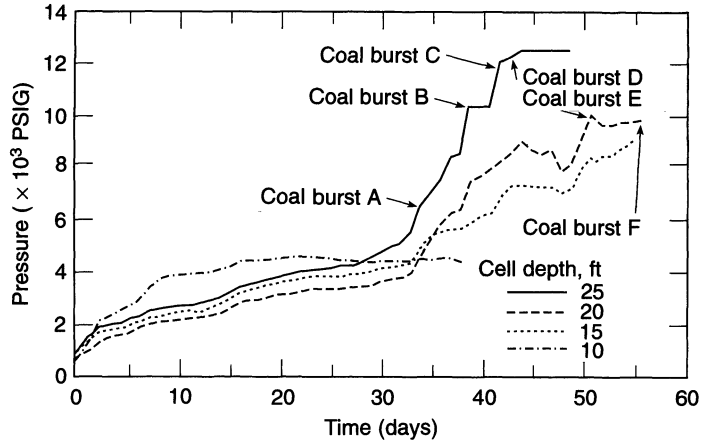

Fig. 10.14 Example of stress monitoring obtained with borehole pressure cells in a room and pillar coal mine in West Virginia. Several cells installed at depths of 10, 15, 20 and 25 ft (3.0, 4.6, 6.1 and 7.6 m) into mine pillars were monitored during extraction and several rockburst events. (After Gilley, Sporcic and Zona, 1964.)

cell can be found in Heasley (1989). Another borehole pressure cell consisting of a flat jack system sandwiched in between solid platens has been proposed by Ishijima *et al.* (1976). In general, all those cells require calibrations which can be done numerically or in the laboratory.

An accurate flat pressure cell was proposed by Swolfs and Brechtel (1977) and further improved by Swolfs and Walsh (1990). The authors used water-filled cells (rubber or welded steel sheets) placed in slender slots with an aspect ratio (thickness over length) of about 0.025. A sensitive pressure gage is used to measure changes in cell pressure. The gap between the cells and the rock is filled with grout or sand (Fig. 10.15). The system also contains a compensator to counterbalance temperature-induced stress changes in the cell. Stress monitoring in a quartz monzonite rock by Swolfs and Brechtel (1977) using two cells buried vertically at a depth of 1.5 m indicated that the cells were able to measure changes in pressure within 96% of the actual changes in horizontal stresses perpendicular to the cells and over a period of 2 years. More recent tests carried out by Swolfs and Walsh (1990) indicated that their system could monitor stress changes associated with Earth tides as small as 0.01 bar (1 kPa).

Another stress monitoring cell based on the flat jack principle is the CALIP (calibratible in place) gage proposed by Keller and Lowry (1990). An exploded view of the cell is shown in Fig. 10.16. The cell consists of a ytterbium strain gage and a small flat jack sandwiched in between two steel straps. After drilling of a 4 in (10.2 cm) hole, the core is split in half and one half is tapered to the host cell. The core is then reassembled and grouted in the hole. The stress normal to the cell is measured by applying a pressure until the strain gage element responds. The pressure when the gage responds is taken as the normal stress acting across the cell.

Another system of hydraulic pressure cells was developed by the US Bureau of Mines to determine both absolute and changes in stress associated with mining in viscoelastic ground (Lu, 1981, 1984, 1986). Two types of borehole cells were used: a cylindrical pressure cell (CPC) which, for all practical purposes, operates like a cylindrical inflatable probe or dilatometer, and a flat pressure cell (BPC) as mentioned above. By using a combination of one CPC and two BPC cells (one in the

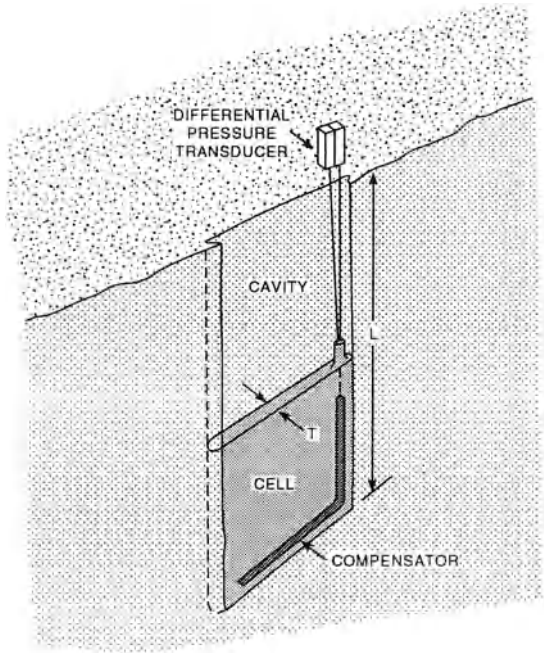

Fig. 10.15 Flat pressure cell stress monitoring system of Swolfs and Walsh (1990). The ratio T/L is the aspect ratio of the slot.

horizontal plane and one in the vertical plane), the vertical and horizontal stress components and any changes of these components can be determined. After applying an initial pressure in the cells, ground equilibrium is reached after a certain time. The cell pressures after equilibrium are used to calculate the absolute vertical and horizontal stresses. In doing so, it is assumed that the vertical and horizontal stresses are principal stresses and that the borehole is parallel to a principal stress direction. Following determination of the absolute stresses, any changes in the cell pressures associated with mining are used for determining variations in stress. Figure 10.17 shows an example of stress monitoring in a coal pillar conducted by Lu (1986). In this example, the initial vertical and horizontal stresses are equal to 5.8 and 5.6 MPa, respectively.

Hydraulic pressure cells are still used today to measure stress changes in rocks and other geomaterials. Various instrument makers carry such cells. Figure 10.18 shows a photograph of a circular pressure cell carried by ROCTEST. One of the most popular cells used

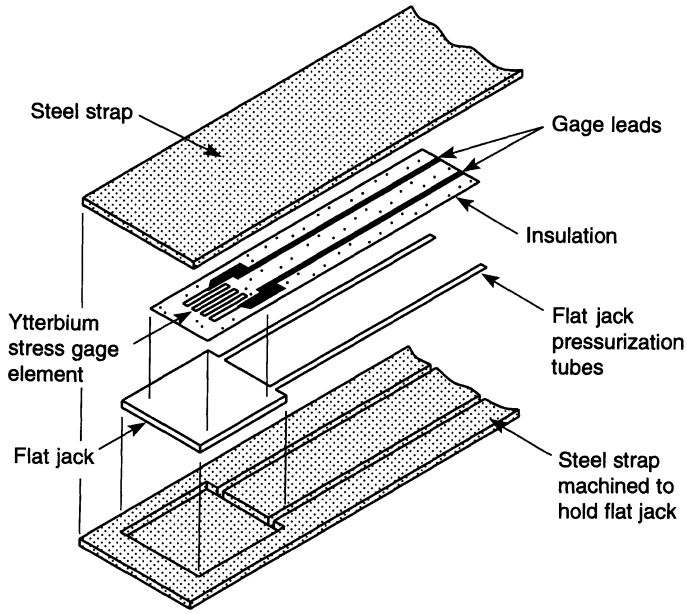

Fig. 10.16 Components of the CALIP gage of Keller and Lowry (1990).

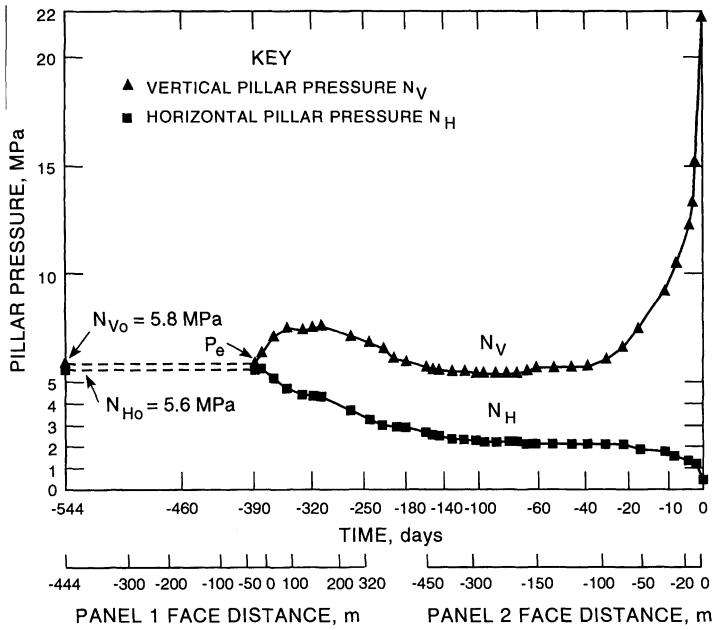

Fig. 10.17 Example of stress monitoring in a coal pillar using a combination of one CPC and two BPC cells. (After Lu, 1986.)

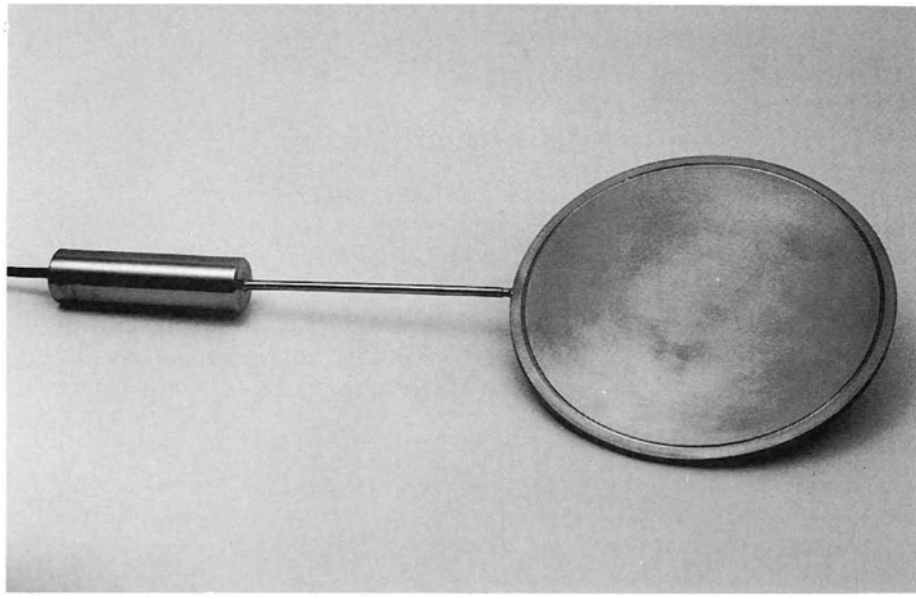

Fig. 10.18 Hydraulic pressure cell. The pressure is measured using a transducer shown on the left of the photograph. (Courtesy of ROCTEST.)

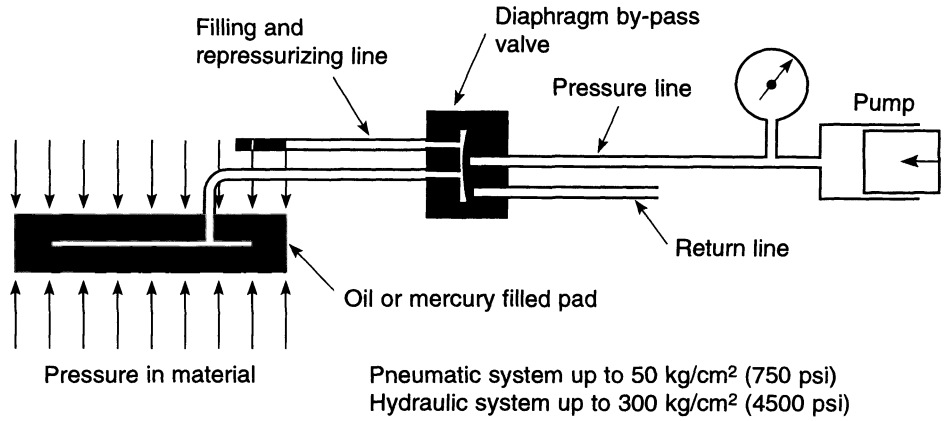

Fig. 10.19 Measurement of normal stress using the Glötzl cell. (From ROCTEST documentation.)

in practice today is the Glötzl (or Gloetzl) cell (Fig. 10.19). The latter (like most modern hydraulic pressure cells) is equipped with a hydraulic diaphragm transducer where the cell pressure is measured by balancing the fluid pressure in the cell by a pressure applied to the reverse side of the transducer diaphragm. Glötzl cells come in different configurations with various sizes and applied pressures (up to 30–40 MPa). The fluid used is either mercury or oil. The cells can be installed in a borehole. After installation, the borehole is backfilled with concrete or a material with a deformability similar to that of the host rock. Single Glötzl cells have been used extensively for measuring stresses in soils, concrete, concrete linings and rocks and at distances not exceeding 50 m into rock masses.

Several hydraulic pressure cells can be assembled to measure stresses in different directions in a given borehole. This set-up provides a means of determining several components of the change in stress tensor. Such a technique was followed, for instance, by Meister *et al.* (1991), who used a combination of four Glötzl cells to measure stress changes in rock salt associated with *in situ* heater experiments in Germany. Another example of stress monitoring with multiple Glötzl cells was reported by Rehbinder (1984). Changes in tangential and axial stresses were monitored in the wall of a large unlined hot-water cavern ($22 \times 18 \times 45$ m) excavated in gneiss at the Avesta plant in Sweden. The cells were grouted in boreholes and were located at distances of 1.3, 3.3 and 6.3 m from the top of the cavern. Stress change monitoring was carried out over a period of 18 months during which the stored water underwent four cycles of heating and cooling. Figure 10.20 shows the variation of the stresses and water temperature with time. It can be seen that the rock stress fluctuations coincide relatively well with the fluctuations of the temperature of the water in the cavern.

10.3 TECHNICAL INFORMATION

Additional information about some of the instrument devices presented in this chapter and any related equipment can be obtained by contacting directly the following manufacturers:

1. ROCTEST, 665 Pine Street, St Lambert, Quebec, J4P 2P4, Canada: pressure cells, Glötzl cell, vibrating wire stressmeter.
2. Glötzl, Baumeßtechnik, Gesellschaft für Baumeßtechnik, 7512 Rheinstetten 4-Fo./Karlsruhe, Germany: Glötzl cells and systems of several Glötzl cells.
3. MINDATA Pty. Ltd., 115 Seaford Road, Seaford 3198, Victoria, Australia: CSIRO HI

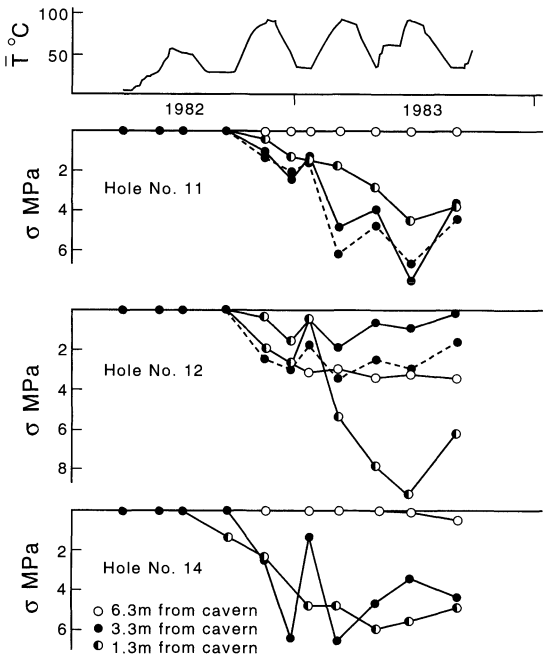

Fig. 10.20 Variation of tangential stress (solid lines) and axial stress (dashed lines) with time measured in three holes above the top of an unlined hot-water cavern at the Avesta plant in Sweden. Glötzl cells were placed at distances of 6.3, 3.3 and 1.3 m from the top of the cavern. The variation of the average stored water temperature with time is shown for comparison. (After Rehbinder, 1984.)

cells, CSIRO Yoke gage, ANZSI cell (also available in the USA through Reliable Geo L.L.C., 241 Lynch Road, Yakima, Washington 98908-9512).

4. GEOKON, Inc., 48 Spencer St, Lebanon, NH 03766, USA: vibrating wire stressmeter, vibrating wire biaxial stressmeter, pressure cells, borehole flat jack cells.

REFERENCES

Amadei, B. (1983) *Rock Anisotropy and the Theory of Stress Measurements*, Lecture Notes in Engineering, Springer-Verlag.

Amadei, B. (1985) Measurement of stress change in rock. *Int. J. Rock Mech. Min. Sci. & Geomech. Abstr.*, **22**, 177–82.

Babcock, C.O. (1974) A new method of analysis to obtain exact solutions for stresses and strains in circular inclusions. US Bureau of Mines Report of Investigation RI 7967.

Babcock, C.O. (1986) Equations for the analysis of borehole pressure cell data, in *Proc. 27th US Symp. Rock Mech.*, Tuscaloosa, SME/AIME, pp. 233–40.

Ballivy, G. *et al.* (1991) Stress variation measurement in a mine pillar, in *Proc. 7th Int. Soc. Rock Mech. (ISRM)*, Aachen, Balkema, Rotterdam, Vol. 1, pp. 427–30.

Barla, G. and Rossi, P.P. (1983) Stress measurement in tunnel lining, in *Proc. Int. Symp. on Field Measurements in Geomechanics*, Zurich, Balkema, Rotterdam, pp. 987–98.

Barron, K. (1965) Glass insert stressmeter. *Trans. Am. Inst. Mining Eng.*, 287–299.

Bauer, E.R., Chekan, G.J. and Hill, J.L. (1985) A borehole instrument for measuring mining-induced pressure changes in underground coal mines, in *Proc. 26th US Symp. Rock Mech.*, Rapid City, Balkema, Rotterdam, pp. 1075–84.

Berry, D.S. (1970) The theory of determination of stress changes in a transversely isotropic medium, using an instrumented cylindrical inclusion. Corps of Engineers, Missouri River Division, Omaha District, Technical Report MRD-1-70.

Blackwood, R.L. and Buckingham, C. (1986) A remotely operated deformation gauge for monitoring stress change in rock, in *Proc. Int. Symp. on Rock Stress and Rock Stress Measurements*, Stockholm, Centek Publ., Luleå, pp. 369–74.

Blejwas, T.E. (1987) Planning a program in experimental rock mechanics for the Nevada Nuclear Waste Storage Investigations Project, in *Proc. 28th US Symp. Rock Mech.*, Tucson, Balkema, Rotterdam, pp. 1043–51.

Blejwas, T.E. (1989) Experiments in rock mechanics for the site characterization of Yucca Mountain, in *Proc. 30th US Symp. Rock Mech.*, Morgantown, Balkema, Rotterdam, pp. 39–46.

Bois, A.-P. (1995) Auscultation des ouvrages en rocher ou en béton à l'aide du cylindre instrumenté de l'Université de Sherbrooke (CIUS), unpublished PhD Thesis (in French), Univ. of Sherbrooke, Dept. of Civil Eng.

Bois, A.-P., Ballivy, G. and Saleh, K. (1994) Monitoring stress changes in three dimensions using a solid cylindrical cell. *Int. J. Rock Mech. Min. Sci. & Geomech. Abstr.*, **31**, 707–18.

Bonnechere, F. and Fairhurst, C. (1971) Results of an in situ comparison of different techniques for

rock stress determination, in *Proc. Int. Symp. on the Determination of Stresses in Rock Masses*, Lab. Nac. de Eng. Civil, Lisbon, pp. 334–58.

Cook, C.W. and Ames, E.S. (1979) Borehole inclusion stressmeter measurements in bedded salt, in *Proc. 20th US Symp. Rock Mech.*, Austin, Center for Earth Sciences and Eng., pp. 481–5.

Corthesy, R. and Gill, D.E. (1990) The modified Doorstopper cell stress measuring technique, in *Proc. Conf. on Stresses in Underground Structures*, Ottawa, CANMET, pp. 23–32.

Coutinho, A. (1949) Theory of an experimental method for determining stresses not requiring an accurate knowledge of the elasticity modulus, in *Proc. Int. Ass. Bridge and Struct. Eng. Cong.*, Liege, pp. 83–103.

Cox, G.F.N. and Johnson, J.B. (1987) Verification tests for a stiff inclusion stress tensor. *Int. J. Rock Mech. Min. Sci. & Geomech. Abstr.*, **24**, 81–8.

Cramer, M.L. *et al.* (1987) Geomechanical testing development for the Basalt Waste Isolation Project, in *Proc. 28th US Symp. Rock Mech.*, Tucson, Balkema, Rotterdam, pp. 1053–62.

Dutta, P. (1985) Some recent developments in vibrating wire rock mechanics instrumentation, in *Proc. 26th US Symp. Rock Mech.*, Rapid City, Balkema, Rotterdam, pp. 1043–54.

Dutta, P. and Hatfield, R.W. (1987) Calibration measurements of rock stress by vibrating wire stressmeter at high temperatures, in *Proc. 2nd Int. Symp. on Field Measurements in Geomechanics*, Kobe, Balkema, Rotterdam, pp. 43–7.

Eshelby, J.D. (1957) The determination of the elastic field of an ellipsoidal inclusion and related problems. *Proc. Roy. Soc. A*, **241**, 376–96.

Fiore, J., Der, V. and Montenyohl, V. (1984) An overview of the OCRM program efforts, in *Proc. 25th US Symp. Rock Mech.*, Evanston, SME/AIME, pp. 1139–52.

Fossum, A.F., Russell, J.E. and Hansen, F.D. (1977) Analysis of a vibrating-wire stress gage in soft rock. *Experim. Mech.*, **17**, 261–4.

Franklin, J. (coordinator) (1980) Suggested methods for pressure monitoring using hydraulic cells. *Int. J. Rock Mech. Min. Sci. & Geomech. Abstr.*, **17**, 117–27.

Gill, D.E. *et al.* (1987) Improvements to standard doorstopper and Leeman cell stress measuring techniques, in *Proc. 2nd Int. Symp. on Field Measurements in Geomechanics*, Kobe, Balkema, Rotterdam, Vol. 1, pp. 75–83.

Gilley, J.L., Sporcic, R. and Zona, A. (1964) Progress in the application of encapsulated cells in a coal mine subject to coal burst, in *Proc. 6th US Symp. Rock Mech.*, Rolla, University of Missouri, pp. 649–67.

Gregory, E.C. and Kim, K. (1981) Preliminary results from the full-scale heater tests at the near-surface test facility, in *Proc. 22nd US Symp. Rock Mech.*, Cambridge, MIT Publ., pp. 143–8.

Gregory, E.C. *et al.* (1983) Applicability of borehole stress measurement instrumentation to closely jointed rock, in *Proc. 24th US Symp. Rock Mech.*, College Station, Association of Eng. Geologists Publ., pp. 283–6.

Hast, N. (1958) The measurement of rock pressures in mines. *Sveriges Geol. Undersökning, Ser. C*, No. 560.

Hawkes, I. (1969) Stress evaluation in low-modulus and viscoelastic materials using photoelastic glass inclusions. *Expl. Mech.*, **9**, 58–66.

Hawkes, I. and Hooker, V.E. (1974) The vibrating wire stressmeter, in *Proc. 3rd Cong. Int. Soc. Rock Mech. (ISRM)*, Denver, National Academy of Sciences, Washington, DC, pp. 439–44.

Heasley, K.A. (1989) Understanding the hydraulic pressure cell, in *Proc. 30th US Symp. Rock Mech.*, Morgantown, Balkema, Rotterdam, pp. 485–92.

Herget, G. (1990) Monitoring equipment for the determination of stress redistribution, in *Proc. Conf. on Stresses in Underground Structures*, Ottawa, CANMET, pp. 175–84.

Herget, G. (1991) Monitoring of excavation performance. CANMET Technical Report MRL 91-082, Ottawa.

Heuze, F.E. (1981) Geomechanics of the Climax 'Mine-By', Nevada Test Site, in *Proc. 22nd US Symp. Rock Mech.*, Cambridge, MIT Publ., pp. 458–64.

Heuze, F.E. *et al.* (1980) In-situ geomechanics, Climax granite. Nevada Test Site. Lawrence Livermore Laboratory Report UCRL 85308.

Hocking, G., Williams, J.R. and Mustoe, G.G.W. (1990) Post-test assessment of simulations for in-situ heater tests in basalt – Part I. Heater test description and rock mass properties. *Int. J. Rock Mech. Min. Sci. & Geomech. Abstr.*, **27**, 143–59.

Hooker, V.E., Aggson, J.R. and Bickel, D.L. (1974) Improvements in the three component borehole deformation gage and overcoring techniques. US Bureau of Mines Report of Investigation RI 7894.

Hustrulid, W.A. (1983) Design of geomechanical experiments for radioactive waste disposal – a rethink, in *Proc. Int. Symp. on Field Measurements in Geomechanics*, Zurich, Balkema, Rotterdam, pp. 1381–408.

Hustrulid, W.A. and McClain, W.C. (1984) Policy questions related to the role of field testing in the establishment of the radioactive waste repository, in *Proc. 25th US Symp. Rock Mech.*, Evanston, SME/AIME, pp. 1161–76.

Ishijima, T. *et al.* (1976) Monitoring of stress relief boring in Akabira coal mine, in *Proc. ISRM Symp. on Investigation of Stress in Rock, Advances in Stress Measurement*, Sydney, The Institution of Engineers, Australia, pp. 100–106.

Jaworski, G.W. *et al.* (1982) Behavior of the rigid inclusion stressmeter in an anisotropic stress field, in *Proc. 23rd US Symp. Rock Mech.*, Berkeley, SME/AIME, pp. 211–18.

Jeger, C. (1971) Interpretation of results of measures with pressiometric caps in order to give an equivalent rheological behavior to a faulted coal-block, in *Proc. Int. Symp. on the Determination of Stresses in Rock Masses*, Lab. Nac. de Eng. Civil, Lisbon, pp. 491–508.

Kaiser, P.K. and Maloney, S. (1992) The role of stress change in underground construction, in *Proc. Eurock '92: Int. Symp. on Rock Characterization*, Chester, UK, British Geotechnical Society, London, pp. 369–401.

Keller, C. and Lowry, W. (1990) The use of the CALIP gauge for those difficult measurements of rock stress, in *Proc. 31st US Symp. Rock Mech.*, Golden, Balkema, Rotterdam, pp. 573–7.

Kim, K. and McCabe, W.M. (1984) Geomechanics characterization of a proposed nuclear waste repository site in basalt, in *Proc. 25th US Symp. Rock Mech.*, Evanston, SME/AIME, pp. 1126–35.

Kohlbeck, F. and Scheidegger, A.E. (1986) Low cost monitoring of strain changes, in *Proc. Int. Symp. on Rock Stress and Rock Stress Measurements*, Stockholm, Centek Publ., Luleå, pp. 121–32.

Lee, F.T., Abel, J. and Nichols, T.C. (1976) The relation of geology to stress changes caused by underground excavation in crystalline rocks at Idaho Springs, Colorado. US Geological Survey Professional Paper 965, Washington.

Leeman, E.R. (1958) The measurement of the stress in the ground surrounding mining excavations. *Ass. Mine Managers S. Afr.*, 331–56.

Leeman, E.R. (1959) The measurement of changes in rock stress due to mining. *Mine Quarry Eng.*, **25**, 300–304.

Leeman, E.R. (1960) Measurement of stress in abutments at depth, in *Proc. Int. Conf. Strata Control*, Paris, pp. 301–14.

Leeman, E.R. (1971) The CSIR Doorstopper and triaxial rock stress measuring instruments. *Rock Mech.*, **3**, 25–50.

Lingle, R. and Nelson, P.H. (1982) In-situ measurements of stress change induced by thermal load: a case history in granitic rock, in *Proc. 23rd US Symp. Rock Mech.*, Berkeley, SME/AIME, pp. 837–45.

Lingle, R., Bakhtar, K. and Barton, N. (1983) Extraordinary geomechanical instrumentation applications, in *Proc. Int. Symp. on Field Measurements in Geomechanics*, Zurich, Balkema, Rotterdam, pp. 1409–17.

Lu, P.H. (1981) Determination of ground pressure existing in a viscoelastic rock mass by use of hydraulic borehole pressure cells, in *Proc. Int. Symp. on Weak Rocks*, Tokyo, Balkema, Rotterdam, pp. 459–65.

Lu, P.H. (1984) Mining induced stress measurement with hydraulic borehole pressure cells, in *Proc. 25th US Symp. Rock Mech.*, Evanston, SME/AIME, pp. 204–11.

Lu, P.H. (1986) A new method of rock stress measurement with hydraulic borehole pressure cells, in *Proc. Int. Symp. on Rock Stress and Rock Stress Measurements*, Stockholm, Centek Publ., Luleå, pp. 237–45.

Maleki, H.N. (1990) Development of modeling procedures for coal mine stability evaluation, in *Proc. 31st US Symp. Rock Mech.*, Golden, Balkema, Rotterdam, pp. 85–92.

Mao, N.-H. (1986) A new approach for calibration and interpretation of IRAD gage vibrating-wire stressmeters, in *Proc. Int. Symp. on Rock Stress and Rock Stress Measurements*, Stockholm, Centek Publ., Luleå, pp. 499–508.

Martin, C.D. and Simmons, G.R. (1993) The Atomic Energy of Canada Limited Underground Research Laboratory: an overview of geomechanics characterization, in *Comprehensive Rock Engineering* (ed. J.A. Hudson), Pergamon Press, Oxford, Chapter 38, Vol. 3, pp. 915–50.

May, A.N. (1962) The application of measurement instrumentation to the determination of stresses encountered in rocks surrounding underground openings. *Instrument Soc. Am. Trans.*, **1**, 161–9.

Meister, D. *et al.* (1991) Geotechnical and geophysical studies of the thermomechanical response of rock with regard to the disposal of heat-producing radioactive waste in boreholes, in *Proc. 7th Cong. Int. Soc. Rock Mech. (ISRM)*, Aachen, Balkema, Rotterdam, Vol. 1, pp. 121–6.

Mills, K.W. and Pender, M.J. (1986) A soft inclusion instrument for in-situ stress measurement in coal, in *Proc. Int. Symp. on Rock Stress and Rock Stress Measurements*, Stockholm, Centek Publ., Luleå, pp. 247–51.

Morgan, H.S. (1984) Analysis of borehole inclusion stress measurement concepts proposed for use in the Waste Isolation Pilot Plant (WIPP), in *Proc. 25th. US Symp. Rock Mech.*, Evanston, SME/AIME, pp. 212–19.

Myrvang, A.M. and Hansen, S.E. (1990) Use of the modified Doorstoppers for rock stress change measurements, in *Proc. 31st US Symp. Rock Mech.*, Golden, Balkema, Rotterdam, pp. 999–1004.

Nichols, T.C., Abel, J.F. and Lee, F.T. (1968) A solid inclusion probe to determine three dimensional stress changes at a point in a rock mass. *US Geol. Surv. Bull.*, 1258-C.

Niwa, Y. and Hirashima, K.I. (1971) The theory of the determination of stress in an anisotropic elastic medium using an instrumented cylindrical inclusion. *Mem. Faculty of Eng., Kyoto University*, Japan, **33**, 221–32.

Obert, L. and Duvall, W.I. (1967) *Rock Mechanics and the Design of Structures in Rock*, Wiley.

Panek, L.A. and Stock, J.A. (1964) Development of a rock stress monitoring station based on the flat slot method of measuring existing rock stress. US Bureau of Mines Report of Investigation RI 6537.

Pariseau, W.G. (1978) A note on monitoring stress changes in situ. *Int. J. Rock Mech. Min. Sci.*, **15**, 161–6.

Park, D.-W. (1986) Development of a new borehole stressmeter and installation tool, in *Proc. Int. Symp. on Rock Stress and Rock Stress Measurements*, Stockholm, Centek Publ., Luleå, pp. 217–25.

Patrick, W.C. (1986) Spent-fuel test-climax: an evaluation of the technical feasibility of geologic storage of spent nuclear fuel in granite. Lawrence Livermore Lab. Report UCRL-53702.

Patrick, W.C. and Rector, N.L. (1983) Reliability of instrumentation in a simulated nuclear-waste repository environment, in *Proc. Int. Symp. on Field Measurements in Geomechanics*, Zurich, Balkema, Rotterdam, pp. 1431–40.

Peng, S.S., Su, W.H. and Okubo, S. (1982) A low cost stressmeter for measuring complete stress changes in underground mining. *Geotech. Test. J.*, **5**, 50–53.

Potts, E.L.J. (1954) Stress distribution rock pressures and support loads. *Colliery Eng.*, 333–9.

Read, R.S. and Martin, C.D. (1992) Monitoring the excavation-induced response of granite, in *Proc. 33rd US Symp. Rock Mech.*, Santa Fe, Balkema, Rotterdam, pp. 201–10.

Rehbinder, G. (1984) Strains and stresses in the rock around an unlined hot water cavern. *Rock Mech. Rock Eng.*, **17**, 129–45.

Roberts, A. *et al.* (1964) A laboratory study of the photoelastic stressmeter. *Int. J. Rock Mech. Min. Sci.*, **1**, 441–57.

Roberts, A. *et al.* (1965) Some field applications of the photoelastic stressmeter. *Int. J. Rock Mech. Min. Sci.*, **2**, 93–103.

Schaller, S., McKay, J. and Hargraves, A.J. (1976) Rock pressure distribution at caved faces of Appin Colliery, in *Proc. ISRM Symp. on Investigation of Stress in Rock, Advances in Stress Measurement*, Sydney, The Institution of Engineers, Australia, pp. 55–62.

Schrauf, T. *et al.* (1979) Instrument evaluation, calibration and installation for the heater experiments at Stripa. Lawrence Berkeley Laboratory, Berkeley, California, Technical Report LBL-8313, SAC-25, UC-70.

Sellers, J.B. (1970) The measurement of rock stress changes using hydraulic borehole gages. *Int. J. Rock Mech. Min. Sci.*, **7**, 423–35.

Sellers, J.B. (1977) The measurement of stress change in rock using the vibrating wire stressmeter, in *Proc. Symp. on Field Measurements in Rock Mechanics*, Zurich, Balkema, Rotterdam, Vol. 1, pp. 275–88.

Skilton, D. (1971) Behavior of rigid inclusion stressmeters in viscoelastic rock. *Int. J. Rock Mech. Min. Sci.*, **8**, 283–9.

Spathis, A.T. (1988) A biaxial viscoelastic analysis of hollow inclusion gauges with implication for stress monitoring. *Int. J. Rock Mech. Min. Sci. & Geomech. Abstr.*, **25**, 473–7.

St John, C.M. and Hardy, M.P. (1982) Geotechnical monitoring of high-level nuclear waste repository performance, in *Proc. 23rd US Symp. Rock Mech.*, Berkeley, SME/AIME, pp. 846–54.

Swolfs, H.S. and Brechtel, C.E. (1977) The direct measurement of long-term stress variations in rock, in *Proc. 18th. US Symp. Rock Mech.*, Golden, Johnson Publ., pp. 4C5-1–4C5-3.

Swolfs, H.S. and Walsh, J.B. (1990) The theory and prototype development of a stress-monitoring system. *Seism. Soc. Am. Bull.*, **80**, 197–208.

Teufel, L.W. and Farrell, H.E. (1990) In situ stress and natural fracture distribution in the Ekofisk field, North Sea. Sandia National Labs Report No. SAND-90-1058C.

Tunbridge, L.W. and Oien, K. (1987) The advantages of vibrating wire instruments in geomechanics, in *Proc. 2nd Int. Symp. on Field Measurements in Geomechanics*, Kobe, Balkema, Rotterdam, pp. 3–15.

Walton, R.J. and Worotnicki, G. (1986) A comparison of three borehole instruments for monitoring the change of rock stress with time, in *Proc. Int. Symp. on Rock Stress and Rock Stress Measurements*, Stockholm, Centek Publ., Luleå, pp. 479–88.

Wilson, A.H. (1961) A laboratory investigation of a high modulus borehole plug gage for the measurement of rock stress, in *Proc. 4th US Symp. Rock Mech.*, University Park, Pennsylvania State University Publ., pp. 185–95.

Wold, M.B. and Pala, J. (1986) Three dimensional stress changes in pillars during longwall mining at Ellalong colliery. CSIRO Division of Geomechanics, Coal Mining Report No. 65.

Worotnicki, G. (1993) CSIRO triaxial stress measurement cell, in *Comprehensive Rock Engineering* (ed. J.A. Hudson), Pergamon Press, Oxford, Chapter 13, Vol. 3, pp. 329–94.

Zimmerman, R.M. (1982) Issues related to field testing in tuff, in *Proc. 23rd US Symp. Rock Mech.*, Berkeley, SME/AIME, pp. 872–80.

THE STATE OF STRESS IN THE EARTH'S CRUST: FROM LOCAL MEASUREMENTS TO THE WORLD STRESS MAP

11

The last 30 years have seen a major advance in our knowledge of *in situ* stresses in rock. A large body of data on the state of stress in the near-surface part of the Earth's crust (upper 4–5 km of the crust) is now available. Regional stress data from various continents have been collected in separate databases and later compiled into a worldwide database. The first part of this chapter deals with the organization and database of the World Stress Map Project, and the 'big picture' of the state of stress in the Earth's crust. The second part of this chapter deals with the effect of scale on *in situ* stresses and *in situ* stress measurements, and the relationship between local stress measurements and the global stress field.

11.1 THE WORLD STRESS MAP

The World Stress Map (WSM) Project is a 'global cooperative effort to compile and interpret data on the orientation and relative magnitudes of the contemporary *in situ* tectonic stress field in the Earth's lithosphere' (Zoback, 1992). The project was initiated in 1986 under the auspices of the International Lithosphere Program and involves more than 30 scientists from about 20 different countries who have been responsible for a systematic compilation of available stress data in their respective geographical regions. The main focus of the project has been the characterization of the state of stress within lithospheric plates. In 1992, over 7300 data points had been compiled in a digital database. The data are available on floppy disk from: NOAA, World Data Center A, 315 Marine Drive, Boulder, CO 80220, USA. In this section we present an overview of the WSM database, and a summary of the major stress patterns in the Earth's crust that have been proposed by Zoback *et al.* (1989), Zoback (1992) and others. More detailed information about the WSM can be found in the papers by Zoback *et al.* (1989) and Zoback (1992).

It should be clear to the reader that most of the data in the WSM database have been collected in the continental part of the Earth's crust. Data from the oceanic part of the Earth's crust are still sparse, except for the North Sea as reported recently by Fejerskov *et al.* (1995), where there exists a good data compilation.

11.1.1 THE WSM DATABASE

The stress data in the WSM are compiled in a digital database. All information regarding stress orientation (such as number of determinations, mean, standard deviation and depth range) is complete. On the other hand, detailed stress magnitude information is not compiled. Stress values at maximum depth and/or stress gradient with depth are sometimes given. Clear changes in stress orientation with depth are also recorded in the database. It is noteworthy that the WSM database complements several more complete regional databases, a list of which can be found in Zoback (1992).

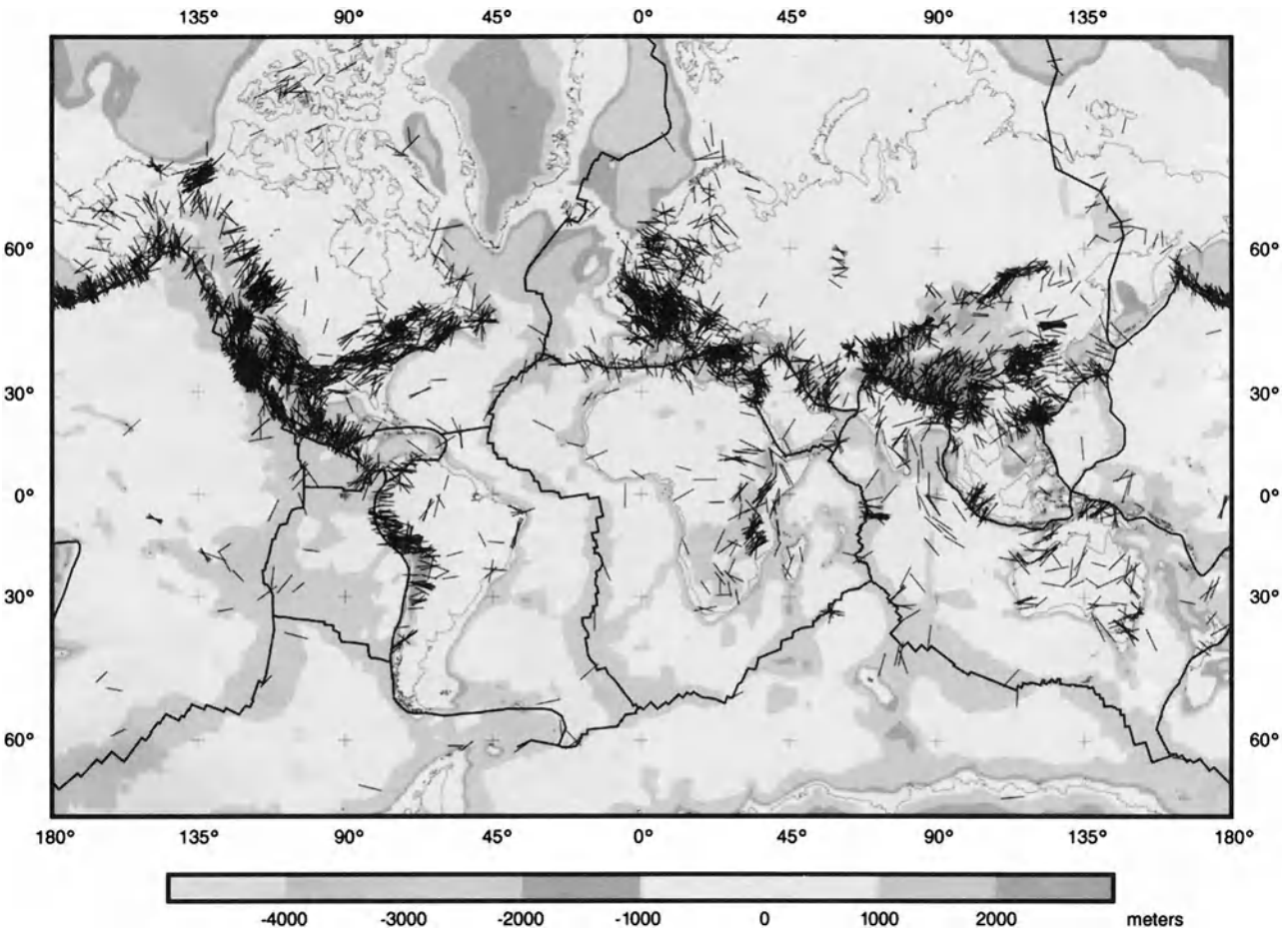

Fig. 11.1 World stress map: orientations of S_{Hmax} plotted on a base of average topography. Line length of data proportional to quality (A–C data plotted, see Table 11.1). The scale at the bottom gives the average topography elevation (in meters relative to sea level). (After Zoback, 1992.)

Table 11.1 Quality ranking system for stress orientations (after Zoback, 1992)

A	*B*	*C*	*D*	*E*
		Focal mechanism (FM)		
Average *P* axis or formal inversion of four or more single-event solutions in close geographical proximity (at least one event $M \geq 4.0$, other events $M \geq 3.0$)	Well-constrained single-event solution ($M \geq 4.5$) or average of two well-constrained single-event solutions ($M \geq 3.5$) determined from first motions and other methods (e.g. moment tensor waveform modeling or inversion)	Single-event solution (constrained by first motion only, often based on author's quality assignment) ($M \geq 2.5$) Average of several well-constrained composites ($M \geq 2.0$)	Single composite solution Poorly constrained single-event solution Single-event solution for $M < 2.5$ event	Large historic event with no reliable focal mechanism Event with *P*-, *T*-, *B*-axes all plunging 25°–40° Event with *P*- and *T*-axes both plunging 40°–50°
		Wellbore breakout (IS-BO)		
Ten or more distinct breakout zones in a single well with s.d. $\leq 12°$ and/or combined length > 300 m Average of breakouts in two or more wells in close geographical proximity with combined length > 300 m and s.d. $\leq 12°$	At least six distinct breakout zones in a single well with s.d. $\leq 20°$ and/or combined length > 100 m	At least four distinct breakouts with s.d. $< 25°$ and/or combined length > 30 m	Less than four consistently oriented breakouts or < 30 m combined length in a single well Breakouts in a single well with s.d. $\geq 25°$	Wells in which no reliable breakouts detected Extreme scatter of orientations, no significant mean determined (s.d. $> 40°$)
		Hydraulic fracture (IS-HF)		
Four or more hydrofrac orientations in a single well with s.d. $\leq 12°$, depth > 300 m Average of hydrofrac orientations for two or more wells in close geographical proximity, s.d. $\leq 12°$	Three or more hydrofrac orientations in a single well with s.d. $< 20°$ Hydrofrac orientations in a single well with $12° <$ s.d. $\leq 25°$	Hydrofrac orientations in a single well with $20° <$ s.d. $< 25°$; distinct hydrofrac orientation change with depth, deepest measurements assumed valid One or two hydrofrac orientations in a single well	Single hydrofrac measurement at < 100 m depth	Wells in which only stress magnitudes measured, no information on orientations

Table 11.1 *Continued*

A	*B*	*C*	*D*	*E*
		Petal centerline fracture (IS-PO)		
		Mean orientation of fractures in a single well with s.d. $< 20°$		
		Overcore (IS-OC)		
Average of consistent (s.d. $\leq 12°$) measurements in two or more boreholes extending more than two excavation radii from the excavation wall and far from any known local disturbances, depth > 300 m	Multiple consistent (s.d. $< 20°$) measurements in one or more boreholes extending more than two excavation radii from excavation well, depth > 100 m	Average of multiple measurements made near surface (depth > 5–10 m) at two or more localities in close proximity with s.d. $\leq 25°$ Multiple measurements at depth > 100 m with $20° <$ s.d. $< 25°$	All near-surface measurements with s.d. $> 15°$, depth < 5 m All single measurements at depth Multiple measurements at depth with s.d. $> 25°$	Multiple measurements at a single site or locality with no significant mean (s.d. $> 40°$)
		Fault slip (G-FS)		
Inversion of fault-slip data for best-fitting mean deviatoric stress tensor using Quaternary age faults	Slip direction on fault plane, based on mean fault attitude and multiple observations of the slip vector; inferred maximum stress at 30° to fault	Attitude of fault and primary sense of slip known, no actual slip vector	Offset core holes Quarry pop-ups Postglacial surface fault offsets	Not compiled
		Volcanic vent alignment[a] *(G-Va)*		
Five or more Quaternary vent alignments or 'parallel' dikes with s.d. $\leq 12°$	Three or more Quaternary vent alignments or 'parallel' dikes with s.d. $< 20°$	Single well-exposed Quaternary dike Single alignment with at least five vents	Volcanic alignment inferred from less than five vents	Not compiled

s.d. = standard deviation.

[a] Volcanic alignments must be based, in general, on five or more vents or cinder cones. Dikes must not be intruding a regional joint set.

Six types of geological and geophysical data grouped into four different categories are used in the WSM as reliable indicators of horizontal tectonic stress orientation: earthquake focal mechanisms, borehole breakouts, *in situ* stress measurements by overcoring and hydraulic fracturing, and young (mostly Quaternary) geological deformation features such as fault slip and volcanic vent alignments. Throughout the WSM Project, it is assumed that the vertical and horizontal stresses are principal stresses and that the orientation of the stress field is therefore defined by the azimuth of the maximum horizontal stress S_{Hmax}.

A quality ranking system was developed to assist in the analysis of the WSM data. Five qualities are used, ranked in the order A > B > C > D > E. The quality ranking scheme is presented in Table 11.1. The ranking criteria include the accuracy of the measurements, the number of determinations, the depth interval and volume of rock sampled, and the general reliability of the particular method as a tectonic stress indicator. For earthquake focal mechanisms, the ranking depends also on the earthquake magnitude, with a higher quality ranking assigned to larger earthquakes.

In general, the A quality data are believed to record the orientation of the horizontal stress field to within ± 10–15°, the B quality data to within ± 15–20° and the C quality data to within ± 25°. The D quality data are considered to give questionable stress orientations and the E quality data yield no reliable information regarding principal stress orientation. In cases where there is a definite change in stress orientation with depth, the deeper data are given a higher-quality ranking.

As of December 1991, of 7328 stress data compiled as part of the WSM Project, 1141 were assigned an E quality. Of the remaining 6214 entries, 4413 were considered to yield reliable (A–C quality) information on stress orientation (Zoback, 1992). Figure 11.1 shows the 1992 version of the global stress data map based on the reliable data. In this figure, the maximum horizontal stress (S_{Hmax}) orientations obtained with the different stress measurement techniques have been plotted on a background of average topography. A more detailed map accompanying the paper of Zoback (1992) is also available in which various colors and symbols are used to represent the ranking system and the different types of data and stress regimes.

The distribution of the reliable data in the WSM database by type of stress indicator is shown in Fig. 11.2 and their distribution with depth is presented in Fig. 11.3.

(a) Earthquake focal plane mechanisms

As shown in Fig. 11.2, focal mechanism data represent a large proportion (54%) of the WSM data. In general, they provide valuable information on the stress regime and the relative magnitude of the principal stresses. The advantage of using well-constrained earthquake focal plane mechanisms to map the tectonic stress field is that earthquakes record stress-induced deformation at mid-crustal depths ranging from about 5 to 20 km (and even deeper), and also involve relatively large volumes of rock. It is important to keep in mind that focal plane mechanisms record deformation and not stress. Also, as discussed in section 2.14.2, for an individual earthquake the actual stress orientation producing slip

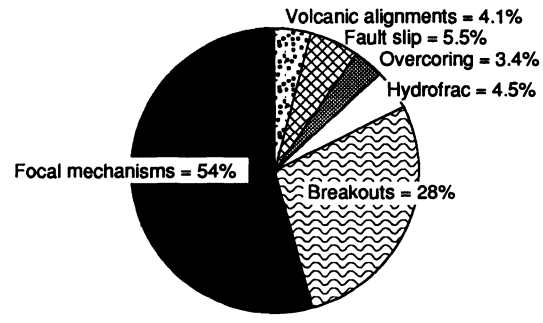

Fig. 11.2 Distribution of reliable (A–C quality) data in WSM database by type of stress indicator. (After Zoback, 1992.)

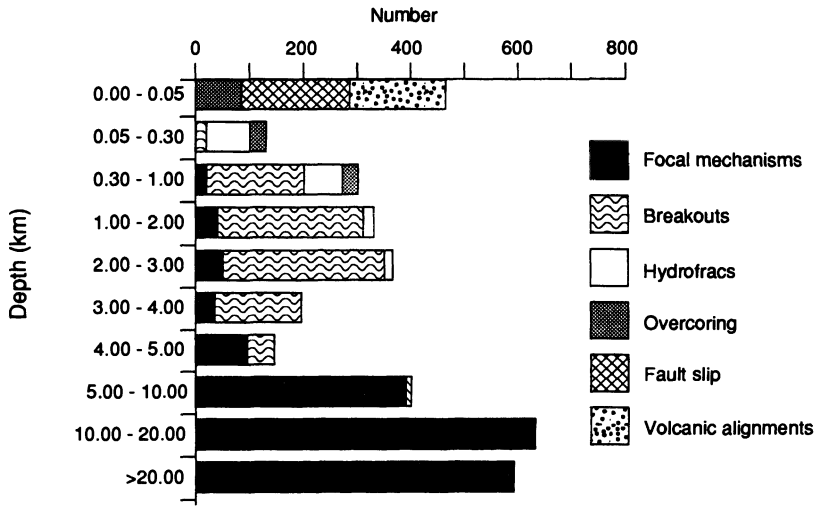

Fig. 11.3 Depth distribution of reliable WSM data. (After Zoback, 1992.)

along a fault may differ from the orientation of the *P*- and *T*-axes. This is the reason why no single-event focal mechanism receives an A quality ranking in the WSM database, regardless of the magnitude of the event and whether it is well constrained or not.

As shown in Table 11.1, the A quality ranking is reserved for stress directions determined from mean *P*- or *T*-axis orientations or inversions for best-fitting stress axes of groups of moderate-sized earthquakes (at least one event with magnitude larger than 4.5) occurring within close geographical proximity, and with a variety of focal mechanisms. Well-constrained mechanisms with B quality ranking are generally available for large magnitude earthquakes, and for those single events with magnitudes larger than 4.5–5.0. Well-constrained focal mechanisms may be available for smaller-magnitude earthquakes in areas of a dense seismic network and detailed crustal structure and velocity information. Single-event mechanisms constrained by body waves from a sparse regional seismic network are given a C rating. Composite focal mechanisms for local diffuse seismicity and/or aftershocks, and single events of small magnitude less than 2.5 are given a D rating.

(b) Fault-slip data

The inversion methods for fault-slip data are essentially the same as those used for focal plane mechanism data and, in both cases, yield principal stress orientations that are generally well constrained. As discussed in section 2.14.1, by recording the orientation and direction of motion of slickenside lineations on a given population of non-parallel fault planes, it is possible to determine the stress field responsible for those lineations. No assumption is made concerning the orientation of the fault planes with respect to the stress axes, so that reactivated faults are accounted for along with newly created ones. A more complex method of analysis of heterogeneous data sets, which allows one to distinguish between successive faulting events is discussed by Angelier (1984).

For the fault-slip technique to work well, it is necessary to document slip directions of similar age on non-parallel fault surfaces of varied orientation at a given location. The most significant limitation of this method is the assumption that all the slickensides in the fault population are related to a given and uniform, but unknown, stress tensor. Further,

all fault motions are assumed to be independent and there is no fault interaction. A final concern is that fault-slip observed at or near the ground surface may only represent the near-surface response to deeper slip events.

As indicated in Table 11.1, the highest-quality ranking of fault-slip data in the WSM database is reserved for inversions of fault striations on fault planes with a variety of attitudes. The slip vectors and mean attitudes of fault planes for historic or prehistoric events are treated as paleofocal mechanisms and are given a B quality. In cases where several tectonic events are recorded at a given outcrop or region, only the youngest event is inserted into the database. The B quality data imply using multiple observations of slip vectors within a major fault zone to define a mean fault attitude and fault vector. The C quality data provide a less accurate estimate of stress orientation, using only the strike of young faults and the primary sense of offset (but not the actual slip vector) on an active fault plane. Data that fall into the D category include offset boreholes along road cuts and surficial post-glacial pop-ups, and offsets of faults in quarries. Stress directions inferred from the trends of joints and joint sets are not considered in the WSM database.

(c) Volcanic vent alignments

As discussed in section 2.14.1, volcanic feeder vents such as dikes and cinder cones tend to propagate perpendicular to the minimum principal far-field stress as natural large-scale hydraulic fracturing experiments. Thus the mean strike of vertical dikes should correspond to the direction of the maximum horizontal stress S_{Hmax}. In order to determine the current state of stress, one must use feeder vents of young age, preferably of Quaternary age; however, paleostresses can similarly be studied using older dikes or cinder cones that are radiometrically dated.

All the data related to volcanic vent alignments included in the WSM database have been dated as Quaternary in age either radiometrically or based on field relationships. Table 11.1 indicates that five or more parallel dikes or cinder cones are given an A quality ranking if the standard deviation of their orientation is less than 12°. In the case of three or more, or less parallel features, a B quality rating is given. The C quality rating is reserved for single well-exposed dikes and single alignments with at least five vents. Finally, the D rating is given for volcanic alignments inferred from less than five vents.

(d) Overcoring stress measurements

As discussed in Chapter 5, overcoring is a well-established technique for determining the state of stress in the Earth's crust. According to Zoback *et al.* (1989), there are two primary drawbacks with this technique which restrict its usefulness as a tectonic stress indicator. First, many measurements have been made near a free surface or close to the ground surface where local topography, rock anisotropy and natural weathering and fracturing might have influenced the recordings. Second, many of these measurements have been made specifically for engineering applications (e.g. tunneling, dam construction and mining) where nearby excavations and related fracturing could perturb the regional stress field.

For all the above reasons, a conservative quality ranking is used when using overcoring data in the WSM database. The D quality ranking is given to all near-surface (< 5–10 m) stress relief measurements. For stress relief measurements made at depths larger than 10 m (or at least one excavation diameter away from the free surface of an opening), the assigned data quality depends on the internal consistency of multiple measurements (Table 11.1). For instance, in Fennoscandia the overcoring data believed to have been influenced by overlying or adjacent excavations in mines or underground chambers are simply not included in the WSM database (Stephansson *et al.*, 1987).

(e) Hydraulic fracturing stress measurements

As discussed in Chapter 4, hydraulic fracturing can be used to measure *in situ* stresses at large depths now reaching 6–9 km (Te Kamp, Rummel and Zoback, 1995). According to Zoback *et al.* (1989), since many of the hydraulic fracturing tests are conducted for engineering purposes, the reliability of the test results to record tectonic stress fields must be evaluated in terms of local site conditions. If this information is not valid, a conservative approach is followed and stress orientations obtained by hydraulic fracturing (for purely engineering studies) are given a D quality rating. As shown in Table 11.1, the highest quality rating, A, for stress orientation requires four or more hydrofrac orientations in a single well with a standard deviation $\leq 12°$ at a depth > 300 m, or alternatively the average of the hydrofrac orientations for two or more wells in close geographical proximity with a standard deviation $\leq 12°$.

(f) Borehole breakouts

Borehole breakouts represent 28% of the WSM database (Fig. 11.2). In addition, the technique probably has the greatest potential for producing new stress orientation data. Breakout data are important for the WSM compilation because they generally sample a depth interval (1–4 km or even deeper, up to 5–6 km) intermediate between the earthquake focal plane mechanisms and the *in situ* stress measurements and near-surface geological observations (Fig. 11.3). They also provide a large number of observations of stress orientation over considerable depth ranges which allows statistical determination of orientation and the scatter about the mean. Statistical analyses of breakout data recorded with borehole televiewers and formation microscanners are of great importance (Barton, Zoback and Burns, 1988) since these instruments generate detailed breakout information. Breakout ranking in Table 11.1 depends largely on the number and combined length of breakouts observed in a single well (or in wells in close proximity), and on the average and standard deviation of the breakout orientation.

11.1.2 DETERMINATION OF STRESS REGIMES AND GLOBAL STRESS PATTERNS

Various analyses of the WSM database have enabled Zoback *et al.* (1989) and Zoback (1992) to draw some general conclusions regarding stress patterns and stress regimes in the Earth's crust. The stress regimes are defined using the model of Anderson (1951), based on the relative magnitude of the vertical stress S_v and the maximum and minimum horizontal stresses S_{Hmax} and S_{hmin}, respectively. The three major stress regimes include (1) the normal faulting stress regime with $S_v > S_{Hmax} > S_{hmin}$, (2) the strike-slip faulting stress regime with $S_{Hmax} > S_v > S_{hmin}$ and (3) the thrust or reverse faulting stress regime with $S_{Hmax} > S_{hmin} > S_v$. These stress regimes and their respective body-wave focal plane mechanisms are shown in Fig. 11.4. In addition to those three basic regimes, Zoback *et al.* (1989) and Zoback (1992) consider transitional stress regimes such as $S_v \approx S_{Hmax} > S_{hmin}$, which produces a combination of normal and strike-slip faulting, and $S_{Hmax} > S_{hmin} \approx S_v$, which produces a combination of strike-slip and thrust faulting.

The mean stress directions and dominant stress regimes for different clusters of data in the WSM database have been plotted by Zoback (1992) and are presented in Fig. 11.5. The arrow size on this figure represents a subjective assessment of quality related to the degree of uniformity of stress orientation and also to the quantity and density of data (see caption of Fig. 11.5).

One of the major conclusions derived from the analysis of the WSM database (and from Figs 11.1 and 11.5) is that broad regions within the interior of many plates of the Earth's lithosphere are characterized by uniformly oriented ($\pm 15°$) and consistently oriented (for

different types of stress indicators and depths) horizontal stress fields. Uniformity in stress orientation has been found in continental regions over distances of up to 5000 km. This regional consistency allows the definition of broad-scale regional stress provinces, also called 'first-order' stress provinces by Zoback (1992). Regions of very uniform horizontal stress orientation include, for instance, eastern North America, the western Canadian Basin, central California, the Andes, western Europe, the Aegean and northeastern China.

Another conclusion derived from the WSM is that most mid-plate or intraplate continental regions are dominated by compressive stress regimes (thrust or a combination of thrust and strike-slip faulting) in which one or both of the horizontal stresses are greater than the vertical stress. On the other hand, continental extensional stress regimes (normal or combined normal and strike-slip faulting), in which the maximum principal stress is vertical, generally occur in topographically high areas.

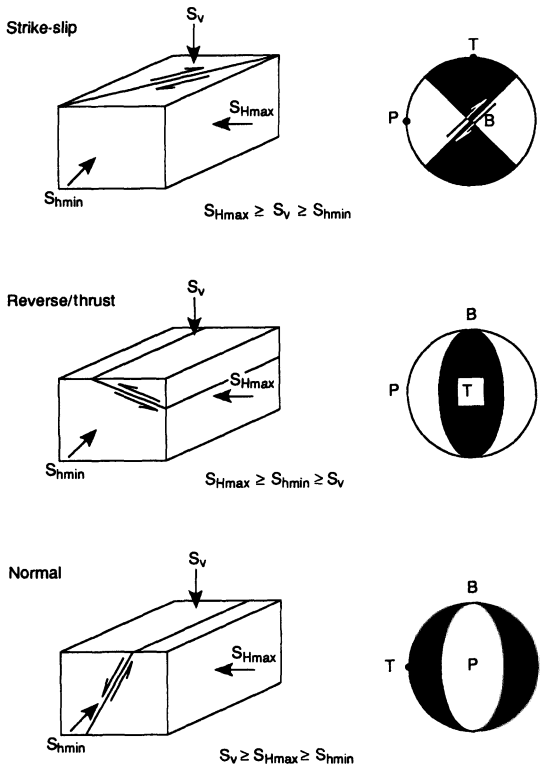

Fig. 11.4 Definition of style of faulting and state of stress, related slip vectors and *P*-, *T*- and *B*-axes. (After Anderson, 1951.)

Correlation between regional intraplate stress orientations and both absolute and relative plate motions has been noted by several authors such as Sbar and Sykes (1973) and later by Zoback and Zoback (1980) for North America, and by Müller *et al.* (1992) for Europe. This observation was reinforced at a larger scale by Zoback *et al.* (1989) and Zoback (1992), who found some correlation between the measured S_{Hmax} orientations and the azimuths of absolute plate velocity predicted with the AM-2 model of Minster and Jordan (1978). This correlation is shown in Fig. 11.5 where plate movements are indicated by thin lines. The correlation has been found to be (1) strong for mid-plate North America and the South American plate, (2) good for western Europe except for the Aegean, and (3) weak for the Pacific plate, much of Asia, the Indian-Australian plate, the African plate and the US Cordillera.

Zoback *et al.* (1989) and Zoback (1992) concluded that the most probable sources of uniform broad-scale stress fields in the lithosphere are the broad-scale forces that either drive or resist plate motion, including slab pull, ridge push, collisional resistance, trench suction and basal drag (Fig. 2.29). The regional stress field (first-order stress pattern) can be perturbed locally by various local phenomena due to a variety of forces acting on the lithosphere and to even more local effects or perturbations related to topography, anisotropy, heterogeneities, erosion, artificial excavation and major faults or shear zones. These more local stresses create so-called 'second-order' stress patterns (Zoback, 1992).

Intraplate areas of active extension are generally associated with regions of high topography, e.g. the high Andes, western US Cordillera, Tibetan plateau and South Africa.

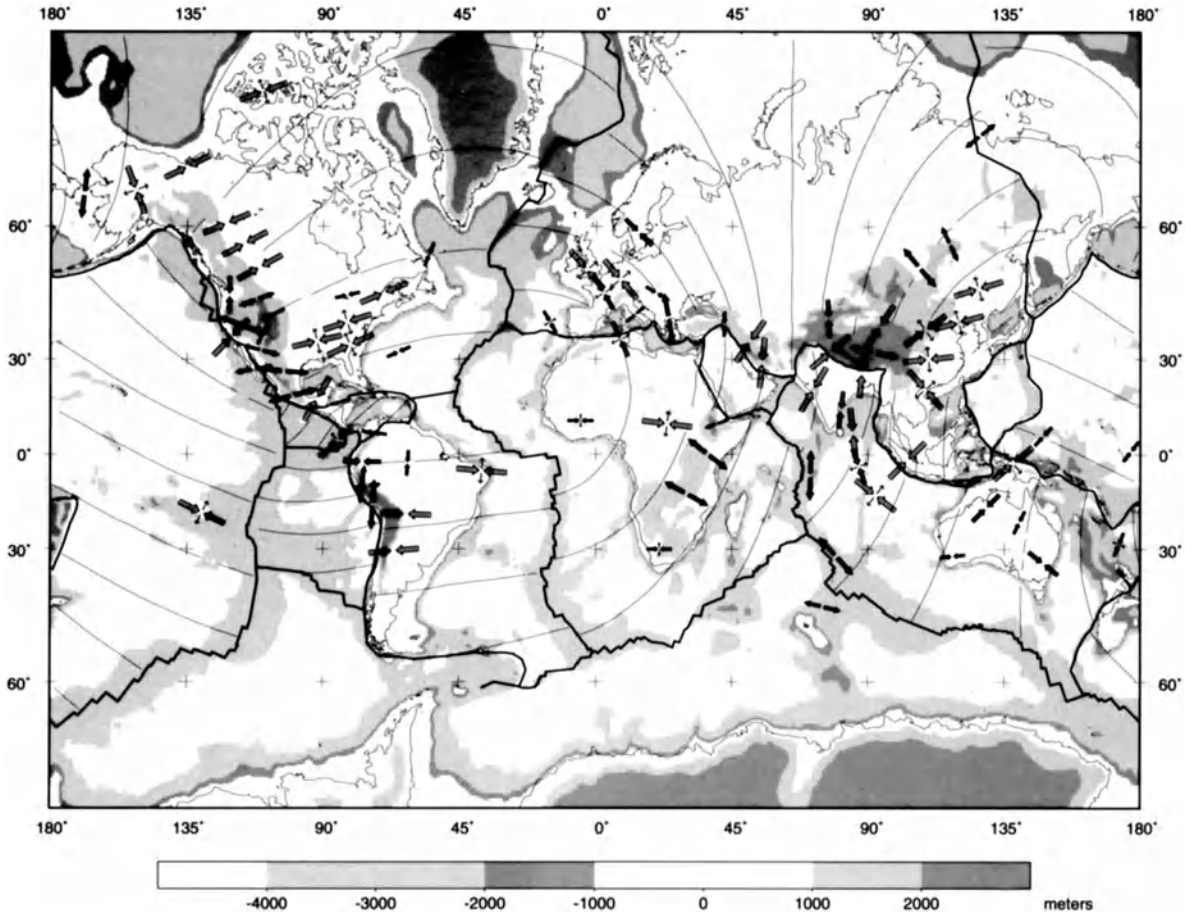

Fig. 11.5 Generalized stress map, mean stress directions based on averages of clusters of data shown in Fig. 11.1. Thin lines indicate absolute velocity trajectories for individual plates based on the AM-2 model of Minster and Jordan (1978). A single set of thick inward-pointing arrows indicates S_{Hmax} orientations in thrust faulting stress regime ($S_{Hmax} > S_{hmin} > S_v$). A single set of outward-pointing arrows indicates S_{hmin} orientations in a normal faulting regime ($S_v > S_{Hmax} > S_{hmin}$). Strike-slip faulting stress regime ($S_{Hmax} > S_v > S_{hmin}$) is indicated by thick inward-pointing arrows (S_{Hmax} direction) and thin outward-pointing arrows (S_{hmin} direction). Symbol sizes in all cases are proportional to the number and consistency of data orientation averaged. The scale at the bottom gives the average topography elevation (in meters relative to sea level). (After Zoback, 1992.)

The extension is believed to be due to buoyancy forces which are responsible for some of the largest local perturbations that have been identified in the data of the WSM database. Second-order stress patterns can also be associated with specific geological or tectonic features such as lithospheric flexure and lateral strength contrasts, as well as lateral density contrasts which give rise to buoyancy forces (see local tectonic stresses in Fig. 2.29). Second-order stresses of flexural type are likely to be generated by sediment loading on continental margins (Stein *et al.*, 1989) and glacial rebound from former glaciations (Gregersen, 1992; Müller *et al.*, 1992; Stephansson, 1988). Regional stress fields globally show numerous examples of stress patterns related to lateral density anomalies, many of which are related to compensate variations in topography. The presence of thin crust and upwelling hot mantle material in the East African rift, Baikal rift and the western US Cordillera causes stress refraction and anomalies compared with the first-order global stress pattern (Zoback, 1992). Crustal contrast at ocean/continent boundaries (Bott and Dean, 1972), lateral variation in crustal strength (Mount and Suppe, 1992; Zoback *et al.*, 1987), crustal inhomogeneities such as thick cratonic lithosphere (Kusznir and Bott, 1977), and orogenic belts (Evans, 1989; Müller *et al.*, 1992) are examples of perturbations that generate second-order stress patterns.

Lateral variations in crustal strength associated with major faults can sometimes dominate first-order stress patterns. The best and largest example is the stress refraction observed adjacent to the San Andreas right-lateral strike-slip fault in California. Based on a number of stress indicators and rock stress measurements, Zoback *et al.* (1987) were able to demonstrate that the direction of maximum horizontal compressive stress in western California is not at an angle of about 30° to 40° to the strike of the San Andreas fault (as expected from frictional faulting theory), but is oriented nearly orthogonal to the strike of the fault (Fig. 11.6). At a distance from the fault area toward the northwest, the stress state is aligned with the stress field for central-eastern California. It has been proposed that the fault-normal crustal compression in central-west California is the result of the extremely low shear strength of the San Andreas fault (weak fault concept) and the slightly convergent relative motion between the Pacific and North American plates. The assumed low shear strength of the fault agrees with the normal conductive heat flow data recorded in shallow boreholes near the San Andreas fault, and *in situ* stress measurements reported by Zoback and Healy (1992) in a 3.5 km deep borehole drilled adjacent to the fault at the Cajon Pass drill site (section 9.5.3).

11.1.3 BRIEF SUMMARY OF STRESS PATTERNS IN CONTINENTS

Regional patterns of currently active tectonic stress are primarily used to evaluate the forces acting on the lithosphere and to investigate intraplate seismicity. However, the data in the WSM database and related maps are well suited to obtain a first impression of the state of stress in the area of an engineering project. Below is a brief description of the state of stress in the major continents as they are known today.

(a) North America

A version of the WSM for North America is shown in Fig. 11.7 and summarized in Table 11.2. The general observation about the state of stress in North America is that it is compressional throughout most of the plate (Zoback and Zoback, 1980, 1991). The primary evidence for this is the fact that earthquake focal plane mechanisms range between strike-slip and reverse faulting throughout the interior of North America. Thus here the stress field is uniform roughly 5000 km in both the E–W and N–S directions. Extensional states of stress are restricted to the western Cordillera, the Texas–Louisiana Gulf Coast, the Aleutian arc and a few intraplate basins (Table 11.2).

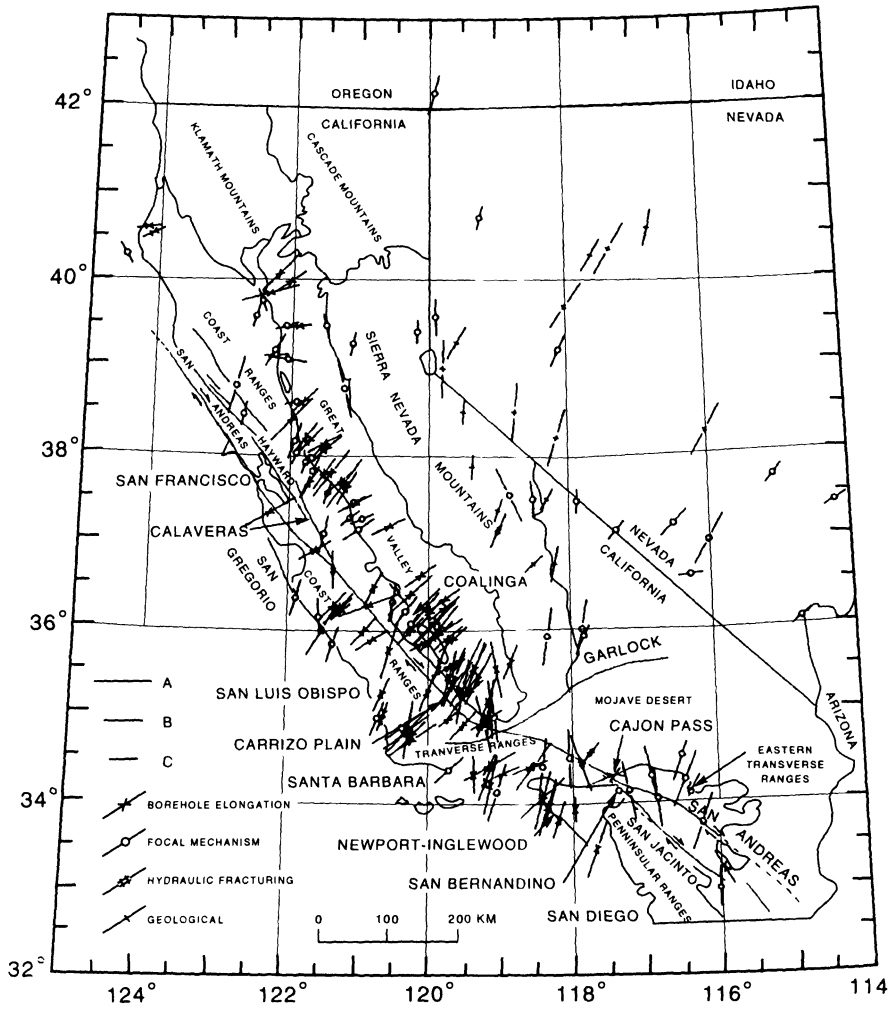

Fig. 11.6 Generalized geological map of California with data points showing the direction of maximum horizontal compression in the crust. The length of the bars attached to each data point is a measure of its quality (A, B or C as defined in Table 11.1). The symbol associated with each data point indicates the type of stress indicator. No focal mechanisms from earthquakes directly on the San Andreas or major, right-lateral strike-slip subsidiary faults are included. (After Zoback *et al.*, 1987.)

Within the Mid-plate stress province in North America, at the center of each region defined by the 20° by 20° latitude and longitude grid in Fig. 11.7, the direction of absolute plate motion of North America coincides with that determined by Minster and Jordan (1978). One cannot simply interpret the generally good correlation between S_{Hmax} and the absolute plate motion directions in North America as proof that the state of stress results from drag forces as the plate moves over a relatively stable asthenosphere (Zoback *et al.*, 1989). It is not possible at this time to say with certainty whether a push from the Mid-Atlantic ridge or a drag from the base of the plate is responsible for the state of stress in the Mid-plate province.

The Texas–Louisiana Gulf Coast stress province is characterized by an extensional state of

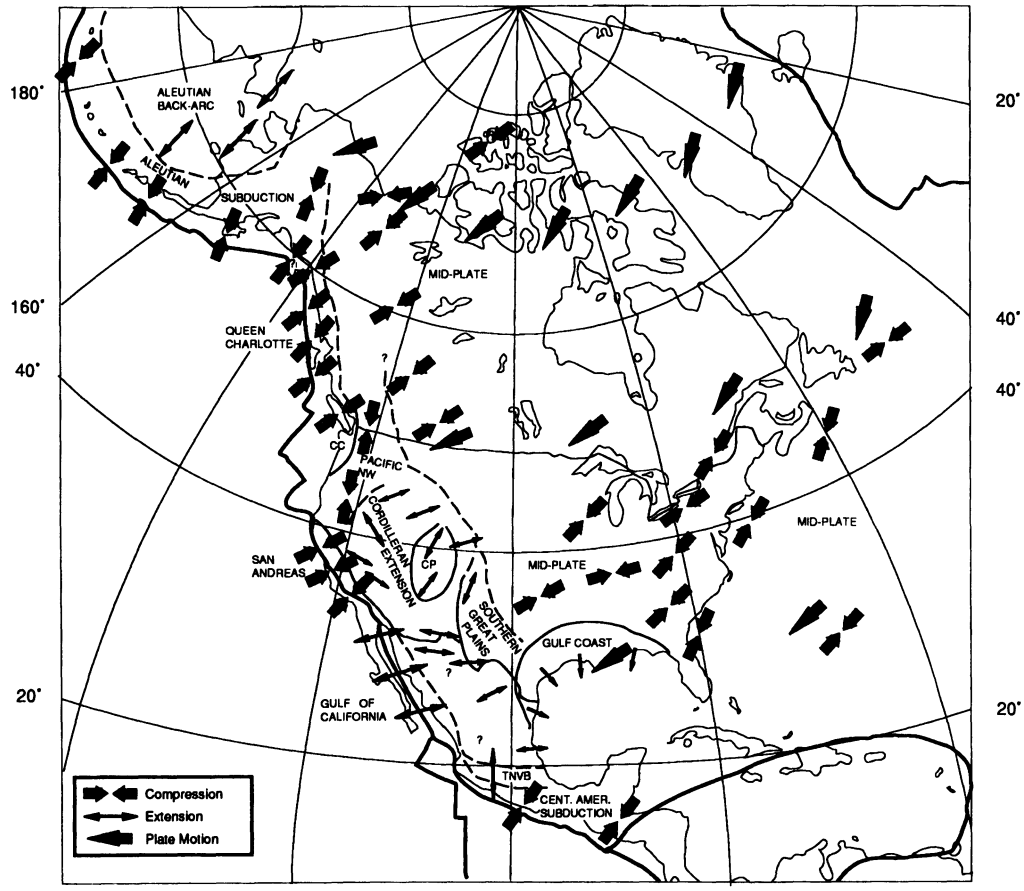

Fig. 11.7 Stress provinces of North America and plate motion. (After Zoback and Zoback, 1991.)

stress. *In situ* stress measurements and fluid pressure data from both onshore and offshore boreholes of the Gulf Coast have been used to show that the state of stress within the sedimentary basin is controlled by the frictional strength of the many normal faults in the area. To what degree the underlying basement rocks are involved in the fault mechanisms is still unknown.

As shown in Table 11.2, six subduction-related stress provinces have been identified in North America (Zoback and Zoback, 1991). The state of stress in continental plates that are overriding the subduction zones can be divided into three distinct regions (Nakamura and Uyeda, 1980): (1) in the accretionary wedge and forearc region, the state of stress is highly compressive and thrust faulting is dominant with the direction of S_{Hmax} parallel to the direction of relative plate motion, (2) in the volcanic arc, the state of stress is typical of strike-slip faulting and the direction of S_{Hmax} is parallel to the direction of plate motion, and (3) an extensional state of stress in the back-arc region, where S_{v} is the maximum principal stress and the direction of the intermediate stress is parallel to the strike of the volcanic arc. Although it is not necessary for all three stress domains to be present in a given plate overriding a subduction zone, this general pattern has been widely observed (Nakamura and Uyeda, 1980).

Table 11.2 Stress provinces of North America (after Zoback and Zoback, 1991)

	Stress regime	*Principal stress direction*		*Remarks*
		Maximum	*Minimum*	
Plate interior provinces				
Midplate	SS/TF[a]	ENE	NNW/ Vertical	Encompasses most of intraplate North America east of US Cordillera including the western Atlantic basin. Earthquake focal plane mechanisms in southwestern Canada are predominantly thrust and those in the United States are predominantly strike-slip. Excellent correlation between direction of maximum horizontal stress with absolute plate motion direction as well as the direction of ridge push from the Mid-Atlantic ridge
Gulf Coast	NF	Vertical	SSE	Extensive gulfward extension and growth faulting within Coastal Plain sediments. State of stress in the underlying basement is not known
Cordilleran extension	NF/SS	Vertical	WNW (WSW–WNW)[b]	Broad region of variable magnitude extension including the Basin and Range, Rio Grande rift, northern Rocky Mountain and Snake River Plain regions of western United States. Extent into Canada and Mexico is uncertain. Correlative with zone of high heat flow, elevation and thin crust. Pronounced strike-slip deformation (with constant S_{hmin} direction) along western boundary of province (Walker Lane). Predominant S_{hmin} direction within the province is WNW but direction varies between WSW and WNW
Colorado plateau/ Southern, Great Plains	NF	Vertical	NNE	Unique extension direction, thicker crust and very low rate of crustal deformation distinguishes the Colorado plateau and Southern Great Plains from the surrounding Cordilleran extension province
Subduction-related provinces				
Aleutian subduction	TF/SS	NNW	Vertical/ ENE	NNW S_{Hmax} direction observed throughout most of Alaska south of the Brooks Range is consistent with the NNW direction of relative motion of the Pacific plate with respect to North America. Thrust faulting along shallow, low-angle subduction zone and within accretionary prism. Strike-slip faulting in volcanic arc. Pronounced oblique subduction in western Aleutians
Aleutian back-arc	NF	Vertical	NNW?	While poorly documented, this province may encompass most of the Bering Sea, Seward Peninsula and parts of northeasternmost Siberia. Direction of minimum horizontal compression is approximately perpendicular to the arc
Central American subduction	TF/SS	NE	Vertical/ NW	S_{Hmax} direction parallel to the direction of relative motion of Cocos plate with respect to North America
Trans-Mexican volcanic belt	NF	Vertical	N (NNE–N)	Pronounced volcanic alignments and grabens define this stress province. Calc-alkalic composition and location of volcanic belt consistent with this zone as a volcanic arc of the Central American subduction zone. Unlike most volcanic arcs, however, the S_{Hmax} direction is normal to the convergence direction rather than parallel to it
Cascade convergence	TF	NE	Vertical	Poorly defined, this province is based on ~ 10 earthquakes in Vancouver Island and sparse breakout data in western Washington and Oregon. The NE S_{Hmax} direction distinguishes the province from the Pacific Northwest province to the east. Apparent S_{Hmax} direction is $\sim 30°$ oblique to convergence direction of the Juan de Fuca plate, suggesting a weak coupling between the state of stress in the North American plate and subduction of the Juan de Fuca plate

Table 11.2 *Continued*

	Stress regime	*Principal stress direction*		*Remarks*
		Maximum	*Minimum*	
Subduction-related provinces–*Continued*				
Pacific Northwest	SS/TF	N	E/Vertical	N–S compression throughout this province is accompanied by strike-slip faulting in the Cascades and active folding and thrust faulting in Puget Sound and Columbia plateau. Source of this N–S compression may be movement of the Pacific plate with respect to North America, perhaps suggesting a weak coupling between the Juan de Fuca plate and North American plates
Transform-related provinces				
San Andreas	SS/TF	NE	NW/ Vertical	This province includes the San Andreas fault zone and a broad zone of crustal shortening adding to it in which S_{Hmax} is oriented at a very high angle to the strike of the fault (~ 85° in central California and ~ 70° in southern California). This is especially surprising as the direction of relative plate motion between the Pacific and North American plates in central California is only slightly convergent. The source of the near fault-normal compression direction is believed to be the result of the San Andreas, and its principal branches, having a markedly lower stress than the surrounding crust
Queen Charlotte	SS/TF	NE	NW/ Vertical	Similar to the San Andreas, the S_{Hmax} direction adjacent to the Queen Charlotte is at a high to the strike of the fault (~ 60 to 70°). However, the data set is quite sparse and based primarily on earthquake focal plane mechanisms. In addition, the Queen Charlotte is oriented obliquely to the direction of relative plate motion and thus accommodates appreciable shorting across it
Gulf of California	SS/NF	N–NW/ Vertical	E/NE	Although generally considered as a zone of mid-ocean spreading, most of the length of the Gulf of California is a transform plate boundary with spreading limited to a number of rather short segments. Geological indicators and earthquake focal plane mechanisms indicate strike-slip and normal faulting in Baja California with an S_{hmin} direction that ranges between NE (fault-normal extension) to E–W, a direction more consistent with that expected from conventional faulting

[a] NF = normal faulting; SS = strike-slip faulting; TF = thrust faulting.
[b] Directions refer to range of stress directions observed throughout a province.

Three separate transform fault-related stress provinces namely, San Andreas, Queen Charlotte and Gulf of California have been identified by Zoback and Zoback (1991). The type of stress regime, principal stress direction and remarks for each of these provinces are presented in Table 11.2. Although the strike of the San Andreas fault in central California is almost parallel to the direction of relative plate movement, the direction of S_{Hmax} is almost perpendicular to the relative plate motion direction (Fig. 11.6).

(b) South America

A compilation of lithospheric stress directions for continental South America and the inferred major patterns of the regional intraplate stress field has been presented by Assumpcao (1992). Stress orientations are based primarily on earthquake focal mechanisms and Quaternary fault slip inversion published in the literature (Fig. 11.1). Here overcoring, hydrofracturing and borehole breakout data are sparse. Although there are no data for large areas of

South America, the present WSM data should be helpful in constraining theoretical models of the plate-driving forces and increase our overall understanding of the state of stress in the Earth's crust.

In western South America, predominant N–S extensional stresses in the High Andes (S_{Hmax} being the intermediate principal stress) and E–W compressional stresses in the sub-Andes (S_{Hmax} being the major principal stress) are now well established. The orientation of the regional lithospheric S_{Hmax} field is remarkably constant and does not seem to be affected by the change of strike of the Andean mountain chain (Assumpcao, 1992). The eastern limit of the Andean E–W stress province seems to coincide with regions of very low seismicity in the Amazonian craton and in the intracratonic Paraná Basin. This may indicate that the Andean E–W stress field decreases in magnitude eastward and is replaced by stresses of different origin in the middle of the continent.

In the central Amazonian region, the distribution of epicenters and the stress data suggest a different stress regime characterized by roughly N–S compression. In northeastern Brazil, strike-slip focal mechanisms and the distribution of seismicity suggest a combination of plate-wide regional forces together with local sources of loading from sediments at the continental margin.

(c) Africa

The plate tectonic setting of Africa, surrounded by mid-ocean ridges and continental collision to the north, suggests a typical mid-plate compressional stress field. New data support this picture and suggest that intra-plate stress fields related to plate-driving forces exist outside the area of high topography (South Africa) and high heat flow (East Africa).

The WSM data within the African plate show dominantly extensional stress regime with normal faulting within the thermally elevated East African rift system. Borehole breakout studies, aligned Quaternary volcanic vents and kinematic analysis of Quaternary faults indicate that the direction of the present-day minimum horizontal stress, S_{hmin}, in Kenya is aligned approximately NW–SE and in central Sudan is nearly N–S (Bosworth, Strecker and Blisniuk, 1992). The regional pattern for S_{hmin} is therefore roughly radially disposed about the Afar plate junction. The data seem to indicate that the central East African stress field underwent a significant rotation during the Quaternary.

The existence of a region in western and north-central Africa of compressional tectonism with an approximately E–W direction of S_{Hmax} has been identified on the basis of more recent data in the WSM database (Zoback, 1992). These new data have also identified a zone of NNW compression along the northern boundary of the African plate consistent with the convergence of Africa and Eurasia (Zoback, 1992).

(d) Europe

The European Stress Data Base (ESDB) forms a subset of the WSM database (Müller *et al.*, 1992). The ESDB contains 1400 data points, including other existing compilations, e.g. the Fennoscandian Rock Stress Data Base by Stephansson *et al.* (1987), the compilation of borehole breakouts from the British islands by Klein and Barr (1986), hydraulic fracturing and hydraulic testing of pre-existing fractures by Cornet and Burlet (1992), and numerous local studies of earthquakes and the interaction of stress and tectonics listed by Müller *et al.* (1992).

From the patterns on the stress map of Europe (Figs 11.8 and 1.7), three main regions of characteristic stress orientation can be identified: (1) western Europe, with an average S_{Hmax} orientation trending NW–SE, (2) northern Europe, including Fennoscandia, with a scattered stress orientation, and (3) eastern Mediterranean (Aegean and western Anatolia), with a nearly E–W direction of

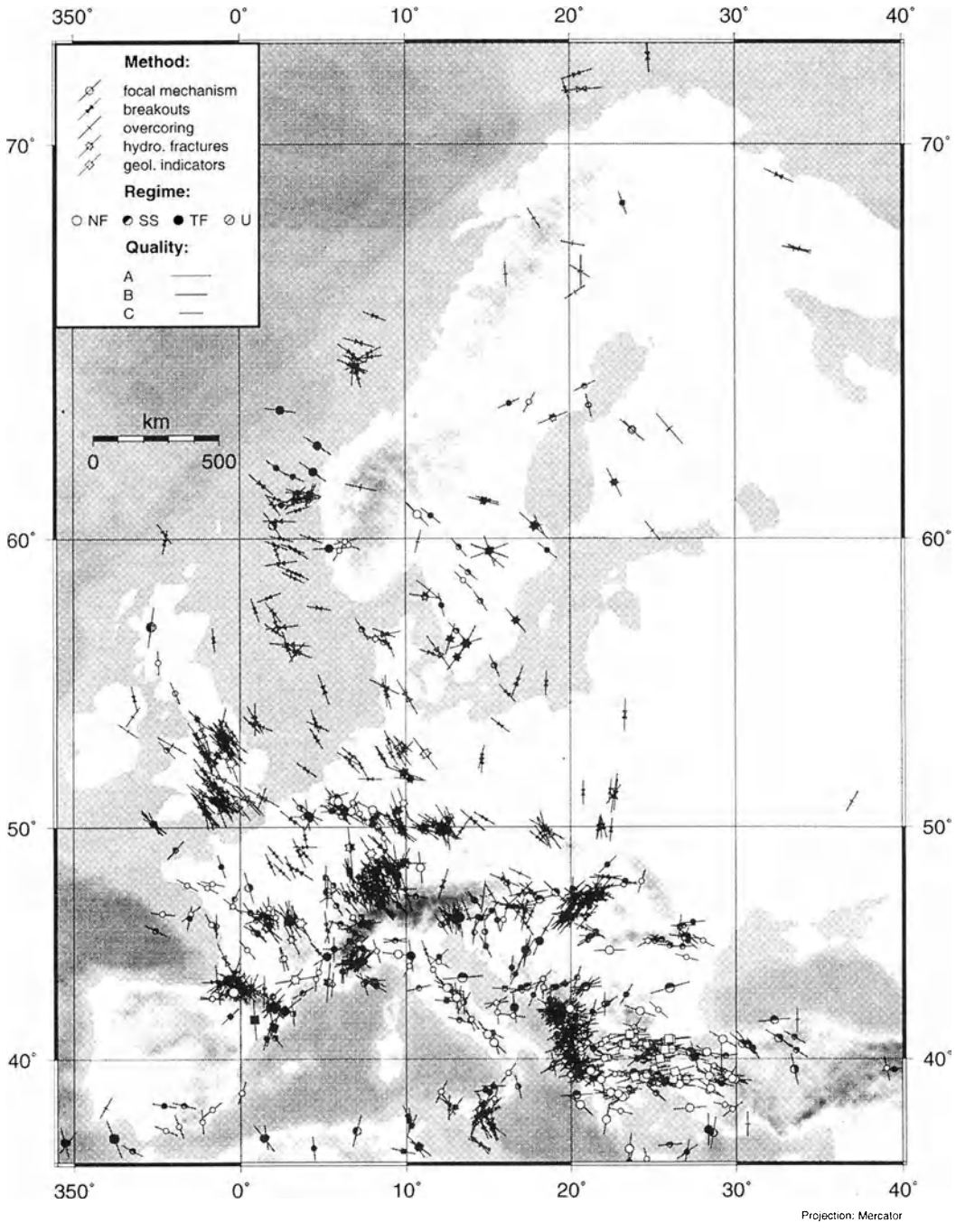

Fig. 11.8 European stress map plotted on a regional topographic base. Maximum horizontal compressive stress orientations are plotted for all data of quality categories A, B and C (Table 11.1). The length of the symbols is proportional to the quality. The different center symbols represent different types of stress indicators as defined in the key. (Courtesy of B. Müller, 1996.)

S_{Hmax}. The different stress fields can be attributed to plate-driving forces acting on the boundaries of the Eurasian plate, locally modified by lithospheric properties in different regions.

In the stress province of western Europe, the direction of maximum horizontal stress shows a uniform NW–SE direction with a mean value of N53°W ± 16°. The boundary of the stress province to the north is governed by the Ringköping–Fyn basement ridge striking WNW–ESE across southern Denmark (Ask, Müller and Stephansson, 1996). Overall, the maximum stress in western Europe is aligned with the direction of the Eurasian plate motion relative to the African plate. As pointed out by Zoback *et al.* (1989) and Müller *et al.* (1992), the uniform stress field coincides with a thin to medium thick lithosphere (50–90 km) and high heat flow ($> 80 \times 10^{-3}$ W/m^2). The persistent S_{Hmax} orientation of western Europe is only locally affected by major geological structures such as the Alps. The Rhine Graben rift system, which is another major structure, appears to have no effect on the stress orientation.

The European stress map (Fig. 11.8) shows that the stress orientation in Fennoscandia is not as consistent as in western Europe. However, there is a slight tendency for the stresses to be aligned in the NW–SE orientation at greater depth, as demonstrated from earthquake focal plane mechanisms by Slunga (1989), Bungum *et al.* (1991) and Gregersen (1992). Rock stress and rock stress problems from overcoring stress measurements in Norway have been discussed by Myrvang (1993). The ridge spreading and the associated ridge push force at the Mid-Atlantic ridge give rise to tectonic stresses, and this is assumed to be one of the contributors to the stress field in Fennoscandia. The following conditions may modify the local stress field and cause some of the observed scatter in the orientation of the principal stresses according to Stephansson (1988, 1993): (1) isostatic response from ice loading, (2) creep of crustal rocks from ice loading, (3) the effect of topography and (4) shear strength variations of faults and joints. The physical properties of geologically old shield areas, like the Fennoscandian Shield, are characterized by thick lithosphere and low heat flow. This reduces the mean stress level of the lithosphere and permits local effects due to lateral inhomogeneities in the crust such as density or strength to have an important influence on the stress field.

The maximum principal stress of the European continent is horizontal except in the Aegean Sea and western Anatolia, the Lower Rhine embayment, the Apennines and western France, where dominantly normal faulting data exist (Fig. 11.8). The E–W direction of S_{Hmax} in the Aegean Sea appears to be associated with African versus Eurasian plate movement.

(e) Indian subcontinent

A map of the orientation of S_{Hmax} in the Indian subcontinent has been prepared by Gowd, Srirama Ra and Gar (1992) using orientations derived from borehole breakouts, hydraulic fracturing and earthquake fault plane mechanisms (Fig. 11.9). Four stress provinces have been identified on the basis of regionally consistent orientations, namely (1) the midcontinent Indian province, (2) the Southern Indian Shield, (3) the Bengal Basin and (4) the Assam wedge. The midcontinental province comprises central and northern India and is characterized by NNE–ENE-oriented S_{Hmax} which is expected to arise from the net resistive forces at the Himalayan collision zone. Much of southern India appears to form the second stress province characterized by NW-oriented S_{Hmax} stresses. This orientation appears to be similar to that of the intraplate stress field prevailing in the central Indian Ocean. The third stress province in the Bengal Basin is fairly complex but shows mainly an E–W orientation of the maximum horizontal principal stress.

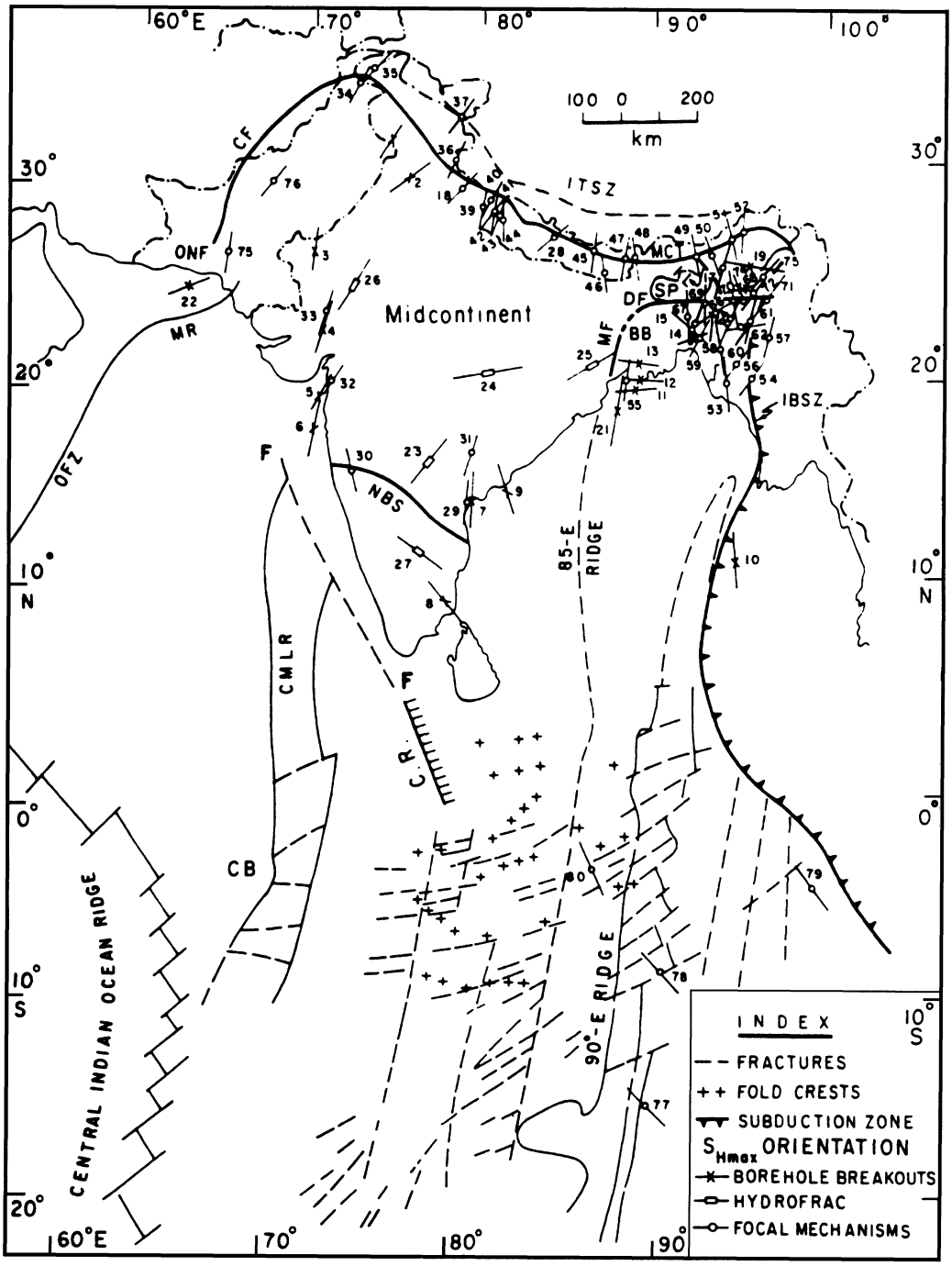

Fig. 11.9 Map of S_{Hmax} orientations in the Indian subcontinent. S_{Hmax} orientation is indicated by a line whose center symbol designates the type of stress indicator. The length of the line indicates quality of the data. Important tectonic and geodynamical features of the Indian plate are also shown on the map. (After Gowd, Srirama Ra and Gar, 1992.)

(f) Australia

The first major compilation of stress measurement data for the Australian continent was published by Worotnicki and Denham (1976). Later, Brown and Windsor (1990) made a compilation of stress data primarily based on near-surface *in situ* measurements, and reached the conclusion that the distribution of measurement sites across the continent as a whole is still too sparse to establish reliable continental or regional trends. Attempts to relate continental stress data to large-scale geological and tectonic features have been generally inconclusive. Brown and Windsor (1990) suggested that the underlying stress directions in Australia reflect those associated with the cratonization of the continent. Hence the situation in the Australian continent, as for Fennoscandia (Stephansson, 1988), Brazil (Assumpcao, 1992), Canada (Adams, 1989) and other shield areas, seems to be characterized by a large scatter in the orientation of the horizontal principal stresses in the upper part of the Earth's crust.

Zoback (1992) reported that stress patterns have been recently clarified somewhat in Australia. New breakout data and thrust faulting focal mechanisms seem to indicate that much of central and northeastern Australia experiences a compressional stress field dominated by a N–NE compression, whereas available data from both the southeastern and southwestern parts of Australia indicate an E–W compression.

(g) China

The data used to infer the present-day stress field in China come from more than 5000 small earthquakes (with a local magnitude $1 < ML < 5$) reported by Xu *et al.* (1992), a large number of *in situ* stress measurements made with overcoring and hydraulic fracturing (Li and Liu, 1986), and borehole breakout studies (Gao, Xu and Chen, 1990). The map of the *P*-axes orientation from focal plane mechanisms studied by Xu *et al.* (1992) suggests that the maximum horizontal principal compressive stress trajectories radiate from the Tibetan plateau to the northern, eastern and the southeastern parts of the mainland (Fig. 11.10). The existence of the broad-scale radial pattern of S_{Hmax} directions seems to indicate that it is quite likely that the indentor effect of plate collision between India and Asia is the driving force.

11.2 EFFECT OF SCALE ON *IN SITU* STRESSES: FACT OR FICTION?

The dependence of rock properties on the geometric dimensions of the sample is called scale effect (Cuisiat and Haimson, 1992). The role of scale on *in situ* stresses in rock needs to be addressed for three main reasons. First, stress is, by definition, a concept that applies to a point in a continuum. Second, all measuring techniques used in practice monitor the response to disturbance of a certain volume of rock (a sample) which can consist of a very large number of points (Table 3.1). The volume can be small, as with hydraulic methods and especially borehole relief methods, or quite large, as with the earthquake focal mechanism method, the under-excavation technique or the bored raise method. The larger the rock volume, the more rock discontinuities and heterogeneities can be expected to be included in that volume and to affect *in situ* stress measurements. In general, large rock volumes give average values of the *in situ* stress field and tend to eliminate the effect of local rock mass irregularities on the stress measurements. On the other hand, small-scale measurements provide a more detailed description of the *in situ* stress field. The rock volume involved in stress measurements defines the stress measurement scale.

A third reason for addressing the problem of scale when dealing with *in situ* stresses is that stress measurements are usually carried out to provide input data for the analysis of problems of various scales. For instance, geophysicists are interested in large-scale problems (of

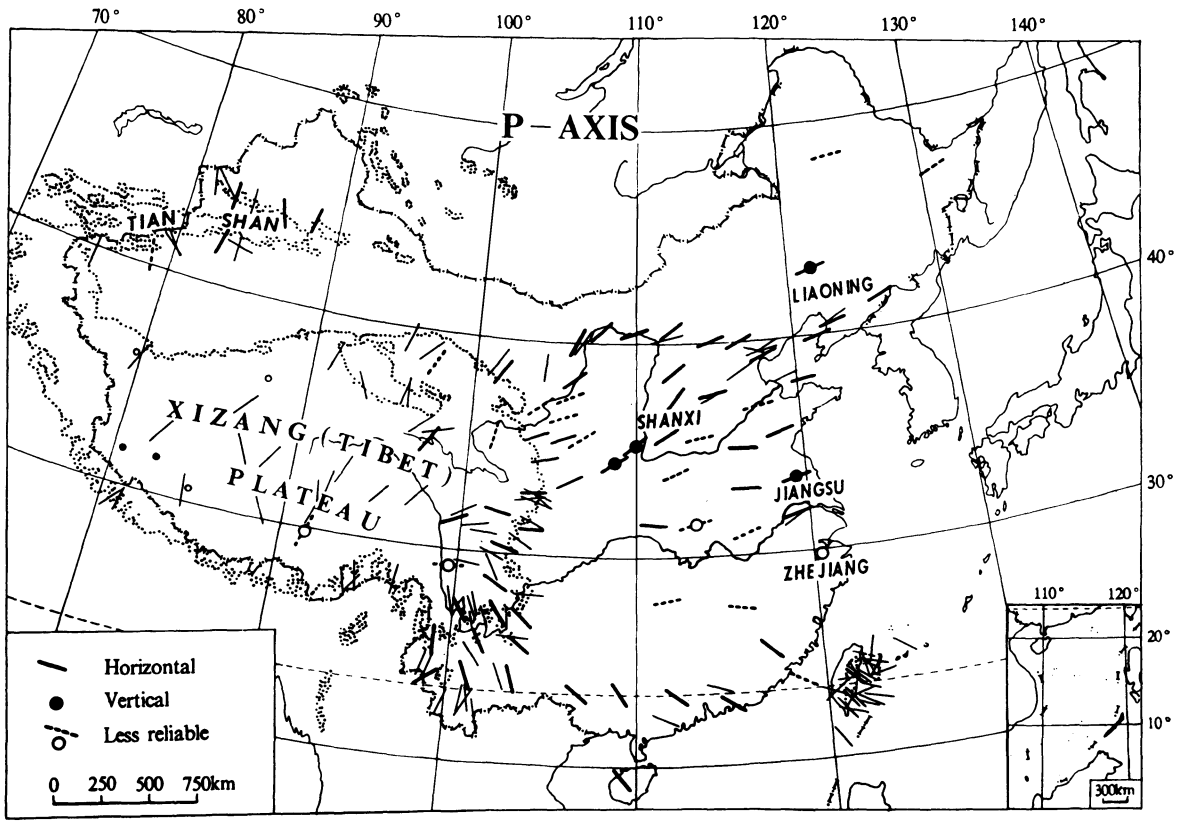

Fig. 11.10 *P*-axes orientation map for China. Bold symbols represent mean directions from multiple earthquake composites while thinner and smaller symbols indicate axes from individual $M \geq 6$ earthquakes. The regions contoured by dotted lines have an elevation higher than 3000 m. A bar crossing a dot means that the *P*-axis is vertical and the direction of the horizontal *B*-axis is represented by the bar. (After Xu *et al.*, 1992.)

the order of several cubic kilometers) such as identifying general stress patterns in a region or over an entire continent. Their problems are essentially at the megascopic or regional scale. Geologists are more interested in smaller-scale problems, such as the influence of a particular geological structure on the stress field. Mining and geotechnical engineers are interested in determining the stress field in a volume of rock interacting with an excavation (of the order of 10^3–10^9 m^3). The problems of interest to engineers and geologists are at the application scale or local scale, which ranges somewhat between the megascopic scale and the mesoscopic scale (i.e. a scale large enough to be observed in its entirety). Stresses at the microscopic scale are of interest to geologists interested in petrography, mineralogy and crystallography. The microscopic scale is also the strain or displacement measurement scale in overcoring techniques.

In general, engineers, geologists and geophysicists are interested in knowing stresses over rock volumes much larger than those involved in the actual *in situ* stress measurements. Unless the stress field is homogeneous over the volume of rock of interest, stresses need to be extrapolated from the measurement scale to the scale of the problem of interest (or application scale). This interpolation process is still a subject of discussion in the rock mechanics and rock engineering literature. Thus a basic question arises: how do we reconcile the state of stress at a point with what we measure *in situ*?

The problem of scale effect in rock mechanics has received quite a large amount of interest over the past decade, as testified by the creation of a special ISRM commission on the subject and the publication of the proceedings of two recent ISRM-sponsored international workshops (Cunha, 1990, 1993). Both workshops addressed the general problem of scale effect with regard to rock deformability, strength, permeability and *in situ* stress. Despite all the research reported in the workshop proceedings and in more recent technical papers, the problem of scale effect with regard to *in situ* stress is still poorly understood and open for discussion and further research. The reader interested in the topic of scale effect and *in situ* stress will find additional information in the papers by Hyett, Dyke and Hudson (1986), Hudson and Cooling (1988), Enever, Walton and Wold (1990), Haimson (1990b) and Cuisiat and Haimson (1992).

When dealing with *in situ* stresses, three types of potential scale effects need to be considered: (1) the effect of scale on stress itself, (2) the effect of scale on stress measurements and (3) the effect of scale on the properties entering into the analysis of *in situ* stress measurements. In discussing these three aspects of scale effect, we will make use (for illustrative purposes) of the simple model of Fig. 2.18 which has been reproduced in Fig. 11.11a. In this model, an idealized rock mass of length L (and unit width) consists of N juxtaposed units, each unit i ($i = 1,N$) having an elastic modulus E_i. The units are all assumed to be horizontal, to have the same width $w_i = L/N$, and to be connected laterally. The rock mass is subject to a vertical force F and is assumed to experience a uniform displacement in the vertical direction over the length L. Using basic strength of materials, the average vertical stress σ_i in each unit is given by equation (2.19) which, for the case considered here, reduces to $\sigma_i = (E_i/E_{av})\sigma_{av}$ where E_{av} is the average modulus over the length L and $\sigma_{av} = F/(L \times 1)$.

11.2.1 EFFECT OF SCALE ON STRESS

By definition, the concept of stress as defined by Cauchy (and summarized in Appendix A and section 1.1), is a limiting concept that is applied at a point around which a small area is defined. In the limiting process, the average force vector per unit area converges to a vector called the stress vector and the resultant moment is assumed to vanish. Stress is also defined within the context of continuum

mechanics, which implies that the material under consideration is continuously distributed throughout its volume and completely fills the space it occupies. Stress is expressed as a piecewise continuous function of space and time (Mase, 1970). Because of its intrinsic definition, stress in any material cannot be scale dependent.

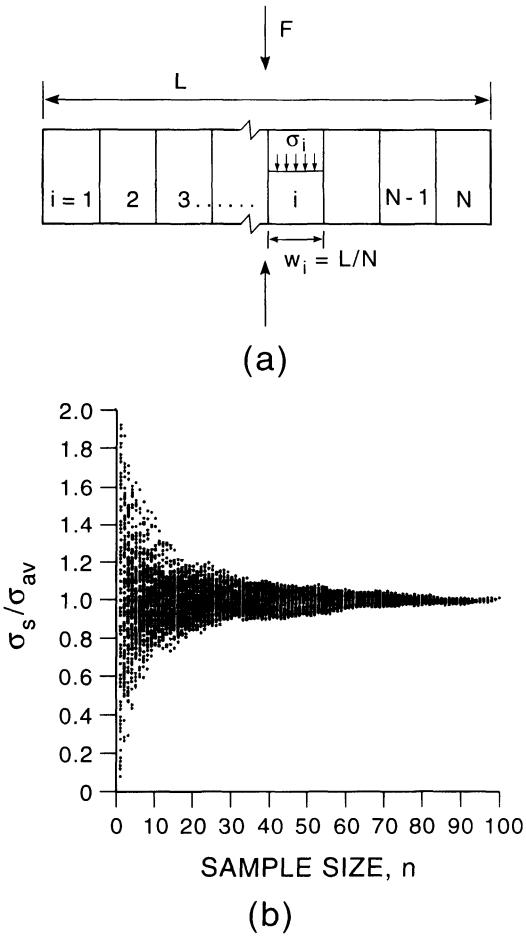

Fig. 11.11 (a) Idealized rock mass of length L (and unit width) consisting of N juxtaposed units, each unit i ($i = 1,N$) having a modulus E_i. The rock mass is subject to a vertical force F distributed over the N units and is assumed to experience a uniform displacement in the vertical direction over the length L. (b) Variation of σ_s/σ_{av} with the number of element n in each sample as n varies between 1 and $N = 100$.

Due to the complex nature of rocks from the micro-scale to the regional scale, *in situ* stresses are intrinsically non-uniform. As discussed in Chapter 2, for given boundary conditions, the magnitude and distribution of *in situ* stresses depend largely on the rock mass structure (petrography, discontinuities, heterogeneities, folds, faults, dikes, fabric, etc.) and on its geological history. When analyzed thoroughly, the *in situ* stress distribution in a rock mass can be so complex that local stresses may be quite different from the average stress. Note that the two are however related, as shown for instance for the model of Fig. 11.11a (equation (2.19)).

In rock masses, stress perturbations occur at the small and large scales. This was clearly emphasized by Enever, Walton and Wold (1990) who presented several case studies in Australia showing how stress measurements by overcoring and hydraulic fracturing can be affected by geological structures at various scales ranging from the regional scale to the local scale. In the model of Fig. 11.11a, the vertical stress in each unit varies with the unit stiffness, yielding larger stresses for the stiffer layers. Since there is no scale in Fig. 11.11a, this figure could be used to describe stress perturbations over the length of a core specimen, a borehole or a tunnel.

The non-uniformity of *in situ* stresses in rock masses at various scales creates, in itself, a natural (intrinsic, inherent) local scale effect which is obviously independent of the method of stress measurement. It is related to the geology and the applied boundary conditions. Nevertheless, it has been found that the non-uniformity does not seem to be as strong at the megascopic or regional scale. As discussed in the previous section, analysis of *in situ* stress data collected worldwide through the WSM Project has shown that large stress provinces (or stress regions) can be identified over which the stress is quite uniform (mostly in orientation) despite topography, local variations in geology and many causes of geological structures and

heterogeneities (Cornet, 1993; Zoback, 1992; Zoback *et al.*, 1989). More specifically, stress regions have been identified (1) in North America (Adams and Bell, 1991; Arjang, 1991; Bell and Babcock, 1986; Haimson, 1990a; Haimson, 1992; Herget, 1993; Plumb and Cox, 1987; Sbar and Sykes, 1973; Zoback, 1989; Zoback and Zoback, 1980), (2) in Europe (Cornet and Burlet, 1992; Gonzalez de Vallejo *et al.*, 1988; Klein and Barr, 1986; Müller *et al.*, 1992; Stephansson, 1993), (3) in Australia (Brown and Windsor, 1990; Enever and Chopra, 1986; Enever, Walton and Windsor, 1990; Enever, Walton and Wold, 1990; Worotnicki and Denham, 1976) and (4) in Asia (Gowd, Srirama Ra and Gar, 1992; Li, 1986; Lin, Yeh and Tsai, 1985; Sugawara and Obara, 1993). Figures 11.12 and 11.13 show two examples of principal stress orientation showing consistency in *in situ* stress orientation over large continental areas. Figure 11.12 depicts the results of four-arm dipmeter surveys of oil well breakouts in the western Canadian Basin reported by Bell and Babcock (1986). Figure 11.13 shows the maximum horizontal stress directions in the eastern part of the USA and Canada inferred from borehole breakouts, hydraulic fracturing and overcoring, reported by Plumb and Cox (1987).

As discussed in section 9.1, the stress measurements at the Underground Research Laboratory (URL) also showed well-defined stress domains bounded by major thrust faults. In each domain the stress field was found to be essentially continuous and predictable using numerical techniques. The block test at the Colorado School of Mines (CSM) Experimental Mine serves as another example showing that, in between well-defined geological boundaries (in this case local fractures) and for known boundary conditions, the local state of stress can be predicted (section 9.2). These two examples, which involve two different scales, can serve as arguments that within well-defined geological boundaries and for adequate boundary conditions, the variation of *in situ* stresses is quite predictable and has nothing to do with scale effect. The quality of the prediction depends of course on the complexity of the rock mass and the constitutive models chosen for its constituents. The prediction can be as simple as that for the model of Fig. 11.11a or may require more complex numerical models such as those used at the URL or with the CSM block.

11.2.2 EFFECT OF SCALE ON STRESS MEASUREMENTS

As discussed in section 3.8, stress measurements involve different rock volumes of several orders of magnitude and therefore different samples of the stress field. Depending on the size of the sample, the rock characteristics (anisotropy, heterogeneity and discontinuities) change. Each rock volume will react differently as the rock is subject to new boundary conditions or disturbance associated with the measurement process itself. Therefore, one should expect different values of the stress field for different rock volumes. However, the case studies presented in Chapter 9, and in particular the URL, seem to indicate otherwise. From these case studies it appears that for a same rock condition and within a well-defined geological domain, different stress measurement techniques give (on average) comparable stress values within the uncertainty expected in stress measurements, i.e. an error of $\pm$ 10–20% for the stress magnitude and an error of $\pm$ 10–20° for the stress orientation.

It must be emphasized that the conclusion about the apparent lack of substantial effect of scale on stress measurements for the URL site was reached based on the results of a large number of small-scale stress measurements (overcoring and hydrofracturing) sampled over the representative domain, and to a lesser extent on a smaller number of large-scale measurements. The small-scale measurements provided multiple samples of the rock mass with a meaningful average despite some clear dispersion. The conclusion was also based on detailed mapping of the site geology at all

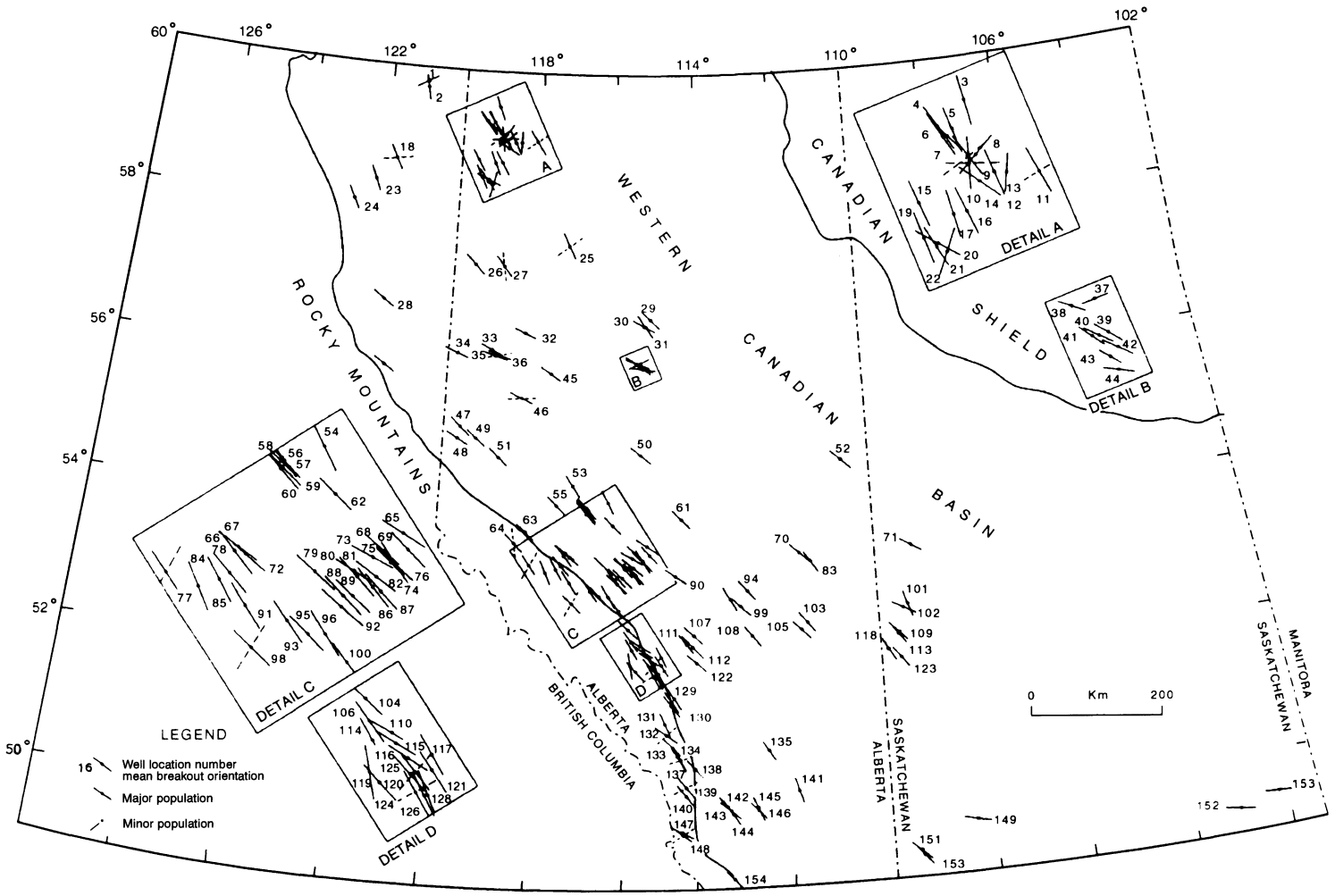

Fig. 11.12 Mean azimuths of major and minor breakout populations for 154 wells in the western Canadian Basin and Rocky Mountains. (After Bell and Babcock, 1986.)

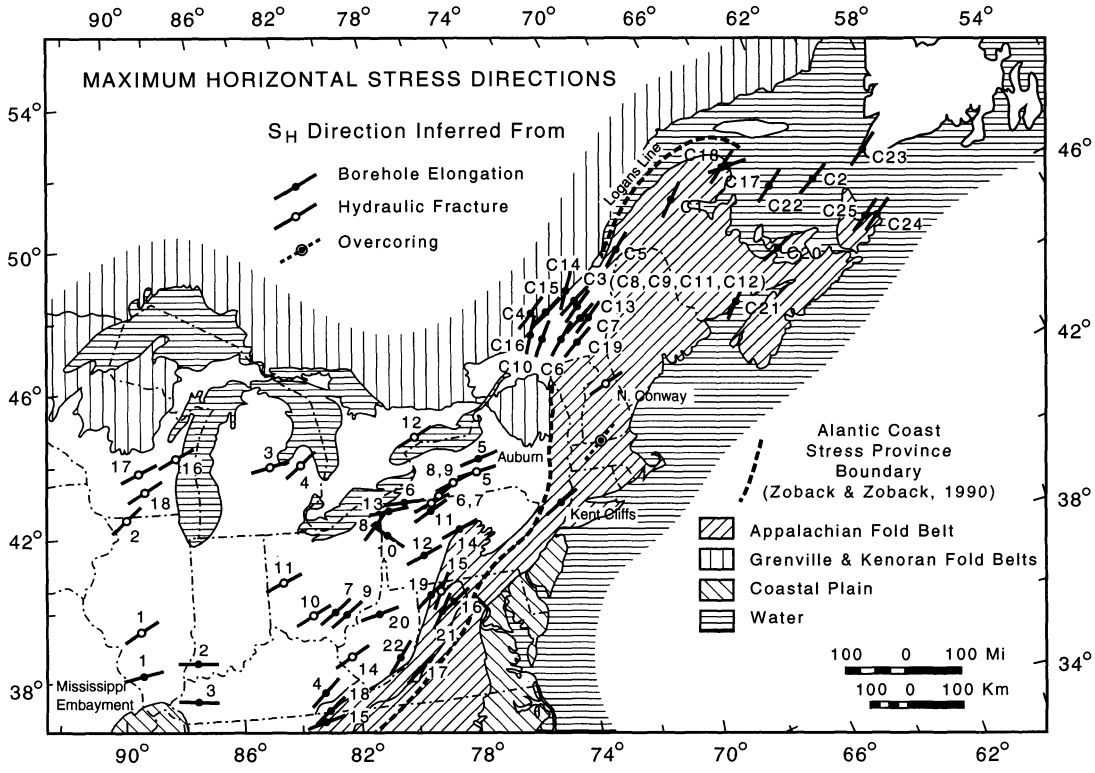

Fig. 11.13 Maximum horizontal stress directions in the eastern part of the USA and Canada inferred from borehole breakouts, hydraulic fracturing and overcoring. (After Plumb and Cox, 1987.)

scales. Extension of the trends observed at the URL site to rocks other than hard and competent granitic rocks, and to other geological environments, must be taken with caution. The extremely low natural fracture frequency encountered at the URL is an exception and is far from being representative of the conditions of hard granitic rocks of Precambrian age. Detailed studies similar to the study at the URL are needed before we can draw more general conclusions on the effect of scale on *in situ* stress and its measurement. It is clear, however, that if geological boundaries are crossed in the process of stress measurement (such as faults, folds, inclusions and dikes), variations in the measured stress field should be expected (Fig. 2.16). Such variations may be interpreted as scale effect but have nothing to do with it.

The importance of rock volume when measuring *in situ* stresses can be illustrated further using again the model of Fig. 11.11a, which is now assumed to consist of $N = 100$ elements. The Young's modulus for each element was determined using a random number generator with values ranging between 1 and 100 GPa. Samples consisting of n consecutive elements ($1 \leq n \leq N$) were taken from the idealized rock mass. For each sample, the mean stress σ_s was determined as the average of all the vertical stresses in the units comprising the sample. Figure 11.11b shows the variation of σ_s/σ_{av} as n varies between 1 and $N = 100$. Figure 11.11b indicates that as n increases, σ_s converges to σ_{av} and the dispersion decreases. If we now use the analogy that each sample is comparable to a rock volume involved in stress measurements, we can predict much

more variation in stress measurements with methods (such as overcoring) that involve small rock volumes than with those methods (such as the under-excavation technique) that involve larger volumes where the effect of rock irregularities has been eliminated. It is noteworthy that the fan-shaped trend in Fig. 11.11b is not surprising and could have been suspected beforehand, due to the nature of the problem being analyzed here and the averaging process selected in making that figure.

If the trend shown in Fig. 11.11b is again transposed to actual stress measurements, there is a rock volume beyond which the stress scatter is minimal (which corresponds to the sample of size L in Fig. 11.11a). This volume is called the representative elementary volume or REV in the literature. Initially used for characterizing the hydraulic properties of rock masses, the REV concept has been extended to *in situ* stresses by Hyett, Dyke and Hudson (1986), Hudson and Cooling (1988), Cuisiat and Haimson (1992) and Cornet (1993). When dealing with *in situ* stresses, the REV has three basic characteristics. First, the REV must be small enough so that over the REV, the variable of interest, e.g. the *in situ* state of stress, is constant, the *in situ* stress tensor is symmetric and *in situ* stress gradients can be neglected. Second, since stresses are assumed to be constant over the REV, the latter must consist of an equivalent continuum material where the rock mass is homogenized. Finally, the REV cannot be used to understand or model phenomena that occur at scales smaller than the REV.

In the model of Fig. 11.11a, the idealized rock mass has only one level of heterogeneity. This model can be extended further to a rock mass with several levels of heterogeneity. An extension of the model of Fig. 11.11a would be, for instance, a rock mass consisting of several sections separated by major discontinuities, each section having the same number of units N. For any sample larger than N, the effect of one or several of the major discontinuities will be felt when calculating the mean stress over the sample. In general, for different scales of interest involving different rock mass volumes, different fan-shaped diagrams similar to that shown in Fig. 11.11b can be constructed (Cuisiat and Haimson, 1992).

Before concluding our discussion on the effect of scale on stress measurements, the importance of scale on the measurement of residual stresses needs to be reiterated. As discussed in more detail in section 2.9.2, there seems to be a consensus in the literature that residual stresses vary with the volume of rock considered, up to a certain volume where there are in equilibrium. As remarked by Hyett, Dyke and Hudson (1986), a rock mass can be considered as being composed of equilibrium volumes at different scales depending on the heterogeneities present. Any volumes smaller than the equilibrium volumes will be affected by the stresses balanced at the scale of the equilibrium volumes. According to Hyett, Dyke and Hudson (1986), the amount of residual stress should increase as the volume of rock decreases from the macro- to the micro-scale. This trend can be attributed to the fact that as the volume increases, discontinuities are more likely to be found and those discontinuities are not able to transmit residual stresses if in tension.

11.2.3 EFFECT OF SCALE ON ROCK PROPERTIES INVOLVED IN THE ANALYSIS OF STRESS MEASUREMENTS

As seen in this book, *in situ* stresses cannot be measured directly but are instead inferred by monitoring how the rock responds to disturbance (relief, pressurization, slotting, excavation, stress concentration, etc.). In order to calculate *in situ* stresses, it is therefore necessary to know the mechanical properties of the rock such as the Young modulus and Poisson ratio for overcoring, the tensile strength for conventional hydraulic fracturing, and the compressive strength for the quantitative analysis of borehole breakouts. There is enough evidence in the literature that these properties are scale dependent. Thus this

phenomenon may have potential for influencing the interpretation of various stress measurements.

As discussed more extensively in Chapter 4 in relation to hydraulic fracturing, the rock tensile strength entering into the equation for the breakdown pressure is affected by scale and in particular by the hole diameter. Several theories have been proposed in the literature to model that effect (see review by Haimson, 1990b and Cuisiat and Haimson, 1992 and section 4.2.4). The scale effect was clearly shown by Enever, Walton and Wold (1990) who calculated the difference between crack initiation and crack reopening pressure (also known as the hydraulic fracture tensile strength) in the laboratory and *in situ*. They found a decrease in tensile strength with an increase in hole diameter. For instance, for a fine-grained low-permeability sandstone, the scale effect was found to operate for a hole diameter of up to about 30 mm. Laboratory tests conducted by Haimson and Zhao (1991) also showed the effect of hole diameter on tensile strength for diameters up to 20 mm. In general, an overestimation of the hydraulic fracture tensile strength would result in an overestimation of the major horizontal *in situ* stress.

As discussed in Chapter 8, the prediction of the initiation of borehole breakouts requires knowledge of the compressive strength of the rock. The results of various load tests conducted in the laboratory on blocks of rock containing a circular borehole have revealed that the tangential stress at the wall of the hole required to cause failure is about two to four times the unconfined compressive strength determined in standard uniaxial compression tests (Carter, 1992; Cuisiat and Haimson, 1992; Guenot, 1987; Haimson, 1990b). The rock compressive strength necessary for borehole wall failure has been found to depend on the borehole diameter, and to decrease with an increase in borehole diameter. For instance, in the tests on Alabama limestone reported by Haimson (1990b), scale effect was observed for holes with diameters as large as 120 mm but mostly for holes with diameters between 20 and 75 mm, where the tangential stress at the borehole wall required to cause spalling could be up to three times the rock's unconfined compressive strength. For diameters larger than 75 mm, the stress at failure was found to be less than the unconfined compressive strength. Similar trends were observed by Martin, Martino and Dzik (1994) who tested blocks of Lac du Bonnet granite in uniaxial compression with boreholes ranging between 5 and 103 mm in diameter. Their test results, shown in Fig. 11.14, indicate that for boreholes with diameters at least equal to 75 mm, the maximum tangential stress required to create borehole sidewall spalling is close to the rock's unconfined compressive strength σ_c (=200 MPa). For smaller diameters, the scale effect is important. A review of other laboratory tests showing the effect of borehole diameter on the sidewall stress required to initiate breakouts under uniaxial, biaxial and triaxial loading conditions can be found in Martin, Martino and Dzik (1994).

The only comprehensive study known to the authors showing the effect of scale on breakouts *in situ* was reported by Martin, Martino and Dzik (1994). Breakouts were observed in boreholes with diameters ranging

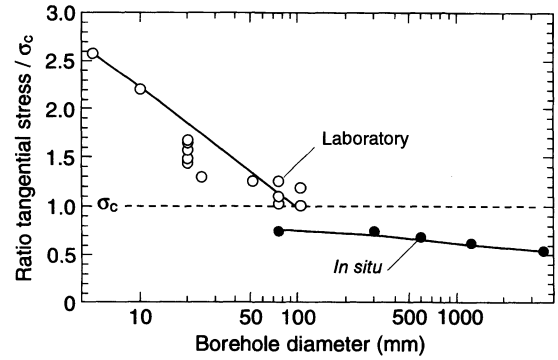

Fig. 11.14 Ratio of maximum tangential borehole wall stress (required to create borehole breakout) to unconfined compressive strength σ_c for various hole diameters tested in the laboratory (5–103 mm) and *in situ* (75–3500 mm) at the URL site. (After Martin, Martino and Dzik, 1994.)

between 75 and 1250 mm drilled to a nominal depth of 5 m from the floor of room 405 at the URL site. The boreholes were drilled in a direction parallel to the minimum *in situ* stress. Breakouts were also observed in the roof (and to a certain extent in the floor) of a horizontal tunnel 46 m long and 3500 mm in diameter, excavated without blasting at the same site and as part of a mine-by experiment. The tunnel was parallel to the intermediate *in situ* stress. Figure 11.14 also shows the ratio of maximum tangential borehole wall stress (determined by elastic three-dimensional analysis) to unconfined compressive strength σ_c for the different hole diameters investigated in the field. This figure indicates a modest scale effect for the *in situ* data and a noticeable change in the effect of scale between the laboratory and *in situ* results. Indeed, it appears that the laboratory and field tests require different strength–scaling laws. This difference has been attributed to different loading paths followed in the laboratory and *in situ* (Martin, 1995). The field tests of Martin, Martino and Dzik (1994) also showed that breakout geometry is affected by the hole diameter, with an increase in breakout length and depth with an increase in hole diameter. Finally, the field tests indicated that failure could initiate at a stress level as low as 50% of the laboratory unconfined compressive strength.

A review of possible explanations and existing models for the effect of scale on breakouts can be found in Haimson (1990b), Martin, Martino and Dzik (1994) and Martin (1995). This scale effect suggests that the classical theory used to analyze borehole breakouts could result in an underestimation of the magnitude of the *in situ* stresses.

REFERENCES

Adams, J. (1989) Crustal stresses in eastern Canada, in *Earthquakes at North Atlantic Passive Margins: Neotectonics and Postglacial Rebound*, Kluwer Academic, Boston, Mass., pp. 355–70.

Adams, J. and Bell, J.S. (1991) Crustal stresses in Canada, in *The Geology of North America*, Decade Map Vol. 1, *Neotectonics of North America*, Geological Society of America, Boulder, Colorado, pp. 367–86.

Anderson, E.M. (1951) *The Dynamics of Faulting and Dyke Formation with Applications to Britain*, Oliver and Boyd, Edinburgh.

Angelier, J. (1984) Tectonic analysis of fault slip data sets. *J. Geophys. Res.*, **89**, 5835–48.

Arjang, B. (1991) Pre-mining stresses at some hard rock mines in the Canadian shield. *Bull. Can. Inst. Mining*, **84**, 80–86.

Ask, M.V.S., Müller, B. and Stephansson, O. (1996) In situ stress determination from breakout analysis in the Tornquist Fan, Denmark, *Terra Nova* (in press).

Assumpcao, M. (1992) The regional intraplate stress field in South America. *J. Geophys. Res.*, **97**, 11889–903.

Barton, C.A., Zoback, M.D. and Burns, K.L. (1988) In-situ stress orientation and magnitude at the Fenton Hill geothermal site, New Mexico, determined from wellbore breakouts. *Geophys. Res. Lett.*, **15**, 467–70.

Bell, J.S. and Babcock, E.A. (1986) The stress regime of the western Canadian Basin and implications for hydrocarbon production. *Bull. Can. Petrol. Geol.*, **34**, 364–78.

Bosworth, W., Strecker, M.R. and Blisniuk, P.M. (1992) Integration of East African paleostress and present-day stress data: implications for continental stress field dynamics. *J. Geophys. Res.*, **97**, 11851–65.

Bott, M.H.P. and Dean, D.S. (1972) Stress systems at young continental margins. *Nature Phys. Sci.*, **235**, 23–5.

Brown, E.T. and Windsor, C.R. (1990) Near surface in-situ stresses in Australia and their influence on underground construction, in *Proc. Tunnelling Conf.*, Sydney, The Institution of Engineers, Australia, pp. 18–48.

Bungum, H. *et al.* (1991) Seismicity and seismotectonics of Norway and nearby continental shelf areas. *J. Geophys. Res.*, **96**, 2249–65.

Carter, B.J. (1992) Size and stress gradient effects on fracture around cavities. *Rock Mech. Rock Eng.*, **25**, 167–86.

Cornet, F.H. (1993) Stresses in rocks and rock masses, in *Comprehensive Rock Engineering* (ed. J.A. Hudson), Pergamon Press, Oxford, Chapter 17, Vol. 3, pp. 297–324.

Cornet, F.H. and Burlet, D. (1992) Stress field determination in France by hydraulic tests in boreholes. *J. Geophys. Res.*, **97**, 11829–49.

Cuisiat, F.D. and Haimson, B.C. (1992) Scale effects in rock mass stress measurements. *Int. J. Rock Mech. Min. Sci. & Geomech. Abstr.*, **29**, 99–117.

Cunha, A.P. (1990) Scale effects in rock masses, in *Proc. 1st Workshop on Scale Effects in Rock Masses*, Loen, Norway, Balkema, Rotterdam.

Cunha, A.P. (1993) Scale effects in rock masses 93, in *Proc. 2nd Workshop on Scale Effects in Rock Masses*, Lisbon, Balkema, Rotterdam.

Enever, J.R. and Chopra, P.N. (1986) Experience with hydraulic fracture stress measurements in granite, in *Proc. Int. Symp. on Rock Stress and Rock Stress Measurements*, Stockholm, Centek Publ., Luleå, pp. 411–20.

Enever, J.R., Walton, R.J. and Windsor, C.R. (1990) Stress regime in the Sydney basin and its implication for excavation design and construction, in *Proc. Tunnelling Conf.*, Sydney, The Institution of Engineers, Australia, pp. 49–59.

Enever, J.R., Walton, R.J. and Wold, M.B. (1990) Scale effects influencing hydraulic fracture and overcoring stress measurements, in *Proc. Int. Workshop on Scale Effects in Rock Masses*, Loen, Norway, Balkema, Rotterdam, pp. 317–26.

Evans, K.F. (1989) Appalachian stress study, 3, regional scale stress variations and their relation to structure and contemporary tectonics. *J. Geophys. Res.*, **94**, 17619–45.

Fejerskov, M. *et al.* (1995) In-situ rock stress pattern on the Norwegian continental shelf and mainland, in *Proc. Workshop on Rock Stresses in the North Sea*, Trondheim, Norway, NTH and SINTEF Publ., Trondheim, pp. 191–201.

Gao, Q.L., Xu, Zh.H. and Chen, J.G. (1990) Horizontal principal stress axes in Sichuan Basin deduced from oil-well breakouts. *Acta Seismol. Sin.*, **12**, 140–47.

Gonzalez de Vallejo, L.I. *et al.* (1988) The state of stress in Spain and its assessment by empirical methods, in *Proc. Int. Symp. Rock Mech. and Power Plant*, Madrid, Balkema, Rotterdam, pp. 165–72.

Gowd, T.N., Srirama Ra, S.V. and Gar, V.K. (1992) Tectonic stress field in the Indian subcontinent. *J. Geophys. Res.*, **97**, 11879–88.

Gregersen, S. (1992) Crustal stress regime in Fennoscandia from focal mechanisms. *J. Geophys. Res.*, **98**, 11821–7.

Guenot, A. (1987) Stress and rupture conditions around oil wellbores, in *Proc. 6th Int. Cong. Rock Mech.*, Montreal, Balkema, Rotterdam, Vol. 1, pp. 109–18.

Haimson, B.C. (1990a) Stress measurements in the Sioux Falls quartzite and the state of stress in the Midcontinent, in *Proc. 31st US Symp. Rock Mech.*, Golden, Balkema, Rotterdam, pp. 397–404.

Haimson, B.C. (1990b) Scale effects in rock stress measurements, in *Proc. Int. Workshop on Scale Effects in Rock Masses*, Loen, Balkema, Rotterdam, pp. 89–101.

Haimson, B.C. (1992) Hydraulic fracturing measurements in New York city reaffirm the uniformity of the stress regime in northeastern United States, in *Proc. 33rd US Symp. Rock Mech.*, Santa Fe, Balkema, Rotterdam, pp. 59–68.

Haimson, B.C. and Zhao, Z. (1991) Effect of borehole size and pressurization rate on hydraulic fracturing breakdown pressure, in *Proc. 31st US Symp. Rock Mech.*, Norman, Balkema, Rotterdam, pp. 191–9.

Herget, G. (1993) Rock stresses and rock stress monitoring in Canada, in *Comprehensive Rock Engineering* (ed. J.A. Hudson), Pergamon Press, Oxford, Chapter 19, Vol. 3, pp. 473–96.

Hudson, J.A. and Cooling, C.M. (1988) In situ rock stresses and their measurement in the UK – Part I. The current state of knowledge. *Int. J. Rock Mech. Min. Sci. & Geomech. Abstr.*, **25**, 363–70.

Hyett, A.J., Dyke, C.G. and Hudson, J.A (1986) A critical examination of basic concepts associated with the existence and measurement of in-situ stress, in *Proc. Int. Symp. on Rock Stress and Rock Stress Measurements*, Stockholm, Centek Publ., Luleå, pp. 387–91.

Klein, R.J. and Barr, M.V. (1986) Regional state of stress in western Europe, in *Proc. Int. Symp. Rock Stress and Rock Stress Measurements*, Stockholm, Centek Publ., Luleå, pp. 33–44.

Kusznir, N.J. and Bott, M.P.H. (1977) Stress concentration in the upper lithosphere caused by underlying visco-elastic creep. *Tectonophysics*, **43**, 247–56.

Li, F. (1986) In-situ stress measurements, stress state in the upper crust and their application to rock engineering, in *Proc. Int. Symp. on Rock Stress and Rock Stress Measurements*, Stockholm, Centek Publ., Luleå, pp. 69–77.

Li, F. and Liu, G. (1986) Stress state in the upper crust of the China mainland. *J. Phys. Earth*, **34**, S71–80.

Lin, C.H., Yeh, Y.H. and Tsai, Y.B. (1985) Determination of regional principal stress directions in Taiwan from fault plane solutions. *Bull. Inst. of Earth Sciences, Academia Sinica*, **5**, 67–85.

Martin, C.D. (1995) Brittle rock strength and failure: laboratory and in situ, in *Proc. 8th Cong. Int. Soc. Rock Mech. (ISRM)*, Tokyo, Balkema, Rotterdam, Vol. 3 (in press).

Martin, C.D., Martino, J.B. and Dzik, E.J. (1994) Comparison of borehole breakouts from laboratory and field tests, in *Proc. Eurock '94: Int. Symp. on Rock Mech. in Petrol. Eng.*, Delft, Balkema, Rotterdam, pp. 183–90.

Mase, G.E. (1970) *Continuum Mechanics*, Schaum's Outline Series, McGraw-Hill.

Minster, J.B. and Jordan, T.H. (1978) Present-day plate motions. *J. Geophys. Res.*, **83**, 5331–54.

Mount, Van S. and Suppe, J. (1992) Present-day stress orientations adjacent to active strike-slip faults: California and Sumatra. *J. Geophys. Res.*, **97**, 11995–2013.

Müller, B. *et al.* (1992) Regional patterns of tectonic stress in Europe. *J. Geophys. Res.*, **97**, 11783–803.

Myrvang, A.M. (1993) Rock stress and rock stress problems in Norway, in *Comprehensive Rock Engineering* (ed. J.A. Hudson), Pergamon Press, Oxford, Chapter 18, Vol. 3, pp. 461–71.

Nakamura, K. and Uyeda, S. (1980) Stress gradient in arc–back arc regions and plate subduction. *J. Geophys. Res.*, **85**, 6419–28.

Plumb, R.A. and Cox, J.W. (1987) Stress directions in eastern North America determined to 4.5 km from borehole elongation measurements. *J. Geophys. Res.*, **92**, 4805–16.

Sbar, M.L. and Sykes, L.R. (1973) Contemporary compressive stress and seismicity in eastern North America: an example of intra-plate tectonics. *Geol. Soc. Am. Bull.*, **84**, 1861–82.

Slunga, R. (1989) Focal mechanisms and crustal stresses in the Baltic shield, in *Earthquakes at North Atlantic Passive Margins: Neotectonics and Postglacial Rebound*, Kluwer Academic, Boston, pp. 261–76.

Stein, S. *et al.* (1989) Passive margin earthquakes, stresses and rheology, in *Earthquakes at North Atlantic Passive Margins: Neotectonics and Postglacial Rebound*, Kluwer Academic, Boston, pp. 231–59.

Stephansson, O. (1988) Ridge push and glacial rebound as rock stress generators in Fennoscandia, in *Geological Kinematics and Dynamics: From Molecules to the Mantle. Bull. Geol. Institutions of Univ. Uppsala*, **14**, 39–48.

Stephansson, O. (1993) Rock stress in the Fennoscandian shield, in *Comprehensive Rock Engineering* (ed. J.A. Hudson), Pergamon Press, Oxford, Chapter 17, Vol. 3, pp. 445–59.

Stephansson, O. *et al.* (1987) Fennoscandian rock stress data base – FRSDB. Technical University of Luleå, Luleå, Sweden, Research Report Lulea 1987:06.

Sugawara, K. and Obara, Y. (1993) Measuring rock stress, in *Comprehensive Rock Engineering* (ed. J.A. Hudson), Pergamon Press, Oxford, Chapter 21, Vol. 3, pp. 533–52.

Te Kamp, L., Rummel, F. and Zoback, M.D. (1995) Hydrofrac stress profile to 9 km at the German KTB site, in *Proc. Workshop on Rock Stresses in the North Sea*, Trondheim, Norway, NTH and SINTEF Publ., Trondheim, pp. 147–53.

Worotnicki, G. and Denham, D. (1976) The state of stress in the upper part of the Earth's crust in Australia according to measurements in mines and tunnels and from seismic observations, in *Proc. ISRM Symp. on Investigation of Stress in Rock, Advances in Stress Measurement*, Sydney, The Institution of Engineers, Australia, pp. 71–82.

Xu, Zh. *et al.* (1992) Tectonic stress field of China inferred from a large number of small earthquakes, *J. Geophys. Res.*, **97**, 11867–77.

Zoback, M.D. and Healy, J.H. (1992) In-situ stress measurements to 3.5 km depth in the Cajon Pass scientific research borehole: implications for the mechanics of crustal faulting. *J. Geophys. Res.*, **97**, 5039–57.

Zoback, M.D. and Zoback, M.L. (1991) Tectonic stress field of North America and relative plate motions, in *The Geology of North America*, Decade Map Vol. 1, *Neotectonics of North America*, Geological Society of America, Boulder, pp. 339–66.

Zoback, M.D. *et al.* (1987) New evidence on the state of stress of the San Andreas fault system. *Science*, **238**, 1105–11.

Zoback, M.L. (1989) State of stress and modern deformation of the northern Basin and Range province. *J. Geophys. Res.*, **94**, 7105–28.

Zoback, M.L. (1992) First- and second-order patterns of stress in the lithosphere: the World Stress Map Project. *J. Geophys. Res.*, **97**, 11703–28.

Zoback, M.L. and Zoback, M.D. (1980) State of stress in the conterminous United States. *J. Geophys. Res.*, **85**, 6113–56.

Zoback, M.L. *et al.* (1989) Global patterns of tectonic stress. *Nature*, **341**, 291–8.

USING STRESSES IN ROCK ENGINEERING, GEOLOGY AND GEOPHYSICS

12

12.1 INTRODUCTION

Rock masses are initially stressed in their natural state. Whether one is interested in natural geological structures (folds, faults, intrusions, etc.) or artificial structures (tunnels, caverns, mines, surface excavations, etc.), a knowledge of the *in situ* or virgin stress field (along with other rock mass properties) is needed when predicting the response of rock masses to the disturbance associated with those structures. The response can take multiple forms such as deformations of the walls of a surface or underground excavation, stresses and breakouts in the walls of a shaft or borehole, creep of a salt pillar, initiation of a microearthquake, shearing of a fault or glacial rebound of a glaciated terrain. Today, there exist a variety of analytical solutions to many of the geological, geophysical and geoengineering problems. Computer-based numerical methods for stress, strain and strength analysis are also available to handle problems with more complex geometries and/or constitutive behavior. Many of the analytical methods and numerical codes use stress (or traction) as a possible boundary condition. Hence, a proper determination, or at least a good estimation, of the state of stress *in situ* is needed in order to reach reliable solutions to the problem of interest.

In this chapter we present several examples of applications showing the role played by *in situ* stresses in civil and mining rock engineering, energy development, and geology and geophysics. For civil engineering projects such as underground excavations and tunnels, we need to know the *in situ* stress field in order to identify zones of compression, tension and stress concentrations for stability analysis. *In situ* stresses are also important for the design of support systems. In mining engineering, stresses need to be taken into account when selecting mining methods and designing mining stopes, pillars and support systems. In both civil and mining engineering, *in situ* stress measurements constitute part of a larger program of data collection (Bawden, 1993; Leijon, 1986). *In situ* stress data along with data on geology, rock mass strength, deformability, permeability, etc. provide the information required to perform analysis and design.

Borehole stability and borehole deviation in oil and gas exploration and production are to a large extent governed by the *in situ* state of stress in geological formations. Thus *in situ* stresses are of the utmost importance in petroleum engineering. Other activities in the oil and gas industry such as drilling, mud selection, casing and borehole stimulation need *in situ* stress data in order to be successful. Thermal energy extraction is another sector of energy development where borehole stability and rock stresses are intimately related. The success of fracture propagation and water injection for energy extraction from a hot dry rock depends largely on the virgin state of stress.

Knowledge of the *in situ* stress field is also important for the fracturing of formations of oil and gas fields to stimulate production. The success of hydraulic fracturing and massive hydraulic fracturing depends to a large extent on the magnitude and distribution of *in situ* stresses in addition to the rock and rock mass properties (deformability, strength, permeability and porosity) and the geological structures. Of particular interest here are induced fracture containment and fracture evolution from one rock stratum to the next in stratified rock masses. Models of fracture propagation in such rock masses require knowledge of the *in situ* stresses in the different rock formations (Hanson *et al.*, 1978, 1980).

The design and location of a radioactive waste repository is determined by a large number of geological conditions and features. The mechanical stability and long-term integrity of a repository is to a large extent governed by the virgin state of stress at the site. Superposition of the virgin stresses onto the stress concentrations resulting from the excavation and the thermal stresses induced by the heat release from the emplaced waste must be such that the rock mass strength is not mobilized. Rock fracturing in the near vicinity of the waste, and displacement along pre-existing fractures, could alter the groundwater flow in the repository area, thus bringing some of the waste in contact with the biosphere (Hansson, Jing and Stephansson, 1995).

In the fields of geology and geophysics, two primary categories of forces are responsible for the state of stress in the upper part of the Earth's lithosphere. The first category consists of tectonic stresses and includes plate boundary forces, broad-scale flexure of the lithosphere and thermoelastic forces in cooling oceanic lithosphere. The second category of stresses is derived from local effects of topography, anisotropy of strength or elastic properties and effects of erosion, glacial rebound and artificial excavations; these forces generate local or 'induced' stresses following the terminology presented by Zoback *et al.* (1989) and Zoback (1992) in the World Stress Map Project (section 11.1; Figure 2.29).

As remarked by Jaeger and Cook (1976) and others, many of the problems of structural geology are similar to those encountered in rock mechanics and rock engineering, except that they are often on a much larger scale. Over the years, a number of mechanistic theories of faulting, folding, thrusting, tectonic fabrics, boudinage and pinch-and-swell structures, mechanics of intrusion, subsidence, etc. have been developed by structural geologists (Johnson, 1970; Mattauer, 1973; Price and Cosgrove, 1990; Ramberg, 1981; Ramsay, 1967). All these might equally well have been developed within the context of rock mechanics and rock engineering.

12.2 STRESSES IN CIVIL ROCK ENGINEERING

In situ stresses play a critical role in civil engineering projects involving rock either as a construction or foundation material. They enter into the design and stability analysis of various underground structures (tunnels, caverns, shafts, etc.). They are also important when selecting the location of pressure tunnels and shafts and other rock cavities used for hydropower or underground storage of compressed natural gas, liquified natural gas (LNG), liquified petroleum gases, compressed air, oil or water, for which rock confinement is critical. Finally, *in situ* stresses may control the stability of surface excavations (natural and artificial).

A large number of well-documented case studies where stresses play a critical role are available in the rock engineering literature. In fact, it is our observation that *in situ* stresses are included more often than not in modern rock engineering design. In this section we present a review of the role played by *in situ* stresses in the behavior of underground and surface excavations, in the selection of pressure tunnels and shafts, and in the underground storage of fluids in unlined caverns.

Several illustrative case studies are also presented.

12.2.1 ROLE OF *IN SITU* STRESSES IN THE BEHAVIOR OF UNDERGROUND EXCAVATIONS

Various stability problems may arise when opening an underground excavation in rock. Hoek and Brown (1980a) defined four major modes of instability: (1) instability due to rock stresses, (2) instability due to adverse structural geology, (3) instability due to weathering and/or swelling and (4) instability due to excessive groundwater pressure or flow. They also noted that there are situations where two or more instability modes could coexist. The pre-excavation *in situ* stresses and their redistribution following excavation contribute to the first mode of instability.

In situ stresses often contribute to the second mode of instability as they can enhance or reduce the role played by the rock fabric and geological structures such as foliations, joints and faults. Compressive stresses provide confinement and therefore tend to lock or clamp the rock mass, thus reducing the effect of blocks, wedges or slabs that would otherwise become unstable by sliding along discontinuities. Block stability is increased further if the discontinuities are rough and are not (or only partially) free to dilate. On the other hand, tensile stresses may open fractures, accelerate the weathering and create more stability problems. Finally, *in situ* stresses affect water flow since compressive stresses make the rock mass tighter and less likely to create seepage problems both during excavation and thereafter.

In situ stresses are mostly included in the analytical/numerical approach of the design of underground excavations. In the empirical approach, which is based on rock mass classifications, *in situ* stresses are 'subjectively' included in the form of scaling factors (Kaiser and Maloney, 1992). For instance, in the Q-rating of Barton, Lien and Lunde (1974), *in situ* stresses are taken into account in the stress reduction factor. In the Geomechanics Classification (Bieniawski, 1984), the RMR-rating is adjusted using a coefficient that varies between 0.6 and 1.2, depending on whether the user judges the stresses to be beneficial or detrimental.

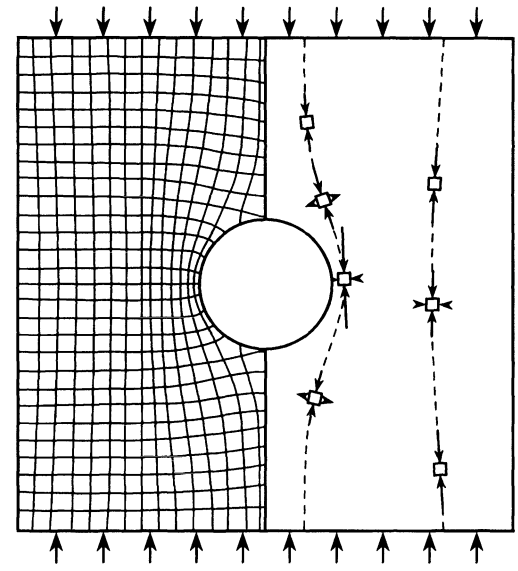

Fig. 12.1 Stress redistribution and principal stress trajectories around a circular opening in a vertically stressed elastic plate. (After Hoek and Brown, 1980a.)

In the analytical/numerical approach to design, stress analyses are usually carried out by considering a region of a rock mass subject to fixed boundary conditions such as tractions (stress) or displacements, or mixed boundary conditions. The stresses measured *in situ* are used as boundary conditions. A variety of analytical solutions (mostly two-dimensional) are available to determine stresses around openings of simple shapes, in homogeneous and continuous rock and subjected to uniform *in situ* stresses at infinity. Figure 12.1 shows the classical example of stress redistribution around a circular opening in a vertically stressed elastic plate. Numerical methods such as the finite element method, boundary element methods, and discrete (distinct) element methods can be used to handle problems with

more complex (two- or three-dimensional) geometries and for rock masses with more complex constitutive behavior. A review of the analytical and numerical methods used in rock mechanics can be found in Obert and Duvall (1967), Jaeger and Cook (1976), Hoek and Brown (1980a), Crouch and Starfield (1983), Brown (1987) and Pande, Beer and Williams (1990), among others. Figure 12.2 shows, as an example, the results of a three-dimensional elastic stress analysis for a power house cavern conducted by Sugawara *et al.* (1986) using a three-dimensional boundary element method. In this example, the boundary stresses used for input were determined using the hemispherically-ended borehole overcoring technique described in section 5.2.2.

Stress analyses are usually conducted to determine stress concentrations, and the type of stress concentration (compression versus tension). Since rock masses are weak in

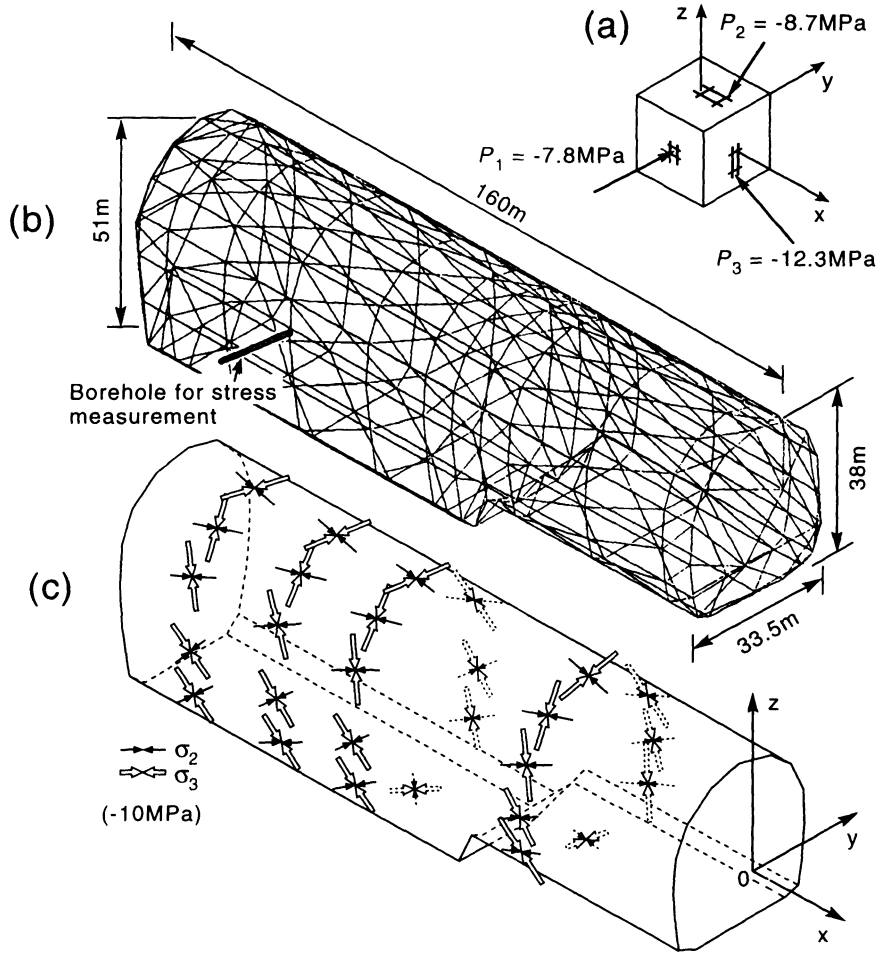

Fig. 12.2 Three-dimensional elastic stress analysis of the Imaichi power house cavern using the boundary element method. (a) Measured *in situ* stress field (compression is negative), (b) three-dimensional boundary element mesh and borehole for stress measurement, (c) distribution of tangential principal stresses on cavern wall. (After Sugawara *et al.*, 1986.)

tension, tensile stresses may open existing fractures or create new ones which could result in block stability problems. On the other hand, the magnitude of compressive stresses in the walls of an excavation may be large enough to overstress the rock and mobilize the rock mass strength locally. This can result in problems such as rockbursts, spalling, buckling and heaving of rock layers, squeezing and excessive deformation in the form of roof closure, sidewall movement and/or ground subsidence. The location, extent and nature of the overstressed zones depend on many parameters such as rock mass properties (strength and deformability), the rock fabric (anisotropy, joints, etc.), the *in situ* stress field (magnitude and orientation), the geometry and depth of the excavation, and external conditions such as the topography (section 2.8) and the method of excavation. High horizontal stresses are likely to create problems in the roof and floor of an underground opening whereas high vertical stresses are likely to create problems in its sidewalls. In mountainous areas with extreme topography and steep valley walls (such as in Norwegian fjords), tunnels parallel to the valleys have been found to experience rockbursts in the tunnel wall and in the part of their roof located the closest to the valley side due to stress concentrations. In very deep excavations, such as the deep mines in South Africa and North America, stability problems can occur all around the excavations. There are also situations where floor and roof stability problems along a section of an underground opening are replaced by sidewall problems (or no stability problems whatsoever) along other sections.

As an example, Fig. 12.3 shows the results of a two-dimensional stress analysis conducted by Eissa (1980) using the boundary element method. The extent of the potential overstressed zone around a horseshoe opening in a biaxial stress field, with a vertical component p and a horizontal component $0.5p$, was determined for different values of the ratio between

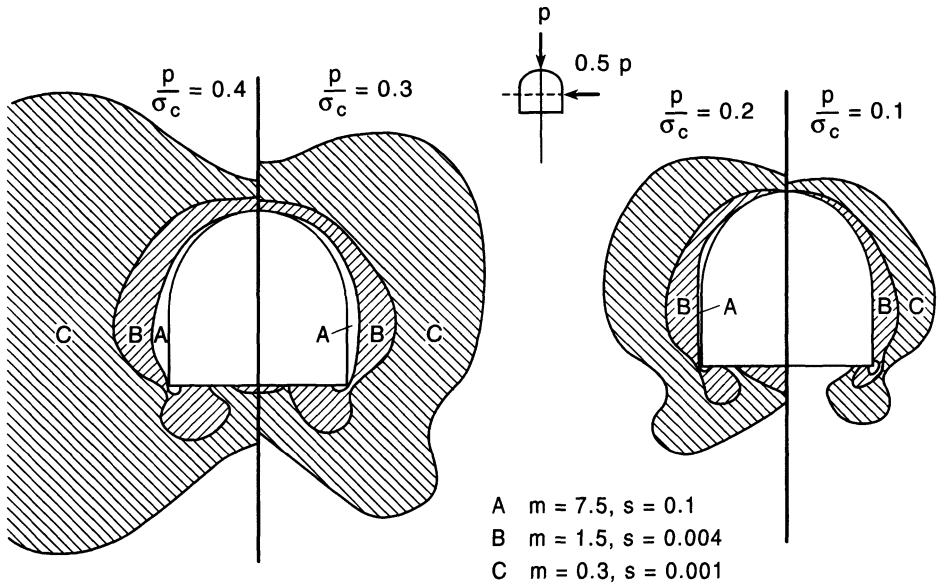

Fig. 12.3 Potential overstressed zones around a horseshoe opening in a biaxial stress field (p, $0.5p$) for different values of the ratio between the vertical stress p and the intact rock compressive strength σ_c. Three rock masses A, B and C are considered with decreasing values of the Hoek and Brown empirical strength parameters m and s. (After Eissa, 1980.)

the vertical stress p and the intact rock compressive strength σ_c. The rock mass was assumed to be under plane strain and its strength was defined using the criterion proposed by Hoek and Brown (1980b) with two parameters, m and s. Three rock masses of decreasing strength were considered and are defined as A, B and C. Figure 12.3 shows clearly an increase in the extent of the overstressed zone around the opening as the rock mass strength decreases. Also, for given values of the parameters m and s, the extent of the overstressed zone increases with the ratio p/σ_c.

The value of the ratio between the vertical stress and the unconfined compressive strength of the intact rock material is critical when assessing the potential for squeezing of weak clay-bearing rocks such as shales, claystones and mudstones. A good example, described by Morton and Provost (1980), is that of the Stillwater tunnel in the USA where squeezing ground was encountered in shale beneath ground cover of the order of 2500 ft (762 m), resulting in a complete stoppage of a tunnel boring machine (TBM). In this case the vertical stress to unconfined compressive strength ratio was of the order of 0.25.

Stress analysis can be used to determine the extent of the zone where stresses have been disturbed by excavation of an underground opening. Such an analysis is important when predicting the interaction between adjacent openings and the interaction between an opening and adjacent geological structures such as faults. Eissa (1980) analyzed the stress distribution around openings of various shapes and under different levels of horizontal and vertical stresses. He concluded that the zone of influence of an opening depends largely on its height to width ratio and the horizontal to vertical *in situ* stress ratio. For all practical purposes stress redistribution takes place over a distance from the wall of the opening of at least 1–1.5 times the opening span. This rule of thumb seems to be realistic when compared to actual stress measurements around openings (e.g. Sugawara and Obara, 1993).

Figure 12.4 shows an illustrative example of stress redistribution measured by Obara *et al.* (1995) in Japan using the conical-ended borehole overcoring technique described in section 5.2.2. A total of 18 overcoring stress measurements were carried out at distances ranging between 0.6 and 29.5 m from the wall of a 6 m span gallery excavated in granodiorite at a depth of 520 m. Three steeply dipping, subparallel faults were found to interact with the gallery, two intersecting the gallery itself (not shown in Fig. 12.4) and one between measurements 6 and 7. Figures 12.4a and 12.4b show the distribution of the principal stresses in the vertical plane and in the horizontal plane, respectively. Here the stress distribution is affected by both the presence of the gallery and the fault(s). The stress measurements at points 17 and 18 (located more than 25 m from the gallery and 20 m from the fault) were taken as *in situ* stress values.

Stress analysis can also help in the selection and design of support systems. For instance, the extent of overstressed rock can be used to determine the length of rock bolts. *In situ* stresses are an integral part of the ground–support interaction model proposed by Brown *et al.* (1983) since they form the 'loading system'. In this model, the extent of the plastic zone around an underground excavation and the displacement of the walls of the opening depend on the magnitude of the *in situ* stresses. As the shape of the ground reaction curve varies with the level of applied stress, so does the amount of support required to reach mechanical equilibrium between the support system and the rock mass.

The distribution and magnitude of *in situ* stresses affect the geometry, shape, dimensioning, excavation sequence and orientation of underground excavations. The main goals when designing underground openings in rock (where stresses are likely to be a problem) are to minimize stress concentrations, create a compressive stress field as evenly distributed as

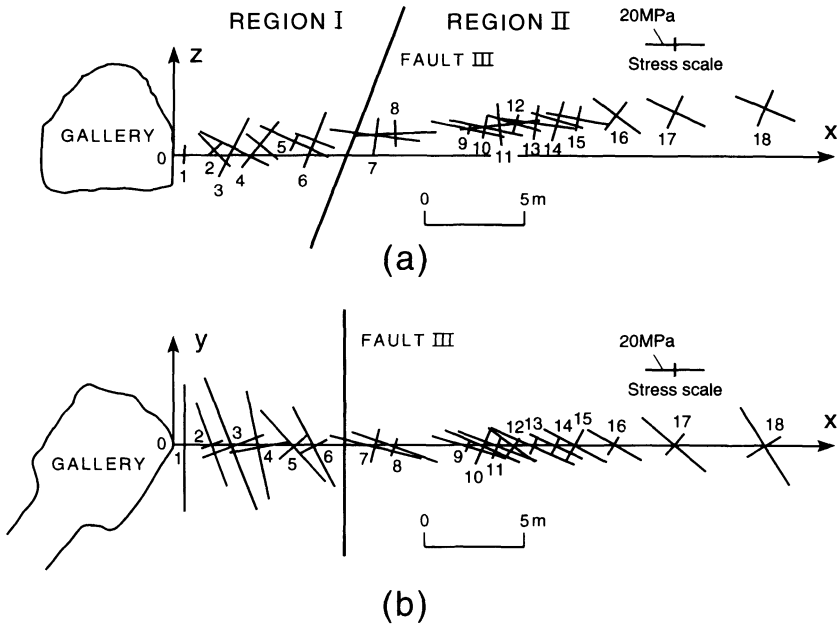

Fig. 12.4 Principal stresses measured in the wall of a gallery. (a) Vertical cross-section, (b) plan view. The stress measurements at points 17 and 18 are used as *in situ* stress values. (After Obara *et al.*, 1995.)

possible (the 'harmonic hole' concept) in the excavation walls and avoid tensile stress regions. This can be done by changing the shape and geometry of the openings as well as their orientation with respect to the known principal *in situ* stresses. The theory of elasticity is often used to that effect. However, as noted by Hoek and Brown (1980a), the harmonic hole concept applies when virgin stresses are low compared with the rock strength. If the virgin stresses are high enough, the harmonic hole concept could result in uniform but large compressive stresses all around the opening, which could create stability problems. In that case, Hoek and Brown (1980a) suggested following a recommendation proposed earlier by Fairhurst (1968) whereby the excavation shape is selected in such a way that the zones of overstressed rock are concentrated in sharp corners and are limited in extent. According to Broch (1993), the same recommendation should be followed for deep caverns where the *in situ* stresses are so high that rockbursts and spalling can be expected.

Stress concentrations based on the two-dimensional theory of elasticity are available for single openings in a uniform *in situ* stress field, or in a stress field increasing linearly with depth. Stress concentration factors are also available for parallel openings of various shapes and for different values of the ratio of the opening span to pillar width (Eissa, 1980; Hoek and Brown, 1980a). Figure 12.5 shows a summary of tangential stress concentrations in the roof and springline of single openings in a uniform *in situ* stress field with vertical component p and horizontal component kp. The rock is assumed to be homogeneous, continuous and linearly elastic. This figure indicates that, within the context of linear elasticity, openings with a major horizontal axis are better suited in stress fields with horizontal stresses higher than the vertical stress. On the other hand, their major axis should be vertical if the vertical stress is larger than the horizontal stress. A general characteristic of stress concentrations around openings in isotropic media is that they are independent of

the elastic properties of the medium. The reader should be aware that this is no longer true if the medium is anisotropic, in which case the stress concentrations depend not only on the rock elastic properties but also on the orientation of the planes of rock anisotropy with respect to the opening (Amadei, 1983). In general, stress concentrations in layered rocks can be quite different from those in isotropic rocks.

Stress concentrations around single or multiple undergound openings can also be (qualitatively) inferred using the 'stream flow' analogy proposed by Hoek and Brown (1980a) for elastic models. The idea is that the applied stress field is analogous to an undisturbed stream flow. In the wall of an excavation (equivalent to a pier in the stream flow), zones of tension may develop and are equivalent to a separation of the stream lines. On the other hand, the zones of compression correspond to a crowding of the stream lines. The stream flow analogy can be useful when trying to understand the overall stress pattern around multiple excavations and stress shadow effects that occur when excavations are in the near vicinity of each other.

The orientation of *in situ* stresses with respect to an excavation can have a large effect on the excavation stability. The excavation layout should be optimized in order to minimize the impact of *in situ* stresses. Geological structures or any other constraints (topography, water, etc.) also need to be taken into account in the optimization process. This has already been discussed in Chapter 1 with regard to the alignment of the penstock manifold at the Helms project (Fig. 1.3) and

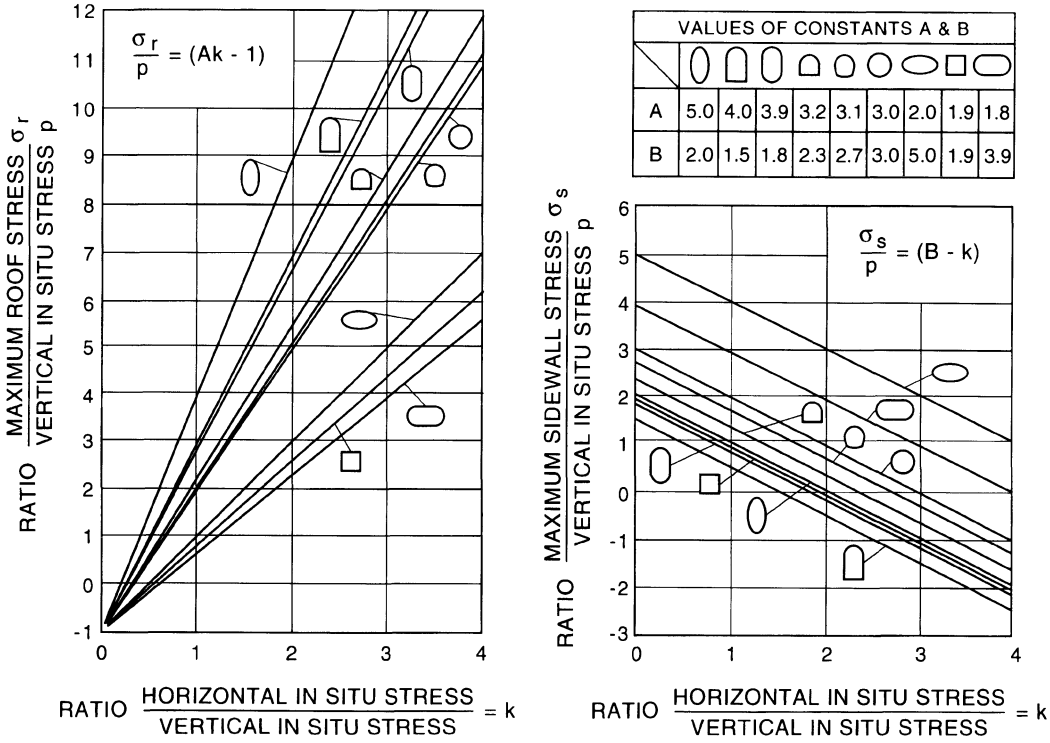

Fig. 12.5 Influence of excavation shape on tangential stress concentrations in the roof (σ_r) and springline (σ_s) of single openings in a uniform *in situ* stress field (p, kp). The rock is assumed to be homogeneous, continuous and linearly elastic. (After Hoek and Brown, 1980a.)

the orientation of the proposed underground nuclear waste repository at Hanford (Fig. 1.5). Various other examples have been reported in the literature. Haimson (1977) showed how *in situ* stresses and rock foliation were accounted for in the design of the underground openings at the Bad Creek pumped storage project in South Carolina.

The stability of rock caverns is very much controlled by their orientation with respect to the *in situ* stress field, along with other factors (Broch, 1993). In general, aligning caverns in rocks with their long axis perpendicular to the largest horizontal *in situ* stress component should be avoided (Broch, 1993; Richards, Sharp and Pine, 1977). Excellent case studies showing the decisive role of *in situ* stresses on cavern orientation selection can be found in Mimaki (1976), Mimaki and Matsuo (1986), Legge, Richards and Pound (1986), Deere *et al.* (1986), and Barla, Sharp and Rabagliati (1991). Figures 12.6a, b show strength/stress contours around a proposed power house cavern in the Niagara Falls area (Haimson, Lee and Huang, 1986). In this example the rock is horizontally stratified and the maximum and minimum horizontal *in situ* stresses are the major and intermediate principal stresses. The stresses around the cavern were determined using the finite element analysis and the strength was defined using the empirical Hoek and Brown (1980b) failure criterion. Figures 12.6a and 12.6b differ in the orientation of the cavern with respect to the horizontal stresses. In Fig. 12.6a the long axis of the opening is perpendicular to the maximum horizontal stress $\sigma_H = 9.2$ MPa. This results in large overstressed zones in the wall and floor of the

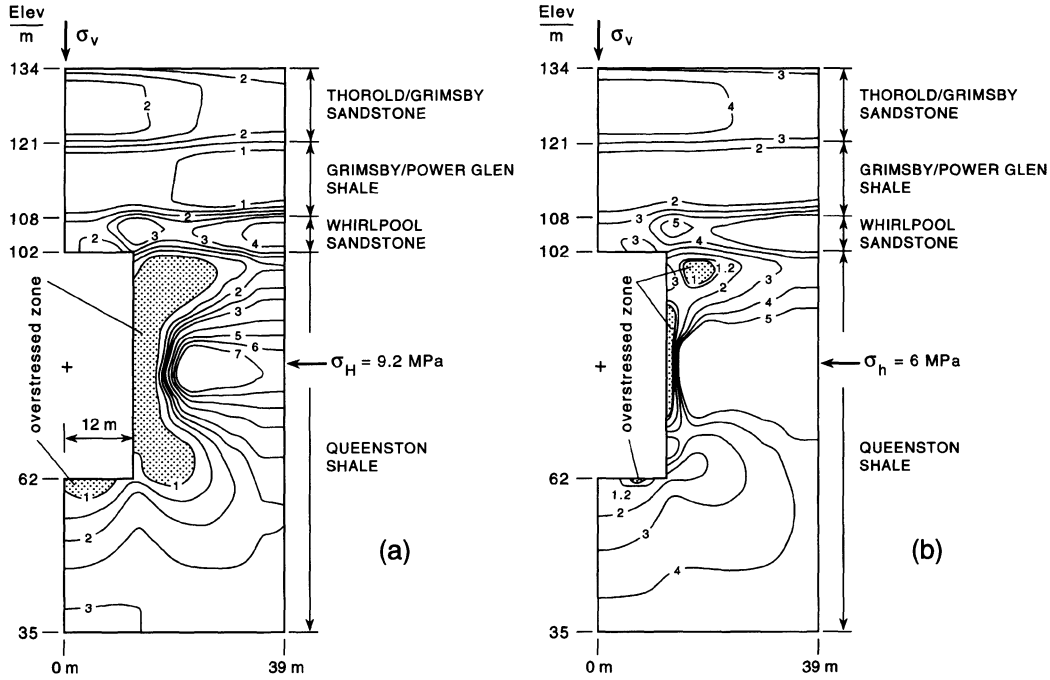

Fig. 12.6 Strength/stress contours around a proposed power house cavern in the Niagara Falls area. (a) Cavern axis perpendicular to the maximum horizontal stress $\sigma_H = 9.2$ MPa resulting in large overstressed zones, (b) cavern axis parallel to the maximum horizontal stress $\sigma_H = 9.2$ MPa and perpendicular to the minimum horizontal stress $\sigma_h = 6.0$ MPa resulting in smaller overstressed zones. (After Haimson, Lee and Huang, 1986.)

opening. On the other hand, in Fig. 12.6b the long axis of the opening is parallel to the maximum horizontal stress $\sigma_H = 9.2$ MPa and perpendicular to the minimum horizontal stress $\sigma_h = 6.0$ MPa. For that orientation the size of the predicted overstressed zone is reduced considerably.

It is usually accepted that stress-related instability problems increase with depth and that structurally controlled problems are more likely to occur at shallow depths. There are many exceptions to this trend, in particular in regions where high horizontal *in situ* stresses exist at shallow depths. As discussed more extensively in section 2.11, this is the case near Lake Ontario (southern Ontario and upper New York State), where stresses of the order of 5–15 MPa have been measured at shallow depths and where stress relief phenomena such as heave of canal and quarry floors, natural pop-ups, rock squeeze, rockbursts, tunnel wall spalling, cracking of tunnel concrete linings and/or movement of the walls of unsupported excavations (tunnels, shafts and canals) have been observed (Asmis and Lee, 1980; Franklin and Hungr, 1978). Rock squeeze applies additional loads to surface and underground structures, which may present considerable difficulties in maintaining operations (Lee and Klym, 1977). It is noteworthy that many of the problems observed near Lake Ontario in Canada and in the USA have also been observed in highly horizontally stressed sedimentary post-Permian rocks in the Sydney Basin in Australia (Enever, Walton and Windsor, 1990). Other examples where high horizontal *in situ* stresses have played a significant role in the stability of civil (and mining) engineering excavations have been reported by Broch and Nielsen (1979), Carlsson and Olsson (1982), Myrvang (1993) and Stephansson (1993) for various underground works in Norway and Sweden.

In high horizontal stress fields, stress-induced instability problems are likely to occur in the roof and floor of excavations in the form of spalling or squeezing due to high stress concentrations. As shown in Fig. 12.5, for the simple case of a circular opening, the maximum tangential stress in the roof and floor of the opening is about three times the horizontal stress if the vertical stress is insignificant. If the opening is close to the surface, the stress concentrations in the roof and floor are no longer equal and depend on the rock cover. For a rock cover equal to 10% of the tunnel diameter, the stress concentration in the roof is about seven times the horizontal stress. Hanssen and Myrvang (1986) reported several examples of tunnels running N–S in the Kobbelv area in northern Norway experiencing heavy spalling in their roofs and floors as they were driven perpendicular to the E–W trending major *in situ* stress component.

If the rock is bedded, layered or stratified, the effect of high horizontal *in situ* stresses will be enhanced and will be expressed in the form of buckling and heaving of roof and floor layers, respectively. Slip along layers may also create large inward and horizontal displacements of the tunnel sidewalls. Several case studies showing this phenomenon were described by Lee (1978) and Franklin and Hungr (1978) for some tunnels in sedimentary rocks in southern Ontario. Guertin and Flanagan (1979) reported several cases of tunnel problems following excavation of tunnels at shallow depths (1–7 m) in a highly stressed (up to 14 MPa) undeformed dolostone in Rochester, New York. Horizontal displacements as large as 40 mm were measured at the tunnel springline, whereas the crown experienced a heave of 0.4 mm. The displacements were accompanied by invert and crown spalling (due to high tangential compressive stresses) and cracking at the springline (due to tangential tensile stresses). All these case studies revealed, among other things, that in stratified rock masses the roof and floor stability problems may not necessarily be the same due to differences in rock layer stiffness and strength.

In general, the presence of high horizontal stresses at any depth should be clearly defined

and properly taken into account in the planning, design and construction of all major rock engineering projects. Failure to anticipate the existence of high stresses may result in structural damage and expensive remedial work as most design methods based only on gravitational loading are invalidated in that case (Franklin and Hungr, 1978). High horizontal stresses may also create problems during excavation. Myrvang (1993) noted several case studies showing the difficulties associated with TBM boring in a rock with violent surface spalling.

Different strategies can be followed to minimize the impact of high horizontal *in situ* stresses. Franklin and Hungr (1978) recommended delaying tunnel lining following excavation. They also suggested maximizing the distance between the location of rock excavation and the nearest rigid support by overexcavation. Linings and supports should either be flexible enough or should be protected by a deformable interface capable of accommodating up to 10 cm of movement of the excavation walls. Monitoring of displacements and rock pressures are also highly recommended. It has also been found that spalling and overbreak in the crown of tunnels can be successfully controlled by using rock bolting with or without shotcrete. In mining, the impact of high ground stresses can be minimized by experimenting with mining sequence and controlled yielding of pillars and closing of excavations.

It must be kept in mind that high horizontal stresses may be beneficial in making the rock tighter, self-supporting and less inclined to create seepage problems. Pathways for contaminant transport are also smaller. In some cases, high horizontal stresses may permit the use of large (mostly unsupported) roof spans in underground caverns, a recent example being the 61 m span underground Olympic ice hockey hall in Lillehammer, Norway (Myrvang, 1993).

The reader should be aware that the effect of *in situ* stresses on the stability of underground openings may vary with time. Stress changes around underground openings may be associated with rock creep, nearby excavations, sequences of excavation, pumping, poor drainage, earthquake loading, blasting, etc. As discussed in Chapter 10, stress changes can be quite complex with some regions of a rock mass experiencing loading and others experiencing unloading. As noted by Kaiser and Maloney (1992), unloading can be critical as some of the previous rock mass confinement is reduced and the rock–support interaction is affected. The role of stress path on the stability of rock masses has been observed in the field but has not received much attention by numerical modelers (Amadei, Robison and Yassin, 1986; Kaiser, 1980; Kaiser and Maloney, 1992; Martin, 1995).

12.2.2 IMPORTANCE OF *IN SITU* STRESSES FOR PRESSURE TUNNELS AND SHAFTS

In situ stresses play an important role in the siting and design of unlined pressure tunnels and shafts. Pressure tunnels and shafts which are unlined over most of their length have been used in various hydroelectric schemes around the world and have been called upon to perform under increasingly higher heads, now approaching 1000 m (Bergh-Christensen, 1986). The first and foremost consideration in the safe design of unlined pressure tunnels is that water leakage by hydraulic opening (hydraulic jacking) of the rock mass must be avoided. Water leakage may lead to disastrous and costly consequences, as illustrated in several case studies (Brekke and Ripley, 1993; Broch, 1984a, b; Haimson, 1992; Marulanda, Ortiz and Gutierrez, 1986; Sharma *et al.*, 1991). Hydraulic jacking can be prevented by positioning unlined pressure openings in competent rock and under enough rock cover to provide confinement and watertight conditions. Another alternative is to use steel liners, which tend to be costly.

Several criteria have been proposed in the literature to determine the safe position of

pressure tunnels and shafts near slopes or valley walls (Brekke and Ripley, 1993; Broch, 1984a). All the criteria emphasize the importance of the topography and its variation over the project layout. One empirical criterion, used successfully in many hydroelectric projects, was first proposed by Bergh-Christensen and Dannevig in 1971 (Broch, 1984a, b). It states that, at each point along the pressure tunnel alignment, the minimum rock cover L, taken as the shortest distance to the valley slope surface and shown in Fig. 12.7, must be equal to

$$L = \frac{\gamma_w h_w F}{\gamma \cos\beta} \tag{12.1}$$

where h_w is the static water head at the point of the tunnel under consideration, β is the average slope angle of the valley side (less than 60°), γ_w and γ are the unit weights of the water and the rock mass, respectively, and F is a safety factor. For a near horizontal topography ($\cos\beta \approx 1$), equation (12.1) reduces to the traditional criterion where the minimum rock cover must be equal to $\gamma_w h_w F/\gamma$, that is, the vertical stress associated with the overburden rock must always exceed the water pressure at any point along the opening.

Another criterion, proposed by Selmer-Olsen, (1974) is based on the concept of using

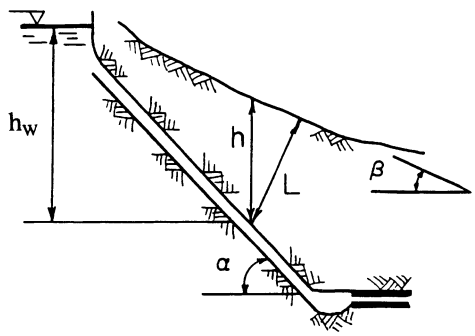

Fig. 12.7 Definition of minimum rock cover in empirical design criterion of Bergh-Christensen and Dannevig. (Source: Broch, E. Copyright 1984, with kind permission from Elsevier Science Ltd, The Boulevard, Langford Lane, Kidlington, UK.)

numerical methods, such as the finite element method, to determine the state of stress *in situ* in valley sides. The selection of the location of a pressure tunnel or shaft is based on the condition that along its alignment the internal water pressure $\gamma_w h_w$ is always less than the minimum *in situ* principal stress σ_3 in the surrounding rock mass (compression being positive). Mathematically, this criterion can be expressed as follows:

$$\sigma_3 > \gamma_w h_w \tag{12.2}$$

Design charts based on the finite element method have been proposed for idealized valley geometries and topographies and idealized rock mass properties.

Using the finite element method to determine the *in situ* state of stress for the purpose of selecting the alignment of pressure tunnels and shafts has several limitations. First, the method is restricted to finite domains. Second, the results tend to be mesh dependent and errors can arise when selecting the boundary conditions of the domain of interest. Third, most pressure tunnel and shaft design charts obtained with the finite element method are based on the assumption that the rock mass is continuous, homogeneous and isotropic. The effect of rock mass fabric such as bedding, foliation or jointing on the *in situ* stress distribution and magnitude is usually not taken into account. Fourth, the model topography is very much simplified and idealized. Fifth, most finite element analyses are two-dimensional and assume a plane strain condition. Finally, the stress perpendicular to the model plane is assumed to be the intermediate principal stress (Broch, 1984a), which is not always mechanically correct even under plane strain.

The design charts based on the finite element method can be replaced by analytical solutions recently proposed by Pan, Amadei and Savage (1994, 1995) and discussed in section 2.8. Recall that those analytical solutions can be used to estimate *in situ* stresses in ridges and valleys with smooth and irregular

topographies and in isotropic or anisotropic rock masses subject to gravity or to combined gravitational and tectonic loading. The use of those solutions for selecting the alignment of unlined pressure tunnels and shafts was explored by Amadei and Pan (1995). It was found that the safe alignment of unlined pressure tunnels or shafts depends greatly on the extent of tensile regions in valley walls, which itself depends on such parameters as the valley geometry, the degree of rock anisotropy, the orientation of the planes of rock anisotropy and the *in situ* loading conditions (gravity or gravity and tectonic).

Figure 12.8 shows the geometry considered by Amadei and Pan (1995) representing a two-dimensional cross-section of an anisotropic rock mass with an irregular topography consisting of long ridges and valleys. An x,y,z coordinate system is attached to the cross-section. Gravity acts in the $-y$ direction and tectonic stresses σ_{xx}^{∞} and σ_{zz}^{∞} act in the horizontal x and z directions, respectively. The rock mass is homogeneous, has a uniform unit weight γ and is transversely isotropic with planes of anisotropy striking perpendicular to the x,y plane and dipping at an angle ψ in the $+x$ direction. For the geometry of Fig. 12.8, at each point P(x,y) in the rock mass, the minimum *in situ* principal stress σ_3 can be determined using the analytical solutions of Pan, Amadei and Savage (1994, 1995).

The no-leakage condition can then be determined by comparing the predicted value of σ_3 with the water pressure at P(x,y) equal to

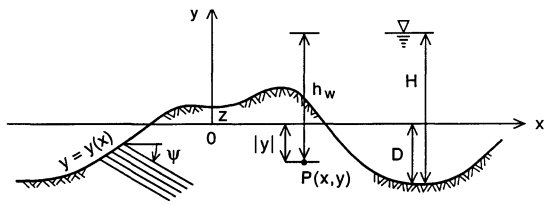

Fig. 12.8 Two-dimensional cross-section of an anisotropic rock mass with irregular topography and definition of variables for no-leakage condition. (After Amadei and Pan, 1995.)

$\gamma_w h_w$. At that point the static water head h_w is equal to $H - y - D$ where H is the maximum static water head and D is a characteristic depth of the topography. Thus the no-leakage criterion defined in equation (12.2) can be rewritten in dimensionless form as follows:

$$S = \frac{\sigma_3}{\gamma D} - \frac{\gamma_w}{\gamma}\left[\frac{H}{D} - \frac{y}{D} - 1\right] > 0 \qquad (12.3)$$

Contour diagrams of S can be generated for different types of topography, rock mass properties, rock mass loading conditions (gravity or gravity and tectonic) and different values of the ratio H/D. The contour $S = 0$ corresponds to the balance between increasing water pressure and increasing minor *in situ* principal stress. The domain $S > 0$ corresponds to the region in the rock mass in which unlined pressure tunnels can be placed without leakage. If a safety factor against leakage F is introduced (usually larger than 1.3), the critical contour is no longer $S = 0$ but $S = S_c$ with

$$S_c = \frac{\sigma_3}{\gamma D} - F\frac{\gamma_w}{\gamma}\left[\frac{H}{D} - \frac{y}{D} - 1\right] \qquad (12.4)$$

Amadei and Pan (1995) have shown that, in general, S and S_c depend on the following parameters: (1) the elastic constants of the rock and the dip angle ψ of the planes of rock anisotropy, (2) the relative density γ/γ_w of the rock, (3) the ratio between the maximum static water head H and a characteristic depth D of the topography, (4) the coordinates x/D and y/D of the point P(x,y) at which the leakage criterion is verified, (5) the parameters describing the topography and its irregularities, (6) the ratios $\sigma_{xx}^{\infty}/\gamma D$ and $\sigma_{zz}^{\infty}/\gamma D$ when tectonic loading is active in the x,z horizontal plane, and (7) the value of the safety factor F.

As an illustrative example, Figs 12.9a–f show contours of the minimum principal stress $\sigma_3/\gamma D$ (Figs 12.9a–c) and contours of S (Figs 12.9d–f) for a symmetric valley for $H/D = 0.5$, 1.0 and 1.5. The rock is strongly anisotropic with $E/E' = G/G' = 3$, $\nu = 0.25$

and $\nu' = 0.15$ (using the notation defined in section 2.5). The planes of anisotropy dip at an angle $\psi = 30°$ in the $+x$ direction. The characteristic depth D is equal to the depth of the valley. The rock mass is (1) under gravity only in Figs 12.9a,d; (2) under gravity and a uniaxial tectonic compressive stress field $\sigma^{\infty}_{xx}/\gamma D = 1$ in Figs 12.9b, e; and (3) under gravity and a biaxial tectonic compressive stress field $\sigma^{\infty}_{xx}/\gamma D = \sigma^{\infty}_{zz}/\gamma D = 1$ in Figs 12.9c, f. Figures 12.9a–f indicate that because the planes of rock anisotropy are inclined, the tensile and no-leakage regions are not symmetric with respect to the axial plane of the valley. Further, the right side of the valley experiences more of a compressive state of stress and is more favorable than the left side with regard to positioning unlined pressure tunnels. Further, the extent of the no-leakage region ($S > 0$) increases as the maximum static water head H decreases, as expected. Finally, addition of far-field compressive stresses reduces the extent of the tensile region in the valley walls and bottom (the tensile region vanishes in Fig. 12.9c), and increases the extent of the no-leakage region on both sides of the valley.

The criteria mentioned above are usually used at the preliminary stage of design of pressure tunnels and shafts. They are useful in assessing the feasibility of a project and in providing recommendations with regard to the maximum length of a pressure opening

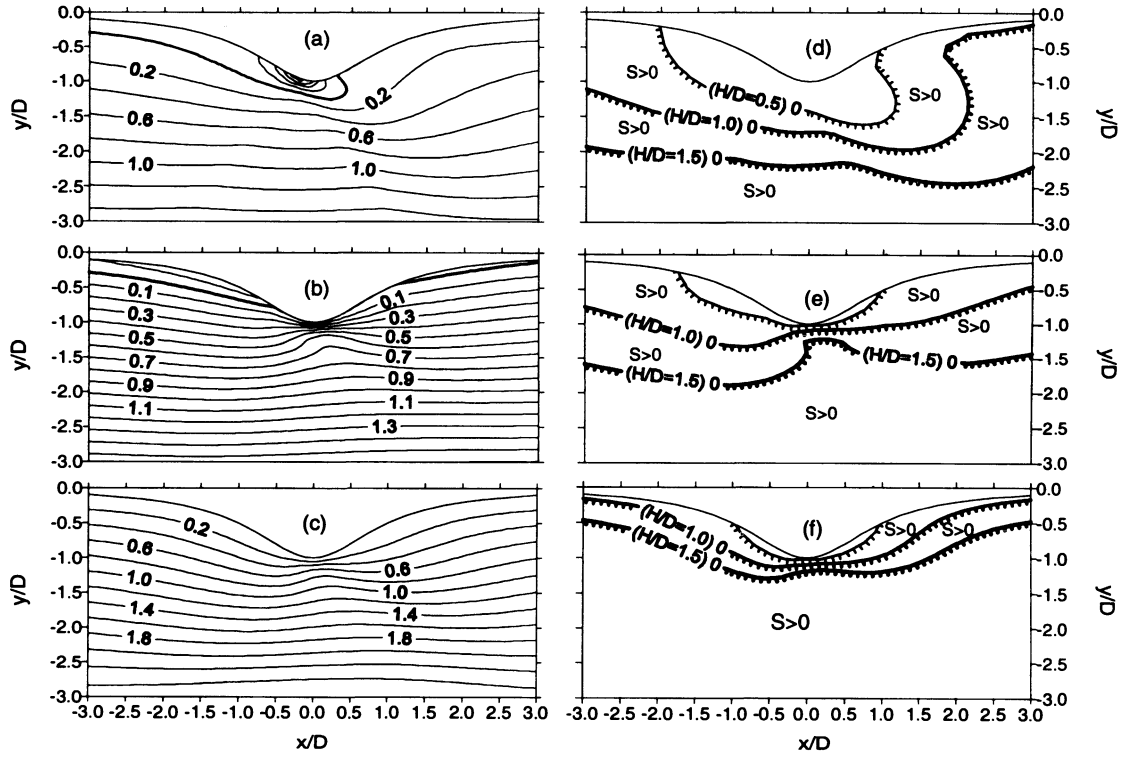

Fig. 12.9 Contours of $\sigma_3/\gamma D$ in (a)–(c) and $S = 0$ in (d)–(f) for a symmetric valley. The contours of $S = 0$ are obtained for $H/D = 0.5$, 1.0 and 1.5. The planes of rock anisotropy dip at 30° to the right. The rock mass is under gravity only in (a) and (d), under gravity and a uniaxial tectonic stress field $\sigma^{\infty}_{xx}/\gamma D = 1$ in (b) and (e), and under gravity and a biaxial tectonic stress field $\sigma^{\infty}_{xx}/\gamma D = \sigma^{\infty}_{zz}/\gamma D = 1$ in (c) and (f). (After Amadei and Pan, 1995.)

which can stay unlined with a minimum risk of water leakage. However, the criteria are based on an estimate of the *in situ* stress field. In order to verify the design assumptions and finalize the design, *in situ* stresses need to be measured. In the past, both overcoring and hydraulic fracturing have been used (Bergh-Christensen, 1986; Enever, Wold and Walton, 1992; Price Jones and Sims, 1984; Vik and Tundbridge, 1986). Overcoring is carried out with some of the techniques described in Chapter 5. Hydraulic fracturing is done in a simplified manner by measuring only the shut-in pressure and by setting that pressure to be equal to the minimum *in situ* stress. As an illustrative example, Fig. 12.10 shows the location of several hydraulic fracturing measurements reported by Bergh-Christensen (1986) and conducted adjacent to a power station near the base of a 1300 m long unlined pressure shaft with a static head of 965 m at the Nauseate–Steggje hydropower project in western Norway. The sandtrap in Fig. 12.10 located at the foot of the pressure shaft has the highest water pressure acting on the unlined rock with a value of 9.64 MPa. The lowest value of the minimum stress σ_3, measured using the shut-in pressures of hydraulic fracturing tests, is 12.3 MPa. Comparison of this pressure with the maximum applied water pressure gives a safety factor of $12.3/9.64 = 1.3$ against hydraulic jacking. This value of the safety factor was found to be in agreement with (1) the safety factor determined using the empirical rule of Bergh-Christensen and Dannevig and equal to 1.3, (2) the safety factor based on finite element charts and equal to 1.4–1.5 and (3) the safety factor determined from the results of overcoring tests and equal to 1.3.

12.2.3 IMPORTANCE OF *IN SITU* STRESSES FOR UNDERGROUND STORAGE OF FLUIDS

In situ stresses, and rock mechanics in general, play a decisive role in the design of unlined rock caverns used for underground storage of fluids such as gas, oil, compressed air, cryogenic liquids and heated water. As for pressure tunnels and shafts, leakage and hydraulic or pneumatic failure must be avoided by providing enough confinement and by requiring that the fluid pressure does not exceed the

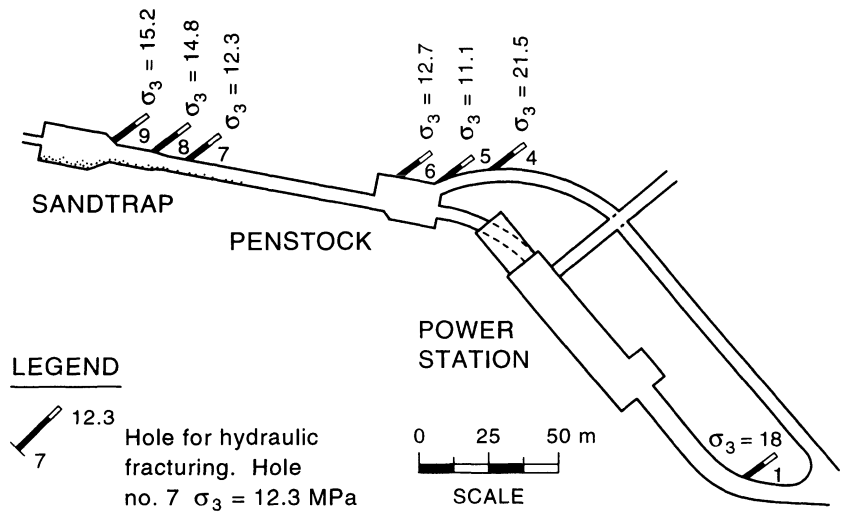

Fig. 12.10 Location of hydraulic fracturing measurements adjacent to a power station near the base of a 1300 m long unlined pressure shaft with a static head of 965 m at the Nauseate–Steggje hydropower project in western Norway. (After Bergh–Christensen, 1986.)

minor principal stress in the rock mass. The construction cost of storage caverns can be reduced if confinement due to sufficiently large *in situ* stresses can be found at shallow depths.

The stress field in the rock around an unlined storage cavern is the combination of four types of stresses: (1) *in situ* stresses, (2) stresses associated with the excavation of the cavern, (3) stresses related to the operation of the cavern (which is often under pressure) and (4) stresses resulting from the interaction between the stored material and the rock in the cavern wall. A good example of the latter corresponds to thermal stresses generated in the walls of LNG storage caverns where the LNG can be at temperatures as low as −250°F (−160°C). Such low temperatures can induce tensile stresses large enough to create thermal cracking of the rock mass, either in the form of new fractures or opening of existing ones, which could result in migration of the stored fluids and further crack propagation (Lindblom, 1977). It is noteworthy that the storage of cryogenic fluids at very low temperatures or, on the other hand, the storage of heated water and oil at temperatures 100–200°F (40–90°C) higher than the ambient temperature induces thermal stresses that vary with time since the temperature distribution in the rock is non-uniform. Such transient effects need to be taken into account when predicting the short- and long-term stability of the wall of storage caverns.

When fluids are stored in unlined caverns excavated in crystalline rocks, most of the leakage is likely to occur along fractures. This problem has been addressed by various authors, in particular in Scandinavian countries. In the case of natural gas (or compressed air), which can be stored at pressures up to 10 MPa, two criteria are used: the gas entry condition and the gas migration condition (Goodall, Åberg and Brekke, 1988). The escape of gas can be reduced or even eliminated using rock confinement by placing storage caverns at large depth (and sometimes at shallow depth when the stresses are high), and by ensuring that the caverns are located deep enough below the water table in order to provide a proper groundwater seal for gas containment (hydrodynamic containment). Sometimes water curtains in the roof or in the roof and walls of the caverns are installed (in the form of parallel drillholes) to provide artificial hydrodynamic containment in addition to that created by the natural water table. This allows gas pressures higher than the natural hydrostatic pressure, thus significantly improving the economics of the storage (Kjorholt and Broch, 1992; Liang and Lindblom, 1994; Lindblom, 1990; Roald, Ustad and Myrvang, 1986). The amount of pressure that can be applied by water curtains is limited by the *in situ* stresses since jacking of the rock mass by opening of the fractures must be avoided (Gustafson, Lindblom and Söder, 1991). The same limitation applies to cryogenic grouting pressures when used to seal rock mass fractures around LNG caverns (Lindblom, 1977).

12.2.4 ROLE OF *IN SITU* STRESSES IN THE BEHAVIOR OF SURFACE EXCAVATIONS

Whether a rock slope is natural or artificial, stress redistribution occurs as a result of the excavation. The final stress field associated with the new topography can be analyzed using the models discussed in section 2.8. At and near the excavation, the principal stresses are essentially parallel and normal to the ground surface. Away from the excavation, the stress field approaches the pre-excavation stress field.

As for underground excavations, instability problems near surface excavations may arise due to the stress redistribution. Excessive compression may lead to local or global slope failure. This can be critical in deep excavations such as open-pit mines where the stresses at the bottom of the pit may be large enough to mobilize the rock compressive strength or create buckling of steeply dipping layers. On the other hand, tension may destabilize the

rock mass, accelerate weathering and create block stability and drainage problems, thus creating a zone near the excavation surface in which the rock mass is looser and discontinuous. In the case of open-pit mining, this may result in an increased risk of bench failure.

Surface excavation of rock masses with high horizontal *in situ* stresses may result in large lateral movement of the excavation walls. The problem is exemplified in horizontally bedded rock formations where slip along bedding planes occurs as stresses are relieved. Such a phenomenon has been well documented for surface excavations in southern Ontario in Canada and upper New York State in the USA (Franklin and Hungr, 1978; Guertin and Flanagan, 1979). Rock movements as large as 23 cm have been reported in open excavations in that geographical area by Rose as early as 1951 (Guertin and Flanagan, 1979). More recent case studies of horizontal displacements due to high stresses can be found in Enever, Walton and Wold (1990) for excavations in the post-Permian rocks in the Sydney Basin. These authors also reported an example of a road cut stability problem where surface spalling was created by stress concentration in highly stressed rock.

Stress redistributions may also create problems in underground excavations located near the walls of surface excavations such as pressure tunnels and shafts (section 12.2.2), underground power stations or mines. Overstressing of tunnel walls and roofs expressed in the form of spalling and rock bursts in mountainous areas with steep valley walls is well documented in the literature (Brekke and Selmer-Olsen, 1966; Broch and Sorheim, 1984; Martna, 1988; Martna and Hansen, 1986, 1987; Myrvang, 1993; Myrvang, Hansen and Sørensen, 1993). Broch and Sorheim (1984) quoted the following rule of thumb for tunneling in mountainous areas in Norway: 'if in a valley side heights above the tunnel of 500 m or more are reached at an angle of 25° or steeper, one should always be prepared for rock stress induced stability problems'.

Myrvang, Hansen and Sørensen (1993) gave an example of stress redistribution around the Bjørnevatn iron ore open-pit mine in Kirkenes in northern Norway. Stress measurements in the near vicinity of the pit revealed sharp increases in stress associated with surface mining (over a period of 19 years) in a rock mass initially subjected to high horizontal *in situ* stresses. Figure 12.11 shows the principal stress distribution predicted by two-dimensional boundary element modeling of an E–W vertical section of the pit, and the location of a ramp for underground mining. Heavy spalling in the roof of the ramp due to stress concentration predicted by the numerical model was also observed during excavation.

Another example illustrating the role played by surface excavation on nearby underground openings was reported by Molinda *et al.* (1992). By conducting a survey on the nature and frequency of coal mine roof failure beneath valleys, they found that 52% of the unstable roof cases in the surveyed mines occurred directly beneath the bottom-most part of the valleys. The survey also showed

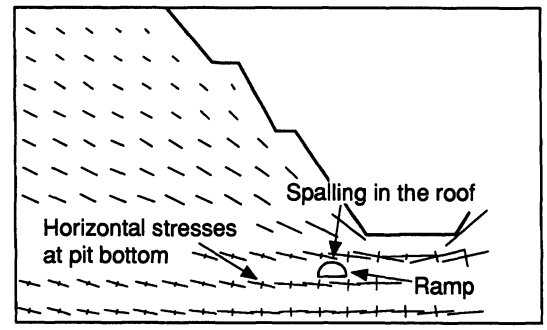

Fig. 12.11 Predicted stress distribution in a vertical E–W section of the Bjørnevatn iron open-pit mine in Kirkenes in northern Norway using the boundary element method. The boundaries of the model were subjected to a 24 MPa horizontal stress to model the *in situ* stress field. (Source: Myrvang, A., Hansen, S.E. and Sørensen, T. Copyright 1993, with kind permission from Elsevier Science Ltd, The Boulevard, Langford Lane, Kidlington, UK.)

that broad, flat-bottomed valleys were more likely to be sites of hazardous roof conditions than narrow-bottomed valleys.

12.3 STRESSES IN MINING ENGINEERING

Over the past 10 years, rock mechanics has become more of a practical tool for surface and underground mine operators. As noted by Bawden (1993), the increased acceptance of rock mechanics techniques in mining is largely due to the development of more sophisticated two- and three-dimensional numerical modeling techniques, the availability of powerful desktop computers and an increased confidence in the ability to determine input parameters for design. Such parameters include rock mass strength and deformability and the *in situ* state of stress, among others. Numerical methods (along with empirical methods) have been found to be very useful in mine planning and sequencing, for the analysis of local areas of potential instability and when assessing the role played by specific geological structures. Numerical analysis can help in the optimization of pillar, stope and shaft location and dimensions. In general, rock mechanics and rock engineering can strongly influence the profitability and survivability of mining operations (Brady and Brown, 1985; Hoek and Brown, 1980a).

Pre-mining stresses form the loading system for underground mine excavations (Bawden, 1993). Redistribution of these stresses due to excavation associated with mining can cause deformation and failure of the rock mass. Analytical methods and numerical methods can be used to predict how the stress redistribution takes place. Obviously, the predictions will only be as good as the original stress input. Data compilations from different geological provinces, such as those presented by Brown and Hoek (1978), Stephansson, Särkkä and Myrvang (1986) and Herget (1993), are often used as a starting point in mine design studies. However, as noted in Chapter 2, the stress field can be extremely variable and simply selecting stress input from published curves of stress versus depth may, in some cases, be misleading and result in serious design errors. Therefore, whenever possible, pre-mining stresses for mine design purposes should be measured.

Many of the trends outlined in the previous section regarding the role played by *in situ* stresses in civil rock engineering projects apply to mining projects as well. Other trends are more specific to mining and the mining methods used. The impact of the pre-mining state of stress with specific reference to the design problems posed in open stoping development has been addressed by Brady and Brown (1985), Bawden (1993) and Barla (1993). The role of *in situ* stresses in mine design was also emphasized: (1) by Krauland (1981) for cut and fill mining, (2) by Ferguson (1993) and Singh, Stephansson and Herdocia (1994) for sublevel caving and block caving, (3) by Hardy and Agapito (1977) for room and pillar mining and (4) by Mills, Pender and Depledge (1986), Gale (1986) and Enever (1993) for coal mining.

As an illustrative example, Gale (1986) presented a case study of optimization of rectangular mine roadway driveage in the southern coalfield in Australia. The *in situ* stress field measured by overcoring was such that the ratio of maximum horizontal stress : minimum horizontal stress : vertical stress could be expressed in the range (1.3–2.0) : 1: (0.82–1.3). The orientation of the roadway axis with respect to the maximum horizontal *in situ* stress σ_1 was found to control the stability of the roadway roof strata. This is shown in Fig. 12.12 where the percentage of roadway driveage affected by shear fracture of roof strata (measured by field survey) at two sites has been plotted versus the angle θ_{SR} between the roadway axis and σ_1. Also plotted on this figure is the theoretical variation of the factor of safety against shear failure for the roof strata (assuming Coulomb failure) versus the angle θ_{SR}. The factors of safety were normalized as a percentage of the maximum value

obtained. Figure 12.12 indicates that the occurrence of shear failure increases as θ_{SR} tends to 90° or, in other words, as the roadway becomes more perpendicular to the major horizontal *in situ* stress component. Thus good stable driveage conditions occur for roadways driven at small angles to σ_1 whereas roadways driven at angles $\theta_{SR} > 45°$ exhibit rock failure.

Another example of mine layout optimization was reported by Mills, Pender and Depledge (1986) for some coal mines in New Zealand. Based on the results of *in situ* stress measurements and the local geology, they concluded that the preferred mining direction should be perpendicular to the major cleat direction of the coal and the largest horizontal *in situ* stress. In order to reduce mine roof stability problems, they recommended using rectangular openings with a horizontal long axis at shallow depths where the horizontal *in situ* stress is about 1.5 times the vertical stress. At larger depths the ratio is about 0.3 and openings with a vertical long axis are better suited. This is a good example showing how the shape of a mining excavation can be varied with depth in order to accommodate changes in the *in situ* stress field.

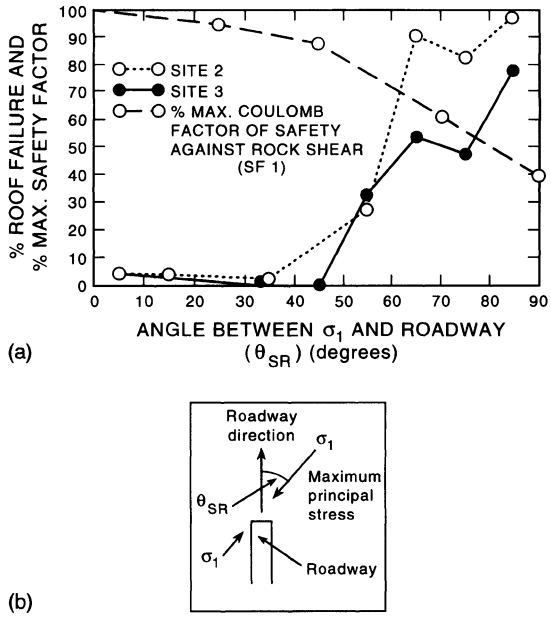

Fig. 12.12 (a) Percentage of roadway driveage affected by shear failure of roof strata at two sites versus the angle θ_{SR} between the roadway axis and σ_1 (see (b)). Also plotted in (a) is a theoretical variation of the factor of safety against shear failure for the roof strata (assuming Coulomb failure) versus the angle θ_{SR}. The factors of safety were normalized as a percentage of the maximum value obtained. (After Gale, 1986.)

Traditionally, most stress measurements for mining engineering purposes are conducted by three-dimensional overcoring techniques from accessible drifts and openings. This allows the possibility of recording any variation in the regional stress field of the mine and provides stress data for detailed design and remedial actions for support. The variation of the *in situ* state of stress at different levels of the iron ore mines at Kiruna and Malmberget of northern Sweden was presented by Leijon (1986) and Leijon and Stillborg (1986). Figure 12.13 is a horizontal section of the 795 m level of the Kiruna mine showing average *in situ* stress measurements at eight locations. This figure indicates the existence of significant stress variations on a scale of several hundred meters across the mine. Such variations, which are often found near orebodies, may create difficulties in the interpretation and application of *in situ* stress data for mine design (Leijon, 1986).

The stress data recorded from the application of two different rock stress measurement techniques at the Luossavaara mine (Leijon and Stillborg, 1986) are used below to demonstrate the procedure used in the design of a crown pillar of a large blasthole open stoping mine.

In the Luossavaara iron ore deposit at Kiruna in northern Sweden, a new bulk mining method called large blasthole open stoping was developed and tested in the mid-1980s. The orebody is 1200 m long, with an average width of 23 m and dips about 60° toward the east. A major crown pillar separating the previously mined upper sections of the

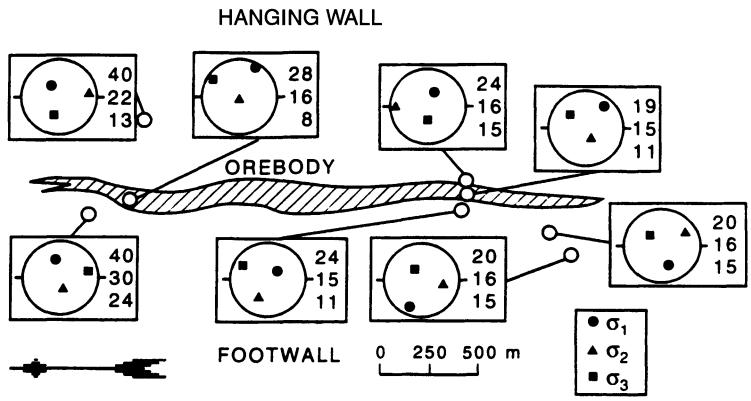

Fig. 12.13 Plan view of the 795 m level of the Kiruna mine showing average *in situ* stress measurements (stresses in MPa) at eight locations. (After Leijon, 1986.)

orebody from the lower stopes had to be designed. The crown pillar not only acted as a support member to provide global stability, but also as a working platform from which drilling was carried out. Two approaches were used in determining the dimensions of the crown pillar, as described by Stillborg (1993).

First, a simple analytical method based on the two-dimensional hanging-wall caving model developed by Brown and Ferguson (1979) was used. The loading is governed by the weight of the wedge of the sliding rock in the hanging wall and the weight of the caved material laying on top of the crown pillar. Using the relevant rock mass strength and geometry, it was concluded that the hanging-wall stability would be ensured if an entire crown pillar thickness of more than 5 m was used. Considering the width of the orebody, the virgin rock stresses and blast-induced fracturing, Stillborg (1993) stated that the top part of the crown pillar should have a minimum thickness of 10 m.

The second method used in the stability analysis of the crown pillar at the Luossavaara mine was assessed by comparing the strength at various points in the pillar to the applied pillar stresses (Stephansson, 1985). A geomechanical model of the crown pillar is presented in Fig. 12.14 and the rock properties for numerical modeling are listed in Table 12.1. The finite element method was used to obtain the stress distribution in crown pillars of different sizes. Pillar stability was determined by using the conventional factor of safety F = strength/stress. Boundary stresses for the two-dimensional finite element analysis were taken from the results of a comparative study of two overcoring stress measurement techniques presented by Leijon and Stillborg (1986; section 9.2). From the compilation of the stress measurement data at the 265 m level, the following *in situ* stresses (in MPa) were applied as boundary stresses to the finite element model:

$$\begin{aligned} \sigma_v &= 0.027z - 0.2 \\ \sigma_H &= 0.05z - 5.1 \end{aligned} \tag{12.5}$$

for the hanging wall,

$$\begin{aligned} \sigma_v &= 0.05z - 5.4 \\ \sigma_H &= 0.05z - 0.1 \end{aligned} \tag{12.6}$$

for the orebody and

$$\begin{aligned} \sigma_v &= 0.036z - 2.0 \\ \sigma_H &= 0.05z - 2.7 \end{aligned} \tag{12.7}$$

for the footwall. The pillar strength was determined using the method presented by Stephansson (1985), which accounts for the fact that large volumes of rock have lower

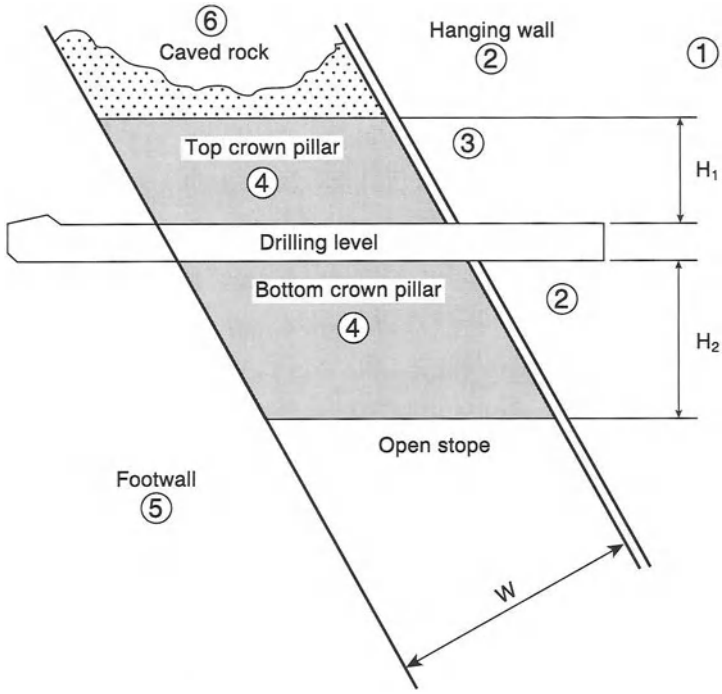

Fig. 12.14 Geomechanical model of the crown pillar at Luossavaara mine. Numbers refer to rocks listed in Table 12.1. (After Stephansson, 1985.)

strength than small laboratory specimens. The volume dependence of strength is determined using the equation

$$\sigma_o = \sigma_c \left(\frac{V_l}{V_i}\right)^{\alpha} \tag{12.8}$$

where σ_o is the unconfined compressive strength of the pillar, σ_c is the average value of the uniaxial compressive strength listed in Table 12.1, V_l is the volume of the laboratory specimens, V_i is the volume of the pillar and α is a coefficient of volume reduction equal to 0.007.

Next, the effect of confinement (or the minor *in situ* principal stress) is accounted for by using the following formula for the strength at any point in the pillar:

$$\sigma_p = \sigma_o + q\sigma_3 \tag{12.9}$$

Table 12.1 Rock properties for numerical modeling of the crown pillar at the Luossavaara mine (after Stephansson, 1985)

Rock type	*Young's modulus (GPa)*	*Uniaxial compressive strength (MPa)*	*Poisson's ratio*	*Unit weight (kg/m^3)*
Quartz-bearing porphyry (1)	57	110	0.16	2700
Foliated quartz-bearing porphyry (2)	38	110	0.16	2700
Chloritized quartz-bearing porphyry (3)	13	20	0.10	2400
Ore (4)	38	100	0.11	4970
Breccia (5)	60	52	0.16	3600
Caved material (6)	0.030	–	0.25	2400

where σ_p is the confined pillar strength, σ_3 is the minimum *in situ* principal stress, and $q = (1 + \sin\phi_b)/(1 - \sin\phi_b)$ where ϕ_b is the base friction angle of the joints in the pillar.

A number of model geometries based on the geomechanical model presented in Fig. 12.14 were run, in which the height of the bottom crown pillar H_2 was varied. Distributions of the pillar strength and factor of safety in the crown pillar for $H_2 = 15$ m are shown in Figs 12.15a and 12.15b, respectively. It can be seen that the pillar strength and factor of safety vary considerably throughout the pillar. Hence it was decided that an overall assessment of the pillar stability could be obtained by considering the factor of safety at the pillar midpoint.

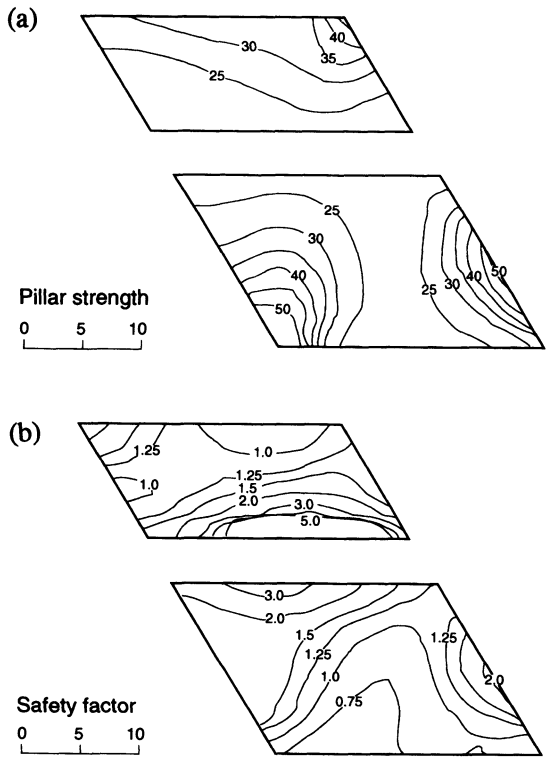

Fig. 12.15 Distribution of pillar strength in MPa in (a) and safety factor in (b) for the top and bottom crown pillars at the Luossavaara mine for a bottom crown pillar height $H_2 = 15$ m. (After Stephansson, 1985.)

Figure 12.16a,b shows variations of the pillar strength and factor of safety determined by finite element analysis at the pillar midpoint for different pillar height to width ratios. These results indicate that for the bottom crown pillar (Fig. 12.16a), both strength and factor of safety increase with increasing height

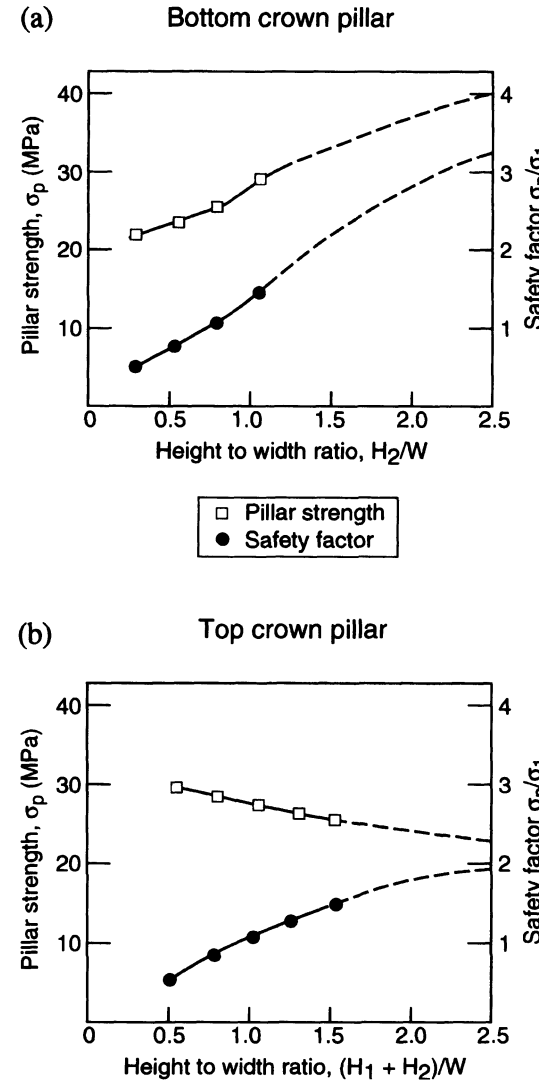

Fig. 12.16 Variation of pillar strength and safety factor at pillar midpoint as a function of pillar height to width ratio. (a) Bottom crown pillar, (b) top crown pillar. (After Stephansson, 1985.)

to width ratio. On the other hand, in the top crown pillar (Fig. 12.16b), the safety factor increases while the strength decreases. This somewhat unusual behavior in the top crown pillar is caused by a decrease in the minor principal stress component as the bottom crown pillar is increased in size, thereby yielding a decreasing strength.

As stated by Hardy and Agapito (1977), a safety factor of 1.2–1.3 is needed for pillars to carry the weight of the overburden of a mine. A safety factor of 1.3 for pillars in general has been suggested by Hoek and Brown (1980a). For the pillar design at the Luossavaara mine, a safety factor of 1.25 was selected. Using the plots in Fig. 12.16 for a top crown pillar thickness $H_1 = 10$ m, and an ore width $W = 20$ m, the thickness of the bottom crown pillar is $H_2 = 15$ m.

In conclusion, this analysis shows that an optimum design of the crown pillar at the 265 m level of the Luossavaara mine for the case of a 10 m high top crown pillar requires a 15 m high bottom crown pillar. This gives a yielding bottom crown pillar with a midspan safety factor of 0.8 and a full overburden support with a safety factor of 1.25 for the top crown pillar. Later mining, where rod and wire extensometers were used for ground control, confirmed the full stability of the crown pillar throughout the large blasthole open stoping of the stopes and pillars (Stillborg, 1993).

12.4 STRESSES IN GEOLOGY AND GEOPHYSICS

In geology and geophysics, a static or dynamic treatment of tectonic evolution is often introduced by considering the mechanical forces that act on the various parts of an arbitrarily limited three-dimensional region of the Earth that contains the structure in question. Such a region is often called a 'tectonic system' (Ramberg, 1981) and is generally affected by different types of mechanical forces which can be divided into surface (boundary) forces and body forces (gravity, inertia and volume changes). These forces create stresses in the system, the distribution and magnitude of which greatly depend on the geometric pattern of the system, the mechanical properties of its constituent rocks and the existence of geological structures.

The fundamental role played by *in situ* stresses in the mechanics of development of geological structures (fractures, faults, folds, intrusions, etc.) has been recognized by structural geologists and geophysicists for a long time. Understanding the processes by which geological structures are formed and emplaced and how they deform and fracture is also of practical value to civil, petroleum and mining engineers. We present below several examples of mechanical analysis of geological structures where *in situ* stresses play a critical role. The reader interested in more specific aspects is referred to the excellent books by Ramsay (1967), Johnson (1970), Mattauer (1973), Ramberg (1981) and Price and Cosgrove (1990), among others.

12.4.1 EMPLACEMENT OF IGNEOUS INTRUSIONS

Igneous materials which are intruded as dikes (discordant sheet intrusions) or sills (concordant sheet intrusions) usually originate from a magma chamber. Until the pressure in the magma chamber exceeds the overburden stress, significant upward migration of the magma in the country rock in the form of sheet intrusions is unlikely to occur. At depth, it is believed that the mechanism for the emplacement of dikes and sills is by means of forceful injection which occurs as a result of hydraulic fracturing of the crust (Price and Cosgrove, 1990). Another mechanism closer to the surface would be passive flow in open fractures. Neglecting stress concentrations at the tip of a propagating intrusion, Price and Cosgrove (1990) proposed the following simple condition for hydraulic fracturing of a magmatic

intrusion:

$$P_m > S_3 + T \tag{12.10}$$

where P_m is the magmatic pressure, S_3 is the total minimum *in situ* principal stress and T is the tensile strength of the rock mass in which fracturing develops. Application of equation (12.10) to the intrusion of a vertical dike gives

$$P_m > S_h + T_h \tag{12.11}$$

where S_h is the minimum principal horizontal stress and T_h is the tensile strength of a given rock type tested or defined in extension parallel to the geological formation, and in the direction of the minimum horizontal stress (Fig. 12.17). If the magmatic pressure P_m is exactly equal to $S_h + T_h$, the pressure is just sufficient to initiate hydraulic fracturing. If the magmatic pressure remains unchanged, it then exceeds the minimum horizontal stress S_h by the magnitude of the tensile strength T_h. This excess of stress will tend to push back the walls of the hydraulic fracture and form a dike of finite width.

The excess of magmatic pressure relative to the least horizontal principal stress, can in some cases be related to the aspect ratio of the dike, e.g. the ratio between its length and maximum width. This relation was suggested by Gudmundsson (1983), who derived an expression between the aspect ratio of a fracture of finite length and the tensile stress at the time of fracture formation, assuming the surrounding rock to be linearly elastic and isotropic with Young's modulus E and Poisson's ratio ν. According to Gudmundsson (1983), the tensile stress T is related to the fracture length L and maximum width W_{max} as follows:

$$T = \frac{E}{2(1-\nu^2)} \frac{W_{max}}{L} \tag{12.12}$$

In the case of a dike, equation (12.12) can be used to determine the effective stress (or the magma overpressure) $T = P_m - S_h$ by measuring the dike's aspect ratio. This approach was followed by Gudmundsson (1983) who mapped 68 extension fractures as part of the Vogar fissure swarm in southeastern Iceland. The average fracture aspect ratio was reported to be equal to 650, $E = 4.85$ GPa and $\nu = 0.25$.

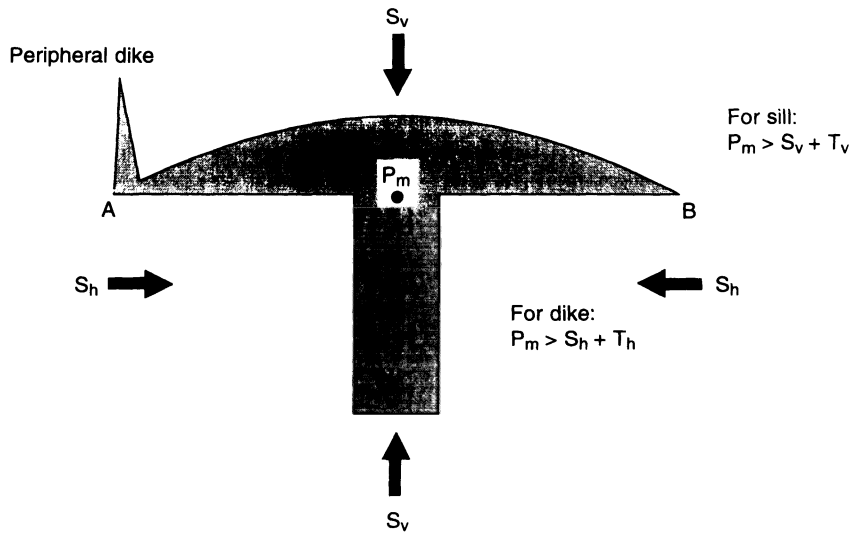

Fig. 12.17 Stress conditions compatible with dike and sill intrusions. (Adapted from Price and Cosgrove, 1990.)

Substituting these values into equation (12.12) gives a tensile stress or magma overpressure at the time of intrusion (if the fractures are interpreted as dikes) of 4 MPa, which is a reasonable value considering the scale effects and the low strength of columnar fractures in basaltic lava flows.

For the emplacement of a horizontal sill, the following condition must be satisfied between the magmatic pressure P_m, the vertical stress S_v and the tensile strength T_v in the vertical direction:

$$P_m > S_v + T_v \tag{12.13}$$

As remarked by Price and Cosgrove (1990), for the emplacement of sills in horizontally bedded or foliated rock formations, the vertical tensile strength is, for all practical cases, close to zero. Thus a sill intrusion into horizontally layered rock masses occurs when $P_m > S_v$.

Sills must be fed with magma from a pipe or a dike. At the junction of the feeder dike and the sill, the conditions governed by equations (12.11) and (12.13) must be satisfied simultaneously (Fig. 12.17). This gives the following relationship:

$$(S_v - S_h) < (T_h - T_v) \tag{12.14}$$

Since, as discussed above, the vertical tensile strength is almost zero, equation (12.14) indicates that sills fed from a dike are emplaced when the difference in magnitude between the vertical and minimum horizontal *in situ* stresses is less than the tensile strength in the horizontal direction, which is itself small (tens of MPa), in particular if the rock mass is jointed (Price and Cosgrove, 1990).

Equation (12.14) gives a possible explanation of the mechanism whereby a dike can become a sill. It can also be used to explain how a sill or laccolith terminates and changes into a dike. Indeed, according to Johnson (1970) and Price and Cosgrove (1990), for the geometry of Fig. 12.17 and for a sill or laccolith inclusion close to the ground surface, deflection of the roof of the inclusion due to increasing magmatic pressure results in a reduction in horizontal stress near the tips of the inclusion (points A and B in Fig. 12.17), which is conducive to the formation of a vertical dike (also called a 'peripheral' dike).

According to Price and Cosgrove (1990), analysis of magmatic intrusions can provide insight into how fluids other than magma can create fracturing *in situ*, and the stress regime of the rock mass at the time of emplacement of the intrusion. However, there is no guarantee that dike and sill structures mapped in the field reflect the present state of stress. On the contrary, large discontinuities in the *in situ* stress field are often measured in rock masses adjacent to dikes, sills and other magmatic intrusions. In many cases this is due to the large contrast in rock stiffness between the hard intrusion and the softer country rock.

12.4.2 SALT DIAPIRS

Diapirs are geological features which result when rocks of relatively low density pierce and rise through overlying rocks of higher density. The largest and most important diapirs are composed of rock salt (or other evaporites) or igneous rocks. Diapiric intrusions of salt may take many forms such as salt pillows, salt walls and salt domes or stocks (Trusheim, 1960). In general, diapir geometry depends upon the thickness, density and viscosity ratio of the source layer and the overburden rock (Ramberg, 1981). Salt diapirs are important in petroleum engineering as they create conditions favorable for the creation of hydrocarbon reservoirs in adjacent sediments.

The driving mechanism of a salt diapir is usually attributed to the buoyancy force of the low-density salt surrounded by denser rocks. Figure 12.18 shows the idealized geometry of an isolated salt stock emplaced into an overburden of denser rock. As shown by Price and

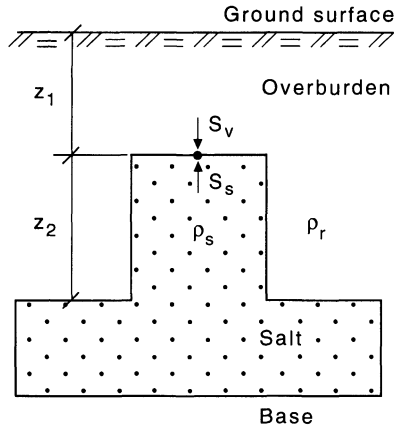

Fig. 12.18 Model of salt piercing through an overburden of denser rock to establish the buoyancy effect. (Adapted from Price and Cosgrove, 1990.)

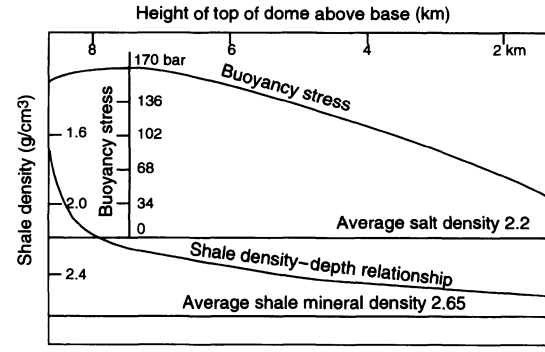

Fig. 12.19 Relationship between buoyancy, pressure and thickness of overburden for probable density distributions. (After Gussow, 1968.)

Cosgrove (1990), in the static case, there is a tendency for the upward pressure S_s at the top of the salt stock to exceed the downward gravitational stress S_v by the amount

$$S_s - S_v = z_2 g(\rho_r - \rho_s) \qquad (12.15)$$

where $(S_s - S_v)$ is the buoyancy stress, ρ_r and ρ_s are the densities of the overburden rock and salt, respectively, and g is the acceleration due to gravity. Equation (12.15) indicates that the buoyancy stress increases with the height of the salt column z_2.

Equation (12.15) was derived assuming that the salt and the country rock have a uniform density. The effect of variable density with depth on the buoyancy stress was analyzed by Gussow (1968) who considered the case of a salt stock rising in a shale formation. Figure 12.19 shows the relationship between buoyancy stress for an average salt density and a depth-dependent shale density. This figure indicates an increase in the buoyancy stress with the height of the stock or dome above the base of the source layer.

When the source layer of salt and the overlying cover rock are perfectly uniform and of constant thickness, there are no buoyancy forces to drive the diapirism. A trigger mechanism is therefore necessary for the buoyancy effect to become sufficiently important for a diapir to evolve. Diapir-generating irregularities are of various kinds, the simplest being a bulge on the top of the source layer. In orogenic environments and tectonically active areas, folds and faults are structures that could start diapirs. Intrusion of the salt along fractures will depend on the *in situ* stress field, very much like the magmatic intrusions mentioned above. Another triggering mechanism may be due to the different stress fields existing in the source layer of salt and the overlying cover rock (Price and Cosgrove, 1990). Stephansson (1972) and Ramberg (1981) studied different initiation mechanisms of diapirs by means of centrifuge models.

In general, the forceful emplacement of a diapir will influence the regional stress field in the vicinity of the diapiric structure. If we assume the rocks to be perfectly elastic or viscous, one can estimate the disturbance of the regional stress field to reach about two structure diameters away from the contact of the source layer and overburden.

12.4.3 DOME STRUCTURES

Domes are geological structures that are formed in part by bending of rock layers due to upward forces. They can be circular or

elliptical in shape and can be formed by different types of tectonic processes such as salt diapirism, sill and laccolith magmatic intrusions and uplifting of basement rock (Withjack and Scheiner, 1982). In general, the process of doming is accompanied by stress redistribution and ultimately faulting as the strength of the overlying cover rock is reached. Various experimental and analytical models of doming have been proposed in the literature, a review of which can be found in Withjack and Scheiner (1982).

A comprehensive analytical and experimental study on the fracture patterns associated with doming was reported by Withjack and Scheiner (1982). Their study emphasized the role played by regional horizontal strain (compression or extension) on the deformation and fracturing of a thick homogeneous layer during vertical doming, for circular and elliptical domes. An innovative experimental technique allowed them to monitor the response of soft clay cakes placed on a rubber sheet that was either extended or compressed horizontally while doming was created by inflating a small balloon placed under the model material. Various fault types and fault patterns were observed for different (horizontal and vertical) strains and strain rates.

Beside laboratory experiments, Withjack and Scheiner (1992) analyzed mathematically the stress distribution in a thick, linearly elastic and isotropic circular or elliptical plate representing a rock layer. Doming was simulated by clamping the edge of the plate and by applying a uniform pressure beneath it. Stresses associated with regional extension or compression were superposed on those related to doming. The mode of faulting at each point in the dome was determined by comparing the predicted principal stresses with those associated with the three basic faulting types of Fig.11.4, assuming the vertical stress to vanish. Figures 12.20a–e show the major principal horizontal stress direction and fault pattern predicted by the analytical model for an elliptical dome when doming occurs by itself, or is accompanied by either extension or compression. In Figs 12.20a–e, zone A corresponds to a region at the crest where both horizontal stresses are tensile, zone B is in the flanks of the dome and is such that one stress is compressive and the second is tensile, and zone C along the dome periphery is such that both stresses are compressive. Zones A, B and C contain normal, strike-slip and reverse (thrust) faults, respectively. Withjack and Scheiner (1982) found a good correlation between the deformation and fracturing modes predicted with the analytical model and those observed experimentally.

Understanding the fracture pattern and stress distribution in a fractured dome structure, which is also a hydrocarbon reservoir, is important to petroleum engineers as both fractures and stress (and their interaction) control reservoir permeability and productivity. An excellent and well-documented case study is that of the Ekofisk field located in the Norwegian sector of the North Sea. The field is an elliptical dome and the reservoir is fractured chalk. An important aspect of that project was to assess the possible effects of changes in pore pressure and reservoir depletion over the past 20 years on the *in situ* stress field and the impact on the reservoir permeability and productivity (Teufel and Farrell, 1990; Teufel, Rhett and Farrell, 1991).

Stress measurements reported by Teufel and Farrell (1990) indicated a strong correlation between the orientation of the maximum horizontal stresses measured *in situ*, the dome structure and radial fractures related to the dome itself. The maximum horizontal stress was found to be parallel to the long axis of the reservoir at the dome crest and to be parallel to the radial fracture pattern on the flanks of the structure (Fig. 1.6). Teufel and Farrell (1990) also noticed a good correlation between the measured fracture and stress patterns and those predicted by the models of Withjack and Scheiner (1982) for an elliptical dome structure.

Over 20 years of petroleum production from the Ekofisk field in the North Sea has resulted in a 21–24 MPa reduction in reservoir pore pressure (Teufel, Rhett and Farrell, 1991). This, in turn, resulted in an increase in the effective vertical stress, pore collapse of the weak chalk, reservoir compaction and sea-floor subsidence. Measurements of shut-in pressure by hydraulic fracturing over a period of 15 years has revealed a change in minimum horizontal stress of about 80% of the net change in pore pressure (Fig. 12.21). Also, the effective minimum horizontal stress has been found to increase at a smaller rate than the effective vertical stress, with a ratio of 0.2.

In spite of the compaction of the chalk formation and the severe subsidence of the ocean floor associated with the reduction in reservoir pore pressure, the Ekofisk field has been able to maintain its reservoir permeability and productivity. According to Teufel, Rhett and Farrell (1991), this can be attributed to an

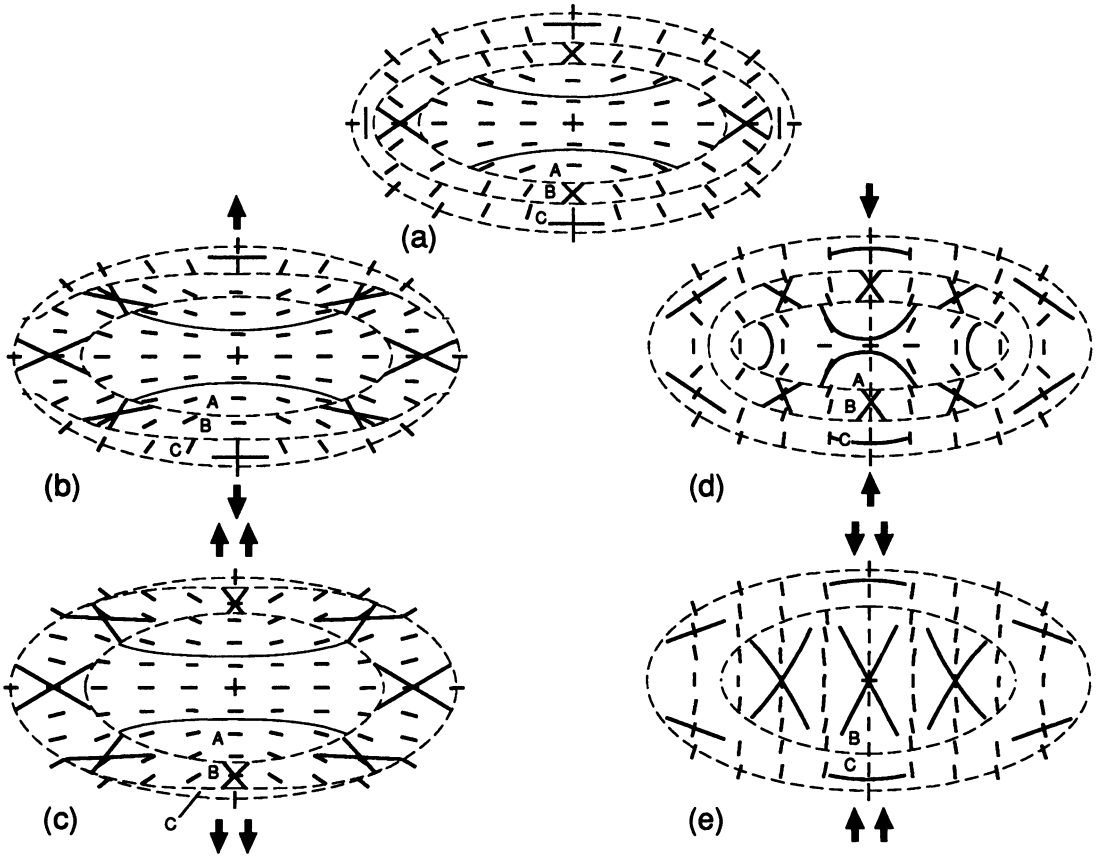

Fig. 12.20 Stress and potential fault patterns for elliptical domes. The short thin lines correspond to the direction of the major principal horizontal stress, and the thick solid lines indicate possible fault trends. Zones A, B and C correspond to normal faults, strike-slip faults and thrust faults, respectively. (a) Elliptical dome without lateral strains, (b) combined doming and uniaxial extension, (c) combined doming with twice as much uniaxial extension as in (b), (d) combined doming and uniaxial compression, (e) combined doming with twice as much uniaxial compression as in (d). Tick marks indicate plate center. (After Withjack and Scheiner, 1982, with permission.)

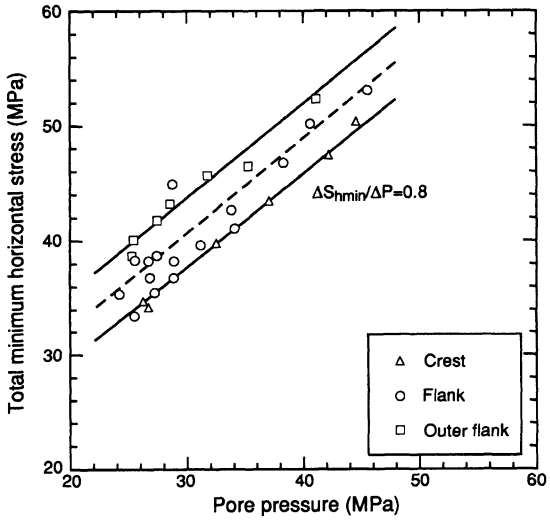

Fig. 12.21 Plot of total minimum horizontal stress versus pore pressure in the Ekofisk field, North Sea, determined from shut-in pressure data of hydraulic fractures. (After Teufel, Rhett and Farrell, 1991.)

increase in reservoir fracture density and reduced matrix block dimensions due to shear failure during reservoir depletion.

12.4.4 SINGLE LAYER BUCKLING

Buckling is defined 'as the flexing or folding of a surface or series of parallel surfaces by a compressive stress directed along the surface or layer' (Price and Cosgrove, 1990). Surface or layer buckling can be found in a wide variety of rock types. The literature about buckling, folding and fold structures is vast and the reader interested in this topic is referred to the books of Johnson (1977), Ramberg (1981) and Price and Cosgrove (1990). In this section we have limited the discussion to single layer folding.

Various theories have been used by geologists to explain the process of folding. In general, most of the theoretical models are much less complex than the geological processes that they are supposed to model (Price and Cosgrove, 1990). One approach to modeling single layer buckling is to use strength of materials and the Euler buckling formula, which states that the critical axial buckling force F_{crit} for an elastic beam of length L, Young's modulus E and moment of inertia I, is equal to

$$F_{crit} = \frac{4\pi^2 EI}{L_e^2} \tag{12.16}$$

(Riley and Zachary, 1989) where L_e is an effective length that depends on the boundary conditions. It is equal to L if the beam has pivoted ends and to $L/2$ if the ends are fixed. The buckling stress is obtained by dividing F_{crit} by the cross-sectional area of the beam. This model is obviously of limited value since it does not consider the interaction of the layer with the surrounding matrix.

More realistic geological simulations of buckling of a single layer were proposed by Biot (1961, 1965). In one of his analytical models, Biot (1961) considered the buckling of a linearly elastic thin plate embedded in an infinite incompressible viscous matrix. He showed that for a given axial stress σ applied to a plate of thickness h, Young's modulus E and Poisson's ratio ν, the dominant wavelength of the folds (i.e. the distance from crest to crest that grows at the fastest rate under the applied stress) is equal to

$$\lambda = \pi h \left(\frac{E}{(1-\nu^2)\sigma} \right)^{1/2} \tag{12.17}$$

The main drawback of this approach is that the wavelength of the elastic layer is independent of the material property of the matrix.

Another buckling model proposed by both Biot (1961) and Ramberg (1961) considers a single (and thin) layer of incompressible purely viscous solid of viscosity η_1 and thickness h immersed in a less viscous and infinite incompressible matrix of viscosity η_2. Equation (12.17) is replaced by

$$\lambda = 2\pi h \left(\frac{\eta_1}{6\eta_2} \right)^{1/3} \tag{12.18}$$

As the wavelength λ and the thickness h are the only data that can be directly observed in the field, structural geologists often express

the fold geometry using a slenderness ratio λ/h which can be calculated using equation (12.18). In view of that equation, the slenderness ratio depends only on the ratio of the viscosities of the layer and the matrix and is independent of the applied stress. This accounts for the different λ/h ratios which often develop in layers of different lithologies (viscosities) under the same compression, and for the different arc lengths of layers with different thicknesses but of same lithology.

Biot (1961, 1965) extended his models to the case of several viscous layers embedded in a viscous matrix and included the effect of gravity and strain rate. In particular, he concluded that viscous mechanisms tend to predominate in tectonic loading of rock layers. Also, it was found that folding may occur under tectonic stresses which are small compared with the rock strength and over reasonable geological time scales. Finally, fold wavelength does not depend on the magnitude of the applied stress unless gravity is taken into account.

Since the 1960s, the Biot theory of single layer buckling has been modified to address several of the assumptions inherent in that theory. More specifically, modifications have been made to take into account the shortening or thickening of a rock layer during folding, the layer thickness (thick plate versus thin plate analysis), the adherence (or slip) between the layer and the matrix, and non-linear viscous behavior of the layer and the matrix. These modifications are discussed more extensively in Price and Cosgrove (1990).

The finite element method has been used extensively on a range of problems associated with single layer buckling. For instance Dieterich and Carter (1969), Hudleston and Stephansson (1973) and Stephansson (1976) used that method of analysis to determine the stress and strain distribution in a single layer buckling fold with initial sinusoidal deflection of the layer. Distributions of principal deviatoric stresses and the maximum shear stress for a single layer fold, assuming a viscosity contrast of 100:1 between the folded layer and the surrounding rock, are shown in Figs 12.22a–c. A pattern of parallel contours of deviatoric stress develops in the hinge zone of the fold but with opposite sign in the inner and outer cores of the hinge (Figs 12.22a, b). This stress difference is able to drive diffusion processes in the rock matrix and can cause migration of oil and gas or geochemical compounds. For the shear stress (Fig. 12.22c), we note a pattern of parallel shear stress contours with increasing value toward the surface of the fold. Driving a horizontal tunnel across an upright fold with a large stiffness contrast between the folded layer and the surrounding rock will generate major differences in the stress pattern around the tunnel which can

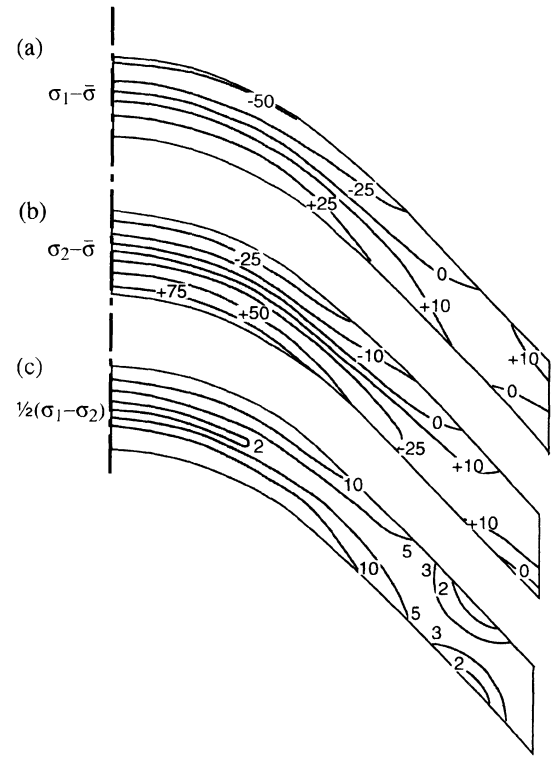

Fig. 12.22 Stress distributions in a single layer fold with a viscosity contrast of 100:1 between the layer and the surrounding rock. (a) Principal maximum deviatoric stress, (b) principal minimum deviatoric stress, (c) maximum shear stress. (After Stephansson, 1976.)

create severe stability and leakage problems (see Fig. 2.19 and related text).

In general, detailed mapping and structural analysis of fold geometry, and of major and minor (linear and planar) geological structures in a given area, allows structural geologists to infer the geometry and symmetry of folded structures. The question then arises as to what can be deduced from the tectonic processes and the stress states that created those structures. As long as the tectonics of young geological formations (with relatively simple fold geometries) is investigated, structural geologists are able to define the virgin stress and the stress history. As one considers the structural geometries that result from the superposition of two or more phases of deformation, or result from deformations widely spaced in time, the definition of the stress states becomes more difficult. The results of such an analysis often show drastic changes in the stress field for the different phases of deformation (Price and Cosgrove, 1990).

12.4.5 NEOTECTONIC OR POSTGLACIAL FAULTING

The siting, characterization and construction of deep repositories for final disposal of spent nuclear fuel and other industrial waste are major topics of interest within nuclear waste programs in several countries. An in-depth analysis of the possible effects of geological and geophysical processes on a final repository is one of the major tasks in those programs. Essential questions are whether recent movements can lead to new fracturing and whether load changes or displacements of large rock blocks can decisively alter the geohydrological or geohydrochemical conditions around a final repository. Rock stress measurements can help provide information about the state of stress in a large rock mass block or the surrounding faults, and thereby provide information about the likelihood for neotectonics, rock mass instability, stress relief, etc., of a potential repository site. This is demonstrated below for the postglacial Lansjärv fault located in the Baltic Shield of northern Sweden.

During the last few decades, there have been a number of discoveries of late Quaternary faults in the Precambrian bedrock of northern Fennoscandia (Fig. 12.23). A recent compilation of mapped and potential faults was presented by Olesen *et al.* (1995). Fault lengths were found to vary from a couple of hundred meters to more than 80 km, and fault scarps were found to range in height from 5 to 10 m with a maximum value of more than 20 m for the long Pärvie fault west of Kiruna. The discovery of the neotectonic faults raised the essential question of whether load changes or rock block movements could decisively alter the geohydrological condition around a potential final repository for radioactive waste. A major study within this framework was directed to the Lansjärv postglacial fault scarps in northern Sweden (Fig. 12.23). The fault complex is composed of four major and several minor fault scarps, together forming a 50 km long fault set with scarp heights of 5–10 m (Bäckblom and Stanfors, 1989).

Based on the results and analysis of geophysical measurements and tectonic interpretations in the Lansjärv area, a site for core drilling a 500 m deep borehole was selected adjacent to the fault. Following geophysical borehole logging, water chemistry analysis, fracture mineral studies and hydrogeological measurements, a series of rock stress measurements was conducted by means of the hydrofracturing method. Measurements were attempted at 27 different levels in the borehole, of which 20 were successful and allowed calculation of stresses and stress ratios (Bjarnason, Zellman and Wickberg, 1989). The measured minimum horizontal stresses were found to be extremely low near the bottom of the borehole and the state of stress in general was found to be much lower and more irregular compared with hydrofracturing data from other parts of the Fennoscandian Shield (Fig. 12.24).

Stress measurements in the vicinity of the postglacial fault at Lansjärv clearly revealed

a stress magnitude anomaly in the bedrock and an almost 90° rotation of the direction of the maximum horizontal stress at a depth of about 400 m below the ground surface. This gives support to the hypothesis of stress relief and faulting accompanying the ice retreat of the late Weichselian glaciation in the Lansjärv area about 7000 years BC. This study demonstrates how rock stress measurements can be used to determine stress relief or stress accumulation in a potential area for radioactive waste disposal.

12.4.6 FAULT SLIP

Analysis of fault slip is of interest to geophysicists and rock engineers. Fault slip can occur naturally by tectonic forces associated with crustal deformation. It can also be triggered artificially by phenomena such as surface storage of water in dam reservoirs, storage of fluids underground, pumping and injection of water, oil and gas extraction and blasting (Goodman, 1993). The potential for an active fault, and therefore ground motion, in the near vicinity of civil engineering structures such as waste repositories or dams needs to be assessed at the preliminary design stage. Whether fault slip occurs due to natural phenomena or human activities, it is controlled by the stresses acting on the fault plane, any change in stress and the fault shear strength.

Simple methods of analysis of slip along a single discontinuity (joint or fault) under axisymmetric loading have been proposed by

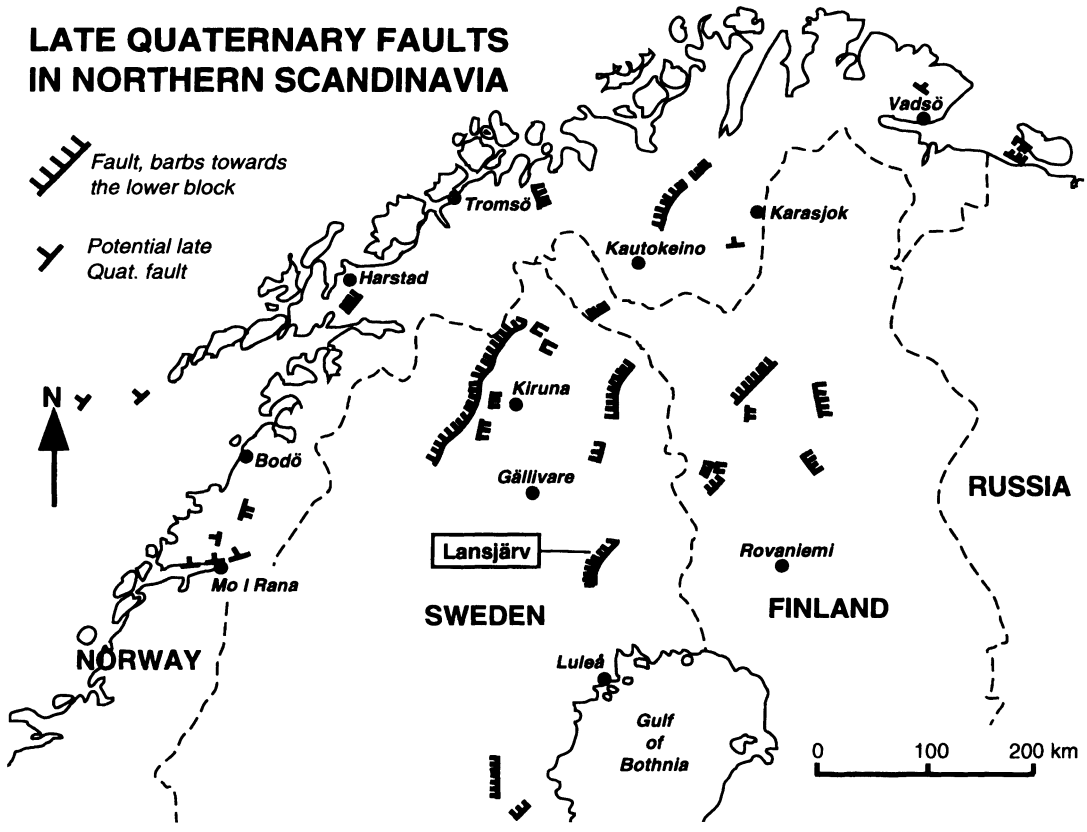

Fig. 12.23 Reported late Quaternary faults in northern Fennoscandia. Stress measurements have been conducted at the Lansjärv fault system south of Gällivare. (After Olesen *et al.*, 1995.)

Jaeger (1960) and Bray (1967). More complex methods of analysis of fault slip under two- and three-dimensional stress fields can be found in Jaeger and Cook (1976), Amadei, Savage and Swolfs (1987), Amadei (1988), Amadei and Savage (1989), Ferrill *et al.* (1995) and Morris, Ferrill and Henderson (1996). Figure 12.25 shows the geometry used by Amadei and co-workers. In this figure the orientation of the fault plane with respect to principal stress directions x,y and z is defined by two angles: a dip azimuth angle β and a dip angle ψ. The principal stresses acting on the fault plane are defined as σ_x, σ_y and σ_z. Using the coordinate transformation rules for stress, the normal stress σ_n and shear stress τ acting on the fault plane can be determined and are equal to (section A.6 in Appendix A)

$$\begin{aligned}\sigma_n &= \sigma_x l^2 + \sigma_y m^2 + \sigma_z n^2 \\ \tau &= [(\sigma_x - \sigma_y)^2 l^2 m^2 + (\sigma_y - \sigma_z)^2 \\ &\quad \times n^2 m^2 + (\sigma_x - \sigma_z)^2 l^2 n^2]^{1/2}\end{aligned} \tag{12.19}$$

where l, m and n are the direction cosines of the normal to the fault plane with respect to the x-, y- and z-axes.

Assuming Coulomb friction, slip along the fault plane occurs when the normal and shear stresses satisfy the following equation:

$$|\tau| = \mu\sigma_n \tag{12.20}$$

where μ is the coefficient of friction along the fault plane. Fault cohesion (cohesive strength) can be accounted for with an additional term on the right-hand side of equation (12.20). Also, if there is water pressure along the fault plane, the normal stress in equation (12.20) must be replaced by an effective stress.

Combining equations (12.19) and (12.20), fault slip can be expressed in the form of a mathematical expression relating the three principal stresses acting on the fault plane, the fault plane orientation angles (β, ψ) and its shear strength properties. That expression must be complemented with the additional

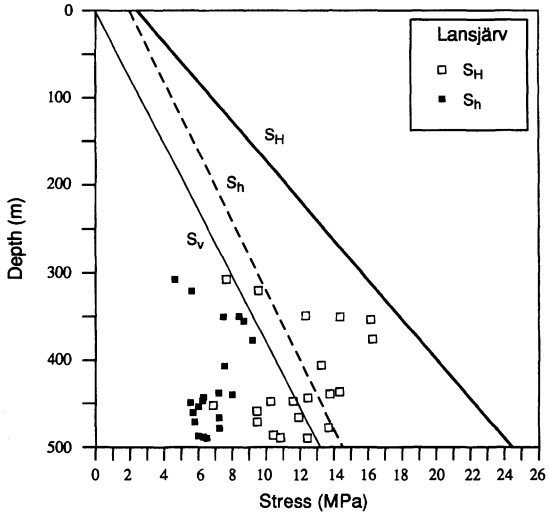

Fig. 12.24 Measured stresses in borehole adjacent to the Lansjärv fault system in northern Sweden. Average stress data from hydraulic fracturing stress measurements in Fennoscandia are presented to illustrate the stress anomaly of a neotectonic fault. (After Bjarnason, Zellman and Wickberg, 1989.)

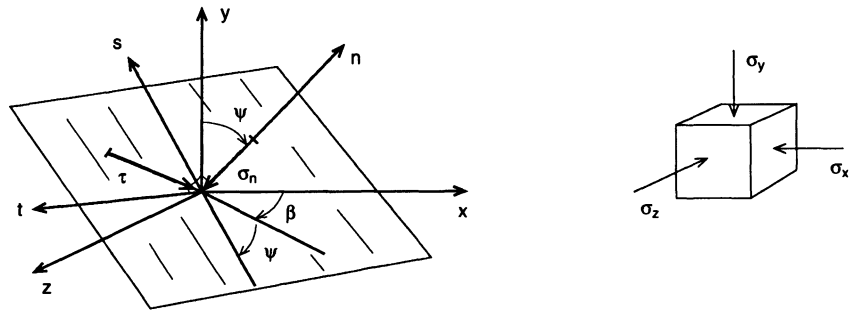

Fig. 12.25 Resolved shear stress τ and normal stress σ_n on a fault plane inclined with respect to a three-dimensional homogeneous principal stress field σ_x, σ_y and σ_z. (After Amadei and Savage, 1989.)

constraint that, in order for slip to occur, the normal stress σ_n must be positive definite. The direction of the shear stress τ on the fault plane (parallel to the slip vector) can also be determined, as well as the type of motion that is likely to occur, e.g. dip-slip (normal or reverse), oblique-slip or strike-slip.

The mathematical analysis outlined above can serve several purposes. First, it can be used to determine, for a fault of given orientation, which stress states could create slip. This approach is discussed more extensively in the papers by Amadei (1988) and Amadei and Savage (1989). Second, it can be used to determine, for a given stress field, the fault plane orientations for which slip could occur. This approach was addressed by Amadei (1988) and Amadei, Savage and Swolfs (1987). It is also called 'slip-tendency analysis' by Ferrill *et al.* (1995) and Morris, Ferrill and Henderson (1996). Finally, the mathematical analysis can be used to solve the inverse problem, i.e. to determine the virgin stress state from slickensides (striae) on a given population of fault planes with various attitudes. This approach, called fault-slip analysis, was followed by Angelier (1984) and co-workers, and is further discussed in section 2.14.1

The slip-tendency analysis of Ferrill *et al.* (1995) and Morris, Ferrill and Henderson (1996) deserves further discussion. Although it is based on the same equations as in the other analyses, it provides a tool for conducting a comprehensive assessment of the risk of fault slip and associated earthquakes on existing faults located in a contemporary stress state. Slip tendency is determined by comparing the value of the ratio $T_s = \tau/\sigma_n$ with the fault's coefficient of friction μ (Ferrill *et al.*, 1995), or by calculating the ratio $T_s/T_{sMAX} = \tau/(\mu\sigma_n)$ (Morris, Ferrill and Henderson, 1996).

A serious advantage of the method of Ferrill *et al.* (1995) and Morris, Ferrill and Henderson (1996) is that slip tendency can be calculated automatically using an interactive computer tool. The stress tensor is specified by choosing values and orientations for the principal stresses. The slip tendency for fault surfaces of any orientation is then calculated and displayed. This slip-tendency display can then be modified by changing the magnitude and orientation of the three principal stresses. The slip tendency and slip vector on any individual fault surface can be determined. The slip-tendency data can also be linked to fault map traces, enabling the user to investigate various stress scenarios and their effects on known or suspected fault geometries. Slip-tendency analysis also provides a means of rapidly assessing which faults are best explained by any given stress state. With a knowledge of both the *in situ* stress state and the distribution of existing faults in a given area, it is possible to assess relative earthquake hazard.

Figure 12.26 gives an example of slip-tendency analysis reported by Morris, Ferrill and Henderson (1996) for faults in the Yucca Mountain area in Nevada. The faults are located in a stress field with principal components $\sigma_1 = 90$ MPa (vertical), $\sigma_2 = 65$ MPa (N25°E–N30°E) and $\sigma_3 = 25$ MPa (N60°W–N65°W) selected on the basis of the results of hydraulic fracturing tests by Stock *et al.* (1985). In Fig. 12.26, the results of the analysis are presented in the form of a shaded stereonet where the degree of shading is scaled with respect to the value of the ratio T_s/T_{sMAX} (which varies between 0 and 100%). Figure 12.26 indicates that faults having N–S to NE–SW azimuths and moderate to large dip angles have a relatively high tendency to slip. Also, strike-slip and normal faults are compatible and can coexist in the contemporary stress state at Yucca Mountain.

12.4.7 INTRAPLATE STRESSES IN THE UPPER EARTH'S CRUST

Various investigations have shown that the Earth's crust can be basically divided into an upper brittle part and a lower ductile part. The strength in the brittle part is essentially controlled by the frictional strength of pre-existing favorably oriented faults. On the

other hand, the strength of the lower ductile part is described by various flow laws (Brudy *et al.*, 1995). In order to verify that the upper crust is in a state of failure equilibrium, *in situ* stress measurements at depth are required. Currently available stress measurements in deep boreholes in intraplate areas include those in Cornwall, England (Pine and Kwakwa, 1989); Fenton Hill, New Mexico (Barton, Zoback and Burns, 1988); Cajon Pass, California (Zoback and Healy, 1992) and the KTB (Kontinentales Tiefbohrprogramm der Bundesrepublik Deutschland) site in the Oberpfalz, Germany (Baumgärtner *et al.*, 1993; Brudy *et al.*, 1995; Te Kamp, Rummel and Zoback, 1995; Zoback *et al.*, 1993). All data of stress versus depth at those sites 'are consistent with the concept that stress magnitudes in the upper crust are in equilibrium with the frictional strength of the crust and that laboratory derived coefficients of friction ranging in the range of 0.6 to 1.0 can be applied to faults *in-situ*' (Brudy *et al.*, 1995). This is demonstrated below for the stress measurements conducted at the KTB drill site in Germany.

The KTB project involved two distinctive phases. In phase I, from September 1987 to April 1989, a pilot hole was drilled through foliated gneisses with sections of amphibolite to a final depth of 4001 m. From October 1990 to December 1994, corresponding to phase II, a main well was drilled down to a final depth of 9101 m (Fig. 12.27). Below a depth of 4 km, nearly all the rock has been found to be massive amphibolite. During phase I, a total of 14 hydrofrac tests were performed by wireline technique and using an inflatable double straddle packer system. Of the 14 tests, seven

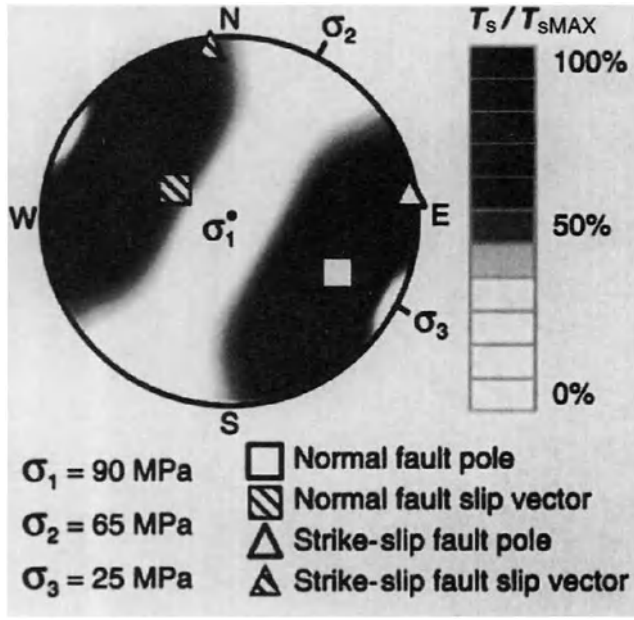

Fig. 12.26 Slip-tendency analysis for Yucca Mountain area faults. Lower hemisphere equal angle plot of poles of surfaces in a three-dimensional state of stress shaded with respect to slip tendency. Superimposed on this plot are poles to two potential slip surfaces with their resolved slip vector orientations to illustrate the coexistence of strike-slip and normal faults in a single stress state. (After Morris, Ferrill and Henderson, 1996.)

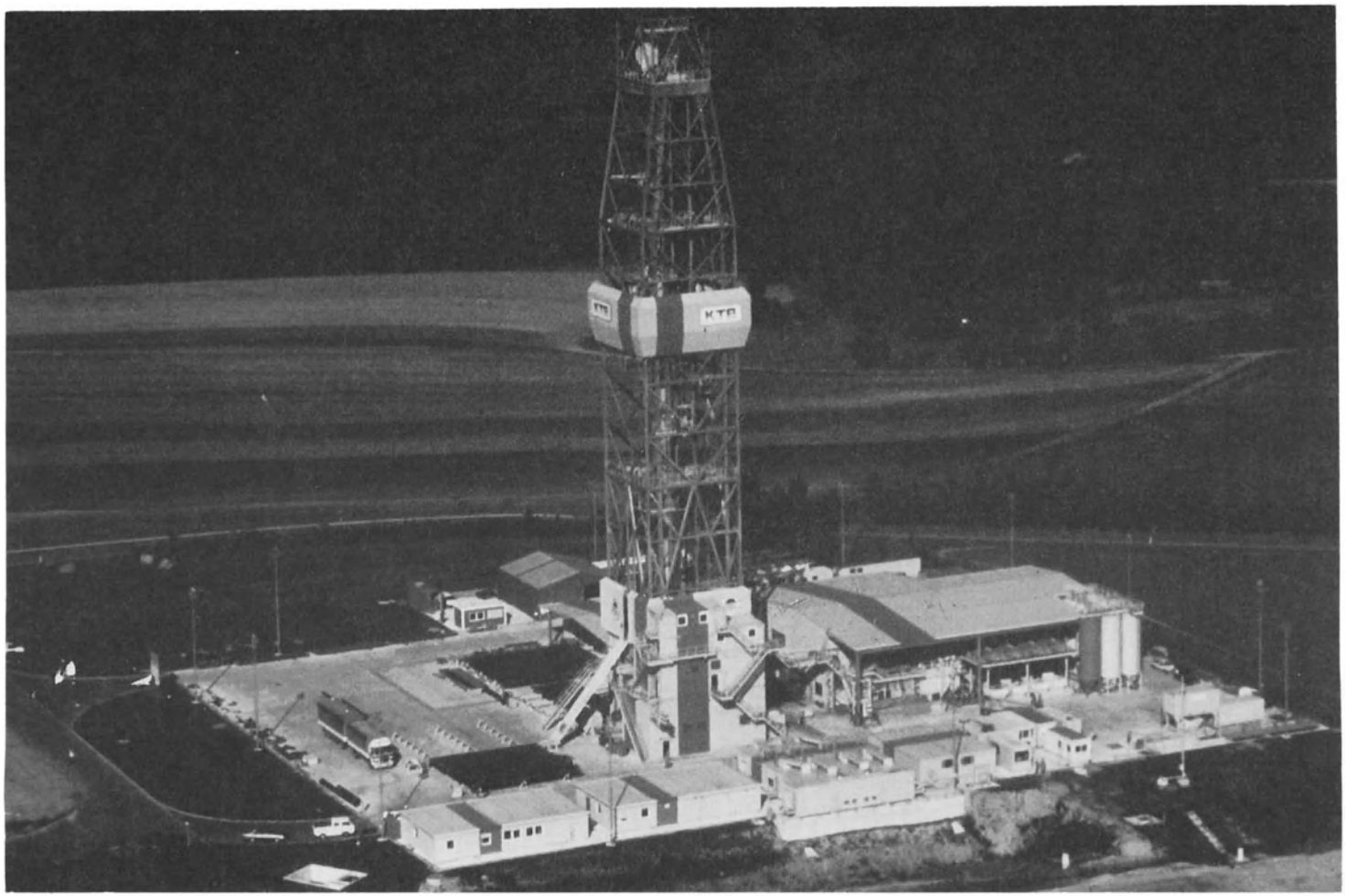

Fig. 12.27 Aerial view of the drilling rig and site of phase II of the KTB continental deep drilling project in Germany. Hydraulic fracturing tests were conducted down to a depth of 9 km, where the maximum and minimum horizontal *in situ* stresses were found to be equal to 285 and 147 MPa, respectively. (Courtesy of J. Lauterjung.)

were successfully completed. In the KTB main borehole, two modified hydrofrac tests were performed at depths of 6 and 9 km where, as described by Te Kamp, Rummel and Zoback (1995), a mechanical casing single packer was set at depth and the remaining open hole section (18 m at 6 km depth and 70 m at 9 km depth) was pressurized. Because the maximum head pressure for fracturing at a depth of 9 km was expected to exceed the upper safety limit of the equipment, an injection fluid with a density of 1.5 g/cm^3 was used. The hydraulic fracturing test at a depth of 9 km represents the deepest reliable stress measurement ever made. The pressure versus time record for that test was found to resemble classical hydrofrac records with a breakdown pressure of 157 MPa, a shut-in pressure of 147 MPa and a refrac pressure of 148 MPa (Figs 3 and 4 in Te Kamp, Rummel and Zoback, 1995). The maximum and minimum horizontal *in situ* stresses were determined to be equal to 285 and 147 MPa, respectively.

A stress profile derived from the hydrofrac tests at the KTB test site is presented in Fig. 12.28. The results indicate a strike-slip type of stress regime ($S_H > S_v > S_h$). The orientation of the hydraulic fracture traces in the pilot hole (depth range 805 to 3011 m) was found to give an average azimuth for the maximum horizontal stress S_H of N149° ± 15°. Using borehole breakouts, Brudy *et al.* (1995) established a profile for the orientation of S_H for the entire depth interval ranging between 3.2 and 8.6 km. They found that, apart from minor local variations, an average orientation of S_H of N160° ± 10° remains essentially constant with depth. This orientation is consistent with other determinations of stress orientation in the area and with the general stress orientation in central Europe described by Müller *et al.* (1992). Brudy *et al.* (1995) also estimated the maximum and minimum principal stresses by analyzing the geometry of breakouts and the orientation of drilling-induced subvertical fractures below a depth of 3 km (Fig. 8.12). These stress estimates complement those measured by hydrofracturing at the depths of 6 and 9 km.

By combining the stresses determined by hydraulic fracturing and those estimated from the breakouts and drilling-induced subvertical fractures, using a Mohr–Coulomb faulting theory and Byerlee's law of friction, both Te Kamp, Rummel and Zoback (1995) and Brudy *et al.* (1995) concluded that for the appropriate pore pressure, the upper Earth's crust supports high shear stresses. They also concluded that stress magnitudes in the crust are limited by the frictional equilibrium on pre-existing optimally oriented faults with laboratory-determined coefficients of friction ranging between 0.6 and 0.8 If the stresses try to exceed this equilibrium state, slip on favorably oriented faults occurs which reduces the stresses back to the equilibrium state.

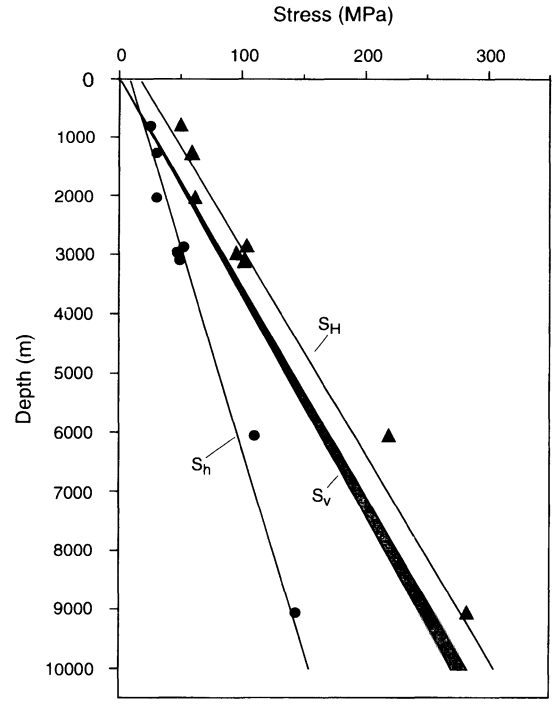

Fig. 12.28 Stress profile evaluated from hydrofrac tests at the KTB site. The vertical stress S_v was calculated as the theoretical overburden stress using density values between 2.8 and 2.9 g/cm^3. (After Te Kamp, Rummel and Zoback, 1995.)

REFERENCES

Amadei, B. (1983) *Rock Anisotropy and the Theory of Stress Measurements*, Lecture Notes in Engineering, Springer-Verlag.

Amadei, B. (1988) Strength of a regularly jointed rock mass under biaxial and axisymmetric loading conditions. *Int. J. Rock Mech. Min. Sci. & Geomech. Abstr.*, **25**, 3–13.

Amadei, B. and Pan, E. (1995) Role of topography and anisotropy when selecting unlined pressure tunnel alignment. *ASCE J. Geotech. Eng. Div.*, **121**, 879–85.

Amadei, B. and Savage, W.Z. (1989) Anisotropic nature of jointed rock mass strength. *ASCE J. Eng. Mech.*, **115**, 525–42.

Amadei, B., Robison, M.J. and Yassin, Y.Y. (1986) Rock strength and the design of underground excavations, in *Proc. Int. Symp. on Large Rock Caverns*, Helsinki, Pergamon Press, Oxford, Vol. 2, pp. 1135–46.

Amadei, B., Savage, W.Z. and Swolfs, H.S. (1987) *In-situ* geomechanics of crystalline and sedimentary rocks. Part IX: prediction of fault slip in a brittle crust under multiaxial loading conditions. US Geological Survey Open File Report 87–503.

Angelier, J. (1984) Tectonic analysis of fault slip data sets. *J. Geophys. Res.*, **89**, 5835–48.

Asmis, H.W. and Lee, C.F. (1980) Mechanistic modes of stress accumulation and relief in Ontario rocks, in *Proc. 13th Can. Symp. Rock Mech.*, Toronto, Canadian Institute of Mining and Metallurgy, CIM Special Vol. 22, pp. 51–5.

Bäckblom, G. and Stanfors, R. (1989) Interdisciplinary study of post-glacial faulting in the Lansjärv area, northern Sweden. Swedish Nuclear Fuel and Waste Management Co., Stockholm, Technical Report 89-31.

Barla, G. (1993) Case study of rock mechanics in the Masua Mine, Italy, in *Comprehensive Rock Engineering* (ed. J.A. Hudson), Pergamon Press, Oxford, Chapter 12, Vol. 5, pp. 291–334.

Barla, G., Sharp, J.C. and Rabagliati, U. (1991) Excavation and support optimisation for a large underground storage facility in weak jointed chalk, in *Proc. 7th Cong. Int. Soc. Rock Mech. (ISRM)*, Aachen, Balkema, Rotterdam, Vol. 2, pp. 1067–72.

Barton, N., Lien, R. and Lunde, J. (1974) Engineering classification of jointed rock masses for the design of tunnel support. *Rock Mech.*, **6**, 189–236.

Barton, C.A., Zoback, M.D. and Burns, K.L. (1988) In-situ stress orientation and magnitude at the Fenton Hill geothermal site, New Mexico, determined from wellbore breakouts. *Geophys. Res. Lett.*, **15**, 467–70.

Baumgärtner, J. *et al.* (1993) Deep hydraulic fracturing stress measurements in the KTB (Germany) and Cajon Pass (USA) scientific drilling projects – a summary, in *Proc. 7th Cong. Int. Soc. Rock Mech. (ISRM)*, Aachen, Balkema, Rotterdam, Vol. 3, pp. 1685–90.

Bawden, W.F. (1993) The use of rock mechanics principles in Canadian underground hard rock mine design, in *Comprehensive Rock Engineering* (ed. J.A. Hudson), Pergamon Press, Oxford, Chapter 11, Vol. 5, pp. 247–90.

Bergh-Christensen, J. (1986) Rock stress measurements for the design of a 965 meter head unlined pressure shaft, in *Proc. Int. Symp. on Rock Stress and Rock Stress Measurements*, Stockholm, Centek Publ., Luleå, pp. 583–90.

Bieniawski, Z.T. (1984) *Rock Mechanics Design in Mining and Tunneling*, Balkema, Rotterdam.

Biot, M.A. (1961) Theory of folding of stratified visco-elastic media and its implications in tectonics and orogenesis. *Geol. Soc. Am. Bull.*, **72**, 1595–620.

Biot, M.A. (1965) Theory of viscous buckling and gravity instability of multilayers with large deformation. *Geol. Soc. Am. Bull.*, **76**, 371–8.

Bjarnason, B., Zellman, O. and Wickberg, P. (1989) Drilling and borehole description, in *Interdisciplinary Study of Post-glacial Faulting in the Lansjärv Area, Northern Sweden*, Swedish Nuclear Fuel and Waste Management Co., Stockholm, Technical Report 89-31.

Brady, B.H.G. and Brown, E.T. (1985) *Rock Mechanics for Underground Mining*, Allen & Unwin, London.

Bray, J.W. (1967) A study of jointed and fractured rock. Part I: fracture patterns and their characteristics. *Rock Mech. and Rock Eng. Geol.*, **5**, 117–36.

Brekke, T. and Ripley, B.D. (1993) Design of pressure tunnels and shafts, in *Comprehensive Rock Engineering* (ed. J.A. Hudson), Pergamon Press, Oxford, Vol. 2, Chapter 14, pp. 349–69.

Brekke, T. and Selmer-Olsen, R. (1966) A survey of the main factors influencing the stability of undergound constructions in Norway, in *Proc. 1st Cong. Int. Soc. Rock Mech. (ISRM)*, Lisbon, Lab. Nac. de Eng. Civil, Lisbon, Vol. II, pp 257–60.

Broch, E. (1984a) Development of unlined pressure shafts and tunnels in Norway. *Underground Space*, **8**, 177–84.

Broch, E. (1984b) Unlined high pressure tunnels in areas of complex topography. *Water Power & Dam Constr.*, **36**, 21–3.

Broch, E. (1993) General report: caverns including civil defense shelters, in *Proc. 7th Cong. Int. Soc. Rock Mech. (ISRM)*, Aachen, Balkema, Rotterdam, Vol. 3, pp. 1613–23.

Broch, E. and Nielsen, B. (1979) Comparison of calculated, measured and observed stresses at the Ortfjell open pit (Norway), in *Proc. 4th Cong. Int. Soc. Rock Mech. (ISRM)*, Montreux, Balkema, Rotterdam, Vol. 2, pp. 49–56.

Broch, E. and Sorheim, S. (1984) Experiences from the planning, construction and supporting of a road tunnel subjected to heavy rockbursting. *Rock Mech. Rock Eng.*, **17**, 15–35.

Brown, E.T. (ed.) (1987) *Analytical and Computational Methods in Engineering Rock Mechanics*, Allen & Unwin, London.

Brown, E.T. and Ferguson, G.A. (1979) Progressive hangingwall caving at Gath's mine, Rhodesia. *Trans. Instn Min. Metall.*, **88**, A92–105.

Brown, E.T. and Hoek, E. (1978) Trends in relationships between measured rock *in-situ* stresses and depth. *Int. J. Rock Mech. Min. Sci. & Geomech. Abstr*, **15**, 211–15.

Brown, E.T. *et al.* (1983) Ground response curve for rock tunnels. *ASCE J. Geotech. Eng. Div.*, **109**, 15–39.

Brudy, M. *et al.* (1995) Application of the integrated stress measurement strategy to the 9 km depth in the KTB boreholes, in *Proc. Workshop on Rock Stresses in the North Sea*, Trondheim, Norway, NTH and SINTEF Publ., Trondheim, pp. 154–64.

Carlsson, A. and Olsson, T. (1982) Rock bursting phenomena in a superficial rock mass in Southern Central Sweden. *Rock Mech.*, **15**, 99–110.

Crouch, S.L. and Starfield, A.M. (1983) *Boundary Element Methods in Solid Mechanics*, Allen & Unwin, London.

Deere, D. *et al.* (1986) Monitoring of the powerhouse cavern for Fortuna hydroproject, in *Proc. Int. Symp. on Large Rock Caverns*, Helsinki, Pergamon Press, Oxford, Vol. 2, pp. 907–20.

Dieterich, J.H. and Carter, N.L. (1969) Stress history of folding. *Am. J. Sci.*, **267**, 129–55.

Eissa, E.A. (1980) Stress analysis of underground excavations in isotropic and stratified rock using the boundary element method, unpublished PhD Thesis, Imperial College, London.

Enever, J.R. (1993) Case studies of hydraulic fracture stress measurements in Australia, in *Comprehensive Rock Engineering* (ed. J.A. Hudson), Pergamon Press, Oxford, Chapter 20, Vol. 3, pp. 498–531.

Enever, J.R., Walton, R.J. and Windsor, C.R. (1990) Stress regime in the Sydney basin and its implication for excavation design and construction, in *Proc. Tunnelling Conf.*, Sydney, The Institution of Engineers, Australia, pp. 49–59.

Enever, J.R., Wold, M.B. and Walton, R.J. (1992) Geotechnical investigations for the assessment of the risk of water leakage from pressure tunnels, in *Proc. 6th Australia–New Zealand Conf. on Geomechanics*.

Fairhurst, C. (1968) Methods of determining in-situ rock stresses at great depths. Corps of Engineers, Omaha, Nebraska, Tech. Report No. 1-68.

Ferguson, G.A. (1993) Caving geomechanics, in *Comprehensive Rock Engineering* (ed J.A. Hudson), Pergamon Press, Oxford, Chapter 14, Vol. 5, pp. 359–92.

Ferrill, D.A. *et al.* (1995) Tectonic processes in the Central Basin and Range region, in *NRC High-Level Radioactive Waste Research at CNWRA*, July–December 1994, Report CNWRA 94-02S prepared by Center for Nuclear Waste Regulatory Analyses, San Antonio, Texas for Nuclear Regulatory Commission.

Franklin, J.A. and Hungr, O. (1978) Rock stresses in Canada: their relevance to engineering projects. *Rock Mech.*, Suppl. **6**, 25–46.

Gale, W.J. (1986) The application of stress measurements to the optimization of coal mine roadway driveage in the Illawarra coal measures, in *Proc. Int. Symp. on Rock Stress and Rock Stress Measurements*, Stockholm, Centek Publ., Luleå, pp. 551–60.

Goodall, D.C., Åberg, B. and Brekke, T.L. (1988) Fundamentals of gas containment in unlined rock caverns. *Rock Mech. Rock Eng.*, **21**, 235–58.

Goodman, R.E. (1993) *Engineering Geology*, Wiley.

Gudmundsson, A. (1983) Stress estimates from the length/width ratios of fractures. *J. Struct. Geol.*, **5**, 623–6.

Guertin, J.D. and Flanagan, R.F. (1979) Construction behavior of a shallow tunnel in highly stressed sedimentary rock, in *Proc. 4th Cong. Int. Soc. Rock Mech. (ISRM)*, Montreux, Balkema, Rotterdam, Vol. 2, pp. 181–8.

Gussow, W.C. (1968) Salt diapirism: importance of temperature and energy source of emplacement, in *Diapirism and Diapirs*, Am. Assoc. Petrol. Geol., pp. 16–52.

Gustafson, G., Lindblom, U. and Söder, C.-O. (1991) Hydrogeological and hydromechanical aspects of

gas storage, in *Proc. 7th Cong. Int. Soc. Rock Mech. (ISRM)*, Aachen, Balkema, Rotterdam, Vol. 1, pp. 99–103.

Haimson, B.C. (1977) Design of underground powerhouses and the importance of pre-excavation stress measurements, in *Proc. 16th US Symp. Rock Mech.*, Minneapolis, ASCE Publ., pp. 197–204.

Haimson, B.C. (1992) Defining pre-excavation stress measurements for meaningful rock characterization, in *Proc. Eurock '92: Int. Symp. on Rock Characterization*, Chester, UK, British Geotechnical Society, London, pp. 221–6.

Haimson, B.C., Lee, C.F. and Huang, J.H.S. (1986) High horizontal stresses at Niagara Falls, their measurement, and the design of a new hydro-electric plant, in *Proc. Int. Symp. on Rock Stress and Rock Stress Measurements*, Stockholm, Centek Publ., Luleå, pp. 615–24.

Hanson, M.E. *et al.* (1978) LLL gas simulation program. Quarterly progress report, April through June 1978. Lawrence Livermore Laboratory Report UCRL-50036-78-2.

Hanson, M.E. *et al.* (1980) LLL gas simulation program. Quarterly progress report, October through December 1979. Lawrence Livermore Laboratory Report UCRL-50036-79-4.

Hanssen, T.H. and Myrvang, A. (1986) Rock stresses and rock stress effects in the Kobbelv area, northern Norway, in *Proc. Int. Symp. on Rock Stress and Rock Stress Measurements*, Stockholm, Centek Publ., Luleå, pp. 625–34.

Hansson, H., Jing, L. and Stephansson, O. (1995) Three-dimensional DEM modelling of coupled thermo-mechanical response for a hypothetical nuclear waste repository, in *Proc. 5th Int. Symp. on Numerical Models in Geomechanics*, Davos, Balkema, Rotterdam, pp. 257–62.

Hardy, M.P. and Agapito, J.F.T. (1977) Pillar design in oil shale mines, in *Proc. 16th US Symp. Rock Mech.*, ASCE, New York, pp. 257–66.

Herget, G. (1993) Rock stresses and rock stress monitoring in Canada, in *Comprehensive Rock Engineering* (ed. J.A. Hudson), Pergamon Press, Oxford, Chapter 19, Vol. 3, pp. 473–96.

Hoek, E and Brown, E.T. (1980a) *Underground Excavations in Rock*, Institution of Mining and Metallurgy, London.

Hoek, E. and Brown, E.T. (1980b) Empirical strength criterion for rock masses. *ASCE J. Geotech. Eng.*, **106**, 1013–35.

Hudleston, P.J. and Stephansson, O. (1973) Layer shortening and fold-shape development in the buckling of single layers. *Tectonophysics*, **17**, 299–321.

Jaeger, J.C. (1960) Shear failure of anisotropic rocks. *Geol. Mag.*, **97**, 65–78.

Jaeger, J.C. and Cook, N.G.W. (1976) *Fundamentals of Rock Mechanics*, 2nd edn, Chapman & Hall, London.

Johnson, A.M. (1970) *Physical Processes in Geology*, Freeman Cooper & Co., San Francisco.

Johnson, A.M. (1977) *Styles of Folding: Mechanics and Mechanisms of Folding of Natural Elastic Materials*, Elsevier.

Kaiser, P.K. (1980) Effect of stress-history on the deformation behavior of underground openings, in *Proc. 13th Can. Symp. Rock Mech.*, Toronto, Canadian Institute of Mining and Metallurgy, CIM Special Vol. 22, pp. 133–40.

Kaiser, P.K. and Maloney, S. (1992) The role of stress change in underground construction, in *Proc. Eurock '92: Int. Symp. on Rock Characterization*, Chester, UK, British Geotechnical Society, London, pp. 396–401.

Kjorholt, H. and Broch, E. (1992) The water curtain – a successful means of preventing gas leakage from high-pressure, unlined rock caverns. *Tunnell. Und. Space Tech.*, **7**, 127–32.

Krauland, N. (1981) FEM model of Näsliden mine – requirements and limitations at start of the Näsliden Project, in *Application of Rock Mechanics to Cut and Fill Mining*, Institution of Mining and Metallurgy, London, pp. 141–4.

Lee, C.F. (1978) Stress induced instability in underground excavations, in *Proc. 19th US Symp. Rock Mech.*, Reno, Univ. of Nevada Publ., pp. 1–9.

Lee, C.F. and Klym, T.W. (1977) Determination of rock squeeze potential for underground power projects, in *Proc. 17th US Symp. Rock Mech.*, Univ. of Utah, SME/AIME, 5A4-1–5A4-6.

Legge, T.F.H., Richards, L.R. and Pound, J.B. (1986) Kiambere hydro electric project cavern: rock mechanics aspects, in *Proc. Int. Symp. on Large Rock Caverns*, Helsinki, Pergamon Press, Oxford, Vol. 1, pp. 159–70.

Leijon, B.A. (1986) Application of the LUT triaxial overcoring technique in Swedish mines, in *Proc. Int. Symp. on Rock Stress and Rock Stress Measurements*, Stockholm, Centek Publ., Luleå, pp. 569–79.

Leijon, B.A. and Stillborg, B.L. (1986) A comparative study between two rock stress measurement techniques at Luossavaara mine. *Rock Mech. Rock Eng.*, **19**, 143–63.

Liang, J. and Lindblom, U. (1994) Critical pressure for gas storage in unlined rock caverns. *Int. J. Rock Mech. Min. Sci. & Geomech. Abstr.*, **31**, 377–81.

Lindblom, U.E. (1977) Rock mechanics research on rock caverns for energy storage, in *Proc. 18th US Symp. Rock Mech.*, Keystone, Johnson Publ., Boulder, 5A2-1–5A2-8.

Lindblom, U.E. (1990) City energy management through underground storage. *Tunnell. Und. Space Tech.*, **5**, 225–32.

Martin, C.D. (1995) Brittle rock strength and failure: laboratory and in situ, in *Proc. 8th Cong. Int. Soc. Rock Mech. (ISRM)*, Tokyo, Balkema, Rotterdam, Vol. 3 (in press).

Martna, J. (1988) Distribution of tectonic stresses in mountainous areas, unpublished paper presented at *Int. Symp. on Tunneling for Water Resources and Power Projects*, New Delhi.

Martna, J. and Hansen, L. (1986) Initial rock stresses around the Vietas headrace tunnels no. 2 and 3, Sweden, in *Proc. Int. Symp. on Rock Stress and Rock Stress Measurements*, Stockholm, Centek Publ., Luleå, pp. 605–13.

Martna, J. and Hansen, L. (1987) Rock bursting and related phenomena in some Swedish water tunnels, in *Proc. 6th Cong. Int. Soc. Rock Mech. (ISRM)*, Montreal, Balkema, Rotterdam, Vol. 2, pp. 1105–10.

Marulanda, A., Ortiz, C. and Gutierrez, R. (1986) Definition of the use of steel liners based on hydraulic fracturing tests. A case history, in *Proc. Int. Symp. on Rock Stress and Rock Stress Measurements*, Stockholm, Centek Publ., Luleå, pp. 599–604.

Mattauer, M. (1973) *Les Déformations des Matériaux de l'Ecorce Terrestre*, Hermann, Paris.

Mills, K.W., Pender, M.J. and Depledge, D. (1986) Measurement of in situ stress in coal, in *Proc. Int. Symp. on Rock Stress and Rock Stress Measurements*, Stockholm, Centek Publ., Luleå, pp. 543–9.

Mimaki, Y. (1976) Design and construction of a large underground power station, in *Design and Construction of Underground Structures*, The Japan Society of Civil Engineers, Tokyo, pp. 115–52.

Mimaki, Y. and Matsuo, K. (1986) Investigation of asymmetrical deformation behavior at the horseshoe-shaped large cavern opening, in *Proc. Int. Symp. on Large Rock Caverns*, Helsinki, Pergamon Press, Oxford, Vol. 2, pp. 1337–48.

Molinda, M. *et al.* (1992) Effects of horizontal stress related to stream valleys on the stability of coal mine openings. US Bureau of Mines Report of Investigation RI 9413.

Morris, A., Ferrill, D.A. and Henderson, D.B. (1996) Slip-tendency analysis and fault reactivation, *Geology*, **24**, 275–8.

Morton, J.D. and Provost, A.J. (1980) Stillwater tunnel: a classroom in engineering geology, in *Proc. 13th Can. Rock Mech. Symp.*, Toronto, Canadian Institute of Mining and Metallurgy, CIM Special Vol. 22, pp. 80–89.

Müller, B. *et al.* (1992) Regional patterns of tectonic stress in Europe. *J. Geophys. Res.*, **97**, 11783–803.

Myrvang, A.M. (1993) Rock stress and rock stress problems in Norway, in *Comprehensive Rock Engineering* (ed. J.A. Hudson), Pergamon Press, Oxford, Chapter 18, Vol. 3, pp. 461–71.

Myrvang, A., Hansen, S.E. and Sørensen, T. (1993) Rock stress redistribution around an open pit mine in hardrock. *Int. J. Rock Mech. Min. Sci. & Geomech. Abstr.*, **30**, 1001–4.

Obara, Y. *et al.* (1995) Measurement of stress distribution around fault and considerations, in *Proc. 2nd Int. Conf. on the Mechanics of Jointed and Faulted Rock*, Vienna, Balkema, Rotterdam, pp. 495–500.

Obert, L. and Duvall, W.I. (1967) *Rock Mechanics and the Design of Structures in Rock*, Wiley, London.

Olesen, O. *et al.* (1995) Neotectonics in the Ranafjorden area, Northern Norway, in *Proc. Workshop on Rock Stresses in the North Sea*, Trondheim, Norway, NTH and SINTEF Publ., Trondheim, pp. 92–9.

Pan, E., Amadei, B. and Savage, W.Z. (1994) Gravitational stresses in long symmetric ridges and valleys in anisotropic rock. *Int. J. Rock Mech. Min. Sci. & Geomech. Abstr.*, **31**, 293–312.

Pan, E., Amadei, B. and Savage, W.Z. (1995) Gravitational and tectonic stresses in anisotropic rock with irregular topography. *Int. J. Rock Mech. Min. Sci. & Geomech. Abstr.*, **32**, 201–14.

Pande, G.N., Beer, G. and Williams, J.R. (1990) *Numerical Methods in Rock Mechanics*, Wiley, London.

Pine, R.J. and Kwakwa, K.A. (1989) Experience with hydrofracture stress measurements to depths of 2.6 km and implications for measurements to 6 km in the Carnmenellis granite. *Int. J. Rock Mech. Min. Sci. & Geomech. Abstr.*, **26**, 565–71.

Price, N.J. and Cosgrove, J.W. (1990) *Analysis of Geological Structures*, Cambridge University Press, Cambridge.

Price Jones, A. and Sims, G.P. (1984) Measurement of in-situ rock stresses for a hydro-electric scheme in Peru, in *Proc. ISRM Symp. on Design and Performance*

of Underground Excavations, Cambridge, British Geotechnical Society, London, pp. 191–8.

Ramberg, H. (1961) Contact strain and fold instability of a multilayered body under compression. *Geol. Rundsch.*, **51**, 405–39.

Ramberg, H. (1981) *Gravity, Deformation and the Earth's Crust*, 2nd edn, Academic Press, London.

Ramsay, J.G. (1967) *Folding and Fracturing of Rocks*, McGraw-Hill, New York.

Richards, L.R., Sharp, J.C. and Pine, R.J. (1977) Design considerations for large unlined caverns at shallow depths in jointed rock, in *Proc. 1st Int. Symp. on Storage in Excavated Rock Caverns*, Stockholm, Pergamon Press, Oxford, Vol. 2, pp. 239–46.

Riley, W.F. and Zachary, L. (1989) *Introduction to Mechanics of Materials*, Wiley, New York.

Roald, S., Ustad, O. and Myrvang, A. (1986) Natural gas storage in hard rock caverns. *Tunnels and Tunnelling*, **18**, 24–5.

Selmer-Olsen, R. (1974) Underground openings filled with high pressure water or air. *Bull. Int. Ass. Eng. Geol.*, **9**, 91–5.

Sharma, V.M. *et al.* (1991) In-situ stress measurement for design of tunnels, in *Proc. 7th Cong. Int. Soc. Rock Mech. (ISRM)*, Aachen, Balkema, Rotterdam, Vol. 2, pp. 1355–8.

Singh, U., Stephansson, O. and Herdocia, A. (1994) Simulation of progressive failure in hanging wall and foot-wall for mining with sub-level caving. *Trans. Inst. Min. Metall., A*, **102**, 188–94.

Stephansson, O. (1972) Theoretical and experimental studies of diapiric structures on Öland. *Bull. Geol. Instn Univ. Uppsala NS*, **3**, 163–200.

Stephansson, O. (1976) Finite element analysis of folds. *Phil. Trans. Roy. Soc. London A*, **283**, 153–61.

Stephansson, O. (1985) Pillar design for large hole open stoping, in *Proc. Int. Symp. on Large Scale Underground Mining*, Centek Publ., Luleå, pp. 185–97.

Stephansson, O. (1993) Rock stress in the Fennoscandian shield, in *Comprehensive Rock Engineering* (ed. J.A. Hudson), Pergamon Press, Oxford, Chapter 17, Vol. 3, pp. 445–59.

Stephansson, O., Särkkä, P. and Myrvang, A. (1986) State of stress in Fennoscandia, in *Proc. Int. Symp. on Rock Stress and Rock Stress Measurements*, Stockholm, Centek Publ., Luleå, pp. 21–32.

Stillborg, B.L. (1993) Rock mass response to large blast hole open stoping, in *Comprehensive Rock Engineering* (ed. J.A. Hudson), Pergamon Press, Oxford, Chapter 17, Vol. 4, pp. 485–511.

Stock, J.M. *et al.* (1985) Hydraulic fracturing stress measurements at Yucca Mountain, Nevada, and relationship to regional stress field. *J. Geophys. Res.*, **90**, 8691–706.

Sugawara, K. and Obara, Y. (1993) Measuring Rock Stress, in *Comprehensive Rock Engineering* (ed. J.A. Hudson), Pergamon Press, Oxford, Chapter 21, Vol. 3, pp. 533–52.

Sugawara, K. *et al.* (1986) Determination of the state of stress in rock by the measurement of strains on the hemispherical borehole bottom, in *Proc. Int. Symp. on Large Rock Caverns*, Helsinki, Pergamon Press, Oxford, Vol. 2, pp. 1039–50.

Te Kamp, L., Rummel, F. and Zoback, M.D. (1995) Hydrofrac stress profile to 9 km at the German KTB site, in *Proc. Workshop on Rock Stresses in the North Sea*, Trondheim, Norway, NTH and SINTEF Publ., Trondheim, pp. 147–53.

Teufel, L.W. and Farrell, H.E. (1990) In situ stress and natural fracture distribution in the Ekofisk field, North Sea. Sandia National Labs Report No. SAND-90-1058C.

Teufel, L.W., Rhett, D.W. and Farrell, H.E. (1991) Effect of reservoir depletion and pore pressure drawdown on in situ stress and deformation in the Ekofisk Field, North Sea, in *Proc. 32nd US Symp. Rock Mech.*, Norman, Balkema, Rotterdam, pp. 63–72.

Trusheim, F. (1960) Mechanism of salt migration in N. Germany. *Am. Assoc. Petrol. Geol. Bull.*, **44**, 1519–40.

Vik, G. and Tundbridge, L. (1986) Hydraulic fracturing – a simple tool for controlling the safety of unlined pressure shafts and headrace tunnels, in *Proc. Int. Symp. on Rock Stress and Rock Stress Measurements*, Stockholm, Centek Publ., Luleå, pp. 591–7.

Withjack, M.O. and Scheiner, C. (1982) Fault patterns associated with domes – an experimental and analytical study. *Am. Assoc. Petrol. Geol. Bull.*, **66**, 302–16.

Zoback, M.D. and Healy, J.H. (1992) In-situ stress measurements to 3.5 km depth in the Cajon Pass scientific research borehole: implications for the mechanics of crustal faulting. *J. Geophys. Res.*, **97**, 5039–57.

Zoback, M.D. *et al.* (1993) Upper-crustal strength inferred from stress measurements to 6 km depth in the KTB borehole. *Nature*, **365**, 633–5.

Zoback, M.L. (1992) First- and second-order patterns of stress in the lithosphere: the World Stress Map Project. *J. Geophys. Res.*, **97**, 11703–28.

Zoback, M.L. *et al.* (1989) Global patterns of tectonic stress. *Nature*, **341**, 291–8.

APPENDIX A ANALYSIS OF STRESS

This appendix provides a summary of the basic concepts of the continuum mechanics description of stress. The writing of this appendix was done based on lecture notes and after consulting several major textbooks on continuum mechanics. The presentation follows in part that used by G.E. Mase in his book entitled *Continuum Mechanics* (Schaum's Outline Series, McGraw-Hill, 1970).

A.1 CAUCHY STRESS PRINCIPLE

Consider a material continuum occupying a region R of space and subjected to body forces $\boldsymbol{b}$ (per unit mass) and surface forces $\bar{\boldsymbol{f}}$ (Fig. A.1). Let x, y, z be a Cartesian coordinate system with unit vectors $\boldsymbol{e}_1$, $\boldsymbol{e}_2$, $\boldsymbol{e}_3$ parallel to the x, y, z directions, respectively.

The material inside an arbitrary volume V in the continuum interacts with the material outside V. For a small surface element ΔS located on the outer surface S of volume V and for a point P located on ΔS, a unit vector $\boldsymbol{n}$ normal to ΔS can be defined. Let $\Delta \boldsymbol{f}$ and $\Delta \boldsymbol{m}$ be respectively the resultant force and moment exerted across ΔS by the material outside of V upon the material within V.

The Cauchy stress principle asserts that the average force per unit area $\Delta f / \Delta S$ tends to a limit $\mathrm{d}f/\mathrm{d}s$ as ΔS tends to zero, whereas $\Delta \boldsymbol{m}$ vanishes in the limiting process. This limit is called the stress vector $\boldsymbol{t}_{(n)}$, i.e.

$$\boldsymbol{t}_{(n)} = \lim_{\Delta S \to 0} \frac{\Delta \boldsymbol{f}}{\Delta S} = \frac{\mathrm{d}\boldsymbol{f}}{\mathrm{d}s} \tag{A.1}$$

The components of the stress vector $\boldsymbol{t}_{(n)}$ in the x, y, z directions are expressed in units of force per unit area. Likewise, the stress vector corresponding to the action across ΔS of the material within volume V upon the material outside that volume is $\boldsymbol{t}_{(-n)}$. By Newton's law of action and reaction

$$\boldsymbol{t}_{(n)} + \boldsymbol{t}_{(-n)} = \boldsymbol{0} \tag{A.2}$$

Equation (A.2) can be formulated as follows: the stress vectors acting on opposite sides of a same surface are equal in magnitude but opposite in direction.

A.2 STATE OF STRESS AT A POINT

The state of stress at point P in Fig. A.1 can be defined by using equation (A.1) for all planes ΔS having point P as an interior point. An alternative is to look at the stress vectors $\boldsymbol{t}_{(e1)}$, $\boldsymbol{t}_{(e2)}$ and $\boldsymbol{t}_{(e3)}$ acting on three orthogonal planes

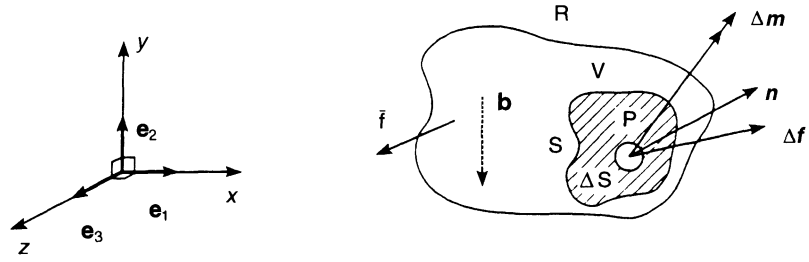

Fig. A.1 Material continuum subjected to body and surface forces.

normal to the x-, y- and z-axes, respectively. These three planes form an infinitesimal stress element around point P.

The nine components of vectors $\boldsymbol{t}_{(e1)}$, $\boldsymbol{t}_{(e2)}$ and $\boldsymbol{t}_{(e3)}$ are the components of a second-order Cartesian tensor also known as the stress tensor σ_{ij} $(i,j = 1\text{–}3)$. The components σ_{11}, σ_{22} and σ_{33} represent three normal stresses σ_x, σ_y and σ_z acting in the x, y and z directions, respectively. The components σ_{ij} $(i \neq j)$ represent six shear stresses τ_{xy}, τ_{yx}, τ_{xz}, τ_{zx}, τ_{yz} and τ_{zy} acting in the x,y; x,z; and y,z planes. Two sign conventions are considered below:

1. Engineering mechanics sign convention. Tensile normal stresses are treated as positive and the direction of positive shear stresses is as shown in Fig. A.2a. The stress vectors $\boldsymbol{t}_{(e1)}$, $\boldsymbol{t}_{(e2)}$ and $\boldsymbol{t}_{(e3)}$ have the following expressions

$$\begin{aligned} \boldsymbol{t}_{(e1)} &= \sigma_x \boldsymbol{e}_1 + \tau_{xy} \boldsymbol{e}_2 + \tau_{xz} \boldsymbol{e}_3 \\ \boldsymbol{t}_{(e2)} &= \tau_{yx} \boldsymbol{e}_1 + \sigma_y \boldsymbol{e}_2 + \tau_{yz} \boldsymbol{e}_3 \\ \boldsymbol{t}_{(e3)} &= \tau_{zx} \boldsymbol{e}_1 + \tau_{zy} \boldsymbol{e}_2 + \sigma_z \boldsymbol{e}_3 \end{aligned} \tag{A.3}$$

2. Rock mechanics sign convention. Compressive normal stresses are treated as positive and the direction of positive shear stresses is as shown in Fig. A.2b. The stress vectors $\boldsymbol{t}_{(e1)}$, $\boldsymbol{t}_{(e2)}$ and $\boldsymbol{t}_{(e3)}$ have the following expressions

$$\begin{aligned} \boldsymbol{t}_{(e1)} &= -\sigma_x \boldsymbol{e}_1 - \tau_{xy} \boldsymbol{e}_2 - \tau_{xz} \boldsymbol{e}_3 \\ \boldsymbol{t}_{(e2)} &= -\tau_{yx} \boldsymbol{e}_1 - \sigma_y \boldsymbol{e}_2 - \tau_{yz} \boldsymbol{e}_3 \\ \boldsymbol{t}_{(e3)} &= -\tau_{zx} \boldsymbol{e}_1 - \tau_{zy} \boldsymbol{e}_2 - \sigma_z \boldsymbol{e}_3 \end{aligned} \tag{A.4}$$

A.3 STATE OF STRESS ON AN INCLINED PLANE

Consider again point P of Fig. A.1 and let σ_{ij} be the stress tensor representing the state of stress at that point. The components of the stress vector $\boldsymbol{t}_{(n)}$ acting on an inclined plane passing through P can be expressed in terms of the σ_{ij} components and the orientation of the plane using a limiting process similar to that used to introduce the stress vector concept. As shown in Fig. A.3, consider a plane ABC of area $\mathrm{d}S$ parallel to the plane of interest passing through P. Let $\boldsymbol{n}$ be the normal to the plane with components n_1, n_2, n_3. The force equilibrium of the PABC tetrahedron leads to the following relation between the (average) stress vectors acting on its forces:

$$\begin{aligned} \boldsymbol{t}_{(n)}\,\mathrm{d}S + \boldsymbol{t}_{(-e1)} n_1\,\mathrm{d}S + \boldsymbol{t}_{(-e2)} n_2\,\mathrm{d}S \\ + \boldsymbol{t}_{(-e3)} n_3\,\mathrm{d}S = \boldsymbol{0} \end{aligned} \tag{A.5}$$

where $n_1\,\mathrm{d}S$, $n_2\,\mathrm{d}S$ and $n_3\,\mathrm{d}S$ are respectively the areas of faces CPB, CPA and APB of the tetrahedron. Using equation (A.2), $\boldsymbol{t}_{(n)}$ can be expressed as follows:

$$\boldsymbol{t}_{(n)} = \boldsymbol{t}_{(e1)} n_1 + \boldsymbol{t}_{(e2)} n_2 + \boldsymbol{t}_{(e3)} n_3 \tag{A.6}$$

The stress acting on plane ABC will approach the stress on the parallel plane passing through P as the tetrahedron in Fig. A.3 is made infinitesimal. In that limiting process, the contribution of any body force acting in the PABC tetrahedron vanishes.

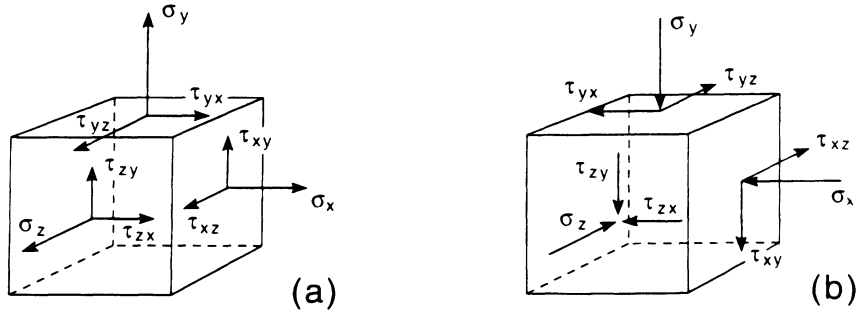

Fig. A.2 Direction of positive normal and shear stresses: (a) engineering mechanics convention, (b) rock mechanics convention.

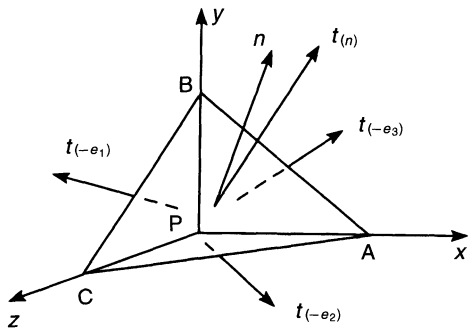

Fig. A.3 State of stress on an inclined plane passing through point P.

Equation (A.6) can also be expressed in terms of the normal and shear stress components at point P. Let t_x, t_y and t_z be the x, y, z components of the stress vector $\boldsymbol{t}_{(n)}$. When using the engineering mechanics sign convention, combining equations (A.3) and (A.6), we have

$$\begin{bmatrix} t_x \\ t_y \\ t_z \end{bmatrix} = \begin{bmatrix} \sigma_x & \tau_{yx} & \tau_{zx} \\ \tau_{xy} & \sigma_y & \tau_{zy} \\ \tau_{xz} & \tau_{yz} & \sigma_z \end{bmatrix} \begin{bmatrix} n_1 \\ n_2 \\ n_3 \end{bmatrix} \tag{A.7a}$$

On the other hand, for the rock mechanics sign convention, combining equations (A.4) and (A.6), we have

$$-\begin{bmatrix} t_x \\ t_y \\ t_z \end{bmatrix} = \begin{bmatrix} \sigma_x & \tau_{yx} & \tau_{zx} \\ \tau_{xy} & \sigma_y & \tau_{zy} \\ \tau_{xz} & \tau_{yz} & \sigma_z \end{bmatrix} \begin{bmatrix} n_1 \\ n_2 \\ n_3 \end{bmatrix} \tag{A.7b}$$

The (3×3) matrix in equations (A.7a) and (A.7b) is a matrix representation of the stress tensor σ_{ij}.

A.4 FORCE AND MOMENT EQUILIBRIUM

For all differential elements in the continuum of Fig. A.1, force and moment equilibrium leads respectively to the equilibrium equations and the symmetry of the stress tensor σ_{ij}.

1. Equations of equilibrium:

$$\begin{aligned} \frac{\partial \sigma_x}{\partial x} + \frac{\partial \tau_{yx}}{\partial y} + \frac{\partial \tau_{zx}}{\partial z} + \rho b_1 &= 0 \\ \frac{\partial \tau_{xy}}{\partial x} + \frac{\partial \sigma_y}{\partial y} + \frac{\partial \tau_{zy}}{\partial z} + \rho b_2 &= 0 \\ \frac{\partial \tau_{xz}}{\partial x} + \frac{\partial \tau_{yz}}{\partial y} + \frac{\partial \sigma_z}{\partial z} + \rho b_3 &= 0 \end{aligned} \tag{A.8}$$

   where ρ is the density and ρb_1, ρb_2, ρb_3 are the components of the body force per unit volume of the continuum in the x, y and z directions, respectively. The positive directions of those components are in the positive x, y and z directions if the engineering mechanics convention for stress is used, and in the negative x, y, z directions if the rock mechanics sign convention is used instead.

2. Symmetry of the stress tensor:

$$\tau_{xy} = \tau_{yx}; \quad \tau_{xz} = \tau_{zx}; \quad \tau_{yz} = \tau_{zy} \tag{A.9}$$

   Equation (A.9) implies that only six stress components are needed to describe the state of stress at a point: three normal stresses and three shear stresses.

A.5 STRESS TRANSFORMATION LAW

Consider two rectangular coordinate systems x, y, z and x', y', z' at point P. The orientation of the x'-, y'-, z'-axes is defined in terms of the direction cosines of unit vectors $\boldsymbol{e}_1'$, $\boldsymbol{e}_2'$ and $\boldsymbol{e}_3'$ in the x, y, z coordinate system, i.e.

$$\begin{aligned} \boldsymbol{e}_1' &= l_{x'}\boldsymbol{e}_1 + m_{x'}\boldsymbol{e}_2 + n_{x'}\boldsymbol{e}_3 \\ \boldsymbol{e}_2' &= l_{y'}\boldsymbol{e}_1 + m_{y'}\boldsymbol{e}_2 + n_{y'}\boldsymbol{e}_3 \\ \boldsymbol{e}_3' &= l_{z'}\boldsymbol{e}_1 + m_{z'}\boldsymbol{e}_2 + n_{z'}\boldsymbol{e}_3 \end{aligned} \tag{A.10}$$

Let $[A]$ be a transformation matrix such that

$$[A] = \begin{bmatrix} l_{x'} & m_{x'} & n_{x'} \\ l_{y'} & m_{y'} & n_{y'} \\ l_{z'} & m_{z'} & n_{z'} \end{bmatrix} \tag{A.11}$$

Matrix $[A]$ is an orthogonal matrix such that $[A]^t = [A]^{-1}$. Using the transformation law for

second-order Cartesian tensors, the components of the stress tensor σ'_{ij} in the x', y', z' coordinate system are related to the components of the stress tensor σ_{ij} in the x, y, z system as follows:

$$\begin{bmatrix} \sigma_{x'} & \tau_{x'y'} & \tau_{x'z'} \\ \tau_{x'y'} & \sigma_{y'} & \tau_{y'z'} \\ \tau_{x'z'} & \tau_{y'z'} & \sigma_{z'} \end{bmatrix} = \begin{bmatrix} l_{x'} & m_{x'} & n_{x'} \\ l_{y'} & m_{y'} & n_{y'} \\ l_{z'} & m_{z'} & n_{z'} \end{bmatrix} \times \begin{bmatrix} \sigma_x & \tau_{xy} & \tau_{xz} \\ \tau_{xy} & \sigma_y & \tau_{yz} \\ \tau_{xz} & \tau_{yz} & \sigma_z \end{bmatrix} \times \begin{bmatrix} l_{x'} & l_{y'} & l_{z'} \\ m_{x'} & m_{y'} & m_{z'} \\ n_{x'} & n_{y'} & n_{z'} \end{bmatrix} \quad \text{(A.12)}$$

Using (6×1) matrix representations of σ'_{ij} and σ_{ij}, equation (A.12) can be rewritten as equation (A.13) or in matrix form:

$$[\sigma]_{x'y'z'} = [T_\sigma][\sigma]_{xyz} \quad \text{(A.14)}$$

Expressions for the direction cosines $l_{x'}$, $m_{x'}$, $n_{x'}$ $\cdots$ are given below for two special cases shown in Figs A.4a and A.4b, respectively. In Fig. A.4a the orientation of the x'-axis is defined using two angles β and δ and the z'-axis lies in the P, x, z plane. The direction cosines are such that

$$\begin{aligned} l_{x'} &= \cos\delta\cos\beta \quad l_{y'} = -\sin\delta\cos\beta \\ l_{z'} &= -\sin\beta \\ m_{x'} &= \sin\delta \quad m_{y'} = \cos\delta \quad m_{z'} = 0 \\ n_{x'} &= \cos\delta\sin\beta \quad n_{y'} = -\sin\delta\sin\beta \\ n_{z'} &= \cos\beta \end{aligned} \quad \text{(A.15)}$$

If we set $\beta = 0$ and $\delta = \theta$ in equation (A.15) and take z' to coincide with the z-axis, x', y', z'

$$\begin{bmatrix} \sigma_{x'} \\ \sigma_{y'} \\ \sigma_{z'} \\ \tau_{y'z'} \\ \tau_{z'x'} \\ \tau_{x'y'} \end{bmatrix} = \begin{bmatrix} l_{x'}^2 & m_{x'}^2 & n_{x'}^2 & 2m_{x'}n_{x'} & 2n_{x'}l_{x'} & 2l_{x'}m_{x'} \\ l_{y'}^2 & m_{y'}^2 & n_{y'}^2 & 2m_{y'}n_{y'} & 2n_{y'}l_{y'} & 2l_{y'}m_{y'} \\ l_{z'}^2 & m_{z'}^2 & n_{z'}^2 & 2m_{z'}n_{z'} & 2n_{z'}l_{z'} & 2l_{z'}m_{z'} \\ l_{y'}l_{z'} & m_{y'}m_{z'} & n_{y'}n_{z'} & m_{y'}n_{z'} + m_{z'}n_{y'} & n_{y'}l_{z'} + n_{z'}l_{y'} & l_{y'}m_{z'} + l_{z'}m_{y'} \\ l_{z'}l_{x'} & m_{z'}m_{x'} & n_{z'}n_{x'} & m_{x'}n_{z'} + m_{z'}n_{x'} & n_{x'}l_{z'} + n_{z'}l_{x'} & l_{x'}m_{z'} + l_{z'}m_{x'} \\ l_{x'}l_{y'} & m_{x'}m_{y'} & n_{x'}n_{y'} & m_{x'}n_{y'} + m_{y'}n_{x'} & n_{x'}l_{y'} + n_{y'}l_{x'} & l_{x'}m_{y'} + l_{y'}m_{x'} \end{bmatrix} \begin{bmatrix} \sigma_x \\ \sigma_y \\ \sigma_z \\ \tau_{yz} \\ \tau_{zx} \\ \tau_{xy} \end{bmatrix} \quad \text{(A.13)}$$

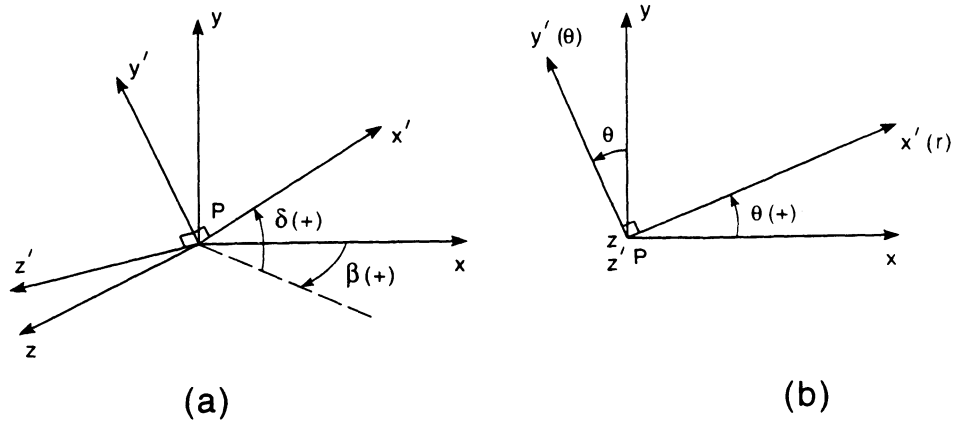

Fig. A.4 Two special orientations of the x'-, y'-, z'-axes with respect to the x, y, z coordinate system.

coincide, for instance, with the radial, tangential and longitudinal axes of a cylindrical coordinate system r, θ, z (Fig. A.4b) with

$$l_{x'} = l_r = \cos\theta \quad l_{y'} = l_\theta = -\sin\theta$$
$$l_{z'} = l_z = 0$$
$$m_{x'} = m_r = \sin\theta \quad m_{y'} = m_\theta = \cos\theta$$
$$m_{z'} = m_z = 0 \qquad \text{(A.16)}$$
$$n_{x'} = n_r = 0 \quad n_{y'} = n_\theta = 0$$
$$n_{z'} = n_z = 1$$

Substituting these direction cosines into equation (A.13) gives the relationship between the stress components in the r, θ, z coordinate system σ_r, σ_θ, σ_z, $\tau_{\theta z}$, τ_{rz}, $\tau_{r\theta}$ and those in the x, y, z coordinate system

$$\begin{bmatrix} \sigma_r \\ \sigma_\theta \\ \sigma_z \\ \tau_{\theta z} \\ \tau_{rz} \\ \tau_{r\theta} \end{bmatrix} = \begin{bmatrix} \cos^2\theta & \sin^2\theta & 0 & 0 & 0 & \sin 2\theta \\ \sin^2\theta & \cos^2\theta & 0 & 0 & 0 & -\sin 2\theta \\ 0 & 0 & 1 & 0 & 0 & 0 \\ 0 & 0 & 0 & \cos\theta & -\sin\theta & 0 \\ 0 & 0 & 0 & \sin\theta & \cos\theta & 0 \\ -\frac{\sin 2\theta}{2} & \frac{\sin 2\theta}{2} & 0 & 0 & 0 & \cos 2\theta \end{bmatrix} \begin{bmatrix} \sigma_x \\ \sigma_y \\ \sigma_z \\ \tau_{yz} \\ \tau_{xz} \\ \tau_{xy} \end{bmatrix} \qquad \text{(A.17)}$$

A.6 NORMAL AND SHEAR STRESSES ON AN INCLINED PLANE

Consider a plane passing through point P and inclined with respect to the x-, y- and z-axes. Let x', y', z' be a Cartesian coordinate system attached to the plane such that the x'-axis is along its outward normal and the y'- and z'-axes are in the plane. The x'-, y'- and z'-axes are oriented as shown in Fig. A.4a with the direction cosines defined in equation (A.15).

The state of stress across the plane is defined by one normal component $\sigma_{x'} = \sigma_n$ and two shear components $\tau_{x'y'}$ and $\tau_{x'z'}$ such that (Fig. A.5)

$$\begin{bmatrix} \sigma_{x'} \\ \tau_{x'y'} \\ \tau_{x'z'} \end{bmatrix} = \begin{bmatrix} l_{x'} & m_{x'} & n_{x'} \\ l_{y'} & m_{y'} & n_{y'} \\ l_{z'} & m_{z'} & n_{z'} \end{bmatrix} \begin{bmatrix} \sigma_x & \tau_{xy} & \tau_{xz} \\ \tau_{xy} & \sigma_y & \tau_{yz} \\ \tau_{xz} & \tau_{yz} & \sigma_z \end{bmatrix} \begin{bmatrix} l_{x'} \\ m_{x'} \\ n_{x'} \end{bmatrix} \qquad \text{(A.18)}$$

Equation (A.18) is the matrix representation of the first, fifth and sixth lines of equation (A.13). The resultant shear stress τ across the plane is equal to

$$\tau^2 = \tau_{x'y'}^2 + \tau_{x'z'}^2 \qquad \text{(A.19)}$$

The stress vector $\boldsymbol{t}_{(n)}$ acting on the plane is such that

$$|\boldsymbol{t}_{(n)}|^2 = \sigma_n^2 + \tau^2 = \sigma_{x'}^2 + \tau_{x'y'}^2 + \tau_{x'z'}^2 \qquad \text{(A.20)}$$

A.7 PRINCIPAL STRESSES

Finding the principal stresses and principal stress directions is equivalent to finding the

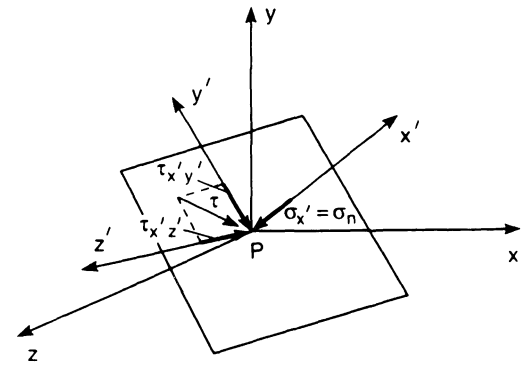

Fig. A.5 Normal and shear components of the stress vector acting on a plane passing through point P.

eigenvalues and corresponding eigenvectors of the stress tensor σ_{ij}. Since this tensor is symmetric, the eigenvalues are real.

The eigenvalues of σ_{ij} are the values of the normal stress σ such that the determinant of $\sigma_{ij} - \sigma\delta_{ij}$ vanishes, i.e.

$$\begin{vmatrix} \sigma_x - \sigma & \tau_{xy} & \tau_{xz} \\ \tau_{xy} & \sigma_y - \sigma & \tau_{yz} \\ \tau_{xz} & \tau_{yz} & \sigma_z - \sigma \end{vmatrix} = 0 \quad \text{(A.21)}$$

Upon expansion, σ has to satisfy the following cubic polynomial:

$$\sigma^3 - I_1\sigma^2 + I_2\sigma - I_3 = 0 \quad \text{(A.22)}$$

where I_1, I_2, I_3 are respectively the first, second and third stress invariants and are equal to

$$\begin{aligned} I_1 &= \sigma_x + \sigma_y + \sigma_z \\ I_2 &= \sigma_y\sigma_z + \sigma_x\sigma_z + \sigma_x\sigma_y \\ &\quad - \tau_{yz}^2 - \tau_{xz}^2 - \tau_{xy}^2 \\ I_3 &= \sigma_x\sigma_y\sigma_z + 2\tau_{xy}\tau_{xz}\tau_{yz} \\ &\quad - (\sigma_x\tau_{yz}^2 + \sigma_y\tau_{xz}^2 + \sigma_z\tau_{xy}^2) \end{aligned} \quad \text{(A.23)}$$

The three roots of equation (A.22) are the principal stresses and are usually denoted as $\sigma_1, \sigma_2, \sigma_3$. For each principal stress σ_k, there is a principal stress direction for which the direction cosines n_{1k}, n_{2k} and n_{3k} are solutions of

$$\begin{bmatrix} \sigma_x - \sigma_k & \tau_{xy} & \tau_{xz} \\ \tau_{xy} & \sigma_y - \sigma_k & \tau_{yz} \\ \tau_{xz} & \tau_{yz} & \sigma_z - \sigma_k \end{bmatrix} \begin{bmatrix} n_{1k} \\ n_{2k} \\ n_{3k} \end{bmatrix} = \begin{bmatrix} 0 \\ 0 \\ 0 \end{bmatrix} \quad \text{(A.24)}$$

with the normality condition

$$n_{1k}^2 + n_{2k}^2 + n_{3k}^2 = 1$$

APPENDIX B DISPLACEMENTS, STRESSES AND STRAINS AROUND A CIRCULAR HOLE: ANISOTROPIC SOLUTION

B.1 GENERAL EXPRESSIONS FOR DISPLACEMENT COMPONENTS

Consider the geometry of Fig. 5.25 (p. 234) and the expression for the traction components X_n, Y_n, Z_n defined in equation (5.10) (p. 237). At any point in the medium, the displacement components u, v, w in the x, y, z directions, respectively, are equal to

$$\begin{aligned} u &= -2\,\mathrm{Re}(p_1\phi_1 + p_2\phi_2 + p_3\phi_3) \\ v &= -2\,\mathrm{Re}(q_1\phi_1 + q_2\phi_2 + q_3\phi_3) \\ w &= -2\,\mathrm{Re}(r_1\phi_1 + r_2\phi_2 + r_3\phi_3) \end{aligned} \tag{B.1}$$

with

$$\begin{aligned} p_k &= \beta_{11}\mu_k^2 + \beta_{12} - \beta_{16}\mu_k + \lambda_k(\beta_{15}\mu_k - \beta_{14}) \\ q_k &= \beta_{12}\mu_k + \frac{\beta_{22}}{\mu_k} - \beta_{26} + \lambda_k\left(\beta_{25} - \frac{\beta_{24}}{\mu_k}\right) \\ r_k &= \beta_{14}\mu_k + \frac{\beta_{24}}{\mu_k} - \beta_{46} + \lambda_k\left(\beta_{45} - \frac{\beta_{44}}{\mu_k}\right) \end{aligned} \tag{B.2a}$$

when $k = 1, 2$ and

$$\begin{aligned} p_3 &= \lambda_3(\beta_{11}\mu_3^2 + \beta_{12} - \beta_{16}\mu_3) + \beta_{15}\mu_3 - \beta_{14} \\ q_3 &= \lambda_3\left(\beta_{12}\mu_3 + \frac{\beta_{22}}{\mu_3} - \beta_{26}\right) + \beta_{25} - \frac{\beta_{24}}{\mu_3} \\ r_3 &= \lambda_3\left(\beta_{14}\mu_3 + \frac{\beta_{24}}{\mu_3} - \beta_{46}\right) + \beta_{45} - \frac{\beta_{44}}{\mu_3} \end{aligned} \tag{B.2b}$$

Sign convention: positive displacement components u, v, w are in the positive x, y, z directions, respectively.

In equations (B.1), (B.2a) and (B.2b):

1. Re denotes the real part of a complex function;
2. μ_1, μ_2, μ_3 and their conjugates $\bar{\mu}_1, \bar{\mu}_2, \bar{\mu}_3$ are complex roots of the equation

$$l_4(\mu)\cdot l_2(\mu) - l_3^2(\mu) = 0 \tag{B.3}$$

with

$$\begin{aligned} l_2(\mu) &= \beta_{55}\mu^2 - 2\beta_{45}\mu + \beta_{44} \\ l_3(\mu) &= \beta_{15}\mu^3 - (\beta_{14} + \beta_{56})\mu^2 + (\beta_{25} + \beta_{46})\mu \\ &\quad - \beta_{24} \\ l_4(\mu) &= \beta_{11}\mu^4 - 2\beta_{16}\mu^3 + (2\beta_{12} + \beta_{66})\mu^2 \\ &\quad - 2\beta_{26}\mu + \beta_{22} \end{aligned}$$

and

$$\beta_{ij} = a_{ij} - \frac{a_{i3}\cdot a_{j3}}{a_{33}} \quad (i, j = 1\text{–}6) \tag{B.4}$$

3. a_{ij} ($i, j = 1$–6) are components of matrix [A] in equation (5.8) (p. 236);
4. $\lambda_1, \lambda_2, \lambda_3$ are such that

$$\lambda_1 = -\frac{l_3(\mu_1)}{l_2(\mu_1)}; \quad \lambda_2 = -\frac{l_3(\mu_2)}{l_2(\mu_2)}; \quad \lambda_3 = -\frac{l_3(\mu_3)}{l_4(\mu_3)} \tag{B.5}$$

5. ϕ_k ($k = 1, 2, 3$) are three analytic functions of the complex variable $z_k = x + \mu_k y$ where x, y are the coordinates of the point in the anisotropic medium at which the displacements are calculated. For the present loading condition, the expressions for the functions ϕ_k are

$$\begin{aligned}
\phi_1 &= \frac{1}{\Delta}\left(\overline{a_1}(\mu_2 - \lambda_2\lambda_3\mu_3) + \overline{b_1}(\lambda_2\lambda_3 - 1)\right. \\
&\quad \left. + \overline{c_1}\lambda_3(\mu_3 - \mu_2)\right)\frac{1}{\xi_1} \\
\phi_2 &= \frac{1}{\Delta}\left(\overline{a_1}(\lambda_1\lambda_3\mu_3 - \mu_1) + \overline{b_1}(1 - \lambda_1\lambda_3)\right. \\
&\quad \left. + \overline{c_1}\lambda_3(\mu_1 - \mu_3)\right)\frac{1}{\xi_2} \\
\phi_3 &= \frac{1}{\Delta}\left(\overline{a_1}(\mu_1\lambda_2 - \mu_2\lambda_1) + \overline{b_1}(\lambda_1 - \lambda_2)\right. \\
&\quad \left. + \overline{c_1}(\mu_2 - \mu_1)\right)\frac{1}{\xi_3}
\end{aligned} \tag{B.6}$$

with

$$\begin{aligned}
\Delta &= \mu_2 - \mu_1 + \lambda_2\lambda_3(\mu_1 - \mu_3) \\
&\quad + \lambda_1\lambda_3(\mu_3 - \mu_2)
\end{aligned} \tag{B.7}$$

and

$$\begin{aligned}
\overline{a_1} &= -\frac{a}{2}(b_{1y} - ia_{1y}) \\
\overline{b_1} &= \frac{a}{2}(b_{1x} - ia_{1x}) \\
\overline{c_1} &= \frac{a}{2}(b_{1z} - ia_{1z})
\end{aligned} \tag{B.8}$$

$a_{1x}, b_{1x}, a_{1y}, b_{1y}, a_{1z}, b_{1z}$ are the coefficients of X_n, Y_n and Z_n defined in equation (5.10) (p. 237). ξ_k ($k = 1, 2, 3$) are functions of the complex variable z_k and are such that

$$\frac{z_k}{a} = \frac{1}{2}(1 - i\mu_k)\xi_k + \frac{1}{2}(1 + i\mu_k)\frac{1}{\xi_k} \tag{B.9}$$

For all points located along the contour of the hole of radius a in Fig. 5.25 (p. 234) ($x = a\cos\theta$, $y = a\sin\theta$), ξ_k is equal to $e^{i\theta}$.

The radial and tangential displacement components are equal to

$$\begin{aligned}
u_r &= u\cos\theta + v\sin\theta; \\
v_\theta &= v\cos\theta - u\,sin\,\theta
\end{aligned} \tag{B.10}$$

B.2 EXPRESSIONS FOR DISPLACEMENT COMPONENTS WHEN HOLE AXIS *z* IS PERPENDICULAR TO A PLANE OF ELASTIC SYMMETRY

If there is a plane of elastic symmetry normal to the z-axis (Fig. 5.26) (p. 236), equations (B.1)–(B.10) still apply with the additional relations

$$\begin{aligned}
&a_{46} = a_{56} = a_{4i} = a_{5i} = 0 \quad (i = 1,2,3) \\
&\beta_{46} = \beta_{56} = \beta_{4i} = \beta_{5i} = 0 \quad (i = 1,2,3) \\
&l_3(\mu) = 0 \\
&\lambda_1 = \lambda_2 = \lambda_3 = r_1 = r_2 = p_3 = q_3 = 0
\end{aligned} \tag{B.11}$$

The problem of elastic equilibrium of an anisotropic medium bounded internally by a hole of circular cross-section with applied stress components X_n, Y_n, Z_n can now be considered as the sum of two uncoupled problems:

1. a plane problem involving the displacement components u,v induced by X_n and Y_n only; μ_1 and μ_2 and their conjugates are the roots of the equation $l_4(\mu) = 0$;
2. an antiplane problem involving the displacement component w induced by Z_n only; μ_3 and its conjugate are the roots of the equation $l_2(\mu) = 0$.

B.3 RADIAL DISPLACEMENT INDUCED BY DRILLING A HOLE IN AN INFINITE ANISOTROPIC MEDIUM

Comparing equation (5.11) (p. 237) with the expressions of X_n, Y_n and Z_n in equation (5.10) and using equation (B.8) we obtain

$$\overline{a_1} = -\frac{a}{2}(\sigma_{yo} - i\tau_{xyo})$$

$$\overline{b_1} = \frac{a}{2}(\tau_{xyo} - i\sigma_{xo}) \qquad \text{(B.12)}$$

$$\overline{c_1} = \frac{a}{2}(\tau_{yzo} - i\tau_{xzo})$$

$\overline{a_1}$, $\overline{b_1}$, $\overline{c_1}$ are then substituted into the expressions of ϕ_1, ϕ_2, ϕ_3 in equation (B.6). Combining equations (B.1) and (B.10), we obtain the expressions for the radial, tangential and longitudinal displacement components induced by drilling a hole of radius a in an already stressed medium. In particular, for a point located at an angle θ from the x-axis along the contour of the hole, we have the radial displacement

$$\frac{u_{rh}}{a} = f_{1h}\sigma_{xo} + f_{2h}\sigma_{yo} + f_{3h}\sigma_{zo} + f_{4h}\tau_{yzo} + f_{5h}\tau_{xzo} + f_{6h}\tau_{xyo} \qquad \text{(B.13)}$$

with

$$f_{1h} = \mathrm{Re}\left\{\frac{1}{\Delta}(\sin\theta\cos\theta + i\cos^2\theta)[p_1(\lambda_2\lambda_3 - 1) + p_2(1 - \lambda_1\lambda_3) + p_3(\lambda_1 - \lambda_2)] + \frac{1}{\Delta}(\sin^2\theta + i\sin\theta\cos\theta)[q_1(\lambda_2\lambda_3 - 1) + q_2(1 - \lambda_1\lambda_3) + q_3(\lambda_1 - \lambda_2)]\right\}$$

$$f_{2h} = \mathrm{Re}\left\{\frac{1}{\Delta}(\cos^2\theta - i\sin\theta\cos\theta) \times [p_1(\mu_2 - \mu_3\lambda_2\lambda_3) + p_2(\lambda_1\lambda_3\mu_3 - \mu_1) + p_3(\mu_1\lambda_2 - \lambda_1\mu_2)] + \frac{1}{\Delta} \times (\sin\theta\cos\theta - i\sin^2\theta)[q_1(\mu_2 - \lambda_2\lambda_3\mu_3) + q_2(\lambda_1\lambda_3\mu_3 - \mu_1) + q_3(\mu_1\lambda_2 - \lambda_1\mu_2)]\right\}$$

$$f_{3h} = 0$$

$$f_{4h} = \mathrm{Re}\left\{\frac{1}{\Delta}(i\cos\theta\sin\theta - \cos^2\theta)[p_1\lambda_3(\mu_3 - \mu_2) + p_2\lambda_3(\mu_1 - \mu_3) + p_3(\mu_2 - \mu_1)] + \frac{1}{\Delta}(i\sin^2\theta - \sin\theta\cos\theta)[q_1\lambda_3(\mu_3 - \mu_2) + q_2\lambda_3(\mu_1 - \mu_3) + q_3(\mu_2 - \mu_1)]\right\}$$

$$f_{5h} = \mathrm{Re}\left\{\frac{1}{\Delta}(\cos\theta\sin\theta + i\cos^2\theta)[p_1\lambda_3(\mu_3 - \mu_2) + p_2\lambda_3(\mu_1 - \mu_3) + p_3(\mu_2 - \mu_1)] + \frac{1}{\Delta}(\sin^2\theta + i\sin\theta\cos\theta)[q_1\lambda_3(\mu_3 - \mu_2) + q_2\lambda_3(\mu_1 - \mu_3) + q_3(\mu_2 - \mu_1)]\right\}$$

$$f_{6h} = \mathrm{Re}\left\{\frac{1}{\Delta}(i\sin\theta\cos\theta - \cos^2\theta) \times [p_1(\lambda_2\lambda_3 - 1 + i(\mu_2 - \lambda_2\lambda_3\mu_3)) + p_2(1 - \lambda_1\lambda_3 + i(\lambda_1\lambda_3\mu_3 - \mu_1)) + p_3(\lambda_1 - \lambda_2 + i(\mu_1\lambda_2 - \mu_2\lambda_1))] + \frac{1}{\Delta}(i\sin^2\theta - \sin\theta\cos\theta) \times [q_1(\lambda_2\lambda_3 - 1 + i(\mu_2 - \lambda_2\lambda_3\mu_3)) + q_2(1 - \lambda_1\lambda_3 + i(\lambda_1\lambda_3\mu_3 - \mu_1)) + q_3(\lambda_1 - \lambda_2 + i(\mu_1\lambda_2 - \mu_2\lambda_1))]\right\} \qquad \text{(B.14)}$$

For small displacement components, the change in hole diameter U_{dh} can be taken equal to $2u_{rh}$.

If there is a plane of elastic symmetry normal to the borehole axis z, conditions (B.11) can be substituted into the expressions for f_{1h}–f_{6h}. This leads to the following expressions

for these coefficients:

$$
\begin{aligned}
f_{1h} &= \mathrm{Re}\Big\{(\sin\theta\cos\theta + i\cos^2\theta) \\
&\quad \times (\beta_{11}(\mu_1+\mu_2) - \beta_{16}) \\
&\quad + (\sin^2\theta + i\cos\theta\sin\theta)\left(\beta_{12} - \frac{\beta_{22}}{\mu_1\mu_2}\right)\Big\} \\
f_{2h} &= \mathrm{Re}\Big\{(\cos^2\theta - i\sin\theta\cos\theta)(\beta_{12} - \beta_{11}\mu_1\mu_2) \\
&\quad + (\sin\theta\cos\theta - i\sin^2\theta) \\
&\quad \times \left(\beta_{22}\frac{(\mu_1+\mu_2)}{\mu_1\mu_2} - \beta_{26}\right)\Big\} \\
f_{3h} &= f_{4h} = f_{5h} = 0 \\
f_{6h} &= \mathrm{Re}\Big\{(i\sin\theta\cos\theta - \cos^2\theta) \\
&\quad \times (i\beta_{12} - \beta_{16} + \beta_{11}(\mu_1+\mu_2) - i\beta_{11}\mu_1\mu_2) \\
&\quad + (i\sin^2\theta - \sin\theta\cos\theta) \\
&\quad \times \left(\beta_{12} - i\beta_{26} + i\beta_{22}\frac{(\mu_1+\mu_2)}{\mu_1\mu_2} - \frac{\beta_{22}}{\mu_1\mu_2}\right)\Big\}
\end{aligned}
\tag{B.15}
$$

When there are three planes of elastic symmetry normal to the x-, y- and z-axes, coefficients β_{16} and β_{26} also vanish and it can be shown that when μ_1 and μ_2 are distinct

$$\mu_1 = i\beta_1; \quad \mu_2 = i\beta_2 \quad (\beta_1, \beta_2 > 0)$$

or

$$
\begin{aligned}
\mu_1 &= \alpha_1 + i\beta_1; \\
\mu_2 &= -\alpha_1 + i\beta_1 \quad (\beta_1 > 0)
\end{aligned}
\tag{B.16}
$$

For both cases, $\mu_1 + \mu_2$ is always purely imaginary and $\mu_1\mu_2$ is always real. In addition,

$$\mu_1\mu_2 = -\left(\frac{\beta_{22}}{\beta_{11}}\right)^{1/2};$$

$$i(\mu_1+\mu_2) = -\left(\frac{2\beta_{12}+\beta_{66}}{\beta_{11}} + 2\left(\frac{\beta_{22}}{\beta_{11}}\right)^{1/2}\right)^{1/2}$$

Substituting these values into equation (B.15), f_{1h}, f_{2h} and f_{6h} are now equal to

$$
\begin{aligned}
f_{1h} &= \sin^2\theta(\beta_{12} + (\beta_{11}\beta_{22})^{1/2}) - \cos^2\theta\,\beta_{11} \\
&\quad \times \left(\frac{2\beta_{12}+\beta_{66}}{\beta_{11}} + 2\left(\frac{\beta_{22}}{\beta_{11}}\right)^{1/2}\right)^{1/2} \\
f_{2h} &= \cos^2\theta(\beta_{12} + (\beta_{11}\beta_{22})^{1/2}) \\
&\quad - \sin^2\theta(\beta_{11}\beta_{22})^{1/2} \\
&\quad \times \left(\frac{2\beta_{12}+\beta_{66}}{\beta_{11}} + 2\left(\frac{\beta_{22}}{\beta_{11}}\right)^{1/2}\right)^{1/2} \\
f_{6h} &= -\sin 2\theta(\beta_{12} + (\beta_{11}\beta_{22})^{1/2}) \\
&\quad - \sin\theta\cos\theta(\beta_{11} + (\beta_{11}\beta_{22})^{1/2}) \\
&\quad \times \left(\frac{2\beta_{12}+\beta_{66}}{\beta_{11}} + 2\left(\frac{\beta_{22}}{\beta_{11}}\right)^{1/2}\right)^{1/2}
\end{aligned}
\tag{B.17}
$$

For an isotropic medium with Young's modulus E and Poisson's ratio ν, $\mu_1 = \mu_2 = i$, $\beta_{16} = \beta_{26} = 0$, $\beta_{11} = \beta_{22} = (1-\nu^2)/E$ and $\beta_{12} = -\nu(1+\nu)/E$ and $\beta_{66} = 2(1+\nu)/E$. This leads to

$$
\begin{aligned}
f_{1h} &= \sin^2\theta\,\frac{(1-\nu-2\nu^2)}{E} \\
&\quad - 2\cos^2\theta\,\frac{(1-\nu^2)}{E} \\
f_{2h} &= \cos^2\theta\,\frac{(1-\nu-2\nu^2)}{E} \\
&\quad - 2\sin^2\theta\,\frac{(1-\nu^2)}{E} \\
f_{6h} &= -\sin 2\theta\,\frac{(3-\nu-4\nu^2)}{E}
\end{aligned}
\tag{B.18}
$$

B.4 RADIAL DISPLACEMENT INDUCED BY APPLICATION OF *IN SITU* STRESS FIELD

As shown by Amadei (1983), the radial displacement induced by application of the *in situ* stress field on the anisotropic medium without

a hole is equal to

$$\frac{u_{ro}}{a} = f_{1o}\sigma_{xo} + f_{2o}\sigma_{yo} + f_{3o}\sigma_{zo} + f_{4o}\tau_{yzo} + f_{5o}\tau_{xzo} + f_{6o}\tau_{xyo} \quad \text{(B.19)}$$

with

$$\begin{aligned} f_{1o} &= -(a_{11}\cos^2\theta + a_{21}\sin^2\theta + a_{61}\sin\theta\cos\theta) \\ f_{2o} &= -(a_{12}\cos^2\theta + a_{22}\sin^2\theta + a_{62}\sin\theta\cos\theta) \\ f_{3o} &= -(a_{13}\cos^2\theta + a_{23}\sin^2\theta + a_{63}\sin\theta\cos\theta) \\ f_{4o} &= -(a_{14}\cos^2\theta + a_{24}\sin^2\theta + a_{64}\sin\theta\cos\theta) \\ f_{5o} &= -(a_{15}\cos^2\theta + a_{25}\sin^2\theta + a_{65}\sin\theta\cos\theta) \\ f_{6o} &= -(a_{16}\cos^2\theta + a_{26}\sin^2\theta + a_{66}\sin\theta\cos\theta) \end{aligned} \quad \text{(B.20)}$$

for points located along the contour of the hole. Again, the change in diameter $U_{do} = 2u_{ro}$.

When there is a plane of elastic symmetry normal to the z-axis, substituting equation (B.11) into (B.20) leads to vanishing values for f_{4o} and f_{5o}. Furthermore, when there are three planes of symmetry normal to the x-, y- and z-axes, coefficients a_{16}, a_{26} and a_{36} also vanish, which gives

$$\begin{aligned} f_{1o} &= -a_{11}\cos^2\theta - a_{21}\sin^2\theta \\ f_{2o} &= -a_{12}\cos^2\theta - a_{22}\sin^2\theta \\ f_{3o} &= -a_{13}\cos^2\theta - a_{23}\sin^2\theta \\ f_{6o} &= -a_{66}\sin\theta\cos\theta \end{aligned} \quad \text{(B.21)}$$

For an isotropic medium, $a_{11} = a_{22} = 1/E$, $a_{12} = a_{23} = a_{13} = -\nu/E$ and $a_{66} = 2(1+\nu)/E$. Then,

$$\begin{aligned} f_{1o} &= -\frac{1}{E}(\cos^2\theta - \nu\sin^2\theta); \\ f_{2o} &= -\frac{1}{E}(\sin^2\theta - \nu\cos^2\theta); \\ f_{3o} &= \frac{\nu}{E} \\ f_{6o} &= -\frac{2(1+\nu)}{E}\sin\theta\cos\theta \end{aligned} \quad \text{(B.22)}$$

B.5 TOTAL RADIAL DISPLACEMENT AROUND THE BOREHOLE CONTOUR

(1) The total radial displacement around the borehole contour is obtained by adding equations (B.13) and (B.19) which gives

$$\frac{U_d}{2a} = f_1\sigma_{xo} + f_2\sigma_{yo} + f_3\sigma_{zo} + f_4\tau_{yzo} + f_5\tau_{xzo} + f_6\tau_{xyo} \quad \text{(B.23)}$$

with $f_1 = f_{1h} + f_{1o} \cdots f_6 = f_{6h} + f_{6o}$. Note that when there is a plane of elastic symmetry normal to the z-axis, both f_4 and f_5 vanish and the shear stresses τ_{xzo} and τ_{yzo} do not contribute to the diametral deformation of the borehole. Then,

$$\frac{U_d}{2a} = f_1\sigma_{xo} + f_2\sigma_{yo} + f_3\sigma_{zo} + f_6\tau_{xyo}$$

For the isotropic case,

$$\begin{aligned} f_1 &= \frac{1}{E}(2\cos 2\theta(\nu^2 - 1) - 1) \\ f_2 &= \frac{1}{E}(2\cos 2\theta(1 - \nu^2) - 1) \\ f_3 &= \frac{\nu}{E} \\ f_6 &= \frac{4}{E}\sin 2\theta(\nu^2 - 1) \end{aligned} \quad \text{(B.24)}$$

(2) Equation (B.23) can also be written as follows:

$$\frac{U_d}{2a} = M_1 + M_2\cos 2\theta + M_3\sin 2\theta \quad \text{(B.25)}$$

by substituting $(1 + \cos 2\theta)/2$, $(1 - \cos 2\theta)/2$ and $\sin 2\theta$ for $\cos^2\theta$, $\sin^2\theta$ and $2\sin\theta\cos\theta$ into the equations for f_{ih} and f_{io} ($i = 1$–6). Coefficients M_1, M_2 and M_3 depend on the six stress components, the elastic properties of the anisotropic medium in the n, s, t coordinate system and the orientation of its planes of anisotropy with respect to the hole.

In particular, when the medium has planes of elastic symmetry normal to the borehole axes x, y, z, M_1, M_2 and M_3 are equal to

$$\begin{aligned}
M_1 = \frac{\sigma_{xo}}{2}\Bigg[&\beta_{12} + (\beta_{11}\beta_{22})^{1/2} - \beta_{11}\Bigg(\frac{2\beta_{12}+\beta_{66}}{\beta_{11}} \\
&+ 2\Big(\frac{\beta_{22}}{\beta_{11}}\Big)^{1/2}\Bigg)^{1/2} - a_{11} - a_{21}\Bigg] + \frac{\sigma_{yo}}{2} \\
&\times \Bigg[\beta_{12} + (\beta_{11}\beta_{22})^{1/2} - (\beta_{11}\beta_{22})^{1/2} \\
&\times \Bigg(\frac{2\beta_{12}+\beta_{66}}{\beta_{11}} + 2\Big(\frac{\beta_{22}}{\beta_{11}}\Big)^{1/2}\Bigg)^{1/2} \\
&- a_{12} - a_{22}\Bigg] - \frac{\sigma_{zo}}{2}(a_{13}+a_{23}) \\
M_2 = \frac{\sigma_{xo}}{2}\Bigg[&-\beta_{12} - (\beta_{11}\beta_{22})^{1/2} - \beta_{11}\Bigg(\frac{2\beta_{12}+\beta_{66}}{\beta_{11}} \\
&+ 2\Big(\frac{\beta_{22}}{\beta_{11}}\Big)^{1/2}\Bigg)^{1/2} - a_{11} + a_{21}\Bigg] + \frac{\sigma_{yo}}{2} \\
&\times \Bigg[\beta_{12} + (\beta_{11}\beta_{22})^{1/2} + (\beta_{11}\beta_{22})^{1/2} \\
&\times \Bigg(\frac{2\beta_{12}+\beta_{66}}{\beta_{11}} + 2\Big(\frac{\beta_{22}}{\beta_{11}}\Big)^{1/2}\Bigg)^{1/2} \\
&- a_{12} + a_{22}\Bigg] - \frac{\sigma_{zo}}{2}(a_{13}-a_{23}) \\
M_3 = -\tau_{xyo}\Bigg[&\beta_{12} + (\beta_{11}\beta_{22})^{1/2} \\
&+ \frac{1}{2}(\beta_{11} + (\beta_{11}\beta_{22})^{1/2}) \\
&\times \Bigg(\frac{2\beta_{12}+\beta_{66}}{\beta_{11}} + 2\Big(\frac{\beta_{22}}{\beta_{11}}\Big)^{1/2}\Bigg)^{1/2} + \frac{a_{66}}{2}\Bigg]
\end{aligned} \tag{B.26}$$

which for an isotropic medium reduces to

$$\begin{aligned}
M_1 &= -\frac{1}{E}(\sigma_{xo} + \sigma_{yo} - \nu\sigma_{zo}) \\
M_2 &= -\frac{2}{E}(1-\nu^2)(\sigma_{xo} - \sigma_{yo}) \\
M_3 &= -\frac{4}{E}(1-\nu^2)\tau_{xyo}
\end{aligned} \tag{B.27}$$

(3) Note that the stress σ_{zo} can be related to the other stress components if the medium without a hole deforms in plane strain when subject to the *in situ* stresses. This gives, according to equation (5.8) (p. 236),

$$\begin{aligned}
\sigma_{zo} = -\frac{1}{a_{33}}&(a_{31}\sigma_{xo} + a_{32}\sigma_{yo} \\
&+ a_{34}\tau_{yzo} + a_{35}\tau_{xzo} + a_{36}\tau_{xyo})
\end{aligned} \tag{B.28}$$

Substituting equation (B.28) into equation (B.26) makes M_1 and M_2 dependent on σ_{xo} and σ_{yo} only. This gives

$$\begin{aligned}
M_1 = \frac{\sigma_{xo}}{2}\Bigg[&\beta_{12} + (\beta_{11}\beta_{22})^{1/2} - \beta_{11}\Bigg(\frac{2\beta_{12}+\beta_{66}}{\beta_{11}} \\
&+ 2\Big(\frac{\beta_{22}}{\beta_{11}}\Big)^{1/2}\Bigg)^{1/2} - a_{11} - a_{21} + \frac{a_{31}}{a_{33}} \\
&\times (a_{13}+a_{23})\Bigg] + \frac{\sigma_{yo}}{2}\Bigg[\beta_{12} + (\beta_{11}\beta_{22})^{1/2} \\
&- (\beta_{11}\beta_{22})^{1/2}\Bigg(\frac{2\beta_{12}+\beta_{66}}{\beta_{11}} + 2\Big(\frac{\beta_{22}}{\beta_{11}}\Big)^{1/2}\Bigg)^{1/2} \\
&- a_{12} - a_{22} + \frac{a_{32}}{a_{33}}(a_{13}+a_{23})\Bigg] \\
M_2 = \frac{\sigma_{xo}}{2}\Bigg[&-\beta_{12} - (\beta_{11}\beta_{22})^{1/2} - \beta_{11}\Bigg(\frac{2\beta_{12}+\beta_{66}}{\beta_{11}} \\
&+ 2\Big(\frac{\beta_{22}}{\beta_{11}}\Big)^{1/2}\Bigg)^{1/2} - a_{11} + a_{21} + \frac{a_{31}}{a_{33}} \\
&\times (a_{13}-a_{23})\Bigg] + \frac{\sigma_{yo}}{2}\Bigg[\beta_{12} + (\beta_{11}\beta_{22})^{1/2} \\
&+ (\beta_{11}\beta_{22})^{1/2}\Bigg(\frac{2\beta_{12}+\beta_{66}}{\beta_{11}} + 2\Big(\frac{\beta_{22}}{\beta_{11}}\Big)^{1/2}\Bigg)^{1/2} \\
&- a_{12} + a_{22} + \frac{a_{32}}{a_{33}}(a_{13}-a_{23})\Bigg]
\end{aligned} \tag{B.29}$$

For an isotropic medium, $\sigma_{zo} = \nu(\sigma_{xo} + \sigma_{yo})$ which gives

$$M_1 = -\frac{1}{E}(1-\nu^2)(\sigma_{xo} + \sigma_{yo}) \tag{B.30}$$

and M_2 and M_3 are defined in equation (B.27).

B.6 GENERAL EXPRESSIONS FOR STRESS COMPONENTS

At any point in the medium, the stress components in the x, y, z coordinate system induced by X_n, Y_n, Z_n are equal to

$$\sigma_{xh} = 2\,\mathrm{Re}[\mu_1^2\phi_1'(z_1) + \mu_2^2\phi_2'(z_2) + \lambda_3\mu_3^2\phi_3'(z_3)]$$

$$\sigma_{yh} = 2\,\mathrm{Re}[\phi_1'(z_1) + \phi_2'(z_2) + \lambda_3\phi_3'(z_3)]$$

$$\tau_{xyh} = -2\,\mathrm{Re}[\mu_1\phi_1'(z_1) + \mu_2\phi_2'(z_2) + \lambda_3\mu_3\phi_3'(z_3)]$$

$$\tau_{xzh} = 2\,\mathrm{Re}[\lambda_1\mu_1\phi_1'(z_1) + \lambda_2\mu_2\phi_2'(z_2) + \mu_3\phi_3'(z_3)]$$

$$\tau_{yzh} = -2\,\mathrm{Re}[\lambda_1\phi_1'(z_1) + \lambda_2\phi_2'(z_2) + \phi_3'(z_3)]$$

$$\sigma_{zh} = -\frac{1}{a_{33}}[a_{31}\sigma_{xh} + a_{32}\sigma_{yh} + a_{34}\tau_{yzh} + a_{35}\tau_{xzh} + a_{36}\tau_{xyh}] \tag{B.31}$$

In equation (B.31), ϕ_k' ($k = 1, 2, 3$) are the derivatives of the three analytic functions ϕ_k, defined in equation (B.6) with respect to the complex variable $z_k = x + \mu_k y$. For the present loading conditions, the expressions for the functions ϕ_k' are

$$\phi_1' = -\frac{1}{a\Delta((z_1/a)^2 - 1 - \mu_1^2)^{1/2}}[\overline{a_1}(\mu_2 - \lambda_2\lambda_3\mu_3) + \overline{b_1}(\lambda_2\lambda_3 - 1) + \overline{c_1}\lambda_3(\mu_3 - \mu_2)]\frac{1}{\xi_1}$$

$$\phi_2' = -\frac{1}{a\Delta((z_2/a)^2 - 1 - \mu_2^2)^{1/2}}[\overline{a_1}(\lambda_1\lambda_3\mu_3 - \mu_1) + \overline{b_1}(1 - \lambda_1\lambda_3) + \overline{c_1}\lambda_3(\mu_1 - \mu_3)]\frac{1}{\xi_2}$$

$$\phi_3' = -\frac{1}{a\Delta((z_3/a)^2 - 1 - \mu_3^2)^{1/2}}[\overline{a_1}(\mu_1\lambda_2 - \mu_2\lambda_1) + \overline{b_1}(\lambda_1 - \lambda_2) + \overline{c_1}(\mu_2 - \mu_1)]\frac{1}{\xi_3} \tag{B.32}$$

For all points located along the contour of the hole ($x = a\cos\theta$, $y = a\sin\theta$), ξ_k is equal to $e^{i\theta}$. Substituting this condition into equation (B.9), the square root terms in (B.32) are equal to

$$\left(\left(\frac{z_k}{a}\right)^2 - 1 - \mu_k^2\right)^{1/2} = i(\sin\theta - \mu_k\cos\theta) \tag{B.33}$$

for $k = 1$, 2 and 3. Combining (B.31), (B.32), (B.8) and (B.33), the stresses can be determined at each point along the wall of the hole.

If there is a plane of elastic symmetry normal to the z-axis (Fig. 5.26) (p. 236), the problem of interest can now be considered as the sum of two uncoupled problems.

1. A plane problem involving the stress components σ_{xh}, σ_{yh}, σ_{zh} and τ_{xyh} induced by X_n and Y_n only. μ_1 and μ_2 and their conjugates are the roots of the equation $l_4(\mu) = 0$.
2. An antiplane problem involving the stress components τ_{xzh}, τ_{yzh} induced by Z_n only. μ_3 and its conjugate are the roots of the equation $l_2(\mu) = 0$.

B.7 STRESSES AROUND A CIRCULAR HOLE DRILLED IN AN INFINITE ANISOTROPIC MEDIUM UNDER A 3D STATE OF STRESS ACTING AT INFINITY

The expressions of $\overline{a_1}$, $\overline{b_1}$, $\overline{c_1}$ defined in (B.12) are substituted into ϕ_1', ϕ_2' and ϕ_3' in (B.32). After mathematical manipulation, it can be shown that the stresses induced by drilling the hole can be expressed as

$$\begin{aligned}
\sigma_{xh} &= f_{11h}\sigma_{xo} + f_{12h}\sigma_{yo} + f_{13h}\sigma_{zo} + f_{14h}\tau_{yzo} + f_{15h}\tau_{xzo} + f_{16h}\tau_{xyo}\\
\sigma_{yh} &= f_{21h}\sigma_{xo} + f_{22h}\sigma_{yo} + f_{23h}\sigma_{zo} + f_{24h}\tau_{yzo} + f_{25h}\tau_{xzo} + f_{26h}\tau_{xyo}\\
\sigma_{zh} &= f_{31h}\sigma_{xo} + f_{32h}\sigma_{yo} + f_{33h}\sigma_{zo} + f_{34h}\tau_{yzo} + f_{35h}\tau_{xzo} + f_{36h}\tau_{xyo}\\
\tau_{yzh} &= f_{41h}\sigma_{xo} + f_{42h}\sigma_{yo} + f_{43h}\sigma_{zo} + f_{44h}\tau_{yzo} + f_{45h}\tau_{xzo} + f_{46h}\tau_{xyo}\\
\tau_{xzh} &= f_{51h}\sigma_{xo} + f_{52h}\sigma_{yo} + f_{53h}\sigma_{zo} + f_{54h}\tau_{yzo} + f_{55h}\tau_{xzo} + f_{56h}\tau_{xyo}\\
\tau_{xyh} &= f_{61h}\sigma_{xo} + f_{62h}\sigma_{yo} + f_{63h}\sigma_{zo} + f_{64h}\tau_{yzo} + f_{65h}\tau_{xzo} + f_{66h}\tau_{xyo}
\end{aligned} \tag{B.34}$$

or in matrix form

$$[\sigma_h]_{xyz} = [F_h][\sigma_o] \tag{B.35}$$

The total stresses are obtained by adding $[\sigma_o]$ to $[\sigma_h]_{xyz}$, that is

$$[\sigma]_{xyz} = [F][\sigma_o] \tag{B.36}$$

with $[F] = [F_h] + [I]$. In equation (B.34), the coefficients f_{ijh} $(i, j = 1\text{–}6)$ are equal to

$$\begin{aligned}
f_{11h} &= -\mathrm{Re}[i\gamma_1\mu_1^2(\lambda_2\lambda_3 - 1) + i\gamma_2\mu_2^2(1 - \lambda_1\lambda_3) \\
&\quad + i\gamma_3\mu_3^2\lambda_3(\lambda_1 - \lambda_2)] \\
f_{12h} &= -\mathrm{Re}[\gamma_1\mu_1^2(\mu_2 - \lambda_2\lambda_3\mu_3) \\
&\quad + \gamma_2\mu_2^2(\lambda_1\lambda_3\mu_3 - \mu_1) \\
&\quad + \gamma_3\mu_3^2\lambda_3(\mu_1\lambda_2 - \mu_2\lambda_1)] \\
f_{13h} &= 0 \\
f_{14h} &= \mathrm{Re}[\gamma_1\mu_1^2\lambda_3(\mu_3 - \mu_2) + \gamma_2\mu_2^2\lambda_3(\mu_1 - \mu_3) \\
&\quad + \gamma_3\mu_3^2\lambda_3(\mu_2 - \mu_1)] \\
f_{15h} &= -\mathrm{Re}[i\gamma_1\mu_1^2\lambda_3(\mu_3 - \mu_2) + i\gamma_2\mu_2^2\lambda_3(\mu_1 - \mu_3) \\
&\quad + i\gamma_3\mu_3^2\lambda_3(\mu_2 - \mu_1)] \\
f_{16h} &= \mathrm{Re}[\gamma_1\mu_1^2(\lambda_2\lambda_3 - 1) + \gamma_2\mu_2^2(1 - \lambda_1\lambda_3) \\
&\quad + \gamma_3\mu_3^2\lambda_3(\lambda_1 - \lambda_2)] + \mathrm{Re}[i\gamma_1\mu_1^2 \\
&\quad \times (\mu_2 - \lambda_2\lambda_3\mu_3) + i\gamma_2\mu_2^2(\lambda_1\lambda_3\mu_3 - \mu_1) \\
&\quad + i\gamma_3\mu_3^2\lambda_3(\mu_1\lambda_2 - \mu_2\lambda_1)]
\end{aligned} \tag{B.37}$$

$$\begin{aligned}
f_{21h} &= -\mathrm{Re}[i\gamma_1(\lambda_2\lambda_3 - 1) + i\gamma_2(1 - \lambda_1\lambda_3) \\
&\quad + i\gamma_3\lambda_3(\lambda_1 - \lambda_2)] \\
f_{22h} &= -\mathrm{Re}[\gamma_1(\mu_2 - \lambda_2\lambda_3\mu_3) + \gamma_2(\lambda_1\lambda_3\mu_3 - \mu_1) \\
&\quad + \gamma_3\lambda_3(\mu_1\lambda_2 - \mu_2\lambda_1)] \\
f_{23h} &= 0 \\
f_{24h} &= \mathrm{Re}[\gamma_1\lambda_3(\mu_3 - \mu_2) + \gamma_2\lambda_3(\mu_1 - \mu_3) \\
&\quad + \gamma_3\lambda_3(\mu_2 - \mu_1)] \\
f_{25h} &= -\mathrm{Re}[i\gamma_1\lambda_3(\mu_3 - \mu_2) + i\gamma_2\lambda_3(\mu_1 - \mu_3) \\
&\quad + i\gamma_3\lambda_3(\mu_2 - \mu_1)] \\
f_{26h} &= \mathrm{Re}[\gamma_1(\lambda_2\lambda_3 - 1) + \gamma_2(1 - \lambda_1\lambda_3) \\
&\quad + \gamma_3\lambda_3(\lambda_1 - \lambda_2)] + \mathrm{Re}[i\gamma_1 \\
&\quad \times (\mu_2 - \lambda_2\lambda_3\mu_3) + i\gamma_2(\lambda_1\lambda_3\mu_3 - \mu_1) \\
&\quad + i\gamma_3\lambda_3(\mu_1\lambda_2 - \mu_2\lambda_1)]
\end{aligned} \tag{B.38}$$

$$\begin{aligned}
f_{41h} &= \mathrm{Re}[i\gamma_1\lambda_1(\lambda_2\lambda_3 - 1) + i\gamma_2\lambda_2(1 - \lambda_1\lambda_3) \\
&\quad + i\gamma_3(\lambda_1 - \lambda_2)] \\
f_{42h} &= \mathrm{Re}[\gamma_1\lambda_1(\mu_2 - \lambda_2\lambda_3\mu_3) + \gamma_2\lambda_2(\lambda_1\lambda_3\mu_3 - \mu_1) \\
&\quad + \gamma_3(\mu_1\lambda_2 - \mu_2\lambda_1)] \\
f_{43h} &= 0 \\
f_{44h} &= -\mathrm{Re}[\gamma_1\lambda_1\lambda_3(\mu_3 - \mu_2) + \gamma_2\lambda_2\lambda_3(\mu_1 - \mu_3) \\
&\quad + \gamma_3(\mu_2 - \mu_1)] \\
f_{45h} &= \mathrm{Re}[i\gamma_1\lambda_3\lambda_1(\mu_3 - \mu_2) + i\gamma_2\lambda_3\lambda_2(\mu_1 - \mu_3) \\
&\quad + i\gamma_3(\mu_2 - \mu_1)] \\
f_{46h} &= -\mathrm{Re}[\gamma_1\lambda_1(\lambda_2\lambda_3 - 1) + \gamma_2\lambda_2(1 - \lambda_1\lambda_3) \\
&\quad + \gamma_3(\lambda_1 - \lambda_2)] - \mathrm{Re}[i\gamma_1\lambda_1 \\
&\quad \times (\mu_2 - \lambda_2\lambda_3\mu_3) + i\gamma_2\lambda_2(\lambda_1\lambda_3\mu_3 - \mu_1) \\
&\quad + i\gamma_3(\mu_1\lambda_2 - \mu_2\lambda_1)]
\end{aligned} \tag{B.39}$$

$$\begin{aligned}
f_{51h} &= -\mathrm{Re}[i\gamma_1\lambda_1\mu_1(\lambda_2\lambda_3 - 1) \\
&\quad + i\gamma_2\lambda_2\mu_2(1 - \lambda_1\lambda_3) + i\gamma_3\mu_3(\lambda_1 - \lambda_2)] \\
f_{52h} &= -\mathrm{Re}[\gamma_1\lambda_1\mu_1(\mu_2 - \lambda_2\lambda_3\mu_3) \\
&\quad + \gamma_2\lambda_2\mu_2(\lambda_1\lambda_3\mu_3 - \mu_1) \\
&\quad + \gamma_3\mu_3(\mu_1\lambda_2 - \mu_2\lambda_1)] \\
f_{53h} &= 0 \\
f_{54h} &= \mathrm{Re}[\gamma_1\lambda_1\lambda_3\mu_1(\mu_3 - \mu_2) + \gamma_2\lambda_2\lambda_3\mu_2(\mu_1 - \mu_3) \\
&\quad + \gamma_3\mu_3(\mu_2 - \mu_1)] \\
f_{55h} &= -\mathrm{Re}[i\gamma_1\lambda_3\lambda_1\mu_1(\mu_3 - \mu_2) \\
&\quad + i\gamma_2\lambda_3\lambda_2\mu_2(\mu_1 - \mu_3) + i\gamma_3\mu_3(\mu_2 - \mu_1)] \\
f_{56h} &= \mathrm{Re}[\gamma_1\lambda_1\mu_1(\lambda_2\lambda_3 - 1) + \gamma_2\lambda_2\mu_2(1 - \lambda_1\lambda_3) \\
&\quad + \gamma_3\mu_3(\lambda_1 - \lambda_2)] + \mathrm{Re}[i\gamma_1\lambda_1\mu_1 \\
&\quad \times (\mu_2 - \lambda_2\lambda_3\mu_3) + i\gamma_2\lambda_2\mu_2(\lambda_1\lambda_3\mu_3 - \mu_1) \\
&\quad + i\gamma_3\mu_3(\mu_1\lambda_2 - \mu_2\lambda_1)]
\end{aligned} \tag{B.40}$$

$$\begin{aligned}
f_{61h} &= \mathrm{Re}[i\gamma_1\mu_1(\lambda_2\lambda_3 - 1) \\
&\quad + i\gamma_2\mu_2(1 - \lambda_1\lambda_3) + i\gamma_3\lambda_3\mu_3(\lambda_1 - \lambda_2)] \\
f_{62h} &= \mathrm{Re}[\gamma_1\mu_1(\mu_2 - \lambda_2\lambda_3\mu_3) + \gamma_2\mu_2(\lambda_1\lambda_3\mu_3 - \mu_1) \\
&\quad + \gamma_3\lambda_3\mu_3(\mu_1\lambda_2 - \mu_2\lambda_1)]
\end{aligned}$$

$$
\begin{aligned}
f_{63h} &= 0 \\
f_{64h} &= -\mathrm{Re}[\gamma_1\lambda_3\mu_1(\mu_3-\mu_2)+\gamma_2\lambda_3\mu_2(\mu_1-\mu_3) \\
&\quad +\gamma_3\lambda_3\mu_3(\mu_2-\mu_1)] \\
f_{65h} &= \mathrm{Re}[i\gamma_1\lambda_3\mu_1(\mu_3-\mu_2) \\
&\quad +i\gamma_2\lambda_3\mu_2(\mu_1-\mu_3)+i\gamma_3\lambda_3\mu_3(\mu_2-\mu_1)] \\
f_{66h} &= -\mathrm{Re}[\gamma_1\mu_1(\lambda_2\lambda_3-1)+\gamma_2\mu_2(1-\lambda_1\lambda_3) \\
&\quad +\gamma_3\lambda_3\mu_3(\lambda_1-\lambda_2)]-\mathrm{Re}[i\gamma_1\mu_1 \\
&\quad \times(\mu_2-\lambda_2\lambda_3\mu_3)+i\gamma_2\mu_2(\lambda_1\lambda_3\mu_3-\mu_1) \\
&\quad +i\gamma_3\lambda_3\mu_3(\mu_1\lambda_2-\mu_2\lambda_1)]
\end{aligned}
\tag{B.41}
$$

$$
f_{3ih} = -\frac{1}{a_{33}}[a_{31}f_{1ih}+a_{32}f_{2ih}+a_{34}f_{4ih} +a_{35}f_{5ih}+a_{36}f_{6ih}] \quad i=1\text{–}6 \tag{B.42}
$$

In equations (B.37)–(B.41), the coefficients γ_k ($k = 1,2,3$) are equal to

$$
\gamma_k = \frac{\sin\theta + i\cos\theta}{\Delta(\sin\theta-\mu_k\cos\theta)} \tag{B.43}
$$

If there is a plane of elastic symmetry normal to the z-axis (Fig. 5.26) (p. 236), equations (B.37)–(B.42) take simpler forms. Let γ be defined as

$$
\gamma = \frac{\sin\theta + i\cos\theta}{(\sin\theta-\mu_1\cos\theta)(\sin\theta-\mu_2\cos\theta)} \tag{B.44}
$$

Equations (B.37)–(B.42) become

$$
\begin{aligned}
f_{11h} &= -\mathrm{Re}[i\gamma((\mu_1+\mu_2)\sin\theta-\mu_1\mu_2\cos\theta)] \\
f_{12h} &= \mathrm{Re}[\mu_1\mu_2\gamma\sin\theta] \\
f_{16h} &= \mathrm{Re}[\gamma((\mu_1+\mu_2)\sin\theta-\mu_1\mu_2\cos\theta)] \\
&\quad -\mathrm{Re}[i\mu_1\mu_2\gamma\sin\theta] \\
f_{13h} &= f_{14h} = f_{15h} = 0
\end{aligned}
\tag{B.45}
$$

$$
\begin{aligned}
f_{21h} &= -\mathrm{Re}[i\gamma\cos\theta] \\
f_{22h} &= -\mathrm{Re}[\gamma(\sin\theta-\cos\theta(\mu_1+\mu_2))] \\
f_{26h} &= \mathrm{Re}[\gamma\cos\theta)] \\
&\quad +\mathrm{Re}[i\gamma(\sin\theta-\cos\theta(\mu_1+\mu_2))] \\
f_{23h} &= f_{24h} = f_{25h} = 0
\end{aligned}
\tag{B.46}
$$

$$
\begin{aligned}
f_{44h} &= -\mathrm{Re}\left[\frac{\sin\theta+i\cos\theta}{\sin\theta-\mu_3\cos\theta}\right] \\
f_{45h} &= \mathrm{Re}\left[i\frac{\sin\theta+i\cos\theta}{\sin\theta-\mu_3\cos\theta}\right] \\
f_{41h} &= f_{42h} = f_{43h} = f_{46h} = 0
\end{aligned}
\tag{B.47}
$$

$$
\begin{aligned}
f_{54h} &= \mathrm{Re}\left[\mu_3\frac{\sin\theta+i\cos\theta}{\sin\theta-\mu_3\cos\theta}\right] \\
f_{55h} &= -\mathrm{Re}\left[i\mu_3\frac{\sin\theta+i\cos\theta}{\sin\theta-\mu_3\cos\theta}\right] \\
f_{51h} &= f_{52h} = f_{53h} = f_{56h} = 0
\end{aligned}
\tag{B.48}
$$

$$
\begin{aligned}
f_{61h} &= \mathrm{Re}[i\gamma\sin\theta] \\
f_{62h} &= -\mathrm{Re}[\mu_1\mu_2\gamma\cos\theta] \\
f_{66h} &= -\mathrm{Re}[\gamma\sin\theta] \\
&\quad +\mathrm{Re}[i\mu_1\mu_2\gamma\cos\theta] \\
f_{63h} &= f_{64h} = f_{65h} = 0
\end{aligned}
\tag{B.49}
$$

If the medium is isotropic with Young's modulus E and Poisson's ratio ν, substituting $\mu_1 = \mu_2 = \mu_3 = i$ in equations (B.45)–(B.49) gives

$$
\begin{aligned}
f_{11h} &= -\cos^4\theta + 2\sin^4\theta - 3\sin^2\theta\cos^2\theta \\
f_{12h} &= -\sin^4\theta + 3\sin^2\theta\cos^2\theta \\
f_{16h} &= -8\sin^3\theta\cos\theta \\
f_{21h} &= 3\sin^2\theta\cos^2\theta - \cos^4\theta \\
f_{22h} &= -\sin^4\theta + 2\cos^4\theta - 3\sin^2\theta\cos^2\theta \\
f_{26h} &= -8\sin\theta\cos^3\theta \\
f_{44h} &= \cos 2\theta \\
f_{45h} &= f_{54h} = -\sin 2\theta \\
f_{55h} &= -\cos 2\theta \\
f_{61h} &= -3\sin^3\theta\cos\theta + \sin\theta\cos^3\theta \\
f_{62h} &= \cos\theta\sin^3\theta - 3\sin\theta\cos^3\theta \\
f_{66h} &= -\sin^4\theta - \cos^4\theta + 6\sin^2\theta\cos^2\theta
\end{aligned}
\tag{B.50}
$$

Once the stress components in the x, y, z coordinate system are determined, the stress components in the r, θ, z cylindrical coordinate

system can be determined by combining equations (B.36) and (A.17). For points along the wall of the hole, $\sigma_r = \tau_{r\theta} = \tau_{rz} = 0$. For the isotropic case, it can be shown that the non-vanishing stress components are equal to

$$\begin{aligned}\sigma_\theta &= \sigma_{xo}(1 - 2\cos 2\theta) \\ &\quad + \sigma_{yo}(1 + 2\cos 2\theta) - 4\tau_{xyo}\sin 2\theta \\ \sigma_z &= \sigma_{zo} - 2\nu\sigma_{xo}\cos 2\theta + 2\nu\sigma_{yo}\cos 2\theta \\ &\quad - 4\nu\tau_{xyo}\sin 2\theta \\ \tau_{\theta z} &= 2\tau_{yzo}\cos\theta - 2\tau_{xzo}\sin\theta\end{aligned} \tag{B.51}$$

B.8 STRAIN COMPONENTS

The strain components in the x, y, z coordinate system can be determined by combining equations (B.36) and (5.8). The strain components in the r, θ, z cylindrical coordinate system can be calculated as follows:

$$[\varepsilon]_{r\theta z} = [T_{r\theta z}][\varepsilon]_{xyz} \tag{B.52}$$

where $[\varepsilon]^t_{xyz} = [\varepsilon_x, \varepsilon_y, \varepsilon_z, \gamma_{yz}, \gamma_{xz}, \gamma_{xy}]$, $[\varepsilon]^t_{r\theta z} = [\varepsilon_r, \varepsilon_\theta, \varepsilon_z, \gamma_{\theta z}, \gamma_{rz}, \gamma_{r\theta}]$ and $[T_{r\theta z}]$ is a (6×6) coordinate transformation matrix for strains equal to

$$\begin{bmatrix} \cos^2\theta & \sin^2\theta & 0 & 0 & 0 & \dfrac{\sin 2\theta}{2} \\ \sin^2\theta & \cos^2\theta & 0 & 0 & 0 & -\dfrac{\sin 2\theta}{2} \\ 0 & 0 & 1 & 0 & 0 & 0 \\ 0 & 0 & 0 & \cos\theta & -\sin\theta & 0 \\ 0 & 0 & 0 & \sin\theta & \cos\theta & 0 \\ -\sin 2\theta & \sin 2\theta & 0 & 0 & 0 & \cos 2\theta \end{bmatrix} \tag{B.53}$$

In the isotropic case, it can be shown that the strain components ε_θ, ε_z and $\gamma_{\theta z}$ are such that

$$\begin{aligned}E\varepsilon_\theta &= \sigma_{xo} + \sigma_{yo} - \nu\sigma_{zo} - 2(1 - \nu^2) \\ &\quad \times [(\sigma_{xo} - \sigma_{yo})\cos 2\theta \\ &\quad + 2\tau_{xyo}\sin 2\theta] \\ E\varepsilon_z &= \sigma_{zo} - \nu(\sigma_{xo} + \sigma_{yo}) \\ E\gamma_{\theta z} &= 4(1 + \nu)[\tau_{yzo}\cos\theta - \tau_{xzo}\sin\theta]\end{aligned} \tag{B.54}$$

AUTHOR INDEX

SUBJECT INDEX